CONCEPTS AND APPLICATIONS OF FINITE ELEMENT ANALYSIS

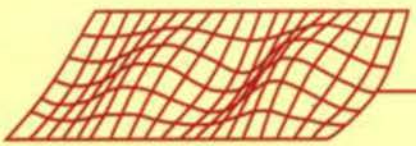

FOURTH EDITION

ROBERT D. COOK • DAVID S. MALKUS
MICHAEL E. PLESHA • ROBERT J. WITT

CONCEPTS AND APPLICATIONS OF FINITE ELEMENT ANALYSIS

FOURTH EDITION

CONCEPTS AND APPLICATIONS OF FINITE ELEMENT ANALYSIS

FOURTH EDITION

Robert D. Cook
David S. Malkus
Michael E. Plesha
Robert J. Witt

University of Wisconsin—Madison

JOHN WILEY & SONS, INC.

Acquisition Editor	Wayne Anderson
Production	Jeanine Furino
Marketing Manager	Katherine Hepburn
Designer	Kevin Murphy
Production Management Services	Publication Services, Inc.

This book was typeset in 10/12 Times Roman by Publication Services, Inc. and printed and bound by Hamilton Printing Company. The cover was printed by The Lehigh Press, Inc.

The paper in this book was manufactured by a mill whose forest management programs include sustained yield harvesting of its timberlands. Sustained yield harvesting principles ensure that the number of trees cut each year does not exceed the amount of new growth.

Copyright © 1974, 1981, 1989, 2002 by John Wiley & Sons. Inc. All rights reserved. ♾

No part of this publication may be reproduced, stored in a retrieval system or transmitted in any form or by any means, electronic, mechanical, photocopying, recording, scanning or otherwise, except as permitted under Sections 107 or 108 of the 1976 United States Copyright Act, without either the prior written permission of the Publisher, or authorization through payment of the appropriate per-copy fee to the Copyright Clearance Center, 222 Rosewood Drive, Danvers, MA 01923, (978) 750-8400, fax (978) 646-8600. Requests to the Publisher for permission should be addressed to the Permissions Department, John Wiley & Sons, Inc., 111 River Street, Hoboken, NJ 07030, (201) 748-6011, fax (201) 748-6008.

To order books or for customer service please, call 1(800)-CALL-WILEY (225-5945).

Library of Congress Cataloging in Publication Data:

Concepts and applications of finite element analysis / Robert D. Cook ... [et al.].--4th ed.
p. cm.
Previous ed. authored by Robert D. Cook, David S. Malkus, Michael E. Plesha.
Includes bibliographical references.
ISBN 978-0-471-35605-9 (cloth : alk. paper)
1. Structural analysis (Engineering) 2. Finite element method. I. Cook, Robert Davis.
II. Cook, Robert Davis. Concepts and applications of finite element analysis.

TA646 .C66 2001
624.1'71--dc21

2001033009

Printed in the United States
20 19 18 17 16 15 14 13 12 11

About the Authors

Robert D. Cook received his Ph.D. in Theoretical and Applied Mechanics from the University of Illinois in 1963. Since then he has been at the University of Wisconsin-Madison, where he is now a professor in the Department of Engineering Physics. His interests include stress analysis and finite element methods. In addition to the present book, he is author of *Finite Element Modeling for Stress Analysis* (Wiley, 1995) and *Advanced Mechanics of Materials* (2nd edition, Prentice-Hall, 1999, With Warren C. Young).

David S. Malkus received his Ph.D. from Boston University in 1976. He spent two years at the National Bureau of Standards and seven years in the Mathematics Department of Illinois Institute of Technology. He is now Professor of Engineering Mechanics at the University of Wisconsin-Madison. His research interests concern application of the finite element method to problems of structural and continuum mechanics, in particular the flow of non-Newtonian fluids. He is a member of the Rheology Research Center (University of Wisconsin-Madison) and the Society of Rheology.

Michael E. Plesha received his B.S. from the University of Illinois at Chicago, and his M.S. and Ph.D. degrees from Northwestern University, the Ph.D. degree in 1983. He has been a faculty member in the Department of Engineering Physics at the University of Wisconsin-Madison since 1983 where he is Professor of Engineering Mechanics. His research areas include constitutive modeling and finite element analysis of contact-friction problems, transient finite element analysis, and discrete element methods.

Robert J. Witt received his Ph.D. in Nuclear Engineering from the Massachusetts Institute of Technology in 1987. He is now an associate professor in the Department of Engineering Physics at the University of Wisconsin-Madison. His research interests are in computational methods of fluid and solid mechanics, with particular application to nuclear systems.

PREFACE

With this new edition we have, as usual, reorganized and thoroughly revised the preceding edition. The more prominent changes are new chapters on modeling, error estimation and convergence; modernization of the chapter on elastic-plastic problems; and inclusion of application problems in which a finite element analysis is planned and executed, and results are critically examined. Much of the latter material comes from the book *Finite Element Modeling for Stress Analysis* (Wiley, 1995; used by permission of the publisher).

This book steers a middle course between books that are quite elementary or favor applications to the exclusion of theory, and books that are strongly theoretical, advanced, or highly detailed. We believe this book is suitable for a first course in the subject and contains enough material for a second course as well. Prerequisites are the usual undergraduate courses in calculus, statics, dynamics, and mechanics of materials. Knowledge of matrix notation and elementary matrix algebra, as summarized in Appendix A, is also assumed. Concepts from other courses are introduced as needed. Prior knowledge of these concepts is not necessary but will, of course, smooth the way. Throughout the book we emphasize the more basic, simple, and useful concepts. Advanced techniques are left to references cited. Tens of thousands of references are available; we cite only those that seem most appropriate or most accessible. In most cases, a citation does not imply priority of discovery.

A course that leans toward practical application may emphasize Chapters 1, 2, 3, 9, and 10. A course more oriented toward theory may emphasize other chapters. Worked-out solutions to analytical problems are available on a CD-ROM that the publisher will provide on request to instructors who adopt the book as a course text. The same CD also contains simple Fortran programs for linear time-independent, buckling, and vibration problems, into which the user can insert test code for element formulation and postprocessing such as stress calculation.

Our experience is that study of the theory of finite elements is not sufficient to produce competence in their use. Accordingly, we hope that students will be required to solve problems using software already written, with proper attention to planning the analysis, anticipating results, and properly checking the results. Computational problems are suggested at the ends of several chapters. These problems are of simple geometry so that time need not be wasted on data input chores. More complicated problems can, of course, be chosen, but even simple problems reveal many misunderstandings about modeling, on the part of graduate students as well as undergraduates.

This book is not directed toward use of any particular software package. However, in association with the book, the publisher offers the finite element software *VisualFEA*, written by J. Y. Lee. This software addresses linear statics and dynamics, some nonlinear structural problems, seepage flow, and steady-state heat conduction. It includes powerful pre- and postprocessing and graphic display, and educational features not found in commercial software.

Our presentation of structural dynamics is partially based on course notes of Ted Belytschko. T. J. R. Hughes provided guidance. Jeff Crowell supplied helpful notes about plasticity. We are grateful to all.

CONTENTS

NOTATION

Chapter 1 INTRODUCTION 1

1.1 Finite Element Analysis 1
1.2 Problem Classification, Modeling, and Discretization 3
1.3 Interpolation. Elements, Nodes, and D.O.F. 5
1.4 Example Applications. History of FEA 8
1.5 Solving a Problem by FEA 11
1.6 Learning and Using FEA 15
Analytical Problems 17

Chapter 2 ONE-DIMENSIONAL ELEMENTS AND COMPUTATIONAL PROCEDURES 19

2.1 Introduction 19
2.2 Bar Element 20
2.3 Beam Element 24
2.4 Bar and Beam Elements of Arbitrary Orientation 29
2.5 Assembly of Elements 32
2.6 Properties of Stiffness Matrices 36
2.7 Boundary Conditions 40
2.8 Exploiting Sparsity. Solving Equations 42
2.9 Mechanical Loads. Stresses 46
2.10 Thermal Loads. Stresses 52
2.11 Structural Symmetry 54
2.12 Review. Remarks Regarding Modeling 57
2.13 An Application 59
Analytical Problems 62
Computational Problems 74

Chapter 3 BASIC ELEMENTS 78

3.1 Preliminaries 78
3.2 Interpolation and Shape Functions 83
3.3 Formulas for Element Matricies 88
3.4 Linear Triangle (CST) 91
3.5 Quadratic Triangle (LST) 95
3.6 Bilinear Rectangle (Q4) 96
3.7 Quadratic Rectangle (Q8, Q9) 100
3.8 Rectangular Solid Elements 102
3.9 Choice of Interpolation Functions 104
3.10 Improved Triangles and Quadrilaterals 106

3.11 Nodal Loads **111**
3.12 Stress Calculation **115**
3.13 Nature of a Finite Element Solution **118**
3.14 Example: A Simple Stress Concentration Problem **119**
3.15 An Application with High Stress Gradient **121**
Analytical Problems **124**
Computational Problems **132**

Chapter 4 FORMULATION TECHNIQUES: VARIATIONAL METHODS 136

4.1 Introduction **136**
4.2 Principle of Stationary Potential Energy **137**
4.3 Problems Having Many D.O.F. **140**
4.4 Potential Energy of an Elastic Body **142**
4.5 The Rayleigh-Ritz Method **146**
4.6 Comments Regarding the Rayleigh-Ritz Method **149**
4.7 Strong Form and Weak Form **151**
4.8 Finite Element Form of the Rayleigh-Ritz Method **156**
4.9 Convergence of Finite Element Solutions **161**
4.10 Additional Formulations. Hybrid Elements **165**
Analytical Problems **171**

Chapter 5 FORMULATION TECHNIQUES: GALERKIN AND OTHER WEIGHTED RESIDUAL METHODS 179

5.1 Galerkin Method **179**
5.2 Methods of Weighted Residuals (MWR) **182**
5.3 Galerkin Finite Element Method in One Dimension **186**
5.4 Integration by Parts **191**
5.5 Galerkin Finite Element Method in Two Dimensions **193**
5.6 A Mixed Formulation **195**
Analytical Problems **198**

Chapter 6 ISOPARAMETRIC ELEMENTS 202

6.1 Introduction **202**
6.2 Bilinear Quadrilateral (Q4) **205**
6.3 Quadrature: [**k**] Obtained by Numerical Integration **209**
6.4 Quadratic Quadrilaterals (Q8, Q9) **213**
6.5 Hexahedral Isoparametric Elements **217**
6.6 Incompatible Modes. Nodeless D.O.F. **219**
6.7 Static Condensation **221**
6.8 Choices in Numerical Integration **223**
6.9 Load Considerations **227**
6.10 Stress Calculation **230**
6.11 Effect of Element Geometry **234**
6.12 Validity of Isoparametric Elements **237**
6.13 Patch Test **238**

6.14 A 2D Application 240
6.15 A 3D Application 244
Analytical Problems 247
Computational Problems 255

Chapter 7 ISOPARAMETRIC TRIANGLES AND TETRAHEDRA 259

7.1 Reference Coordinates. Shape Functions 259
7.2 Element Characteristic Matrices 262
7.3 Analytical Integration. Area and Volume Coordinates 264
7.4 Numerical Integration 266
Analytical Problems 268

Chapter 8 COORDINATE TRANSFORMATION AND SELECTED ANALYSIS OPTIONS 271

8.1 Transformation: Introduction and Vector Forms 271
8.2 Strain, Stress, and Material Property Transformation 273
8.3 Transformation of the Characteristic Matrix 275
8.4 Changing the Directions of Restraints 276
8.5 Connecting Dissimilar Elements. Rigid Elements 278
8.6 Higher Derivatives as Nodal D.O.F. 282
8.7 Fracture Mechanics. Singularity Elements 283
8.8 Elastic Foundations. Infinite Media 286
8.9 Structural Modification. Reanalysis 292
8.10 Tests of Element Quality 293
Analytical Problems 295
Computational Problems 299

Chapter 9 ERROR, ERROR ESTIMATION, AND CONVERGENCE 300

9.1 Sources of Error 300
9.2 Ill-Conditioning 302
9.3 The Condition Number 306
9.4 Diagonal Decay Test 308
9.5 Residuals 309
9.6 Discretization Error. Convergence Rate 310
9.7 Multimesh Extrapolation 315
9.8 Mesh Revision Methods 318
9.9 Gradient (Stress) Recovery and Smoothing 320
9.10 *A-Posteriori* Error Estimate 326
9.11 Adaptive Meshing 329
Analytical Problems 331
Computational Problems 335

Chapter 10 MODELING CONSIDERATIONS AND SOFTWARE USE 336

10.1 Introduction 336
10.2 Physical Behavior Versus Element Behavior 337
10.3 Element Shapes and Interconnection 340

10.4 Test Cases and Pilot Studies **342**
10.5 Material Properties **344**
10.6 Loads and Reactions **347**
10.7 Connections in Structures **348**
10.8 Boundary Conditions **352**
10.9 Repetitive Symmetry **354**
10.10 Stress Concentrations. Submodels **356**
10.11 Substructures **358**
10.12 Planning an Analysis **360**
10.13 Common Mistakes **363**
10.14 Checking the Model **365**
10.15 Critique of Computed Results **366**
10.16 Design Optimization **369**
10.17 Software **370**
10.18 Concluding Remarks **371**
Analytical Problems **371**
Computational Problems **372**

Chapter 11 FINITE ELEMENTS IN STRUCTURAL DYNAMICS AND VIBRATIONS 373

11.1 Introduction **373**
11.2 Dynamic Equations. Mass and Damping Matrices **374**
11.3 Mass Matrices: Consistent, Diagonal, and Other **377**
11.4 Natural Frequencies and Modes **383**
11.5 Damping **388**
11.6 Reduction of the Number of D.O.F. **390**
11.7 Response History: Modal Methods **394**
11.8 Response History: Ritz Vectors **398**
11.9 Component Mode Synthesis (CMS) **400**
11.10 Harmonic Response **405**
11.11 Response History: Direct Integration Methods **407**
11.12 Explicit Direct Integration **409**
11.13 Implicit Direct Integration **416**
11.14 Direct Integration: Stability and Accuracy Analysis **421**
11.15 Analysis by Response Spectra **426**
11.16 Remarks. Modeling Considerations **429**
11.17 An Application: Vibration and Harmonic Response **436**
11.18 An Application: Response History **439**
Analytical Problems **444**
Computational Problems **451**

Chapter 12 HEAT TRANSFER AND SELECTED FLUID PROBLEMS 454

12.1 Heat Transfer: Introduction **454**
12.2 Finite Element Formulation **459**
12.3 Radiation. Nonlinear Heat Transfer Problems **462**
12.4 Transient Thermal Analysis **464**
12.5 Modeling Considerations. Remarks **467**

12.6 An Application **469**
12.7 Acoustic Frequencies and Modes **474**
12.8 Fluid-Structure Interaction **477**
12.9 Plane Incompressible Irrotational Flow **480**
Analytical Problems **482**
Computational Problems **486**

Chapter 13 CONSTRAINTS: PENALTY FORMS, LOCKING, AND CONSTRAINT COUNTING 489

13.1 Explicit Constraints. Transformation Equations **489**
13.2 Lagrange Multipliers to Enforce Constraints **492**
13.3 Penalty Functions to Enforce Constraints **493**
13.4 Implicit Penalty Constraints and Locking **495**
13.5 Constraint Counting **499**
13.6 Remarks About Techniques for Incompressible Media **502**
Analytical Problems **504**

Chapter 14 SOLIDS OF REVOLUTION 508

14.1 Introduction. Elasticity Relations for Axial Symmetry **508**
14.2 Axisymmetric Solid Elements **510**
14.3 An Application **512**
14.4 Loads Without Axial Symmetry: Introduction **516**
14.5 Loads Without Axial Symmetry: Some Details of FEA **521**
Analytical Problems **524**
Computational Problems **527**

Chapter 15 PLATE BENDING 530

15.1 Introduction. Plate Behavior **530**
15.2 C^1 (Kirchhoff) Plate Elements **536**
15.3 C^0 (Mindlin) Plate Elements **542**
15.4 Mindlin Beam. More Devices for C^0 Plate Elements **547**
15.5 Boundary Conditions. Test Problems **551**
15.6 An Application **553**
Analytical Problems **556**
Computational Problems **559**

Chapter 16 SHELLS 561

16.1 Introduction **561**
16.2 Circular Arches and Arch Elements **563**
16.3 Shells of Revolution **570**
16.4 General Shells: Three- and Four-Node Elements **574**
16.5 General Shells: Curved Isoparametric Elements **578**
16.6 Test Cases. Remarks **583**
16.7 An Axisymmetric Shell Application **586**
Analytical Problems **588**
Computational Problems **591**

Chapter 17 NONLINEARITY: AN INTRODUCTION 595

17.1 Nonlinear Problems **595**
17.2 Some Solution Methods **596**
17.3 Plasticity: Introduction **602**
17.4 Plasticity: General Formulation for Small Strains **606**
17.5 Plasticity: Formulation for Von Mises Theory **609**
17.6 Plasticity: Some Computational Procedures **612**
17.7 Nonlinear Dynamic Problems **616**
17.8 Problems of Gaps and Contact **619**
17.9 Geometric Nonlinearity **621**
17.10 Modeling Considerations. Remarks **626**
Analytical Problems **630**
Computational Problems **636**

Chapter 18 STRESS STIFFNESS AND BUCKLING 639

18.1 Introduction. Energy Considerations **639**
18.2 Bar and Beam Elements **642**
18.3 Plate Elements **645**
18.4 A General Formulation **646**
18.5 Calculation of Buckling Loads **648**
18.6 Remarks on Stress Stiffness and Its Uses **650**
18.7 Remarks and Examples **653**
Analytical Problems **656**
Computational Problems **661**

Appendix A MATRICES: SELECTED DEFINITIONS AND MANIPULATIONS 663

Appendix B SIMULTANEOUS ALGEBRAIC EQUATIONS 668

B.1 Overview **668**
B.2 Direct Solvers **668**
B.3 Iterative Solvers **671**

Appendix C EIGENVALUES AND EIGENVECTORS 675

C.1 Overview **675**
C.2 The Standard Eigenproblem **675**
C.3 The General Eigenproblem **676**
C.4 Solution Algorithms **679**

REFERENCES 682

INDEX 711

NOTATION

Symbols used throughout most of the book are listed. Symbols less frequently used, or that have different meanings in different contexts, are defined where they are used. Matrices and vectors are identified by boldface type.

MATHEMATICAL SYMBOLS

$[\ ], \lceil\ \rfloor$	Rectangular matrix or square matrix, diagonal matrix
$\{\ \}, \lfloor\ \rfloor$	Column vector, row vector
$[\ ]^T$	Matrix transpose (thus $\{\ \} = \lfloor\ \rfloor^T$)
$[\ ]^{-1}, [\ ]^{-T}$	Matrix inverse, transpose of inverse ($\equiv$ inverse of transpose)
$\|\ \|$	Norm of a matrix or vector
$\cdot$	Time differentiation; for example, $\dot{u} = du/dt$, $\ddot{u} = d^2u/dt^2$
,	Partial differentiation if the following subscript is a letter; for example $w_{,x} = \partial w/\partial x$, $w_{,xy} = \partial^2 w/\partial x \partial y$
$\left\{\dfrac{\partial \Pi}{\partial \mathbf{a}}\right\}$	Represents $\left\lfloor \dfrac{\partial \Pi}{\partial a_1}\ \dfrac{\partial \Pi}{\partial a_2}\ \cdots\ \dfrac{\partial \Pi}{\partial a_n} \right\rfloor^T$, where $\Pi = \Pi(a_1, a_2, \cdots, a_n)$

LATIN SYMBOLS

A	Area or cross-sectional area
$\{\mathbf{a}\}$	Generalized d.o.f. (also known as generalized coordinates)
B	Bulk modulus, $B = E/(3 - 6\nu)$
$[\mathbf{B}]$	Spatial derivatives of field variables are $[\mathbf{B}]\{\mathbf{d}\}$
C^m	Field continuity of degree m (Section 3.2)
$[\mathbf{C}]$	Damping matrix; constraint matrix
D	Displacement; flexural rigidity of a plate or a shell
$\{\mathbf{D}\}, \{\mathbf{d}\}$	Nodal d.o.f. of structure and element, respectively
$\{\bar{\mathbf{D}}\}$	Amplitudes of nodal d.o.f. (as in vibration or buckling)
d.o.f.	Degree(s) of freedom
E	Modulus of elasticity
$[\mathbf{E}]$	Matrix of elastic stiffnesses; $[\mathbf{E}] = E$ in one dimension
$\{\mathbf{F}\}$	Body forces per unit volume
f	Cyclic frequency of vibration, $f = \omega/2\pi$; flux
G	Shear modulus
h	Characteristic length; convective heat transfer coefficient
I	Moment of inertia of cross-sectional area
$\lceil \mathbf{I} \rfloor$	Unit matrix, also called identity matrix
J	Determinant of $[\mathbf{J}]$
$[\mathbf{J}]$	Jacobian matrix (Section 6.2)
k	Spring stiffness, or bar stiffness AE/L, or thermal conductivity
$[\mathbf{K}], [\mathbf{k}]$	Conventional stiffness matrix of structure, element
$[\mathbf{K}_\sigma], [\mathbf{k}_\sigma]$	Stress stiffness matrix of structure, element

L, L_T	Length of element, length of structure
l, m, n	Direction cosines
$[\mathbf{M}], [\mathbf{m}]$	Mass matrix of structure, element
N_{els}	Number of elements
$[\mathbf{N}]$	Shape (or basis, or interpolation) functions
O	Order; for example $O(h^2)$ = a term of order h^2
$[\mathbf{0}], \{\mathbf{0}\}$	Null matrix, null vector
$\{\mathbf{P}\}$	Externally applied concentrated loads on structure nodes
p	Pressure; degree of a complete polynomial
q	Distributed load, per unit length or per unit area
$\{\mathbf{R}\}$	Total load on structure nodes; $\{\mathbf{R}\} = \{\mathbf{P}\} + \sum\{\mathbf{r}_e\}$
$\{\mathbf{r}_e\}$	Loads applied to nodes by an element (Section 2.5)
S	Surface or surface area
T	Temperature
t	Thickness; time
$[\mathbf{T}]$	Transformation matrix
U, U_0	Strain energy, strain energy per unit volume
u, v, w	Displacement components in coordinate directions
$\{\mathbf{u}\}$	Vector of displacements, $\{\mathbf{u}\} = \lfloor u \;\; v \;\; w \rfloor^T$
V	Volume
x, y, z	Cartesian coordinates

GREEK SYMBOLS

α	Coefficient of thermal expansion; penalty number
$[\mathbf{\Gamma}]$	Jacobian matrix inverse, $[\mathbf{\Gamma}] = [\mathbf{J}]^{-1}$
$\{\boldsymbol{\varepsilon}\}, \{\boldsymbol{\varepsilon}_0\}$	Vector of strains, vector of initial strains
η	A global error measure, computed from the gradient field
$\theta_x, \theta_y, \theta_z$	Rotation components about coordinate axes
$[\boldsymbol{\kappa}], \{\boldsymbol{\kappa}\}$	Matrix of thermal conductivities, vector of curvatures
λ	Eigenvalue; Lagrange multiplier
ν	Poisson's ratio
ξ	Damping ratio (ratio of actual damping to critical damping)
ξ, η, ζ	Reference coordinates of isoparametric elements
Π	A functional; for example Π_p = potential energy functional
ρ	Mass density
$\{\boldsymbol{\sigma}\}, \{\boldsymbol{\sigma}_0\}$	Vector of stresses, vector of initial stresses
σ_e	von Mises stress, Eq. 3.12-2 (also called effective stress)
$[\mathbf{\Phi}]$	Modal matrix
$\{\mathbf{\Phi}\}$	Surface tractions
$\omega, \lceil \boldsymbol{\omega}^2 \rfloor$	Circular frequency in radians per second, spectral matrix

CHAPTER 1

INTRODUCTION

This chapter outlines the finite element method—what it is, to what problems it may be applied, and how it should be used. Details of these matters and appropriate theory occupy the remainder of the book.

1.1 FINITE ELEMENT ANALYSIS

Finite element analysis (FEA), also called the finite element method (FEM), is a method for numerical solution of field problems. A field problem requires that we determine the spatial distribution of one or more dependent variables. Thus we may seek the distribution of temperature in the piston of an engine, or we may seek the distribution of displacements and stresses in a paving slab. Mathematically, a field problem is described by differential equations or by an integral expression. Either description may be used to formulate finite elements. Finite element (FE) formulations, in ready-to-use form, are contained in general-purpose FEA programs. It is possible to use FEA programs while having little knowledge of the analysis method or the problem to which it is applied, inviting consequences that may range from embarrassing to disastrous.

Individual finite elements can be visualized as small pieces of a structure. The word "finite" distinguishes these pieces from infinitesimal elements used in calculus. In each finite element a field quantity is allowed to have only a simple spatial variation, perhaps described by polynomial terms up to x^2, xy, and y^2. The actual variation in the region spanned by an element is almost certainly more complicated, so FEA provides an approximate solution. Elements are connected at points called *nodes* (Fig. 1.1-1). The assemblage of elements is called a finite element structure, the word "structure" being used in a general sense to mean a defined body or region. The particular arrangement of elements is called a *mesh*. Numerically, an FE mesh is represented by a system of algebraic equations to be solved for unknowns at nodes. Nodal unknowns are values of the field quantity and, depending on element type, perhaps also its first derivatives. The solution for nodal quantities, when combined with the assumed field in any given element, completely determines the spatial variation of the field in that element. Thus the field quantity over the entire structure is approximated element by element, in piecewise fashion. Although an FEA solution is not exact (unless the problem is so simple that FEA is probably inappropriate), the solution can be improved by using more elements to represent the structure.

FEA has advantages over most other numerical analysis methods, including versatility and physical appeal.

- FEA is applicable to any field problem: heat transfer, stress analysis, magnetic fields, and so on.
- There is no geometric restriction. The body or region analyzed may have any shape.

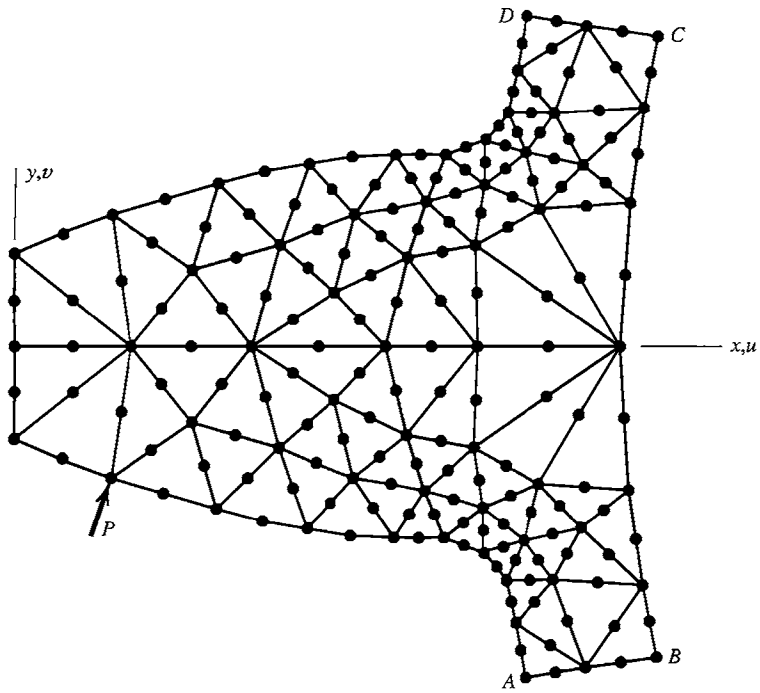

Figure 1.1-1. A two-dimensional model of a gear tooth. All nodes and elements lie in the plane of the figure. Supports are not shown.

- Boundary conditions and loading are not restricted. For example, in stress analysis, any portion of a body may be supported, while distributed or concentrated forces may be applied to any other portion.
- Material properties are not restricted to isotropy and may change from one element to another or even within an element.
- Components that have different behaviors, and different mathematical descriptions, can be combined. Thus a single FE model might contain bar, beam, plate, cable, and friction elements.
- An FE structure closely resembles the actual body or region to be analyzed.
- The approximation is easily improved by grading the mesh so that more elements appear where field gradients are high and more resolution is required.

Other numerical methods have arisen since FEA appeared, but at present only FEA can confidently claim all these attributes.

Overview of the Book. The rest of this chapter elaborates on the foregoing remarks in an introductory way. The most easily understood finite elements are those for structures composed of axial elements and beams. They are discussed in Chapter 2, along with some FEA procedures used with all element types. Simple triangular and rectangular elements for plane problems are discussed in Chapter 3. General formulation methods for finite elements are treated in Chapters 4 and 5. Chapters 6 and 7 discuss arbitrarily shaped quadrilateral elements and elements that may have curved sides. Chapters 8 through 10 discuss modeling procedures, sources of error, and how a sequence of analyses with successively

refined meshes may be deemed to be adequately converged. Chapters 11 through 13 deal with the application of FEA to dynamics and vibrations, thermal problems, and a few problems that involve fluids and incompressible media. Chapters 14 through 18 are devoted to topics in structural mechanics, including material nonlinearity. Appendices deal with matrix manipulations, equation solving, and eigenvalue extraction.

Over many years, element formulations and analysis procedures have been modified, extended, and fine-tuned to improve performance. Throughout the book we emphasize the more basic concepts, elements, and procedures. Refinements are often beyond the scope of this book but are included in commercial software and are described in references cited.

1.2 PROBLEM CLASSIFICATION, MODELING, AND DISCRETIZATION

Classification. The first step in solving a problem is to identify it. What are the more important physical phenomena involved? Is the problem time-independent or time-dependent? (In stress analysis terminology, we ask whether the problem is static or dynamic.) Is nonlinearity involved, so that iterative solution is necessary? What results are sought from analysis? What accuracy is required? Answers to such questions influence how much information must be gathered to carry out an analysis, how the problem is modeled, and what method of solution is adopted.

A complicated problem may not lie entirely in one category. An example is a fluid-structure interaction problem, such as earthquake excitation of a storage tank that contains liquid. Motion of the liquid makes a thin-walled tank deflect, and deflection modifies the liquid motion. Therefore, structural displacement and fluid motion fields cannot be considered separately; calculations must take their interaction into account. This example involves what may be called *direct* or *mutual* coupling, in which each field influences the other. There is also what may be called *indirect* or *sequential* coupling, in which only one field influences the other. An example is ordinary analysis for thermal stresses, where temperature influences stresses but stresses have negligible influence on temperature.

Modeling. An analytical method is applied to a model problem rather than to an actual physical problem. Even laboratory experiments use models unless the actual physical structure is tested. A model for analysis can be devised after the physical nature of the problem has been understood. In modeling, the analyst seeks to exclude superfluous detail but include all essential features, so that analysis of the model is not unnecessarily complicated yet provides results that describe the actual problem with sufficient accuracy. A geometric model becomes a *mathematical model* when its behavior is described, or approximated, by selected differential equations and boundary conditions. The equations, depending on their particular forms, may incorporate restrictions such as homogeneity, isotropy, constancy of material properties, and smallness of strains and rotations.

It is important to recognize that FEA is *simulation,* not reality. FEA is applied to the mathematical model. Even very accurate FEA may be at odds with physical reality if the mathematical model is inappropriate or inadequate.

A mathematical model is an idealization, in which geometry, material properties, loads, and/or boundary conditions are simplified based on the analyst's understanding of what

features are important or unimportant in obtaining the results required. As examples in stress analysis, material may be regarded as homogeneous, isotropic, and linearly elastic (although common materials are otherwise); a load distributed over a small area may be regarded as concentrated at a point (which is not physically possible); a support may be designated as fixed (although no support is completely rigid); a reentrant corner may be introduced but high stresses there ignored (if stresses elsewhere are sought); and an almost-flat structure may be modeled as two-dimensional (if stress variation in the thickness direction is considered to be practically zero, or regarded as linear as it often is for bending). Behavior of an axisymmetric pressure vessel might be described by equations of axisymmetric elasticity or by equations of axisymmetric shells, depending on whether the wall thickness is judged to be thick or relatively thin. Modeling decisions such as these precede FEA.

Discretization. A mathematical model is *discretized* by dividing it into a mesh of finite elements. Thus a fully continuous field is represented by a piecewise continuous field defined by a finite number of nodal quantities and simple interpolation within each element. Clearly, discretization introduces another approximation. Relative to reality, two sources of error have now been introduced: *modeling error* and *discretization error.* Modeling error can be reduced by improving the model; discretization error can be reduced by using more elements. Even if discretization error could be reduced to zero, reality is not perfectly represented because modeling error remains. Also, as a computer does arithmetic, it introduces *numerical error* by using numbers of finite precision to represent data and the results of manipulation. Numerical error is usually small but can be made large by some physical situations and by poor discretization.

As a very simple example of modeling and discretization, consider a tapered support post, as in Fig. 1.2-1. Its cross-sectional area varies from A_b at the bottom to A_t at the top. In modeling, we elect to show the ground as a rigid support. Once we have omitted deformation of the ground from the model, deflection at the top is due entirely to shortening of the post, and stresses at the bottom differ in magnitude and distribution from stresses in the actual post. We may presume that the state of stress is uniaxial at every cross section, which is an acceptable approximation if taper is slight. In the mathematical model of uniaxial stress, the axial coordinate is the only independent variable. This representation is consistent with uniform stress across the bottom. Similarly, in this model the manner of load distribution on top does not matter; only its magnitude P is important. The distributed load of the post's own weight usually may be neglected. We may also assume that the model material is homogeneous and linearly elastic. Thus, if the material is concrete, we ignore its cemented-particle structure and consequent local stress variations, and ignore nonlinearity in its stress-strain relation.

For uniaxial stress and linear elasticity, we can obtain a valid discretized model by representing the tapered model by a stack of uniform members, each of elastic modulus E but different cross-sectional area A, as shown in Fig. 1.2-1. Discretization error can be reduced by increasing the number of members. This manner of discretizing a tapered structure is not at all new, but it can be regarded as a simple instance of FEA, as explained in the next section.

After completing an analysis, it is important to *check the results.* In Fig. 1.2-1 it is obvious that, prior to discretization, axial stresses throughout the model have magnitudes between P/A_b and P/A_t. Even simple checks such as this may detect a large error, due perhaps to a blunder in data input.

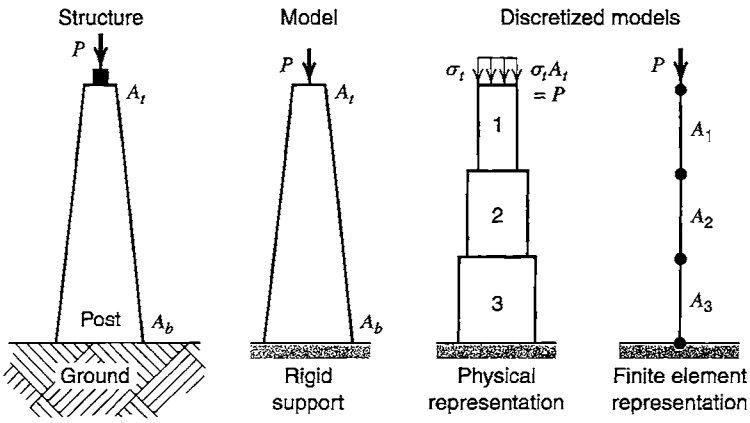

Figure 1.2-1. Steps in modeling and FE analysis of a tapered support post.

1.3 INTERPOLATION. ELEMENTS, NODES, AND D.O.F.

The essence of FEA is *approximation by piecewise interpolation of a field quantity.* Usually, polynomial interpolation is used. Here we illustrate the method by applying it to the tapered bar shown in Fig. 1.3-1, modeled as a problem of uniaxial stress. We will briefly describe a bar element and the nature of results it provides. The results have features in common with results produced by most other FE analyses, however complicated the physical problem may be.

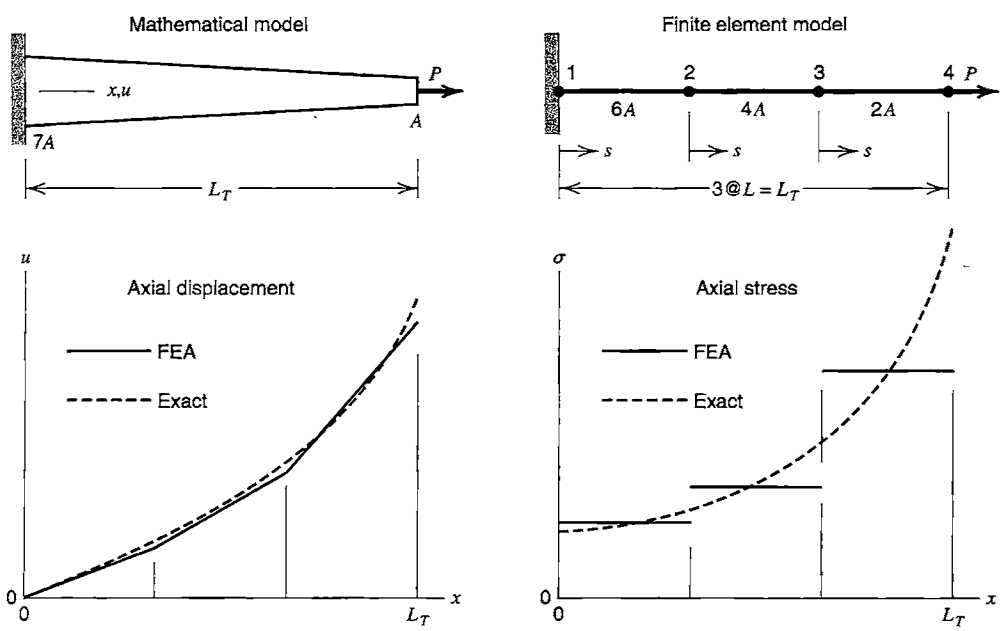

Figure 1.3-1. A tapered bar, discretized by three uniform two-node elements.

Bar Element. Figure 1.3-1 shows a discretization of a tapered bar into three elements, each uniform, linearly elastic, and of length L. The field quantity is axial displacement u. Along a typical element, say the middle one, u is stated in terms of nodal displacements u_2 and u_3 by the equation

$$u = \left(1 - \frac{s}{L}\right)u_2 + \frac{s}{L}u_3 \tag{1.3-1}$$

where s is an axial coordinate along the element. Clearly, Eq. 1.3-1 expresses a linear variation of u with s that has values $u = u_2$ at $s = 0$ and $u = u_3$ at $s = L$. The same form applies to the rightmost element, but with nodal displacements u_3 and u_4. Similarly the form applies to the leftmost element, but with $u_1 = 0$ because the left end of the structure is fixed. Linear displacement $u = u(s)$ dictates that axial strain ε is constant over an element. From the stress-strain relation $\sigma = E\varepsilon$ and the elementary definition of strain as change in length divided by original length, and with $u_1 = 0$, we obtain the following expressions for axial stress in the respective elements of Fig. 1.3-1.

$$\sigma_{1\text{–}2} = E\frac{u_2}{L} \qquad \sigma_{2\text{–}3} = E\frac{u_3 - u_2}{L} \qquad \sigma_{3\text{–}4} = E\frac{u_4 - u_3}{L} \tag{1.3-2}$$

The problem of Fig. 1.3-1 is simple enough that the FE solution can be obtained without matrix formulations and systematic manipulation procedures. Instead we solve for nodal displacements using methods of elementary mechanics of materials, as follows.

The three bar elements are each uniform, of respective cross-sectional areas $6A$, $4A$, and $2A$, which are cross-sectional areas of the tapered bar at element midpoints. Nodal displacements can be obtained from the elementary expression for elongation of a bar under axial load. Thus

$$u_1 = 0 \qquad u_2 = \frac{PL}{6AE} \qquad u_3 = u_2 + \frac{PL}{4AE} \qquad u_4 = u_3 + \frac{PL}{2AE} \tag{1.3-3}$$

These displacements can be expressed in terms of overall length L_T by the substitution $L = L_T/3$. Next, element stresses can be obtained from Eqs. 1.3-2. To check results, we can simply divide load P by element cross-sectional areas, because this simple problem is statically determinate.

Results are plotted in Fig. 1.3-1. The displacement plot is reminiscent of using straight lines for numerical interpolation between points on a continuous curve, but here points do not lie on the correct curve. In other words, nodal values of field quantities are not exact. The cause is discretization error. Only for certain very simple problems are nodal values exact. "Exact" means full agreement with behavior of the mathematical model, not necessarily agreement with physical reality. The stairstep axial stress plot shows that stresses in this example are accurate at element centers. Elsewhere stresses are represented less accurately than displacements, as should be expected in FEA results because most types of finite elements are based on displacement fields, and stresses are usually computed from displacement gradients.

An alternative form of Eq. 1.3-1 is

$$u = a_1 + a_2 s \tag{1.3-4}$$

where a_1 and a_2 are constants that can be expressed in terms of u_2 and u_3 by requiring that $u = u_2$ at $s = 0$ and $u = u_3$ at $s = L$. The a_i are known as *generalized coordinates* or *generalized degrees of freedom.* The term "degrees of freedom" is abbreviated "d.o.f." and is explained at the end of this section.

Other Elements. From Figs. 1.1-1 and 1.3-1 one may surmise (incorrectly) that an FE discretization is obtained by conceptually sawing an actual structure into small fragments and then reconnecting them at convenient points. If applied to the gear tooth of Fig. 1.1-1, this process would result in triangular fragments connected at corner and midside nodes. Such a patchwork would be weaker than the actual structure, with strain concentrations near nodes, sliding of some fragments on one another, and gaps between others. These defects do not arise in FEA because elements are based on simple fields, which do not contain terms capable of representing a strain concentration, and which provide interelement compatibility.[1] Fields used for some simple two-dimensional elements are as follows. In subsequent chapters we explain how these fields are used in FEA.

Figure 1.3-2a shows a three-node triangular element that can represent a two-dimensional field $\phi = \phi(x,y)$. As examples, ϕ might represent temperature, voltage, hydraulic head in seepage flow, or lateral deflection of an inflated membrane. In the form of Eq. 1.3-4, the element field is

$$\phi = a_1 + a_2x + a_3y \tag{1.3-5}$$

The three a_i can be expressed in terms of values of ϕ at the three element nodes, as will be shown in Chapter 3. Figure 1.3-2b shows that a mesh of these elements approximates a smooth function $\phi = \phi(x,y)$ by a surface of triangular facets. The four-node rectangular element shown in Fig. 1.3-2b has the field

$$\phi = a_1 + a_2x + a_3y + a_4xy \tag{1.3-6}$$

and the six-node triangular element with midside nodes has the field

$$\phi = a_1 + a_2x + a_3y + a_4x^2 + a_5xy + a_6y^2 \tag{1.3-7}$$

The four-node rectangular element displays $\phi = \phi(x,y)$ over the element as a surface that may be flat or warped. The six-node triangular element can display a parabolic ϕ surface. In all these elements, the variation of ϕ along an element edge is completely determined by values of ϕ at nodes on that edge. Therefore, adjacent elements that share nodes along a common edge automatically display the same function ϕ along the entire shared edge, and no incompatibilities such as gaps appear between elements.

Summing up, we may say that FEA is an analysis method in which a field variable is approximated by connecting simple interpolation functions, each defined over a small region. The region is called a *finite element.* The interpolation function (such as Eq. 1.3-5) is adapted to the number of nodes in the element type, and amplitudes of the a_i are determined by numerical values of the field quantity at specific points called *nodes.* Elements

[1]Some elements, discussed subsequently, are *incompatible.* Along element edges, but not at nodes, gaps or overlaps can appear between adjacent elements. Such elements are formulated in a way that enhances coarse-mesh accuracy and causes incompatibilities to tend toward zero as a mesh is refined.

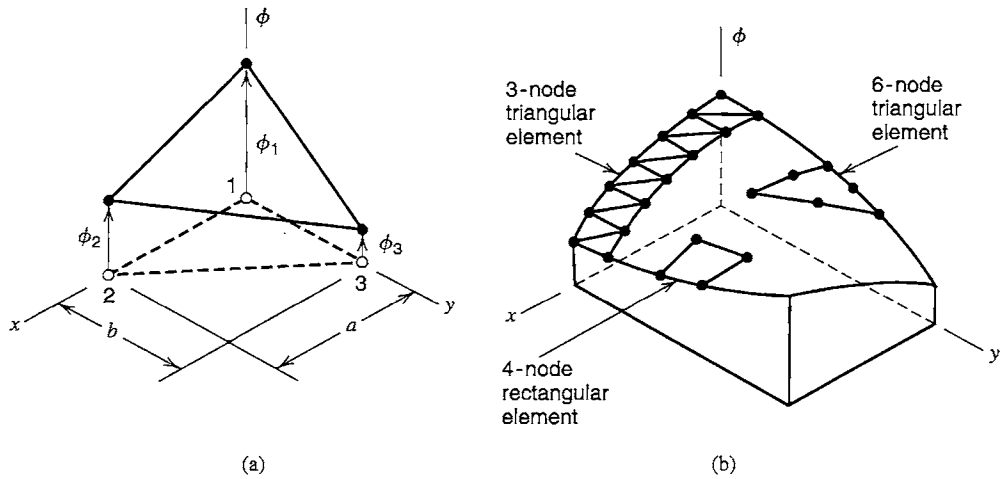

Figure 1.3-2. (a) A three-node triangular element. (b) A smooth function $\phi = \phi(x,y)$ can be approximated by various element types.

are connected at nodes, where they share values of the field quantity (and may also share one or more of derivatives of the field quantity, depending on element type). Nodes are also locations where loads are applied and boundary conditions are imposed.

Degrees of Freedom (d.o.f.). Degrees of freedom are independent quantities that govern the spatial variation of a field. For example, Eq. 1.3-7 defines a field $\phi = \phi(x,y)$ that has six d.o.f., namely the six a_i. Six nodal d.o.f. ϕ_i can be used instead to define the same field. Each element in Fig. 1.1-1 has 12 d.o.f., namely six nodal displacements u_i that govern the x-direction displacement field $u = u(x,y)$ and six nodal displacements v_i that govern the y-direction displacement field $v = v(x,y)$. The u_i and v_i are displacements of specific points; in general the a_i are not.

1.4 EXAMPLE APPLICATIONS. HISTORY OF FEA

Applications. Figure 1.4-1 shows an application of FEA that dates from 1965 [1.1]. The structure is an axisymmetric solid, whose axis of revolution lies above the cross section shown. Each finite element is a toroidal ring of triangular cross section. Each element has a node (or in this case a nodal circle) at each vertex. Field quantities at each node are temperature for heat conduction analysis, and radial and axial displacements for stress analysis. The same discretization can be used for both analyses. Computed nodal temperatures are transferred to the stress analysis model and used to determine thermal stresses.

In Fig. 1.4-2, FEA is applied to an induction motor. Only part of the motor is shown; symmetry is exploited by modeling only a repetitive portion. The mesh of triangular elements spans spaces between pole pieces as well as the pole pieces themselves. For magnetostatic analysis, nodal unknowns are values of the magnetic potential.

Examples of FEA could be given from many other areas of application. The concept of piecewise interpolation is common to all of them. However, familiarity with concepts of FEA does not confer competence in all applications. For example, the problem of Fig. 1.4-1

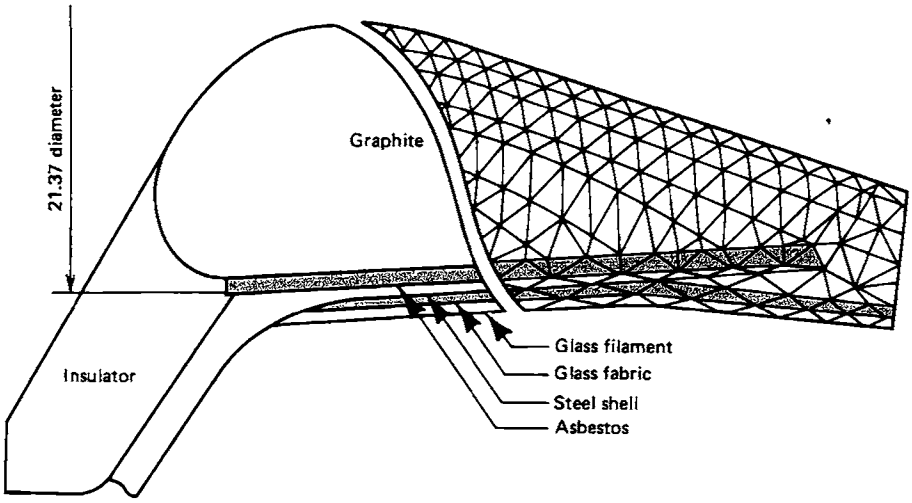

Figure 1.4-1. Cross section of a multi-material rocket nozzle, showing construction (left portion) and possible finite element mesh (right portion), from [1.1].

poses no great challenge to today's stress analyst, but if presented with the magnetics problem of Fig. 1.4-2, a stress analyst may not know what kind of result to seek or what input data is required. *It is important to understand the physics of the problem.*

FEA was accepted by industry soon after its introduction, for reasons suggested by the foregoing two applications. Finite elements can represent structures of arbitrarily complex geometry. A discretized model resembles the actual body or region. Each element can be

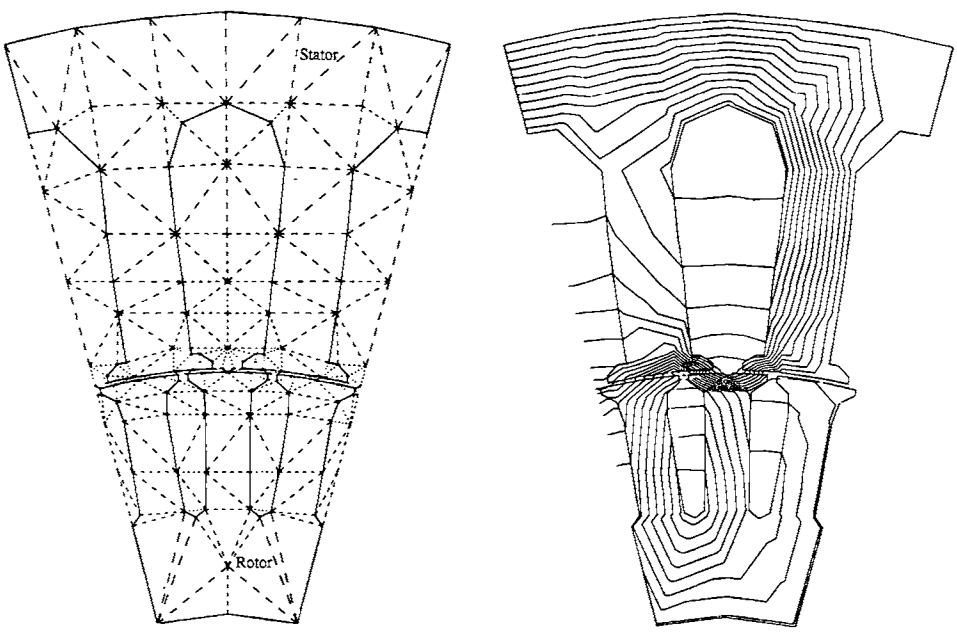

Figure 1.4-2. Part of an induction motor. Computed magnetic flux contours for zero rotor speed are shown by the right-hand figure. (*Courtesy of A. O. Smith Corp., Data Systems Division, Milwaukee, Wisconsin.*)

regarded as a piece of the actual structure (but having idealized behavior). Systematic procedures of FEA allow calculations to be almost completely automated. Unfortunately, automation makes it possible to do FEA with so little understanding that results may be worthless. Some critics say that *most* FEA results are worthless. *It is important to understand how finite elements behave, and important to check for errors.*

History. In 1851, to derive the differential equation of the surface of minimum area bounded by a given closed curve in space, Schellbach discretized a surface into right triangles and wrote a finite difference expression for the total discretized area [1.2]. He proposed no other application or generalization of the idea. FEA is now regarded as a way to *avoid* differential equations by replacing them with an approximating set of algebraic equations.

Starting in 1906, researchers noted that a framework having many bars in a regular pattern behaves much like an isotropic elastic body [1.3,1.4]. Application to problems of plane elasticity and plate bending was reported in 1941 [1.5]. This work exploits well-known methods for analysis of framed structures but cannot be applied to bodies of arbitrary shape. Also, rather than discretization of a continuum into smaller pieces, structural members of a different type are substituted. The framework method may be regarded as a precursor to FEA rather than an early form of it.

The FE method as we know it today seems to have originated with Courant in his 1943 paper, which is the written version of a 1941 lecture to the American Mathematical Society [1.6]. Courant determined the torsional rigidity of a hollow shaft by dividing the cross section into triangles and interpolating a stress function ϕ linearly over each triangle from values of ϕ at net-points (or nodes, as we now call them). He does not mention Schellbach's work. Courant notes that the method "suggests a *wide generalization* which provides great flexibility and seems to have considerable practical value." Practical applications did not appear until aeronautical engineers developed the method, apparently without knowing of Courant's work.

Engineers in the aeronautical industry made remarkable progress in the early to mid-1950s, although some of the work was not published until much later due to company policies. Early in this period, equations from conventional analysis methods were solved on the small computers then available. In the United States, conventional methods proved inadequate for wings of low aspect ratio, so Turner devised a three-node triangular element to model the wing skin [1.7]. In England, Taig did similar work [1.8]. In Germany, Argyris included FEA concepts in a set of influential papers about matrix procedures [1.9]. Details may be found in the references cited; see also [1.10–1.13].

The name "finite element" was coined by Clough in 1960. Many new elements for stress analysis were soon developed, largely by intuition and physical argument. In 1963, FEA acquired respectability in academia when it was recognized as a form of the Rayleigh-Ritz method, a classical approximation technique. Thus FEA was seen not just as a special trick for stress analysis but as a widely applicable method having a sound mathematical basis. Papers about heat conduction and seepage flow using FEA appeared in 1965. General-purpose computer programs for FEA emerged in the late 1960s and early 1970s. Since the late 1970s, computer graphics of increasing power have been attached to FE software, making FEA attractive enough to be used in actual design. Previously, FEA was so tedious that it was used mainly to verify a design already completed or to study a structure that had failed.

Computational demands of practical FEA are so extensive that computer implementation is mandatory. Analyses that involve more than 100,000 d.o.f. are not uncommon. It is no accident that developments in computers and programming languages were contemporaneous with early developments in FEA.

The first textbook about FEA appeared in 1967 [1.14]. By 1995, Mackerle [1.15] estimated that about 3800 papers about FEA were being published annually, and that the cumulative total of FEA publications amounted to some 380 books, 400 conference proceedings, and 56,000 papers (excluding papers on fluid mechanics). Mackerle also counted 310 general-purpose FE computer programs.

1.5 SOLVING A PROBLEM BY FEA

Solving a practical problem by FEA involves learning about the problem, preparing a mathematical model, discretizing it, having the computer do calculations, and checking results. Most often, more than one cycle through these steps is required. Time spent by the computer is a small fraction of time spent by the analyst, but the analyst must have an understanding of what the computer is doing. Material of the present section is discussed in detail in Chapter 10.

Problem Classification. As summarized in Section 1.2, the analyst must understand the nature of the problem. Without this step a proper model cannot be devised, nor can FEA software be told what to do. At present, software does not automatically decide that nonlinear analysis is to be undertaken if stresses are high enough to produce yielding, that buckling is to be considered if thin sections carry compressive load, and so on. Although the trend is for software to be given more decision-making capability, the analyst should not abdicate control. Software has limitations and almost certainly contains errors, yet the engineer, not the software provider, is legally responsible for results obtained.

Mathematical Model. Before undertaking FE discretization and a numerical solution, we devise a model problem for analysis. This step involves deciding what features are important to the purpose at hand, so that unnecessary detail can be omitted, and deciding what theory or mathematical formulation describes behavior. Thus we may ignore geometric irregularities, regard some loads as concentrated, and say that some supports are fixed. Material may be idealized as linear and isotropic. Depending on the dimensions, loading, and boundary conditions of this idealization, we may decide that behavior is described by beam theory, by plate-bending theory, by equations of plane elasticity, or by some other analysis theory. The simplified problem, with the analysis theory to be applied in solving it, constitutes the mathematical model.

Because subsequent FEA is approximate and pertains only to the mathematical model, FEA is two or three steps removed from reality. Modeling decisions are influenced by what information is sought, what accuracy is required, the anticipated expense of FEA, and its capabilities and limitations. Also, initial modeling decisions are provisional. It is likely that results of the first FEA will suggest refinements, in geometry (perhaps by restoring geometric irregularities previously omitted), in applicable theory (perhaps by adding in-plane stretching terms to plate-bending theory), and so on.

As an example of modeling, consider the very simple problem depicted in Fig. 1.5-1a. The ring thickness (measured normal to the figure) is uniform and is considerably less than the ring diameter. The material is considered linearly elastic, homogeneous, and isotropic. We ask for stresses and deflections due to the ring's own weight as it rests on the ground. It is easy to arrive at the plane model in Fig. 1.5-1b, in which symmetry about the vertical centerline has been exploited. Details of pressure applied by the ground have been discarded, replaced by a point support. If mean radius R is perhaps $5t$ or more, the largest stresses in the actual problem are circumferential flexural stresses. Then the theoretically infinite stresses at D associated with a point support are not important (and could only be calculated as high stresses by conventional finite elements). A two-dimensional model is adequate. Instead, if the physical structure is not a ring but a long, thin-walled pipe, should the model be three-dimensional? Probably not. Stress analysts recognize that deflections and stresses are essentially constant along the length, that they vary only near ends, and that the variation has only a small effect on the largest magnitudes of deflection and stress. However, in a long pipe the situation is more nearly plane strain than plane stress. Thus the model is changed, and appropriate data must be supplied to software and appropriate analysis options chosen.

The foregoing conceptual models become complete mathematical models when we decide on the appropriate analysis theory. For a slender ring, it can be beam theory. For a not-so-slender ring, plane elasticity theory is appropriate. For a thin-walled pipe in which end effects are to be represented, thin-shell theory is appropriate. Elements based on the respective theories would be used for FEA of the respective mathematical models.

Why not use a three-dimensional model? After all, reality is always three dimensional, and elements for three-dimensional FEA are available. The reason is cost. Demands on the analyst's time and computer resources are likely to increase by a factor of 10 or more in going from two dimensions to three.

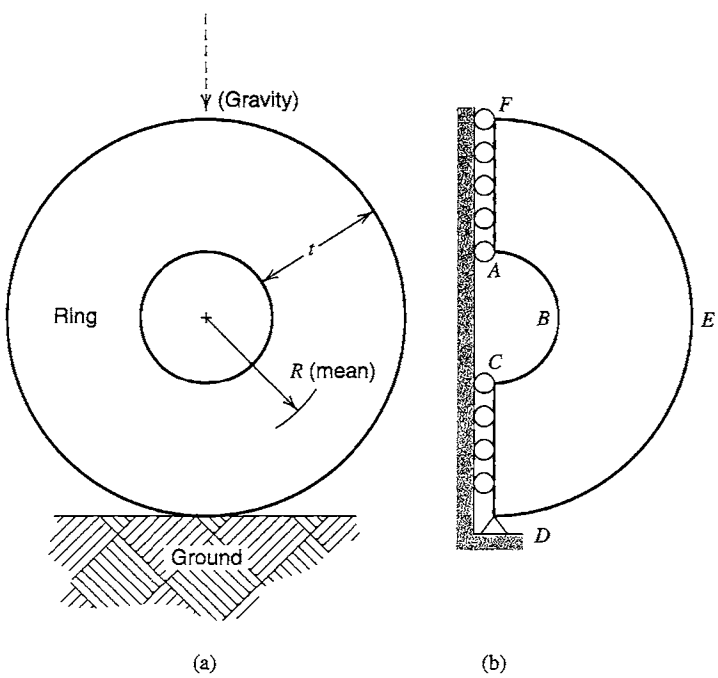

Figure 1.5-1. (a) Ring in the vertical plane that rests on the ground, loaded by its own weight. (b) Mathematical model.

A gear tooth poses a more complicated problem than the ring. In Fig. 1.1-1, supports are not shown. Is it satisfactory to impose full fixity along *ABCD*, where elastic support is actually provided by the remainder of the gear? An actual gear is not of uniform thickness; is a two-dimensional model satisfactory? Is load P uniformly distributed in the z-direction across the tooth? If not, stresses will be considerably higher, and the situation cannot be considered two-dimensional.

Preliminary Analysis. Before going from a mathematical model to FEA, at least one preliminary solution should be obtained, using whatever means are conveniently available—simple analytical calculations, handbook formulas, trusted previous solutions, or experiment. Some of this effort may lead to a better mathematical model. Subsequently it will be used to check computed results. If we do this work before FEA rather than after, we reduce a natural tendency to find answers that support whatever FEA results have already been obtained, especially if it took considerable effort to get them. It is easy to make mistakes in supplying data to software, and even a crude preliminary solution may detect a result that errs greatly due to a mistake in data input.

Preliminary analysis for the ring problem of Fig. 1.5-1 is easy if R is considerably greater than t. Formulas for deflection and stress in a slender ring are available in handbooks [1.16]. If R is comparable to t, these formulas are approximate but still useful for checking.

Finite Element Analysis. Use of general-purpose FEA software involves the following steps.

- *Preprocessing:* Input data describes geometry, material properties, loads, and boundary conditions. Software can automatically prepare much of the FE mesh, but must be given direction as to the type of element and the mesh density desired. That is, the analyst must choose one or more element formulations that suit the mathematical model, and state how large or how small elements should be in selected portions of the FE model. All data should be reviewed for correctness before proceeding.
- *Numerical analysis:* Software automatically generates matrices that describe the behavior of each element, combines these matrices into a large matrix equation that represents the FE structure, and solves this equation to determine values of field quantities at nodes. Substantial additional calculations are performed if behavior is nonlinear or time-dependent.
- *Postprocessing:* The FEA solution and quantities derived from it are listed or graphically displayed. This step is also automatic, except that the analyst must tell the software what lists or displays to prepare. In stress analysis, typical displays include the deformed shape, with deformations exaggerated and probably animated, and stresses of various types on various planes.

Check the Results. First, we examine results qualitatively and ask if they "look right"—that is, are there obvious errors? Have we solved the problem we intended to solve, or some other problem? Boundary conditions are often misrepresented; does the deformed FE structure show displacements where there should not be any? Are expected symmetries present in the results? If answers to such questions are satisfactory, FEA results are compared with

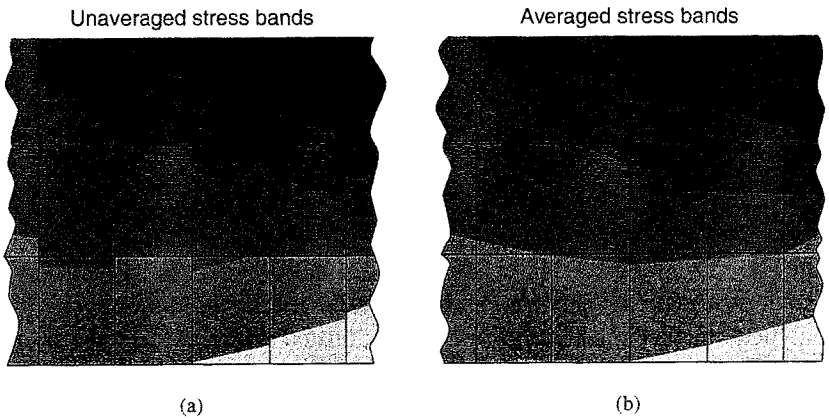

Figure 1.5-2. Stress bands in a portion of a mesh of rectangular elements. (a) Without nodal averaging, interelement discontinuity suggests how good or bad results are. (b) After nodal averaging, continuity prevails, but important information is lost.

solutions from preliminary analysis, and with any other useful information that may be available.

For example, let us qualitatively examine the problem of Fig. 1.5-1. Points along *CD* and *AF* should move downward but not left or right. Points along *BE* should move downward and rightward. Vertical stresses should be compressive near *B* and *D*. Horizontal stresses should be tensile near *A* and *C*, compressive near *D* and *F*. Stresses normal to boundaries *ABC* and *DEF* should be zero, but will not be exactly so because the solution is approximate. Similarly, due to symmetry, shear stress should be zero along *CD* and *AF*, and stress contours of flexural stress should be normal to *CD* and *AF*, but will not be exactly so.

One way to judge the adequacy of a discretization is to look at plots of stress (or plots of heat flux in thermal analysis). Software can plot either stress contours or "stress bands," which are zones of color. Different colors are used for different levels of stress. Stress is related to gradients of the field quantity, and gradients in a given element depend on field quantities at nodes attached to that element only. Therefore, as will be shown subsequently, stress bands are discontinuous across interelement boundaries. Strong discontinuities indicate too coarse a discretization, whereas practically continuous bands suggest unnecessarily fine discretization [1.17]. In Fig. 1.5-2a, bands are discontinuous but not badly so, and the discretization may be adequate for the purpose intended.

Software can be instructed to display bands computed from nodal average values of stress (or of flux). Thus interelement discontinuities are removed. The resulting picture is visually more pleasing, but information useful in judging the quality of computed results is lost. Bands plotted from nodal averages, Fig. 1.5-2b, may suggest that results are of higher quality than is actually the case.

Expect to Revise. Rarely is the first FE analysis satisfactory. Obvious blunders must be corrected. Uncomfortably large discrepancies between what is expected and what is computed demand explanation. Either physical understanding or the FE model, or both, may be at fault. Disagreements must be satisfactorily resolved by repair of the mathematical model and/or the FE model. After another analysis cycle, the discretization may be judged

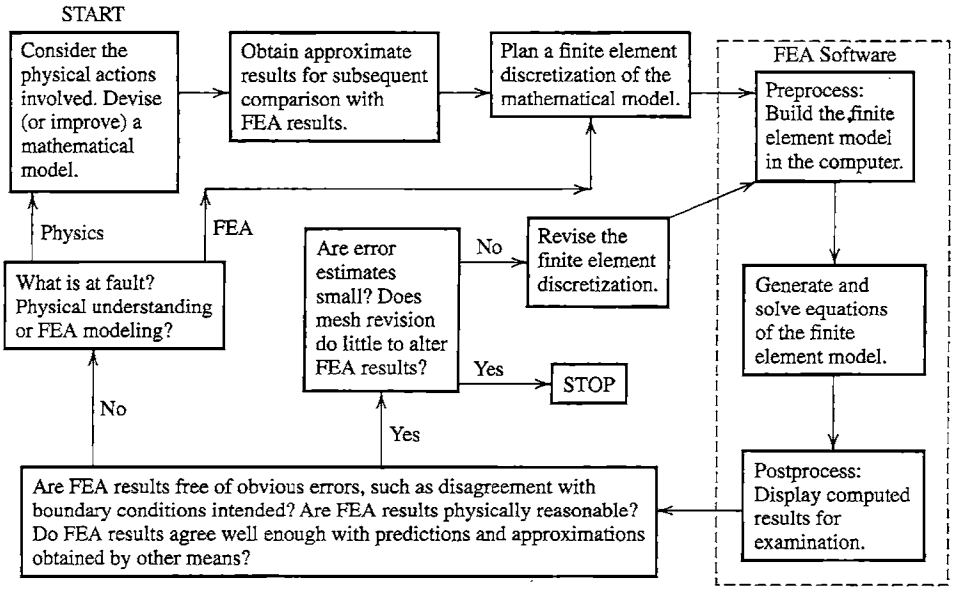

Figure 1.5-3. Outline of a finite element analysis project.

inadequate, perhaps being too coarse in some places. Then mesh revision is required, followed by another analysis.

In analyzing a new problem, it is almost always appropriate to begin with a simple FE model, to which detail is added as the analyst learns more. Each revision is an expected step on the way to an adequate solution, not a penalty for failure in the preceding attempt.

The flow of an analysis project by FEA is outlined in Fig. 1.5-3.

1.6 LEARNING AND USING FEA

Why study the theory of FEA? Satisfactory elements and versatile analysis procedures are already available in widely used software, and software has become so accommodating that even an inept user can obtain a result. Seasoned practitioners stress that *reliable* results are obtained only when the analyst understands the problem, how to model it, behavior of finite elements, assumptions and limitations built into the software, input data formats, and when the analyst checks for errors at all stages. It is not realistic to demand that analysts understand details of all elements and procedures, but misuse of FEA can be avoided only by those who understand fundamentals. For example, it is important to realize that each individual element has very limited ability to represent spatial variation of the field quantity, and to understand how this ability differs from one element type to another.

Older engineers sometimes complain that younger engineers have naive faith in computer programs, value computer skills over analytical skills, and lack the ability to produce "ballpark" answers. Such deficits can be overcome while learning FEA. A student can use FEA to analyze problems for which results are already available and known to be reliable, discovering and fixing the inevitable mistakes in modeling, data input, and software options until computed results agree with established results. Problems for which results are not available can be solved analytically—crudely if necessary—and then solved by FEA, with the process repeated until results are reconciled. This exercise will improve

analytical skills as well as FE skills. Initial failure to achieve agreement may be discouraging, but it is more instructive than success.

A study of computer misuse in engineering [1.18] considers cases in which incorrect results caused damage in the form of expensive delay, a need to redesign, poor performance, or even collapse. Of 52 cases cited, 7 were due to hardware error, 13 to software error, 30 to user error, and 2 to other causes. User error was usually associated with poor modeling, and sometimes with poor understanding of software limitations and input data formats. Most errors could have been caught early had users been careful to check results. Often, after damage was done, the cause of the trouble was found by consultants who used hand calculation to check computer output.

A cautionary example is depicted in Fig. 1.6-1. Here a straight beam with hinge supports is loaded by a pressure pulse that causes yielding of the material and vibration of the beam. Analysis seeks to track lateral displacement at the midpoint as a function of time. Results plotted come from 10 reputable analysis codes operated by users regarded as expert [1.19]. Yet if any of the curves is correct, we cannot tell which one it is. Admittedly, the problem is difficult: results indicate "strong sensitivities of both physical and computational nature" [1.19]. This example reminds us that analysis software is based on theory and approximation, and that a user may push the software beyond its range of validity [1.20].

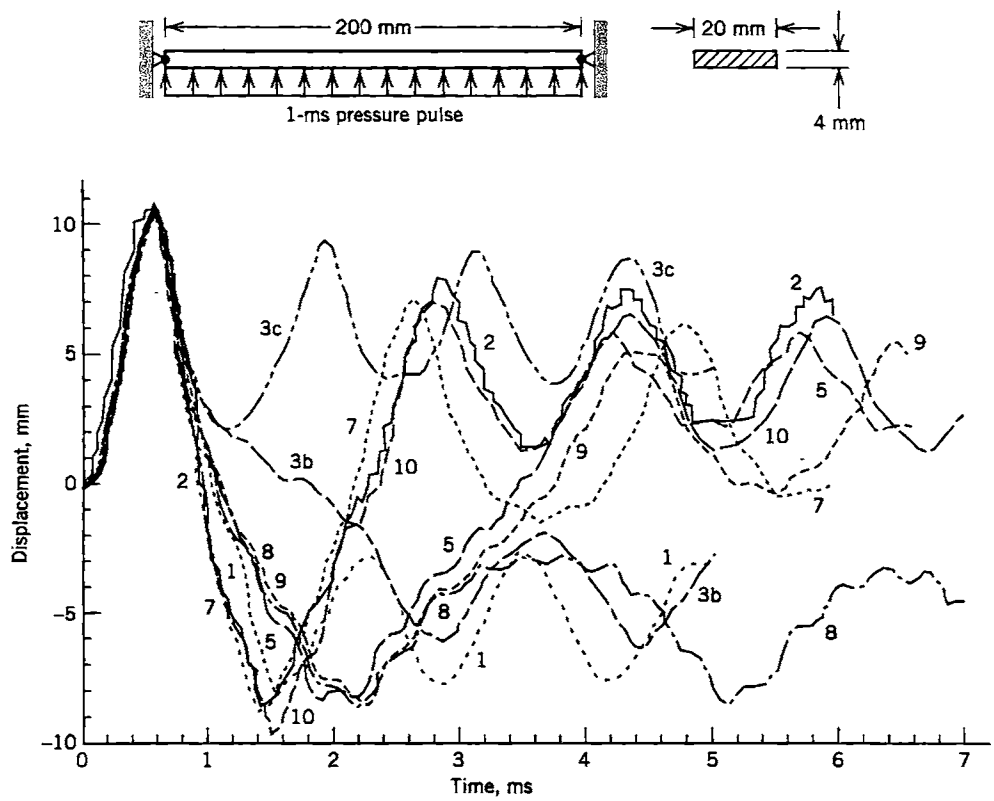

Figure 1.6-1. Lateral midpoint displacement versus time for a beam loaded by a pressure pulse [1.19], reproduced courtesy of ASME. The material is elastic–perfectly plastic. Plots were generated by various analysts and various software packages.

ANALYTICAL PROBLEMS

1.3-1 (a) For the problem of Fig. 1.3-1, determine both exact and finite element values of axial displacement u at $x = L_T/3$, $x = 2L_T/3$, and $x = L_T$. Hence, verify the plots of u versus x.
(b) In similar fashion, verify the plots of σ versus x in Fig. 1.3-1.

1.3-2 Strain ε_x is given by the expression $\varepsilon_x = \partial u/\partial x$. What expression for ε_x is obtained when u in a four-node plane element is given by the right-hand side of Eq. 1.3-6? For a mesh of such elements, what can you say about interelement continuity of ε_x?

1.3-3 (a) In a three-node triangle, field quantity ϕ can be written as $\phi = a_1 + a_2x + a_3y$, where the a_i are generalized d.o.f. For the particular shape of triangle shown, express ϕ in the form $\phi = f_1\phi_1 + f_2\phi_2 + f_3\phi_3$, where the f_i are functions of x, y, a, and b. *Suggestion:* Obtain three equations for the a_i from the conditions $\phi = \phi_1$ at $x = y = 0$, $\phi = \phi_2$ at $x = a$ and $y = 0$, and $\phi = \phi_3$ at $x = 0$ and $y = b$.
(b, c, d) In similar fashion, obtain expressions $\phi = f_1\phi_1 + f_2\phi_2 + f_3\phi_3$ for the triangles shown.

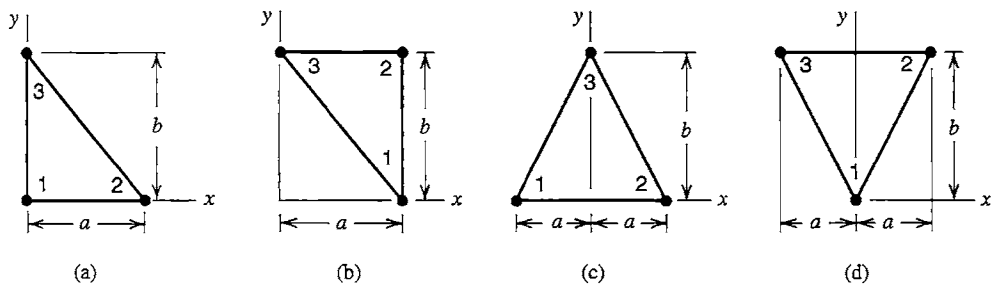

Problem 1.3-3

1.3-4 For the plane quadrilateral element shown, imagine that field quantity ϕ has the form $\phi = a_1 + a_2x + a_3y + a_4xy$, where the a_i are generalized d.o.f. How does ϕ vary with x or y along each side? Do you think this element will be compatible with neighboring elements that may be attached to it?

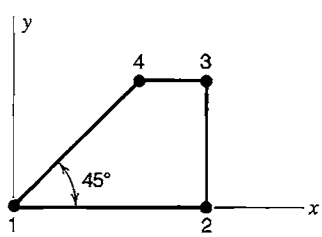

Problem 1.3-4

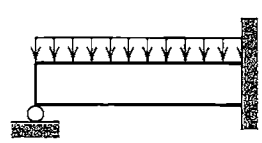

Problem 1.4-1

1.4-1 The sketch shows a propped cantilever beam under uniformly distributed load, as it might be sketched in a book about mechanics of materials. What idealizations of reality may have been introduced in arriving at this model?

1.4-2 A cylindrical pipe, shown in cross section, has nominal temperatures T_1 on the inside and T_2 on the outside. The standard analytical solution for temperature T at arbitrary radius r in the pipe is

$$T = T_1 + (T_2 - T_1)\frac{\ln(r/r_1)}{\ln(r_2/r_1)}$$

However, actual circumstances may differ sufficiently from the ideal that this equation is not accurate enough, and temperature distribution must instead be determined from FEA. What are some of these circumstances?

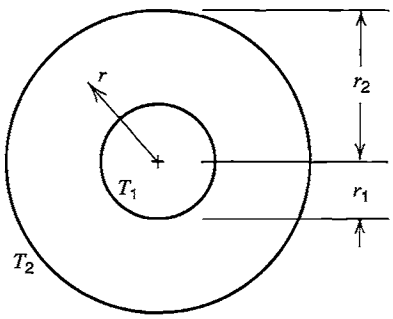

Problem 1.4-2

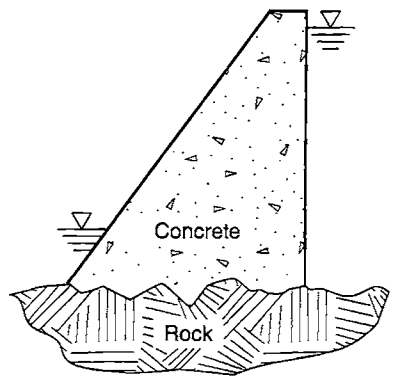

Problem 1.4-3

1.4-3 The sketch shows the cross section of a concrete gravity dam. The ∇ symbols indicate water surfaces. Imagine that stress analysis for loading due to hydraulic pressure is required. Has anything of importance been omitted from the sketch? What considerations influence the mathematical model devised? What additional information will be needed before undertaking numerical analysis?

1.4-4 In the gravity dam of Problem 1.4-3, imagine that the rock is slightly porous and that analysis for seepage flow under the dam is required. Answer the questions posed in Problem 1.4-3.

1.4-5 Two steel plates are connected by a single rivet to form a lap joint, as shown. Axial load is applied. If accurate and detailed stress analysis is required, what aspects of material properties, geometry, and loading must be considered in planning an analysis?

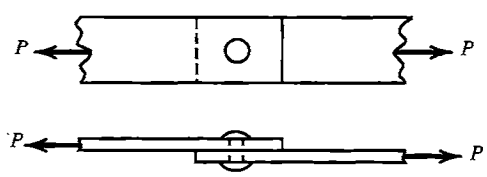

Problem 1.4-5

CHAPTER 2

ONE-DIMENSIONAL ELEMENTS AND COMPUTATIONAL PROCEDURES

We consider straight elements that have a node at each end, and apply physical arguments to obtain matrices that represent element behavior. Then we use these comparatively simple elements and matrices to explain computational procedures that are generally applicable in FEA, regardless of element type. Thus in this chapter we survey the entire computational process of linear static FEA: formulation of element matrices, their assembly into a structural matrix, application of loads and boundary conditions, solution of structural equations, and extraction of gradients (element strains and stresses, in this chapter).

2.1 INTRODUCTION

One-dimensional elements include a straight bar loaded axially, a straight beam loaded laterally, a bar that conducts heat or electricity, and so on. In structural terminology, a *bar* can resist only axial load, whereas a *beam,* in its most general sense, can resist axial, lateral, and twisting loads. In time-independent analysis, a truss of n members can be modeled by n bar elements, and a frame having n straight members usually requires n beam elements. A beam continuous over two or more supports can usually be modeled using one beam element per span between supports. Thus, when one-dimensional elements are used for static analysis, the discretization phase of modeling becomes trivial, and for stress analysis the name "matrix methods of structural mechanics" may be used in preference to "FEA." However, bar and beam elements are provided in FEA software and are much used, both as stand-alone elements and in combination with finite elements of other types. For example, beam elements can be attached to plate elements to model stiffened plates. ?

In this chapter we restrict our attention to linear problems, which means that material properties are essentially unchanged by loading (by force or moment, by temperature, by voltage, and so on). In mechanical problems, linearity also requires that deformations be small enough that equilibrium equations can be written using original geometry rather than deformed geometry. That is, we exclude nonlinear behavior such as yielding of steel, crumbling of concrete, opening or closing of gaps, and lateral deflection large enough to generate membrane-stretching action. Also, we consider only steady-state problems, which are called *static* or (more properly) *quasistatic* in structural mechanics. As an approximation, if a structure is loaded by a cyclic force whose frequency is less than about one-quarter the structure's lowest natural frequency of vibration, the loading can be regarded as quasistatic, and analysis of the type described in the present chapter is acceptable. ? ?

A finite element has a *characteristic matrix,* which is a stiffness matrix for load-deformation analysis, a conductivity matrix for heat conduction analysis, and so on. One-dimensional elements are simple enough that the characteristic matrix can usually be formulated by the

"direct method"; that is, by physical reasoning. Symbolic methods of element formulation, discussed in subsequent chapters, are applicable to one-dimensional elements but are usually not needed for this purpose.

A one-dimensional element often incorporates the exact variation of the field quantity. For example, the usual mathematical model of a uniform beam loaded by concentrated lateral forces displays a cubic variation of lateral displacement between load points. The standard beam element is also based on a cubic field, so an FE model built of beam elements, with nodes at load points, provides results in exact agreement with the mathematical model. Exact agreement is generally not achieved by an FE model of a plane or solid continuum, where element displacement fields are only approximate.

Regardless of the number or types of elements used, the computational procedure for time-independent FEA is as follows:

1. Generate matrices that describe element behavior.
2. Connect elements together, which implies assembly of element matrices to obtain a structure matrix.
3. Provide some nodes with loads.
4. Provide other nodes with boundary conditions, which may be called *support conditions* in structural mechanics.
5. The structure matrix and the array of loads are parts of a system of algebraic equations. Solve these equations to determine nodal values of field quantities.
6. Compute gradients: strains in structural mechanics, heat flux in thermal analysis, and so on.

In this chapter we use one-dimensional elements as vehicles for explanation of these procedures.

In this and subsequent chapters, we make displacements visible in drawings by showing them greatly exaggerated, following the usual practice.

2.2 BAR ELEMENT

Consider a uniform prismatic elastic bar element of length L and elastic modulus E. Often a bar element is represented as a line, as in Fig. 2.2-1, but the element has cross-sectional area A. A node is located at each end. For now, we allow nodes to displace only in the axial direction. Axial displacements at nodes are u_1 and u_2. Internal axial stress σ can be related to nodal forces F_1 and F_2 by free-body diagrams, Fig. 2.2-1a. In turn σ is related to elastic modulus E and axial strain $\varepsilon = (u_2 - u_1)/L$, as shown in Fig. 2.2-1b. Note that we adopt a sign convention in which *nodal forces and nodal displacements are positive in the same direction.* From Fig. 2.2-1 we obtain

$$\begin{aligned} \frac{AE}{L}(u_1 - u_2) &= F_1 \\ \frac{AE}{L}(u_2 - u_1) &= F_2 \end{aligned} \quad \text{or} \quad \begin{bmatrix} k & -k \\ -k & k \end{bmatrix} \begin{Bmatrix} u_1 \\ u_2 \end{Bmatrix} = \begin{Bmatrix} F_1 \\ F_2 \end{Bmatrix} \quad \text{where} \quad k = \frac{AE}{L} \tag{2.2-1}$$

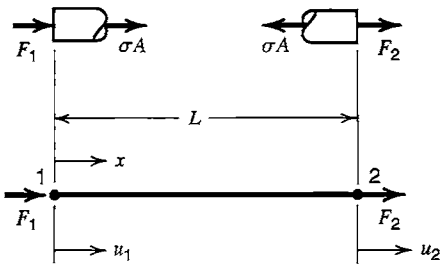

(a)

$$F_1 + A\sigma = 0 \qquad F_2 - A\sigma = 0$$

$$\sigma = E\epsilon \qquad \epsilon = \frac{u_2 - u_1}{L}$$

$$F_1 + AE\,\frac{u_2 - u_1}{L} = 0$$

$$F_2 - AE\,\frac{u_2 - u_1}{L} = 0$$

(b)

Figure 2.2-1. (a) A two-node bar element, showing internal stress σ and nodal d.o.f. u_1 and u_2. (b) Equilibrium equations, stress-strain relation, strain-displacement relation, and nodal forces F_1 and F_2.

Obviously, for this element, equilibrium requires $F_1 = -F_2$. The matrix equation in Eqs. 2.2-1 is abbreviated as

$$[\mathbf{k}]\{\mathbf{d}\} = -\{\mathbf{r}\} \tag{2.2-2}$$

where $[\mathbf{k}]$ is called the *element stiffness matrix*. For the present two-node bar element with only axial displacements at nodes, $[\mathbf{k}]$ is the 2 by 2 matrix in Eq. 2.2-1. Vector $\{\mathbf{r}\}$ in Eq. 2.2-2 has a negative sign because we will use $\{\mathbf{r}\}$ to mean loads associated with element deformation that are applied *by* an element *to* structure nodes to which the element will be connected. Thus forces $-\{\mathbf{r}\} = \lfloor F_1 \;\; F_2 \rfloor^T$ are applied *to* the element.

Note that AE/L can be regarded as k, the stiffness of a linear spring. A bar and a spring have the same behavior under axial load and are represented by the same stiffness matrix.

In the stiffness matrix of Eq. 2.2-1, we see an instance of the following general rule.

A column of $[\mathbf{k}]$ *is the vector of loads that must be applied to an element at its nodes to maintain a deformation state in which the corresponding nodal d.o.f. has unit value while all other nodal d.o.f. are zero.*

For example, let $u_1 = 0$ and $u_2 = 1$ in Eq. 2.2-1, so that the multiplication $[\mathbf{k}]\{\mathbf{d}\}$ produces the second column of $[\mathbf{k}]$. Thus,

$$-\{\mathbf{r}\} = \begin{bmatrix} k & -k \\ -k & k \end{bmatrix} \begin{Bmatrix} 0 \\ 1 \end{Bmatrix} = k \begin{Bmatrix} -1 \\ 1 \end{Bmatrix} = \frac{AE}{L} \begin{Bmatrix} -1 \\ 1 \end{Bmatrix} \tag{2.2-3}$$

which corresponds to Fig. 2.2-1a when $\varepsilon = u_2/L$.

Heat Conduction. Let a uniform bar have cross-sectional area A, thermal conductivity k, and insulation that prevents heat transfer across its lateral surface (Fig. 2.2-2). According to the Fourier heat conduction equation, the rate of axial heat flow, q, is

$$q = -Ak\frac{dT}{dx} \tag{2.2-4}$$

where T is temperature relative to an arbitrarily chosen reference temperature (0 °C, perhaps). SI units for q are W (watts). The negative sign indicates that the direction of heat flow is opposite to the temperature gradient dT/dx. Here dT/dx is independent of x because the bar is uniform and its lateral surface is insulated. Specifically, $dT/dx = (T_2 - T_1)/L$.

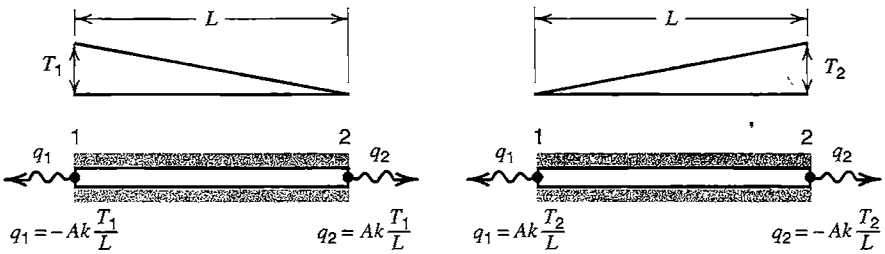

Figure 2.2-2. Nodal heat flow in a uniform bar of cross-sectional area A whose lateral surface is perfectly insulated. Flows are shown for $T_1 > 0$ with $T_2 = 0$ and for $T_1 = 0$ with $T_2 > 0$.

In formulating the element we adopt the convention that heat flow q at ends of the bar is positive when heat flows *out* of the element, and thus positive when heat flows *into* structure nodes to which the element will be connected. This sign convention is analogous to that used with $\{\mathbf{r}\}$ in Eq. 2.2-2. We relate nodal temperatures to nodal heat flows by equations shown in Fig. 2.2-2. In matrix form, the equations in Fig. 2.2-2 are

$$\begin{bmatrix} Ak/L & -Ak/L \\ -Ak/L & Ak/L \end{bmatrix} \begin{Bmatrix} T_1 \\ T_2 \end{Bmatrix} = -\begin{Bmatrix} q_1 \\ q_2 \end{Bmatrix} \tag{2.2-5}$$

in which the square matrix is the element conductivity matrix, analogous to the stiffness matrix of structural mechanics. In analogy to the argument associated with Eq. 2.2-3, a column of a conductivity matrix can be regarded as the vector of nodal heat flows associated with unit value of the corresponding nodal temperature and zero values of all other nodal temperatures (relative to the reference temperature).

Equation 2.2-5 is also applicable to a flat sheet of material whose opposite surfaces have different but uniform temperatures. Then L represents the sheet thickness. If $A = 1$ in Eq. 2.2-4, q can be interpreted as heat flow per unit area (see Eq. 2.2-9).

Structure Equations. Consider a structure built of two uniform elastic bars attached end to end, as shown in Fig. 2.2-3a. Only axial displacements are allowed. Stiffnesses of the respective elements are k_1 and k_2. The structure stiffness equation is

$$\begin{bmatrix} k_1 & -k_1 & 0 \\ -k_1 & k_1 + k_2 & -k_2 \\ 0 & -k_2 & k_2 \end{bmatrix} \begin{Bmatrix} u_1 \\ u_2 \\ u_3 \end{Bmatrix} = \begin{Bmatrix} F_1 \\ F_2 \\ F_3 \end{Bmatrix} \quad \text{or} \quad [\mathbf{K}]\{\mathbf{D}\} = \{\mathbf{R}\} \tag{2.2-6}$$

$[\mathbf{K}]$ is called either the *structure* stiffness matrix or the *global* stiffness matrix. This particular $[\mathbf{K}]$ is easily obtained by applying the general rule stated above Eq. 2.2-3. Thus, as shown in latter portions of Fig. 2.2-3, we activate each d.o.f. in turn, giving unit value to the activated d.o.f. while other d.o.f. are zero, and calculate the nodal forces required for static equilibrium. For each d.o.f. activated, we array nodal forces in a column, ordered by d.o.f. number, with negative sign if directed opposite to nodal displacement. Each such array is a column of $[\mathbf{K}]$.

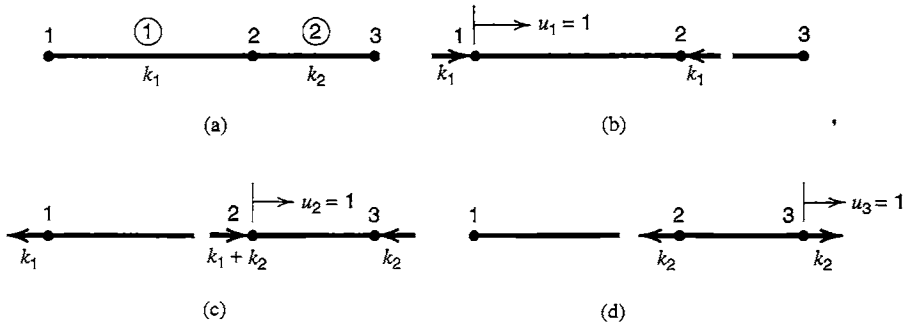

Figure 2.2-3. (a) Structure formed by two bar elements. (b,c,d) Nodal forces associated with unit displacement of each d.o.f. in turn.

An alternative way to obtain [**K**] is as follows. Imagine that the two elements in Fig. 2.2-3a are not yet connected but are provided with numbered ends: 1 and 2 for element 1, and 2 and 3 for element 2. Separately, when expanded to "structure size," stiffness matrices for elements 1 and 2 can be written

$$\begin{array}{c} \begin{array}{ccc} u_1 & u_2 & u_3 \end{array} \\ \begin{bmatrix} k_1 & -k_1 & 0 \\ -k_1 & k_1 & 0 \\ 0 & 0 & 0 \end{bmatrix} \\ \text{Element 1} \end{array} \quad \text{and} \quad \begin{array}{c} \begin{array}{ccc} u_1 & u_2 & u_3 \end{array} \\ \begin{bmatrix} 0 & 0 & 0 \\ 0 & k_2 & -k_2 \\ 0 & -k_2 & k_2 \end{bmatrix} \\ \text{Element 2} \end{array} \tag{2.2-7}$$

where appended column headings u_1, u_2, and u_3 indicate d.o.f. activated to generate matrix columns. Added zeros in the matrix for (say) element 1 can be explained as follows. The row of zeros indicates that because element 1 is not connected to node 3, displacement of any node cannot cause element 1 to produce a force at node 3. The column of zeros indicates that displacement u_3 does not strain element 1, so element 1 applies no force to any node. Clearly, addition of the two matrices in Eq. 2.2-7 produces [**K**] of Eq. 2.2-6. In general, one can imagine a physical space, initially empty except for numbered nodes in their proper positions, that becomes a structure as elements are added. Simultaneously the structure stiffness matrix [**K**] becomes populated by addition of stiffness coefficients from elements. This process of building a structure matrix [**K**] from constituent element matrices [**k**] is called *assembly*.

Support conditions, more generally called *boundary conditions*, are discussed in Section 2.7. For now we note only that if, for example, the left end of the structure in Fig. 2.2-3a is attached to a rigid support, then $u_1 = 0$, and the structure stiffness matrix that relates the remaining "active" d.o.f. u_2 and u_3 is

$$\begin{bmatrix} k_1 + k_2 & -k_2 \\ -k_2 & k_2 \end{bmatrix} \begin{Bmatrix} u_2 \\ u_3 \end{Bmatrix} = \begin{Bmatrix} F_2 \\ F_3 \end{Bmatrix} \tag{2.2-8}$$

from which u_2 and u_3 can be determined when loads F_2 and F_3 on structure nodes 2 and 3 are prescribed. As with other stiffness matrices, columns of [**K**] in Eq. 2.2-8 can be obtained by activating d.o.f. in turn and calculating nodal loads required to maintain equilibrium.

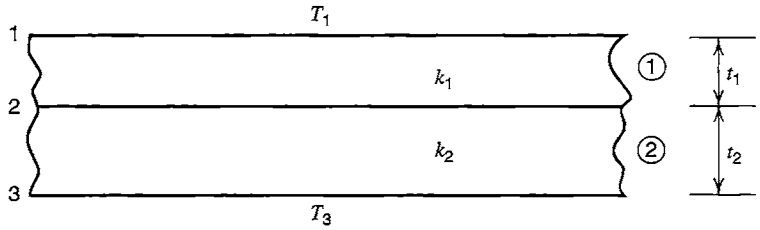

Figure 2.2-4. A two-material layered construction with temperatures T_1 and T_3 at outer surfaces.

Structure matrices for problems of other types are assembled in similar fashion. For the thermal problem of Fig. 2.2-4, the structure equation for heat conduction is

$$\begin{bmatrix} k_1/t_1 & -k_1/t_1 & 0 \\ -k_1/t_1 & (k_1/t_1)+(k_2/t_2) & -k_2/t_2 \\ 0 & -k_2/t_2 & k_2/t_2 \end{bmatrix} \begin{Bmatrix} T_1 \\ T_2 \\ T_3 \end{Bmatrix} = \begin{Bmatrix} f_1 \\ f_2 \\ f_3 \end{Bmatrix} \tag{2.2-9}$$

where k_1 and k_2 are thermal conductivities of layers 1 and 2, and f_1, f_2, and f_3 are net rates of heat flow *per unit area,* positive when directed *into* imagined structure nodes at upper, intermediate, and lower surfaces, respectively. In the absence of a heat source or a heat sink along the interface between layers, continuity requires that $f_2 = 0$. If T_1 and T_3 are prescribed, unknowns are T_2, f_1, and f_3. Further, if $T_1 > T_3$, it will be found that f_1 is positive, and $f_3 = -f_1$ because the problem is steady-state.

When [**K**] is assembled for an FE structure, however complex, computer software uses the addition process just described, but without formal expansion of element matrices to "structure size." Generation of [**K**] is accomplished by starting with a null matrix [**K**] and then, for each element in turn, adding element stiffness coefficients to locations in [**K**] dictated by the numerical labels assigned to structure nodes to which the element is attached. In Section 2.5 we will consider these details of assembly, and we will subsequently discuss loading, boundary conditions, solving equations for nodal quantities, and extracting element strains (or gradients) from the nodal solution.

2.3 BEAM ELEMENT

2D Beam Element. Let a uniform beam lie on the x axis. A 2D beam element has a node at each end. Each node has two d.o.f., namely, lateral translation and rotation (Fig. 2.3-1a). Nodal rotations contain subscript z to denote that their vector representations point along the z axis, which is normal to the xy plane. Nodal loads, each positive if acting in the same direction as its corresponding d.o.f., are shown in Fig. 2.3-1b. To begin, we restrict lateral displacements to the xy plane and consider bending deformations only, assuming that transverse shear deformation can be ignored. That is, we use elementary beam theory, which is more formally known as *Euler-Bernoulli beam theory.* Transverse shear deformation is taken into account by *Timoshenko beam theory* [2.1], a name usually applied when beam vibration is studied. We will use the name for statically loaded beams as well.

Beam element stiffness matrices discussed in the present section are subject to restrictions stated in the *Cautions* subsection that follows Eq. 2.3-8.

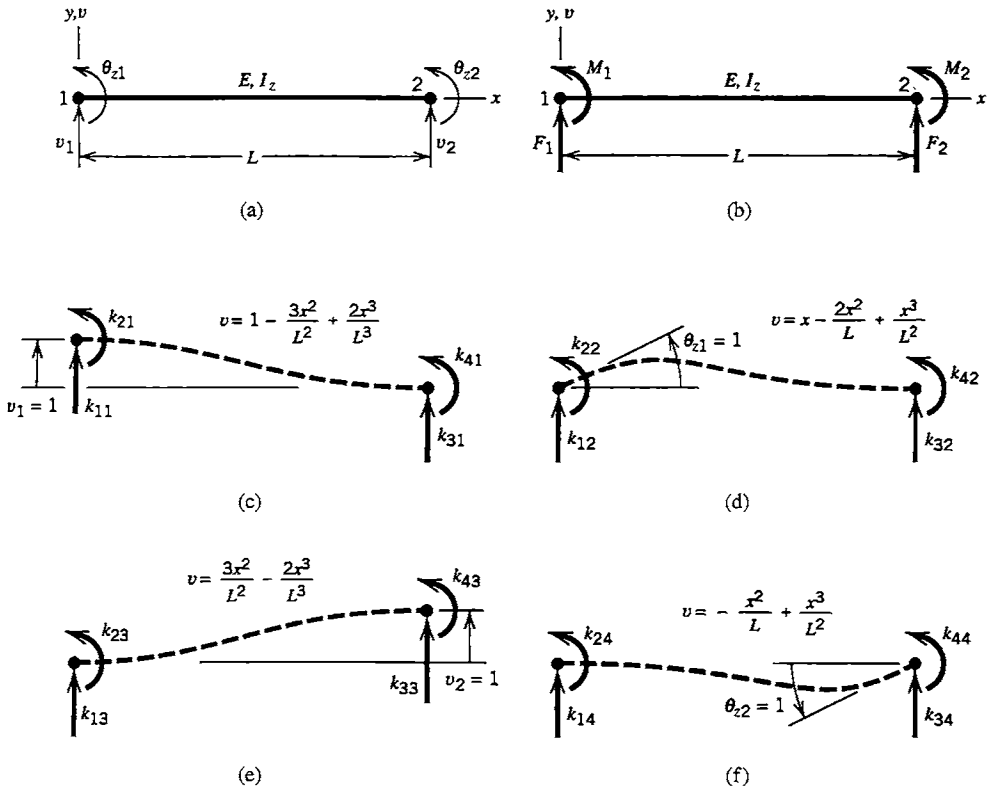

Figure 2.3-1. (a) Beam element in the xy plane and its nodal d.o.f. (b) Nodal loads associated with nodal d.o.f. (c–f) Dashed lines show lateral displacements due to bending associated with activation of each d.o.f. in turn. Formulas shown for $v = v(x)$ are obtained from elementary beam theory.

With axial deformation d.o.f. omitted, the stiffness matrix of a 2D beam element is 4 by 4. It can be constructed column by column. The jth column is the vector of nodal loads associated with unit value of the jth d.o.f. and zero values for all other d.o.f. The load vector contains moments as well as forces. To obtain the column associated with v_1 we calculate nodal loads shown in Fig. 2.3-1c. These loads are named k_{11}, k_{21}, k_{31}, and k_{41} to indicate that they will appear in rows 1, 2, 3, 4 and in column 1 of element stiffness matrix [**k**]. Loads are shown in the positive sense; that is, in the same direction as their associated d.o.f. To obtain k_{11} and k_{21} we can apply handbook formulas of elementary beam theory by regarding Fig. 2.3-1c as a cantilever beam fixed at node 2 and loaded at node 1 by force k_{11} and moment k_{21} such that $v_1 = 1$ and $\theta_{z1} = 0$. Thus

$$v_1 = 1: \quad \frac{k_{11}L^3}{3EI_z} - \frac{k_{21}L^2}{2EI_z} = 1 \qquad \theta_{z1} = 0: \quad -\frac{k_{11}L^2}{2EI_z} + \frac{k_{21}L}{EI_z} = 0 \qquad (2.3\text{-}1)$$

where E is the elastic modulus and I_z is the moment of inertia of the beam cross-sectional area about a centroidal axis parallel to the z axis. Equations 2.3-1 yield

$$k_{11} = \frac{12EI_z}{L^3} \qquad k_{21} = \frac{6EI_z}{L^2} \qquad (2.3\text{-}2)$$

Now that k_{11} and k_{21} are known, k_{31} and k_{41} can be determined from considerations of static equilibrium. We elect to sum y-direction forces and moments about node 2:

$$k_{11} + k_{31} = 0 \qquad k_{21} + k_{41} - k_{11}L = 0 \tag{2.3-3}$$

From Eqs. 2.3-2 and 2.3-3 we obtain

$$k_{31} = -\frac{12EI_z}{L^3} \qquad k_{41} = \frac{6EI_z}{L^2} \tag{2.3-4}$$

Similar analysis of the latter three parts of Fig. 2.3-1 provides terms in the latter three columns of [**k**]. The complete 2D beam element stiffness matrix is

$$[\mathbf{k}] = \begin{bmatrix} \frac{12EI_z}{L^3} & \frac{6EI_z}{L^2} & \frac{-12EI_z}{L^3} & \frac{6EI_z}{L^2} \\ \frac{6EI_z}{L^2} & \frac{4EI_z}{L} & \frac{-6EI_z}{L^2} & \frac{2EI_z}{L} \\ \frac{-12EI_z}{L^3} & \frac{-6EI_z}{L^2} & \frac{12EI_z}{L^3} & \frac{-6EI_z}{L^2} \\ \frac{6EI_z}{L^2} & \frac{2EI_z}{L} & \frac{-6EI_z}{L^2} & \frac{4EI_z}{L} \end{bmatrix} \begin{matrix} v_1 \\ \theta_{z1} \\ v_2 \\ \theta_{z2} \end{matrix} \tag{2.3-5}$$

The column of symbols on the right is appended merely to indicate that [**k**] operates on the column vector of element d.o.f. $\{\mathbf{d}\} = \lfloor v_1 \;\; \theta_{z1} \;\; v_2 \;\; \theta_{z2} \rfloor^T$. A different ordering of d.o.f. in $\{\mathbf{d}\}$ would change the ordering of coefficients in [**k**] but not their numerical values.

If the left end of the beam element is fixed so that $v_1 = 0$ and $\theta_{z1} = 0$, we obtain a structure with "active" d.o.f. v_2 and θ_{z2}. The stiffness matrix of this one-element cantilever beam is the lower right 2 by 2 submatrix in Eq. 2.3-5.

Generalizations. To allow the beam element to stretch as well as bend, we add axial translations u_1 and u_2 to the array of nodal d.o.f., and expand [**k**] to size 6 by 6 by including axial stiffness coefficients AE/L from Eq. 2.2-1. Also, we modify the bending stiffness terms to account for transverse shear deformation, thus producing a Timoshenko beam element. Its derivation, not presented here, may be found in several references, including [2.2–2.5]. See also Section 4.10. For deformation in the xy plane,

$$[\mathbf{k}] = \begin{bmatrix} X & 0 & 0 & -X & 0 & 0 \\ 0 & Y_1 & Y_2 & 0 & -Y_1 & Y_2 \\ 0 & Y_2 & Y_3 & 0 & -Y_2 & Y_4 \\ -X & 0 & 0 & X & 0 & 0 \\ 0 & -Y_1 & -Y_2 & 0 & Y_1 & -Y_2 \\ 0 & Y_2 & Y_4 & 0 & -Y_2 & Y_3 \end{bmatrix} \begin{matrix} u_1 \\ v_1 \\ \theta_{z1} \\ u_2 \\ v_2 \\ \theta_{z2} \end{matrix} \tag{2.3-6}$$

where

$$X = \frac{AE}{L} \qquad Y_1 = \frac{12EI_z}{(1+\phi_y)L^3} \qquad Y_2 = \frac{6EI_z}{(1+\phi_y)L^2}$$
$$Y_3 = \frac{(4+\phi_y)EI_z}{(1+\phi_y)L} \qquad Y_4 = \frac{(2-\phi_y)EI_z}{(1+\phi_y)L} \qquad \phi_y = \frac{12EI_z k_y}{AGL^2} \tag{2.3-7}$$

and A/k_y is the effective shear area for transverse shear deformation in the y direction. Commonly accepted factors are $k_y = 1.2$ for a solid rectangular cross section, $k_y = 2.0$ for a thin-walled tube of circular cross section, and so on. More nearly exact factors appear in [2.1]. Note that as an element becomes more and more slender, ϕ_y approaches zero, so that flexure coefficients Y_i reduce to coefficients seen in Eq. 2.3-5, where transverse shear deformation is neglected.

In Eq. 2.3-5, a rotational d.o.f. defines the nodal value of both beam slope dv/dx and rotation of the beam cross section. If transverse shear deformation is present, beam slope and cross-section rotation differ. Then θ_{z1} and θ_{z2} must be regarded as rotations of beam cross sections at nodes.

3D Beam Element. We allow six d.o.f. per node: three translations and three rotations, as shown in Fig. 2.3-2. The w and θ_y d.o.f. account for lateral deflection in the zx plane. The θ_x d.o.f. account for twist about the x axis, for which the stiffness coefficient is GK/L, where K is a property of the shape and size of the cross section. (Only for a circular cross section, either solid or a tube, does K become equal to J, the polar moment of inertia of the cross-sectional area about its centroid. For thin-walled open cross sections, such as those of standard I beams and channels, K is a small fraction of J.) Partitioned by nodes for the sake of clarity, $[\mathbf{k}]$ is

$$[\mathbf{k}] = \left[\begin{array}{cccccc|cccccc}
X & 0 & 0 & 0 & 0 & 0 & -X & 0 & 0 & 0 & 0 & 0 \\
 & Y_1 & 0 & 0 & 0 & Y_2 & 0 & -Y_1 & 0 & 0 & 0 & Y_2 \\
 & & Z_1 & 0 & -Z_2 & 0 & 0 & 0 & -Z_1 & 0 & -Z_2 & 0 \\
 & & & S & 0 & 0 & 0 & 0 & 0 & -S & 0 & 0 \\
 & & & & Z_3 & 0 & 0 & 0 & Z_2 & 0 & Z_4 & 0 \\
 & & & & & Y_3 & 0 & -Y_2 & 0 & 0 & 0 & Y_4 \\
\hline
 & & & & & & X & 0 & 0 & 0 & 0 & 0 \\
 & & & & & & & Y_1 & 0 & 0 & 0 & -Y_2 \\
 & & \text{symmetric} & & & & & & Z_1 & 0 & Z_2 & 0 \\
 & & & & & & & & & S & 0 & 0 \\
 & & & & & & & & & & Z_3 & 0 \\
 & & & & & & & & & & & Y_3
\end{array}\right]
\begin{array}{c} u_1 \\ v_1 \\ w_1 \\ \theta_{x1} \\ \theta_{y1} \\ \theta_{z1} \\ u_2 \\ v_2 \\ w_2 \\ \theta_{x2} \\ \theta_{y2} \\ \theta_{z2} \end{array} \tag{2.3-8}$$

where $S = GK/L$, X and Y_i terms are defined in Eq. 2.3-7, and Z_i terms are defined as in Eq. 2.3-7 but with interchange of subscripts. For example, $Z_1 = 12EI_y/(1+\phi_z)L^3$ and

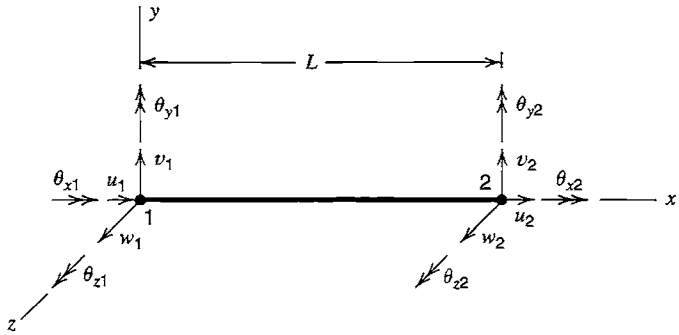

Figure 2.3-2. Beam element on the x axis of a rectangular coordinate system, with nodal d.o.f. used to define axial displacement, twisting, and lateral deflection in the y and z directions.

$\phi_z = 12EI_yk_z/AGL^2$. Sign differences among Y_i and Z_i terms in Eq. 2.3-8 arise because of the positive directions assigned for nodal rotations in Fig. 2.3-2. For example, θ_{y1} produces negative z-direction lateral displacement, whereas θ_{z1} produces positive y-direction lateral displacement. In all cases, positive senses of nodal forces and moments have the same directions as their associated d.o.f. in Fig. 2.3-2.

When elements are assembled, as in Fig. 2.3-3a, element d.o.f. at a shared node are merged into a single set of "global" d.o.f. This process requires that "local" d.o.f. of each element (shown in Fig. 2.3-2) are mated to appropriate local d.o.f. of a connecting element. At node B in Fig. 2.3-3a, for example, the axial translation d.o.f. of element AB is a lateral translation d.o.f. of element BC. In terms of d.o.f. in Fig. 2.3-2, u_2 of element AB must be identified as the same d.o.f. as v_1 of element BC, and so on, which is most easily accomplished by applying a coordinate transformation to the d.o.f. of element AB before assembly of elements (see Section 2.4).

Cautions. It is assumed in the preceding development that axes y and z are principal centroidal axes of the cross section. This assumption is true in the elementary case where $y = z = 0$ at the centroid and the cross section has at least one symmetry axis that is coincident with either axis y or axis z. If the cross section is unsymmetric, principal axes must be established by calculation [2.6]. If y and z were not principal axes, different terms would appear in Eq. 2.3-8, and there would be fewer zero coefficients, because activation of a d.o.f. would produce more nodal forces and moments.

When a member of noncircular cross section is twisted, cross sections "warp"; that is, cross sections do not remain plane. Channels, I beams, and other thin-walled open members have low torsional stiffness, and their cross sections tend to warp appreciably when the member is twisted. Restraint of warping may have a large effect. For example, let member AB in Fig. 2.3-3b be an I beam five times as long as it is deep, with torque T

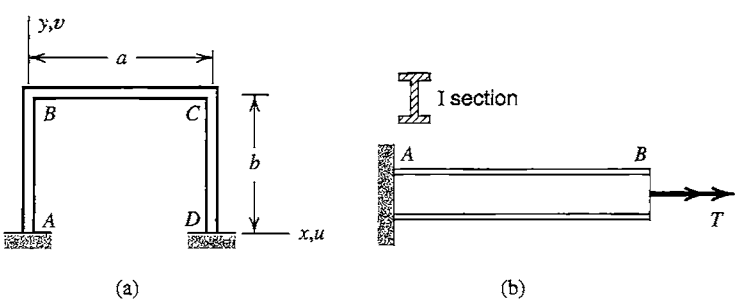

Figure 2.3-3. (a) A plane frame built of beam elements AB, BC, and CD. (b) A beam fixed at A and loaded by torque T at B.

applied at end B. Complete restraint of warping at end A reduces rotation at B by about half and introduces axial normal stresses much larger than the torsional shear stress. In Fig. 2.3-3a, warping is at least partially restrained at lettered nodes, and such restraint influences response due to loads normal to the plane of the frame.

To account for full or partial restraint of warping, another d.o.f. must be added at each node, so that [**k**] for a 3D beam element becomes a 14 by 14 matrix. The added d.o.f. are rates of twist $d\theta_x/dx$ at nodes, each associated with a load term called a *bimoment.* Unfortunately, commercial software typically allows only six displacement d.o.f. per node, so restraint of warping is ignored in beam elements.

Software may accept nodes on an x axis that does not pass through centroids of cross sections. Software may also accept a general shape for the cross section of a thin-walled member, so if that software is supplied with data about cross section geometry, it computes cross-sectional properties such as moments and product of inertia, sectorial properties, and locations of centroid and shear center. (The shear center is the point in a cross section through which transverse forces must be directed if a prismatic beam is to bend without twisting.) If centroid and shear center do not coincide, or if they do not lie on the x axis, coordinate transformation is required in formulating the element stiffness matrix, which is then more complicated than shown in Eq. 2.3-8. Similar considerations influence the mass matrix used for dynamics. If cross sections have shear centers that do not coincide with their centroids, a structure built of such members, even if planar and loaded in its plane, usually requires the d.o.f. of Eq. 2.3-8; the d.o.f. of Eq. 2.3-6 do not suffice.

Equation 2.3-8 is correct for a member of circular cross section, for which cross sections have no tendency to warp. It is also correct for a member whose cross section has two axes of symmetry (so that its shear center and its centroid coincide), whose centroid is on the x axis, and whose cross sections are free to warp when the element is twisted about its axis. The theory of finite elements for thin-walled open members is discussed in many references, of which we cite [2.7-2.12].

2.4 BAR AND BEAM ELEMENTS OF ARBITRARY ORIENTATION

Elements discussed in Sections 2.2 and 2.3 lie along the x axis. For general use, elements must be capable of assuming any orientation in space. This capability can be provided by simple manipulation of element matrices already derived. For this purpose we regard the stiffness matrices of Eqs. 2.2-1 and 2.3-8 as stiffness matrices [**k**′] that lie on the x' axis of a "local" coordinate system $x'y'z'$, which is arbitrarily oriented in a global coordinate system xyz. To obtain an element matrix [**k**] that operates on d.o.f. referred to global coordinates xyz, we apply a rotational coordinate transformation to [**k**′].

The following rotational transformations do not alter intrinsic element properties. Rather, they alter the formal expression of element properties so that they agree with use of d.o.f. whose arrows are parallel to global coordinate directions rather than to local coordinate directions.

Bar Element. Consider first a two-dimensional transformation. Starting with a bar element along a local axis x' in the xy plane, we seek the stiffness matrix of a bar element arbitrarily oriented in the xy plane, so that it operates on the four nodal d.o.f. shown in

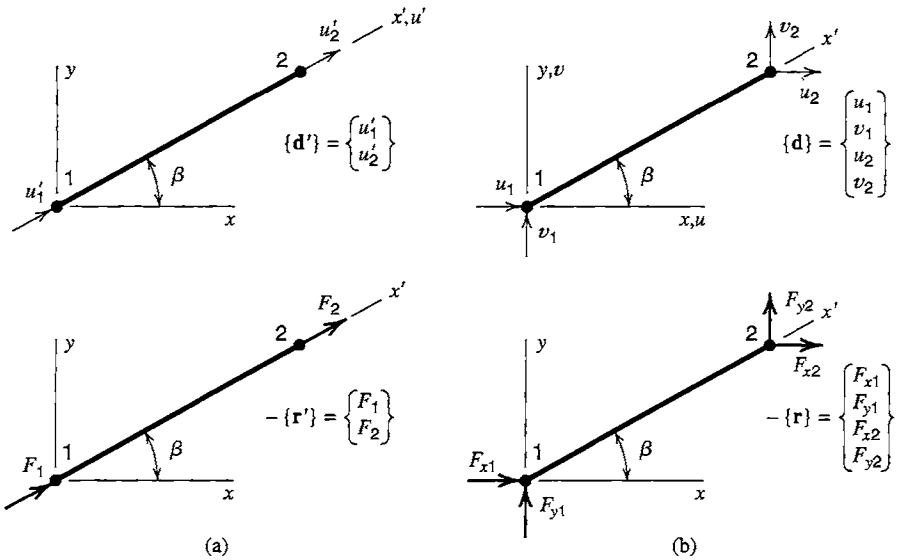

Figure 2.4-1. (a) Local nodal d.o.f. and loads of a bar element lying on a local axis x'. (b) Global nodal d.o.f. and loads of a bar element that lies in the plane of global axes xy.

Fig. 2.4-1b. The relation between local and global d.o.f. is easily written by resolving global d.o.f. into local components at a node, then adding collinear components; for example, $u_1' = u_1 \cos\beta + v_1 \sin\beta$ (Fig. 2.4-2a). In matrix format, displacement arrays in Fig. 2.4-1 have the relation

$$\{\mathbf{d}'\} = [\mathbf{T}]\{\mathbf{d}\} \tag{2.4-1}$$

in which transformation matrix $[\mathbf{T}]$ is

$$[\mathbf{T}] = \begin{bmatrix} c & s & 0 & 0 \\ 0 & 0 & c & s \end{bmatrix} \quad \text{where} \quad c = \cos\beta \quad \text{and} \quad s = \sin\beta \tag{2.4-2}$$

Relations between local and global nodal loads are established by resolving nodal loads F_1 and F_2 into components parallel to x and y axes (Fig. 2.4-2b). Thus force arrays in Fig. 2.4-1 have the relation

$$\{\mathbf{r}\} = [\mathbf{T}]^T\{\mathbf{r}'\} \tag{2.4-3}$$

(The inverse relationship, $\{\mathbf{r}'\} = [\mathbf{T}]\{\mathbf{r}\}$, has the same form as Eq. 2.4-1; see Section 8.1 for virtual work arguments.) The element stiffness relation in local coordinates is

$$\text{Local:} \quad [\mathbf{k}']\{\mathbf{d}'\} = -\{\mathbf{r}'\} \tag{2.4-4}$$

The negative sign is explained following Eq. 2.2-2. In Eq. 2.4-4 we substitute $\{\mathbf{d}'\} = [\mathbf{T}]\{\mathbf{d}\}$ from Eq. 2.4-1, premultiply both sides by $[\mathbf{T}]^T$, and then, on the right-hand side, substitute for $[\mathbf{T}]^T\{\mathbf{r}'\}$ from Eq. 2.4-3. Thus Eq. 2.4-4 is transformed to

$$\text{Global:} \quad [\mathbf{k}]\{\mathbf{d}\} = -\{\mathbf{r}\} \quad \text{where} \quad [\mathbf{k}] = [\mathbf{T}]^T[\mathbf{k}'][\mathbf{T}] \tag{2.4-5}$$

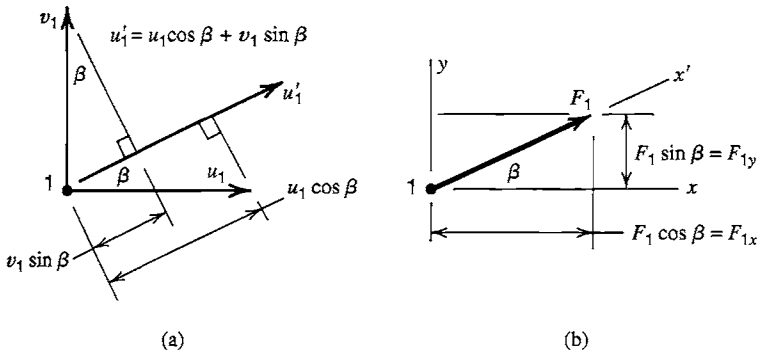

Figure 2.4-2.
(a) Contributions of u_1 and v_1 to u_1'.
(b) Resolution of F_1 into F_{x1} and F_{y1}.

(This triple product form for [**k**] is not restricted to rotational transformation. For other changes of d.o.f., as described in Chapter 8, [**T**] is again the matrix that multiplies "new" d.o.f. {**d**} to produce "old" d.o.f. {**d**′}, as in Eq. 2.4-1.)

For the bar problem, [**k**′] is the 2 by 2 matrix of Eq. 2.2-1. The same element in global coordinates xy operates on d.o.f. $\{\mathbf{d}\} = \lfloor u_1 \;\; v_1 \;\; u_2 \;\; v_2 \rfloor^T$, for which [**k**] is the 4 by 4 matrix

$$[\mathbf{k}] = k \begin{bmatrix} c^2 & cs & -c^2 & -cs \\ cs & s^2 & -cs & -s^2 \\ -c^2 & -cs & c^2 & cs \\ -cs & -s^2 & cs & s^2 \end{bmatrix} \quad \text{where} \quad \begin{aligned} c &= \cos\beta \\ s &= \sin\beta \end{aligned} \tag{2.4-6}$$

and axial stiffness k of the bar is $k = AE/L$. Note that if node numbers are interchanged, $\sin\beta$ and $\cos\beta$ both change sign, and the same [**k**] is produced.

Equation 2.4-6 can also be obtained directly by applying the rule stated following Eq. 2.2-2: obtain a column of [**k**] by activating the corresponding d.o.f. and calculating nodal loads needed to preserve the deformation state. Thus, displacement $u_1 = 1$ produces axial shortening $\delta = -\cos\beta$ and axial compressive force of magnitude $k \cos\beta$. The x and y components of end loads that equilibrate this force appear as column 1 of [**k**].

A bar element arbitrarily oriented in global coordinates xyz has a 6 by 6 stiffness matrix that operates on nodal d.o.f. $\{\mathbf{d}\} = \lfloor u_1 \;\; v_1 \;\; w_1 \;\; u_2 \;\; v_2 \;\; w_2 \rfloor^T$, where u, v, and w are displacement components in x, y, and z directions respectively. The argument that leads to Eq. 2.4-5 remains applicable even though an additional d.o.f. is present at each node. Again, Eq. 2.4-5 states the transformation, and again [**k**′] is as stated in Eq. 2.2-1, but now the transformation matrix is

$$[\mathbf{T}] = \begin{bmatrix} l_1 & m_1 & n_1 & 0 & 0 & 0 \\ 0 & 0 & 0 & l_1 & m_1 & n_1 \end{bmatrix} \tag{2.4-7}$$

where l_1, m_1, and n_1 are direction cosines of local member axis x' with respect to global axes x, y, and z (Fig. 2.4-3). If the element happens to lie in the xy plane, then $l_1 = \cos\beta$, $m_1 = \sin\beta$, and $n_1 = 0$, and nonzero terms in the 6 by 6 matrix [**k**] agree with terms in Eq. 2.4-6. Whether in two dimensions or three, matrix [**k**] is completely defined by A, E, and global coordinates of the two end nodes.

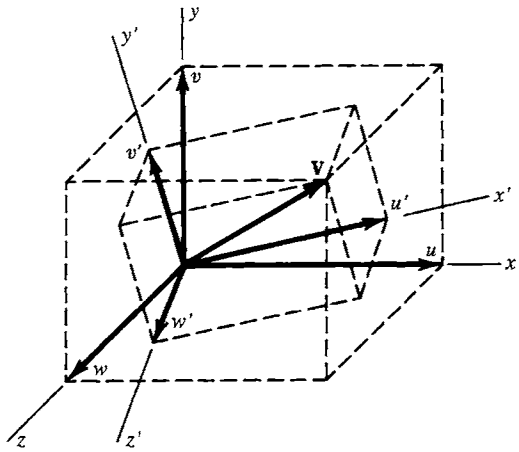

Direction cosines between axes:

	x	y	z
x'	l_1	m_1	n_1
y'	l_2	m_2	n_2
z'	l_3	m_3	n_3

Figure 2.4-3. A vector **V** can be expressed in terms of components uvw in global system xyz or in terms of components $u'v'w'$ in local system $x'y'z'$.

Beam Element. Now Eq. 2.3-8 must be regarded as $[\mathbf{k}']$, the stiffness matrix of an element that lies along a local axis x', with its nodal d.o.f. represented by arrows that point in local directions x', y', and z'. Components of translation and rotation transform from global to local directions in the same way; for example,

$$u_1' = l_1 u_1 + m_1 v_1 + n_1 w_1 \quad \text{and} \quad \theta_{x1}' = l_1 \theta_{x1} + m_1 \theta_{y1} + n_1 \theta_{z1} \tag{2.4-8}$$

Transformation of the stiffness matrix from local to global d.o.f. is as stated by Eq. 2.4-5, and the transformation matrix is

$$\underset{12\times 12}{[\mathbf{T}]} = \begin{bmatrix} \Lambda & 0 & 0 & 0 \\ 0 & \Lambda & 0 & 0 \\ 0 & 0 & \Lambda & 0 \\ 0 & 0 & 0 & \Lambda \end{bmatrix} \quad \text{where} \quad [\Lambda] = \begin{bmatrix} l_1 & m_1 & n_1 \\ l_2 & m_2 & n_2 \\ l_3 & m_3 & n_3 \end{bmatrix} \tag{2.4-9}$$

Local directions should be suited to the element geometry so that cross-sectional properties of a beam element can be stated without confusion. For example, one might define the $x'y'$ plane as being coincident with the web of an I beam. The direction of local axis x' is defined by global coordinates of the two beam nodes, which may be placed at centroids of end cross sections. If coordinates are supplied for a third point that is not collinear with the end nodes, there is enough information to establish the orientation of the $x'y'$ plane in global coordinates xyz, and hence to establish direction z'. Direction cosines of axis y' are provided by the cross product of unit vectors in z' and x' directions.

2.5 ASSEMBLY OF ELEMENTS

In this section we elaborate on the rationale and procedure of assembling elements to produce a set of equations that describes the structure. Concepts discussed are not limited to structures built of bars and beams. The same procedures are applicable regardless of prob-

lem type, element type, and number of nodes per element. When stiffness matrices and load terms are assembled, boundary conditions may also be treated. The details of boundary conditions and loads are discussed in subsequent sections.

Equilibrium Equations. We regard each structure node as a small connector to which elements are attached, and we argue that assembly of elements and load terms produces a set of equations stating that each node is in equilibrium. Loads applied to a node come from element deformation, from initial stress in elements, from external loads distributed over elements, and from loads applied directly to nodes. In Eq. 2.2-2, $-\{\mathbf{r}\}$ represents loads applied *to* an element at its nodes to maintain its deformed state. Equal and opposite loads $\{\mathbf{r}\}$ are applied *by* an element to the structure nodes to which it is connected. That is, loads applied to structure nodes include:

$$\text{Loads on structure nodes from element deformation: } \{\mathbf{r}\} = -[\mathbf{k}]\{\mathbf{d}\} \tag{2.5-1}$$

Additional loads applied to structure nodes by an element (from sources other than element deformation) include loads due to temperature and the action of gravity. For example, heating a truss member creates an outward push against nodes, and element weight pushes down on nodes. Structural supports apply loads directly to nodes. We adopt the following symbolism for such additional loads applied to structure nodes:

$$\begin{aligned} &\text{Loads applied by an element when its d.o.f. are zero: } \{\mathbf{r}_e\} \\ &\text{External loads applied directly to structure nodes: } \{\mathbf{P}\} \end{aligned} \tag{2.5-2}$$

These loads may have components in each coordinate direction and, in general, include moments as well as forces.

The matrix equation that places structure nodes in equilibrium is

$$\sum_{i=1}^{N_{\text{els}}} \{\mathbf{r}\}_i + \sum_{i=1}^{N_{\text{els}}} \{\mathbf{r}_e\}_i + \{\mathbf{P}\} = \{\mathbf{0}\} \tag{2.5-3}$$

where N_{els} is the number of elements in the structure. To repeat, we regard each structure node as a small connector that must be in static equilibrium under the action of all loads applied to it. Substitution from Eq. 2.5-1 yields

$$[\mathbf{K}]\{\mathbf{D}\} = \{\mathbf{R}\} \qquad \text{where} \qquad \begin{aligned} [\mathbf{K}] &= \sum_{i=1}^{N_{\text{els}}} [\mathbf{k}]_i \\ \{\mathbf{R}\} &= \{\mathbf{P}\} + \sum_{i=1}^{N_{\text{els}}} \{\mathbf{r}_e\}_i \end{aligned} \tag{2.5-4}$$

Summations imply the expansion of element matrices to "structure size," as in Eqs. 2.2-7, so that $\{\mathbf{d}\}_i$ of each element i becomes identical to $\{\mathbf{D}\}$, the vector of d.o.f. for the entire

structure. Loads $\{\mathbf{R}\}$ are applied *to* (not by) structure nodes and include all loads other than loads $-[\mathbf{K}]\{\mathbf{D}\}$ applied to nodes by elastic deformation of structural members. The foregoing development shows that $[\mathbf{K}]\{\mathbf{D}\} = \{\mathbf{R}\}$ is a set of equilibrium equations.

Similar argument may be applied to a nonstructural problem. For example, in steady-state heat conduction analysis, equilibrium of a node means that the net heat flow into (or out of) a structure node is zero. With the convention that heat flow into a structure node is positive, Eq. 2.2-5 is the thermal analog of Eq. 2.5-1. For example, a vector $\{\mathbf{r}_e\}$ may account for heating due to electric current flow, and a vector $\{\mathbf{P}\}$ may account for convection heat transfer at nodes on the surface of a solid body.

Assembly and Structure Node Numbers. The following example shows that locations to which terms of element matrices $[\mathbf{k}]_i$ are assigned in a structure matrix $[\mathbf{K}]$ depend on structure node numbering. For this purpose the number of nodes per element does not matter, and we need not know how any $[\mathbf{k}]_i$ is derived. We consider three-node triangular elements. For illustration only, we allow matrices to be unsymmetric, and we give names to individual coefficients in each $[\mathbf{k}]_i$ to show more clearly what becomes of them upon assembly. We show that formal expansion of $[\mathbf{k}]_i$ to "structure size" is not required.

In Fig. 2.5-1, let there be one d.o.f. per node. For the respective elements, in the element numbering system,

For triangular element 1: For triangular element 2:

$$[\mathbf{k}]_1\{\mathbf{d}\}_1 = \begin{bmatrix} a_1 & a_2 & a_3 \\ a_4 & a_5 & a_6 \\ a_7 & a_8 & a_9 \end{bmatrix} \begin{Bmatrix} d_1 \\ d_2 \\ d_3 \end{Bmatrix} \qquad [\mathbf{k}]_2\{\mathbf{d}\}_2 = \begin{bmatrix} b_1 & b_2 & b_3 \\ b_4 & b_5 & b_6 \\ b_7 & b_8 & b_9 \end{bmatrix} \begin{Bmatrix} d_1 \\ d_2 \\ d_3 \end{Bmatrix} \tag{2.5-5}$$

where the a's and b's are symbolic names for coefficients in element matrices $[\mathbf{k}]_1$ and $[\mathbf{k}]_2$. The loads applied to elements by structure nodes are $-\{\mathbf{r}\}$, where $-\{\mathbf{r}\} = [\mathbf{k}]\{\mathbf{d}\}$. To identify the same loads when structure node numbers are substituted for element node numbers, we add superscript s. Thus, for element 1,

Element node numbering: Structure node numbering:

$$\begin{aligned} -r_1 &= a_1d_1 + a_2d_2 + a_3d_3 \\ -r_2 &= a_4d_1 + a_5d_2 + a_6d_3 \\ -r_3 &= a_7d_1 + a_8d_2 + a_9d_3 \end{aligned} \quad \text{and} \quad \begin{aligned} -r_1^s &= a_1D_1 + a_2D_4 + a_3D_2 \\ -r_4^s &= a_4D_1 + a_5D_4 + a_6D_2 \\ -r_2^s &= a_7D_1 + a_8D_4 + a_9D_2 \end{aligned} \tag{2.5-6}$$

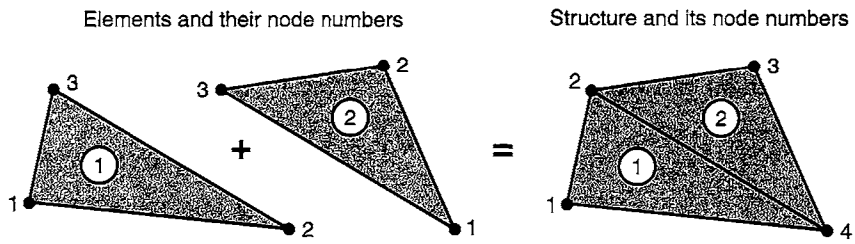

Figure 2.5-1. A hypothetical four-node structure built of two triangular three-node elements. Each node has one d.o.f.

To the latter group of equations we can add the equation $r_3^s = 0$, because structure node 3 is not attached to element 1. For the same reason, D_3 produces no load at any node of element 1. After these additions, and rearrangement to place the D's in numerical order, we have for element 1

$$\begin{Bmatrix} -r_1^s \\ -r_2^s \\ -r_3^s \\ -r_4^s \end{Bmatrix} = \begin{bmatrix} a_1 & a_3 & 0 & a_2 \\ a_7 & a_9 & 0 & a_8 \\ 0 & 0 & 0 & 0 \\ a_4 & a_6 & 0 & a_5 \end{bmatrix} \begin{Bmatrix} D_1 \\ D_2 \\ D_3 \\ D_4 \end{Bmatrix} \tag{2.5-7}$$

in which the 4 by 4 matrix is $[\mathbf{k}]_1$. Element 2 can be treated similarly.

The net load associated with each node can be written in terms of a's, b's, and D's. For example, the net load applied by structure node 4 to the two elastically deformed elements is

$$-r_4^s = (a_4D_1 + a_6D_2 + 0 + a_5D_4) + (0 + b_3D_2 + b_2D_3 + b_1D_4) \tag{2.5-8}$$

By writing the net nodal loads in structure node number order and gathering coefficients of each D_i, we conclude that, because $[\mathbf{k}]_1$ and $[\mathbf{k}]_2$ have the same size and operate on the same vector $\{\mathbf{D}\}$, we can write $[\mathbf{K}]\{\mathbf{D}\} = (\sum[\mathbf{k}])\{\mathbf{D}\}$, where

$$[\mathbf{K}] = [\mathbf{k}]_1 + [\mathbf{k}]_2 = \begin{bmatrix} a_1 & a_3 & 0 & a_2 \\ a_7 & a_9 & 0 & a_8 \\ 0 & 0 & 0 & 0 \\ a_4 & a_6 & 0 & a_5 \end{bmatrix} + \begin{bmatrix} 0 & 0 & 0 & 0 \\ 0 & b_9 & b_8 & b_7 \\ 0 & b_6 & b_5 & b_4 \\ 0 & b_3 & b_2 & b_1 \end{bmatrix} \tag{2.5-9}$$

We see that coefficients originally below the diagonal of an element matrix $[\mathbf{k}]$ may be assigned to locations above the diagonal of $[\mathbf{K}]$. Whether or not this happens, it is the *structure* numbers of element nodes that determine where element coefficients are placed in structure matrix $[\mathbf{K}]$. This fact may be demonstrated by cyclically permuting element node numbers; for example, by permuting node numbers in element 1 of Fig. 2.5-1 so that the lower left node becomes element node 2. Then the first of Eqs. 2.5-6 becomes $-r_2 = a_1d_2 + a_2d_3 + a_3d_1$, but if structure node numbers are unchanged, Eq. 2.5-7 is again obtained.

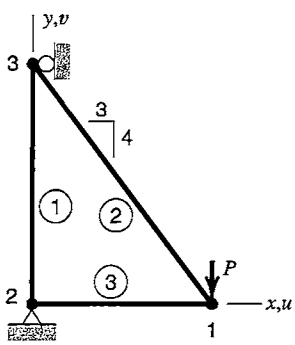

Figure 2.5-2. A plane three-bar truss loaded by force P.

What if there are n d.o.f. per node rather than a single d.o.f. per node? Then, in Eq. 2.5-7, each $-r_i^s$ and each D_i becomes a column array of n terms, and each a_i becomes an n by n submatrix. As an example, consider the three-bar plane truss of Fig. 2.5-2, for which $n = 2$. Imagine that supports are temporarily removed. With displacements confined to the xy plane, Eq. 2.4-6 provides the stiffness matrix of each element, with k the axial stiffness A_iE_i/L_i of element i. Element node numbers may be chosen in either order. For example, if the order is 1–3 for element 2, then angle β lies in the second quadrant, so $\sin\beta = 0.8$ and $\cos\beta = -0.6$. If the order is 3–1, then angle β lies in the fourth quadrant, so $\sin\beta = -0.8$ and $\cos\beta = 0.6$. Either way, the same $[\mathbf{k}]$ is obtained for element 2. After assembly of elements, structure equations $[\mathbf{K}]\{\mathbf{D}\} = \{\mathbf{R}\}$ are

$$\begin{bmatrix} k_3+0.36k_2 & -0.48k_2 & -k_3 & 0 & -0.36k_2 & 0.48k_2 \\ -0.48k_2 & 0.64k_2 & 0 & 0 & 0.48k_2 & -0.64k_2 \\ -k_3 & 0 & k_3 & 0 & 0 & 0 \\ 0 & 0 & 0 & k_1 & 0 & -k_1 \\ -0.36k_2 & 0.48k_2 & 0 & 0 & 0.36k_2 & -0.48k_2 \\ 0.48k_2 & -0.64k_2 & 0 & -k_1 & -0.48k_2 & k_1+0.64k_2 \end{bmatrix} \begin{Bmatrix} u_1 \\ v_1 \\ u_2 \\ v_2 \\ u_3 \\ v_3 \end{Bmatrix} = \begin{Bmatrix} 0 \\ -P \\ p_2 \\ q_2 \\ p_3 \\ 0 \end{Bmatrix} \tag{2.5-10}$$

in which load P is negative because it is directed opposite to the direction of d.o.f. v_1. Load terms p_2, q_2, and p_3 are horizontal and vertical forces applied to nodes 2 and 3 by supports. (Analogous assembly of beam elements is illustrated by Eq. 2.9-7.) Boundary conditions shown in Fig. 2.5-2 dictate that $u_2 = v_2 = u_3 = 0$. Treatment of boundary conditions is discussed in Section 2.7.

The foregoing procedure, in which element coefficients are added to locations in $[\mathbf{K}]$ and $\{\mathbf{R}\}$ dictated by structure node numbering, is called the *direct stiffness method.* An alternative procedure, called congruent transformation, is more formal but less suited to computer implementation. It is used in the latter equations of Section 4.8.

Discussion of assembly leads directly to implementation procedures in computer software, for details of which see the third edition of this book; also [2.13–2.15]. In software, the assembly process is likely to be augmented to allow connection of elements with different numbers of d.o.f. per node and to allow certain boundary conditions to be imposed as part of the assembly process.

Thus far we have included no more d.o.f. than necessary in our arguments. Subsequently, we must be aware that software typically allows three translations and three rotations per node. Some of these d.o.f. may be irrelevant in a given problem, and those may have to be suppressed to provide adequate support to a structure so that a solution can be obtained.

2.6 PROPERTIES OF STIFFNESS MATRICES

Element and structure stiffness matrices already seen—in Eqs. 2.2-1, 2.2-6, 2.3-5, and 2.5-10, for example—have properties such as symmetry, positive diagonal terms, and zeros

off-diagonal. We now discuss these and other properties, and when they can be expected for stiffness matrices in general. Characteristic matrices for nonstructural problems have analogous properties.

Nonnegative $\mathbf{K}_{ii}$. Imagine that all d.o.f. in $\{\mathbf{D}\}$ are zero but a single d.o.f. D_i. Then the product $[\mathbf{K}]\{\mathbf{D}\}$ yields $R_i = K_{ii}D_i$ as the externally applied load that corresponds to D_i. It is physically unreasonable that a single load in a given direction would produce a displacement component in the opposite direction. Therefore, diagonal coefficients K_{ii} cannot be negative; that is, $K_{ii} \geq 0$. If $K_{ii} = 0$, we infer either that no element is attached to d.o.f. i or that there is a mechanism that involves d.o.f. i (see below).

Symmetry. The stiffness matrix of any element or structure is symmetric if loads are linearly related to displacements. This property can be proven by applying the *Betti-Maxwell reciprocal theorem,* which states that if two sets of loads act on a linearly elastic structure, work done by the first set of loads in acting through displacements produced by the second set of loads is equal to work done by the second set in acting through displacements produced by the first set. That is, if loads $\{\mathbf{R}\}_1$ and $\{\mathbf{R}\}_2$ produce the respective displacements $\{\mathbf{D}\}_1$ and $\{\mathbf{D}\}_2$, then

$$\{\mathbf{R}\}_1^T\{\mathbf{D}\}_2 = \{\mathbf{R}\}_2^T\{\mathbf{D}\}_1 \tag{2.6-1}$$

Substitution for $\{\mathbf{R}\}_1$ and $\{\mathbf{R}\}_2$ yields

$$([\mathbf{K}]\{\mathbf{D}\}_1)^T\{\mathbf{D}\}_2 = ([\mathbf{K}]\{\mathbf{D}\}_2)^T\{\mathbf{D}\}_1 \quad \text{or} \quad \{\mathbf{D}\}_1^T[\mathbf{K}]^T\{\mathbf{D}\}_2 = \{\mathbf{D}\}_2^T[\mathbf{K}]^T\{\mathbf{D}\}_1 \tag{2.6-2}$$

Both sides of the latter equation are scalars, so either side can be transposed without changing anything. Transposing the right-hand side and then gathering terms, we obtain

$$\{\mathbf{D}\}_1^T[\mathbf{K}]^T\{\mathbf{D}\}_2 = \{\mathbf{D}\}_1^T[\mathbf{K}]\{\mathbf{D}\}_2 \quad \text{or} \quad \{\mathbf{D}\}_1^T([\mathbf{K}]^T - [\mathbf{K}])\{\mathbf{D}\}_2 = 0 \tag{2.6-3}$$

Because neither $\{\mathbf{D}\}_1$ nor $\{\mathbf{D}\}_2$ is null, the expression in parentheses must vanish. Therefore $[\mathbf{K}]^T = [\mathbf{K}]$, which means that $[\mathbf{K}]$ is symmetric.

Sparsity. A global stiffness coefficient K_{ij} is zero unless at least one element is attached to both d.o.f. i and d.o.f. j. For example, in Eq. 2.2-6, $K_{13} = 0$, because d.o.f. u_1 in Fig. 2.2-3 is attached to element 1 only. (Occasionally K_{ij} is zero even when both d.o.f. are present in the element, perhaps because of element orientation. An example appears in Eq. 2.5-10, where there is a zero in column 4 of row 1. The horizontal member is attached to both u_1 and v_2, yet $K_{14} = 0$, which indicates that displacement v_2 does not cause a horizontal force to appear at node 1.)

A matrix is called "sparse" if it contains many zeros. The stiffness matrices of example structures considered thus far are not sparse, but only because the structures contain few elements. A practical FE structure may contain hundreds or thousands of elements, and more than 99% of coefficients in its stiffness matrix may be zero. To avoid storing and processing vast numbers of zeros in $[\mathbf{K}]$, general-purpose software uses special storage formats and algorithms adapted to these formats.

Singularity: No Support. Until boundary conditions are imposed, a structure is free to "float" in space; that is, the structure is unsupported and can undergo rigid-body motion. Rigid-body motion includes translation and rotation. When we consider rotation of a structure (or any of its parts), it is important to recognize that, in commonplace linear analysis, deformations and rotations are assumed to be small, and $[\mathbf{K}]$ is constructed using the original *undeformed* geometry. Figure 2.6-1 shows rigid-body rotation of a bar about its left end. Approximations $u_2 \approx -L\theta^2/2$ and $v_2 \approx L\theta$ are valid only for small θ, and come from substitution of series for $\sin\theta$ and $\cos\theta$ and truncation of each resulting expression to a single term. For small θ, u_2 is negligible in comparison with v_2, and $\theta \approx v_2/L$. For this reason, if v_2 is the only nonzero d.o.f. and $v_2 << L$, this displacement state may be regarded as rigid-body rotation about node 1. Note that if $\theta = \pi/2$, actual displacements in $\{\mathbf{d}\}$ are $u_2 = -L$ and $v_2 = L$, but then $[\mathbf{k}]\{\mathbf{d}\} \neq \{\mathbf{0}\}$ because $[\mathbf{k}]$ is not valid for so large a rotation.

If $\{\mathbf{D}\}$ represents a small rigid-body displacement, then $[\mathbf{K}]\{\mathbf{D}\} = \{\mathbf{0}\}$; no loads are required. Imagine that the supports of the plane truss in Fig. 2.5-2 are temporarily removed so that all nodal displacements in the xy plane are allowed. Four examples of plane rigid-body displacement for this structure are then

$$\begin{aligned} \{\mathbf{D}\}_1 &= \lfloor c \;\; 0 \;\; c \;\; 0 \;\; c \;\; 0 \rfloor^T & \{\mathbf{D}\}_2 &= \lfloor 0 \;\; c \;\; 0 \;\; c \;\; 0 \;\; c \rfloor^T \\ \{\mathbf{D}\}_3 &= \lfloor c \;\; c \;\; c \;\; c \;\; c \;\; c \rfloor^T & \{\mathbf{D}\}_4 &= \lfloor 4\theta \;\; 3\theta \;\; 4\theta \;\; 0 \;\; 0 \;\; 0 \rfloor^T \end{aligned} \tag{2.6-4}$$

where c is a small displacement and θ is a small angle of rotation. Respectively, these four displacement vectors represent translation along the x axis, translation along the y axis, translation along the direction $x = y$, and small rotation about node 3.

For any structure, infinitely many rigid-body displacement vectors can be written, but for plane motion only three are linearly independent. For motion in 3D space, six are linearly independent. In Eqs. 2.6-4 the first three nodal displacement vectors are linearly dependent, because $\{\mathbf{D}\}_1 + \{\mathbf{D}\}_2 = \{\mathbf{D}\}_3$. A linearly independent set could be composed of $\{\mathbf{D}\}_4$ and any two of the first three vectors.

For the plane truss of Fig. 2.5-2, with supports removed, the equation $[\mathbf{K}]\{\mathbf{D}\}_3 = \{\mathbf{0}\}$ with $c = 1$ in $\{\mathbf{D}\}_3$ says that terms in a row of $[\mathbf{K}]$ sum to zero. For the beam element whose $[\mathbf{k}]$ is stated in Eq. 2.3-5, row sums provided by the multiplication $[\mathbf{k}]\lfloor 1 \;\; 1 \;\; 1 \;\; 1 \rfloor^T$ are not zero, because $\{\mathbf{D}\} = \lfloor 1 \;\; 1 \;\; 1 \;\; 1 \rfloor^T$ is not rigid-body motion; it is a nodal displacement vector that both translates the element laterally and bends it into an "S" shape.

The stiffness matrix of an unsupported structure is *singular,* so structural equations have no unique solution vector $\{\mathbf{D}\}$. If asked to solve for $\{\mathbf{D}\}$ when $[\mathbf{K}]$ is singular, software may complain of an attempt to divide by zero or issue some other error message, and stop

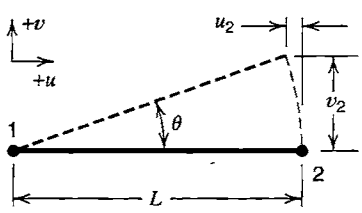

$$u_2 = -L(1 - \cos\theta) \approx -\frac{L\theta^2}{2}$$
$$v_2 = L\sin\theta \approx L\theta$$
$$\text{hence } \theta \approx \frac{v_2}{L}$$

Figure 2.6-1. Rigid-body rotation through angle θ. The stated displacement approximations are valid for small θ.

without providing a solution. Other software may automatically insert a "fix" and continue processing without explanation of the trouble.

Singularity: Inadequate Support; Mechanisms. An inadequately supported structure has a singular [**K**]. The truss of Fig. 2.5-2, for example, would be inadequately supported if the restraint shown at node 3 were removed, because the truss could then rotate as a rigid body about node 2.

The quadratic form that represents strain energy U in a linearly elastic structure is $U = \{\mathbf{D}\}^T[\mathbf{K}]\{\mathbf{D}\}/2$. In general, there exists a $\{\mathbf{D}\}$ for which $U = 0$ if the structure has no support, has only partial support, or contains a mechanism. A *mechanism,* also called an *instability,* is a displacement mode that is not rigid-body motion but for which $U = 0$.

An example of a structure that contains a mechanism is depicted in Fig. 2.6-2a, where axial load is applied to two bars connected end to end. Physically, this structure is stable when supported and loaded as shown. However, a lateral load applied at node 2 would not be resisted. Resistance would appear if lateral displacement became large, but this effect is not taken into account by linear theory, which is based on original (undeformed) geometry. It does not matter that no lateral load is actually applied at node 2: [**K**] is singular, and no unique solution for $\{\mathbf{D}\}$ can be obtained.

It is a simple matter to solve the cantilever beam problem of Fig. 2.6-2b by using beam elements. However, an analyst accustomed to two-dimensional problems may restrain only d.o.f. u, v, and θ_z at node 1. These restraints are inadequate, because the structure is still free to have the rigid-body motions of translation normal to the xy plane and rotation about the x and y axes. An analyst must remember that general-purpose software allows six displacement d.o.f. per node, so six rigid-body motions must be suppressed to achieve adequate support of a structure.

Software may help by automatically suppressing nodal d.o.f. w, θ_x, and θ_y if input data states that the problem is plane. If the problem is a plane truss, whose bars are assumed to be connected by frictionless pins at nodes, what about nodal d.o.f. θ_z? Resistance to θ_z d.o.f. is absent from element stiffness matrices (Eq. 2.4-6), so the structure stiffness matrix would be singular, because it contains zero rows and columns in positions that correspond to the θ_z d.o.f. Rather than assuming that software will automatically suppress the θ_z d.o.f. for a truss in the xy plane, a cautious analyst will determine what the software actually does. If documentation is unclear, a simple test problem should resolve the matter.

Note that suppression of d.o.f. θ_z at nodes of a plane truss neither prevents the truss from having rigid-body rotation in the xy plane nor prevents elements from rotating with respect to one another. Here one can regard a node as a frictionless pin that connects elements but can rotate freely in the joint (until θ_z is suppressed). For a plane *frame,* whose members are rigidly connected together at nodes, elements resist θ_z and share a single θ_z d.o.f. at nodes where they are connected, so suppression of θ_z at all nodes would prevent all joints from rotating, which is probably not intended.

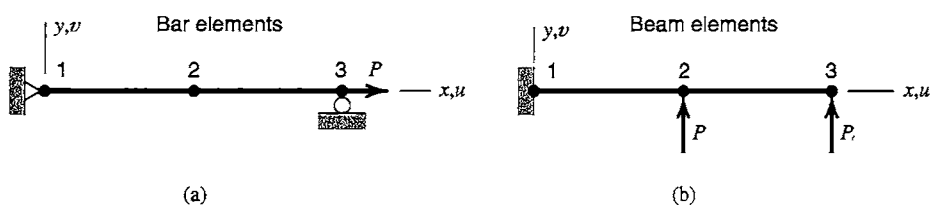

Figure 2.6-2. Two-element structures built of (a) bar elements and (b) beam elements.

2.7 BOUNDARY CONDITIONS

Formal Explanation. Let a structure be fully assembled. By partitioning, accompanied by such rearrangement of matrix coefficients as may be necessary, we can write structural equations $[\mathbf{K}]\{\mathbf{D}\} = \{\mathbf{R}\}$ for an unsupported structure as

$$\begin{bmatrix} \mathbf{K}_{11} & \mathbf{K}_{12} \\ \mathbf{K}_{21} & \mathbf{K}_{22} \end{bmatrix} \begin{Bmatrix} \mathbf{D}_x \\ \mathbf{D}_c \end{Bmatrix} = \begin{Bmatrix} \mathbf{R}_c \\ \mathbf{R}_x \end{Bmatrix} \tag{2.7-1}$$

where subscript c denotes known quantities, and subscript x denotes unknown quantities. Thus, where loads $\{\mathbf{R}_c\}$ are prescribed, the corresponding d.o.f. $\{\mathbf{D}_x\}$ are unknown, and where d.o.f. $\{\mathbf{D}_c\}$ are prescribed, the corresponding loads $\{\mathbf{R}_x\}$ are unknown. Typically $\{\mathbf{R}_x\}$ represents support reactions, and the corresponding d.o.f. $\{\mathbf{D}_c\}$ are zero, because they represent motions prevented by supports. However, prescribed nonzero d.o.f. are also acceptable. In expanded form, Eq. 2.7-1 is

$$[\mathbf{K}_{11}]\{\mathbf{D}_x\} + [\mathbf{K}_{12}]\{\mathbf{D}_c\} = \{\mathbf{R}_c\} \tag{2.7-2a}$$

$$[\mathbf{K}_{21}]\{\mathbf{D}_x\} + [\mathbf{K}_{22}]\{\mathbf{D}_c\} = \{\mathbf{R}_x\} \tag{2.7-2b}$$

Submatrix $[\mathbf{K}_{11}]$ is nonsingular if prescribed d.o.f. $\{\mathbf{D}_c\}$ are sufficient in number and arrangement to prevent rigid-body motion. Then unknown d.o.f. $\{\mathbf{D}_x\}$ can de determined from Eq. 2.7-2a:

$$\{\mathbf{D}_x\} = [\mathbf{K}_{11}]^{-1}(\{\mathbf{R}_c\} - [\mathbf{K}_{12}]\{\mathbf{D}_c\}) \tag{2.7-3}$$

Finally, loads $\{\mathbf{R}_x\}$ can be determined from Eq. 2.7-2b by substitution of d.o.f. $\{\mathbf{D}_x\}$, which are now known. Loads $\{\mathbf{R}_x\}$ are computed from elastic deformations and do not include external loads transmitted directly to supports. For example, to account for bar weights W_1, W_2, and W_3 in the truss of Fig. 2.5-2, half the weight of a bar is assigned to its two end nodes and is included in the contents of $\{\mathbf{R}_c\}$. However, the term in $\{\mathbf{R}_x\}$ that represents vertical support reaction at node 2 does not include $W_1/2$ and $W_3/2$ applied at node 2.

An Alternative Procedure. Again imagine that structure equations $[\mathbf{K}]\{\mathbf{D}\} = \{\mathbf{R}\}$ have been assembled, but no boundary conditions have yet been imposed. In software, the rearrangement operations needed to obtain the partitioned format of Eq. 2.7-1 are awkward and time-consuming. Instead we wish to impose boundary conditions without destroying the symmetry of $[\mathbf{K}]$, changing its size, or rearranging its terms. The method we now describe is applicable to any type of problem—structural, thermal, and so on.

An arbitrary 3 by 3 example system suffices to explain the method. Let the global equations be

$$\begin{bmatrix} K_{11} & K_{12} & K_{13} \\ K_{21} & K_{22} & K_{23} \\ K_{31} & K_{32} & K_{33} \end{bmatrix} \begin{Bmatrix} D_1 \\ D_2 \\ D_3 \end{Bmatrix} = \begin{Bmatrix} R_1 \\ R_2 \\ R_3 \end{Bmatrix} \tag{2.7-4}$$

in which $K_{ij} = K_{ji}$ because [**K**] is symmetric. For any d.o.f. i we can prescribe either D_i or R_i (but not both). Assume, for example, that R_1 and R_3 are known and the condition $D_2 = \Delta_2$ is to be imposed, where Δ_2 is a prescribed quantity (rather than an unknown). The corresponding load term R_2 is therefore unknown. As a first step we take known products $K_{i2}\Delta_2$ to the right-hand side. Thus

$$\begin{bmatrix} K_{11} & 0 & K_{13} \\ K_{21} & 0 & K_{23} \\ K_{31} & 0 & K_{33} \end{bmatrix} \begin{Bmatrix} D_1 \\ D_2 \\ D_3 \end{Bmatrix} = \begin{Bmatrix} R_1 - K_{12}\Delta_2 \\ R_2 - K_{22}\Delta_2 \\ R_3 - K_{32}\Delta_2 \end{Bmatrix} \tag{2.7-5}$$

Now, however, the matrix lacks symmetry, and the term $R_2 - K_{22}\Delta_2$ contains a mixture of known and unknown quantities. We remedy these troubles by replacing the second equation with the trivial equation $D_2 = \Delta_2$. Thus, Eq. 2.7-5 becomes

$$\begin{bmatrix} K_{11} & 0 & K_{13} \\ 0 & 1 & 0 \\ K_{31} & 0 & K_{33} \end{bmatrix} \begin{Bmatrix} D_1 \\ D_2 \\ D_3 \end{Bmatrix} = \begin{Bmatrix} R_1 - K_{12}\Delta_2 \\ \Delta_2 \\ R_3 - K_{32}\Delta_2 \end{Bmatrix} \tag{2.7-6}$$

(An alternative is to zero out the second row and column, but leave K_{22} in place and replace R_2 by $K_{22}\Delta_2$.) Equation 2.7-6 can be modified again in similar fashion if D_1 or D_3 is also prescribed. The procedure of Eq. 2.7-6 is particularly simple when d.o.f. Δ_i are to be suppressed; that is, when $\Delta_i = 0$.

As an example application, let boundary conditions $u_2 = v_2 = u_3 = 0$ depicted in Fig. 2.5-2 be imposed on Eq. 2.5-10. The method of Eq. 2.7-6 leads to the result

$$\begin{bmatrix} k_3 + 0.36k_2 & -0.48k_2 & 0 & 0 & 0 & 0.48k_2 \\ -0.48k_2 & 0.64k_2 & 0 & 0 & 0 & -0.64k_2 \\ 0 & 0 & 1 & 0 & 0 & 0 \\ 0 & 0 & 0 & 1 & 0 & 0 \\ 0 & 0 & 0 & 0 & 1 & 0 \\ 0.48k_2 & -0.64k_2 & 0 & 0 & 0 & k_1 + 0.64k_2 \end{bmatrix} \begin{Bmatrix} u_1 \\ v_1 \\ u_2 \\ v_2 \\ u_3 \\ v_3 \end{Bmatrix} = \begin{Bmatrix} 0 \\ -P \\ 0 \\ 0 \\ 0 \\ 0 \end{Bmatrix} \tag{2.7-7}$$

This set of equations may be solved to obtain the desired values of u_1, v_1, and v_3 (and, of course, the expected results $u_2 = v_2 = u_3 = 0$).

The method of Eq. 2.7-6 is somewhat wasteful of storage space if many d.o.f. must be set to zero. Programming procedures that omit suppressed d.o.f. from the assembly process are described in the third edition of this book and in [2.13–2.15]. For a plane frame problem, d.o.f. w_i, θ_{xi}, and θ_{yi} can be suppressed by omitting them during assembly, so that the assembled matrix [**K**] operates only on the in-plane d.o.f. u_i, v_i, and θ_{zi}. For a plane truss problem, θ_{zi} can also be suppressed, so that u_i and v_i are the only d.o.f. retained. Finally, some of the remaining d.o.f. must be prescribed in order to prevent rigid-body motion of

the structure. In Fig. 2.5-2, these remaining boundary conditions are $u_2 = v_2 = u_3 = 0$, and if these d.o.f. are suppressed by discarding them during the assembly process, the final set of equations is

$$\begin{bmatrix} k_3 + 0.36k_2 & -0.48k_2 & 0.48k_2 \\ -0.48k_2 & 0.64k_2 & -0.64k_2 \\ 0.48k_2 & -0.64k_2 & k_1 + 0.64k_2 \end{bmatrix} \begin{Bmatrix} u_1 \\ v_1 \\ v_3 \end{Bmatrix} = \begin{Bmatrix} 0 \\ -P \\ 0 \end{Bmatrix} \tag{2.7-8}$$

Unknown d.o.f. u_1, v_1, and v_3 can now be calculated. Equations 2.7-7 and 2.7-8, of course, provide the same results. Support reactions p_2, q_2, and p_3 can be obtained from Eq. 2.5-10 by premultiplying solution vector $\{\mathbf{D}\}$ by rows 3, 4, and 5 of $[\mathbf{K}]$. Information in these rows is discarded when boundary conditions are imposed as shown in Eq. 2.7-7 and Eq. 2.7-8. However, software should have provision for saving or reconstructing information in affected rows of $[\mathbf{K}]$ so that support reactions can be calculated (but see remarks that follow Eq. 2.7-3).

Boundary conditions can also be treated by Lagrange multipliers and by the penalty method. They are discussed in Sections 13.2 and 13.3.

2.8 EXPLOITING SPARSITY. SOLVING EQUATIONS

Structure nodes can be numbered in arbitrary sequence. A different sequence produces a different topology of the structure matrix; that is, coefficients are assigned to different locations in the array. We seek a topology that favors compact storage and rapid solution of the structural equations [2.15]. We can choose any of several solution algorithms, influenced by matrix topology, the number of equations, and whether they are ill-conditioned or not. A software user may be obliged to choose among available options or take an active role if difficulties develop. Discussion in the present section is supplemented in Appendix B.

Numbering and Sparsity. Consider the structure in Fig. 2.8-1, which consists of two-node elements that may represent beam elements, electrical resistors, pipes in a distribution system, and so on. The physical problem does not matter for our discussion. However, for explanation we imagine that there is a single d.o.f. per node. For the node numberings of Figs. 2.8-1a and 2.8-1b respectively, we obtain the structure matrices

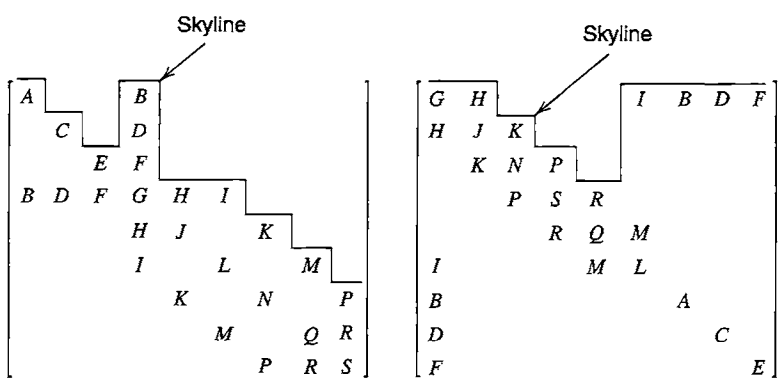

(2.8-1)

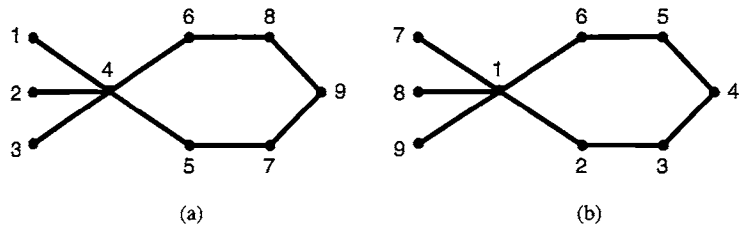

Figure 2.8-1. Different node numberings for an assembly of two-node elements.

in which nonzero coefficients are represented by capital letters and zero coefficients are represented by blanks. The *skyline* encloses the uppermost nonzero coefficients in each column. Although the same coefficients appear in each matrix, topologies differ.

Because of symmetry, only the upper triangle of the matrix need be stored to retain all information in the matrix. Also, in solving equations we need process only entries below the skyline, down to and including the diagonal. Therefore, we can store all needed coefficients in a one-dimensional array, taking columns in order, and including information from the skyline down to the diagonal. Zeros between the skyline and the diagonal are retained because a direct (noniterative) equation solver creates *fills;* that is, it converts most zeros under the skyline to nonzero coefficients. Unlike zeros, which can be skipped during numerical processing, fills must be processed, and storage space must be reserved for them. For the numbering of Fig. 2.8-1a, we store the one-dimensional array

$$\lfloor A \;\; C \;\; E \;\; B \;\; D \;\; F \;\; G \;\; H \;\; J \;\; I \;\; 0 \;\; L \;\; K \;\; 0 \;\; N \;\; M \;\; 0 \;\; Q \;\; P \;\; R \;\; S \rfloor \tag{2.8-2}$$

The number of terms stored in this format is sometimes called the *profile* of the matrix. In equation solving, this storage format is associated with the name *active column storage.* Software must be told which terms in the one-dimensional array are diagonal terms of the n by n structure matrix. This information is supplied by an auxiliary array of n numbers that lists the height of each column. For Fig. 2.8-1a, this array is $\lfloor 1 \;\; 1 \;\; 1 \;\; 4 \;\; 2 \;\; 3 \;\; 3 \;\; 3 \;\; 3 \rfloor$. The sum of these numbers, 21, is the matrix profile. The second matrix in Eq. 2.8-1 has a profile of 39, which reflects the poor numbering arrangement of Fig. 2.8-1b.

General-purpose software usually includes a renumbering option that examines the node numbering provided by input data, renumbers nodes for efficient storage and equation solving, and then converts back to the input numbering for presentation of results. References include [2.16].

Solution of Equations. Formally, the solution of structure equations $[\mathbf{K}]\{\mathbf{D}\} = \{\mathbf{R}\}$ is written as $\{\mathbf{D}\} = [\mathbf{K}]^{-1}\{\mathbf{R}\}$. The latter equation should be regarded as saying "solve for $\{\mathbf{D}\}$" rather than requiring that $[\mathbf{K}]$ be inverted. The inverse is not needed in order to solve for $\{\mathbf{D}\}$. Also, $[\mathbf{K}]^{-1}$ is full even when $[\mathbf{K}]$ is sparse, so inversion is time-consuming and too demanding of storage space.

In structural mechanics, $\{\mathbf{D}\}$ represents nodal displacements, so we require that the structure be *kinematically* determinate; that is, the structure can have no rigid-body modes or mechanisms. Because unknowns are displacements rather than forces, static indeterminacy does not make a problem more complicated. Indeed, if a high degree of static indeterminacy arises because of many supports, the problem becomes simpler because there are fewer nontrivial equations.

Equation solvers can be classified as either *direct* or *iterative.* In a direct solution such as Gauss elimination, the number of operations required depends on matrix topology and

the number of equations and can be calculated in advance. In an iterative solution, the number of operations required is uncertain. Iterative cycling continues until a convergence test is satisfied.

A direct solver is efficient when the matrix profile is small, as it is for the cantilever beam in Fig. 2.8-2a. Then nonzero entries in the structure matrix are tightly clustered along its diagonal, so elimination produces few fills (none, in this particular example). In contrast, the structure of Fig. 2.8-2b creates a matrix that is sparse but has large profile, so storage demands and processing effort become large if the number of nodes is large. A matrix of large profile also has a large *semibandwidth,* which we denote by b. For each row i, semibandwidth b_i is equal to the number of columns from the diagonal to the rightmost nonzero term. In the first matrix of Eqs. 2.8-1, b_i for the respective rows is 4, 3, 2, 3, 3, 3, 3, 2, 1. A root-mean-square average of the b_i may be taken as a representative b for the entire matrix: $b = 2.79$ in this example. If matrix order n is large and b is much smaller than n, the computational effort required for a direct solution is approximately proportional to nb^2.

When using a direct solver, we need not assemble the entire structure matrix before starting to solve equations. Steps of assembly can alternate with steps of solution. When enough elements have been assembled to complete the initial portion of the structure matrix, solution begins, then temporarily ceases when more of the matrix must be built by assembly. Names associated with this approach are *frontal method* or *wavefront method,* because d.o.f. currently active can be visualized as a "wave" or "front" that passes over the structure as the assembly-solution alternation progresses. The order in which equations are processed depends on element numbering, not node numbering. Efficiency is increased by element numbering that decreases front size. A frontal solution requires less storage than building the entire structure matrix before starting the solution, but it is more complicated to program.

Iterative solvers converge more slowly as the *condition number* of the structure matrix increases [2.13,2.15,2.17]. For the present discussion, the condition number can be thought of as the square of the ratio of the highest to the lowest vibration frequencies (see also Section 9.3). The beam of Fig. 2.8-2a produces a large condition number: in the mode of highest frequency, every element assumes an "S" shape; in the mode of lowest frequency, the entire beam flaps in a "diving board" mode. On the other hand, the structure of Fig. 2.8-2b has a comparatively low condition number. Condition number is influenced by the types of elements used; it is increased by larger aspect ratio (that is, elongation) of the structure and by larger aspect ratio of individual elements. Practical iterative solvers employ "preconditioners" that provide more rapid convergence.

Iterative solvers have the advantage that they are not obliged to convert zeros under the skyline to nonzero terms. Thus, there is no need to reserve storage space for fills or to pro-

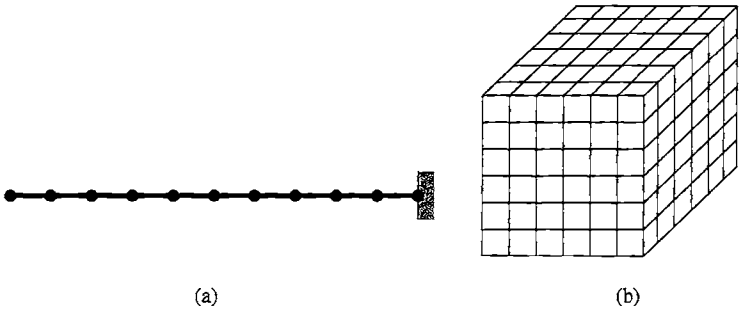

Figure 2.8-2. (a) A cantilever built of many beam elements. (b) A cube built of many cubical elements.

cess them. Indeed, [**K**] need not even be assembled. Information needed for iteration consists of nodal forces associated with deformations. These forces can be computed element by element as needed, often by procedures that require less computation than generating [**k**] and the product [**k**]{**d**} for each element. Iterative solvers are particularly well suited to vector and parallel computation, which achieve greatest efficiency when special data storage schemes are used. An iterative solver can be considerably faster than a direct solver if there are a great many d.o.f., equations are well conditioned, and [**K**] would have a large profile even if nodes were optimally numbered.

If solutions for many different load vectors {**R**} on the same structure are needed, a direct solver has the advantage that after [**K**] has been processed by the solver, each additional load vector is processed with very little additional effort. An iterative solver may require a complete new solution for each additional load vector, although some progress toward removing this drawback has been made [2.18].

Gauss Elimination. A direct equation solver uses Gauss elimination, Cholesky decomposition, or another of many methods that are closely related. In Gauss elimination, equations [**K**]{**D**} = {**R**} are solved for {**D**} by reducing [**K**] to upper triangular form, then solving for unknowns in reverse order by back substitution. With reference to the example of Fig. 2.8-3, steps of the process are as follows.

The first row of [**K**] in Fig. 2.8-3a is multiplied by the factor $K_{21}/K_{11} = -6/18$ and subtracted from row 2, and multiplied by the factor $K_{31}/K_{11} = -6/18$ and subtracted from row 3. Similarly we subtract $(K_{21}/K_{11})R_1$ from R_2 and $(K_{31}/K_{11})R_1$ from R_3. Thus the first unknown D_1 is eliminated from subsequent equations, as if we had done the formal algebra of solving the first equation for D_1 and substituting it into subsequent equations, resulting in Fig. 2.8-3b. Row 4 is not changed by elimination of D_1; software would exploit this circumstance by skipping calculations because $K_{41} = 0$. Next, D_2 is eliminated by similar treatment

Original equations:

$$\begin{bmatrix} 18 & -6 & -6 & 0 \\ -6 & 12 & 0 & -6 \\ -6 & 0 & 12 & -6 \\ 0 & -6 & -6 & 12 \end{bmatrix} \begin{Bmatrix} D_1 \\ D_2 \\ D_3 \\ D_4 \end{Bmatrix} = \begin{Bmatrix} 60 \\ 0 \\ 20 \\ 0 \end{Bmatrix}$$

(a)

After one elimination:

$$\begin{bmatrix} 18 & -6 & -6 & 0 \\ 0 & 10 & -2 & -6 \\ 0 & -2 & 10 & -6 \\ 0 & -6 & -6 & 12 \end{bmatrix} \begin{Bmatrix} D_1 \\ D_2 \\ D_3 \\ D_4 \end{Bmatrix} = \begin{Bmatrix} 60 \\ 20 \\ 40 \\ 0 \end{Bmatrix}$$

(b)

After two eliminations:

$$\begin{bmatrix} 18 & -6 & -6 & 0 \\ 0 & 10 & -2 & -6 \\ 0 & 0 & 9.6 & -7.2 \\ 0 & 0 & -7.2 & 8.4 \end{bmatrix} \begin{Bmatrix} D_1 \\ D_2 \\ D_3 \\ D_4 \end{Bmatrix} = \begin{Bmatrix} 60 \\ 20 \\ 44 \\ 12 \end{Bmatrix}$$

(c)

After three eliminations:

$$\begin{bmatrix} 18 & -6 & -6 & 0 \\ 0 & 10 & -2 & -6 \\ 0 & 0 & 9.6 & -7.2 \\ 0 & 0 & 0 & 3 \end{bmatrix} \begin{Bmatrix} D_1 \\ D_2 \\ D_3 \\ D_4 \end{Bmatrix} = \begin{Bmatrix} 60 \\ 20 \\ 44 \\ 45 \end{Bmatrix}$$

(d)

Solve for unknowns by back substitution:

$D_4 = 45/3 = 15$

$D_3 = (44 + 7.2D_4)/9.6 = (44 + 108)/9.6 = 15.83$

$D_2 = (20 + 2D_3 + 6D_4)/10 = (20 + 31.67 + 90)/10 = 14.17$

$D_1 = (60 + 6D_2 + 6D_3)/18 = (60 + 85 + 95)/18 = 13.33$

(e)

Figure 2.8-3. Example of solving simultaneous linear algebraic equations by Gauss elimination.

of equations 3 and 4 in Fig. 2.8-3b, for which the multiplying factors are $K_{32}/K_{22} = -2/10$ and $K_{42}/K_{22} = -6/10$, resulting in Fig. 2.8-3c. Finally, D_3 is eliminated from equation 4 in Fig. 2.8-3c using the multiplying factor $K_{43}/K_{33} = -7.2/9.6$, resulting in Fig. 2.8-3d. [**K**] is now triangularized, and unknowns are determined in reverse order by back substitution as shown in Fig. 2.8-3e.

Coefficient K_{23} is a "fill" because it becomes nonzero, but the zero above the skyline, K_{14}, remains zero. Skyline topology is not changed by forward reduction, and the portion of the matrix below the eliminated equations remains symmetric. Therefore, a multiplying factor such as K_{21}/K_{11} could as well be written K_{12}/K_{11}. In other words, information stored and processed can reside entirely in the upper triangle of [**K**], from the skyline down to and including the diagonal. Note also that information needed to process terms on the right-hand side is retained in the triangularized matrix, which means that additional right-hand sides can be processed very quickly.

The foregoing illustration uses "pivots on the diagonal," which means that the ith equation is used to eliminate the ith unknown. This procedure is convenient in programming, but it requires that stiffness coefficient K_{ii} be nonzero when used to eliminate the ith unknown. Such will be the case if the structure is adequately supported and contains no mechanism and if displacements are used as nodal d.o.f. With some alternative FE formulations and some methods of imposing constraints, some diagonal coefficients are zero when equation solving begins (Sections 5.6 and 13.2).

2.9 MECHANICAL LOADS. STRESSES

Loads applied directly to structure nodes are added directly to the structure load vector (loads $\{\mathbf{P}\}$ in Eq. 2.5-4). In the present section we consider *element* loads $\{\mathbf{r}_e\}$ produced by externally applied forces and/or moments that act within elements, at locations other than structure nodes. We also consider how stresses in bar and beam elements may be calculated. Similar discussion of loads and stresses caused by temperature change appears in the following section.

Introductory Remarks. In Fig. 2.5-2, imagine that load P is omitted and that the structure is instead loaded by the weight of its own members. Let respective members have weights W_1, W_2, and W_3. Then it is physically reasonable to say that nodal loads consist of downward forces $(W_2 + W_3)/2$ at node 1, $(W_1 + W_3)/2$ at node 2, and $(W_1 + W_2)/2$ at node 3. Thus we have "lumped" gravity loads at node points. Even if members are pin-connected at nodes, the structure is not strictly a truss, because members do not carry purely axial load; all nonvertical members also carry gravity loads that cause them to bend and develop flexural stress. If members are rigidly connected together at nodes, then the structure is a frame, and the foregoing lumped or "reduced" loading ignores moments that members also apply to structure nodes. These moments are part of the "consistent" loading discussed in what follows. Reduced loading is likely to be a good approximation for a structure that contains many members; in that case, flexural stress is apt to be negligible in truss members, and nodal moment loads contributed by weights of frame members are apt to be negligible. If desired, flexural stress in a truss member can be computed by regarding it as a simply supported beam loaded by its own weight. Flexural stress is superposed on axial stress due to nodal displacements.

"Lost" Loads. With $P = 0$ and reduced loading as described in the foregoing paragraph, the load vector on the right-hand side of Eq. 2.7-8 becomes

$$\begin{bmatrix} 0 & -\frac{1}{2}(W_2 + W_3) & -\frac{1}{2}(W_1 + W_2) \end{bmatrix}^T$$

Thus, the downward load $(W_1 + W_3)/2$ at node 2 is "lost" from the equation system and does not affect computed displacements and member forces. This load is "lost" because the support reacts against it directly. To determine the vertical reaction at node 2 after nodal d.o.f. have been calculated, we can add $(W_1 + W_3)/2$ to the value of q_2 determined from Eq. 2.5-10. Temperature change also contributes to support reactions if supports act to inhibit displacements associated with temperature change.

Consistent Nodal Loads. For uniform bar and beam elements, element loads can be treated by methods of elementary mechanics of materials, to obtain a "consistent" set of loads that act on structure nodes. This set of loads is the same as the set produced by formal procedures of FEA described in Section 3.3, where the terminology "consistent" is explained. For some structures, including those built of uniform bar or uniform beam elements, consistent nodal loading leads to computed nodal displacements that agree exactly with displacements at these locations in the mathematical model [2.5]. This behavior continues to prevail in uniform beams even when transverse shear deformation terms are included in element $[\mathbf{k}]$'s and in the vector of consistent nodal loads [2.5]. In what follows, we omit transverse shear deformation in beams.

Loads on Bar Elements. Let a uniformly distributed axial load q act on a uniform bar fixed at both ends (Fig. 2.9-1a). This is a simple, statically indeterminate problem in mechanics of materials, whose solution shows that reactions on the bar are $qL/2$ at each end. Regarding the bar as a single element whose end nodes are fixed, we obtain nodal loads $qL/2$ at each end. Similarly, if a concentrated axial load P acts at, for example, $x = L/3$ on the element (Fig. 2.9-1b), nodal loads are $2P/3$ on the left node and $P/3$ on the right node, both acting in the same direction as P. Loads $qL/2$, $2P/3$, and $P/3$ in Fig. 2.9-1a and 2.9-1b are "consistent" element loads $\{\mathbf{r}_e\}$ applied to nodes by the element. They are directed opposite to end reactions on the statically indeterminate bar.

Stresses in Bar Elements. In a bar element, axial stress due to nodal displacements is calculated by determining elongation e, axial strain $\varepsilon = e/L$, and axial stress $\sigma = E\varepsilon$. Specifically, for a bar element of arbitrary orientation in xyz coordinates,

$$\sigma = \frac{E}{L}\left[(u_2 - u_1)l + (v_2 - v_1)m + (w_2 - w_1)n\right] \tag{2.9-1}$$

where l, m, and n are direction cosines of the bar axis, as used in Section 2.4. Numerical values of all nodal d.o.f. in the structure appear in $\{\mathbf{D}\}$ after global equations have been solved. Values of d.o.f. associated with the element at hand are extracted from $\{\mathbf{D}\}$.

When mechanical loads produce nonzero element loads $\{\mathbf{r}_e\}$, we may (optionally) add the "fixed-ended" element stresses now described. Let the bar in Fig. 2.9-1a be regarded as a one-element structure. Then, according to Eq. 2.9-1, axial stress is zero because both nodes are fixed. However, if we add the stress σ_x shown, which is the analytically obtained

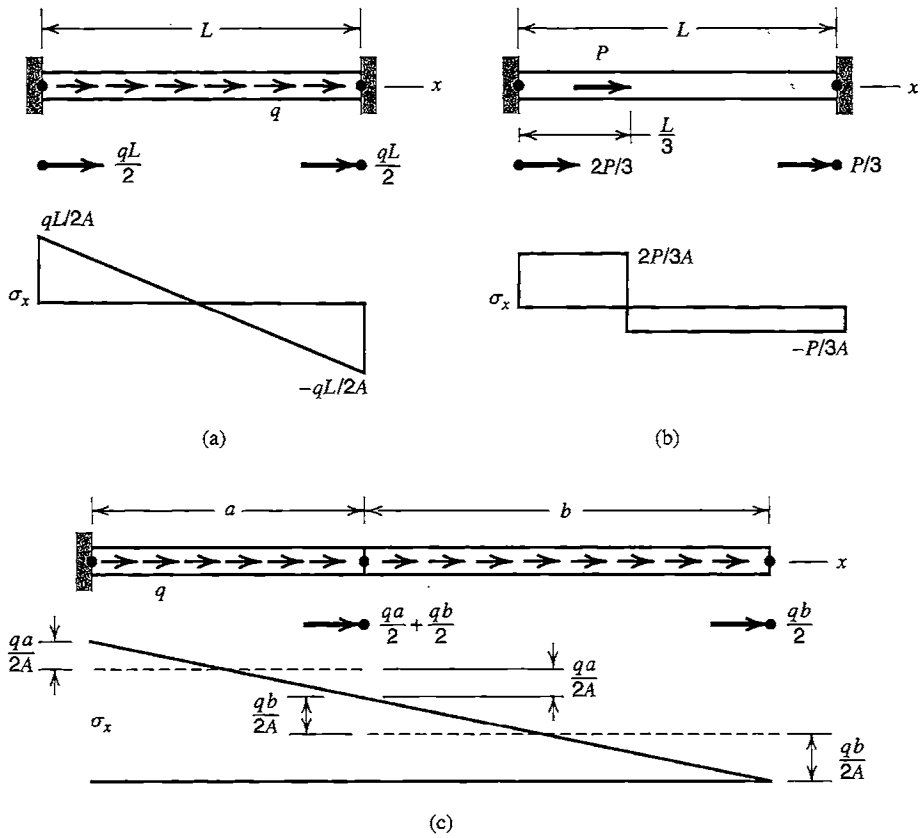

Figure 2.9-1. Nodal loads and stress fields that result from axial loads applied to bar elements between nodes.

stress distribution in the bar with both ends fixed, we obtain the correct result. Stated more generally, stresses are more accurately calculated by superposing stresses calculated by FEA (stresses due to nodal displacements) and separately calculated stresses associated with mechanical loading of the element while all of its d.o.f. are fixed. For thermal loading, element stresses *must* be included; see Section 2.10.

When elements are assembled, loads contributed by adjacent elements combine at shared nodes, as shown in Fig. 2.9-1c for a uniformly distributed load. No load is shown at the leftmost node, because that node is fixed. If a load were applied there, it would become a "lost" load, discarded in the process of imposing boundary conditions. Stress σ_x shown by dashed lines is produced by nodal displacements. Superposition of fixed d.o.f. element stresses yields the solid line, which is exact.

Remark. The foregoing superposition procedure of stress calculation can also be applied to beam elements. For elements other than bars and beams it is not easy to separately calculate element stresses due to mechanical load when all element d.o.f. are fixed. Accordingly, this element stress field is likely to be included only for beam elements. Its contribution to total stress tends toward zero as element size is reduced. Inclusion of these element stresses usually enhances accuracy in a coarse mesh, but omission does not prevent convergence toward correct stresses as the mesh is refined.

Loads on Beam Elements. A uniformly distributed load on a uniform beam with both ends fixed produces support reactions that can be calculated by elementary beam theory. If reversed in direction, these reactions comprise the nodal loads shown in Fig. 2.9-2a, which are

$$\{\mathbf{r}_e\} = \begin{Bmatrix} -qL/2 \\ -qL^2/12 \\ -qL/2 \\ qL^2/12 \end{Bmatrix} \tag{2.9-2}$$

in which negative signs indicate loads directed opposite to the positive senses of their respective d.o.f. When elements are assembled, moment loads at interior nodes tend to cancel (Fig. 2.9-2b).

Load vectors $\{\mathbf{r}_e\}$ can easily be written for other loadings on a fixed-fixed beam, such as a concentrated force or moment at arbitrary x, or a linearly varying distributed load. General-purpose software typically is capable of computing load vectors for such loadings on beams. It may also be capable of using the corresponding fixed-end element moment fields in stress calculation, in the manner previously described for element stress fields of bar elements. Thus, for uniformly distributed loading, the element moment field M shown in Fig. 2.9-2a would be added to the bending moment produced by nodal displacements.

Stresses in Beam Elements. We consider stress calculation in the local coordinate system of Fig. 2.3-2. Thus, the first step is calculation of local d.o.f. by the transformation $[\mathbf{T}]\{\mathbf{d}\}$, where $[\mathbf{T}]$ is given by Eq. 2.4-9. Numerical values of d.o.f. $\{\mathbf{d}\}$, for the element at hand and referred to the global coordinate system, can be extracted from $\{\mathbf{D}\}$ after global equations have been solved.

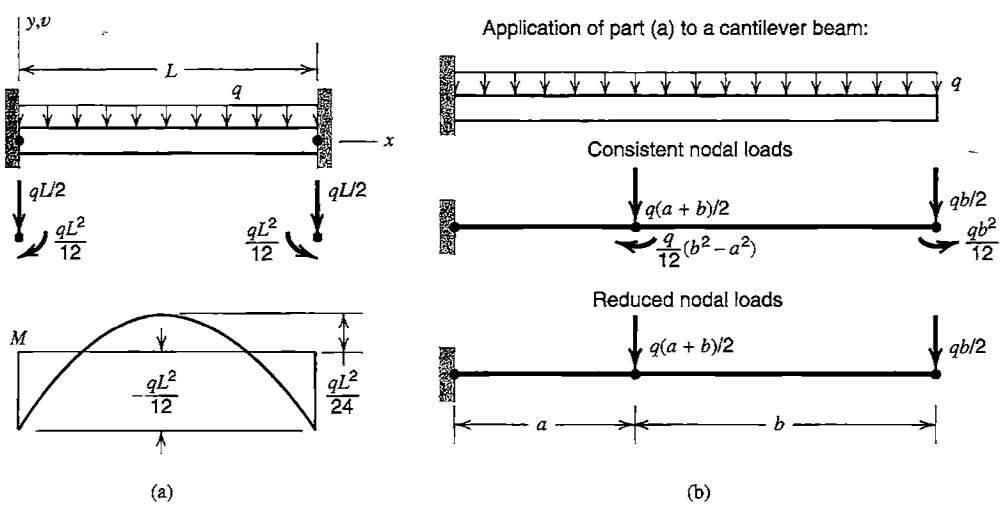

Figure 2.9-2. Nodal loads and bending moment field that result from lateral loads applied to beam elements between nodes.

Nodal displacements produce a cubic lateral displacement field $v = v(x)$ in a 2D element, as shown in Fig. 2.3-1. The bending moment due to nodal displacements is calculated from the curvature of this field. As shown in elementary beam theory, the bending moment field $M_z = M_z(x)$ and transverse shear force field V_y are

$$M_z = EI_z \frac{d^2 v}{dx^2} \quad \text{and} \quad V_y = \frac{dM_z}{dx} = EI_z \frac{d^3 v}{dx^3} \tag{2.9-3}$$

Figure 2.3-1 provides lateral displacement $v = v(x)$ for unit values of the respective nodal d.o.f. By differentiation we obtain curvature d^2v/dx^2 and hence bending moment $M_z = M_z(x)$ in terms of nodal d.o.f.

$$M_z = EI_z\left[\left(-\frac{6}{L^2}+\frac{12x}{L^3}\right)v_1 + \left(-\frac{4}{L}+\frac{6x}{L^2}\right)\theta_{z1} + \left(\frac{6}{L^2}-\frac{12x}{L^3}\right)v_2 + \left(-\frac{2}{L}+\frac{6x}{L^2}\right)\theta_{z2}\right] \tag{2.9-4}$$

Then dM_z/dx is the expression for V_y in terms of nodal d.o.f.

The 3D beam element described by Eq. 2.3-8 and Fig. 2.3-2 can also display axial force N, torque T about its axis, bending moment M_y about the y axis, and transverse shear force V_z, where

$$N = AE\frac{u_2 - u_1}{L} \qquad T = GK\frac{\theta_{x2} - \theta_{x1}}{L} \qquad M_y = EI_y \frac{d^2 w}{dx^2} \qquad V_z = EI_y \frac{d^3 w}{dx^3} \tag{2.9-5}$$

Lateral displacement $w = w(x)$ is a cubic field governed by nodal d.o.f. w_1, θ_{y1}, w_2, and θ_{y2}. Bending moment $M_y = M_y(x)$ is provided by an equation like Eq. 2.9-4, with signs of nodal rotations reversed. Normal and shear stresses associated with the forces and moments of Eqs. 2.9-3 and 2.9-5 are

$$\begin{aligned} \sigma_x &= \frac{N}{A} - \frac{M_z y}{I_z} - \frac{M_y z}{I_y} & \tau_T &= \frac{T c_T}{K} \\ \tau_y &= c_y \frac{V_y}{A} & \tau_z &= c_z \frac{V_z}{A} \end{aligned} \tag{2.9-6}$$

The locations of these maximum values of the three shear stresses depend on the shape of the cross section. If the cross section is a solid circle of radius R, then $A = \pi R^2$, $I_y = I_z = \pi R^4/4$, $K = \pi R^4/2$, $c_T = R$, and $c_y = c_z = 4/3$. Maximum magnitudes of flexural stress appear at $y = \pm R$ due to M_z and at $z = \pm R$ due to M_y. The maximum magnitude of τ_T appears on the outer surface. Maximum magnitudes of τ_y and τ_z appear on the neutral surface of bending. If the cross section is a solid square with sides of length a parallel to the y and z axes, then $A = a^2$, $I_y = I_z = a^4/12$, $K = 0.1406a^4$, $c_T = 0.675a$, and $c_y = c_z = 1.500$. The maximum magnitude of τ_T appears on the outer surface at the four locations closest to the centroid of the square cross section. Data such as this, appropriate to each element cross section present in the FE model, must be provided to software if it is to calculate stresses in beam elements correctly. Software may report σ_x at four points on a cross section. Often these points are flange tips of an I section. Some software may (misleadingly) use polar moment J of the cross section rather than K in Eq. 2.9-6, and adjust c_T accordingly.

Consistent vs. Reduced Loads. A nodal load vector that omits moment terms may be called "reduced" or "lumped." Thus, the reduced load form of $\{\mathbf{r}_e\}$ in Eq. 2.9-2 is $\lfloor -qL/2 \;\; 0 \;\; -qL/2 \;\; 0 \rfloor^T$, which leads to the reduced nodal loading shown in Fig. 2.9-2b. For this two-element structure, after displacement boundary conditions have been imposed, equations $[\mathbf{K}]\{\mathbf{D}\} = \{\mathbf{R}\}$ for reduced nodal loading are

$$EI_z \begin{bmatrix} 12/a^3 + 12/b^3 & -6/a^2 + 6/b^2 & -12/b^3 & 6/b^2 \\ -6/a^2 + 6/b^2 & 4/a + 4/b & -6/b^2 & 2/b \\ -12/b^3 & -6/b^2 & 12/b^3 & -6/b^2 \\ 6/b^2 & 2/b & -6/b^2 & 4/b \end{bmatrix} \begin{Bmatrix} v_2 \\ \theta_{z2} \\ v_3 \\ \theta_{z3} \end{Bmatrix} = \begin{Bmatrix} -q(a+b)/2 \\ 0 \\ -qb/2 \\ 0 \end{Bmatrix} \tag{2.9-7}$$

As L shrinks in Eq. 2.9-2, moment terms tend toward zero more rapidly than force terms. Omission of moment terms does not prevent convergence toward correct results as a mesh is refined. Indeed, accuracy in a given mesh is sometimes greater if moment terms are omitted. In Fig. 2.9-3, a circular arch is modeled by a coarse mesh of straight elements. Because elements are of unequal length in the mesh shown, nodal moments remain at the two uppermost nodes after elements are assembled. These moments are slightly detrimental. Moments at the two lowermost nodes are clearly detrimental, because the actual structure can have no bending moment at a pinned support. And, in bending moment calculation, the element bending moment fields of Fig. 2.9-3c should not be included. There is no bending moment in the actual arch, and there will not be any in the FE model if reduced loading is used and element moment fields are omitted from moment calculation.

In general, for any type of element, we define reduced loading as nodal loads computed as if the element had no rotational d.o.f. Thus, for example, transverse load P at $x = L/3$ on a beam element produces reduced nodal loads $2P/3$ at node 1 and $P/3$ at node 2, as if ends of the beam were simply supported rather than fixed. This result is not the same as would be obtained by omitting nodal moments after they are calculated, because nodal forces are changed by restraint of end rotation when the load is off-center.

Elements for beams, plates, and shells all have rotational d.o.f., which are ignored in the calculation of reduced nodal loads. Whether reduced loading leads to better or worse results than consistent loading depends on the nature of the problem, what results are sought, and

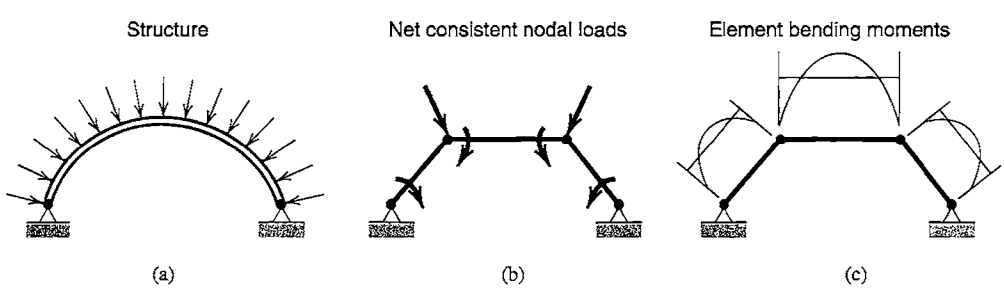

Figure 2.9-3. (a) Uniformly distributed load on a circular two-hinged arch. (b) Loading on a coarse-mesh FE model. Element lengths are unequal. (c) Element bending moment fields, calculated as in Fig. 2.9-2a.

what calculation options are chosen. For example, in the problem of Fig. 2.9-2b, suppose we omit the moment field of Fig. 2.9-2a from final moment calculation. Then consistent loading leads to exact nodal displacements but approximate bending moments at nodes, whereas reduced loading leads to approximate nodal displacements but exact bending moments at nodes. Either loading system produces convergence toward correct results as the mesh is refined.

2.10 THERMAL LOADS. STRESSES

Thermal Stress Problems. Stresses in an elastic FE model produced by a temperature field are calculated as follows. The procedure is not restricted to bar and beam elements. It is used for all finite elements that are based on displacement fields and use nodal displacements as d.o.f. The following steps are carried out automatically by software.

1. In each element, compute "initial" stresses, which are stresses produced by the temperature field when all displacements are prohibited. Also compute loads applied to nodes by initial stresses. (See Sections 3.1 and 3.3 for a general treatment of initial stresses $\{\sigma_0\}$.)
2. Assemble the elements and loads calculated in Step 1. The result is a structure whose nodes as yet have no displacements but are loaded by initial stresses produced by temperature changes.
3. Solve for nodal d.o.f. produced by loads of Step 2, and compute element strains and stresses they produce. Superpose on these stresses the initial stresses calculated in Step 1.

If mechanical loads are also applied, they may be superposed on thermal loads in Step 2. An example will follow.

Remarks. A temperature field can be defined relative to an arbitrary reference temperature. Absolute temperatures are not needed for thermal stress analysis (but *are* needed to calculate temperatures when heat is transferred by radiation). If the reference temperature chosen is 0 °C, then temperatures are simply stated in degrees Celsius. The computation procedure provides *changes* in stress associated with the temperature field. Residual stresses that may exist at the reference temperature play no role in computation and must be superposed on computed thermal stresses.

A temperature gradient does not necessarily produce stress. Consider a body that is homogeneous, isotropic, and linearly elastic, whose supports do nothing to inhibit deformations caused by temperature change. Then, if the temperature field is linear in rectangular Cartesian coordinates and the coefficient of thermal expansion is independent of temperature, there are no thermal stresses. For example, if a uniform and simply supported straight beam is caused to have a linear temperature variation from upper surface to lower surface, the beam deforms to a circular arc but remains free of stress.

Due to temperature change T, initial stress in a bar element is $\sigma_0 = -E\varepsilon_0$, where initial strain ε_0 is αT. However, if coefficient of thermal expansion α is temperature-dependent, ε_0 must be computed as the integral of $\alpha\, dT$ from the initial temperature to the final temperature.

And, if T is not constant along the length of the bar, it is best to use average temperature in the final stress calculation of step 3 [2.19].

Example. A uniform bar of length $2L$ fixed at both ends is modeled by two elements, as shown in Fig. 2.10-1. Lateral deflection d.o.f. are set to zero; thus we avoid the possibility of a hinge at node 2. Initially the bar is isothermal at temperature $T = 0$. Then the bar is loaded by axial force P and by linear temperature variation from T_2 to T_3 in the right element only. Initial stress exists only in the right element. From node 2 to node 3, based on the average temperature $(T_2 + T_3)/2$, initial stress σ_0 is

$$\sigma_0 = -E\alpha\frac{T_2 + T_3}{2} \qquad \text{(right element only)} \tag{2.10-1}$$

where α is the coefficient of thermal expansion. The heated element applies forces of magnitude F to nodes 2 and 3, where

$$F = |A\sigma_0| = AE\alpha\frac{T_2 + T_3}{2} \tag{2.10-2}$$

Before fixed-end conditions are imposed, and with support reactions H_1 and H_3 included, equations $[\mathbf{K}]\{\mathbf{D}\} = \{\mathbf{R}\}$ are

$$\frac{AE}{L}\begin{bmatrix} 1 & -1 & 0 \\ -1 & 2 & -1 \\ 0 & -1 & 1 \end{bmatrix}\begin{Bmatrix} u_1 \\ u_2 \\ u_3 \end{Bmatrix} = \begin{Bmatrix} H_1 \\ P - AE\alpha(T_2 + T_3)/2 \\ H_3 + AE\alpha(T_2 + T_3)/2 \end{Bmatrix} \tag{2.10-3}$$

Boundary conditions $u_1 = 0$ and $u_3 = 0$ can be imposed according to the scheme of Eq. 2.7-6. Thus Eq. 2.10-3 becomes

$$\frac{AE}{L}\begin{bmatrix} 1 & 0 & 0 \\ 0 & 2 & 0 \\ 0 & 0 & 1 \end{bmatrix}\begin{Bmatrix} u_1 \\ u_2 \\ u_3 \end{Bmatrix} = \begin{Bmatrix} 0 \\ P - AE\alpha(T_2 + T_3)/2 \\ 0 \end{Bmatrix} \tag{2.10-4}$$

from which

$$u_1 = 0 \qquad u_2 = \frac{PL}{2AE} - \frac{\alpha L(T_2 + T_3)}{4} \qquad u_3 = 0 \tag{2.10-5}$$

Reactions H_1 and H_3, if desired, can now be obtained by returning to the first and third of Eqs. 2.10-3 with the known values of u_1, u_2, and u_3. These results are

$$H_1 = -\frac{P}{2} + \frac{AE\alpha(T_2 + T_3)}{4} \qquad \text{and} \qquad H_3 = -\frac{P}{2} - \frac{AE\alpha(T_2 + T_3)}{4} \tag{2.10-6}$$

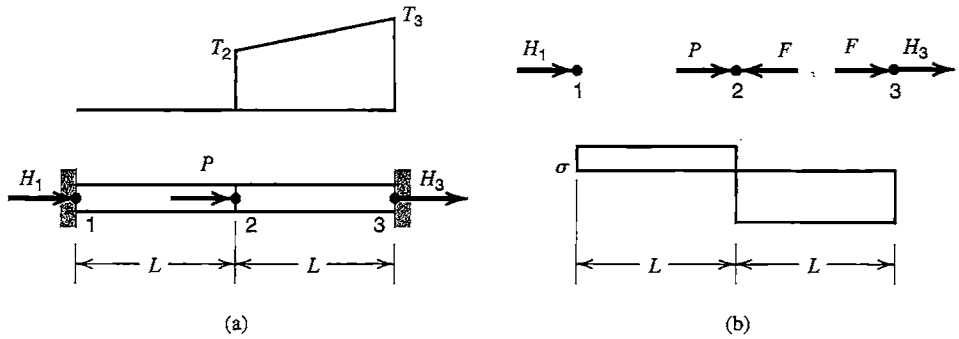

Figure 2.10-1. (a) Bar fixed at both ends, loaded by force P and a temperature field. (b) Nodal loads and final axial stress distribution.

Final stresses in the two elements are

$$\begin{aligned} \sigma_{1-2} &= E\frac{u_2-u_1}{L} + (\text{zero}) = \frac{P}{2A} - \frac{E\alpha(T_2+T_3)}{4} \\ \sigma_{2-3} &= E\frac{u_3-u_2}{L} + \sigma_0 = -\frac{P}{2A} - \frac{E\alpha(T_2+T_3)}{4} \end{aligned} \tag{2.10-7}$$

For uniform temperature $(T_2 + T_3)/2$ in the right element, the correctness of these results can easily be verified by methods of elementary mechanics of materials.

What if the linearly varying temperature shown in Fig. 2.10-1 is used, rather than the average temperature $(T_2 + T_3)/2$? Then, with displacements suppressed throughout the structure, the right element has initial stresses $\sigma_0 = -E\alpha T_2$ at node 2 and $\sigma_0 = -E\alpha T_3$ at node 3 instead of the σ_0 given by Eq. 2.10-1. Force F remains as stated by Eq. 2.10-2 because it depends on the integral of initial stresses over element length (see Eq. 3.3-8). Therefore Eqs. 2.10-2 through 2.10-6 are unchanged, σ_{1-2} remains as stated in Eqs. 2.10-7, but σ_{2-3} becomes

$$\begin{aligned} &\text{At node 2:} \quad \sigma_{2-3} = E\frac{u_3-u_2}{L} - E\alpha T_2 = -\frac{P}{2A} - \frac{E\alpha(3T_2-T_3)}{4} \\ &\text{At node 3:} \quad \sigma_{2-3} = E\frac{u_3-u_2}{L} - E\alpha T_3 = -\frac{P}{2A} - \frac{E\alpha(3T_3-T_2)}{4} \end{aligned} \tag{2.10-8}$$

Clearly these results are incorrect, because in this problem axial stress must be constant throughout each element. In this example at least, it is better to use average element temperature in final stress calculation. Further discussion of thermal stress problems appears in Section 3.12.

2.11 STRUCTURAL SYMMETRY

If symmetry is recognized and exploited, the size of the FE model is reduced. Thus less computation is required and, usually of more importance, there is less input data to be prepared and checked by the analyst. Reflective and skew symmetry are discussed in the present section. Axial and repetitive symmetry are discussed in subsequent chapters. References include [2.20–2.22].

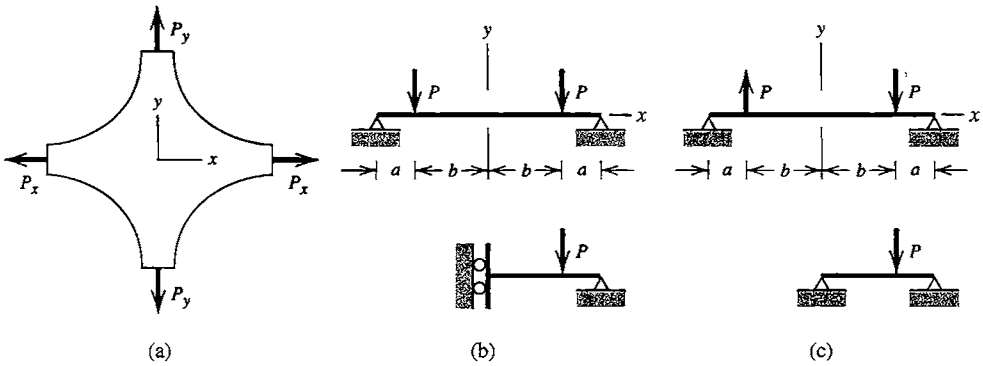

Figure 2.11-1. (a) Plane structure having reflective symmetry about $x = 0$ and $y = 0$ planes. (b) Beam under symmetric loading. (c) Beam under antisymmetric loading.

A structure has *reflective* or *mirror* symmetry if there is symmetry of geometry, support conditions, and elastic properties with respect to a plane. Reflective symmetry of structure *and loads* is shown in Fig. 2.11-1a: if reflected by the plane $x = 0$, the left half yields the right half, and vice versa. There is also reflective symmetry about the $y = 0$ plane. One can say that reflection brings the structure and its loads into "self coincidence." Analysis of either half provides a complete solution, because symmetric loading on a symmetric structure produces symmetric results.

If $P_x = P_y$ in Fig. 2.11-1a, planes $x = 0$, $y = 0$, $x = y$, and $x = -y$ are all planes of reflective symmetry, and we need analyze only one-eighth of the structure, using, for example, the segment in the first octant between lines $y = 0$ and $x = y$, with boundary conditions on the two lines such as to allow only radial motion from the origin $x = y = 0$. Load on this octant is $P_x/2$, because the original load P_x is bisected by the symmetry plane $y = 0$. (In a related example, if a stiffening beam under a floor slab is longitudinally bisected by a plane of symmetry, only half its stiffness is retained in the portion analyzed.)

The symmetric beam problem of Fig. 2.11-1b can be solved by analysis of either half, with rotation θ_z prevented at $x = 0$. The beam problem in Fig. 2.11-1c is *antisymmetric* because of the loading. Reflection about the plane $x = 0$, followed by *reversal* of all loads, results in self-coincidence. Analysis of either half as a simply supported beam provides a complete solution. These examples are simple, but it is not hard to see that, if the structure were large and complicated, it would be a waste of effort and storage space to ignore symmetry and prepare a model of the entire structure.

The following rules help in setting correct displacement boundary conditions for reflective symmetry. The conditions stated apply *only* to boundary nodes of the FE model that lie in a plane of reflective symmetry of the entire structure. If the problem is *symmetric,*

S1. Translational motion has no component normal to a plane of symmetry.

S2. Rotation vectors have no components in a plane of symmetry.

If the problem is *antisymmetric,* that is, symmetric except that loads must be reversed to achieve self-coincidence,

A1. Translational motion has no component in a plane of antisymmetry.

A2. Rotation vectors have no components normal to a plane of antisymmetry.

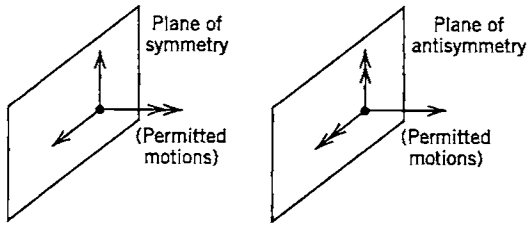

Figure 2.11-2. Degrees of freedom permitted (that is, not restrained) at a node in a plane of symmetry or antisymmetry. A double-headed arrow represents a rotational d.o.f.

Figure 2.11-2 depicts these rules in terms of d.o.f. *permitted* rather than d.o.f. restrained. Software may be able to insert appropriate boundary conditions automatically at nodes in a symmetry plane after input data defines the plane in question and states whether symmetry or antisymmetry prevails.

Figure 2.11-3a depicts an example problem in which symmetry concepts can be applied even though symmetry is not obvious at the outset [2.21]. By representing the original loading as the sum of symmetric and antisymmetric parts, we obtain the cases in Figs. 2.11-3b and 2.11-3c. Superposition of solutions of the latter two cases provides the solution of the original problem. Thus, bending moments in Fig. 2.11-3a are $M_1 = M_4$, $M_2 = M_5 + M_7$, and $M_3 = M_4$. We have traded one analysis of the entire structure for two analyses of half the structure, with different loading and support conditions.

Skew or *inversion* symmetry is illustrated in Fig. 2.11-4. In Fig. 2.11-4a, a half-revolution about the z axis (normal to the figure) results in self-coincidence. The same result would be produced by two successive reflections, about the $x = 0$ and $y = 0$ planes. In Fig. 2.11-4b,

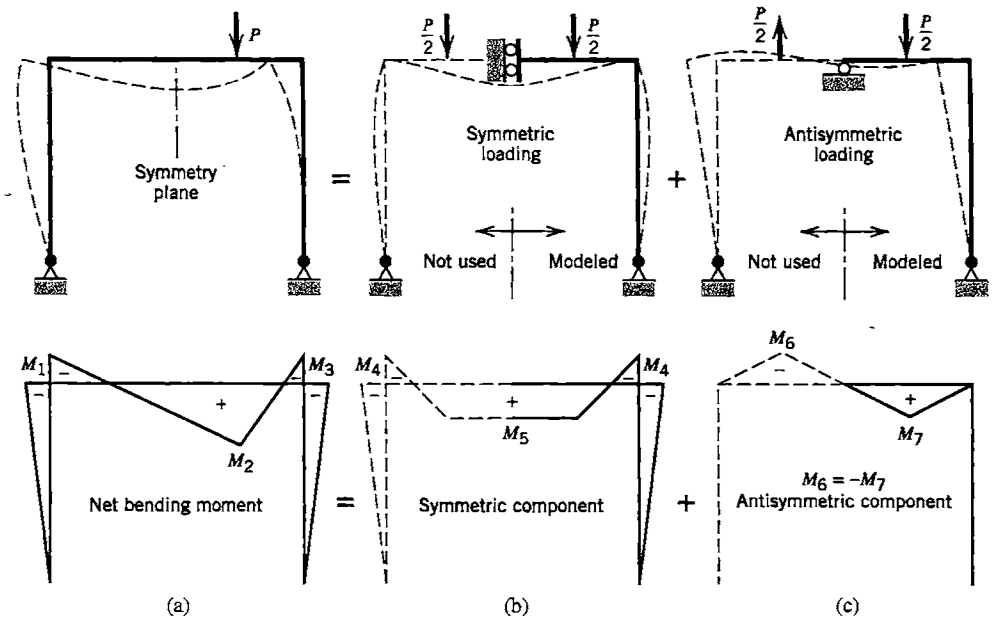

Figure 2.11-3. Modeling a plane frame problem as the sum of symmetric and antisymmetric cases. (Reproduced from C. Meyer, *Finite Element Idealization,* American Society of Civil Engineers, New York, 1987, by permission of the publisher.)

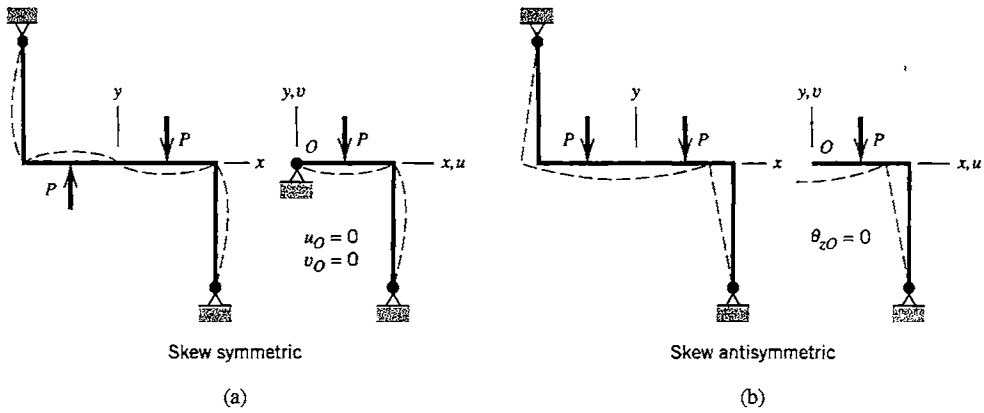

Figure 2.11-4. Skew symmetry of a plane frame, with loads that are (a) skew symmetric, and (b) skew antisymmetric.

a half-revolution followed by reversal of loads results in self-coincidence. In each case only half the structure need be analyzed. Boundary conditions for skew symmetry are discussed in detail in [2.22].

If symmetries are suspected but their nature is unclear, one may elect to do a coarse-mesh analysis of the structure in order to see whether computed results confirm or refute existence of the suspected symmetries.

Caution. Symmetry should be invoked sparingly and carefully in problems of vibration and buckling. For example, a uniform simply supported beam has symmetry about its center but has *anti*symmetric vibration modes as well as symmetric vibration modes. If half the beam were analyzed, the support conditions of Fig. 2.11-1b would permit only symmetric modes, whereas the support conditions of Fig. 2.11-1c would permit only antisymmetric modes. Similarly, unsymmetric modes are prominent in analyses for vibration and buckling of a shell of revolution. Caution is also needed in static problems that involve nonlinearity, because symmetries that are present when loading begins may subsequently disappear.

2.12 REVIEW. REMARKS REGARDING MODELING

Let us solve the truss problem of Fig. 2.5-2 by hand calculation. After all boundary conditions have been imposed, the structural equations are Eqs. 2.7-8. Triangularizing these equations by Gauss elimination, for the special case $k = AE/L$ the same for each member, we obtain

$$k\begin{bmatrix} 1.3600 & -0.4800 & 0.4800 \\ 0 & 0.4706 & -0.4706 \\ 0 & 0 & 1.0000 \end{bmatrix}\begin{Bmatrix} u_1 \\ v_1 \\ v_3 \end{Bmatrix} = \begin{Bmatrix} 0 \\ -P \\ -P \end{Bmatrix} \tag{2.12-1}$$

Hence, by back substitution, we obtain the nodal displacements

$$u_1 = -0.7500\frac{P}{k} \qquad v_1 = -3.125\frac{P}{k} \qquad v_3 = -\frac{P}{k} \tag{2.12-2}$$

These displacements agree with displacements obtained by classical analysis, using, for example, Castigliano's second theorem. Discretization error is zero in this problem, so FEA results should agree with results of classical analysis to one part in a million or better, the discrepancy being due to truncation or rounding error during formation of [**K**] and solution of equations. Recall that all these results presume that stiffness $k = AE/L$ is large enough that displacements are much smaller than overall dimensions of the truss, so that linear small-deflection theory is applicable.

The foregoing example problem can easily be solved by standard analytical methods, but for a truss or frame of even modest complexity (especially if it is statically indeterminate), hand calculation becomes very tedious, with ample opportunity to make sign and manipulation errors. For this reason, FEA software may be the preferred analysis tool for all but the simplest trusses and frames. Hand calculation is used to obtain approximate results as a check on FEA results.

By using the mesh generation capabilities of general-purpose software, a user can easily fill a region with elements. A novice user may activate this capability when its use is unwarranted or even wrong. If each member of our example truss were meshed with two or more bar elements connected end to end, FEA would yield either no result or a nonsensical result due to numerical difficulties such as a "small pivot" or "divide by zero" error. This kind of failure would arise because each junction between generated elements acts as a hinge, thus creating a mechanism. No additional information is to be gained from multiple collinear truss elements: each truss member experiences uniform strain, which is exactly modeled by a single bar element.

Similarly, a general-purpose FE software package contains an extensive element library that permits a user to choose among dozens of element types. A novice user may choose complicated elements, even if they contain features inappropriate for the problem at hand. Thus it may be tempting to use beam elements to model a truss, especially because each truss member can then be meshed using many beam elements connected end to end without creating a mechanism. If joints of the truss are indeed frictionless pins that connect truss members, then beam elements are inappropriate, because they prevent relative rotation between truss members at nodes, thus converting the truss to a frame. Bar elements, though simple, are the appropriate choice for truss analysis.

Figure 2.12-1 depicts a uniform beam that is continuous over simple supports at A, C, E, and G. Spans AB, BC, CD, DE, and EF can each be modeled by a single beam element. In these spans, use of more than one element per span is acceptable but not helpful, because the cubic lateral displacement field of a single beam element provides an exact representation of a mathematical model. Such is not the case in spans FG and GH, where, unless the element moment field depicted in Fig. 2.9-2a is included in the stress calculation phase, exact results for bending moment and flexural stress are only approached by using more and more elements in spans FG and GH.

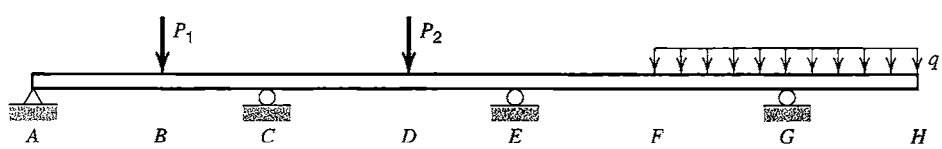

Figure 2.12-1. A uniform straight beam continuous over several simple supports.

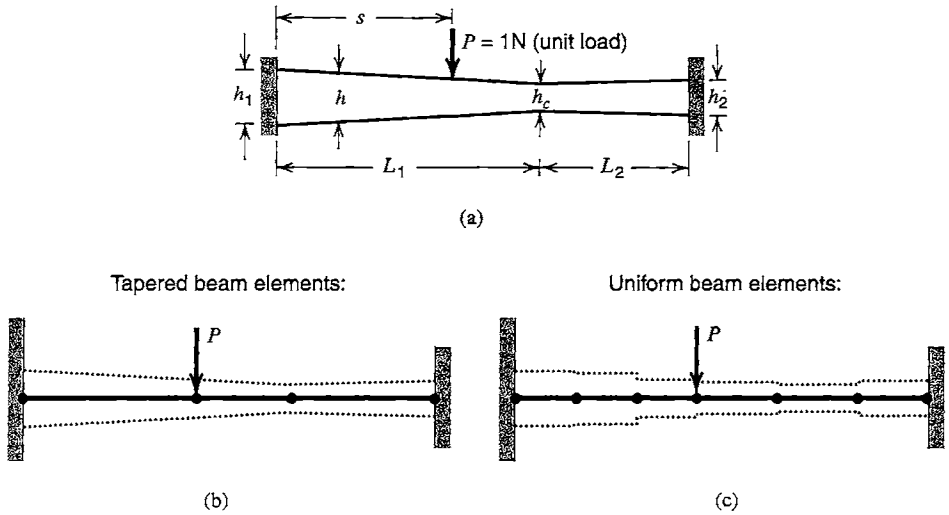

Figure 2.12-2. (a) A tapered plane beam of uniform thickness. (b,c) FE models that use tapered and uniform elements respectively. Element depths are suggested by dotted lines.

Consider next the tapered beam shown in Fig. 2.12-2. Only for some special cases (such as $h_1 = h_2$ and $s = L_1 = L_2$) is it possible to exploit symmetry. There is unlikely to be a convenient analytical solution. More importantly, in obtaining results for comparison with FEA results, there may be no unique or obvious choice among analytical approximations. Also, many different types of elements (not only beam elements) might be used to construct the FE model. Beam elements are appropriate only if the structure is slender. This example is representative of professional practice in that *engineering judgment* must be used to construct the FE model *and* to check FEA results.

To obtain approximate results for comparison with results of FEA, we might replace the actual taper by a uniform depth h_{ave} based on some average of the continuously varying depth. Handbook results are available for a uniform beam with fixed ends and a single off-center load [1.16]. Alternatively, we might assume (incorrectly) that the portion of the structure to the right of load P prevents rotation at load P, and use handbook results for a simple tapered beam with one end fixed and rotation prevented at the other end [1.16]. In FEA analysis, if the element library contains a tapered beam element, we might use the model of Fig. 2.12-2b. Otherwise, we may use a number of uniform elements to model each simple taper (Fig. 2.12-2c).

The following example problem illustrates further aspects of modeling using beam elements.

2.13 AN APPLICATION

We consider an example problem, with emphasis on FE modeling and checking results rather than on FE theory. The physical structure is a flat oval bar loaded in its own plane (Fig. 2.13-1). Deflections and stresses of greatest magnitude are sought. The solution strategy suggested in Section 1.5 is used in the following analysis.

Preliminary Analysis. The structure is roughly circular. Therefore a crude model is a circular ring, having the same perimeter as the oval and loaded by concentrated forces as

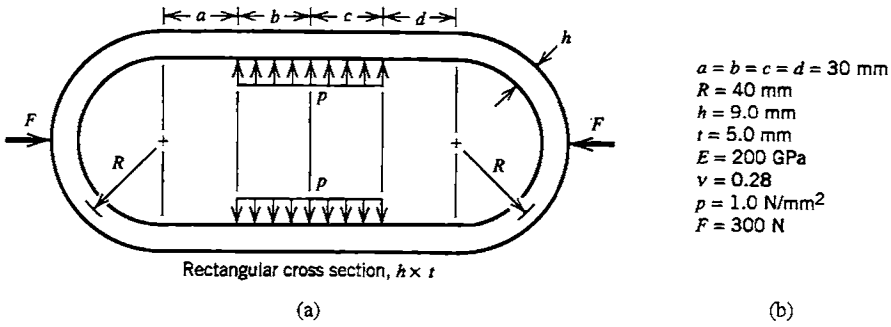

Figure 2.13-1. (a) Plane structure under mechanical loading. (b) Data used in the numerical example.

shown in Fig. 2.13-2. Data are such that the substitute ring has radius $r = 78.2$ mm, and pressure load produces forces $F = pt(b + c) = 300$ N. Handbook formulas [1.16] state deflections due to flexure and bending moments in a circular ring loaded by two diametrically opposing forces. By superposing two such cases, one with inward forces F and the other with outward forces F but 90 degrees away, we obtain

$$\delta = 0.143\frac{Fr^3}{EI} = 0.338 \text{ mm} \qquad \text{and} \qquad M = 0.5Fr = 11{,}730 \text{ N} \bullet \text{mm} \tag{2.13-1}$$

as magnitudes of radial deflection and bending moments at loaded points on the substitute ring. At these locations, direct circumferential stress and bending stress have magnitudes

$$\sigma_a = \frac{F/2}{ht} = 3.33 \text{ MPa} \qquad \text{and} \qquad \sigma_b = \frac{M(h/2)}{I} = 174 \text{ MPa} \tag{2.13-2}$$

These results are estimates of uncertain accuracy. If they differ greatly from FEA results subsequently computed, we must question the computed results, the physical understanding on which the estimates are based, or both.

We should also anticipate how the structure will deform. This matter is discussed in connection with the critique of FEA results.

Finite Element Analysis. Because of symmetry about horizontal and vertical centerlines, only one quadrant need be analyzed (Fig. 2.13-3). Supports shown are consistent with horizontal displacement allowed at end A, vertical displacement allowed at end D, and neither A nor D allowed to rotate about the z axis (normal to the xy plane).

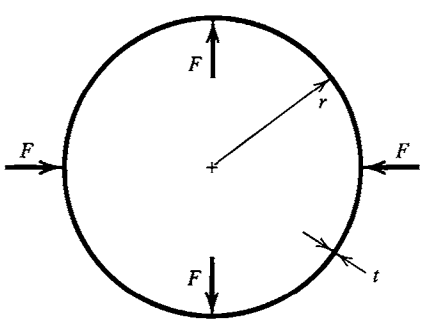

Figure 2.13-2. Simple mathematical model for approximate analysis, with $r = R + (a + b + c + d)/\pi$.

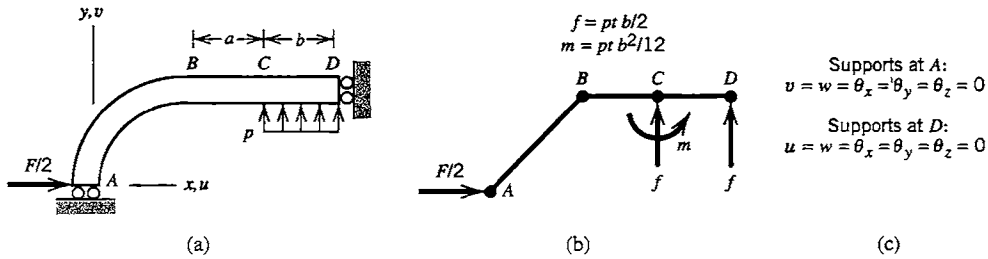

Figure 2.13-3. (a) Quadrant modeled. (b) Coarse-mesh FE model with consistent nodal loads. (c) Boundary conditions.

Our mathematical model is the plane oval shape shown in Fig. 2.13-1, with the assumption that behavior is described by flexure theory. Accordingly, beam elements are used for FEA. A coarse-mesh FE model is shown in Fig. 2.13-3b. Portion *BD* is modeled by two elements, *BC* and *CD*, so that nodal loads described in Fig. 2.9-2a can be computed, and applied as shown in Fig. 2.13-3b. No moment load is needed at *D*, because it would be reacted by the support instead of acting to deform the structure. Rigid-body motions w, θ_x, and θ_y of the model must be restrained, even though there are no loads that would make these d.o.f. nonzero at any node. Support conditions indicated in Fig. 2.13-3c allow only translation u at *A* and only translation v at *D*, with the result that all displacements of the FE model are confined to the xy plane. The same result would be obtained if we were to omit restraint of w, θ_x, and θ_y at either *A* or *D*. The remaining fixity at the other end would provide adequate restraint, because loads have no tendency to produce z-direction displacements.

Critique of Results. Before examining the computed output, we sketch an intuitive approximation of the displaced shape, as shown dashed in Fig. 2.13-4a. Software will plot the computed displaced shape, scaled up so as to be easily visible, and animated so that the model is seen to move back and forth between its original configuration and its displaced configuration. We should see reasonable agreement between the anticipated and computed shapes. In particular, point *A* should move only to the right, point *D* should move only upward, and neither point should rotate. (In checking the displaced shape we must allow for the inability of most software to plot anything but a straight line between two nodes; actual cubic curves are not displayed.) Thus, we visually check that intended boundary conditions have indeed been imposed. Upon examining a list of computed values of nodal d.o.f., we should see that w, θ_x, and θ_y are zero at all nodes. We also compare displacements u_A and v_D with the approximate displacements, Eq. 2.13-1.

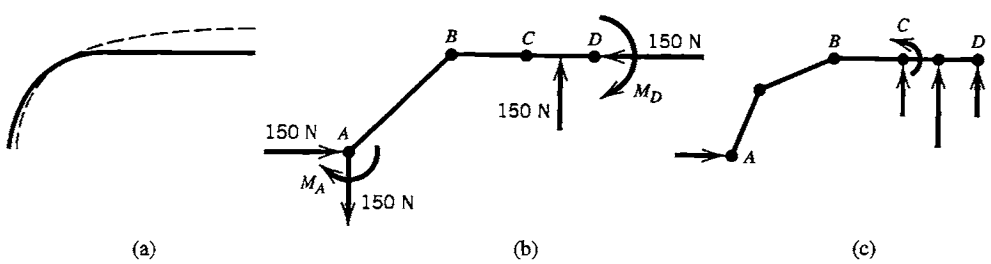

Figure 2.13-4. (a) Original centerline (solid) and deformed centerline (dashed) of the quadrant modeled. (b) Free-body diagram, showing loads applied to the quadrant modeled. (c) Refined FE model with consistent nodal loads.

If the foregoing examination discloses no obvious error in displacements, we proceed to examine stresses. We should find that the direct axial component $\sigma_a = N/A$ is tensile at A and compressive at D, while the bending component $\sigma_b = Mc/I$ is tensile on the inside at A and tensile on the outside at D. A summary of computed results for the coarse-mesh FE model of Fig. 2.13-3b is as follows:

$$\begin{aligned} u_A &= 0.135 \text{ mm} & (\sigma_a)_A &= 0 & (\sigma_b)_A &= \pm 166 \text{ MPa} \\ v_D &= 0.316 \text{ mm} & (\sigma_a)_D &= -3.33 \text{ MPa} & (\sigma_b)_D &= \pm 117 \text{ MPa} \end{aligned} \tag{2.13-3}$$

Software may report σ_a and σ_b individually, report their algebraic sum at beam surfaces, or both. The value of σ_a at A at first looks wrong; why is it zero? Elementary statics, applied to Fig. 2.13-4b, shows that member AB carries transverse shear force but zero axial force because of its 45° orientation. Therefore $(\sigma_a)_A = 0$ is correct for this particular FE model.

An improved mesh for the same problem is shown in Fig. 2.13-4c. Now arc AB is modeled by two chords rather than one, which is the most significant improvement. Portion BC is not refined, because doing so would make no difference. This portion is straight and no loads are applied between B and C, so it has cubic lateral deflection and a single beam element can represent it exactly. Computed results from the improved mesh are

$$\begin{aligned} u_A &= 0.121 \text{ mm} & (\sigma_a)_A &= 1.80 \text{ MPa} & (\sigma_b)_A &= \pm 163 \text{ MPa} \\ v_D &= 0.349 \text{ mm} & (\sigma_a)_D &= -3.33 \text{ MPa} & (\sigma_b)_D &= \pm 116 \text{ MPa} \end{aligned} \tag{2.13-4}$$

These results are in reasonable agreement with Eqs. 2.13-1 and 2.13-2, and in good agreement with Eqs. 2.13-3 except for σ_a at A, which is a small stress for which the discrepancy has been satisfactorily explained. We conclude that computed results from the refined mesh are reliable, although one more mesh refinement and reanalysis might provide additional confidence.

It would be instructive to repeat the analysis using reduced nodal loads ($m = 0$ in Fig. 2.13-3b). Other concerns about modeling may be raised, as follows. Truly concentrated loads are not possible; therefore, the horizontal forces F in Fig. 2.13-1 are idealizations whose actual distribution should perhaps be represented more precisely. The ratio h/R is probably small enough that transverse shear deformation is negligible, but it does no harm to use elements that include it. We have assumed from the outset that the material is linearly elastic. Stresses are not large and the elastic modulus suggests that the material is steel, so the assumption of linearity appears reasonable. Our linear analysis also assumes that deformations are small enough that equilibrium equations $[\mathbf{K}]\{\mathbf{D}\} = \{\mathbf{R}\}$, which are based on original geometry, remain sufficiently accurate after deformations have been produced by load. This assumption is seen to be true for this problem, because u_A and v_D are much smaller than overall dimensions of the structure. A problem that is nonlinear, because the material yields or because deformations are large, is much harder to solve, because information needed in the solution—namely, material properties at all locations, the deformed geometry, or both—is not known in advance.

ANALYTICAL PROBLEMS

2.2-1 (a) Consider a two-node bar element, as in Fig. 2.2-1, but let cross-sectional area A vary linearly with x from A_0 at $x = 0$ to cA_0 at $x = L$, where c is a constant. Write

the element stiffness matrix, first as in Eq. 2.2-1 using the average A, then using the exact relation between axial load and change in length of the member. Evaluate both matrices numerically for the case $c = 2$.

(b) A bar of length L_T has linearly varying cross-sectional area A, from A_0 at the left end to $3A_0$ at the right end. The bar is stretched by axial forces P at each end. The bar is modeled by the "average A" elements of part (a). Calculate the elongation of the bar, using one, two, three, then four elements of equal length. What is the percentage error in each case?

2.2-2 (a,b) In each of the two plane structures shown, rigid blocks are connected by linear springs. Imagine that only horizontal displacements are allowed. In each case, write the structure equilibrium equations $[\mathbf{K}]\{\mathbf{D}\} = \{\mathbf{R}\}$ in terms of spring stiffnesses k_i, displacement d.o.f. u_i, and applied loads F_i.

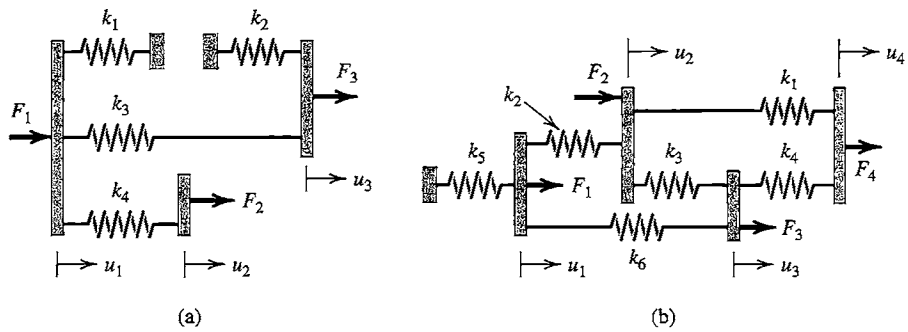

Problem 2.2-2

2.2-3 The plane structure shown consists of a rigid, weightless bar and linear springs of stiffnesses k_1 and k_2. Only small vertical displacements are permitted. Stiffness matrix $[\mathbf{K}]$ of this structure is 2 by 2 but can have various forms, depending on the choice of d.o.f. Determine $[\mathbf{K}]$ for each of the following choices of lateral translation d.o.f. (a) v_1 at $x = 0$ and v_2 at $x = L$, as shown. (b) v_1 at $x = 0$ and v_A at $x = L/2$. (c) v_2 at $x = L$ and v_B at $x = 2L$.

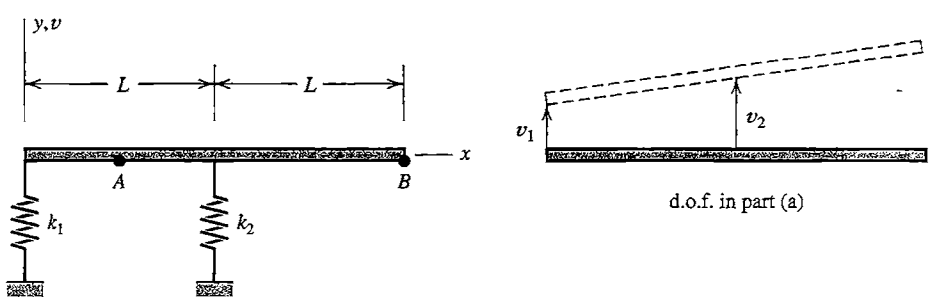

Problem 2.2-3

2.2-4 Consider a cable element of length L under constant tension T, as shown. Assume that lateral deflection v is linear in x and that $v \ll L$. What is the 2 by 2 stiffness matrix that operates on d.o.f. v_1 and v_2? (The matrix will contain T. Lateral forces F_1 and F_2 will be collinear with the d.o.f.)

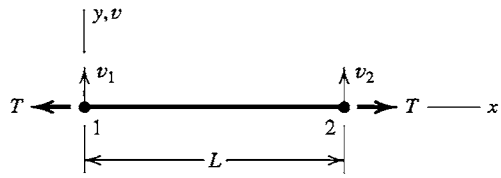

Problem 2.2-4

2.2-5 In Fig. 2.2-4, let $k_1 = k_2 = k$ and $t_1 = t_2 = t$.
(a) Let $T_1 = 0$ °C and $T_3 = 200$ °C. Solve for T_2 and the unknown rates of heat flow in terms of k and t.
(b) Let $T_1 = 400$ °C and let f_3 have the prescribed value $\bar{f}$. What are the unknowns? Solve for them in terms of k, t, and $\bar{f}$.

2.3-1 For the structure described in Problem 2.2-3, determine [**K**] for each of the following choices of d.o.f. (a) Lateral displacement v_1 at $x = 0$ and small rotation θ about $x = 0$. (b) Lateral displacement v_B at $x = 2L$ and small rotation θ about $x = 2L$.

2.3-2 (a,b) The plane structures shown consist of rigid weightless bars connected by linear springs, each of stiffness k. Degrees of freedom are horizontal translations u_i and small rotations θ_i for $i = 1,2$, as shown. Vertical motion and out-of-plane displacements are not allowed. In each case determine the 4 by 4 structure stiffness matrix in terms of k and b.

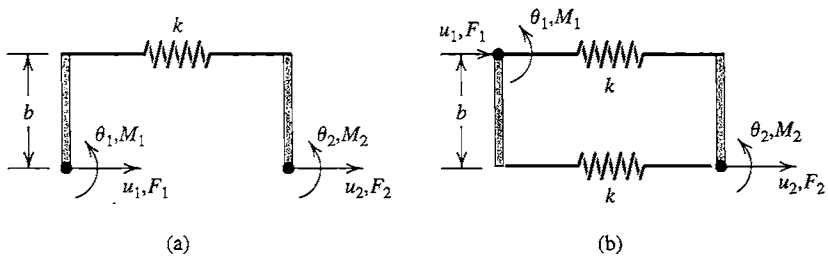

Problem 2.3-2

2.3-3 The plane structures shown consist of rigid weightless members and springs. In each case determine the stiffness matrix that operates on the two d.o.f. shown.
(a) Spring k_A resists translation; spring k_B resists relative rotation between bars AB and BC. Each bar has length $5L$ and slides without friction on the horizontal surface.
(b) Rotation θ is small. Assume that the roller can apply upward or downward force to the trapezoidal block.

2.3-4 To elevate the end of a cantilever beam without rotating it, as shown, force and moment are required. From the information shown, fill in as many numerical values as you can in an element stiffness matrix that operates on nodal d.o.f. $\{\mathbf{d}\} = \lfloor v_1 \;\; \theta_{z1} \;\; v_2 \;\; \theta_{z2} \rfloor^T$, where v_1 and v_2 are measured in millimeters. Do not use beam deflection formulas or Eq. 2.3-5. Instead rely on the given data, physical argument, statics, and the symmetry of [**k**]. Ignore transverse shear deformation.

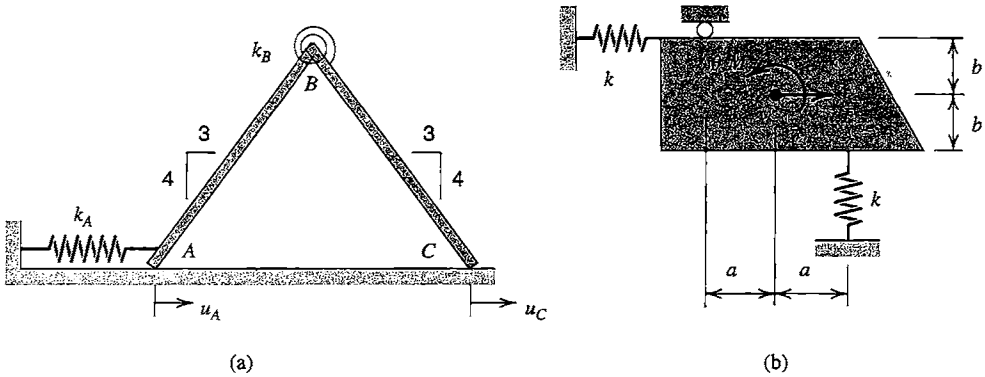

Problem 2.3-3

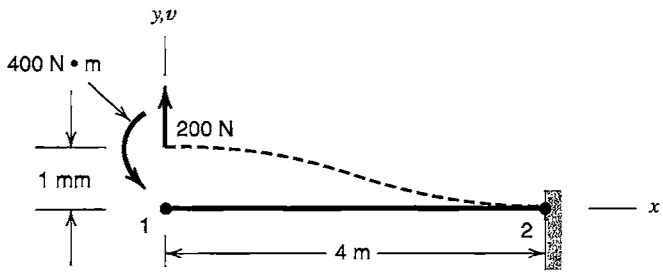

Problem 2.3-4

2.3-5 Using Eqs. 2.3-1 to 2.3-4 as a guide, apply elementary beam theory to derive the following columns of [**k**] in Eq. 2.3-5. (a) Column 2. (b) Column 3. (c) Column 4.

2.3-6 (a,b) The slender plane beams shown have both axial and bending stiffness. Without calculation, determine the *algebraic sign* of each coefficient in the element stiffness matrix [**k**] associated with the d.o.f. shown (or enter zero if the coefficient is null). Assume that displacements and rotations are small, and that nodal forces and moments have the same positive senses as their corresponding nodal d.o.f.

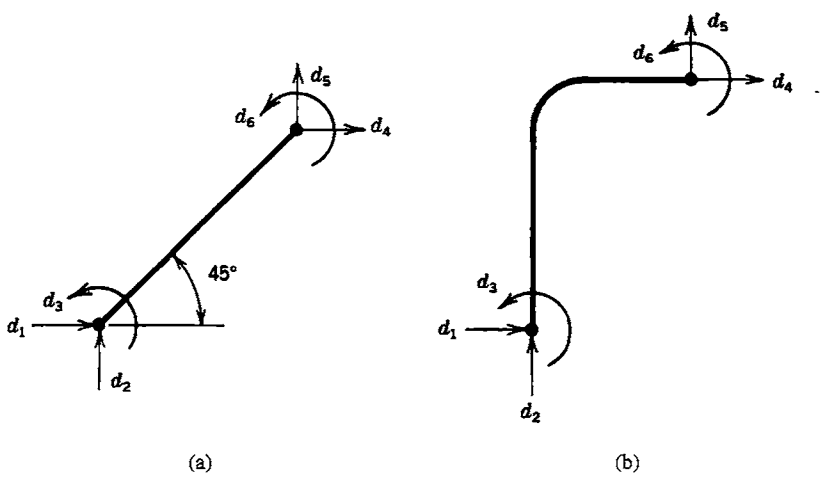

Problem 2.3-6

2.3-7 (a) Let a uniform beam element have simply supported ends. Apply end loads such that bending moment is constant along the beam. Use Eq. 2.3-6 to show that there is no transverse shear deformation in this case.
(b) Let a uniform cantilever beam be supported at the loaded end so that this end cannot rotate, as shown. For the cross section shown, and with $E = 2G$, use Eq. 2.3-6 to calculate the lateral deflection at node 2 in terms of P and E. Consider $L = 8$ mm, $L = 16$ mm, and $L = 32$ mm. In each case, what fraction of the deflection is due to transverse shear deformation?
(c) For the beam of part (b), verify that lateral deflection according to Eq. 2.3-6 agrees with mechanics of materials theory for the two limiting cases $L \to 0$ and $L \to \infty$.

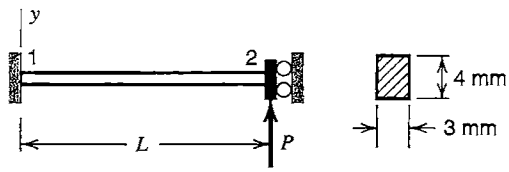

Problem 2.3-7(b)

2.3-8 Two identical cantilever beams lie in the xy plane and are welded together where they meet at right angles, as shown. Set up a 2 by 2 matrix that operates on lateral deflection and rotation d.o.f. at B. Note that rotations about x and y axes are equal in magnitude at B. Solve for the lateral deflection at the loaded point. Neglect transverse shear deformation but include torsional stiffness. If the two beams have I sections, what can be said about the calculated deflection as compared with the actual deflection, and why?

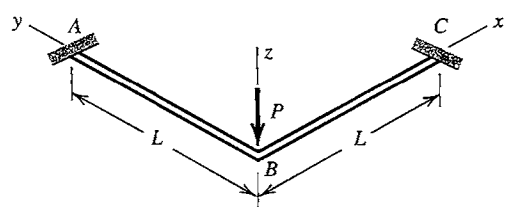

Problem 2.3-8

2.4-1 For a bar element arbitrarily oriented in the xy plane, Fig. 2.4-1b, determine [**k**] by activating each d.o.f. in turn, rather than by using the transformation of Eq. 2.4-5.

2.4-2 (a) Derive a 4 by 4 stiffness matrix for a uniform bar element, using the d.o.f. shown.
(b) Obtain the same result by coordinate transformation of the 2 by 2 matrix in Eq. 2.2-1.

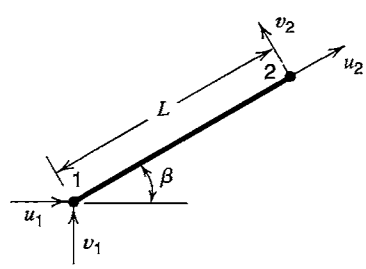

Problem 2.4-2

2.4-3 (a) For a two-node bar element arbitrarily oriented in space, determine the 6 by 6 matrix [**k**] by activating each d.o.f. in turn, rather than by using the transformation of Eq. 2.4-5.
(b) Verify the result of part (a) by carrying out the coordinate transformation.

2.4-4 Obtain the stiffness matrices requested in the following problems by applying coordinate transformation to the stiffness matrix determined in Problem 2.2-3(a):
(a) Problem 2.2-3(b) (b) Problem 2.2-3(c)
(c) Problem 2.3-1(a) (d) Problem 2.3-1(b)

2.5-1 In Fig. 2.5-1, permute element node labels so that element nodes are numbered as shown in the sketch for the present problem. Maintain structure node numbers as shown in Fig. 2.5-1. Show that [**K**] of Eq. 2.5-9 is again obtained.

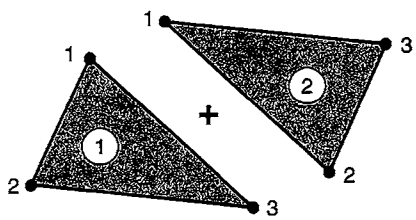

Problem 2.5-1

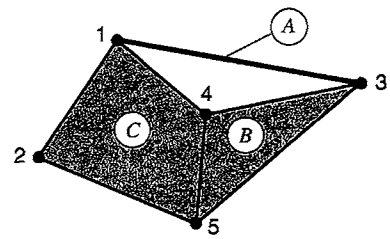

Problem 2.5-2

2.5-2 The structure shown consists of a two-node element A, a three-node element B, and a four-node element C. There is one d.o.f. per node. Place letters A, B, and C in appropriate positions in arrays [**K**] and {**R**} to indicate the locations to which contributions from element matrices are assigned.

2.5-3 Two collinear cantilever beams are connected by a frictionless hinge, as shown. Flexural stiffness EI_z is the same for both beams. Load P and deformations are confined to the xy plane. Write the stiffness matrix that operates on the "active" d.o.f. Ignore transverse shear deformation.

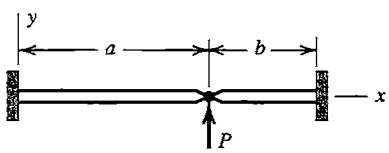

Problem 2.5-3

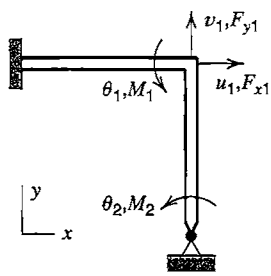

Problem 2.5-4

2.5-4 For the frame shown, write equilibrium equations [**K**]{**D**} = {**R**} using d.o.f. $\{\mathbf{D}\} = \lfloor u_1 \;\; v_1 \;\; \theta_{z1} \;\; \theta_{z2} \rfloor^T$. Both members are slender and have the same E, I, A, and L. Express matrix coefficients in terms of L, $a = AE/L$, and $b = EI/L^3$.

2.5-5 For the plane frame of Fig. 2.3-3(a), assume that members are slender and have the same EI_z, and that axial deformations are negligible in comparison with bending deformations. Let loads and deformations be confined to the plane of the frame.

Write the structure stiffness matrix that operates on "active" d.o.f. $\{\mathbf{D}\} = \lfloor u_B \;\; \theta_{zB} \;\; \theta_{zC} \rfloor^T$.

2.5-6 Imagine that a beam element has positive directions for nodal loads and nodal d.o.f. as shown in the sketch. How does this arrangement alter [**k**] of Eq. 2.3-5? What is awkward about this arrangement?

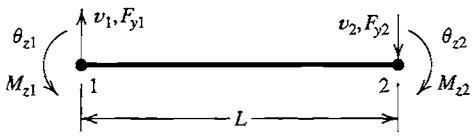

Problem 2.5-6

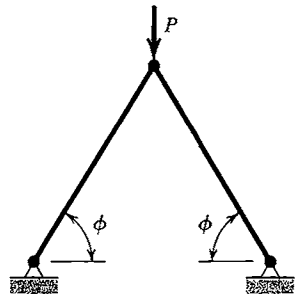

Problem 2.5-7

2.5-7 Displacements of the two-member truss shown are confined to the plane of the figure. Both members have the same A, E, and L. Obtain the 2 by 2 stiffness matrix that operates on horizontal and vertical displacements of the top node. Solve for these displacements, and for axial stress in members, when downward load P is applied.

2.6-1 Let each of the following beam elements lie along the x axis. Write the most general nodal displacement vector that describes a small rigid-body motion of the element. (a) 2D element (see Eq. 2.3-6). (b) 3D element (see Eq. 2.3-8).

2.6-2 For the 2D beam element cited in Problem 2.6-1(a), write the nodal displacement vector $\{\mathbf{d}\}$ that describes a rigid-body rotation of 180° about node 1. For this vector, $[\mathbf{k}]\{\mathbf{d}\}$ is not zero. Why?

2.6-3 Remove supports from the truss of Fig. 2.5-2. Use $L = 5a$ as the length of bar 2, where a is a constant having units of length. Write rigid-body displacement vectors for the following small motions (a), (b), and (c) in the plane of the truss. Show that each vector produces zero forces $\{\mathbf{R}\}$.

(a) Translation in the direction of bar 2

(b) Rotation about node 3

(c) Rotation about the point $x = 3a, y = 4a$

(d) Are the foregoing three displacement vectors linearly independent?

(e) Let the nodal displacement vector be $\{\mathbf{D}\} = \lfloor -7 \;\; -3 \;\; -4 \;\; 0 \;\; 0 \;\; -4 \rfloor^T$. Is the product $[\mathbf{K}]\{\mathbf{D}\}$ equal to zero? Does this $\{\mathbf{D}\}$ represent rigid-body motion?

2.6-4 For the quarter-circle curved beam element shown, use the d.o.f. indicated and confine displacements to the xy plane.

(a) Do individual rows (or columns) of [**k**] sum to zero? Why or why not? (Do not construct [**k**] to answer.)

(b) Write the most general nodal displacement vector that expresses rigid-body motion.

(c) Write $\{\mathbf{d}\}$ (all six terms) such that $[\mathbf{k}]\{\mathbf{d}\} = \{\mathbf{0}\}$. There are infinitely many possibilities; write three $\{\mathbf{d}\}$'s that are linearly independent.

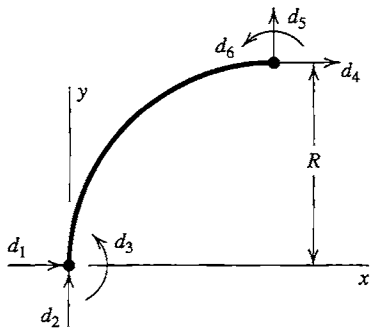

Problem 2.6-4

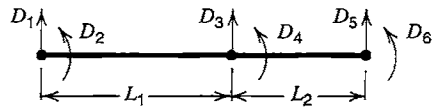

Problem 2.6-5

2.6-5 (a,b) Repeat the instructions of Problem 2.6-4(a,b) with reference to the uniform two-element beam structure shown.
(c) Sketch the deformation mode that corresponds to a $\{\mathbf{D}\}$ that makes each nodal load R_i in $\{\mathbf{R}\}$ equal to the sum of the K_{ij} in row i. Show the R_i by sketching properly oriented arrows on the structure.

2.6-6 Write the most general nodal displacement vector $\{\mathbf{d}\}$ that expresses rigid-body motion in the xy plane for the following truss elements:
(a) The bar element of Fig. 2.4-1b with $\beta = 0$
(b) The bar element of Fig. 2.4-1b with $\beta > 0$
(c) The bar element of Problem 2.4-2

2.6-7 (a) There must be n_R restraints to prevent rigid-body motion, where $n_R = 3$ for 2D (plane) motion and $n_R = 6$ for motion in 3D space. However, the d.o.f. to be restrained cannot be chosen arbitrarily. Explain why. Also, provide 2D and 3D examples for which n_R restraints are inadequate.
(b) The choice of restraints adequate to prevent rigid-body motion is not unique. For the two-element cantilever beam of Fig. 2.6-2b, starting with no supports, write six sets of boundary conditions, each adequate to prevent rigid-body motion in 3D space and yet also adequate to model a plane problem. Avoid unnecessary restraint.

2.6-8 For a given $\{\mathbf{D}\}$, why does the form $\{\mathbf{D}\}^T[\mathbf{K}]\{\mathbf{D}\}/2$ represent strain energy in a structure? *Suggestion:* Consider work done by applied loads.

2.7-1 In each of the following beam problems, confine displacements to the xy plane, use a single element, and ignore transverse shear deformation. Write $[\mathbf{K}]\{\mathbf{D}\} = \{\mathbf{R}\}$ with $\{\mathbf{D}\} = \lfloor v_2 \;\; \theta_{z2} \rfloor^T$. Impose d.o.f. at node 2 by using the method of Eq. 2.7-6. Solve by matrix operations; then check results by elementary beam theory.
(a) A cantilever beam is fixed at its left end. A lateral displacement $\bar{v}_2$ is imposed at its right end. What is the associated force, and what is θ_{z2}?
(b) A simply supported beam is forced to rotate $\bar{\theta}_{z1}$ units at its left end. What is the associated moment, and what is θ_{z2}?

2.7-2 (a) Let AE/L be the same for each bar of the plane truss in Fig. 2.5-2. Remove load P. Using the method of Eq. 2.7-6, impose the following displacements at node 1: $u_1 = c$ (where c is a small number), and $v_1 = 0$. Determine v_3 and the x and y components of load applied at node 1.

(b) Use the results of part (a) in Eq. 2.5-10 to determine support reactions at nodes 2 and 3.

(c) Show that the forces of parts (a) and (b) place the truss in static equilibrium.

2.8-1 Renumber nodes in Fig. 2.8-1a as follows: 7 becomes 6, 9 becomes 7, and 6 becomes 9. Numbers of other nodes are not changed. What now are the maximum semibandwidth and the profile of [**K**]? How many "fills" will Gauss elimination produce?

2.8-2 (a,b) Reverse the node numbering in Fig. 2.8-1a, so that 9 becomes 1, 8 becomes 2, and so on. Do likewise for Fig. 2.8-1b. In each case, answer the questions posed in Problem 2.8-1.

2.8-3 (a) Assume that the structure shown has one d.o.f. per node, and that each straight line between nodes is a two-node element. Try to assign a node numbering that minimizes the largest semibandwidth b_{max}. For this numbering, what are b_{max}, profile p, and the number of "fills" created by Gauss elimination?

(b) Repeat part (a), but now try to assign an alternative numbering that maximizes b_{max}.

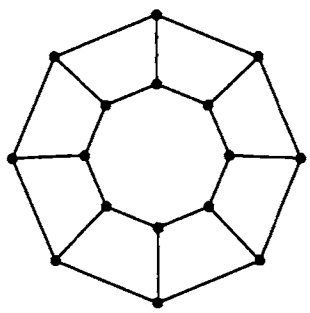

Problem 2.8-3

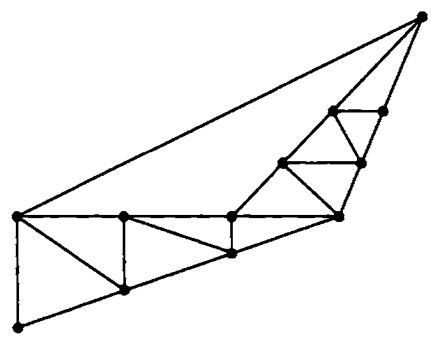

Problem 2.8-4

2.8-4 (a,b) Repeat Problem 2.8-3 with reference to the structure shown.

2.8-5 The stiffness matrix of Fig. 2.8-3a can be provided by an actual structure. Devise such a structure, using linear springs and rigid blocks, in the manner of structures considered in Problem 2.2-2.

2.8-6 Apply Gauss elimination to the stiffness equations that represent the inadequately supported plane structures shown. In what equation does trouble appear, in the form of a zero diagonal term? Could the step number be predicted in advance?

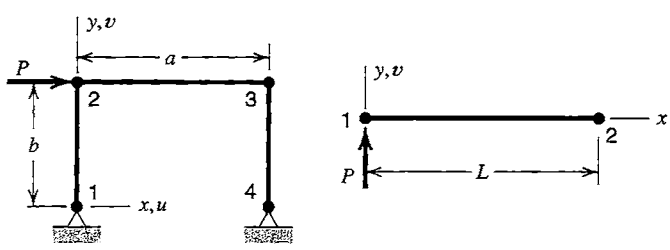

Problem 2.8-6

(a) Each of the three bar elements has the same A and E. Each node acts as a hinge connection. There are four active d.o.f.
(b) Use Eq. 2.3-5 to represent the unsupported beam.

2.8-7 The sketch shows an axially loaded structure and its structural equations after boundary conditions have been imposed.
(a) Use Gauss elimination to solve for u_2, u_3, and u_4.
(b) After the first elimination, what physical interpretation can be given to K_{22}? And what interpretation to K_{33} after the second elimination?
(c) Structural equations can be written in the following form:

$$u_2 = (24 + 6u_3)/12 \qquad u_3 = (24 + 6u_2 + 6u_4)/12 \qquad u_4 = u_3$$

In Gauss-Seidel iteration, one solves the equations serially, using the most recently calculated values of the u_i in each equation. Thus, in the first iteration, starting with $u_2 = u_3 = u_4 = 0$, one obtains $u_2 = 2$ from the first equation, then $u_3 = 3$ from the second equation, then $u_4 = 3$ from the fourth equation. Carry out another three cycles of this process. (*Note:* There are ways to greatly increase the convergence rate.)

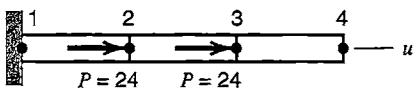

$$\begin{bmatrix} 12 & -6 & 0 \\ -6 & 12 & -6 \\ 0 & -6 & 6 \end{bmatrix} \begin{Bmatrix} u_2 \\ u_3 \\ u_4 \end{Bmatrix} = \begin{Bmatrix} 24 \\ 24 \\ 0 \end{Bmatrix}$$

Problem 2.8-7

2.8-8 (a) For the structure of Problem 2.2-2(a), let all springs have the same stiffness k. Let all loads be zero but F_2. Use Gauss elimination to determine the displacement d.o.f. in terms of k and F_2.
(b) For the same structure, change the loading so that all loads are zero but F_1. Determine the displacement d.o.f. in terms of k and F_1. However, rather than starting over, use the triangularized matrix of part (a) to reduce the load vector, then back-substitute.

2.8-9 (a,b) Repeat the instructions of Problem 2.8-8, but with reference to the structure of Problem 2.2-2(b).

2.8-10 (a) In Fig. 2.5-2, let $k = AE/L$ be the same for each member of the truss. Use Gauss elimination to determine u_1, v_1, and v_3 in terms of stiffness k and load P.
(b) Use Eq. 2.5-10 and the results of part (a) to determine the support reactions. Verify that these reactions and load P place the truss in static equilibrium.

2.9-1 The uniform bar shown carries uniformly distributed axial load q over its right half. Determine the axial stress distribution in the bar, both with and without element stress fields that exist when all nodal d.o.f. are zero. (a) Use one element of length $2L$. (b) Use two elements, each of length L.

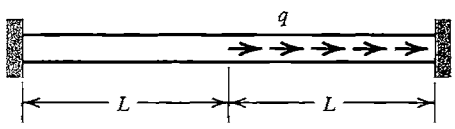

Problem 2.9-1

2.9-2 (a,b) Repeat Problem 2.9-1, but remove the support at the right end of the bar.

2.9-3 Solve the problem of Fig. 2.9-2(a) using two elements of equal length in span L. Plot bending moment M in the beam using (a) M as produced by nodal d.o.f. only, and (b) M as produced by nodal d.o.f. in combination with element M fields that exist when all nodal d.o.f. are zero.

2.9-4 Distributed lateral force q and the slender cantilever beam are both uniform (see sketch). Determine the tip deflection and root bending moment using consistent nodal loads produced by q. Omit element M fields that exist when all nodal d.o.f. are zero. Then repeat the calculation, this time using reduced nodal loads. (a) Use a single element. (b) Use two elements of equal length.

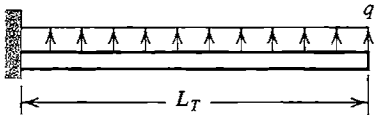

Problem 2.9-4

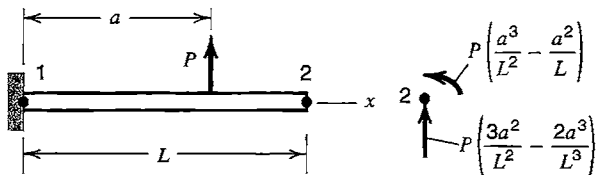

Problem 2.9-5

2.9-5 The uniform slender cantilever beam shown carries a concentrated lateral force P. Model the beam by a single element.
(a) Calculate nodal d.o.f. v_2 using consistent nodal loads (shown in the sketch). Express the answer in terms of P, L, E, I, and a.
(b) Again calculate v_2, now using reduced nodal loading (only force Pa/L at $x = L$).
(c) For part (a) and for part (b), calculate the ratio of the calculated v_2 to the exact v_2 according to elementary beam theory. Plot these ratios versus a/L for $0 < a < L$.
(d) Use the nodal d.o.f. of part (a) to calculate bending moment $M = EIv_{,xx}$ at the left end, without including the bending moment that exists when all nodal d.o.f. are zero. Repeat for part (b). In each case compute the ratio of calculated end moment to exact end moment, and plot these ratios versus a/L for $0 < a < L$.

2.10-1 Repeat the example problem of Section 2.10, but alter support conditions by letting the bar be fixed at its left end and free at its right end.

2.10-2 The bar shown is confined between rigid walls. Cross-sectional area A varies linearly from A_0 to $1.6A_0$. The bar is uniformly heated an amount ΔT from its stress-free temperature. Calculate stresses in a model that contains three uniform elements, each of length $L_T/3$ and having the respective cross-sectional areas $1.1A_0$, $1.3A_0$, and $1.5A_0$. On axes x (abscissa) and $\alpha L\ \Delta T$ (ordinate), plot exact results and FE results.

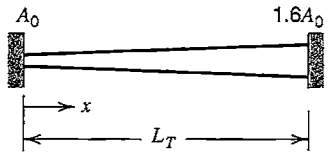

Problem 2.10-2

2.10-3 Remove load P in Fig. 2.5-2. Heat bar 2 only, an amount T degrees. Use the three-step method described in Section 2.10 to determine nodal displacements and element stresses. Let bar 2 have length $5a$, where a is a constant.

2.10-4 (a,b) Each beam shown is slender and has a solid rectangular cross section of dimensions $2c$ by t. Each is loaded by a temperature field that is constant along the beam but varies from $+T$ on the top surface to $-T$ on the lower surface. In each case use a single element and the three-step method described in Section 2.10 to determine stress σ_x on the top surface as a function of x, E, α, T, and dimensions.

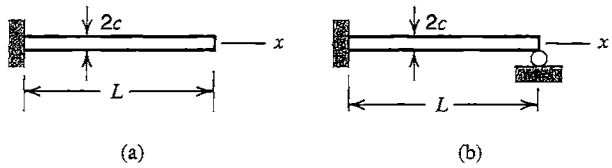

Problem 2.10-4

2.11-1 For the slender beam shown, decompose the problem into the sum of symmetric and antisymmetric cases, then use beam theory to determine the deflection of load P in terms of P, L, E, and I. Check the result by a handbook formula of beam theory.

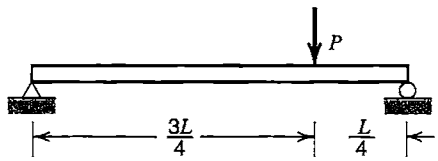

Problem 2.11-1

2.11-2 The ring shown is loaded in its plane by moments M_0 at opposite ends of a diameter. For a complete solution, only the first quadrant need be modeled and analyzed. What boundary conditions and loads are appropriate?

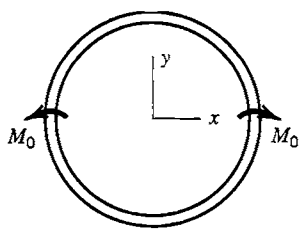

Problem 2.11-2

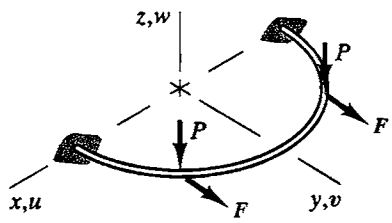

Problem 2.11-3

2.11-3 The half-ring shown lies in the xy plane and is symmetric about the yz plane. Loads P and F are applied at points equidistant from the yz plane and act parallel to it. Symmetry conditions are to be exploited by analysis of only the half of the ring that lies in the first quadrant. Fixed support is provided at the xz plane.
(a) At the yz plane, what displacement boundary conditions must be imposed on the quadrant analyzed? At this location, which of the nodal loads are known to be zero?
(b) Reverse the directions of loads P and F in the first quadrant only, and answer the questions posed in part (a).

2.11-4 The model shown is a square grillage of uniformly spaced beam elements that lie in the xy plane and are welded together at nodes. Assume that all elements are identical and that nodal d.o.f. are lateral (z direction) displacements w_i and rotations θ_{xi} and θ_{yi}. Supports impose $w_i = 0$ at all nodes i on the square boundary of

the grillage. Internal nodes are not restrained. In each part of this problem, lateral (z direction) forces of magnitude P act on internal nodes as described below. State what portion of the grillage constitutes the smallest acceptable model, and what its boundary conditions must be, if:

(a) Each node carries a load P, all acting in the same direction.

(b) Loads P act upward for $y > 0$, act downward for $y < 0$, and are omitted on $y = 0$.

(c) Loads P alternate in direction by quadrant. That is, they act upward in the first and third quadrants, downward in the second and fourth quadrants, and are omitted on x and y axes.

(d) Loads P alternate in direction by octant.

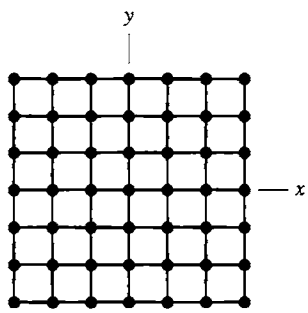

Problem 2.11-4

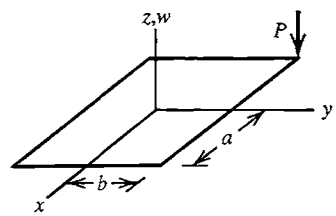

Problem 2.11-5

2.11-5 The sketch represents a uniform rectangular plate with lateral load P applied at one corner. Imagine that the FE mesh (not shown) is uniform and is supported by a uniform elastic foundation. The d.o.f. at each node are lateral displacement w_i and rotations θ_{xi} and θ_{yi}. Describe how the entire plate under the given loading can be analyzed for lateral deflection $w = w(x,y)$ by analyzing a single quadrant four times, each time using different loading and/or support conditions, or then superposing results.

COMPUTATIONAL PROBLEMS

In the following problems, compute peak values of displacement and stress or bending moment. Exploit symmetry where possible. When mesh refinement is used, estimate the maximum percentage error of results provided by the finest FE mesh. Where dimensions or loads are not assigned, choose values that seem reasonable or convenient. Where material properties are needed but not stated, use properties of steel. Apply the analysis methodology suggested in Section 1.5.

C2.1 (a) Does the software you use include transverse shear deformation in beam elements? Rather than consulting program documentation, find out by devising and running simple cantilever beam test cases.

(b) Similarly, consider uniformly distributed load on a beam. Analyze it using consistent nodal loads, then reduced nodal loads (Section 2.9). Then analyze again, this time obtaining loads automatically by using the gravity load option in FE software. Which nodal load formulation appears to be coded in the software?

C2.2 Use FEA software to determine displacements due to load P in Problem 2.5-7. Compare computed results with results determined by hand calculation in Problem 2.5-7. In computation, include cases for which angle ϕ is very small.

C2.3 A stepladder contains a linkage mechanism that permits the ladder to be folded, as shown. As a simple idealization, a stepladder can be analyzed as a plane structure.
(a) Do an analysis for a load P acting downward on top of the ladder. Use the simplest workable FE model. Both bar and beam elements may be needed.
(b) Do an analysis for load P on a step of the ladder. Modify the FE model of part (a) only to the extent necessary.
(c) Repeat the foregoing stepladder analyses, but improve the model by making it a three-dimensional structure. Obtain dimensions by measuring an actual stepladder.

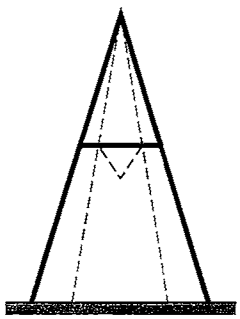

Problem C2.3

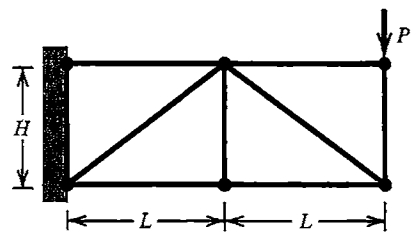

Problem C2.4

C2.4 Members of the plane structure shown may be bars connected by pins to create a truss, or beams rigidly connected at joints to create a frame. For the frame model, nodal rotations at the wall may be either permitted or prohibited. Investigate how displacements and stresses differ between the truss model and the frame model. Assume that all members have a square cross section, b units on a side. Suggested cases include $b = 5$ mm, $b = 15$ mm, and $b = 30$ mm; also $H = 120$ mm and $L = 160$ mm. Unit load $P = 1.0$ N is convenient.

C2.5 Members of the plane structure shown may be bars connected by pins to create a truss or beams rigidly connected at joints to create a frame. Investigate how displacements and stresses differ between the truss model and the frame model. Assume that all members have a square cross section. Dimensions shown are in meters. Loading may be by uniformly distributed load q or by the weight of the structure itself. Obtain nodal loads by the reduced approach described in Section 2.9. (It is also instructive to omit diagonals from the frame model, so that upper and lower chords are connected only by vertical members.)

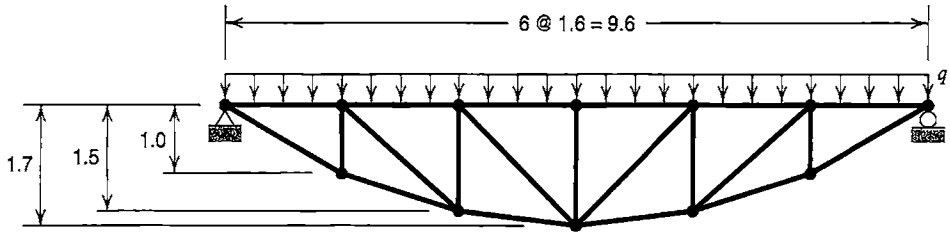

Problem C2.5

C2.6 Analyze the circular ring shown in Fig. 2.13-2, but with loads F directed normal to the plane of the ring and alternating in direction from one load to the next. Let $r = 80$ mm, and let the cross section be circular and of diameter 6.0 mm.

C2.7 Consider the tapered beam shown in Fig. 2.12-2a. Let the beam have unit thickness normal to the figure, and let depth h vary linearly in the axial direction. Confine displacements to the plane of the figure. Suggested cases include the following.
(a) $L_1 = L_2 = s = 200$ mm, $h_1 = h_2 = 40$ mm, $h_c = 20$ mm
(b) $L_1 = L_2 = s = 200$ mm, $h_1 = h_2 = 20$ mm, $h_c = 40$ mm
(c) $L_1 = 200$ mm, $L_2 = 0$, $s = 80$ mm, $h_1 = 40$ mm, $h_2 = h_c = 20$ mm

C2.8 (a,b,c) Repeat Problem C2.7, now letting an end of the beam be simply supported.

C2.9 Consider the problem of a plane beam on a continuous "Winkler" elastic foundation [2.6]. The foundation can be represented by discrete springs that connect nodes of an FE beam model to a rigid support (see sketch). This is not the best FE representation of the problem, but it is instructive to discover how displacements and bending moments in the FE beam model converge toward exact results as the mesh is refined. Analytical solutions for straight beams with various arrangements of loading and support are available [1.16]. A circular ring built of straight elements can also be investigated, under loads normal to the plane of the ring.

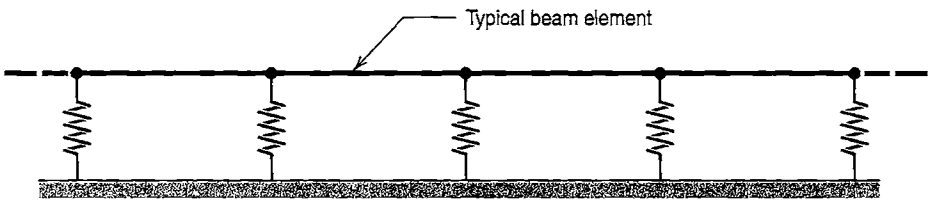

Problem C2.9

C2.10 Idealize a bicycle wheel as a planar structure having 36 radial spokes. Properties are as follows [2.23]. Spokes: diameter = 2.1 mm, $E = 210$ GPa, length = 309.4 mm from the center of the wheel to the centroidal axis of the rim cross section. Rim: $A = 138.4$ mm^2, $E = 70$ GPa, $\nu = 0.33$, centroidal I of $A = 1469$ mm^4, $I/c = 176$ mm^3 (for stress calculation). Assume that initial tension in the spokes is sufficient to maintain tension in every spoke when load is applied. Consider the following loadings:
(a) A vertical force of 490 N applied by the road.
(b) A force of 100 N applied tangentially by caliper brakes at the top of the wheel.

C2.11 The structure shown has unit thickness normal to the figure. Depth h of the cross section varies linearly in the circumferential direction. Confine displacements to the plane of the figure. Some possible choices of geometry are as follows.
(a) $\phi_1 = 45°$, $\phi_2 = 90°$, $R = 500$ mm, $h_1 = h_2 = 30$ mm
(b) $\phi_1 = 20°$, $\phi_2 = 40°$, $R = 500$ mm, $h_1 = h_2 = 30$ mm
(c) $\phi_1 = 20°$, $\phi_2 = 90°$, $R = 500$ mm, $h_1 = h_2 = 30$ mm
(d) $\phi_1 = 20°$, $\phi_2 = 90°$, $R = 500$ mm, $h_1 = 30$ mm, $h_2 = 10$ mm

C2.12 Problem C2.11 can be repeated with either end or both ends simply supported. Uniform or nonuniform temperature change can be applied. Additional loadings may include prescribed zero or nonzero values of translational and/or rotational d.o.f. at one end.

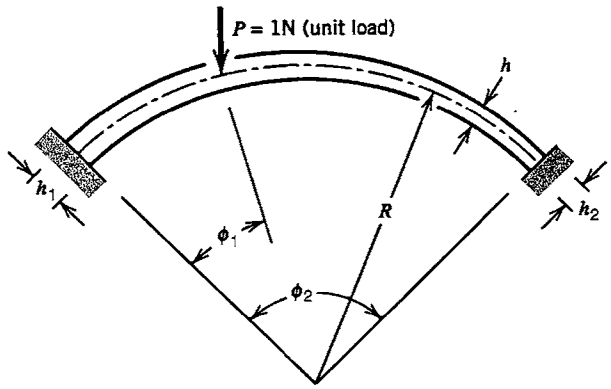

Problem C2.11

C2.13 Uniform pipes, each fixed at one end, lie in a horizontal *xy* plane and intersect at right angles, where they are welded together (see sketch). A steel rod *BD* of cross-sectional area 100 mm^2 connects *B* to fixed support *D*. The pipes have the hollow circular cross section shown. All members are steel. Determine the largest deflections and largest stresses in each member.

(a) Omit pipe *AB*, so that only pipe *BC* is present, supported by hanger *BD*.

(b) Include both pipes and hanger *BD* in the analysis.

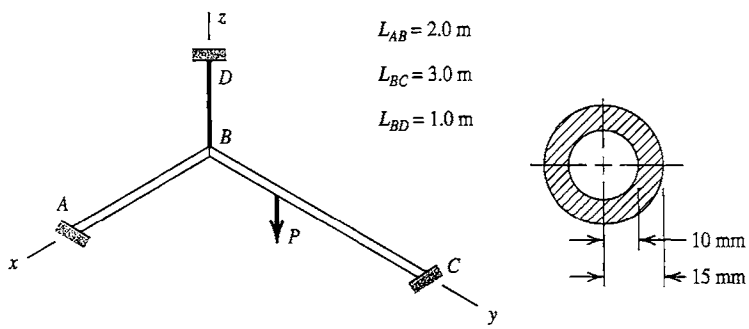

Problem C2.13

C2.14 Apply loading directed normal to the plane of the structure analyzed in Problem C2.4. Load(s) may be applied to joints or to members between joints. Let members have a circular cross section.

C2.15 Use the structure geometry described in Problem C2.11, but orient load *P* so that it acts normal to the plane of the figure. Let *h* represent the diameter of a solid circular cross section. Alternative loadings and support conditions suggested in Problem C2.12 may also be addressed. End loading may include torque or prescribed angle of twist.

CHAPTER 3

BASIC ELEMENTS

Most elements in common use are displacement-based. This chapter discusses interpolation and simple elements based on displacement fields, and shows how their stiffness matrices are formulated. Additional formulation procedures, and similar elements of more general shape, are discussed in subsequent chapters.

An understanding of element displacement fields, and especially of shortcomings an element may have because of its displacement field, is needed in order to prepare a good FE model and to properly check computed results.

3.1 PRELIMINARIES

Few elements can be formulated using the direct method, as applied to bars and beams in Chapter 2. In general, formulation of elements for structural mechanics relies on long-established tools of stress analysis, including stress-strain relations, strain-displacement relations, and energy considerations [3.1]. In this chapter we state formulas in rectangular Cartesian coordinates. Analogous formulas in polar and cylindrical coordinates are stated where needed. Formulations for problems other than structural mechanics appear in subsequent chapters.

Stress-Strain Relations. Let $\{\boldsymbol{\sigma}\}$ be the array of stresses and $\{\boldsymbol{\varepsilon}\}$ the array of strains. Subscripts zero indicate initial values. Constitutive matrix $[\mathbf{E}]$ contains elastic constants. For linearly elastic conditions, stress-strain relations can be stated in the matrix forms

$$\{\boldsymbol{\sigma}\} = [\mathbf{E}]\{\boldsymbol{\varepsilon}\} + \{\boldsymbol{\sigma}_0\} \quad \text{or} \quad \{\boldsymbol{\sigma}\} = [\mathbf{E}](\{\boldsymbol{\varepsilon}\} - \{\boldsymbol{\varepsilon}_0\})$$
$$\text{where} \quad \{\boldsymbol{\sigma}_0\} = -[\mathbf{E}]\{\boldsymbol{\varepsilon}_0\} \tag{3.1-1}$$

This relation is valid in one, two, or three dimensions. For a uniaxial stress state, with no initial stress, it is simply $\sigma = E\varepsilon$, where E is the elastic modulus. In two dimensions, with x and y as the in-plane coordinates, Eq. 3.1-1 is

Stresses = Constitutive matrix × Strains + Initial stresses

$$\begin{Bmatrix} \sigma_x \\ \sigma_y \\ \tau_{xy} \end{Bmatrix} = \begin{bmatrix} E_{11} & E_{12} & E_{13} \\ E_{21} & E_{22} & E_{23} \\ E_{31} & E_{32} & E_{33} \end{bmatrix} \begin{Bmatrix} \varepsilon_x \\ \varepsilon_y \\ \gamma_{xy} \end{Bmatrix} + \begin{Bmatrix} \sigma_{x0} \\ \sigma_{y0} \\ \tau_{xy0} \end{Bmatrix} \tag{3.1-2}$$

Constitutive matrix [**E**] is symmetric; $E_{ij} = E_{ji}$. [**E**] can represent isotropic or anisotropic material properties. For isotropy and plane stress conditions ($\sigma_z = \tau_{yz} = \tau_{zx} = 0$), [**E**] and its inverse are

$$[\mathbf{E}] = \frac{E}{1-\nu^2}\begin{bmatrix} 1 & \nu & 0 \\ \nu & 1 & 0 \\ 0 & 0 & (1-\nu)/2 \end{bmatrix} \qquad [\mathbf{E}]^{-1} = \begin{bmatrix} 1/E & -\nu/E & 0 \\ -\nu/E & 1/E & 0 \\ 0 & 0 & 1/G \end{bmatrix} \tag{3.1-3}$$

where ν is Poisson's ratio and $G = 0.5E/(1+\nu)$ is the shear modulus. (For plane *strain* conditions, namely $\varepsilon_z = \gamma_{yz} = \gamma_{zx} = 0$, see Eq. 3.4-11). Inverting Eq. 3.1-1, we obtain

General form:

$$\{\boldsymbol{\varepsilon}\} = [\mathbf{E}]^{-1}\{\boldsymbol{\sigma}\} + \{\boldsymbol{\varepsilon}_0\}$$

For isotropy and plane stress conditions:

$$\begin{aligned} \varepsilon_x &= \sigma_x/E - \nu\sigma_y/E + \varepsilon_{x0} \\ \varepsilon_y &= -\nu\sigma_x/E + \sigma_y/E + \varepsilon_{y0} \\ \gamma_{xy} &= \tau_{xy}/G + \gamma_{xy0} \end{aligned} \tag{3.1-4}$$

Initial strains $\{\boldsymbol{\varepsilon}_0\}$ may have various causes, including temperature change and swelling due to moisture or radiation. If convenient, in order to account for initial effects from the simultaneous action of two or more sources, $\{\boldsymbol{\varepsilon}_0\}$ and $\{\boldsymbol{\sigma}_0\}$ can both appear in the stress-strain relation. If the material is isotropic and initial strains are produced by temperature change T, then $\varepsilon_{x0} = \varepsilon_{y0} = \alpha T$ and $\gamma_{xy0} = 0$, where α is the coefficient of thermal expansion, here assumed to be independent of temperature. Temperature T is measured relative to a reference temperature, perhaps room temperature, at which the body may be regarded as free of stress.

In three dimensions, [**E**] is a symmetric 6 by 6 array that relates stresses $\{\boldsymbol{\sigma}\} = \lfloor \sigma_x \;\; \sigma_y \;\; \sigma_z \;\; \tau_{xy} \;\; \tau_{yz} \;\; \tau_{zx} \rfloor^T$ and strains $\{\boldsymbol{\varepsilon}\} = \lfloor \varepsilon_x \;\; \varepsilon_y \;\; \varepsilon_z \;\; \gamma_{xy} \;\; \gamma_{yz} \;\; \gamma_{zx} \rfloor^T$. For the case of isotropy and initial strains caused by temperature change T, nonzero entries in [**E**] and $\{\boldsymbol{\varepsilon}_0\}$ are

$$\begin{aligned} E_{11} = E_{22} = E_{33} &= (1-\nu)c & \varepsilon_{x0} &= \alpha T \\ E_{44} = E_{55} = E_{66} &= G & \varepsilon_{y0} &= \alpha T \\ E_{12} = E_{21} = E_{13} = E_{31} = E_{23} = E_{32} &= \nu c & \varepsilon_{z0} &= \alpha T \end{aligned} \tag{3.1-5a}$$

$$\text{where} \quad c = \frac{E}{(1+\nu)(1-2\nu)} \quad \text{and} \quad G = \frac{E}{2(1+\nu)} \tag{3.1-5b}$$

Analogous coefficients for an orthotropic material are stated in Eqs. 10.5-1.

Temperature may vary from one part of a body to another, and it may happen that material properties are temperature-dependent. Then [**E**] must contain terms appropriate to the temperature at the location where [**E**] is used. And, if α is a function of temperature, αT must be replaced by $\alpha_{\text{ave}}T$, so that $\alpha_{\text{ave}}T$ is equal to the integral of $\alpha\, dT$ over the temperature range imposed. If material properties are *stress*-dependent, the problem is nonlinear (see Chapter 17).

Strain-Displacement Relations. A displacement field describes how a body deforms as well as how it displaces. Strain-displacement relations extract the strain field contained in a displacement field and play a prominent role in formulating commonly used elements.

To obtain formulas, we use engineering definitions of strain. *Normal strain* is change in length divided by original length; *shear strain* is the amount of change in a right angle. Deformations shown in Fig. 3.1-1 provide formulas shown for strains ε_x, ε_y, and γ_{xy} in the xy plane. In general, x-direction displacement u and y-direction displacement v are functions of the coordinates; $u = u(x,y)$ and $v = v(x,y)$. Therefore, we must use partial derivatives. Doing so, and letting Δx and Δy approach zero, we obtain the *two-dimensional strain-displacement relations*

$$\varepsilon_x = \frac{\partial u}{\partial x} \qquad \varepsilon_y = \frac{\partial v}{\partial y} \qquad \gamma_{xy} = \frac{\partial u}{\partial y} + \frac{\partial v}{\partial x} \tag{3.1-6}$$

Subsequently it will be convenient to use a comma to denote partial differentiation with respect to the subscript that follows. In this notation, Eqs. 3.1-6 are

$$\varepsilon_x = u_{,x} \qquad \varepsilon_y = v_{,y} \qquad \gamma_{xy} = u_{,y} + v_{,x} \tag{3.1-7}$$

In *three* dimensions, displacements in coordinate directions x, y, and z are $u = u(x,y,z)$, $v = v(x,y,z)$, and $w = w(x,y,z)$, and Eqs. 3.1-7 are supplemented by the relations

$$\varepsilon_z = w_{,z} \qquad \gamma_{yz} = v_{,z} + w_{,y} \qquad \gamma_{zx} = w_{,x} + u_{,z} \tag{3.1-8}$$

In matrix operator format, for 2D and 3D cases respectively, the strain-displacement relations are

$$\begin{Bmatrix} \varepsilon_x \\ \varepsilon_y \\ \gamma_{xy} \end{Bmatrix} = \begin{bmatrix} \dfrac{\partial}{\partial x} & 0 \\ 0 & \dfrac{\partial}{\partial y} \\ \dfrac{\partial}{\partial y} & \dfrac{\partial}{\partial x} \end{bmatrix} \begin{Bmatrix} u \\ v \end{Bmatrix} \qquad \begin{Bmatrix} \varepsilon_x \\ \varepsilon_y \\ \varepsilon_z \\ \gamma_{xy} \\ \gamma_{yz} \\ \gamma_{zx} \end{Bmatrix} = \begin{bmatrix} \dfrac{\partial}{\partial x} & 0 & 0 \\ 0 & \dfrac{\partial}{\partial y} & 0 \\ 0 & 0 & \dfrac{\partial}{\partial z} \\ \dfrac{\partial}{\partial y} & \dfrac{\partial}{\partial x} & 0 \\ 0 & \dfrac{\partial}{\partial z} & \dfrac{\partial}{\partial y} \\ \dfrac{\partial}{\partial z} & 0 & \dfrac{\partial}{\partial x} \end{bmatrix} \begin{Bmatrix} u \\ v \\ w \end{Bmatrix} \tag{3.1-9}$$

Symbolically, for both of Eqs. 3.1-9 and for strain-displacement relations in general, we write

$$\{\boldsymbol{\varepsilon}\} = [\partial]\{\mathbf{u}\} \tag{3.1-10}$$

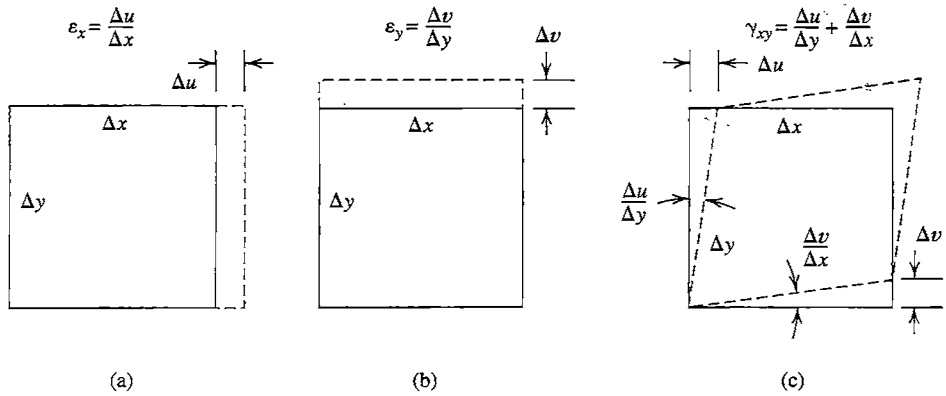

Figure 3.1-1. An infinitesimal rectangle, subjected to (a) x-direction normal strain, (b) y-direction normal strain, and (c) shear strain.

Compatibility. When a body is deformed without breaking, no cracks appear in stretching, no kinks appear in bending, and material particles do not interpenetrate. Stated more elegantly, the *compatibility condition* requires that displacements be continuous and single-valued functions of position.

In a plane problem, the *compatibility equation* is $\varepsilon_{x,yy} + \varepsilon_{y,xx} = \gamma_{xy,xy}$ [3.1,3.2]. This equation states the relation among strains that must exist if the compatibility condition is to be satisfied. There are additional equations for a three-dimensional problem. Arbitrarily assumed expressions for ε_x, ε_y, and γ_{xy} may not satisfy the compatibility equation, but arbitrarily assumed displacement fields are certain to satisfy it, provided they are single-valued and continuous, as may be verified by substituting Eqs. 3.1-6 into the compatibility equation. One reason for the widespread use of displacement-based finite elements, which use assumed polynomials as displacement fields, is the ease with which compatibility can be satisfied. ?

Equilibrium Equations. Figure 3.1-2a shows stresses that act on a differential element in a two-dimensional problem. In rectangular Cartesian coordinates, we now develop equations stating that the differential element is in equilibrium under forces applied to it. Forces come from stresses on the sides and from body forces.

Body forces, F_x and F_y in x and y directions respectively, are defined as forces per unit volume, positive when acting in positive coordinate directions. Body forces can be produced by gravity, acceleration, a magnetic field, and so on. On each differential element of volume ($dV = t\,dx\,dy$, where t = thickness), F_x and F_y produce differential forces $F_x\,dV$ and $F_y\,dV$. In general, body forces and stresses are functions of the coordinates. Thus, for example, $\sigma_{x,x}$ is the *rate* of change and $\sigma_{x,x}\,dx$ is the *amount* of change in σ_x over distance dx. For uniform thickness t, static equilibrium of forces in the x direction requires that

$$-\sigma_x t\,dy - \tau_{xy} t\,dx + (\sigma_x + \sigma_{x,x}\,dx)t\,dy + (\tau_{xy} + \tau_{xy,y}\,dy)t\,dx + F_x t\,dx\,dy = 0 \qquad (3.1\text{-}11)$$

There is a corresponding y-direction equation of equilibrium. After simplification, the *differential equations of equilibrium* for a plane (2D) problem are as follows. For reference, analogous equations for a solid (3D) problem are also stated here.

$$
\begin{array}{lll}
 & \text{2D:} & \text{3D:} \\
x \text{ direction:} & \sigma_{x,x} + \tau_{xy,y} + F_x = 0 & \sigma_{x,x} + \tau_{xy,y} + \tau_{zx,z} + F_x = 0 \\
y \text{ direction:} & \tau_{xy,x} + \sigma_{y,y} + F_y = 0 & \tau_{xy,x} + \sigma_{y,y} + \tau_{yz,z} + F_y = 0 \\
z \text{ direction:} & \text{(not used)} & \tau_{zx,x} + \tau_{yz,y} + \sigma_{z,z} + F_z = 0
\end{array}
\tag{3.1-12}
$$

Although derived for static conditions, Eqs. 3.1-12 can also be used if acceleration is present, provided that F_x, F_y, and F_z include d'Alembert or "effective" body forces per unit volume. For example, if there is x-direction acceleration a_x, then F_x must include the inertial force term $-\rho a_x$, where ρ is the mass density. Whether in two dimensions or three, equilibrium equations can be symbolized as

$$[\partial]^T\{\boldsymbol{\sigma}\} + \{\mathbf{F}\} = \{\mathbf{0}\} \tag{3.1-13}$$

where $[\partial]$ is given in Eqs. 3.1-9 and, in 2D and 3D rectangular Cartesian coordinates respectively, $\{\mathbf{F}\}$ is $\lfloor F_x \quad F_y \rfloor^T$ or $\lfloor F_x \quad F_y \quad F_z \rfloor^T$.

Boundary Conditions. Boundary conditions include prescriptions of displacements or stresses on sides or surfaces of a body. For example, in the plane problem of Fig. 3.1-2b, the rigid support implies that $u = v = 0$ along the left side. Stress boundary conditions prevail along the remaining sides: $\tau_{xy} = 0$ and $\sigma_y = -p$ along the top side, $\sigma_x = 0$ and $\tau_{xy} = 0$ along the right side, and $\sigma_n = 0$ and $\tau_{ns} = 0$ along the bottom side.

In general, distributed load can act tangent to a boundary as well as normal to it. On any boundary, including one not perpendicular to a coordinate axis, normal and tangential loads can be expressed as *surface tractions,* which are forces per unit of surface area, directed parallel to the coordinate axes. In rectangular Cartesian coordinates xyz, surface tractions $\{\boldsymbol{\Phi}\}$ are

$$\{\boldsymbol{\Phi}\} = \begin{Bmatrix} \Phi_x \\ \Phi_y \\ \Phi_z \end{Bmatrix} \qquad \text{where} \qquad \begin{aligned} \Phi_x &= l\sigma_x + m\tau_{xy} + n\tau_{zx} \\ \Phi_y &= l\tau_{xy} + m\sigma_y + n\tau_{yz} \\ \Phi_z &= l\tau_{zx} + m\tau_{yz} + n\sigma_z \end{aligned} \tag{3.1-14}$$

in which l, m, and n are direction cosines of a vector normal to the surface. When Eqs. 3.1-14 are satisfied, each differential element of the surface is in equilibrium under the action of surface tractions and internal stresses (evaluated at the surface). Such is also the case on a portion of the boundary where displacements rather than tractions are prescribed, but tractions applied by a support are not known *a priori* and are usually not calculated in the course of a solution. ?

Exact and Approximate Solutions. An exact solution must satisfy compatibility, equilibrium, and boundary conditions. For example, if we begin with a compatible displacement field, we can obtain strains from Eq. 3.1-10 and then stresses from Eq. 3.1-1. If these stresses satisfy Eq. 3.1-13 at every point throughout the volume of a body, and all boundary conditions are satisfied, then we have obtained the exact solution of the mathematical model (which is subject to basic assumptions such as linearity of the stress-strain relation and smallness of displacements). This is easy to say but difficult to do. Exact solutions are known only for simple combinations of geometry, loading, and support conditions.

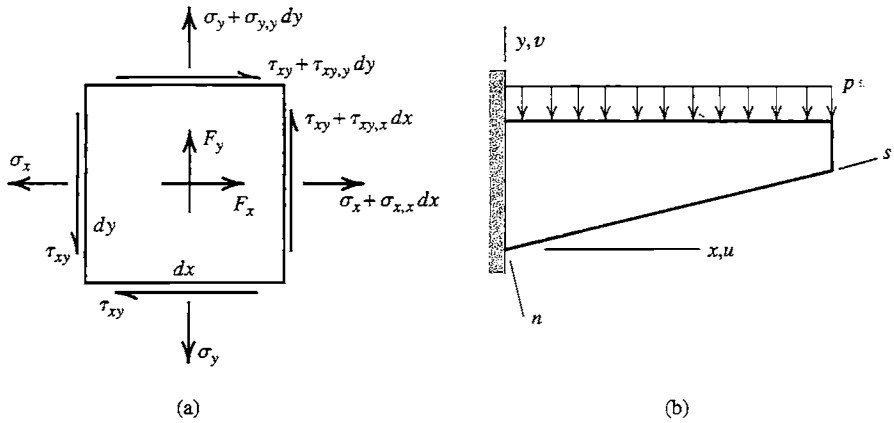

Figure 3.1-2. (a) Stresses and body forces that act on a plane differential element of uniform thickness. (b) Tapered cantilever beam with pressure p on its top surface.

Finite elements based on displacement fields do not satisfy equilibrium conditions at every material point. Instead, displacement-based elements satisfy Eqs. 3.1-13 and 3.1-14 in an integral or average sense. The matter is more fully explained in Chapters 4 and 5, where generally applicable methods of formulating approximate solutions are discussed.

Other Problems. The foregoing formulas of structural mechanics have counterparts in other areas. Details appear as needed in subsequent chapters. Here we briefly compare basic equations of structural mechanics and heat conduction. First we note that heat conduction is a *scalar* problem because the field quantity, temperature T, has no direction associated with it. In contrast, the displacement field of structural mechanics is a vector field having components in coordinate directions. The following list is for static (steady-state) conditions:

Quantity	Structural mechanics	Heat conduction
Independent variables	Coordinates x, y, z	Coordinates x, y, z
Dependent variable(s)	Displacements u, v, w	Temperature T
Field gradient	Strains $\varepsilon_x, \varepsilon_y, \gamma_{xy}$, etc.	$\{\nabla T\} = \lfloor T_{,x} \quad T_{,y} \quad T_{,z} \rfloor^T$
Constitutive matrix	Elastic constants $[\mathbf{E}]$	Thermal conductivities $[\boldsymbol{\kappa}]$
Induced field	Stresses $\{\boldsymbol{\sigma}\} = [\mathbf{E}]\{\boldsymbol{\varepsilon}\}$	Heat fluxes $\{\mathbf{f}\} = -[\boldsymbol{\kappa}]\{\nabla T\}$
Surface load	Tractions $\{\boldsymbol{\Phi}\}$ on boundary	Normal flux f_n at a boundary
Internal load	Body forces F_x, F_y, F_z	Internal heat generation Q
Equilibrium equation	$[\partial]^T\{\boldsymbol{\sigma}\} + \{\mathbf{F}\} = \{\mathbf{0}\}$	$f_{x,x} + f_{y,y} + f_{z,z} - Q = 0$

3.2 INTERPOLATION AND SHAPE FUNCTIONS

To *interpolate* is to devise a continuous function that satisfies prescribed conditions at a finite number of points. In FEA, the points are nodes of an element, and the prescribed

conditions are nodal values of a field quantity (and perhaps its derivatives as well). Nodal values are rarely exact, and even when they are, interpolation generally provides approximate values at other locations. In FEA, the interpolating function is almost always a polynomial, which automatically provides a single-valued and continuous field.

In terms of generalized d.o.f. a_i, an interpolating polynomial with dependent variable ϕ and independent variable x can be written in the form

$$\phi = \sum_{i=0}^{n} a_i x^i \qquad \text{or} \qquad \phi = \lfloor \mathbf{X} \rfloor \{\mathbf{a}\} \tag{3.2-1a}$$

in which

$$\lfloor \mathbf{X} \rfloor = \begin{bmatrix} 1 & x & x^2 & & x^n \end{bmatrix} \quad \text{and} \quad \{\mathbf{a}\} = \begin{bmatrix} a_0 & a_1 & a_2 & & a_n \end{bmatrix}^T \tag{3.2-1b}$$

where $n = 1$ for linear interpolation, $n = 2$ for quadratic interpolation, and so on. The a_i can be expressed in terms of nodal values of ϕ, which appear at known values of x. The relation between nodal values $\{\boldsymbol{\phi}_e\}$ and the a_i is symbolized as

$$\{\boldsymbol{\phi}_e\} = [\mathbf{A}]\{\mathbf{a}\} \tag{3.2-2}$$

where each row of $[\mathbf{A}]$ is $\lfloor \mathbf{X} \rfloor$ evaluated at the appropriate nodal location (examples follow). From Eqs. 3.2-1 and 3.2-2 we obtain

$$\phi = \lfloor \mathbf{N} \rfloor \{\boldsymbol{\phi}_e\} \qquad \text{where} \qquad \lfloor \mathbf{N} \rfloor = \lfloor \mathbf{X} \rfloor [\mathbf{A}]^{-1} = \begin{bmatrix} N_1 & N_2 & \cdots \end{bmatrix} \tag{3.2-3}$$

An individual N_i in matrix $\lfloor \mathbf{N} \rfloor$ is called a *shape function.* The name *basis function* is sometimes used instead. Each N_i states the interpolated $\phi = \phi(x)$ when the corresponding ϕ_i is unity and all other ϕ_i are zero. In FEA, assembly of elements causes element nodal values $\{\boldsymbol{\phi}_e\}$ to appear in $\{\mathbf{D}\}$, the global vector of d.o.f. Thus, in FEA, $\{\boldsymbol{\phi}_e\}$ for each element is determined by solving global equations $[\mathbf{K}]\{\mathbf{D}\} = \{\mathbf{R}\}$.

Degree of Continuity. Field quantity ϕ is interpolated in piecewise fashion over an FE mesh. That is, each "interpolation piece" is defined only within its element. So while ϕ can be guaranteed to vary smoothly *within* each element, the transition *between* elements may not be smooth. The symbol C^m is used to describe the continuity of a piecewise field. A field is C^m continuous if its derivatives up to and including degree m are interelement-continuous. Thus, in one dimension, $\phi = \phi(x)$ is C^0 continuous if ϕ is continuous but $\phi_{,x}$ is not, and $\phi = \phi(x)$ is C^1 continuous if both ϕ and $\phi_{,x}$ are continuous but $\phi_{,xx}$ is not. These two cases are illustrated in Fig. 3.2-1, where $x = a$ represents an interelement boundary. In general, it is necessary that derivatives of ϕ of order m be included as nodal d.o.f. if field ϕ is to be C^m continuous.

The C^m terminology is also applied to element types. In Chapter 2 we encountered the bar element and the beam element, which are types of "C^0 element" and "C^1 element" respectively. Usually, C^0 elements are used to model plane and solid bodies. C^1 elements are used to model beams, plates, and shells, thus providing interelement continuity of slope. !?

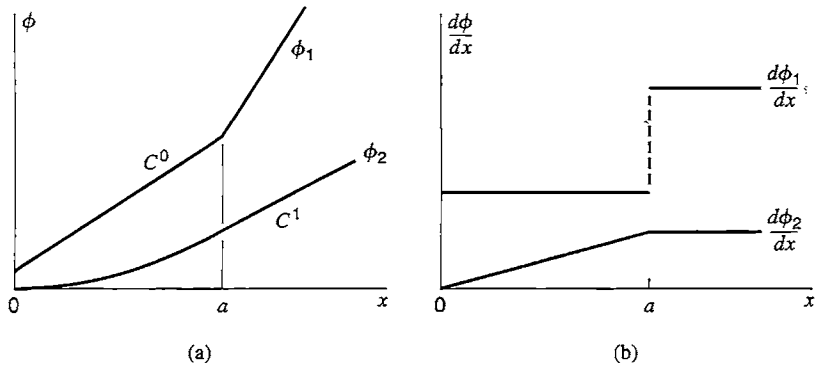

Figure 3.2-1. Function ϕ_1 is C^0 continuous. Function ϕ_2 is C^1 continuous.

C^0 Interpolation. We begin with linear interpolation between points (x_1,ϕ_1) and (x_2,ϕ_2), for which $\lfloor \mathbf{X} \rfloor = \lfloor 1 \quad x \rfloor$ in Eq. 3.2-1. Evaluating $\lfloor \mathbf{X} \rfloor$ at points 1 and 2, we obtain

$$\begin{Bmatrix} \phi_1 \\ \phi_2 \end{Bmatrix} = [\mathbf{A}] \begin{Bmatrix} a_0 \\ a_1 \end{Bmatrix} \qquad \text{where} \qquad [\mathbf{A}] = \begin{bmatrix} 1 & x_1 \\ 1 & x_2 \end{bmatrix} \tag{3.2-4}$$

Inverting $[\mathbf{A}]$ and using Eq. 3.2-3, we obtain

$$[\mathbf{A}]^{-1} = \frac{1}{x_2 - x_1} \begin{bmatrix} x_2 & -x_1 \\ -1 & 1 \end{bmatrix} \qquad \text{and} \qquad \lfloor \mathbf{N} \rfloor = \begin{bmatrix} \dfrac{x_2 - x}{x_2 - x_1} & \dfrac{x - x_1}{x_2 - x_1} \end{bmatrix} \tag{3.2-5}$$

The two linear shape functions N_1 and N_2 are shown in Fig. 3.2-2a. This example displays the simplest interpolation used in FEA. In formulating properties of a two-node element of length L, we will use $x_1 = 0$, $x_2 = L$, and nodal d.o.f. ϕ_1 and ϕ_2.

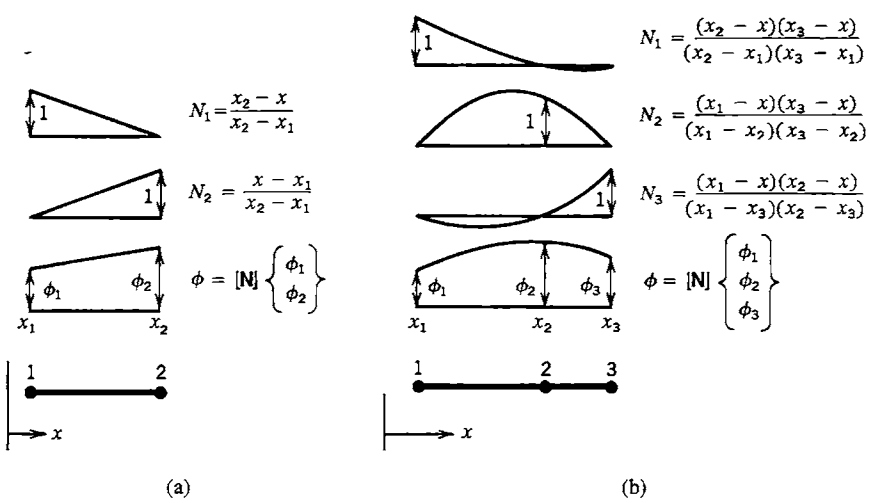

Figure 3.2-2. (a) Linear interpolation and shape functions. (b) Quadratic interpolation and shape functions.

Quadratic interpolation fits a parabola to the points (x_1,ϕ_1), (x_2,ϕ_2), and (x_3,ϕ_3). These points need not be equidistant. Now $\lfloor \mathbf{X} \rfloor = \lfloor 1 \quad x \quad x^2 \rfloor$, and Eq. 3.2-2 becomes

$$\begin{Bmatrix} \phi_1 \\ \phi_2 \\ \phi_3 \end{Bmatrix} = [\mathbf{A}] \begin{Bmatrix} a_0 \\ a_1 \\ a_2 \end{Bmatrix} \qquad \text{where} \qquad [\mathbf{A}] = \begin{bmatrix} 1 & x_1 & x_1^2 \\ 1 & x_2 & x_2^2 \\ 1 & x_3 & x_3^2 \end{bmatrix} \tag{3.2-6}$$

Equation 3.2-3 yields $\lfloor \mathbf{N} \rfloor$, whose individual shape functions are shown in Fig. 3.2-2b.

Results shown in Fig. 3.2-2 can be regarded as particular instances of *Lagrange's interpolation formula,* which provides the following shape functions for a curve fitted to ordinates at n points.

$$N_1 = \frac{(x_2-x)(x_3-x)\cdots(x_n-x)}{(x_2-x_1)(x_3-x_1)\cdots(x_n-x_1)}, \qquad N_2 = \frac{(x_1-x)(x_3-x)\cdots(x_n-x)}{(x_1-x_2)(x_3-x_2)\cdots(x_n-x_2)}, \qquad \text{etc.} \tag{3.2-7a}$$

or more generally

$$N_k = \frac{(x_1-x)(x_2-x)\cdots[x_k-x]\cdots(x_n-x)}{(x_1-x_k)(x_2-x_k)\cdots[x_k-x_k]\cdots(x_n-x_k)} \tag{3.2-7b}$$

in which the bracketed terms are omitted to obtain the kth shape function. For linear interpolation, N's and x's having subscripts greater than 2 do not appear; for quadratic interpolation, N's and x's having subscripts greater than 3 do not appear; and so on. The foregoing shape functions have the following characteristics:

- All shape functions N_i, along with function ϕ itself, are polynomials of the same degree.
- For any shape function N_i, $N_i = 1$ when $x = x_i$ and $N_i = 0$ when $x = x_j$ for any integer $j \neq i$. That is, N_i is unity at its own node but is zero at other nodes.
- C^0 shape functions sum to unity; that is, $\sum N_i = 1$. This conclusion is implied by Eq. 3.2-3, because we must obtain $\phi = 1$ when $\{\boldsymbol{\phi}_e\}$ is a column of 1's.

Lagrange's interpolation formula uses only ordinates ϕ_i in fitting a curve. Slope information is not used, so Lagrange interpolation may display slopes at nodes other than those desired (see Fig. 3.2-3a). Use of both ordinate and slope information in curve fitting, sometimes called *Hermitian* interpolation, is described as follows.

C^1 Interpolation. Consider a cubic curve $\phi = \phi(x)$, whose shape is determined by four data items. We take these items to be ordinates ϕ_i and small slopes $(d\phi/dx)_i$ at either end of a line of length L, as shown in Fig. 3.2-3b. Now $\lfloor \mathbf{X} \rfloor = \lfloor 1 \quad x \quad x^2 \quad x^3 \rfloor$, and upon evaluating ϕ and $\phi_{,x}$ at $x = 0$ and at $x = L$, Eq. 3.2-2 becomes

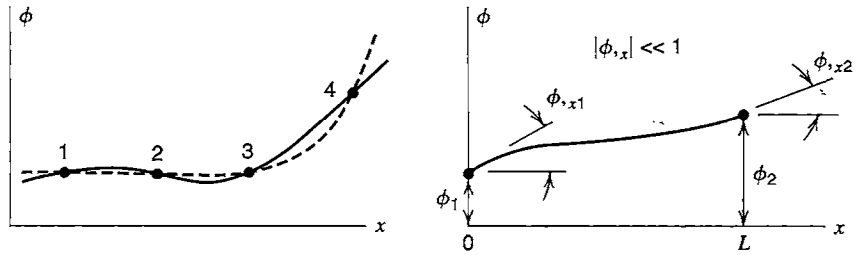

(a) (b)

Figure 3.2-3. (a) The solid line is a C^0 cubic interpolation fitted to ordinates of four points on the dashed line. (b) A cubic interpolation curve based on ordinate and slope information at end points.

$$\begin{Bmatrix} \phi_1 \\ \phi_{,x1} \\ \phi_2 \\ \phi_{,x2} \end{Bmatrix} = [\mathbf{A}] \begin{Bmatrix} a_0 \\ a_1 \\ a_2 \\ a_3 \end{Bmatrix} \qquad \text{where} \qquad [\mathbf{A}] = \begin{bmatrix} 1 & 0 & 0 & 0 \\ 0 & 1 & 0 & 0 \\ 1 & L & L^2 & L^3 \\ 0 & 1 & 2L & 3L^2 \end{bmatrix} \tag{3.2-8}$$

The four shape functions produced by Eq. 3.2-3 turn out to be the four lateral displacement nodes of a beam shown in Fig. 2.3-1. These shape functions are repeated in Fig. 3.2-4, where their behavior at end points is listed. In Section 3.3 we illustrate how these shape functions can be used to generate the stiffness matrix of a beam element.

2D and 3D Interpolation. Interpolations described thus far use a single independent variable. In two- or three-dimensional problems, two or three independent variables are needed. These interpolations are extensions of one-dimensional interpolations and are described where they are used. When there are two or three *dependent* variables, such as displacement components in 2D or 3D problems, usually all components are interpolated using the same shape functions, as we will see shortly.

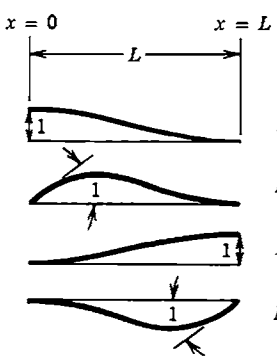

	At $x = 0$		At $x = L$	
	N_i	$N_{i,x}$	N_i	$N_{i,x}$
$N_1 = 1 - \frac{3x^2}{L^2} + \frac{2x^3}{L^3}$	1	0	0	0
$N_2 = x - \frac{2x^2}{L} + \frac{x^3}{L^2}$	0	1	0	0
$N_3 = \frac{3x^2}{L^2} - \frac{2x^3}{L^3}$	0	0	1	0
$N_4 = -\frac{x^2}{L} + \frac{x^3}{L^2}$	0	0	0	1

Figure 3.2-4. Shape functions of a cubic curve fitted to ordinates and slopes at $x = 0$ and $x = L$.

3.3 FORMULAS FOR ELEMENT MATRICES

In this section we use the principle of virtual work to obtain formulas for the element stiffness matrix and for load vectors associated with initial strains, body forces, and surface tractions. These results apply to commonly used elements, which are based on interpolation of displacements from nodal d.o.f. The same results can be obtained by alternative methods discussed in Chapters 4 and 5 that yield further insight into the nature of FEA and permit its extension to problems other than structural mechanics. The virtual work approach provides essential formulas without requiring much mathematics.

A *virtual displacement* is an imaginary and very small change in the configuration of a system. For analysis purposes we imagine that a virtual displacement takes place relative to the equilibrium configuration (when all loads have been fully applied), and that the displacement is admissible. An *admissible displacement* does not violate compatibility or displacement boundary conditions. Neither loads nor stresses are altered by a virtual displacement. The *principle of virtual work,* also known as the *principle of virtual displacements,* can be stated in the form [3.2]

?

$$\int \{\delta\boldsymbol{\varepsilon}\}^T\{\boldsymbol{\sigma}\}\, dV = \int \{\delta\mathbf{u}\}^T\{\mathbf{F}\}\, dV + \int \{\delta\mathbf{u}\}^T\{\boldsymbol{\Phi}\}\, dS \tag{3.3-1}$$

Here $\{\delta\boldsymbol{\varepsilon}\}$ is the vector of strains produced by Eqs. 3.1-9 and virtual displacement $\{\delta\mathbf{u}\}$, where $\{\delta\mathbf{u}\} = \lfloor \delta u \quad \delta v \quad \delta w \rfloor^T$. The symbol δ has the same meaning as d for differential, but by convention δ is used when displacements are virtual. In words, Eq. 3.3-1 says that for any quasistatic and admissible virtual displacement $\{\delta\mathbf{u}\}$ from an equilibrium configuration, the increment of strain energy stored is equal to the increment of work done by body forces $\{\mathbf{F}\}$ in volume V and surface tractions $\{\boldsymbol{\Phi}\}$ on surface S.

Equation 3.3-1 can also be obtained by multiplying the left-hand sides of the equilibrium equations, Eq. 3.1-13, by $\{\delta\mathbf{u}\}^T$, integrating over the volume, and using integration by parts to change the form. This approach, described in the latter part of Section 4.7, makes plausible the statement that displacement-based finite elements satisfy differential equations of equilibrium in an average or integral sense.

Let displacements $\{\mathbf{u}\}$ be interpolated over an element in the same way as ϕ in Eq. 3.2-3, that is

$$\{\mathbf{u}\} = [\mathbf{N}]\{\mathbf{d}\} \qquad \text{where} \qquad \{\mathbf{u}\} = \lfloor u \quad v \quad w \rfloor^T \tag{3.3-2}$$

and $\{\mathbf{d}\}$ lists the nodal displacement d.o.f. of an element. Examples appear in subsequent sections. Strains are determined from displacements according to Eq. 3.1-10; that is $\{\boldsymbol{\varepsilon}\} = [\partial]\{\mathbf{u}\}$. Hence

$$\{\boldsymbol{\varepsilon}\} = [\mathbf{B}]\{\mathbf{d}\} \qquad \text{where} \qquad [\mathbf{B}] = [\partial][\mathbf{N}] \tag{3.3-3}$$

Matrix $[\mathbf{B}]$ is called the *strain-displacement matrix.* From Eqs. 3.3-2 and 3.3-3 we obtain

$$\{\delta\mathbf{u}\}^T = \{\delta\mathbf{d}\}^T[\mathbf{N}]^T \qquad \text{and} \qquad \{\delta\boldsymbol{\varepsilon}\}^T = \{\delta\mathbf{d}\}^T[\mathbf{B}]^T \tag{3.3-4}$$

From Eq. 3.1-1 (the stress-strain relation, now including both initial strain and initial stress for the sake of generality), and Eqs. 3.3-1, 3.3-3, and 3.3-4, we obtain

$$\{\delta\mathbf{d}\}^T\left(\int [\mathbf{B}]^T[\mathbf{E}][\mathbf{B}]\,dV\,\{\mathbf{d}\} - \int [\mathbf{B}]^T[\mathbf{E}]\{\boldsymbol{\varepsilon}_0\}\,dV + \int [\mathbf{B}]^T\{\boldsymbol{\sigma}_0\}\,dV\right.$$
$$\left. - \int [\mathbf{N}]^T\{\mathbf{F}\}\,dV - \int [\mathbf{N}]^T\{\boldsymbol{\Phi}\}\,dS\right) = 0 \tag{3.3-5}$$

Vectors $\{\delta\mathbf{d}\}$ and $\{\mathbf{d}\}$ do not appear within integrals because they are not functions of the coordinates. Equation 3.3-5 must be true for *any* admissible virtual displacement $\{\delta\mathbf{d}\}$ from the equilibrium configuration. Therefore Eq. 3.3-5 yields

$$[\mathbf{k}]\{\mathbf{d}\} = \{\mathbf{r}_e\} \tag{3.3-6}$$

where the element stiffness matrix is

$$[\mathbf{k}] = \int [\mathbf{B}]^T[\mathbf{E}][\mathbf{B}]\,dV \tag{3.3-7}$$

and the vector of loads applied to structure nodes by elements, due to all sources but element deformation, is

$$\{\mathbf{r}_e\} = \int [\mathbf{N}]^T\{\mathbf{F}\}\,dV + \int [\mathbf{N}]^T\{\boldsymbol{\Phi}\}\,dS + \int [\mathbf{B}]^T[\mathbf{E}]\{\boldsymbol{\varepsilon}_0\}\,dV - \int [\mathbf{B}]^T\{\boldsymbol{\sigma}_0\}\,dV \tag{3.3-8}$$

This equation defines "consistent" nodal loads, which means that $\{\mathbf{r}_e\}$ is determined by use of the same shape functions as are used to determine the element stiffness matrix. Examples of consistent loads $\{\mathbf{r}_e\}$ for bar and beam elements appear in Section 2.9.

Assembly of elements to form an FE structure can be indicated by adding a summation sign before the entire left-hand side of Eq. 3.3-5. Thus we are led to the assembly process described in Section 2.5. That is, element matrices are conceptually expanded to "structure size" and their terms rearranged as necessary, followed by addition of overlapping terms. In this step we can also add concentrated loads $\{\mathbf{P}\}$ applied directly to nodes. The result is structure equations $[\mathbf{K}]\{\mathbf{D}\} = \{\mathbf{R}\}$, as stated by Eq. 2.5-4.

In a particular problem, any integral on the right-hand side of Eq. 3.3-8 may vanish. Even when present, an integral may vanish for most elements. For example, $\{\boldsymbol{\sigma}_0\}$ may be nonzero only for elements in a portion of the structure, and $\{\boldsymbol{\Phi}\}$ is nonzero only for element surfaces that lie on the boundary of the structure and are loaded by surface traction.

Bar Element. A simple example confirms that Eqs. 3.3-7 and 3.3-8 provide the same results as obtained in Chapter 2. For the bar element in Fig. 3.3-1a, we set $x_1 = 0$ and $x_2 = L$ in Fig. 3.2-2a. Axial displacement is linearly interpolated from nodal d.o.f. u_1 and u_2. Thus the shape function and strain-displacement matrices are

$$\lfloor\mathbf{N}\rfloor = \begin{bmatrix} \dfrac{L-x}{L} & \dfrac{x}{L} \end{bmatrix} \qquad \lfloor\mathbf{B}\rfloor = \frac{d}{dx}\lfloor\mathbf{N}\rfloor = \begin{bmatrix} \dfrac{-1}{L} & \dfrac{1}{L} \end{bmatrix} \tag{3.3-9}$$

With E and A both constant, Eq. 3.3-7 yields the element stiffness matrix

$$[\mathbf{k}] = \int_0^L \lfloor \mathbf{B} \rfloor^T E \lfloor \mathbf{B} \rfloor A \, dx = \frac{AE}{L}\begin{bmatrix} 1 & -1 \\ -1 & 1 \end{bmatrix} \tag{3.3-10}$$

which agrees with $[\mathbf{k}]$ in Eq. 2.2-1. In Eq. 3.3-8, $\{\mathbf{\Phi}\}\, dS$ becomes force P and $\lfloor \mathbf{N} \rfloor$ is evaluated at $x = L/3$. If there is also initial stress σ_0 due to a uniform temperature change T, Eq. 3.3-8 yields

$$\{\mathbf{r}_e\} = \lfloor \mathbf{N}_{L/3} \rfloor^T P - \int_0^L \lfloor \mathbf{B} \rfloor^T (-E\alpha T) A \, dx = \begin{Bmatrix} 2P/3 \\ P/3 \end{Bmatrix} + EA\alpha T \begin{Bmatrix} -1 \\ 1 \end{Bmatrix} \tag{3.3-11}$$

which agrees with the results in Figs. 2.9-1a and 2.10-1b.

An initial lack of fit, as for a bar initially ΔL units too long, is accommodated by taking the initial stress as $\sigma_0 = -E\varepsilon_0 = -E(\Delta L/L)$. This initial stress can be superposed on initial stress due to a temperature change.

Beam Element. As another simple example, we can confirm the results obtained in Chapter 2 for a uniform beam element without transverse shear deformation.

In formulating a beam element, we deal with bending moment M and curvature κ rather than stress and strain. In the first integral of Eq. 3.3-1, the integrand becomes $(\delta\kappa)^T M \, dx$. For a uniform beam element, Fig. 3.3-1b,

$$M = EI_z\kappa \qquad \kappa = \frac{d^2 v}{dx^2} \qquad v = \lfloor \mathbf{N} \rfloor \{\mathbf{d}\} \qquad \kappa = \lfloor \mathbf{B} \rfloor \{\mathbf{d}\} \tag{3.3-12}$$

where $v = v(x)$ is lateral displacement. Nodal d.o.f. are $\{\mathbf{d}\} = \lfloor v_1 \quad \theta_{z1} \quad v_2 \quad \theta_{z2} \rfloor^T$. Using shape functions listed in Fig. 3.2-4, we obtain

$$\lfloor \mathbf{B} \rfloor = \frac{d^2}{dx^2}\lfloor \mathbf{N} \rfloor = \left\lfloor -\frac{6}{L^2} + \frac{12x}{L^3} \quad -\frac{4}{L} + \frac{6x}{L^2} \quad \frac{6}{L^2} - \frac{12x}{L^3} \quad -\frac{2}{L} + \frac{6x}{L^2} \right\rfloor \tag{3.3-13}$$

With E and I_z both constant, the element stiffness matrix is

$$[\mathbf{k}] = \int_0^L \lfloor \mathbf{B} \rfloor^T EI_z \lfloor \mathbf{B} \rfloor \, dx = \frac{EI_z}{L^3}\begin{bmatrix} 12 & 6L & -12 & 6L \\ 6L & 4L^2 & -6L & 2L^2 \\ -12 & -6L & 12 & -6L \\ 6L & 2L^2 & -6L & 4L^2 \end{bmatrix} \tag{3.3-14}$$

?

which agrees with $[\mathbf{k}]$ in Eq. 2.3-5.

To obtain nodal loads produced by the uniform downward load q in Fig. 3.3-1b, we use the second integral in Eq. 3.3-8, with $\{\mathbf{\Phi}\} = -q$ and $dS = dx$. Results turn out to be the same as shown in Eq. 2.9-2 and Fig. 2.9-2a. To similarly treat thermal load, we use the third integral in Eq. 3.3-8, with $\{\boldsymbol{\sigma}_0\}$ replaced by m_0 and dV replaced by dx. If for example

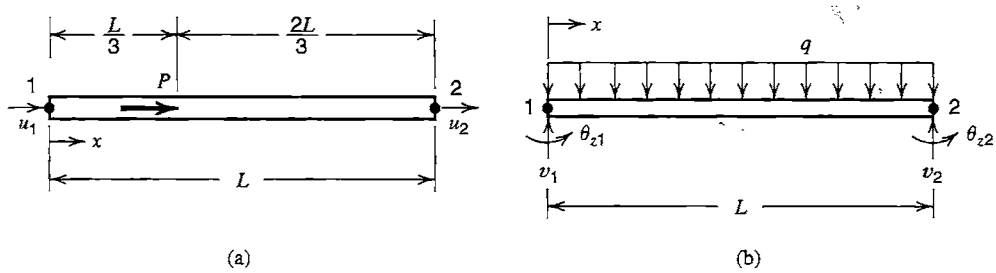

Figure 3.3-1. (a) Uniform bar element with concentrated load P at the one-third point. (b) Uniform beam element with uniformly distributed downward load of intensity q.

the beam cross section has two axes of symmetry and depth $2c$, and temperature varies linearly from $-T$ at the upper surface to $+T$ at the lower surface, then

$$m_0 = -EI_z\kappa_0 \qquad \kappa_0 = \frac{\alpha T}{c} \qquad \{\mathbf{r}_e\} = \frac{EI_z\alpha T}{c}\lfloor 0 \quad -1 \quad 0 \quad 1\rfloor^T \tag{3.3-15}$$

This load vector consists of equal and opposite moments applied to nodes at element ends.

3.4 LINEAR TRIANGLE (CST)

A *linear triangle* is a plane triangle whose field quantity varies linearly with Cartesian coordinates x and y. In stress analysis, a linear displacement field produces a constant strain field, so the element may be called a *constant-strain triangle* (CST).

For convenience of explanation only, we place node 1 at $x = y = 0$ and side 1-2 along a local x axis (Fig. 3.4-1). This choice [3.3] causes no loss of generality in a scalar field element, but would require a final coordinate transformation to obtain a generally applicable element for stress analysis. A formulation that accommodates an element arbitrarily oriented in global coordinates appears in Chapter 7.

Scalar Field Element. In terms of generalized d.o.f. a_i, field quantity ϕ is interpolated over the element by the polynomial

$$\phi = \lfloor 1 \quad x \quad y \rfloor \begin{Bmatrix} a_1 \\ a_2 \\ a_3 \end{Bmatrix} \tag{3.4-1}$$

Evaluating this expression at the nodes in Fig. 3.4-1, and noting that $x_1 = y_1 = y_2 = 0$, we obtain

$$\begin{Bmatrix} \phi_1 \\ \phi_2 \\ \phi_3 \end{Bmatrix} = [\mathbf{A}]\begin{Bmatrix} a_1 \\ a_2 \\ a_3 \end{Bmatrix} \qquad \text{where} \qquad [\mathbf{A}] = \begin{bmatrix} 1 & 0 & 0 \\ 1 & x_2 & 0 \\ 1 & x_3 & y_3 \end{bmatrix} \tag{3.4-2}$$

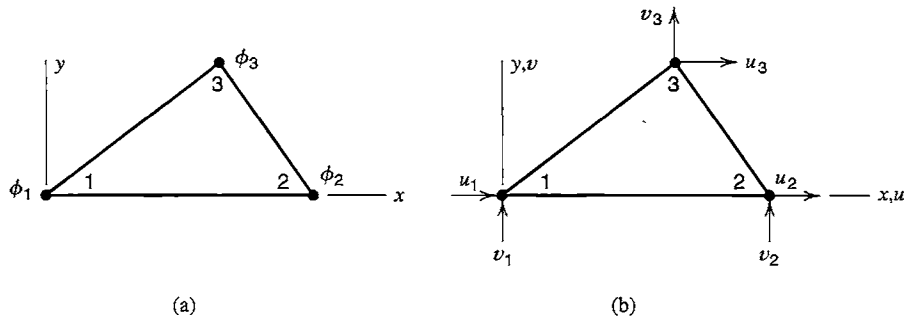

Figure 3.4-1. Linear triangles. (a) Scalar field element. (b) CST element for 2D stress analysis.

Matrix [**A**] is already triangularized, allowing solution for a_i's in terms of ϕ_i's by forward substitution, analogous to the back substitution of Gauss elimination (Section 2.8). Thus we obtain

$$a_1 = \phi_1 \qquad a_2 = \frac{\phi_2 - \phi_1}{x_2} \qquad a_3 = \frac{(x_3 - x_2)\phi_1}{x_2 y_3} - \frac{x_3 \phi_2}{x_2 y_3} + \frac{\phi_3}{y_3} \tag{3.4-3}$$

Hence, for the element in Fig. 3.4-1a, the interpolated field $\phi = \lfloor \mathbf{N} \rfloor \{\mathbf{d}\}$ is

$$\phi = \underbrace{\lfloor 1 \quad x \quad y \rfloor [\mathbf{A}]^{-1}}_{\lfloor \mathbf{N} \rfloor} \begin{Bmatrix} \phi_1 \\ \phi_2 \\ \phi_3 \end{Bmatrix} \quad \text{where} \quad [\mathbf{A}]^{-1} = \begin{bmatrix} 1 & 0 & 0 \\ \dfrac{-1}{x_2} & \dfrac{1}{x_2} & 0 \\ \dfrac{x_3 - x_2}{x_2 y_3} & \dfrac{-x_3}{x_2 y_3} & \dfrac{1}{y_3} \end{bmatrix} \tag{3.4-4}$$

Gradients of the field are

$$\begin{Bmatrix} \phi_{,x} \\ \phi_{,y} \end{Bmatrix} = [\mathbf{B}] \begin{Bmatrix} \phi_1 \\ \phi_2 \\ \phi_3 \end{Bmatrix} \quad \text{where} \quad [\mathbf{B}] = \begin{Bmatrix} \partial/\partial x \\ \partial/\partial y \end{Bmatrix} \lfloor \mathbf{N} \rfloor \tag{3.4-5}$$

Specifically, for the element in Fig. 3.4-1a,

$$[\mathbf{B}] = \begin{bmatrix} 0 & 1 & 0 \\ 0 & 0 & 1 \end{bmatrix} [\mathbf{A}]^{-1} = \begin{bmatrix} \dfrac{-1}{x_2} & \dfrac{1}{x_2} & 0 \\ \dfrac{x_3 - x_2}{x_2 y_3} & \dfrac{-x_3}{x_2 y_3} & \dfrac{1}{y_3} \end{bmatrix} \tag{3.4-6}$$

For heat conduction analysis in the xy plane, ϕ represents temperature, and the conductivity matrix of the element is

$$[\mathbf{k}] = \int [\mathbf{B}]^T[\kappa][\mathbf{B}]\, t\, dA \tag{3.4-7}$$

where $[\kappa]$ is a matrix of material conductivities, t is the element thickness, and A is the area of the triangle. If $[\kappa]$ and t are independent of x and y, then $[\mathbf{k}]$ is the simple 3 by 3 matrix $[\mathbf{B}]^T[\kappa][\mathbf{B}]\, t\, A$.

Stress Analysis Element (CST). The interpolation of Eq. 3.4-1 is applied to both displacement components, u and v. Six generalized d.o.f. a_i are now required.

$$u = \lfloor 1 \quad x \quad y \rfloor \begin{Bmatrix} a_1 \\ a_2 \\ a_3 \end{Bmatrix} \qquad v = \lfloor 1 \quad x \quad y \rfloor \begin{Bmatrix} a_4 \\ a_5 \\ a_6 \end{Bmatrix} \tag{3.4-8}$$

Because displacement functions are linear in x and y, all lines in the element, including its sides, remain straight as the element deforms. From Eqs. 3.1-6, element strains are constants:

$$\varepsilon_x = a_2 \qquad \varepsilon_y = a_6 \qquad \gamma_{xy} = a_3 + a_5 \tag{3.4-9}$$

Accordingly, this element may be called a CST, for "constant-strain triangle." Its strain-displacement matrix $[\mathbf{B}]$ can be obtained from information already obtained for the scalar field element, Eqs. 3.4-1 to 3.4-6. For the choice of axes in Fig. 3.4-1b,

$$\begin{Bmatrix} \varepsilon_x \\ \varepsilon_y \\ \gamma_{xy} \end{Bmatrix} = \underbrace{\begin{bmatrix} \frac{-1}{x_2} & 0 & \frac{1}{x_2} & 0 & 0 & 0 \\ 0 & \frac{x_3 - x_2}{x_2 y_3} & 0 & \frac{-x_3}{x_2 y_3} & 0 & \frac{1}{y_3} \\ \frac{x_3 - x_2}{x_2 y_3} & \frac{-1}{x_2} & \frac{-x_3}{x_2 y_3} & \frac{1}{x_2} & \frac{1}{y_3} & 0 \end{bmatrix}}_{[\mathbf{B}]} \begin{Bmatrix} u_1 \\ v_1 \\ u_2 \\ v_2 \\ u_3 \\ v_3 \end{Bmatrix} \tag{3.4-10}$$

The strain-displacement matrix for an arbitrary choice of axes appears in Section 7.2. If element thickness t and constitutive matrix $[\mathbf{E}]$ are constant, Eq. 3.3-7 yields the 6 by 6 element stiffness matrix as $[\mathbf{k}] = [\mathbf{B}]^T[\mathbf{E}][\mathbf{B}]tA$. In the following section, the performance of the CST is compared with that of another triangular element.

Element Defects. The linear triangle was the first element devised for plane stress analysis [1.7]. It does not work very well. In bending, a mesh of these elements is undesirably stiff. Correct results are approached as a mesh is refined, but convergence is slow. In plane strain conditions, a mesh can "lock" so that it cannot deform at all.

Consider the beam in Fig. 3.4-2a, which is loaded in pure bending. Each CST in the model displays constant σ_x, rather than the linear variation of σ_x with y that an exact solution requires. Therefore σ_x along the x axis is not zero as expected from beam theory. ?

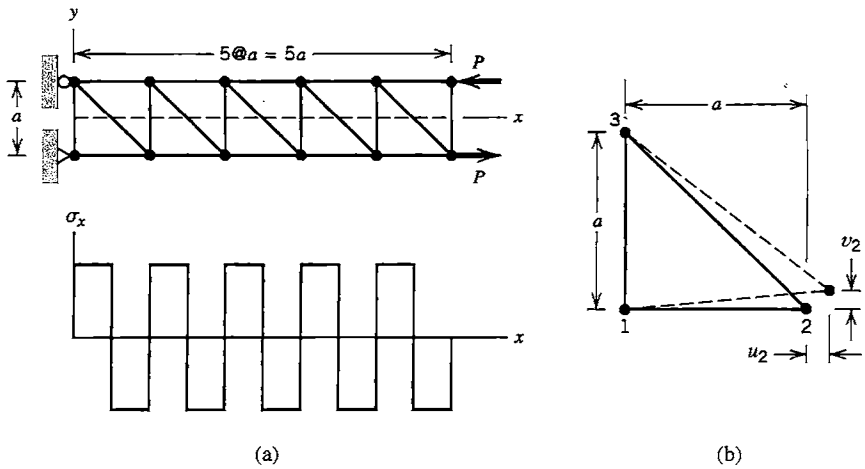

Figure 3.4-2. (a) Stress σ_x along the x axis in a beam modeled by CSTs and loaded in pure bending. (b) Deformation of the lower-left CST in the model.

Rather, σ_x displays the square-wave pattern shown. This CST model predicts y-direction deflections and σ_x stresses that are only about one-quarter the correct values. The inability of the CST to represent linearly varying stress and strain is partly to blame for this poor result. But the CST also displays a spurious shear stress. Consider the lower left element in the model, shown in Fig. 3.4-2b, which has nonzero d.o.f. u_2 and v_2, as it should. Applying Eq. 3.4-10 to this element, with $x_2 = a$ and $x_3 = 0$, we obtain $\varepsilon_x = u_2/a$, $\varepsilon_y = 0$, and $\gamma_{xy} = v_2/a$. The element displays transverse shear strain, which should not be present. Spurious shear strain absorbs energy, so that if a given deformation is prescribed, the load needed to produce it is larger than the correct value. This is a reason for the excessive stiffness in bending of the CST.

Locking of the mesh can occur when CSTs are used to model a rubberlike material in the plane strain condition. *Plane strain* exists when strain normal to the analysis plane is constrained to be zero. When $\varepsilon_z = 0$, matrix [**E**] of Eq. 3.1-3 must be replaced by

$$[\mathbf{E}] = \frac{E}{(1+\nu)(1-2\nu)}\begin{bmatrix} 1-\nu & \nu & 0 \\ \nu & 1-\nu & 0 \\ 0 & 0 & (1-2\nu)/2 \end{bmatrix} \tag{3.4-11}$$

With $\varepsilon_z = 0$, consider the volumetric strain $\Delta V/V = \varepsilon_x + \varepsilon_y$. When ν approaches 0.5, as it does for a rubberlike material, the pressure required to produce volumetric strain approaches infinity. As a result, a stiffness matrix has nearly infinite resistance to nodal displacements that produce volumetric strain. In Fig. 3.4-3 for example, any in-plane displacement of node 5 would create volumetric strain in element 1-4-5 and/or element 1-5-2. Therefore, as ν approaches 0.5, node 5 becomes almost immovable. The argument then extends to nodes 6, 8, and so on, with the final conclusion that the entire mesh is practically rigid or "locked." The corresponding scalar field element, Eqs. 3.4-1 to 3.4-7, does not display a mode analogous to volumetric strain, and does not lock.

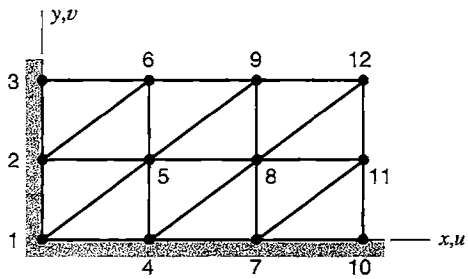

Figure 3.4-3. A mesh of CSTs that may lock under plane strain conditions.

As commonly used in FEA, the term "locking" refers to excessive stiffness in one or more deformation modes. With elements whose shape can be nonrectangular, large aspect ratio may interact unfavorably with nonrectangularity to exacerbate locking behavior. Usually, locking does not imply complete rigidity. Thus, locking may not preclude convergence with mesh refinement, but may preclude reasonable accuracy in coarse to intermediate mesh densities. Procedures for dealing with locking include supplementing the element displacement field with additional modes and use of reduced numerical integration rules to evaluate Eq. 3.3-7. None of these procedures is applicable to the constant strain triangle.

3.5 QUADRATIC TRIANGLE (LST)

A quadratic triangle is shown in Fig. 3.5-1a. It has side nodes in addition to vertex nodes. For stress analysis, nodal d.o.f. are u_i and v_i at each node, $i = 1,2,...,6$, for a total of 12 d.o.f. per element. In terms of generalized d.o.f. a_i, the element displacement field is the complete quadratic

$$\begin{aligned} u &= a_1 + a_2x + a_3y + a_4x^2 + a_5xy + a_6y^2 \\ v &= a_7 + a_8x + a_9y + a_{10}x^2 + a_{11}xy + a_{12}y^2 \end{aligned} \tag{3.5-1}$$

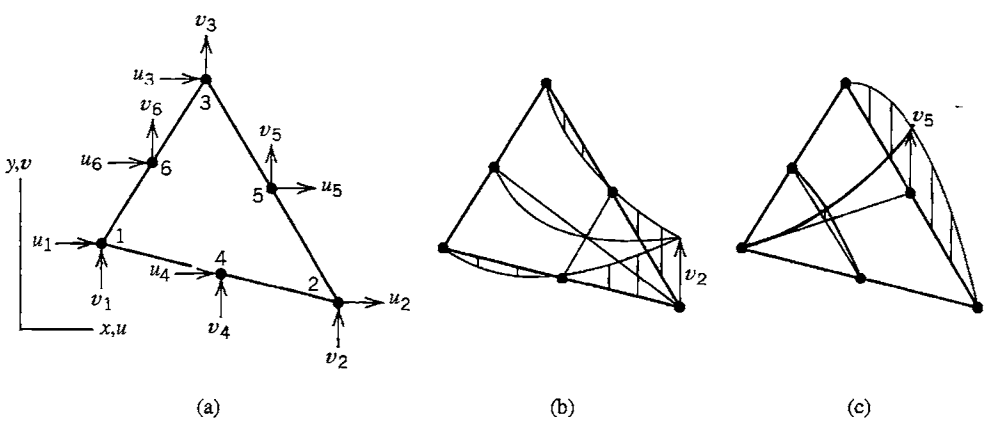

Figure 3.5-1. (a) Quadratic triangle (LST) and its 12 nodal d.o.f. (b,c) Displacement modes associated with vertex and side d.o.f. (For visualization only, displacement is imagined to take place normal to the plane of the element.)

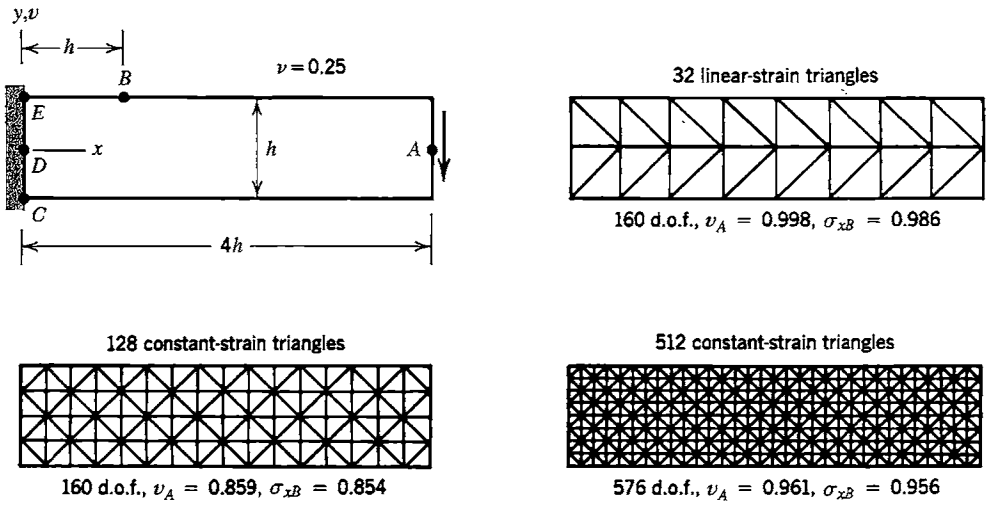

Figure 3.5-2. Tip deflection v_A and flexural stress σ_x at point B in an isotropic cantilever beam of uniform thickness [3.4].

From Eqs. 3.1-6 and 3.5-1, element strains are

$$\begin{aligned} \varepsilon_x &= a_2 + 2a_4x + a_5y \\ \varepsilon_y &= a_9 + a_{11}x + 2a_{12}y \\ \gamma_{xy} &= (a_3 + a_8) + (a_5 + 2a_{10})x + (2a_6 + a_{11})y \end{aligned} \tag{3.5-2}$$

If required by the problem being modeled, element strains can vary linearly within the element. Hence the element may be called an LST, for "linear-strain triangle." Because displacement functions are quadratic in x and y, all lines in the element, including its sides, can deform into quadratic curves (Fig. 3.5-1b,c). One can show that the element models pure bending exactly by applying the argument associated with Eqs. 3.7-3 and 3.7-4.

In Fig. 3.5-2, CST and LST elements are used to solve a cantilever beam problem. Transverse tip load is parabolically distributed over depth h on the right end. Each numerical result in Fig. 3.5-2 is the ratio of computed result to exact result as predicted by theory of elasticity [3.1]. Despite having many more d.o.f., even the finer CST mesh is less accurate than the LST mesh. In modeling this particular problem, the only shortcoming of the LST is that γ_{xy} is represented as linear rather than quadratic in y.

Discussion of the LST element continues in Chapter 7, where element formulation is completed and also extended to allow sides to have initial curvature (that is, before loads are applied).

3.6 BILINEAR RECTANGLE (Q4)

The bilinear rectangle is a four-node plane element having eight d.o.f. (Fig. 3.6-1). The name "Q4" identifies the element as a quadrilateral having four nodes. In terms of generalized d.o.f. a_i, its displacement field and associated strain field are

$$u = a_1 + a_2x + a_3y + a_4xy \qquad \varepsilon_x = a_2 + a_4y$$
$$v = a_5 + a_6x + a_7y + a_8xy \qquad \varepsilon_y = a_7 + a_8x \qquad (3.6\text{-}1)$$
$$\gamma_{xy} = (a_3 + a_6) + a_4x + a_8y$$

Shape functions can be determined by the same argument as used in Eqs. 3.2-1 to 3.2-3, but it is more instructive to apply Lagrange's interpolation formula, Eq. 3.2-7, as follows. Consider x-direction displacement u. First, we interpolate linearly along top and bottom sides to obtain side displacements u_{12} and u_{43}. Thus, in Eq. 3.2-7, $x_1 = -a$ and $x_2 = a$, so that

$$u_{12} = \frac{a-x}{2a}u_1 + \frac{a+x}{2a}u_2 \qquad u_{43} = \frac{a-x}{2a}u_4 + \frac{a+x}{2a}u_3 \qquad (3.6\text{-}2)$$

Next, we interpolate linearly in the y direction between u_{12} and u_{43}.

$$u = \frac{b-y}{2b}u_{12} + \frac{b+y}{2b}u_{43} \qquad (3.6\text{-}3)$$

Substitution of Eqs. 3.6-2 into Eq. 3.6-3 yields $u = \sum N_i u_i$, in which N_i is a shape function of the rectangular four-node element. This development results in N_i that can be produced as products of linear shape functions obtainable from Eq. 3.2-7. Indeed such *Lagrange product formulas* can be used as shape functions for *Lagrange elements.* Quadratic and higher-order Lagrange elements have side and internal nodes if two-dimensional, and edge, surface, and internal nodes if three-dimensional. For the rectangular four-node element, shape functions N_i are

$$N_1 = \frac{(a-x)(b-y)}{4ab} \qquad N_2 = \frac{(a+x)(b-y)}{4ab}$$
$$N_3 = \frac{(a+x)(b+y)}{4ab} \qquad N_4 = \frac{(a-x)(b+y)}{4ab} \qquad (3.6\text{-}4)$$

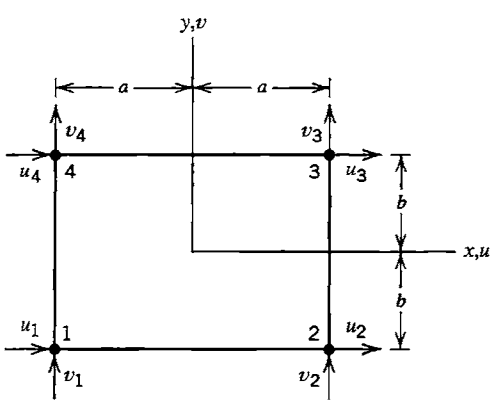

Figure 3.6-1. Bilinear quadrilateral (Q4) and its eight nodal d.o.f.

The element is called "bilinear" because its shape functions are products of one-dimensional linear polynomials. The N_i contain only one quadratic term, namely xy. Shape functions display the three properties noted following Eqs. 3.2-7. The complete element displacement field, $\{\mathbf{u}\} = [\mathbf{N}]\{\mathbf{d}\}$, is

$$\begin{Bmatrix} u \\ v \end{Bmatrix} = \begin{bmatrix} N_1 & 0 & N_2 & 0 & N_3 & 0 & N_4 & 0 \\ 0 & N_1 & 0 & N_2 & 0 & N_3 & 0 & N_4 \end{bmatrix} \begin{Bmatrix} u_1 \\ v_1 \\ u_2 \\ \vdots \\ v_4 \end{Bmatrix} \tag{3.6-5}$$

Element strains in terms of nodal d.o.f. are $\{\boldsymbol{\varepsilon}\} = [\mathbf{B}]\{\mathbf{d}\}$. From Eqs. 3.1-9, 3.6-4, and 3.6-5,

$$[\mathbf{B}] = \frac{1}{4ab}\begin{bmatrix} -(b-y) & 0 & (b-y) & 0 & (b+y) & 0 & -(b+y) & 0 \\ 0 & -(a-x) & 0 & -(a+x) & 0 & (a+x) & 0 & (a-x) \\ -(a-x) & -(b-y) & -(a+x) & (b-y) & (a+x) & (b+y) & (a-x) & -(b+y) \end{bmatrix} \tag{3.6-6}$$

The element stiffness matrix is

$$\underset{8\times 8}{[\mathbf{k}]} = \int_{-b}^{b}\int_{-a}^{a} \underset{8\times 3}{[\mathbf{B}]^T}\underset{3\times 3}{[\mathbf{E}]}\underset{3\times 8}{[\mathbf{B}]}\, t\, dx\, dy \tag{3.6-7}$$

where t is the element thickness. The integrand contains x and y to first and second powers and is easily evaluated.

The foregoing Q4 element is restricted to rectangular shape, which is a severe limitation. An isoparametric formulation of the element, discussed in Section 6.2, removes the shape restriction. An element of general quadrilateral shape has behavior similar to that of the rectangular element.

Element Defects. Like the CST, the Q4 element cannot exhibit pure bending. When bent, it displays shear strain as well as the expected bending strain. This *parasitic shear* absorbs strain energy, so that if a given bending deformation is prescribed, the bending moment needed to produce it is larger than the correct value. In other words, the Q4 element exhibits *shear locking* behavior. The argument is quantified as follows.

As shown in Section 4.4, strain energy U in a linearly elastic body of volume V, without initial stress or strain, can be evaluated from the expression

$$U = \frac{1}{2}\int \{\boldsymbol{\varepsilon}\}^T[\mathbf{E}]\{\boldsymbol{\varepsilon}\}dV \qquad \text{where, for the 2D case,} \qquad \{\boldsymbol{\varepsilon}\} = \lfloor \varepsilon_x \quad \varepsilon_y \quad \gamma_{xy} \rfloor^T \tag{3.6-8}$$

and, for isotropy and plane stress conditions, $[\mathbf{E}]$ is given by Eq. 3.1-3. For a plane element of thickness t, the volume increment is $dV = t\, dx\, dy$. In pure bending, as shown in Fig. 3.6-2a, a block of material has strains

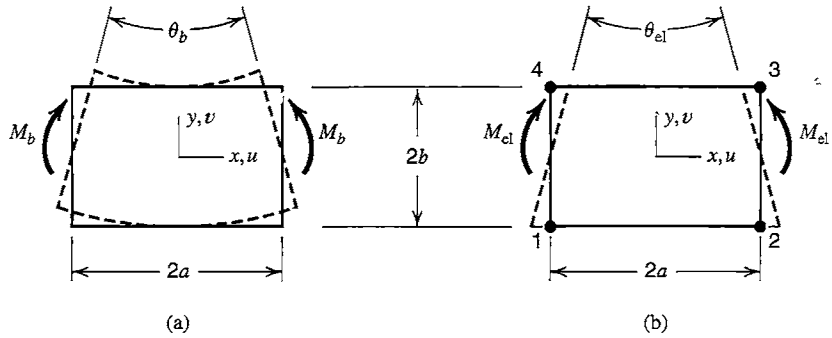

Figure 3.6-2. (a) Deformation mode of a rectangular block of material in pure bending. (b) Deformation mode of the Q4 element under bending load.

$$\varepsilon_x = -\frac{\theta_b y}{2a} \qquad \varepsilon_y = \nu\frac{\theta_b y}{2a} \qquad \gamma_{xy} = 0 \tag{3.6-9}$$

When a Q4 element is bent, as shown in Fig. 3.6-2b, its top and bottom sides remain straight, and each node has only horizontal displacement of magnitude $\theta_{el}b/2$. Hence, from the strain-displacement relation $\{\boldsymbol{\varepsilon}\} = [\mathbf{B}]\{\mathbf{d}\}$, element strains are

$$\varepsilon_x = -\frac{\theta_{el} y}{2a} \qquad \varepsilon_y = 0 \qquad \gamma_{xy} = -\frac{\theta_{el} x}{2a} \tag{3.6-10}$$

We see that ε_x in the element is exact and that ε_y is approximate (but exact if $\nu = 0$). Of greatest concern is the nonzero shear strain γ_{xy}, which should be zero in bending. Bending deformation of a Q4 element automatically generates this spurious shear strain, which is therefore identified as parasitic shear. Equations 3.6-8 and 3.6-9 yield strain energy U_b in the actual block of material, and Eqs. 3.6-8 and 3.6-10 yield strain energy U_{el} in the element. Work done by a moment load is equal to strain energy stored, so that $M_b\theta_b/2 = U_b$ and $M_{el}\theta_{el}/2 = U_{el}$. If $\theta_{el} = \theta_b$, then $M_{el} > M_b$ and $U_{el} > U_b$. Or, if $M_b = M_{el}$, then the ratio of rotations produced is

$$\frac{\theta_{el}}{\theta_b} = \frac{1-\nu^2}{1+\dfrac{1-\nu}{2}\left(\dfrac{a}{b}\right)^2} \tag{3.6-11}$$

The $(a/b)^2$ term is present only because of parasitic shear. The ratio θ_{el}/θ_b approaches zero as aspect ratio a/b increases without limit. This condition is called *shear locking*. Bending is not prohibited by shear locking, but bending tends to be excluded from element behavior because it is penalized by high strain energy in the unwanted shear mode.

Figure 3.6-3 depicts an FE model that tests element bending capability. Stress σ_x in each element is independent of x, as might be anticipated by inspection of Eqs. 3.6-1 or Eq. 3.6-6. Except at element centers, shear stress τ_{xy} on the x axis is dominated by the parasitic shear effect, which is more pronounced in elements that have greater bending deformation. If elements are square and Poisson's ratio is 0.3, transverse tip deflection and σ_x at point A (where $x = a$) are each about two-thirds their correct values. (For $a/b = 1$ and

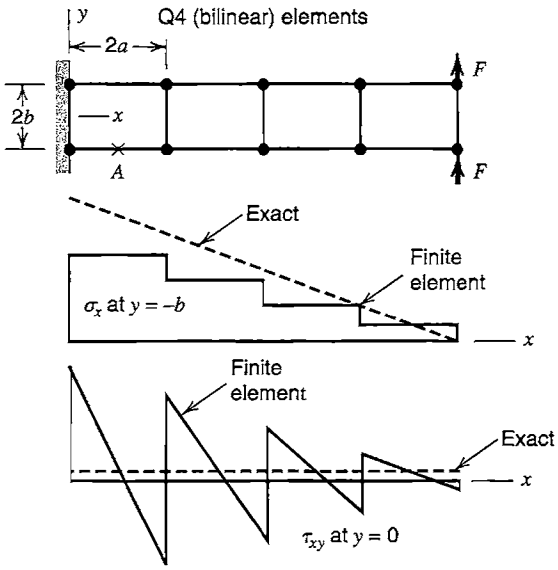

Figure 3.6-3. Cantilever beam modeled by Q4 elements, showing qualitative variation of axial stress σ_x on the lower surface and shear stress τ_{xy} on the x axis.

$0 < \nu < 0.5$, Eq. 3.6-11 yields $0.600 < \theta_{el}/\theta_b < 0.686$, with $\theta_{el}/\theta_b = 0.674$ for $\nu = 0.300$.) An additional example problem appears in Fig. 3.7-2.

Remedies for the parasitic shear effect in four-node quadrilaterals are discussed in Section 3.10.

3.7 QUADRATIC RECTANGLE (Q8, Q9)

A quadratic rectangle is obtained by adding side nodes to the linear rectangle, much as side nodes are added to the CST to obtain the LST triangular element. Here we describe the displacement field and the strain field. Shape functions and procedures of element formulation are discussed in Section 6.4, where the element is allowed to be an arbitrarily shaped quadrilateral and to have curved sides.

In terms of generalized d.o.f. a_i, the displacement field of the element in Fig. 3.7-1 is

$$\begin{aligned} u &= a_1 + a_2x + a_3y + a_4x^2 + a_5xy + a_6y^2 + a_7x^2y + a_8xy^2 \\ v &= a_9 + a_{10}x + a_{11}y + a_{12}x^2 + a_{13}xy + a_{14}y^2 + a_{15}x^2y + a_{16}xy^2 \end{aligned} \tag{3.7-1}$$

We use the name "Q8" for this eight-node quadrilateral. The name "serendipity" is also used; the reader is invited to read the dictionary definition. By letting x or y be constant, we see from Eqs. 3.7-1 that lines in the element, including element sides, can become quadratic curves in the deformed element. From Eqs. 3.1-6 and 3.7-1, element strains are

$$\begin{aligned} \varepsilon_x &= a_2 + 2a_4x + a_5y + 2a_7xy + a_8y^2 \\ \varepsilon_y &= a_{11} + a_{13}x + 2a_{14}y + a_{15}x^2 + 2a_{16}xy \\ \gamma_{xy} &= (a_3 + a_{10}) + (a_5 + 2a_{12})x + (2a_6 + a_{13})y + a_7x^2 + 2(a_8 + a_{15})xy + a_{16}y^2 \end{aligned} \tag{3.7-2}$$

As an option, a ninth node can be placed at $x = y = 0$, to produce an element we call Q9. This node is internal to the element; it is not connected to any other element. With a ninth node, u and v of Eq. 3.7-1 are augmented by modes $u = a_{17}x^2y^2$ and $v = a_{18}x^2y^2$, and strain expressions are augmented by terms that contain a_{17} and a_{18}. Element Q9 is a "Lagrange" element, whose shape functions can be obtained as Lagrange product formulas, as noted for element Q4 following Eq. 3.6-3. Element Q9 is *biquadratic,* as its shape functions are products of one-dimensional quadratic functions. In the stiffness matrix formula, Eq. 3.3-7, the size of [**E**] is 3 by 3, while [**B**] is 3 by 16 for the Q8 element and 3 by 18 for the Q9 element. Thus the respective stiffness matrices are 16 by 16 and 18 by 18.

A quadratic rectangle does not display the parasitic shear effect that plagues the bilinear element when it is bent. To show that this is so, let a cantilever beam such as that in Fig. 3.6-3 be built of Q8 elements and carry counterclockwise tip moment rather than transverse tip force. The exact displacement field and strains are [3.1]

$$u = -Cxy \qquad v = \frac{C}{2}(x^2 + \nu y^2) \qquad \text{and} \qquad \varepsilon_x = -Cy \qquad \varepsilon_y = \nu Cy \qquad \gamma_{xy} = 0 \tag{3.7-3}$$

where C is a constant. In Eqs. 3.7-1, the a_i can assume values such that Eqs. 3.7-3 are produced. Specifically, let all a_i be zero except for

$$a_5 = -C \qquad a_{12} = \frac{C}{2} \qquad a_{14} = \nu\frac{C}{2} \tag{3.7-4}$$

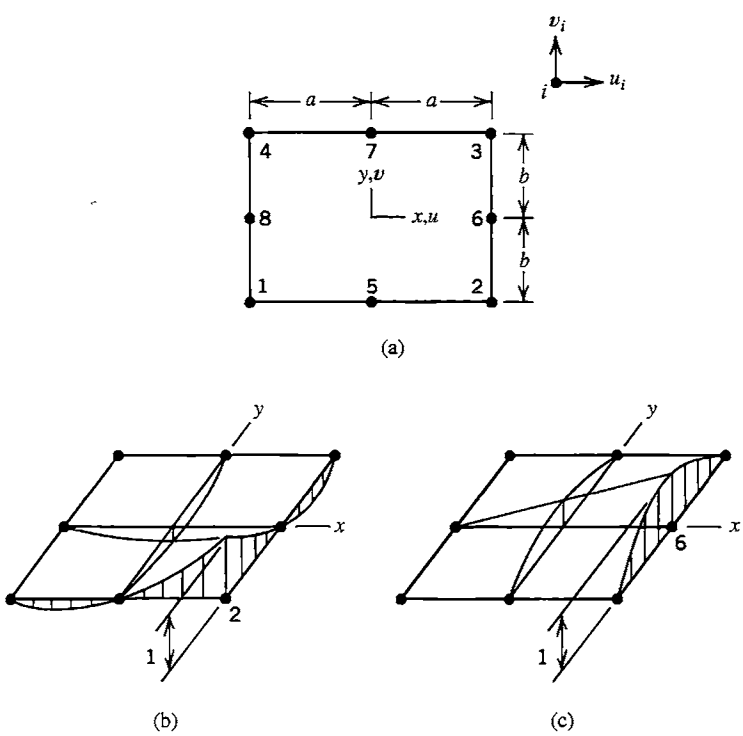

Figure 3.7-1. (a) A quadratic quadrilateral. (b,c) Displacement modes associated with vertex and side d.o.f. (For visualization only, displacement is imagined to take place normal to the plane of the element.)

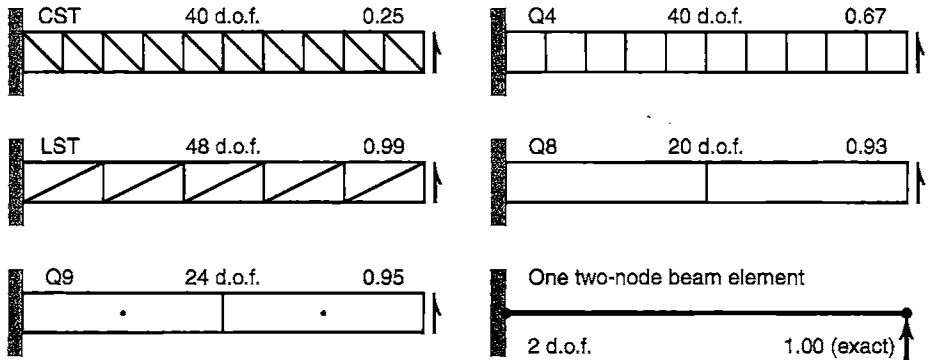

Figure 3.7-2. Tip-loaded cantilever beams of aspect ratio 10 and Poisson's ratio $\nu = 0.30$. Transverse tip displacement is reported as the ratio of computed value to exact value.

Hence Eqs. 3.7-2 yield $\varepsilon_x = -Cy$, $\varepsilon_y = \nu Cy$, and $\gamma_{xy} = 0$, which are the correct strains. The a_{12} term allows the a_5 term to exist without creating nonzero γ_{xy} in the element. Accordingly, one expects Q8 and Q9 elements to perform well in applications where bending is important.

Numerical examples appear in Fig. 3.7-2. The cantilever beam is of uniform thickness and ten times as long as it is deep. Transverse tip displacement is reported as the ratio of computed value to exact value. As might be expected, the Q9 element performs better than the Q8 element. These two elements are further discussed in Chapter 6, where nonrectangular shapes are allowed and stiffness matrices are generated by using numerical integration. In the terminology of Chapter 6, data in Fig. 3.7-2 is obtained from "fully integrated" elements. The standard two-node beam element in Fig. 3.7-2 provides an exact result despite having only two nonzero d.o.f. This model serves as a reminder that standard beam elements are most appropriate for this particular problem. Other parts of Fig. 3.7-2 show how some other elements perform, but these FE models are not recommended for a cantilever beam.

3.8 RECTANGULAR SOLID ELEMENTS

Rectangular solid elements, sometimes called "brick" elements, are direct extensions of rectangular plane elements. Two brick elements are shown in Fig. 3.8-1. In the first, the eight-node solid, x-direction displacement u is described by the polynomial displacement field

$$u = a_1 + a_2x + a_3y + a_4z + a_5xy + a_6yz + a_7zx + a_8xyz \tag{3.8-1}$$

Similar expressions are used for displacements v and w, for a total of 24 d.o.f. in the element. In terms of shape functions, the element displacement field $\{\mathbf{u}\} = [\mathbf{N}]\{\mathbf{d}\}$ is

$$\begin{Bmatrix} u \\ v \\ w \end{Bmatrix} = \begin{bmatrix} N_1 & 0 & 0 & N_2 & 0 & 0 & N_3 & 0 & 0 & \cdots \\ 0 & N_1 & 0 & 0 & N_2 & 0 & 0 & N_3 & 0 & \cdots \\ 0 & 0 & N_1 & 0 & 0 & N_2 & 0 & 0 & N_3 & \cdots \end{bmatrix} \begin{Bmatrix} u_1 \\ v_1 \\ w_1 \\ u_2 \\ \vdots \\ w_8 \end{Bmatrix} \tag{3.8-2}$$

where individual shape functions N_i have the form

$$\frac{(a \pm x)(b \pm y)(c \pm z)}{8abc} \tag{3.8-3}$$

Algebraic signs are all negative for N_2, all positive for N_8, and so on (to choose signs, recall that $N_i = 1$ when x, y, and z assume the coordinates of node i.) The element may be called "trilinear" because each of its shape functions contains the product of three linear functions. On any element surface, such as the surface $z = c$, Eqs. 3.8-1 and 3.8-3 yield forms used for the four-node rectangular element, Eqs. 3.6-1 and 3.6-4. The strain-displacement matrix is $[\mathbf{B}] = [\partial][\mathbf{N}]$, where $[\partial]$ is given by the latter rectangular array in Eq. 3.1-9. The element stiffness matrix is

$$\underset{24\times 24}{[\mathbf{k}]} = \int_{-c}^{c}\int_{-b}^{b}\int_{-a}^{a} \underset{24\times 6}{[\mathbf{B}]^T} \underset{6\times 6}{[\mathbf{E}]} \underset{6\times 24}{[\mathbf{B}]}\, dx\, dy\, dz \tag{3.8-4}$$

The 20-node solid, shown in Fig. 3.8-1b, has corner nodes and midside nodes. Its x-direction displacement u is described by the polynomial displacement field

$$\begin{aligned} u = {} & a_1 + a_2x + a_3y + a_4z + a_5x^2 + a_6y^2 + a_7z^2 + a_8xy + a_9yz + a_{10}zx + a_{11}x^2y + a_{12}xy^2 \\ & + a_{13}y^2z + a_{14}yz^2 + a_{15}z^2x + a_{16}zx^2 + a_{17}xyz + a_{18}x^2yz + a_{19}xy^2z + a_{20}xyz^2 \end{aligned} \tag{3.8-5}$$

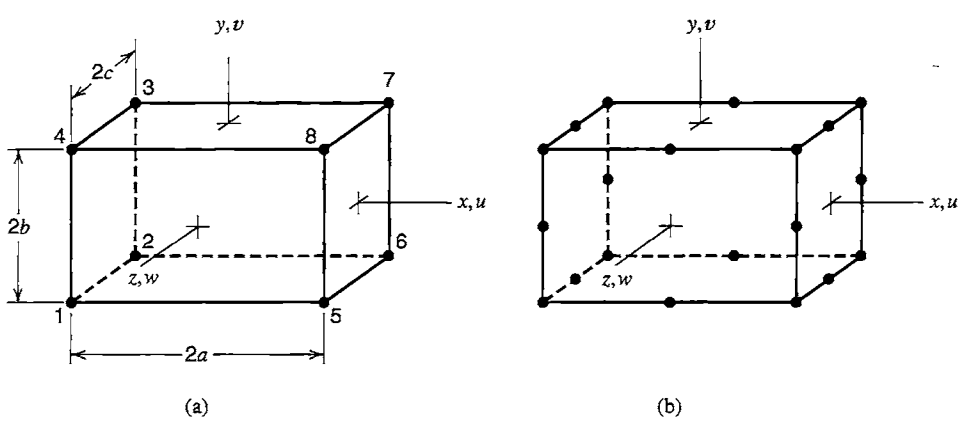

Figure 3.8-1. Rectangular solid elements. (a) Eight-node trilinear element, which has 24 d.o.f. (b) Twenty-node solid element, which has 60 d.o.f.

In order to provide interelement compatibility, the three cubic terms x^3, y^3, and z^3 do not appear. Instead the three quartic terms x^2yz, xy^2z, and xyz^2 are used. Similar expressions are used for displacements v and w, for a total of 60 d.o.f. in the element. The element stiffness matrix formula resembles Eq. 3.8-4, except that $[\mathbf{B}]$ is a 6 by 60 matrix and $[\mathbf{k}]$ is a 60 by 60 matrix.

Behavior of the foregoing solid elements resembles that of their plane counterparts, elements Q4 and Q8. Solid elements can display bending modes such as seen in Fig. 3.6-2 but with z-direction variation, and can display a twisting mode about each coordinate axis. As described in the present chapter, these solid elements are restricted to rectangular (brick-like) shape. A formulation that permits nonrectangular shapes is discussed in Section 6.5.

3.9 CHOICE OF INTERPOLATION FUNCTIONS

In this section we review elements discussed in the present chapter, with attention to choices made and reasons for them.

The choice of interpolation field may appear to be somewhat arbitrary. For a three-node triangle, instead of the linear displacement field of Eqs. 3.4-8, why not use a quadratic such as $u = a_1x^2 + a_2xy + a_3y^2$ and similarly for v? The linear field is chosen because an element must be able to display rigid body motion and constant strain states if mesh refinement is to produce convergence toward correct results. Thus the lowest-order terms of a polynomial field must not be omitted. For a three-node triangle, which has the displacement field of Eqs. 3.4-8, constant strain states are given in Eqs. 3.4-9, and rigid body motions are a_1 (x-direction translation), a_4 (y-direction translation), and $a_5 - a_3$ (rigid body rotation, defined as $(v_{,x} - u_{,y})/2$ in the theory of elasticity [3.1]). The necessary constant strain and rigid body motion capabilities are not provided by the polynomial $a_1x^2 + a_2xy + a_3y^2$. Interpolation fields for all displacement-based elements discussed will be seen to contain constant and linear terms. For elements that must bend, such as elements for beams, plates, and shells, convergence requirements demand that constant curvature also be possible. For example, see $\lfloor \mathbf{X} \rfloor$ used for a beam element, just preceding Eq. 3.2-8. (Convergence is discussed further in Sections 4.9, 6.13, and 9.6.)

Another attribute of satisfactory polynomial displacement fields is *balance;* that is, the field should favor neither x nor y. Plane elements use the polynomial terms shown in Fig. 3.9-1. Thus, in element Q4 for example, among the three possible quadratic terms x^2, y^2, and xy, balance requires that we choose the latter. Were we to use either x^2 or y^2 rather than xy, the magnitude of curvature produced in a square element loaded by couple-forces on opposite sides would depend on whether the couple-forces are applied to x-parallel sides or to y-parallel sides. Similar considerations influence the choice of higher-order terms in plane elements Q8

Terms	CST	LST	Q4	Q8(Q9)
Constant	1	1	1	1
Linear	x y	x y	x y	x y
Quadratic	-----	x^2 xy y^2	xy	x^2 xy y^2
Cubic	----------	----------	----------	x^2y xy^2
Quartic	----------	----------	----------	(x^2y^2)

Figure 3.9-1. Terms used in interpolation functions for various plane elements.

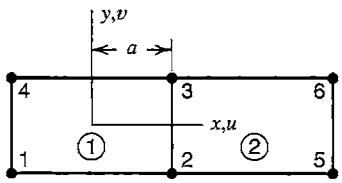

Figure 3.9-2. Adjacent elements.

and Q9 and in solid elements. In general, choices made in element formulation should provide elements with *geometric isotropy* or *frame invariance,* so that behavior of an FE structure is independent of how local xy coordinates of its elements are oriented with respect to a global coordinate system. An FE model that is sensitive to coordinate system orientation is said to display *artificial bias* or *induced anisotropy* [3.3].

One might propose that terms be combined, for example, by replacing xy by $x^2 + y^2$ in the Q4 element. This choice provides balance but makes elements incompatible. The argument is as follows. With the usual displacement field, Eq. 3.6-1, consider an element side such as side $x = a$ of element 1 of Fig. 3.9-2. On that side, displacement u is linear in y and is completely determined by nodal d.o.f. u_2 and u_3 (see Eq. 3.6-4). In a neighboring Q4 element to the right, element 2 in Fig. 3.9-2, u is linear in y along the left side and is completely determined by the same two nodal d.o.f., u_2 and u_3. Thus both elements provide the same displacement $u = u(y)$ along the shared side, so there is no gap or overlap between adjacent Q4 elements. But if xy were replaced by $x^2 + y^2$ in the displacement field, u on side $x = a$ in element 1 would be quadratic in y and could not be completely determined by d.o.f. u_2 and u_3 alone, which implies that u on this side would also depend on d.o.f. at nodes 1 and 4. Thus if all d.o.f. of nodes 2, 3, 5, and 6 in Fig. 3.9-2 are zero, but d.o.f. are nonzero at nodes 1 and 4, displacements could not be the same in elements 1 and 2 along sides that connect nodes 2 and 3. A similar argument can be used with the Q8 element, to show that x^3 and y^3 should not replace x^2y and xy^2 in the displacement expression.

Other objections can be raised to replacing xy by $x^2 + y^2$ in the Q4 element. Normal strains would then be $\varepsilon_x = a_2 + 2a_4x$ and $\varepsilon_y = a_7 + 2a_8y$. Comparing these strains with those in Eq. 3.6-1, we see that the ability to represent bending deformation has been lost. Also, if we attempt to determine shape functions by using the procedure of Eqs. 3.2-1 to 3.2-3, we discover that matrix [**A**] is singular and therefore not invertible.

In two dimensions, a polynomial is of degree n if it contains a term of the form $x^l y^m$, where l and m are nonnegative integers and $l + m = n$. The polynomial is *complete* if it contains *all* combinations of l and m for which $l + m \leq n$. For example, a complete quadratic, $n = 2$, has the form $u = a_1 + a_2x + a_3y + a_4x^2 + a_5xy + a_6y^2$. A complete polynomial of degree n in two dimensions contains $(n + 1)(n + 2)/2$ terms (see Fig. 3.9-3). In three dimensions, similar remarks apply, so that a complete quadratic contains 10 terms, which include a constant term, the linear terms x, y, and z, and the quadratic terms x^2, y^2, z^2, xy, yz, and zx. A complete polynomial of degree n in three dimensions contains $(n + 1)(n + 2)(n + 3)/6$ terms (see Fig. 3.9-4).

Pascal triangle:	Degree and number of terms:	
1	0 (constant)	1 term
$x \quad y$	1 (linear)	3 terms
$x^2 \quad xy \quad y^2$	2 (quadratic)	6 terms
$x^3 \quad x^2y \quad xy^2 \quad y^3$	3 (cubic)	10 terms
$x^4 \quad x^3y \quad x^2y^2 \quad xy^3 \quad y^4$	4 (quartic)	15 terms
$x^5 \quad x^4y \quad x^3y^2 \quad x^2y^3 \quad xy^4 \quad y^5$	5 (quintic)	21 terms

Figure 3.9-3. Pascal triangle, showing the number of terms in complete polynomials in two independent variables x and y.

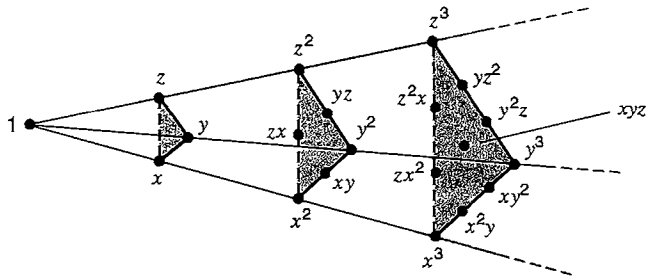

Figure 3.9-4. Pyramid showing the number of terms in complete polynomials in three independent variables x, y, and z.

An element whose displacement expression is a complete polynomial automatically has a balanced field. The CST element uses a complete linear polynomial; the LST element uses a complete quadratic polynomial. Equation 3.8-1, for the eight-node solid element, is an incomplete cubic. It is complete only through linear terms because it contains only three of the quadratic terms and only one cubic term. Nevertheless it is balanced because it favors no coordinate direction over another.

The number of independent displacement modes an element can display is equal to the number of its d.o.f. In the CST, all six of its d.o.f. are needed to endow the essential modes of rigid-body motion and constant strain. The eight-node solid element has 24 d.o.f., of which six are needed for rigid-body motion (three translations and three rotations) and another six for constant strain states. This leaves 12 independent deformation modes associated with bending, twisting, and other non-constant strain states.

3.10 IMPROVED TRIANGLES AND QUADRILATERALS

Ways to improve the performance of three-node triangles and four-node quadrilaterals include addition of *drilling* d.o.f. Four-node quadrilaterals can also be improved by addition of incompatible modes and by "underintegration" of the element stiffness matrix. Depending on element type, these procedures reduce or even eliminate parasitic shear strain. The procedures are applied to stress analysis elements but not to scalar field elements because a gradient term analogous to shear strain does not appear in scalar field problems.

Drilling d.o.f. A drilling d.o.f. in a plane element is a rotational d.o.f. whose vector is normal to the analysis plane. An appeal of drilling d.o.f. is that they can enable elements having only corner nodes to provide acceptable performance while using fewer d.o.f. than elements having both corner and side nodes. For example, a triangular element having drilling d.o.f. and only vertex nodes performs much better than the six-d.o.f. CST, although not as well as the 12-d.o.f. LST. Another part of their appeal occurs in shell analysis. A shell element can easily be formed as the combination of a plane element and an element for plate bending. Unless drilling d.o.f. are present in the plane element, this combination leaves rotational d.o.f. normal to the element unused and their possible benefit to in-plane (membrane) performance unexploited. A shell element that uses all six d.o.f. at each node is perhaps best suited to analysis of folded plates, where many elements are coplanar. In modeling a continuously curved shell, drilling d.o.f. may interact unfavorably with bending deformation [3.3].

In their simplest implementation, drilling d.o.f. in a plane element remove two d.o.f. at the middle of each side while adding one rotational d.o.f. at each corner. Thus, plane elements LST and Q8 can be converted to elements that have corner nodes only, with three d.o.f. per node. In a large plane mesh of LSTs, the conversion reduces the total number of d.o.f. by a factor of 5/8. For Q8 elements the reduction factor is 1/2. The 20-node solid element of Fig. 3.8-1b can be converted by removing translational d.o.f. at the 12 midedge nodes and adding three rotational d.o.f. at each corner node. Thus the number of d.o.f. in a large 3D mesh is reduced by a factor of 1/2.

Consider a typical side of a plane element, Fig. 3.10-1a, in which δ is the component of side-normal displacement due to drilling d.o.f. ω_i and ω_j at nodes i and j. We regard δ as quadratic in side-tangent coordinate s. Thus, δ and its midside value δ_m are

$$\delta = \frac{s(L-s)}{2L}(\omega_j - \omega_i) \qquad \delta_m = \frac{L}{8}(\omega_j - \omega_i) \tag{3.10-1}$$

If $\omega_i = \omega_j$, the side remains straight. If $\omega_i = -\omega_j$, then δ_m can be regarded as the midspan deflection of a simply supported beam of length L, loaded by end moments such that end rotations are of equal magnitude but opposite sign. The form of Eq. 3.10-1 can be modified by substituting the x and y components of δ_m and L, specifically $\delta_m \cos\beta = u_m$, $\delta_m \sin\beta = v_m$, $L\cos\beta = y_j - y_i$, and $L\sin\beta = x_i - x_j$. Side-tangent displacement at midside is taken as the average of side-tangent displacements at the corner nodes at the two ends of the side. Thus, after adding the contribution to displacement from nodes i and j, we obtain the midside displacement components

$$\begin{Bmatrix} u_m \\ v_m \end{Bmatrix} = \frac{1}{2}\begin{Bmatrix} u_i \\ v_j \end{Bmatrix} + \frac{1}{2}\begin{Bmatrix} u_i \\ v_j \end{Bmatrix} + \frac{\omega_j - \omega_i}{8}\begin{Bmatrix} y_j - y_i \\ x_i - x_j \end{Bmatrix} \tag{3.10-2}$$

The complete relation between d.o.f. in elements LST and TR in Fig. 3.10-1 can be written

$$\lfloor u_1 \quad v_1 \quad u_2 \qquad u_6 \quad v_6 \rfloor^T = \underset{12\times 9}{[\mathbf{T}]} \lfloor u_1 \quad v_1 \quad \omega_1 \quad u_2 \quad v_2 \quad \omega_2 \quad u_3 \quad v_3 \quad \omega_3 \rfloor^T \tag{3.10-3}$$

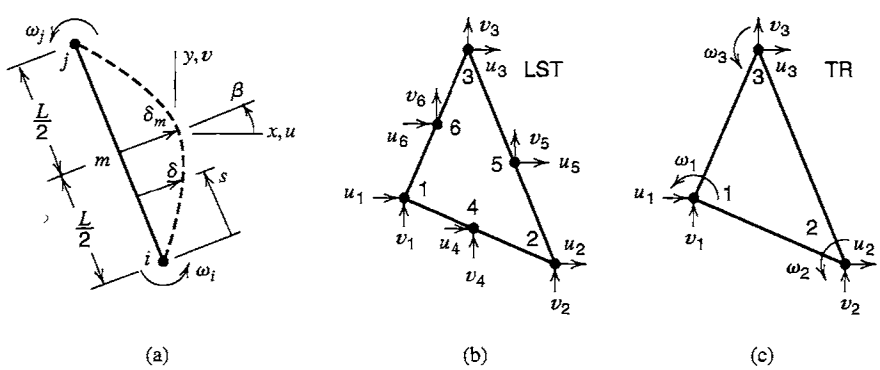

Figure 3.10-1. (a) Side displacement associated with drilling d.o.f. ω_i and ω_j. (b) A linear strain triangle (LST). (c) Triangular element with drilling d.o.f. (TR).

Transformation matrix [**T**] contains six 1's to state that $u_i = u_i$ and $v_i = v_i$ for $i = 1,2,3$, and contains information from Eq. 3.10-2 to relate the six translational d.o.f. at midside nodes to translational and drilling d.o.f. at vertex nodes. Because Eq. 3.10-3 has the same form as Eq. 2.4-1, we could obtain the 9 by 9 stiffness matrix [**k**] of element TR in Fig. 3.10-1 by applying the transformation of Eq. 2.4-5, specifically $[\mathbf{k}] = [\mathbf{T}]^T[\mathbf{k}'][\mathbf{T}]$, where in the present case $[\mathbf{k}']$ is the 12 by 12 stiffness matrix of element LST. Computationally, it is more efficient to use Eq. 3.3-7 with $[\mathbf{B}] = [\mathbf{B}'][\mathbf{T}]$, where, in the present example, strain-displacement matrices are denoted as [**B**] for element TR and $[\mathbf{B}']$ for element LST.

Clearly the same kind of transformation can be applied to element Q8 to obtain a 12-d.o.f. plane element with two translational and one drilling d.o.f. at each of its four corners. If the cantilever beam of Fig. 3.7-2 is modeled by 10 square elements of this type, with all d.o.f. at the support set to zero so that the model contains 60 d.o.f., transverse tip displacement is about 90% of the correct value.

In the preceding development, drilling d.o.f. have been given the symbol ω rather than θ because they are not true rotations, which are defined as $(v_{,x} - u_{,y})/2$ in the theory of elasticity. The matter is discussed in [3.5].

In the foregoing formulation of drilling d.o.f., the consistent load vector of Eq. 3.3-8 includes nodal moments as well as nodal forces. Thus, a uniformly distributed load q directed normal to an element side of length L produces nodal forces $qL/2$ and nodal moments $qL^2/12$, as shown in Fig. 2.9-2a.

A "zero-energy mode" is possible in elements with drilling d.o.f. Equation 3.10-2 shows that if translational d.o.f. are zero at corner nodes and $\omega_i = \omega_j$, then $u_m = v_m = 0$. The result is that a mesh of elements formulated in this way displays no strain energy if all drilling d.o.f. in the mesh are equal. Therefore the structure stiffness matrix is singular. Singularity can be avoided by setting one drilling d.o.f. in the mesh to zero. An alternative for four-node quadrilateral elements is to invoke a penalty constraint (Section 13.3) by associating strain energy with the function $\omega_1 - \omega_2 + \omega_3 - \omega_4$ [3.3]. This function, being zero for rigid body motion and constant strain modes, does not corrupt the element or structure stiffness matrix.

Because of the zero-energy mode, element TR of Fig. 3.10-1c has only 8 d.o.f. available to model deformation, despite having a total of 9 nodal d.o.f. The analogous four-node quadrilateral has 11 d.o.f. available, out of a total of 12 d.o.f. at nodes. Therefore both of these elements use incomplete quadratic fields, because a complete 2D quadratic, Eq. 3.5-1, has 12 d.o.f.

Since the original formulation [3.5], described by Eqs. 3.10-1 to 3.10-3, elements with drilling d.o.f. have been considerably improved. Of many papers, we cite [3.6–3.10]. Numerical results reported in Fig. 3.10-2 come from [3.9], whose element is better than the foregoing element TR.

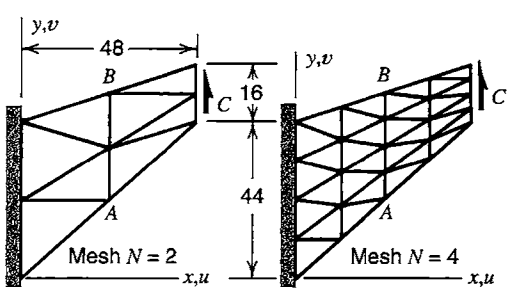

Mesh	CST[a]	Ref. 3.9[b]
$N = 2$	0.502	0.852
$N = 4$	0.765	0.954
$N = 8$	0.921	0.989

[a]No drilling d.o.f.; 6 d.o.f./el.
[b]Drilling d.o.f.; 9 d.o.f./el.

Figure 3.10-2. A swept panel with uniformly distributed load along the right side and Poisson's ratio $\nu = 0.333$. Numerical results report the computed y-direction deflection at C (exact = 1.000). The element with drilling d.o.f. is that of [3.9].

Incompatible Modes (Q6 Element). The shear-locking defect of element Q4 is explained in connection with Fig. 3.6-2. This defect is associated with an element displacement field that contains no terms quadratic in x and y, and can be remedied simply by adding the desired modes [3.11]. Thus the displacement field of element Q6 becomes

$$u = \sum_{i=1}^{4} N_i u_i + \left(1-\xi^2\right)a_1 + \left(1-\eta^2\right)a_2 \qquad \xi = \frac{x}{a}$$

$$\text{where} \qquad (3.10\text{-}4)$$

$$v = \sum_{i=1}^{4} N_i v_i + \left(1-\xi^2\right)a_3 + \left(1-\eta^2\right)a_4 \qquad \eta = \frac{y}{b}$$

The four N_i are shape functions of the Q4 element, Eqs. 3.6-4, and the four a_i are generalized d.o.f. The a_i are not associated with any node nor are they connected to d.o.f. of any other element. In this way they resemble d.o.f. at the internal node of element Q9 (Section 3.7). The a_i are appended to the array of element nodal d.o.f. $\{\mathbf{d}\}$. Physically, displacement modes associated with the a_i are displacements *relative* to the displacement field dictated by the summations in Eqs. 3.10-4. The element described by Eqs. 3.10-4 is given the name Q6 to indicate that it is a quadrilateral and has six shape functions. Details of element formulation appear in Section 6.6, where a general quadrilateral shape is permitted, and the swept panel of Fig. 3.10-2 is used in a numerical example.

Element Q6 is called "incompatible" because of behavior illustrated in Fig. 3.10-3b. With the loading shown, a gap appears between elements. If forces were reversed, elements would overlap. (With the same loading, Q4 elements remain compatible but their behavior is overly stiff.) For pure bending of the upper element in Fig. 3.10-3b, corner nodes have no vertical displacement and $a_1 = a_2 = 0$ in Eqs. 3.10-4. With c a constant, nonzero d.o.f. of this deformation field are

$$u_1 = c \quad u_2 = -c \quad u_3 = c \quad u_4 = -c \quad a_3 = \frac{a}{2b}c \quad a_4 = \nu\frac{b}{2a}c \qquad (3.10\text{-}5)$$

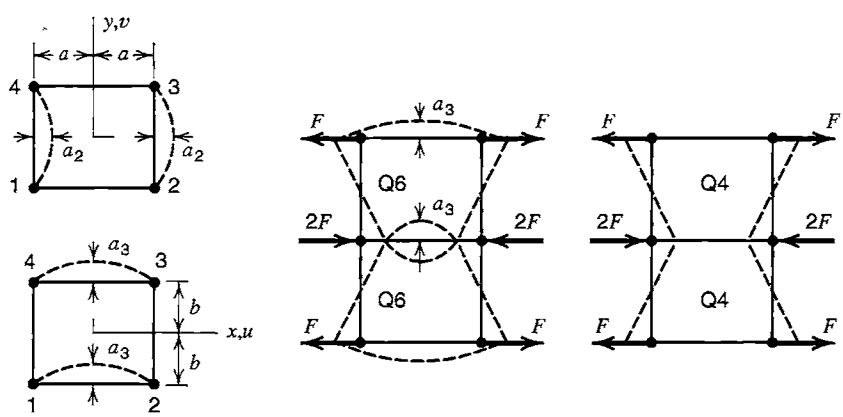

Figure 3.10-3. (a) Displacement modes $u = (1-\eta^2)a_2$ and $v = (1-\xi^2)a_3$ in the Q6 element. (b) Incompatibility between adjacent Q6 elements. (c) No incompatibility between adjacent Q4 elements.

In general, strains in the rectangular Q6 element are

$$\varepsilon_x = u_{,x} = \sum_{i=1}^{4} \frac{\partial N_i}{\partial x} u_i - \frac{2x}{a^2} a_1 \qquad \varepsilon_y = v_{,y} = \sum_{i=1}^{4} \frac{\partial N_i}{\partial y} v_i - \frac{2y}{b^2} a_4$$

$$\gamma_{xy} = u_{,y} + v_{,x} = \sum_{i=1}^{4} \left(\frac{\partial N_i}{\partial y} u_i + \frac{\partial N_i}{\partial x} v_i \right) - \frac{2y}{b^2} a_2 - \frac{2x}{a^2} a_3 \tag{3.10-6}$$

From Eqs. 3.10-5 and 3.10-6 we obtain the correct strain field for the pure bending mode of the upper element in Fig. 3.10-3b:

$$\varepsilon_x = \frac{cy}{ab} \qquad \varepsilon_y = -\nu \frac{cy}{ab} \qquad \gamma_{xy} = 0 \tag{3.10-7}$$

In this bending mode, a_3 makes it possible for γ_{xy} to vanish, and a_4 makes it possible for the relation $\varepsilon_y = -\nu\varepsilon_x$ to exist. Respectively, d.o.f. a_2 and a_1 play similar roles in bending fields rotated 90° to those shown in Fig. 3.10-3b. Note, however, that pure bending is represented exactly only if element sides are oriented with respect to the moment field as shown in Fig. 3.6-2.

No gaps or overlaps appear in a physical continuum. Why then do incompatible elements provide a satisfactory model? It is because repeated mesh refinement causes elements to approach a state of constant strain. Initially straight lines, such as sides of undeformed elements, *remain* straight when deformation is such as to produce a state of constant strain. Thus an FE model composed of Q6 elements allows exact results to be approached as the mesh is refined. Convergence may be "from above" because a coarse mesh of Q6 elements may be overly flexible. In contrast, Q4 elements converge "from below" because they are always too stiff (or at best exact, in a field of constant strain).

If the beam problem of Fig. 3.6-3 is solved again, now using Q6 elements, results are as shown in Fig. 3.10-4. Transverse tip deflection is only about 1% too small. Axial stress σ_x is exact along the vertical (y-parallel) centerline of each element. Transverse shear stress is the average value everywhere, specifically $\tau_{xy} = 2F/A = F/bt$, without the spurious x-direction variation seen in Fig. 3.6-3. In an actual beam τ_{xy} varies quadratically with y, but its representation in the Q6 element contains no quadratic terms. Neither Q4 nor Q6 elements display the correct linear variation of σ_x with x, as can be anticipated by examining element displacement fields. Further discussion of the Q6 element appears in Section 6.6.

Underintegration. In computing stiffness matrix [**k**] of a quadrilateral element, the integral in Eq. 3.3-7 can be evaluated numerically rather than analytically (Section 6.3). The simplest and cheapest form of numerical integration is *one-point quadrature,* which produces an element that resists only constant strain states. Thus the element has zero-energy modes that correspond to bending modes of deformation. These models must be suppressed if the element is to be usable, so a stabilization scheme is invoked. Discussion appears in Section 6.8, where pertinent references are cited.

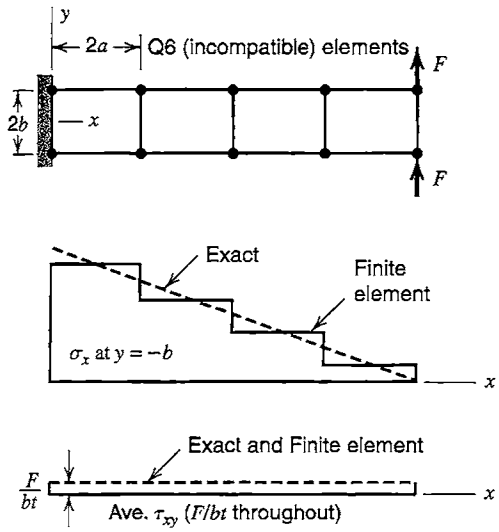

Figure 3.10-4. A cantilever beam modeled by Q6 elements, showing qualitative variation of axial stress σ_x on the lower surface and average shear stress τ_{xy} on the x axis (compare with Fig. 3.6-3).

3.11 NODAL LOADS

Equation 3.3-8 states how body forces and surface tractions are converted to consistent nodal loads. In the present section we consider mechanical loads and show that consistent nodal loads are also work-equivalent, and provide results for selected loadings on elements discussed in the present chapter. Thermal loads can be represented by either $\{\boldsymbol{\sigma}_0\}$ or $\{\boldsymbol{\varepsilon}_0\}$ in Eq. 3.3-8; see Section 2.10 for one-dimensional examples and Section 6.10 for further discussion.

Consistent (Work-Equivalent) Loads. We can show that work W done by nodal loads $\{\mathbf{r}_e\}$ in moving through nodal displacements $\{\mathbf{d}\}$ is equal to work done by distributed loads $\{\mathbf{F}\}$ and $\{\boldsymbol{\Phi}\}$ in moving through the displacement field defined by $\{\mathbf{d}\}$ and element shape functions. Work done by nodal loads is $W = \{\mathbf{d}\}^T\{\mathbf{r}_e\}$. We substitute for $\{\mathbf{r}_e\}$ from Eq. 3.3-8, and in integrals note that $\{\mathbf{d}\}^T[\mathbf{N}]^T = \{\mathbf{u}\}^T$. Thus

$$W = \{\mathbf{d}\}^T\{\mathbf{r}_e\} = \int \{\mathbf{u}\}^T\{\mathbf{F}\}\, dV + \int \{\mathbf{u}\}^T\{\boldsymbol{\Phi}\}\, dS \tag{3.11-1}$$

Integrals sum the work of load increments $\{\mathbf{F}\}\, dV$ and $\{\boldsymbol{\Phi}\}\, dS$ in moving through displacements $\{\mathbf{u}\}$ produced by nodal d.o.f. Equation 3.11-1 shows that loads $\{\mathbf{r}_e\}$, as consistently defined by Eq. 3.3-8, are work-equivalent to distributed loads.

Consistent nodal loads are also *statically equivalent* to the original distributed loading, which means that both load systems have the same resultant force and the same moment about an arbitrarily located point. That this is so can be seen by considering work-equivalence of the load systems during a rigid-body translation and a small rotation about an arbitrarily located point.

Side and internal displacements of element Q6, discussed in Section 3.10, are influenced by generalized d.o.f. a_1 to a_4, so one might expect that these d.o.f. would influence nodal loads associated with body force and surface traction and should be included in load

vector $\{\mathbf{r}_e\}$. In practice, incompatible modes of the Q6 element are ignored in nodal load calculation, so that nodal loads for Q4 and Q6 elements are identical. With this simplification, Q6 elements pass the "patch test," discussed in Section 6.13, which is regarded as an essential test of element reliability.

Examples. Equation 3.3-8 can be used to account for concentrated loads as well as distributed loads. A force F applied at a point on surface S is regarded as the limiting case of intense pressure over infinitesimal area, so that $\{\mathbf{\Phi}\}\ dS$ approaches F. Thus, for surface traction,

$$\text{Distributed traction } \{\mathbf{\Phi}\}: \qquad \{\mathbf{r}_e\} = \int [\mathbf{N}]^T \{\mathbf{\Phi}\}\, dS \qquad \text{Concentrated force } F: \qquad \{\mathbf{r}_e\} = [\mathbf{N}_*]^T F \tag{3.11-2}$$

where $[\mathbf{N}_*]$ is obtained by evaluating $[\mathbf{N}]$ at coordinates of the point to which force F is applied. A similar argument can be used if force F acts within an element, now regarding F as a limiting case of the body force term $\{\mathbf{F}\}\ dV$.

As example applications of Eqs. 3.11-2, consider the loadings shown in Fig. 3.11-1. Load $q = q(x)$ is force per unit length, so that pressure on the side is q/t, where t is element thickness. For plane elements, only side displacements enter into Eqs. 3.11-2, so the same nodal loads are obtained whether elements in Fig. 3.11-1a are Q4, Q6, or CST elements (recall that incompatible modes, if present, are not loaded). Shape functions on the loaded side can be obtained by evaluating Eqs. 3.6-4 at $y = b$. Here we reorder individual shape functions merely for the convenience of reading nodal loads left to right along the loaded side. Thus, for the upper side in Fig. 3.11-1a,

$$[\mathbf{N}] = \frac{1}{2a}\lfloor a - x \quad a + x \rfloor \qquad \{\mathbf{\Phi}\} = \frac{1}{t}[\mathbf{N}]\begin{Bmatrix} q_4 \\ q_3 \end{Bmatrix} \tag{3.11-3}$$

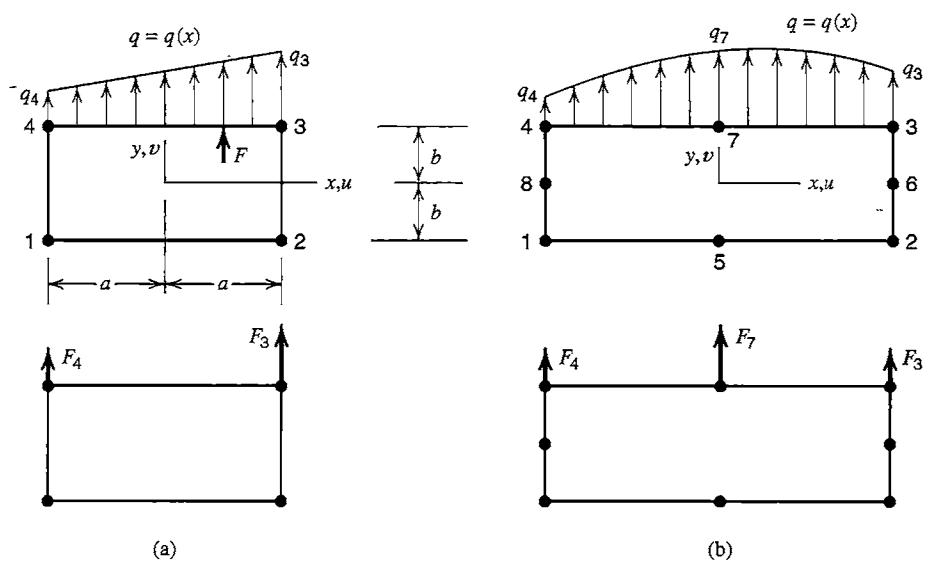

Figure 3.11-1. Distributed loads q on sides of Q4 and Q8 elements, and their nodal force equivalents.

and $dS = t\,dx$. To account for the concentrated force at $x = a/2$ in Fig. 3.11-1a we evaluate $[\mathbf{N}_*]$ in Eq. 3.11-2 at $x = a/2$. Hence, nodal loads associated with the linear side in Fig. 3.11-1a are

$$\begin{Bmatrix} F_4 \\ F_3 \end{Bmatrix} = \int_{-a}^{a} [\mathbf{N}]^T[\mathbf{N}]\,dx \begin{Bmatrix} q_4 \\ q_3 \end{Bmatrix} + [\mathbf{N}_{a/2}]^T F = \frac{a}{3}\begin{bmatrix} 2 & 1 \\ 1 & 2 \end{bmatrix}\begin{Bmatrix} q_4 \\ q_3 \end{Bmatrix} + \frac{F}{4}\begin{Bmatrix} 1 \\ 3 \end{Bmatrix} \tag{3.11-4}$$

These loads have the same magnitude as reactions on a simply supported beam of length $2a$, loaded as side 4-3 is loaded.

Side load $q = q(x)$ in Fig. 3.11-1b is treated similarly. Shape functions on this side can be obtained from Lagrange's formula, Eqs. 3.2-7, using $x_1 = -a$, $x_2 = 0$, and $x_3 = a$. Arranging individual N_i to suit the node order 4-7-3, we have

$$[\mathbf{N}] = \frac{1}{2a^2}\begin{bmatrix} x(x-a) & 2(a^2-x^2) & x(x+a) \end{bmatrix} \qquad \{\mathbf{\Phi}\} = \frac{1}{t}[\mathbf{N}]\begin{Bmatrix} q_4 \\ q_7 \\ q_3 \end{Bmatrix} \tag{3.11-5}$$

Hence, nodal loads associated with a quadratic variation on a quadratic side are

$$\begin{Bmatrix} F_4 \\ F_7 \\ F_3 \end{Bmatrix} = \int_{-a}^{a} [\mathbf{N}]^T[\mathbf{N}]\,dx \begin{Bmatrix} q_4 \\ q_7 \\ q_3 \end{Bmatrix} = \frac{a}{15}\begin{bmatrix} 4 & 2 & -1 \\ 2 & 16 & 2 \\ -1 & 2 & 4 \end{bmatrix}\begin{Bmatrix} q_4 \\ q_7 \\ q_3 \end{Bmatrix} \tag{3.11-6}$$

If loading is uniform, then $q_4 = q_7 = q_3$, and Eq. 3.11-6 says that of the total force on the side, one-sixth is allocated to each end node and two-thirds to the midside node.

The foregoing results do not require that side traction act normal to the side. For example, if uniform side-tangent traction q acts on collinear sides of equal length and having midside nodes, nodal loads shown in Fig. 3.11-2 are obtained.

Body force is treated by the first integral in Eq. 3.3-8. Consider the weight W of an element. Contents of body force array $\{\mathbf{F}\}$ are obtained by dividing W by element volume and, if W does not act parallel to a coordinate axis, resolving W into axis-parallel components. Example results appear in Fig. 3.11-3. The fraction of total weight assigned to each node is independent of element orientation, but nodal loads shown are correct only if elements are of uniform material and thickness, quadrilaterals are rectangular, and side nodes

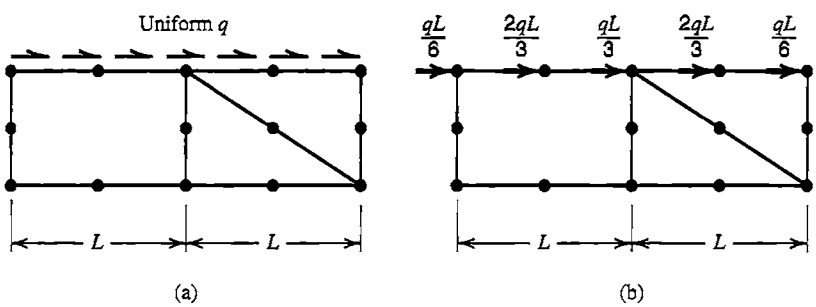

Figure 3.11-2. Allocation of uniformly distributed side-tangent load to uniformly spaced nodes.

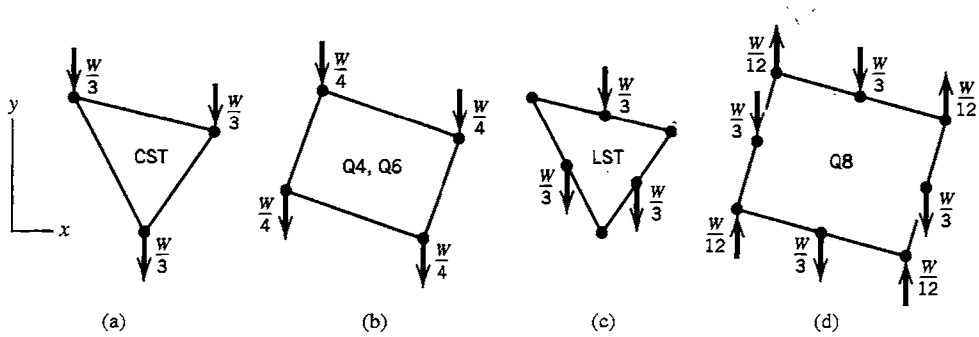

Figure 3.11-3. Consistent nodal loads associated with element weight W in the negative y direction, for triangular and rectangular quadrilateral elements of uniform thickness.

are at midside. In Figs. 3.11-3c and 3.11-3d we see some surprises. Vertex nodes of the LST element are not loaded. Corner nodes of the Q8 element carry *upward* loads, but the sum of all eight nodal loads is W, acting downward, as must be the case. A uniform traction on a surface of a solid element creates nodal loads like those in Fig. 3.11-3. For example, if uniform pressure p acts on a rectangular surface of the solid element in Fig. 3.8-1b, so as to produce total force F on the surface, then $F/3$ is allocated to each of the four midside nodes and $F/12$ in the opposite direction to each corner node.

Remarks. A given nodal load may represent any of several distributed loadings. Figure 3.11-4 shows two of the many load distributions that have P as their consistent and statically equivalent nodal load. This being so, all these loadings produce identical deformations in the FE model. In a physical continuum the different loadings would produce different results, but only close to the loaded area, in accord with Saint-Venant's principle. This example reminds us that fine detail cannot be modeled by a coarse mesh.

A nodal moment can be applied to a beam element, whose nodes have rotational d.o.f. Excluding elements with drilling d.o.f., elements discussed in this chapter have only translational d.o.f., and so cannot resist a nodal moment load. A moment load can be applied to these elements only as couple-forces. For example, in Fig. 3.11-4, a clockwise couple PL would result if a leftward force P were added at node A. Although moment can be applied to a node that has drilling d.o.f., accurate results in the neighborhood of the loaded node are not to be expected.

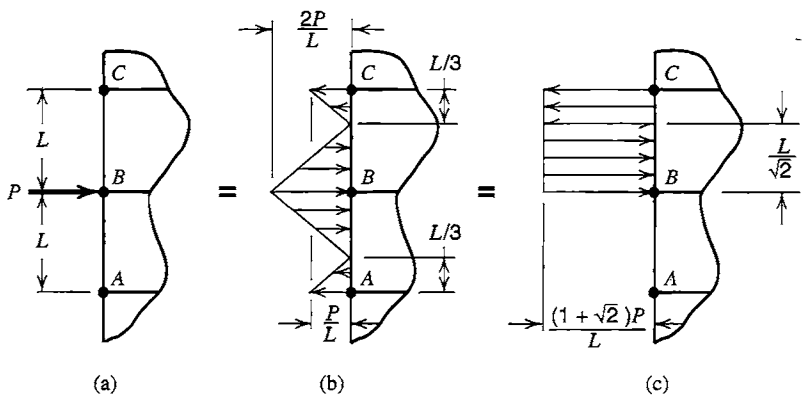

Figure 3.11-4. (a) Force P normal to a side formed by elements having corner nodes only. (b,c) Two load distributions that are statically equivalent to force P.

Most FE software is capable of calculating nodal loads of proper magnitude and direction. The user need only describe the direction, spatial variation, and intensity of distributed surface traction and body force, and the spatial variation and intensity of initial stresses or initial strains. Software does not require that loaded sides be collinear or of the same length.

3.12 STRESS CALCULATION

Structural d.o.f. $\{\mathbf{D}\}$ are calculated by solving structural equations $[\mathbf{K}]\{\mathbf{D}\} = \{\mathbf{R}\}$. Vector $\{\mathbf{D}\}$ contains nodal d.o.f. $\{\mathbf{d}\}$ of every element. Nodeless or internal d.o.f. of elements such as Q6 and Q9 may appear in $\{\mathbf{D}\}$ or may be eliminated before assembly and later recovered by separate element-by-element calculations (see Section 6.7). Stresses in each element can be calculated according to Eq. 3.1-1, with $\{\boldsymbol{\varepsilon}\} = [\mathbf{B}]\{\mathbf{d}\}$. Thus for isotropy, plane stress conditions, and initial strains due to temperature change T with temperature-independent coefficient of thermal expansion α, element stresses in the analysis plane are

$$\begin{Bmatrix} \sigma_x \\ \sigma_y \\ \tau_{xy} \end{Bmatrix} = \frac{E}{1-\nu^2}\begin{bmatrix} 1 & \nu & 0 \\ \nu & 1 & 0 \\ 0 & 0 & (1-\nu)/2 \end{bmatrix}\left([\mathbf{B}]\{\mathbf{d}\} - \begin{Bmatrix} \alpha T \\ \alpha T \\ 0 \end{Bmatrix}\right) \tag{3.12-1}$$

Matrix $[\mathbf{B}]$ is a function of the coordinates and must be evaluated at the location in the element where stresses are desired. Step 3 on page 52 uses Eq. 3.12-1.

Typically, temperature is a function of the coordinates. An example problem in Section 2.10 suggests that if the element temperature field T is of higher degree than the element strain field, then the degree of T in Eq. 3.12-1 should be reduced to that of the element strain field in order to improve the accuracy of computed stresses. However, the following counterexample can be given. Imagine that $\nu = 0$ and $F = 0$ in Fig. 3.6-3, and impose the temperature field $T = (b^2 - 3y^2)T_0$, where T_0 is a constant. Nodal forces and displacements are zero, and use of this temperature variation in Eq. 3.12-1 provides the correct σ_x but an incorrect σ_y. If we simplify the temperature field so that, like the strain field, it contains no quadratic terms, then the best-fit temperature field is $T = 0$, which leaves the body free of stress. Clearly, neither way of treating temperature is best in all cases. Both ways provide convergence toward exact results with repeated mesh refinement. References include [2.19,3.12,3.13]. Further discussion of thermal stress appears in Section 6.10.

Strain fields (and hence stress fields) are likely to display greater error than the displacement field. This behavior is apparent in the problem of Fig. 3.10-4, where nodal d.o.f. are almost exact but σ_x varies in stairstep fashion. The reason for this behavior is that strain-displacement matrix $[\mathbf{B}]$ is obtained by differentiation of the displacement field, and differentiation discloses differences. As an example, imagine that a simply supported beam element displays a quadratic lateral displacement, while the exact lateral displacement is a half sine wave. If plotted, the two $v = v(x)$ functions appear almost identical. Not so the bending moment, calculated as $M_z = EI_z(d^2v/dx^2)$; it is constant throughout the beam element, while the exact bending moment field is a half sine wave.

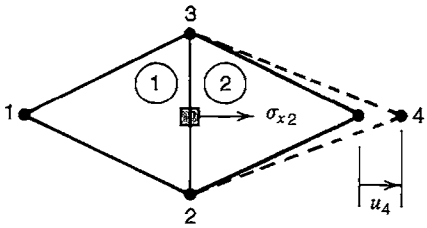

Figure 3.12-1. Stress appears in element 2 but not in element 1. The differential element (shaded) spans the interelement boundary.

Computed stresses are usually most accurate at locations within an element rather than on its boundaries. This is unfortunate because stresses of greatest interest usually appear at boundaries. Therefore, stresses may be calculated at certain points within an element, then extrapolated to element boundaries (Section 6.10), or treated by smoothing schemes that span a "patch" of elements (Section 9.9).

Elements discussed in the present chapter are C^0 elements, which means that gradients of element fields are in general not continuous across boundaries between elements. Therefore, computed stresses are in general not interelement-continuous. This behavior is immediately apparent in the pair of CST elements shown in Fig. 3.12-1. Because u_4 is the only nonzero nodal displacement, the left element is free of stress while stress σ_{x2} prevails throughout the right element. Discontinuous stress fields also appear in Figs. 3.6-3 and 3.10-4.

In general, adjacent elements display different states of stress at a node they share. As it is not known which of these stress states is most accurate, the average stress at a node is more to be trusted than stress at the node in any element attached to that node. Typically, software computes average stresses at nodes, and uses them to plot stress bands (or stress contours). These bands are interelement-continuous, and have a more pleasing appearance than discontinuous element-by-element stress bands. However, because pronounced stress discontinuity provides a visual warning that the mesh is too coarse to provide reliable results, element-by-element stress bands are more useful to the analyst. Example stress bands appear in Fig. 1.5-2. The reader may wish to review the discussion in that section of Chapter 1. Stresses produced by smoothing operations are discussed in Section 9.9.

There are other circumstances in which stresses should not be averaged at nodes. Parts joined by shrink fit, such as a disk on a shaft, have different circumferential stresses on either side of the interface between parts. An average circumferential stress would not be the correct circumferential stress in either part. A discontinuity of thickness or modulus also causes a discontinuity in stress. As examples, in Fig. 3.12-2a, σ_x is discontinuous at $x = 0$ because x-direction force must be continuous but thicknesses differ. At $x = 0$ in Fig. 3.12-2b, σ_y (normal to the xz plane) is discontinuous because both parts must have the same strain ε_y but $E_1\varepsilon_y \neq E_2\varepsilon_y$. In Fig. 3.12-2c, different local coordinate systems have been established in adjacent elements, and an average such as $(\sigma_x + \sigma_n)/2$ has no physical meaning. If elements of different type are somehow connected, such as a beam element and a plane element, an average stress at a node shared by the two is not likely to be meaningful.

Some stress quantities are *invariant;* that is, they have the same numerical value regardless of the coordinate system in which they are computed. One such quantity is the von Mises or "effective" stress σ_e, which is used to predict the onset of yielding when material behaves in a ductile fashion. In terms of general stress components and principal stresses respectively, σ_e is

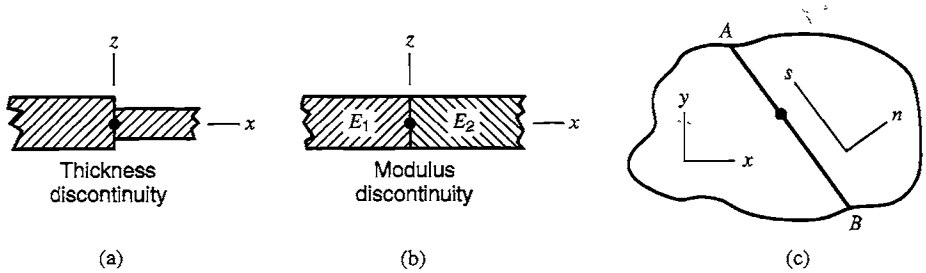

Figure 3.12-2. Some situations in which stresses should not be averaged at a node. (a,b) Plane elements seen in cross section, with Cartesian coordinates xyz. (c) Plane elements seen in plan view, with interelement boundary AB.

$$\sigma_e = \frac{1}{\sqrt{2}}\left[(\sigma_x-\sigma_y)^2 + (\sigma_y-\sigma_z)^2 + (\sigma_z-\sigma_x)^2 + 6\left(\tau_{xy}^2 + \tau_{yz}^2 + \tau_{zx}^2\right)\right]^{1/2} \quad (3.12\text{-}2a)$$

$$\sigma_e = \frac{1}{\sqrt{2}}\left[(\sigma_1-\sigma_2)^2 + (\sigma_2-\sigma_3)^2 + (\sigma_3-\sigma_1)^2\right]^{1/2} \quad (3.12\text{-}2b)$$

in which σ_1, σ_2, and σ_3 are the principal stresses at the point in question, where (conventionally) label σ_1 is assigned to the algebraically largest and σ_3 to the algebraically smallest. Principal stresses can be determined from the six stresses in $\{\boldsymbol{\sigma}\}$ by standard methods [2.6]. Equation 3.12-2 reduces to $\sigma_e = \sigma_1$ if σ_1 is uniaxial, that is, if $\sigma_2 = \sigma_3 = 0$. Note that σ_e may exceed the magnitude of σ_1, for example, when $\sigma_1 = -\sigma_3$. Also, σ_e is always positive and does not identify the algebraic signs of stresses that contribute to it. Another stress invariant is the *stress intensity* S_I, where

$$S_I = \sigma_1 - \sigma_3 \quad (3.12\text{-}3)$$

Thus, by definition, S_I is twice the maximum shear stress. Like σ_e, it serves as a yield criterion. Note that S_I is *not* the stress intensity factor used in fracture mechanics. No direction is associated with σ_e. The orientation of planes that carry the maximum shear stress $S_I/2$ can be determined, but usually this information is not of interest.

The von Mises stress σ_e is often computed, and its element-by element contours plotted, because it is a scalar measure of the intensity of the *entire* state of stress. Contours of some other stress, such as σ_x, might be similarly informative in one part of the model but less so in another part because a stress other than σ_x is dominant there. Symmetry in the FE model should provide symmetry in contours of σ_e or S_I.

If a body is in a state of uniform stress, its FE model should display complete uniformity of the stress field, so that computed results display no stress contours. This will not happen if the model contains a patch of elements with improper connections, some of which are shown for plane elements in Fig. 3.12-3. Along CD for example, elements LST and Q4 should apply to one another nodal loads consistent with uniform traction, but from the discussion in Section 3.11 we realize that because nodal loads on sides of elements that meet along CD must be proportioned differently, the desired nodal loads cannot exist. A disturbed and incorrect stress pattern will result. If poor connections are localized in a model, the region of inaccurate stresses will also be localized, in accord with Saint-Venant's principle. One can also note that displacements are incompatible along CD and

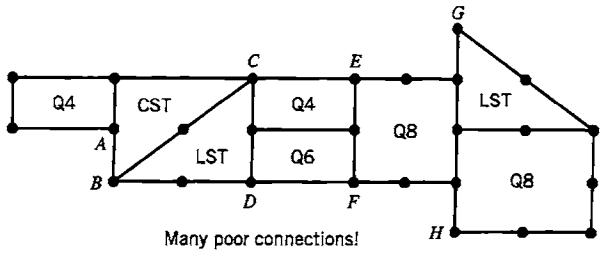

Figure 3.12-3. Examples of how *not* to connect plane elements.

also along *EF*, being quadratic in elements LST and Q8 but linear in element Q4 and a *different* quadratic displacement in element Q6. Along *GH*, all three sides can displace to become parabolic segments, but because the segments are offset, sides cannot be compatible. At node *A* there is no connection at all because element CST has no side node. Some of these faulty connections can be made to work properly by imposing constraints, which are discussed in Chapter 13.

Software may report stresses with reference to global coordinates or with reference to local coordinates such as used for the beam element in Fig. 2.3-2. In a beam, flexural stress is referred to local coordinates because it is a normal stress in the beam's axial direction. Elements for plates and shells may be arbitrarily oriented in global coordinates, but their membrane and bending components of stress are computed in local coordinates tangent to the element surface. A software user must consult documentation to understand how local axes are oriented in the global system.

Elements discussed thus far, and indeed most elements in common use, are based on displacement fields. There are other formulation methods, some based on simultaneous use of separate fields for displacement and stress. Although such elements may have displacement d.o.f., element stresses are not calculated by the same formulas as used for displacement-based elements. A casual software user may be unaware of the basis of element formulation. In any case the analyst should study documentation and run simple test cases in order to appreciate how an element behaves before using it in applications.

3.13 NATURE OF A FINITE ELEMENT SOLUTION

In an exact solution, every differential element of material is in equilibrium, compatibility prevails everywhere, and all boundary conditions on stress and displacement are met. A solution by FEA, being approximate, does not satisfy these requirements in every way. In what follows we note the extent to which the requirements are met in static FEA when elements are based on displacement fields.

- *Compatibility prevails at nodes.* At connection points (nodes), elements have identical displacement components. A partial connection implies a relaxation of this statement. For example, let two adjacent elements have three translational and three rotational d.o.f. per node. If only the translational d.o.f. are connected where elements meet at a node, the node acts like a ball-and-socket joint.
- *Compatibility may or may not be satisfied across interelement boundaries.* Compatibility prevails when displacements along an element side are entirely determined by d.o.f. of nodes on that side, and adjacent elements share these nodes and all their d.o.f. Such is not the case for element Q6, and it is not the case for some elements often used

for plates and shells. It is also not the case when element types are mixed and elements are poorly connected, as in Fig. 3.12-3. For properly connected elements that are valid in the patch-test sense (including element Q6), incompatibilities tend toward zero as the mesh is repeatedly refined.

- *Compatibility is satisfied within elements.* Internal compatibility requires only that the element displacement field be continuous and single-valued. These conditions are automatically satisfied by polynomial displacement fields.
- *Equilibrium of nodal forces and moments is satisfied.* Solution vector $\{\mathbf{D}\}$ satisfies structural equations $\{\mathbf{R}\} - [\mathbf{K}]\{\mathbf{D}\} = \{\mathbf{0}\}$, which state that each node is in static equilibrium under the action of applied loads $\{\mathbf{R}\}$ and elastically-generated internal loads $-[\mathbf{K}]\{\mathbf{D}\}$.
- *Equilibrium is usually not satisfied at or across interelement boundaries.* Computed stresses usually do not satisfy Eqs. 3.1-14. For example, in an FE model of the structure in Fig. 3.1-2b, computed results will not display $\sigma_n = 0$ and $\tau_{ns} = 0$ along the lower side. A lack of equilibrium across interelement boundaries is displayed by the differential element in Fig. 3.12-1, on which all stresses are zero except for $\sigma_{x2} > 0$ on its right side. A similar situation appears in Fig. 3.10-4. These disagreements with boundary and interelement equilibrium tend toward zero as the mesh is repeatedly refined.
- *Equilibrium is usually not satisfied within elements.* Computed stresses usually do not satisfy the differential equations of equilibrium, Eqs. 3.1-13, except in an average or integral sense over the element volume, as noted before Eq. 3.3-2. An exception is the CST element, for which Eqs. 3.1-13 are always satisfied. But equilibrium across interelement boundaries is poorly modeled by CST elements, and Fig. 3.7-2 shows that CST elements may perform poorly. Clearly, good element behavior requires more than satisfaction of Eqs. 3.1-13. However, with any acceptable element, Eqs. 3.1-13 become more nearly satisfied as a mesh is repeatedly refined.

3.14 EXAMPLE: A SIMPLE STRESS CONCENTRATION PROBLEM

We illustrate the behavior of LST elements by applying them to a plane problem for which results are already known. Imagine that a circular hole exists in an isotropic infinite plate that is subjected to uniform uniaxial far-field stress σ_∞. Unless we wish to use special "infinite" elements, discussed in Section 8.8, we must develop a model with a finite domain. Because horizontal and vertical axes through the center of the hole are axes of symmetry, only one quadrant of the problem need be modeled (Fig. 3.14-1a). Saint-Venant's principle suggests that stress disturbance due to the hole extends no more than a few diameters from the hole. Thus it is perhaps reasonable to use a $10R$ by $10R$ domain to represent one quadrant. Then, for this geometry, the tabulated stress concentration factor is 2.722 [1.16]; hence $\sigma_{y\max} = 2.722(\sigma_\infty/0.9) = 3.025\sigma_\infty$. According to the theory of elasticity [3.1], for a circular hole in an *infinite* plate under plane stress conditions, the maximum normal stress is $\sigma_y = 3\sigma_\infty$ where the hole intersects the x-axis in Fig. 3.14-1a, and the minimum normal stress is $\sigma_x = -\sigma_\infty$ where the hole intersects the y-axis.

Our mathematical model consists of a central circular hole of radius R in a $20R$ by $20R$ square plate under plane stress conditions, which implies that the hole diameter in the

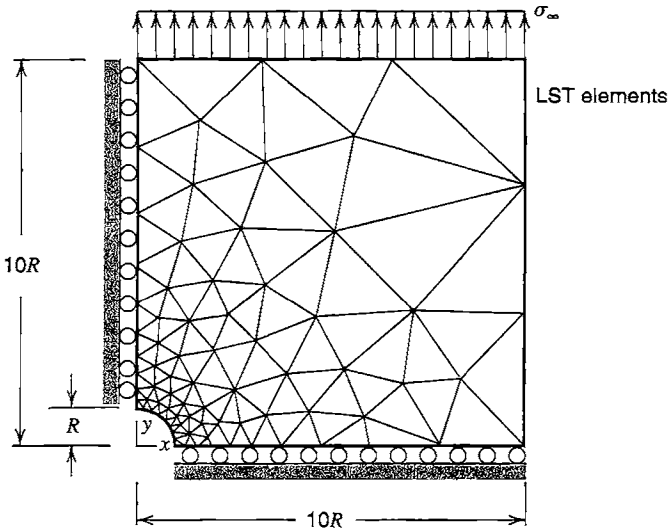

(a)

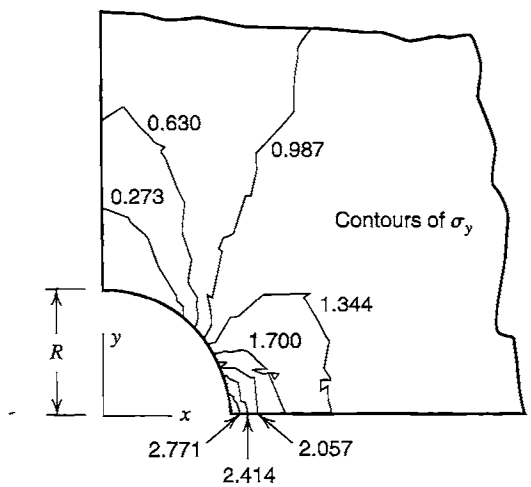

(b)

Figure 3.14-1. (a) FE domain, mesh, and boundary conditions for modeling a hole in an infinite plate. (b) Unaveraged contours of σ_y from a portion of the mesh in part (a).

physical structure should be greater than the plate thickness so that stress components with z subscripts are indeed negligible. On the quadrant shown in Fig. 3.14-1a we apply stress boundary conditions of zero traction on the arc that defines the hole and on the side $x = 10R$, and y-direction traction σ_∞ on the side $y = 10R$. Thus we assume that these conditions on the finite mathematical model are very nearly consistent with stresses along these lines in the infinite domain. Displacement boundary conditions are $u = 0$ on $x = 0$ and $v = 0$ on $y = 0$, as indicated by rollers. These displacement conditions are exact, and no additional approximation is implied by exploiting symmetry and analyzing a quadrant.

For FE analysis of this mathematical model, LST elements under plane stress conditions are used. Stress gradients are expected to be much larger near the hole than farther away, so elements are graded in size as shown in Fig. 3.14-1a. The mesh was generated by software. Eight uniform divisions were prescribed on the circular arc that defines the hole,

and three uniform divisions on the outer boundaries. The software generated a mesh of 122 LST elements with 279 nodes (558 d.o.f.), not accounting for any reduction due to imposition of boundary conditions. The material is isotropic, with $E = 200$ GPa and $\nu = 0.3$.

FEA provides stresses throughout the model. Unaveraged contours of σ_y in the vicinity of the hole are shown in Fig. 3.14-1b. The list of stresses tabulated by the software shows that the largest σ_y is $3.128\sigma_\infty$ and the smallest σ_x is $-1.091\sigma_\infty$. Each of these stresses appears in the anticipated location. Although these values are close to expectations, Fig. 3.14-1b shows obvious inter-element discontinuities in unaveraged σ_y contours around the hole. Far from the hole (not shown in Fig. 3.14-1b), the σ_y distribution appears uniform, which suggests that both the location of the far-field boundary and the coarseness of the far-field mesh are acceptable. To improve results we might refine elements near the hole, but no refinement appears necessary near the outer boundary.

The software used provides a numerical measure of how well averaged and unaveraged stress fields agree. This measure, described in Section 9.10 and symbolized by η, becomes zero if the two fields are identical. FE discretization is often considered acceptable if $\eta < 0.05$. For the LST mesh of Fig. 3.14-1a, we obtain $\eta = 0.012$.

In theory, stresses are independent of E and ν. FEA stresses are indeed independent of E, but changing ν from 0.3 to zero changes $\sigma_{y\max}$ from $3.128\sigma_\infty$ to $3.122\sigma_\infty$ in the mesh used here. Mesh refinement should reduce the disagreement.

3.15 AN APPLICATION WITH HIGH STRESS GRADIENT

The preceding example may suggest that any plane problem can be satisfactorily solved by elements discussed in this chapter if the mesh is sufficiently dense in regions where strain gradients are high. Figure 3.15-1 depicts an apparently simple problem that will disabuse us of this notion. The problem is a reminder that we must think carefully about each problem despite the power of FEA.

Figure 3.15-1 depicts a bimetal body, consisting of two different but isotropic metals bonded together in an unstressed state at room temperature. Material moduli, Poisson ratios, and thermal expansion coefficients differ, with $E_s > E_a$, $\nu_s < \nu_a$, and $\alpha_s < \alpha_a$, where subscripts s and a denote steel and aluminum, respectively. We seek stresses that result from unconstrained and uniform heating to 100 °C above the stress-free temperature. Our choice for the mathematical model is a body of uniform thickness 20 mm normal to the xy plane, with plane stress conditions in the xy plane (despite the appreciable thickness).

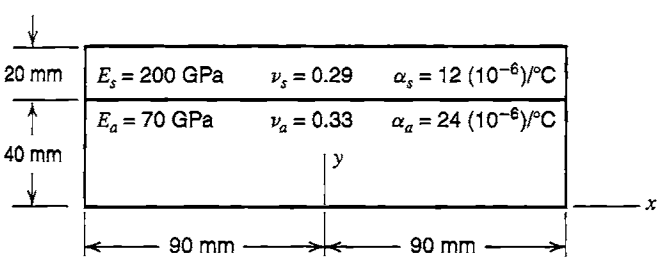

Figure 3.15-1. Geometry and material properties of a bimetal problem.

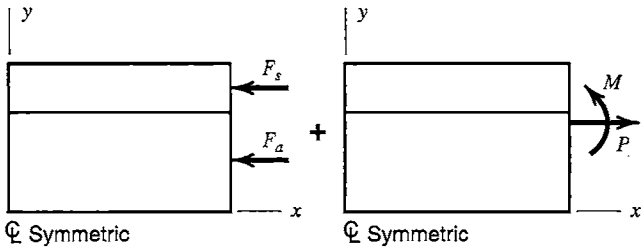

Figure 3.15-2. Preliminary analysis of the bimetal problem, using superposition. The y axis is an axis of symmetry.

Preliminary Analysis. Because $\alpha_s < \alpha_a$, we expect the structure to bend in the xy plane, placing the upper surface of the top layer in compression and the lower surface of the bottom layer in tension. For preliminary analysis we assume that stresses do not vary along the length, and apply elementary mechanics of materials, summarized as follows. If axial expansion is prevented, initial axial stresses -240 MPa and -168 MPa appear in the steel and aluminum layers respectively, with associated axial compressive forces of restraint $F_s = 96{,}000$ N and $F_a = 134{,}400$ N in the respective layers (Fig. 13.5-2). Next we remove axial restraint by applying these forces in the opposite sense, and use the transformed section method for stress analysis. Transforming (say) the steel portion, we obtain an aluminum T-section beam, whose upper part has dimension $20(200/70) = 57.14$ mm normal to the xy plane and whose centroidal axis is 37.647 mm from the base. Loads are centroidal force $P = F_a + F_b = 230{,}400$ N in axial tension and moment $M = 1{,}186{,}000$ N • mm that bends the beam concave up. With $I = 568{,}300$ mm^4, the resulting axial stress on the top of the T-section is $P/A - Mc/I = 71.9$ MPa. Transforming back to the original steel and superposing the initial stress, we obtain $71.9(200/70) - 240 = -34$ MPa as the estimate of the final axial stress on top of the actual bimetal beam in its central portion, away from end effects. Similar analysis provides the estimate 29 MPa on the bottom of the bimetal beam.

Finite Element Analysis. Figure 3.15-3a depicts the initial FE model as well as the resulting deflection profile under thermal load. Roller supports along the y axis provide symmetry about the vertical centerline of the structure. The single roller support at the lower right corner permits unconstrained expansion of the structure while preventing rigid body translation in the y direction. A coarse mesh of Q8 elements is used. The maximum computed deflection is approximately 0.25 mm in the x direction, as shown (not to scale).

Critique of Results. The displaced shape, Fig. 3.15-3a, is reasonable: the body expands in both x and y directions and becomes concave up, as expected. But it appears that the upper left corner, on the y axis, has zero vertical displacement. Has a mistake been made in boundary conditions, so that vertical displacement is prevented at this node? A simple calculation shows that the zero-displacement result is only fortuitous. Returning to the T-section beam of preliminary analysis, we calculate that moment $M = 1{,}186{,}000$ N • mm creates downward displacement $ML^2/8EI = 0.121$ mm at the middle of a simply supported beam of length $L = 180$ mm, while thermal expansion creates upward displacement $(40\alpha_a + 20\alpha_s)100 = 0.120$ mm. Thus the two motions very nearly cancel.

Figure 3.15-3b shows unaveraged contours of σ_x. On the y axis, tabulated values of σ_x produced by the FE software indicate that $\sigma_x = 29.4$ MPa at $y = 0$ and $\sigma_x = -34.0$ MPa at $y = 60$ mm, in almost exact agreement with stresses obtained in preliminary analysis. As

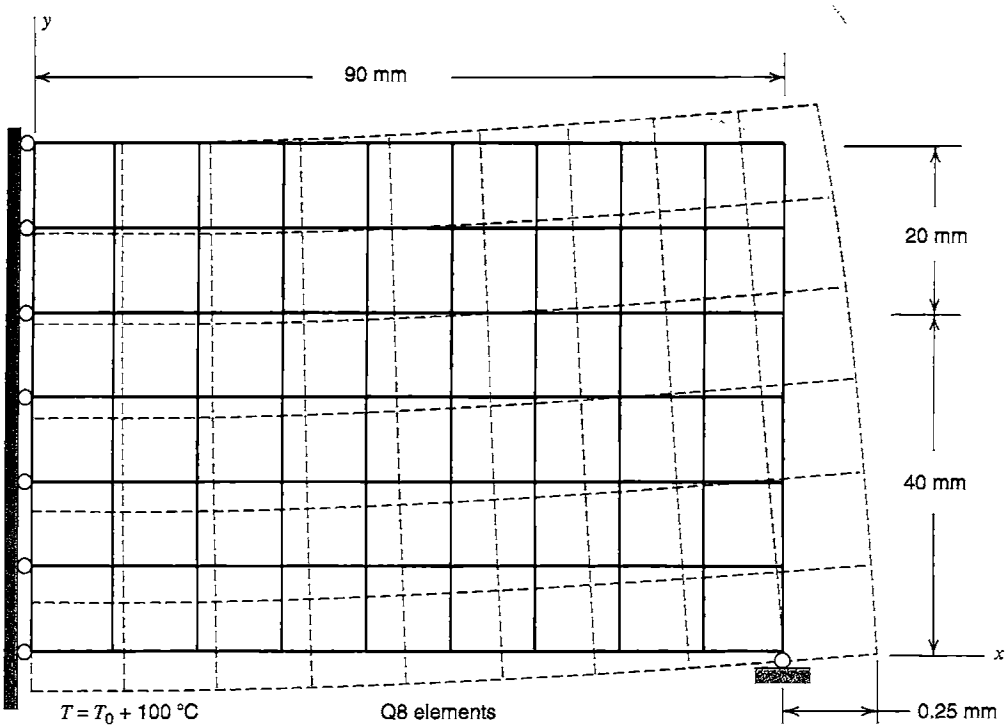

(a)

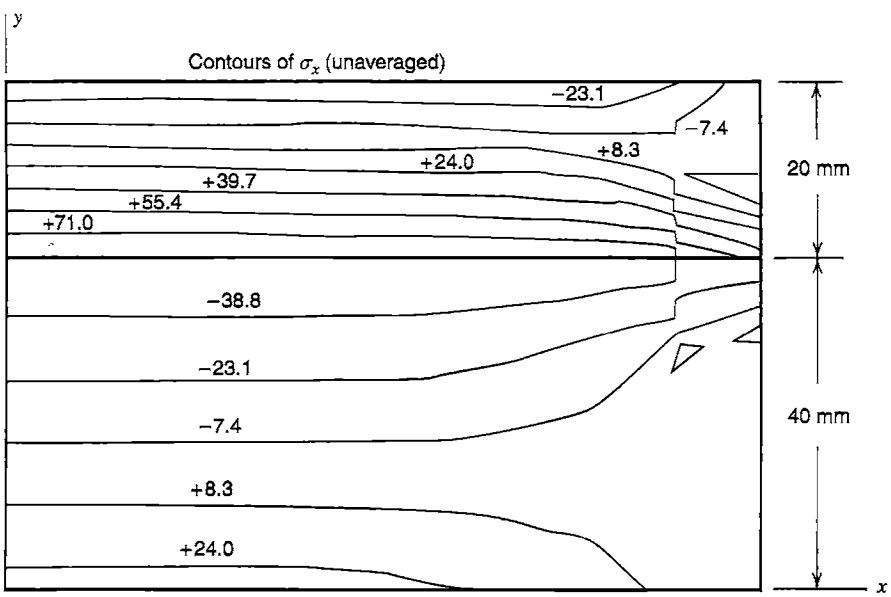

(b)

Figure 3.15-3. (a) FE domain, mesh, boundary conditions, and displacement profile in the bimetal body after a uniform temperature increase of 100 °C. (b) Unaveraged contours of σ_x from the mesh in part (a).

expected, there is a discontinuous transition between tensile and compressive σ_x as we move through the material interface from top to bottom. Particularly in this case, plotting averaged values of σ_x would eliminate important information. Because the right boundary is a free surface, we expect σ_x to approach zero there, and σ_x contours indicate that σ_x does indeed approach zero everywhere on the right boundary except for a small region around the material interface.

Based on these results, it would appear that the FE model is good. However, near where the material interface meets the right-hand boundary, we see large discontinuities in σ_x contours. Contour plots of σ_y and τ_{xy} (not shown) display enormous strain gradients through individual elements adjacent to the material interface at the right boundary. Furthermore, we find that repeated mesh refinement fails to alleviate the problem. What is wrong? It happens that this simple-looking problem has a stress singularity at the boundary on the material interface [3.14,3.15]. For most combinations of material properties, the singular stress field is proportional to $1/r^{\rho}$, where r is radial distance measured from an origin at the right boundary on the material interface and ρ is a coefficient that depends on the relative material properties. Because interpolation functions of the elements used are incapable of modeling this behavior, repeated mesh refinement never achieves infinite stress at $r = 0$.

Note that modeling choices may significantly affect results away from the singularity. Imagine, for example, that the roller support in Fig. 3.15-3a is replaced by a pin, so that $u = v = 0$ at the lower right corner. In this case, the tendency toward outward expansion would be prevented by horizontal force applied by the support, significantly altering deformation and stress in the central portion of the structure, and producing a stress singularity at the pin, for which again mesh refinement would not result in convergence of stresses. Of course, a pin support is inconsistent with our intention to analyze unrestrained thermal loading of the bimetal bar.

Because the actual body is rather thick normal to the xy plane, our plane-stress mathematical model differs from reality, but provides no information about the magnitude of the difference. A 3D analysis would display nonzero stresses σ_z, τ_{yz}, and τ_{zx}, and values of σ_x, σ_y, and τ_{xy} somewhat different than those computed in plane analysis. In a 3D model, a stress singularity analogous to that observed at a point in the plane model would be expected along the rectangular boundary line where the material interface meets the outer surfaces.

We conclude by reminding ourselves that considerable frustration can be avoided by ensuring that we understand the nature of the problem before we begin numerical analysis.

ANALYTICAL PROBLEMS

3.1-1 (a) By writing equations analogous to Eq. 3.1-11, derive differential equations of equilibrium for the three-dimensional case.
(b) Use a free-body diagram to derive the two-dimensional form of stress boundary conditions, Eqs. 3.1-14.

3.1-2 Imagine that stresses in the xy plane are reported to be $\sigma_x = -6a_1x^2$, $\sigma_y = 12a_1x^2$, and $\tau_{xy} = 12a_1y^2$, where a_1 is a constant.

(a) Consider the square region $0 \le x \le b$, $0 \le y \le b$. Write expressions for tractions Φ_x and Φ_y on each side of this square, in terms of x, y, b, and a_1.
(b) If body forces are zero, is this state of stress in fact possible? Explain.

3.1-3 Determine if the following stress field is a valid solution of a plane elasticity problem: $\sigma_x = 3a_1x^2y$, $\sigma_y = a_1y^3$, and $\tau_{xy} = -3a_1xy^2$, where a_1 is a constant. The body is isotropic and linearly elastic, and body forces are zero.

3.1-4 (a) Consider volume V of a differential element and its change ΔV under stress. Show that $\Delta V/V = \varepsilon_x + \varepsilon_y + \varepsilon_z$ if strains are small.
(b) Let hydrostatic pressure p be applied. Obtain an expression for $(\Delta V/V)/p$.
(c) Hence, show that a rubberlike material is almost incompressible.

3.1-5 Let displacements in an isotropic body in a state of plane stress be as stated by Eqs. 3.5-1. What relation among constants a_i is needed if differential equations of equilibrium are to be satisfied?

3.2-1 In Fig. 3.2-2b, let $x_1 = 0$, $x_2 = 2$, and $x_3 = 3$. Then use this data in the following.
(a) Verify numerically that shape functions sum to unity.
(b) What should the sum of x derivatives of the shape functions be? Verify the property numerically.

3.2-2 Shape functions of C^0 elements satisfy the relation $\sum N_i = 0$, but such is not the case for shape functions of a C^1 element such as a plane beam. Why?

3.2-3 In Fig. 3.2-3a, let numbered points have respective x_i of 1, 3, 5, and 8, and respective ϕ_i of 2, 2, 2, and 5.
(a) Use Lagrange's formula to obtain an interpolating polynomial.
(b) What values of ϕ does the formula predict at $x = 0$, at $x = 2$, at $x = 4$, and at $x = 7$?

3.2-4 Invert matrix [**A**] of Eq. 3.2-8. Hence verify the shape functions shown in Fig. 3.2-4. *Suggestion:* Regard Eqs. 3.2-8 as four equations to be solved for the four a_i. Arrange results in matrix format, identify a 4 by 4 matrix as $[\mathbf{A}]^{-1}$, then use Eq. 3.2-3 to obtain $\lfloor \mathbf{N} \rfloor$.

3.2-5 Imagine that a curve $\phi = \phi(x)$ is to be fitted to three data values: ϕ_1 and $\phi_{,x1}$ at $x = 0$ and ϕ_2 at $x = L$ (analogous to Fig. 3.2-3b but with $\phi_{,x2}$ unspecified). Determine the shape functions. Also sketch them and check their behavior at $x = 0$ and at $x = L$ (in the manner of Fig. 3.2-4).

3.2-6 Imagine that, at points A, B, and C in the sketch, both ordinate and slope data are known. Slope data are indicated by short lines through data points. Without calculation, sketch
(a) a Lagrange interpolation curve through all three points.
(b) a piecewise interpolation of C^0 continuity.
(c) a piecewise interpolation of C^1 continuity.

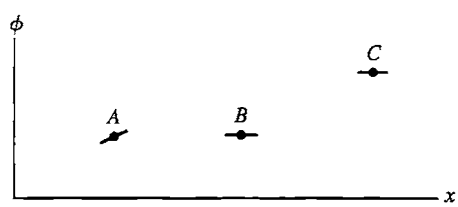

Problem 3.2-6

3.3-1 (a) The shape function matrix for a bar element of length L can be written as $\lfloor \mathbf{N} \rfloor = \lfloor 1 \quad x \rfloor [\mathbf{A}]^{-1}$, where $[\mathbf{A}]^{-1}$ is given by Eq. 3.2-4 with $x_1 = 0$ and $x_2 = L$. Hence $\lfloor \mathbf{B} \rfloor = \lfloor 0 \quad 1 \rfloor [\mathbf{A}]^{-1}$, and the element stiffness matrix is

$$[\mathbf{k}] = [\mathbf{A}]^{-T} \int_0^L \begin{Bmatrix} 0 \\ 1 \end{Bmatrix} AE \lfloor 0 \quad 1 \rfloor \, dx [\mathbf{A}]^{-1}$$

Use this form to generate $[\mathbf{k}]$ of a uniform bar element, Eq. 3.3-10.
(b) Using a similar form for a uniform beam element, verify $[\mathbf{k}]$ of Eq. 3.3-14.

3.3-2 (a) Imagine that, at each end node, a uniform bar element is to have not only axial displacement d.o.f., but axial strain d.o.f. as well, so that $\{\mathbf{d}\} = \lfloor u_1 \quad \varepsilon_{x1} \quad u_2 \quad \varepsilon_{x2} \rfloor^T$. Derive the resulting 4 by 4 element stiffness matrix.
(b) How can this element be used to model a bar that carries concentrated axial loads, or has abrupt changes in elastic modulus or in cross-sectional area?

3.3-3 A uniform bar element of length L has a node at each end and a node at the middle, as shown. Determine the element stiffness matrix that operates on nodal d.o.f. u_1, u_2, and u_3.

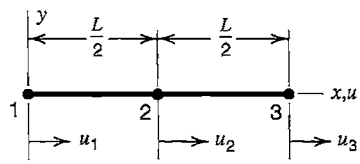

Problem 3.3-3

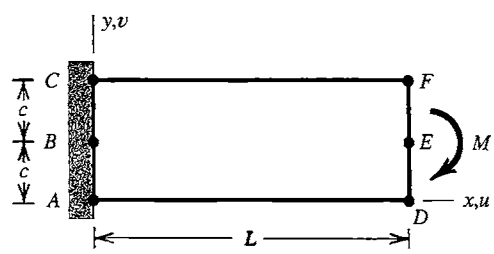

Problem 3.4-1

3.4-1 The cantilever beam shown is tip-loaded by moment M. Use beam theory to compute displacement components of points D, E, and F. Then regard these results as nodal displacements, and use them to compute stresses $\{\boldsymbol{\sigma}\} = [\mathbf{E}][\mathbf{B}]\{\mathbf{d}\}$ in elements defined as follows. Assume that $\nu = 0$. What becomes of the ratio τ_{xy}/σ_x as L/c becomes large?
(a) A CST element whose nodes are A, D, and F.
(b) A CST element whose nodes are A, D, and C.

3.4-2 Repeat Problem 3.4-1, but replace moment M by transverse tip force P in the y direction. Neglect transverse shear deformation in computing displacements of lettered nodes.

3.4-3 (a) Two nodes of an isosceles CST element are fixed, as shown. Let $\nu = 0$, and determine the 2 by 2 stiffness matrix associated with d.o.f. at the unrestrained node.
(b) A plane square region of uniform thickness is divided into eight congruent CST elements, as shown. Load P in the y direction is applied to the node at $x = y = 0$. If $\nu = 0$, what is the displacement of load P?

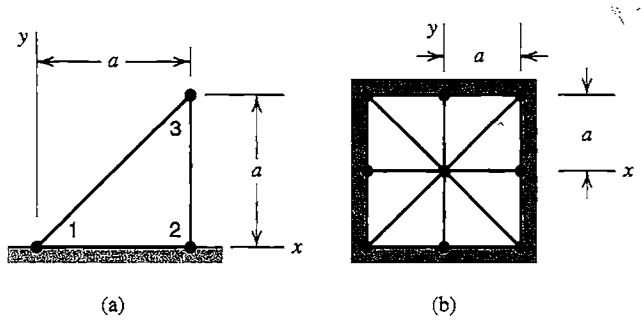

Problem 3.4-3

3.4-4 The x-direction displacement field of the CST shown is

$$u = \frac{y}{b}u_1 + \frac{1}{2}\left(1 - \frac{x}{a} - \frac{y}{b}\right)u_2 + \frac{1}{2}\left(1 + \frac{x}{a} - \frac{y}{b}\right)u_3$$

and similarly for y-direction displacement v. For constant thickness and $\nu = 0$, determine the 2 by 2 submatrix of [**k**] that operates on d.o.f. at node 1.

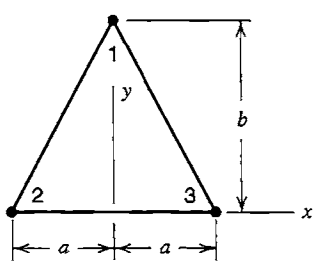

Problem 3.4-4

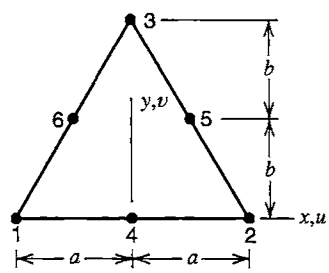

Problem 3.5-1

3.5-1 (a) For the LST element shown, determine shape function N_3 in terms of y and b (see Fig. 3.5-1 for a hint).
(b) Shape function N_4 for this element is $N_4 = 1 - (y/b) - (x/a)^2 + (y/2b)^2$. Show that N_4 is unity at node 4 and zero at all other element nodes.
(c) Let u_3, v_3, u_4, and v_4 be the only nonzero d.o.f. In terms of these d.o.f., x, y, a, and b, what is the element strain field?

3.6-1 Let a plane element be isotropic, and body forces F_x and F_y be constant. In terms of F_x, F_y, E, and ν, what must the values of a_4 and a_8 in Eqs. 3.6-1 be if the differential equations of equilibrium are to be satisfied?

3.6-2 For the Q4 element of Fig. 3.6-1, let the linear displacement field $u = a_1 + a_2x + a_3y$, $v = a_4 + a_5x + a_6y$ be prescribed. Nodal d.o.f. $\{\mathbf{d}\}$ are consistent with this field; that is, $u_1 = a_1 - a_2a - a_3b$, and so on.
(a) Show that with these nodal d.o.f., Eq. 3.6-5 yields the prescribed u and v fields.
(b) Similarly, show that $[\mathbf{B}]\{\mathbf{d}\}$ yields the constant strain state $\varepsilon_x = a_2$, $\varepsilon_y = a_6$, and $\gamma_{xy} = a_3 + a_5$.

3.6-3 (a) In Problem 3.4-1, consider a Q4 element whose nodes coincide with lettered points A, D, F, and C. Compute element stresses using the procedure described in Problem 3.4-1. For convenience, use the coordinate system of Fig. 3.6-1.
(b) Repeat part (a), but replace moment M by transverse tip force in the y direction. Neglect transverse shear deformation in computing displacements of lettered nodes.

3.6-4 Element j is a Q4 element that is to be attached to structure nodes 19, 20, 30, and 31, as shown. Assume that the structure stiffness matrix is to be stored as a full matrix, without use of a sparse-matrix storage format. D.o.f. are u and v at each node. What is the numerical contribution of element j to the single coefficient of [**K**] at the intersection of
(a) row 48 and column 39?
(b) row 37 and column 37?
(c) row 59 and column 61?

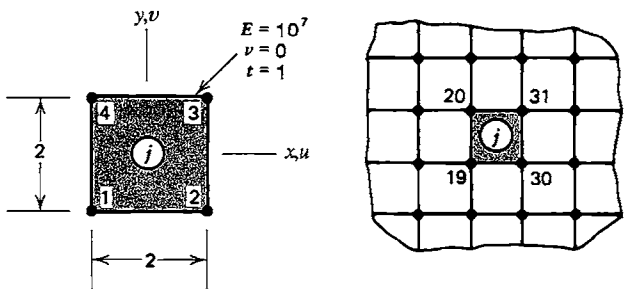

Problem 3.6-4

3.6-5 Let axes x and y originate at node 1 of a Q4 element, as shown. Write shape functions appropriate to this choice of axes.

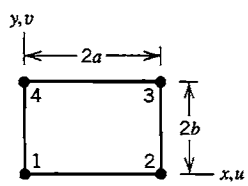

Problem 3.6-5

3.6-6 Reconsider Problem 3.4-3(b). Now divide the square structure into four square Q4 elements of equal area and solve for the displacement of the middle node in response to the load applied there.

3.6-7 A cantilever beam is loaded by transverse tip force. Consider the two different arrangements of sixteen Q4 elements shown. Transverse tip deflection is to be calculated.

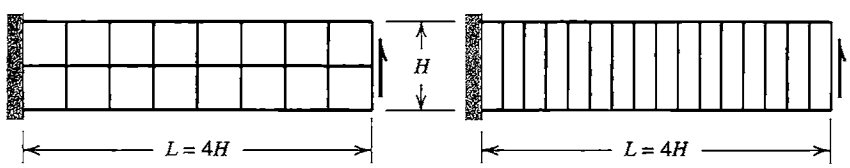

Problem 3.6-7

(a) Which mesh can be expected to provide the more accurate result, and why?
(b) Without undertaking actual FE analysis, estimate the percentage error expected from each mesh. For simplicity, let $\nu = 0$.

3.7-1 The element shown has three linear sides and one quadratic side. Determine the five shape functions N_i. *Suggestion:* Apply the method used to obtain Eqs. 3.6-4.

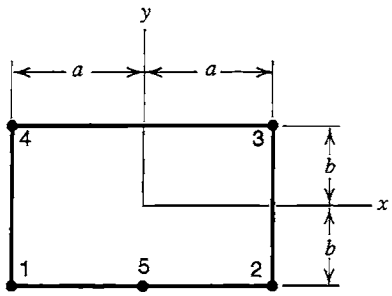

Problem 3.7-1

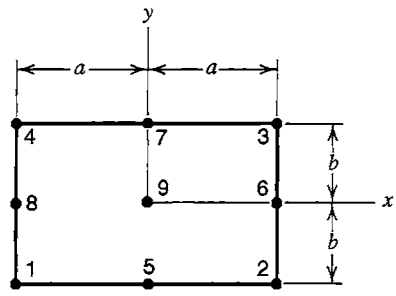

Problem 3.7-2

3.7-2 (a) Determine shape functions for the Q9 element shown.
(b) Show how N_1 varies over the element by making a sketch like that in Fig. 3.7-1b. Make similar sketches for shape functions N_8 and N_9.

3.8-1 A cantilever beam is loaded by lateral force at midspan, as shown in part (a) of the sketch. Parts (b), (c), and (d) show three different FE models, each containing 12 eight-node solid elements. Rank the three models from best to worst according to their expected accuracy in predicting the transverse tip displacement. Also sketch a mesh that contains the same type and number of elements as the meshes shown, but is superior to all of them for this particular problem.

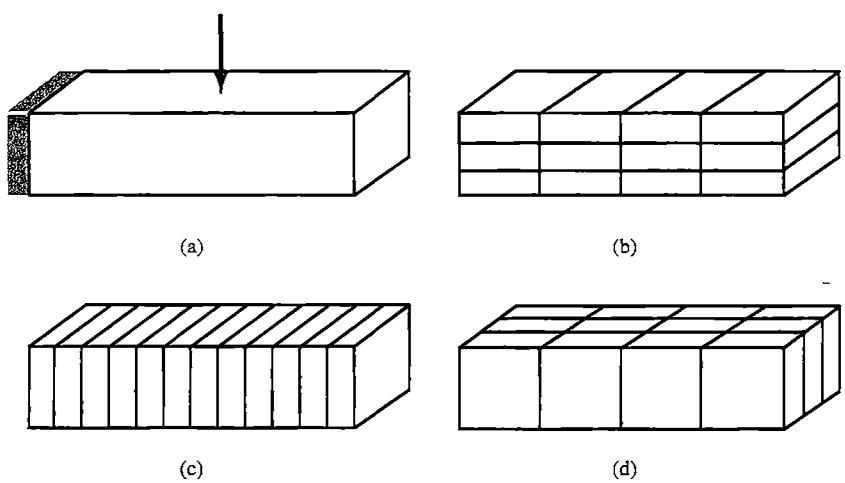

Problem 3.8-1

3.9-1 For a standard beam element, given by Eqs. 3.3-13 and 3.3-14, verify that $[\mathbf{B}]\{\mathbf{d}\}$ and $[\mathbf{k}]\{\mathbf{d}\}$ are both zero when $\{\mathbf{d}\}$ represents the rigid body motion of
(a) lateral translation.
(b) rotation about the left end.

3.9-2 For a beam element with a node at each end, as in Fig. 3.3-1b, consider the lateral displacement field

$$v = \frac{L-x}{L}v_1 + \frac{x}{2}\left(\frac{L-x}{L}\right)\theta_{z1} + \frac{x}{L}v_2 - \frac{x}{2}\left(\frac{L-x}{L}\right)\theta_{z2}$$

(a) Show that this field includes the required rigid body motion capability.
(b) If nodal d.o.f. consistent with a state of constant curvature are imposed, is the correct $v_{,xx}$ in fact obtained?
(c) Determine [**k**] based on the given field. What defects does this [**k**] have?

3.9-3 Bar elements shown are uniform and have nodes 1 and 2. Let the axial displacement field have forms defined as follows. In each case, express u in terms of nodal d.o.f. u_1 and u_2. Then determine the strain-displacement matrix and the element stiffness matrix in terms of A, E, and L. What defects do you see in these results, and what is their source?
(a) $u = a_1 + a_2x^2$.
(b) $u = a_1x + a_2x^2$.

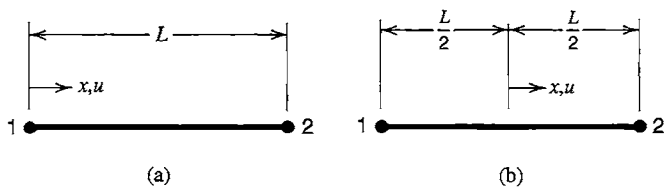

Problem 3.9-3

3.9-4 (a) For the two-element bar model shown, compute axial displacement at $x = 2L$ and axial stress at $x = 0$. Use the element stiffness matrix obtained in Problem 3.9-3a. Evaluate axial stress in an element by $\sigma_x = E\lfloor\mathbf{B}\rfloor\{\mathbf{d}\}$. Are the results correct?
(b) Repeat part (a), now using the element stiffness matrix obtained in Problem 3.9-3b.

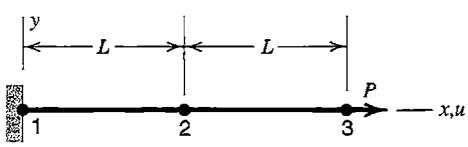

Problem 3.9-4

3.9-5 The eight-node solid element of Fig. 3.8-1a has six rigid body modes, six constant strain modes, and 12 nonuniform strain modes, for a total of 24 independent modes. Using sketches, describe four independent nonuniform strain modes that involve only x-direction nodal displacements.

3.10-1 In terms of the coordinates of vertex nodes of the triangle in Fig. 3.10-1, establish the contents of matrix [**T**] in Eq. 3.10-3.

3.10-2 Let a plane element have three or more sides, side lengths L_i, midside normal displacements δ_{mi}, and all translational d.o.f. at corners set to zero (see Fig. 3.10-1).

Show that use of a drilling d.o.f. at each corner implies the constraint equation $\sum(\delta_{mi}/L_i) = 0$, where the summation includes all sides.

3.11-1 Show that nodal forces calculated according to Eq. 3.11-6 are statically equivalent to the following loadings on a side of a rectangular plane body of unit thickness.
(a) $q_4 = \sigma$, $q_7 = 0$, and $q_3 = -\sigma$ (corresponding to a flexural stress distribution with node 7 on the neutral axis).
(b) $q_4 = 0$, $q_7 = \sigma/2$, and $q_3 = \sigma$ (corresponding to a flexural stress distribution with node 4 on the neutral axis).
(c) $q_4 = q_3 = 0$ and $q_7 = \tau$ (corresponding to a transverse shear stress distribution in a beam of rectangular cross section).

3.11-2 If load q is constant, the integrand in Eq. 3.11-6 becomes $[\mathbf{N}]^T q\, dx$. Using the integral, verify that the total force F on a straight side with a midside node is allocated as $F/6$, $2F/3$, and $F/6$ to the respective nodes.

3.11-3 Use the virtual work argument to determine nodal moment $qL^2/12$ associated with uniformly distributed transverse load q on a beam element (as shown in Eq. 2.9-2 and Fig. 2.9-2a). That is, calculate work done as q moves through the displacement created by virtual nodal rotation $\delta\theta_{z1}$ and beam shape function N_2, and equate it to work done by the nodal moment in acting through rotation $\delta\theta_{z1}$.

3.11-4 For the following loads on a beam element, determine the consistent nodal load vector. Also show that this load vector is statically equivalent to the given load.
(a) Uniformly distributed transverse load q acts on the left half of the element only.
(b) Concentrated moment M_c is applied at midspan.

3.11-5 In Fig. 3.11-1a, let force F act at $x = a/2$ as shown, but let the side have three nodes, as in Fig. 3.11-1b. What are the three resulting nodal loads on this side? Show that these loads are statically equivalent to F.

3.11-6 In Fig. 3.11-4c, show by use of Eq. 3.11-2 that distance $L/\sqrt{2}$ and load intensity $(1 + \sqrt{2})P/L$ constitute a loading that is statically equivalent to force P at point B.

3.11-7 A 10-unit force acts at point Q in the Q4 element shown. Determine the load vector $\{\mathbf{r}_e\}$.

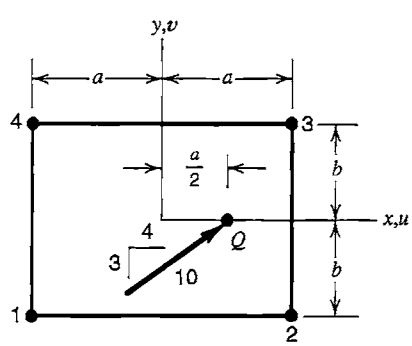

Problem 3.11-7

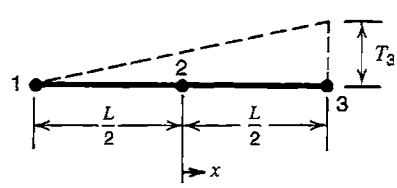

Problem 3.11-8

3.11-8 A uniform bar element has a node at each end and a node at the middle, as shown. Each node has an axial displacement d.o.f. A temperature change that varies linearly from 0 to T_3 is imposed. Determine the load vector $\{\mathbf{r}_e\}$.

3.11-9 Show that initial stresses $\{\boldsymbol{\sigma}_0\}$ on a C^0 element lead to nodal loads $\{\mathbf{r}_e\}$ that are self-equilibrating. That is, show that nodal forces in $\{\mathbf{r}_e\}$ provide a zero resultant.

3.11-10 Let temperature change T in the Q4 element of Fig. 3.6-1 have the form $T = T_0 x$, where T_0 is a constant. Material properties and thickness are constant over the element. Determine the load vector $\{\mathbf{r}_e\}$.

3.11-11 A bar of length L_T carries linearly varying axial load, as shown, where c is a constant. Consider FE models that have one, two, and finally three elements (of equal length in each case), using axial displacements as nodal d.o.f.
(a) Determine the consistent nodal load vector $\{\mathbf{r}_e\}$ for each of the three models.
(b) For each of the three models, solve for axial deflection at $x = L_T$. Also determine axial stress at $x = 0$ from the calculation $\sigma_x = E\lfloor\mathbf{B}\rfloor\{\mathbf{d}\}$.

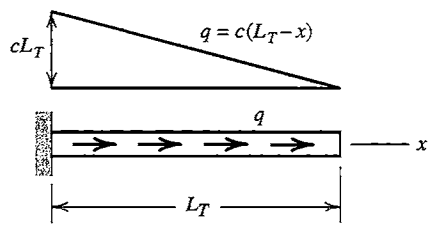

Problem 3.11-11

COMPUTATIONAL PROBLEMS

In the following problems compute significant values of displacement and/or stress, as appropriate. Exploit symmetry where possible. When mesh refinement is used, estimate the maximum percentage error of results provided by the finest FE mesh. Where dimensions or loads are not assigned, choose values that seem reasonable or convenient. Where material properties are needed but not stated, use properties of steel. Apply the analysis methodology suggested in Section 1.5.

C3.1 (a) The rectangular plane structure shown can be modeled by CST or LST triangular elements. Uniformly distributed pressure p is applied to the right edge as shown. Imagine that region AB is a soft but linearly elastic medium. Represent this medium by discrete linear springs that extend from the rigid support to structure nodes. Choose spring stiffnesses such that each element displays uniform uniaxial stress $\sigma_x = -p$.
(b) Alter part (a) by removing load p and by replacing medium AB by the supports shown. Apply the temperature change $T = T_0 x$, where T_0 is a constant. Then repeat the calculations, now using $T = T_0 y$. Are results reasonable? If results differ for the two thermal loadings, explain why.

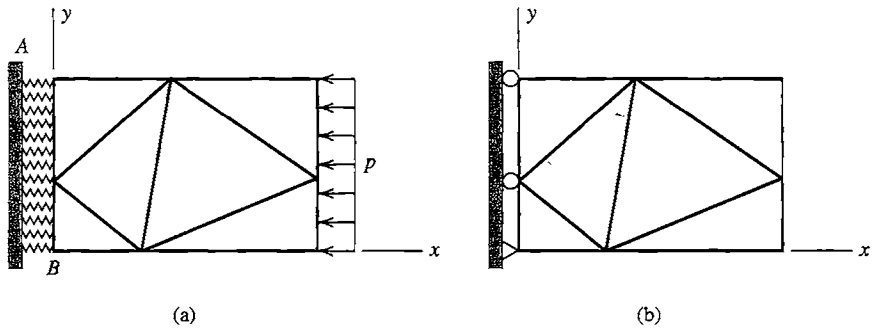

Problem C3.1

C3.2 A handbook such as [1.16] provides analytically and empirically determined stress concentration factors that can be used to improve FE modeling skills. Analyze the following cases, all of which appear in Table 37 of [1.16]. Use a dense mesh of elements where stress concentration is expected and a coarse mesh far from the area of concentration.
(a) Two U-notches in a member of rectangular section.
(b) Square shoulder with fillet in a member of rectangular section.
(c) Elliptical hole in an infinite plate.
(d) Infinite row of circular holes in an infinite plate.

C3.3 In Section 3.14, although agreement between the FE model and theory is acceptable, there is still an error (about 3%) between the peak stress expected and that computed by FEA. Modify the FE model to improve agreement. What is the effect of extending the domain further toward infinity? What is the effect of generating a more dense or less distorted mesh in the vicinity of the hole?

C3.4 A rectangular body 3.0 m in length and 1.0 m high is modeled as a cantilever beam. Let $E = 200$ GPa, $\nu = 0.3$, and thickness $= 1.0$ mm. Load the beam by a transverse tip force of 10^4 N uniformly distributed over the 1.0 m dimension. Generate an FE model of this beam using a small number of regularly shaped elements. Compare the distributions of σ_y and τ_{xy} generated by LST, Q4, Q6, and Q8 elements. How and why are these distributions consistent with properties of these elements as discussed in Sections 3.5, 3.6, 3.7, and 3.10?

C3.5 A centrally loaded beam is supported at both ends, as shown. Compute stress-σ_x at $x = 0$ on top and bottom surfaces. Compare these results with stress from the flexure formula, $\sigma_x = Mc/I$.
(a) Choose numerical values such as $P = 1$, $L = 12$, and various values of H in the range $4 < H < 36$ [1.16]. Build the FE model of plane elements.
(b) Model the structure by a minimal number of beam elements (see Eq. 2.3-6). Compare results with results obtained in part (a).
(c) Repeat part (a) but make the right-hand support like the left, so as to impose the restraints $u = v = 0$ at both lower corners.

C3.6 (a) In reality, a "fixed support" cannot be achieved. Assume that the cantilever beam shown is attached to a very large plane body that has the same thickness and elastic properties as the beam. By what amount is the tip rotation $\theta_z = ML/EI$ increased by deformation of the support [1.16,3.16]?

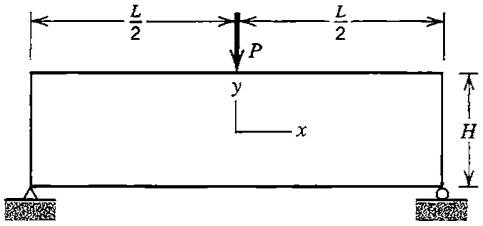

Problem C3.5

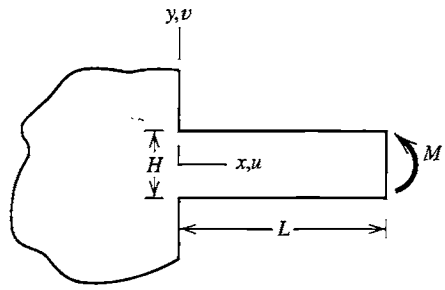

Problem C3.6

(b) Model the beam-to-plane connection of part (a) in the manner shown by Fig. 8.5-2b. Investigate the adequacy of this model.

C3.7 The structures shown consist of bars of square cross section (indicated by double lines) securely connected to flat panels of the same material. Centerlines of bars and midsurfaces of panels lie in the same plane. Let FE models consist of plane elements of thickness t and bar elements of cross-sectional area A. In part (a) of the sketch, $H_1 + H_2 \approx 3L$, $L \approx 500t$, and $A \approx (H_1 + H_2)t$ are suggested. Is it reasonable to neglect bending stiffness of the bars? Find out by repeating the analysis with bending stiffness included.

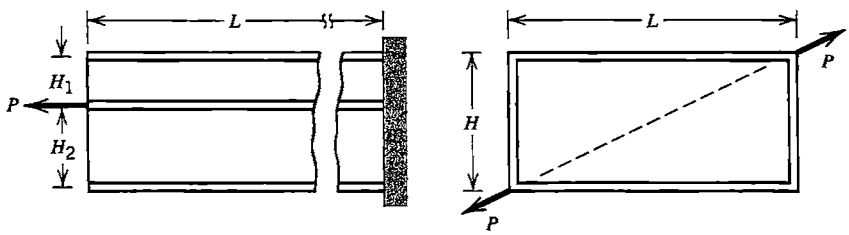

(a) (b)

Problem C3.7

C3.8 The cantilevered block of material shown is loaded by a uniformly distributed z-direction load q along line AA. Construct an FE model of 3D elements. As support conditions in the plane $y = 0$, apply q in the negative z direction along the line $z = h/2$, set $u = v = w = 0$ at $x = y = z = 0$, $w = 0$ at $x = b$ on the x axis, and $v = 0$ at all nodes in the $y = 0$ plane. Include $b >> h$ as one of the cases analyzed. Be sure to examine results near $x = 0$ or $x = b$.

C3.9 Consider the application of torque to the rectangular block sketched for Problem C3.8. Let the block be twisted about a y-parallel axis. As support conditions in the plane $y = 0$, set $v = 0$ at the midpoint of each edge, and set $u = w = 0$ at all nodes in the $y = 0$ plane. Devise a simple (if approximate) way to apply the twisting load to end $y = L$.

C3.10 Any of the preceding computational problems can be modified by making the material orthotropic. As a possible choice for plane problems, with n and s principal axes of the material, let $E_n = 8E_s$ and $G = 2E_s$, with zero Poisson ratios. Thus [E] becomes a diagonal matrix. Axes n and s may be oriented arbitrarily with respect to global axes.

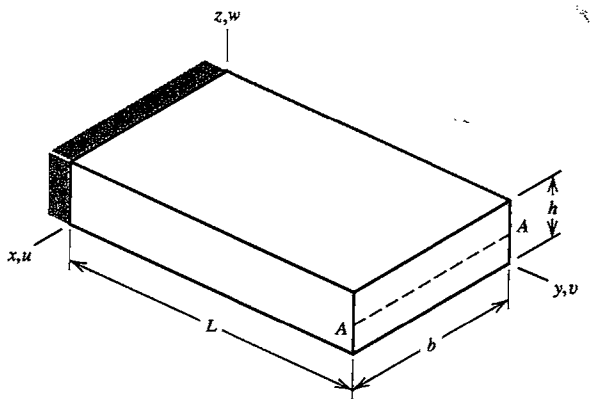

Problem C3.8

CHAPTER 4

FORMULATION TECHNIQUES: VARIATIONAL METHODS

Integral expressions called *functionals* are presented in this chapter. We seek values of d.o.f. that make these functionals either stationary or minimum. Functionals provide a powerful technique for generating finite element approximations. In structural mechanics, the most commonly used functional is that of potential energy. Other functionals, including one for heat conduction and other phenomena described by differential equations of the same form, are also presented.

4.1 INTRODUCTION

In preceding chapters, element stiffness matrices $[\mathbf{k}]$ are formulated either by direct physical argument or by using the principle of virtual work. Direct argument is limited to simple problems and simple elements. Virtual work is powerful and has physical appeal, but does not provide a framework for producing more general FE approximations. In this chapter we present a general and systematic procedure for producing FE approximations using the *Rayleigh-Ritz* method. The procedure requires only that a functional be available. In our terminology, a *functional* is an integral expression that implicitly contains the governing differential equations for a particular problem. Early sections of this chapter focus on structural mechanics. Later sections treat other physical problems.

The Rayleigh-Ritz method has a classical form and an FE form. In the classical form, an approximating field is defined over the entire domain of a problem. In the FE form, the approximating field is defined in piecewise fashion over subdomains, where each subdomain is a finite element. In both cases the approximating field is defined in terms of independent d.o.f. such that the configuration of the system always satisfies compatibility and does not violate essential boundary conditions (such as support conditions in structural mechanics).[1] In the classical form, d.o.f. may not have a straightforward physical interpretation, in which case we call them *generalized* d.o.f. In the FE form, d.o.f. are nodal values of the approximating field, and perhaps also nodal values of one or more spatial derivatives of the field, such as nodal rotations of a plate element.

Governing differential equations plus boundary conditions are said to state a problem in *strong form*. An integral expression such as a functional that implicitly contains the differential equations is called the *weak form*. The strong form states conditions that must be met at every material point, whereas the weak form states conditions that must be met only in an average or integral sense. Although the terminology of *weak form* and *strong form* may suggest inferiority of the weak form, both are valid statements of a problem. Indeed,

[1] Incompatible elements, introduced in Section 3.10 and further discussed in Section 6.6, provide limited relaxation of the continuity requirement.

in Section 4.7 we show that the weak form implies the strong form when infinitely many d.o.f. are present, as is the case prior to the discretization that accompanies FEA. The weak form provides a convenient starting point for producing finite element approximations.

A functional, such as that for potential energy Π_p, contains integrals that span the entire domain of a problem. After expressing the field quantity in terms of assumed modes and their associated d.o.f. and carrying out integrations, the Π_p expression becomes an algebraic function of a finite number of d.o.f. For an initially discrete structure such as a truss, the Π_p expression need not be written in integral form. We will consider these initially discrete forms first, then address the more general integral forms later in this chapter.

Physical insight was responsible for the early rapid development of the FE method and its appeal to stress analysts. A more mathematical approach augments physical understanding by placing FEA on a sound theoretical foundation, thus allowing statements to be made regarding bounds and convergence, and suggesting solution tactics that are not apparent from physical reasoning alone.

4.2 PRINCIPLE OF STATIONARY POTENTIAL ENERGY

In the present section we consider time-independent problems of structural mechanics. We define a *system* as the physical structure, its supports, and loads applied to it. The *configuration* of a system is the set of positions of all particles of the structure. Let the system have a reference configuration C_R and a displaced configuration C_D. A system is called *conservative* if work done by internal forces and work done by external loads are each independent of the path taken between C_R and C_D. In an elastic structure, work done by internal forces is equal in magnitude to the change in strain energy.

The linear spring of Fig. 4.2-1 is a simple example. Let C_R and C_D refer to unstretched and stretched configurations, respectively. If the spring dissipates no energy, then the work of internal forces (that is, strain energy in the spring) depends only on stretch D, not on whether the passage from C_R to C_D is via path A or path B. Similarly, if external load P has constant magnitude and constant direction, it does work equal to PD regardless of the path taken from C_R to C_D. We conclude that because internal forces and external forces are both conservative, so is the system. If $C_R = C_D$—that is, if the original configuration is restored after displacement—then $PD = 0$ and zero net work is done by all forces, regardless of the path taken.

Boundary conditions are of two types: *essential* (or *principal*) and *nonessential* (often called *natural*). In FEA, essential boundary conditions are prescribed values of nodal d.o.f., and nonessential boundary conditions are prescribed values of higher derivatives of the field quantity than are usually used as nodal d.o.f. (more detail and rigor appears

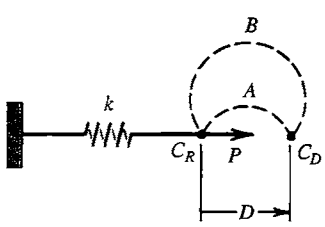

Figure 4.2-1. A linear spring of stiffness k loaded by a constant horizontal force P. Dashed lines A and B are possible displacement paths of the loaded point.

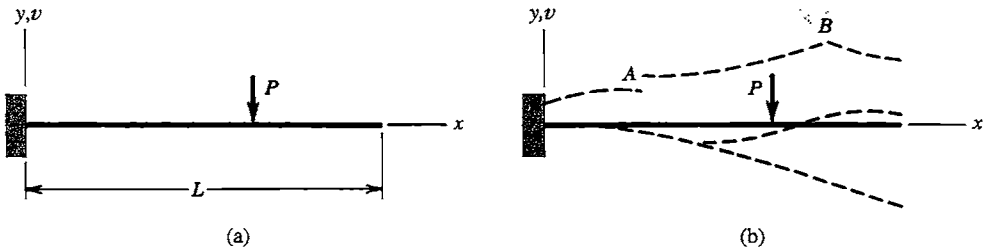

Figure 4.2-2. (a) A cantilever beam. (b) An inadmissible configuration (upper dashed line) and two admissible configurations (lower dashed lines).

in Section 4.7). For example, if we use standard Euler-Bernoulli beam elements (transverse shear deformation neglected), nodal d.o.f. are lateral deflection v and its first derivative, $v_{,x}$. When these elements are used to analyze the beam of Fig. 4.2-2a, essential boundary conditions (which may also be called *geometric, kinematic,* or *displacement* boundary conditions in this problem) are $v = 0$ and $v_{,x} = 0$ at $x = 0$. Nonessential boundary conditions are $v_{,xx} = 0$ and $v_{,xxx} = 0$ at $x = L$, because bending moment $M = EIv_{,xx}$ and transverse shear force $V = EIv_{,xxx}$ are both zero at $x = L$. Because $v_{,xx}$ and $v_{,xxx}$ are not used as nodal d.o.f., an FE solution that uses standard beam elements usually does not satisfy nonessential boundary conditions exactly.

An *admissible* configuration is any configuration that satisfies internal compatibility (described in Section 3.1) and essential boundary conditions. Examples of admissible and inadmissible configurations appear in Fig. 4.2-2b. The uppermost curve, which is inadmissible, has four faults: it violates the two essential boundary conditions $v = 0$ and $v_{,x} = 0$ at $x = 0$, and it violates internal compatibility because of the discontinuity at A and the cusp (or kink) at B. The lower two curves are *both* admissible, but only the lowest one seems physically reasonable. An admissible configuration need not satisfy nonessential boundary conditions. Thus, at $x = L$, neither of the two lower curves need satisfy $v_{,xx} = 0$ or $v_{,xxx} = 0$.

A conservative mechanical system has potential energy that can be expressed in terms of its initial and final configurations, without reference to whatever deformation history or path takes the system from initial to final configuration [4.1]. Potential energy, which is also known as *total* potential energy, includes (a) strain energy of elastic distortion, and (b) potential possessed by applied loads, by virtue of their having the capacity to do work if displaced through a distance. The *principle of stationary potential energy* states that

> *Among all admissible configurations of a conservative system, those that satisfy the equations of equilibrium make the potential energy stationary with respect to small admissible variations of displacement.*

This principle is applicable whether or not the load-versus-deformation relation is linear. If the stationary condition is a relative minimum, the equilibrium state is stable. Loads and internal stresses are assumed to remain unchanged during the small variation of displacement.

Example: Linear Spring with Axial Load. A very simple system is shown in Fig. 4.2-3. Its potential energy Π_p has two parts:

$$\Pi_p = U + \Omega \tag{4.2-1}$$

where U is the strain energy of the system, and Ω is the potential of applied loads. In the example of Fig. 4.2-3

$$U = \frac{1}{2}kD^2 \quad \text{and} \quad \Omega = -PD \tag{4.2-2}$$

The load is regarded as always acting at its full value P. In moving through displacement D it does work in the amount PD, thereby *losing* potential of equal amount; hence the negative sign in the expression $\Omega = -PD$. The potential energy

$$\Pi_p = \frac{1}{2}kD^2 - PD \tag{4.2-3}$$

can be regarded as the total internal and external work done in changing the configuration from the reference state $D = 0$ to the displaced state $D \neq 0$. Note that if P were directed toward the left, while D remains positive toward the right, then Ω would become $+PD$. In essence this is the same as increasing the potential energy of a weight by raising it.

If only displacements along the x axis are allowed, then the single d.o.f. D defines all admissible configurations. The equilibrium configuration D_{eq} is found from the stationary value of Π_p:

$$d\Pi_p = (kD_{eq} - P)dD = 0 \qquad \text{hence} \qquad D_{eq} = P/k \tag{4.2-4}$$

The equation $(kD_{eq} - P)dD = 0$ is an instance of the virtual work principle: zero net work is done by all forces, internal and external, during a small admissible displacement dD from the equilibrium configuration. This is graphically apparent in Fig. 4.2-4, where we also see that Π_p is a relative minimum, which means that the equilibrium state is stable.

The reference datum for Ω can be arbitrarily changed by a constant without changing the equilibrium configuration. For example, if we say that Ω is zero at the equilibrium configuration, then $\Omega = P(D_{eq} - D)$. The added constant PD_{eq} disappears in the process of writing $d\Pi_p = 0$, and the same value of D_{eq} is again obtained.

Conservation of Energy. We could bypass the stationary potential energy principle and imagine that D is produced by a gradually increasing load whose final value is P. Thus, equating work done by the load to strain energy stored in the linear spring, we have

$$\frac{1}{2}PD_{eq} = \frac{1}{2}kD_{eq}^2 \qquad \text{from which} \qquad D_{eq} = \frac{P}{k} \tag{4.2-5}$$

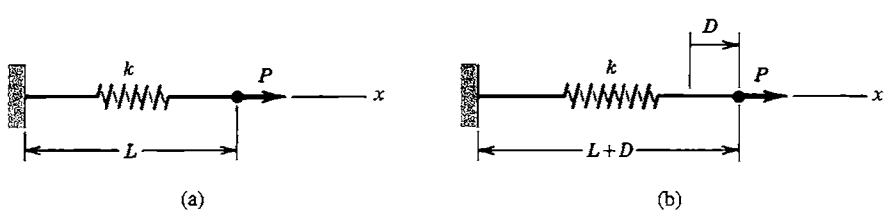

Figure 4.2-3. (a) Unstretched (reference) configuration of a linear spring of stiffness k. (b) Configuration after the spring is stretched an amount D due to application of force P.

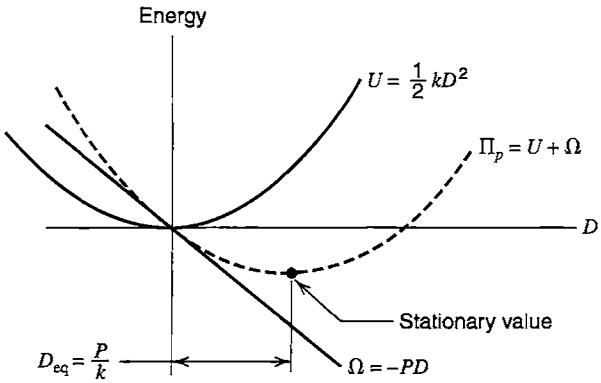

Figure 4.2-4. Graphical representation of energy relations for the problem of Fig. 4.2-3.

This energy balance argument is valid but rarely helpful. It yields but one equation, even if there are a great many d.o.f. that must be determined.

Factors of one-half are present in Eq. 4.2-5 only because force is directly proportional to extension in a linear spring. In Eq. 4.2-2, we write $\Omega = -PD$ rather than $\Omega = -\frac{1}{2}PD$ because load P is regarded as always acting at full intensity in the stationary potential energy principle. Potential Ω is *independent* of properties of the spring.

4.3 PROBLEMS HAVING MANY D.O.F.

A finite element discretization typically uses hundreds or thousands of d.o.f. They may be the x and y displacements of nodes (as in a plane stress problem), or lateral displacement v and its first derivative $v_{,x}$ at nodes (as in a beam problem), and so on. Let n be the number of d.o.f. that must be determined, and let them be collected in the structure displacement vector $\{\mathbf{D}\} = \lfloor D_1 \;\; D_2 \;\; \cdots \;\; D_n \rfloor^T$. In what follows we assume that support conditions are already imposed, so that arbitrary values of the D_i always give admissible configurations.

Potential Π_p is a function of the D_i. Symbolically, $\Pi_p = \Pi_p(D_1, D_2, \ldots, D_n)$. Applying the principle of stationary potential energy, we obtain

$$d\Pi_p = 0 \qquad \text{where} \qquad d\Pi_p = \frac{\partial \Pi_p}{\partial D_1} dD_1 + \frac{\partial \Pi_p}{\partial D_2} dD_2 + \cdots + \frac{\partial \Pi_p}{\partial D_n} dD_n \tag{4.3-1}$$

The stationary principle states that equilibrium prevails when $d\Pi_p = 0$ for *any* small admissible variation of the configuration. We can imagine that only dD_1 is nonzero, or that only dD_2 and dD_3 are nonzero, and so on. For any and all such choices, $d\Pi_p$ must vanish. This is possible only if all coefficients of the dD_i vanish separately. Thus, for $i = 1, 2, 3, \ldots, n$,

$$\frac{\partial \Pi_p}{\partial D_i} = 0 \qquad \text{or, in alternative notation,} \qquad \left\{\frac{\partial \Pi_p}{\partial \mathbf{D}}\right\} = \{\mathbf{0}\} \tag{4.3-2}$$

These are n equations to be solved for the n values of d.o.f. D_i that define the static equilibrium configuration.

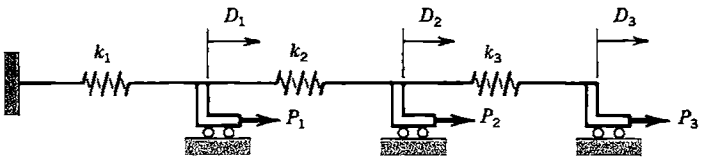

Figure 4.3-1. A three-d.o.f. system consisting of three linear springs and three axial loads P_1, P_2, and P_3. Springs are unstretched when $D_1 = D_2 = D_3 = 0$.

Example: Springs in Series. The structure shown in Fig. 4.3-1 has potential energy

$$\Pi_p = \frac{1}{2}k_1D_1^2 + \frac{1}{2}k_2(D_2 - D_1)^2 + \frac{1}{2}k_3(D_3 - D_2)^2 - P_1D_1 - P_2D_2 - P_3D_3 \tag{4.3-3}$$

where d.o.f. D_i are axial displacements relative to a point fixed in space, such as the left support. Equations 4.3-2 and 4.3-3 yield, for $i = 1, 2, 3$,

$$\begin{aligned} k_1D_1 - k_2(D_2 - D_1) - P_1 &= 0 \\ k_2(D_2 - D_1) - k_3(D_3 - D_2) - P_2 &= 0 \\ k_3(D_3 - D_2) - P_3 &= 0 \end{aligned} \tag{4.3-4}$$

In the matrix form $[\mathbf{K}]\{\mathbf{D}\} = \{\mathbf{R}\}$, Eqs. 4.3-4 are

$$\begin{bmatrix} k_1 + k_2 & -k_2 & 0 \\ -k_2 & k_2 + k_3 & -k_3 \\ 0 & -k_3 & k_3 \end{bmatrix} \begin{Bmatrix} D_1 \\ D_2 \\ D_3 \end{Bmatrix} = \begin{Bmatrix} P_1 \\ P_2 \\ P_3 \end{Bmatrix} \tag{4.3-5}$$

The correctness of stiffness matrix $[\mathbf{K}]$ in Eq. 4.3-5 can be checked by the procedure of activating one d.o.f. at a time, as described in Sections 2.2 and 2.3.

Remarks. From the foregoing example we draw the following conclusions, which are true in general:

1. A system that has linear load versus displacement characteristics has a symmetric stiffness matrix;[2] that is, $K_{ij} = K_{ji}$. This happens because each symmetrically located pair of off-diagonal coefficients comes from a single term in Π_p whose form is a constant times D_iD_j. Thus $K_{ij} = \partial^2\Pi_p/\partial D_i\partial D_j = \partial^2\Pi_p/\partial D_j\partial D_i = K_{ji}$, where K_{ij} multiplies D_j in the ith row of equations $[\mathbf{K}]\{\mathbf{D}\} = \{\mathbf{R}\}$ and K_{ji} multiplies D_i in the jth row.
2. If D_i is a nodal displacement (or rotation), the equation $\partial\Pi_p/\partial D_i = 0$ is a nodal equilibrium equation stating that forces (or moments) applied to the node sum to zero in the direction of D_i. Included in the sum are (a) loads from external sources and (b) loads from internal sources, due to deformation of structural components (and perhaps also due to thermal load, body force, etc.).
3. Static indeterminacy does not alter the procedure or make a problem more difficult. For example, in Fig. 4.3-1 we could connect a fourth spring between the left support

[2]These remarks on symmetry also apply to a special class of nonlinear materials, called hyperelastic, for which a strain energy density function U_0 can be defined.

and node 3. Then Π_p would be augmented by $k_4 D_3^2/2$, and the last stiffness coefficient in Eq. 4.3-5 would be changed from k_3 to $k_3 + k_4$, but no additional d.o.f. would be needed.

4. The potential energy of a linearly elastic structure can be written in the form

$$\Pi_p = U + \Omega \quad \text{where} \quad U = \frac{1}{2}\{\mathbf{D}\}^T[\mathbf{K}]\{\mathbf{D}\} \quad \text{and} \quad \Omega = -\{\mathbf{D}\}^T\{\mathbf{R}\} \tag{4.3-6}$$

If $U = 0$, then either $\{\mathbf{D}\}$ is null, $\{\mathbf{D}\}$ expresses a mechanism, or $\{\mathbf{D}\}$ expresses a rigid-body motion. If the structure is stable and is supported so that mechanisms and rigid-body motion are not possible (as in Eqs. 4.3-3 and 4.3-5), then $\frac{1}{2}\{\mathbf{D}\}^T[\mathbf{K}]\{\mathbf{D}\} > 0$ for any nonzero $\{\mathbf{D}\}$, and $[\mathbf{K}]$ is said to be *positive definite*.

4.4 POTENTIAL ENERGY OF AN ELASTIC BODY

The potential energy of an elastic body consists of strain energy contained in elastic distortions and potential energy of applied loads. The total potential energy expression, which we call Π_p, can be used to formulate element stiffness matrices and element load vectors. Simple FE formulations based on Π_p appear later in this chapter and additional formulations appear in subsequent chapters.

In this section we present formulas, argue their validity, show that special cases yield correct results, and consider examples. Derivations and detailed arguments appear elsewhere [4.1-4.3].

The energy that must be supplied to deform a unit volume of material is

$$\begin{aligned} U_0 &\neq \int \{\boldsymbol{\sigma}\}^T\{d\boldsymbol{\varepsilon}\} \qquad \sigma_{ij} = \frac{\partial U_0}{\partial \varepsilon_{ij}} \\ &\neq \int \sigma_x\, d\varepsilon_x + \int \sigma_y\, d\varepsilon_y + \int \sigma_z\, d\varepsilon_z + \int \tau_{xy}\, d\gamma_{xy} + \int \tau_{yz}\, d\gamma_{yz} + \int \tau_{zx}\, d\gamma_{zx} \end{aligned} \tag{4.4-1}$$

U_0 is called *strain energy per unit volume* or *strain energy density*. If the material is elastic, U_0 is energy stored in the material and recovered as work when the loading is removed. In this case U_0 may be called *elastic strain energy density*.

A linearly elastic material, without initial stress or strain, has the stress-strain relation $\{\boldsymbol{\sigma}\} = [\mathbf{E}]\{\boldsymbol{\varepsilon}\}$, in which $[\mathbf{E}]$ is symmetric. Material behavior may be isotropic, in which case the contents of $[\mathbf{E}]$ are given by Eq. 3.1-3 or Eq. 3.1-5, or anisotropic, in which case $[\mathbf{E}]$ is more complicated. Combination of the expression $\{\boldsymbol{\sigma}\} = [\mathbf{E}]\{\boldsymbol{\varepsilon}\}$ with Eq. 4.4-1 and integration yields the strain energy density

$$U_0 = \frac{1}{2}\{\boldsymbol{\sigma}\}^T\{\boldsymbol{\varepsilon}\} = \frac{1}{2}\{\boldsymbol{\varepsilon}\}^T[\mathbf{E}]\{\boldsymbol{\varepsilon}\} \tag{4.4-2}$$

For a linearly elastic material with initial stresses $\{\boldsymbol{\sigma}_0\}$ and initial strains $\{\boldsymbol{\varepsilon}_0\}$, the stress-strain relation is

$$\{\boldsymbol{\sigma}\} = [\mathbf{E}](\{\boldsymbol{\varepsilon}\} - \{\boldsymbol{\varepsilon}_0\}) + \{\boldsymbol{\sigma}_0\} \tag{4.4-3}$$

Combination of Eqs. 4.4-1 and 4.4-3 and integration yields a more general expression for strain energy density:

$$U_0 = \frac{1}{2}\{\boldsymbol{\varepsilon}\}^T[\mathbf{E}]\{\boldsymbol{\varepsilon}\} - \{\boldsymbol{\varepsilon}\}^T[\mathbf{E}]\{\boldsymbol{\varepsilon}_0\} + \{\boldsymbol{\varepsilon}\}^T\{\boldsymbol{\sigma}_0\} \tag{4.4-4}$$

In writing Eqs. 4.4-2 and 4.4-4, a constant of integration that is not a function of strains has been omitted. It is superfluous because it disappears during the differentiation process that makes Π_p stationary. That these integrations are correct may be shown by applying differentiation rules stated in Appendix A.

Now consider a body of linearly elastic material. If there are no initial stresses or initial strains, then the *total strain energy* contained in the body, U, is obtained from Eq. 4.4-2 as follows:

$$U = \int U_0\, dV = \frac{1}{2}\int \{\boldsymbol{\sigma}\}^T\{\boldsymbol{\varepsilon}\} dV = \frac{1}{2}\int \{\boldsymbol{\varepsilon}\}^T[\mathbf{E}]\{\boldsymbol{\varepsilon}\}\, dV \tag{4.4-5}$$

When initial stresses or initial strains are present somewhere in the body, Eq. 4.4-4 is integrated to give

$$U = \int U_0\, dV = \int\left(\frac{1}{2}\{\boldsymbol{\varepsilon}\}^T[\mathbf{E}]\{\boldsymbol{\varepsilon}\} - \{\boldsymbol{\varepsilon}\}^T[\mathbf{E}]\{\boldsymbol{\varepsilon}_0\} + \{\boldsymbol{\varepsilon}\}^T\{\boldsymbol{\sigma}_0\}\right) dV \tag{4.4-6}$$

Now consider a body of linearly elastic material that carries conservative loads. Using notation adopted in Section 3.3, the expression for its potential energy is

$$\begin{aligned}\Pi = &\int\left(\frac{1}{2}\{\boldsymbol{\varepsilon}\}^T[\mathbf{E}]\{\boldsymbol{\varepsilon}\} - \{\boldsymbol{\varepsilon}\}^T[\mathbf{E}]\{\boldsymbol{\varepsilon}_0\} + \{\boldsymbol{\varepsilon}\}^T\{\boldsymbol{\sigma}_0\}\right) dV - \int \{\mathbf{u}\}^T\{\mathbf{F}\}\, dV \\ &- \int \{\mathbf{u}\}^T\{\boldsymbol{\Phi}\}\, dS - \{\mathbf{D}\}^T\{\mathbf{P}\}\end{aligned} \tag{4.4-7}$$

The integrand of the first integral is U_0, the strain energy per unit volume. Integrals that contain body forces $\{\mathbf{F}\}$ and surface tractions $\{\boldsymbol{\Phi}\}$ represent work done (hence potential lost) by $\{\mathbf{F}\}$ and $\{\boldsymbol{\Phi}\}$ as the body deforms. In the last integral, $\{\mathbf{u}\}$ is evaluated on the surface S to which $\{\boldsymbol{\Phi}\}$ is applied. With u, v, and w being displacements in the x, y, and z directions respectively, potential energy changes associated with $\{\mathbf{F}\}$ and $\{\boldsymbol{\Phi}\}$, per unit volume and per unit area respectively, are

$$-\{\mathbf{u}\}^T\{\mathbf{F}\} = -F_x u - F_y v - F_z w \quad \text{and} \quad -\{\mathbf{u}\}^T\{\boldsymbol{\Phi}\} = -\Phi_x u - \Phi_y v - \Phi_z w \tag{4.4-8}$$

In writing Eq. 4.4-8, it is assumed that positive senses of $\{\mathbf{F}\}$ and $\{\boldsymbol{\Phi}\}$ correspond to positive displacement directions (which are taken to be in positive coordinate directions). For example, F_x, Φ_x, and u are all considered positive when acting in the $+x$ direction.

The final term in Eq. 4.4-7, $-\{\mathbf{D}\}^T\{\mathbf{P}\} = -D_1P_1 - D_2P_2 - \cdots - D_nP_n$, accounts for work done, hence potential lost, by prescribed concentrated forces and/or moments (of known magnitude) applied to the body. As usual, forces and moments share the same positive sense as their corresponding displacements and rotations. In writing this term, we assume that at the location of every load or moment P_i, there is a degree of freedom D_i, so that work done is simply D_iP_i. (Treatment of concentrated loads and/or moments that are not located at nodes is addressed in Section 3.11). We exclude from this list unknown loads applied by d.o.f. that are prescribed, such as d.o.f. set to zero as support conditions. In FEA, prescribed nonzero d.o.f. create strains that are accounted for by the first term in the first integral of Eq. 4.4-7.

In a typical problem, many of the load terms $\{\boldsymbol{\varepsilon}_0\}$, $\{\boldsymbol{\sigma}_0\}$, $\{\mathbf{F}\}$, $\{\boldsymbol{\Phi}\}$, and $\{\mathbf{P}\}$ are zero. For example, if initial stress is due to localized heating, $\{\boldsymbol{\sigma}_0\}$ is zero throughout most of the body. If gravity or acceleration loads are considered unimportant, $\{\mathbf{F}\} = \{\mathbf{0}\}$. Surface tractions $\{\boldsymbol{\Phi}\}$ usually act on only a portion of surface S and may be absent altogether. Indeed, *all* these load terms might be zero if nonzero values of one or more d.o.f. are prescribed instead.

Equation 4.4-7 is not restricted to rectangular coordinates. It requires only that x, y, and z refer to three mutually perpendicular directions at each material point.

Particular Cases. In its most general form, Eq. 4.4-7 includes all six strains in $\{\boldsymbol{\varepsilon}\}$ and material property matrix $[\mathbf{E}]$ is 6 by 6. Its coefficients are stated in Eq. 3.1-5 for the case of isotropy. If the problem is one of plane stress or plane strain, then $\{\boldsymbol{\varepsilon}\} = \lfloor \varepsilon_x \;\; \varepsilon_y \;\; \gamma_{xy} \rfloor^T$ is used for analysis and $[\mathbf{E}]$ is a 3 by 3 matrix. For an isotropic material, terms in $[\mathbf{E}]$ are given by Eq. 3.1-3 for plane stress and by Eq. 3.4-11 for plane strain.

The simplest special case is that of uniaxial stress. For this particular case, and perhaps for others as well, it may be easier to derive the strain energy expression afresh, as follows, rather than extract it from Eq. 4.4-7. Equation 4.4-3 becomes $\sigma_x = E\varepsilon_x - E\varepsilon_{x0} + \sigma_{x0}$ and U_0 becomes $U_0 = \frac{1}{2}\sigma_x\varepsilon_x = \frac{1}{2}E\varepsilon_x^2 - \varepsilon_x E\varepsilon_{x0} + \varepsilon_x\sigma_{x0}$. After integration and inclusion of load terms, we obtain in place of Eq. 4.4-7

$$\Pi_p = \int_0^L \left(\frac{1}{2}E\varepsilon_x^2 - \varepsilon_x E\varepsilon_{x0} + \varepsilon_x\sigma_{x0}\right) A\,dx - \int_0^L uF_x A\,dx - \{\mathbf{D}\}^T\{\mathbf{P}\} \tag{4.4-9}$$

where E = elastic modulus, $dV = A\,dx$, A = cross-sectional area, and L = length. In the second integral, the integrand could be regarded as $uF_x\,dV$ or as $uq\,dx$, where $q = F_xA$: axial body force F_x and axial line load q have the same effect when the body is mathematically one-dimensional.

In Euler-Bernoulli beam theory, Fig. 4.4-1b, transverse shear deformation is neglected and normal stress σ_x is regarded as the only nonzero stress. Therefore the expression for strain energy in an Euler-Bernoulli beam can be derived from Eq. 4.4-9. Let b represent the width of the beam cross section. Because $\varepsilon_x = u_{,x}$ and $u = -yv_{,x}$, the first term in Eq. 4.4-9 yields

$$\int \frac{1}{2}E\varepsilon_x^2\,dV = \int\int \frac{1}{2}E(-yv_{,xx})^2 b\,dy\,dx = \int \frac{1}{2}EI_z v_{,xx}^2\,dx \tag{4.4-10}$$

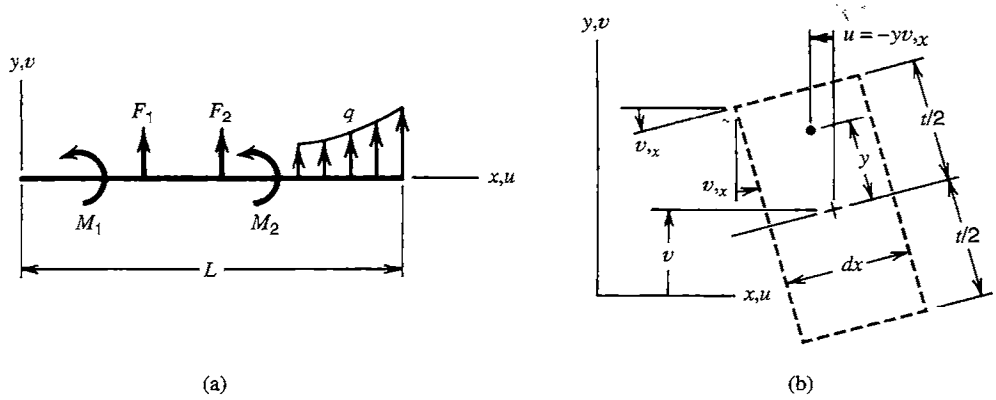

Figure 4.4-1. (a) A beam loaded by lateral forces F_i, moments M_i, and distributed lateral load q (force per unit length). (b) A slice cut from the beam, shown after it has undergone lateral deflection v and small rotation $v_{,x}$. Transverse shear deformation is ignored.

where, if the cross section is rectangular, $I_z = bt^3/12$ is the moment of inertia of cross-sectional area A about the centroidal z axis. If terms analogous to ε_{x0} and σ_{x0} are omitted (the reader may add these terms as an exercise), the expression for potential energy of a straight Euler-Bernoulli beam is

$$\Pi_p = \int_0^L \frac{1}{2} E I_z v_{,xx}^2 dx - \int_0^L vq\, dx - \{\boldsymbol{v}\}^T\{\mathbf{F}\} - \{\boldsymbol{\theta}\}^T\{\mathbf{M}\} \tag{4.4-11}$$

where $\{\boldsymbol{v}\}^T = \lfloor v_1 \;\; v_2 \;\; \cdots \rfloor$ and $\{\boldsymbol{\theta}\}^T = \lfloor \theta_{z1} \;\; \theta_{z2} \;\; \cdots \rfloor$ are lateral deflections and rotations ($\theta_z = v_{,x}$) at locations where lateral forces $\{\mathbf{F}\}$ and moments $\{\mathbf{M}\}$ are applied. The second integral in Eq. 4.4-11 accounts for work done by lateral force increments $q\,dx$ during lateral displacement v. Axial stress in the beam is $\sigma_x = E\varepsilon_x = Eu_{,x} = -Eyv_{,xx}$.

Plates in bending are analogous to beams in that strain energy is conveniently expressed in terms of curvatures rather than strains. Specifically, in a thin plate having lateral deflection $w = w(x,y)$, strain energy can be expressed in terms of $w_{,xx}$, $w_{,yy}$, and $w_{,xy}$ instead of ε_x, ε_y, and γ_{xy}.

Example: Bar under Axial Load. Let the uniform bar of Fig. 4.4-2 carry an end load P and be uniformly heated T degrees. Let D designate the end displacement produced by P and T. With $\varepsilon_{x0} = 0$, $\sigma_{x0} = -E\alpha T$, and $\varepsilon_x = D/L$, Eq. 4.4-9 becomes

$$\Pi_p = \int_0^L \left[\frac{1}{2}E\left(\frac{D}{L}\right)^2 + \frac{D}{L}(-E\alpha T)\right] A\, dx - DP = \frac{EAD^2}{2L} - DEA\alpha T - DP \tag{4.4-12}$$

End displacement D is found from the equation $d\Pi_p/dD = 0$:

$$D = \frac{PL}{AE} + \alpha TL \tag{4.4-13}$$

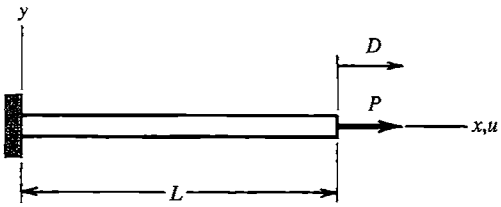

Figure 4.4-2. Uniform bar under axial load P.

Finally, axial stress σ_x is, with $\varepsilon_x = D/L$,

$$\sigma_x = E\varepsilon_x + \sigma_{x0} = E\left(\frac{P}{AE} + \alpha T\right) + (-E\alpha T) = \frac{P}{A} \tag{4.4-14}$$

which is the result expected.

4.5 THE RAYLEIGH-RITZ METHOD

Deformation of a structure composed of discrete members, such as a truss or a frame, can be represented exactly by a finite number of d.o.f. These d.o.f. are displacements of the joints. A continuum, such as an elastic solid, has an infinite number of d.o.f., namely the displacements of every particle of material. Behavior of a continuum is described by partial differential equations. For all but the simplest problems there is little hope of discovering a stress field or a displacement field that solves the differential equations and satisfies boundary conditions. The need to solve differential equations can be avoided by applying the Rayleigh-Ritz method to a functional, such as Π_p, that describes the mathematical model. The result is a substitute model that has a finite number of d.o.f. and is described by algebraic equations rather than by differential equations. A Rayleigh-Ritz solution is rarely exact but becomes more accurate as more d.o.f. are used.

The Rayleigh-Ritz method has a classical form and an FE form. It was originated in the 1870s for studies of vibration problems by Lord Rayleigh. He used an approximating field that contained a single d.o.f. In 1909, Ritz generalized the method by building an approximating field from several functions, each satisfying essential (kinematic) boundary conditions, and each associated with a separate d.o.f. Ritz applied the method to equilibrium problems and to eigenvalue problems. In general, the Rayleigh-Ritz method is a procedure for determining parameters in an approximating field so as to achieve an extremum of a function F of the field. Examples of F include Π_p and the Rayleigh quotient of structural dynamics. The procedure for an equilibrium (time-independent) problem is described here.

Consider an elastic solid. Displacements and stresses produced by applied loads are required. In general, a point has displacement components u, v, and w. A Rayleigh-Ritz solution begins with approximating fields for these components. Each field is a series, whose typical term is a function of the coordinates, $f_i = f_i(x,y,z)$, times an amplitude a_i whose value is yet to be determined. The a_i may be called *generalized coordinates* or *generalized d.o.f.* We write

$$u = \sum_{i=1}^{l} a_i f_i \qquad v = \sum_{i=l+1}^{m} a_i f_i \qquad w = \sum_{i=m+1}^{n} a_i f_i \tag{4.5-1}$$

Each function $f_i = f_i(x,y,z)$ must be *admissible;* that is, each must satisfy compatibility conditions and essential boundary conditions. It is not required that any f_i satisfy nonessential boundary conditions, but doing so yields a more accurate approximation for a given number of d.o.f. Usually, but not necessarily, the f_i are polynomials, which automatically satisfy compatibility conditions. The analyst must estimate how many terms are needed in each series in order to achieve the accuracy required. Thus the series in Eq. 4.5-1 are truncated rather than infinite, having, respectively, l, $m - l$, and $n - m$ terms, for a total of n terms.

D.o.f. of the problem are the n amplitudes a_i. They are determined as follows. Substitute Eqs. 4.5-1 into the strain-displacement relations (Eqs. 3.1-9) to determine strains $\{\boldsymbol{\varepsilon}\}$, then use Eq. 4.4-7 to evaluate Π_p. Thus Π_p becomes a function of d.o.f. a_i, just as Π_p is a function of d.o.f. D_i in Eq. 4.3-1. According to the principle of stationary potential energy, the equilibrium configuration is defined by the n algebraic equations

$$\frac{\partial \Pi_p}{\partial a_i} = 0 \quad \text{for} \quad i = 1, 2, \ldots, n \tag{4.5-2}$$

After Eqs. 4.5-2 are solved for numerical values of the a_i, the displacement fields of Eqs. 4.5-1 are completely defined. Differentiation of displacement fields yields strains, and subsequently using these strains in the stress-strain relations provides stresses.

The foregoing procedure has two principal steps. First, establish a trial family of admissible solutions. Second, apply a criterion to select the best form of the family. Here the criterion is that Π_p be stationary. Alternative criteria are available, such as methods of weighted residuals (Chapter 5).

Equations 4.5-1 create a substitute problem because the infinitely many d.o.f. of the original mathematical model are replaced by the finite number of d.o.f. in the Rayleigh-Ritz model. A Rayleigh-Ritz solution is usually approximate because there is no combination of the assumed functions f_i that is capable of exactly representing displacements of the original mathematical model. The solution process selects amplitudes a_i so as to combine functions f_i to best advantage. When Π_p is the functional, this means determining the combination of d.o.f. a_i so that Π_p is as small as possible, which implies that the underlying differential equations of equilibrium and stress boundary conditions are approximated with increasing accuracy as more and more terms $a_i f_i$ are added to the series.

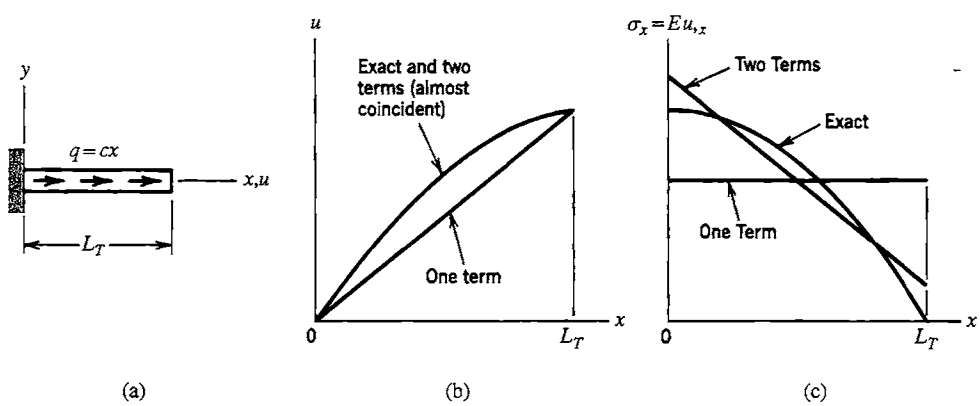

Figure 4.5-1. (a) Uniform bar under linearly varying distributed axial load of intensity $q = cx$, where c is a constant. (b) Exact and approximate axial displacements. (c) Exact and approximate axial stresses.

Equations 4.5-2 are found to be stiffness equations. They can be written in the usual form $[\mathbf{K}]\{\mathbf{D}\} = \{\mathbf{R}\}$, where $\{\mathbf{D}\} = \lfloor a_1 \;\; a_2 \;\; \cdots \;\; a_n \rfloor^T$. Not all D_i have units of displacement and not all R_i have units of force, but each product $R_i D_i$ has units of work or energy.

Example: Bar under Axial Load. Consider the uniform bar of Fig. 4.5-1a. Axial load q is linearly distributed along the length of the bar according to $q = cx$, where c is a constant that has units of force divided by the square of length. Axial displacement u and axial stress σ_x in this mathematical model are to be computed by the Rayleigh-Ritz method.

Axial strain is $\varepsilon_x = u_{,x}$. Thus Eq. 4.4-9 becomes

$$\Pi_p = \int_0^{L_T} \frac{1}{2} E u_{,x}^2 A \, dx - \int_0^{L_T} u \, cx \, dx \tag{4.5-3}$$

Equation 4.5-1 becomes, with $f_i = x^i$ in this case,

$$u = \sum_{i=1}^{n} a_i f_i = a_1 x + a_2 x^2 + a_3 x^3 + \cdots + a_n x^n \tag{4.5-4}$$

Note that there is no initial term a_0: the displacement mode $u = a_0$ is inadmissible because it violates the essential boundary condition, namely $u = 0$ at $x = 0$.

The simplest approximation results from using only the first term of the series, $u = a_1 x$. From Eqs. 4.5-2 and 4.5-3,

$$\Pi_p = \frac{AEL_T}{2} a_1^2 - \frac{cL_T^3}{3} a_1 \tag{4.5-5a}$$

$$\frac{d\Pi_p}{da_1} = 0 \qquad \text{yields} \qquad a_1 = \frac{cL_T^2}{3AE} \tag{4.5-5b}$$

$$\text{hence} \qquad u = \frac{cL_T^2}{3AE} x \quad \text{and} \quad \sigma_x = E u_{,x} = \frac{cL_T^2}{3A} \tag{4.5-5c}$$

Before commenting on these results we consider a two-term solution, using the field $u = a_1 x + a_2 x^2$. After substituting into Eq. 4.5-3 and writing $\partial \Pi_p / \partial a_1 = 0$ and $\partial \Pi_p / \partial a_2 = 0$, we obtain

$$AEL_T \begin{bmatrix} 1 & L_T \\ L_T & 4L_T^2/3 \end{bmatrix} \begin{Bmatrix} a_1 \\ a_2 \end{Bmatrix} = \frac{cL_T^3}{12} \begin{Bmatrix} 4 \\ 3L_T \end{Bmatrix} \quad \text{or} \quad \begin{Bmatrix} a_1 \\ a_2 \end{Bmatrix} = \frac{cL_T}{12AE} \begin{Bmatrix} 7L_T \\ -3 \end{Bmatrix} \tag{4.5-6a}$$

$$\text{hence} \qquad u = \frac{cL_T}{12AE}(7L_T x - 3x^2) \quad \text{and} \quad \sigma_x = E u_{,x} = \frac{cL_T}{12A}(7L_T - 6x) \tag{4.5-6b}$$

Figures 4.5-lb and 4.5-1c show the exact and approximate results. As expected, two-term results (Eqs. 4.5-6) are better than one-term results (Eqs. 4.5-5). With the body force term $F = cx/A$, the differential equation of equilibrium (Eq. 3.1-12) becomes

$$\sigma_{x,x} + \frac{cx}{A} = 0 \quad \text{or} \quad AEu_{,xx} + cx = 0 \tag{4.5-7}$$

where the latter equation results from the substitution $\sigma_x = Eu_{,x}$. Neither Eq. 4.5-7, nor the natural boundary condition $\sigma_x = 0$ at $x = L_T$, is satisfied by the foregoing two approximate solutions.

Notice that approximate displacements are more accurate than approximate stresses. This is to be expected, because stresses are calculated from derivatives of the approximating field. (To see that differentiation exacerbates discrepancies, consider the functions $f_1 = 4x(1 - x)$ and $f_2 = \sin \pi x$. In the range $0 < x < 1$, functions f_1 and f_2 look much alike, but successive derivatives of f_1 and f_2 have less and less resemblance.)

The mathematically exact solution of the problem of Fig. 4.5-la is obtained by solving Eq. 4.5-7 with boundary conditions $u = 0$ at $x = 0$ and $\sigma_x = 0$ at $x = L$. Thus

$$u = \frac{c}{6AE}(3L_T^2 x - x^3) \tag{4.5-8}$$

Use of the series $u = a_1 x + a_2 x^2 + a_3 x^3$ in the Rayleigh-Ritz method produces

$$a_1 = \frac{cL_T^2}{2AE} \qquad a_2 = 0 \qquad a_3 = -\frac{c}{6AE} \tag{4.5-9}$$

which is the exact solution. Use of still more terms leads again to the exact solution: one obtains the same a_1, a_2, and a_3 as in Eq. 4.5-9 and $a_4 = a_5 = a_6 = \cdots = a_n = 0$. In general, the Rayleigh-Ritz method yields the exact solution if the approximating field is capable of representing the exact field by appropriate choice of d.o.f. a_i. In practice this circumstance is rare.

4.6 COMMENTS REGARDING THE RAYLEIGH-RITZ METHOD

Approximating fields must be admissible and should be easy to use. Only polynomials, and occasionally sine and cosine functions, are simple enough to be practicable. Beyond this there are no easy answers to important questions: What form of assumption for the field is best? How many terms should be used? How accurate are computed results? These difficulties and uncertainties appear in both the classical Rayleigh-Ritz method and its FE form, and are increased for multidimensional problems.

In seeking the exact solution of a mathematical model, imagine that several numerical solutions are obtained, each time with another term added to the assumed field (as in Eqs. 4.5-5 and 4.5-6, for example). Thus we generate a sequence of trial solutions. We expect the sequence to converge: to the exact Π_p, to exact displacements, and to exact stresses. A necessary condition for convergence is that the trial field be *complete.*

Completeness is achieved if the exact displacements, *and* their derivatives that appear in Π_p, can be matched arbitrarily closely if enough terms appear in the trial field. In this sense, the word "completeness" has a different, more liberal meaning than when used to describe the completeness of a polynomial.

Completeness demands that the lowest-order admissible terms be included. For example, consider the tip-loaded bar of Fig. 4.4-2. If we omit the term a_1x from Eq. 4.5-4, we omit the very term that contains the exact answer, namely $u = (P/AE)x$. Thus completeness is destroyed, and the sequence of approximate solutions does not produce the exact answer even if the number of terms approaches infinity. This is easy to see: if Eq. 4.5-4 begins with a_2x^2, then $\sigma_x = Eu_{,x} = 0$ at $x = 0$, which is incorrect. The term a_1x provides the essential *constant-strain capability.* (In a finite element context, this requirement means that each element must be capable of representing a state of constant strain.) Completeness also requires that no series terms be omitted. Referring again to Eq. 4.5-4, a two-term approximation should be $a_1x + a_2x^2$, not $a_1x + a_3x^3$, and not $a_1x + a_4x^4$, and so on.

Note that polynomial terms in an element field are not chosen with the sole purpose of including all terms of a given degree. While it is mandatory to include certain lower degree terms, as described by Requirement 1 in Section 4.9, the choice of which higher degree terms to include is based on considerations of interelement compatibility and frame invariance, as discussed in Section 3.9. For example, each field of the nine-node plane element noted following Eq. 3.7-2 contains two of the four cubic terms and one of the five quadratic terms, and therefore the polynomial is complete only through quadratic terms.

In comparison with the mathematical model, a compatible Rayleigh-Ritz solution is either exact or too stiff. This happens because the numerically modeled structure is permitted to displace only into shapes that can be described by superposing the finite number of functions f_i retained in the assumed displacement field. Therefore, the correct shape is excluded, unless the problem is so simple that the assumed field happens to contain it. Effectively, for most practical problems, the assumed field imposes constraints that prevent the structure from deforming the way it wants to. Constraints stiffen a structure. In effect, the solution method creates a substitute mathematical model that is stiffer than the original mathematical model. Thus, as d.o.f. are added, an FE solution approaches the mathematically exact solution "from below."

In practical problems the Rayleigh-Ritz solution is approximate. Because stiffness is generally overpredicted, a Rayleigh-Ritz solution underpredicts displacements, *in an average sense,* when loads are prescribed and d.o.f. are either free or prescribed as zero. Specifically, if the structure is loaded by a single concentrated force (or moment), then displacement (or rotation) at the loaded point is certain to be underpredicted, or at best exact in a very simple problem, but never overpredicted. If the problem has multiple loads (and/or body forces and surface tractions) and d.o.f. are either free or are prescribed as zero, then the solution will underpredict displacements in some regions and may overpredict displacements in others. However, displacements are underpredicted in the sense that total work done by loads in undergoing displacements predicted by a Rayleigh-Ritz solution is less than the exact work (or at best equal to it, but never greater). Therefore, computed strain energy in the structure is a lower bound on the exact value.

Conversely, if the only loads are those implicitly associated with supports and prescribed nonzero values of some d.o.f., we generally find that these loads are overpredicted in an average sense. For problems involving both prescribed loads and prescribed nonzero displacements, we can say only that overall stiffness is overestimated.

Stresses are calculated from displacements, so we expect that a too-stiff structure will underestimate stress magnitudes when loading consists of prescribed forces and/or moments. However, as seen in Fig. 4.5-1c, approximate stresses may be too low in one region but too high in another, even when stress is derived from an approximate displacement field that is everywhere too low. Accordingly, a rule about stress magnitudes would be either so crude or so equivocal as to be of little value.

4.7 STRONG FORM AND WEAK FORM

The principle of stationary potential energy is one of many stationary principles of mathematical physics. Central to each is a functional, of which Π_p is one. In this section we first state, without derivation, rules that provide the governing differential equations contained in a particular functional. Then, for the example of an axially loaded bar, we use the calculus of variations to show that the functional contains the differential equations and nonessential boundary conditions.

Consider the functional Π_p, given by Eq. 4.4-7. It depends on displacements $\{\mathbf{u}\}$ and strains $\{\boldsymbol{\varepsilon}\}$, which are derivatives of displacements $\{\mathbf{u}\}$. The term "functional" indicates that Π_p depends not on $\{\mathbf{u}\}$ and its derivatives at a particular point, but upon their integrated effect over a region of interest. The stationary condition $d\Pi_p = 0$ may be applied directly to Eq. 4.4-7, without first expressing Π_p in terms of a finite number of d.o.f. This is accomplished using the *calculus of variations,* details of which are beyond the scope of this book [4.1-4.3]. End results of using Eq. 4.4-7 and setting $d\Pi_p$ to zero are found to be the differential equations of equilibrium (in general, Eqs. 3.1-12) and the nonessential boundary conditions (in general, stress boundary conditions, Eqs. 3.1-14). Thus, if the field $\{\mathbf{u}\}$ is admissible, the statement $d\Pi_p = 0$ implies all additional components of a valid solution. In an approximation that uses a finite number of d.o.f., equilibrium conditions and stress boundary conditions are satisfied only in an average or integral sense, not at every point.

In other physical problems there exist other functionals Π. Instead of displacements $\{\mathbf{u}\}$, the primary field may be temperature, pressure, or voltage, or another field variable. In each case the functional Π can be tested for correctness by applying the calculus of variations to see if the condition $d\Pi = 0$ yields the appropriate governing differential equations and nonessential boundary conditions.

Boundary Conditions. There are two classes of boundary conditions: *essential* and *nonessential.* Despite implications of this nomenclature, both classes are equally important. The distinction relates to how boundary conditions are treated and approximated with variational methods. For a problem having one dependent field variable, the rule is as follows. Let $2m$ be the highest-order derivative of the dependent field variable in the governing differential equation. Derivatives of order m then appear in the functional. Essential boundary conditions involve derivatives of order zero through $m - 1$, the zeroth derivative being the dependent variable itself. Nonessential boundary conditions involve derivatives of order m and higher, up to and including $2m - 1$. The following are examples.

Problem	Bar (Fig. 4.5-1a)	Beam bending	2D heat conduction
Differential equation	$AEu_{,xx} + q = 0$	$EIv_{,xxxx} - q = 0$	$k\nabla^2 T + Q - c\rho\dot{T} = 0$
$2m, m-1, 2m-1$	2, 0, 1	4, 1, 3	2, 0, 1
Essential B.C.	On u only	On v and $v_{,x}$	On T only
Nonessential B.C.	On $\sigma_x = Eu_{,x}$	On $M = EIv_{,xx}$ and $V = EIv_{,xxx}$	On heat flux $f_B = k(T_{,x}l + T_{,y}m)$

In these examples the dependent field variables are axial displacement u, lateral displacement v, and temperature T. Nonessential boundary conditions apply to axial stress σ_x, bending moment M, transverse shear force V, and inward heat flux f_B. In the heat conduction example, k is thermal conductivity, $\dot{T}$ is the time derivative of T, and l and m are direction cosines of a normal to the boundary.

The foregoing remarks are little changed if there is more than one field. Imagine, for example, that there are dependent field variables u and v, with second derivatives $u_{,xx}$, $u_{,xy}$, $u_{,yy}$, $v_{,xx}$, $v_{,xy}$, and $v_{,yy}$ in the governing differential equations and first derivatives $u_{,x}$, $u_{,y}$, $v_{,x}$, and $v_{,y}$ in the functional. Then $2m = 2$ and $m = 1$ for both u and v. Essential boundary conditions are prescriptions of u and v at particular locations. Nonessential boundary conditions involve first derivatives of u and v, either individually or in combination.

Functionals and Governing Differential Equations. Imagine that a functional Π depends on two dependent field variables, $u = u(x,y)$ and $v = v(x,y)$, in which independent variables x and y are Cartesian coordinates:

$$\Pi = \iint F(x, y, u, v, u_{,x}, u_{,y}, v_{,x}, v_{,y}, \ldots, v_{,yy})\, dx\, dy \tag{4.7-1}$$

We assume that the integral is defined throughout its domain. In beam bending, for example, we must exclude a field that displays discontinuities such as at A and B in Fig. 4.2-2b. Similarly, in eventual FE applications, interpolating polynomials must satisfy smoothness requirements. There are as many *Euler equations* as there are dependent field variables. An Euler equation is a governing differential equation of the physical problem. If F contains no derivatives higher than second order, methods of calculus of variations extract from Eq. 4.7-1 the Euler equations

$$\frac{\partial F}{\partial u} - \frac{\partial}{\partial x}\frac{\partial F}{\partial u_{,x}} - \frac{\partial}{\partial y}\frac{\partial F}{\partial u_{,y}} + \frac{\partial^2}{\partial x^2}\frac{\partial F}{\partial u_{,xx}} + \frac{\partial^2}{\partial x \partial y}\frac{\partial F}{\partial u_{,xy}} + \frac{\partial^2}{\partial y^2}\frac{\partial F}{\partial u_{,yy}} = 0 \tag{4.7-2a}$$

$$\frac{\partial F}{\partial v} - \frac{\partial}{\partial x}\frac{\partial F}{\partial v_{,x}} - \frac{\partial}{\partial y}\frac{\partial F}{\partial v_{,y}} + \frac{\partial^2}{\partial x^2}\frac{\partial F}{\partial v_{,xx}} + \frac{\partial^2}{\partial x \partial y}\frac{\partial F}{\partial v_{,xy}} + \frac{\partial^2}{\partial y^2}\frac{\partial F}{\partial v_{,yy}} = 0 \tag{4.7-2b}$$

Equations 4.7-1 and 4.7-2 both describe the same problem, Eq. 4.7-1 being called the "weak form" and Eqs. 4.7-2 the "strong form."

As a specific example of Eq. 4.7-2, consider the axially loaded uniform bar described by Fig. 4.5-la. Here there is one independent variable, x, one dependent variable, u, and no

second derivative. Equation 4.7-1 reduces to the Π_p stated in Eq. 4.5-3. There is but one Euler equation, Eq. 4.7-2a, which reduces to

$$\frac{\partial F}{\partial u} - \frac{d}{dx}\frac{\partial F}{\partial u_{,x}} = 0 \qquad \text{in which} \qquad F = \frac{1}{2}AEu_{,x}^2 - u\,cx \tag{4.7-3}$$

Derivatives in the Euler equation are

$$\frac{\partial F}{\partial u} = -cx \qquad \text{and} \qquad \frac{d}{dx}\frac{\partial F}{\partial u_{,x}} = \frac{d}{dx}(AEu_{,x}) = AEu_{,xx} \tag{4.7-4}$$

from which we obtain the differential equation of equilibrium, Eq. 4.5-7, as expected.

As another example, consider time-dependent heat conduction in an isotropic plane medium. A suitable functional is

$$\Pi = \iint\left(\frac{1}{2}kT_{,x}^2 + \frac{1}{2}kT_{,y}^2 - QT + c\rho T\dot{T}\right)dx\,dy \quad \text{or} \quad \Pi = \iint F\,dx\,dy \tag{4.7-5}$$

in which T = temperature, k = thermal conductivity, Q = rate of internal heat generation per unit volume, ρ = mass density, c = specific heat, and $\dot{T}$ is the time derivative $\partial T/\partial t$. Unit thickness is assumed. (Equation 4.7-5 omits certain boundary terms of practical interest. See Section 12.2 for a more detailed treatment.) There is one dependent field variable, T, and one Euler equation, which is

$$\frac{\partial F}{\partial T} - \frac{\partial}{\partial x}\frac{\partial F}{\partial T_{,x}} - \frac{\partial}{\partial y}\frac{\partial F}{\partial T_{,y}} = 0 \tag{4.7-6}$$

where F is the integrand of Eq. 4.7-5. If k is constant, Eqs. 4.7-5 and 4.7-6 yield

$$k(T_{,xx} + T_{,yy}) + Q - c\rho\dot{T} = 0 \tag{4.7-7}$$

as the differential equation that describes time-dependent temperature distribution in the region of interest.

Although there is always a differential equation associated with a functional, the reverse is not necessarily true. For example, a differential equation that contains an odd-numbered derivative does not have an associated functional of the form of Eq. 4.7-1. For problems of this type, weighted residual methods of Chapter 5 are effective. A functional always produces a Rayleigh-Ritz solution $[\mathbf{K}]\{\mathbf{D}\} = \{\mathbf{R}\}$ in which $[\mathbf{K}]$ is a symmetric matrix. Weighted residual methods may or may not produce a symmetric $[\mathbf{K}]$, depending on the particular method chosen. If an odd-numbered derivative is present in the differential equation, $[\mathbf{K}]$ is not symmetric.

The calculus of variations also produces natural boundary conditions. In the example that follows, we see how they arise. More thorough explanation appears in [4.1–4.3].

Variational Methods: A Brief Example. Figure 4.7-1 shows a uniform bar loaded by a distributed axial load $q = q(x)$ and prescribed stress σ_L at $x = L$. We will use this problem, with the calculus of variations, to show that the functional for potential energy, Π_p, contains

the governing differential equation and the nonessential boundary condition. The argument will suggest the origin of terms seen in Eqs. 4.7-3 and 4.7-4. The development will also produce the virtual work equation, and will suggest a powerful alternative formulation, namely the weighted residual method, which is discussed in Chapter 5.

In Eq. 4.4-9, let $\varepsilon_x = u_{,x}$, $F_x = q/A$, $D = u_L$, and $P = A\sigma_L$. Thus the potential energy functional for the uniform bar in Fig. 4.7-la is

$$\Pi_p = \frac{AE}{2}\int_0^L u_{,x}^2\, dx - \int_0^L qu\, dx - (A\sigma_L)u_L \tag{4.7-8}$$

We presume that $u = u(x)$ is an admissible displacement field for this problem. That is, u is continuous and satisfies the essential boundary condition $u = 0$ at $x = 0$. Let u be perturbed by an amount δu, which we elect to write as $\delta u = e\eta$, where e is a small number and $\eta = \eta(x)$ is an admissible function. Thus the perturbed field $u + e\eta$ is also admissible and satisfies the same essential boundary condition as u. Using this perturbed field in Eq. 4.7-8, $u_{,x}$ becomes $u_{,x} + e\eta_{,x}$, u_L becomes $u_L + e\eta_L$ (where η_L is η at $x = L$), and Π_p becomes $\Pi_p + \delta\Pi_p$. The change in potential is $(\Pi_p + \delta\Pi_p) - \Pi_p$, from which

$$\delta\Pi_p = e\left[AE\int_0^L u_{,x}\eta_{,x}\, dx - \int_0^L q\eta\, dx - (A\sigma_L)\eta_L\right] + e^2\frac{AE}{2}\int_0^L \eta_{,x}^2\, dx \tag{4.7-9}$$

This variational expression can be formally compared to a Taylor series for $f(x+h)$ from which the expansion-point (equilibrium) value $f(x)$ is subtracted, and the result truncated at the quadratic term (which contains h^2). In this analogy, Π_p corresponds to $f(x)$, $\Pi_p + \delta\Pi_p$ to $f(x+h)$, and $e\eta$ to h. This process is called "linearization" of the functional or "variational differentiation."

According to the potential energy principle, stable equilibrium occurs when Π_p is a relative minimum. This implies that $\delta\Pi_p > 0$ for any admissible η. In Eq. 4.7-9, the latter term is never negative due to the squared terms e^2 and $\eta_{,x}^2$, and the former term changes sign when e changes sign. We conclude that if $\delta\Pi_p$ is to be positive for all small values of e, the bracketed expression in Eq. 4.7-9 must vanish. Setting this expression to zero and integrating its first term by parts according to the standard formula $\int u\,dv = -\int v\,du + uv$ with $dv = \eta_{,x}dx$, we obtain

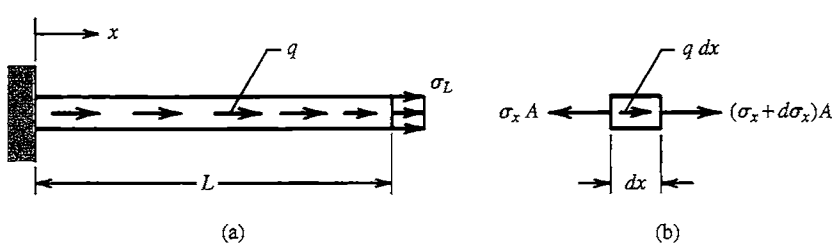

Figure 4.7-1. (a) Uniform elastic bar loaded by distributed axial load q and end stress σ_L. (b) Forces that act on a differential element of the bar.

$$0 = -AE\int_0^L u_{,xx}\eta\,dx + \left[AEu_{,x}\,\eta\right]_0^L - \int_0^L q\eta\,dx - (A\sigma_L)\eta_L \tag{4.7-10}$$

Because η is an admissible function, $\eta = 0$ at $x = 0$, so Eq. 4.7-10 becomes

$$0 = -\int_0^L (AEu_{,xx} + q)\eta\,dx + A\left[E(u_{,x})_L - \sigma_L\right]\eta_L \tag{4.7-11}$$

Because η is admissible but otherwise arbitrary, an arbitrary value of η_L can be assigned while infinitely many functions $\eta = \eta(x)$ are yet possible in the range $0 < x < L$. Therefore, Eq. 4.7-11 can be satisfied only if the coefficients of η and η_L vanish separately. Thus we obtain

$$AEu_{,xx} + q = 0 \quad \text{for} \quad 0 < x < L \tag{4.7-12a}$$

$$Eu_{,x} - \sigma_L = 0 \quad \text{at} \quad x = L \tag{4.7-12b}$$

Equation 4.7-12a is the governing differential equation of equilibrium. It can be written in the alternative form $A\sigma_{x,x} + q = 0$, and can also be derived by considering the equilibrium of axial forces in Fig. 4.7-lb. Equation 4.7-12b is the nonessential (or *natural*) boundary condition, which states that $\varepsilon_x = \sigma_L/E$ at $x = L$. The same approach is used in two- and three-dimensional problems, where the divergence theorem is used in place of integration by parts to obtain traction boundary conditions, Eq. 3.1-14.

The definitions of essential and natural boundary conditions can be sharpened. Essential boundary conditions are those enforced on the trial functions to make them admissible. Natural boundary conditions are enforced on the solution by making the functional stationary. Natural boundary conditions do not explicitly appear in a functional, but nonetheless are contained in it. For example, in the expression for Π_p, Eq. 4.7-8, the natural boundary condition $Eu_{,x} = \sigma_L$ at $x = L$ does not appear. Making Π_p stationary and integrating by parts leads to Eq. 4.7-11, where the natural boundary condition, Eq. 4.7-12b, is revealed.

The vanishing of the bracketed expression in Eq. 4.7-9 can be regarded as an expression of the virtual work principle, which states that the total work of internal and external forces must vanish for any admissible infinitesimal displacement from an equilibrium configuration. In Eq. 4.7-9, internal forces $AEu_{,x}\,dx = A\sigma_x\,dx$ do work (and store strain energy) when strains $\eta_{,x}$ occur, and external forces $q\,dx$ and $A\sigma_L$ do work (and lose potential energy) when positive displacements η and η_L occur.

The vanishing of the bracketed expression in Eq. 4.7-9 can also be obtained by working backward, as follows. Imagine that we seek an approximate solution $\tilde{u} = \tilde{u}(x)$. An example is the admissible polynomial $\tilde{u} = a_1x + a_2x^2 + a_3x^3 + \cdots$, where the a_i are generalized d.o.f. Because $\tilde{u}$ does not satisfy Eq. 4.7-12a for all x, a *residual*, $R = R(x) = AE\tilde{u}_{,xx} + q \neq 0$, is left over. Nevertheless, we can select the a_i so as to satisfy Eq. 4.7-12a in an average or integral sense by writing

$$\int_0^L (AE\tilde{u}_{,xx} + q)\eta\,dx = 0 \tag{4.7-13}$$

where $\eta = \eta(x)$ may now be called a "weight function." Applying integration by parts to Eq. 4.7-13, using the formula presented immediately before Eq. 4.7-10 but now with $dv = \tilde{u}_{,xx}\, dx$, we obtain

$$-AE\int_0^L \tilde{u}_{,x}\,\eta_{,x}\, dx + \left[AE\tilde{u}_{,x}\,\eta\right]_0^L + \int_0^L q\eta\, dx = 0 \tag{4.7-14}$$

But $\eta = 0$ at $x = 0$. In addition, at $x = L$ we may replace $E\tilde{u}_{,x}$ by σ_L, thus introducing the nonessential boundary condition. Equation 4.7-14 becomes

$$-AE\int_0^L \tilde{u}_{,x}\eta_{,x}\, dx + \int_0^L q\eta\, dx + (A\sigma_L)\eta_L = 0 \tag{4.7-15}$$

which agrees with the vanishing of the bracketed expression in Eq. 4.7-9. Equation 4.7-15 can be identified as an application of the method of weighted residuals, which is a way of formulating an approximate solution when one knows the differential equation but not the functional or the variational principle. If $\eta_i = \partial\tilde{u}/\partial a_i$, then the method is known as the *Galerkin method,* for which Eq. 4.7-15 yields as many equations as there are a_i to be determined. A more detailed discussion appears in Chapter 5.

The progression from Eq. 4.7-13 to Eq. 4.7-15 is an instance of starting with the strong form and obtaining a weak form from it. Equation 4.7-15 can be regarded as an instance of the virtual work principle, in which η is a virtual displacement from an equilibrium configuration. A general expression of the virtual work principle can be obtained by multiplying left-hand sides of equilibrium equations (Eqs. 3.1-12) by the respective virtual displacements δu, δv, and δw, adding the results, integrating over the volume of the body, and using Green's theorem to integrate by parts [2.2,4.4].

4.8 FINITE ELEMENT FORM OF THE RAYLEIGH-RITZ METHOD

In this section we use the Rayleigh-Ritz method to develop FE methods for plane heat conduction and multidimensional elasticity. As in preceding sections of this chapter, we form a functional Π, make Π stationary with respect to the nodal d.o.f., then solve the resulting equations $[\mathbf{K}]\{\mathbf{D}\} = \{\mathbf{R}\}$ for d.o.f. $\{\mathbf{D}\}$. In an actual computer program, equations $[\mathbf{K}]\{\mathbf{D}\} = \{\mathbf{R}\}$ would be developed directly, without using Π at all.

Piecewise Interpolation. Solution by FEA involves dividing a domain into subdomains and defining a separate interpolation for each, as opposed to the classical Rayleigh-Ritz method of regarding the entire structure as a single domain and spanning it with a single trial function. An additional step in FEA, replacing generalized d.o.f. by nodal d.o.f., does not change the concept but makes FEA practical by facilitating computer implementation.

Consider the bar shown in Fig. 4.8-1a, which is discretized into subdomains, each of length L. Linear interpolants in terms of generalized d.o.f. a_i for the two subdomains shown are given in Fig. 4.8-1b. With axial strain $\varepsilon_x = u_{,x}$, the potential energy expression,

Eq. 4.4-9 (with zero initial stress and strain) is broken into subdomain contributions and becomes, for N_{els} subdomains, or elements as we will now call them,

$$\Pi_p = \sum_{i=1}^{N_{\text{els}}} \int_{L_i} \frac{1}{2} E u_{,x}^2 A \, dx - \sum_{i=1}^{N_{\text{els}}} \int_{L_i} u F_x A \, dx - \{\mathbf{D}\}^T \{\mathbf{P}\} \tag{4.8-1}$$

As in Section 4.5, Π_p is a function of generalized d.o.f. a_i. However, generalized d.o.f. have disadvantages. First, they have no straightforward physical meaning. For example, a_1 and a_3 in Fig. 4.8-1a each have units of length, and a_2 and a_4 are dimensionless. More seriously, use of d.o.f. a_i makes it awkward to ensure interelement compatibility and to impose essential boundary conditions. For the bar shown in Fig. 4.8-1a, continuity of displacement at the point x_i requires $a_1 + a_2 x_i = a_3 + a_4 x_i$, and each additional interelement connection brings a similar constraint. Also, most problems have essential boundary conditions, whose enforcement brings yet more equations of constraint. It is difficult to treat these constraints in software. In practical application, nodal d.o.f. replace generalized d.o.f.

For the bar shown in Fig. 4.8-1b, Fig. 3.2-2a is used to write linear interpolants for the two elements that share point x_i. In contrast to Fig. 4.8-1a, d.o.f. in Fig. 4.8-1b are displacements of discrete points, namely the nodes. By using the same nodal displacement u_i in each of the interpolants, enforcement of continuity of displacement between elements is automatic. Also, imposition of essential boundary conditions is straightforward. Equation 4.8-1 is still used, except now Π_p is a function of nodal d.o.f. u_i and is made stationary with respect to these d.o.f. by writing the equations $\partial \Pi_p / \partial u_i = 0$.

In the remainder of this section we use the Rayleigh-Ritz method to develop finite element methods for heat conduction and structural mechanics.

FEA in Heat Conduction. A functional for plane heat conduction in an isotropic material of unit thickness is given in Eq. 4.7-5. With $T = T^T$, $T_{,x}^2 = T_{,x}^T T_{,x}$, and $T_{,y}^2 = T_{,y}^T T_{,y}$, Eq. 4.7-5 can be written as

$$\Pi = \iint \frac{1}{2} (T_{,x}^T T_{,x} + T_{,y}^T T_{,y}) k \, dx \, dy - \iint T^T Q \, dx \, dy + \iint T^T \dot{T} c\rho \, dx \, dy \tag{4.8-2}$$

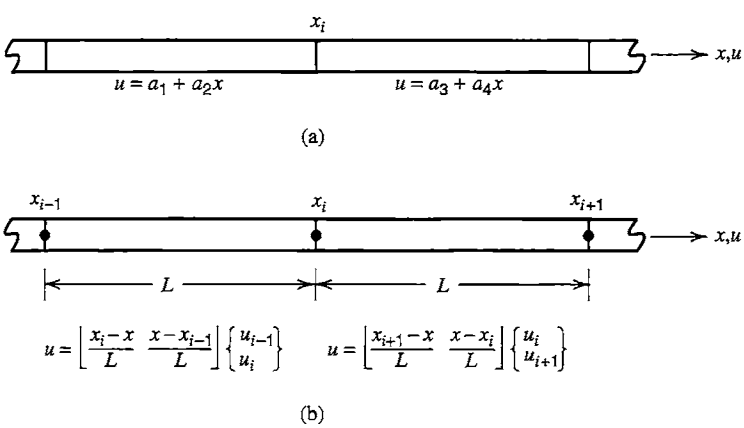

Figure 4.8-1. (a) Elastic bar discretized into subdomains, which can be called finite elements. (b) Finite element discretization using linear interpolation between nodes.

The transposition symbol is placed on the scalar fields T, $T_{,x}$, and $T_{,y}$ to make it easier to differentiate subsequent matrix expressions when making Π stationary. In this discussion we view Eq. 4.8-2 as being written for a single finite element.

Consider a plane element having n nodes. For example, if the element has corner nodes only, then $n = 3$ for a triangle and $n = 4$ for a rectangle. Let temperature T within the element be interpolated from n nodal temperatures $\{\mathbf{T}_e\}$,

$$T = \underset{1\times n}{\lfloor \mathbf{N} \rfloor} \underset{n\times 1}{\{\mathbf{T}_e\}} \tag{4.8-3}$$

where each of the n shape functions in $\lfloor \mathbf{N} \rfloor$ is a function of x and y. Differentiations of Eq. 4.8-3 yield

$$T_{,x} = \lfloor \mathbf{N}_{,x} \rfloor \{\mathbf{T}_e\} \qquad T_{,y} = \lfloor \mathbf{N}_{,y} \rfloor \{\mathbf{T}_e\} \qquad \dot{T} = \lfloor \mathbf{N}_{,x} \rfloor \{\dot{\mathbf{T}}_e\} \tag{4.8-4}$$

in which, for example,

$$\lfloor \mathbf{N}_{,x} \rfloor = \lfloor N_{1,x} \;\; N_{2,x} \;\; \cdots \;\; N_{n,x} \rfloor \tag{4.8-5}$$

In differentiating Eq. 4.8-3 to arrive at Eqs. 4.8-4, shape functions $\lfloor \mathbf{N} \rfloor$ are functions of space only, and nodal temperatures $\{\mathbf{T}_e\}$ are functions of time only. Thus, temperature T and the time rate of change of temperature $\dot{T}$ are interpolated from nodal values $\{\mathbf{T}_e\}$ and $\{\dot{\mathbf{T}}_e\}$ by means of the same shape functions.

Substitution of Eqs. 4.8-3 and 4.8-4 into Eq. 4.8-2 yields, for a single element,

$$\Pi = \frac{1}{2}\{\mathbf{T}_e\}^T[\mathbf{k}]\{\mathbf{T}_e\} + \{\mathbf{T}_e\}^T[\mathbf{c}]\{\dot{\mathbf{T}}_e\} - \{\mathbf{T}_e\}^T\{\mathbf{r}_Q\} \tag{4.8-6}$$

in which we have defined terms as follows:

$$[\mathbf{k}] = \iint \left(\lfloor \mathbf{N}_{,x} \rfloor^T \lfloor \mathbf{N}_{,x} \rfloor + \lfloor \mathbf{N}_{,y} \rfloor^T \lfloor \mathbf{N}_{,y} \rfloor \right) k \, dx \, dy \tag{4.8-7a}$$

$$[\mathbf{c}] = \iint \lfloor \mathbf{N} \rfloor^T \lfloor \mathbf{N} \rfloor c\rho \, dx \, dy \tag{4.8-7b}$$

$$\{\mathbf{r}_Q\} = \iint \lfloor \mathbf{N} \rfloor^T Q \, dx \, dy \tag{4.8-7c}$$

Finite element equations are obtained by making Π stationary with respect to variations of nodal temperature. Using differentiation rules stated in Appendix A, we obtain

$$\left\{ \frac{\partial \Pi}{\partial \mathbf{T}_e} \right\} = \{\mathbf{0}\} \quad \text{yields} \quad [\mathbf{k}]\{\mathbf{T}_e\} + [\mathbf{c}]\{\dot{\mathbf{T}}_e\} = \{\mathbf{r}_Q\} \tag{4.8-8}$$

To obtain global equations, we conceptually expand arrays in Eq. 4.8-8 to structure size for each element, then assemble elements, to obtain

$$[\mathbf{K}]\{\mathbf{T}\} + [\mathbf{C}]\{\dot{\mathbf{T}}\} = \{\mathbf{R}_Q\} \tag{4.8-9}$$

in which $\{\mathbf{T}\}$ contains all nodal temperatures of the structure. Alternatively, Eq. 4.8-9 is also obtained by assembling all element contributions to Π first, followed by making Π stationary with respect to the global vector of nodal temperatures $\{\mathbf{T}\}$. This process is illustrated in the structural mechanics example that follows.

For the sake of having notation like that used in structural mechanics, we can write $[\mathbf{k}]$ of Eq. 4.8-7a in the form

$$[\mathbf{k}] = \iint [\mathbf{B}]^T k [\mathbf{B}] t \, dx \, dy \qquad \text{where} \qquad [\mathbf{B}] = \begin{bmatrix} \mathbf{N}_{,x} \\ \mathbf{N}_{,y} \end{bmatrix} \tag{4.8-10}$$

and thickness t has been taken as unity in the preceding development.

FEA in Structural Mechanics. The functional for quasistatic, linearly elastic problems of structural mechanics is given by Eq. 4.4-7, which is written as follows for an assembly of N_{els} elements. Integrations span individual elements, and results are added.

$$\begin{aligned} \Pi_p = & \sum_{i=1}^{N_{\text{els}}} \int \left(\frac{1}{2} \{\boldsymbol{\varepsilon}\}^T [\mathbf{E}] \{\boldsymbol{\varepsilon}\} - \{\boldsymbol{\varepsilon}\}^T [\mathbf{E}] \{\boldsymbol{\varepsilon}_0\} + \{\boldsymbol{\varepsilon}\}^T \{\boldsymbol{\sigma}_0\} \right) dV \\ & - \sum_{i=1}^{N_{\text{els}}} \int \{\mathbf{u}\}^T \{\mathbf{F}\} dV - \sum_{i=1}^{N_{\text{els}}} \int \{\mathbf{u}\}^T \{\boldsymbol{\Phi}\} dS - \{\mathbf{D}\}^T \{\mathbf{P}\} \end{aligned} \tag{4.8-11}$$

Displacements $\{\mathbf{u}\}$ within element i are interpolated from element nodal d.o.f. $\{\mathbf{d}\}_i$ by

$$\{\mathbf{u}\} = [\mathbf{N}]\{\mathbf{d}\}_i \tag{4.8-12}$$

where $[\mathbf{N}]$ is the shape function matrix. For elasticity problems in one, two and three dimensions, $\{\mathbf{u}\}$ is a scalar, a 2 by 1 vector, and a 3 by 1 vector, respectively, and $\{\boldsymbol{\varepsilon}\}$ and $\{\boldsymbol{\sigma}\}$ are scalars, 3 by 1 vectors, and 6 by 1 vectors, respectively. The size and specific form of $[\mathbf{N}]$ depends on the dimensionality of the problem, the shape of element, and the number of nodes per element. These details must eventually be addressed, but need not be specified yet.

Strains are obtained from displacements by differentiation according to Eqs. 3.1-10 and 3.3-3, here repeated:

$$\{\boldsymbol{\varepsilon}\} = [\boldsymbol{\partial}]\{\mathbf{u}\} \quad \text{yields} \quad \{\boldsymbol{\varepsilon}\} = [\mathbf{B}]\{\mathbf{d}\} \qquad \text{where} \qquad [\mathbf{B}] = [\boldsymbol{\partial}]\{\mathbf{N}\} \tag{4.8-13}$$

Specific forms of $[\mathbf{E}]$ and $[\boldsymbol{\partial}]$ for elasticity are given in Section 3.1. Other problems of structural mechanics such as bending of beams and plates can also be represented by these equations provided appropriate definitions of $\{\boldsymbol{\varepsilon}\}$ and $\{\boldsymbol{\sigma}\}$ are used (for example, see Eq. 3.3-12). Substitution of Eqs. 4.8-12 and 4.8-13 into Eq. 4.8-11 provides

$$\Pi_p = \frac{1}{2}\sum_{i=1}^{N_{\text{els}}} \{\mathbf{d}\}_i^T[\mathbf{k}]_i\{\mathbf{d}\}_i - \sum_{i=1}^{N_{\text{els}}} \{\mathbf{d}\}_i^T\{\mathbf{r}_e\}_i - \{\mathbf{D}\}^T\{\mathbf{P}\} \tag{4.8-14}$$

where $[\mathbf{k}]_i$ and $\{\mathbf{r}_e\}_i$ are respectively the stiffness matrix and load vector of element i:

$$[\mathbf{k}]_i = \int [\mathbf{B}]^T[\mathbf{E}][\mathbf{B}]\, dV \tag{4.8-15a}$$

$$\{\mathbf{r}_e\}_i = \int [\mathbf{B}]^T[\mathbf{E}]\{\boldsymbol{\varepsilon}_0\}\, dV - \int [\mathbf{B}]^T\{\boldsymbol{\sigma}_0\}\, dV + \int [\mathbf{N}]^T\{\mathbf{F}\}\, dV + \int [\mathbf{N}]^T\{\boldsymbol{\Phi}\}\, dS \tag{4.8-15b}$$

These results agree with Eqs. 3.3-7 and 3.3-8.

Equations 4.8-11 to 4.8-15 show that strain energy in an individual element due to its nodal displacements $\{\mathbf{d}\}$ is

$$U = \frac{1}{2}\{\mathbf{d}\}^T[\mathbf{k}]\{\mathbf{d}\} \tag{4.8-16}$$

Π_p given by Eq. 4.8-14 is to be made stationary with respect to global d.o.f. $\{\mathbf{D}\}$, but the first two terms in Eq. 4.8-14 are functions of element d.o.f. $\{\mathbf{d}\}_i$, which are a subset of the global d.o.f. These sets of d.o.f. are related by the transformation

$$\{\mathbf{d}\}_i = [\mathbf{L}]_i\{\mathbf{D}\} \tag{4.8-17}$$

Matrix $[\mathbf{L}]_i$ has size m_i by m where m_i is the number of d.o.f. in element i and m is the total number of global d.o.f. $[\mathbf{L}]_i$ contains only zeros and ones. For example, in Fig. 1.3-1, $\{\mathbf{D}\} = \lfloor u_1 \;\; u_2 \;\; u_3 \;\; u_4 \rfloor^T$ and for element 2, which has nodes 2 and 3, $\{\mathbf{d}\}_2 = \lfloor u_2 \;\; u_3 \rfloor^T$ and all coefficients of the 2 by 4 matrix $[\mathbf{L}]_2$ are zero except for $L_{12} = L_{23} = 1$. If the structure has many elements, each $[\mathbf{L}]_i$ is very sparse. Substitution of Eq. 4.8-17 into Eq. 4.8-14 yields

$$\Pi_p = \frac{1}{2}\{\mathbf{D}\}^T\left(\sum_{i=1}^{N_{\text{els}}} [\mathbf{L}]_i^T[\mathbf{k}]_i[\mathbf{L}]_i\right)\{\mathbf{D}\} - \{\mathbf{D}\}^T\sum_{i=1}^{N_{\text{els}}} [\mathbf{L}]_i^T\{\mathbf{r}_e\}_i - \{\mathbf{D}\}^T\{\mathbf{P}\} \tag{4.8-18}$$

Making Π_p stationary with respect to global d.o.f. $\{\mathbf{D}\}$ yields the structure equations

$$\left(\sum_{i=1}^{N_{\text{els}}} [\mathbf{L}]_i^T[\mathbf{k}]_i[\mathbf{L}]_i\right)\{\mathbf{D}\} = \{\mathbf{P}\} + \sum_{i=1}^{N_{\text{els}}} [\mathbf{L}]_i^T\{\mathbf{r}_e\}_i \tag{4.8-19}$$

Products $[\mathbf{L}]_i^T[\mathbf{k}]_i[\mathbf{L}]_i$ have size m by m, and products $[\mathbf{L}]_i^T\{\mathbf{r}_e\}_i$ have size m by 1, where m is the number of global d.o.f. By properly locating element coefficients in global-size

arrays, Eq. 4.8-17 accomplishes the same function as expansion of element matrices to structure size. In computer implementation the matrix multiplications $[\mathbf{L}]_i^T [\mathbf{k}]_i[\mathbf{L}]_i$ and $[\mathbf{L}]_i^T \{\mathbf{r}_e\}_i$ are not performed. Instead terms in each $[\mathbf{k}]_i$ and each $\{\mathbf{r}_e\}_i$ are added directly to appropriate locations in global matrix $[\mathbf{K}]$ and vector $\{\mathbf{R}\}$. In other words, in practice assembly is accomplished by the direct stiffness method (Section 2.5) rather than by the computationally inefficient "congruent transformation" procedure using $[\mathbf{L}]_i$ matrices. Finally, Eq. 4.8-18 can be written in the form

$$\Pi_p = \frac{1}{2}\{\mathbf{D}\}^T[\mathbf{K}]\{\mathbf{D}\} - \{\mathbf{D}\}^T\{\mathbf{R}\} \tag{4.8-20}$$

where $\{\mathbf{R}\}$ includes both $\{\mathbf{P}\}$ and contributions from element load vectors $\{\mathbf{r}_e\}$.

Remarks. The foregoing derivations show that an FE formulation is available from only two basic ingredients—namely, a functional that describes the physical problem and a nodal interpolation based on shape function matrix $[\mathbf{N}]$ that describes the element. From these we obtain definitions of element matrices such as Eqs. 4.8-7 and 4.8-15. To obtain explicit forms for element matrices one must next attend to specifics by choosing the element shape, number of d.o.f., distribution of d.o.f. over the element, and the shape function matrix $[\mathbf{N}]$. These choices have great influence on efficiency of calculation and accuracy of results.

Division of a domain into finite elements produces *spatial discretization* but not *temporal discretization*. For example, the expression for potential Π for plane transient heat conduction, Eq. 4.8-2, implicitly contains a single governing partial differential equation where temperature T is a function of coordinates x and y and time t. Using Eq. 4.8-3, we arrive at Eq. 4.8-8, which is a system of simultaneous first-order ordinary differential equations where nodal temperatures $\{\mathbf{T}_e\}$ are discrete in space, but are still continuous functions of time. Thus, we have taken a single partial differential equation, and using the FE method, have replaced it by a system of ordinary differential equations. Because nodal temperatures are still continuous functions of time, Eq. 4.8-8 may be called a *semi-discretization*. In Chapter 11 we describe methods that allow Eq. 4.8-8 to be solved in step-by-step fashion, using increments of time.

4.9 CONVERGENCE OF FINITE ELEMENT SOLUTIONS

An acceptable FE formulation converges to the exact solution of the mathematical model as the mesh is indefinitely refined (neglecting errors due to finite precision computer arithmetic). A satisfactory rate of convergence is also important, so that acceptable accuracy will not require extremely many d.o.f. Some elements converge more rapidly than others. In this section we first discuss convergence of a general multidimensional potential field problem, then specialize the discussion to structural mechanics.

Potential Field Problems. Let the field variable be $\phi = \phi(x,y,z)$, and let there be a functional $\Pi = \Pi(\phi)$ that yields the governing differential equation of the physical

problem from the stationary condition $\delta\Pi = 0$. Problems in this category include steady-state heat conduction, bending of thin flat plates, potential flow of fluids, electrostatics, torsion of shafts with noncircular cross section, and others. Let m be the highest-order derivative of ϕ that appears in Π. The value of m can be determined by examination of either the governing differential equation or its associated functional Π. If derivatives of order $2m$ appear in the differential equation, then derivatives of order m appear in Π. (If an odd-order derivative appears in the differential equation, no variational principle exists, but an FE formulation can still be obtained by Galerkin or related methods; see Chapter 5.)

In the following discussion we assume that calculations are done in exact arithmetic and that geometry of the mathematical model comes to be represented exactly as the mesh is refined. Let polynomial expressions be used to interpolate ϕ within elements from nodal values of ϕ. If ϕ and its spatial derivatives are to approach mathematically exact values as an FE mesh is repeatedly refined, then:

1. Within each element the assumed field for ϕ must contain a complete polynomial of degree m or higher.
2. Across boundaries between elements there must be continuity of ϕ and derivatives of ϕ through order $m - 1$.
3. Each element must be capable of exactly representing states of
   (a) uniform ϕ, and
   (b) uniform value of any derivative of ϕ through order m.

As an example, if $\phi = \phi(x,y)$ and Π contains first derivatives of ϕ, then $m = 1$, and the lowest degree polynomial field that is acceptable is the complete linear form $\phi = a_0 + a_1x + a_2y$. Only ϕ itself need be continuous across interelement boundaries. Each element must be capable of exactly representing a constant value of ϕ, a constant value of $\phi_{,x}$, and a constant value of $\phi_{,y}$.

An interpolation that satisfies Requirement 1 provides a ϕ that is a single-valued function of position; therefore continuity of ϕ within an element is guaranteed. Requirements 2 and 3 must be met in the limit of mesh refinement. Incompatible elements, such as plane element Q6 discussed in Sections 3.10 and 6.6, may violate Requirements 2 and 3 in a general mesh, when elements are of general shape. Yet if mesh refinement causes element shapes to become parallelograms, incompatibilities disappear and a mesh of Q6 elements will satisfy these requirements and converge properly. (The modified Q6 element, called QM6 in Section 6.6, meets requirement 3 when of general quadrilateral shape.) For incompatible elements, satisfaction of Requirement 1 does not guarantee satisfaction of Requirements 2 and 3. The ability of elements to meet all three requirements can be checked computationally by applying the *patch test,* as described in Section 6.13.

Elements that do not satisfy Requirements 1–3 may yet provide convergence, but not to correct results in all applications. Correct convergence is guaranteed if elements satisfy Requirements 1–3 as the mesh is refined (assuming that computer arithmetic and geometric representation introduce no errors). Requirements 1–3 say nothing about the *rate* of convergence or the accuracy provided by a coarse mesh. However, if the requirements are met at all stages of refinement, either as existing elements are subdivided or as polynomial terms are added to existing elements, then there will be *monotonic* convergence of structural strain energy, or of a comparable global quantity in a nonstructural problem [4.5].

Subdivision of elements and addition of terms are ways of assuring that the previous interpolation field or trial space is a subset of the new. Further discussion of mesh refinement appears in Sections 9.6, 9.7, 9.8, and 9.11.

Structural Mechanics. The order of differentiation m can be determined from the strain energy term in Π_p. For stretching of a bar, we see from Eq. 4.7-8 that $m = 1$. A two-node bar element is based on a linear interpolation field, and axial displacements of adjacent elements have the same value at nodes where elements are joined, so Requirements 1 and 2 are clearly met. Order of differentiation m may have two values for a single problem. For example, a thin flat plate that must both stretch and bend has $m = 1$ for in-plane displacements u and v, and $m = 2$ for lateral displacement w associated with bending. Therefore, Requirement 2 demands interelement continuity of u, v, w, $w_{,x}$, and $w_{,y}$, at least in the limit of mesh refinement.

In structural mechanics, Requirement 3a states that an element must be capable of rigid-body motion without developing strain, and Requirement 3b states that the element must be capable of representing a state of uniform strain. Requirement 3 can be physically explained as follows. An individual element undergoes rigid-body motion with superposed strain. Mesh refinement by subdivision causes each element to occupy a smaller portion of the structure. If there are no singularities and material properties vary smoothly, an element approaches a state of uniform strain. That is, if a strain gradient exists, the variation of strain over the element becomes less and less significant in comparison with the average (uniform) strain the element displays. Indeed, an element may lack the ability to display a strain gradient and yet provide correct convergence. This behavior can be seen in Fig. 1.3-1, where axial stress (or strain) in two-node bar elements produces a stairstep approximation that converges toward the correct stress distribution as more elements are used. Note that hypothetical bar elements based on the incomplete axial displacement field $u = a_0 + a_2x^2$ would fail: axial strain is $\varepsilon_x = 2a_2x$, the constant-strain capability is missing, and the element would always display $\varepsilon_x = 0$ at its left end, where $x = 0$. Such a defect is not correctable by mesh refinement.

In two or three dimensions, rigid-body motion consists of translation and rotation. For rigid-body translation, strain measures such as Eqs. 3.1-9 and 3.3-12 provide zero strains, even for large translations. For rigid-body rotation, strain measures used in this book provide zero strains only if the rotation is small. As an example, consider the constant-strain triangle, introduced in Section 3.4, subjected to the motion

$$\begin{Bmatrix} u \\ v \end{Bmatrix} = \begin{bmatrix} a_1 & \cos\theta - 1 & -\sin\theta \\ a_4 & \sin\theta & \cos\theta - 1 \end{bmatrix} \begin{Bmatrix} 1 \\ x \\ y \end{Bmatrix} \tag{4.9-1}$$

Here, x and y are the original coordinates of any point in the element, and u and v are its displacement components. Use of Eq. 4.9-1 to compute the displacement of nodes 1, 2, and 3 in turn provides the displaced position shown in Fig. 4.9-1, where it is seen that a_1 and a_4 are rigid-body translations in the x and y directions respectively, and θ is a clockwise rigid-body rotation about the origin. With Eqs. 3.1-6, this displacement field yields strains $\varepsilon_x = \varepsilon_y = \cos\theta - 1$ and $\gamma_{xy} = 0$. Because the displacement is a rigid-body motion, we expect all strain components to be zero, but such is the case only if θ is small.

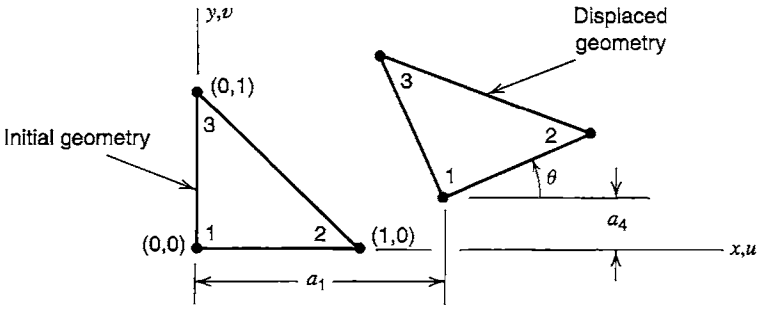

Figure 4.9-1. Constant strain triangle element subjected to a rigid body motion consisting of translations a_1 and a_4 in the x and y directions, and rotation θ about node 1.

Strain measures that provide zero strains for large rigid-body rotations are desirable, but they are complicated and nonlinear. Their use is usually reserved for problems where rotations are expected to be large.

Convergence Rate. The rate of convergence of a particular type of element can be obtained by analysis, as in Section 9.6, or by a study of results provided by a sequence of successively refined meshes, as in Section 9.7. Simple geometric arguments also provide insight, as follows.

Consider piecewise linear interpolation, with an FE mesh of sufficient refinement that nodal d.o.f. can be considered exact and assume that the exact displacement function $u = u(x)$ can be regarded as having quadratic variation over the span h of element 1-2 shown in Fig. 4-9-2a. Quadratic curve ABC has the form $u = a + bx + cx^2$, where a, b, and c are constants. The approximating dashed line has the form $\tilde{u} = a + (b + ch)x$. Error e of the linear FE approximation is greatest at midpoint D, where

$$e_D = u_D - u_B = \frac{u_A + u_C}{2} - u_B = \frac{ch^2}{4} = \frac{h^2}{8}u'' \tag{4.9-2}$$

in which u'' is the curvature $d^2u/dx^2 = 2c$. Error of the linear approximation in representing the gradient $u' = du/dx$ is greatest at A and C, where values of u' have equal magnitude and opposite sign. At A, where $du/dx = b$, gradient error is

$$e'_A = \frac{u_C - u_A}{h} - b = hc = \frac{h}{2}u'' \tag{4.9-3}$$

Equations 4.9-2 and 4.9-3 show that the linear function and its first derivative have errors proportional to u'' of the exact function, which depends on the first higher-order term *not* contained in the linear FE approximation. We also see that if element length h is halved, the error of u is quartered and the error of du/dx is halved. Using the symbol O for "order," we say that error is $O(h^2)$ for the function itself and $O(h)$ for its first derivative, and the convergence rate is 2 (quadratic) for the function itself and 1 (linear) for its first derivative.

In similar fashion one can approximate a cubic function $u = u(x)$ by a quadratic curve whose values at nodes 1, 2, and 3 are exact (Fig. 4.9-2b). For solid and dashed curves, respectively,

$$u = a + bx + cx^2 + dx^3 \tag{4.9-4a}$$

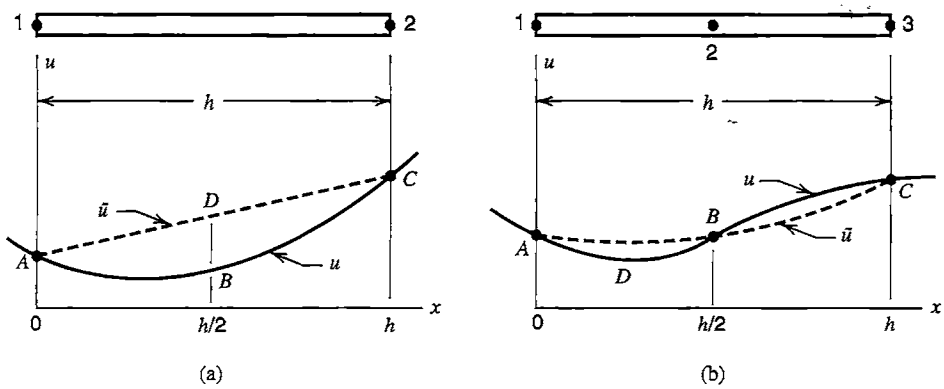

Figure 4.9-2. Functions $u = u(x)$ shown by solid curves, and their approximation by FE interpolation (dashed lines).

$$\tilde{u} = a + \left(b - \frac{1}{2}dh^2\right)x + \left(c + \frac{3}{2}dh\right)x^2 \tag{4.9-4b}$$

Error $e = \tilde{u} - u$ at D, where $x = h/4$, and gradient error $e' = \tilde{u}' - u'$ at A, are respectively

$$e_D = -\frac{3dh^3}{64} = -\frac{h^3}{128}u''' \quad \text{and} \quad e'_A = -\frac{dh^2}{2} = -\frac{h^2}{12}u''' \tag{4.9-5}$$

where $u''' = 6d$ is d^3u/dx^3 of the cubic curve. Here, as in Fig. 4.9-2a, we see that errors are related to the first higher-order term *not* contained in the FE approximation.

A generalization of these results is as follows. Let p be the degree of the highest order *complete* polynomial contained in the FE interpolation field and let h be a linear measure of element size. Then the error is $O(h^{p+1})$ for the field quantity and is $O(h^{p+1-r})$ for the rth derivative of the field quantity, and the convergence rate is $p + 1$ for the field quantity and $p + 1 - r$ for the rth derivative of the field quantity.

4.10 ADDITIONAL FORMULATIONS. HYBRID ELEMENTS

Formulation Methods. Elements discussed thus far are called "displacement elements," meaning that they are based on assumed displacement fields. Displacement elements are the most widely used element type in structural mechanics. Their matrices, such as stiffness matrices, can be obtained from the potential energy expression, Eq. 4.4-7. Several other functionals are available. Each can produce finite elements, some of which perform very well and are incorporated in general-purpose software. A software user may be unaware of the functional basis for elements used.

Classic functionals in structural mechanics are those of strain energy and complementary strain energy. The strain energy functional is based on a strain field that satisfies compatibility conditions *a priori* and yields equilibrium equations when strains are varied. The complementary strain energy functional is based on a stress field that satisfies equilibrium conditions *a priori* and yields compatibility equations when stresses are varied. More

recently, many additional functionals have been devised, some of which use Lagrange multipliers to impose the constraints of equilibrium and compatibility, in an integral sense rather than at every point. Such a formulation does not favor equilibrium over compatibility or vice versa, and permits simultaneous use of an assumed stress field and an assumed displacement field in FE solutions. The associated element is called a mixed element [2.20]. A mixed element may have only displacement d.o.f., but typically it has d.o.f. of different types. Examples include elements for fluid flow that have both velocity and pressure d.o.f. and plate bending elements that have both lateral displacement and bending moment d.o.f. A mixed formulation for a two-node bar element is derived by the Galerkin method in Section 5.6.

A hybrid element is a mixed element for which fields within an element and on its boundaries are independently assumed. Thus one might use assumed stresses within an element and assumed displacements on its boundary (as in the original hybrid element [4.6]) or use independent displacement fields within the element and on its boundary. Element formulation can be based on a mixed functional or, for the simplest type of hybrid element, on a complementary strain energy functional [4.6]. In structural mechanics the usual result is an element stiffness matrix. Thus a hybrid element included in general-purpose software is likely to have only the usual displacement d.o.f. A sampling of the many publications about hybrid elements is [2.20,4.6–4.10]. In following subsections we discuss the simplest type of hybrid element in more detail.

A *Trefftz element* is formulated by using a field within the element that satisfies governing differential equations of the problem a priori. In structural mechanics this field is a displacement field. For example, in plate bending the lateral displacement field w satisfies the differential equation $\nabla^4 w = q/D$, where q is lateral load. Optionally, the internal field can include terms that account for a geometric irregularity such as a hole, or for the singularity associated with a crack or a concentrated load. Interelement continuity and boundary conditions are satisfied approximately, either in an integral sense or pointwise. Element matrices can be derived from a functional, which has a hybrid form that uses assumed boundary displacements between nodes. The resulting hybrid-Trefftz elements can be connected to conventional finite elements. Trefftz elements may be relatively insensitive to geometric distortion. They have also been called "large" elements because typically few are needed. Each element spans a substantial portion of the region analyzed, may have a complicated shape if necessary, and has many nodes on its boundary. As compared with models built of conventional elements, a Trefftz element model requires fewer nodes for comparable accuracy, thus reducing data preparation effort and computation time. A Trefftz element solution can be regarded as a kind of boundary element method (BEM) solution, Section 8.8, but does not require the "fundamental solution" used in BEM, has less mathematical complexity, produces symmetric coefficient matrices, and requires no integration to evaluate results inside the domain. Drawbacks, shared with BEM, include having matrices that are not sparse, and having to base the formulation on governing differential equations. Of some 200 papers about the Trefftz method in engineering, including applications to time-dependent, nonlinear, and nonstructural problems, we cite [4.11–4.14].

Hybrid Element Formulation. Here we elect to describe the original form of assumed-stress hybrid elements [4.6]. Accordingly we use a complementary energy principle and an internal stress field that satisfies differential equations of equilibrium

a priori. (The equilibrium requirement can be relaxed by using alternative functionals that allow equilibrium within an element to be satisfied in an average sense rather than at every point [4.8,4.9].)

For a linearly elastic material, complementary strain energy per unit volume is

$$U_0^* = \frac{1}{2}\{\boldsymbol{\sigma}\}^T[\mathbf{E}]^{-1}\{\boldsymbol{\sigma}\} \tag{4.10-1}$$

Within the element, the assumed stress field is

$$\{\boldsymbol{\sigma}\} = [\mathbf{P}]\{\boldsymbol{\beta}\} \tag{4.10-2}$$

where $\{\boldsymbol{\beta}\}$ contains parameters β_i that are yet to be determined, and $[\mathbf{P}]$ is a function of the coordinates whose form is such that differential equations of equilibrium are satisfied (examples follow). We omit body force terms. Complementary strain energy in an element of volume V, from Eqs. 4.10-1 and 4.10-2, is

$$U^* = \int U_0^*\, dV = \frac{1}{2}\{\boldsymbol{\beta}\}^T[\mathbf{H}]\{\boldsymbol{\beta}\} \qquad \text{where} \qquad [\mathbf{H}] = \int [\mathbf{P}]^T[\mathbf{E}]^{-1}[\mathbf{P}]\, dV \tag{4.10-3}$$

Let $\{\boldsymbol{\Phi}\}$ represent tractions on element boundary S, obtained by evaluating Eq. 4.10-2 on the boundary. Also let boundary displacements $\{\mathbf{u}_b\}$ be interpolated from element nodal d.o.f. $\{\mathbf{d}\}$. These relations are symbolized as

$$\{\boldsymbol{\Phi}\} = [\mathbf{R}]\{\boldsymbol{\beta}\} \qquad \text{and} \qquad \{\mathbf{u}_b\} = [\mathbf{L}]\{\mathbf{d}\} \tag{4.10-4}$$

Total complementary energy in the element is U^* minus work done by tractions $\{\boldsymbol{\Phi}\}$ in moving through displacements $\{\mathbf{u}_b\}$; that is

$$\Pi_c = U^* - \int \{\boldsymbol{\Phi}\}^T\{\mathbf{u}_b\}\, dS \qquad \text{or} \qquad \Pi_c = \frac{1}{2}\{\boldsymbol{\beta}\}^T[\mathbf{H}]\{\boldsymbol{\beta}\} - \{\boldsymbol{\beta}\}^T[\mathbf{G}]\{\mathbf{d}\} \tag{4.10-5}$$

where

$$[\mathbf{G}] = \int [\mathbf{R}]^T[\mathbf{L}]\, dS \tag{4.10-6}$$

To make Π_c stationary with respect to small changes in stress, we write

$$\frac{\partial \Pi_c}{\partial \beta_i} = 0 \quad \text{for} \quad i = 1, 2, \ldots, n \quad \text{or} \quad \left\{\frac{\partial \Pi_c}{\partial \boldsymbol{\beta}}\right\} = \{\mathbf{0}\} \tag{4.10-7}$$

from which

$$[\mathbf{H}]\{\boldsymbol{\beta}\} = [\mathbf{G}]\{\mathbf{d}\} \quad \text{or} \quad \{\boldsymbol{\beta}\} = [\mathbf{H}]^{-1}[\mathbf{G}]\{\mathbf{d}\} \tag{4.10-8}$$

At this point one can say that we have asked for the stress field within an element when boundary displacements $\{\mathbf{u}_b\}$ are defined by a chosen interpolation $\{\mathbf{u}_b\} = [\mathbf{L}]\{\mathbf{d}\}$ from

nodal displacement d.o.f. $\{\mathbf{d}\}$, and answered by determining parameters β_i that define a best-fit stress field contained in the approximation $\{\boldsymbol{\sigma}\} = [\mathbf{P}]\{\boldsymbol{\beta}\}$. Substitution of $\{\boldsymbol{\beta}\}$ from Eq. 4.10-8 into Eq. 4.10-3 yields

$$U^* = \frac{1}{2}\{\mathbf{d}\}^T[\mathbf{k}]\{\mathbf{d}\} \qquad \text{where} \qquad [\mathbf{k}] = [\mathbf{G}]^T[\mathbf{H}]^{-1}[\mathbf{G}] \tag{4.10-9}$$

Here we have identified $[\mathbf{k}]$ as a stiffness matrix because the form of U^* matches the form of strain energy U in an element, Eq. 4.8-16. Note that because we deal here with a linearly elastic material, strain energy and complementary energy are equal, $U = U^*$. After assembling the global stiffness matrix $[\mathbf{K}]$ from element stiffness matrices $[\mathbf{k}]$ in the usual way, and solving the global system $[\mathbf{K}]\{\mathbf{D}\} = \{\mathbf{R}\}$ for $\{\mathbf{D}\}$, nodal displacement d.o.f. $\{\mathbf{d}\}$ are known for each element. Element stresses are obtained from Eqs. 4.10-2 and 4.10-8:

$$\{\boldsymbol{\sigma}\} = [\mathbf{P}][\mathbf{H}]^{-1}[\mathbf{G}]\{\mathbf{d}\} \tag{4.10-10}$$

A hybrid element becomes stiffer as the number of β_i increases, and usually becomes more flexible as the element boundary is permitted more complicated displacement patterns. However, no bound can be set; we cannot say in general that a model built of hybrid elements will be either stiffer or more flexible than the mathematically exact solution.

Four-Node Plane Hybrid Element. For the stress field $\{\boldsymbol{\sigma}\} = \lfloor \sigma_z \quad \sigma_y \quad \tau_{xy} \rfloor^T = [\mathbf{P}]\{\boldsymbol{\beta}\}$ of a plane element, acceptable choices of $[\mathbf{P}]$ include

$$\begin{array}{cc} \text{Five-}\beta\text{ element} & \text{Seven-}\beta\text{ element} \\ [\mathbf{P}] = \begin{bmatrix} 1 & y & 0 & 0 & 0 \\ 0 & 0 & 1 & x & 0 \\ 0 & 0 & 0 & 0 & 1 \end{bmatrix} & [\mathbf{P}] = \begin{bmatrix} 1 & x & y & 0 & 0 & 0 & 0 \\ 0 & 0 & 0 & 1 & x & y & 0 \\ 0 & -y & 0 & 0 & 0 & -x & 1 \end{bmatrix} \end{array} \tag{4.10-11}$$

Both assumptions satisfy the differential equations of equilibrium, Eqs. 3.1-12, when body forces are zero. In general, the number of deformation modes an element resists is equal to the rank of $[\mathbf{k}]$, which does not exceed the number of β_i. A four-node, three-β plane element has rank three and resists only constant stress states. It does not resist the two bending modes numbered 7 and 8 in Fig. 6.8-1. In what follows we consider the five-β element.

In evaluating $[\mathbf{H}]$, Eq. 4.10-3, $dV = t\,dx\,dy$, where t = element thickness. Integration can be performed numerically as described in Section 6.3. Formulation of $[\mathbf{G}]$, Eq. 4.10-6, proceeds as follows. Surface tractions shown in Fig. 4.10-1a are, from Eq. 3.1-14,

$$\begin{aligned} \Phi_x &= l\sigma_x + m\tau_{xy} \\ \Phi_y &= l\tau_{xy} + m\sigma_y \end{aligned} \quad \text{where, for side } ij, \quad \begin{aligned} l &= l_{ij} = \cos\alpha_{ij} = (y_j - y_i)/L_{ij} \\ m &= m_{ij} = \sin\alpha_{ij} = (x_i - x_j)/L_{ij} \end{aligned} \tag{4.10-12}$$

Matrix $[\mathbf{R}]$ for the five-β element is, from Eqs. 4.10-11 and 4.10-12,

$$\underset{8\times5}{[\mathbf{R}]} = \begin{bmatrix} l_{12} & l_{12}y_{12} & 0 & 0 & m_{12} \\ 0 & 0 & m_{12} & m_{12}x_{12} & l_{12} \\ l_{23} & l_{23}y_{23} & 0 & 0 & m_{23} \\ \vdots & \vdots & \vdots & \vdots & \vdots \end{bmatrix} \quad \text{where} \quad \begin{aligned} x_{ij} &= x_i - s\sin\alpha_{ij} \\ y_{ij} &= y_i + s\cos\alpha_{ij} \end{aligned} \tag{4.10-13}$$

in which s is a side-tangent coordinate as shown in Fig. 4.10-1a. With u_{ij} and v_{ij} the x-parallel and y-parallel displacements along side ij, the second of Eqs. 4.10-4 becomes

$$\begin{Bmatrix} u_{12} \\ v_{12} \\ u_{23} \\ v_{23} \\ u_{34} \\ v_{34} \\ u_{41} \\ v_{41} \end{Bmatrix} = [\mathbf{L}] \begin{Bmatrix} u_1 \\ v_1 \\ u_2 \\ v_2 \\ u_3 \\ v_3 \\ u_4 \\ v_4 \end{Bmatrix}$$

$$\text{where} \quad \underset{8\times8}{[\mathbf{L}]} = \begin{bmatrix} 1-\dfrac{s}{L_{12}} & 0 & \dfrac{s}{L_{12}} & 0 & 0 & 0 & 0 & 0 \\ 0 & 1-\dfrac{s}{L_{12}} & 0 & \dfrac{s}{L_{12}} & 0 & 0 & 0 & 0 \\ 0 & 0 & 1-\dfrac{s}{L_{23}} & 0 & \dfrac{s}{L_{23}} & 0 & 0 & 0 \\ \vdots & \vdots & \vdots & \vdots & \vdots & & & \vdots \end{bmatrix} \tag{4.10-14}$$

In the integral that provides [**G**], Eq. 4.10-6, dS becomes $t\,ds$, where t = element thickness. Limits of integration are 0 to L_{12} for side 12, 0 to L_{23} for side 23, and so on. Manipulations are straightforward but tedious and result in a matrix [**G**] whose terms are simple functions of the nodal coordinates. For the present five-β element, with uniform thickness t,

$$\underset{5\times8}{[\mathbf{G}]} = \frac{t}{6}\begin{bmatrix} Y_1 & 0 & Y_2 & 0 & Y_3 & 0 & Y_4 & 0 \\ Z_1 & 0 & Z_2 & 0 & Z_3 & 0 & Z_4 & 0 \\ 0 & X_1 & 0 & X_2 & 0 & X_3 & 0 & X_4 \\ 0 & W_1 & 0 & W_2 & 0 & W_3 & 0 & W_4 \\ X_1 & Y_1 & X_2 & Y_2 & X_3 & Y_3 & X_4 & Y_4 \end{bmatrix} \tag{4.10-15a}$$

$$\text{where} \quad \begin{aligned} Y_j &= 3(y_k - y_i) & Z_j &= y_k(y_j + y_k) - y_i(y_i + y_j) \\ X_j &= 3(x_i - x_k) & W_j &= x_i(x_i + x_j) - x_k(x_j + x_k) \end{aligned} \tag{4.10-15b}$$

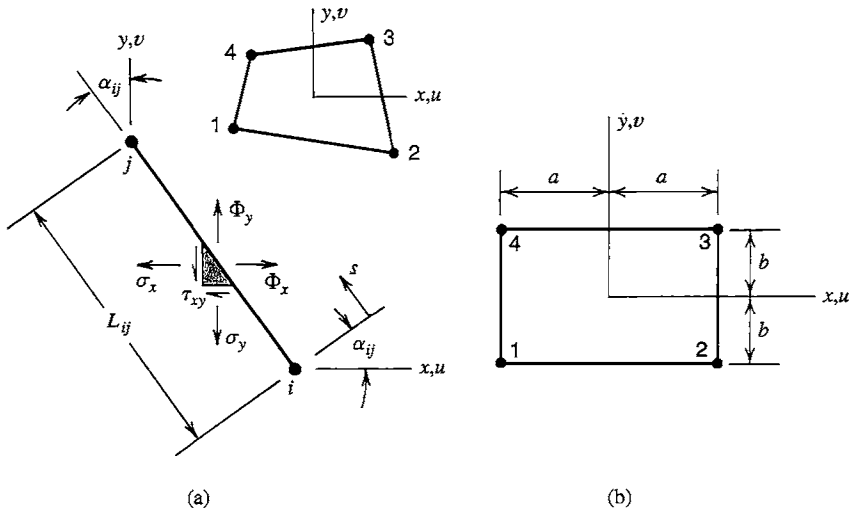

Figure 4.10-1. (a) Four-node plane element, with boundary tractions Φ_x and Φ_y and notation for a typical side ij. (b) The special case of a rectangular element.

Subscripts i, j, k are cyclically permuted in the sequence 1,2,3,4 with $i = j - 1$ and $k = j + 1$. Thus, for example, $Y_1 = 3(y_2 - y_4)$. For rectangular geometry, Fig. 4.10-1b, the present element is identical to the Q6 element discussed in Sections 3.10 and 6.6 [4.15].

Shear-Flexible Beam Element. An advantage of the assumed-stress hybrid formulation is the ease with which it includes transverse shear deformation effects in beam, plate and shell elements. Here we formulate a uniform plane beam element, shown in Fig. 4.10-2 [2.3]. For simplicity we omit axial deformation terms.

Complementary strain energy in a uniform beam element is

$$
\begin{aligned}
U^* &= \frac{1}{2EI_z}\int_0^L M^2 dx + \frac{k_y}{2AG}\int_0^L V^2 dx \\
&= \frac{1}{2}\int_0^L \begin{Bmatrix} M \\ V \end{Bmatrix}^T \begin{bmatrix} 1/EI_z & 0 \\ 0 & k_y/(AG) \end{bmatrix} \begin{Bmatrix} M \\ V \end{Bmatrix} dx
\end{aligned}
\tag{4.10-16}
$$

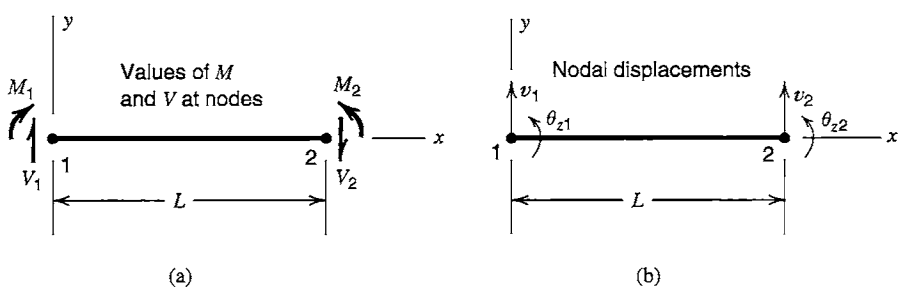

Figure 4.10-2. Plane beam element, showing (a) values of bending moment M and transverse shear force V at nodes, and (b) nodal displacement d.o.f.

Where E = elastic modulus, G = shear modulus, I_z = moment of inertia of cross-sectional area A about a centroidal z axis, and k_y = shear factor that accounts for the y-direction variation of τ_{xy} (for example, k_y = 1.2 for a solid rectangular cross section). Within the element, the assumed field for bending moment M and transverse shear force V is

$$\begin{Bmatrix} M \\ V \end{Bmatrix} = [\mathbf{P}] \begin{Bmatrix} \beta_1 \\ \beta_2 \end{Bmatrix} \qquad \text{where} \qquad [\mathbf{P}] = \begin{bmatrix} 1 & x \\ 0 & 1 \end{bmatrix} \tag{4.10-17}$$

This assumption satisfies the equilibrium equation $dM/dx = V$ of beam theory. The square matrix in Eq. 4.10-16 plays the same role as $[\mathbf{E}]^{-1}$ in Eq. 4.10-3. Therefore

$$\left.\begin{aligned} [\mathbf{H}] &= \int_0^L [\mathbf{P}]^T [\mathbf{E}]^{-1} [\mathbf{P}]\, dx \\ \text{Define} \quad \phi_y &= \frac{12EI_z k_y}{AGL^2} \end{aligned}\right\} \text{hence } [\mathbf{H}]^{-1} = \frac{12EI_z}{(1+\phi_y)L^2} \begin{bmatrix} \dfrac{L}{3} + \dfrac{EI_z k_y}{AGL} & -\dfrac{1}{2} \\ -\dfrac{1}{2} & \dfrac{1}{L} \end{bmatrix} \tag{4.10-18}$$

Nodal values of M and V, with signs chosen to agree with directions of nodal d.o.f., are

$$\begin{Bmatrix} V_1 \\ -M_1 \\ -V_2 \\ M_2 \end{Bmatrix} = [\mathbf{R}] \begin{Bmatrix} \beta_1 \\ \beta_2 \end{Bmatrix} \qquad \text{where} \qquad [\mathbf{R}] = \begin{bmatrix} 0 & 1 \\ -1 & 0 \\ 0 & -1 \\ 1 & L \end{bmatrix} \tag{4.10-19}$$

In the second of Eqs. 4.10-4, element d.o.f. are $\{\mathbf{d}\} = \lfloor v_1 \;\; \theta_{z1} \;\; v_2 \;\; \theta_{z2} \rfloor^T$ and $[\mathbf{L}]$ is a unit matrix because $\{\mathbf{u}_b\} = \{\mathbf{d}\}$. Hence Eq. 4.10-6 yields $[\mathbf{G}] = [\mathbf{R}]^T$ and Eqs. 4.10-9 and 4.10-18 yield the stiffness matrix of a Timoshenko beam element

$$[\mathbf{k}] = \frac{12EI_z}{(1+\phi_y)L^2} \begin{bmatrix} 1/L & 1/2 & -1/L & 1/2 \\ 1/2 & (4+\phi_y)L/12 & -1/2 & (2-\phi_y)L/12 \\ -1/L & -1/2 & 1/L & -1/2 \\ 1/2 & (2-\phi_y)L/12 & -1/2 & (4+\phi_y)L/12 \end{bmatrix} \tag{4.10-20}$$

This result agrees with Eqs. 2.3-6 and 2.3-7. As the element becomes more and more slender, ϕ_y approaches zero, and $[\mathbf{k}]$ reduces to the familiar stiffness matrix of a beam that has only bending deformation, without exhibiting shear locking or ill-conditioning of $[\mathbf{k}]$.

ANALYTICAL PROBLEMS

4.2-1 The system shown consists of a rigid half-cylinder that can roll without friction on a horizontal surface, a linear spring of stiffness k, and a force P of constant magnitude that can move around the cylinder but is always directed at point C on the cylinder.

Show that work done by P when point C undergoes a horizontal displacement D is path-dependent, and hence the system is not conservative.

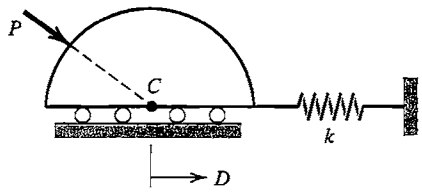

Problem 4.2-1

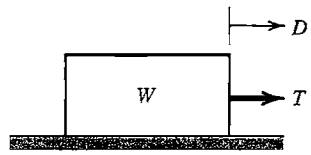

Problem 4.2-2

4.2-2 The block shown has weight W and rests on a rough horizontal surface having friction coefficient μ. A horizontal force T is applied to produce sliding displacement D. Show that the system is not conservative.

4.2-3 Load P applied to the tip of the column shown is called a *follower load:* it always has the same orientation θ as the tip. By considering work done by P in undergoing small displacements v and θ from initial position to final position, show that the system is not conservative. Neglect work associated with displacement of P in the x direction.

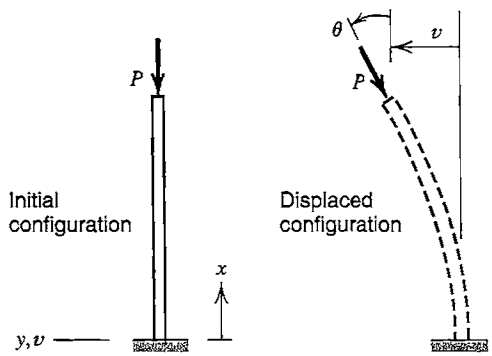

Problem 4.2-3

4.2-4 Redefine Ω to be $\Omega = P(D_{eq} - D)$ as suggested near the end of Section 4.2. Revise Fig. 4.2-4 as required.

4.2-5 Reverse the direction of load P in Fig. 4.2-3. Solve for the equilibrium value of D by use of Π_p. Revise Fig. 4.2-4 as required.

4.2-6 Imagine that the spring in Fig. 4.2-3 is not linear but exerts a force proportional to the square of its stretch. Write an expression for Π_p, and from it determine the equilibrium value of D.

4.3-1 Redefine D_2 and D_3 in Fig. 4.3-1 so that D_2 is an axial displacement *relative* to D_1 and D_3 is an axial displacement *relative* to D_2. Write an expression for Π_p, analogous to Eq. 4.3-3. For the special case $k_1 = k_2 = k_3 = k$ and $P_1 = P_2 = P_3 = P$, solve for the D_i and show that they give the same *absolute* axial displacements as Eq. 4.3-3.

4.3-2 Displacement d.o.f. d_i at ends of a uniform bar element have the directions shown. Write an expression for Π_p in terms of these d.o.f. From the stationary condition $d\Pi_p = 0$, obtain the element stiffness matrix that operates on these four d.o.f.

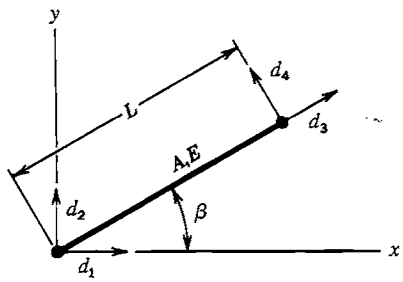

Problem 4.3-2

4.3-3 Use the method of stationary potential energy to derive stiffness matrices for the structures described in (a) Problem 2.2-2, (b) Problem 2.2-3, (c) Problem 2.3-2, and (d) Problem 2.3-3.

4.3-4 Verify that Eqs. 4.3-5 and 4.3-6 yield Eq. 4.3-3.

4.4-1 Write Eq. 4.4-2 for an isotropic material in a condition of plane stress in the xy plane (for which [E] is 3 by 3). Specialize this expression for the case of uniaxial stress σ_x. Check your result against the corresponding term in Eq. 4.4-9.

4.4-2 In the beam formulation described by Fig. 4.4-lb, let initial strain and initial stress be given by $\varepsilon_0 = -y\kappa_0$ and $\sigma_0 = -m_0 y/I_z$, respectively. Here κ_0 is initial curvature and m_0 is initial moment, both considered positive when associated with a concave-up condition of the beam. Starting with Eq. 4.4-9, determine the contributions of κ_0 and m_0 to Eq. 4.4-11.

4.4-3 Repeat the example of Eqs. 4.4-12 to 4.4-14, but account for heating by use of ε_0 rather than σ_0.

4.5-1 Verify that the first of Eqs. 4.5-6a is indeed given by the conditions $\partial\Pi_p/\partial a_1 = 0$ and $\partial\Pi_p/\partial a_2 = 0$.

4.5-2 Verify that the a_i of Eq. 4.5-9 result from the use of the three-term polynomial $u = a_1x + a_2x^2 + a_3x^3$ in a Rayleigh-Ritz solution.

4.5-3 Consider the two approximate solutions and the one exact solution in Section 4.5 (Eqs. 4.5-5c, 4.5-6b, and 4.5-8). At what point or points on the bar is the differential equation of equilibrium satisfied by each solution?

4.5-4 Consider a uniform cantilever beam of length L, fixed at end $x = 0$ and carrying a transverse force F at $x = L$.

(a) Let the lateral displacement field be $v = a_1x^3$, where a_1 is a generalized d.o.f. Is this field admissible? Explain.

(b) Write a polynomial field for v that is better than that of part (a). Let the field contain three terms, each of the form a_ix^j, where $i = 1,2,3$ and j is an integer such that the term is admissible.

(c) Without calculation, can you predict the quality of the answers obtainable from the field of part (b) and the numerical value of any of the a_i?

(d) Use the field of part (a) to calculate the deflection of force F.

4.5-5 A uniformly loaded beam of uniform flexural stiffness EI is simply supported at its ends $x = 0$ and $x = L$. In parts (a) and (b), determine the deflection and bending

moment predicted at $x = L/2$ by a Rayleigh-Ritz solution that has a single d.o.f. Compare exact and approximate results.
(a) Use the single-d.o.f. algebraic expression $v = a_1 x(L - x)$.
(b) Use one term of a sine series.
(c) Why should you anticipate that part (b) will provide a more accurate result than part (a)?

4.5-6 The uniform cantilever beam shown carries uniformly distributed load of intensity q, tip force P_L, and tip moment M_L. In parts (a) and (b), compute Rayleigh-Ritz approximations for displacement and rotation of the tip. Compare these results with formulas from beam theory, and explain why the Rayleigh-Ritz result is or is not exact.
(a) Use one term of a polynomial series.
(b) Use two terms of a polynomial series.
(c) In part (a), for which of the given loadings is the displacement field $v(x)$ exact *throughout* the beam? Explain.

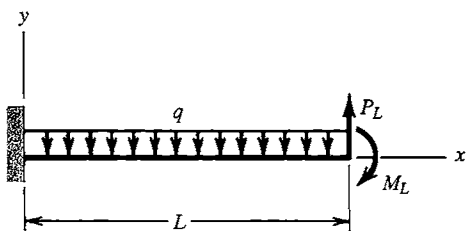

Problem 4.5-6

4.5-7 If loads P_L and M_L in Problem 4.5-6 were applied at $x = L/2$ rather than at the tip, how many polynomial terms would be needed to obtain the exact displacement at $x = L$? Explain.

4.5-8 A beam with uniform EI and length L has a pin support at $x = 0$, a roller support at $x = L/2$, and is loaded by a transverse tip force P at $x = L$. Starting with a complete quadratic polynomial trial function, determine the tip displacement using the Rayleigh-Ritz method. What is the percentage error of this result, and of the associated bending moment at $x = L/2$?

4.5-9 The beam shown has uniform EI. Starting with the trial function $v = a_0 + a_1 x + a_2 x^2$ for lateral displacement, make the function admissible, then use the Rayleigh-Ritz method to determine v at $x = L$ and the largest bending moment. What are the percentage errors of these results?

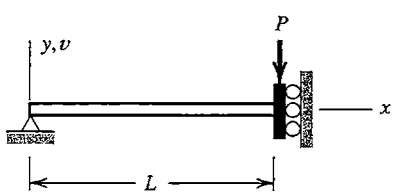

Problem 4.5-9

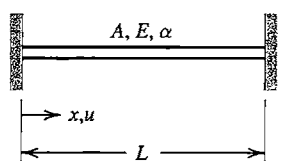

Problem 4.5-10

4.5-10 The uniform bar shown has modulus E, cross sectional area A, and coefficient of thermal expansion α. At a reference temperature of zero, the bar is stress-free and

exactly fits between the two rigid walls. The bar is then subjected to a temperature field $T(x)$ that varies linearly from zero at $x = 0$ to T_0 at $x = L$ where $T_0 > 0$. Starting with a complete quadratic polynomial trial function, use the Rayleigh-Ritz method to predict the axial displacement field $u(x)$ and the axial stress field.

4.5-11 Consider a straight column with uniform A and EI that supports an axial load P (positive in tension) as shown. Potential energy for small deflections is

$$\Pi_p = \int_0^L \frac{AE}{2} u_{,x}^2 \, dx + \int_0^L \frac{P}{2} v_{,x}^2 \, dx + \int_0^L \frac{EI}{2} v_{,xx}^2 \, dx - P\delta$$

Using the Rayleigh-Ritz method, with separate trial functions for u and v, estimate the buckling load for the column. Use the simplest possible kinematically admissible polynomial trial functions for u and v. Express the result in terms of constants such as A, EI, L, etc. One of the resulting equations will allow one of the generalized d.o.f. to be zero. Rather than accept this solution (physically, it means the column remains straight and does not buckle), let the d.o.f. be nonzero; hence obtain an equation for the buckling load.

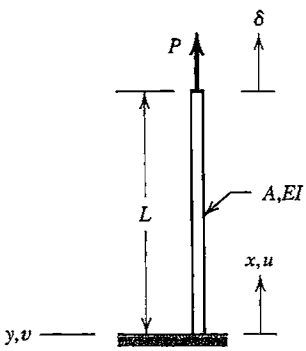

Problem 4.5-11

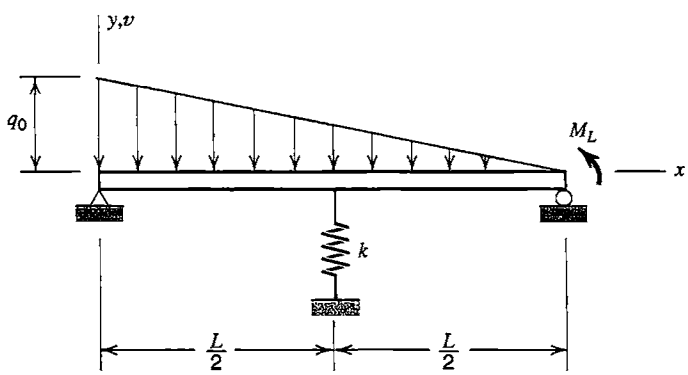

Problem 4.5-12

4.5-12 The simply supported beam shown has uniform EI and supports a linearly varying distributed load of intensity q_0 at the left-hand end, and a moment M_L at the right-hand end. It also has an elastic spring support of stiffness k at midspan. Use the Rayleigh-Ritz method with the simplest possible trial function to determine an approximate deflection field $v(x)$.

4.5-13 A uniform beam is simply supported and carries a force P at its center. Use the Rayleigh-Ritz method with the infinite series

$$v = \sum a_i \sin\frac{i\pi x}{L} \quad \text{with} \quad i = 1, 3, 5, \ldots$$

to compute deflection and bending moment at the center. Compare exact and approximate results for 1, 2, 3, and 4 terms retained.

4.5-14 Repeat Problem 4.5-13 with load P replaced by a uniformly distributed downward load of intensity q.

4.6-1 (a) Compute work done by applied load $q = cx$ in going through the exact displacement u of Eq. 4.5-8.
(b) Similarly, compute the work done by load q in each of the two approximate solutions (Eqs. 4.5-5 and 4.5-6). What conclusion can be drawn?

4.6-2 (a) Compute strain energy associated with the exact solution given in Eq. 4.5-8. How is this energy related to work computed in Problem 4.6-1a, and why?
(b) Similarly, compute strain energy associated with the two approximate solutions (Eqs. 4.5-5 and 4.5-6), and compare answers with work values computed in Problem 4.6-1b.

4.7-1 Consider the functional $\Pi = \int F\,dx$ in which $F = c_1\phi_{,xx}^2 + c_2\phi_{,x}^2 + c_3\phi^2 + c_4\phi + c_5$ and the five c_i are constants. Determine the Euler equation using (a) Eq. 4.7-2a and (b) the calculus of variations as demonstrated for Eq. 4.7-8.

4.7-2 A certain physical problem has the functional

$$\Pi_p = \int_0^L \left(\frac{1}{2}\phi_{,x}^2 - 50\phi\right) dx$$

Determine the Euler equation for this functional. Then solve the Euler equation with the essential boundary conditions $\phi = 0$ at $x = 0$ and $\phi = 20$ at $x = L$ to determine ϕ as a function of x and L.

4.7-3 Discard terms that contain $\{\mathbf{F}\}$ and $\{\mathbf{M}\}$ from Eq. 4.4-11, and use Eq. 4.7-2a to obtain the Euler equation of a uniform beam under lateral load q. What is the Euler equation if EI_z is not constant?

4.7-4 Repeat Problem 4.7-3 using the calculus of variations (as demonstrated for Eq. 4.7-8).

4.7-5 The potential energy of an isotropic plate of uniform thickness that carries lateral pressure q is

$$\Pi_p = \frac{D}{2}\iint\left\{(w_{,xx} + w_{,yy})^2 - 2(1-\nu)\left[w_{,xx}w_{,yy} - w_{,xy}^2\right] - \frac{2qw}{D}\right\} dx\,dy$$

where w is the lateral deflection, D is a constant called *flexural rigidity* and ν is Poisson's ratio. Use Eq. 4.7-2a to show that the Euler equation is $\nabla^4 w = q/D$, where ∇^4 is the biharmonic operator.

4.7-6 Consider the functional

$$\Pi = \int\left(\frac{M^2}{2EI} + M_{,x}v_{,x} + qv\right) dx$$

for a uniform beam that carries distributed lateral load q. Bending moment M and lateral deflection v are independent fields. Derive the two Euler equations using Eqs. 4.7-2. Do the Euler equations have the form expected from beam theory?

4.7-7 The *rigid* bar shown rests on an elastic foundation. When displaced laterally an amount v, the foundation applies a force $kv\,dx$ to a length dx of the bar, where k is a constant. Determine the 2 by 2 stiffness matrix that operates on v_i and v_j. *Suggestion:* Express strain energy U in terms of k, L, v_i and v_j, then write U in the form $\{\mathbf{d}\}^T[\mathbf{k}]\{\mathbf{d}\}/2$, and identify $[\mathbf{k}]$.

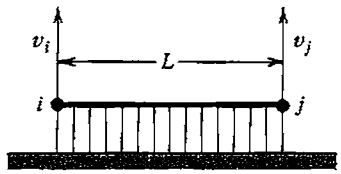

Problem 4.7-7

4.8-1 For each of the following problems, obtain finite element formulations in a form analogous to Eqs. 4.8-7 and 4.8-8. Details such as specific element shape functions are not required.

(a) Plane beam (use the integrals in Eq. 4.4-11).

(b) Plane beam (see Problem 4.7-6). Use two interpolating fields, one for M that depends on nodal moments $\{\mathbf{M}_e\}$ and one for v that depends on nodal lateral deflections $\{\boldsymbol{v}_e\}$.

(c) Acoustic modes of gas or fluid in a cavity with rigid walls. The functional is

$$\Pi = \int\left(p_{,x}^2 + p_{,y}^2 + p_{,z}^2 - \frac{\omega^2}{c^2}p^2\right) dV$$

where $p = p(x,y,z)$ is the amplitude of gas or fluid pressure that varies with time, ω is the circular frequency, and c is the speed of sound. Let $p = \lfloor \mathbf{N} \rfloor \{\mathbf{p}_e\}$, where $\{\mathbf{p}_e\}$ represents nodal pressures.

(d) Isotropic plate with lateral pressure (see Problem 4.7-5).

4.9-1 Verify numerically that Eq. 4.9-1 yields the displacement shown in Fig. 4.9-1. Use $\theta = 30°$. Also, by comparing element edge lengths before and after displacement, verify that the displacement is a rigid-body motion.

4.9-2 It is proposed that a beam element be based on a cubic polynomial but that d.o.f. are to be lateral displacements v_i, where $i = 1,2,3,4$. Nodes are to be at either end and at the third-points (that is, at $x = 0, L/3, 2L/3, L$). What convergence criterion is violated by this element?

4.9-3 In three dimensions, which of the cubic terms would you add to a complete quadratic field (10 terms), if there is to be no directional bias and the total number of terms in the field is to be (a) 11, (b) 13, (c) 14, (d) 16, (e) 17, (f) 19?

4.9-4 Consider a uniform straight bar of length L that is supported against rigid body motion, and is loaded by a smoothly varying distributed axial force q. The bar is to be modeled using two meshes. The first uses n linear-displacement bar elements, where n is an even number. The second mesh uses $n/2$ quadratic-displacement bar elements. The number and locations of nodes for each mesh are the same.

(a) Which mesh will likely provide the more accurate displacement and stress results? Explain.

(b) If each mesh is refined by subdividing elements into two, by what factors will errors in displacements and stresses likely be reduced for each of the finer meshes?

4.10-1 Letting thickness be constant and Poisson's ratio be zero, evaluate matrix [**H**] for the rectangular element in Fig. 4.10-1b.

4.10-2 Use the hybrid formulation to obtain the 4 by 4 stiffness matrix of a slender beam element (analogous to Eq. 4.10-20). However, from the outset, include only the energy of bending.

CHAPTER 5

FORMULATION TECHNIQUES: GALERKIN AND OTHER WEIGHTED RESIDUAL METHODS

Approximate solutions, including FE solutions, can be constructed from governing differential equations. This chapter discusses the Galerkin method, which is commonly used for this purpose, and summarizes related methods. Examples include a "mixed" formulation and nonstructural problems.

5.1 GALERKIN METHOD

Introduction. Thus far we have formulated finite elements by direct physical argument (Chapter 2), by a virtual work argument (Chapter 3), and by variational arguments applied to functionals such as potential energy (Chapter 4). Virtual work and variational arguments are classical analysis tools, and remain adequate for FE formulation of most problems in structural mechanics. In other problem areas, functionals analogous to potential energy are less well known and may not have a clear physical meaning. Also, for some applications the functional needed for a variational approach cannot be written. A case in point is fluid mechanics, where, for some types of flow, all that is available are differential equations and boundary conditions. FE formulations for such problems can still be obtained, using *weighted residual methods,* of which the *Galerkin method* is the most widely used. Like a variational statement of a problem, a Galerkin statement incorporates differential equations in their weak form, as described in Chapter 4, so that they are satisfied over a domain in an integral or average sense rather than at every point. A relation between the Galerkin method and the principle of virtual work is noted at the end of Section 4.7.

In this section and the next we adopt the following notation:

x	independent variables, for example, coordinates of a material point
$u = u(x)$	dependent variables, for example, displacements of a material point
$\tilde{u} = \tilde{u}(x)$	an approximate solution; $\tilde{u} = u$ if exact
f	a function of x (which may be constant or zero)
D	a differential operator

The mathematical statement of a physical problem is

$$\text{In domain } V: \qquad Du - f = 0 \tag{5.1-1}$$

As an example, for steady-state heat conduction in an isotropic material without internal heat generation, D is the harmonic operator ∇^2, u is temperature T, and $f = 0$. The problem is stated in strong form by Eq. 5.1-1 and appropriate boundary conditions, which imply that the differential equation must be satisfied at every internal point and boundary conditions at every boundary point. In general an approximating function $\tilde{u}$ does not satisfy Eq. 5.1-1 at every point. Thus a residual $R = R(x)$ remains:

$$\text{Residual in domain } V: \qquad R = D\tilde{u} - f \tag{5.1-2}$$

Let $\tilde{u}$ be a linear combination of basis functions. Typically $\tilde{u}$ is a polynomial of n terms whose ith term is multiplied by a generalized d.o.f. a_i. The n values of the a_i are to be selected so that R is small (in some sense). According to a weighted residual method, values of the a_i that are best (in some sense) satisfy the following expression of governing equations in their weak form.

$$\int W_i R \, dV = 0 \qquad \text{for} \qquad i = 1, 2, \ldots, n \tag{5.1-3}$$

where each $W_i = W_i(x)$ is a *weight function*. In the Galerkin weighted residual method, each W_i is the multiplier of the corresponding a_i in $\tilde{u}$. Other weighted residual methods are discussed in Section 5.2.

One-Dimensional Example. Figure 5.1-1 depicts a uniform bar under axial load and shows the derivation of its governing differential equation. The *exact* solution for axial displacement $u = u(x)$ is easily obtained by integrating the differential equation. Thus

$$u = \frac{P}{AE}x + \frac{cL_T^2}{2AE}x - \frac{c}{6AE}x^3 \tag{5.1-4}$$

We now pretend not to know this result and instead seek an approximate solution. From Fig. 5.1-1 and Eq. 5.1-3, a Galerkin statement of the problem is

$$\int_0^{L_T} W_i \left(\frac{d^2\tilde{u}}{dx^2} + \frac{cx}{AE} \right) dx = 0 \tag{5.1-5}$$

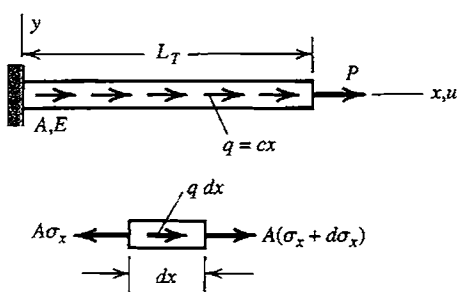

(a)

$$\left.\begin{aligned} A\frac{d\sigma_x}{dx} + q &= 0 \\ \sigma_x = E\varepsilon_x = E\frac{du}{dx} \end{aligned}\right\} AE\frac{d^2u}{dx^2} + q = 0$$

For the problem shown:

$$\frac{d^2u}{dx^2} + \frac{cx}{AE} = 0 \quad \text{for } 0 < x < L_T$$

$$AE\frac{du}{dx} = P \quad \text{at } x = L_T$$

(b)

Figure 5.1-1. (a) Uniform elastic bar, loaded by axial tip force P and by linearly-varying axial force $q = cx$, where c is a constant. A = cross-sectional area, E = elastic modulus. (b) Derivation of governing equations.

The next step is to alter the form by applying integration by parts. This step serves to introduce natural boundary conditions. Also, the order of differentiation in integrals is reduced, so that the assumed form of $\tilde{u}$ can be of lower order than required in Eq. 5.1-5. This feature becomes important in the FE form of the method, discussed in subsequent sections, where we prefer that FE models have interelement continuity requirements that involve only low-order derivatives. Accordingly we apply the formula for integration by parts in one dimension, specifically

$$d\,(uv) = u\,dv + v\,du \qquad \text{from which} \qquad \int u\,dv = uv - \int v\,du \tag{5.1-6}$$

With $u = W_i$ in Eq. 5.1-6, Eqs. 5.1-5 and 5.1-6 yield

$$\int_0^{L_T}\left(-\frac{dW_i}{dx}\frac{d\tilde{u}}{dx} + W_i\frac{cx}{AE}\right)dx + \left[W_i\frac{d\tilde{u}}{dx}\right]_0^{L_T} = 0 \tag{5.1-7}$$

For the approximate axial displacement, we elect to use a two-d.o.f. trial function $\tilde{u}$. This function, and weight functions W_i extracted from it, are

$$\tilde{u} = a_1x + a_2x^2 \qquad \begin{matrix} W_1 = x \\ W_2 = x^2 \end{matrix} \qquad \text{hence} \qquad \begin{matrix} dW_1/dx = 1 \\ dW_2/dx = 2x \end{matrix} \tag{5.1-8}$$

where the a_i are generalized d.o.f. Note that trial function $\tilde{u}$ is *admissible* because W_1 and W_2 both satisfy the essential boundary condition of zero axial displacement at $x = 0$. At $x = L_T$ we apply the natural boundary condition that axial strain $d\tilde{u}/dx$ is equal to P/AE. From Eqs. 5.1-7 and 5.1-8, with $i = 1$ and then $i = 2$,

$$\begin{aligned} &\int_0^{L_T}\left[(-1)(a_1 + 2a_2x) + x\frac{cx}{AE}\right]dx + L_T\frac{P}{AE} = 0 \\ &\int_0^{L_T}\left[(-2x)(a_1 + 2a_2x) + x^2\frac{cx}{AE}\right]dx + L_T^2\frac{P}{AE} = 0 \end{aligned} \tag{5.1-9}$$

From which

$$\begin{aligned} a_1 &= \frac{P}{AE} + \frac{7cL_T^2}{12AE} \qquad & \qquad \tilde{u} &= \frac{P}{AE}x + \frac{7cL_T^2}{12AE}x - \frac{cL_T}{4AE}x^2 \\ a_2 &= -\frac{cL_T}{4AE} \qquad \text{hence} & \qquad \tilde{\sigma} &= E\tilde{u}_{,x} = \frac{P}{A} + \frac{7cL_T^2}{12A} - \frac{cL_T}{2A}x \end{aligned} \tag{5.1-10}$$

A numerical comparison of these results with other approximate results appears subsequently, in Table 5.2-1. Equations 5.1-10 are seen to agree with results for the same problem obtained by the Rayleigh-Ritz method (Eqs. 4.5-6).

Remarks. The foregoing Galerkin method, in which weight functions W_i are also used as multipliers of numerical coefficients a_i, is more specifically known as the Bubnov-Galerkin method. We follow the common practice of calling it simply the Galerkin method. There is a variant of the Galerkin method called the Petrov-Galerkin method, in which some or all of the W_i are chosen to differ from multipliers of the a_i, and which consequently provides results that differ from those obtained from a functional (if the necessary functional exists). The Petrov-Galerkin method is used in fluid mechanics.

If a functional can be constructed that yields the governing differential equations of the problem, as described in Chapter 4, then the Galerkin method and the Rayleigh-Ritz method yield identical results when both use the same approximating function $\tilde{u}$. It is easy to show that this is so for the foregoing example. The potential energy expression for the bar problem of Fig. 5.1-1 is

$$\Pi_p = \int_0^{L_T} \left(\frac{1}{2} AE\tilde{u}_{,x}^2 - cx\tilde{u} \right) dx - P\tilde{u}_{L_T} \tag{5.1-11}$$

With a two-parameter approximating function $\tilde{u}$, the Rayleigh-Ritz solution for these parameters is obtained from the equations $\partial \Pi_p / \partial a_1 = 0$ and $\partial \Pi_p / \partial a_2 = 0$. Thus

$$\begin{aligned} \int_0^{L_T} \left(AE\tilde{u}_{,x} \frac{\partial \tilde{u}_{,x}}{\partial a_1} - cx \frac{\partial \tilde{u}}{\partial a_1} \right) dx - P\left(\frac{\partial \tilde{u}}{\partial a_1} \right)_{L_T} &= 0 \\ \int_0^{L_T} \left(AE\tilde{u}_{,x} \frac{\partial \tilde{u}_{,x}}{\partial a_2} - cx \frac{\partial \tilde{u}}{\partial a_2} \right) dx - P\left(\frac{\partial \tilde{u}}{\partial a_2} \right)_{L_T} &= 0 \end{aligned} \tag{5.1-12}$$

With $\tilde{u} = a_1 x + a_2 x^2$, these two equations are found to be the same as Eqs. 5.1-9.

5.2 METHODS OF WEIGHTED RESIDUALS (MWR)

The Galerkin method is but one of many methods of weighted residuals (MWR), all of which are intended to select parameters in approximating trial functions so as to obtain the best approximation (in some sense). In order to explain MWR briefly, we expand our definition of "residual" to include the boundary residual. (With the Galerkin method a boundary residual need not be stated explicitly because integration by parts invokes natural boundary conditions, as seen in Eq. 5.1-7.) Presuming that the approximate solution $\tilde{u}$ is a function of coordinates x and n generalized d.o.f. $\{\mathbf{a}\} = \lfloor a_1 \ a_2 \cdots a_n \rfloor^T$, whose numerical values are to be determined, we write

$$R = R(\{\mathbf{a}\},x) = D\tilde{u} - f \qquad \text{(residual in domain } V) \tag{5.2-1a}$$

$$R_S = R_S(\{\mathbf{a}\},x) = D_S\tilde{u} - g \qquad \text{(residual on boundary } S \text{ of } V) \tag{5.2-1b}$$

where D_S is a differential operator. We seek to minimize residuals according to some definition, while providing enough equations to solve for the n values of the a_i. Among MWR, the Galerkin method and the following methods are perhaps best known.

In the *collocation* method, also called *point collocation,* residuals are set to zero at n different locations x_i.

$$R(\{\mathbf{a}\},x_i) = 0 \qquad \text{for} \qquad i = 1, 2, \ldots, j-1 \tag{5.2-2a}$$

$$R_S(\{\mathbf{a}\},x_i) = 0 \qquad \text{for} \qquad i = j, j+1, \ldots, n \tag{5.2-2b}$$

where $j < n$, else conditions on boundary S do not appear. The distribution of collocation points may be almost uniform or may be more dense in regions of greatest interest.

In the *subdomain* method, also called *subdomain collocation,* integrals of the residual over n different portions of V and S are set to zero.

$$\int R(\{\mathbf{a}\},x)\, dV_i = 0 \qquad \text{for} \qquad i = 1, 2, \ldots, j-1 \tag{5.2-3a}$$

$$\int R_S(\{\mathbf{a}\},x)\, dS_i = 0 \qquad \text{for} \qquad i = j, j+1, \ldots, n \tag{5.2-3b}$$

In the *least squares* method, also called *continuous least squares,* the a_i are chosen to minimize a function I.

$$\frac{\partial I}{\partial a_i} = 0 \qquad \text{for} \qquad i = 1, 2, \ldots, n \tag{5.2-4}$$

in which function I is formed by integrating squares of the residuals.

$$I = \int [R(\{\mathbf{a}\},x)]^2\, dV + \alpha \int [R_S(\{\mathbf{a}\},x)]^2\, dS \tag{5.2-5}$$

where α is an arbitrary multiplier that serves to achieve dimensional homogeneity and can also serve as a penalty number. Larger values of α increase the importance of R_S relative to R.

In *least squares collocation,* also called *point least squares* and *overdetermined collocation,* Eq. 5.2-4 is still used, but I is defined as the sum of squared residuals at m points, where $m \geq n$:

$$I = \sum_{i=1}^{j-1} [R(\{\mathbf{a}\}, x_i)]^2 + \alpha \sum_{i=j}^{n} [R_S(\{\mathbf{a}\}, x_i)]^2 \tag{5.2-6}$$

Equation 5.2-6 yields n equations for the n coefficients a_i, even when $m > n$. If $m = n$, the method reduces to simple collocation.

Remarks. The commonality shared by Galerkin and other MWR is that they all can be loosely symbolized as

$$\int W_i R_\Gamma\, d\Gamma = 0 \tag{5.2-7}$$

where R_Γ represents R (and perhaps also R_S) and Γ represents V (and perhaps also S). The various MWR differ in how W_i is defined [5.1–5.4]. In the Galerkin method, $W_i = \partial\tilde{u}/\partial a_i$. In collocation or subdomain methods, the W_i are unit delta or step functions that are nonzero at certain points or over certain subregions. In least squares methods, $W_i = \partial R/\partial a_i$ [5.5].

In words, Eq. 5.2-7 says that residual R_Γ, weighted by factor W_i, has an average value of zero over region Γ. Obtaining a solution from Eq. 5.2-7 is analogous to obtaining a solution from the variational statement $\delta\Pi = 0$ in a problem for which a functional Π is available.

All MWR yield a set of algebraic equations of the form $[\mathbf{A}]\{\mathbf{a}\} = \{\mathbf{c}\}$, to be solved for the a_i in the approximating function $\tilde{u}$. The set of equations is linear if D is a linear operator [2.14,5.1]. In the (Bubnov-) Galerkin method and all least squares methods, coefficient matrix $[\mathbf{A}]$ is symmetric. Collocation, subdomain, and Petrov-Galerkin methods may produce an unsymmetric $[\mathbf{A}]$. Unless $\tilde{u}$ contains the exact solution, a given $\tilde{u}$ will in general produce different solutions for different choices of collocation points, subdomains, or α in Eqs. 5.2-5 and 5.2-6.

Least squares methods tend to produce an ill-conditioned $[\mathbf{A}]$, and despite the "tuning" allowed by coefficient α, the solution may be too strongly influenced by unimportant residuals. Because weights are $W_i = \partial R/\partial a_i$, both R and W_i contain derivatives of the field quantity of the same order. Therefore, in the continuous least squares method, integration by parts cannot reduce the order of differentiation in integrals. Thus if derivatives of order $2m$ appear in R, an FE formulation would require that $\tilde{u}$ display interelement continuity of derivatives of order $2m - 1$. The required order of interelement continuity can be reduced by reformulating the problem as a set of first order differential equations.

Example Solutions. Again we consider the problem depicted in Fig. 5.1-1, and use the admissible trial function stated in Eq. 5.1-8. Thus

$$\left.\begin{aligned} \frac{d^2u}{dx^2} + \frac{cx}{AE} &= 0 \\ \tilde{u} &= a_1x + a_2x^2 \end{aligned}\right\} \qquad \begin{aligned} &\text{Interior residual:} \quad R = 2a_2 + \frac{cx}{AE} \\ &\text{Boundary residual:} \quad R_S = a_1 + 2a_2L_T - \frac{P}{AE} \end{aligned} \tag{5.2-8}$$

The essential boundary condition, $u = 0$ at $x = 0$, is satisfied by $\tilde{u}$ and so does not appear in R_S. Here $R_S = 0$ implies that $\tilde{\varepsilon} = P/AE$ at $x = L_T$.

For a collocation solution, we arbitrarily elect to evaluate R at $x = L_T/3$. Hence the equations $R = 0$ and $R_S = 0$ yield

$$a_1 = \frac{P}{AE} + \frac{cL_T^2}{3AE} \qquad a_2 = -\frac{cL_T}{6AE} \tag{5.2-9}$$

For a subdomain solution, we elect to integrate R over the entire length, from $x = 0$ to $x = L_T$. Thus Eq. 5.2-3a and $R_S = 0$ yield

$$a_1 = \frac{P}{AE} + \frac{cL_T^2}{2AE} \qquad a_2 = -\frac{cL_T}{4AE} \tag{5.2-10}$$

In a least squares solution, the two terms in Eq. 5.2-5 have the same dimensions if we use $\alpha = 1/L_T$. Thus

$$I = \int_0^{L_T}\left(2a_2 + \frac{cx}{AE}\right)^2 dx + \frac{1}{L_T}\left(a_1 + 2a_2L_T - \frac{P}{AE}\right)^2 \tag{5.2-11}$$

in which the last term is already "integrated" over the area at $x = L_T$. The equations $\partial I/\partial a_1 = 0$ and $\partial I/\partial a_2 = 0$ are found to yield the results stated in Eqs. 5.2-10.

For a solution by least squares collocation, we elect to evaluate R at $x = L_T/3$ and at $x = L_T$. Residual R_S is stated in Eq. 5.2-8. For dimensional homogeneity, we choose $\alpha = 1/L_T^2$. The three residuals can be written in the form

$$\begin{Bmatrix} R_1 \\ R_2 \\ R_S/L_T \end{Bmatrix} = \begin{bmatrix} 0 & 2 \\ 0 & 2 \\ 1/L_T & 2 \end{bmatrix} \begin{Bmatrix} a_1 \\ a_2 \end{Bmatrix} - \begin{Bmatrix} -cL_T/3AE \\ -cL_T/AE \\ P/AEL_T \end{Bmatrix} \tag{5.2-12}$$

If all three residuals were set to zero the system of equations would be overdetermined (more equations than unknowns). A least squares solution requires that we form $I = R_1^2 + R_2^2 + R_S^2/L_T^2$ and then apply Eq. 5.2-4 for $i = 1$ and $i = 2$. We introduce symbols $[\mathbf{Q}]$, $\{\mathbf{a}\}$, and $\{\mathbf{b}\}$ for the respective arrays on the right-hand side of Eq. 5.2-12, and obtain a least-squares solution for $\{\mathbf{a}\} = \lfloor a_1 \;\; a_2 \rfloor^T$ in matrix format as follows.

$$I = \{\mathbf{R}\}^T\{\mathbf{R}\} \quad \text{where} \quad \{\mathbf{R}\} = [\mathbf{Q}]\{\mathbf{a}\} - \{\mathbf{b}\} \tag{5.2-13a}$$

$$I = \{\mathbf{a}\}^T[\mathbf{Q}]^T[\mathbf{Q}]\{\mathbf{a}\} - 2\{\mathbf{a}\}^T[\mathbf{Q}]^T\{\mathbf{b}\} + \{\mathbf{b}\}^T\{\mathbf{b}\} \tag{5.2-13b}$$

$$\left\{\frac{\partial I}{\partial \mathbf{a}}\right\} = \{\mathbf{0}\} \quad \text{yields} \quad [\mathbf{A}]\{\mathbf{a}\} = \{\mathbf{c}\} \quad \text{where} \quad \begin{aligned} [\mathbf{A}] &= [\mathbf{Q}]^T\,[\mathbf{Q}] \\ \{\mathbf{c}\} &= [\mathbf{Q}]^T\,\{\mathbf{b}\} \end{aligned} \tag{5.2-13c}$$

In writing Eq. 5.2-13b we have used the relation $\{\mathbf{b}\}^T[\mathbf{Q}]\{\mathbf{a}\} = \{\mathbf{a}\}^T[\mathbf{Q}]^T\{\mathbf{b}\}$. Transposition is valid because each of the two matrix triple products is a scalar. In the solution $\{\mathbf{a}\} = [\mathbf{A}]^{-1}\{\mathbf{c}\}$, coefficient matrix $[\mathbf{A}]$ is symmetric and of the same order as $\{\mathbf{a}\}$. Applying Eq. 5.2-13c to Eq. 5.2-12, we obtain

$$a_1 = \frac{P}{AE} + \frac{2cL_T^2}{3AE} \qquad a_2 = -\frac{cL_T}{3AE} \tag{5.2-14}$$

The Galerkin solution, from Eq. 5.1-10, is

$$a_1 = \frac{P}{AE} + \frac{7cL_T^2}{12AE} \qquad a_2 = -\frac{cL_T}{4AE} \tag{5.2-15}$$

Sample results from the foregoing solutions appear in Table 5.2-1, for the special case $P = 0$ and with unit values of A, E, c, and L_T. Recall that a given $\tilde{u}$ provides different results for different choices of collocation points or subdomains.

TABLE 5.2-1. RESULTS FOR THE PROBLEM OF FIG. 5.1-1, WITH $\tilde{u} = a_1x + a_2x^2$ AND FOR THE SPECIAL CASE $P = 0, A = E = c = L_T = 1$.

Quantity and location	Exact	Collocation	Subdomain and least squares	Least squares collocation	Galerkin
u at $x = L_T/2$	0.2292	0.1250	0.1875	0.2500	0.2292
u at $x = L_T$	0.3333	0.1667	0.2500	0.3333	0.3333
$u_{,x}$ at $x = 0$	0.5000	0.3333	0.5000	0.6667	0.5833
$u_{,x}$ at $x = L_T/2$	0.3750	0.1667	0.2500	0.3333	0.3333
$u_{,x}$ at $x = L_T$	0	0	0	0	0.0833

5.3 GALERKIN FINITE ELEMENT METHOD IN ONE DIMENSION

In this section, one-dimensional examples are used to illustrate the FE form of the Galerkin method. The interpretation of terms that result from integration by parts, and the assembly of elements to form a structure, are explained in the first example.

Uniform Bar, Axial Load. For arbitrary distributed axial load $q = q(x)$, the governing differential equation in terms of axial displacement u, derived in Fig. 5.1-1, is

$$AEu_{,xx} + q = 0 \tag{5.3-1}$$

At arbitrary x, axial force in the bar is

$$F = AEu_{,x} \tag{5.3-2}$$

At a free end, the natural boundary condition is $F = 0$. At a fixed end, the essential boundary condition is $u = 0$.

Let the bar be divided into N_{els} elements of length L. Typical elements are shown in Fig. 5.3-1. Let each element have a linear axial displacement field. Thus, in a typical two-d.o.f. element with end nodes 1 and 2, the approximating function is[1]

$$\tilde{u} = \lfloor \mathbf{N} \rfloor \{\mathbf{d}\} \quad \text{in which} \quad \begin{aligned} \lfloor \mathbf{N} \rfloor &= \left\lfloor \frac{L-x}{L} \;\; \frac{x}{L} \right\rfloor \\ \{\mathbf{d}\} &= \lfloor u_1 \;\; u_2 \rfloor^T \end{aligned} \tag{5.3-3}$$

where $x = 0$ at the left end of an element. Thus, in each element, x differs by a constant from the global x in Fig. 5.3-1a. D.o.f. u_1 and u_2 are coefficients of displacement modes in the approximating function and therefore play the same role as the a_i in Sections 5.1 and 5.2. Accordingly, weights W_i used in the Galerkin method are

[1]In preceding chapters, where the difference between exact and approximate solutions is not an essential concept of the solution method, this approximating field is written without an overbar, as $u = \lfloor \mathbf{N} \rfloor \{\mathbf{d}\}$.

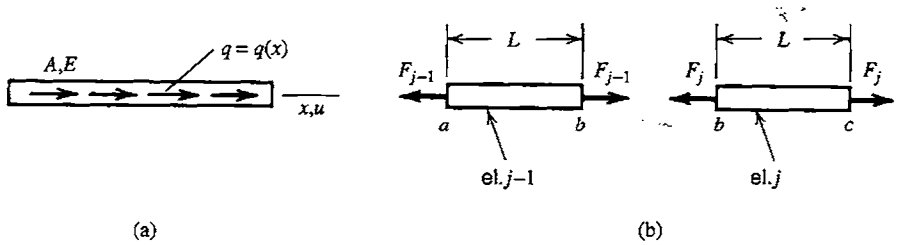

Figure 5.3-1. (a) Uniform elastic bar under distributed axial load $q = q(x)$. A = cross-sectional area, E = elastic modulus. (b) Adjacent elements $j-1$ and j. Node b is shared after assembly of elements.

$$W_i = \frac{\partial \tilde{u}}{\partial d_i} = N_i \qquad \text{where} \qquad N_1 = \frac{L-x}{L} \quad \text{and} \quad N_2 = \frac{x}{L} \tag{5.3-4}$$

The Galerkin residual equation, Eq. 5.1-3, becomes a sum over the N_{els} elements of the structure.

$$\sum_{j=1}^{N_{\text{els}}} \int_0^L N_i(AE\tilde{u}_{,xx} + q)\, dx = 0 \tag{5.3-5}$$

where index i ranges over all element shape functions; $i = 1, 2$ for the bar element. When elements have been assembled, activation of a single d.o.f. activates shape functions associated with that d.o.f. in elements that share the d.o.f. Thus in the present bar example, linear ramps or "hat functions" are created by activation of a single d.o.f. (Fig. 5.3-2). We see that there are as many shape functions on the structural level as there are d.o.f., and therefore as many Galerkin residual equations as there are d.o.f. With AE constant, integration by parts of the first term in Eq. 5.3-5 yields

$$\int_0^L N_i AE\tilde{u}_{,xx}\, dx = \left[N_i AE\tilde{u}_{,x}\right]_0^L - \int_0^L N_{i,x} AE\tilde{u}_{,x}\, dx \tag{5.3-6}$$

(If AE is not constant, the differential equation is $d(AEu_{,x})/dx + q = 0$. An equation of this form is treated subsequently; see Eq. 5.3-21). From Eq. 5.3-2, the natural boundary condition at element ends is $F = AE\tilde{u}_{,x}$. Substituting this and Eq. 5.3-6 into Eq. 5.3-5, we obtain

$$\sum_{j=1}^{N_{\text{els}}} \int_0^L (-N_{i,x} AE\tilde{u}_{,x} + N_i q)\, dx + \sum_{j=1}^{N_{\text{els}}} \left[N_i F\right]_0^L = 0 \tag{5.3-7}$$

as the Galerkin residual equation. A benefit of integration by parts is that now only first-order derivatives appear, so spatial derivatives of the approximating function need not be interelement-continuous [5.6] (continuity requirements are discussed in Section 4.9).

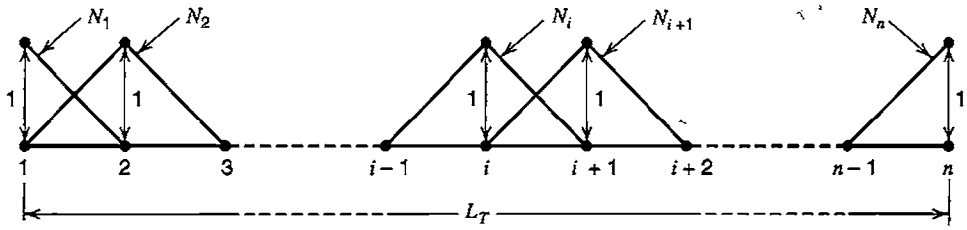

Figure 5.3-2. Shape functions active on the structural level after bar elements have been assembled. The number of these shape functions, and the number of d.o.f., is $N_{\text{els}} + 1$.

Therefore C^0 elements may be used, as indeed we have already assumed by writing Eqs. 5.3-3. For a typical bar element we adopt the notation

$$\lfloor \mathbf{B} \rfloor = \lfloor \mathbf{N}_{,x} \rfloor \qquad \text{hence} \qquad \tilde{u}_{,x} = \lfloor \mathbf{B} \rfloor \{\mathbf{d}\} = \lfloor -1/L \quad 1/L \rfloor \begin{Bmatrix} u_1 \\ u_2 \end{Bmatrix} \tag{5.3-8}$$

Thus Eq. 5.3-7 becomes, after rearrangement,

$$\sum_{j=1}^{N_{\text{els}}} \underbrace{\int_0^L \lfloor \mathbf{B} \rfloor^T AE \lfloor \mathbf{B} \rfloor \, dx}_{[\mathbf{k}]_j} \{\mathbf{d}\}_j = \sum_{j=1}^{N_{\text{els}}} \underbrace{\int_0^L \lfloor \mathbf{N} \rfloor^T q \, dx}_{\{\mathbf{r}_e\}_j} + \sum_{j=1}^{N_{\text{els}}} \Big[\lfloor \mathbf{N} \rfloor^T F \Big]_0^L \tag{5.3-9}$$

Except for the last summation, which is discussed in what follows, Eq. 5.3-9 is clearly the standard structure stiffness equation $[\mathbf{K}]\{\mathbf{D}\} = \{\mathbf{R}\}$, that is

$$\left(\sum_{j=1}^{N_{\text{els}}} [\mathbf{k}]_j \right) \{\mathbf{D}\} = \sum_{j=1}^{N_{\text{els}}} \{\mathbf{r}_e\}_j + \{\mathbf{P}\} \tag{5.3-10}$$

where $\{\mathbf{D}\}$ replaces $\{\mathbf{d}\}$ because of the usual expansion of element matrices to "structure size."

We must explain how the last summation in Eq. 5.3-9 can be regarded as $\{\mathbf{P}\}$, the vector of externally-applied concentrated axial loads [5.6]. At ends of a typical element, $x = 0$ and $x = L$ respectively,

$$\lfloor \mathbf{N} \rfloor_0 = \lfloor 1 \quad 0 \rfloor \quad \text{and} \quad \lfloor \mathbf{N} \rfloor_L = \lfloor 0 \quad 1 \rfloor \tag{5.3-11}$$

For two adjacent elements $j - 1$ and j, Fig. 5.3-1b, the last summation in Eq. 5.3-9 produces the terms

$$\begin{array}{l} \text{node } a \text{ - - - - -} \\ \text{node } b \text{ - - - - -} \\ \text{node } c \text{ - - - - - - - - - - - -} \end{array} \begin{array}{c} -\begin{Bmatrix} 1 \\ 0 \end{Bmatrix} F_{j-1} + \left(\begin{Bmatrix} 0 \\ 1 \end{Bmatrix} F_{j-1} - \begin{Bmatrix} 1 \\ 0 \end{Bmatrix} F_j \right) + \begin{Bmatrix} 0 \\ 1 \end{Bmatrix} F_j \\ \text{- - - - - - - -} \end{array} \tag{5.3-12}$$

At a typical node b, assembly of elements produces the resultant axial force $F_{j-1} - F_j$. This resultant appears in parentheses in Eq. 5.3-12 and is identified as representing an externally-applied axial force P. Of course, P may be zero, in which case $F_{j-1} = F_j$. For the problem of Fig. 5.1-1, load vector $\{\mathbf{P}\}$ would be null except for force P associated with the rightmost node. (Expression 5.3-12 is not used in actual computation; it serves only to explain the transition from Eq. 5.3-9 to Eq. 5.3-10.)

Beam Dynamics. In this example we omit most of the summation signs that indicate assembly of elements, and also omit detailed explanation of nodal loads (as in Eq. 5.3-12). Thus we emphasize the formulation of element matrices by the Galerkin method.

Consider a uniform straight elastic beam of flexural stiffness EI, length L, and mass ρ_L per unit length. Transverse shear deformation will be neglected. The following well-known relations provide the governing differential equation. With $v = v(x)$ the lateral displacement, the moment-curvature relation is $M = EIv_{,xx}$. Also, $M_{,x} = V$ and $V_{,x} = q$, where V is transverse shear force and $q = q(x)$ is distributed lateral load per unit length. The effective inertia load is therefore $q = -\rho_L \ddot{v}$, where $\ddot{v} = d^2v/dt^2$ and t represents time. Putting all this together, we obtain

$$EIv_{,xxxx} + \rho_L \ddot{v} = 0 \tag{5.3-13}$$

Natural boundary conditions are

$$EIv_{,xx} - M_B = 0 \quad \text{and} \quad EIv_{,xxx} - V_B = 0 \tag{5.3-14}$$

where M_B and V_B are prescribed values of bending moment and transverse shear force at ends of the beam. Essential boundary conditions consist of prescribed values of v and $v_{,x}$. In an element, the approximating lateral displacement field $\tilde{v} = \tilde{v}(x)$ and weight functions $W_i = W_i(x)$ are

$$\tilde{v} = \lfloor \mathbf{N} \rfloor \{\mathbf{d}\} \quad \text{and} \quad W_i = N_i \tag{5.3-15}$$

where $\{\mathbf{d}\} = \lfloor v_1 \ \theta_{z1} \ v_2 \ \theta_{z2} \rfloor^T$ and the N_i are the usual cubic shape functions (for which see Fig. 2.3-1 or Fig. 3.2-4). The Galerkin residual equation for a single element of length L is

$$\int_0^L \lfloor \mathbf{N} \rfloor^T (EI\tilde{v}_{,xxxx} + \rho_L \ddot{\tilde{v}})\, dx = 0 \tag{5.3-16}$$

With EI constant, two integrations by parts of the fourth-derivative term in Eq. 5.3-16 yield

$$\int_0^L \lfloor \mathbf{N} \rfloor^T \tilde{v}_{,xxxx}\, dx = \int_0^L \lfloor \mathbf{N}_{,xx} \rfloor^T \tilde{v}_{,xx}\, dx + \Big[\lfloor \mathbf{N} \rfloor^T \tilde{v}_{,xxx} - \lfloor \mathbf{N}_{,x} \rfloor^T \tilde{v}_{,xx} \Big]_0^L \tag{5.3-17}$$

Substitution of Eqs. 5.3-14 and 5.3-17 in Eq. 5.3-16 yields

$$\int_0^L \left(\lfloor \mathbf{N}_{,xx} \rfloor^T EI\tilde{v}_{,xx} + \rho_L \lfloor \mathbf{N} \rfloor^T \ddot{\tilde{v}} \right) dx = -\left[\lfloor \mathbf{N} \rfloor^T V_B - \lfloor \mathbf{N}_{,x} \rfloor^T M_B \right]_0^L \tag{5.3-18}$$

Terms V_B and M_B become part of the load vector $\{\mathbf{R}\}$. The argument is analogous to that used with Eqs. 5.3-11 and 5.3-12. From Eq. 5.3-15,

$$\ddot{\tilde{v}} = \lfloor \mathbf{N} \rfloor \{\ddot{\mathbf{d}}\} \quad \text{and} \quad \tilde{v}_{,xx} = \lfloor \mathbf{B} \rfloor \{\mathbf{d}\} \quad \text{where} \quad \lfloor \mathbf{B} \rfloor = \lfloor \mathbf{N}_{,xx} \rfloor \tag{5.3-19}$$

Substituting Eq. 5.3-19 into Eq. 5.3-18 and assembling elements, we obtain

$$\sum_{j=1}^{N_{\text{els}}} \underbrace{\int_0^L \lfloor \mathbf{B} \rfloor^T EI \lfloor \mathbf{B} \rfloor \, dx}_{[\mathbf{k}]_j} \{\mathbf{d}\}_j + \sum_{j=1}^{N_{\text{els}}} \underbrace{\int_0^L \rho_L \lfloor \mathbf{N} \rfloor^T \lfloor \mathbf{N} \rfloor \, dx}_{[\mathbf{m}]_j} \{\ddot{\mathbf{d}}\}_j = \{\mathbf{R}\} \tag{5.3-20}$$

With element matrices expanded to "structure size," Eq. 5.3-20 is recognized as the standard equation of motion $[\mathbf{K}]\{\mathbf{D}\} + [\mathbf{M}]\{\ddot{\mathbf{D}}\} = \{\mathbf{R}\}$, where $[\mathbf{K}]$ and $[\mathbf{M}]$ are respectively the structure stiffness and mass matrices and $\{\mathbf{R}\}$ represents loads that may vary with time.

Heat Flow in a Bar. We consider axial heat flow in a tapered bar with insulated lateral surface, as shown in Fig. 5.3-3a. Axial heat flux f obeys the Fourier heat conduction equation, $f = -kT_{,x}$, where k is the thermal conductivity of the material. The negative sign indicates that heat flow is opposite to the direction of temperature increase. Units, for f and k respectively, are W/m^2 and $\text{W/m} \cdot {}^\circ\text{C}$. In a steady-state condition with no internal heat sources or sinks, the net rate of heat flow out of a differential element is zero. Thus, from Fig. 5.3-3b, $d(Af)/dx = 0$. Combination of this equation and the Fourier equation yields the governing differential equation

$$\frac{d}{dx}(AkT_{,x}) = 0 \tag{5.3-21}$$

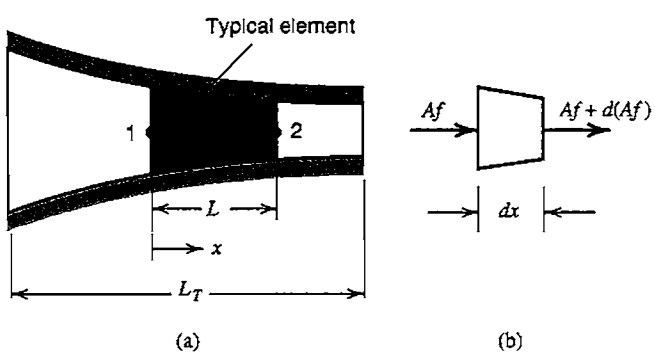

Figure 5.3-3. (a) Axial heat flow in a tapered bar with insulated lateral surface. A typical element is shown shaded. (b) Heat flow through a diferential element.

in which A, k, and T may be functions of x. The approximating temperature field in an element is $\tilde{T} = \lfloor \mathbf{N} \rfloor^T \{\mathbf{T}_e\}$, where, for an element having two nodes and two d.o.f., nodal d.o.f. are temperatures $\{\mathbf{T}_e\} = \lfloor T_1 \;\; T_2 \rfloor^T$ and shape functions N_i are stated in Eq. 5.3-4. We write the Galerkin residual equation, integrate by parts, and substitute the natural boundary condition $f = -k\tilde{T}_{,x}$ at element ends. Thus we obtain two Galerkin residual equations on the element level, one for each of two shape functions N_i.

$$\int_0^L \lfloor \mathbf{N} \rfloor^T \frac{d}{dx}(Ak\tilde{T}_{,x})\, dx = \begin{Bmatrix} 0 \\ 0 \end{Bmatrix} \quad \text{or}$$
$$-\int_0^L \lfloor \mathbf{N}_{,x} \rfloor^T (Ak\tilde{T}_{,x})\, dx - \Big[\lfloor \mathbf{N} \rfloor^T Af\Big]_0^L = \begin{Bmatrix} 0 \\ 0 \end{Bmatrix} \tag{5.3-22}$$

With $\tilde{T}_{,x} = \lfloor \mathbf{N}_{,x} \rfloor \{\mathbf{T}_e\}$, the element equation becomes

$$\int_0^L \lfloor \mathbf{N}_{,x} \rfloor^T Ak \lfloor \mathbf{N}_{,x} \rfloor\, dx \{\mathbf{T}_e\} = -\begin{Bmatrix} 0 \\ 1 \end{Bmatrix} A_2 f_2 + \begin{Bmatrix} 1 \\ 0 \end{Bmatrix} A_1 f_1 = \begin{Bmatrix} A_1 f_1 \\ -A_2 f_2 \end{Bmatrix} \tag{5.3-23}$$

where fluxes f_1 and f_2 at element ends are considered positive when heat flows in the positive x direction. We adopt the convention that heat flow is positive when flowing *into* nodes of the structure. Thus the amount of heat flow, $q = |Af|$ in magnitude, is positive when directed *out* of element ends. From Eq. 5.3-23 we obtain, for a single element in which A and k are constant,

$$\begin{bmatrix} Ak/L & -Ak/L \\ -Ak/L & Ak/L \end{bmatrix} \begin{Bmatrix} T_1 \\ T_2 \end{Bmatrix} = -\begin{Bmatrix} q_1 \\ q_2 \end{Bmatrix} \tag{5.3-24}$$

which agrees with Eq. 2.2-5.

5.4 INTEGRATION BY PARTS

Galerkin formulations make frequent use of integration by parts. Some useful formulas are now reviewed.

Let $\mathbf{i}$, $\mathbf{j}$, and $\mathbf{k}$ be unit vectors in the coordinate directions. Also let F_1, F_2, and F_3 be independent functions of the coordinates, and

$$\mathbf{F} = F_1\mathbf{i} + F_2\mathbf{j} + F_3\mathbf{k} \qquad \text{and} \qquad \boldsymbol{\nu} = l\mathbf{i} + m\mathbf{j} + n\mathbf{k} \tag{5.4-1}$$

where function $\mathbf{F}$ is defined in a volume V, $\boldsymbol{\nu}$ is an outward normal on surface S of V, and l, m, and n are direction cosines of $\boldsymbol{\nu}$. The divergence theorem states that

$$\int \nabla \cdot \mathbf{F}\, dV = \int \mathbf{F} \cdot \boldsymbol{\nu}\, dS \tag{5.4-2}$$

where $\nabla \bullet \mathbf{F}$ is the divergence of $\mathbf{F}$, for example

$$\text{Rectangular coordinates:} \quad \nabla \bullet \mathbf{F} = \frac{\partial F_1}{\partial x} + \frac{\partial F_2}{\partial y} + \frac{\partial F_3}{\partial z} \tag{5.4-3a}$$

$$\text{Cylindrical coordinates:} \quad \nabla \bullet \mathbf{F} = \frac{1}{r}\frac{\partial}{\partial r}(rF_1) + \frac{1}{r}\frac{\partial F_2}{\partial \theta} + \frac{\partial F_3}{\partial z} \tag{5.4-3b}$$

In Eq. 5.4-2, $\mathbf{F}$ and its first partial derivatives must be continuous in V and on S, and integration must proceed over all boundaries, interior as well as exterior.

Let P and Q be functions of the coordinates. Then, for example, $(PQ)_{,x} = P_{,x}Q + PQ_{,x}$. Therefore

$$\int PQ_{,x}\, dV = -\int P_{,x}Q\, dV + \int (PQ)_{,x}\, dV \tag{5.4-4}$$

If we regard PQ as F_1 in Eq. 5.4-3a and let $F_2 = F_3 = 0$, Eq. 5.4-2 allows us to replace the last integral in Eq. 5.4-4 by a surface integral. Thus we obtain the following formula for integration by parts in rectangular coordinates.

$$\int PQ_{,x}\, dV = -\int P_{,x}Q\, dV + \int PQl\, dS \tag{5.4-5}$$

Analogous formulas for y and z derivatives are easily written.

The same procedure can be applied in cylindrical coordinates. For example,

$$\int \frac{1}{r}\frac{\partial}{\partial r}(rPQ)\, dV = \int \left[\frac{\partial P}{\partial r}Q + P\frac{1}{r}\frac{\partial}{\partial r}(rQ)\right] dV \tag{5.4-6}$$

We let $F_1 = PQ$ and $F_2 = F_3 = 0$ in Eq. 5.4-3b, solve for the last term in Eq. 5.4-6, and apply Eq. 5.4-2. Thus

$$\int P\frac{1}{r}\frac{\partial}{\partial r}(rQ)\, dV = -\int \frac{\partial P}{\partial r}Q\, dV + \int PQl\, dS \tag{5.4-7}$$

In similar fashion,

$$\int \frac{1}{r}P\frac{\partial Q}{\partial \theta}\, dV = -\int \frac{1}{r}\frac{\partial P}{\partial \theta}Q\, dV + \int PQm\, dS \tag{5.4-8}$$

Formulas for integration by parts in two dimensions can be obtained directly from the preceding formulas by setting $F_3 = 0$ in Eqs. 5.4-3 and presuming that integration with respect to z has already been done across a unit thickness.

5.5 GALERKIN FINITE ELEMENT METHOD IN TWO DIMENSIONS

Quasiharmonic Equation. A *quasiharmonic* equation describes many scalar field problems such as heat conduction, fluid film lubrication, electric fields, and seepage flow in porous media. In this section we formulate element matrices by the Galerkin method without considering details of physical problems.

Let a plane region have volume V, boundary S in the xy plane, and unit thickness in the z direction. For steady-state conditions, the governing equation and natural boundary condition are respectively

$$\text{In } V: \quad \frac{\partial}{\partial x}(k_x\phi_{,x}) + \frac{\partial}{\partial y}(k_y\phi_{,y}) + Q = 0 \tag{5.5-1}$$

$$\text{On } S: \quad lk_x\phi_{,x} + mk_y\phi_{,y} - f_B = 0 \tag{5.5-2}$$

where $\phi = \phi(x,y)$ is the dependent variable and l and m are direction cosines of an outward normal to S. Known quantities k_x, k_y, and Q may be either constants or functions of x and y. In the natural boundary condition, f_B is a prescribed boundary flux, which we consider positive when directed into V. Essential boundary conditions, which prevail over only a portion of S, consist of prescribed values of ϕ. If $k_x = k_y = k$, a constant, Eq. 5.5-1 becomes the Poisson equation, $k\nabla^2\phi + Q = 0$. If also $Q = 0$, Eq. 5.5-1 becomes Laplace's equation, $\nabla^2\phi = 0$. A function ϕ that satisfies $\nabla^2\phi = 0$ is called *harmonic*.

A discretized approximation is usually taken as C^0 continuous in the scalar field variable $\tilde{\phi}$. Thus there is one d.o.f. per node, and the approximating field in an n-d.o.f. element is

$$\tilde{\phi} = \lfloor \mathbf{N} \rfloor \{\boldsymbol{\phi}_e\} = \lfloor N_1 \quad N_2 \quad \cdots \quad N_n \rfloor \{\boldsymbol{\phi}_e\} \tag{5.5-3}$$

where $\{\boldsymbol{\phi}_e\}$ is the vector of element nodal d.o.f. On the element level there are n Galerkin residual equations.

$$\iint \lfloor \mathbf{N} \rfloor^T \left[\frac{\partial}{\partial x}(k_x\tilde{\phi}_{,x}) + \frac{\partial}{\partial y}(k_y\tilde{\phi}_{,y}) + Q\right] dx\,dy = \begin{Bmatrix} 0 \\ 0 \\ \vdots \\ 0 \end{Bmatrix} \tag{5.5-4}$$

Integration by parts, as in Eq. 5.4-5 for example, yields

$$\iint \lfloor \mathbf{N} \rfloor^T \frac{\partial}{\partial x}(k_x\tilde{\phi}_{,x})\,dx\,dy = -\iint \lfloor \mathbf{N}_{,x} \rfloor^T k_x\tilde{\phi}_{,x}\,dx\,dy + \int \lfloor \mathbf{N} \rfloor^T k_x\tilde{\phi}_{,x} l\,dS \tag{5.5-5a}$$

$$\iint \lfloor \mathbf{N} \rfloor^T \frac{\partial}{\partial y}(k_y\tilde{\phi}_{,y})\,dx\,dy = -\iint \lfloor \mathbf{N}_{,y} \rfloor^T k_y\tilde{\phi}_{,y}\,dx\,dy + \int \lfloor \mathbf{N} \rfloor^T k_y\tilde{\phi}_{,y} m\,dS \tag{5.5-5b}$$

where, in the last integral of each equation, $\lfloor \mathbf{N} \rfloor^T$ is evaluated on S. Substitution of Eqs. 5.5-5 and 5.5-2 into Eq. 5.5-4 yields

$$\iint\left(-\lfloor \mathbf{N}_{,x}\rfloor^T k_x \tilde{\phi}_{,x} - \lfloor \mathbf{N}_{,y}\rfloor^T k_y \tilde{\phi}_{,y} + \lfloor \mathbf{N}\rfloor^T Q\right) dx\,dy = -\int \lfloor \mathbf{N}\rfloor^T f_B\, dS \tag{5.5-6}$$

Finally, substitution of $\tilde{\phi}_{,x} = \lfloor \mathbf{N}_{,x}\rfloor\{\phi_e\}$ and $\tilde{\phi}_{,y} = \lfloor \mathbf{N}_{,y}\rfloor\{\phi_e\}$ into Eq. 5.5-6 yields

$$\begin{aligned}\left[\iint\left(\lfloor \mathbf{N}_{,x}\rfloor^T k_x \lfloor \mathbf{N}_{,x}\rfloor + \lfloor \mathbf{N}_{,y}\rfloor^T k_y \lfloor \mathbf{N}_{,y}\rfloor\right) dx\,dy\right]\{\phi_e\} \\ = \iint \lfloor \mathbf{N}\rfloor^T Q\, dx\,dy + \int \lfloor \mathbf{N}\rfloor^T f_B\, dS\end{aligned} \tag{5.5-7}$$

Or, in our customary notation, $[\mathbf{k}]\{\phi_e\} = \{\mathbf{r}_e\}$.

Plane Elasticity. The foregoing manipulations are little changed in application to problems of plane stress or plane strain. We summarize as follows. The governing differential equations are equilibrium equations, and natural boundary conditions involve surface tractions. That is, from Eqs. 3.1-12 and 3.1-14,

$$\begin{aligned}\sigma_{x,x} + \tau_{xy,y} + F_x &= 0 \\ \tau_{xy,x} + \sigma_{y,y} + F_y &= 0\end{aligned} \quad \text{and} \quad \begin{aligned}\Phi_x &= l\sigma_x + m\tau_{xy} \\ \Phi_y &= l\tau_{xy} + m\sigma_y\end{aligned} \tag{5.5-8}$$

where F_x and F_y are body forces per unit volume, and l and m are direction cosines of an outward normal to boundary S in the xy plane. Essential boundary conditions consist of prescribed values of displacement components u and v. In an element, the approximating displacement field can be written as

$$\{\tilde{\mathbf{u}}\} = \begin{Bmatrix}\tilde{u} \\ \tilde{v}\end{Bmatrix} = \begin{bmatrix}\lfloor \mathbf{N}\rfloor & \lfloor \mathbf{0}\rfloor \\ \lfloor \mathbf{0}\rfloor & \lfloor \mathbf{N}\rfloor\end{bmatrix}\{\mathbf{d}\} \tag{5.5-9}$$

where $\{\mathbf{d}\} = \lfloor u_1\ u_2 \cdots u_n\ v_1\ v_2 \cdots v_n\rfloor^T$ and $\lfloor \mathbf{N}\rfloor = \lfloor N_1\ N_2 \cdots N_n\rfloor$ for an n-node element. With two differential equations and an n-node element, there are $2n$ Galerkin residual equations on the element level, namely

$$\iint \lfloor \mathbf{N}\rfloor^T (\tilde{\sigma}_{x,x} + \tilde{\tau}_{xy,y} + F_x)\, dx\,dy = \begin{Bmatrix}0 \\ 0 \\ \vdots \\ 0\end{Bmatrix} \tag{5.5-10a}$$

$$\iint \lfloor \mathbf{N}\rfloor^T (\tilde{\tau}_{xy,x} + \tilde{\sigma}_{y,y} + F_y)\, dx\,dy = \begin{Bmatrix}0 \\ 0 \\ \vdots \\ 0\end{Bmatrix} \tag{5.5-10b}$$

in which $\tilde{\sigma}_x$, $\tilde{\sigma}_y$, and $\tilde{\tau}_{xy}$ are stress fields produced by the approximating displacement field. There are four terms in Eqs. 5.5-10 to be integrated by parts. For example, the first such integration yields

$$\iint \lfloor \mathbf{N} \rfloor^T \tilde{\sigma}_{x,x}\, dx\, dy = -\iint \lfloor \mathbf{N}_{,x} \rfloor^T \tilde{\sigma}_x\, dx\, dy + \int \lfloor \mathbf{N} \rfloor^T \tilde{\sigma}_x l\, dS \tag{5.5-11}$$

Natural boundary conditions are introduced by this process. Next we express $\tilde{\sigma}_x$, $\tilde{\sigma}_y$, and $\tilde{\tau}_{xy}$ in terms of $\tilde{u}$ and $\tilde{v}$ by substitution of Eqs. 5.5-9, strain-displacement relations, and stress-strain relations into the first of Eqs. 5.5-8. Thus

$$\{\tilde{\boldsymbol{\varepsilon}}\} = [\boldsymbol{\partial}]\{\tilde{\mathbf{u}}\} \quad \text{or} \quad \{\tilde{\boldsymbol{\varepsilon}}\} = [\mathbf{B}]\{\mathbf{d}\} \tag{5.5-12}$$

$$\{\tilde{\boldsymbol{\sigma}}\} = [\mathbf{E}](\{\tilde{\boldsymbol{\varepsilon}}\} - \{\boldsymbol{\varepsilon}_0\}) + \{\boldsymbol{\sigma}_0\} \tag{5.5-13}$$

where $[\boldsymbol{\partial}]$ is the 3 by 2 differential operator defined in Eq. 3.1-9. The final result agrees with Eqs. 4.8-15.

5.6 A MIXED FORMULATION

In structural mechanics it is common to use a displacement-based FE approximation. To obtain it we can apply the Galerkin method to one or more governing differential equations expressed in terms of displacements. These equations are obtained by combining subsidiary relations: the differential equations of equilibrium, stress-strain relations, and strain-displacement relations. A *mixed* formulation can be obtained by applying the Galerkin method directly to subsidiary relations, either combining them partially or not at all. In the resulting FE formulation, the list of nodal d.o.f. contains displacements *and* other field quantities that otherwise would enter only as natural boundary conditions. To illustrate a mixed formulation, in this section we construct the coefficient matrix for a uniform bar element that has axial displacement and axial stress as d.o.f. at each node.

Let us combine the stress-strain relation $\sigma_x = E\varepsilon_x$ and the strain-displacement relation $\varepsilon_x = du/dx$. Then, for the bar in Fig. 5.6-1a, the equilibrium and stress-displacement relations are

$$\text{Axial equilibrium:} \quad \frac{d\sigma_x}{dx} + \frac{q}{A} = 0 \tag{5.6-1}$$

$$\text{Stress-displacement:} \quad \frac{du}{dx} - \frac{\sigma_x}{E} = 0 \tag{5.6-2}$$

Approximating fields for axial stress and axial displacement are independent. For a two-node element, we adopt the interpolations

$$\tilde{\sigma}_x = \lfloor \mathbf{N} \rfloor^T \begin{Bmatrix} \sigma_1 \\ \sigma_2 \end{Bmatrix} \quad \tilde{u} = \lfloor \mathbf{N} \rfloor^T \begin{Bmatrix} u_1 \\ u_2 \end{Bmatrix} \quad \text{where} \quad \lfloor \mathbf{N} \rfloor = \begin{bmatrix} \dfrac{L-x}{L} & \dfrac{x}{L} \end{bmatrix} \tag{5.6-3}$$

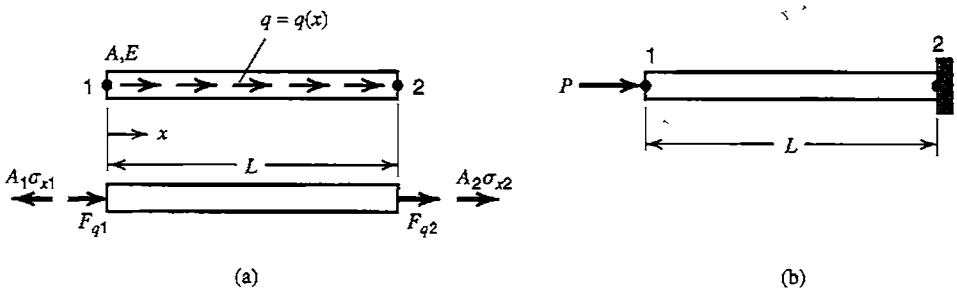

Figure 5.6-1. (a) Axially loaded bar, showing end forces associated with axial stress and axial load. (b) One-element model of a uniform bar.

In the present example, stress and displacement fields use the same interpolating polynomial and the same nodal locations. In general, interpolants and node sets may differ for the fields used in formulation.

Galerkin residual equations on the element level are

$$\int_0^L \lfloor \mathbf{N} \rfloor^T \left(\frac{d\tilde{\sigma}_x}{dx} + \frac{q}{A} \right) A\, dx = \begin{Bmatrix} 0 \\ 0 \end{Bmatrix} \qquad \int_0^L \lfloor \mathbf{N} \rfloor^T \left(\frac{d\tilde{u}}{dx} - \frac{\tilde{\sigma}_x}{E} \right) A\, dx = \begin{Bmatrix} 0 \\ 0 \end{Bmatrix} \tag{5.6-4}$$

In the first of these two equations, we change the form of the first term by applying integration by parts. Thus the equation becomes

$$\int_0^L \lfloor \mathbf{N}_{,x} \rfloor^T \tilde{\sigma}_x A\, dx = \Big[\lfloor \mathbf{N} \rfloor^T A \tilde{\sigma}_x \Big]_0^L + \int_0^L \lfloor \mathbf{N} \rfloor^T q\, dx \tag{5.6-5}$$

Substituting $\tilde{\sigma}_x$ from Eq. 5.6-3 into Eq. 5.6-5, we obtain

$$\underbrace{\int_0^L \lfloor \mathbf{N}_{,x} \rfloor^T \lfloor \mathbf{N} \rfloor A\, dx}_{[\mathbf{k}_{u\sigma}]} \begin{Bmatrix} \sigma_1 \\ \sigma_2 \end{Bmatrix} = \begin{Bmatrix} -A_1 \sigma_{x1} \\ A_2 \sigma_{x2} \end{Bmatrix} + \begin{Bmatrix} F_{q1} \\ F_{q2} \end{Bmatrix} \tag{5.6-6}$$

where F_{q1} and F_{q2} are nodal forces that result from the distributed axial load q (Fig. 5.6-1a). Substituting $\tilde{\sigma}_x$ and $\tilde{u}$ from Eq. 5.6-3 into the second of Eqs. 5.6-4, we obtain

$$\underbrace{\int_0^L \lfloor \mathbf{N} \rfloor^T \lfloor \mathbf{N}_{,x} \rfloor A\, dx}_{[\mathbf{k}_{\sigma u}]} \begin{Bmatrix} u_1 \\ u_2 \end{Bmatrix} - \underbrace{\int_0^L \lfloor \mathbf{N} \rfloor^T \lfloor \mathbf{N} \rfloor \frac{A}{E}\, dx}_{[\mathbf{k}_{\sigma\sigma}]} \begin{Bmatrix} \sigma_1 \\ \sigma_2 \end{Bmatrix} = \begin{Bmatrix} 0 \\ 0 \end{Bmatrix} \tag{5.6-7}$$

In terms of matrices defined in Eqs. 5.6-6 and 5.6-7, FE equations for a single element are

$$\begin{bmatrix} -[\mathbf{k}_{\sigma\sigma}] & [\mathbf{k}_{\sigma u}] \\ [\mathbf{k}_{u\sigma}] & [\mathbf{0}] \end{bmatrix} \begin{Bmatrix} \sigma_1 \\ \sigma_2 \\ u_1 \\ u_2 \end{Bmatrix} = \begin{Bmatrix} 0 \\ 0 \\ -A_1\sigma_{x1} + F_{q1} \\ A_2\sigma_{x2} + F_{q2} \end{Bmatrix} \quad \text{in which} \quad [\mathbf{k}_{u\sigma}] = [\mathbf{k}_{\sigma u}]^T \tag{5.6-8}$$

When two elements are connected together, $A_2\sigma_{x2}$ from one element cancels $A_1\sigma_{x1}$ from the next element at nodes where no external force is applied.

As a simple example application, consider the one-element model of a uniform bar shown in Fig. 5.6-1b. Essential boundary conditions are prescribed values of σ and u at nodes. In Fig. 5.6-1b, prescribed nodal d.o.f. are $\sigma_1 = -P/A$ and $u_2 = 0$. Loads F_{q1} and F_{q2} are zero. Equation 5.6-8 becomes

$$\begin{bmatrix} -AL/3E & -AL/6E & -A/2 & A/2 \\ -AL/6E & -AL/3E & -A/2 & A/2 \\ -A/2 & -A/2 & 0 & 0 \\ A/2 & A/2 & 0 & 0 \end{bmatrix} \begin{Bmatrix} -P/A \\ \sigma_2 \\ u_1 \\ 0 \end{Bmatrix} = \begin{Bmatrix} 0 \\ 0 \\ P \\ A\sigma_{x2} \end{Bmatrix} \tag{5.6-9}$$

Unknowns σ_2 and u_1 are obtained from the second and third equations.

$$\begin{bmatrix} -AL/3E & -A/2 \\ -A/2 & 0 \end{bmatrix} \begin{Bmatrix} \sigma_2 \\ u_1 \end{Bmatrix} = \begin{Bmatrix} -PL/6E \\ P - P/2 \end{Bmatrix} \quad \text{hence} \quad \begin{Bmatrix} \sigma_2 \\ u_1 \end{Bmatrix} = \begin{Bmatrix} -P/A \\ PL/AE \end{Bmatrix} \tag{5.6-10}$$

These results are exact. The first of Eqs. 5.6-9 is identically satisfied, and the last yields $\sigma_{x2} = -P/A$.

Remarks. The foregoing formulation has the advantage of giving σ_x the same status as u, rather than obtaining σ_x as $\sigma_x = Eu_{,x}$ as in the more common displacement-based formulation. Thus the σ_x field can be linear within an element rather than constant, as it is in the displacement formulation. Interelement continuity of σ_x is provided, which is desirable in a uniform member but is incorrect if there is a step change in cross-sectional area at a node. There are also twice as many d.o.f. per element as in the usual displacement formulation.

A mixed formulation can also be obtained from a functional. Indeed several functionals are available and various mixed formulations can be obtained from them [2.13,2.14,5.7]. It has been shown that displacement-based methods and mixed methods are related [5.8]. If both use the same kinematical description, then for each numerical integration scheme (that is, for each discrete-quadrature rule) used in the displacement-based method, there exists an internal force distribution in a mixed method such that both methods provide the same results.

For the axially-loaded bar of Fig. 5.6-1, the mixed formulation described above can be obtained from the functional

$$\Pi = \int FA\,dx \qquad \text{where} \qquad F = \sigma_x \frac{du}{dx} - \frac{\sigma_x^2}{2E} - \frac{q}{A}u \tag{5.6-11}$$

Straightforward application of Eqs. 4.7-2 shows that F provides both the equilibrium equation and the stress-displacement equation:

$$\frac{\partial F}{\partial \sigma_x} - \frac{d}{dx}\frac{\partial F}{\partial \sigma_{x,x}} = 0 \quad \text{yields} \quad \frac{du}{dx} - \frac{\sigma_x}{E} = 0 \tag{5.6-12a}$$

$$\frac{\partial F}{\partial u} - \frac{d}{dx}\frac{\partial F}{\partial u_{,x}} = 0 \quad \text{yields} \quad -\frac{q}{A} - \frac{d\sigma_x}{dx} = 0 \tag{5.6-12b}$$

These equations agree with Eqs. 5.6-1 and 5.6-2.

ANALYTICAL PROBLEMS

5.1-1 Show that the approximate result stated in Eq. 5.1-10 is also produced by the $\tilde{u}$ field of Eq. 5.1-8 and the potential energy expression stated in Eq. 5.1-11.

5.1-2 Consider a uniform, simply supported beam of length L. For each of the following loadings, use the Galerkin method to determine generalized d.o.f. a in the approximating lateral deflection field $\tilde{v} = ax(L-x)$. At midspan, determine the percentage errors of deflection $\tilde{v}$ and bending moment $\tilde{M} = EI\tilde{v}_{,xx}$.
(a) Sinusoidal distributed lateral load $q = q_o \sin(\pi x/L)$ over $0 < x < L$.
(b) Uniformly distributed lateral load $q = q_o$ over $0 < x < L$.

5.2-1 Verify that despite collocation at $x = L_T/3$, the $\tilde{u}$ field of Eqs. 5.2-8 and the a_i of Eqs. 5.2-9 do not yield $\tilde{u} = u$ at $x = L_T/3$. Does this indicate that something is wrong? Explain.

5.2-2 Solve the problem depicted in Fig. 5.1-1, but change the distributed load to $q = c$, a constant. Again assume that $\tilde{u} = a_1 x + a_2 x^2$. Determine generalized d.o.f. a_1 and a_2 by (a) collocation, (b) subdomain, (c) least squares, (d) least squares collocation, and (e) Galerkin methods. In collocation solutions, use the same points as chosen in the example solutions of Section 5.2.

5.2-3 Consider the differential equation $u_{,xx} + 4u = 12$ in the range $0 < x < 1$, with essential boundary conditions $u = 3$ at $x = 0$ and $u = 1$ at $x = 1$. There are no natural boundary conditions. The exact solution is $u = 3 - 2.1995 \sin 2x$. An admissible one-parameter approximating polynomial is $\tilde{u} = 3 - 2x + a(x^2 - x)$. Determine parameter a by (a) collocation, (b) subdomain, (c) least squares, (d) least squares collocation, and (e) Galerkin methods. Choose points at $x = 0.5$ in part (a) and at $x = 1/3$ and $x = 2/3$ in part (d). In each case calculate the percentage error of $\tilde{u}$ at $x = 0.5$ and at $x = 0.7$.

5.2-4 Consider the differential equation $u_{,x} + 2u - 16x = 0$ in the range $0 < x < 1$, with the boundary condition $u = 0$ at $x = 0$. The exact solution is $u = 4(e^{-2x} - 1) + 8x$. An admissible two-parameter approximating polynomial is $\tilde{u} = a_1 x + a_2 x^2$. Determine a_1 and a_2. Also determine percentage errors of $\tilde{u}$ at $x = 0.5$ and at $x = 0.7$.
(a) Use least squares collocation, with collocation points at $x = 0.25$, $x = 0.50$, and $x = 0.75$.
(b) Use the Galerkin method.

5.2-5 Solve the problem depicted in Fig. 5.1-1 in each of the following ways. Again use the approximating polynomial $\tilde{u} = a_1x + a_2x^2$. Compare results with those stated in Table 5.2-1.

(a) Use collocation, with the sampling point at $x = L_T/2$.

(b) Use subdomain and integrate over the span $0 < x < L_T/2$.

(c) Use least squares collocation. Evaluate R at $x = 0, x = L_T/2$, and $x = L_T$.

(d) Omit residual R_2 in Eq. 5.2-12.

(e) Why, in this particular problem, is the solution provided by least squares collocation independent of α?

5.3-1 The uniform elastic bar shown is loaded by axial force P at its left end. The bar is embedded in an elastic medium that applies end load F and distributed axial load q, both of which are directly proportional to axial displacement u of the bar. Use the Galerkin method to establish matrices of a one-element FE formulation based on a linear axial displacement field.

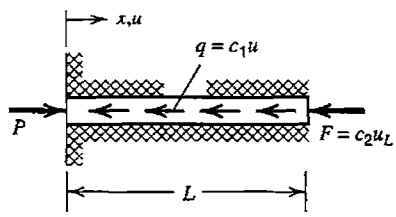

Problem 5.3-1

5.3-2 A cable of negligible flexural stiffness carries axial tension and contacts an elastic foundation of modulus B (force per unit length per unit of lateral deflection w). The sketch shows the cable in its deflected position. Left and right ends of the cable are loaded by the respective lateral forces F_L and F_R. Cable tension can be considered constant over the span shown, and equal to horizontal forces T, because $|w_{,x}| << 1$.

(a) Show that the governing differential equation is $Tw_{,xx} - Bw = 0$.

(b) Use the Galerkin method to establish formulas for element matrices in terms of shape functions and constants. Clearly identify the stiffness matrix and the load vector (which is expressed in terms of F_L and F_R).

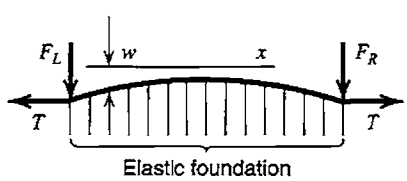

Problem 5.3-2

5.3-3 The equation of motion of a string is $Tw_{,xx} - \rho_L\ddot{w} = 0$, where T = constant axial tension, w = small lateral displacement, x = axial coordinate, ρ_L = mass per unit length, and $\ddot{w} = d^2w/dt^2$.

(a) Use the Galerkin method to establish matrices of a two-d.o.f. element.

(b) Consider a simply supported uniform string of length $2L$. Model it by two elements, each of length L and of the type formulated in part (a). Solve for the fundamental frequency of vibration. (The exact answer is $\omega^2 = \pi^2T/4\rho_LL^2$.)

5.3-4 Let F = constant axial force, positive in tension, q = distributed lateral load, and B = elastic foundation modulus (force per unit length per unit of lateral deflection v). The differential equation of a uniform beam becomes $EIv_{,xxxx} - q - Fv_{,xx} + Bv = 0$. Use the Galerkin method to formulate expressions for element matrices associated with F and B in a form analogous to that in Eq. 5.3-20.

5.3-5 For the beam problem, Eqs. 5.3-13 to 5.3-20, demonstrate the treatment of interelement bending moments and transverse shear forces, in the fashion of Eq. 5.3-12.

5.3-6 Let end cross sections of element 1-2 in Fig. 5.3-3 have the respective areas A_1 and A_2. If A between element ends is a linear function of x, what equation replaces Eq. 5.3-24? Assume that k is constant.

5.3-7 Starting with Eq. 5.3-23, demonstrate the assembly of element thermal "load" vectors. Use Eq. 5.3-12 as a guide.

5.5-1 Show that Eq. 5.5-7 can also be obtained from Eq. 5.5-3 and the stationary condition of the functional

$$\Pi = \frac{1}{2}\iint\left(k_x\phi_{,x}^2 + k_y\phi_{,y}^2 - 2Q\phi\right)dx\,dy - \int f_B\phi\,dS$$

5.5-2 The Helmholz equation, $p_{,xx} + p_{,yy} + p_{,zz} + (\omega/c)^2 p = 0$, governs acoustic modes of vibration in a cavity with rigid walls. Here $p = p(x,y,z)$ is the amplitude of sinusoidally varying pressure, ω is the circular frequency, and c is the speed of sound in the medium. The boundary condition is $p_{,n} = 0$, where n is an axis normal to the wall. Let the assumed pressure amplitude field be $p = \lfloor \mathbf{N} \rfloor \{\mathbf{p}_e\}$. By using the Galerkin method, derive formulas for element matrices in terms of shape functions and constants.

5.5-3 In cylindrical coordinates and with $k_x = k_y = k$ = constant, Eq. 5.5-1 becomes

$$\frac{1}{r}\frac{\partial}{\partial r}\left(r\frac{\partial\phi}{\partial r}\right) + \frac{1}{r^2}\frac{\partial^2\phi}{\partial\theta^2} + \frac{\partial^2\phi}{\partial z^2} + \frac{Q}{k} = 0$$

For a solid of revolution, the natural boundary condition is $k(l\phi_{,r} + n\phi_{,z}) - f_B = 0$, where l and n are direction cosines of a normal to the surface of the solid. Use the Galerkin method to formulate equations analogous to Eqs. 5.5-7.

5.5-4 The differential equation for wind-driven circulation in a shallow lake is

$$\psi_{,xx} + \psi_{,yy} + A\psi_{,x} + B\psi_{,y} + C = 0$$

where ψ is the stream function and A, B, and C are functions of x and y. Coordinates x and y are horizontal, tangent to the lake surface. With h = depth, depthwise average velocities are $u = \psi_{,y}/h$ and $v = -\psi_{,x}/h$. The boundary condition is $\psi_{,n} = 0$, where n is a direction normal to the shoreline. Use the Galerkin method to derive formulas for element matrices in terms of shape functions and constants [5.9].

5.5-5 Complete the development outlined in Eqs. 5.5-8 to 5.5-13; that is, verify that Eqs. 4.8-15 are indeed produced.

5.5-6 An isotropic flat disk is used as a flywheel. The disk has unit thickness and spins about a central axis normal to its plane at constant angular velocity ω. The differential equation of equilibrium is

$$\frac{1}{r}\frac{d}{dr}(r\sigma_r) - \frac{\sigma_\theta}{r} + \rho\omega^2 r = 0$$

where σ_r = radial stress, σ_θ = circumferential stress, and ρ = mass density. An FE formulation can be based on annular elements of inner radius r_i and outer radius r_o. Nodal d.o.f. are radial displacements, one at $r = r_i$ and another at $r = r_o$. Use the Galerkin method to derive formulas for element matrices in terms of shape functions and constants.

5.5-7 Differential equations of equilibrium for an elastic axisymmetric solid under axisymmetric load but without body forces are

$$\frac{1}{r}\frac{\partial(r\sigma_r)}{\partial r} + \frac{\partial\tau_{rz}}{\partial z} - \frac{\sigma_\theta}{r} = 0 \quad \text{and} \quad \frac{1}{r}\frac{\partial(r\tau_{zr})}{\partial r} + \frac{\partial\sigma_z}{\partial z} = 0$$

For a displacement-based formulation, use arguments analogous to those of Eqs. 5.5-8 to 5.5-13 to generate element matrices in terms of shape functions and constants.

5.6-1 Use the FE formulation of Eq. 5.6-8 to solve for nodal stresses and nodal displacements in the uniform two-element bar shown. (Four unknowns remain after boundary conditions are imposed.)

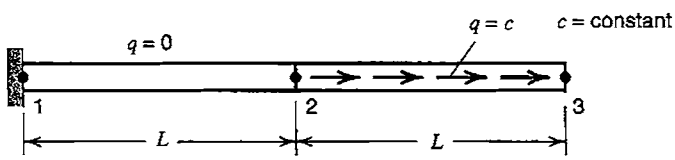

Problem 5.6-1

5.6-2 For the "mixed" beam formulation described in Problem 4.7-6, use the Galerkin method to obtain expressions for element matrices in terms of shape functions and constants. Governing equations are $v_{,xx} - M/EI = 0$ and $M_{,xx} - q = 0$. Consider a four-d.o.f. beam element of length L, and assume that M and v fields use linear interpolation from nodal d.o.f. at element ends. Apply the formulation to a one-element cantilever beam that carries uniformly distributed lateral load q and transverse tip force P.

5.6-3 Verify that the functional of Eq. 5.6-11 produces the same FE formulation as stated in Eqs. 5.6-6 and 5.6-7.

CHAPTER 6

ISOPARAMETRIC ELEMENTS

The isoparametric formulation permits quadrilateral and hexahedral elements to have nonrectangular shapes. It is a versatile formulation, providing plane, solid, plate, and shell elements. Isoparametric elements based on assumed displacement fields are discussed in the present chapter, with emphasis on plane elements and structural mechanics. Numerical integration, used in element formulation, is described and its possible pitfalls discussed. The patch test, considered the arbiter of validity for any type of element, is described.

6.1 INTRODUCTION

This chapter generalizes elements introduced in Chapter 3. Except for triangles, elements in Chapter 3 are restricted to rectangular shape. Rectangular elements are easy to formulate, but are usually impractical because it is difficult to mesh a complicated geometry using only rectangular elements, especially if the mesh must be graded from coarse to fine in order to capture detail in critical regions. Isoparametric elements, discussed in this chapter, can be nonrectangular and can even have curved sides. They use auxiliary coordinates, or reference coordinates, which we call $\xi\eta$ in two dimensions and $\xi\eta\zeta$ in three dimensions. Reference coordinates map the physical element into a reference element that is a square or a cube. In element formulation, the price paid for generality of physical element shape is having to deal with coordinate transformation. Also, because transformation produces algebraic forms that are awkward to integrate exactly, more costly numerical integration is used instead.

For elements described in this chapter, shape functions are used to interpolate both the displacement field (or some other field variable) and element geometry. That is, displacement of a point within an element can be expressed in terms of nodal d.o.f. and shape functions $[\mathbf{N}]$, which are functions of reference coordinates. Similarly, the global position (coordinates) of a point within the element can be expressed in terms of global nodal positions and shape functions $[\tilde{\mathbf{N}}]$, which are also functions of reference coordinates. Symbolically,

- Nodal d.o.f. $\{\mathbf{d}\}$ define displacements $\lfloor u \quad v \quad w \rfloor$ of a point within the element; that is, $\lfloor u \quad v \quad w \rfloor^T = [\mathbf{N}]\{\mathbf{d}\}$.
- Nodal coordinates $\{\mathbf{c}\}$ define coordinates $\lfloor x \quad y \quad z \rfloor$ of a point within the element; that is, $\lfloor x \quad y \quad z \rfloor^T = [\tilde{\mathbf{N}}]\{\mathbf{c}\}$.

Shape function matrices $[\mathbf{N}]$ and $[\tilde{\mathbf{N}}]$ are functions of ξ, η, and ζ. An element is called *isoparametric,* which means "same parameter," if $[\mathbf{N}]$ and $[\tilde{\mathbf{N}}]$ are identical. If $[\tilde{\mathbf{N}}]$ is of lower degree than $[\mathbf{N}]$, the element is called *subparametric.* If $[\tilde{\mathbf{N}}]$ is of higher degree than $[\mathbf{N}]$, the element is called *superparametric.*

The isoparametric formulation began with four-node plane elements, originated by Taig in 1958 [1.8]. Publication outside of company reports began with Irons in 1966 [6.1]. Irons developed elements having curved sides and is credited with the name "isoparametric."

Example: Bar Element. A straight bar element does not show the practical value of the isoparametric formulation, but illustrates its manipulations in a simple context. The element depicted in Fig. 6.1-1a has an internal node that may or may not lie at its physical center. Reference coordinate ξ is a *natural* or *intrinsic* coordinate. It is attached to the bar and remains axial regardless of how the bar may be oriented in global coordinates. Nodes 1 and 3 always lie at $\xi = -1$ and $\xi = +1$, regardless of the physical length L. Node 2 always lies at $\xi = 0$, the center of the mapped element.

There are three nodal coordinates x_i and three axially directed nodal d.o.f. u_i. Thus the element is isoparametric rather than subparametric or superparametric. Three x_i (or three u_i) define a quadratic interpolation. An arbitrary point on the bar has physical coordinate x and displacement u (or field quantity ϕ in a nonstructural context). In terms of generalized d.o.f. a_i,

$$x = \lfloor 1 \quad \xi \quad \xi^2 \rfloor \begin{Bmatrix} a_1 \\ a_2 \\ a_3 \end{Bmatrix} \qquad \text{and} \qquad u = \lfloor 1 \quad \xi \quad \xi^2 \rfloor \begin{Bmatrix} a_4 \\ a_5 \\ a_6 \end{Bmatrix} \tag{6.1-1}$$

One way to obtain the shape function matrix is to follow the procedure associated with Eqs. 3.2-3 and 3.2-6, now using natural coordinate ξ rather than x. Thus

$$\begin{Bmatrix} x_1 \\ x_2 \\ x_3 \end{Bmatrix} = \begin{bmatrix} 1 & -1 & 1 \\ 1 & 0 & 0 \\ 1 & 1 & 1 \end{bmatrix} \begin{Bmatrix} a_1 \\ a_2 \\ a_3 \end{Bmatrix} \qquad \text{hence} \qquad x = \underbrace{\lfloor 1 \quad \xi \quad \xi^2 \rfloor \begin{bmatrix} 1 & -1 & 1 \\ 1 & 0 & 0 \\ 1 & 1 & 1 \end{bmatrix}^{-1}}_{\lfloor \mathbf{N} \rfloor} \begin{Bmatrix} x_1 \\ x_2 \\ x_3 \end{Bmatrix} \tag{6.1-2}$$

Another way we may obtain shape functions is by a combination of intuition, inspection, and trial, as follows. We note that linear ramps seen in Fig. 3.2-2a are described by the forms $\frac{1}{2}(1 - \xi)$ and $\frac{1}{2}(1 + \xi)$. These forms have magnitude $\frac{1}{2}$ at $\xi = 0$. We require that each shape function N_i have unit value at node i and vanish at every other node. Accordingly, if we have already guessed that $N_2 = 1 - \xi^2$, we obtain $N_1 = \frac{1}{2}(1 - \xi) - \frac{1}{2}N_2$ and $N_3 = \frac{1}{2}(1 + \xi) - \frac{1}{2}N_2$. By either this procedure or that of Eq. 6.1-2, we obtain

$$x = \lfloor \mathbf{N} \rfloor \lfloor x_1 \quad x_2 \quad x_3 \rfloor^T \qquad \text{and} \qquad u = \lfloor \mathbf{N} \rfloor \lfloor u_1 \quad u_2 \quad u_3 \rfloor^T \tag{6.1-3}$$

where the shape function matrix is

$$\lfloor \mathbf{N} \rfloor = \left\lfloor \frac{1}{2}\left(-\xi + \xi^2\right) \quad 1 - \xi^2 \quad \frac{1}{2}\left(\xi + \xi^2\right) \right\rfloor \tag{6.1-4}$$

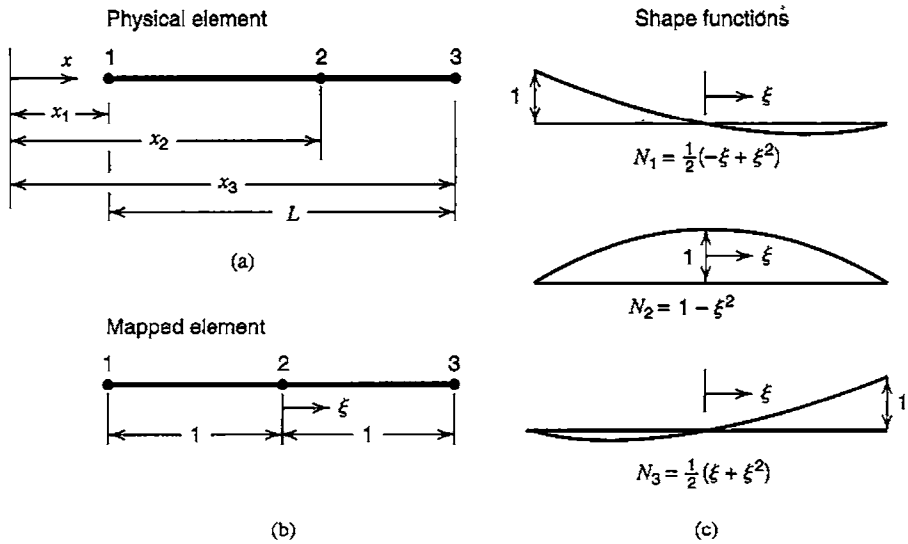

Figure 6.1-1. A three-node (quadratic) bar element.

The same shape functions are provided by Lagrange interpolation functions, using ξ rather than x (see Fig. 3.2-2b and Eqs. 3.2-7). For a given ξ, Eqs. 6.1-3 and 6.1-4 provide physical coordinate x and axial displacement u in terms of nodal values.

Axial strain in the element is

$$\varepsilon_x = \frac{du}{dx} = \left(\frac{d}{dx}\lfloor \mathbf{N} \rfloor\right)\begin{Bmatrix} u_1 \\ u_2 \\ u_3 \end{Bmatrix} \qquad \text{where} \qquad \frac{d}{dx} = \frac{d\xi}{dx}\frac{d}{d\xi} \tag{6.1-5}$$

The chain rule for d/dx must be invoked because $\lfloor \mathbf{N} \rfloor$ is expressed in terms of ξ rather than x. Because $d\xi/dx$ is not immediately available, we must begin with its inverse, $dx/d\xi$, from the first of Eqs. 6.1-3. Let J denote this inverse. Thus

$$J = \frac{dx}{d\xi} = \frac{d}{d\xi}\lfloor \mathbf{N} \rfloor \begin{Bmatrix} x_1 \\ x_2 \\ x_3 \end{Bmatrix} = \begin{bmatrix} \frac{1}{2}(-1 + 2\xi) & -2\xi & \frac{1}{2}(1 + 2\xi) \end{bmatrix} \begin{Bmatrix} x_1 \\ x_2 \\ x_3 \end{Bmatrix} \tag{6.1-6}$$

J may be called a Jacobian. It can be regarded as a scale factor that describes the physical length dx associated with a reference length $d\xi$. Axial strain in the element is $\varepsilon_x = (du/d\xi)/J = \lfloor \mathbf{B} \rfloor \lfloor u_1 \quad u_2 \quad u_3 \rfloor^T$, where

$$\lfloor \mathbf{B} \rfloor = \frac{1}{J}\frac{d}{d\xi}\lfloor \mathbf{N} \rfloor = \frac{1}{J}\begin{bmatrix} \frac{1}{2}(-1 + 2\xi) & -2\xi & \frac{1}{2}(1 + 2\xi) \end{bmatrix} \tag{6.1-7}$$

The element stiffness matrix, from Eq. 3.3-7 or Eq. 4.8-15a, is

$$[\mathbf{k}] = \int_0^L \lfloor \mathbf{B} \rfloor^T E \lfloor \mathbf{B} \rfloor A \, dx = \int_{-1}^{1} \lfloor \mathbf{B} \rfloor^T A E \lfloor \mathbf{B} \rfloor J \, d\xi \tag{6.1-8}$$

Only if node 2 is at the physical midpoint of the element does J reduce to the constant value $J = L/2$. Then ξ is simply the dimensionless axial coordinate $\xi = 2x/L$. The specific form of J depends on the specific numerical values of x_1, x_2, and x_3. In general, J is a function of ξ. Thus $\lfloor \mathbf{B} \rfloor$ contains ξ in both numerator and denominator of every term, and Eq. 6.1-8 cannot conveniently be integrated in closed form. In practice, integration is usually performed by Gauss quadrature, which is a numerical integration procedure described in Section 6.3.

6.2 BILINEAR QUADRILATERAL (Q4)

The plane element discussed here is a generalization of the rectangular Q4 element discussed in Section 3.6 that removes the restriction to rectangular shape. The shear-locking defect noted in Section 3.6 also appears in the present element. An improved formulation, called Q6 in Section 3.10, is discussed in Section 6.6. In the present section the structural element is considered first. A scalar field element is extracted from it as a special case.

Figure 6.2-1a shows the actual physical element. In physical space, reference coordinates ξ and η need not be orthogonal and need not be parallel to Cartesian coordinates x and y. Element sides are bisected by axes ξ and η. Sides have coordinates $\xi = \pm 1$ and $\eta = \pm 1$, regardless of the shape or physical size of the element and regardless of its orientation in Cartesian coordinates. The point $\xi = \eta = 0$ is nominally the element center, but in general it is not the centroid of the physical element. Mapped into $\xi\eta$ space, the element is always a square two units on a side, as shown in Fig. 6.2-1b. Displacements u and v are directed parallel to x and y axes, not parallel to ξ and η axes. In terms of generalized d.o.f., displacements have the form seen in Eqs. 3.6-1, with x and y replaced by ξ and η. Thus, for example, $u = a_1 + a_2\xi + a_3\eta + a_4\xi\eta$, where the a_i are generalized d.o.f.

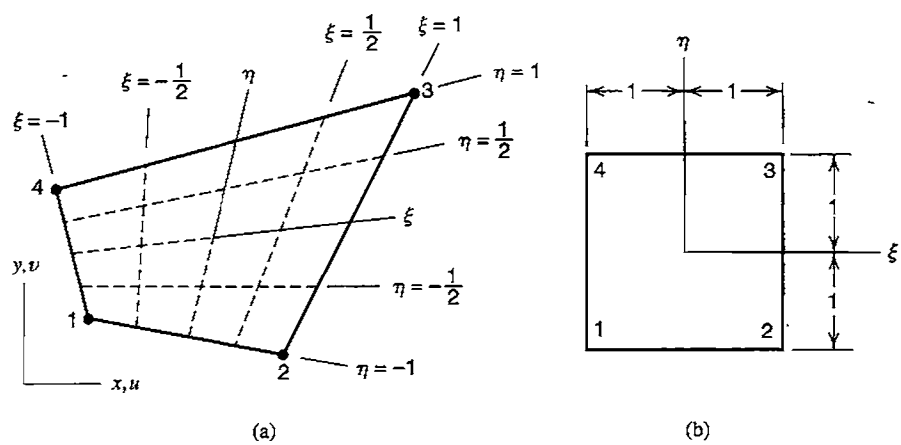

Figure 6.2-1. (a) Four-node plane element in physical space. (b) The same element, mapped into $\xi\eta$ space.

Because the element is isoparametric, the same shape functions are used to interpolate both coordinates and displacements of a point within the element from coordinates and displacements of nodes. Thus

$$\begin{Bmatrix} x \\ y \end{Bmatrix} = \begin{Bmatrix} \sum N_i x_i \\ \sum N_i y_i \end{Bmatrix} = [\mathbf{N}]\{\mathbf{c}\} \qquad \text{and} \qquad \begin{Bmatrix} u \\ v \end{Bmatrix} = \begin{Bmatrix} \sum N_i u_i \\ \sum N_i v_i \end{Bmatrix} = [\mathbf{N}]\{\mathbf{d}\} \tag{6.2-1}$$

where index i in summations runs from 1 to 4, and

$$\begin{aligned} \{\mathbf{c}\} &= \lfloor x_1 \quad y_1 \quad x_2 \quad y_2 \quad x_3 \quad y_3 \quad x_4 \quad y_4 \rfloor^T \\ \{\mathbf{d}\} &= \lfloor u_1 \quad v_1 \quad u_2 \quad v_2 \quad u_3 \quad v_3 \quad u_4 \quad v_4 \rfloor^T \\ [\mathbf{N}] &= \begin{bmatrix} N_1 & 0 & N_2 & 0 & N_3 & 0 & N_4 & 0 \\ 0 & N_1 & 0 & N_2 & 0 & N_3 & 0 & N_4 \end{bmatrix} \end{aligned} \tag{6.2-2}$$

Individual shape functions can be obtained from Eqs. 3.6-4 by setting $a = 1$, $b = 1$, $x = \xi$, and $y = \eta$. Thus

$$\begin{aligned} N_1 &= \tfrac{1}{4}(1-\xi)(1-\eta) \qquad & N_2 &= \tfrac{1}{4}(1+\xi)(1-\eta) \\ N_3 &= \tfrac{1}{4}(1+\xi)(1+\eta) \qquad & N_4 &= \tfrac{1}{4}(1-\xi)(1+\eta) \end{aligned} \tag{6.2-3}$$

As a check, one may note that each N_i is unity when ξ and η assume the coordinates of node i, but zero when ξ and η assume the coordinates of any other node.

For a given physical element, the orientation of $\xi\eta$ axes with respect to xy axes is dictated by the shape functions and node numbering. If node numbers in Fig. 6.2-1 were permuted so that the counterclockwise sequence became 4-1-2-3 starting from the lower left node, axis ξ would appear where axis η now appears, and axis η would be directed in the present $-\xi$ direction. Figure 6.2-1b would not be changed.

Transformation. Strain-displacement matrix [**B**] cannot be written as easily as the foregoing equations because it involves gradients, and an operator such as $\partial/\partial x$ is not simply a constant times $\partial/\partial\xi$. In what follows we consider a function $\phi = \phi(\xi,\eta)$ and examine its derivatives with respect to x and y. Here ϕ may represent either u or v. Except for Eq. 6.2-6, the following transformation equations apply to a plane element having any number of nodes.

Derivatives with respect to x and y are not available directly. Instead we begin with derivatives with respect to ξ and η.

$$\begin{aligned} \frac{\partial\phi}{\partial\xi} &= \frac{\partial\phi}{\partial x}\frac{\partial x}{\partial\xi} + \frac{\partial\phi}{\partial y}\frac{\partial y}{\partial\xi} \\ \frac{\partial\phi}{\partial\eta} &= \frac{\partial\phi}{\partial x}\frac{\partial x}{\partial\eta} + \frac{\partial\phi}{\partial y}\frac{\partial y}{\partial\eta} \end{aligned} \qquad \text{or} \qquad \begin{Bmatrix} \phi_{,\xi} \\ \phi_{,\eta} \end{Bmatrix} = [\mathbf{J}]\begin{Bmatrix} \phi_{,x} \\ \phi_{,y} \end{Bmatrix} \tag{6.2-4}$$

where [J] is called the *Jacobian matrix.*

$$[\mathbf{J}] = \begin{bmatrix} x_{,\xi} & y_{,\xi} \\ x_{,\eta} & y_{,\eta} \end{bmatrix} = \begin{bmatrix} \sum N_{i,\xi} x_i & \sum N_{i,\xi} y_i \\ \sum N_{i,\eta} x_i & \sum N_{i,\eta} y_i \end{bmatrix} \tag{6.2-5}$$

From Eqs. 6.2-1 and 6.2-2, for the special case of the four-node plane element,

$$[\mathbf{J}] = \frac{1}{4}\begin{bmatrix} -(1-\eta) & (1-\eta) & (1+\eta) & -(1+\eta) \\ -(1-\xi) & -(1+\xi) & (1+\xi) & (1-\xi) \end{bmatrix} \begin{bmatrix} x_1 & y_1 \\ x_2 & y_2 \\ x_3 & y_3 \\ x_4 & y_4 \end{bmatrix} = \begin{bmatrix} J_{11} & J_{12} \\ J_{21} & J_{22} \end{bmatrix} \tag{6.2-6}$$

The desired derivatives with respect to x and y are obtained from Eq. 6.2-4:

$$\begin{Bmatrix} \phi_{,x} \\ \phi_{,y} \end{Bmatrix} = \underbrace{\begin{bmatrix} \Gamma_{11} & \Gamma_{12} \\ \Gamma_{21} & \Gamma_{22} \end{bmatrix}}_{[\Gamma]} \begin{Bmatrix} \phi_{,\xi} \\ \phi_{,\eta} \end{Bmatrix} \quad \text{where} \quad [\Gamma] = [\mathbf{J}]^{-1} = \frac{1}{J}\begin{bmatrix} J_{22} & -J_{12} \\ -J_{21} & J_{11} \end{bmatrix} \tag{6.2-7}$$

and J is the determinant of the Jacobian matrix,

$$J = \det[\mathbf{J}] = J_{11}J_{22} - J_{21}J_{12} \tag{6.2-8}$$

Often J is referred to simply as the Jacobian. It can be regarded as a scale factor that multiplies $d\xi\, d\eta$ to produce the physical area increment $dx\, dy$. (As a commonplace example of J, recall the relation between Cartesian and polar coordinates, $dx\, dy = r\, dr\, d\theta$. Here $J = r$.) In general, J is a function of ξ and η, but for rectangles and parallelograms it is the constant value $J = A/4$, where A is the area of the physical element.

[B] Matrix and Stiffness Matrix. In the element strain-displacement relation $\{\boldsymbol{\varepsilon}\} = [\mathbf{B}]\{\mathbf{d}\}$, matrix [**B**] is equal to the product of the three rectangular matrices in the following three equations. Equation 6.2-9 states the plane strain-displacement relations (Eqs. 3.1-7). Equation 6.2-10 is an expanded form of Eq. 6.2-7. Equation 6.2-11 results from differentiation of the second of Eqs. 6.2-1. The final result is a [**B**] matrix analogous to that seen in Eq. 3.6-6.

$$\{\boldsymbol{\varepsilon}\} = \begin{Bmatrix} \varepsilon_x \\ \varepsilon_y \\ \gamma_{xy} \end{Bmatrix} = \begin{bmatrix} 1 & 0 & 0 & 0 \\ 0 & 0 & 0 & 1 \\ 0 & 1 & 1 & 0 \end{bmatrix} \begin{Bmatrix} u_{,x} \\ u_{,y} \\ v_{,x} \\ v_{,y} \end{Bmatrix} \tag{6.2-9}$$

$$\begin{Bmatrix} u_{,x} \\ u_{,y} \\ v_{,x} \\ v_{,y} \end{Bmatrix} = \begin{bmatrix} \Gamma_{11} & \Gamma_{12} & 0 & 0 \\ \Gamma_{21} & \Gamma_{22} & 0 & 0 \\ 0 & 0 & \Gamma_{11} & \Gamma_{12} \\ 0 & 0 & \Gamma_{21} & \Gamma_{22} \end{bmatrix} \begin{Bmatrix} u_{,\xi} \\ u_{,\eta} \\ v_{,\xi} \\ v_{,\eta} \end{Bmatrix} \tag{6.2-10}$$

$$\begin{Bmatrix} u_{,\xi} \\ u_{,\eta} \\ v_{,\xi} \\ v_{,\eta} \end{Bmatrix} = \begin{bmatrix} N_{1,\xi} & 0 & N_{2,\xi} & 0 & N_{3,\xi} & 0 & N_{4,\xi} & 0 \\ N_{1,\eta} & 0 & N_{2,\eta} & 0 & N_{3,\eta} & 0 & N_{4,\eta} & 0 \\ 0 & N_{1,\xi} & 0 & N_{2,\xi} & 0 & N_{3,\xi} & 0 & N_{4,\xi} \\ 0 & N_{1,\eta} & 0 & N_{2,\eta} & 0 & N_{3,\eta} & 0 & N_{4,\eta} \end{bmatrix} \underset{8\times 1}{\{\mathbf{d}\}} \tag{6.2-11}$$

where $N_{1,\xi} = -(1-\eta)/4$, and so on. The stiffness matrix of an element of thickness t, from Eq. 3.3-7 or Eq. 4.8-15a, is

$$\underset{8\times 8}{[\mathbf{k}]} = \iint \underset{8\times 3}{[\mathbf{B}]^T} \underset{3\times 3}{[\mathbf{E}]} \underset{3\times 8}{[\mathbf{B}]} t\, dx\, dy = \int_{-1}^{1}\int_{-1}^{1} \underset{8\times 3}{[\mathbf{B}]^T} \underset{3\times 3}{[\mathbf{E}]} \underset{3\times 8}{[\mathbf{B}]}\, t\, J\, d\xi\, d\eta \tag{6.2-12}$$

If element thickness t is variable and defined by thicknesses t_i at nodes i, thickness at an arbitrary location can be obtained by shape function interpolation, $t = \sum N_i t_i$.

Remarks. Starting from (say) the lower left node in Fig. 6.2-1a, nodes may be numbered 1-2-3-4, 2-3-4-1, 3-4-1-2, or 4-1-2-3. However, when using the N_i of Eqs. 6.2-3, the cyclic order must be maintained and must run counterclockwise if J is not to become negative over part or all of the element. Subject to these restrictions, a change in element node numbering affects only the locations of the k_{ij} in $[\mathbf{k}]$. The node numbering change does not affect numerical values of the k_{ij} or the positions in the global $[\mathbf{K}]$ to which they are assigned (provided that global node numbers are not changed).

In the first integral of Eq. 6.2-12 it is implied that $[\mathbf{B}]$ is a function of x and y. In the second integral, $[\mathbf{B}]$ and J are in general functions of both ξ and η. Equations 6.2-7 and 6.2-10 show that the B_{ij} contain functions of ξ and η in their numerators and in their denominators. For this reason it is convenient to evaluate integrals numerically, as described in Section 6.3, rather than analytically.

Scalar Field Element. Let ϕ be a field quantity, such as temperature if the problem is heat conduction. At a node i there is now a single d.o.f. ϕ_i. The scalar element can be extracted from the structural element by giving u the new name ϕ, discarding v, and compacting arrays. Thus, Eq. 6.2-7 and the compacted form of Eq. 6.2-11 yield

$$\begin{Bmatrix} \phi_{,x} \\ \phi_{,y} \end{Bmatrix} = \underbrace{\begin{bmatrix} \Gamma_{11} & \Gamma_{12} \\ \Gamma_{21} & \Gamma_{22} \end{bmatrix} \begin{bmatrix} N_{1,\xi} & N_{2,\xi} & N_{3,\xi} & N_{4,\xi} \\ N_{1,\eta} & N_{2,\eta} & N_{3,\eta} & N_{4,\eta} \end{bmatrix}}_{[\mathbf{B}]} \begin{Bmatrix} \phi_1 \\ \phi_2 \\ \phi_3 \\ \phi_4 \end{Bmatrix} \tag{6.2-13}$$

The element characteristic matrix, which for heat conduction problems is a conductivity matrix, is stated by Eq. 3.4-7. For the present four-node plane element,

$$\underset{4\times 4}{[\mathbf{k}]} = \int \underset{4\times 2}{[\mathbf{B}]^T} \underset{2\times 2}{[\kappa]} \underset{2\times 4}{[\mathbf{B}]}\, t\, dA = \int_{-1}^{1}\int_{-1}^{1} \underset{4\times 2}{[\mathbf{B}]^T} \underset{2\times 2}{[\kappa]} \underset{2\times 4}{[\mathbf{B}]}\, t\, J\, d\xi\, d\eta \tag{6.2-14}$$

where $[\kappa]$ contains material conductivities.

6.3 QUADRATURE: [k] OBTAINED BY NUMERICAL INTEGRATION

Quadrature is a name used for numerical integration. There are many quadrature rules. Each operates by evaluating (or *sampling*) the function at specific points, multiplying the resulting number by an appropriate weighting factor, and adding results. As applied to integration of a stiffness matrix, each different stiffness coefficient k_{ij} in [k] counts as a function that must be integrated over the element length, area, or volume. In the following discussion we call the function ϕ, where $\phi = \phi(\xi)$ in one dimension, $\phi = \phi(\xi,\eta)$ in plane problems, and $\phi = \phi(\xi,\eta,\zeta)$ in 3D problems. In this chapter we apply quadrature to quadrilaterals and hexahedra. Triangles and tetrahedra are considered in Chapter 7.

Here we discuss only Gauss quadrature, as it is the quadrature rule most often used in generating element matrices. This method locates sampling points and assigns weights so as to minimize integration error when the integrand is a general polynomial. Thus, for a given level of accuracy, Gauss quadrature uses fewer sampling points than other quadrature rules.

One Dimension. An integral having limits $x = x_1$ and $x = x_2$ can be transformed to an integral having limits $\xi = -1$ and $\xi = 1$ by making a substitution such as $x = \frac{1}{2}(1-\xi)x_1 + \frac{1}{2}(1+\xi)x_2$, which is appropriate for a two-node element. Thus

$$I = \int_{x_1}^{x_2} f\, dx \qquad \text{becomes} \qquad I = \int_{-1}^{1} \phi\, d\xi \tag{6.3-1}$$

The integrand is changed in form, from $f = f(x)$ to $\phi = \phi(\xi)$, where ϕ incorporates the Jacobian of the transformation, $J = dx/d\xi$, which becomes $J = (x_2 - x_1)/2$ for a two-node element. The latter form of Eq. 6.3-1 makes it possible to write convenient quadrature formulas. The isoparametric formulation incorporates the limit change.

For the simplest numerical integration, we sample (evaluate) ϕ at the midpoint of the interval and multiply by the length of the interval (Fig. 6.3-1b). Thus we approximate area under the curve by a rectangle of height ϕ_1 and length 2, so that $I \approx 2\phi_1$. This result is exact if $\phi = \phi(\xi)$ happens to describe a straight line of any finite slope. Generalization of the procedure provides the quadrature formula

$$I = \int_{-1}^{1} \phi\, d\xi \approx W_1\phi_1 + W_2\phi_2 + \cdots + W_n\phi_n \tag{6.3-2}$$

Examples using $n = 1$, $n = 2$, and $n = 3$ appear in Fig. 6.3-1. Table 6.3-1 lists Gauss quadrature data through order 3, where the "degree of precision" is the degree of the

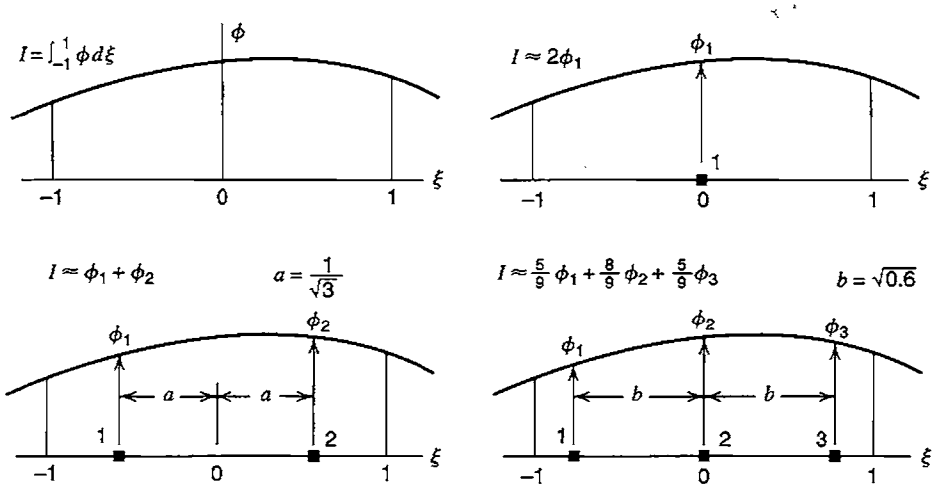

Figure 6.3-1. Integration of a function $\phi = \phi(\xi)$ in one dimension by Gauss quadrature of orders 1, 2, and 3. Gauss points are numbered.

highest-order polynomial in ξ that is integrated exactly by Eq. 6.3-2 for a given n. Much more extensive tabulations are available [6.2], but Gauss rules of high order are not often applied to finite elements. Note that sampling points ("Gauss points") are located symmetrically with respect to the center of the interval and that symmetrically paired points have the same weight W. These data are sometimes called Gauss-Legendre coefficients because sampling point locations are roots of Legendre polynomials.

Example. Consider the third-degree polynomial $\phi = a_0 + a_1\xi + a_2\xi^2 + a_3\xi^3$, where the a_i are constants. The exact integral from $\xi = -1$ to $\xi = 1$ is

$$I = \int_{-1}^{1} \phi\, d\xi = 2a_0 + \frac{2}{3}a_2 \tag{6.3-3}$$

The one-point rule provides the approximation $I_1 \approx 2a_0$. From the two-point rule, with $\xi_1 = -p$, $\xi_2 = p$, where $p = 1/\sqrt{3}$, we obtain

$$I_2 = 1.0(a_0 - a_1p + a_2p^2 - a_3p^3) + 1.0(a_0 + a_1p + a_2p^2 + a_3p^3) = 2a_0 + \frac{2}{3}a_2 \tag{6.3-4}$$

TABLE 6.3-1 SAMPLING POINT LOCATIONS AND WEIGHT FACTORS FOR GAUSS QUADRATURE OVER THE INTERVAL $\xi = -1$ TO $\xi = +1$.

Order n	Degree of precision	Sampling point locations ξ_i	Weight factors W_i
1	1	0.	2.
2	3	$\pm 0.57735\ 02691\ 89626 = \pm 1/\sqrt{3}$	1.
3	5	$\pm 0.77459\ 66692\ 41483 = \pm\sqrt{0.6}$	$0.55555\ 55555\ 55555 = 5/9$
		0.	$0.88888\ 88888\ 88888 = 8/9$

In this example we see an instance of a general rule: a polynomial of degree $2n - 1$ is integrated exactly by n-point Gauss quadrature. Use of more than n points will still produce the exact result.

Two and Three Dimensions. Multidimensional Gauss rules, called Gaussian product rules, are obtained by successive application of one-dimensional Gauss rules. In two dimensions, consider the function $\phi = \phi(\xi,\eta)$. We elect to integrate first with respect to ξ and then with respect to η. Thus

$$I = \int_{-1}^{1}\int_{-1}^{1} \phi(\xi,\eta)\, d\xi\, d\eta \approx \int_{-1}^{1}\left[\sum_i W_i \phi(\xi_i,\eta)\right] d\eta$$
$$\approx \sum_j W_j \left[\sum_i W_i \phi(\xi_i,\eta_j)\right] = \sum_i \sum_j W_i W_j \phi(\xi_i,\eta_j) \tag{6.3-5}$$

Figure 6.3-2 shows what two-dimensional polynomials in ξ and η are integrated exactly by Eq. 6.3-5. The figure represents a polynomial in an integrand ϕ, not the polynomial in a displacement field. A complete polynomial has degree $l + m$. We see that, for example, all quartic terms except ξ^4 and η^4 are integrated exactly by a 2 by 2 Gauss rule.

For a one-point rule, $\phi = \phi_1$ is evaluated at $\xi = \eta = 0$, and $I \approx 4\phi_1$ in two dimensions. For the four-point rule depicted in Fig. 6.3-3a, $W_i W_j = 1$ at each Gauss point. Hence Eq. 6.3-5 yields

$$I \approx \phi_1 + \phi_2 + \phi_3 + \phi_4 \tag{6.3-6}$$

where ϕ_i is the numerical value of ϕ at the ith Gauss point. For the nine-point rule depicted in Fig. 6.3-3b, Eq. 6.3-5 yields

$$I \approx \frac{25}{81}(\phi_1 + \phi_3 + \phi_7 + \phi_9) + \frac{40}{81}(\phi_2 + \phi_4 + \phi_6 + \phi_8) + \frac{64}{81}\phi_5 \tag{6.3-7}$$

In three dimensions, Gauss quadrature takes the form

$$I = \int_{-1}^{1}\int_{-1}^{1}\int_{-1}^{1} \phi(\xi,\eta,\zeta)\, d\xi\, d\eta\, d\zeta \approx \sum_i \sum_j \sum_k W_i W_j W_k\, \phi(\xi_i,\eta_j,\zeta_k) \tag{6.3-8}$$

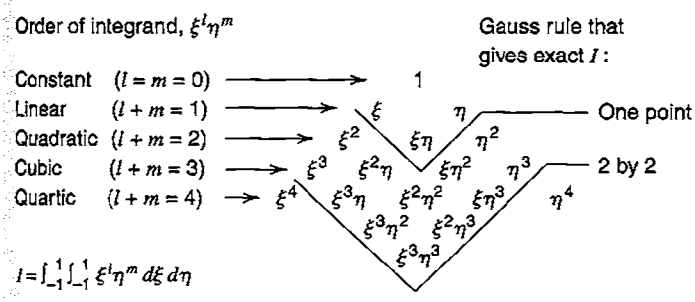

Figure 6.3-2. Exactness of Gauss quadrature in two dimensions. Polynomial terms in the Pascal triangle down to the V-shaped lines are integrated exactly by Gauss rules of orders 1 and 2, respectively.

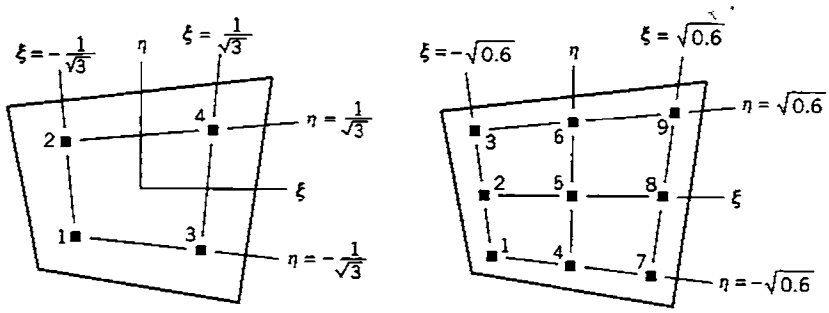

(a) (b)

Figure 6.3-3. Sampling point locations for integration of a function $\phi = \phi(\xi,\eta)$, using Gauss rules of orders 2 (four points) and 3 (nine points).

If $\phi = 1$ in Eq. 6.3-2, then $I = 2$, and we see that $\sum W_i = 2$ for a Gauss rule of any order. Similarly, products W_iW_j in Eq. 6.3-5 sum to 4, and products $W_iW_jW_k$ in Eq. 6.3-8 sum to 8. If $\phi = J$, the Jacobian of the transformation, then integration provides the length, area, or volume of the physical element (not the mapped element).

Stiffness Matrix Integration. We consider use of numerical integration to generate [**k**] of a plane element. Table 6.3-2 summarizes steps of the numerical integration process. The process is the same if the element has more than four nodes. Then arrays [**B**] and [**k**] become larger, but regardless of matrix order, each coefficient k_{ij} is treated like ϕ in Eq. 6.3-5. Jacobian matrix [**J**] is 2 by 2 for any plane element. Fortran coding may be found in [2.13–2.15] and in the second and third editions of this book.

TABLE 6.3-2 COMPUTATIONAL PROCEDURE FOR GENERATING THE STIFFNESS MATRIX OF A PLANE ISOPARAMETRIC ELEMENT BY NUMERICAL INTEGRATION.

(a) Numerical integration procedure

Clear the array that will contain [**k**]; call it array KE in what follows
Loop on integration points in the ξ direction ($i = 1$ to n_i)
Set sampling point location $\xi = \xi_i$ and associated weight factor W_i
Loop on integration points in the η direction ($j = 1$ to n_j)
Set sampling point location $\eta = \eta_j$ and associated weight factor W_j
Call shape function subroutine to calculate element matrix [**B**], thickness t, and Jacobian J, all at point (ξ_i,η_j).
Calculate product $[\mathbf{B}]^T[\mathbf{E}][\mathbf{B}]t\,JW_iW_j$ and add it to array KE
End loop on index j
End loop on index i

(b) Shape function subroutine to generate [**B**], t, and J at a given point

Calling routine supplies coordinates ξ and η at which [**B**], t, and J are to be calculated. At this point:
Calculate shape functions N_i and their ξ and η derivatives
Calculate thickness $t = \sum N_it_i$ from nodal thicknesses t_i
Calculate Jacobian matrix [**J**], its determinant J, and its inverse [Γ]
Calculate strain-displacement matrix [**B**] (for the four-node plane element, see Eqs. 6.2-9 to 6.2-11)

Remarks. Operations summarized in Table 6.3-2a involve as many calls to Table 6.3-2b, and as many matrix multiplications $[\mathbf{B}]^T[\mathbf{E}][\mathbf{B}]$, as there are sampling points in the integration rule. The symmetry of $[\mathbf{k}]$ enables some saving in matrix multiplication. For the four-node quadrilateral, only 36 coefficients k_{ij} appear in the upper or lower triangle of the 8 by 8 matrix $[\mathbf{k}]$. Despite such savings, computational expense is not trivial. Also, for all but rectangular and parallelogram elements, terms to be integrated are not polynomials but rational functions (ratios of polynomials), which are not integrated exactly by a quadrature rule of any finite order. Accuracy of integration increases as more points are used. Should we use a low order rule to reduce computational expense, or a high order rule to gain accuracy? The answer is not easily given. Too low an order renders $[\mathbf{k}]$ rank-deficient, so that one or more deformation modes are met with no elastic resistance. Too high an order may stiffen higher-order displacement modes to an extent that accuracy of FEA suffers. *Accuracy of integration is not the same as accuracy of element behavior.* These matters are discussed in Section 6.8.

Gauss quadrature is widely used but is not the only quadrature method available. For quadratic solid elements, a 14-point rule is available [6.3]. It is intermediate in computational expense to 2 by 2 by 2 and 3 by 3 by 3 Gauss rules. There are special formulas for triangles and pyramids [6.4]. For analysis of plastically deforming plate and shell elements, a sampling point should lie on each surface, where yielding begins in bending. Then thickness-direction integration may be done by Simpson's rule or a special rule that spaces sampling points more closely near surfaces.

As usual, material property matrix $[\mathbf{E}]$ is not restricted to isotropy. Contents of $[\mathbf{E}]$ can be taken as functions of ξ and η to accommodate properties that vary over an element. Anisotropy with principal directions parallel to lines of constant ξ or constant η can also be accommodated [6.5]. Material properties of solid elements can be treated similarly.

6.4 QUADRATIC QUADRILATERALS (Q8, Q9)

Eight-Node Element (Q8). By adding a node to each side of a four-node quadrilateral, we obtain an eight-node plane element that can assume shapes such as shown in Fig. 6.4-1. A curved element side provides a good geometric fit to a curved structure boundary. The

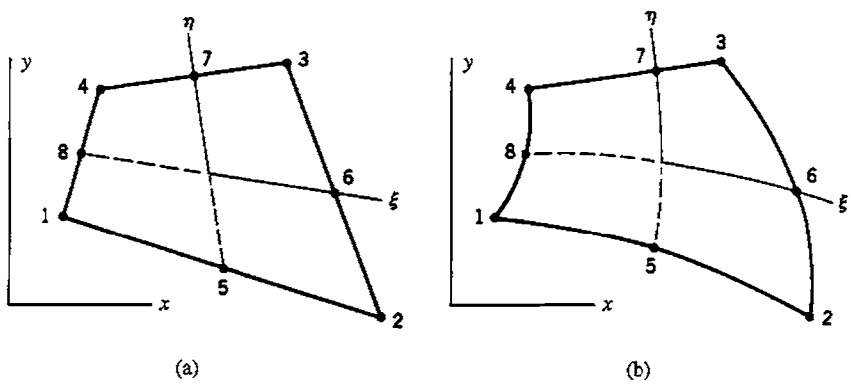

Figure 6.4-1. Eight-node plane serendipity elements in Cartesian coordinates xy. Elements shown have (a) straight sides and midside nodes, and (b) some curved sides and off-center nodes.

mapped element in $\xi\eta$ coordinates remains a two-unit square, with sides at $\xi = \pm 1$ and $\eta = \pm 1$, and midside nodes on ξ and η axes. The displaced shape of an initially straight side can be a straight line or a quadratic curve. An initially curved side need not have a quadratic displacement. In a field of constant strain, its displacement would be a linear function of x and y.

The rectangular form of this element was introduced in Section 3.7. Shape functions can be obtained by the "[A] matrix" method of Section 3.2, applied to Eq. 3.7-1 with x and y replaced by ξ and η. The following alternative argument is more intuitive and perhaps easier. In Fig. 6.4-2a, shape function N_5 of node 5 is obtained by interpolating quadratically in ξ and linearly in η, taking care that $N_5 = 1$ at node 5 and $N_5 = 0$ at all other nodes. In Fig. 6.4-2b, N_8 is obtained in similar fashion. Next, we observe that $N_{(c)}$, which corresponds to N_1 of a four-node element, has ordinate 0.5 at nodes 5 and 8. The function $N_{(c)} - \frac{1}{2}N_5 - \frac{1}{2}N_8$ is therefore zero at all nodes but node 1, where it is unity. Therefore it is shape function N_1 of the Q8 element. Proceeding similarly for remaining nodes, we obtain the complete set of Q8 shape functions, which is

$$
\begin{aligned}
N_1 &= \frac{1}{4}(1-\xi)(1-\eta) - \frac{1}{2}(N_8 + N_5) & N_5 &= \frac{1}{2}(1-\xi^2)(1-\eta) \\
N_2 &= \frac{1}{4}(1+\xi)(1-\eta) - \frac{1}{2}(N_5 + N_6) & N_6 &= \frac{1}{2}(1+\xi)(1-\eta^2) \\
N_3 &= \frac{1}{4}(1+\xi)(1+\eta) - \frac{1}{2}(N_6 + N_7) & N_7 &= \frac{1}{2}(1-\xi^2)(1+\eta) \\
N_4 &= \frac{1}{4}(1-\xi)(1+\eta) - \frac{1}{2}(N_7 + N_8) & N_8 &= \frac{1}{2}(1-\xi)(1-\eta^2)
\end{aligned}
\tag{6.4-1}
$$

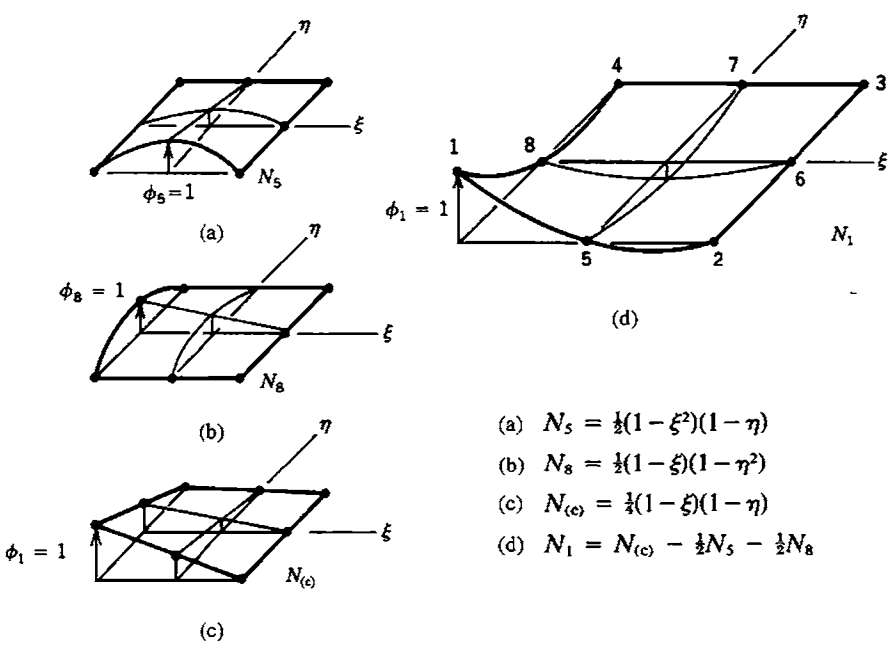

Figure 6.4-2. Selected shape functions for the eight-node plane quadrilateral. (For visualization only, displacement is imagined to take place normal to the plane of the element.)

The foregoing element is known as a member of the "serendipity" element family. In terms of generalized d.o.f. a_i, the displacement field is

$$\begin{aligned} u &= a_1 + a_2\xi + a_3\eta + a_4\xi^2 + a_5\xi\eta + a_6\eta^2 + a_7\xi^2\eta + a_8\xi\eta^2 \\ v &= a_9 + a_{10}\xi + a_{11}\eta + a_{12}\xi^2 + a_{13}\xi\eta + a_{14}\eta^2 + a_{15}\xi^2\eta + a_{16}\xi\eta^2 \end{aligned} \tag{6.4-2}$$

This displacement field contains all coefficients of a quadratic polynomial in ξ and η. Cubic terms $\xi^2\eta$ and $\xi\eta^2$ are present, but cubic terms ξ^3 and η^3 are absent.

Nine-Node Element (Q9). Addition of an internal node (node 9) at $\xi = \eta = 0$ makes the element a *Lagrange* element (Fig. 6.4-3a). Element geometry is completely defined by the eight boundary nodes, using the shape functions of Eqs. 6.4-1. Coordinates x_9 and y_9 of the internal node need not be specified by the software user.

Shape functions of the nine-node element can be obtained by forming products of one-dimensional Lagrange interpolants (Eqs. 3.2-7), in the manner of Eqs. 3.6-2 and 3.6-3. A more intuitive procedure is as follows. The shape function associated with node 9 is

$$N_9 = (1 - \xi^2)(1 - \eta^2) \tag{6.4-3}$$

which may be called a "bubble function" because it resembles a bubble blown over a rectangular opening in a flat plate, as shown in Fig. 6.4-3b. The bubble function mode is analogous to the mode $(1 - \xi^2)$ associated with node 2 in the bar element of Fig. 6.1-1. The first eight shape functions of the Q9 element can be obtained by modifying the N_i of Eqs. 6.4-1 so that each is zero at $\xi = \eta = 0$. Thus, because N_5 through N_8 in Eqs. 6.4-1 equal $\frac{1}{2}$ at $\xi = \eta = 0$, we need only subtract $N_9/2$ from each in order to obtain N_5 through N_8 of the Q9 element. Similarly, N_1 through N_4 in Eqs. 6.4-1 equal negative $\frac{1}{4}$ at $\xi = \eta = 0$, so we must add $N_9/4$. The complete set of shape functions is shown in Table 6.4-1. In these shape functions, remember that N_5 through N_8 include N_9. Thus, for example, when written out, N_1 is

$$\begin{aligned} N_1 = {} & \frac{1}{4}(1-\xi)(1-\eta) - \frac{1}{2}\left[\frac{1}{2}(1-\xi^2)(1-\eta) - \frac{1}{2}N_9\right] \\ & - \frac{1}{2}\left[\frac{1}{2}(1-\xi)(1-\eta^2) - \frac{1}{2}N_9\right] - \frac{1}{4}N_9 \end{aligned} \tag{6.4-4}$$

Table 6.4-1 is explained as follows. The element may have from four to nine nodes. When all nine nodes are included, all nine N_i of Table 6.4-1 are included. The Q8 element of Eqs. 6.4-1 is produced by omitting node 9 and its shape function N_9. The four-node element Q4 of Section 6.2 is produced by omitting nodes 5 through 9 and their shape functions. Elements having 5, 6, or 7 nodes, which can serve as transition elements that connect Q4 elements to Q8 or Q9 elements, are obtained by including only one, two, or three side nodes and their shape functions. (Commercial software is likely to create such transition elements by starting with a Q8 element and then applying constraints that force one or more sides to remain straight, and is not likely to include Q9 elements.)

TABLE 6.4-1 SHAPE FUNCTIONS OF A PLANE QUADRILATERAL THAT HAS FROM FOUR TO NINE NODES. NODE 9, IF PRESENT, IS LOCATED AT $\xi = \eta = 0$.

	Include only if node i is present in the element				
	$i = 5$	$i = 6$	$i = 7$	$i = 8$	$i = 9$
$N_1 = \frac{1}{4}(1-\xi)(1-\eta)$	$-\frac{1}{2}N_5$			$-\frac{1}{2}N_8$	$-\frac{1}{4}N_9$
$N_2 = \frac{1}{4}(1+\xi)(1-\eta)$	$-\frac{1}{2}N_5$	$-\frac{1}{2}N_6$			$-\frac{1}{4}N_9$
$N_3 = \frac{1}{4}(1+\xi)(1+\eta)$		$-\frac{1}{2}N_6$	$-\frac{1}{2}N_7$		$-\frac{1}{4}N_9$
$N_4 = \frac{1}{4}(1-\xi)(1+\eta)$			$-\frac{1}{2}N_7$	$-\frac{1}{2}N_8$	$-\frac{1}{4}N_9$
$N_5 = \frac{1}{2}(1-\xi^2)(1-\eta)$					$-\frac{1}{2}N_9$
$N_6 = \frac{1}{2}(1+\xi)(1-\eta^2)$					$-\frac{1}{2}N_9$
$N_7 = \frac{1}{2}(1-\xi^2)(1+\eta)$					$-\frac{1}{2}N_9$
$N_8 = \frac{1}{2}(1-\xi)(1-\eta^2)$					$-\frac{1}{2}N_9$
$N_9 = (1-\xi^2)(1-\eta^2)$					

Remarks. Except that some matrices have larger size, Eq. 6.2-12 (or Eq. 6.2-14 for a scalar element) also apply to Q8 and Q9 elements. For the Q8 element, $[\mathbf{k}]$ is 16 by 16, $[\mathbf{B}]$ is 3 by 16, and $[\mathbf{E}]$ remains 3 by 3. Equation 6.2-5 continues to provide $[\mathbf{J}]$, but index i now runs from 1 to 16 (as it does also for the Q9 element, whose node at $\xi = \eta = 0$ is not used in defining element shape). Equation 6.2-11 has 16 columns for the Q8 element, because $\{\mathbf{d}\}$ is 16 by 1. Table 6.3-2 remains applicable.

A Q8 element can exactly represent a state of pure bending only if it is rectangular. A Q9 element can do so even if it is nonrectangular, provided that sides are straight and side nodes are at midsides as in Fig. 6.4-1a [6.6]. In general, the accuracy of computed results decreases as elements shapes depart from being compact and rectangular. Element Q9 is much less sensitive than element Q8 to nonrectangularity, curvature of sides, and placement

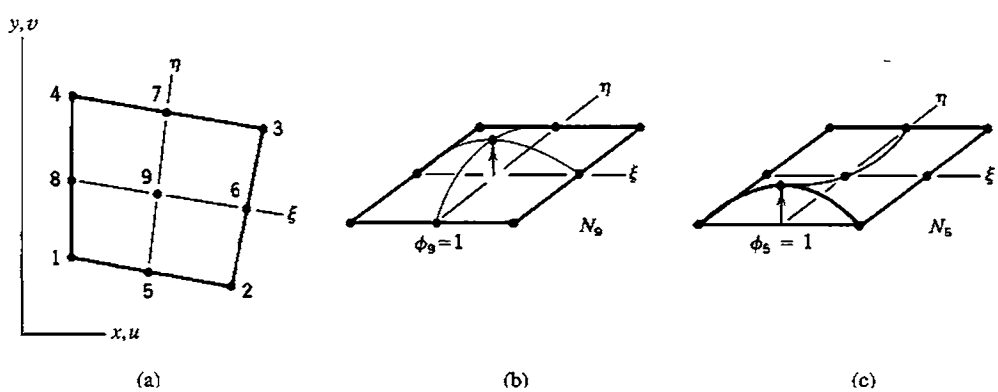

Figure 6.4-3. (a) Nine-node plane Lagrange element in Cartesian coordinates xy. (b) Shape functions N_9 and N_5. (For visualization only, displacement is imagined to take place normal to the plane of the element.)

of side nodes away from midsides. These benefits may be attributed to the quartic term $\xi^2\eta^2$, which appears in the displacement field of element Q9 but is absent from Eqs. 6.4-2. Neither Q8 nor Q9 contains the cubic terms ξ^3 and η^3.

Q8 and Q9 elements are called quadratic because a *complete* polynomial of second degree, but no higher, appears in their shape functions. Is it better to use one Q8 or Q9 (quadratic) element rather than four four-node (linear) elements? Let us assume that the four-node element is the "modified Q6 form" (QM6) form that does not suffer from parasitic shear (see Section 6.6). Then there may not be a strong case to be made either way. MacNeal [3.3] considers computational expense and accuracy of computed results, and notes that, in practice, linear and quadratic elements seem to have almost equal use.

6.5 HEXAHEDRAL ISOPARAMETRIC ELEMENTS

Solid isoparametric elements are formulated by direct extension of the procedure used for plane elements. The eight-node solid element shown in Fig. 6.5-1a is analogous to the four-node plane Q4 element of Section 6.2, and also has the defect of shear locking. With restriction to rectangular shape, this element is discussed in Section 3.8. In the present section the shape restriction is avoided. If midedge nodes are added to the element, Fig. 6.5-1b, we obtain a 20-node solid element analogous to plane element Q8 of Section 6.4. Regardless of the number of nodes or possible curvature of edges and faces, faces of a hexahedron lie at $\xi = \pm 1$, $\eta = \pm 1$, and $\zeta = \pm 1$.

For a solid isoparametric element having any number of nodes, geometry and displacements are given by

$$\begin{Bmatrix} x \\ y \\ z \end{Bmatrix} = \sum_i N_i \begin{Bmatrix} x_i \\ y_i \\ z_i \end{Bmatrix} \quad \text{and} \quad \begin{Bmatrix} u \\ v \\ w \end{Bmatrix} = \sum_i N_i \begin{Bmatrix} u_i \\ v_i \\ w_i \end{Bmatrix} \tag{6.5-1}$$

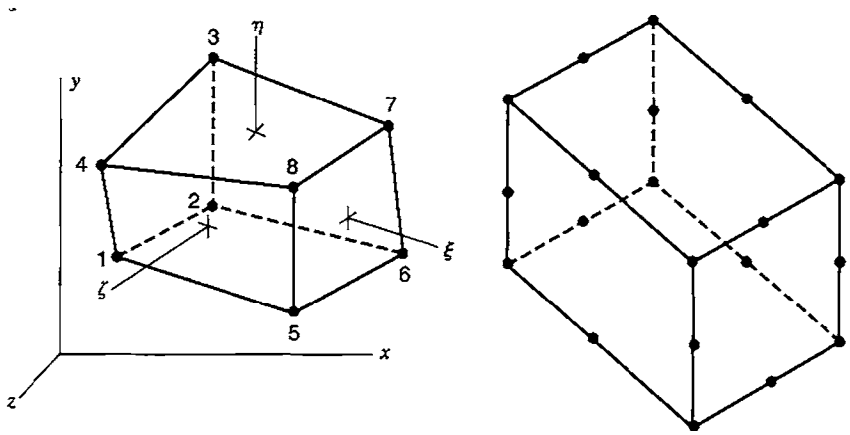

(a) (b)

Figure 6.5-1. (a) Eight-node hexahedron, also known as a linear hexahedron and as a trilinear solid element. (b) 20-node hexahedron, shown as rectangular.

Analogously to Eq. 6.2-5, the Jacobian matrix is

$$[\mathbf{J}] = \begin{bmatrix} x_{,\xi} & y_{,\xi} & z_{,\xi} \\ x_{,\eta} & y_{,\eta} & z_{,\eta} \\ x_{,\zeta} & y_{,\zeta} & z_{,\zeta} \end{bmatrix} = \sum_i \begin{bmatrix} N_{i,\xi}x_i & N_{i,\xi}y_i & N_{i,\xi}z_i \\ N_{i,\eta}x_i & N_{i,\eta}y_i & N_{i,\eta}z_i \\ N_{i,\zeta}x_i & N_{i,\zeta}y_i & N_{i,\zeta}z_i \end{bmatrix} \tag{6.5-2}$$

where index i ranges over the number of nodes in the element. Analogously to Eq. 6.2-9, the strain-displacement relation, Eqs. 3.1-7 and 3.1-8, can be written in the form

$$\begin{Bmatrix} \varepsilon_x \\ \varepsilon_y \\ \varepsilon_z \\ \gamma_{xy} \\ \gamma_{yz} \\ \gamma_{zx} \end{Bmatrix} = \begin{bmatrix} 1 & 0 & 0 & 0 & 0 & 0 & 0 & 0 & 0 \\ 0 & 0 & 0 & 0 & 1 & 0 & 0 & 0 & 0 \\ 0 & 0 & 0 & 0 & 0 & 0 & 0 & 0 & 1 \\ 0 & 1 & 0 & 1 & 0 & 0 & 0 & 0 & 0 \\ 0 & 0 & 0 & 0 & 0 & 1 & 0 & 1 & 0 \\ 0 & 0 & 1 & 0 & 0 & 0 & 1 & 0 & 0 \end{bmatrix} \begin{Bmatrix} u_{,x} \\ u_{,y} \\ u_{,z} \\ v_{,x} \\ \vdots \\ w_{,z} \end{Bmatrix} \tag{6.5-3}$$

For the eight node solid of Fig. 6.5-1a, i ranges from 1 to 8 in Eqs. 6.5-1 and 6.5-2. In terms of generalized d.o.f. a_i, displacement u has the form

$$u = a_1 + a_2\xi + a_3\eta + a_4\zeta + a_5\xi\eta + a_6\eta\zeta + a_7\zeta\xi + a_8\xi\eta\zeta \tag{6.5-4}$$

The same form is used for displacements v and w. Equation 6.5-4 contains all linear terms, three of the six quadratic terms (ξ^2, η^2, and ζ^2 are not present), and only $\xi\eta\zeta$ from the 10 cubic terms. From Eq. 3.8-3, shape functions of the eight-node hexahedron are

$$N_1 = \frac{1}{8}(1-\xi)(1-\eta)(1+\zeta), \qquad N_2 = \frac{1}{8}(1-\xi)(1-\eta)(1-\zeta),$$
$$N_3 = \frac{1}{8}(1-\xi)(1+\eta)(1-\zeta), \tag{6.5-5}$$

and so on. Equation 6.2-10 is expanded so that the square matrix is 9 by 9, and Eq. 6.2-11 is expanded so that the rectangular matrix is 9 by 24. The stiffness matrix of the eight-node element is given by

$$\underset{24\times 24}{[\mathbf{k}]} = \int_{-1}^{1}\int_{-1}^{1}\int_{-1}^{1} \underset{24\times 6}{[\mathbf{B}]^T} \underset{6\times 6}{[\mathbf{E}]} \underset{6\times 24}{[\mathbf{B}]} \; J\, d\xi\, d\eta\, d\zeta \tag{6.5-6}$$

where J is the determinant of $[\mathbf{J}]$ in Eq. 6.5-2.

For the 20-node solid of Fig. 6.5-1b, i ranges from 1 to 20 in Eqs. 6.5-1 and 6.5-2. Displacements u, v, and w each have the following 20 modes in their displacement expressions: a constant term, all three linear terms (ξ, η, ζ), all six quadratic terms (ξ^2, η^2, ζ^2, $\xi\eta$, $\eta\zeta$, $\zeta\xi$), seven of the ten cubic terms ($\xi^2\eta$, $\xi\eta^2$, $\eta^2\zeta$, $\eta\zeta^2$, $\zeta^2\xi$, $\zeta\xi^2$, $\xi\eta\zeta$), and three

quartic terms ($\xi^2\eta\zeta$, $\xi\eta^2\zeta$, $\xi\eta\zeta^2$). Shape functions appear in books such as [2.14,3.3,4.4]. Stiffness matrix integration is as stated by Eq. 6.5-6, but with "24" changed to "60."

The 20-node solid is a serendipity element. If a node is added to the middle of each face and an internal node is added at $\xi = \eta = \zeta = 0$, we obtain a 27-node Lagrange element, whose stiffness matrix is 81 by 81.

6.6 INCOMPATIBLE MODES. NODELESS D.O.F.

The four-node plane element and the eight-node solid element both exhibit shear locking. That is, due to spurious shear strain, they are excessively stiff when asked to display the beam-bending mode that is so important in structural mechanics. A remedy for the problem is to add bending modes to element displacement fields. Thus we obtain the Q6 element, as discussed for rectangular shapes in Section 3.10. Unfortunately, when directly extended to nonrectangular shapes, the element has a defect that makes it unsuitable for general use. In the present section we describe the defect and how it may be overcome.

Figure 3.10-3 shows incompatible modes added to the four-node plane element. Similar modes can be added to the eight-node solid element. Thus, displacement fields for these elements become

Eight-node solid element →

Four-node plane element →

$$
\begin{aligned}
u &= \sum_i N_i u_i + (1-\xi^2)a_1 + (1-\eta^2)a_2 + (1-\zeta^2)a_7 \\
v &= \sum_i N_i v_i + (1-\xi^2)a_3 + (1-\eta^2)a_4 + (1-\zeta^2)a_8 \\
w &= \sum_i N_i w_i + (1-\xi^2)a_5 + (1-\eta^2)a_6 + (1-\zeta^2)a_9
\end{aligned}
\tag{6.6-1}
$$

For the plane element, index i runs from 1 to 4 and shape functions N_i are given by Eqs. 6.2-3. For the solid element, index i runs from 1 to 8 and shape functions N_i are given by Eqs. 6.5-5. The a_i are generalized d.o.f. They may also be called "nodeless" d.o.f. Displacement modes associated with the a_i are usually called "incompatible" or "nonconforming" because, at locations other than nodes, they allow overlaps or gaps between adjacent elements. Element stiffness matrices can be generated by numerical integration in the usual way, with the [**B**] matrix expanded:

$$[\mathbf{B}] = [\mathbf{B}_d \ \mathbf{B}_a] \tag{6.6-2}$$

where $[\mathbf{B}_d]$ operates on nodal d.o.f. and $[\mathbf{B}_a]$ operates on nodeless d.o.f. Thus $[\mathbf{B}_d]$ is identical to the entire matrix [**B**] of an element without nodeless d.o.f. Jacobian calculations are based only on nodal coordinates and are unchanged (Eqs. 6.2-4 to 6.2-8, for example). In generating $[\mathbf{B}_d \ \mathbf{B}_a]$ for the four-node element, Eqs. 6.2-9 and 6.2-10 are unchanged. Four columns are appended to the rectangular matrix in Eq. 6.2-11; these columns multiply the

a_i and contain zeros, -2ξ, and -2η. For example, the $u_{,\xi}$ expression now contains the term $-2\xi a_1$, and so on.

However, Q6 elements formulated in this way fail to represent constant stress (or constant strain) states unless they are rectangular. Specifically, let a mesh of nonrectangular elements be loaded in such a way that a state of constant stress should prevail. If incompatible modes are *not* present in element formulations, which is the same as setting the a_i to zero, elements respond properly and display the constant state. If incompatible modes *are* present, elements do not respond properly. Nodeless d.o.f. a_i should be zero but they are not.

A remedy for the defect is as follows [6.7]. Let a vector of constants $\{\boldsymbol{\sigma}_0\}$ represent any state of uniform stress, and consider the load vector $\{\mathbf{r}_e\}$ in Eq. 3.3-8. We desire that d.o.f. a_i remain zero when a typical element displays an arbitrary constant stress state $\{\boldsymbol{\sigma}_0\}$. This requires that load terms associated with the a_i be zero; that is, we require

$$\int [\mathbf{B}_a]^T \{\boldsymbol{\sigma}_0\}\, dV = \{\mathbf{0}\} \qquad \text{hence} \qquad \int [\mathbf{B}_a]^T dV = [\mathbf{0}] \tag{6.6-3}$$

Or, for plane and solid isoparametric elements respectively,

$$\int_{-1}^{1}\int_{-1}^{1} [\mathbf{B}_a]^T t\, J\, d\xi\, d\eta = [\mathbf{0}] \qquad \int_{-1}^{1}\int_{-1}^{1}\int_{-1}^{1} [\mathbf{B}_a]^T J\, d\xi\, d\eta\, d\zeta = [\mathbf{0}] \tag{6.6-4}$$

For parallelograms of uniform thickness and for parallelepipeds, thickness t and Jacobian J are constant and $[\mathbf{B}_a]$ contains first powers of ξ and η (and ζ for solid elements), so that Eqs. 6.6-4 are satisfied automatically. For elements of more general shape, expressions in the integrand are more complicated. But even for generally shaped elements, we can contrive to satisfy Eqs. 6.6-4 by modifying the computation of $[\mathbf{B}_a]$ (but not of $[\mathbf{B}_d]$) in the following way. At all integration points, use the value of $[\mathbf{J}]$ and its determinant J (and thickness t for a plane element) at the element center, $\xi = \eta = \zeta = 0$. Thus Eqs. 6.6-4 continue to contain first powers of isoparametric coordinates and therefore integrate to zero. Thus modified, the plane Q6 element is often called the QM6 element. An alternative explanation of the QM6 element appears in [6.8]. If a Q6 or QM6 element is rectangular, it has the same element stiffness matrix as the five-β hybrid element discussed in Section 4.10.

Remarks. Degrees of freedom a_i can be carried into array $\{\mathbf{D}\}$ that lists structural d.o.f., but more commonly the a_i are "condensed" before elements are assembled. This matter is discussed in Section 6.7, where d.o.f. a_i of Eqs. 6.6-1 would constitute the contents of array $\{\mathbf{d}_c\}$.

Arbitrarily shaped QM6 elements pass the patch test (described in Section 6.13), thus guaranteeing convergence toward exact results with mesh refinement. Briefly, the patch test requires that all elements in a mesh display the expected state of constant stress or strain when conditions at nodes on the boundary of the mesh are appropriately prescribed, perhaps by imposing nodal displacements consistent with uniform ε_x. If instead distributed load is prescribed and Eq. 3.3-8 is used to calculate nodal loads, load terms associated with incompatible d.o.f. must be omitted during element formulation and during subsequent stress calculation if the patch test is to be passed. Thus, for load terms, the QM6 element is treated as if it were a Q4 element.

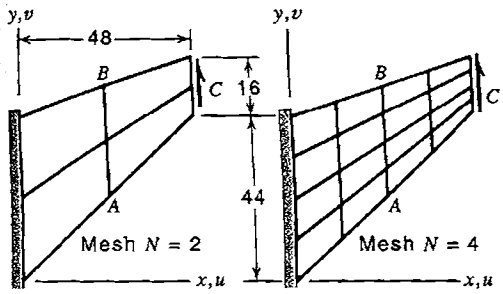

	Mesh	$N = 2$	$N = 4$
QM6	v_C	0.884	0.967
	σ_A	0.840	0.978
	σ_B	0.788	0.926
Q4	v_C	0.498	0.769
	σ_A	0.558	0.830
	σ_B	0.457	0.753

Figure 6.6-1. A swept panel with uniformly distributed load along the right side and Poisson's ratio $\nu = 0.333$. Numerical results [6.7] are y-direction deflection at the right side, maximum normal stress at A, and minimum normal stress at B (exact = 1.000).

The remedy that converts a Q6 element to a QM6 element is a kind of "selective integration," which means use of different integration rules to treat different parts of the stiffness matrix integrand. Selective integration is often applied to elements for plates and shells and to elements used for nearly incompressible materials.

A mesh of incompatible elements may be either too stiff or too flexible. That is, we cannot guarantee a lower bound on computed displacements, as we can for (say) constant-strain triangles. For engineers, lack of a bound on displacements is usually less important than accuracy of computed results. Incompatible elements are usually more accurate than their parent elements that have only nodal d.o.f.

Stresses in an incompatible element are computed using all element d.o.f., including the a_i. Again, the a_i are not loaded, so they assume values dictated by nodal d.o.f. and coefficients in [**k**]. Stress and displacement results from Q4 and QM6 elements are compared in Fig. 6.6-1. This is the same problem as used in Fig. 3.10-2.

6.7 STATIC CONDENSATION

When elements are assembled to form global equations $[\mathbf{K}]\{\mathbf{D}\} = \{\mathbf{R}\}$, all element d.o.f. can be carried into $\{\mathbf{D}\}$, and their associated load terms into $\{\mathbf{R}\}$. These d.o.f. include internal and nodeless d.o.f. such as shown in Fig. 6.7-1. In practice, these d.o.f. are "condensed" before assembly of elements. In this context, condensation has the effect of altering the order in which d.o.f. are processed in solving global equations. Only coefficients that multiply element boundary d.o.f. are assembled into the global matrix [**K**], so that less storage space is needed. The manipulations of static condensation introduce no additional approximation into FEA. It is called "static" condensation to distinguish it from a similar process in dynamics, where both [**K**] and mass matrix [**M**] are reduced in size. However, in dynamics, condensation introduces an additional approximation, which appears in [**M**]. Static condensation can be regarded as a special case of *substructuring* (Section 10.11).

In another application of static condensation, imagine that the last three (rotational) d.o.f. of the 3D beam element, at node 2 in Eq. 2.3-8, are condensed. Then when this element is assembled into the structure, only translational d.o.f. at node 2 are connected to the structure node. At 2 the element can rotate on the structure node, effectively creating a ball-and-socket joint.

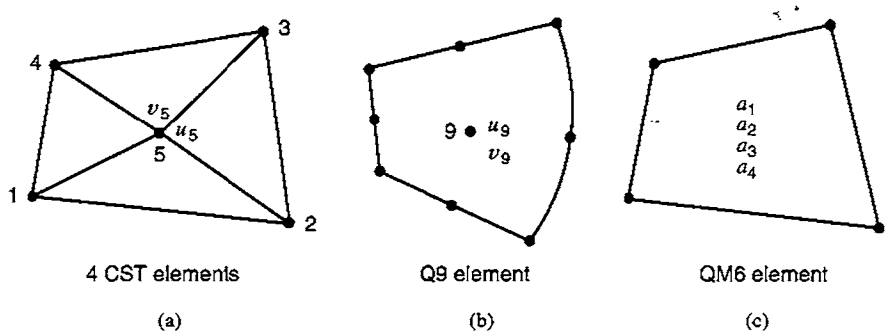

Figure 6.7-1. Examples of elements that have internal or nodeless d.o.f. The d.o.f. identified are usually treated by static condensation.

Static condensation is formally stated as follows. Let equations $[\mathbf{k}]\{\mathbf{d}\} = \{\mathbf{r}\}$ represent a portion of the entire structure. The portion may be a macroelement built of subelements (Fig. 6.7-1a) or a single element that contains internal or nodeless d.o.f. (Fig. 6.7-1b,c). Let d.o.f. $\{\mathbf{d}\}$ be partitioned, $\{\mathbf{d}\} = \lfloor \mathbf{d}_r \;\; \mathbf{d}_c \rfloor^T$, where $\{\mathbf{d}_r\}$ are boundary d.o.f. to be retained and $\{\mathbf{d}_c\}$ are internal or nodeless d.o.f. to be condensed. Loads $\{\mathbf{r}\}$, which are often zero, are similarly partitioned. Thus equations $[\mathbf{k}]\{\mathbf{d}\} = \{\mathbf{r}\}$ become

$$\begin{bmatrix} \mathbf{k}_{rr} & \mathbf{k}_{rc} \\ \mathbf{k}_{cr} & \mathbf{k}_{cc} \end{bmatrix} \begin{Bmatrix} \mathbf{d}_r \\ \mathbf{d}_c \end{Bmatrix} = \begin{Bmatrix} \mathbf{r}_r \\ \mathbf{r}_c \end{Bmatrix} \tag{6.7-1}$$

The lower partition is solved for $\{\mathbf{d}_c\}$, which is then substituted into the upper partition. Thus

$$\{\mathbf{d}_c\} = -[\mathbf{k}_{cc}]^{-1}([\mathbf{k}_{cr}]\{\mathbf{d}_r\} - \{\mathbf{r}_c\}) \tag{6.7-2}$$

$$\underbrace{([\mathbf{k}_{rr}] - [\mathbf{k}_{rc}][\mathbf{k}_{cc}]^{-1}[\mathbf{k}_{cr}])}_{\text{condensed } [\mathbf{k}]}\{\mathbf{d}_r\} = \underbrace{\{\mathbf{r}_r\} - [\mathbf{k}_{rc}][\mathbf{k}_{cc}]^{-1}\{\mathbf{r}_c\}}_{\text{condensed } \{\mathbf{r}\}} \tag{6.7-3}$$

Next follows the standard assembly and solution procedure. Condensed $[\mathbf{k}]$ and $\{\mathbf{r}\}$ arrays are assembled to produce global equations $[\mathbf{K}]\{\mathbf{D}\} = \{\mathbf{R}\}$, in which $\{\mathbf{D}\}$ contains d.o.f. $\{\mathbf{d}_r\}$ of all elements. After solving global equations for $\{\mathbf{D}\}$, d.o.f. $\{\mathbf{d}_r\}$ are known, and d.o.f. $\{\mathbf{d}_c\}$ can be recovered by solving Eq. 6.7-2. Subsequent stress computation makes use of $\{\mathbf{d}_c\}$ as well as $\{\mathbf{d}_r\}$.

Partitioning used in Eqs. 6.7-2 and 6.7-3 is a conceptual convenience rather than a computational necessity. D.o.f. to be condensed can appear anywhere in the array of element d.o.f. and can be processed in any order. When these d.o.f. appear last in the array, as shown in Eq. 6.7-1, condensation can be accomplished by Gauss elimination, starting with the last d.o.f. and working upward, and stopping the process when all d.o.f. $\{\mathbf{d}_c\}$ have been eliminated. What remains is the condensed $[\mathbf{k}]$ in the upper left portion of the element stiffness array and the condensed $\{\mathbf{r}\}$ in the upper portion of the element load array. Further details about static condensation appear in [2.20,6.9,6.10].

6.8 CHOICES IN NUMERICAL INTEGRATION

Except for special geometries such as rectangular and parallelogram elements, with uniformly spaced side nodes (if present), numerical integration of element stiffness coefficients cannot provide exact results. Accuracy of integration can be increased by using more integration points. Will more points also increase the accuracy of computed FE results? Not necessarily. FE results may become more accurate if the order of quadrature is *reduced.* But use of a low order quadrature rule may allow elements to have one or more spurious modes, with consequences that may or may not be serious, depending on the physical problem and the nature of the spurious mode. Spurious modes can be avoided by using some tricks in element formulation, but each trick may introduce some other trouble. These matters are summarized in the present section.

Full Integration. We define "full integration" as a quadrature rule of sufficient accuracy to exactly integrate all stiffness coefficients k_{ij} of an undistorted element. Quadrilateral and hexahedral elements are undistorted if they are rectangular and side nodes (if present) are uniformly spaced along straight sides or straight edges. The Jacobian J of an undistorted element is constant within the element. Consequently all terms in the stiffness matrix integrand are polynomials rather than ratios of polynomials. The simplest example of this behavior appears in Eqs. 6.1-6 to 6.1-8 when $x_2 = (x_1 + x_3)/2$. Equations in Section 6.2 show that the $[\mathbf{B}]$ matrix of a four-node plane rectangle is a linear function of ξ and η. Then, if thickness is uniform and $[\mathbf{E}]$ is constant, the stiffness matrix integrand $[\mathbf{B}]^T[\mathbf{E}][\mathbf{B}]\, t\, J$ contains squares of ξ and η. Therefore an order 2 Gauss rule (four points) integrates $[\mathbf{k}]$ exactly. Similarly, $[\mathbf{k}]$ of an eight-node rectangular solid element is integrated exactly by an order 2 Gauss rule (eight points). The $[\mathbf{B}]$ matrix of an undistorted eight- or nine-node plane element contains squares of ξ and η, so fourth powers appear in the integrand and a 3 by 3 Gauss rule provides exact integration.

If element geometry is distorted, "full integration" is taken to mean the integration rule that would be exact if element geometry were not distorted. Thus, for an arbitrarily shaped eight-node solid element, an order 2 Gauss rule is considered full integration.

Underintegration and Spurious Modes. Use of an integration rule of less than full order is called "underintegration" or "reduced" integration. Underintegration reduces computation time, which may be an important consideration in some analyses that are nonlinear and/or dynamic. Also, underintegration may improve the accuracy of computed FE results by offsetting the overstiffness associated with compatible elements based on assumed displacement fields. Underintegration has a softening effect because some polynomial terms vanish at Gauss points of a low-order rule and therefore make no contribution to strain energy. But underintegration introduces the defect variously known as spurious mode, singular mode, zero-energy deformation mode, hourglass mode, kinematic mode, instability, and mechanism. An element whose stiffness matrix incorporates a spurious mode has no resistance to nodal loads that tend to activate the mode. Mathematically, an underintegrated $[\mathbf{k}]$ is called rank-deficient, which means that its order minus the number of possible rigid-body motions is greater than its rank.

Consider independent displacement modes of a four-node plane element, as shown in Fig. 6.8-1. Modes 1 through 3 are rigid-body modes. They display no strain energy. Modes 4 through 6 are constant-strain modes, and modes 7 and 8 are bending modes. Full integration for this element is a 2 by 2 Gauss rule, which provides an element stiffness matrix that

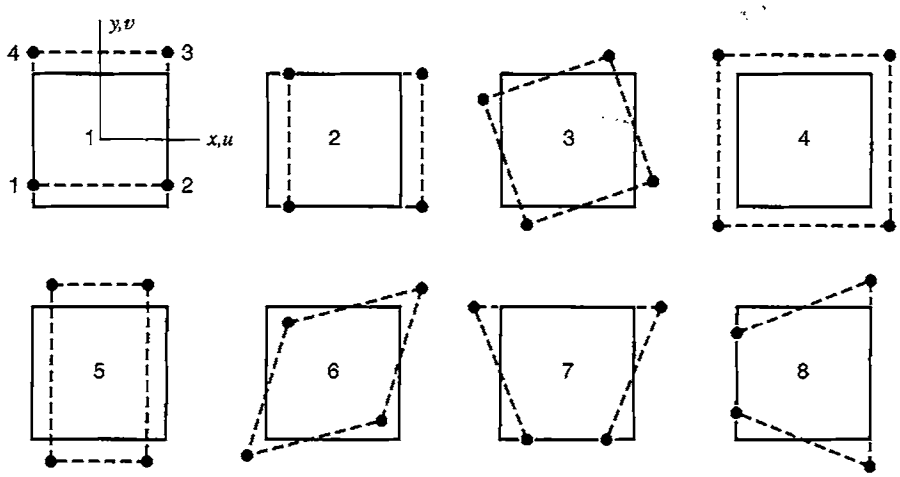

Figure 6.8-1. Independent displacement modes of a four-node plane element.

resists modes 4 through 8, as it should. Underintegration for this element is a single Gauss point at the element center, where modes 7 and 8 produce no strain. An underintegrated [**k**] contains only information that can be detected at sampling points of the integration rule. Therefore underintegration of the four-node element provides a [**k**] for which modes 7 and 8 offer no resistance to applied loads; that is, they are spurious modes. Nonrectangular elements also display these spurious modes under one-point quadrature. Spurious modes may appear in combination with one another and may be superposed on rigid-body modes and on modes that resist deformation.

When elements having spurious modes are connected to produce a mesh, the assembly may or may not provide poor results, depending on the nature of the mode and the information sought. For example, let a bar be modeled by four-node plane elements, each integrated using one Gauss point (Fig. 6.8-2a). All nodes at the support are fixed, thus

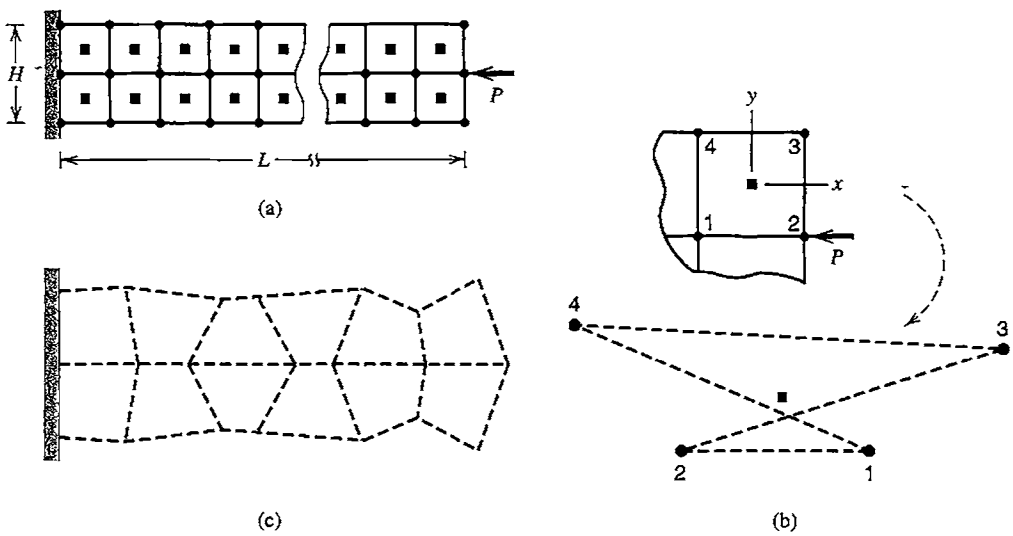

Figure 6.8-2. Four-node square elements with reduced integration. (a) Static axial load. (b) Dashed lines show deformation mode of the upper right element in a 2 by 14 mesh. (c) A computed vibration mode.

suppressing the mechanism and rendering the structure stable. However, there is a "near mechanism:" restraint provided by the support is felt less and less with increasing distance from it. Figure 6.8-2b shows computed deformation of the upper-right element of a 2 by 14 mesh of square elements. If L/H is large enough, computed axial displacement of the loaded node may be greater than the length of the bar! Despite unrealistically large nodal displacements, at the central Gauss point in each element, computed displacements and stresses may be reasonable because spurious displacements and associated strains are not sensed at these locations (Fig. 6.8-2b). When the mesh shown is used in a vibration problem [6.11], one of the computed vibration modes is the physically unreasonable mode shown in Fig. 6.8-2c, whose frequency is less than that of some physically reasonable lateral displacement vibration modes of a cantilever beam. Spurious modes are troublesome in this element because they are *communicable.* A communicable spurious mode is a mode for which elements connected together participate in the mode rather than offering elastic resistance to it because of the connection. An example of a *non*communicable mode is described in what follows.

When eight- and nine-node plane elements are underintegrated by using four Gauss points, the elements have spurious modes as shown in Fig. 6.8-3. Spurious modes that appear only in the nine-node element are communicable. The "hourglass" mode of Fig. 6.8-3d is noncommunicable: there is no way that adjacent elements can both display this mode while remaining connected (in considering this statement, note that signs of all nodal displacements can be reversed without changing the mode; strains at Gauss points of a 2 by 2 rule remain zero). If eight-node elements with 2 by 2 integration are used for the problems of Fig. 6.8-2, computed

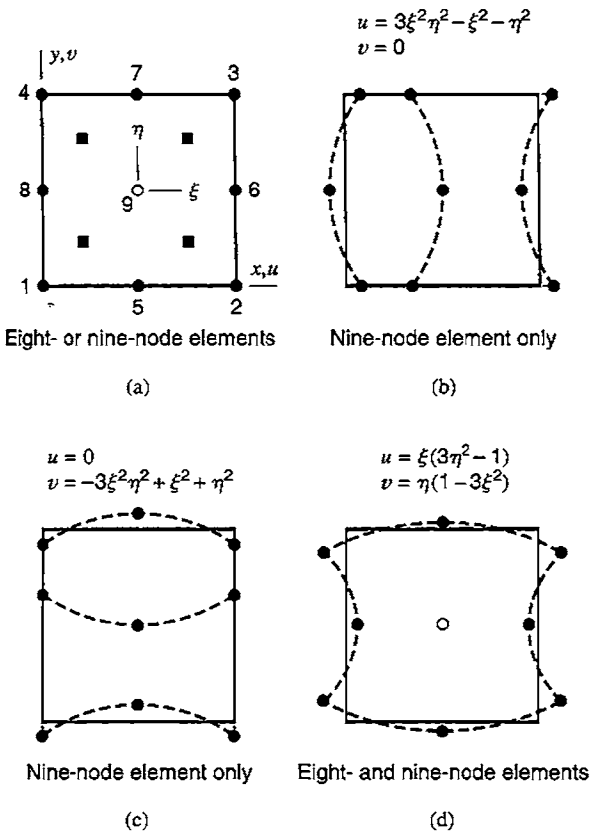

Figure 6.8-3. Spurious modes in plane quadratic elements when a 2 by 2 Gauss rule is used for stiffness matrix integration. Elements shown are initially square. Equations for u and v indicate form, not amplitude.

TABLE 6.8-1 GAUSS QUADRATURE RULES AND SPURIOUS MODES ASSOCIATED WITH THE RESULTING STIFFNESS MATRIX.

	Gauss quadrature rule		Spurious modes from reduced quadrature	
Element type	Full	Reduced	Number	Type
4-node plane	2×2	1-point	2	$\xi\eta$ for u and v
8-node plane	3×3	2×2	1	Fig. 6.8-3d
9-node plane	3×3	2×2	3	Fig. 6.8-3b,c,d
8-node solid	2×2×2	1-point	12	$\xi\eta$, $\eta\zeta$, $\zeta\xi$, $\xi\eta\zeta$ for u, v, w
20-node solid	3×3×3	2×2×2	6	See [3.3,6.12]

results are much better than results provided by four-node elements with one-point quadrature or by nine-node elements with four-point quadrature [6.11]. These results suggest that underintegration may be acceptable if it introduces only noncommunicable spurious modes.

The number of spurious modes in an underintegrated element can usually be counted in the following way. The number of strains sampled at a Gauss point is three in a plane element and six in a solid element. In a reduced but regular rule, which uses the same number of Gauss points in each direction, n-point integration provides $3n$ (plane element; PE) or $6n$ (solid element; SE) items of independent information. If, as usual, the rank of material property matrix $[\mathbf{E}]$ is equal to its order, then the rank of $[\mathbf{k}]$ is $3n$ (PE) or $6n$ (SE). There are 3 (PE) or 6 (SE) possible rigid-body motions. The number of spurious modes is equal to the order of $[\mathbf{k}]$ minus $3n + 3$ (PE) or $6n + 6$ (SE). If $[\mathbf{k}]$ is fully integrated so that there are no spurious modes, some items of information are redundant, and the rank of $[\mathbf{k}]$ is equal to its order minus the number of rigid-body modes. The foregoing way of counting may overestimate the rank of $[\mathbf{k}]$ if different numbers of Gauss points are used in different directions, or if another kind of quadrature is used.

Table 6.8-1 provides selected results related to spurious modes of stiffness matrices integrated by reduced Gauss quadrature. Elements need not be rectangular for these modes to appear. One of the spurious modes of an unsupported 20-node solid element with 2 by 2 by 2 Gauss quadrature is shown in Fig. 6.8-4b. This is an "hourglass" mode like that in

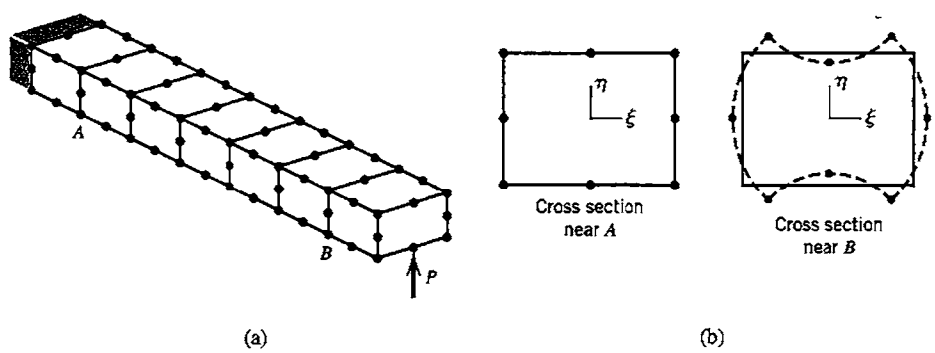

Figure 6.8-4. (a) Cantilever beam modeled by 20-node solid elements. (b) Near-instability is possible far from the fixed end when 2 by 2 by 2 Gauss quadrature is used.

Fig. 6.8-3d, and is communicable in certain meshes. In Fig. 6.8-4a this mode tends to appear at the loaded end, where restraint provided by the fixed support is not strongly felt.

Software providers are obliged to make their products as foolproof as reasonably possible. Therefore underintegration is not often used for stiffness matrices of plane and solid elements, except perhaps the eight-node plane element, whose spurious mode under 2 by 2 Gauss quadrature is noncommunicable. The dangers of underintegration appear to be greatest in dynamics, where "phantom" modes can be confused with physical modes and can provoke substantial error.

Selective Integration and Substitution. For the four-node plane element, an obvious benefit of one-point integration is that the resulting [**k**] is not stiffened by spurious shear strain because bending modes 7 and 8 of Fig. 6.8-1 produce zero shear strain at the element center. To avoid the accompanying defect of spurious modes, one can adopt *selective* integration, which in this case involves use of one Gauss point at $\xi = \eta = 0$ to evaluate the contribution of shear strain to [**k**] while using the usual four Gauss points to evaluate the contribution of normal strains to [**k**]. An alternative, called *selective substitution,* uses the usual four Gauss points for all terms but substitutes shear strain at $\xi = \eta = 0$ in place of actual shear strains at Gauss points. Both schemes, selective integration and selective substitution, pass patch tests, but they differ for an anisotropic material for which [**E**] is a full matrix, which couples all stresses to all strains [3.3]. A disadvantage of both schemes is that they produce elements that are not *frame-invariant* (discussed in Section 3.9). Frame invariance of shear strain is guaranteed by consistent use of the same shape functions for all components of displacement [3.3]. Selective integration and selective substitution are inconsistent. To restore frame invariance, one can add coding to software that supplies a local xy coordinate system whose orientation does not change, or changes by a multiple of 90°, when element nodes are renumbered.

Similar tricks can be applied to plane elements having more than four nodes and to solid elements, but the procedures become increasingly complicated [3.3].

Stabilization. Nonlinear solutions and explicitly integrated dynamic solutions are computationally expensive because they are solved by taking a sequence of many steps, with each step typically demanding the evaluation of element stiffness coefficients. Expense can be reduced substantially by reducing the number of Gauss points per element. Thus, numerical analysts have been prompted to use a minimal number of Gauss points per element and to restrain spurious modes by computationally inexpensive "stabilization" devices. Stabilization is often applied to four-node plane elements, four-node shell elements, and eight-node solid elements, with one-point quadrature used in each case.

A good stabilization scheme is computationally inexpensive, leaves rigid-body and constant-strain modes intact so that elements can pass patch tests, and requires no decisions by the software user. A great many papers have addressed the matter. Variational principles other than minimum potential energy are often used. References include [3.3,6.13–6.15].

6.9 LOAD CONSIDERATIONS

Nodal loads due to force and pressure are discussed in Section 3.11 with restriction to straight edges, side nodes at midsides, and rectangular elements. In the present section

we consider nodal loads due to tractions on curved edges and curved faces, and show how the calculation of nodal loads due to body forces and initial stresses can be incorporated in the numerical integration process that provides the element stiffness matrix. Repeating the basic equation (Eq. 3.3-8), nodal loads $\{\mathbf{r}_e\}$ due to body forces $\{\mathbf{F}\}$ per unit volume, surface traction $\{\mathbf{\Phi}\}$, initial strains $\{\boldsymbol{\varepsilon}_0\}$, and initial stresses $\{\boldsymbol{\sigma}_0\}$, are

$$\{\mathbf{r}_e\} = \int [\mathbf{N}]^T\{\mathbf{F}\}dV + \int [\mathbf{N}]^T\{\mathbf{\Phi}\}dS + \int [\mathbf{B}]^T[\mathbf{E}]\{\boldsymbol{\varepsilon}_0\}dV - \int [\mathbf{B}]^T\{\boldsymbol{\sigma}_0\}dV \qquad (6.9\text{-}1)$$

If an element has incompatible modes, no load terms should be associated with their d.o.f. Thus, load terms for the QM6 element Section 6.6 are the same as those of the Q4 element of Section 6.2. Loads are omitted from incompatible modes so that elements will pass patch tests, which are discussed in Section 6.13.

Edge Traction. Consider, for example, edge $\eta = 1$ of a quadratic element, shown in Fig. 6.9-1a. Applied loads consist of edge-tangent stress τ and edge-normal stress σ. On this edge, shape functions N_i are zero for $i = 1,2,5,6,8$. Therefore the only nonzero contributions from the second integral in Eq. 6.9-1 are associated with nodes 4, 7, and 3, and are

$$\underset{6\times 1}{\{\mathbf{r}_e\}} = \int_{\text{Edge 4-7-3}} \begin{bmatrix} N_4 & 0 & N_7 & 0 & N_3 & 0 \\ 0 & N_4 & 0 & N_7 & 0 & N_3 \end{bmatrix}_{\eta=1}^T \begin{Bmatrix} \Phi_x \\ \Phi_y \end{Bmatrix} t\,ds \qquad (6.9\text{-}2)$$

where t is element thickness and ds is an increment of edge length. Increments of x- and y-parallel force components are

$$\begin{Bmatrix} \Phi_x \\ \Phi_y \end{Bmatrix} t\,ds = \begin{Bmatrix} \tau t\,ds\cos\beta - \sigma t\,ds\sin\beta \\ \sigma t\,ds\cos\beta + \tau t\,ds\sin\beta \end{Bmatrix} = \begin{Bmatrix} \tau\,dx - \sigma\,dy \\ \sigma\,dx - \tau\,dy \end{Bmatrix} t \qquad (6.9\text{-}3)$$

Along edge $\eta = 1$, with substitution of Jacobian terms from Eq. 6.2-4,

$$dx = x_{,\xi}\,d\xi = J_{11}d\xi \qquad \text{and} \qquad dy = y_{,\xi}\,d\xi = J_{12}d\xi \qquad (6.9\text{-}4)$$

Hence Eq. 6.9-2 yields x and y components of nodal load at node i.

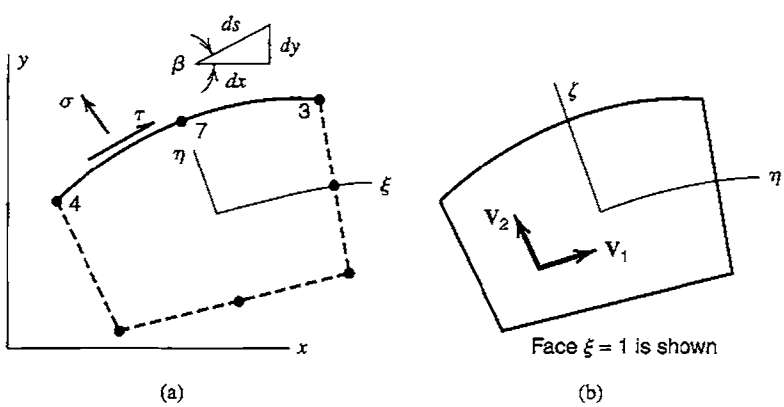

Figure 6.9-1. (a) Prescribed tractions normal and tangent to an edge of a plane element. (b) A face of a solid element, with vectors $\mathbf{V}_1$ and $\mathbf{V}_2$ tangent to the face at an arbitrary point on the face.

$$r_{xi} = \int_{-1}^{1} N_i(\tau J_{11} - \sigma J_{12})t\, d\xi$$
$$r_{yi} = \int_{-1}^{1} N_i(\sigma J_{11} + \tau J_{12})t\, d\xi \tag{6.9-5}$$

where i is 4, 7, or 3, and N_i , t, and Jacobian terms are evaluated on $\eta = 1$. Numerical evaluation of these integrals proceeds in the manner of Eq. 6.3-2.

Surface Traction. To illustrate the method, we consider only a traction σ normal to the $\xi = 1$ face of a hexahedron element. The face need not be plane, and the number of nodes on this face need not enter the argument. The main task is to evaluate the $\{\Phi\}\, dS$ term in Eq. 6.9-1, where dS is an element of area on the face. For this evaluation we need direction cosines of a normal to the face. Let $\mathbf{V} = x\mathbf{i} + y\mathbf{j} + z\mathbf{k}$ be an arbitrary vector on face $\xi = 1$. where $\mathbf{i}$, $\mathbf{j}$, and $\mathbf{k}$ are the usual unit vectors in x, y, and z directions. In Fig. 6.9-1b, face-tangent vectors $\mathbf{V}_1$ and $\mathbf{V}_2$ at an arbitrary point on the face are

$$\mathbf{V}_1 = \frac{\partial \mathbf{V}}{\partial \eta} d\eta = (x,_\eta \mathbf{i} + y,_\eta \mathbf{j} + z,_\eta \mathbf{k})\, d\eta = (J_{21}\mathbf{i} + J_{22}\mathbf{j} + J_{23}\mathbf{k})\, d\eta$$
$$\mathbf{V}_2 = \frac{\partial \mathbf{V}}{\partial \zeta} d\zeta = (x,_\zeta \mathbf{i} + y,_\zeta \mathbf{j} + z,_\zeta \mathbf{k})\, d\zeta = (J_{31}\mathbf{i} + J_{32}\mathbf{j} + J_{33}\mathbf{k})\, d\zeta \tag{6.9-6}$$

Direction cosines l, m, and n of a normal to the face are obtained from the cross product.

$$l\mathbf{i} + m\mathbf{j} + n\mathbf{k} = \frac{\mathbf{V}_1 \times \mathbf{V}_2}{|\mathbf{V}_1 \times \mathbf{V}_2|} = \frac{\mathbf{V}_1 \times \mathbf{V}_2}{dS} \tag{6.9-7}$$

Thus $l\, dS = (J_{22}J_{33} - J_{23}J_{32})\, d\eta\, d\zeta$, and so on. Now $\{\Phi\}\, dS = \lfloor l \;\; m \;\; n \rfloor^T \sigma\, dS$, where $l\,\sigma\, dS$, $m\,\sigma\, dS$, and $n\,\sigma\, dS$ are the x, y, and z components of the normal force increment $\sigma\, dS$, respectively. The x, y, and z components of load at node i are

$$\begin{Bmatrix} r_{xi} \\ r_{yi} \\ r_{zi} \end{Bmatrix} = \int_{-1}^{1}\int_{-1}^{1} N_i \sigma \begin{Bmatrix} J_{22}J_{33} - J_{23}J_{32} \\ J_{23}J_{31} - J_{21}J_{33} \\ J_{21}J_{32} - J_{22}J_{31} \end{Bmatrix} d\eta\, d\zeta \tag{6.9-8}$$

where all shape functions and Jacobian terms are evaluated at $\xi = 1$, and i ranges over all nodes on face $\xi = 1$ ($i = 5,6,7,8$ for the element in Fig. 6.5-1a). Numerical evaluation of Eq. 6.9-8 proceeds in the manner of Eq. 6.3-5.

Body Force and Initial Stress. For a plane problem, in a format suited to numerical integration, Eqs. 6.3-5 and 6.9-1 yield

$$\{\mathbf{r}_e\} = \sum_i \sum_j \left([\mathbf{N}]^T\{\mathbf{F}\} - [\mathbf{B}]^T\{\boldsymbol{\sigma}_0\}\right) t J W_i W_j \tag{6.9-9}$$

The calculation of Eq. 6.9-9 can be fit into Table 6.3-2 as follows.

- At the outset of Table 6.3-2a, clear the array that will contain $\{\mathbf{r}_e\}$; call it RE. In the innermost loop (spanned by indices i and j that identify the current Gauss point) and after the call to the shape function subroutine calculate $\left([\mathbf{N}]^T\{\mathbf{F}\} - [\mathbf{B}]^T\{\boldsymbol{\sigma}_0\}\right)tJW_iW_j$ and add these results to array RE.
- If $\{\mathbf{F}\}$ and $\{\boldsymbol{\sigma}_0\}$ are uniform throughout the element, they can be supplied directly to the foregoing calculation. If instead values of $\{\mathbf{F}\}$ and $\{\boldsymbol{\sigma}_0\}$ are supplied at nodes, append to the shape-function subroutine given in Table 6.3-2b, calculation of their values at the current location by shape function interpolation, in the manner already shown for thickness t.

6.10 STRESS CALCULATION

Stress calculation is also discussed in Section 3.12. In the present section we continue the discussion, with emphasis on techniques useful for numerically integrated elements. Element stresses, as calculated from the element displacement field, are given by the equation

$$\{\boldsymbol{\sigma}\} = [\mathbf{E}]([\mathbf{B}]\{\mathbf{d}\} - \{\boldsymbol{\varepsilon}_0\}) + \{\boldsymbol{\sigma}_0\} \tag{6.10-1}$$

Mechanical strains, associated with element d.o.f. $\{\mathbf{d}\}$, are given by the term $[\mathbf{B}]\{\mathbf{d}\}$, where $\{\mathbf{d}\}$ includes any nodeless d.o.f. that may be present, such as those of elements discussed in Section 6.6. Typically, an initial condition such as a temperature field is included as *either* initial strains $\{\boldsymbol{\varepsilon}_0\}$ *or* initial stresses $\{\boldsymbol{\sigma}_0\}$, but not both. Both might be used if two initial conditions are present simultaneously. Matrix $[\mathbf{B}]$ is a function of the coordinates, so appropriate locations for stress calculation must be chosen. Then $[\mathbf{B}]$ can be calculated from a shape function subroutine as summarized in Table 6.3-2b.

Stresses at Gauss Points. Element Q4 has the defect of displaying spurious shear stress when bent, as shown in Fig. 3.6-3. In Fig. 3.6-3 we see that a vertical line through the element center displays the correct shear stress. If an element were bent by moments applied to the other two opposite sides, the correct shear stress would appear only along a horizontal centerline. These observations suggest that in general use, shear stress in element Q4 should be calculated at the center, $\xi = \eta = 0$, which happens to be the Gauss point location of the lowest order quadrature rule. Similar remarks apply to the basic eight-node hexahedron element.

Spurious shear stress can be avoided in four-node quadrilaterals and eight-node hexahedra by adding incompatible modes (Section 6.6). But for most elements, it often happens that stresses (especially shear stresses) computed according to Eq. 6.10-1 are more accurate at Gauss point locations than elsewhere in an element. Indeed, stresses at $\xi = \eta = 0$ in the Q4 element, and at Gauss points of a four-point rule in the Q8 element, are "superconvergent" in the sense that their accuracy may be comparable to that of computed displacements at these locations, rather than of lower accuracy as is usually the case at other locations. Figure 6.8-2b shows an example of this behavior. This observation does not imply that stiffness matrix integration and stress calculation must use the same order rule. Stresses may be calculated at Gauss points of a lower-order rule than used for integration.

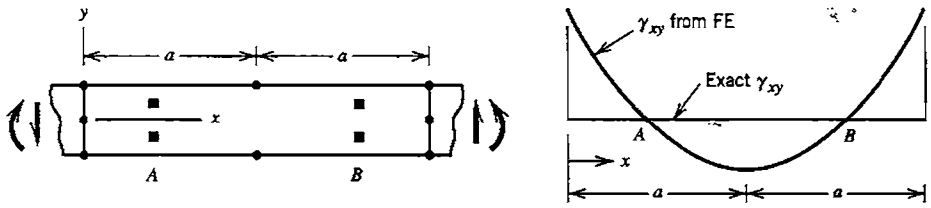

(a) (b)

Figure 6.10-1. (a) Portion of a beam, modeled by an eight-node plane element. Squares indicate Gauss points. (b) Distribution of transverse shear strain along the x axis.

In brief, an analytical argument that locates optimal stress points is as follows [3.3,6.16,6.17]. Impose on an element a complete polynomial displacement field $\{\mathbf{f}_h\}$ whose degree is one higher than the degree of the highest-order *complete* polynomial in the actual element field. For example, impose a complete cubic field on a Q8 element. Obtain nodal d.o.f. $\{\mathbf{d}_h\}$ by evaluating $\{\mathbf{f}_h\}$ at nodal locations. Now seek locations in the element where strains of field $\{\mathbf{f}_h\}$ are the same as strains $[\mathbf{B}]\{\mathbf{d}_h\}$, where $[\mathbf{B}]$ is calculated from the (lower-order) element displacement field. These locations are found to be Gauss point locations in lower-order elements, but slightly different locations in higher-order elements (which are seldom used). As an example, consider Eqs. 4.9-4. Locations at which $du/dx = d\bar{u}/dx$ are at distances $(h/2)/\sqrt{3}$ from the element center. These are Gauss point locations of an order 2 rule.

In Q8 and Q9 elements, which are commonly integrated using four-point and nine-point rules respectively, stresses computed by applying Eq. 6.10-1 at locations of the four-point rule may have only one-tenth the error of stresses computed from the same formula at other locations [6.17]. Figure 6.10-1 shows computed transverse shear strain in a beam modeled by Q8 elements. This strain varies quadratically with x and may be wildly inaccurate except at points A and B, whose x coordinates are those of Gauss points of a four-point rule. This example suggests that strains (or stresses) be calculated at the four Gauss points indicated, then interpolated or extrapolated to other points in the element. Similarly, computed stresses in the analogous 20- or 21-node hexahedron are often most accurate at locations of the eight-point Gauss rule, and can be extrapolated from these points to other element locations.

In Fig. 6.10-1b, we see that γ_{xy} is too large at $x = 0$ and at $x = 2a$. It is also too large at these locations in adjacent elements on either side, so that nodal averaging at shared nodes is of no benefit to accuracy. In this example, ε_x does not behave as badly as γ_{xy} and so would not benefit as much by extrapolation.

Extrapolation Calculations. Imagine that stresses have been calculated at four Gauss points in a plane element (points 1,2,3,4 in Fig. 6.10-2). Dimensionless coordinates r and s are respectively proportional to ξ and η. At (say) point 3, $r = s = 1$ and $\xi = \eta = 1/\sqrt{3}$. Therefore the factor of proportionality is $\sqrt{3}$, so that

$$r = \sqrt{3}\,\xi \qquad \text{and} \qquad s = \sqrt{3}\,\eta \tag{6.10-2}$$

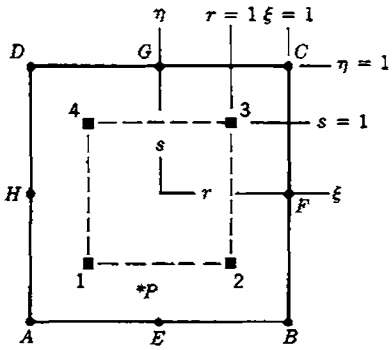

Figure 6.10-2. Reference coordinate systems rs and $\xi\eta$ used in extrapolation of stresses from Gauss points. Squares show Gauss points of a 2 by 2 rule.

Stress at an arbitrary point P in the element can be obtained by the usual shape function formula, with shape functions N_i evaluated at the coordinates of point P:

$$\sigma_P = \sum N_i \sigma_i \qquad \text{for} \qquad i = 1,2,3,4 \tag{6.10-3}$$

where σ is σ_x, σ_y, or τ_{xy}. The N_i are bilinear shape functions as given by Eq. 6.2-3, but with ξ and η replaced by r and s; that is

$$N_1 = \frac{1}{4}(1-r)(1-s), \qquad N_2 = \frac{1}{4}(1+r)(1-s), \qquad \ldots \tag{6.10-4}$$

For example, let us calculate stress σ_x at corner A from the σ_x values at Gauss points 1,2,3,4. We substitute $r = s = -\sqrt{3}$, and obtain from Eq. 6.10-3

$$\sigma_{xA} = 1.866\sigma_{x1} - 0.500\sigma_{x2} + 0.134\sigma_{x3} - 0.500\sigma_{x4} \tag{6.10-5}$$

In a solid element, the formula analogous to Eq. 6.10-3 contains trilinear N_i like those in Eq. 6.5-5, but uses coordinates $r = \sqrt{3}\,\xi$, $s = \sqrt{3}\,\eta$, and $t = \sqrt{3}\,\zeta$. The physical element need not be a square or a cube in order for these formulas to be applied.

Remarks. Stresses at nodes are usually of more interest than stresses at Gauss points, for two reasons. First, nodes appear on surfaces, where stresses are usually higher than at interior locations. Second, elements that share a node usually do not predict the same set of stresses at the shared node, so the discrepancy can be used as a measure of error. In a four-node rectangle (and in an eight-node rectangular hexahedron), stresses calculated directly at a node agree with stresses extrapolated to the node from four (or eight) Gauss points. For general element shapes they disagree, more strongly as element geometry becomes more distorted.

A stress field based on sampling points of an order 2 Gauss rule is a smoothed field. In a quadratic element it is of lower order than the field based on stresses at nodes of a quadratic element. There is no guarantee that the smoothed field will display superior accuracy at locations other than Gauss points. Examining the von Mises stress σ_e (Eq. 3.12-2) at a location of stress concentration and using eight-node quadrilateral elements, Tenchev [6.18] found that the von Mises stress σ_e calculated directly at a node had about one-third the error

of σ_e calculated at the node by extrapolation from four Gauss points. He proposed the following empirical formula. If σ_{eN} and σ_{eG} are respectively the von Mises stresses calculated directly at nodes and by extrapolation to nodes from four Gauss points, then the revised nodal stress, here called σ^*_{eN}, is

$$\sigma^*_{eN} = \frac{\sigma_{eN} + \sigma_{eG}}{3 - \dfrac{\sigma_{eN}}{\sigma_{eG}}} \qquad \begin{array}{l} \text{To be used when } \sigma_{eG} < \sigma_{eN} < 2\sigma_{eG} \\ \text{Otherwise use } \sigma_{eN} \text{ at the node} \end{array} \tag{6.10-6}$$

In test cases using eight-node plane elements, the respective errors of σ^*_{eN}, σ_{eN}, and σ_{eG} are, on average, about 7%, 15%, and 40% [6.18]. The difference between σ_{eN} and σ^*_{eN} could be used as an error measure.

An Alternative Method. Stress calculation that avoids Eq. 6.10-1 has been proposed [6.8]. It starts with calculation of element nodal forces $\{\mathbf{r}\} = [\mathbf{k}]\{\mathbf{d}\}$, in which element d.o.f. $\{\mathbf{d}\}$ are available after global equations have been solved. Then we seek a stress field $\{\boldsymbol{\sigma}\}$ that equilibrates $\{\mathbf{r}\}$, where

$$\{\boldsymbol{\sigma}\} = [\mathbf{P}]\{\boldsymbol{\beta}\} \tag{6.10-7}$$

For example, with a four-node plane quadrilateral, we might adopt the form

$$\begin{Bmatrix} \sigma_x \\ \sigma_y \\ \tau_{xy} \end{Bmatrix} = [\mathbf{P}] \begin{Bmatrix} \beta_1 \\ \beta_2 \\ \vdots \\ \beta_7 \end{Bmatrix} \qquad \text{where} \qquad [\mathbf{P}] = \begin{bmatrix} 1 & x & y & 0 & 0 & 0 & 0 \\ 0 & 0 & 0 & 1 & x & y & 0 \\ 0 & -y & 0 & 0 & 0 & -x & 1 \end{bmatrix} \tag{6.10-8}$$

The β_i are quantities to be determined. Note that these equations are written in a form that satisfies the differential equations of equilibrium, Eqs. 3.1-12 or 3.1-13. Body forces are omitted. Although body forces may produce important loads on the structure, usually they can be ignored on the element level in stress calculation. From Eqs. 6.9-1 and 6.10-7 we obtain

$$\{\mathbf{r}_e\} = -[\mathbf{Q}]\{\boldsymbol{\beta}\} \qquad \text{where} \qquad [\mathbf{Q}] = \int [\mathbf{B}]^T[\mathbf{P}]\, dV \tag{6.10-9}$$

For a four-node quadrilateral, $[\mathbf{B}]$ is 3 by 8 and $[\mathbf{Q}]$ is therefore 8 by 7. The nodal equilibrium equation is $\{\mathbf{r}\} + \{\mathbf{r}_e\} = \{\mathbf{0}\}$, from which we solve for $\{\boldsymbol{\beta}\}$. If this equation is written for a four-node plane element, with $[\mathbf{P}]$ given by Eq. 6.10-8, the equation system is overdetermined (more equations than unknowns). Seeking a least-squares fit of the β_i, we solve for $\{\boldsymbol{\beta}\}$ from the equation

$$[\mathbf{Q}^T\mathbf{Q}]\{\boldsymbol{\beta}\} = [\mathbf{Q}]^T\{\mathbf{r}\} \qquad \text{where} \qquad \{\mathbf{r}\} = [\mathbf{k}]\{\mathbf{d}\} \tag{6.10-10}$$

Finally we return to Eq. 6.10-7 to obtain element stresses. The reader may recognize Eqs. 6.10-7 and 6.10-8 from the assumed-stress hybrid formulation discussed in Section 4.10.

Stresses $\{\boldsymbol{\sigma}\} = [\mathbf{P}]\{\boldsymbol{\beta}\}$ may be more accurate than stresses determined from Eq. 6.10-1 because nodal forces equilibrate loads applied to the element, and may have little error even if poor element shapes render Eq. 6.10-1 inaccurate, or if overly stiff element formulations cause computed displacements to be underestimated (as in Fig. 3.6-3). From the latter possibility we infer that stresses $\{\boldsymbol{\sigma}\} = [\mathbf{P}]\{\boldsymbol{\beta}\}$ may be overestimated if an overly stiff structure is loaded by prescribed displacements rather than by forces.

To accommodate thermal stresses in the calculation $\{\boldsymbol{\sigma}\} = [\mathbf{P}]\{\boldsymbol{\beta}\}$, an ad hoc procedure has been suggested [6.8]. For example, in a plane problem let temperature change T have the form

$$T = a_1 + a_2 x + a_3 y \tag{6.10-11}$$

where the a_i are constants. Let the material be isotropic. Assume that dimensional changes are unrestrained and that no shear strain develops. Hence, displacements can be obtained by integration of Eqs. 3.1-7 and 3.1-8 with $\gamma_{xy} = \gamma_{yz} = \gamma_{zx} = 0$. Thus, using Eq. 6.10-11, with α the coefficient of thermal expansion,

$$u = \alpha\left(a_1 x + \frac{1}{2}a_2 x^2 + a_3 xy - \frac{1}{2}a_2 y^2\right) \quad v = \alpha\left(a_1 y + a_2 xy + \frac{1}{2}a_3 y^2 - \frac{1}{2}a_3 x^2\right) \tag{6.10-12}$$

These displacements are evaluated at element nodes, providing a vector of nodal displacements $\{\mathbf{d}_T\}$. Element nodal forces in Eq. 6.10-10 are then computed as $\{\mathbf{r}\} = [\mathbf{k}](\{\mathbf{d}\} - \{\mathbf{d}_T\})$ rather than as simply $\{\mathbf{r}\} = [\mathbf{k}]\{\mathbf{d}\}$. Results of test cases appear in [6.8].

6.11 EFFECT OF ELEMENT GEOMETRY

Computed results become less accurate when element shapes are distorted from being compact and straight-sided. Here "distortion" refers to *initial* element shape, before loading creates displacements. Only for large-displacement nonlinear problems might displacements be so great as to change element shapes from good to bad. In linear analysis, which is much more common, analysis is based on *original* geometry. Test cases can be used to display the extent of accuracy loss due to element distortion. Cases presented here emphasize the bending capability of elements and may not fairly represent element capabilities in other situations.

Figure 6.11-1 shows the effect of distortion on four-node elements integrated by four-point Gauss quadrature. Units are omitted, as they are unnecessary for our purpose. At corner B, the exact axial stress is $\sigma_{xB} = 300$. At the middle of the lower side of the leftmost square element, where $x = 1$, the exact axial stress is $\sigma_x = 270$, and here the QM6 element is exact. With transverse shear deformation included, beam theory yields the lateral tip deflection $v_C = 1.031$. We see that QM6 elements suffer less from distortion than do Q4 elements, and that the effect of distortion is to stiffen elements.

A similar test case is reported in Table 6.11-1, where eight- and nine-node elements are used. Point B is a Gauss point of a 2 by 2 quadrature rule. Load P is allocated to nodes on the right end in the proportion 1:8:1, which is consistent with a parabolic distribution of transverse shear force. In the trapezoidal-element case two corner nodes are moved, to

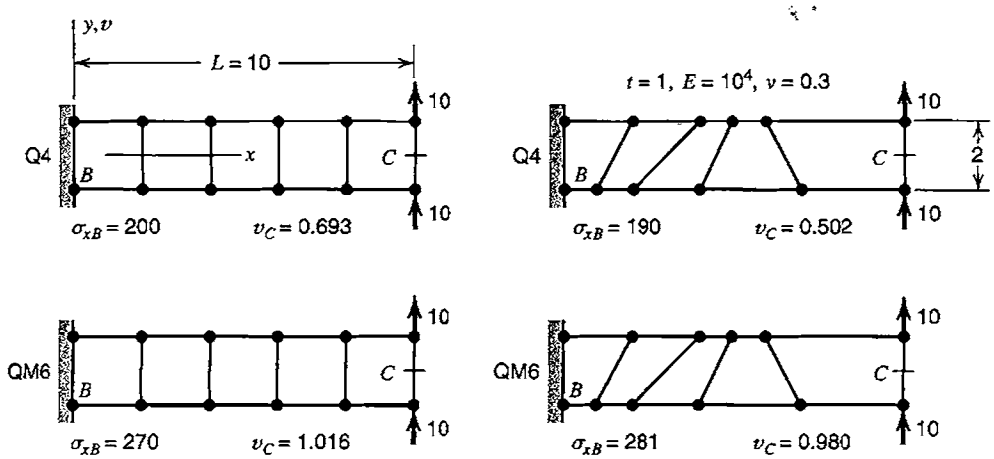

Figure 6.11-1. Stresses and deflections in FE models of a cantilever beam. Four-node elements and four-point Gauss quadrature are used. Exact $\sigma_{xB} = 300$; exact $v_C = 1.031$.

$3L/4$ on top and to $L/4$ on the bottom. In the curved-side case, one side node is moved a distance $L/20$ to the left. Side nodes are at midpoints of sides. Computed results are reported as fractions of correct values according to beam theory with transverse shear deformation neglected. We see that elements are stiffened by distortion and by an increase in the order of Gauss quadrature.

If elements are rectangular and side nodes (if included) are at midsides, and if coordinate systems $\xi\eta\zeta$ and xyz are parallel, then displacement fields such as Eq. 6.4-2 have the same form in both coordinate systems. Because Eqs. 6.4-2 include all quadratic terms, we

TABLE 6.11-1 STRESSES AND DEFLECTIONS IN TWO-ELEMENT CANTILEVER BEAMS UNDER TRANSVERSE TIP LOAD P. EXACT VALUES BY BEAM THEORY ARE UNITY (NEGLECTING TRANSVERSE SHEAR DEFORMATION).

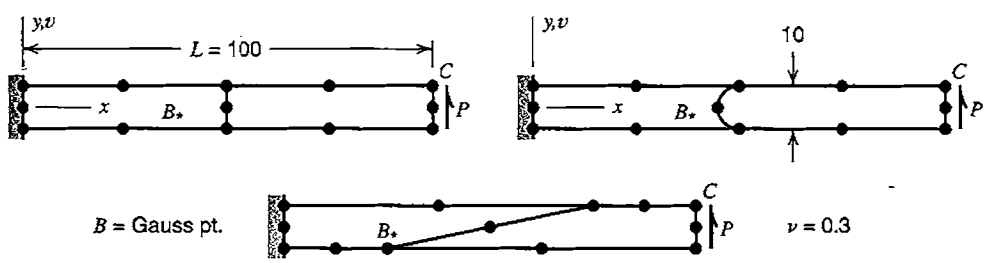

Element type, integration rule	Rectangular elements σ_{xB}	Rectangular elements v_C	Trapezoidal elements σ_{xB}	Trapezoidal elements v_C	Curved sides σ_{xB}	Curved sides v_C
8-node, 2×2	1.000	0.968	0.051	0.362	−0.048	0.430
8-node, 3×3	1.129	0.930	0.048	0.161	0.050	0.221
9-node, 2×2	1.000	1.006	1.125	1.109	0.958	0.955
9-node, 3×3	1.141	0.954	0.687	0.791	0.705	0.737

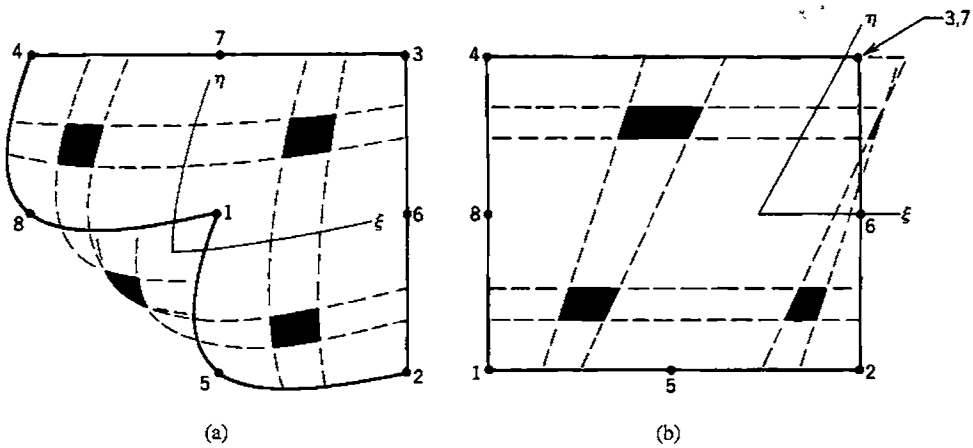

Figure 6.11-2. Badly shaped eight-node elements. Gauss points of a 2 by 2 rule are bounded by dashed lines of constant ξ and constant η. (a) Node 1 is moved to the center of the original rectangle. (b) Node 7 is moved from top midside to corner 3.

expect the element to be capable of modeling pure bending exactly, and such is indeed the case if elements are rectangular. For the eight-node element this capability is lost if corner angles depart from 90°, if sides are curved, and/or if side nodes are not at midsides. The nine-node plane element is similarly affected by side node placement, but not by angular distortion alone.

Analysis [6.19,6.20] shows that shape distortion may render an element capable of exactly displaying only a linear field. Thus, only constant-strain fields can be represented exactly. This does not mean that distortion reduces an isoparametric element to the level of a constant-strain triangle. Higher-order displacement modes continue to be present, but can represent the desired field only approximately. Performance improves as higher-order modes are added, as seen in Table 6.11-1.

Table 6.11-1 suggests that 2 by 2 integration is preferable to 3 by 3 integration, for both eight- and nine-node elements. Such is not necessarily the case; see Section 6.8.

Extreme shape distortions are shown in Fig. 6.11-2. In each of these two examples, a Gauss point lies outside the element, and the Jacobian J is negative there. An acceptably shaped element should not display negative J at any Gauss point location. Indeed, in a well-shaped element J does not change much from one location to another. If badly shaped elements are surrounded by elements of reasonable shapes, one expects that computed results will be locally poor but acceptable not far away, in accord with Saint-Venant's principle.

Practical Implications. Computed results are most accurate when elements are compact and straight-sided. Increasing elongation, nonrectangularity, side curvature, and off-centering of side nodes are all likely to increase error. There is rarely a need to locate a side node other than at midside. Although an element side may be curved in order to fit a curved boundary, other element sides (internal to the mesh) should remain straight.

Commercial software commonly checks the geometry of each element [6.21]. Before analysis begins, elongation and other geometric distortions can be examined and each assigned a numerical value. Depending on where the numerical values appear in empirically devised scales, an element can be accepted without comment by the software, or the user might be warned of a poor shape, or the software may refuse to continue with analysis until shapes it considers unacceptable are corrected. The "poor shape" threshold may be

high, so that software may accept elements having great enough distortion to introduce significant errors.

Additional remarks pertinent to element geometry appear in Sections 10.3 and 10.14.

6.12 VALIDITY OF ISOPARAMETRIC ELEMENTS

In a sufficiently small region of a continuum, strain variations become negligible in comparison with mean values of strain. Accordingly, if computed FE results are to converge toward exact results as a mesh is refined ad infinitum, each element must be capable of displaying constant states of strain. We wish to show that isoparametric elements have this capability [6.22]. In more general terms, we wish to show that isoparametric elements have the ability to represent constant gradients of the field quantity.

Let $\phi = \phi(x,y,z)$ be a linear field in Cartesian coordinates, specifically

$$\phi = a_1 + a_2 x + a_3 y + a_4 z \tag{6.12-1}$$

where the a_i are constants. This form is representative of displacement u, v, or w in a field of constant strain. Thus a_1 is associated with rigid-body translation and the remaining a_i are associated with constant strain and/or rigid-body rotation. Let this field be evaluated at specific points i, to provide specific field values $\phi_i = \phi(x_i,y_i,z_i)$. If points i are nodes of an element, the ϕ_i are nodal d.o.f. Within the element,

$$\phi = \sum N_i \phi_i \tag{6.12-2}$$

We will show that Eqs. 6.12-1 and 6.12-2 provide the same field. Thus we show that when nodal d.o.f. consistent with a constant gradient are imposed, an isoparametric element displays that state. As the first step of the argument, we evaluate Eq. 6.12-1 at nodes i and substitute into Eq. 6.12-2. Thus

$$\phi = a_1 \sum N_i + a_2 \sum N_i x_i + a_3 \sum N_i y_i + a_4 \sum N_i z_i \tag{6.12-3}$$

But, if the element is isoparametric, coordinates are interpolated in the same way as ϕ, that is

$$x = \sum N_i x_i \qquad y = \sum N_i y_i \qquad z = \sum N_i z_i \tag{6.12-4}$$

Therefore, if $\sum N_i = 1$, Eq. 6.12-2 reduces to Eq. 6.12-1 as claimed. To see that $\sum N_i = 1$, we note that Eqs. 6.12-4 are applicable regardless of where the element is located in Cartesian coordinates xyz. Imagine that there is a second Cartesian system XYZ, translated along the x axis a distance h, so that $x = X + h$. Hence

$$x = \sum N_i x_i = \sum N_i X_i + h \sum N_i = X + h \sum N_i = (x - h) + h \sum N_i \tag{6.12-5}$$

from which we obtain $h = h \sum N_i$ and therefore conclude that $\sum N_i = 1$.

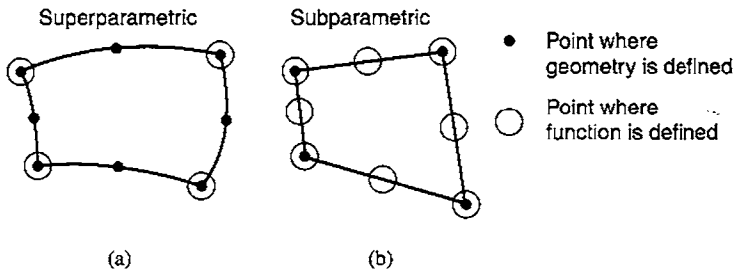

Figure 6.12-1. Examples of superparametric and subparametric plane elements.

The foregoing argument says nothing about accuracy in a coarse mesh, rate of convergence with mesh refinement, or the extent to which element distortion reduces the efficacy of higher-order terms in the approximating field. It shows only that the approximating field of an isoparametric element contains a complete linear polynomial, which is necessary for convergence toward exact results as a mesh is refined. It is also necessary that elements are either compatible or become compatible as a mesh is refined. All these requirements are checked by the patch test discussed in Section 6.13.

Superparametric and Subparametric Elements. These elements are defined in Section 6.1. Examples appear in Fig. 6.12-1. The foregoing argument fails for a superparametic element. For the element in Fig. 6.12-1a, each summation in Eq. 6.12-3 spans four terms, while each summation in Eq. 6.12-4 spans eight terms. Reduction to Eq. 6.12-1 is not obtained. In stress analysis this means that a superparametric element cannot represent a state of constant strain. Moreover, because displacement gradients also define rotation, a superparametric element will display strain when asked to undergo rigid body rotation. An inability to display rigid-body motion may be disastrous.

For the subparametric element in Fig. 6.12-1b, each summation in Eq. 6.12-3 spans eight terms, while each summation in Eq. 6.12-4 spans four terms. At first glance it appears that reduction to Eq. 6.12-1 is not obtained. However, we do indeed obtain Eq. 6.12-1: with straight sides and side nodes at midsides, four-node and eight-node interpolations define the same geometry, as may be checked by use of Eqs. 6.4-1 with $x_5 = \frac{1}{2}(x_1 + x_2)$, $y_5 = \frac{1}{2}(y_1 + y_2)$, and so on. With geometry restricted in this way, the eight-node element becomes the subparametric element of Fig. 6.12-1b. Subparametric mapping allows exact representation of some states that would only be approximated with isoparametric mapping. Thus, with a ninth node added, at $\xi = \eta = 0$ so that geometric mapping is unchanged, the element in Fig. 6.4-1a can exactly represent linearly-varying states of strain; the element in Fig. 6.4-1b cannot.

6.13 PATCH TEST

Imagine that a problem is solved repeatedly, each time using a finer FE mesh. Will the sequence of solutions converge toward exact displacements, strains, and stresses? The answer is *yes* provided that the elements used pass *patch tests,* which ask if an assembly of elements can display a constant state of strain.

The patch test was originated by Irons and has since been analyzed, discussed, and reinterpreted at length [3.3,6.6]. Here we describe a "numerical experiment" form of the patch test. It is easily applied using software into which the element has been coded. Because

software typically reports stresses rather than strains, we can examine computed stresses, which are directly proportional to their associated strains if the material is isotropic, Poisson's ratio is zero, and stresses are computed as $\{\boldsymbol{\sigma}\} = [\mathbf{E}]\{\boldsymbol{\varepsilon}\}$. Although the patch test is performed using specific (but arbitrary) element geometries, passing the test is sufficient to guarantee that, when the element is used in other shapes and in other problems, computed results will converge toward exact results with mesh refinement (provided that the element is stable; see subsequent discussion).

Procedure. To perform a patch test, one builds a simple FE model, that is, a "patch" of elements, such that at least one node is internal to the patch (rather than on its boundary). The patch is provided with just enough support to prevent rigid-body motion. Element shapes should be irregular because some element types pass the test if they are rectangular but fail otherwise. The boundary of the patch can be a rectangle, with uniformly spaced nodes if desired. To one or more boundaries of the patch, we apply work-equivalent nodal loads (Section 3.11) consistent with a state of constant stress. Incompatible modes, if present, are ignored in determining these loads. A node internal to an element, if present, is neither loaded nor restrained. An example of a loaded patch of four-node plane elements appears in Fig. 6.13-1a. The roller support on the left edge permits Poisson-effect strain ε_y. If ν is not zero, it would be incorrect to prohibit y-direction motion at both of the supports shown. The choice of uniform nodal spacing along left and right edges makes it easy to determine the nodal loads $F = \frac{1}{2}(\sigma_x H t)$ shown, which are consistent with uniform uniaxial stress σ_x in a plane body of uniform thickness t. One computes results for the patch model as if it were any other FE model. Exact results are the value of σ_x used to determine loads F and zero for all other stresses. If computed results are correct at all points, say at all corners of each element, the patch test is passed. By "correct" we mean exact to the limit of computer accuracy.

One can also test a plane patch for proper calculation of constant σ_y and constant τ_{xy}. A patch of solid elements should be able to properly display each of the six constant stresses. Elements for plate bending analysis should be able to display constant bending moments M_x and M_y and constant twisting moment M_{xy}.

One might also examine computed nodal displacements. If these are correct but stresses are not, one suspects that the stress calculation algorithm is in error.

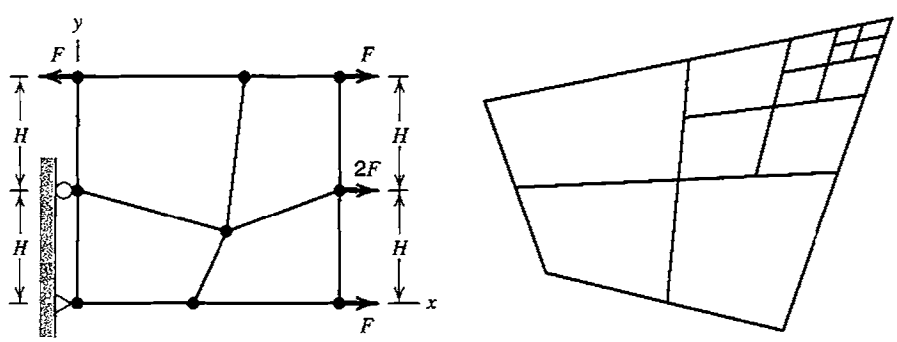

Figure 6.13-1. (a) A patch test for σ_x in plane four-node elements. (b) Repeated subdivision of a trapezoid produces parallelograms.

Stability. It is possible for an element to pass a patch test even though it is unstable because it contains a spurious mode. Typically, the cause of element instability is use of too few Gauss points for integration of $[\mathbf{k}]$. If a patch of elements contains an instability, software should complain that a zero pivot was encountered in attempting to solve the equation system $[\mathbf{K}]\{\mathbf{D}\} = \{\mathbf{R}\}$. One can also detect instability by perturbing the loads used in a patch test. Instability is present if a small change in the magnitude of a load produces a large change in computed nodal displacements. As another alternative, eigenvalues of $[\mathbf{K}]$ for the patch can be extracted. All should be positive if the patch is just-adequately supported against rigid-body motion. A zero eigenvalue then indicates the presence of a spurious mode (see Sections 6.8 and 8.10).

"Weak" Patch Test. Conceivably, a sequence of mesh refinements will produce convergence toward exact results even when the elements used fail a patch test. This is possible if elements are formulated in a such way that they fail patch tests when they are of general shape, but pass if they are parallelograms or parallelepipeds. Correct convergence is possible because repeated subdivision of arbitrary shapes eventually creates parallelograms and parallelepipeds (Fig. 6.13-1b). An element that passes a patch test when it has a shape that results from repeated mesh subdivision, for which the Jacobian J becomes essentially constant over the element, is said to have passed a "weak" patch test. Clearly there are practical difficulties in conducting a weak patch test [6.23].

Remarks. As described above, the patch test examines only states of constant stress or strain. A test for correct representation of a more complicated state such as linear variation of stress or strain is called a "higher-order" patch test. An FE model of a prismatic beam loaded in pure bending constitutes a higher-order patch test.

A stable element that passes the patch test is able to display (a) rigid-body motion without strain, (b) states of constant strain, and (c) compatibility with adjacent elements when a state of constant strain prevails in adjacent elements. Meeting these requirements is sufficient to guarantee that a mesh of these elements will converge to exact results in problems other than a patch test as the mesh is refined ad infinitum [6.6].

Passing constant-strain patch tests shows that an element is valid in the sense that there is proper convergence with mesh refinement. The test says nothing about how well an element works in other applications. An element that passes may display poor accuracy in a coarse mesh or display slow convergence with mesh refinement.

For the developer of new elements, patch tests are essential. They have shown that suspect formulations such as some incompatible or underintegrated elements are in fact valid. The student of FEA and the practitioner learning to use new software may also find patch tests useful because they are simple, input data is easy to prepare, and exact results are known.

6.14 A 2D APPLICATION

A square plate of uniform thickness contains a central circular hole. Geometry and elastic properties are depicted in Fig. 6.14-1a. Uniform pressure p acts on the boundary of the hole, and plane stress conditions prevail. Magnitudes and locations of significant principal stresses are to be determined.

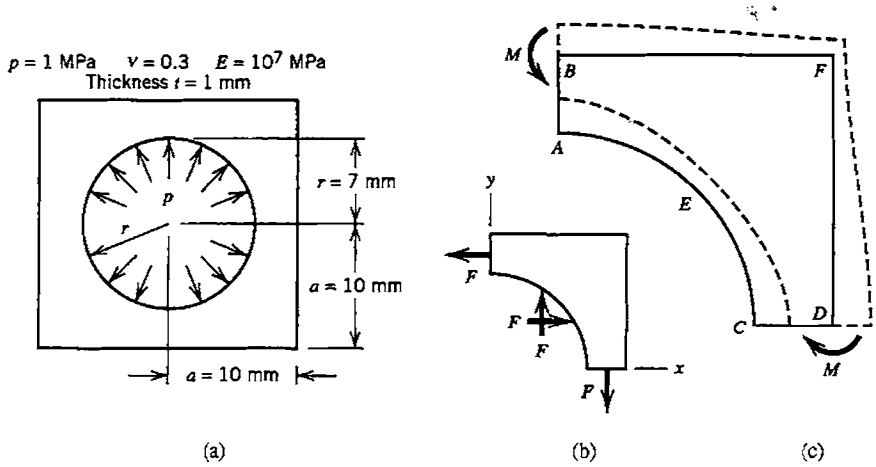

Figure 6.14-1. (a) Flat plate with central hole loaded by uniform pressure. (b) Forces that act on one quadrant. (c) The anticipated displaced shape, greatly exaggerated, is shown by dashed lines.

Preliminary Analysis. Before undertaking FE analysis we examine the problem in a physical way and make simple calculations, in order to anticipate where stresses will be largest, prepare a good FE model, and obtain approximate results for subsequent comparison with FE results.

Geometry, elastic properties, and loading are all symmetric with respect to both horizontal and vertical centerlines. Deflections and stresses have these same symmetries, so analysis can be restricted to a single quadrant. Forces F that act on a representative quadrant are shown in Fig. 6.14-1b. Using statics, we easily calculate the exact value of F. The average normal stress on horizontal and vertical cross sections then follows.

$$F = prt = 7\,\text{N} \qquad \text{and} \qquad \sigma_{\text{ave}} = \frac{F}{(a-r)t} = 2.3\,\text{MPa} \tag{6.14-1}$$

Deformations will be symmetric with respect to horizontal and vertical centerlines, and we expect that pressure will push the slender parts further outward than the more massive corners. Thus we anticipate the displaced shape shown in Fig. 6.14-1c. We see that slender parts have acquired inward curvature, which must be associated with bending moments M in the directions shown. Resulting flexural stresses will be tensile on the outside, compressive on the inside, and will add algebraically to σ_{ave} of Eq. 6.14-1. Hence it appears that the principal stresses sought may appear at B and D rather than at A and C. But there is another possibility. Because arc AEC bends outward, there will be tensile flexural stress at E. Therefore points B, E, and D are all candidates for locations of the normal stress of greatest magnitude.

Finite Element Analysis. Our mathematical model is the geometric shape shown in Fig. 6.14-1a, with internal pressure loading, and with behavior described by plane theory of elasticity. We might elect to model only one octant, because diagonals are also axes of symmetry. We elect instead to model a quadrant, because support conditions are more straightforward and computed results can be checked for anticipated symmetries about a diagonal. For the sake of illustration, we deliberately choose a *very coarse* mesh

of four-node QM6 elements for the *initial* FE analysis, fully expecting to use information it provides in a second analysis. The model and its boundary conditions are shown in Fig. 6.14-2a. The mesh is symmetric about diagonal EF and is most coarse near corner F where stress gradients are expected to be low. Having stated to the software used that the problem is plane and QM6 elements are to be used, nodal translations w_i and all rotational d.o.f. are suppressed automatically. The only boundary conditions that the user need impose explicitly are $u_i = 0$ at nodes i along AB and $v_i = 0$ at nodes i along CD. Nodal loads due to pressure p along AEC are calculated automatically.

Critique of Results. Computed displacements are examined first, scaled up so as to be easily visible, and animated on the monitor. We see that nodes along AB have only y-direction displacement, nodes along CD have only x-direction displacement, all displacements are symmetric about diagonal EF, and the anticipated displaced shape prevails (shown by dashed lines in Fig. 6.14-1c). These results are appropriate to the model we intended to describe to the software, so no blunder is yet in evidence. For a more precise inspection, the list of nodal displacements is inspected. For the symmetric mesh used, symmetries such as $v_A = u_C$ appear with many digits of accuracy.

Discussion of maximum magnitudes of normal stress is postponed until results from a finer mesh have been obtained. For now, using the coarse mesh, we examine contours of the von Mises stress σ_e (Eq. 3.12-2). Contours plotted from nodal average stresses and from element-by-element (unaveraged) stresses are plotted in Figs. 6.14-2b and 6.14-2c. As expected, contours of σ_e are symmetric about diagonal EF. Aside from reflecting the coarseness of the mesh, averaged contours give little indication that results are unreliable. But unaveraged contours show *severe* interelement discontinuities. Interelement changes in stress are comparable to the stresses themselves! It is now obvious that the coarse-mesh results are not to be trusted.

The quadrant is now modeled by a finer mesh, again using four-node QM6 elements. This time, just to see what happens, the mesh is made asymmetric about the diagonal. (We remark that automated meshing tools in software, not used in this example problem, often do not recognize or exploit structural symmetries.) Elements are smallest near points A, B, C, D, and E, where larger stresses and stress gradients are expected. Elements near E are more slender in the radial direction because Fig. 6.14-2 suggests that stress gradients are much larger in the radial direction than in the circumferential direction. The displaced

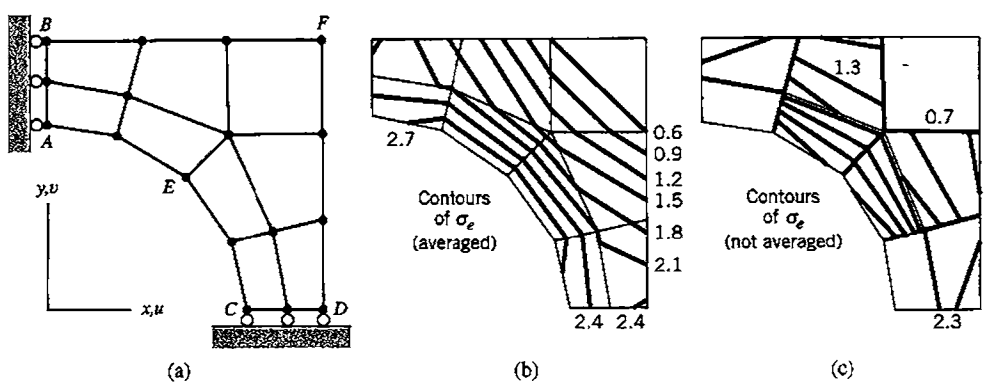

Figure 6.14-2. (a) Coarse-mesh FE model, showing boundary conditions. (b) Contours of von Mises stress σ_e, from nodal averages, in MPa. (c) Contours of σ_e, without nodal averaging, from individual elements.

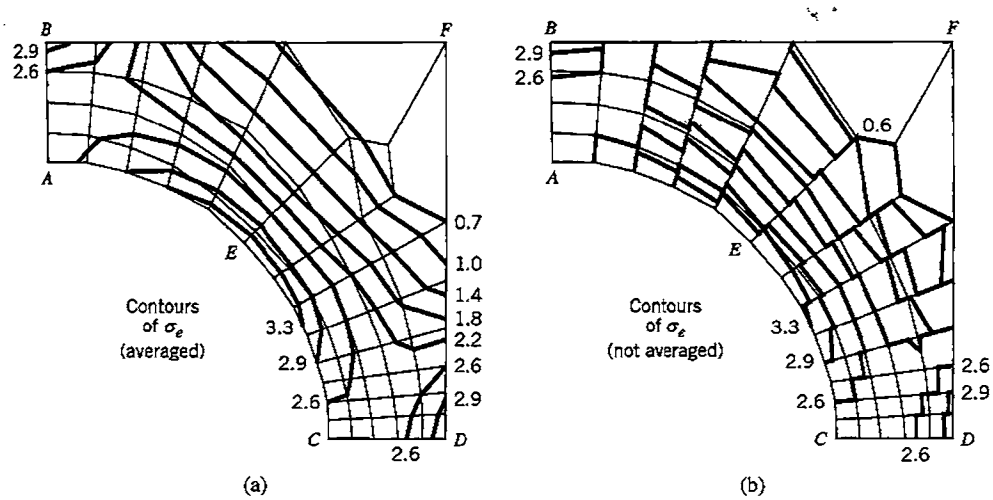

Figure 6.14-3. Contours of von Mises stress σ_e from a finer mesh, in MPa. (a) From nodal average stresses. (b) Without nodal averaging, from individual elements.

shape again appears satisfactory. The list of nodal displacements shows that deformation is not quite symmetric about the diagonal, owing to asymmetry of the mesh. Averaged and unaveraged plots of von Mises stress σ_e are shown in Fig. 6.14-3. Results are greatly improved over the coarse mesh, but unaveraged contours still have significant interelement discontinuity. Even averaged contours show appreciable changes in direction where they cross some interelement boundaries. Also, σ_e contours do not intersect lines of symmetry *AB*, *CD*, and *EF* at right angles. All this suggests a need for even more mesh refinement.

Numerical results from both meshes are listed in Table 6.14-1. These numbers are obtained directly from output files, not by visual inspection of displacement plots and stress plots. Displacement results are reasonable. They show that dimensions *AB* and *CD* have contracted, as should be expected from the combination of compressive radial loading and the Poisson effect with circumferential tension. Computed displacements show that the finer mesh is the more flexible of the two. Such is usually the case but cannot be guaranteed because QM6 elements are incompatible. At corner *F*, where stresses are zero

TABLE 6.14-1 DISPLACEMENT AND MAXIMUM PRINCIPAL STRESS AT SELECTED POINTS IN FIG. 6.14-2 (COARSE MESH) AND FIG. 6.14-3 (FINER MESH). UNITS: mm FOR DISPLACEMENT, MPa FOR STRESS.

Node	Coarse mesh			Finer mesh		
i	$10^6 u_i$	$10^6 v_i$	σ_1	$10^6 u_i$	$10^6 v_i$	σ_1
A	0	2.08	2.11	0	2.28	1.92
B	0	1.78	2.28	0	1.96	3.01
C	2.08	0	2.11	2.34	0	1.84
D	1.78	0	2.28	2.01	0	3.12
E	1.22	1.22	2.68	1.27	1.24	3.16
F	0.97	0.97	0.38	0.98	1.00	0.21

according to theory, computed stresses are small and decrease with mesh refinement, as expected. At a point such as A, σ_x (not shown in Table 6.14-1) is *almost* equal to maximum principal stress σ_1 at A. Theoretically, $\sigma_x = \sigma_1$ at A. The discrepancy is due to τ_{xy}, which is small but not quite zero as theory says it should be on an axis of symmetry. The average normal stress from points A and B or C and D is in satisfactory agreement with Eq. 6.14-1. The largest principal stress σ_1 anywhere in the structure is at B and D or at E and has a numerical value of about 3.1 MPa. We cannot be sure of the location or the stress without further mesh refinement.

An error measure for the stress field, discussed in Section 9.10, gives $\eta = 0.373$ for the coarse mesh and $\eta = 0.183$ for the finer mesh. Because $\eta < 0.05$ is desired, these measures also indicate a need for further refinement. The next mesh should build on information in Fig. 6.14-3 by making elements smallest where stresses and stress gradients are largest. By plotting a particular stress or a particular displacement versus element size, as obtained from two or more meshes, one can extrapolate to zero element size, and thus obtain a predicted result for infinite mesh refinement (Section 9.7). Thus the percentage error of a result from a given mesh can be estimated.

We may now admit that FEA is probably not needed for this problem. Reference 6.24 provides experimentally-determined factors from which we obtain $\sigma_1 = 2.9$ MPa at B and D and $\sigma_1 = 2.7$ MPa at E. It is prudent to ask at the outset if a computational solution is really needed, as it is not a trivial task.

6.15 A 3D APPLICATION

A curved beam of uniform trapezoidal cross section is bent in its own plane by moments M (Fig. 6.15-1). Although structure geometry is generated by revolving the cross section about an axis of revolution, the problem is not axisymmetric because displacements have circumferential components as well as radial and axial components. Accordingly, analysis uses 3D solid elements rather than solid of revolution elements. Structure geometry can nevertheless be described in cylindrical coordinates.

We seek stresses of greatest magnitude for the trapezoidal cross section shown in Fig. 6.15-2a. Stresses in the curved beam do not vary with θ, so only a typical slice between two closely-spaced radial planes need be analyzed (Fig. 6.15-2b). Bending moment M must be applied indirectly because we do not know in advance what circumferential stresses it produces and therefore cannot apply appropriate nodal loads. Instead we will prescribe *displacements,* such that radial plane sections remain plane

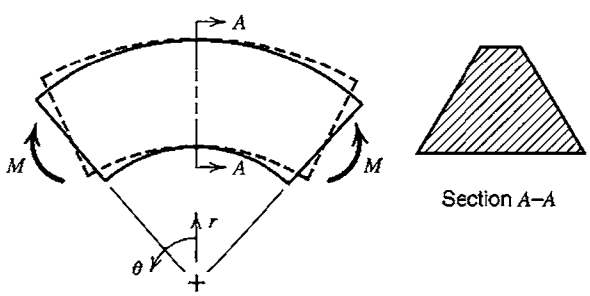

Figure 6.15-1. A curved beam of trapezoidal cross section, bent in its own plane by moments M. The deflected shape is shown by dashed lines.

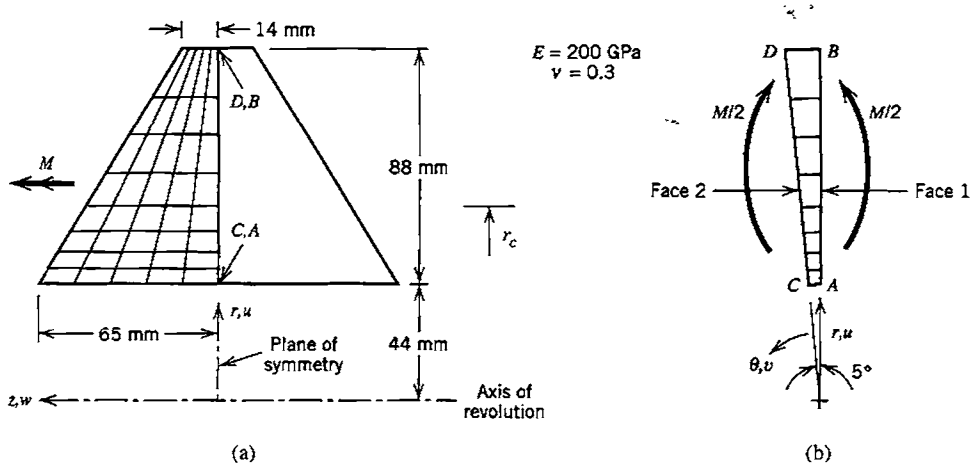

Figure 6.15-2. (a) Cross section of the curved beam. The FE mesh is needed in only the left half. (b) The FE model viewed parallel to the axis of revolution.

and moment load is applied without accompanying net force. From computed stresses we will determine M. Stresses associated with a prescribed moment M_p can then be determined by multiplying computed stresses by the ratio M_p/M.

Preliminary Analysis. The simplest approximate solution comes from the straight-beam flexure formula $\sigma = Mc/I$, which yields $\sigma = 8.94(10^{-6})\,M$ at the inside edge, in MPa if M is in N • mm. A formula for circumferential stress in a curved beam is readily available [1.16,2.6]. It yields, at the inside edge,

$$\text{Curved beam theory, along } r = 44 \text{ mm:} \quad \sigma_\theta = 13.46(10^{-6})M \tag{6.15-1}$$

in MPa if M is in N • mm. We will return to this result for comparison with FE results after M is known. Might Eq. 6.15-1 be adequate? Perhaps, but FEA may show otherwise. An assumption underlying the curved beam formula is that a cross section does not distort in its own plane, so that stresses do not vary in the z direction, parallel to the axis of revolution. FEA contains no such restriction and may therefore provide different results.

Finite Element Analysis. Our mathematical model is the wedge between faces 1 and 2 in Fig. 6.15-2b, with displacements to be prescribed on these faces, and with behavior described by 3D theory of elasticity. There is symmetry about a z-constant plane that contains points $ABCD$ (Fig. 6.15-2), so only half the cross section need be meshed. Curved beam theory predicts that stress gradients will be highest on the edge nearest the center of curvature. Accordingly the mesh is graded so that elements nearer the inner edge span a smaller radial distance. In Fig. 6.15-2b, face 1 and its nodes are merely rotated 5° to produce face 2. The slice between faces 1 and 2 contains a single layer of straight-sided eight-node solid elements, each containing nine internal d.o.f. a_i (Eq. 6.6-1). As boundary conditions, nodal d.o.f. in radial, circumferential, and axial directions are prescribed as follows:

Face 1	Face 2
$u = 0$ at node A	
$v = 0$ at all nodes	$v = 0.0001(r_c - r)$ at all nodes
$w = 0$ at nodes along AB	$w = 0$ at nodes along CD

All remaining nodal d.o.f. are unrestrained. Setting $u = 0$ at A prevents rigid body motion in the r direction, and setting $v = 0$ at all nodes on face 1 prevents circumferential motion of face 1. Setting $w = 0$ at nodes on $ABCD$ imposes symmetry about the middle $r\theta$ plane. The expression $v = 0.0001(r_c - r)$, where 0.0001 is an arbitrarily-chosen factor, causes face 2 to remain plane as it rotates about a z-parallel axis at $r = r_c$. At the outset the appropriate value of r_c is unknown. Therefore *two* preliminary FE analyses are performed, respectively using the arbitrarily chosen values $r_c = 60$ mm and $r_c = 70$ mm. Neither of these r_c values is correct, so each of the two preliminary FE analyses results in a radial reaction R_A at A, which should not exist because the desired loading is pure bending. The respective R_A values are computed by the software as 2001 N and 357 N. By linear extrapolation, $R_A = 0$ when $r_c = 72.2$ mm. The value $r_c = 72.2$ mm is used in a third and final FE analysis, which provides a $R_A \approx 0$, as expected. Circumferential support reactions on face 1 produce a moment about a z-parallel axis, which is automatically computed by the software. This moment is doubled to provide moment M applied to the *entire* cross section.

Critique of Results. The deformed shape of the cross section is shown in Fig. 6.15-3a. Animation of the display on the computer monitor shows that intended boundary conditions have indeed been enforced. On physical grounds we argue that the deformed shape is reasonable, as follows. As expected, radial stress is tensile, so the 88-mm dimension becomes larger. As expected, circumferential stress σ_θ is, respectively, tensile and compressive on inner and outer portions of the cross section, while stress σ_z parallel to axis of revolution z is small. Therefore the Poisson effect should cause inner and outer portions,

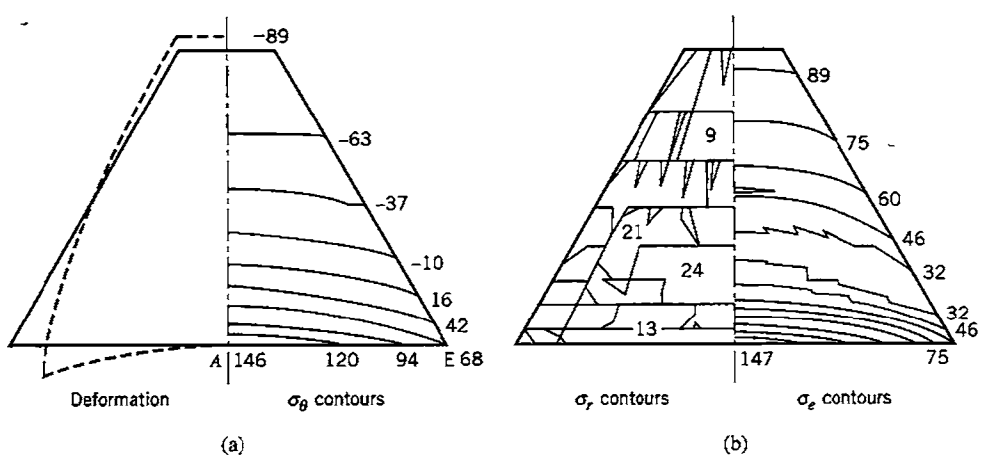

Figure 6.15-3. Results from FE analysis: deformed cross section and unaveraged stress contours. Stress units are MPa. (Stresses shown in the right half are mirrored from FE results actually computed in the left half.)

respectively, to contract and expand in the z direction, as is indeed observed. Circumferential tension on the inner portion pulls material toward the center of curvature. Outer corners are more flexible than the central portion, so it is proper that corner E moves inward relative to central point A. As expected, σ_θ contours are more closely spaced at smaller values of r.

Material that moves radially inward while bounded by faces 1 and 2 in Fig. 6.15-2b must shorten circumferentially. Thus, compressive strain is superposed on the tensile strain caused by flexing. Radial deflection provides greatest "stress relief" to material that deflects farthest. For this reason, Fig. 6.15-3a shows smaller circumferential stress at E than at A. FEA yields $\sigma_\theta = 146$ MPa at A and $\sigma_\theta = 65$ MPa at E. The software uses σ_θ stresses to compute moment $M/2$ on face 1 of the FE model in Fig. 6.15-2. Thus we obtain $M = 8.804(10^6)$ N • mm. With this M, the curved beam formula (Eq. 6.15-1) yields $\sigma_\theta = 119$ MPa, which is in approximate agreement with the average of FE stresses at A and E, which is $(146 + 65)/2 = 106$ MPa. The neutral axis is the locus of points where σ_θ is zero. We see from FEA that the neutral axis is curved, contrary to the assumption made in mechanics of materials theory.

No interelement discontinuity of σ_θ contours is visible in Fig. 6.15-3a. The reason is that σ_θ is dominated by circumferential strain $\varepsilon_\theta = (u/r) + (\partial v/\partial\theta)/r$ [3.1], but $\partial v/\partial\theta = 0$ in this FE solution, so that ε_θ is proportional to displacements on face 2, which are of course interelement-continuous. Figure 6.15-3b shows that contours of radial stress σ_r are badly discontinuous. But the largest σ_r is about 25 MPa, which is much less than the largest σ_θ. Therefore the plot of von Mises stress σ_e, Fig. 6.15-3b, shows small to moderate discontinuities. The error measure discussed in Section 9.10 gives $\eta = 0.05$, an acceptably small value. We conclude that results are reliable, at least for stress σ_θ.

ANALYTICAL PROBLEMS

6.1-1 (a) Complete calculations begun in Eq. 6.1-2, and so obtain shape functions N_i.
(b) Verify that the same result is provided by Lagrange interpolation.

6.1-2 (a) Verify that if nodes in Fig. 6.1-1a are uniformly spaced, then $J = L/2$.
(b) If ε_x at node 1 is to remain finite, how far from the center can node 2 be moved?

6.1-3 Determine the 3 by 3 stiffness matrix if nodes of the element in Fig. 6.1-1a are uniformly spaced. Let A and E be constant and perform integrations explicitly.

6.1-4 Omit the internal node in Fig. 6.1-1a, so that the element becomes a bar with end nodes only. Using natural coordinate ξ, derive the 2 by 2 stiffness matrix of a uniform element.

6.1-5 In Fig. 6.1-1a, let $x_3 - x_2 = L/4$ and $x_2 - x_1 = 3L/4$. If only node 3 has axial displacement ($u_1 = u_2 = 0, u_3 \neq 0$) what is strain ε_x at each node?

6.2-1 For the element in Fig. 6.2-1a, let $x = \lfloor 1 \;\; \xi \;\; \eta \;\; \xi\eta \rfloor \lfloor a_1 \;\; a_2 \;\; a_3 \;\; a_4 \rfloor^T$.
(a) Write matrix $[\mathbf{A}]$ in the relation $\lfloor x_1 \;\; x_2 \;\; x_3 \;\; x_4 \rfloor^T = [\mathbf{A}] \lfloor a_1 \;\; a_2 \;\; a_3 \;\; a_4 \rfloor^T$.
(b) By inspection of Eqs. 6.2-3, write $[\mathbf{A}]^{-1}$ in the relation
$x = \lfloor 1 \;\; \xi \;\; \eta \;\; \xi\eta \rfloor [\mathbf{A}]^{-1} \lfloor x_1 \;\; x_2 \;\; x_3 \;\; x_4 \rfloor^T$.
(c) Check answers to parts (a) and (b) by seeing if $[\mathbf{A}][\mathbf{A}]^{-1} = \lceil \mathbf{I} \rfloor$.

6.2-2 Sketch a quadrilateral with corners properly lettered and $\xi\eta$ axes properly oriented if shape functions are written as $N_A = \frac{1}{4}(1-\xi)(1+\eta)$, $N_B = \frac{1}{4}(1+\xi)(1+\eta)$, $N_C = \frac{1}{4}(1-\xi)(1-\eta)$, $N_D = \frac{1}{4}(1+\xi)(1-\eta)$.

6.2-3 Natural coordinates other than the $\xi\eta$ system shown in Fig. 6.2-1 may be chosen. One alternative is the rs system shown. Write shape functions of the bilinear element in terms of r and s.

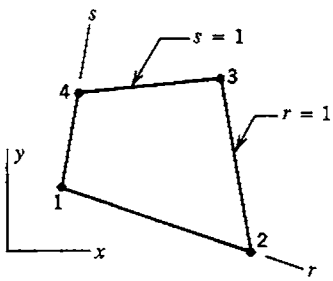

Problem 6.2-3

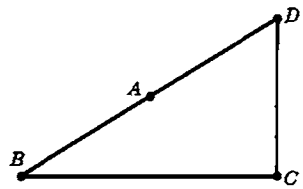

Problem 6.2-4

6.2-4 For the element shown, let $\xi = \eta = -1$ at (a) point A, (b) point B, (c) point C, and (d) point D. In each case sketch the three lines $\xi = -0.5, 0.0, 0.5$ and the three lines $\eta = -0.5, 0.0, 0.5$. Shape functions are as stated in Eqs. 6.2-3.

6.2-5 Sketch a four-node plane element for which J is a function of ξ but not of η.

6.2-6 Consider elements that are square and two units on a side. Node numberings shown for two such elements create difficulties. For each, determine [J] and J, using the shape functions of Eqs. 6.2-3. What do the node numberings shown imply about the $\xi\eta$ axes of the first element and the shape of the second?

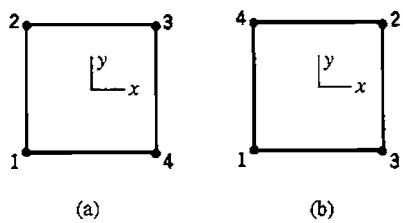

Problem 6.2-6

6.2-7 Evaluate [J] and J for each of the four elements shown. Also determine the ratio of element area to the area of a square two units on a side. How is this ratio related to J, and why?

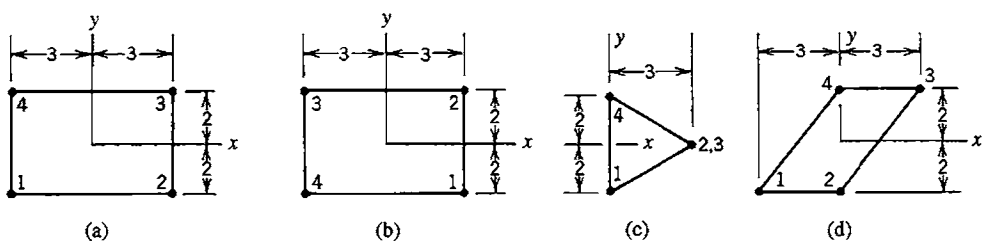

Problem 6.2-7

6.3-1 Derive locations and weights of an order 2 Gauss rule by requiring that it integrate exactly the polynomial $\phi = a_1 + a_2\xi + a_3\xi^2 + a_4\xi^3$ in the interval $-1 \le \xi \le 1$. Assume that sampling points and weights are symmetric with respect to the middle of the interval.

6.3-2 In Problem 6.2-3, what are the r and s coordinates of the Gauss points of an order 2 rule? And what are the associated weights W_i ? (Integration is from 0 to 1 for both r and s.)

6.3-3 Write an expression for integral I, analogous to Eq. 6.3-7, for a 2 by 3 Gauss rule.

6.3-4 Let 3 by 3 by 3 Gauss quadrature be applied to a hexahedral element. What numerical values of weight products $W_iW_jW_k$ appear? How many points are associated with each of these numerical values? Check that your answers provide the correct volume of an element for which $J = 1$.

6.3-5 The area shown is composed of a trapezoid and a rectangle. Evaluate the area using Gauss rules of order 1, 2, and 3, and determine the percentage error of each result.

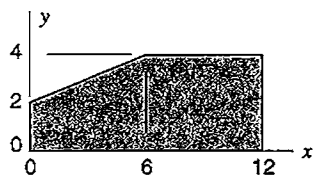

Problem 6.3-5

6.3-6 Use one-, two-, and then three-point Gauss quadrature to integrate the following functions. Determine the percentage error of each result.
(a) $\phi = \xi^2 + \xi^3$ over the interval $\xi = -1$ to $\xi = +1$.
(b) $\phi = \cos 1.5\xi$ over the interval $\xi = -1$ to $\xi = +1$.
(c) $\phi = (1 - \xi)/(2 + \xi)$ over the interval $\xi = -1$ to $\xi = +1$.
(d) $\phi = 1/x$ over the interval $x = 1$ to $x = 7$.

6.3-7 Use Gauss quadrature to evaluate the integral

$$I = \int_{-1}^{1}\int_{-1}^{1} \frac{3 + \xi^2}{2 + \eta^2}\, d\xi\, d\eta$$

Use (a) one point, (b) four points, and (c) nine points. Determine the percentage error of each result.

6.3-8 (a) Determine the element stiffness matrix of a two-node uniform bar element of length L by two-point Gauss quadrature. The result should agree with Eq. 2.2-1.
(b) Repeat part (a), but let the cross-sectional area vary linearly from A_1 at node 1 to A_2 at node 2.
(c) Repeat part (b), but use one-point Gauss quadrature.

6.3-9 Repeat Problem 6.1-3, but use two-point Gauss quadrature rather than explicit integration.

6.3-10 Obtain stiffness coefficients k_{ij} of a uniform beam element by two-point Gauss quadrature rather than explicit integration. Neglect transverse shear deformation. The strain-displacement matrix is stated in Eq. 3.3-13. It is helpful to note that

sampling points are at $1/\sqrt{3}$ times $L/2$ from the center, and that $x = (1 + \xi)\, L/2$.

6.4-1 Consider two adjacent plane quadratic elements, as shown. Show that shape functions in Table 6.4-1 provide interelement continuity of the field quantity along the shared boundary.

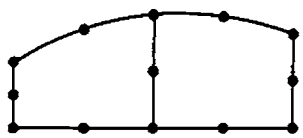

Problem 6.4-1

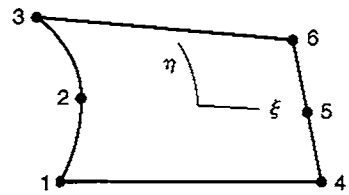

Problem 6.4-2

6.4-2 Shape functions for the element shown can be generated by "sweeping" a quadratic in η over the ξ-direction span of the element. Proceeding in this way, and using the node numbering shown, write the six shape functions.

6.4-3 For the plane quadratic Lagrange element (nine nodes), sketch shape function N_1 in the manner of Fig. 6.4-2d. Decide whether N_1 is positive or negative in each quadrant by evaluating N_1 at $\xi = \pm\frac{1}{2}$ and $\eta = \pm\frac{1}{2}$.

6.4-4 Sketch an eight-node plane element for which J is a function of η but not of ξ, if (a) the element is rectangular, and (b) the element has two curved sides.

6.4-5 Consider the nine-node plane element whose shape functions are given by Table 6.4-1. Any of nodes 5 through 9 may be omitted. In similar fashion, can corner node 1 be omitted, to produce a valid element with (say) straight sides? *Suggestion:* At corner 1, consider displacement parallel to a side.

6.4-6 Consider the standard C^1 beam element, which has translational and rotational d.o.f. at each of the two end nodes. Imagine that a lateral displacement mode is to be added, analogous to the bubble function mode of Eq. 6.4-3, such that activation of the mode does not destroy continuity with another beam element that may be attached to either end. Suggest a suitable shape function.

6.6-1 If, after computation of nodal d.o.f. in a mesh of QM6 elements, nodeless d.o.f. a_i of Eq. 6.6-1 are omitted from stress computation, what consequences are to be expected? Consider, for example, the square-element case in Fig. 6.11-1.

6.6-2 All three elements in the beam shown are plane QM6 elements. Examine displacements along sides of element 2 under the moment loading shown to demonstrate that pure bending cannot be modeled exactly by a QM6 element of trapezoidal shape.

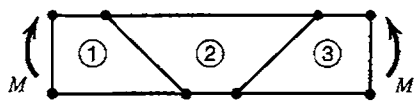

Problem 6.6-2

6.7-1 Apply condensation to the set of three equations shown in Problem 2.8-7. Let $\{\mathbf{d}_r\}$ be the single d.o.f. u_4. Solve for u_4, then recover the remaining two d.o.f. in $\{\mathbf{d}_c\}$ by use of Eq. 6.7-2. Check that results satisfy the original equations.

6.7-2 Let the three-node bar element of Fig. 6.1-1a be uniform, with node 2 at the midpoint. The first row of its stiffness matrix $[\mathbf{k}]$ is $(AE/3L)\lfloor 7 \quad -8 \quad 1 \rfloor$. Matrix $[\mathbf{k}]$ operates on d.o.f. $\lfloor u_1 \quad u_2 \quad u_3 \rfloor^T$.
(a) Without calculation, fill in the remainder of $[\mathbf{k}]$. *Suggestion:* Consider symmetry of element behavior, symmetry of $[\mathbf{k}]$, and rigid body translation.
(b) Determine the 2 by 2 stiffness matrix produced by condensation of u_2.
(c) Let the bar carry a uniformly distributed axial load of intensity q. Starting with the 3 by 1 consistent load vector $\{\mathbf{r}_e\} = (qL/6)\lfloor 1 \quad 4 \quad 1 \rfloor^T$, obtain the condensed load vector associated with d.o.f. u_1 and u_3. Solve for u_3 if $u_1 = 0$, then recover the condensed d.o.f. u_2 and finally check nodal loads computed as $[\mathbf{k}]\{\mathbf{d}\}$.

6.7-3 The sketch shows two uniform beam elements connected at node 2. Prior to making the connection, d.o.f. θ_{z2} in element 1-2 is condensed, so that node 2 is a hinge connection. Starting with the stiffness matrix of Eq. 2.3-5 (same as Eq. 3.3-14), obtain the condensed 3 by 3 stiffness matrix of the left hand element.

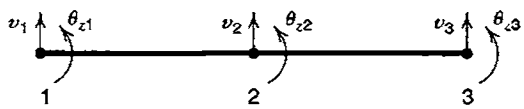

Problem 6.7-3

6.7-4 Consider a uniform beam element that deforms in the xy plane and can resist bending and axial deformation. Let the element be connected to a rotational spring at each end, as shown, with respective spring stiffnesses k_1 and k_2 (moment per radian). Let β_{z1} and β_{z2} be *structure* node rotations. Element rotational d.o.f. θ_{z1} and θ_{z2} are to be connected to structure d.o.f. β_{z1} and β_{z2} through the rotational springs, so that $\beta_{z1} \neq \theta_{z1}$ and $\beta_{z2} \neq \theta_{z2}$. Translational d.o.f. are to be connected directly, as usual. Describe steps in writing an 8 by 8 element stiffness matrix that operates on d.o.f. $\lfloor u_1 \quad v_1 \quad \theta_{z1} \quad u_2 \quad v_2 \quad \theta_{z2} \quad \beta_{z1} \quad \beta_{z2} \rfloor^T$ and obtaining from it a 6 by 6 matrix that operates on d.o.f. $\lfloor u_1 \quad v_1 \quad \beta_{z1} \quad u_2 \quad v_2 \quad \beta_{z2} \rfloor^T$ and is a function of A, E, I, L, k_1, and k_2.

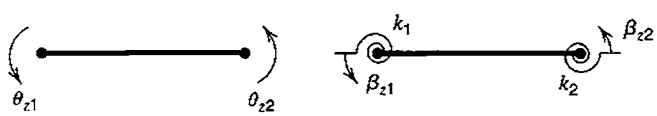

Problem 6.7-4

6.8-1 In Fig. 6.1-1a, let $x_3 - x_2 = L/3$ and $x_2 - x_1 = 2L/3$. Use one-point Gauss quadrature to determine the 3 by 3 stiffness matrix of an element with uniform A and E.

6.8-2 If element thickness can vary and is computed as $t = \sum N_i t_i$ from nodal values t_i, what order of Gauss quadrature is needed to compute the exact volume of (a) a four-node plane element, and (b) an eight-node plane element?

6.8-3 Show that the volume of an eight-node solid element is computed exactly by an order two Gauss rule.

6.8-4 Let the following plane elements be rectangular, with side nodes (if present) uniformly spaced, and element thickness computed as $t = \sum N_i t_i$ from nodal values

t_i. In each case, determine the order of Gauss quadrature needed to exactly evaluate stiffness coefficients k_{ij}. (a) Four-node element. (b) Eight-node element.

6.8-5 In Fig. 6.11-1, imagine that the order of Gauss quadrature is changed from 2 to 3. What will be the qualitative change in computed deflection for each of the four test cases?

6.8-6 Verify that expressions for u and v in Fig. 6.8-3d yield zero strain at the four Gauss points of a square element.

6.8-7 For each of the following elements, write (if possible) a vector $\{\mathbf{d}\}$ of nodal d.o.f. that represents a spurious mode under one-point Gauss quadrature.
(a) The three-node bar element of Fig. 6.1-1.
(b) A standard four-d.o.f. beam element (see Eq. 2.3-5 or Eq. 3.3-14).

6.8-8 For the following elements and nonuniform Gauss quadrature rules, what is the rank of $[\mathbf{k}]$, and what are disadvantages of using the rule?
(a) 2 by 1 rule in a Q4 plane element.
(b) 2 by 1 rule in a QM6 plane element.
(c) 2 by 3 rule in a Q8 plane element.

6.8-9 The four-node element shown was initially a square, two units on a side. Nodal displacement components, each of magnitude c in both x and y directions, create the displaced shape indicated by dashed lines.
(a) Determine strains $\{\boldsymbol{\varepsilon}\} = [\mathbf{B}]\{\mathbf{d}\}$, and show that they are zero at the center of the element.
(b) Show that nodal displacement vector $\{\mathbf{d}\}$ can be obtained by combining modes 7 and 8 of Fig. 6.8-1 with a rigid body rotation.

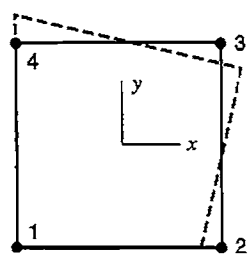

Problem 6.8-9

6.8-10 Let an eight-node solid element be rectangular and two units on a side, so that $\xi = x$, $\eta = y$, and $\zeta = z$.
(a) Consider only the x-direction displacement u. Let $\{\mathbf{d}_x\}$ represent nodal d.o.f. u_i. For each spurious mode under one-point Gauss quadrature that involves only the u_i, sketch the deformed element and write the corresponding $\{\mathbf{d}_x\}$ (of arbitrary magnitude).
(b) Similarly, considering only the u_i, write $\{\mathbf{d}_x\}$ for each independent rigid body mode and constant-strain mode.
(c) Show that the $\{\mathbf{d}_x\}$ vectors of part (a) are orthogonal to those of part (b).

6.8-11 There exists a six-point quadrature rule for hexahedra that uses a sampling point at the middle of each face [6.25]. What are the weight factors W_i? What spurious modes are possible for a rectangular eight-node element whose $[\mathbf{k}]$ is integrated by this rule? Can a mesh of these elements also display these mechanisms?

6.9-1 Let uniform traction act normal to a surface of a quadratic solid Lagrange element that is rectangular and has uniformly spaced nodes. In the consistent element load vector $\{\mathbf{r}_e\}$, what fraction of the total force appears at each of the nine nodes on the surface?

6.9-2 (a) Calculate nodal loads at all three nodes of the bar element considered in Problem 6.10-1b.
(b) Calculate the nodal load associated with d.o.f. a_1 in Problem 6.10-2.

6.10-1 Let the three-node bar element of Fig. 6.1-1a be uniform and have uniformly spaced nodes. See Problem 6.7-2 for information about the element stiffness matrix. Calculate and sketch the axial stress distribution along the fixed-ended element shown for each of the following loadings, and compare calculated results with exact results.
(a) Axial load P is applied at node 2.
(b) Uniformly distributed axial load of intensity q acts along the entire bar.

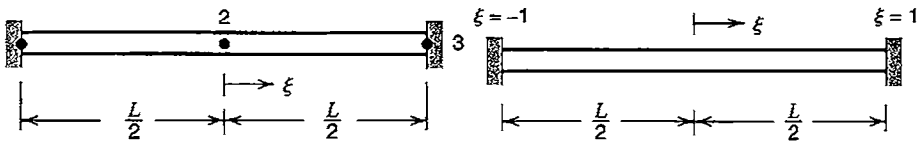

Problem 6.10-1 **Problem 6.10-2**

6.10-2 A beam of uniform bending stiffness EI is fixed at both ends, as shown. Model the beam by a single element, to which the lateral displacement mode $a_1(1 + \cos \pi\xi)$ has been added, where a_1 is a nodeless d.o.f. Uniformly distributed lateral load of intensity q acts along the entire beam.
(a) Determine the stiffness coefficient associated with a_1.
(b) Determine the predicted lateral deflection at midspan and its percentage error with respect to the exact value.
(c) Determine the predicted bending moment at midspan and at ends and the percentage error of each.

6.10-3 Repeat Problem 6.10-2 with load q replaced by concentrated lateral load P at midspan.

6.10-4 Use the shape functions of Eqs. 6.2-3 to show that $\gamma_{xy} = -c\xi$ on the line $\eta = 0$ in Fig. 3.6-2b, where c is a positive constant. For simplicity, assume that elements are square.

6.10-5 (a) Verify the numerical factors in Eq. 6.10-5.
(b) Apply Eq. 6.10-3 to nodes B, C, and D in Fig. 6.10-2. Thus obtain numerical factors, as in Eq. 6.10-5.
(c) Similarly, apply Eq. 6.10-3 to nodes E, F, G, and H in Fig. 6.10-2.

6.10-6 Write a formula analogous to Eq. 6.10-3 that uses stresses σ_i at the eight Gauss points of an order 2 rule in a hexahedron. Use it to write expressions analogous to Eq. 6.10-5 for σ_x at the following locations in the eight-node element of Fig. 6.5-1a: (a) node 8, and (b) the middle of face $\xi = 1$.

6.10-7 In a plane four-node element of parallelogram shape, stresses calculated directly at nodes agree exactly with stresses extrapolated to nodes from four Gauss points. Agreement is not obtained if the element has an arbitrary quadrilateral shape. Why?

6.10-8 Imagine that a plane bilinear element is not of constant thickness. What role does thickness variation play in stress calculation according to Eq. 6.10-1? Suggest an ad hoc adjustment for thickness variation that might improve the accuracy of computed stresses.

6.10-9 The uniform bar element shown has three nodes, whose axial displacements are $u_1 = 0, u_2 = 0$, and $u_3 = 0.001L$.
(a) Calculate axial strain ε_x directly at nodes.
(b) Calculate axial strain ε_x at Gauss points of an order 2 rule.
(c) Calculate ε_x at each node by extrapolation of ε_x values at the two Gauss points.
(d) Write Eq. 6.10-6 for strain ε_x rather than stress σ_e, and recalculate ε_x at node 3.

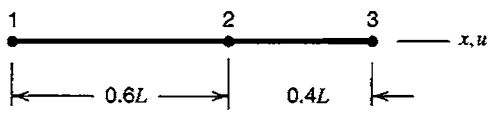

Problem 6.10-9

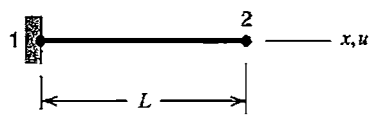

Problem 6.10-10

6.10-10 (a) Node 2 of the uniform bar element shown has axial displacement u_2. Show that stress calculation associated with Eqs. 6.10-7 and 6.10-10 provides $\sigma_x = Eu_2/L$, as expected.
(b) For the three-node bar element of Fig. 6.1-1, ε_x is linear in ξ if $x_2 = (x_1 + x_3)/2$. Hence it may at first seem appropriate to use $\sigma_x = \beta_1 + \beta_2 x$ in Eq. 6.10-7. Why is this expression in fact unacceptable?

6.11-1 In Fig. 6.11-2a, locate the point described by (a) $\xi = -1$ and $\xi = -1/\sqrt{3}$, and (b) $\eta = 0$ and $\eta = -1$.

6.11-2 Starting with a rectangular four-node plane element, move nodes 3 and 4 together so they coincide on the η axis.
(a) Sketch the resulting element and the four Gauss points of an order 2 rule, in the manner of Fig. 6.11-2.
(b) What is the smallest Jacobian J in the element? Among the four Gauss points, what is the ratio $J_{\max}/J_{\min}$?

6.11-3 Starting with a square four-node plane element two units on a side, create a triangle by moving node 3 so that nodes 2, 3, and 4 are collinear and uniformly spaced.
(a) Sketch the resulting element and the four Gauss points of an order 2 rule, in the manner of Fig. 6.11-2.
(b) What is the numerical value of Jacobian J at each node?

6.12-1 (a) Verify that $\sum N_i = 1$ for the N_i of Eqs. 6.2-3 and 6.4-1.
(b) From $\sum N_i = 1$ we obtain $\sum N_{i,\xi} = 0$ and $\sum N_{i,\eta} = 0$. Show that the N_i of Eqs. 6.2-3 satisfy the latter summations.

6.12-2 Let geometry of a three-node bar element be defined by three x_i, as in Fig. 6.1-1a. Interpolate axial displacement linearly in ξ over the element, from displacements u_1 and u_3 of end nodes. Thus the element is superparametric. Determine the expression for axial strain ε_x. Hence, show that the element fails unless node 2 lies at the middle of the bar.

6.13-1 Assume that the patch test is passed for the mesh in Fig. 6.13-1a. If all nine nodes are assigned displacements consistent with a field of constant strain, what loads at the internal node should result from the calculation $[\mathbf{K}]\{\mathbf{D}\}$, and why?

6.13-2 Sketch an assembly of hexahedral elements that could be conveniently used for a patch test. Let elements have corner nodes only. Show supports and nodal loads appropriate to testing proper representation of uniform stress σ_z.

COMPUTATIONAL PROBLEMS

In the following problems compute significant values of displacement and/or stress, as appropriate. Exploit symmetry where possible. When mesh refinement is used, estimate the maximum percentage error of results provided by the finest FE mesh. Where dimensions or loads are not assigned, choose values that seem reasonable or convenient. Where material properties are needed but not stated, use properties of steel. Apply the analysis methodology suggested in Section 1.5.

C6.1 (a) Construct a mesh of several elements, suitable for a patch test, that incorporates one of the "poor connections" depicted in Fig. 3.12-3. See if the patch test is passed. If not, to what extent is the effect of a poor connection localized?
(b) Apply uniform pressure to one face of a rectangular 20-node brick (Fig. 6.5-1b). Fix all d.o.f. at all nodes on the opposite face. Is uniform stress computed for $\nu > 0$? Or for $\nu = 0$? For $\nu > 0$, fix the smallest number of d.o.f. consistent with uniform stress, and recalculate. (How many d.o.f. are fixed?) What does the software do if less than six d.o.f. are fixed?

C6.2 One can undertake a systematic study of the effects of mesh distortion [6.26]. For example, if the plane beams shown are modeled by Q4 or QM6 elements, one could vary ϕ (or ℓ/H) while keeping ℓ/H (or ϕ) constant. Using triangular or quadrilateral elements with side nodes, one might vary ϕ or s/H. Possible loadings include tip moment and transverse tip force.

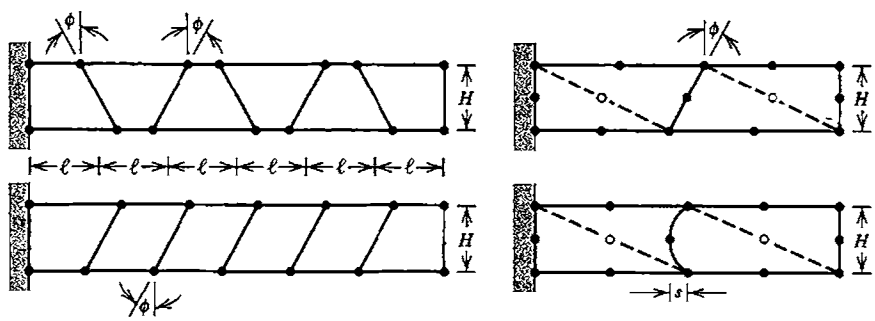

Problem C6.2

C6.3 As a variant of Problem C6.2, use plane strain conditions, maintain a chosen mesh geometry, and investigate what happens as Poisson's ratio approaches 0.5.

C6.4 The rectangular plate shown contains a hole and is securely bonded to a rigid base on the bottom and to a rigid bar on top. Peak values of von Mises stress σ_e are

sought. Load the model by prescribed motion of the rigid bar (x- or y-direction translation, rotation about an end, and so on).

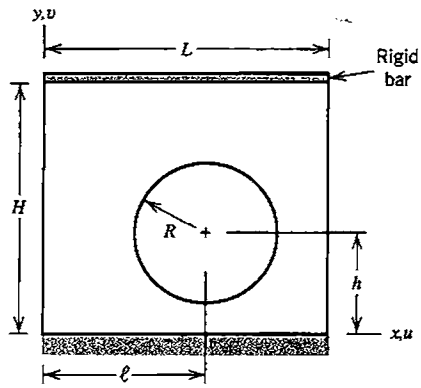

Problem C6.4

C6.5 (a) In Problem C6.4, reinforce the hole by increasing the z-direction thickness of material out to a radius of $1.3R$ or so.
(a) In Problem C6.4, omit the rigid bar, and load the structure by increasing the temperature of material around the hole, out to a radius of $1.3R$ or so.

C6.6 Regard a thick deposit of soil or rock as a continuous elastic medium, loaded by its own weight. Excavate a vertical cut of height H and/or a tunnel of radius R, as shown. What is the change in the state of stress and the final state of stress? Assume that plane strain conditions prevail in the z direction.

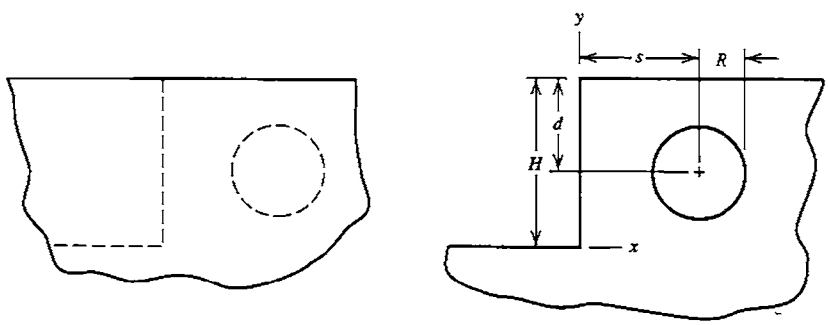

Problem C6.6

C6.7 Use plane elements in rectangular coordinates to solve the problem of a circular disk with a central circular hole, loaded by internal or external pressure, or by temperature change that depends only on the radial coordinate. Use a wedge-shaped mesh like that in Fig. 6.15-2b (but plane), with nodes permitted to have only radial displacement.

C6.8 Experimentally-determined stress concentration factors have been tabulated for plane-stress conditions in many geometries [1.16,6.24]. Some specific suggestions appear in Problem C3.2. The factors can be verified by FEA, using elements described in this chapter and progressive mesh refinement, until the error is less than (say) 5%.

C6.9 A castellated beam is a weight-saving design that has holes in the web. It can be made by cutting a standard beam along a zigzag path in the web, shifting the two pieces, and welding them back together, as shown. Investigate stresses in the castellated beam, using typical cases of support and loading.

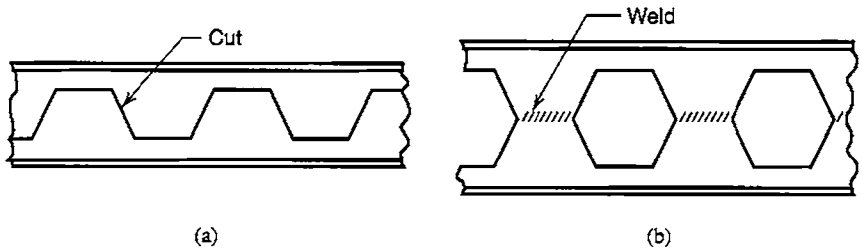

Problem C6.9

C6.10 If software permits a change in the order of Gauss quadrature, its effect can be investigated in various problems, including the test cases of Figs. 3.7-2, 6.6-1, 6.8-2, 6.8-4, 6.11-1, and Table 6.11-1.

C6.11 A thick plate contains a circular hole of small radius, as shown. Well away from the hole, the plate is in a state of pure shear. Investigate the state of stress on the boundary of the hole. Also observe the effect of Poisson's ratio.

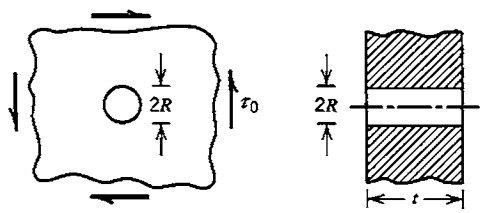

Problem C6.11

C6.12 Consider a prismatic cantilever beam whose (solid) cross section is a right triangle or a half-circle, as shown.

(a) Investigate deflections and stresses produced by transverse tip load P applied at the location shown.

(b) Determine the location along the x axis through which load P must pass if the beam is to bend without twisting.

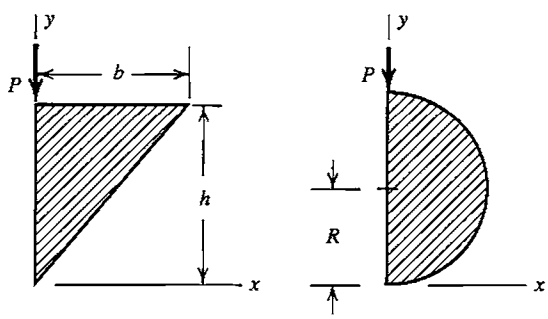

Problem C6.12

C6.13 The sketch shows a massive coil spring, formed by bending a bar of rectangular cross section into a helix. Loading is by axial forces F applied at ends (not shown). Consider a wedge-shaped portion of a coil that spans angle $\Delta\theta$, as shown. If angle α is small, we may assume that $u = 0$ on cross sections that form faces of the wedge [3.1]. Also, $w = 0$ on $\theta = 0$ and $w = c\theta$ on $\theta = \Delta\theta$, where c is a constant. Circumferential displacement is $v = v(r,z)$. Impose u and w displacement boundary conditions, solve for stresses, and calculate F from computed reactions at restrained nodes.

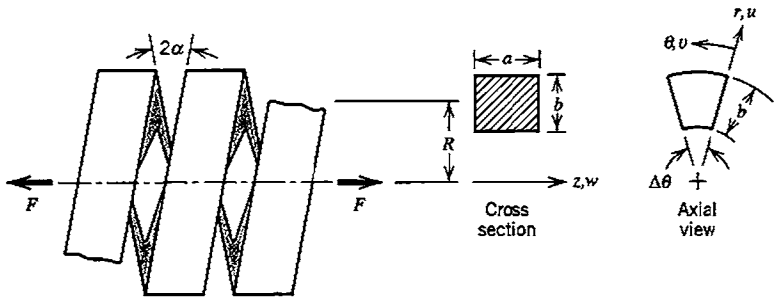

Problem C6.13

CHAPTER 7

ISOPARAMETRIC TRIANGLES AND TETRAHEDRA

If formulated using coordinates and methods similar to those discussed in Chapter 6, triangles can have curved sides and tetrahedra can have curved edges and faces. For these general shapes, element matrices are formulated using numerical integration. Elements having straight edges and uniform spacing of edge nodes (if present) can be regarded as special cases and can be integrated exactly using special formulas.

7.1 REFERENCE COORDINATES. SHAPE FUNCTIONS

The constant-strain triangle (CST) and the linear-strain triangle (LST) were introduced in Sections 3.4 and 3.5, where polynomial fields for displacement and strain were presented, but details of element formulation were not provided. These details are now considered, in a format that allows elements that have side nodes to have curved sides. Analogous tetrahedral elements are also considered. Like coordinates $\xi\eta$ and $\xi\eta\zeta$ used in Chapter 6, reference coordinates rs and rst used in the present chapter are *natural* or *intrinsic* coordinate systems (Fig. 7.1-1). They are attached to the element and maintain their position with respect to it regardless of element orientation in global coordinates. Also, an element's physical size and shape have no effect on the numerical values of reference coordinates at which nodes appear. Thus, physical elements of various sizes and shapes are all mapped into the same size and shape in reference coordinates. Elements considered in the present chapter are *isoparametric;* that is, element shape and element field quantity are defined by the same interpolation.

When used for stress analysis problems, the three-node triangle and the four-node tetrahedron are susceptible to shear locking behavior. Higher-order elements—the six-node triangle and ten-node tetrahedron—are preferable choices for stress analysis. Three-node triangles are acceptable for scalar field problems, where a gradient term analogous to shear strain does not arise.

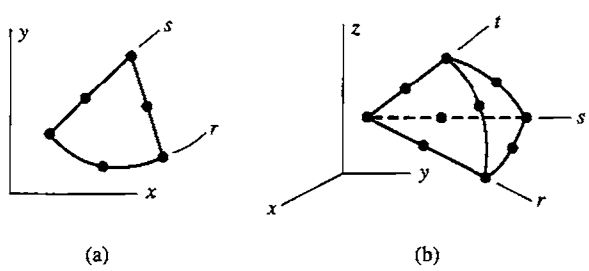

Figure 7.1-1. Quadratic elements in Cartesian coordinates, showing reference coordinate systems rs and rst. (a) Six-node triangle. (b) Ten-node tetrahedron.

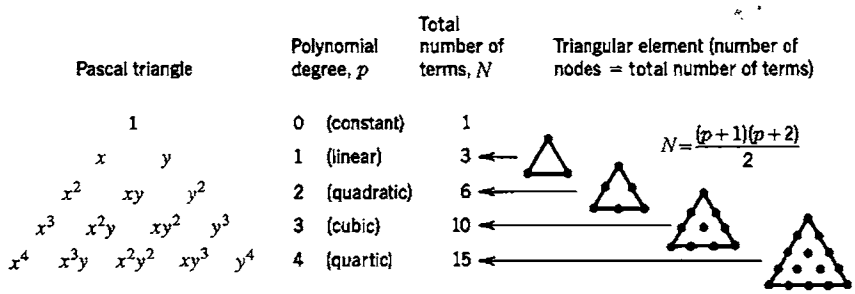

Figure 7.1-2. Relation between type of plane triangular element and number of polynomial coefficients used for interpolation.

Triangles. If side and internal nodes have a regular pattern, one can generate a family of straight-sided triangles such that each contains a *complete* polynomial in Cartesian coordinates (Fig. 7.1-2). In what follows we consider only linear and quadratic triangles.

When mapped into reference coordinates rs, three- and six-node triangles have nodes at locations shown in Fig. 7.1-3, regardless of the size and shape of the physical element. Shape functions of the three-node triangle in Fig. 7.1-3a are

$$N_1 = 1 - r - s \qquad N_2 = r \qquad N_3 = s \tag{7.1-1}$$

We see that $N_i = 1$ at node i and $N_i = 0$ at other nodes, as required of shape functions. Equations $N_1 = 0, N_2 = 0$, and $N_3 = 0$ are each the equation of one side of the triangle. Indeed, each of the equations $N_i = 0$ is the equation of a line that passes through nodes where the ith shape function must be zero. For higher-order members of the family, each shape function is the *product* of functions that might be called "line functions." When each line function is equated to zero, it becomes the equation of a line that passes through nodes where the ith shape function must be zero [3.3]. Applying this concept to the six-node triangle in Fig. 7.1-3b, and multiplying by numerical constants as necessary to provide $N_i = 1$ at node i, we obtain

$$\begin{aligned} N_1 &= (1-r-s)(1-2r-2s) & N_2 &= r(2r-1) & N_3 &= s(2s-1) \\ N_4 &= 4r(1-r-s) & N_5 &= 4rs & N_6 &= 4s(1-r-s) \end{aligned} \tag{7.1-2}$$

The process can be extended to additional elements of the family shown in Fig. 7.1-2.

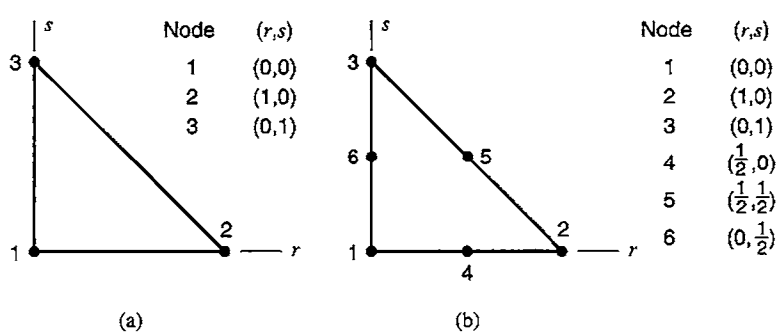

Figure 7.1-3. Linear and quadratic triangular elements, mapped into reference coordinates rs. Coordinates r and s of element nodes are shown.

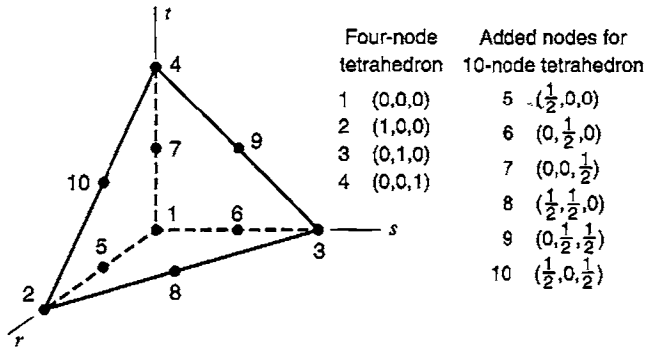

Figure 7.1-4. Tetrahedral element, showing reference coordinates r, s, and t of element nodes for the four-node form and for the ten-node form.

Tetrahedra. By retaining only vertex nodes in Fig. 7.1-4, we obtain a four-node tetrahedron. Its shape functions are

$$N_1 = 1 - r - s - t \qquad N_2 = r \qquad N_3 = s \qquad N_4 = t \tag{7.1-3}$$

Each shape function, if equated to zero, is the equation of the tetrahedron face that does *not* pass through the node in question [3.3]. To obtain each shape function N_i of the ten-node tetrahedron, we can take the product of two functions, each of which describes a face or other plane that passes through nodes other than node i. For example, planes $1 - r - s - t = 0$ and $r = 0$ are planes not passing through node 5; the product of their left-hand sides yields N_5 (after multiplication by 4 so that $N_5 = 1$ at the coordinates of node 5). The complete set of shape functions for the ten-node tetrahedron is

$$\begin{aligned}
N_1 &= (1-r-s-t)(1-2r-2s-2t) \\
N_2 &= r(2r-1) \qquad N_5 = 4r(1-r-s-t) \qquad N_8 = 4rs \\
N_3 &= s(2s-1) \qquad N_6 = 4s(1-r-s-t) \qquad N_9 = 4st \\
N_4 &= t(2t-1) \qquad N_7 = 4t(1-r-s-t) \qquad N_{10} = 4tr
\end{aligned} \tag{7.1-4}$$

Higher-order tetrahedra can have internal nodes. Thus we can generate a family of tetrahedra analogous to the family of triangles shown in Fig. 7.1-2, each of which contains a complete polynomial of degree p. The relation between p and N, where N is both the number of nodes in the tetrahedron and the total number of terms in the complete polynomial, is $N = (p+1)(p+2)(p+3)/6$.

Isoparametric Elements. An element is isoparametric if its geometry and its field quantity ϕ use the same set of shape functions to interpolate from nodal values. Thus

$$x = \sum_i N_i x_i \qquad y = \sum_i N_i y_i \qquad z = \sum_i N_i z_i \qquad \phi = \sum_i N_i \phi_i \tag{7.1-5}$$

where i ranges over the number of nodes. For a plane element, the z equation is omitted.

7.2 ELEMENT CHARACTERISTIC MATRICES

The element characteristic matrix is a stiffness matrix for structural mechanics problems. For heat conduction, which is a scalar field problem, it is an element conductivity matrix. For either structural or scalar problems, manipulations used for triangles and tetrahedra are very similar to manipulations used for quadrilaterals and hexahedra in Chapter 6. Therefore, extensive explanation is not provided here. In what follows we emphasize the scalar field problem. The structural problem can be addressed by expanding arrays in a way that should be apparent from study of Section 6.2.

Most manipulation is occupied with expressing derivatives of a field quantity ϕ with respect to Cartesian coordinates when ϕ is stated in terms of the reference coordinates. The procedure is most easily explained using the simplest element, as follows.

Linear Triangle. The principal task is to establish matrix [**B**] that provides gradients in terms of nodal d.o.f. ϕ_1, ϕ_2, and ϕ_3.

$$\begin{Bmatrix} \phi_{,x} \\ \phi_{,y} \end{Bmatrix} = [\mathbf{B}] \begin{Bmatrix} \phi_1 \\ \phi_2 \\ \phi_3 \end{Bmatrix} \tag{7.2-1}$$

where $\phi_{,x} = \partial\phi/\partial x$ and $\phi_{,y} = \partial\phi/\partial y$. Shape functions N_i are stated in terms of r and s rather than x and y, so we first write, using Eqs. 7.1-5,

$$\begin{Bmatrix} \phi_{,r} \\ \phi_{,s} \end{Bmatrix} = [\mathbf{J}] \begin{Bmatrix} \phi_{,x} \\ \phi_{,y} \end{Bmatrix} \quad \text{where} \quad [\mathbf{J}] = \begin{bmatrix} x_{,r} & y_{,r} \\ x_{,s} & y_{,s} \end{bmatrix} = \begin{bmatrix} \sum N_{i,r}x_i & \sum N_{i,r}y_i \\ \sum N_{i,s}x_i & \sum N_{i,s}y_i \end{bmatrix} \tag{7.2-2}$$

These relations are analogous to those for a quadrilateral, Eqs. 6.2-4 and 6.2-5. Analogously to Eq. 6.2-6, we obtain an expression for Jacobian matrix [**J**] of a three-node triangle from Eqs. 7.1-1 and 7.2-2.

$$[\mathbf{J}] = \begin{bmatrix} -1 & 1 & 0 \\ -1 & 0 & 1 \end{bmatrix} \begin{bmatrix} x_1 & y_1 \\ x_2 & y_2 \\ x_3 & y_3 \end{bmatrix} = \begin{bmatrix} x_{21} & y_{21} \\ x_{31} & y_{31} \end{bmatrix} \quad \text{where} \quad \begin{aligned} x_{ij} &= x_i - x_j \\ y_{ij} &= y_i - y_j \end{aligned} \tag{7.2-3}$$

The Jacobian inverse is

$$[\mathbf{J}]^{-1} = \frac{1}{|\mathbf{J}|} \begin{bmatrix} y_{31} & -y_{21} \\ -x_{31} & x_{21} \end{bmatrix} \quad \text{where} \quad |\mathbf{J}| = x_{21}y_{31} - x_{31}y_{21} \tag{7.2-4}$$

It can be shown that $|\mathbf{J}| = 2A$, where A is the area of the triangle (Problem 7.2-1). Area calculated in this way is positive if nodes are numbered counterclockwise around the triangle. Gradients of the field quantity in Cartesian coordinates are, from Eqs. 7.2-2 and 7.2-3,

$$\begin{Bmatrix} \phi_{,x} \\ \phi_{,y} \end{Bmatrix} = [\mathbf{J}]^{-1} \begin{Bmatrix} \phi_{,r} \\ \phi_{,s} \end{Bmatrix} \qquad \begin{Bmatrix} \phi_{,r} \\ \phi_{,s} \end{Bmatrix} = \begin{bmatrix} -1 & 1 & 0 \\ -1 & 0 & 1 \end{bmatrix} \begin{Bmatrix} \phi_1 \\ \phi_2 \\ \phi_3 \end{Bmatrix}$$

$$\text{hence} \quad \begin{Bmatrix} \phi_{,x} \\ \phi_{,y} \end{Bmatrix} = \underbrace{[\mathbf{J}]^{-1} \begin{bmatrix} -1 & 1 & 0 \\ -1 & 0 & 1 \end{bmatrix}}_{[\mathbf{B}]} \begin{Bmatrix} \phi_1 \\ \phi_2 \\ \phi_3 \end{Bmatrix} \tag{7.2-5}$$

Written out, matrix [**B**] for the three-node triangle in a scalar field problem is

$$[\mathbf{B}] = \frac{1}{2A} \begin{bmatrix} -y_{31} + y_{21} & y_{31} & -y_{21} \\ x_{31} - x_{21} & -x_{31} & x_{21} \end{bmatrix} = \frac{1}{2A} \begin{bmatrix} y_{23} & y_{31} & y_{12} \\ x_{32} & x_{13} & x_{21} \end{bmatrix} \tag{7.2-6}$$

where $2A = x_{21}y_{31} - x_{31}y_{21}$. With [$\kappa$] a 2 by 2 array of material constants and t the element thickness, the characteristic matrix of a scalar element is

$$[\mathbf{k}] = \int [\mathbf{B}]^T [\kappa][\mathbf{B}]\, t\, dA \tag{7.2-7}$$

If [κ] and t are constant over the element, integration is trivial; we obtain $[\mathbf{k}] = [\mathbf{B}]^T[\kappa][\mathbf{B}]tA$. For higher-order elements the integrand is a function of r and s. Such integrals are addressed in Sections 7.3 and 7.4.

The element stiffness matrix is needed for structural problems. For the three-node triangle, it is

$$[\mathbf{k}] = \int [\mathbf{B}]^T [\mathbf{E}][\mathbf{B}]\, t\, dA \quad \text{where } [\mathbf{B}] = \frac{1}{2A} \begin{bmatrix} y_{23} & 0 & y_{31} & 0 & y_{12} & 0 \\ 0 & x_{32} & 0 & x_{13} & 0 & x_{21} \\ x_{32} & y_{23} & x_{13} & y_{31} & x_{21} & y_{12} \end{bmatrix} \tag{7.2-8}$$

Quadratic Triangle. For the six-node triangle of Fig. 7.1-3b, shape functions are given by Eqs. 7.1-2. Equation 7.2-2 remains valid, but now each summation has six terms rather than three. For example, term $J_{11} = x_{,r}$ of the 2 by 2 Jacobian matrix [**J**] is

$$\frac{\partial x}{\partial r} = (4r + 4s - 3)x_1 + (4r - 1)x_2 - 4(2r + s - 1)x_4 + 4sx_5 - 4sx_6 \tag{7.2-9}$$

(The multiplier of x_3 is zero.) The expression for $\partial\phi/\partial r$ is the same as Eq. 7.2-9, with the x_i replaced by nodal d.o.f. ϕ_i. For straight sides and midside nodes, [**J**] is given by Eq. 7.2-3.

Tetrahedra. By direct extension of the foregoing, coordinates r and s are supplemented by coordinate t, and field quantity ϕ is a function of r, s, and t. The shape and displacement interpolations of Eqs. 6.5-1 are applicable, with the N_i taken from Eq. 7.1-3, or Eq. 7.1-4, and so on. Equation 6.5-2 for Jacobian matrix [**J**] applies if ξ, η, and ζ are replaced by r, s, and t, respectively. The element characteristic matrix is

$$[\mathbf{k}] = \int [\mathbf{B}]^T [\kappa][\mathbf{B}]\, dV \tag{7.2-10}$$

Remarks. One may ask if triangular elements can be obtained by "degrading" or "degenerating" a quadrilateral element, for example, by coalescing two nodes of a four-node quadrilateral to obtain a three-node triangle. Indeed this appears to work. Upon assigning the same coordinates to the superposed nodes and gathering terms, shape functions of the linear triangle are obtained [2.14]. However, shape functions of a six-node triangle are *not* obtained by simply coalescing all three nodes on one side of an eight-node quadrilateral [7.1,7.2]. To avoid trouble, software users should not create triangles by supplying data that superposes nodes. It is better to use triangles and tetrahedra that are formulated as such.

7.3 ANALYTICAL INTEGRATION. AREA AND VOLUME COORDINATES

An element characteristic matrix such as Eq. 7.2-7 can be integrated analytically, rather than numerically, if element geometry is suitably restricted. Specifically, we require that element sides be straight and side nodes (if present) be uniformly spaced, so that Jacobian J is constant throughout the element. Thus, all terms to be integrated are products of reference coordinates, and we can obtain a closed-form expression for $[\mathbf{k}]$. Analytical integration formulas for triangles are expressed in terms of *area coordinates,* discussed next. Similar coordinates and formulas for tetrahedra are summarized at the end of this section.

The six-node triangle with straight sides and midside nodes has been studied with the intent of efficiently generating its characteristic (or stiffness) matrix in closed form [3.4,7.3,7.4]. Reference [7.5] addresses related tetrahedra, and claims that generating the stiffness matrix of the ten-node tetrahedron in closed form is 133 times faster than generating it by four-point quadrature.

Many triangular elements have been developed using area coordinates rather than coordinates rs of Fig. 7.1-1. Area coordinates may also be called *areal, triangular,* or *trilinear* coordinates. Although known in mathematics for many years [7.6], they seem to have been reinvented when finite element theory found a need for them.

Area Coordinates. In Fig. 7.3-1a, an arbitrarily located point P divides triangle 1-2-3 into the three subareas A_1, A_2, and A_3. Area coordinates are defined as ratios of areas:

$$\xi_1 = \frac{A_1}{A} \qquad \xi_2 = \frac{A_2}{A} \qquad \xi_3 = \frac{A_3}{A} \tag{7.3-1}$$

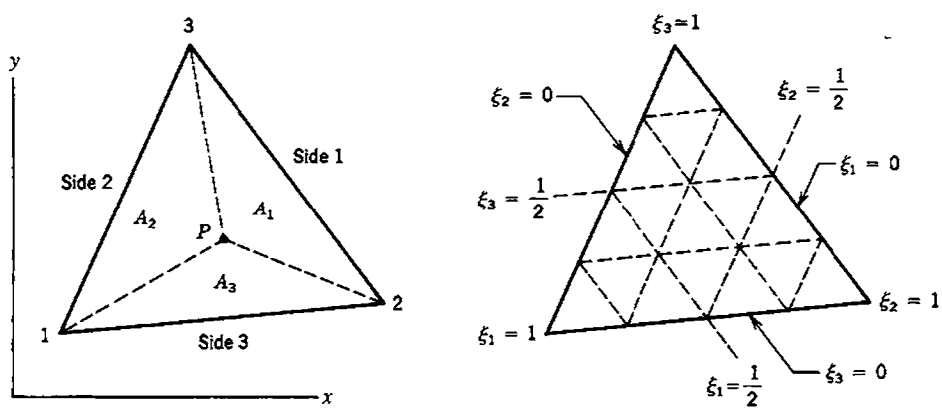

Figure 7.3-1. Area coordinates $\xi_1\xi_2\xi_3$ in a triangle.

where A is the area of triangle 1-2-3. Because $A = A_1 + A_2 + A_3$, the ξ_i are not independent. They satisfy the constraint relation

$$\xi_1 + \xi_2 + \xi_3 = 1 \tag{7.3-2}$$

The centroid of a straight-sided triangle is located at $\xi_1 = \xi_2 = \xi_3 = \frac{1}{3}$. In terms of nodal coordinates, plane geometry shows that Cartesian coordinates of the centroid are $(x_1 + x_2 + x_3)/3$ and $(y_1 + y_2 + y_3)/3$.

Area coordinates can also be stated as ratios of lengths. For example, in Fig. 7.3-1, let L_{23} be the length of side 2-3, s the distance from point P to side 2-3, and h the distance from vertex 1 to side 2-3. Then $A_1 = L_{23}s/2$, $A = L_{23}h/2$, and $\xi_1 = A_1/A = s/h$.

The relation between area coordinates $\xi_1\xi_2\xi_3$ and coordinates rs of Fig. 7.1-3 is easily established by regarding area coordinates as ratios of lengths. In Fig. 7.1-3, sides 1-2 and 1-3 are each one unit long. Therefore $\xi_2 = r/1 = r$ and $\xi_3 = s/1 = s$. Finally, $\xi_1 = 1 - \xi_2 - \xi_3$. In summary,

$$\xi_1 = 1 - r - s \qquad \xi_2 = r \qquad \xi_3 = s \tag{7.3-3}$$

Thus, shape functions of the linear element, given in Fig. 7.1-3a and Eqs. 7.1-1, are $N_1 = \xi_1$, $N_2 = \xi_2$, and $N_3 = \xi_3$. Shape functions of the quadratic triangle, given in Fig. 7.1-3b and Eqs. 7.1-2, are

$$\begin{aligned} N_1 &= \xi_1(2\xi_1 - 1) & N_2 &= \xi_2(2\xi_2 - 1) & N_3 &= \xi_3(2\xi_3 - 1) \\ N_4 &= 4\xi_1\xi_2 & N_5 &= 4\xi_2\xi_3 & N_6 &= 4\xi_3\xi_1 \end{aligned} \tag{7.3-4}$$

By use of Eqs. 7.3-3, all terms in the integrand of the element characteristic matrix can be expressed in terms of area coordinates rather than in terms of r and s.

Equations 7.3-1 to 7.3-4 do not require that sides of a triangle be straight or that side nodes be uniformly spaced. But when these conditions prevail, Jacobian J is constant throughout the element, all terms to be integrated are polynomials in area coordinates, and integration formulas that follow can be used.

Integration Formulas. Consider first integration along a side of the triangle, which is useful for calculation of consistent nodal loads when traction is applied to the side. For example, consider side 3 of the triangle in Fig. 7.3-1. There $\xi_3 = 0$, so the variation of a quantity along this side is a function ξ_1 and ξ_2. Integrations involve various products of ξ_1 and ξ_2, all of which can be evaluated by use of the formula

$$\int_L \xi_1^k \xi_2^l \, dL = L\frac{k!\,l!}{(1+k+l)!} \tag{7.3-5}$$

where k and l are nonnegative integers and L is the length of the side. The formula yields length L itself if k and l are both zero. As further examples,

$$\int_L \xi_2^2 \, dL = L\frac{2!}{3!} = \frac{L}{3} \qquad \text{and} \qquad \int_L \xi_1\xi_2^2 \, dL = L\frac{2!}{4!} = \frac{L}{12} \tag{7.3-6}$$

Similarly, the formula for integration over triangle area A is

$$\int_A \xi_1^k \xi_2^l \xi_3^m \, dA = 2A \frac{k!\,l!\,m!}{(2+k+l+m)!} \tag{7.3-7}$$

which appropriately yields area A when $k = l = m = 0$. Alternative forms of this formula, in both two and three dimensions, allow the integrand to be expressed in terms of Cartesian coordinates rather than area or volume coordinates [4.4,7.7].

Tetrahedra. *Volume coordinates* in a tetrahedron are analogous to area coordinates in a triangle. A point within the tetrahedron divides it into subvolumes V_1, V_2, V_3, and V_4. Taking the ratio of each subvolume to total volume V, we obtain the volume coordinates $\xi_i = V_i/V$, where $i = 1,2,3,4$. These volume coordinates satisfy the constraint relation $\xi_1 + \xi_2 + \xi_3 + \xi_4 = 1$. The relation between volume coordinates $\xi_1\xi_2\xi_3\xi_4$ and coordinates rst of Fig. 7.1-4 is obtained by the same kind of argument that provides Eqs. 7.3-3. Thus,

$$\xi_1 = 1 - r - s - t \qquad \xi_2 = r \qquad \xi_3 = s \qquad \xi_4 = t \tag{7.3-8}$$

Therefore, shape functions of the four-node tetrahedron are $N_1 = \xi_1$, $N_2 = \xi_2$, $N_3 = \xi_3$, and $N_4 = \xi_4$. The integration formula in volume coordinates, which is useful when edges are straight and edge nodes are uniformly spaced, is

$$\int_V \xi_1^k \xi_2^l \xi_3^m \xi_4^n \, dV = 6V \frac{k!\,l!\,m!\,n!}{(3+k+l+m+n)!} \tag{7.3-9}$$

7.4 NUMERICAL INTEGRATION

When element sides are curved or side nodes are not uniformly spaced, we call the triangle "distorted." Then Jacobian J is not constant over an element, and terms in integrands become ratios of polynomials. In these cases numerical integration is appropriate. Numerical integration involves multiplying the value of the integrand at prescribed locations by suitable weight factors and adding results. Every matrix coefficient in the integrand is treated in this way. The same concept is applied to quadrilaterals in Section 6.3. However, for triangles and tetrahedra, weight factors are defined individually rather than as products of one-dimensional weights. Also, a variety of integration rules is available, and there is disagreement among authors as to which rules are best.

For stress calculation in quadrilaterals and hexahedra, it is often beneficial to evaluate stresses at Gauss quadrature points and use these values to extrapolate to other locations in the element (Section 6.10). In a six-node triangle with straight sides and midside nodes, the displacement field is a complete quadratic in global Cartesian coordinates, hence the strain field is a complete linear field, so linear extrapolation from all sets of three noncollinear points in the element provides the same result. An analogous situation prevails in higher-order triangles and in tetrahedra. In "patch recovery" methods of stress calculation, numerical experiment suggests that optimal stress locations for general states of stress are at centers of three-node triangles and at side nodes of six-node triangles (see Section 9.9).

TABLE 7.4-1 SELECTED FORMULAS FOR NUMERICAL INTEGRATION OVER A TRIANGULAR AREA, EQ. 7.4-1 [6.4]

No. of points	Figure	Degree of precision	Coordinates (r_i,s_i)	Weights W_i
1	7.4-1a	1	$\left(\frac{1}{3},\frac{1}{3}\right)$	1.0
3	7.4-1b	2	$\left(\frac{2}{3},\frac{1}{6}\right),\left(\frac{1}{6},\frac{1}{6}\right),\left(\frac{1}{6},\frac{2}{3}\right)$	$\frac{1}{3}$
3	7.4-1c	2	$\left(\frac{1}{2},0\right),\left(0,\frac{1}{2}\right),\left(\frac{1}{2},\frac{1}{2}\right)$	$\frac{1}{3}$
4	7.4-1d	3	$\left(\frac{1}{3},\frac{1}{3}\right)$	$-\frac{27}{48}$
			$\left(\frac{3}{5},\frac{1}{5}\right),\left(\frac{1}{5},\frac{1}{5}\right),\left(\frac{1}{5},\frac{3}{5}\right)$	$\frac{25}{48}$

Triangles. Let $\phi = \phi(r,s)$ represent a single coefficient of the characteristic element matrix integrand $[\mathbf{B}]^T[\boldsymbol{\kappa}][\mathbf{B}]t$ in Eq. 7.2-7. Then, for n sampling points,

$$\int_A \phi\, dA \approx \sum_{i=1}^{n} \phi_i J_i W_i \qquad \text{where} \qquad J_i = \frac{1}{2}|\mathbf{J}|_i \tag{7.4-1}$$

The factor $\frac{1}{2}$ appears because the area of the mapped triangle in reference coordinates rs is $\frac{1}{2}$. For a triangle with either straight or curved sides, $[\mathbf{J}]$ is given by Eq. 7.2-2. For an *undistorted* triangle of area A in Cartesian coordinates, $|\mathbf{J}| = 2A$ throughout the triangle (as shown, for example, by letting sides 1-2 and 1-3 in Fig 7.1-3a have physical lengths of unity, so that $A = \frac{1}{2}$, and applying Eq. 7.2-4). Hence, because $\sum W_i = 1$ (as in Table 7.4-1), Eq. 7.4-1 correctly yields $\int dA = A$ when $\phi = 1$.

Table 7.4-1 lists data of some lower-order numerical integration formulas for plane triangles [6.4] for use in Eq. 7.4-1. Locations of sampling points in the mapped triangle are shown in Fig. 7.4-1. Sampling points are uniformly distributed over the triangle in the sense of having locations that are symmetric in area coordinates. The *degree of precision* is the degree of the highest-order polynomial terms in r and s that are integrated exactly by the formula. Specifically, a rule having degree of precision k exactly integrates all terms of the form $r^l s^m$ when $l + m \le k$ (including $l = 0$ or $m = 0$), and is inexact for at least one term $r^l s^m$ when $l + m > k$. Discussion and additional rules appear in many references, including [2.13,2.14,3.3,4.4,7.9,7.10]. Rules of higher order are sometimes favored for the specific heat matrix in heat conduction analysis. Considerations related to the better choice among competing rules are summarized in [7.11].

Each of the three-point rules has its advocates [7.10,7.12]. Numerical coefficients of the four-point rule are stated incorrectly in some older references. In consequence this rule may have been unjustly criticized by those who used it. A computer subroutine that uses the three-point interior rule appears in [7.13].

Tetrahedra. Let $\phi = \phi(r,s,t)$ represent a single coefficient of the characteristic element matrix integrand $[\mathbf{B}]^T[\boldsymbol{\kappa}][\mathbf{B}]$ in Eq. 7.2-10. Then, with n the number of sampling points,

$$\int_V \phi\, dV \approx \sum_{i=1}^{n} \phi_i J_i W_i \qquad \text{where} \qquad J_i = \frac{1}{6}|\mathbf{J}|_i \tag{7.4-2}$$

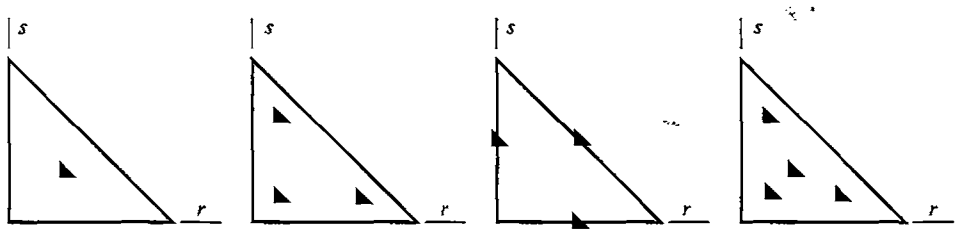

Figure 7.4-1. Locations of sampling points for numerical integration rules in Table 7.4-1.

The factor of $\frac{1}{6}$ appears because the volume of the mapped tetrahedron in reference coordinates rst is $\frac{1}{6}$. For an undistorted tetrahedron of unit volume V in Cartesian coordinates, $|\mathbf{J}| = 6V$ throughout the tetrahedron. Hence, because $\sum W_i = 1$ (as in Table 7.4-2), Eq. 7.4-2 correctly yields $\int dV = V$ when $\phi = 1$.

Table 7.4-2 lists data of some lower-order numerical integration formulas for tetrahedra [7.11] for use in Eq. 7.4-2. The degree of precision is defined in the same way as for Table 7.4-1, so that a rule of precision k exactly integrates all terms of the form $r^l s^m t^n$ when $l + m + n \leq k$. Additional rules appear in many references, including [3.3,4.4,6.4, 7.9,7.11,7.14].

ANALYTICAL PROBLEMS

7.1-1 Derive the shape functions of Eq. 7.1-1 by starting with $\phi = a_1 + a_2 r + a_3 s$ and applying the "[A] matrix procedure" (see Section 3.2).

7.1-2 Show that if the quadratic triangle (Fig. 7.1-1a) has straight sides and midside nodes, then its geometric mapping is linear. In other words, show that, as applied to geometry, Eqs. 7.1-2 reduce to Eqs. 7.1-1.

TABLE 7.4-2 SELECTED FORMULAS FOR NUMERICAL INTEGRATION OVER A TETRAHEDRAL VOLUME, EQ. 7.4-2 [7.11]

No. of points	Degree of precision	Coordinates (r_i,s_i,t_i)	Weights W_i
1	1	$\left(\frac{1}{4},\frac{1}{4},\frac{1}{4}\right)$	1.0
4	2	$(a,b,b),(b,b,b),(b,b,a),(b,a,b)$	$\frac{1}{4}$
		where $a = \dfrac{5+3\sqrt{5}}{20}$, $b = \dfrac{5-\sqrt{5}}{20}$	
5	3	$\left(\frac{1}{4},\frac{1}{4},\frac{1}{4}\right)$	$-\frac{4}{5}$
		$\left(\frac{1}{2},\frac{1}{6},\frac{1}{6}\right), \left(\frac{1}{6},\frac{1}{6},\frac{1}{6}\right), \left(\frac{1}{6},\frac{1}{6},\frac{1}{2}\right), \left(\frac{1}{6},\frac{1}{2},\frac{1}{6}\right)$	$\frac{9}{20}$

7.1-3 For the ten-node triangle shown, determine shape functions $N_i(r,s)$ for nodes 1, 2, 4, 5, 6, and 10.

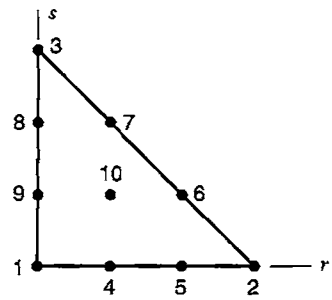

Problem 7.1-3

7.1-4 Let a triangular element be allowed to have 3, 4, 5, or 6 nodes. Postulate that a table like Table 6.4-1 is valid for this situation. Write out the table, and verify that it correctly provides shape functions of vertex nodes when side nodes 4, 5, and 6 are all present.

7.2-1 Show that $|\mathbf{J}| = 2A$ for a three-node triangle of arbitrary shape, where $|\mathbf{J}|$ is given by Eq. 7.2-4. *Suggestion:* Place the triangle in the first quadrant, drop lines from vertices to the x axis, and work with trapezoidal areas thus created.

7.2-2 Show that Eq. 7.2-6 provides [**B**] as stated in Eq. 3.4-6 for the element of Fig. 3.4-1.

7.2-3 For the triangle shown, determine the [**B**] matrix of a scalar element using bilinear shape functions (Eqs. 6.2-3). Show that Eq. 7.2-6 provides the same [**B**] matrix.

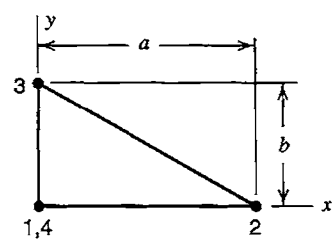

Problem 7.2-3

7.3-1 Working entirely in area coordinates, show that $\sum N_i = 1$ for the six shape functions of Eqs. 7.3-4.

7.3-2 A ten-node triangular element has a node at its centroid. In area coordinates, its shape function is $N_{10} = 27\xi_1\xi_2\xi_3$. Let ϕ be the field variable. Imagine that, with $\phi = 0$ at all nodes on the boundary of the element, nonzero ϕ_{10} produces ordinate $\phi = \phi_a$ at a point midway between node 10 and a vertex of the triangle. What is the volume under the ϕ surface, in terms of ϕ_a and triangle area A?

7.3-3 Consider a straight-sided triangle whose centroid is at the origin of Cartesian coordinates xy. Use area coordinates to derive the formula

$$\int_A x^2\, dA = \frac{A}{12}(x_1^2 + x_2^2 + x_3^2)$$

(Related formulas for triangles appear in [7.7].)

7.3-4 In terms of area coordinates ξ_i and generalized d.o.f. a_i, the polynomial field of a six-node triangle has the form

$$\phi = a_1\xi_1^2 + a_2\xi_2^2 + a_3\xi_3^2 + a_4\xi_1\xi_2 + a_5\xi_2\xi_3 + a_6\xi_3\xi_1$$

Using the "[A] matrix procedure" of Section 3.2, derive the element shape functions (Eqs. 7.3-4).

7.3-5 Let side 1-4-2 of a quadratic triangle be straight and of length L, with node 4 at midside. Also let an x axis be coincident with side 1-4-2. Use area coordinates evaluated on side 1-4-2 to determine the consistent nodal loads that result from the following distributed loads on this edge.
(a) Uniform traction normal to the side.
(b) Traction that is tangent to the side and varies parabolically, being zero at nodes 1 and 2 and maximum at node 4.
(c) Traction normal to the edge that varies linearly from $+\bar{\sigma}$ at node 2 to $-\bar{\sigma}$ at node 1.

7.3-6 Let uniform pressure p act normal to one face of a quadratic tetrahedron that has straight edges and midedge nodes. What are the consistent loads at nodes on this face?

7.4-1 Consider a straight-sided triangle of area $A = 0.5$, and the function

$$\phi = a_1 r + a_2 r^2 + a_3 rs + a_4 r^3 + a_5 rs^2$$

where the a_i are constants.
(a) Obtain the exact integral $I = \int \phi \, dA$ over area A by use of Eq. 7.3-7.
(b-e) Approximate I by use of the first, second, third, and fourth numerical formulas in Table 7.4-1.

7.4-2 By use of each numerical formula in Table 7.4-1, obtain four approximations for the integral of the function $\phi = (1 + rs)^{-1}$ over a triangle. Let $A = 1$.

7.4-3 Let a quadratic triangular element have curved sides and variable thickness t, where t is interpolated from thickness t_i at the six nodes, $t = \sum N_i t_i$. If the exact element volume is to be determined by numerical integration, what degree of precision must the numerical integration formula have?

7.4-4 Consider a flat-faced tetrahedron of volume $V = \frac{1}{6}$, and the function

$$\phi = a_1 r + a_2 r^2 + a_3 rs + a_4 r^3 + a_5 rs^2 + a_6 rst$$

where the a_i are constants.
(a) Obtain the exact integral $I = \int \phi \, dV$ over volume V by use of Eq. 7.3-9.
(b–d) Approximate I by use of the first, second, and third numerical formulas in Table 7.4-2.

CHAPTER 8

COORDINATE TRANSFORMATION AND SELECTED ANALYSIS OPTIONS

The chapter first considers how to change the coordinate system in which vectors, stresses, material properties, and stiffness matrices are described, and then discusses special element types and procedures of practical interest, including rigid links, joining of dissimilar or offset elements, elastic foundations, boundaries at infinity, reanalysis, and tests of element quality.

8.1 TRANSFORMATION: INTRODUCTION AND VECTOR FORMS

Some applications of transformation are in accommodating anisotropic material properties that are arbitrarily oriented in global coordinates and in forcing adjacent elements of different type to share the same d.o.f. In transformations, the form $[\mathbf{Q}] = [\mathbf{T}]^T[\mathbf{Q}'][\mathbf{T}]$ appears often. Here $[\mathbf{Q}']$ is the matrix to be transformed and $[\mathbf{T}]$ is the transformation matrix. The result of transformation, matrix $[\mathbf{Q}]$, is symmetric if $[\mathbf{Q}']$ is symmetric. Depending upon the application, $[\mathbf{T}]$ may be rectangular or square. If square, it may not be orthogonal. $[\mathbf{T}]$ is likely to be sparse if it is a large matrix. Then the formal matrix multiplication $[\mathbf{T}]^T[\mathbf{Q}'][\mathbf{T}]$ is wasteful of time and storage space, and can be replaced by coding adapted to the forms of $[\mathbf{T}]$ and $[\mathbf{Q}']$.

Matrices $[\mathbf{Q}]$ and $[\mathbf{Q}']$ are usually stiffness matrices, or analogous characteristic matrices in a nonstructural problem. Sometimes $[\mathbf{Q}']$ can be taken as either an element matrix or the corresponding structure matrix. Computer programming is usually easiest when transformations are done *before* elements are assembled, so that several small matrices are transformed rather than one large matrix.

Small errors and inconsistencies in $[\mathbf{T}]$ can degrade accuracy by making elements unable to represent constant states, including the state of rigid-body motion without strain. To minimize this source of error, transformation matrices (and constraint equations) should be written and manipulated with as much numerical precision as is granted to coefficients K_{ij} in the element characteristic matrix.

2D and 3D Vectors. Let $\mathbf{V}$ be a vector quantity (Fig. 8.1-1). It may represent position, or displacement, or heat flux, and so on. Components of $\mathbf{V}$ parallel to primed axes are u', v', and w'. We wish to express u', v', and w' in terms of direction cosines and u, v, and w, which are components of $\mathbf{V}$ parallel to unprimed axes.

Component u' can be regarded as the sum of x'-parallel components of u, v, and w. That is, $u' = l_1u + m_1v + n_1w$. Components v' and w' can be similarly expressed. In matrix format, these relations are

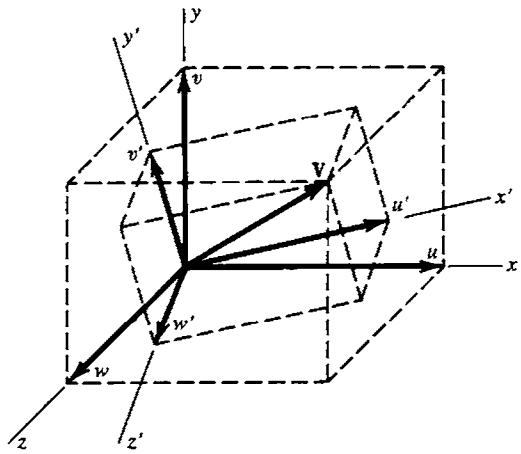

Direction cosines between axes:

	x	y	z
x'	l_1	m_1	n_1
y'	l_2	m_2	n_2
z'	l_3	m_3	n_3

Figure 8.1-1. A vector **V** can be expressed in terms of components uvw in system xyz or in terms of components $u'v'w'$ in system $x'y'z'$ Direction cosines are cosines of angles between axes.

$$\begin{Bmatrix} u' \\ v' \\ w' \end{Bmatrix} = [\Lambda]\begin{Bmatrix} u \\ v \\ w \end{Bmatrix} \qquad \text{where} \qquad [\Lambda] = \begin{bmatrix} l_1 & m_1 & n_1 \\ l_2 & m_2 & n_2 \\ l_3 & m_3 & n_3 \end{bmatrix} \tag{8.1-1}$$

Matrix $[\Lambda]$ is often called a *rotation matrix.* It is an *orthogonal* matrix; that is, $[\Lambda]^{-1} = [\Lambda]^T$. Hence the inverse of the transformation in Eq. 8.1-1 is

$$\begin{Bmatrix} u \\ v \\ w \end{Bmatrix} = [\Lambda]^T\begin{Bmatrix} u' \\ v' \\ w' \end{Bmatrix} \tag{8.1-2}$$

Let **V** represent the nodal displacement vector $\{\mathbf{d}\}$ or $\{\mathbf{d}'\}$. Vectors $\{\mathbf{d}\} = \lfloor u \quad v \quad w \rfloor^T$ and $\{\mathbf{d}'\} = \lfloor u' \quad v' \quad w' \rfloor^T$ are the same, but expressed in different coordinate systems. ("Displacement" may include rotation, provided it is small. Large rotations do not combine vectorially.) Corresponding nodal force vectors $\{\mathbf{r}\}$ and $\{\mathbf{r}'\}$ can be expressed in terms of components in the same way as displacements. According to Eqs. 8.1-1 and 8.1-2, these vectors obey the transformation rules

$$\{\mathbf{d}'\} = [\Lambda]\{\mathbf{d}\} \qquad \text{and} \qquad \{\mathbf{d}\} = [\Lambda]^T\{\mathbf{d}'\} \tag{8.1-3}$$

$$\{\mathbf{r}'\} = [\Lambda]\{\mathbf{r}\} \qquad \text{and} \qquad \{\mathbf{r}\} = [\Lambda]^T\{\mathbf{r}'\} \tag{8.1-4}$$

Equations 8.1-3 and 8.1-4 require only that xyz and $x'y'z'$ each be a set of mutually orthogonal directions. In some applications it might be convenient if one system is Cartesian and the other cylindrical.

More General Expressions. If nodal displacements and their corresponding forces have the respective relations

$$\{\mathbf{d}'\} = [\mathbf{T}]\{\mathbf{d}\} \qquad \text{and} \qquad \{\mathbf{r}'\} = [\mathbf{T}]\{\mathbf{r}\} \tag{8.1-5}$$

where $[\mathbf{T}]$ may not be orthogonal or even square, the form seen in the second of Eq. 8.1-4 continues to apply; that is, $\{\mathbf{r}\} = [\mathbf{T}]^T\{\mathbf{r}'\}$. The argument is as follows. Because $\{\mathbf{r}\}$ and $\{\mathbf{r}'\}$ describe the same resultant force, work done during a virtual displacement must be independent of the coordinate system in which work is computed. Let $\{\delta\mathbf{d}\}$ and $\{\delta\mathbf{d}'\}$ be descriptions of the same virtual displacement, in unprimed and primed coordinate systems respectively. Writing the virtual work equality and using the relation $\{\delta\mathbf{d}'\}^T = \{\delta\mathbf{d}\}^T[\mathbf{T}]^T$, we obtain

$$\{\delta\mathbf{d}\}^T\{\mathbf{r}\} = \{\delta\mathbf{d}'\}^T\{\mathbf{r}'\} \qquad \text{or} \qquad \{\delta\mathbf{d}\}^T\{\mathbf{r}\} = \{\delta\mathbf{d}\}^T[\mathbf{T}]^T\{\mathbf{r}'\} \tag{8.1-6}$$

from which

$$\{\delta\mathbf{d}\}^T\Big(\{\mathbf{r}\} - [\mathbf{T}]^T\{\mathbf{r}'\}\Big) = 0 \qquad \text{therefore} \qquad \{\mathbf{r}\} = [\mathbf{T}]^T\{\mathbf{r}'\} \tag{8.1-7}$$

The latter equation results from the consideration that the equation before it must be true for *any* virtual displacement $\{\delta\mathbf{d}\}$. The foregoing arguments apply also at the global level, so that we may also write $\{\mathbf{D}'\} = [\mathbf{T}]\{\mathbf{D}\}$ and $\{\mathbf{R}\} = [\mathbf{T}]^T\{\mathbf{R}'\}$.

8.2 STRAIN, STRESS, AND MATERIAL PROPERTY TRANSFORMATION

We seek the relation between quantities expressed in one coordinate system and the same quantities expressed in another coordinate system. Transformation of strains $\{\boldsymbol{\varepsilon}\}$ and stresses $\{\boldsymbol{\sigma}\}$ in two dimensions leads to equations that may be represented graphically by Mohr circles. In this section we emphasize three-dimensional transformation, for which there is no graphical representation. Material properties are represented by matrix $[\mathbf{E}]$ of elastic constants. Arrays $\{\boldsymbol{\varepsilon}\}$, $\{\boldsymbol{\sigma}\}$, and $[\mathbf{E}]$ have counterparts in problems other than structural mechanics.

Strains. Strain transformations are transformations of displacement derivatives. Thus, to relate ε_x' in coordinates $x'y'z'$ to ε_x in coordinates xyz, we must relate $\partial u'/\partial x'$ to $\partial u/\partial x$ and to other derivatives of u, v, and w. From Eq. 8.1-1,

$$\frac{\partial u'}{\partial x'} = l_1\frac{\partial u}{\partial x'} + m_1\frac{\partial v}{\partial x'} + n_1\frac{\partial w}{\partial x'} \tag{8.2-1}$$

For the term $\partial u/\partial x'$, by chain rule differentiation with $\partial x/\partial x' = l_1$, $\partial y/\partial x' = m_1$, and $\partial z/\partial x' = n_1$, we obtain

$$\frac{\partial u}{\partial x'} = l_1\frac{\partial u}{\partial x} + m_1\frac{\partial u}{\partial y} + n_1\frac{\partial u}{\partial z} \tag{8.2-2}$$

Applying this process to other displacement derivatives as well provides

$$\underbrace{\left\lfloor \frac{\partial u'}{\partial x'} \;\; \frac{\partial u'}{\partial y'} \;\; \frac{\partial u'}{\partial z'} \;\; \cdots \;\; \frac{\partial w'}{\partial z'} \right\rfloor^T}_{9\times 1} = \begin{bmatrix} l_1\mathbf{\Lambda} & m_1\mathbf{\Lambda} & n_1\mathbf{\Lambda} \\ l_2\mathbf{\Lambda} & m_2\mathbf{\Lambda} & n_2\mathbf{\Lambda} \\ l_3\mathbf{\Lambda} & m_3\mathbf{\Lambda} & n_3\mathbf{\Lambda} \end{bmatrix} \underbrace{\left\lfloor u_{,x} \;\; u_{,y} \;\; u_{,z} \;\; \cdots \;\; w_{,z} \right\rfloor^T}_{9\times 1} \tag{8.2-3}$$

where $[\mathbf{\Lambda}]$ is given by Eq. 8.1-1. The 9 by 9 square matrix in Eq. 8.2-3 is orthogonal.

A state of strain can be expressed as $\{\boldsymbol{\varepsilon}'\}$ in $x'y'z'$ coordinates or as $\{\boldsymbol{\varepsilon}\}$ in xyz coordinates. Next we introduce strain-displacement relations (Eqs. 3.1-6 to 3.1-8) into Eq. 8.2-3. After straightforward but tedious expansion and gathering of terms, we obtain

$$\{\boldsymbol{\varepsilon}'\} = [\mathbf{T}_\varepsilon]\{\boldsymbol{\varepsilon}\} \tag{8.2-4}$$

where $\{\boldsymbol{\varepsilon}\} = \lfloor \varepsilon_x \;\; \varepsilon_y \;\; \varepsilon_z \;\; \gamma_{xy} \;\; \gamma_{yz} \;\; \gamma_{zx} \rfloor^T$, and similarly for $\{\boldsymbol{\varepsilon}'\}$. The strain transformation matrix is

$$[\mathbf{T}_\varepsilon] = \left[\begin{array}{ccc|ccc} l_1^2 & m_1^2 & n_1^2 & l_1m_1 & m_1n_1 & n_1l_1 \\ l_2^2 & m_2^2 & n_2^2 & l_2m_2 & m_2n_2 & n_2l_2 \\ l_3^2 & m_3^2 & n_3^2 & l_3m_3 & m_3n_3 & n_3l_3 \\ \hline 2l_1l_2 & 2m_1m_2 & 2n_1n_2 & l_1m_2+l_2m_1 & m_1n_2+m_2n_1 & n_1l_2+n_2l_1 \\ 2l_2l_3 & 2m_2m_3 & 2n_2n_3 & l_2m_3+l_3m_2 & m_2n_3+m_3n_2 & n_2l_3+n_3l_2 \\ 2l_3l_1 & 2m_3m_1 & 2n_3n_1 & l_3m_1+l_1m_3 & m_3n_1+m_1n_3 & n_3l_1+n_1l_3 \end{array}\right] \tag{8.2-5}$$

Here the engineering definition of shear strain is used, for example, $\gamma_{xy} = u_{,y} + v_{,x}$. Partitioning seen in Eq. 8.2-5 is used in what follows.

Stresses. Consider internal work per unit volume, done by stresses during a prescribed virtual displacement. This work must be the same whether it is computed in the xyz system or the $x'y'z'$ system. Writing the virtual work equality and using Eq. 8.2-4, we obtain

$$\{\delta\boldsymbol{\varepsilon}\}^T\{\boldsymbol{\sigma}\} = \{\delta\boldsymbol{\varepsilon}'\}^T\{\boldsymbol{\sigma}'\} \qquad \text{or} \qquad \{\delta\boldsymbol{\varepsilon}\}^T\{\boldsymbol{\sigma}\} = \{\delta\boldsymbol{\varepsilon}\}^T[\mathbf{T}_\varepsilon]^T\{\boldsymbol{\sigma}'\} \tag{8.2-6}$$

The latter equation must be true for *any* virtual strain vector $\{\delta\boldsymbol{\varepsilon}\}$. Thus, in the same way as we obtain Eq. 8.1-7 from Eq. 8.1-6, we obtain the stress transformation relations

$$\{\boldsymbol{\sigma}\} = [\mathbf{T}_\varepsilon]^T\{\boldsymbol{\sigma}'\} \qquad \text{and} \qquad \{\boldsymbol{\sigma}'\} = [\mathbf{T}_\varepsilon]^{-T}\{\boldsymbol{\sigma}\} \tag{8.2-7}$$

where $\{\boldsymbol{\sigma}\} = \lfloor \sigma_x \;\; \sigma_y \;\; \sigma_z \;\; \tau_{xy} \;\; \tau_{yz} \;\; \tau_{zx} \rfloor^T$, and similarly for $\{\boldsymbol{\sigma}'\}$. Matrix $[\mathbf{T}_\varepsilon]^{-T}$ is easily stated. After assigning names $\mathbf{T}_{11}$, $\mathbf{T}_{12}$, $\mathbf{T}_{21}$, and $\mathbf{T}_{22}$ to the 3 by 3 submatrices in Eq. 8.2-5, one discovers that

$$\text{if} \qquad [\mathbf{T}_\varepsilon] = \begin{bmatrix} \mathbf{T}_{11} & \mathbf{T}_{12} \\ \mathbf{T}_{21} & \mathbf{T}_{22} \end{bmatrix} \qquad \text{then} \qquad [\mathbf{T}_\varepsilon]^{-T} = \begin{bmatrix} \mathbf{T}_{11} & 2\mathbf{T}_{12} \\ \tfrac{1}{2}\mathbf{T}_{21} & \mathbf{T}_{22} \end{bmatrix} \tag{8.2-8}$$

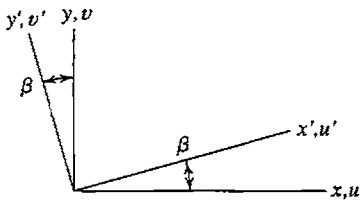

	x	y	z
x'	$l_1 = \cos\beta$	$m_1 = \sin\beta$	$n_1 = 0$
y'	$l_2 = -\sin\beta$	$m_2 = \cos\beta$	$n_2 = 0$
z'	$l_3 = 0$	$m_3 = 0$	$n_3 = 1$

Figure 8.2-1. Rotation of axes in two dimensions, a special case of Fig. 8.1-1.

Thus $[\mathbf{T}_\varepsilon]^{-T}$ is obtained from $[\mathbf{T}_\varepsilon]$ in Eq. 8.2-5 by moving the factors of 2 to their symmetrically located positions above the diagonal.

Material Properties. For a given set of material properties, the stress-strain relation can be written as $\{\boldsymbol{\sigma}\} = [\mathbf{E}]\{\boldsymbol{\varepsilon}\}$ in the xyz system or as $\{\boldsymbol{\sigma}'\} = [\mathbf{E}']\{\boldsymbol{\varepsilon}'\}$ in the $x'y'z'$ system. Imagine that $[\mathbf{E}']$ is known and that $[\mathbf{E}]$ is desired. By substitution from Eqs. 8.2-4, 8.2-7, and the relation $\{\boldsymbol{\sigma}'\} = [\mathbf{E}']\{\boldsymbol{\varepsilon}'\}$,

$$\{\boldsymbol{\sigma}\} = [\mathbf{T}_\varepsilon]^T\{\boldsymbol{\sigma}'\} = [\mathbf{T}_\varepsilon]^T[\mathbf{E}']\{\boldsymbol{\varepsilon}'\} = [\mathbf{T}_\varepsilon]^T[\mathbf{E}'][\mathbf{T}_\varepsilon]\{\boldsymbol{\varepsilon}\} \tag{8.2-9}$$

Finally, because $\{\boldsymbol{\sigma}\} = [\mathbf{E}]\{\boldsymbol{\varepsilon}\}$, we obtain

$$[\mathbf{E}] = [\mathbf{T}_\varepsilon]^T[\mathbf{E}'][\mathbf{T}_\varepsilon] \tag{8.2-10}$$

As in Eqs. 8.1-3 and 8.1-4, xyz and $x'y'z'$ need only be a set of mutually perpendicular directions.

Plane Problems. A two-dimensional problem is a special case in which $n_3 = 1$ and $l_3 = m_3 = n_1 = n_2 = 0$ (Fig. 8.2-1). Also, $\{\boldsymbol{\varepsilon}\} = \lfloor \varepsilon_x \ \varepsilon_y \ \gamma_{xy} \rfloor^T$, $\{\boldsymbol{\sigma}\} = \lfloor \sigma_x \ \sigma_y \ \tau_{xy} \rfloor^T$, $[\mathbf{E}]$ is 3 by 3, and transformation matrices are

$$[\mathbf{T}_\varepsilon] = \begin{bmatrix} c^2 & s^2 & cs \\ s^2 & c^2 & -cs \\ -2cs & 2cs & c^2-s^2 \end{bmatrix} \quad \text{and} \quad [\mathbf{T}_\varepsilon]^{-T} = \begin{bmatrix} c^2 & s^2 & 2cs \\ s^2 & c^2 & -2cs \\ -cs & cs & c^2-s^2 \end{bmatrix} \tag{8.2-11}$$

where $c = \cos\beta$ and $s = \sin\beta$.

8.3 TRANSFORMATION OF THE CHARACTERISTIC MATRIX

The element characteristic matrix $[\mathbf{k}]$ is a stiffness matrix in structural mechanics. For other problem areas, relations having the same form as those that follow can be written. Expressions stated in terms of element matrices could also be stated in terms of structure matrices. In a scalar field problem, $[\mathbf{k}]$ need not be transformed.

In two coordinate systems such as xyz and $x'y'z'$, the element stiffness relation can be stated as

$$[\mathbf{k}]\{\mathbf{d}\} = -\{\mathbf{r}\} \qquad \text{or as} \qquad [\mathbf{k}']\{\mathbf{d}'\} = -\{\mathbf{r}'\} \tag{8.3-1}$$

In Eq. 8.3-1, $\{\mathbf{r}\}$ and $\{\mathbf{r}'\}$ are loads associated with element deformation. The negative sign is used because, as explained following Eq. 2.2-2, $\{\mathbf{r}\}$ and $\{\mathbf{r}'\}$ are defined as loads applied *by* an element *to* structure nodes. Matrices $[\mathbf{k}]$ and $[\mathbf{k}']$ express the same information, but with reference to two different vectors of nodal d.o.f., namely $\{\mathbf{d}\}$ and $\{\mathbf{d}'\}$. Let us assume that $[\mathbf{k}']$ is known and that $[\mathbf{k}]$ is desired. The necessary transformation is derived by substituting Eqs. 8.1-5 and 8.1-7 into the stiffness relation.

$$[\mathbf{k}]\{\mathbf{d}\} = -\{\mathbf{r}\} = -[\mathbf{T}]^T\{\mathbf{r}'\} = [\mathbf{T}]^T[\mathbf{k}']\{\mathbf{d}'\} = [\mathbf{T}]^T[\mathbf{k}'][\mathbf{T}]\{\mathbf{d}\} \tag{8.3-2}$$

As the relation $[\mathbf{k}]\{\mathbf{d}\} = [\mathbf{T}]^T[\mathbf{k}'][\mathbf{T}]\{\mathbf{d}\}$ must be true for *any* $\{\mathbf{d}\}$, we obtain

$$[\mathbf{k}] = [\mathbf{T}]^T[\mathbf{k}'][\mathbf{T}] \tag{8.3-3}$$

Or, if the argument is applied on the global level, we obtain $[\mathbf{K}] = [\mathbf{T}]^T[\mathbf{K}'][\mathbf{T}]$.

The transformation of Eq. 8.3-3 can be regarded as changing neither element properties nor element orientation in global coordinates, but rather as changing the *formal expression* of element properties to agree with a change in d.o.f. from $\{\mathbf{d}'\}$ to $\{\mathbf{d}\}$. In the relation $\{\mathbf{d}'\} = [\mathbf{T}]\{\mathbf{d}\}$, transformation matrix $[\mathbf{T}]$ must be known but need have no special form. Applications of Eq. 8.3-3 appear in Section 2.4 and in the following two sections.

8.4 CHANGING THE DIRECTIONS OF RESTRAINTS

If a support allows a node to move only in one direction, and that direction is parallel to a translational d.o.f. already defined, the boundary condition is simple: we merely suppress all other translational d.o.f. at the node. If the permitted motion is in some other direction, a transformation of the following kind is useful. (An ad hoc way of treating this support condition may lead to trouble; see Fig. 9.2-3c.)

We take as an example the plane structure of Fig. 8.4-1a, which may be either a truss or a frame. Before boundary conditions are imposed, structural equations $[\mathbf{K}']\{\mathbf{D}'\} = \{\mathbf{R}'\}$, subsequently to be transformed, are

$$\begin{bmatrix} \mathbf{K}_{11} & \mathbf{K}_{12} & \mathbf{K}_{13} & \mathbf{K}_{14} \\ \mathbf{K}_{21} & \mathbf{K}_{22} & \mathbf{0} & \mathbf{K}_{24} \\ \mathbf{K}_{31} & \mathbf{0} & \mathbf{K}_{33} & \mathbf{K}_{34} \\ \mathbf{K}_{41} & \mathbf{K}_{42} & \mathbf{K}_{43} & \mathbf{K}_{44} \end{bmatrix} \begin{Bmatrix} \mathbf{D}_1 \\ \mathbf{D}_2 \\ \mathbf{D}_3 \\ \mathbf{D}_4 \end{Bmatrix} = \begin{Bmatrix} \mathbf{R}_1 \\ \mathbf{R}_2 \\ \mathbf{R}_3 \\ \mathbf{R}_4 \end{Bmatrix} \tag{8.4-1}$$

Merely to avoid clutter, we have not attached a prime symbol to each submatrix. If formulated in global coordinates xy in the usual way, each $\{\mathbf{D}_i\}$ contains translational d.o.f. u_i and v_i in x and y directions at nodes. Rotational d.o.f. θ_{zi} are also present if the structure is a frame. At nodes 1 and 2, support conditions indicate that u and v are zero. At node 3, the roller support demands the awkward condition $v_3 = -u_3 \tan \beta$. If at node 3 we replace u_3 and v_3 by translational d.o.f. U_3 and V_3 parallel to axes of the rs coordinate system, the boundary condition becomes simply $V_3 = 0$. We now regard submatrices associated with

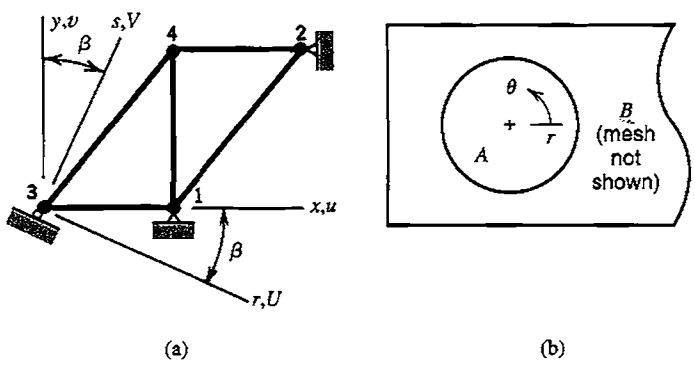

Figure 8.4-1. (a) A plane truss or plane frame, in which node 3 is allowed to move in only the r direction. (b) Pin A occupies a large circular hole in plane bar B.

node 3 as primed arrays that require transformation. Transformation $\{\mathbf{D}_3'\} = [\mathbf{T}_3]\{\mathbf{D}_3\}$ among d.o.f. at node 3 is, for plane truss and plane frame problems respectively,

$$\begin{Bmatrix} u_3 \\ v_3 \end{Bmatrix} = \underbrace{\begin{bmatrix} c & s \\ -s & c \end{bmatrix}}_{[\mathbf{T}_3]} \begin{Bmatrix} U_3 \\ V_3 \end{Bmatrix} \quad \text{or} \quad \begin{Bmatrix} u_3 \\ v_3 \\ \theta_{z3} \end{Bmatrix} = \underbrace{\begin{bmatrix} c & s & 0 \\ -s & c & 0 \\ 0 & 0 & 1 \end{bmatrix}}_{[\mathbf{T}_3]} \begin{Bmatrix} U_3 \\ V_3 \\ \theta_{z3} \end{Bmatrix} \tag{8.4-2}$$

where $c = \cos\beta$ and $s = \sin\beta$. Transformation matrix $[\mathbf{T}]$ for the entire structure is a unit matrix except for $[\mathbf{T}_3]$ on the diagonal. With $\lceil \mathbf{I} \rfloor$ a 2 by 2 or a 3 by 3 unit matrix (for plane truss and plane frame respectively), $[\mathbf{T}]$ is

$$[\mathbf{T}] = \lceil \mathbf{I} \quad \mathbf{I} \quad \mathbf{T}_3 \quad \mathbf{I} \rfloor \tag{8.4-3}$$

Using $[\mathbf{K}']$ and $[\mathbf{T}]$ from Eqs. 8.4-1 and 8.4-3 in Eq. 8.3-3, we obtain the transformed structure stiffness matrix

$$[\mathbf{T}]^T[\mathbf{K}'][\mathbf{T}] = \begin{bmatrix} \mathbf{K}_{11} & \mathbf{K}_{12} & \mathbf{K}_{13}\mathbf{T}_3 & \mathbf{K}_{14} \\ \mathbf{K}_{21} & \mathbf{K}_{22} & \mathbf{0} & \mathbf{K}_{24} \\ \mathbf{T}_3^T\mathbf{K}_{31} & \mathbf{0} & \mathbf{T}_3^T\mathbf{K}_{33}\mathbf{T}_3 & \mathbf{T}_3^T\mathbf{K}_{34} \\ \mathbf{K}_{41} & \mathbf{K}_{42} & \mathbf{K}_{43}\mathbf{T}_3 & \mathbf{K}_{44} \end{bmatrix} \tag{8.4-4}$$

which operates on a displacement vector $\{\mathbf{D}\}$ whose translational d.o.f. at node 3 are U_3 and V_3. From Eq. 8.1-7, transformed loads at node 3 are $\{\mathbf{R}_3\} = [\mathbf{T}_3]^T\{\mathbf{R}_3'\}$. The transformed stiffness matrix and load vector can be transformed again in the same way if there is an additional inclined support.

In the preceding explanation, transformation is done at the structure level. In programming, this approach becomes awkward because $[\mathbf{K}]$ is stored in a compact format. It is preferable to transform individual element matrices before assembly. Thus, in the foregoing example, we transform element matrices $[\mathbf{k}']$ of elements 3-1 and 3-4 according to Eq. 8.3-3, using the transformation matrix $[\mathbf{T}] = \lceil \mathbf{T}_3 \quad \mathbf{I} \rfloor$. If d.o.f. of node 3 were to appear second rather than first in $\{\mathbf{d}\}$, we would use $[\mathbf{T}] = \lceil \mathbf{I} \quad \mathbf{T}_3 \rfloor$ instead.

Another possible application is shown in Fig. 8.4-1b. Imagine that plane bar B is free to rotate without friction on pin A, which for the time being is to be regarded as rigid. Pin A need not be meshed. D.o.f. of nodes of bar B that lie on the circular boundary can be transformed to the polar coordinate system shown. Then only radial displacements at these nodes are set to zero.

8.5 CONNECTING DISSIMILAR ELEMENTS. RIGID ELEMENTS

By "dissimilar elements" we mean elements whose d.o.f. are of different type and/or of different location. As examples, we may wish to connect a beam element (having rotational d.o.f.) to a plane element (having translational d.o.f. only), or we may wish to connect two FE meshes whose nodal locations are such that nodes of one mesh cannot be superposed on nodes of the other. The latter situation also arises in *submodeling* and *substructuring* (Sections 10.10 and 10.11, where references are cited).

A way of dealing with these situations is to impose constraints that force d.o.f. of mating elements or meshes to have a prescribed relation to one another. Constraints of this kind can be imposed on a stiffness matrix by the transformation $[\mathbf{k}] = [\mathbf{T}]^T[\mathbf{k}'][\mathbf{T}]$. In establishing transformation matrix $[\mathbf{T}]$, it is convenient to think in terms of a rigid link or a rigid element that contains the d.o.f. to be related. (Constraints are discussed in a more general way in Chapter 13.)

Simple Examples. In Fig. 8.5-1a, one end of a plane beam element that has both bending and axial stiffness is to be attached at an arbitrary location on one side of a four-node plane quadrilateral that has no rotational d.o.f. The beam element has the stiffness relation $[\mathbf{k}']\{\mathbf{d}'\} = \{\mathbf{r}'\}$, where

$$\{\mathbf{d}'\} = \lfloor u_5 \quad v_5 \quad \theta_{z5} \quad u_6 \quad v_6 \quad \theta_{z6} \rfloor^T \tag{8.5-1}$$

New d.o.f. of the beam element are to be

$$\{\mathbf{d}\} = \lfloor u_2 \quad v_2 \quad u_3 \quad v_3 \quad u_6 \quad v_6 \quad \theta_{z6} \rfloor^T \tag{8.5-2}$$

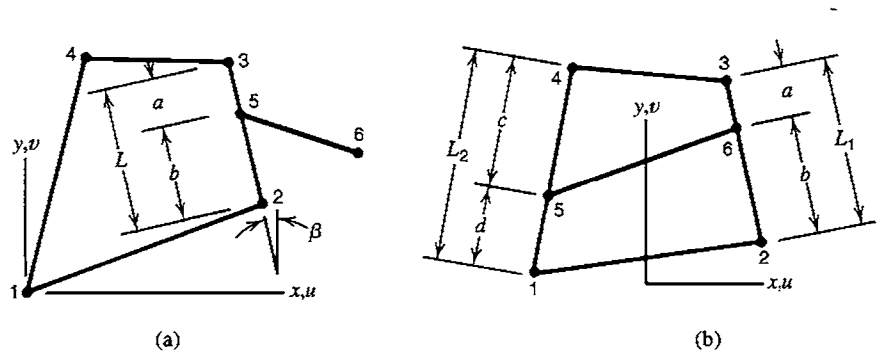

Figure 8.5-1. (a) Plane beam element 5-6 is connected to four-node plane element 1-2-3-4. (b) Two-node bar element 5-6 is connected to four-node plane element 1-2-3-4.

We now require that translation of node 5 be linearly interpolated along side 2-3 from translational d.o.f. at nodes 2 and 3. Rotation at node 5 is defined as the difference between the side-normal displacements at nodes 2 and 3, divided by the distance L between them. Thus, in the relation $\{\mathbf{d}'\} = [\mathbf{T}]\{\mathbf{d}\}$, transformation matrix $[\mathbf{T}]$ is

$$\underset{6\times 7}{[\mathbf{T}]} = \begin{bmatrix} \mathbf{T}_5 & \mathbf{0} \\ \mathbf{0} & \mathbf{I} \end{bmatrix} \quad \text{where} \quad [\mathbf{T}_5] = \frac{1}{L}\begin{bmatrix} a & 0 & b & 0 \\ 0 & a & 0 & b \\ \cos\beta & \sin\beta & -\cos\beta & -\sin\beta \end{bmatrix} \tag{8.5-3}$$

and $\lceil \mathbf{I} \rfloor$ is the unit matrix $\lceil 1 \quad 1 \quad 1 \rfloor$. The transformed beam element matrix is 7 by 7, and operates on d.o.f. of nodes 2, 3, and 6. After solution for nodal d.o.f., original d.o.f. of the beam element can be recovered by the operation $\{\mathbf{d}'\} = [\mathbf{T}]\{\mathbf{d}\}$, for use in stress calculation.

A second simple example is that of Fig. 8.5-1b. A two-force member, such as a portion of a reinforcing bar in concrete, is to be connected to points arbitrarily located on opposite sides of a four-node plane element. As originally formulated, the 2 by 2 matrix $[\mathbf{k}']$ of the bar element operates on d.o.f. u_5, v_5, u_6, and v_6. By transformation, we seek the 8 by 8 matrix $[\mathbf{k}] = [\mathbf{T}]^T[\mathbf{k}'][\mathbf{T}]$ of the bar element, which operates on d.o.f. u_i and v_i of the four-node element, where $i = 1,2,3,4$. Matrix $[\mathbf{T}]$ is 4 by 8, and contains terms like those seen in the first two rows of $[\mathbf{T}_5]$ in Eq. 8.5-3. References that deal with 3D situations and full bonding between concrete and reinforcement include [8.1].

The examples of Fig. 8.5-1 invoke constraint transformation as a way of connecting elements whose nodes do not coincide. Transformation may not be needed if nodes coincide, even if elements to be connected do not have the same set of nodal d.o.f. Consider Fig. 8.5-2a. The connection at A is a hinge because the beam has a rotational d.o.f. but plane elements do not (unless the plane elements happen to have drilling d.o.f., but then such a connection is not recommended). The hinge is avoided by the ad hoc arrangement in Fig. 8.5-2b, where the beam has been extended into the plane body by adding two beam elements AB and BC. Adding only one beam element, AB, is also plausible [8.2]. Translational d.o.f. are shared by plane elements and beam elements at nodes A, B, and C. Rotational d.o.f. at these nodes are associated with only the beam elements. One should not expect that stresses will be accurately computed near node A.

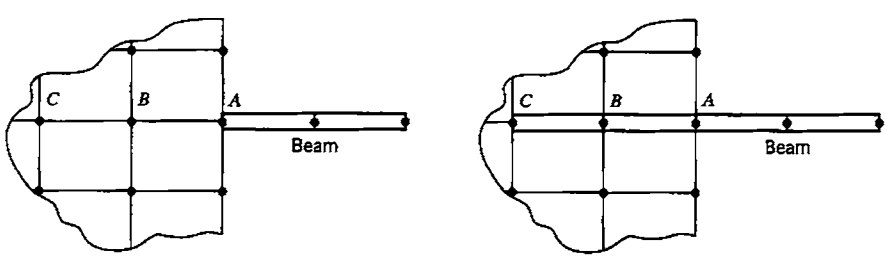

(a) (b)

Figure 8.5-2. Connecting a 2D beam element to a mesh of four-node plane elements. (a) Hinge mechanism. No moment is transferred at A. (b) Moment is transferred between the beam and the plane mesh.

The method described in the preceding paragraph can also be applied to analogous axisymmetric problems. Then Fig. 8.5-2 would represent a cross section that contains the axis of revolution and shows the connection of a flat annular plate and an axisymmetric solid.

Eccentric Stiffeners. Plates are often reinforced by attaching beams to one side of the plate (Fig. 8.5-3). Beam nodes and plate nodes do not coincide, but are typically separated by a distance that is small in comparison with other dimensions ($b << L$ in Fig. 8.5-3). Adjacent nodes such as 1 and 3 can then be regarded as joined by a rigid link, whose displacement components completely define displacements of plate and beam nodes at ends of the link. Displacements of the link can be stated in terms of d.o.f. of a node placed anywhere along it. In what follows we take this node to be coincident with the plate node. Thus the plate midsurface becomes the reference plane of the assembled structure. Stiffness matrices of beam elements are transformed. Beam d.o.f. become "slave" to plate d.o.f., and beam d.o.f. do not appear explicitly in the global array of d.o.f.

Let the plate shown in Fig. 8.5-3b be an element having a node at each corner, and the beam an element having a node at each end. Both elements have both bending stiffness and membrane (or axial) stiffness. Imagine that a rigid weightless link joins nodes 1 and 3, and that a similar link joins nodes 2 and 4. In the following equation we assume that rotations are small and include only d.o.f. needed to describe deformation in the xz plane. At the left end, the transformation is

$$\begin{Bmatrix} u_3 \\ w_3 \\ \theta_{y3} \end{Bmatrix} = [\mathbf{T}_b]\begin{Bmatrix} u_1 \\ w_1 \\ \theta_{y1} \end{Bmatrix} \qquad \text{where} \qquad [\mathbf{T}_b] = \begin{bmatrix} 1 & 0 & -b \\ 0 & 1 & 0 \\ 0 & 0 & 1 \end{bmatrix} \tag{8.5-4}$$

A similar transformation applies at the right end, with subscripts 1 and 3 replaced by 2 and 4. Let primed arrays refer to the original beam element, when it is associated with d.o.f. at nodes 3 and 4. When associated with d.o.f. at nodes 1 and 2, arrays $[\mathbf{k}]$ and $\{\mathbf{r}\}$ of the beam element are

$$\begin{aligned} [\mathbf{k}] &= [\mathbf{T}]^T[\mathbf{k}'][\mathbf{T}] \\ \{\mathbf{r}\} &= [\mathbf{T}]^T\{\mathbf{r}'\} \end{aligned} \qquad \text{where} \qquad [\mathbf{T}] = \begin{bmatrix} \mathbf{T}_b & \mathbf{0} \\ \mathbf{0} & \mathbf{T}_b \end{bmatrix} \tag{8.5-5}$$

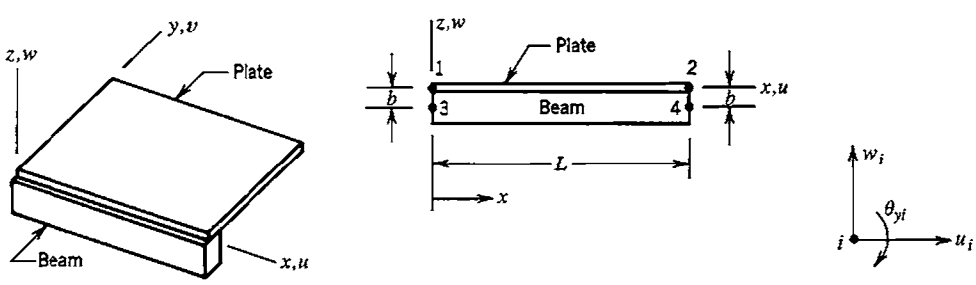

(a) (b) (c)

Figure 8.5-3. (a) A beam element attached to a plate element along one edge. (b) Side view. (c) Typical node, showing d.o.f. used in the transformation.

Clearly this procedure can be extended to account for twisting of the stiffener, and to deal with a stiffener that is arbitrarily oriented in space or with rigid links that are not perpendicular to either element. If elements to be connected do not use parallel directions of d.o.f., the rotation transformation discussed in Section 8.1 must also be used.

When the transformation of Eqs. 8.5-4 and 8.5-5 is applied to a standard beam element, to make its d.o.f. slave to d.o.f. of a plate element, the beam-plate assembly displays the correct stiffness in states of pure stretching and pure bending. But if curvature varies with x, the assembly is too flexible. Consider the deformation state $u_1 = u_2 = w_1 = w_2 = 0$, $\theta_{y1} = \theta_{y2}$, which bends both beam and plate elements into S shapes, without axial strain in either. Thus, rather than sharing a common neutral axis, beam and plate cross sections each rotate about neutral axes at their own centroids. Thus flexural stiffness is underestimated. In applications, repeated mesh subdivision causes each element to approach a state of constant curvature, for which adjacent beam and plate elements share a common neutral axis, as they should. Discussion of eccentric stiffeners, and a remedy for the foregoing defect of transformation, appears in [2.17,8.3–8.5].

Rigid Elements. In the preceding discussion we introduced imaginary rigid links to make d.o.f. of one element "slave" to d.o.f. of another element. Generalizing, we can imagine a rigid element of any shape and size, to be used as a device for enforcing a relation among two or more d.o.f. Such a relationship is sometimes called a *multipoint constraint.*

Another application of rigid elements appears when an element or patch of elements happens to be far stiffer then the mesh in which it is embedded. This situation may provoke numerical errors of the type discussed in Section 9.2. These errors can be avoided by representing the stiff region as perfectly rigid. Again transformation relations provide a way to enforce the rigidity constraint.

As an example, imagine that triangle 1-2-3 in Fig. 8.5-4a is to be idealized as perfectly rigid. Thus it has only rigid-body motion in the xy plane, which is defined by only three d.o.f., say u_1, v_1, and u_2. These d.o.f. are related to the original six d.o.f. by the transformation

$$\{\mathbf{d}'\} = [\mathbf{T}]\{\mathbf{d}\} \qquad \text{or} \qquad \begin{Bmatrix} u_1 \\ v_1 \\ u_2 \\ v_2 \\ u_3 \\ v_3 \end{Bmatrix} = \begin{bmatrix} 1 & 0 & 0 \\ 0 & 1 & 0 \\ 0 & 0 & 1 \\ -a/b & 1 & a/b \\ 1 & 0 & 0 \\ -a/b & 1 & a/b \end{bmatrix} \begin{Bmatrix} u_1 \\ v_1 \\ u_2 \end{Bmatrix} \tag{8.5-6}$$

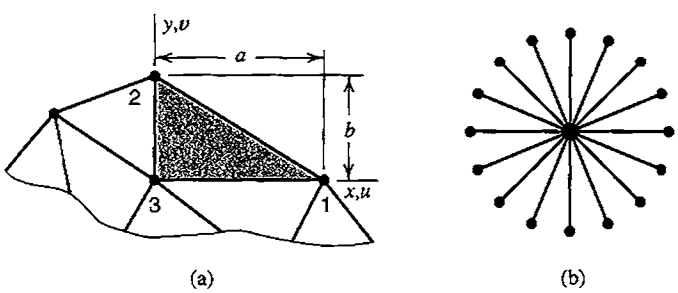

Figure 8.5-4. (a) Rigid element 1-2-3 in a mesh of plane elastic elements. (b) Fanlike array of rigid links.

in which $u_3 = u_1$ and $v_2 = v_3 = v_1 - \theta_z a$, where $\theta_z = (u_1 - u_2)/b$ is a small rigid-body rotation. This transformation removes d.o.f. v_2, u_3, and v_3 from the array of structure d.o.f. Elastic properties of element 1-2-3 do not matter; they are overridden by the rigid-body constraint. Equation 8.5-6 can be used to construct a transformation matrix applicable to the entire structure, although it is probably better to apply these relations before assembly, to each element that contains one of the d.o.f. to be removed.

The choice $\{\mathbf{d}\} = \lfloor u_1 \quad v_1 \quad u_2 \rfloor^T$ is not unique. It would not even be acceptable if node numbers of the rigid triangle were permuted from 1-2-3 to 2-3-1, so that $y_2 - y_1 = 0$. Then there would be a division by zero in Eq. 8.5-6, and the use of u_1 and u_2 as independent d.o.f. would contradict the statement that the triangle is rigid. Clearly the d.o.f. to be retained must be chosen carefully.

A possible drawback of rigid elements is that they cannot expand or contract with temperature change. Another possible drawback, encountered in dynamic problems, is that transformation converts a diagonal element mass matrix $[\mathbf{m}']$ to a nondiagonal mass matrix $[\mathbf{m}]$.

The plane problem discussed in connection with Fig. 8.4-1b can be treated using a fanlike array of rigid links (Fig. 8.5-4b). One such link connects each node on the circular boundary of bar B to a node at the center of pin A. At this node, rotation is permitted but translation is prevented.

Various other applications of rigid links might be imagined. The effect of a spot weld that connects overlapping plates might be approximated by connecting two adjacent nodes, one in each plate and on the plate midsurface, by a rigid link oriented normal to the plate midsurfaces. Such a model concentrates moment transfer to a single node on each midsurface. The moment could be spread by adding a fanlike array of rigid links in each plate (Fig. 8.5-4b). Each array would be centered at a midsurface node, have the same diameter as the spot weld, and replace plate material over that diameter. The connector between central midsurface nodes might be a beam element rather than a rigid link.

8.6 HIGHER DERIVATIVES AS NODAL D.O.F.

Displacement-based elements in common use have translations and rotations as nodal d.o.f. In terms of axes xyz, these motions are displacements u, v, and w along axes and rotations θ_x, θ_y, and θ_z about axes. Thus, d.o.f. of a typical plane element in the xy plane are nodal values of u and v, and d.o.f. of a typical plate bending element in the xy plane are nodal values of w, θ_x, and θ_y. For these elements, higher-derivative nodal d.o.f. would include strain components $u_{,x}$, $u_{,y}$, $v_{,x}$, and $v_{,y}$ for the plane element and curvatures $w_{,xx}$, $w_{,yy}$, and $w_{,xy}$ for the plate bending element. In years past, elements with nodal d.o.f. such as these were proposed in many research papers.

Elements having many d.o.f. per node are necessarily based on high-order fields. Thus, for a given number of elements, they provide better accuracy than conventional elements. Strain (or curvature) terms used for calculation of stresses (or bending moments) appear in the vector of nodal d.o.f. Therefore, strains $\{\boldsymbol{\varepsilon}\} = [\mathbf{B}]\{\mathbf{d}\}$ may be computed more accurately than in conventional elements. Furthermore, displacement derivatives used in strain calculation are available directly at nodes, which are locations where the conventional calculation $\{\boldsymbol{\varepsilon}\} = [\mathbf{B}]\{\mathbf{d}\}$ is not particularly accurate.

However, elements having higher-order d.o.f. can be awkward to use. Where there is an abrupt change of thickness or material properties, interelement continuity of higher derivatives must *not* be enforced. For example, if a plate has a step change in thickness, bending moment is continuous across the step but curvature is not. To avoid enforcing continuity of curvature, in one of a pair of elements that share the step as an interelement boundary, curvature d.o.f. at nodes on the step can be condensed before assembly of elements. In addition to the trouble of doing the condensation, we reduce the benefit of higher-derivative d.o.f. in the very place where it might be most appreciated—near a high stress gradient.

Boundary conditions become awkward because the physical meaning of higher-derivative d.o.f. and their associated loads is often obscure. For example, if a plane element includes $u_{,x}$, $u_{,y}$, $v_{,x}$, and $v_{,x}$ as nodal d.o.f., a stress-free boundary dictates a constraint relation among these d.o.f. but does not dictate the numerical value of any of them.

Software is usually coded in such a way that the vector of d.o.f. at each node is limited in size, perhaps to three translations, three rotations, temperature, and pressure. Thus an element with a sizeable list of d.o.f. at each node could not easily be added to the software.

In summary, higher-derivative d.o.f. tend to make FEA awkward in application to problems for which it is best suited—problems that require a mixture of element types, have abrupt changes in geometry, or have components that meet at sharp angles rather than with smooth curves.

8.7 FRACTURE MECHANICS. SINGULARITY ELEMENTS

A body can fail due to sudden propagation of an existing crack of macroscopic size, even if behavior is ductile when no crack is present. *Fracture mechanics* deals with the conditions under which cracks may suddenly propagate [8.6]. In analysis, one might ask for the load that will produce failure, or for the allowable size of a crack when a known load must be sustained.

Fracture mechanics is a separate discipline with its own extensive literature. Also, many papers have been written about FE applications to fracture mechanics. In this section we present only an introductory discussion.

Three different crack deformation modes can be identified (Fig. 8.7-1). It is possible for these modes to appear in combination. Mode I, the crack-opening mode, is most common. Stresses rise sharply with decreasing distance from a crack tip, and can be quantified by a *stress intensity factor K*:

$$K_{\mathrm{I}} = \beta\sigma\sqrt{\pi a} \tag{8.7-1}$$

where subscript I indicates that the factor applies to mode I. As shown in Fig. 8.7-2, stress σ in Eq. 8.7-1 is the stress sufficiently far from the crack to not be influenced by it, and a is the conventional symbol for crack length ($2a$ for a central crack and a for an edge crack). Dimensionless factor β depends on geometry. In Fig. 8.7-2, β depends on the ratio a/w and is not the same for the two cracks shown. A stress intensity factor is *not* a stress concentration factor; their definitions are fundamentally different. Also, K_{I} has units $\mathrm{MPa}\sqrt{\mathrm{m}}$, while a stress concentration factor is dimensionless. Although stresses are high near a crack tip, σ in Eq. 8.7-1 is the far-field stress, and no stress concentration factor is invoked in Eq. 8.7-1.

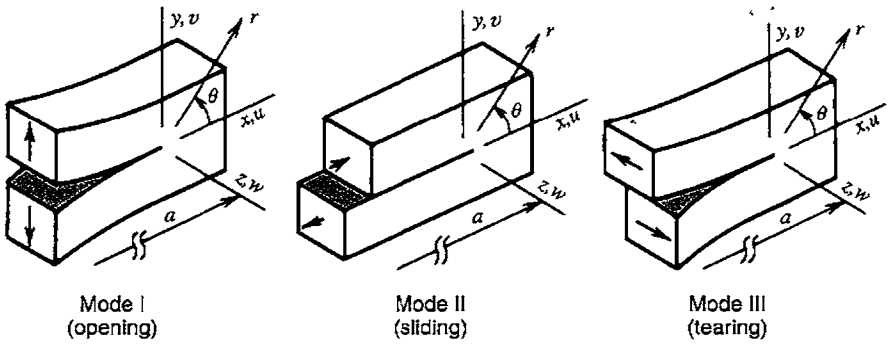

Figure 8.7-1. Deformation modes in the immediate neighborhood of a crack tip.

Fracture impends when K_I reaches a critical value K_{Ic}, which is called *fracture toughness* and, like K_I, has units MPa$\sqrt{\text{m}}$. If some conditions are met, K_{Ic} can be regarded as a material property, for which numerical values are tabulated. The conditions are that crack length a and specimen thickness t must both be at least $2.5(K_{Ic}/\sigma_Y)^2$, where σ_Y is the yield strength in a tension test. For smaller values of a and t, fracture toughness is a function of a and t. With $K_I = K_{Ic}$ in Eq. 8.7-1, one could solve for the stress σ or the crack length a that will produce fracture. Or, if σ and a are provided, one could solve for the required K_{Ic}.

Stress intensity factors, especially for mode I cracks, are tabulated for simple geometries and loadings. For arbitrary geometries and loadings, FEA provides a way to compute stress intensity factors. To calculate the load that will produce failure, one can apply an arbitrary reference load, determine the stress intensity factor, then multiply the reference load by the ratio of fracture toughness to computed stress intensity factor. Also, FEA can provide the stress field near a crack or a pattern of cracks in a body of arbitrary geometry.

Theory shows that, for linearly elastic conditions, stresses near a crack tip are inversely proportional to $\sqrt{r}$, where r is distance from the crack tip. Although conventional elements cannot represent a $1/\sqrt{r}$ stress field, they can be used to obtain a stress intensity factor because the calculations required depend on conditions *near* the crack tip but not *at* it. However, elements that can represent a $1/\sqrt{r}$ stress field provide greater accuracy for a given number of elements, or comparable accuracy with a smaller number of elements. It happens that conventional elements that have side nodes become capable of representing a $1/\sqrt{r}$ stress field when the side nodes are properly placed.

Quarter Point Elements. An isoparametric element having side nodes can be made to incorporate the desired stress field merely by moving side nodes so they appear at quarter points rather than at midsides. To illustrate this behavior in the simplest way, we consider the three-node bar element discussed in Section 6.1. This element is shown again in Fig. 8.7-3, but now with nodes at $x_1 = 0$, $x_2 = L/4$, and $x_3 = L$. Equations 6.1-3 and 6.1-4 yield

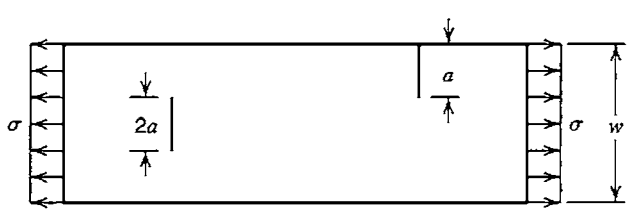

Figure 8.7-2. Flat plate of width w with a central crack and an edge crack. In-plane stress σ is uniform well away from the cracks.

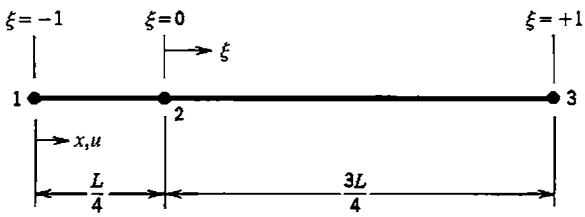

Figure 8.7-3. Three-node bar element with node 2 at the quarter point.

$$x = \frac{L}{4}(1+\xi)^2 \qquad \text{or} \qquad \xi = 2\sqrt{\frac{x}{L}} - 1 \tag{8.7-2}$$

Equations 6.1-6 and 6.1-7 yield J and $\lfloor \mathbf{B} \rfloor$, from which ξ may be eliminated by means of Eq. 8.7-2. The resulting expression for axial strain is

$$\varepsilon_x = \left[\left(\frac{2}{L} - \frac{3}{2\sqrt{Lx}}\right) \quad \left(-\frac{4}{L} + \frac{2}{\sqrt{Lx}}\right) \quad \left(\frac{2}{L} - \frac{1}{2\sqrt{Lx}}\right)\right] \begin{Bmatrix} u_1 \\ u_2 \\ u_3 \end{Bmatrix} \tag{8.7-3}$$

Equation 8.7-3 shows that if $x << L$, then ε_x (and consequently σ_x) varies inversely with $\sqrt{x}$. That is, the desired singularity is present. The element retains the ability to represent rigid-body motion without strain ($\varepsilon_x = 0$ when $u_1 = u_2 = u_3$), and the ability to represent a constant strain state ($\varepsilon_x = c$ when $u_i = cx_i$).

Six-node plane triangles behave the same way. Therefore, it is appropriate to surround a crack tip by a disklike patch in which element sides emanating from the crack tip have their nodes at quarter points, as shown in Fig. 8.7-4b. For best accuracy it is recommended that each triangle be straight-sided, isosceles, with side node at midside on the side opposite the crack, $l < a/8$, and $30° < \alpha < 40°$ [8.7]. The $1/\sqrt{r}$ stress variation appears on all rays that emanate from the crack tip. The same is true of a triangle created by collapsing an eight-node quadrilateral so that nodes 1, 4, and 8 in Fig. 6.4-1 are superposed so that they have the same coordinates *and* the same displacement components. The eight-node quadrilateral with quarter-point nodes on two of its four sides is not quite as successful. In three dimensions, curved crack fronts lead to some difficulties. References include [8.8].

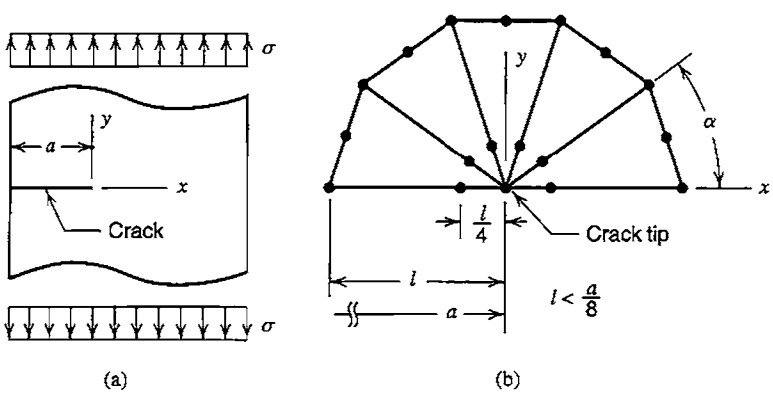

Figure 8.7-4. (a) Flat bar loaded in tension, with edge crack of length a. (b) Mesh of quarter-point triangular elements around the crack tip. Symmetry can be exploited by modeling only the $y > 0$ portion of the bar.

The advantage of quarter-point elements is that they are created merely by input data that specifies nodal positions of elements already contained in standard software. Quarter-point elements pass patch tests, so proper convergence with mesh refinement is assured. Of course, alternatives exist. Hybrid elements have been devised that have displacement d.o.f. and an internal stress field that incorporates the desired singularity. Boundary elements, discussed in the following section, also serve.

Calculation of K_I. There are three ways to calculate a stress intensity factor. Each is preceded by analysis of the cracked body. Then the factor can be calculated by the crack-opening displacement method, the stiffness-derivative method, or the J-integral method. The crack-opening displacement method is simplest but least accurate. The other two alternatives have approximately equal accuracy [8.8]. The J-integral method is often used, but the stiffness-derivative method is much more easily explained. As applied to calculation of K_I in a plane body, it proceeds as follows.

Potential energy in the body is, from Eq. 4.8-20,

$$\Pi_p = \frac{1}{2}\{\mathbf{D}\}^T[\mathbf{K}]\{\mathbf{D}\} - \{\mathbf{D}\}^T\{\mathbf{R}\} \tag{8.7-4}$$

Now let the crack be extended a small amount Δa while the structure and its supports and loads are unchanged. A possible choice for Δa is 10^{-6} times a typical element span [8.8]. Because of Δa, the stiffness matrix becomes $[\mathbf{K} + \Delta\mathbf{K}]$ and displacements become $\{\mathbf{D} + \Delta\mathbf{D}\}$. Hence

$$\Pi_p + \Delta\Pi_p = \frac{1}{2}\{\mathbf{D} + \Delta\mathbf{D}\}^T[\mathbf{K} + \Delta\mathbf{K}]\{\mathbf{D} + \Delta\mathbf{D}\} - \{\mathbf{D} + \Delta\mathbf{D}\}^T\{\mathbf{R}\} \tag{8.7-5}$$

$$\Delta\Pi_p = (\Pi_p + \Delta\Pi_p) - \Pi_p = \frac{1}{2}\{\mathbf{D}\}^T[\Delta\mathbf{K}]\{\mathbf{D}\} \tag{8.7-6}$$

where the latter equation is obtained from the former by discarding higher-order terms and using the relation $[\mathbf{K}]\{\mathbf{D}\} = \{\mathbf{R}\}$. To compute $\Delta\Pi_p$ numerically, we can solve $[\mathbf{K}]\{\mathbf{D}\} = \{\mathbf{R}\}$ for $\{\mathbf{D}\}$, then use Eq. 8.7-6. Matrix $[\Delta\mathbf{K}]$ is likely to be very sparse because a small extension of the crack need change only the mesh near the crack tip. Then $\Delta\Pi_p$ can be computed using $[\Delta\mathbf{k}]$ matrices of the altered elements rather than $[\Delta\mathbf{K}]$. With t = structure thickness and ν = Poisson's ratio, equations of fracture mechanics theory that provide stress intensity factor K_I are

$$\text{Plane strain: } K_I^2 = -\frac{E}{(1-\nu^2)t}\frac{\Delta\Pi_p}{\Delta a} \qquad \text{Plane stress: } K_I^2 = -\frac{E}{t}\frac{\Delta\Pi_p}{\Delta a} \tag{8.7-7}$$

The negative sign appears because $\Delta\Pi_p$ is negative when Δa is positive.

8.8 ELASTIC FOUNDATIONS. INFINITE MEDIA

Sometimes one structure is elastically supported by another. An example is a paving slab, supported by soil whose behavior can be idealized as a simple elastic foundation. Or, a

region of interest may be surrounded by a medium of such great extent that it can be regarded as infinite. The physical problem need not be one of structural mechanics. In any case the supporting or surrounding medium must be represented in a way that does not require a large number of d.o.f., does not reflect waves if the medium is infinite and the problem is dynamic, and has adequate accuracy. The intent of modeling is to represent the effect of the medium on the region of interest, not to analyze the medium itself.

Elastic Foundations. A simple kind of elastic support can be modeled by connecting nodes on a structure surface to adjacent nodes on a fixed surface by means of discrete linear springs, but this is an awkward and error-prone model. To model an elastic layer of uniform stiffness, discrete springs must have stiffnesses that depend on the spacing of nodes on the structure surface. And, if structure elements are solids and have edge nodes, some spring stiffness must be *negative* to model uniform pressure in response to uniform displacement. Note, for example, that total force due to uniform pressure on an eight-node rectangular face is allocated to nodes in the same proportion as shown for total force W in Fig. 3.11-3d.

The Winkler foundation model is easy to formulate using energy concepts like those in Section 4.8. The Winkler model postulates a foundation that resists only displacement normal to its surface, with resisting pressure $p = \beta w$, where β is the foundation modulus and w is lateral deflection at the foundation surface. This model deflects only where load is applied. The surrounding foundation is utterly unaffected (Fig. 8.8-1a). An area dA of the foundation surface acts like a linear spring of stiffness $k = p\,dA/w = \beta w\,dA/w = \beta\,dA$. Strain energy in a linear spring is $\frac{1}{2}kw^2$. Now consider a structural element, perhaps a plate bending element or one face of a 3D solid element, that has area A in contact with the foundation. Lateral deflection of area A, normal to the foundation, is $w = \lfloor \mathbf{N}_f \rfloor \{\mathbf{d}_f\}$, where $\{\mathbf{d}_f\}$ contains d.o.f. of element nodes in contact with the foundation. Strain energy U in the foundation over area A is

$$U = \frac{1}{2}\int \beta w^2 dA = \frac{1}{2}\int w^T \beta w\, dA = \frac{1}{2}\{\mathbf{d}_f\}^T[\mathbf{k}_f]\{\mathbf{d}_f\} \tag{8.8-1}$$

in which the Winkler foundation stiffness matrix for the element is

$$[\mathbf{k}_f] = \int \beta \lfloor \mathbf{N}_f \rfloor^T \lfloor \mathbf{N}_f \rfloor\, dA \tag{8.8-2}$$

If, for example, the problem is that of a beam on a Winkler foundation, $\lfloor \mathbf{N}_f \rfloor$ is identical to shape function matrix $\lfloor \mathbf{N} \rfloor$ of the beam, whose individual N_i appear in Fig. 3.2-4, and $dA = b\,dx$, where b is the width of the beam face in contact with the foundation. Matrix $[\mathbf{k}_f]$ has the same form as the mass matrix $[\mathbf{m}]$ used in dynamics. (Note that if the problem is indeed dynamic, a foundation contributes mass as well as stiffness.)

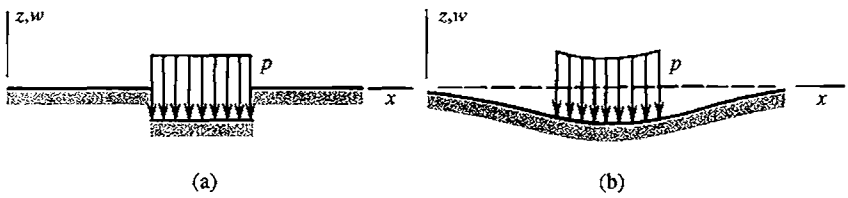

Figure 8.8-1. Deflections of elastic foundations under uniform pressure p applied directly to the foundation. (a) Winkler foundation. (b) Elastic solid foundation.

Matrix $[\mathbf{k}_f]$ is inexact because $\lfloor \mathbf{N}_f \rfloor$ is inexact. For a beam, $\lfloor \mathbf{N}_f \rfloor$ contains cubic polynomials, but the exact deflection of a beam on a Winkler foundation is expressed in terms of exponential and trigonometric functions [2.6]. With $[\mathbf{k}_f]$ based on cubic shape functions, convergence occurs with mesh refinement, but a rather fine mesh may be needed to determine bending moments accurately. Stiffness matrices for beams on elastic foundations, based on theoretically exact lateral displacement functions, are much more accurate in a coarse mesh. Formulations are also available for related two-parameter foundation models. Of many references, [8.9–8.11] are typical.

The Winkler foundation model may be adequate for many problems. Another possible foundation model, not nearly as simple, is the elastic solid (Fig. 8.8-1b). Here the entire foundation surface deforms in response to load at any point. Accordingly, the foundation couples all d.o.f. on the foundation surface, and the foundation stiffness matrix is full rather than sparse. Sparsity can be restored by introducing some approximations [8.12]. For both Winkler and elastic solid foundation models, it is assumed that no part of the structure separates from the foundation. Separation would make the problem nonlinear, because the extent of contact and contact pressures are both unknown at the outset.

Infinite Elements. A problem may involve a medium that is practically unbounded but cannot be properly represented by an elastic foundation. Examples include an underground structure, a wing moving through air, and a marine structure subject to wave action. A numerical model of the surrounding medium must be terminated somewhere short of infinity. In a conventional FE model, Fig. 8.8-2b, it is not obvious where a rigid supporting boundary should be placed. If too close to the load, accuracy suffers. If too far away, many elements are used to represent regions of little interest. To reduce the number of d.o.f., we can model the region of interest by a comparatively small mesh of conventional elements, and attach this mesh to a layer of "infinite" elements (Fig. 8.8-2c).

One way to formulate an infinite element is to use shape functions that cause the field quantity to approach the far-field value at infinity, while retaining the finite size of the element. Another way is to use conventional shape functions to describe variation of the field quantity, but describe element geometry by other shape functions that place one side of the element at infinity. The latter way is simpler. It produces what are called "mapped" infinite elements. The following one-dimensional mapped element is not of practical use but provides a simple introduction [8.13].

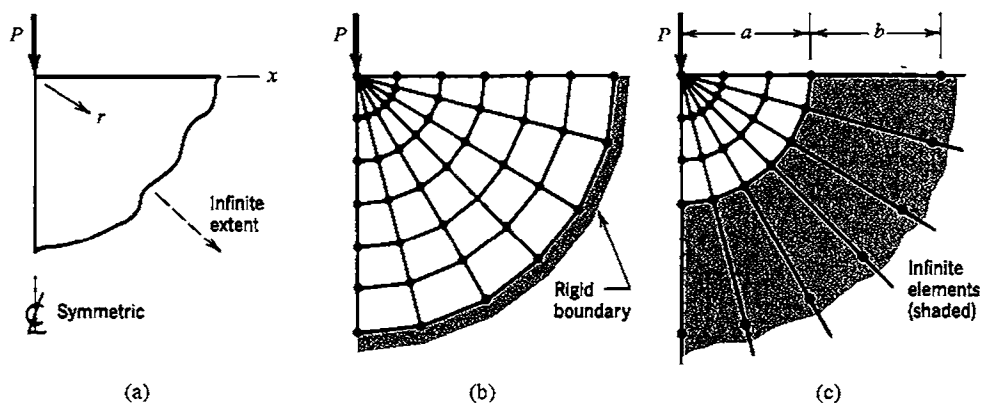

Figure 8.8-2. (a) Load P on a plane or axisymmetric body of infinite extent below the x axis. (b) Large mesh of conventional elements. (c) Smaller mesh, bounded by infinite elements.

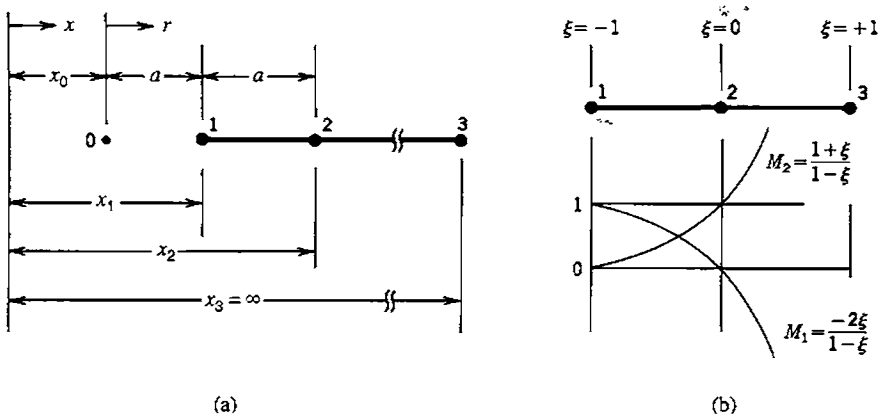

Figure 8.8-3. (a) One-dimensional element in physical space. (b) The same element as mapped using reference coordinate ξ.

Element 1-2-3 in Fig. 8.8-3 is one-dimensional. Distance a between nodes 1 and 2 can be regarded as a characteristic length of the element. With M_i used to mean the ith geometric shape function, element 1-2-3 has the geometry

$$x = M_1 x_1 + M_2 x_2 \qquad \text{where} \qquad \begin{aligned} M_1 &= -\frac{2\xi}{1-\xi} \\ M_2 &= \frac{1+\xi}{1-\xi} \end{aligned} \tag{8.8-3}$$

from which $x = x_1$ at $\xi = -1$ and $x = x_2$ at $\xi = 0$. As ξ approaches $+1$, x approaches infinity. Therefore node 3 need not be explicitly present in Eq. 8.8-3. A field variable ϕ can be interpolated using standard shape functions. For the present three-node element, from Eq. 6.1-4,

$$\phi = \underbrace{\lfloor \tfrac{1}{2}(-\xi+\xi^2) \quad 1-\xi^2 \quad \tfrac{1}{2}(\xi+\xi^2) \rfloor}_{\lfloor \mathbf{N} \rfloor} \begin{Bmatrix} \phi_1 \\ \phi_2 \\ \phi_3 \end{Bmatrix} \tag{8.8-4}$$

Degree of freedom ϕ_3 may be set to zero as a boundary condition. Formulation of element matrices, Eqs. 6.1-6 to 6.1-8 for a structural element, proceeds in normal fashion except that mapping functions M_1 and M_2 from Eqs. 8.8-3 are used to construct Jacobian J. For example, matrix $\lfloor \mathbf{B} \rfloor$ is

$$\lfloor \mathbf{B} \rfloor = \frac{1}{J}\frac{d}{d\xi}\lfloor \mathbf{N} \rfloor \qquad \text{where} \qquad J = \frac{dM_1}{d\xi}x_1 + \frac{dM_2}{d\xi}x_2 \tag{8.8-5}$$

To obtain an expression that shows how field quantity ϕ is represented, we first solve Eq. 8.8-3 for ξ in terms of x, then substitute $x = x_0 + r$, $x_1 = x_0 + a$, and $x_2 = x_0 + 2a$ from Fig. 8.8-3. Thus

$$\xi = \frac{x - x_2}{x - 2x_1 + x_2} = 1 - \frac{2a}{r} \tag{8.8-6}$$

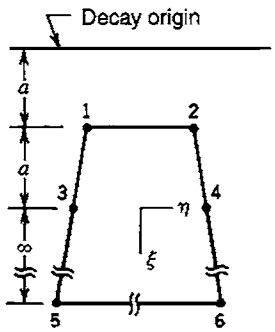

Mapping functions

$$M_1 = \frac{-2\xi}{1-\xi}\frac{1-\eta}{2}$$

$$M_2 = \frac{-2\xi}{1-\xi}\frac{1+\eta}{2}$$

$$M_3 = \frac{1+\xi}{1-\xi}\frac{1-\eta}{2}$$

$$M_4 = \frac{1+\xi}{1-\xi}\frac{1+\eta}{2}$$

Shape functions

$$N_1 = \tfrac{1}{4}(-\xi + \xi^2)(1-\eta)$$

$$N_2 = \tfrac{1}{4}(-\xi + \xi^2)(1+\eta)$$

$$N_3 = \tfrac{1}{2}(1-\xi^2)(1-\eta)$$

$$N_4 = \tfrac{1}{2}(1-\xi^2)(1+\eta)$$

$$N_5 = \tfrac{1}{4}(\xi + \xi^2)(1-\eta)$$

$$N_6 = \tfrac{1}{4}(\xi + \xi^2)(1+\eta)$$

Figure. 8.8-4. A two-dimensional infinite element.

Substitution of Eq. 8.8-6 into Eq. 8.8-4 yields

$$\phi = \phi_3 + (-\phi_1 + 4\phi_2 - 3\phi_3)\frac{a}{r} + (2\phi_1 - 4\phi_2 + 2\phi_3)\frac{a^2}{r^2} \tag{8.8-7}$$

As r approaches infinity, ϕ approaches ϕ_3 (which is perhaps set to zero as a boundary condition). The constant value $\phi = c$ prevails if $\phi_1 = \phi_2 = \phi_3 = c$. Linear variations of ϕ with r are not represented by Eq. 8.8-7. In general, the two parenthetic expressions in Eq. 8.8-7 do not vanish, so ϕ becomes infinite at point 0, where $r = 0$. Point 0 is therefore a pole or singular point about which field quantity ϕ decays. This suggests that in a problem such as that of Fig. 8.8-2c, in which there is indeed a singularity at $r = 0$, one should use $a = b$.

An element that can be used in either plane or axisymmetric problems is shown in Fig. 8.8-4. It extends to infinity in the ξ direction and can be regarded as an extension of the element of Fig. 8.8-3. If field variable ϕ is set to zero at element nodes 5 and 6, N_5 and N_6 need not appear in element formulation and d.o.f. ϕ_5 and ϕ_6 need not be carried into $\{\mathbf{D}\}$. Interelement boundaries of infinite elements should be approximately radial from the region of highest stress gradient, and with increasing distance from this region should "fan out" rather than intersect.

Additional information appears in many references, including [8.13,8.14]. Corrected functions for 3D infinite elements appear in [8.15]. References pertinent to wave problems, for which a nonreflecting boundary at infinity is desired, include [8.16–8.18].

Boundary Elements. A body analyzed by the boundary element method (BEM) need be discretized only on its boundary, not both boundary and interior as is the case for FEM. Thus in a BEM solution of the problem in Fig. 8.8-2, one would see nodes along the x axis but no nodes below it. In a solid body, BEM places nodes on surfaces but none within.

While FEM leads to global matrices that are sparse and symmetric, BEM leads to matrices that are full and unsymmetric but smaller than matrices of FEM. The reduction in size comes from having to mesh only the boundary, which computationally reduces a 3D problem to a 2D problem or a 2D problem to a 1D problem. For 3D problems that strain computer resources when analyzed by FEM, size reduction can be important. For most problems, the advantage of BEM in reducing data preparation effort is perhaps less than first appears: regardless of the solution method, the geometry of the problem must be described, and FEM software can automatically fill a defined region with elements.

Formulation of BEM starts with a *fundamental solution,* which is a solution for what may be called a point load. In elastic problems the load is a point force of unit magnitude;

in heat conduction it is unit flux at a point; in electrostatics it is a unit charge. The fundamental solution satisfies the governing differential equations of the problem and may therefore be considered exact. The fundamental solution applies to an unbounded medium, and incorporates a singularity at the load point, but the resulting BEM can be applied to problems that display neither. In practice, advantages of BEM relative to FEM are greatest when modeling problems having boundaries at infinity. When applied to bounded problems, BEM works best when there is a low ratio of surface to volume. Thus, BEM is not well-suited to plates and shells, which have a high ratio of surface to volume, and no engineer would use BEM to analyze a truss or a frame. References for BEM include [8.19–8.23].

Advantages of BEM relative to FEM include:

- Singularities, such as stresses at reentrant corners and at crack tips, can be included in the fundamental solution, without need for special elements or special adjustments (such as quarter-point finite elements used in fracture mechanics).
- Similarly, boundaries at infinity are automatically included, without need for special formulations such as infinite elements.
- Incompressible materials can be treated without encountering numerical difficulties associated with ill conditioning.
- Stresses at a boundary, where they are usually of greatest interest, are more accurately computed.

Disadvantages of BEM relative to FEM include:

- BEM is not applicable to problems where the fundamental solution is unknown. Thus BEM is not applicable to every problem that involves anisotropy, inhomogeneity, or nonlinearity.
- The mathematics of BEM are comparatively difficult. The physical appeal of FEM, with its discrete regions and interpolation fields that can be visualized, is absent from BEM.
- At present, techniques and software for BEM are not as well-developed and widely available as they are for FEM.

It is not necessary to do an analysis entirely by FEM or entirely by BEM. There are ways to couple the two methods in a single analysis, so that each is used to represent portions of the model to which it is best suited [8.24–8.27].

Related Options. A recent method for treatment of unbounded media combines features of FEM and BEM [8.28–8.31]. It is associated with the names "scaled boundary finite element method" and "consistent infinitesimal finite element cell method." According to [8.28], discretization is performed only on the structure-medium interface, thus producing a model that has one less spatial dimension than the physical structure. The procedure is said to be rigorous in the radial direction and exact in the finite-element sense in the circumferential direction. In contrast to BEM, the method does not require a fundamental solution. It accommodates anisotropic materials and can incorporate boundaries extending to infinity without additional computational effort. Derivation is based on FE formulation procedures and on similarity.

Trefftz elements are similar to boundary elements in that they are formulated using functions that exactly satisfy differential equations of the problem. A summary appears in Section 4.10.

8.9 STRUCTURAL MODIFICATION. REANALYSIS

Imagine that an analysis has been performed. Then the structure is altered: by changing some dimensions, by changing some materials, or by revising the FE mesh. Response of the altered structure is desired. The obvious way to obtain it is complete re-solution, by generating matrix equations for the altered structure and solving them. *Reanalysis methods* are intended to provide or closely approximate the new solution with less computational effort than complete re-solution, by operating on information available from the previous solution. The savings in effort are likely to be greatest when a small portion of a large structure is modified. Reanalysis may be appropriate during repeated modifications to meet limits on allowable stresses or deflections, in optimal design, in alteration of the FE model to match test data, and in parametric studies (in which the analyst seeks response to systematic variation of a quantity).

A statement of the time-independent reanalysis problem is as follows. Before and after structural modification, global equations are

$$\text{Before:} \quad [\mathbf{K}]\{\mathbf{D}\} = \{\mathbf{R}\} \qquad \text{After:} \quad [\mathbf{K}^*]\{\mathbf{D}^*\} = \{\mathbf{R}\} \tag{8.9-1}$$

Here $[\mathbf{K}^*]$ incorporates the structural modification, and $\{\mathbf{D}^*\}$ is the modified response we seek. We regard $\{\mathbf{R}\}$ as unchanged. This of course requires that loads on the structure remain the same. It also requires that the way that loads are expressed as nodal quantities in $\{\mathbf{R}\}$ remain the same. If this is not so, $\{\mathbf{R}\}$ is modified but remains statically equivalent to its original form.

In an eigenproblem, before and after structural modification, global equations are

$$\text{Before:} \ ([\mathbf{K}] - \lambda[\mathbf{M}])\{\bar{\mathbf{D}}\} = \{\mathbf{0}\} \qquad \text{After:} \ ([\mathbf{K}^*] - \lambda^*[\mathbf{M}^*])\{\bar{\mathbf{D}}^*\} = \{\mathbf{0}\} \tag{8.9-2}$$

in which eigenvalues λ and eigenvectors $\{\bar{\mathbf{D}}\}$ are both altered by modifications in structure matrices $[\mathbf{K}]$ and $[\mathbf{M}]$. The goal of reanalysis is to obtain λ^* and $\{\bar{\mathbf{D}}^*\}$ more efficiently than would be possible by complete re-solution of the eigenproblem.

There are many approaches to reanalysis [8.32–8.37]. Broadly, all approaches can be placed in one of two groups.

- *Direct methods* produce exact results. They involve a finite and predictable number of steps, and work best when only a small portion of the structure is modified.
- *Iterative methods* produce approximate results. They converge at a rate that is case-dependent. Large differences between $[\mathbf{K}]$ and $[\mathbf{K}^*]$ make iterations converge slowly or even diverge.

A very simple iterative method is as follows. We write $[\mathbf{K}^*] = [\mathbf{K}] + [\Delta\mathbf{K}]$, where $[\Delta\mathbf{K}]$ incorporates the structural modifications (and may be a very sparse matrix). Then, from Eq. 8.9-1, we write the form

$$[\mathbf{K}]\{\mathbf{D}^*\}_{i+1} = \{\mathbf{R}^*\}_i \qquad \text{where} \qquad \{\mathbf{R}^*\}_i = \{\mathbf{R}\} - [\Delta\mathbf{K}]\{\mathbf{D}^*\}_i \tag{8.9-3}$$

In the first iteration, $i = 1$ and $\{\mathbf{D}^*\}_1 = \{\mathbf{D}\}$, the solution vector of the unmodified structure. After $\{\mathbf{R}^*\}_i$ is established, solving for $\{\mathbf{D}^*\}_{i+1}$ is computationally the same as solving the original system for a new load vector, which is done very efficiently.

Substructuring (Section 10.11) can be a useful tool in reanalysis. If modifications are confined to a single substructure, and consequences of modification are to be examined in only that substructure, then the analyst need compute only internal d.o.f. of the one substructure and attachment d.o.f. Internal d.o.f. of other substructures need not be computed.

8.10 TESTS OF ELEMENT QUALITY

Many element formulations have been proposed. Even for (say) four-node plane elements that have two displacement d.o.f. per node, several alternatives are available. How can we choose the best? If we were to solve a set of test-case problems [6.26], using candidate elements in each, we would gather anecdotal evidence from which we might reach the ambiguous conclusion that an element best in one case is not best in another.

In what follows we consider more systematic tests of element quality. They cannot identify the "best element," but provide some guidance, and may be helpful in identifying element deficiencies. These tests supplement the patch test, described in Section 6.13.

Eigenvalue Test. We first describe the calculations, then how to interpret results [8.38]. Let loads $-\{\mathbf{r}\}$ be applied to element nodes, and let them be proportional to nodal displacements $\{\mathbf{d}\}$ through a factor λ. Thus

$$[\mathbf{k}]\{\mathbf{d}\} = -\{\mathbf{r}\} = \lambda\{\mathbf{d}\} \qquad \text{or} \qquad \Big([\mathbf{k}] - \lambda[\mathbf{I}]\Big)\{\mathbf{d}\} = \{\mathbf{0}\} \tag{8.10-1}$$

This is an eigenproblem. The λ_i are eigenvalues of $[\mathbf{k}]$. There are as many λ_i as there are d.o.f. in $\{\mathbf{d}\}$. To each λ_i there corresponds an eigenvector $\{\mathbf{d}\}_i$. If each $\{\mathbf{d}\}_i$ is scaled so that $\{\mathbf{d}\}_i^T\{\mathbf{d}\}_i = 1$, then premultiplication of Eq. 8.10-1 by $\{\mathbf{d}\}_i^T$ yields

$$\{\mathbf{d}\}_i^T[\mathbf{k}]\{\mathbf{d}\}_i = \lambda_i \qquad \text{or} \qquad 2U_i = \lambda_i \tag{8.10-2}$$

where U_i is strain energy in the element when its nodal d.o.f. are the scaled displacements $\{\mathbf{d}\}_i$ (see Eq. 4.8-16). To solve Eq. 8.10-2 using standard FE software, one can leave all element d.o.f. unrestrained, associate a unit mass with each d.o.f., and compute natural frequencies ω_i of the element, where $\omega_i^2 = \lambda_i$. Note that λ_i is not changed if algebraic signs of all d.o.f. in $\{\mathbf{d}\}_i$ are reversed.

Equation 8.10-2 shows that λ_i should be zero when $\{\mathbf{d}\}_i$ represents any rigid-body motion. Three linearly independent rigid-body motions are possible in a plane. Therefore three of the λ_i should be zero for a plane element. Six should be zero for a solid element or a shell element, but only one for a solid- or shell-of-revolution element (if only axisymmetric states are permitted). A spurious mode (mechanism) also yields a zero eigenvalue. Computation does not automatically present zero-energy modes as x-direction translation, rotation about the z axis, and so on. Rather, these motions may appear in combination, although the combinations are such as to preserve the linear independence of modes.

In testing an element, we ask if there are as many zero eigenvalues as there should be. Too few indicates that the element lacks a desired capability for rigid-body motion without strain. Too many indicates the presence of one or more spurious modes. Nonzero eigenvalues are

real and positive if [**k**] is positive semidefinite. If eigenvalues change when the element is reoriented in global coordinates, the element is not frame-invariant; that is, it has artificial anisotropy. Similar modes, such as flexural modes of the square isotropic elements in Fig. 8.10-1, should have equal eigenvalues.

Eigenvalues of [**k**] can sometimes be used to compare different formulations of a given element type, for example isoparametric versus hybrid formulations of a four-node plane element. Properly formulated elements of the same shape, size, and material properties should be equally stiff in their constant-strain modes. Their stiffness matrices should therefore have eigenvalues in common. Stiffnesses, and therefore eigenvalues, may differ in higher modes. For compatible elements based on assumed displacement fields, the λ_i either provide strain energy $2U_i$ exactly or are upper bounds. Therefore, when comparing elements of the same shape, size, [**E**], node placement, and number and type of d.o.f., the element with the lowest strain energy is best. The stiffness matrix of this element has the lowest trace (tr[**k**] equals the sum of the λ_i). The trace is not a good indicator if any λ_i is not an upper bound, which happens, for example, if the element contains a spurious mode.

Eigenvalues and eigenvectors of several elements have been published; see [8.40] and papers it cites.

Remarks. In another energy-based test [8.41,8.42], a polynomial displacement field is imagined imposed on a continuum. In a region of the continuum subsequently to be spanned by a finite element, strain energy is calculated using classical formulas (Eq. 4.4-5). Also, at points where element nodes will be located, displacements are calculated. These displacements are then imposed as nodal d.o.f., and element strain energy is calculated. Strain energies of continuum and element are compared. The better the match, the more capable the element. The comparison is repeated, using various other displacement fields.

In the *single-element* test, a one-element model, of (say) a cantilever beam of length L and depth D loaded in pure bending, is analyzed using standard software. The exact solution is known. The rate at which accuracy declines as aspect ratio L/D increases is a measure of element sensitivity to geometric distortion. This test can also be used to compare competing elements, such as different formulations of four-node plane elements. It is not a general test, as it falls in the category of applying FEA to a specific problem whose solution is known.

In testing an element, no single test is likely to be decisive, except perhaps in discovering a fatally flawed element. Tests of element quality are probably of more value to element developers than to users of FEA software. Nevertheless, users may want to try patch tests and single-element tests as ways to learn how to use a new software package because these tests are easy to perform and exact results are known in advance.

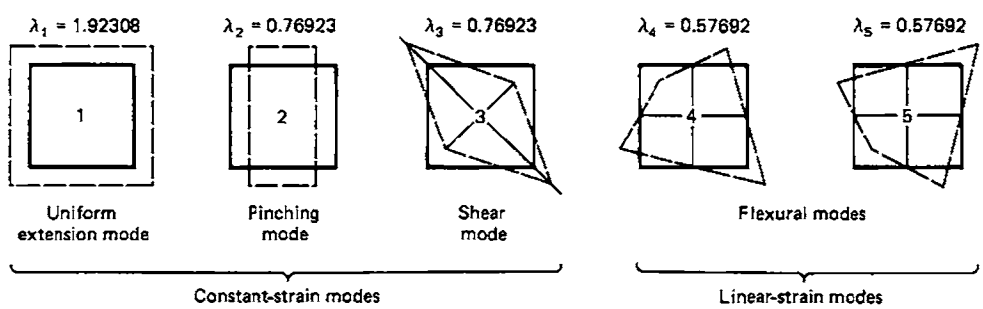

Figure 8.10-1. Nonzero eigenvalues and their corresponding eigenvectors (deformation modes) of a square bilinear element in plane strain [8.39]. $E = 1.0$, $\nu = 0.3$, side length $= 1.0$.

ANALYTICAL PROBLEMS

8.1-1 If a vector **V** has length L, then $\mathbf{V} \cdot \mathbf{V} = L^2$ regardless of the coordinate system in which **V** is described. Hence, using Eq. 8.1-1, show that $\sum l_i^2 = 1$, $\sum l_i m_i = 0$, and so on (six such relations altogether).

8.1-2 (a) Let $x' = -x$ and $y' = -y$. What is [**A**] in Eq. 8.1-1? Both coordinate systems are right-handed.
(b) Similarly, what is [**A**] if $x' = y$ and $z' = z$?

8.2-1 Let [**E**′] be 3 by 3, as for a plane stress problem. Show that Eq. 8.2-10 yields [**E**′] = [**E**] if the material is isotropic.

8.2-2 Consider a plane problem for which the 3 by 3 matrix [**E**′] is diagonal, with $E'_{11} = E_a$, $E'_{22} = E_b$, and $E'_{33} = G$. What are the terms in [**E**] for an arbitrary angle β in Fig. 8.2-1? As a partial check on your answer, try the case $\beta = \pi/2$.

8.2-3 Is $[\mathbf{T}_\varepsilon]$ of Eq. 8.2-11 an orthogonal matrix? Why or why not?

8.3-1 Let a uniform bar element of axial stiffness $k = AE/L$ be allowed only x-direction displacements (along its axis). Its stiffness matrix [**k**] operates on nodal displacements u_1 and u_2. Transform [**k**] so that it operates on nodal d.o.f. u_1 and u_r, where u_r is the displacement of node 2 relative to node 1.

8.3-2 A three-node bar element and its shape functions N_i are shown in Fig. 6.1-1. Imagine that d.o.f. u_2 is to be replaced by u_r, where u_r is the displacement of a central node 2 relative to $\frac{1}{2}(u_1 + u_3)$, which would be the displacement at the center if only the two end nodes were present. Write the transformation matrix and use it to determine the new shape functions.

8.3-3 Let Fig. 8.4-1a represent a plane truss whose nodal d.o.f. are u_i and v_i at each node i. Imagine that supports are not yet present, so that [**K**] is 8 by 8. Let [**k**′] be the 4 by 4 stiffness matrix of bar 4-2. Write a transformation matrix [**T**] such that $[\mathbf{T}]^T[\mathbf{k}'][\mathbf{T}]$ is an 8 by 8 matrix that can be added directly to the 8 by 8 array reserved for the structure stiffness matrix, which operates on d.o.f.

$$\begin{bmatrix} u_1 & v_1 & u_2 & \cdots & v_4 \end{bmatrix}^T$$

[For additional transformation questions, see Problems 2.4-2 and 2.4-4 of Chapter 2.]

8.4-1 Let Fig. 8.4-1a represent a plane truss for which axial stiffness $k = AE/L$ is the same for each member. Also let the three interior angles in each panel be 45°, 45°, and 90°. Apply a downward load P at node 4 and set $u_4 = 0$. If $\beta = \arctan 0.75$, what is the force in member 3-1 in terms of P?

8.4-2 Imagine that, at a certain joint in a 3D truss, motion is to be prohibited along a line whose direction cosines are l_1, l_2, and l_3. Motion is to be permitted in all directions normal to the line. Original d.o.f. are translations of joints in x, y, and z directions.
(a) Explain precisely how to define suitable new directions for d.o.f. at the joint, and write the transformation matrix at the joint.
(b) Check the result for the special case $l_2 = 1$.

8.4-3 The right end of the cantilever beam shown slides without friction on a rigid wall. Represent the cantilever as a single plane beam element with axial, transverse, and rotational d.o.f. at the right end. Neglect transverse shear deformation.

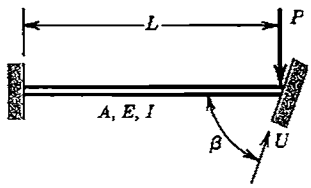

Problem 8.4-3

(a) Transform and impose boundary conditions. Thus, obtain a 2 by 2 matrix [**K**] that operates on tangential displacement U and rotation θ at the right end.
(b) In addition, let the condition $\theta = 0$ be imposed. Solve for U.

8.5-1 The element shown is of arbitrary quadrilateral shape and is formulated as a bilinear element (Section 6.2). A constant-strain triangle (six d.o.f.; lettered nodes) is to be attached, so that lettered nodes lie at $\xi = \pm 0.5$ and $\eta = \pm 0.5$ in the quadrilateral. Degees of freedom $\{\mathbf{d}'\}$ of lettered nodes are to be made slave to d.o.f. $\{\mathbf{d}\}$ of numbered nodes. Write [**T**] in the relation $\{\mathbf{d}'\} = [\mathbf{T}]\{\mathbf{d}\}$.

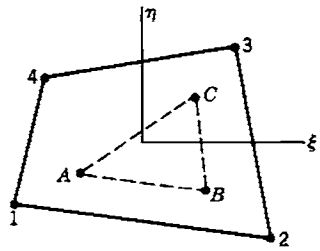

Problem 8.5-1

8.5-2 At node 5 of the plane beam element in Fig. 8.5-1a, let forces F_x and F_y and moment M_5 (counterclockwise) be applied. How are these loads distributed to nodes 2 and 3 by the transformation of Eq. 8.5-3? Show that these loads are statically equivalent to the original loads.

8.5-3 Write the transformation matrix for the problem described in connection with Fig. 8.5-1b.

8.5-4 Plane element 1 in the sketch is bilinear (Section 6.2). It has d.o.f. u_i and v_i at each node i. Plane element 2 has d.o.f. u_i, v_i and counterclockwise rotation θ_i at each node. Consider stiffness matrices $[\mathbf{k}_1]$ and $[\mathbf{k}_2]$ for the respective elements.
(a) Write a transformation matrix $[\mathbf{T}_1]$ that could be used to convert $[\mathbf{k}_1]$ so that it operates on the d.o.f. of element 2.
(b) Write a transformation matrix $[\mathbf{T}_2]$ that could be used to convert $[\mathbf{k}_2]$ so that it operates on the d.o.f. of element 1.
(c) Should $[\mathbf{T}_1][\mathbf{T}_2]$ and $[\mathbf{T}_2][\mathbf{T}_1]$ be unit matrices? Devise an argument that says so.
(d) Evaluate the products $[\mathbf{T}_1][\mathbf{T}_2]$ and $[\mathbf{T}_2][\mathbf{T}_1]$ and explain the results.

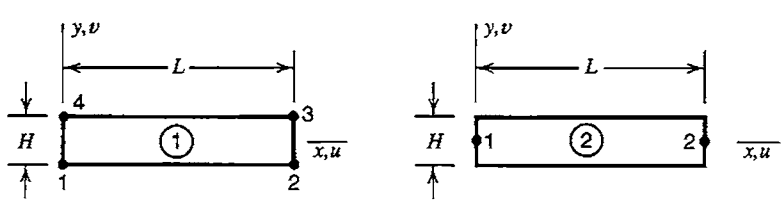

Problem 8.5-4

8.5-5 Element ij shown is a 2D beam element that has both axial and bending stiffness. At each of nodes i, j, 1, and 2, d.o.f. are u, v, and counterclockwise rotation θ. Imagine that d.o.f. at nodes i and j are to be made slave to d.o.f. at nodes 1 and 2 via rigid links $i1$ and $j2$. Write the 6 by 6 transformation matrix [**T**].

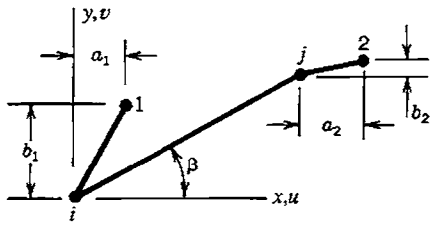

Problem 8.5-5

8.5-6 Consider a beam element ij, arbitrarily oriented in space. D.o.f. at node i are $\lfloor u_i \quad v_i \quad w_i \quad \theta_{xi} \quad \theta_{yi} \quad \theta_{zi} \rfloor^T$, where θ d.o.f. vectors point in positive coordinate directions. D.o.f. at node j are similar. The element is to be made slave to d.o.f. at other nodes (nodes 1 and 2, say) via rigid links $i1$ and $j2$, which are arbitrarily oriented. Write the 12 by 12 transformation matrix in terms of the x, y, and z coordinates of the nodes.

8.5-7 (a) Rewrite Eq. 8.5-6 if the d.o.f. to be retained are changed from u_1, v_1, and u_2 to u_2, u_3, and v_3.
(b) Rewrite Eq. 8.5-6 if the triangle is of arbitrary shape, with nodal coordinates x_i and $y_i (i = 1,2,3)$.

8.6-1 The structure shown is built of four-node plane elements. Imagine that nodal d.o.f. consist of u, v, $u_{,x}$, $v_{,x}$, $u_{,y}$, and $v_{,y}$. Pressure p acts along edge AB. Edge BC is fixed. What boundary conditions should be imposed on nodal d.o.f. along edges AB, BC, CD, and DA? Assume that the material is isotropic. What would be different if the material were anisotropic?

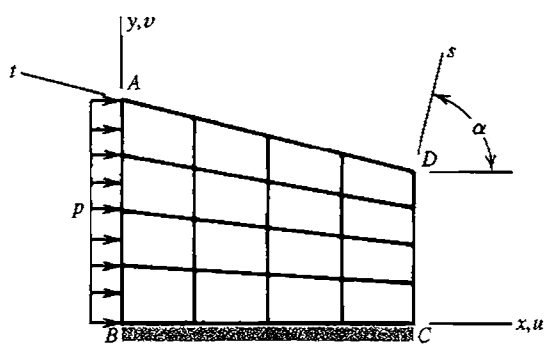

Problem 8.6-1

8.6-2 (a) A uniform bar element has four d.o.f., namely axial displacement and axial strain at each node, as shown. Derive the 4 by 4 element stiffness matrix [**k**]. Use the displacement method, as in Chapter 3, rather than the mixed formulation of Section 5.6.
(b) Use [**k**] from part (a) to solve for ε_{x1} and u_2 in the one-element problem shown. Impose known values of u_1 and ε_{x2} as boundary conditions.

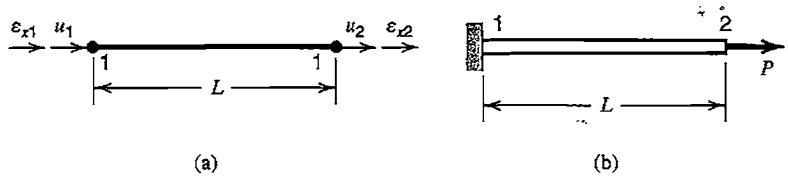

Problem 8.6-2

8.7-1 Consider the uniform bar element of Fig. 8.7-3, but place node 2 at the third point rather than the quarter point. At what value of x/L is a stress singularity indicated?

8.8-1 The plane beam element shown has d.o.f. $\{\mathbf{d}\} = \lfloor w_1 \quad \theta_1 \quad w_2 \quad \theta_2 \rfloor^T$, where θ is a counterclockwise rotation. The element has width b in contact with a Winkler foundation of modulus β. Determine the foundation matrix $[\mathbf{k}_f]$ produced by each of the following assumptions for lateral displacement w. Are all of them valid?

(a) Let w be cubic in x, as in the standard beam element.

(b) Let w be quadratic in x, so that $Lw = (L-x)w_1 + xw_2 + \frac{1}{2}x(L-x)(\theta_1 - \theta_2)$.

(c) Let w be linear in x (independent of θ_1 and θ_2).

(d) Let w be independent of x.

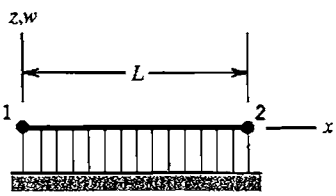

Problem 8.8-1

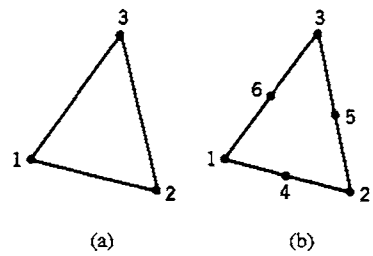

Problem 8.8-2

8.8-2 The sketches represent plan views of triangular elements that rest on a Winkler foundation of modulus β. The type of element is not important in this problem. Assume that deflection w normal to the foundation depends only on nodal values of w. Determine the foundation matrix $[\mathbf{k}_f]$ for

(a) the three-node element.

(b) the six-node element, if sides are straight and side nodes are at midsides.

8.8-3 Imagine that a Winkler elastic foundation having translational modulus β is somehow augmented by a layer that has rotational modulus α (having units of force divided by length). What formula for $[\mathbf{k}_f]$ replaces Eq. 8.8-2? (A symbolic result is desired, with terms defined, rather than specifics of a particular element.)

8.8-4 For the element of Fig. 8.8-3a, let element geometry be defined by Eq. 8.8-3, while field quantity ϕ is defined by the linear interpolation $\phi = \frac{1}{2}(1-\xi)\phi_1 + \frac{1}{2}(1+\xi)\phi_3$. Determine:

(a) Field variable ϕ as a function of r (analogous to Eq. 8.8-7).

(b) Jacobian J as a function of ξ and a.

(c) The element stiffness matrix $[\mathbf{k}]$ (regard the element as a bar).

8.8-5 (a) For the plane infinite element shown, let field variable ϕ depend on nodal values ϕ_1, ϕ_2, ϕ_5, and ϕ_6 (not on ϕ_3 or ϕ_4). All six nodes are used to define geometry. Write mapping functions and shape functions for this element.
(b) Let sides 1-3-5 and 2-4-6 be parallel. Evaluate $[\mathbf{J}]^{-1}$ and J.
(c) If $\phi_5 = \phi_6 = 0$, what 2 by 2 element characteristic matrix $[\mathbf{k}]$ operates on ϕ_1 and ϕ_2? Again let sides 1-3-5 and 2-4-6 be parallel. Also let t = element thickness and k = material property, both uniform over the element.

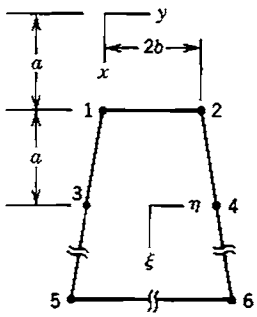

Problem 8.8-5

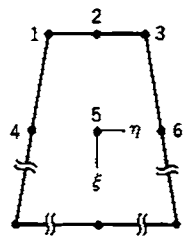

Problem 8.8-6

8.8-6 Write mapping functions for the plane infinite element shown.

8.9-1 Consider the application of Eq. 8.9-3 to a one-d.o.f. problem, as follows.
(a) Let $K = 0.5$, $K^* = 0.8$, and $R = 2$. Starting with the solution $D = 4$ for the original problem (before modification), apply five iterative cycles. Do results appear to be converging correctly?
(b) For what range of values $\Delta K/K$ does the iterative method converge?

COMPUTATIONAL PROBLEMS

C8.1 Model the T-section cantilever beam shown by using separate sets of beam elements, one set for the cross of the T and the other for the stem. Use one, then two, then four elements along the length in each set. Make nodes of the stem slave to nodes of the cross. Let Poisson's ratio be zero. Compare computed values of tip displacement and rotation with values predicted by beam theory.

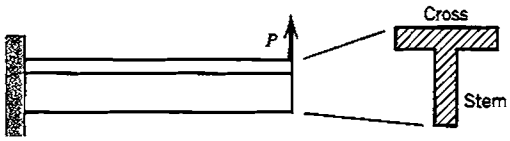

Problem C8.1

C8.2 Consider the cantilever beam of Problem C8.1, but model it by conventional beam elements and support its lower surface by an elastic medium. Model the medium by conventional plane elements, with a fixed support at finite distance, in the manner of Fig. 8.8-2b. Also model the medium using infinite elements, or whatever comparable option software provides. Attempt to obtain comparable accuracy from the two models, and compare their size and convenience.

CHAPTER 9

ERROR, ERROR ESTIMATION, AND CONVERGENCE

The first part of this chapter discusses numerical error and how it can be detected and reduced. Discretization error and convergence rate are considered next. The latter part of the chapter discusses *a posteriori* estimates of discretization error that can be included in software, and use of error estimates in constructing an improved FE model. Greatest emphasis is given to time-independent linear problems.

9.1 SOURCES OF ERROR

Results computed by FEA contain error, except in instances where the mathematical model is so simple that FEA is unnecessary. By "error" we mean disagreement between FEA results and the exact solution of the mathematical model. Sources of error are noted later in this section. In subsequent sections of this chapter we will assume that several possible sources of error are absent. Specifically, we will assume that the software is appropriate to the task at hand and is free of bugs; that the prescribed geometry, boundary conditions, loads, and material properties of the FE model are suited to the problem at hand; that the user has made no blunders in data input to the software; and that the proper general types of element have been selected (such as solid rather than plane, as may be appropriate). Thus, after the following descriptions of modeling error, user error, and bugs, we omit discussion of these items from the remainder of this chapter (but return to them in Chapter 10).

What remains are specific choices of element types, element sizes and shapes, and how certain boundary conditions and constraints are imposed. In addition to their influence on discretization error, these choices can increase or decrease the numerical error associated with having to store and process numbers of less-than-infinite precision.

Error Classification. Possible sources of error can be grouped in the following way. Related remarks appear in Chapter 1, which the reader may wish to review. Terminology used here is not universally adopted.

Modeling error refers to the difference between a physical system and its mathematical model. What is analyzed is not the actual problem, but its mathematical model, which is a simplification in which fine detail of the actual problem is omitted and what remains is described by an accepted mathematical formulation (such as plane theory of elasticity, or thin-plate theory, or equations of heat conduction, and so on). Details of fasteners, small holes, other geometric irregularities, and minor nonuniformity of material properties are probably ignored, at least in initial analyses. Loads are simplified. Boundary conditions are idealized, as by stating that supports are rigid. The problem is often represented as plane rather than three-dimensional, or as linear rather than nonlinear, or as time-independent

rather than dynamic, and so on. In summary, modeling error refers to reasonable and considered approximations made deliberately rather than by mistake, and to uncertainties, often about the actual nature of loads and boundary conditions.

User error refers to mistakes made by the software user after the physical problem has been understood, the questions to be answered by analysis have been decided, and an appropriate mathematical model has been created. Included in user error are choosing the wrong general element type (plate elements where shell elements are needed, perhaps), choosing poor element sizes and shapes, and outright blunders in data input so that the model described is not the model intended. One might also include in this category an inability to interpret computed results, so that consequences of early mistakes escape notice.

Bugs exist in the software. A bug may halt execution, perhaps in the preprocessing phase. A more dangerous bug is one that allows execution to continue but creates inaccuracy that is serious but not so great as to be immediately obvious.

Discretization error is error introduced by representing the mathematical model by an FE model. The number of d.o.f. is infinite in the mathematical model but finite in an FE model. The FEA solution is influenced by the number of elements used, the number of nodes per element, the nature of element shape functions, integration rules used with isoparametric elements, and other formulation details of particular elements.

Truncation error or *rounding error* refers to loss of information due to truncation or rounding of numbers to fit a finite computer word length. This kind of error is present in element and structure matrices before a solution algorithm is applied. As an example, let $x = 1.23456$ and $y = 1.23455$ be six-digit representations of numbers having more than six digits. The result $x - y = 1(10)^{-5}$ is unreliable in even its single digit. Here trouble appears after subtraction, but its source is truncation error in x and y, despite each being represented with five reliable digits.

Manipulation error is introduced as equations are processed; for example, results of multiplication are truncated or rounded. Manipulation error may be minor if global equations $[\mathbf{K}]\{\mathbf{D}\} = \{\mathbf{R}\}$ are solved once, as in time-independent analysis. In some dynamic and nonlinear problems, where each step builds on the step before and a calculation sequence must be executed repeatedly, manipulation errors may accumulate.

Numerical error, as the term is used in this chapter, is the combined result of truncation (or rounding) error and manipulation error.

Although error is unavoidable in FE computations, there is no excuse for gratuitous errors. Numerical constants such as π and Gauss point locations and weights should be stated with as many accurate digits as computer words allow. To avoid possibly serious errors of manipulation and especially truncation, FEA typically requires 12 to 14 digits per word. Therefore, on most computers, numbers must be stored and manipulated in double-precision arithmetic. Some computers have extended-precision registers but truncate results to single-word size (or double in double-precision arithmetic), so that truncation error dominates numerical error.

Error Tests. The remainder of this chapter emphasizes numerical error (Sections 9.2 to 9.5), discretization error (Sections 9.6 to 9.11), and tests for these errors. When significant numerical error is detected, the FE model should be revised, and analysis repeated. Significant discretization error can often be detected by postprocessing, whereupon the mesh must be revised and analysis repeated. Cycles of postprocessing, mesh revision, and

reanalysis can be repeated automatically by software until a user-defined error tolerance is reached. Modeling error, user error, and software bugs are discussed in Chapter 10.

The term "ill-conditioned" is often used in discussions of numerical error. As applied to a matrix, the term means that small numerical changes in matrix coefficients produce large changes in computed results. However, we cannot say that a matrix is ill-conditioned until we state what is to be done with it. A matrix that is well-conditioned for equation-solving can be ill-conditioned for eigenvalue extraction, and vice versa.

There is no single foolproof test of solution accuracy short of knowing the correct result by other means. An error test that detects trouble in one situation may fail to detect trouble in another, or may warn of trouble that does not develop. A plausible error test may be useless. For example, consider the Hilbert matrix [**H**], whose general term is $H_{ij} = 1/(i+j-1)$. [**H**] is notoriously ill-conditioned for equation-solving, and for this reason is sometimes used as a test case. In one study [9.1], a tenth order Hilbert matrix was represented in single-precision arithmetic, its inverse $[\mathbf{H}]^{-1}$ computed, and finally the original matrix recovered as $([\mathbf{H}]^{-1})^{-1}$. It was found that $[\mathbf{H}] = ([\mathbf{H}]^{-1})^{-1}$ to seven-digit accuracy, yet $[\mathbf{H}]^{-1}$ had coefficients in error by seven orders of magnitude.

9.2 ILL-CONDITIONING

A set of equations is ill-conditioned if the solution vector is sensitive to small changes in the coefficient matrix or in the vector of constants. In FEA the coefficient matrix [**K**] is likely to be more troublesome than the vector of constants {**R**}. A coefficient matrix that is ill-conditioned for equation-solving is almost singular.

Consider the two-d.o.f. structure in Fig. 9.2-1, whose global equations $[\mathbf{K}]\{\mathbf{D}\} = \{\mathbf{R}\}$ are

$$\begin{bmatrix} k_1 & -k_1 \\ -k_1 & k_1+k_2 \end{bmatrix} \begin{Bmatrix} u_1 \\ u_2 \end{Bmatrix} = \begin{Bmatrix} P \\ 0 \end{Bmatrix} \quad \text{or} \quad \begin{aligned} k_1u_1 - k_1u_2 &= P \qquad (9.2\text{-}1a) \\ -k_1u_1 + (k_1+k_2)u_2 &= 0 \qquad (9.2\text{-}1b) \end{aligned}$$

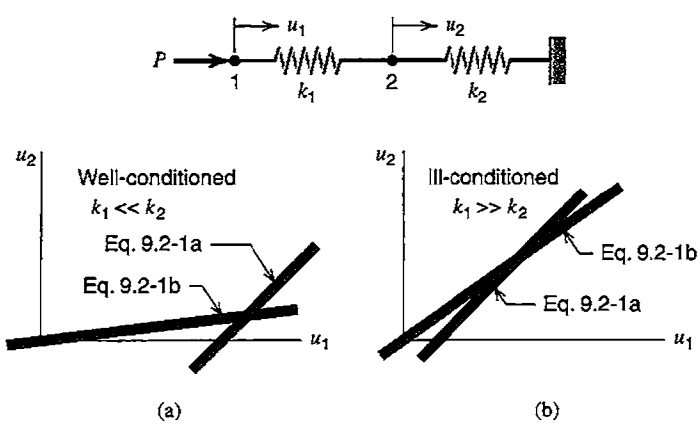

Figure 9.2-1. A two-d.o.f. structure built of linear springs. (a) Flexible part supported by stiff part. (b) Stiff part supported by flexible part.

Each of the two equations plots as a straight line in a u_1u_2 coordinate system. These are the solid lines in Fig. 9.2-1. Shaded bands that surround the lines suggest inexactness associated with use of a finite number of digits (or bits) to represent numerical coefficients in computer memory. The exact solution is represented by the point where the solid lines cross. The calculated solution is represented by a point somewhere in the region where the shaded bands overlap. We see that this region is small if $k_1 << k_2$ but large if $k_1 >> k_2$. If $k_1 >> k_2$ the rows of [**K**] are almost linearly dependent; that is, one row is almost a scalar multiple of the other. Then a small change in k_2 or P creates significant changes in u_1 and u_2.

In an elimination solution of Eqs. 9.2-1 we add the first equation to the second, which converts the second equation to

$$\left[(k_1 + k_2) - k_1\right] u_2 = P \tag{9.2-2}$$

which would be exactly the correct result, $k_2u_2 = P$, if k_1 and k_2 were represented to infinite precision. But if, for example, $k_1 = 1.000000$ and $k_2 = 4.444444(10^{-6})$ and computer words were to store the equivalent of seven digits, then Eq. 9.2-2 would yield $1.000004 - 1.000000 = 4(10^{-6})$; that is, only one significant digit would remain. With only six digits stored, the result would be $1.00000 - 1.00000 = 0$. Physically, this result implies that the stiff spring has no support whatever and is free to move as a rigid body. Software should respond to such a result by complaining that the coefficient matrix is singular. Note that the case $k_1 << k_2$ does not provoke this kind of trouble.

In terms of the error classification of Section 9.2, we deal here with *truncation error.* Although the manipulations of equation-solving make the difficulty obvious, its source is insufficient information in the original stiffness coefficients. Information needed for an accurate solution may occupy only the last few bits of computer words. Subsequent manipulation, however careful or extensive, cannot recover information absent at the outset because of truncation.

The greatest danger of ill-conditioning is not that equation-solving may fail, but that it may *succeed,* without warning messages or with warning messages not heeded by the software user, and produce a solution whose errors are serious but not so extreme as to make it obvious that something is wrong.

Situations Susceptible to Ill-Conditioning. In structural mechanics, the physical situation most likely to provoke trouble, of which the structure in Fig. 9.2-1b is a simple example, is *a stiff region supported by a much more flexible region.* Then the stiffer region has a rigid-body component of deformation so large that it overwhelms other deformation components needed for accurate computation of strains. A similar situation may appear in other problem areas. For example, the situation analogous to Fig. 9.2-1b in heat conduction is a region of high conductivity attached to a region of low conductivity whose boundary has prescribed temperature. In structural mechanics, as Poisson's ratio approaches 0.5 in plane strain and solid problems, elements become extremely stiff in resisting volume change, but retain their ability to deform in other modes. In all problems of stiff regions supported by flexible regions, essential information is relegated to the latter bits of computer words. These bits may be so few in number that at least some of the computed solution is seriously in error.

The anticipated trouble may not ensue if loads are self-equilibrating. For example, if a leftward load P is added at node 2 in Fig. 9.2-1b, the *relative* displacement of nodes 1 and 2 will be accurately computed even if the rigid-body displacement components of u_1 and u_2 contain significant error. More generally, self-equilibrating loads sometimes permit accurate computation of gradients (or stresses).

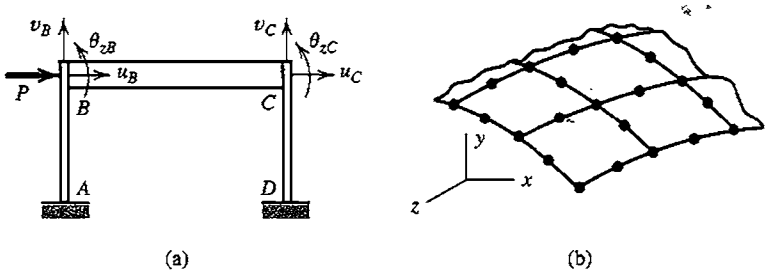

Figure 9.2-2. Potentially ill-conditioned systems. (a) A plane frame. (b) A portion of a thin shell modeled by eight-node shell elements.

Further examples of troublesome structures appear in Fig. 9.2-2. The plane frame of Fig. 9.2-2a appears to be a trivial problem. But typically the axial stiffness of beam BC is much greater than the sidesway stiffness of columns AB and CD. Computed values of lateral displacement d.o.f. u_B and u_C may lack sufficient accuracy, especially if we intend to use their difference to accurately compute the axial component of stress in the beam as $\sigma_a = E(u_C - u_B)/L$. As a practical matter, σ_a is likely to be negligible in comparison with flexural stress. If we are willing to say it is zero, the beam can be provided with infinite axial stiffness (see Section 8.5). Thus we eliminate either u_B or u_C from the problem, and so eliminate this source of ill-conditioning. Similar concerns arise in the analysis of a piping network, whose individual members have axial stiffness much larger than their bending stiffness.

In shell analysis, elements display both membrane stiffness and flexural stiffness. Membrane stiffness of a shell is analogous to axial stiffness of a beam. The ratio of membrane stiffness to flexural stiffness is very large in a thin shell. Accordingly, in Fig. 9.2-2b, we again see the case of a high-stiffness region embedded in a low-stiffness region. Great mesh refinement, intended to decrease discretization error, may increase numerical error to such an extent that computed results become less accurate rather than more (Sections 9.3 and 9.4).

A Special Case. The plane three-member structure in Fig. 9.2-3a has linear springs of stiffnesses k and αk. If α is large, a stiff portion (the spring of stiffness αk) is supported by a flexible portion (the springs of stiffness k). Stiffness equations $[\mathbf{K}]\{\mathbf{D}\} = \{\mathbf{R}\}$ for this problem are

$$\begin{bmatrix} k\left(1+\alpha c^2\right) & k\alpha cs \\ k\alpha cs & k\left(1+\alpha s^2\right) \end{bmatrix} \begin{Bmatrix} u_1 \\ v_1 \end{Bmatrix} = \begin{Bmatrix} P \\ 0 \end{Bmatrix} \quad \text{where} \quad \begin{aligned} c &= \cos\beta \\ s &= \sin\beta \end{aligned} \tag{9.2-3}$$

In $u_1 v_1$ space, straight lines that represent these two equations have the respective slopes

$$\frac{dv_1}{du_1} = -\frac{1+\alpha c^2}{\alpha cs} \quad \text{and} \quad \frac{dv_1}{du_1} = -\frac{\alpha cs}{1+\alpha s^2} \tag{9.2-4}$$

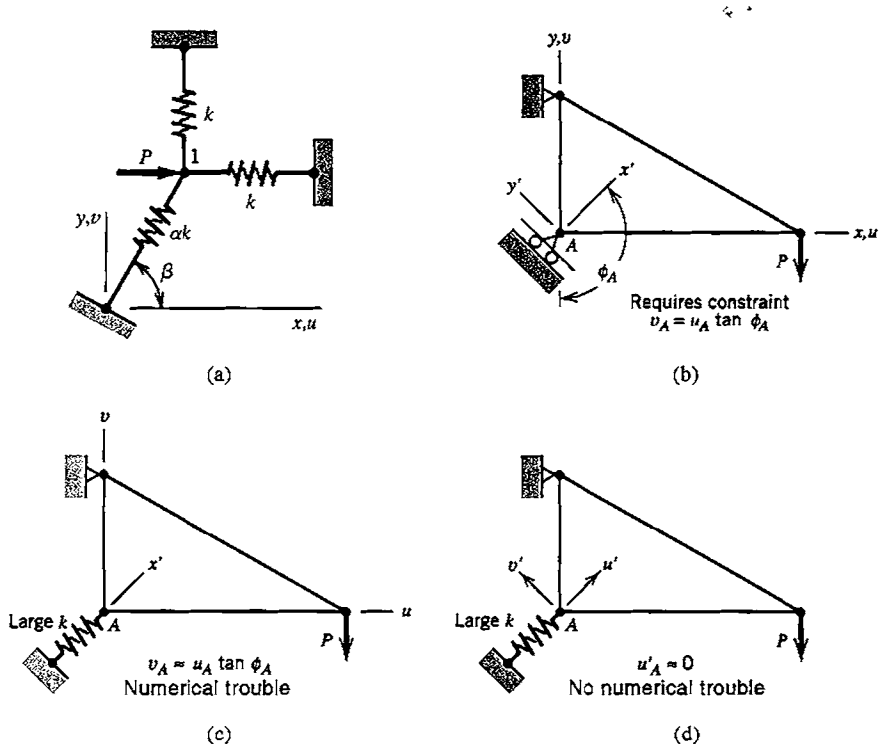

Figure 9.2-3. (a) Plane three-spring structure, with d.o.f. u_1 and v_1 at node 1. (b) Plane three-bar truss, with roller support at node A. (c,d) Ways of imposing the boundary condition approximately.

If α is large, the two lines have nearly the same slope, and equations $[\mathbf{K}]\{\mathbf{D}\} = \{\mathbf{R}\}$ are ill-conditioned. However, there are two exceptions: for $\beta = 0$ and for $\beta = \pi/2$, the lines intersect at right angles, even if α is large. For these angles, the equations remain well-conditioned for any value of α. Note that for these angles the off-diagonal terms $k\alpha cs$ vanish from $[\mathbf{K}]$, so the cancellation error described by Eq. 9.2-2 does not arise.

The foregoing considerations can be applied to the problem in Fig. 9.2-3b, where motion of node A is to be prohibited in direction x' but permitted in direction y'. One option, which does not lead to ill-conditioning, is to introduce d.o.f. u'_A and v'_A in directions x' and y' respectively, using a transformation described in Section 8.4, then impose $u'_A = 0$. It is tempting to avoid the transformation, and enforce the support condition approximately, by the simple trick of installing a very stiff spring in direction x', as shown in Fig. 9.2-3c. But then, if d.o.f. u_A and v_A are retained as d.o.f. at node A, large off-diagonal terms appear in the structure stiffness matrix and ill-conditioning is introduced, as described in connection with Eq. 9.2-3. A very stiff spring in direction x' can be used at node A without ill-conditioning if d.o.f. u'_A and v'_A are adopted at node A. With this option, a large stiffness term appears only on-diagonal, as is the case with $\beta = 0$ or $\beta = \pi/2$ in Eq. 9.2-3.

"Relative" and "Hierarchic" d.o.f. For the problem of Fig. 9.2-1, let us introduce the "relative" d.o.f. $u_r = u_1 - u_2$ in place of d.o.f. u_1. Thus Eqs. 9.2-1 are replaced by

$$\begin{bmatrix} k_1 & 0 \\ 0 & k_2 \end{bmatrix} \begin{Bmatrix} u_r \\ u_2 \end{Bmatrix} = \begin{Bmatrix} P \\ P \end{Bmatrix} \tag{9.2-5}$$

Equations 9.2-5 are well-conditioned for all values of k_1 and k_2. Equations 9.2-5 must be obtained by introducing u_r as a d.o.f. in element formulation, perhaps via transformation of standard element matrices prior to assembly. No purpose would be served by introducing u_r via transformation of assembled structural matrices, Eqs. 9.2-1, because the coefficient $k_1 + k_2$ already contains the error we seek to avoid.

In the context of p refinement, discussed in Section 9.8, added relative d.o.f. are known as "hierarchic" d.o.f. Hierarchic d.o.f. do not replace d.o.f. already present, but are added to an element to increase the degree of its polynomial field (as in Eq. 9.8-1).

9.3 THE CONDITION NUMBER

The condition number of a matrix $[\mathbf{K}]$, denoted here as $C(\mathbf{K})$, provides an estimate of the number of digits of accuracy that may be lost in solving equations $[\mathbf{K}]\{\mathbf{D}\} = \{\mathbf{R}\}$. The actual loss is usually less than the estimate, so accurate calculation of $C(\mathbf{K})$ is not necessary.

Definition and Calculation. The condition number of $[\mathbf{K}]$, also called its spectral condition number, is defined as

$$C(\mathbf{K}) = \frac{\lambda_{\max}}{\lambda_{\min}} \tag{9.3-1}$$

where $\lambda_{\max}$ and $\lambda_{\min}$ are the largest and smallest eigenvalues of $[\mathbf{K}]$. In some cases, $C(\mathbf{K})$ may be "artificially" high in the sense that it predicts much greater loss of accuracy than is actually realized. For example, in Fig. 9.2-1, $C(\mathbf{K})$ is large when $k_1 << k_2$ and when $k_1 >> k_2$, yet only the case $k_1 >> k_2$ leads to numerical error in equation solving. One can arrange for the condition number to be large only when equations are truly ill-conditioned by scaling $[\mathbf{K}]$ so that its diagonal coefficients are unity, then computing $\lambda_{\max}$ and $\lambda_{\min}$ from the scaled matrix $[\mathbf{K}_s]$. The scaling matrix $\lceil \mathbf{S} \rfloor$ is diagonal and is constructed from diagonal coefficients in $[\mathbf{K}]$. Thus the eigenvalue problem becomes

$$\left([\mathbf{K}_s] - \lambda \lceil \mathbf{I} \rfloor\right)\{\mathbf{D}\} = \{\mathbf{0}\} \qquad \text{where} \qquad [\mathbf{K}_s] = \lceil \mathbf{S} \rfloor [\mathbf{K}] \lceil \mathbf{S} \rfloor \quad \text{and} \quad S_{ii} = \frac{1}{\sqrt{K_{ii}}} \tag{9.3-2}$$

Here $\lceil \mathbf{I} \rfloor$ is a unit matrix. The form of Eq. 9.3-2 can be changed, without changing the eigenvalues, by substituting $\{\mathbf{D}\} = \lceil \mathbf{S} \rfloor^{-1}\{\mathbf{D}_s\}$ and premultiplying by $\lceil \mathbf{S} \rfloor^{-1}$. Thus

$$\left([\mathbf{K}] - \lambda \lceil K_{11} \;\; K_{22} \;\; \cdots \;\; K_{nn} \rfloor\right)\{\mathbf{D}_s\} = \{\mathbf{0}\} \tag{9.3-3}$$

In vibrations terminology, Eq. 9.3-3 says that eigenvalues $\lambda_i = \omega_i^2$ of the scaled matrix $[\mathbf{K}_s]$ can be determined from natural frequencies ω_i of a structure having the original stiffness matrix $[\mathbf{K}]$ and a diagonal "mass" matrix that is simply the diagonal of $[\mathbf{K}]$. This viewpoint shows why an isolated stiff region raises the condition number: an isolated large "mass" K_{ii} reduces the lowest frequency but has little effect on the highest.

The computational cost of solving an eigenproblem is greater than the cost of solving equations $[\mathbf{K}]\{\mathbf{D}\} = \{\mathbf{R}\}$. Fortunately, $\lambda_{\max}$ and $\lambda_{\min}$ need not be accurately known. A satisfactory *a priori* estimate of $\lambda_{\max}$ can be obtained from the Gerschgorin bound, Eq. 11.12-17.

However, *a priori* estimates of $\lambda_{\min}$ are not nearly as reliable. An approximation of the condition number of the scaled matrix $[\mathbf{K}_s]$ is $C(\mathbf{K}_s) = (r_i)_{\max}$, where r_i is the diagonal decay ratio defined in Eq. 9.4-1 [9.2]. This estimate is of course *a posteriori* rather than *a priori*.

Interpretation. As coefficient matrix $[\mathbf{K}]$ is processed in solving equations $[\mathbf{K}]\{\mathbf{D}\} = \{\mathbf{R}\}$, truncation error in original stiffness coefficients leads to loss of accuracy in the modified coefficients. If d digits are used to represent each number, modified coefficients are accurate to d_{acc} digits, where

$$d_{\text{acc}} = d - d_{\text{loss}} \quad \text{in which} \quad d_{\text{loss}} \le \log_{10} C(\mathbf{K}_s) \tag{9.3-4}$$

Thus if $d = 14$ and $C(\mathbf{K}_s) = 10^8$, then $d_{\text{acc}} \ge 6$. The " $\le$ " symbol in Eq. 9.3-4 indicates that $\log_{10} C(\mathbf{K}_s)$ may overestimate the number of digits lost. Typically $C(\mathbf{K}_s)$ is in the millions, but the potential loss of accuracy stated by Eq. 9.3-4 does not materialize. One reason is that Eq. 9.3-4 takes no account of loads $\{\mathbf{R}\}$. Loss of accuracy is most likely when the shape of $\{\mathbf{R}\}$ resembles one of the last eigenvectors $\{\mathbf{V}\}_i$ in Eq. 9.3-5 below, or is approximately a linear combination of them, but contains errors or small load components that resemble the first eigenvector [9.3]. In practice, the shape of $\{\mathbf{R}\}$ more often resembles a linear combination of the lowest eigenvectors.

The theory behind Eq. 9.3-4 is summarized as follows [9.4]. Let $[\mathbf{K}]$ have eigenvalues λ_i and associated eigenvectors $\{\mathbf{V}\}_i$ normalized so that $\{\mathbf{V}\}_i^T\{\mathbf{V}\}_i = 1$. Then for an n by n matrix $[\mathbf{K}]$ that is symmetric and positive definite,

$$[\mathbf{K}] = \sum_{i=1}^{n} \lambda_i \{\mathbf{V}\}_i \{\mathbf{V}\}_i^T \quad \text{and} \quad [\mathbf{K}]^{-1} = \sum_{i=1}^{n} \frac{1}{\lambda_i} \{\mathbf{V}\}_i \{\mathbf{V}\}_i^T \tag{9.3-5}$$

$[\mathbf{K}]$ is dominated by $\lambda_{\max}$ and $[\mathbf{K}]^{-1}$ by $\lambda_{\min}$. Information needed to compute $\lambda_{\min}$ is contained in the rightmost bits of coefficients K_{ij}. For every power of 10 in the ratio $\lambda_{\max}/\lambda_{\min}$, the dominant lowest mode of $[\mathbf{K}]^{-1}$ is represented by about one less digit as information drops off the ends of computer words.

Parameters That Influence $C(\mathbf{K})$. The severity of ill-conditioning is related to the type of problem and characteristics of the FE model. According to Fried [9.5],

$$C(\mathbf{K}) = b\left(\frac{h_{\max}}{h_{\min}}\right)^{2m-1} N_{\text{els}}^{2m/n} \tag{9.3-6}$$

where

b = a positive number

$h_{\max}, h_{\min}$ = maximum and minimum node spacings in the mesh

N_{els} = number of elements in the FE model

$2m$ = differential equation order

n = dimensionality of the FE mesh

To elaborate, for a problem that uses displacements as dependent variables and as nodal d.o.f., [**K**] is a stiffness matrix. In the differential equation(s) that describe the problem, $2m$ is the order of the highest displacement derivative. A measure of the number of elements per side of the FE mesh is $N_{es} = N_{els}^{1/n}$. Thus $C(\mathbf{K})$ is proportional to N_{es} raised to the power $2m$. As examples of exponent $2m/n$ in Eq. 9.3-6, for an axially-loaded bar, $2m/n = 2/1$; for a beam, $2m/n = 4/1$; in plane stress or plane strain, $2m/n = 2/2$; in 3D solids, $2m/n = 2/3$; in thin-plate bending, $2m/n = 4/2$. For plane strain conditions, and in solids of revolution and 3D solids, b in Eq. 9.3-6 is proportional to $1/(1 - 2\nu)$. As Poisson's ratio ν approaches 0.5, a near-incompressibility constraint is enforced, and $C(\mathbf{K})$ becomes very large [9.6].

Equation 9.3-6 can be useful in predicting the effect on $C(\mathbf{K})$ of changes in the FE model. For example, in a beam problem, if the length ratio h_{max}/h_{min} of elements is changed from 1/1 to 10/1, $C(\mathbf{K})$ increases by a factor of 1000. If the number of elements is doubled, $C(\mathbf{K})$ increases by a factor of 16. If *both* these changes are made, $C(\mathbf{K})$ increases by a factor of 16,000.

A formula that provides upper and lower bounds on $C(\mathbf{K})$ is available [9.5], but it is not attractive for use in FEA software because of computational expense.

9.4 DIAGONAL DECAY TEST

Here we describe the diagonal decay test as a way of detecting numerical error during the process of solving equations $[\mathbf{K}]\{\mathbf{D}\} = \{\mathbf{R}\}$ by Gauss elimination. Like other tests for numerical error it is not infallible, but it is simple and has very little computational expense.

Let [**K**] be symmetric and positive definite. As equations are processed—that is, as unknowns are eliminated—diagonal coefficients K_{ii} that correspond to a d.o.f. i yet to be eliminated are reduced in magnitude by subtraction operations but remain positive. An example of this behavior appears in Fig. 2.8-3. Another example appears in Eqs. 9.2-1 and 9.2-2, where elimination of u_1 reduces the second diagonal coefficient from $k_1 + k_2$ to k_2.

The diagonal decay test is applied to each diagonal coefficient just before it is used as the pivot in eliminating another unknown [9.7]. Let P_{ii} be the value of the ith diagonal coefficient at this instant. With K_{ii} the original value of this coefficient, the diagonal decay ratio is

$$r_i = \frac{K_{ii}}{P_{ii}} \tag{9.4-1}$$

For each power of 10 in r_i, up to that number of accurate digits may have been lost from the original diagonal coefficient. For example, if $r_i = 10^8$, then K_{ii} may have lost as many as eight digits of accuracy by the time it becomes P_{ii} and is about to be used to eliminate the ith unknown. It is possible to obtain $r_i = \infty$, which indicates that boundary conditions are inadequate; in structural mechanics terms, rigid-body motion is possible (even a small negative value of r_i is possible, owing to numerical error). If the result $r_i = \infty$ appears, it may not do so until the last step of elimination, because restraint of the last d.o.f. suffices to prevent singularity in some problems. Some software may be coded to insert a boundary condition when $r_i = \infty$ is detected, thus imposing the programmer's conjecture of what physical problem was intended by the software user.

TABLE 9.4-1. CANTILEVER BEAM OF N_{els} EQUAL-LENGTH ELEMENTS, SHOWING COMPUTED LATERAL TIP DEFLECTION v AND DIAGONAL DECAY RATIOS r_i IN THE LAST THREE EQUATIONS PROCESSED ($i = 2n - 2, i = 2n - 1$, AND $i = 2n$).

Total length = 1000

$EI = 8(10^6)$

$v_{\text{exact}} = 1.0000$

Tip-to-root numbering
$2n$ nonzero d.o.f.

Root-to-tip numbering
$2n$ nonzero d.o.f.

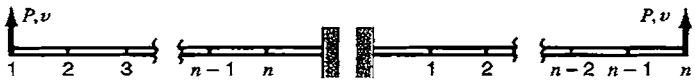

Number of elements	v	r_{2n-2}	r_{2n-1}	r_{2n}	v	r_{2n-2}	r_{2n-1}	r_{2n}
$N_{\text{els}} = n = 10$	1.0000	8.0	2.0	8.0	1.0000	5.3	$1(10^3)$	$4(10^1)$
$N_{\text{els}} = n = 100$	1.0000	8.0	2.0	8.0	0.9992	7.7	$1(10^6)$	$4(10^2)$
$N_{\text{els}} = n = 1000$	1.0000	8.0	2.0	8.0	0.1197	8.0	$2(10^8)$	$2(10^3)$

Table 9.4-1 shows applications of the diagonal decay test. Beam elements in this example do not allow for transverse shear deflection. In $\{\mathbf{D}\}$, the ordering of nodal d.o.f. v and $\theta = dv/dx$ is $\{\mathbf{D}\} = \lfloor v_1 \;\; \theta_1 \;\; v_2 \;\; \cdots \;\; \theta_{2n-2} \;\; v_{2n} \;\; \theta_{2n} \rfloor^T$. Analyses were performed on a machine that carries about 11 digits per computer word. The diagonal decay test is successful in this example; r_i becomes large only when there is substantial error in the computed tip deflection v. The condition number of $[\mathbf{K}]$, after scaling as in Eq. 9.3-2, is about 10^{12} for the case $N_{\text{els}} = 1000$, regardless of whether node numbering is tip-to-root or root-to-tip. Yet the severe loss of accuracy predicted by this large condition number does not appear for the tip-to-root numbering.

The example of Table 9.4-1 uses elements of equal length. Now, for the case $N_{\text{els}} = 1000$, let elements have varied lengths in the range $L = 0.99999$ to $L = 1.00001$. Then the tip-to-root numbering gives tip deflection $v = 1.027$ while diagonal decay ratios are essentially unchanged from the values of 8.0 and 2.0 seen in Table 9.4-1. Thus we see that there can be substantial accuracy loss that is not detected by the diagonal decay test.

It is the *decay* of diagonal coefficients that is significant, not their smallness. Small diagonal coefficients *per se* do not provoke large error. Similarly, large diagonal coefficients *per se* are not harmful (as in Eqs. 9.2-1 and 9.2-2 for the case $k_1 << k_2$, even if the node numbering were reversed). However, when a large diagonal coefficient is accompanied by large off-diagonal coefficients, its elimination causes considerable diagonal decay in other equations that also contain the large off-diagonal coefficients (as in Eqs. 9.2-1 and 9.2-2 for the case $k_1 >> k_2$).

9.5 RESIDUALS

Imagine that equations $[\mathbf{K}]\{\mathbf{D}\} = \{\mathbf{R}\}$ have been solved for $\{\mathbf{D}\}$. Then one can solve for the vector of residuals, $\{\Delta\mathbf{R}\}$:

$$\{\Delta\mathbf{R}\} = \{\mathbf{R}\} - [\mathbf{K}]\{\mathbf{D}\} \tag{9.5-1}$$

If solution vector $\{\mathbf{D}\}$ is not contaminated by numerical error, then $\{\Delta\mathbf{R}\} = \{\mathbf{0}\}$. More likely, numerical error is present; then $\{\Delta\mathbf{R}\}$ is a measure of error. A scalar form of this error measure is

$$e = \frac{\{\mathbf{D}\}^T\{\Delta\mathbf{R}\}}{\{\mathbf{D}\}^T\{\mathbf{R}\}} \tag{9.5-2}$$

Physically, e is the ratio of work done by residual loads to work done by actual loads when both act through displacements $\{\mathbf{D}\}$.

Unfortunately, when ill-conditioned equations are solved by Gauss elimination, residuals tend to be small whether solution vector $\{\mathbf{D}\}$ is accurate or not [9.8]. It is possible for the less accurate of two solution vectors to have the smaller residuals. Although a small $\{\Delta\mathbf{R}\}$ does not guarantee accuracy, a *large* $\{\Delta\mathbf{R}\}$ is a reliable indicator that something is wrong.

In structural mechanics, a small $\{\Delta\mathbf{R}\}$ has the physical meaning that applied loads $\{\mathbf{R}\}$ are very nearly in static equilibrium with resisting forces $[\mathbf{K}]\{\mathbf{D}\}$. Equilibrium can be satisfied even if $\{\mathbf{D}\}$ is much smaller than it should be in the physical problem because of an overly stiff discretization (as in Fig. 3.4-2, for example).

Numerical error in the solution of equations $[\mathbf{K}]\{\mathbf{D}\} = \{\mathbf{R}\}$ can be reduced by the following iterative improvement scheme. Calling the original solution $\{\mathbf{D}\}_1$, we successively calculate the residual vector, increments in the solution vector, and an updated solution vector. The sequence of calculations is repeated until convergence ($i = 1,2,\ldots,n$).

$$\{\Delta\mathbf{R}\}_i = \{\mathbf{R}\} - [\mathbf{K}]\{\mathbf{D}\}_i \qquad [\mathbf{K}]\{\Delta\mathbf{D}\}_i = \{\Delta\mathbf{R}\}_i \qquad \{\mathbf{D}\}_{i+1} = \{\mathbf{D}\}_i + \{\Delta\mathbf{D}\}_i \tag{9.5-3}$$

For this process to provide improved accuracy, $[\mathbf{K}]$ in the first of Eqs. 9.5-3 must be represented to greater precision than was used to determine the original solution vector $\{\mathbf{D}\}_1$. In the second of Eqs. 9.5-3 one can use the original (less precise) $[\mathbf{K}]$, whose factored form is already available from the process of solving for $\{\mathbf{D}\}_1$. Convergence is toward the solution of equations $[\mathbf{K}]\{\mathbf{D}\} = \{\mathbf{R}\}$ with the more precise representation of $[\mathbf{K}]$.

If a set of equations is seriously ill-conditioned, it is better to rework the model to improve its condition than to make heroic attempts to improve a poor solution. "If a thing is not worth doing, it is not worth doing well" [9.8].

9.6 DISCRETIZATION ERROR. CONVERGENCE RATE

Discretization error refers to the difference between a mathematical model and its discretized (finite element) model. In this section we discuss the relation between mesh refinement and the convergence of FE results toward results implicit in the mathematical model. Convergence *per se* says nothing about how well the mathematical model represents reality.

Arguments that follow are an elaboration of arguments associated with Fig. 4.9-2. The arguments are built on a fundamental proposition of FE error analysis: that for a *sufficiently refined mesh,* error in an FE solution can be bounded by the error in a shape function interpolation that is exact at nodes [9.9]. This proposition does not require that the FE

solution be exact at nodes; such is the case only for special situations [2.5]. It does require a *sufficiently refined mesh,* which is a mesh of sufficient refinement that the "true" convergence rate has been established (see also Fig. 9.7-1). Thus we exclude FE models having large discretization error (as in Fig. 3.4-2, for example). We also require that nodal loads be consistently applied, as described in Section 3.11.

Error Analysis. Discretization error can sometimes be determined by an order of error analysis. Consider the axially loaded uniform bar of Fig. 9.6-1a. From the differential element, the equation of axial equilibrium is $A\sigma_{x,x} + q = 0$. Or, substituting the stress-strain relation $\sigma_x = Eu_{,x}$, the equilibrium equation is

$$u_{,xx} + \frac{q}{AE} = 0 \tag{9.6-1}$$

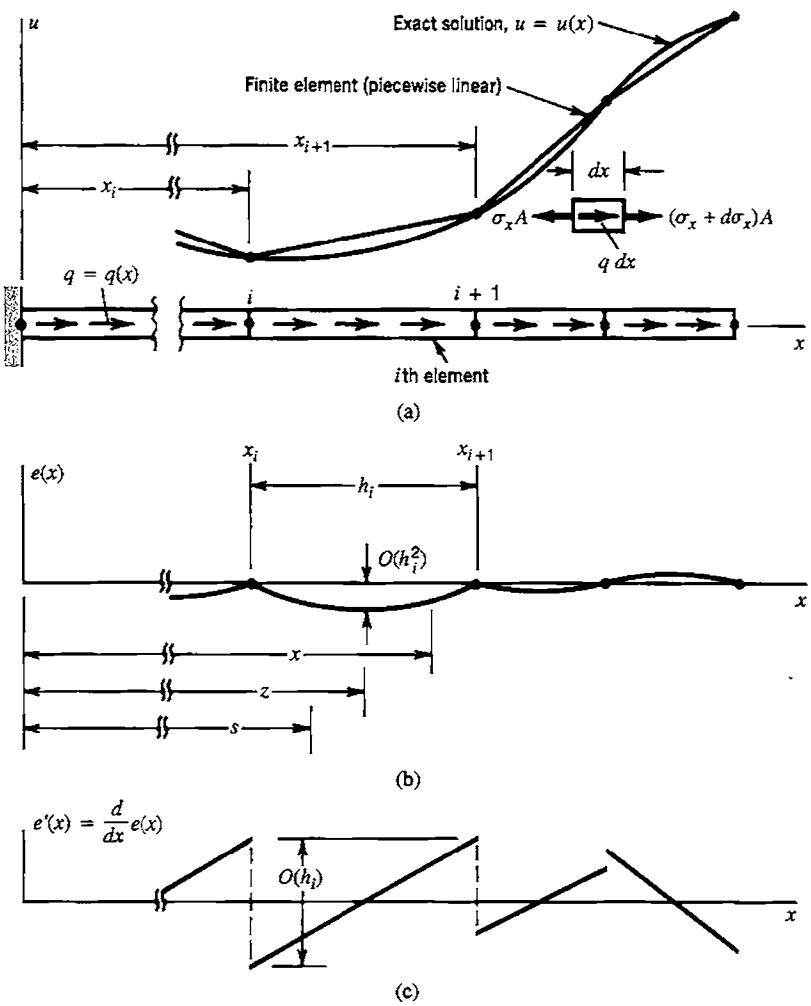

Figure 9.6-1. Behavior of the error in an FE model of a uniform bar under distributed axial load q. Exact axial displacement is $u = u(x)$ and its error is $e = e(x)$.

Let the FE model consist of standard two-node bar elements. If the load integral is evaluated consistently (as stated by Eq. 3.3-8 and by Eq. 4.8-15b) and A and E are constant, then nodal displacements u_i of the FE model are exact [2.5]. Because the exact solution is in general not piecewise linear, the FE solution has error *between* nodes. The nature of the error in the bar problem is characteristic of its nature in more complicated and realistic FE problems. Subsequent discussion is most directly applicable to linear elasticity problems with smooth (but possibly varying) elastic coefficients, with distributed (not point) loading, in bodies without strong singularities (no cracks).

In the bar problem we analyze the error of linear interpolation in the ith element, between nodes at x_i and x_{i+1}. Displacement error $e = e(x)$ is

$$e(x) = u(x) - \left[u_i\left(1 - \frac{x - x_i}{h_i}\right) + u_{i+1}\left(\frac{x - x_i}{h_i}\right)\right] \tag{9.6-2}$$

where $u(x)$ is the exact solution and $h_i = x_{i+1} - x_i$ is element length. Also, $u_i = u(x_i)$ and $u_{i+1} = u(x_{i+1})$. At nodes, $e(x) = 0$. Element lengths need not be equal. Within elements, $e(x)$ is a smooth function. At nodes, there are discontinuities in the first derivative $e'(x)$, as shown in Fig. 9.6-1c. (In the remainder of this section we use the notation $e_{,x} = e'$, $e_{,xx} = e''$, and so on.)

An upper bound on $e(x)$ is provided by the following argument [9.9]. Let z be an axial coordinate in the range $x_i \le z \le x_{i+1}$ such that $e'(z) = 0$. That there is such a point is obvious from Fig. 9.6-1b and follows rigorously from Rolle's theorem of elementary calculus. In what follows we assume that $u''(x)$ is continuous between nodes. The change in e' can be obtained by integrating e''. Thus from Eq. 9.6-2, with s a dummy variable and $e'(z) = 0$,

$$e'(x) - e'(z) = e'(x) = \int_z^x e''(s)\, ds = \int_z^x u''(s)\, ds \tag{9.6-3}$$

because linear terms in Eq. 9.6-2 do not contribute to $e''(x)$. Also,

$$\left|\int_z^x u''(s)\, ds\right| \le \int_z^x |u''(s)|\, ds \le \int_{x_i}^{x_{i+1}} |u''(s)|\, ds \le h_i \left(\max_{x_i \le x \le x_{i+1}} |u''(x)|\right) \tag{9.6-4}$$

Therefore, on the ith element, the error in strains, $e'(x)$, is bounded by

$$|e'(x)| \le h_i \left(\max_{x_i \le x \le x_{i+1}} |u''(x)|\right) \tag{9.6-5}$$

We can also bound displacement error $e(x)$ by observing that it must have greatest magnitude at $x = z$, where $e'(z) = 0$. If z is not at the element midpoint it must be closer to either x_i or x_{i+1}. Assume that z is closer to x_i, and compute $e(x_i)$ by a three-term Taylor series, with exact remainder, expanded about $x = z$.

$$e(x_i) = e(z) + (x_i - z)e'(z) + \frac{1}{2}(x_i - z)^2 e''(s) \tag{9.6-6}$$

where s is the remainder evaluation point on element i. But $e(x_i) = 0$, $e'(z) = 0$, and $e''(s) = u''(s)$ from Eq. 9.6-2, so

$$e(z) = -\frac{1}{2}(x_i - z)^2 u''(s) \tag{9.6-7}$$

According to the assumption that z is closer to x_i than to x_{i+1}, we conclude that $|z - x_i| \le h_i/2$. Therefore, on the ith element, the error in displacement, $e(x)$, is bounded by

$$e(x) \le \frac{1}{8} h_i^2 \left(\max_{x_i \le x \le x_{i+1}} |u''(x)| \right) \tag{9.6-8}$$

One may verify that the same result is obtained when z is assumed to be closer to x_{i+1} than to x_i.

We note that the existence of a z for which the error in strain is zero is the rationale for the existence of optimal points for stress calculation (see Section 6.10).

Salient points of the foregoing discussion are:

- Strain error in a linear element is proportional to element size, and displacement error is proportional to the square of element size.
- Error estimates are proportional to derivatives one order higher than the degree of the shape function (second derivatives for the bar, whose shape functions are linear).
- Displacements are most accurate at or near nodes. Strains are most accurate in element interiors.

Using the notation "O" for "order," we say that Eq. 9.6-5 displays discretization error $O(h)$ in strain and Eq. 9.6-8 displays discretization error $O(h^2)$ in displacement. Thus if $h = \max(h_i)$ is halved to create two elements from one, error in strain is approximately halved and error in displacement is approximately quartered.

More General Statements. We define symbols as follows.

h = approximate "characteristic length" of an element: length of a linear element; length of the longest line segment that fits within a plane or solid element (various definitions are possible)
p = degree of highest *complete* polynomial in the element field quantity
$2m$ = order of the highest derivative of the field quantity in the governing differential equation

The word "complete" in the definition of p is important. For example, $p = 1$ for the basic four-node plane element (Fig. 3.6-1 and Eqs. 3.6-1). In this element all constant and linear terms are present, but only xy among the three quadratic terms x^2, y^2, and xy.

An element whose field quantity contains a complete polynomial of degree p errs in representing polynomial terms of degree $p + 1$ and greater. If no singularities are present, it is reasonable to assume that most error is due to the lowest-degree term omitted, namely the term of degree $p + 1$. From this argument we conclude that in the absence of a singularity, discretization error (and convergence rate) are as follows:

- $O(h^{p+1})$ in representation of the field quantity
- $O(h^{p+1-r})$ in representing the rth derivative of the field quantity
- $O(h^{2(p+1-m)})$ in representing strain energy (in structural mechanics)

Exponent $2(p + 1 - m)$ appears in the latter expression because derivatives of degree m appear in formulas for strain (or curvature), which are then squared in expressions for strain energy. In order-of-error expressions, h can be replaced by $N_{\text{els}}^{-1/n}$, where N_{els} and n are respectively the number of elements in the FE model and the dimensionality of the model. The substitution is justified by noting that h is inversely related to the number of elements per side, N_{es}, which is approximately $N_{\text{els}}^{1/n}$.

In the one-dimensional example of Fig. 9.6-1, $p = 1$, $r = 1$ for strain calculation, and $2m = 2$. In plane bodies modeled by three-node triangles, and in solid bodies modeled by four-node tetrahedra, the field quantity is a complete linear polynomial, so $p = 1$. Also, $r = 1$ for gradient (strain or stress) calculation, and $2m = 2$ for problems such as heat conduction and stress analysis. The same numbers apply to conventional four-node quadrilaterals and eight-node bricks without internal "nodeless" d.o.f. These elements have more polynomial terms than triangles and tetrahedra, but not enough to form complete quadratic polynomials (Fig. 3.9-1). Discretization error is less, and therefore convergence rate is higher, with higher-order elements: if in a plane problem we change from four-node elements to eight-node elements, the order of error in the field quantity is changed from $O(h^2)$ to $O(h^3)$. With mesh subdivision that reduces h by half, the *amount* of error is reduced by a factor of four for a mesh of four-node elements and a factor of eight for a mesh of eight-node elements. In a beam problem, the numbers are $p = 3$ for standard two-node beam elements, $r = 2$ for curvature calculation, and $2m = 4$. The displacement error is $O(h^4)$ and the error of bending moment computed from curvature is $O(h^2)$. Recall that these estimates presume that nodal loads are calculated in consistent fashion. Thus, for a uniformly loaded cantilever beam, in an FE model with uniformly spaced nodes, the tip node carries force load and moment load.

Error estimates for derivatives of the field quantity may be pessimistic. For example, in the bar of Fig. 9.6-1, error estimates for $u_{,x}$ apply at nodes, where error in $u_{,x}$ is greatest. If instead $u_{,x}$ were computed at element midpoints, error would be less; $O(h^2)$ rather than $O(h)$. In other words, at bar element midpoints, gradients would converge at the same rate as the field quantity. In general, if there are points in an FE mesh where stresses have the same order of error as displacements, stresses at these points are said to display "superconvergence."

Finally we remark that some of the potential discretization error is reduced if structure volume is correctly represented. Thus if the boundary of a plane body is circular, and is modeled by a mesh of straight-sided elements, the polygonal outer boundary of the FE model should not lie entirely within the circle nor entirely outside it.

Singularities. We have seen that error bounds are proportional to the $(p + 1)$-order partial derivative of the exact field quantity (Eqs. 9.6-5 and 9.6-8, for example). If the problem to be solved displays an infinite value of this derivative, the error bound does not rigorously apply. For example, in bodies with cracks, displacement derivatives through second are infinite at a crack tip. Therefore, even for linear elements, for which $p = 1$, our estimates do not apply in the neighborhood of a crack tip. If we do not know the order of the lowest singular derivative, we cannot estimate the factor by which error will be reduced by subdividing the mesh.

Although singularities may slow convergence, singularities in derivatives higher than second do not *prevent* convergence. A complete polynomial of degree p necessarily contains a complete polynomial of degree $p - \mu$, where μ is a number such that $0 < \mu \leq p$. If the $(p + 1 - \mu)$-order derivative in the exact solution is the highest-order derivative that is

nonsingular, we can repeat our previous estimates with p replaced by $p - \mu$ to deduce that the field quantity has error $O(h^{p+1-\mu})$, its first derivative has error $O(h^{p-\mu})$, and so on. The implication is that for each derivative of order $p + 1$ or less that is singular in the exact solution, the FE solution may lose a power of h in accuracy. This estimate is often pessimistic. But when it holds, elements of degree $p - \mu$ will have the same order of error as elements of degree p, and the lower-degree elements have less computational expense.

As an application of concepts in the preceding paragraph, consider again the axially loaded bar, now with a step change in loading *within an element.* Specifically, for the element whose node numbers are i and $i + 1$, let $x_i < x_q < x_{i+1}$, and let the distributed axial load be

$$q = 0 \quad \text{for} \quad x \le x_q \qquad \text{and} \qquad q = 1 \quad \text{for} \quad x > x_q \tag{9.6-9}$$

Then from Eq. 9.6-1, $u_{,xx}$ is defined for all x, $\max|u''(x)| = 1/AE$, and Eqs. 9.6-5 and 9.6-8 are applicable. However, $u'''(x)$ is a delta function at $x = x_q$, so $\max|u'''(x)|$ is undefined. Accordingly, error estimates remain as stated in Eqs. 9.6-5 and 9.6-8, whether the element is linear, quadratic, or of yet higher degree. The $O(h^3)$ displacement accuracy one would normally expect from a quadratic element is not available. Full accuracy could be recovered by placing an interelement boundary at the step change in load. Generalizing, we expect that accuracy may decline substantially in the neighborhood of sudden changes *within* elements, of loading, material properties, or thickness.

9.7 MULTIMESH EXTRAPOLATION

Let ϕ represent a quantity of interest, calculated at some location in an FE mesh. Here ϕ may be the field quantity itself, one of its derivatives, or a quantity such as stress, which is proportional to a combination of derivatives. Let $O(h^q)$ be the order of error of ϕ, where h is a measure of element size as defined in Section 9.6. Assume that convergence is monotonic and that q is known. A plot of ϕ versus h^q is a straight line (Fig. 9.7-1a). Let ϕ_1 and ϕ_2 be values calculated from two meshes that have the respective size measures h_1 and h_2. By linear extrapolation to the ϕ axis, we obtain

$$\phi_\infty = \frac{\phi_1 h_2^q - \phi_2 h_1^q}{h_2^q - h_1^q} \qquad \text{or} \qquad \phi_\infty = \frac{\phi_1 - \phi_2 (h_1/h_2)^q}{1 - (h_1/h_2)^q} \tag{9.7-1}$$

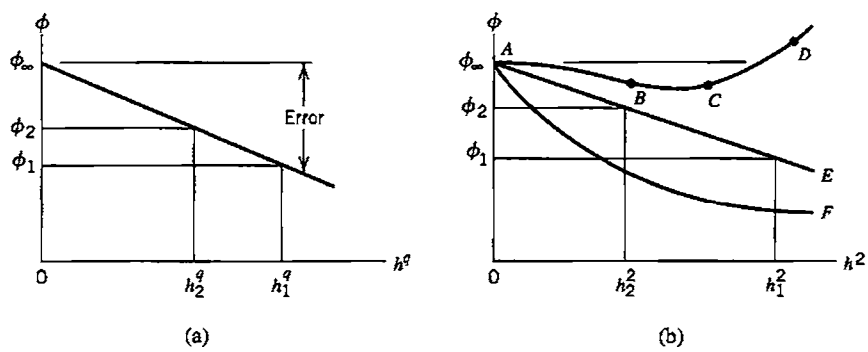

Figure 9.7-1. (a) Error in ϕ is proportional to h^q. (b) Error is nonmonotonic in curve $ABCD$ and proportional to h^2 in curve AE. Curve AF would plot as a straight line if the abscissa were h.

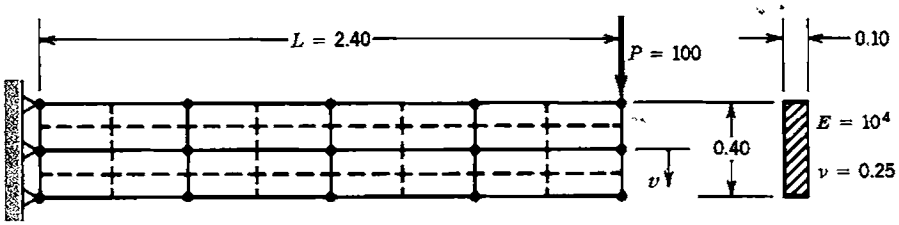

Figure 9.7-2. Regular mesh refinement of an end-loaded cantilever beam. Solid lines show mesh $N_{\text{els}} = 8$. Solid lines plus dashed lines suggest mesh $N_{\text{els}} = 32$. Four-node plane elements are used in both cases.

where ϕ_∞ corresponds to element size $h = 0$; in other words, ϕ_∞ corresponds to an infinitely refined mesh. Equation 9.7-1 is known as Richardson's extrapolation formula [5.1]. Restrictions apply, as follows.

What rigor there is in Eq. 9.7-1 depends on completely regular mesh refinement. That is, in each refinement, nodes and interelement boundaries of the coarser mesh are preserved, while new nodes, elements, and interelement boundaries are added. Corner nodes stay corner nodes and side nodes stay side nodes (Fig. 9.7-2). Element types are not changed. In all refinements, the quantity of interest must appear at a fixed location in the mathematical model, and at a fixed position relative to an element (always at a corner node, say). Without these restrictions, convergence may not be monotonic, in which case Eq. 9.7-1 does not apply.

Nonmonotonic convergence may result from a mesh of incompatible elements, such as QM6 elements discussed in Section 6.6. Also, rectangular QM6 elements contain a complete quadratic displacement expression and indeed behave like quadratic elements. But with increasing shape distortion they tend to lose quadratic capability and behave more like Q4 (linear) elements, as noted in Section 6.11. For these reasons q is not easy to predict.

If q is not known in advance, it can be established graphically by seeking an exponent q such that ϕ versus h^q plots as a straight line. Strictly, restrictions noted in the foregoing paragraph must be observed. At least three different meshes are needed so that we may distinguish a curve from a straight line (such as AF versus AE in Fig. 9.7-1b). If the original mesh is too coarse, ϕ from this mesh may not lie on a straight line for any value of q. If too few data points are calculated or an incorrect value of q is used, the extrapolated result may be less accurate than the result at either data point (as would be the result calculated from a straight line through C and D in Fig. 9.7-1, for example). In view of the many uncertainties, rather than regarding ϕ_∞ as exact, it seems preferable to regard

$$e = \frac{\phi_2 - \phi_\infty}{\phi_\infty} 100\% \tag{9.7-2}$$

as an estimate of the percentage error of ϕ_2.

Example: Regular Refinement. Lateral deflection at the tip of the cantilever beam in Fig. 9.7-2 was calculated using 8, 32, and 128 four-node plane elements. Each finer mesh is a regular subdivision of the preceding mesh. Each mesh was analyzed using three different kinds of four-node plane elements based on the bilinear shape functions of Eqs. 6.2-3: full integration (four Gauss points), reduced integration (one Gauss point), and reduced integration with spurious "hourglass" modes stabilized by one of the control devices cited in Section 6.8. Boundary conditions at the left end of the beam are sufficient to prevent mechanisms of the mesh that would otherwise be possible with reduced integration.

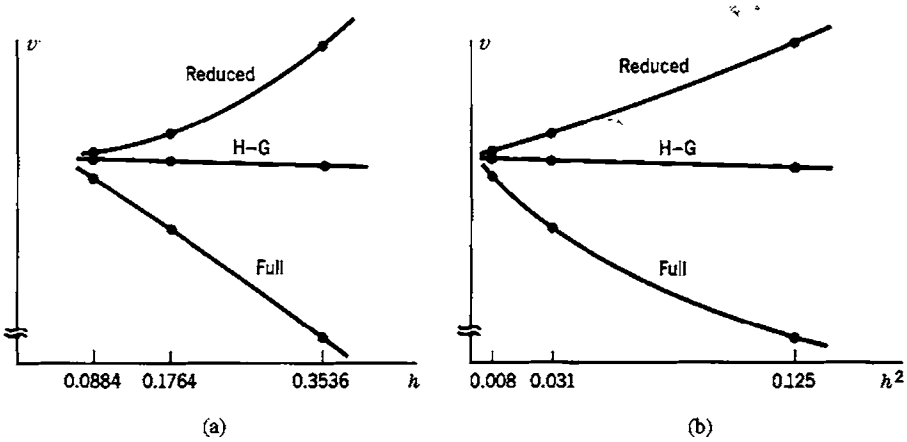

Figure 9.7-3. Plots of data from Table 9.7-1, for the problem of Fig. 9.7-2. (a) Tip deflection versus h. (b) Tip deflection versus h^2.

Computed results plotted in Fig. 9.7-3 suggest that error is approximately $O(h)$ for the full integration case and approximately $O(h^2)$ for the reduced integration case. If we assume that $O(h^2)$ applies to all cases and therefore apply Eq. 9.7-1 with $q = 2$, we obtain results stated in Table 9.7-1. Beam theory, including transverse shear deformation, predicts lateral tip deflection $\frac{PL^3}{3EI} + \frac{6PL}{5AG} = 8.640 + 0.180 = 8.820$.

Example: Irregular Refinement. We seek the largest principal stress in the cantilever beam of Fig. 9.7-4. The left end is completely fixed. Load P is uniformly distributed across the right end. The upper half is modeled, with all nodes on the x axis allowed only vertical displacement. Elements are fully-integrated four-node plane elements based on the bilinear shape functions of Eqs. 6.2-3. Meshes shown violate rules of regular mesh refinement. Also, meshes are poor in that they are unnecessarily fine far from the hole and undesirably coarse close to the hole. Plotted as $\sigma_{\max}$ in Fig. 9.7-4 is the largest normal stress at an element center, regardless of the element in which it appears.

With irregular refinement, it is unclear how size measures h_1, h_2, and h_3 of successive meshes should be defined. With N_{els} the number of elements in the mesh, the abscissa $1/\sqrt{N_{\text{els}}}$ used in Fig. 9.7-4 is approximately the reciprocal of the number of elements per side of the mesh. Thus the abscissa measure corresponds to h^1. A least-squares fit of a straight line to the three data points yields the estimate $\sigma_{\max} = 93.3$. Photoelastic data indicate that $\sigma_{\max} = 98.4$, at the top of the hole [1.16]. The extrapolated result is remarkably good, although such a good result may be somewhat fortuitous. At least, plotted results show that none of the three meshes by itself provides a satisfactory result.

TABLE 9.7-1. TIP DEFLECTION v OF THE BEAM IN FIG. 9.7-2, USING EQ. 9.7-1 WITH $q = 2$. ELEMENT SIZE h IS TAKEN AS $h = 1/\sqrt{N_{\text{els}}}$.

Mesh data		Computed deflection			Extrapolated deflection		
N_{els}	$h = N_{\text{els}}^{-1/2}$	Full	Reduced	H-G	Full	Reduced	H-G
8	0.3536	4.562	11.440	8.572			
					7.978	8.617	8.768
32	0.1768	7.124	9.323	8.719			
					8.695	8.788	8.788
128	0.0884	8.302	8.922	8.771			

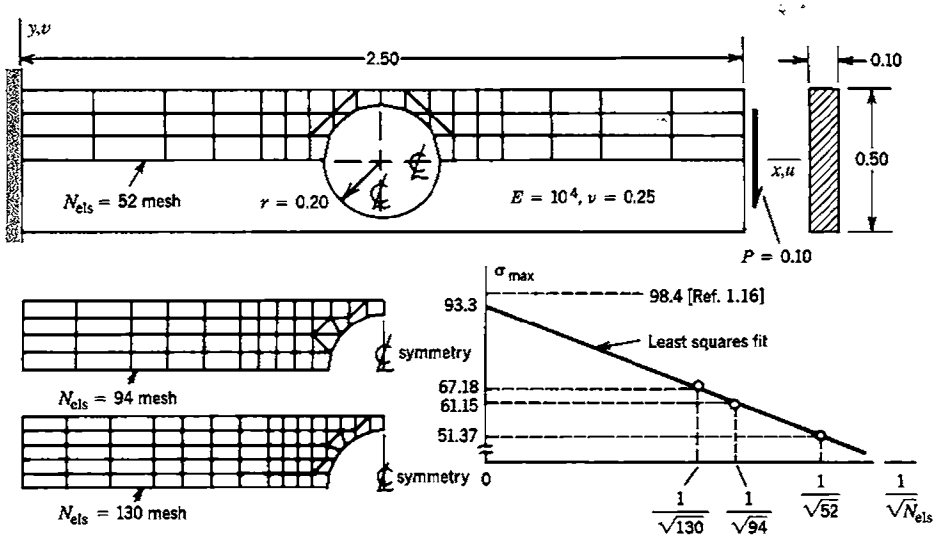

Figure 9.7-4. Irregular mesh refinement of a cantilever beam with a large central hole. Each mesh is symmetric about both centerlines. (The authors thank S.-C. Liang and D. Rusche for doing the calculations.)

9.8 MESH REVISION METHODS

In this and subsequent sections of the present chapter we consider how an FE mesh may be revised so as to provide improved results in the next cycle of analysis. The goal is to achieve the necessary accuracy by using only as many d.o.f. as necessary. Analysis of the current mesh provides both an error estimate and guidance for mesh revision. We begin by classifying the ways in which a mesh may be refined. We say "refined" because mesh revision typically involves refinement of a coarse mesh, but it is possible that revision will involve coarsening in some regions.

***h* Refinement.** Here h refers to a linear dimension that characterizes the size of an element, such as its largest span, or perhaps the square root of the area of a plane element, or the cube root of the volume of a solid element. An h refinement consists of adding elements of the same type (Fig. 9.8-1b). Figure 9.7-2 shows uniform h refinement; Figs. 9.7-4 and 9.8-1b show nonuniform h refinement. Figure 6.13-1b shows h refinement by repeated subdivision of some existing elements. This kind of refinement is sometimes called "enrichment."

***p* Refinement.** Here p refers to the degree of the highest *complete* polynomial in the element field quantity. A p refinement consists of increasing p within elements without changing the number of elements. This may be accomplished by adding d.o.f. to existing nodes, adding nodes on existing interelement boundaries, and/or adding internal d.o.f. The p refinement in Fig. 9.8-1c is nonuniform because elements are not all refined in the same way.

***r* Refinement.** Here r means "rearrange." Thus an r refinement consists of relocating nodes, without changing the number of elements or the polynomial degree of their field quantities (Fig. 9.8-1d).

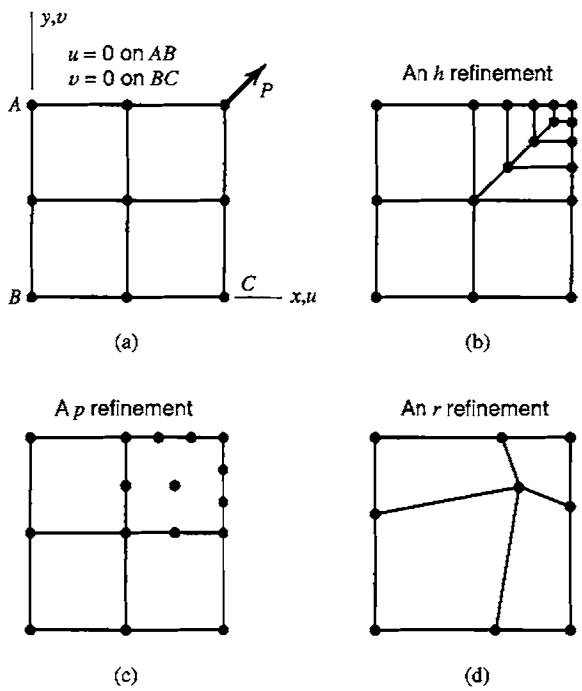

Figure 9.8-1. (a) Initial mesh for a square plate with in-plane corner load P. (b) A possible h refinement. (c) A possible p refinement. (d) A possible r refinement.

Remarks. If done manually, h refinement requires no change in existing FEA software. If automated, h refinement requires only that existing FEA software be used after a remeshing algorithm has adjusted the mesh. In remeshing, a well-shaped element should not be replaced by two or more badly shaped elements. With clever programming, if refinement is confined to a small portion of the FE model, some intermediate results used in analysis of the preceding mesh, such as stiffness matrices of unaffected elements, can be reused rather than redone. Refinement by the h method can be indefinitely repeated, limited only by computational expense, computer storage capacity, and possibly an eventual loss of accuracy due to numerical error.

Automation of p refinement requires substantial changes in conventional software. Refinement can continue, using successively higher degrees of element shape functions, until the highest degrees coded in the software have been used. For computational economy, a refined mesh can reuse some calculations used in the preceding mesh if added shape functions are presented in "hierarchic" form, so that existing element shape functions retain their original forms [4.4]. For example, Eqs. 6.1-3 and 6.1-4 can be replaced by

$$u = \lfloor \mathbf{N} \rfloor \{\mathbf{d}\} = \left\lfloor \frac{1}{2}(1-\xi) \quad (1-\xi^2) \quad \frac{1}{2}(1+\xi) \right\rfloor \begin{Bmatrix} u_1 \\ a_2 \\ u_3 \end{Bmatrix} \tag{9.8-1}$$

where a_2 is a hierarchic d.o.f. whose physical meaning is displacement relative to a linear variation dictated by u_1 and u_3. Thus, linear shape functions of a two-node element are not changed by addition of the hierarchic shape function $1 - \xi^2$. If d.o.f. in $\{\mathbf{d}\}$ are ordered so that each added hierarchic d.o.f. is appended to the end of the list, then, with each addition of a hierarchic d.o.f., rows and columns are added to the element stiffness matrix without altering rows and columns already present.

As d.o.f. are added, p refinement has a higher convergence rate than h refinement, especially if a singularity is present [4.4]. Also, in hierarchic form a p refinement produces a $[\mathbf{K}]$ of lower condition number than an h refinement having the same number of d.o.f. On the other hand, h refinement is better suited to a massively parallel computer, which can simultaneously generate thousands of elements of the same type [9.10]. The p method, by selectively adding d.o.f., tends to generate elements of many types.

The r method allows only limited improvement because the number of d.o.f. is unchanged. Accordingly, although optimization of node placement is possible, it is expensive and rarely worthwhile. In structural mechanics, an interesting feature of an r-optimized mesh is that interelement boundaries tend to follow principal stress trajectories. References include [9.10–9.12].

Of course, the foregoing methods of mesh refinement can be used in combination, and usually are. Typically h refinement is accompanied by repositioning of nodes, so that it is really an hr refinement (as for example in going from Fig. 6.14-2 to Fig. 6.14-3, or in the meshes of Fig. 9.7-4). Another effective combination is hp refinement, whose convergence rate as d.o.f. are added is greater than that of h refinement alone or p refinement alone.

Other Methods. After an initial analysis, one can elect to isolate a portion of the original FE structure, and refine only that portion. On the boundary of the portion isolated, displacements calculated from the initial analysis are imposed. This method is called *submodeling* and is discussed in Section 10.10. A conceptually similar method is that of overlaying a portion of the FE model by a supplementary mesh that has enhanced capability for resolving fine detail [9.13–9.15].

Multigrid methods are superficially similar to overlays, but are apt to be regarded as techniques of iterative equation-solving rather than as techniques of mesh refinement. They are summarized in Section B.3 of Appendix B.

9.9 GRADIENT (STRESS) RECOVERY AND SMOOTHING

The basic way to determine a gradient field is to calculate it in element-by-element fashion. A familiar example is the strain field calculated from element nodal d.o.f. $\{\mathbf{d}\}$, namely $\{\boldsymbol{\varepsilon}\} = [\mathbf{B}]\{\mathbf{d}\}$ as in Eq. 3.3-3. Commonly used elements are of the C^0 type (or C^1 for some plate and shell elements), and therefore do not display interelement continuity of strain (or curvature) fields. Alternative methods of gradient calculation can be more accurate, and many of them provide interelement continuity. They may be known collectively as *smoothing* operations, and have been intensively studied. In the following discussion we do not attempt to cite all references or decide which smoothing scheme works best. An important concept is that the discrepancy between an element-by-element field and a smoothed field can serve as a measure of discretization error. For this purpose, and for then deciding how the discretization can be improved, the smoothed field is regarded as the most accurate result the current mesh can provide.

The following explanations are oriented toward stress analysis problems in one and two dimensions. Other applications are noted subsequently. The following symbols are used.

$\{\boldsymbol{\varepsilon}\}$, $\{\boldsymbol{\sigma}\}$	Strain and stress fields calculated element-by-element in basic fashion; that is $\{\boldsymbol{\varepsilon}\} = [\mathbf{B}]\{\mathbf{d}\}$ and $\{\boldsymbol{\sigma}\} = [\mathbf{E}]\{\boldsymbol{\varepsilon}\}$
$\{\boldsymbol{\varepsilon}^*\}$, $\{\boldsymbol{\sigma}^*\}$	Strain and stress fields produced by a smoothing operation
σ, σ^*	One of the stresses in $\{\boldsymbol{\sigma}\}$ or $\{\boldsymbol{\sigma}^*\}$

Numerical error measures constructed by comparison of smoothed and unsmoothed fields are considered in Section 9.10.

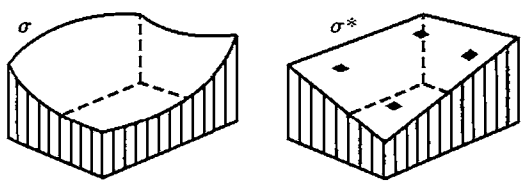

Figure 9.9-1. Element stress field σ and element-smoothed stress field σ^* in a quadrilateral element, depicted normal to the element plane.

Element Smoothing. Stresses and strains in an element may be most accurate at Gauss points of a low-order rule, such as at the four Gauss points of an order 2 rule in an eight-node quadrilateral element. Equations 6.10-3 and 6.10-4 describe the element stress field based on these four Gauss point stresses, which we now call an "element-smoothed" field [9.16]. Element smoothing does not remove stress discontinuities between elements. In general, the element field $\{\boldsymbol{\sigma}\} = [\mathbf{E}][\mathbf{B}]\{\mathbf{d}\}$ and the element-smoothed stress field differ (Fig. 9.9-1). With a plane element and extrapolation from four Gauss points, the element-smoothed field is a bilinear polynomial. The element field $\{\boldsymbol{\sigma}\} = [\mathbf{E}][\mathbf{B}]\{\mathbf{d}\}$ is of higher order if there are more than four nodes, and is usually a *different* bilinear polynomial if the element has four nodes but is not a parallelogram. The difference between element and element-smoothed fields can provide a useful element-by-element graphical display. If the difference is plotted as color contours or color bands, then elements of the mesh having the most varied colors are elements most in need of refinement or perhaps shape improvement [9.17]. Although any stress (or strain) component can be used in constructing the display, the von Mises stress σ_e is a reasonable choice because it incorporates all stress components. Other stress components provide different displays.

Nodal Averaging Methods. Let a stress such as the von Mises stress σ_e (Eq. 3.12-2) be computed at each node in each element, either directly at nodes or by extrapolation to nodes from Gauss points. At a node shared by n elements there are in general n different values of σ_e. The nodal average is

$$(\sigma_e)_{\text{ave}} = \frac{1}{n}\sum_{i=1}^{n}(\sigma_e)_i \tag{9.9-1}$$

In constructing nodal averages, one must avoid averaging across physically valid discontinuities such as a sudden change in material property or thickness, for which an average has no useful physical meaning. Also, the average is not necessarily a good estimate of actual stress. For example, if all elements display the stress variation seen in Fig. 6.10-1b, then all contributions to the average are overestimates. Variants of Eq. 9.9-1 include weighting element contributions according to proximity of the element centroid to the node in question.

A smoothed field that is interelement-continuous can be constructed from nodal average stresses. The same shape functions used to interpolate the field quantity from nodal d.o.f. can be applied to nodal average stresses. Thus, the portion of a smoothed stress field over a single element is

$$\sigma^* = \lfloor \mathbf{N} \rfloor \{\boldsymbol{\sigma}_n^*\} \tag{9.9-2}$$

where σ^* is any stress (σ_x, or σ_y, etc.) and $\{\boldsymbol{\sigma}_n^*\}$ is the vector of nodal averages of this stress for the element at hand. A one-dimensional example appears in Fig. 9.9-2a.

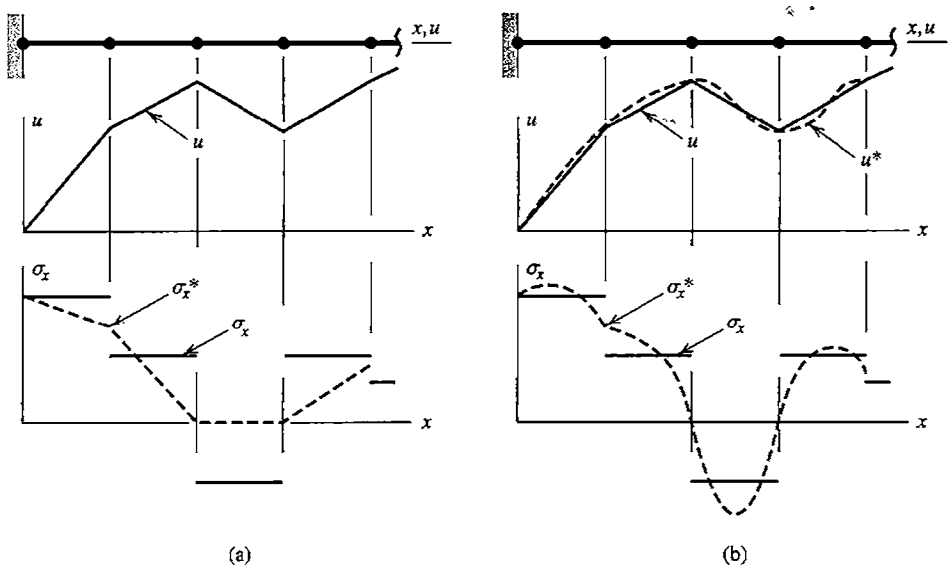

Figure 9.9-2. Uniform bar modeled by linear elements, showing a possible axial displacement field, the resulting element-by-element stress field, and smoothed stress field from (a) Eq. 9.9-2, and (b) Eq. 9.9-3.

The method of Eq. 9.9-1 has been used since the advent of FEA to provide stresses at nodes, and Eq. 9.9-2 for graphical display of smoothed stress fields, such as seen in Fig. 1.5-2b. The *un*smoothed field of Fig. 1.5-2a is a better display for engineering purposes, as it provides a whole-field portrayal of where mesh refinement is needed, specifically in areas where stress bands show greatest interelement discontinuity.

Another smoothing option is to begin by improving the displacement field, then differentiate it to obtain a smoothed strain field [9.18]. Consider, for example, several two-node bar elements connected end to end. At node 1 of a typical element, where $x = 0$, axial displacement is u_1, and axial strain can be taken as the nodal average value ε_{x1}^*. Similarly, at node 2, nodal values are u_2 and ε_{x2}^*. These nodal values define a smoothed function $u^* = u^*(x)$. Specifically, using cubic shape functions from Fig. 3.2-4,

$$u^* = N_1 u_1 + N_2 \varepsilon_{x1}^* + N_3 u_2 + N_4 \varepsilon_{x2}^* \quad \text{and} \quad \sigma_x^* = E\varepsilon_x^* = E\frac{du^*}{dx} \tag{9.9-3}$$

An example of this calculation appears in Fig. 9.9-2b. The method can be extended to C^1 problems such as plates, where second-derivative quantities must be smoothed [9.19].

Loubignac proposed a simple procedure for obtaining more accurate stresses, based on nodal average stresses and iteration that adjusts nodal d.o.f. until the averaged stress field and the last integral in Eq. 3.3-8 produce nodal loads that equilibrate externally applied loads at every node [9.20]. Crisfield states that in some cases the method does not converge [2.17].

Global Smoothing. An early proposal was to determine nodal values of a smoothed stress field by a least-squares fit, minimizing the square of the difference between the smoothed field and the element-by-element field [9.16]. To do so, we write the function

$$F_G = \sum \int (\sigma^* - \sigma)^2 \, dV \tag{9.9-4}$$

where σ and σ^* both pertain to a single stress, such as σ_e. As in Eq. 9.9-2, σ^* can be interpolated from nodal stresses in element-by-element fashion as $\sigma^* = \lfloor \mathbf{N} \rfloor \{\boldsymbol{\sigma}_n^*\}$, but in the present formulation, nodal stresses $\{\boldsymbol{\sigma}_n^*\}$ are as yet unknown. Stress σ is one of the stresses in $\{\boldsymbol{\sigma}\} = [\mathbf{E}][\mathbf{B}]\{\mathbf{d}\}$. Integration in Eq. 9.9-4 is over an element. Summation spans all elements of the structure, whereupon nodal stresses $\{\boldsymbol{\sigma}_n^*\}$can be listed in a global vector $\{\boldsymbol{\sigma}_n^*\}_G$. Hence, in the manner of Eq. 5.2-13,

$$\frac{\partial F_G}{\partial \{\boldsymbol{\sigma}_n^*\}_G} = \{\mathbf{0}\} \qquad \text{yields} \qquad \left(\sum \int \lfloor \mathbf{N} \rfloor^T \lfloor \mathbf{N} \rfloor \, dV\right) \{\boldsymbol{\sigma}_n^*\}_G = \sum \int \lfloor \mathbf{N} \rfloor^T \sigma \, dV \quad (9.9\text{-}5)$$

which is to be solved for $\{\boldsymbol{\sigma}_n^*\}_G$. The global coefficient matrix, in parentheses, has the form of a mass matrix. The same coefficient matrix is used for every stress component. The method is sometimes called "global L_2 projection" (see Eq. A.23, Appendix A). Despite its formal appeal, it is not favored because of its computational expense and because it is often not as accurate as methods discussed next.

Patch Recovery. A small number of contiguous elements, called a "patch," is selected. Stresses in elements of the patch are used to construct a smoothed field applicable to the patch. Either stress or strain can be smoothed. Choosing stress, we let the smoothed stress field over the patch be represented as

$$\sigma^* = \lfloor \mathbf{P} \rfloor \{\mathbf{a}\} \tag{9.9-6}$$

where σ^* is any one of the stress components (σ_x, or σ_y, etc.), $\lfloor \mathbf{P} \rfloor$ contains terms of a polynomial, and $\{\mathbf{a}\}$ contains generalized coordinates to be determined. Different values of the a_i in $\{\mathbf{a}\}$ are obtained for different stress components. In a plane problem, possible choices of the polynomial matrix are

$$\begin{aligned} &\text{Bilinear:} \quad \lfloor \mathbf{P} \rfloor = \lfloor 1 \;\; x \;\; y \;\; xy \rfloor && (\{\mathbf{a}\} \text{ contains } a_1 \text{ through } a_4) \\ &\text{Quadratic:} \quad \lfloor \mathbf{P} \rfloor = \lfloor 1 \;\; x \;\; y \;\; x^2 \;\; xy \;\; y^2 \rfloor && (\{\mathbf{a}\} \text{ contains } a_1 \text{ through } a_6) \end{aligned} \tag{9.9-7}$$

A bilinear $\lfloor \mathbf{P} \rfloor$, being an incomplete polynomial, provides results dependent on the orientation of xy axes relative to the patch, and results may be poor for some orientations.

To determine $\{\mathbf{a}\}$ and thus define the smoothed stress field, we select a patch, such as one of those shown in Fig. 9.9-3, and assign a coordinate system xy. The origin of coordinates can be located arbitrarily, but should be close to the patch to avoid possible numerical difficulty associated with a small patch far from the origin, for which coordinates of points in the patch would have small percentage differences. The element stress field σ is sampled at locations where it is likely to be most accurate. Typically these locations are Gauss points of various integration rules (shown by open squares and open triangles in Fig. 9.9-3). Next, at each sampling point (x_i, y_i) we square the difference between element stress σ and the as yet unknown smoothed stress σ^* from Eq. 9.9-6, and add the squares. Thus we obtain the function [9.21]

$$F_P = \sum_{i=1}^{nsp} (\sigma^* - \sigma)_i^2 \tag{9.9-8}$$

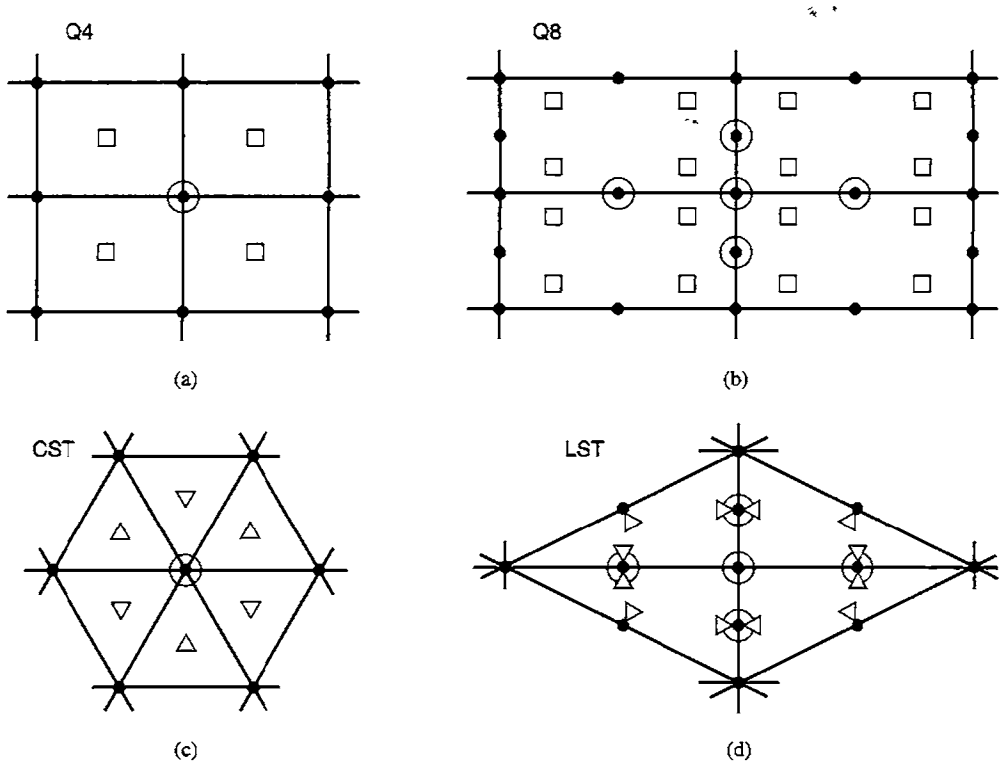

Figure 9.9-3. Patch recovery using plane elements. △, □ = locations where stress (or another gradient) is sampled. • = nodes. ⊙ = nodes where stresses σ^* are most accurately provided by the patch. Element names are explained in Chapter 3.

Here *nsp* is the number of sampling points in the patch (in the respective parts of Fig. 9.9-3, *nsp* is 4, 16, 6, and 12). Substitution from Eq. 9.9-6, followed by minimization of F_P with respect to the a_i in the manner of Eq. 9.9-5, yields

$$[\mathbf{A}]\{\mathbf{a}\} = \{\mathbf{b}\} \qquad \text{where} \qquad \begin{aligned} [\mathbf{A}] &= \sum_{i=1}^{nsp} \lfloor \mathbf{P} \rfloor_i^T \lfloor \mathbf{P} \rfloor_i \\ \{\mathbf{b}\} &= \sum_{i=1}^{nsp} \lfloor \mathbf{P} \rfloor_i^T \sigma_i \end{aligned} \tag{9.9-9}$$

from which $\{\mathbf{a}\}$ is determined. We require that *nsp* be equal to or greater than the number of terms in $\{\mathbf{a}\}$. If greater, the equation system is overdetermined, and yields a_i that provide a least-squares fit. The same matrix $[\mathbf{A}]$ is used for each stress component in the stress field, such as σ_x, σ_y, and τ_{xy} in a plane stress problem. Unlike Eq. 9.9-5, no integration is involved, and the fitted field is confined to a patch of elements rather than the entire structure. Patch recovery has also been applied to calculation of the field quantity itself [9.22].

When $\{\mathbf{a}\}$ has been computed, the smoothed stress σ^* can be evaluated at any point in the patch by substituting the x and y coordinates of the point into Eq. 9.9-6. Nodes surrounded by open circles in Fig. 9.9-3 are considered good choices for this evaluation. The entire structure can be spanned by many partially overlapping "recovery patches" (taking care that no patch straddles a known stress discontinuity, such as an interface between different materials). When this process is applied to quadratic and higher order elements, nodes internal to the mesh and most nodes on its boundary receive σ^* stresses from more than one patch. The several values at a node can be averaged [9.21]. Stresses σ^* at boundary nodes are not likely to be as accurate as stresses at internal nodes. If σ^* stresses have been calculated at all nodes, stress within each element can be obtained from Eq. 9.9-2 if so desired.

According to the discussion in Section 9.6, element stresses $\{\boldsymbol{\sigma}\} = [\mathbf{E}][\mathbf{B}]\{\mathbf{d}\}$ in a plane problem have convergence rate $O(h^p)$, where p is the degree of the highest complete polynomial in the element displacement field. It happens that stresses σ^* provided by patch recovery are superconvergent; that is, their convergence rate is at least $O(h^{p+1})$ [9.21]. For linear elements Q4 and CST in Fig. 9.9-3, the rate is $O(h^2)$; for quadratic elements Q8 and LST, the rate is $O(h^3)$ for points on the boundary and $O(h^4)$ for points internal to the mesh. The $O(h^4)$ rate has been termed "ultraconvergent" [9.21]. In this case, reduction of element size by half reduces stress error by a factor of 16.

The accuracy of stresses provided by patch recovery can sometimes be improved, especially at nodes on a boundary of the mesh, by taking equilibrium equations into account [9.23,9.24]. This can be accomplished by applying the left hand side of Eq. 3.1-13 to the smoothed stress field, integrating over the patch, and adding the resulting term to the right hand side of Eq. 9.9-8. Thus all components of a stress field are treated simultaneously by the patch recovery process. The method can be regarded as augmentation of F_P, Eq. 9.9-8, by a constraint function that penalizes departure from equilibrium conditions (see Section 13.3). Inclusion of equilibrium equations produces a coefficient matrix analogous to $[\mathbf{A}]$ in Eq. 9.9-9, but less likely to be ill-conditioned. A 1997 study of error estimators [9.25] finds that including equilibrium conditions as in [9.23] produces a smoothing method that is sensitive to element shape distortion, and concludes that the most reliable method is the original patch recovery method of [9.21] (Eqs. 9.9-6 to 9.9-9).

Variants of patch recovery [9.24,9.26] include relating stresses from overlapping patches at shared stress recovery points in a way other than simple averaging, and avoiding subsequent representation of stresses in element-by-element fashion (Eq. 9.9-2), which provides an interpolation different from that of the patch. Additional procedures are reported in [9.27,9.28].

As described above, a patch is centered about a node, as seen in Fig. 9.9-3. An alternative is to center a patch about an element, as shown in Fig. 9.9-4, so as to obtain a stress field over the central element directly, without first determining smoothed stresses at element nodes [9.26]. For elements whose displacement fields contain a complete polynomial of degree p, degree $p + 1$ may be appropriate for the fitted polynomial (Eq. 9.9-6). Smoothed fields determined by use of several element-centered patches are not interelement-continuous. If stresses on interelement boundaries are required, simple averaging of smoothed fields is suggested [9.26].

Further improvements and additional schemes are likely to be suggested in the future. Any method of stress calculation that differs from element stresses $\{\boldsymbol{\sigma}\} = [\mathbf{E}][\mathbf{B}]\{\mathbf{d}\}$ and provides improved results is a candidate for study and can serve as a basis for estimation of discretization error.

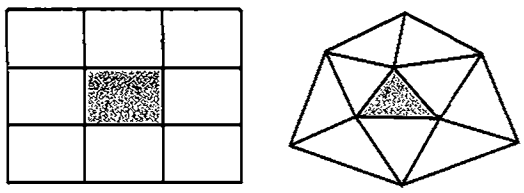

(a) (b)

Figure 9.9-4. Element-centered patches for (a) quadrilateral elements, and (b) triangular elements.

Other Applications. In heat conduction analysis, flux is a first-derivative quantity that corresponds to stress in structural mechanics. Flux smoothing in a plane steady-state problem with isotropic material may incorporate the equilibrium equation $f_{x,x} + f_{y,y} = 0$, where f_x and f_y are flux components in x and y directions [9.23]. In problems of stress analysis where bending appears, first derivatives of lateral displacement may already be inter-element-continuous, depending on element type. Then smoothing is applied to second and perhaps also third derivative quantities; that is, to bending moments and transverse shear forces [9.29,9.30]. Eigenvalue problems, such as the calculation of natural frequencies of vibration and buckling loads, have been addressed by smoothing of the type depicted in Fig. 9.9-2b and also by patch smoothing of displacement fields [9.18,9.19,9.22,9.31]. In problems of acoustic vibration, C^0 elements have a single pressure d.o.f. at each node, so smoothing is used to obtain an improved pressure field.

9.10 *A POSTERIORI* ERROR ESTIMATE

A finite element solution contains enough information to estimate its own error. That is, *a posteriori* error estimation is possible. The estimate is based on the difference between an element-by-element field and an alternative field, presumably more accurate and usually obtained by a smoothing operation. Information obtained in constructing the estimate can be used to improve the FE mesh, as described in Section 9.11.

An error measure can be based on any component of the stress field and can be defined in various ways. A simple way to quantify the discrepancy among contributions to nodal average stress from the n elements that share the node, from Eq. 9.9-1, is $\frac{1}{n}\sum\left|(\sigma_e)_{\text{ave}} - (\sigma_e)_i\right|$. This result might be divided by the maximum σ_e in the mesh, in order to avoid ascribing importance to large stress differences when the stresses themselves are not large enough to cause concern. Rather than using such a node by node error measure, it is more common to determine an error measure for each element and combine the element measures into a global error measure. The explanation that follows uses terminology of time-independent and isothermal stress analysis. Other applications are noted subsequently.

ZZ Error Estimate. The following form of error estimate is often called the ZZ (or the Z^2) error estimate after its originators, Zienkiewicz and Zhu [9.32,9.33]. Using element-by-element strains $\{\boldsymbol{\varepsilon}\} = [\mathbf{B}]\{\mathbf{d}\}$, we obtain the strain energy in each element from Eq. 4.4-5. The sum of element strain energies, multiplied by 2, is defined as the square of the *global strain energy norm,* $\|U\|$.

$$\|U\|^2 = \sum_{i=1}^{m} \int \{\boldsymbol{\varepsilon}\}_i^T [\mathbf{E}] \{\boldsymbol{\varepsilon}\}_i \, dV \tag{9.10-1}$$

where m is the number of elements in the region of the structure whose error is to be estimated. This region need not include all elements in the structure. Using the difference between the smoothed strain field $\{\boldsymbol{\varepsilon}^*\}$ and element-by-element strains $\{\boldsymbol{\varepsilon}\} = [\mathbf{B}]\{\mathbf{d}\}$, we define the *global energy error norm* $\|e\|$, which is called the error estimator. Its square is

$$\|e\|^2 = \sum_{i=1}^{m} \int (\{\boldsymbol{\varepsilon}^*\}_i - \{\boldsymbol{\varepsilon}\}_i)^T [\mathbf{E}](\{\boldsymbol{\varepsilon}^*\}_i - \{\boldsymbol{\varepsilon}\}_i)\, dV \tag{9.10-2}$$

Because $\{\boldsymbol{\sigma}\} = [\mathbf{E}]\{\boldsymbol{\varepsilon}\}$ and $\{\boldsymbol{\sigma}^*\} = [\mathbf{E}]\{\boldsymbol{\varepsilon}^*\}$, Eqs. 9.10-1 and 9.10-2 can also be stated in terms of stresses.

$$\|U\|^2 = \sum_{i=1}^{m} \int \{\boldsymbol{\sigma}\}_i^T [\mathbf{E}]^{-1} \{\boldsymbol{\sigma}\}_i\, dV \tag{9.10-3}$$

$$\|e\|^2 = \sum_{i=1}^{m} \int (\{\boldsymbol{\sigma}^*\}_i - \{\boldsymbol{\sigma}\}_i)^T [\mathbf{E}]^{-1} (\{\boldsymbol{\sigma}^*\}_i - \{\boldsymbol{\sigma}\}_i)\, dV \tag{9.10-4}$$

Because $\|U\|^2$ and $\|e\|^2$ depend on squares and products of stresses, $\|U\|$ and $\|e\|$ are in a sense representative of stresses themselves (or, more generally, of gradients of the field quantity).

As alternatives to $\|U\|$ and $\|e\|$ in subsequent calculations one can work with L_2 norm quantities (defined in Appendix A). They are obtained from the foregoing expressions by omitting the weighting matrix $[\mathbf{E}]$. Specifically

$$\|U\|_{L_2}^2 = \sum_{i=1}^{m} \int \{\boldsymbol{\sigma}\}_i^T \{\boldsymbol{\sigma}\}_i\, dV \tag{9.10-5}$$

$$\|e\|_{L_2}^2 = \sum_{i=1}^{m} \int (\{\boldsymbol{\sigma}^*\}_i - \{\boldsymbol{\sigma}\}_i)^T (\{\boldsymbol{\sigma}^*\}_i - \{\boldsymbol{\sigma}\}_i)\, dV \tag{9.10-6}$$

Relative error can be defined as

$$\eta = \left[\frac{\|e\|^2}{\|U\|^2 + \|e\|^2} \right]^{1/2} \tag{9.10-7}$$

where η can be used to quantify the discretization error over a patch of elements or possibly the entire mesh. The denominator of Eq. 9.10-7 is an estimate of the exact error energy, which is unknown. As an alternative denominator, one might use $\|U^*\|^2$, which can be calculated by replacing $\{\boldsymbol{\varepsilon}\}$ by $\{\boldsymbol{\varepsilon}^*\}$ in Eq. 9.10-1. Unless error is large, as from a mesh that is much too coarse, $\|U^*\|^2 \approx \|U\|^2 + \|e\|^2$. Note that η is a relative error estimate that applies to the *original* element-by-element field, not to the improved field produced by a smoothing operation. The possible range of η is $0 < \eta < 1$. An acceptable value of η is often taken as $\eta \leq 0.05$.

Remarks. The foregoing error estimates pertain to gradients of the field quantity, not to the field quantity itself, and to an assembly of elements, not to individual elements or to stress at a particular point. If the foregoing equations were applied to individual elements so as to obtain $\|U\|_i$ and $\|e\|_i$ for each element i, one would usually encounter highly stressed and lightly stressed elements that have almost equal element norms $\|e\|_i$, so that η_i might be higher in lightly stressed elements. Such information would not be helpful.

Because the global $\|e\|$ is a measure of interelement gradient discontinuity before smoothing, stress smoothing and error measure should not be based on a mesh or patch that spans a physically realistic stress discontinuity associated with a step change in thickness, a change of material, a shrink-fit connection, and so on. However, use of the error estimator in the presence of singularities has been studied [9.34,9.35].

For application to plate bending, $\|e\|$ over a patch of m elements can be defined as

$$\|e\|^2 = \sum_{i=1}^{m} \int (\{\mathbf{M}^*\} - \{\mathbf{M}\})^T [\mathbf{D}]^{-1} (\{\mathbf{M}^*\} - \{\mathbf{M}\})\, dA \tag{9.10-8}$$

where $\{\mathbf{M}^*\}$ is the smoothed bending moment field, $[\mathbf{D}]$ is the matrix of flexural rigidities, and A is element area. The expression for $\|U\|^2$ is analogous to Eq. 9.10-3 and is obtained by omitting $\{\mathbf{M}^*\}$ terms from Eq. 9.10-8. For application to thick plates, where transverse shear deformation is taken into account, the contribution of transverse shear force is also included in energy norms [9.36]. For application to shells, Eq. 9.10-8 is augmented by Eq. 9.10-4, using stresses that arise from membrane forces [9.37]. The expression for $\|U\|^2$ is similarly augmented.

As a simplification in calculation, smoothing and error estimation might be based on $\|U\|_{L_2}^2$ and $\|e\|_{L_2}^2$ of Eqs. 9.10-5 and 9.10-6, using only the von Mises stress σ_e. Thus [9.38]

$$\|u\|_{L_2}^2 = \sum_{i=1}^{m} \int \sigma_e^2\, dV \qquad \text{and} \qquad \|e\|_{L_2}^2 = \sum_{i=1}^{m} \int (\sigma_e^* - \sigma_e)^2\, dV \tag{9.10-9}$$

Other Applications. In heat conduction, Eqs. 9.10-3 to 9.10-7 can be used if symbols are redefined. Stress vectors $\{\boldsymbol{\sigma}\}$ and $\{\boldsymbol{\sigma}^*\}$ are replaced by vectors of heat flux, respectively associated with element-by-element and smoothed calculation, and $[\mathbf{E}]$ is replaced by a matrix of thermal conductivities. If the overall problem is the two-stage problem of thermal stress analysis, error analysis and mesh revision should be undertaken in the temperature analysis stage and again in the subsequent stress analysis stage, because a mesh suitable for one stage may not be suitable for the other. Error analysis and mesh revision applied only in one stage cannot correct poor results from the other stage.

For each mode of a vibration problem, smoothing can be used in calculating both numerator and denominator of the Rayleigh quotient, which produces a more accurate value of the natural frequency of that mode. Thus we obtain a global estimate of error in the original calculation and an improved value of the result sought. The method has also been applied to buckling problems. References include [9.18,9.19,9.22,9.31,9.39].

In the mode superposition approach to structural dynamics, the ZZ estimator and associated mesh improvement have been applied to each mode retained in the analysis [9.40].

Applications in fluid dynamics are surveyed in [9.41].

9.11 ADAPTIVE MESHING

The goal of adaptive meshing is to achieve a desired accuracy by revising a mesh, where necessary and to the extent necessary. Usually a few cycles of analysis and mesh revision are needed. Automation of the process requires numerical indication of where and how to revise the discretization, software for automatic meshing, and a termination criterion. The following scheme, suggested by Zienkiewicz and Zhu, is often used [4.4,9.32,9.33,9.36]. It is not restricted to stress analysis problems.

A possible termination criterion is that the final value of η (Eq. 9.10-7) must not exceed an allowable value η_{all} in either the final mesh or a portion of it for which η is computed. The average value of $\|U\|^2 + \|e\|^2$ per element, in combination with η_{all}, provides an allowable value of $\|e\|$ in an element. Thus from Eq. 9.10-7, with m the number of elements in the region whose error is to be estimated,

$$\text{In a single element:} \qquad \|e\|_{\text{all}} = \eta_{\text{all}}\left[\frac{\|U\|^2 + \|e\|^2}{m}\right]^{1/2} \tag{9.11-1}$$

The ratio of the actual value of $\|e\|$ in a typical element i to the allowable value is

$$\xi_i = \frac{\|e\|_i}{\|e\|_{\text{all}}} \qquad \text{where} \qquad \|e\|_i^2 = \int (\{\sigma^*\}_i - \{\sigma\}_i)^T [\mathbf{E}]^{-1} (\{\sigma^*\}_i - \{\sigma\}_i)\, dV \tag{9.11-2}$$

With the h method of mesh revision, the result $\xi_i < 1$ indicates that the element is larger than necessary. The result $\xi_i > 1$ indicates that more elements are needed in this location. Because usual practice is to begin with a coarse mesh, few if any elements will have $\xi_i < 1$ after the first analysis cycle. These elements, if any, might be ignored, with attention directed toward refinement of elements for which $\xi_i > 1$. With h a characteristic element dimension, such as defined early in Section 9.8, the desired new size of element i is taken as

$$(h_i)_{\text{new}} = \frac{(h_i)_{\text{old}}}{\xi_i^{\alpha}} \qquad \text{where} \qquad \begin{array}{lll} \alpha = 1/p & \text{not adjacent to a singularity} \\ \alpha = 1/\lambda & \text{adjacent to a singularity} \end{array} \tag{9.11-3}$$

Here p is the degree of the highest complete polynomial in the element field quantity ($p = 1$ for a four-node bilinear quadrilateral, $p = 2$ for an eight-node quadrilateral, and so on), and λ is the strength of the singularity (if present). For a sharp crack, $\lambda = 0.5$, and indeed for adaptive meshing $\lambda = 0.5$ can be used as an adequate approximation for any singularity [4.4].

With successive cycles of analysis, error estimation, and mesh revision, the foregoing procedure drives the mesh toward a condition in which $\|e\|_i$ has the same value in all elements, which is a possible definition of an optimal mesh. Again a helpful graphical display comes to mind: different colors can be assigned to different numerical ranges of $\|e\|_i$. Then, in a satisfactory mesh, all elements display the same color.

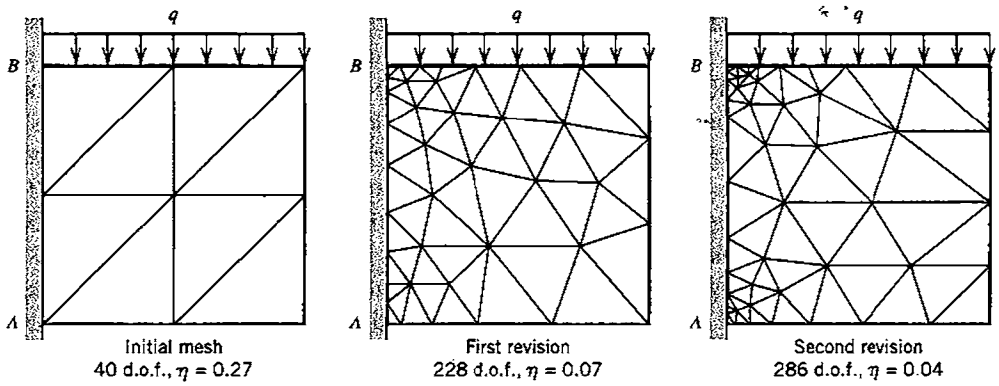

Figure 9.11-1. Results of an adaptive solution in a plane region using linear-strain triangles. Poisson's ratio is 0.3. All d.o.f. along AB are set to zero. Each mesh revision aimed at $\eta = 0.05$. [From J. Z. Zhu and O. C. Zienkiewicz, "Adaptive Techniques in the Finite Element Method," *Communications in Applied Numerical Methods*, Vol. 4, No. 2, 1988, pp. 197–204. © John Wiley & Sons Ltd. Reproduced by permission.]

After mesh revision, FEA and error estimation are repeated, followed by another mesh revision and reanalysis if necessary. Iteration can be stopped, and results deemed satisfactory, when η defined by Eq. 9.10-7 falls below the user-defined value η_{all}, a typical value for which is 0.05 (5%). This criterion is based on energy norms and does not guarantee that individual stresses all have the same accuracy. One can require that other criteria for termination also be satisfied, and can adopt equations other than Eq. 9.11-3 for revision of element size. These efforts include defining a permissible error at the element level, revising the shape of elements as well as their size to take advantage of stress gradients not being the same in all directions, and other techniques [9.32,9.42–9.44].

Figure 9.11-1 is an example of adaptive mesh refinement. The goal of reducing η to less than 0.05 is achieved quickly. However, the two reentrant corners are singular points, where stresses are theoretically infinite. Repeated cycles of error estimation and adaptive meshing will continue to refine the mesh in these locations. Although the global η is low enough, one may wish to exclude such singular points from the region treated by adaptive meshing. Another common example of a singular point is the location where a concentrated load is applied.

With the p method of refinement, in which d.o.f. are added to existing elements, procedures of error estimation and mesh revision are not as simple as with the h method. Calculation of energy error norms may rely on the estimated effect of adding one or more d.o.f. References include [4.4,9.34,9.45].

Remarks. What mesh is appropriate if the structure must be analyzed for more than one set of loads? The foregoing mesh revision strategies produce a different mesh for each different load case. It would be less time consuming for both analyst and computer if a single mesh revision constituted an improvement for all load cases. A possible strategy is to estimate appropriate element sizes for each load case separately, using, for example, Eq. 9.11-3, then generate a new mesh in which element size at every location is the smallest of the several estimates.

Mesh refinement is not merely filling a defined region with more elements. When elements and nodes are added along a curved boundary, the curve of the mathematical model should be matched, not the crude approximation of it that may be represented by a coarse mesh of straight-sided elements. And, in any part of the FE model, a revised mesh must have elements that are satisfactorily shaped and graded, lest the new mesh be worse than the old despite having more d.o.f. If the initial mesh is based on simplified geometry, such as ignoring the curves of fillets, adaptive meshing may produce convergence toward incorrect results.

We have not discussed how an improved mesh is to be generated. Mesh generation has become a technical specialty, with many techniques proposed and a substantial literature, of which [9.46,9.47] is a very small sampling. Available software can accept input regarding required element sizes in various parts of the FE model, and produce a graded mesh that satisfies the requirements of Eq. 9.11-3. However, a computer-generated mesh may not be a good mesh. It may contain many badly shaped elements. Such a mesh can be manually improved prior to analysis, unless adaptive meshing is automated, in which case one trusts that computer-generated meshes are adequate.

Software having automatic adaptive capability does much to reduce the labor of preparing meshes and altering them to make the next analysis more accurate. However, by seeming to guarantee an accurate result, adaptive capability may promote careless mistakes such as applying the wrong loads or prescribing the wrong boundary conditions. There is no benefit in iteratively improving a solution to the wrong problem. Error estimation does not relieve the analyst of responsibility for defining the problem properly and critically examining computed results.

ANALYTICAL PROBLEMS

9.2-1 Consider the equations $x + y = 2$ and $x + 1.01y = 2.01$. Obtain the solution of these equations. Then alter the second equation, first to (a) $x + 1.02y = 2.01$, then to (b) $x + 1.01y = 2.02$. Obtain the solution in each case, thus illustrating sensitivity of the equation set to small changes in (a) the coefficient matrix, and (b) the vector of constants.

9.2-2 In Eq. 9.2-3, determine the reduced coefficient K_{22} produced by applying one step of Gauss elimination so as to eliminate u_1. Show that the result suggests that numerical error is likely if α is large.

9.2-3 The sketch shows a two-element model of a uniform plane beam. The beam is fixed at the left end and simply supported at the right end. Show that global equations become ill-conditioned if scalar multiplier α becomes small.

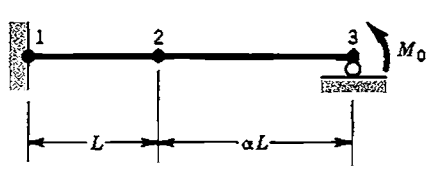

Problem 9.2-3

9.2-4 The left end of the uniform plane beam shown rests on a soft spring of stiffness k. Rotation is prevented at the left end. Adopt a one-element model, and as nodal d.o.f. use lateral deflections w_1 and w_2 and rotation θ_2 (θ_1, at the left end, is suppressed).
(a) Solve for nodal d.o.f. due to load P. Show that the equations become ill-conditioned if $k << EI/L^3$.
(b) For the four-d.o.f. beam element before the condition $\theta_1 = 0$ is imposed, adopt d.o.f. w_1, θ_1, w_{21} and θ_{21}, where w_{21} and θ_{21} are the "relative" d.o.f. $w_{21} = w_2 - (w_1 + L\theta_1)$ and $\theta_{21} = \theta_2 - \theta_1$. Then impose the condition $\theta_1 = 0$, include the soft spring and load P, and solve for nodal d.o.f. Are these equations ill-conditioned if $k << EI/L^3$?

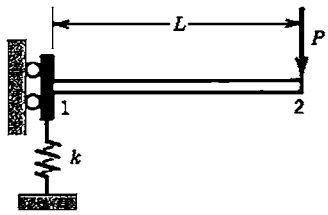

Problem 9.2-4

9.3-1 (a) Let $k_1 = 10k_2$ in Fig. 9.2-1. Determine condition numbers of the unscaled matrix [**K**] and the scaled matrix [$\mathbf{K}_s$].
(b) Repeat part (a), now with $k_2 = 10k_1$.

9.3-2 (a) The system shown has nodal d.o.f. u_1 and u_2 and springs of stiffnesses k and ck. For what value of scalar c is the condition number of the unscaled stiffness matrix a minimum, and what is this minimum value?
(b) Repeat part (a), using the scaled stiffness matrix.

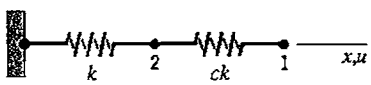

Problem 9.3-2

9.3-3 Let $\beta = 45°$ in Fig. 9.2-3a. Determine $C(\mathbf{K})$ in terms of α using (a) the unscaled matrix [**K**], and (b) the scaled matrix [$\mathbf{K}_s$].

9.3-4 A uniform plane beam is modeled by a single beam element. What is the condition number of the scaled stiffness matrix if the beam is (a) simply supported, and (b) cantilevered? (There are two nonzero d.o.f. in each case.)

9.4-1 (a) Write [**K**] for the structure shown, in which each spring has stiffness $k = 100$. Nodal d.o.f. are axial displacements u_i. By examination of the first few steps of a Gauss elimination solution for u_{101}, deduce an expression for the reduced diagonal coefficient P_{ii} of Eq. 9.4-1 in terms of k and i. Hence, what are the diagonal decay ratios after the 99th and 100th eliminations?
(b) Repeat part (a), but now number nodes from right to left, so that node 1 carries load P.

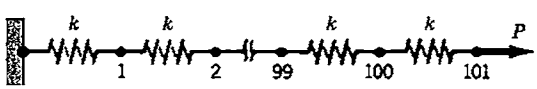

Problem 9.4-1

9.4-2 In each part of this problem, imagine that the analyst has forgotten to specify any displacement boundary conditions, so that the structure is unsupported. In what equation (first, second, ..., last) of the system $[\mathbf{K}]\{\mathbf{D}\} = \{\mathbf{R}\}$ will the diagonal decay test detect trouble?

(a) Springs in series, as in Problem 9.4-1.
(b) The plane beams of Table 9.4-1.
(c) A plane frame having the usual three d.o.f. per node.
(d) A solid of revolution (two d.o.f. at each node; radial and axial translations).
(e) A plane structure (two d.o.f. at each node; x- and y-direction translations).

9.4-3 Determine the diagonal decay ratio in terms of α and the sine and cosine of β for the problem described by Fig. 9.2-3a. Show that the ratio is not large if $\beta = 0$ or if $\beta = \pi/2$.

9.4-4 With unit axial loads at nodes 2 and 3 of the structure shown, the exact structure equations are $8006.6u_2 - 8000.0u_3 = 1$ and $-8000.0u_2 + 8000.0u_3 = 1$. Determine u_2 and u_3 to eight decimal places. Then calculate approximate values of these d.o.f. under the assumption that a hypothetical computer rounds numbers to four digits after each operation of Gauss elimination. Does the accuracy loss agree with that predicted by (a) the diagonal decay ratio, and (b) the condition number of the (scaled) stiffness matrix?

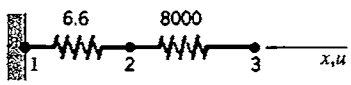

Problem 9.4-4

9.5-1 Consider the two equations $1.78u_1 + 1.06u_2 = 2.88$ and $0.94u_1 + 0.56u_2 = 1.52$. What is the exact solution? Are the equations ill-conditioned? What residual vector $\{\Delta\mathbf{R}\}$ is given by the approximate solution $u_1 = 1.88$, $u_2 = -0.44$, and what is e of Eq. 9.5-2? Are residual tests useful in this example?

9.5-2 Consider the ill-conditioned equations $u_1 + u_2 = 2$, $u_1 + 1.0001u_2 = 2.0001$. What residual vector $\{\Delta\mathbf{R}\}$ and what e are given by the approximate solution $u_1 = 2$, $u_2 = 0$, and by the approximate solution $u_1 = u_2 = 1.1$? Which of the two approximate solutions is more nearly correct?

9.5-3 Imagine that a single linear spring of stiffness $k = 28$ N/m is loaded by a force of 0.5 N. Using the approximate value $k^{-1} \approx 0.040$ m/N, we compute the approximate displacement $u \approx 0.020$ m. Improve this result by using the iterative method of Eq. 9.5-3, using the correct k and the approximate k^{-1}.

9.5-4 Consider the two equations $(u_1/3) - (u_2/3) = 1$, $-(u_1/3) + (7u_2/12) = 0$. Let the coefficient matrix and its inverse be approximated as

$$[\mathbf{K}] \approx \begin{bmatrix} 0.3 & -0.3 \\ -0.3 & 0.5 \end{bmatrix} \quad \text{and} \quad [\mathbf{K}]^{-1} \approx \begin{bmatrix} 8.0 & 5.0 \\ 5.0 & 5.0 \end{bmatrix}$$

(a) Using the approximate matrices, apply three cycles of iteration according to Eqs. 9.5-3. Do calculated values of u_1 and u_2 appear to be converging to correct results?
(b) Again apply three cycles of iteration, now using the approximate $[\mathbf{K}]^{-1}$ but the *correct* $[\mathbf{K}]$ in Eqs. 9.5-3. Assess the results.

9.6-1 Consider a one-dimensional element of length h whose nodal d.o.f. are u_i and $u_i' = (du/dx)_i$ at nodes $i = 1$ and $i = 2$. At $x = h/2$, using shape functions in Fig. 3.2-4, we obtain $u = \frac{1}{2}(u_1 + u_2) + \frac{h}{8}(u_1' + u_2')$. Expand u_1, u_2, u_1', and u_2' as series to show that $u + e = u + O(h^4)$, and determine the exact form of the error term $e = O(h^4)$.

9.7-1 Recompute the six "extrapolated results" in Table 9.7-1, this time using $q = 1$ in Eq. 9.7-1.

9.7-2 Verify that $\sigma_{\max} = 93.3$ is the value predicted at $N_{\text{els}} = \infty$ in Fig. 9.7-4 by linear regression (least squares fit of a straight line to the data points).

9.7-3 What value of $\sigma_{\max}$ is predicted by linear extrapolation in Fig. 9.7-4? Use Eq. 9.7-1 with $q = 1$ and all three possible combinations of the three data points (two of them for each extrapolation). What is the average of all three $\sigma_{\max}$ values?

9.7-4 Imagine that for plane meshes having $N_{\text{els}} = 100$, 200, and 400 elements, computed values of displacement at a certain point are respectively 4.16, 4.64, and 4.76 units. What displacement is predicted by extrapolation to zero element size?

9.7-5 Use Eq. 9.7-1, with a value of q appropriate to the quantity to be extrapolated, to predict converged values of displacement and/or stress reported in the following example problems.
(a) Constant-strain triangle results in Fig. 3.5-2.
(b) "CST" results in Fig. 3.10-2.
(c) "Ref. 3.9" results in Fig. 3.10-2.
(d) "QM6" results in Fig. 6.6-1.
(e) "Q4" results in Fig. 6.6-1.

9.7-6 Imagine that the problem of Fig. 9.7-4 is solved twice, using nine-node plane elements each time. Mesh 2 is created by regular refinement of mesh 1, quadrupling the number of elements. For the respective meshes, computed values of lateral tip displacement and maximum stress are

Mesh 1	$v = 0.0035$	$\sigma_{\max} = 74.23$
Mesh 2	$v = 0.0041$	$\sigma_{\max} = 89.03$

Use these data to estimate the percentage error of v and $\sigma_{\max}$ in mesh 2.

9.7-7 In Table 6.14-1, use multimesh extrapolation to estimate the percentage error of the maximum normal stress in the finer mesh. Do the meshes used constitute regular refinements? If not, devise a suitable measure of h.

9.7-8 Imagine that eight-node brick elements having only translational d.o.f. at nodes are used to analyze a 3D elasticity problem. Three meshes are used, with results as follows for displacement at a certain point.

Mesh 1	2014 d.o.f.	1.10 mm
Mesh 2	3342 d.o.f.	1.17 mm
Mesh 3	4560 d.o.f.	1.20 mm

(a) Do these meshes seem to constitute regular mesh refinements? Why or why not?
(b) Use the data to graphically estimate the rate of convergence. Is this rate consistent with the type of element used?
(c) Use multimesh extrapolation to estimate the percentage error in the finest mesh.

9.9-1 (a) Show that minimization of F_G in Eq. 9.9-4 leads to the second of Eqs. 9.9-5.
(b) Show that minimization of F_P in Eq. 9.9-8 leads to Eq. 9.9-9.

9.9-2 (a) The sketch shows two linear elements, 1-2 and 2-3. Gauss points of an order 1 rule in each element are lettered. A smoothed stress field, $\sigma_x^* = a_0 + a_1 x$, is to be obtained by use of Eq. 9.9-9. Establish matrix [**A**] and constant vector {**b**}. Let $\sigma_{xA} = 1$ and $\sigma_{xB} = 3$.
(b) What value of σ_x^* at $x = L$ is predicted by the calculations of part (a)?

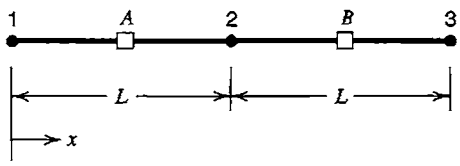

Problem 9.9-2

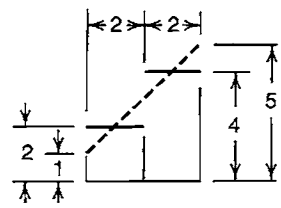

Problem 9.10-1

9.10-1 Imagine that the sketch represents stresses along two bar elements, each of length $L = 2$, unit cross-sectional area, and the same elastic modulus. The elements lie within an FE model of several bar elements. Solid horizontal lines represent axial stresses $\sigma_i = E(u_{i+1} - u_i)/L_i$ in individual elements. The inclined dashed line represents axial stress computed from nodal average stresses. For these two elements, use Eqs. 9.10-1, 9.10-2, and 9.10-7 to calculate $\|U\|^2, \|e\|^2$, and η. Is $\|U\|^2 + \|e\|^2$ equal to $\|U^*\|^2$ of the average stress field?

9.10-2 A straight uniform bar extends from $x = 0$ to $x = 4$. For each of the following FE meshes, linear (two-node) bar elements are used. Axial displacements u_i at nodes lie on the curve $u = 2x - 0.1x^3$. Determine the exact energy norm, then from the FE model determine $\|U\|, \|e\|, \|U\|^2 + \|e\|^2$, and η. For simplicity, assume that A and E are both unity, and determine the smoothed gradient field from nodal averages (as in Fig. 9.9-2a).
(a) Use two elements, each of length 2.
(b) Use four elements, each of length 1.
(c) What convergence rate of axial stress is suggested by the change in $\|e\|$ from part (a) to part (b)?

9.10-3 In parts (a) and (b) of Problem 9.10-2, determine $\|U^*\|$, the energy norm of the smoothed stress field constructed from nodal average stresses. What is the reason for the discrepancy between $\|U^*\|^2$ and $\|U\|^2 + \|e\|^2$?

COMPUTATIONAL PROBLEMS

Use the adaptive meshing capability of software to seek quite accurate results to some problems. Candidate applications in preceding chapters include those of Figs. 3.10-2, 3.14-1, 3.15-1, 6.14-1, and 6.15-1. If all elements of a mesh are allowed to contribute to the error estimate, what is the observed effect of singularities on the computational process?

CHAPTER 10

MODELING CONSIDERATIONS AND SOFTWARE USE

10.1 INTRODUCTION

Overview. In this chapter we discuss representing a physical problem by an FE model, choosing elements and analysis options that are suitable, finding and correcting errors, and interpreting results. It is emphasized that satisfactory analysis requires a physical grasp of the problem to be solved, care in planning and execution, and willingness to check for inadequacies and revise as necessary.

Some material pertinent to this chapter is summarized in Chapter 1, Sections 1.2 and 1.5, which the reader should review. Other pertinent material in preceding chapters will be cited as appropriate. Modeling for problems of vibration, dynamic response, nonlinearity, and buckling is discussed in subsequent chapters.

Advice in the present chapter does not fall neatly into categories, so its arrangement by sections is somewhat arbitrary. The sections and their contents should not be regarded as checklists to be followed by rote in every problem. If a list of modeling rules were prepared, each rule might have an exception that could be exploited to advantage in particular situations by a skillful analyst. Modeling advice should be regarded more as concepts than as rules. Ideally, the reader has access to FEA software, and performs numerical experiments to test the advice and develop the ability to apply it in a variety of situations.

Remarks. For analytical or numerical solutions, an early step is the simulation of physical reality by a mathematical model, as defined in Section 1.2. Thus we create an abstraction intended to represent essential features of the physical problem. Fine detail actually present may be ignored. Typically ignored are such things as detail in connections and small geometric irregularities. However, detail is important if the connection itself is to be studied, and small irregularities can have a large influence on the behavior of thin-walled structures such as panels and shells. Thus we see that a list of modeling rules cannot suit all situations, and that physical understanding is essential. The devising of a mathematical model need not imply a particular method of solution, but familiarity with available tools (such as FEA) may influence the amount of detail included and the kind of answers sought.

Preparation of an adequate model requires a grasp of the problem area, be it stress analysis, heat transfer, magnetic fields, and so on. Skill in one area does not confer skill in another, either in creating the model, in converting it to an FE representation, or in checking computed results. In any discipline, the necessary knowledge base includes basic theory and the essentials of classical analysis tools, because their assumptions *and restrictions* are incorporated in FEA software. As a simple example, in classical beam theory, stress calculation requires homogeneous material and deflection calculation requires small deflections. The same restrictions apply to standard beam elements. Knowing the

limitations of theory and analysis tools makes it less likely that software will be pushed beyond its range of applicability. It is entirely possible for an unprepared software user to misunderstand the problem, prepare the wrong mathematical model, discretize it inappropriately, fail to check computed output, and yet accept nonsensical results that appear in beguiling graphical display.

In short, we advise that physical understanding of the problem and the essentials of its theory, combined with planning, careful work, and the patience to search for errors at all stages, are skills at least as important to a satisfactory outcome as familiarity with FE theory. FEA is a solution technique that removes many limitations of classical solution techniques, but FEA does not bypass the underlying theory or the need to devise a satisfactory model, and in addition requires some familiarity with element capabilities and limitations and with possible pitfalls of numerical analysis on a computer. Posing the wrong questions and modeling a problem other than the problem intended are defects that cannot be cured by refinement of an FE mesh.

We suggest that it is more productive to begin with a plan, which can be modified as more is learned during the course of the project, than to plunge headlong, hoping that the bother of planning can be avoided. Essential components of planning include deciding what results are required and how computed results will be checked. There is a natural tendency to accept computed results merely because considerable effort is required to obtain them. To counter this tendency, approximate results should be in hand *before* doing FEA. The thought needed to obtain approximate results will improve analysis skills and will also produce a better model.

We repeat our suggestion that the reader review Sections 1.2 and 1.5.

10.2 PHYSICAL BEHAVIOR VERSUS ELEMENT BEHAVIOR

What general sorts of elements should be used—beam, plane, shell, or solid? If plane, should elements be triangular or quadrilateral? With or without side nodes? How many elements, and how should the mesh be graded? Such questions arise as we begin to discretize the mathematical model. To answer these types of questions, we must understand how the structure (or its mathematical model) is *likely* to behave and how elements are *able* to behave. We must recall that the essence of the FE method is *piecewise polynomial interpolation.* An element can represent a field variation no more complicated than the interpolation contained in its formulation. Therefore, in structural mechanics we rarely use basic three-node triangles and four-node tetrahedra because they cannot represent the linear variations of strain so often encountered in stress analysis, and because these elements suffer from shear locking (described in Section 3.6). Shortcomings of these element types are of much less concern in a scalar field problem such as heat conduction, where greatest interest may be in the field itself rather than its gradients, and there is no difficulty analogous to shear locking.

Thin-Walled Construction. A typical first course in stress analysis treats deformation and stress in straight members subjected to stretching, bending, and twisting, with a circular cross section required for analysis of twisting. An analyst with only this background may be unaware that thin-walled members often have additional deformation modes, which may produce the largest stresses. The additional modes cannot be represented by standard beam elements.

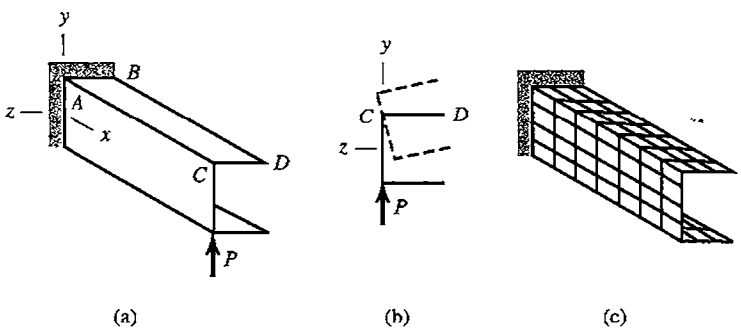

Figure 10.2-1. (a) Thin-walled channel loaded by transverse tip force P in the plane of the web. (b) Deflection of the tip cross section is shown by dashed lines. (c) FE model of the beam, built of shell elements.

The cantilever beam of Fig. 10.2-1 is a case in point. A typical cross section has a *shear center,* located in the xz plane and having a positive z coordinate, through which transverse load must be directed if the beam is to bend without twisting [1.16,2.6]. With load P located as shown, the beam twists as well as bends, and cross sections warp as predicted by Saint-Venant torsion theory. The fixed support prevents warping at $x = 0$. Restraint of warping reduces the amount of twisting and introduces normal stresses not predicted by elementary beam theory or by elementary torsion theory. For pure torque loading, these normal stresses can be larger than the torsional shear stresses. For the problem of Fig. 10.2-1a, a standard beam element, Eq. 2.3-8, is not capable of providing either the correct torsional stiffness or the correct stresses. Instead the beam must be modeled in the manner shown by Fig. 10.2-1c, where individual elements display both membrane and bending stiffness.

Even if load P is directed through the shear center so that the beam does not twist, a thin-walled open cross section with wide flanges displays a shear lag effect [1.16]. That is, in Fig. 10.2-1, shear stress τ_{zx} in very wide flanges produces x-direction deformation such that plane cross sections do not remain plane when the beam is bent by transverse load. Again the standard beam element is not capable of representing this effect, and again an FE model such as that in Fig. 10.2-1c is appropriate.

Examples of thin-walled curved beams appear in Fig. 10.2-2. With moment M directed as shown, circumferential stresses σ_θ are tensile on the side closest to the center of curvature and compressive on the side farthest away. On a typical slice spanned by arc $d\theta$,

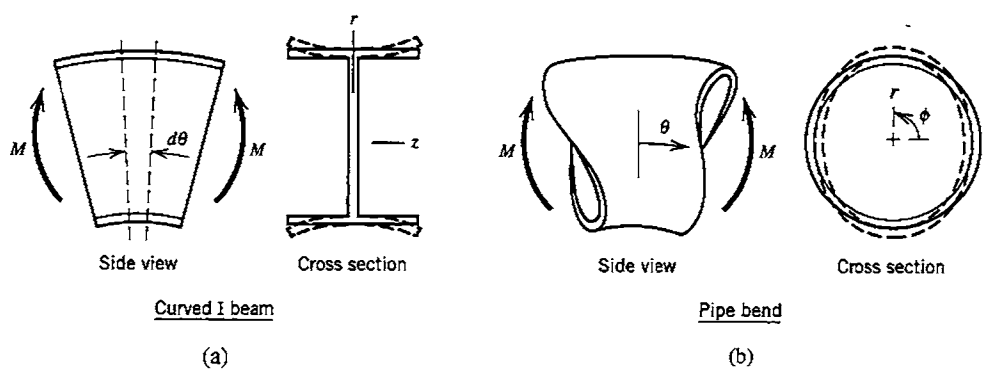

Figure 10.2-2. Thin-walled curved beams bent in the planes of their curved axes by moments M. Dashed lines show deformations in the plane of a cross section.

Fig. 10.2-2a, forces produced by σ_θ have radial components, directed outward on the outer flange and inward on the inner flange for the direction of M shown. These radial components produce the "flapping" deformation of flanges indicated by dashed lines, which reduces the stiffness seen by moments load M and produces z-direction stress σ_z that may be larger than circumferential stress σ_θ [1.16,2.6]. Deformations and signs of stresses are reversed if the direction of M is reversed. Ordinary beam elements, even if formulated as initially curved, do not account for these actions. An FE model similar to that in Fig. 10.2-1c is appropriate.

The physical action in Fig. 10.2-2b is similar to that in Fig. 10.2-2a. Deformation in the $r\phi$ plane is called *ovalization* [10.1]. Again an FE model analogous to that in Fig. 10.2-1c can be used, but the problem is frequently encountered in the analysis of piping networks, so commercial software is likely to include a special pipe-bend element that accounts for ovalization.

A shell carries load by a combination of bending action and membrane action. Figure 10.2-3 shows an axisymmetric problem of a thin-walled shell. Support reactions M_0 and V_0 are uniformly distributed around the circular base. Near the base, axial flexural stress σ_x is large but highly localized, so that it has steep gradients. Standard cylindrical shell elements are quite capable of modeling the problem properly, but an unprepared software user may not realize how localized the flexural stresses are, and consequently may use a mesh so coarse that flexural stresses appear negligible. High local flexural stress is to be expected in thin shells at or very near line loads, supports, reinforcements, or changes in curvature (such as the juncture between a cylindrical shell and an ellipsoidal end cap). An analyst must learn enough about shell behavior to be able to anticipate where flexural stresses may be large and localized [1.16,2.6,10.2].

Behavior of a thin-walled structure may be strongly influenced by imperfections in geometry or misalignment in connections. Imperfections are often introduced during manufacture or assembly, and may be overlooked in analysis because they are small and their type, magnitude, and location can at best only be estimated in advance of construction. Yet their presence may greatly reduce load-carrying capacity. Unfortunately, they usually make response nonlinear, so that analysis becomes much more difficult.

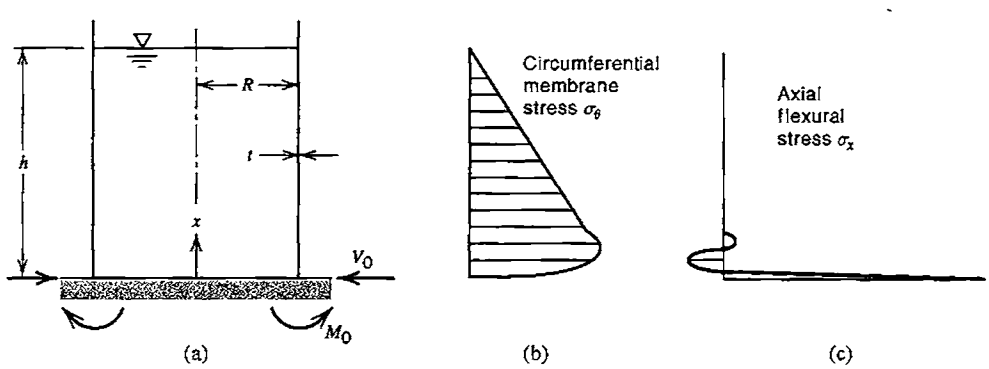

Figure 10.2-3. (a) Thin-walled cylindrical tank filled with liquid to depth h. (b) Circumferential membrane stress. (c) Axial flexural stress.

Nonlinearity. The term "nonlinearity" means that response is not directly proportional to the action that produces it. In reality, nonlinearity is always present. We are fortunate that nonlinear effects are small enough that they can be ignored in many common problems. When nonlinearity is important, software does not automatically detect that it should be taken into account and proceed to do the appropriate analysis. At present, the analyst must recognize that nonlinearity may be important, activate nonlinear analysis, supply whatever additional data may be needed to accomplish it, and usually supply guidance at various stages of solution, because various nonlinear procedures can be invoked and intelligent choices are needed. In nonlinear analysis, a single solution of the usual equations $[\mathbf{K}]\{\mathbf{D}\} = \{\mathbf{R}\}$ is inadequate because $[\mathbf{K}]$ and/or $\{\mathbf{R}\}$ are functions of $\{\mathbf{D}\}$. A sequence of analyses is required, in which $[\mathbf{K}]$ and/or $\{\mathbf{R}\}$ are updated after each analysis.

In structural mechanics, nonlinearity is usually classified as *material* or *geometric*. The two types may appear in combination. *Material nonlinearity* includes yielding. When bending is present, yielding begins at a surface and propagates toward the neutral axis of bending and the thickness-direction distribution of stress is not a straight line. Therefore, an element formulation that provides the correct resistance to bending must incorporate an appropriate thickness-direction integration scheme. An example of *geometric nonlinearity* is a thin flat disk, clamped around its circular boundary, and loaded by lateral pressure. If lateral deflection at the center is more than about half the thickness, the disk develops membrane stretching forces that carry a considerable portion of the load [1.16,2.6,10.2]. In order to double the deflection, the load must more than double. An FE model built of plate elements that resist only bending deformation can provide only a linear solution, which will overestimate the actual deflection. *Contact nonlinearity* is a type of geometric nonlinearity in which deformable bodies are pressed together or a gap may open or close.

In heat conduction, material properties such as thermal conductivity may be sufficiently temperature-dependent that nonlinear analysis is required. In electromagnetic problems, there may be a nonlinear relationship between magnetic flux and magnetic field, or between electric flux and electric field. In fluid mechanics, a convective term is nonlinearly related to velocity. The variety of possible nonlinearities in FEA is so large that a single solution procedure does not work well for all problems. In most nonlinear problems the solution process is likely to require guidance from the analyst.

10.3 ELEMENT SHAPES AND INTERCONNECTION

Element Shapes. Elements that satisfactorily portray geometry may not serve well in FEA because they are badly shaped for analytical purposes. Computed FE results tend to be most accurate when elements are compact, without great elongation, skew, or warping. Distortions such as those shown in Fig. 10.3-1 usually degrade accuracy. The amount of degradation caused by a given distortion varies with element type, mesh arrangement, and physical problem. *Combinations* of these distortions may be especially detrimental. Distortion usually degrades field gradients such as stresses more than it degrades displacements, natural frequencies, mode shapes, or temperatures. Distorted plane and solid elements can display a constant field and a linearly varying field, but have less ability to represent more complicated variations. Elements are usually less sensitive to shape distortion if they have side (or edge) nodes in addition to corner nodes. Elements that have one or more internal d.o.f. are also less sensitive. Examples that show some of these effects numerically appear in Section 6.11. Numerical examples for plate problems appear in [10.3].

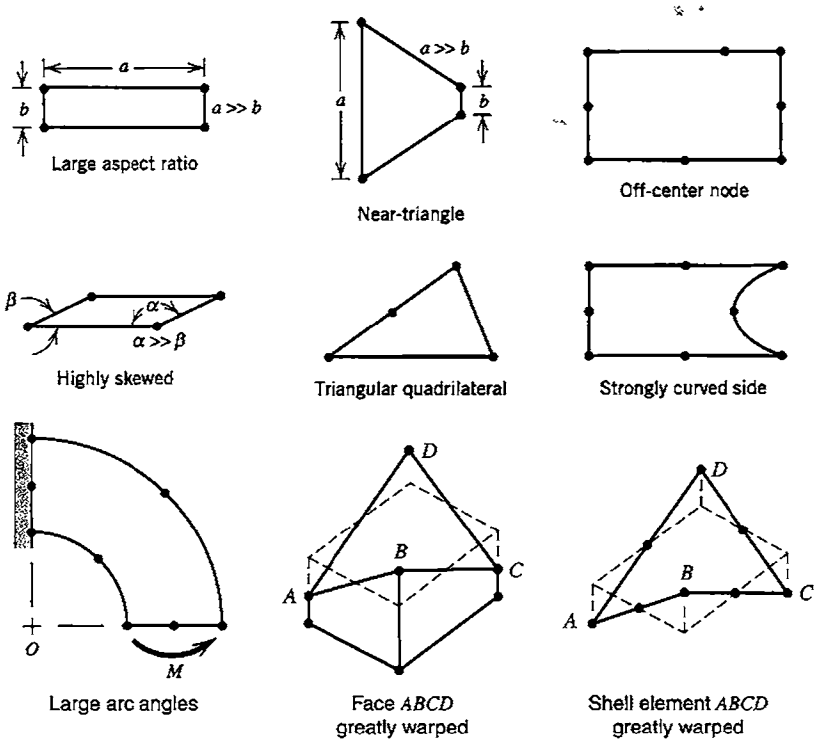

Figure 10.3-1. Element shape distortions that usually reduce accuracy.

Deliberate geometric distortion can be beneficial if used with understanding and care. Quarter-point elements are suited to fracture mechanics (Section 8.7). Elements having side nodes can better fit a curved boundary than elements having only corner nodes. In Fig. 10.3-1, a single quadratic element is used to model a quarter-circle curved beam loaded by moment M. Usually it is unwise to use curved sides that span a 90° arc, but computed results for this particular problem have surprising accuracy [10.3]. The reason is that the isoparametric transformation produces a singularity at the center of curvature O, which is exactly where stress analysis theory predicts infinite stress. However, note that curved edges of this element are parabolas, not the circular arcs intended.

In three dimensions, making a surface or element warped rather than flat is likely to decrease accuracy. Warping may be necessary to model shell geometry, but can seriously degrade results if the shell is thin. Also, in modeling a shell of revolution, the meridional arc spanned by a shell element should subtend an angle no greater than roughly 12°. A similar recommendation can be made for the arc spanned by a general shell element. A more specific numerical recommendation would not be suited to all element formulations or all modeling situations.

Abrupt changes in element size should be avoided (Fig. 10.3-2). Even if element aspect ratios are satisfactory in the "poor" arrangement, a disturbance appears in the gradient field in

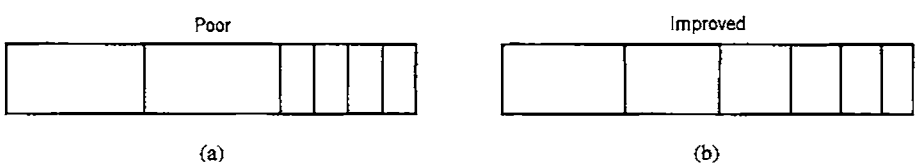

Figure 10.3-2. Changes in element size are (a) too abrupt and (b) much improved.

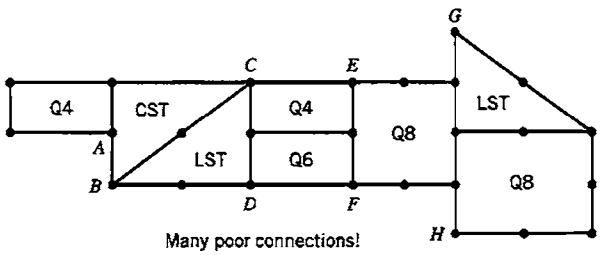

Figure 10.3-3. Examples of how *not* to connect elements (same as Fig. 3.12-3).

the neighborhood of an abrupt element size change. Changes in element type (such as triangular to quadrilateral), abrupt changes in element size, poorly shaped elements, and inappropriate element connections (Fig. 10.3-3) all may produce artificial disturbances in the gradient field that may mistakenly be accepted as physically realistic. The 2D examples shown in Fig. 10.3-3 have counterparts in 3D. Particular care should be taken to avoid such defects in regions where gradients are large and where accuracy is important. Great experience is not needed to identify a mesh that "looks bad" in some way. If a mesh looks bad, it is probably deficient.

Commercial software includes tests of element shape and element connections, and warns the user of situations considered questionable or unacceptable (see Section 10.14). Of course, the user cannot assume that such checks are infallible.

Figure 10.3-4a depicts a corner in a plane structure. A beam-element model does not capture details of stress distribution at the corner. If these details are important, one way to study them is by *submodeling* (Section 10.10).

10.4 TEST CASES AND PILOT STUDIES

All valid elements pass patch tests (Section 6.13). Beyond this, we would like to know how well specific element types perform in solving real problems. We would like assurance that potential defects—such as locking, high sensitivity to shape distortion, spurious modes, or even nonconvergence—are not present, regardless of the problem to which the element is applied. Elements that do well are called *robust,* meaning that they are not only free of fatal defects, but are also relatively insensitive to small changes unrelated to the physical problem, such as changes in element geometry, how loads are applied (such as by omitting the nodal moment component of consistent nodal loading), and Poisson's ratio ν (in a problem that should be independent of ν).

Test cases are often used in FE research papers. In presenting new formulations, authors tend to use test cases already used by other authors. In this way a set of test cases has arisen by default. These cases have been criticized as reporting few if any bad results, perhaps because authors correct only those troubles they happen to find, and because not enough different conditions are tested [6.26].

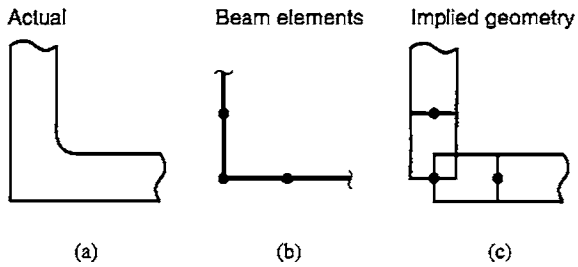

Figure 10.3-4. Modeling of a corner in a plane structure.

A good set of test cases exercises all behaviors an element purports to model. A set of test cases was proposed in 1985 [6.26]. Each test case was solved using various element formulations, each appropriate for the problem at hand (plane stress, or plate bending, etc.). FE results for a typical test case range from poor to good, depending on element formulation. In comparing test-case results provided by different software packages, one may find that superficially identical elements, such as four-node plane quadrilaterals, behave differently due to differences in basic formulation or different choices of add-on features intended to improve performance.

Another effort to establish a rational set of test cases has been undertaken by NAFEMS (National Agency for Finite Elements Methods and Standards). Aims of the organization include setting FE standards and testing procedures, and coordinating the evaluation of FE software. The numerous NAFEMS test cases are called *benchmarks* and have the following characteristics: each uses a single element type; data preparation is straightforward; geometry, loading, and boundary conditions are unambiguous; and each case has a single well-defined result (such as deflection at a single point, or a set of vibration frequencies) known from classical analysis or perhaps from *soundly justified* computation [10.4]. Commercial software packages can be compared by applying them to a benchmark. Such comparisons have occasionally appeared in NAFEMS publications.

Vendors of commercial software maintain extensive sets of test cases. They are used to verify a new version of the software by making sure it can solve all the test cases, and solve them at least as well as the preceding version. New cases may be added as part of an effort to isolate and fix a defect reported by users. Users may wish to examine the vendor's manual of test cases, both to understand element performance and to learn how to use the software. Patch tests and single-element tests, described in Sections 6.13 and 8.10, can also be useful in learning how to use software.

As a direct way to answer questions about element performance, the analyst can devise and run simple test cases, exploring such things as convergence rate with mesh refinement, the effects of element shape distortion, and mesh arrangement. For example, consider the square region shown in Fig. 10.4-1. The physical problem does not concern us here. The first two meshes are part of a series of subdivisions from which convergence rate can be determined. Mesh (c) will show some effects of distorting mesh (a). Meshes (a), (d), and (e) each have eight elements, each a 90° isosceles triangle, but in different arrangements. Results from (d) will not display symmetry about horizontal and vertical centerlines, even if demanded by the physical problem. If all d.o.f. are suppressed on the square boundary, the four corner elements in (e) are completely inactive, effectively reducing the FE model to a smaller and differently oriented four-element square.

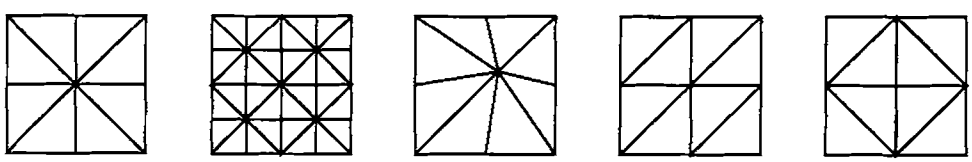

(a) (b) (c) (d) (e)

Figure 10.4-1. Coarse meshes in a square region. The meshes might be used in studies of convergence rate, mesh distortion, and mesh arrangement.

Computed results can be influenced by the interaction of mesh layout and how the load vector is calculated. Imagine that there is uniformly distributed load in Fig. 10.4-1, and that one-third of the total force F on a triangle is allocated to each of its vertices. Then, after assembly of elements, net loads applied to central nodes in Fig. 10.4-1 are $8F/3$ in part (a), $6F/3$ in part (d), and $4F/3$ in part (e).

Pilot Studies. A *pilot study* is a simplified analysis of a more complicated problem, performed with a simplified model and perhaps with limited analysis goals. Software capabilities required in the full-blown analysis can be tested. One might even insert intentional errors, to see if software error traps will detect them [2.21]. The benefit of a pilot study is the reduction of effort associated with less input data to prepare, while still providing a way to preview structural behavior, test-model idealizations such as joints and boundary conditions, detect blunders such as incorrect units for input data, and provide insight into what computational options may be appropriate. There is also less output to examine, so the analyst can better plan what output to request from the full-scale analysis and can answer questions as to its meaning (for example, are stresses presented in global or local coordinates, and if the latter, in what local system?). Pilot studies are particularly appropriate with dynamic or nonlinear problems, where response may be hard to foresee and there are many computational options.

Pilot studies and simple test cases are strongly recommended as a way to answer "what if" questions about modeling, or to test the software and discover if it behaves as expected. Sometimes software is directed into computational paths not anticipated by its developers, and a satisfactory outcome is in doubt. Pilot studies can test software efficiency, accuracy, and ease of use. One is likely to see some behavior at odds with expectations, and perhaps at odds with descriptions in the documentation.

10.5 MATERIAL PROPERTIES

Material data for isotropic materials is comparatively easy to obtain and easy to convey to the software. Data for anisotropic materials is more difficult on both counts. Consider, for example, the stress-strain-temperature relations for an orthotropic material, with principal directions x, y, and z.

$$\begin{aligned}
\varepsilon_x &= +\frac{1}{E_x}\sigma_x - \frac{\nu_{yx}}{E_y}\sigma_y - \frac{\nu_{zx}}{E_z}\sigma_z + \alpha_x T & \gamma_{xy} &= \frac{\tau_{xy}}{G_{xy}} \\
\varepsilon_y &= -\frac{\nu_{xy}}{E_x}\sigma_x + \frac{1}{E_y}\sigma_y - \frac{\nu_{zy}}{E_z}\sigma_z + \alpha_y T & \gamma_{yz} &= \frac{\tau_{yz}}{G_{yz}} \\
\varepsilon_z &= -\frac{\nu_{xz}}{E_x}\sigma_x - \frac{\nu_{yz}}{E_y}\sigma_y + \frac{1}{E_z}\sigma_z + \alpha_z T & \gamma_{zx} &= \frac{\tau_{zx}}{G_{zx}}
\end{aligned} \tag{10.5-1}$$

Not all material constants in Eqs. 10.5-1 are independent. Maxwell's reciprocal theorem shows that the matrix of constants must be symmetric. Therefore,

$$E_x\nu_{yx} = E_y\nu_{xy} \qquad E_y\nu_{zy} = E_z\nu_{yz} \qquad E_z\nu_{xz} = E_x\nu_{zx} \tag{10.5-2}$$

Thus Eqs. 10.5-1 contain nine independent elastic constants and three independent coefficients of thermal expansion (assumed temperature-independent in Eqs. 10.5-1). A general anisotropic material has 21 independent elastic constants. It may not be easy to obtain numerical values for all needed constants, or to state them properly as input data, not mixing them up, and with attention to principal directions of an orthotropic material that may be differently oriented in different parts of the structure. Nominally isotropic materials may be slightly nonlinear, and tabulated properties are typically average values. Properties may vary substantially because of changes in composition, method of manufacture, and heat treatment.

Substitute Properties. Corrugations, indentations, or perforations are often present, and can have a large effect on stiffness. If such geometric disturbances are numerous and have a regular pattern, they can be "smeared" to provide a substitute structure without these geometric disturbances but having modified elastic constants. A common example is a flat plate perforated by a regular pattern of circular holes. Substitute elastic constants depend on the size and spacing of holes, whether the hole pattern is square or triangular, and elastic constants of the actual material [10.5]. When properties needed are not tabulated, they can be calculated as now described by means of a plane-stress example [10.6,10.7].

Consider in-plane behavior of a perforated plate, Fig. 10.5-1. Isolate a typical repeating portion such as *ABCDE*, and model it by an FE mesh (not shown in Fig. 10.5-1). Let there be three different displacement states of the FE model, $i = 1$, 2, and 3, with each state i described by a set of d.o.f. $\{\mathbf{D}\}_i$ associated with a particular state of constant strain in the *substitute* plate (which has no holes). In what follows, we elect to use constant-strain states of unity. Accordingly, on boundary *ABCDE* of the FE model of the actual plate with holes, selected d.o.f. in $\{\mathbf{D}\}_i$ are prescribed as follows (see Section 2.11 for discussion of symmetry and antisymmetry conditions).

State	Strain	d.o.f.	On *AB*	On *BC*	On *CD*	On *DE*
$\{\boldsymbol{\varepsilon}\}_1$	$\varepsilon_x = 1$	$\{\mathbf{D}\}_1$	$v = 0$	$u = 0$	$v = 0$	$u = a$
$\{\boldsymbol{\varepsilon}\}_2$	$\varepsilon_y = 1$	$\{\mathbf{D}\}_2$	$v = 0$	$u = 0$	$v = b$	$u = 0$
$\{\boldsymbol{\varepsilon}\}_3$	$\gamma_{xy} = 1$	$\{\mathbf{D}\}_3$	$u = 0$	$v = 0$	$u = b$	$v = 0$

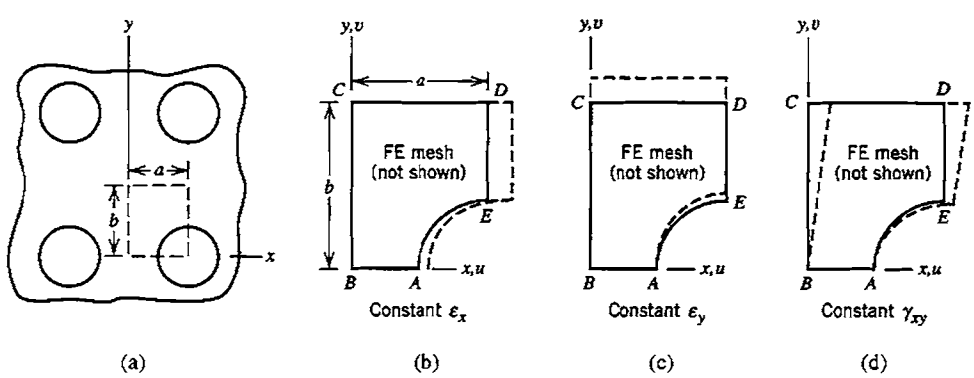

Figure 10.5-1. (a) Portion of a plate with a regular pattern of holes. (b,c,d) A typical repeating geometry, showing deformations used in computing effective elastic properties.

All d.o.f. not prescribed, whether internal to the FE mesh or on its boundary, are unrestrained. We solve the three FE problems $[\mathbf{K}]\{\mathbf{D}\}_i = \{\mathbf{R}\}_i$, $i = 1,2,3$, for d.o.f. in each $\{\mathbf{D}\}_i$ that are not prescribed and for nodal forces in each $\{\mathbf{R}\}_i$ that are associated with prescribed d.o.f. For internal d.o.f. and for boundary d.o.f. that are not prescribed, nodal forces in $\{\mathbf{R}\}_i$ are zero. Therefore, nonzero entries in $\{\mathbf{R}\}_i$ are externally applied boundary forces associated with prescribed d.o.f. For $i = 1$,

$$\{\mathbf{R}\}_1 = [\mathbf{K}]\{\mathbf{D}\}_1 \tag{10.5-3}$$

When subjected to the same boundary displacements as the actual plate, nodal forces in the substitute (unperforated) plate are

$$\{\mathbf{R}^*\}_1 = [\mathbf{K}^*]\{\mathbf{D}\}_1 \quad \text{or} \quad \{\mathbf{R}^*\}_1 = \left[\sum \int [\mathbf{B}]^T[\mathbf{E}][\mathbf{B}]\, dV\right]\{\mathbf{D}\}_1 \tag{10.5-4}$$

where $[\mathbf{K}^*]$ is the stiffness matrix of the substitute plate, symbolized in the latter equation as the sum of element stiffness matrices. Actually, $[\mathbf{K}^*]$ is not constructed; $[\mathbf{K}^*]$ and discretization of the substitute plate are introduced here only as conceptual conveniences. Also, in writing $[\mathbf{K}^*]\{\mathbf{D}\}_1$ we imagine that $\{\mathbf{D}\}_1$ contains d.o.f. on sides of an a by b rectangle of the substitute plate. In order for stiffness of the actual plate, as averaged over many holes, to be the same as stiffness of the substitute plate, we require that work done by $\{\mathbf{D}\}_1$ be the same in actual and substitute plates. Thus $\frac{1}{2}\{\mathbf{D}\}_1^T\{\mathbf{R}\}_1 = \frac{1}{2}\{\mathbf{D}\}_1^T\{\mathbf{R}^*\}_1$, and because $[\mathbf{B}]\{\mathbf{D}\}_1 = \lfloor 1 \quad 0 \quad 0 \rfloor^T \equiv \{\boldsymbol{\varepsilon}\}_1$, Eq. 10.5-4 yields

$$\{\mathbf{D}\}_1^T\{\mathbf{R}\}_1 = \sum \int \{\boldsymbol{\varepsilon}\}_1^T [\mathbf{E}]\{\boldsymbol{\varepsilon}\}_1\, dV = E_{11}V \tag{10.5-5}$$

from which $E_{11} = \{\mathbf{D}\}_1^T\{\mathbf{R}\}_1/V$, where V is the volume of the substitute plate, namely ab times thickness t in the present example. Thus we have obtained the first term in the 3 by 3 matrix $[\mathbf{E}]$ of the substitute plate. In similar fashion we write $\frac{1}{2}\{\mathbf{D}\}_2^T\{\mathbf{R}\}_1 = \frac{1}{2}\{\mathbf{D}\}_2^T\{\mathbf{R}^*\}_1$, and because $\{\mathbf{D}\}_2^T[\mathbf{B}]^T = \lfloor 0 \quad 1 \quad 0 \rfloor \equiv \{\boldsymbol{\varepsilon}\}_2^T$, Eq. 10.5-4 yields

$$\{\mathbf{D}\}_2^T\{\mathbf{R}\}_1 = \sum \int \{\boldsymbol{\varepsilon}\}_2^T [\mathbf{E}]\{\boldsymbol{\varepsilon}\}_1\, dV = E_{21}V \tag{10.5-6}$$

from which $E_{21} = \{\mathbf{D}\}_2^T\{\mathbf{R}\}_1/V$. Proceeding similarly for the remaining terms, we obtain

$$[\mathbf{E}] = \frac{1}{V}\begin{Bmatrix} \{\mathbf{D}\}_1^T \\ \{\mathbf{D}\}_2^T \\ \{\mathbf{D}\}_3^T \end{Bmatrix}\Big[\{\mathbf{R}\}_1 \;\; \{\mathbf{R}\}_2 \;\; \{\mathbf{R}\}_3\Big] \tag{10.5-7}$$

as the material property matrix of the substitute plate that has no geometric disturbances. Because $[\mathbf{E}]$ is symmetric, its upper or lower triangle can be filled in after the other triangle has been computed as described above.

Analogous arguments can be made if properties are referred to polar or cylindrical coordinates [10.6]. Flexural stiffness coefficients can be determined in similar fashion, by applying unit curvature states and calculating associated nodal moments.

Null Properties. In some analyses, one may wish to remove elements from the structure if certain conditions are satisfied; for example, if a portion of the structure melts. Actual removal is awkward, but elements can be effectively inactivated by multiplying their moduli by a small factor such as 10^{-6}. Elements previously inactivated in this way can be reactivated by multiplying their moduli by 10^6, perhaps to model solidification, or addition of a layer of material. Software may provide for automatic application of these multipliers when user-prescribed conditions are detected.

10.6 LOADS AND REACTIONS

According to classical linear theories of beams, plates, and solids, at a point loaded by concentrated normal force P there is:

- Finite displacement and finite stress in a beam loaded laterally by P
- Finite displacement and infinite stress in a flat plate loaded laterally by P
- Infinite displacement and infinite stress where P acts on a 2D or 3D solid

These seemingly contradictory assertions result from differences in the mathematical models, which incorporate different premises about the nature of stress fields in each class of problem. The premises are also incorporated in finite elements for each class of problem. Thus, if mesh refinement is indefinitely repeated in the neighborhood of force P, bending moments in a plate continue to increase, and displacements and stresses in a solid continue to increase. Of course, a concentrated force is a convenient fiction. All real forces are distributed over an area greater than zero. In FEA, various distributed loads equivalent to P can be constructed (Fig. 3.11-4).

The easiest way to apply a concentrated force at a prescribed location is to arrange the FE mesh so that a node appears at this location. A concentrated moment load cannot be applied at a node unless the node includes the appropriate rotational d.o.f. If nodes have only translational d.o.f., a moment must be applied as couple-forces on a pair of nodes. In field problems such as heat conduction and fluid flow, the analogue of a concentrated force is a source or a sink, and the analogue of a moment is a doublet.

If axisymmetric conditions prevail, what appears to be a concentrated load on a solid or shell of revolution depicted in cross section is interpreted by FEA as a line load on a nodal circle. Such a load, expressed in force units, may be distributed on a 1-radian slice or on the entire circumference, depending on the convention adopted by the software. In the latter case, a uniform line load of intensity q around a circle of radius r is described as a force of magnitude $2\pi rq$, even if the load is radially directed so that its resultant is statically equivalent to zero.

External loads impart no stiffness to the FE model. Therefore, if an attached part is replaced by the load or loads it presumably applies, stiffness associated with the attached part is lost.

Software converts distributed loads to statically equivalent nodal loads. If elements have rotational d.o.f., as is the case for plate or shell elements, equivalent nodal loads may or may not include nodal moments (described in Section 2.9). One can easily discover whether the software includes nodal moments by running suitable test cases, using perhaps a single element, and comparing computed results with theoretical results.

Although reactions are computed quantities rather than input quantities, they can be regarded as loads. Reactions appear at d.o.f. that have been suppressed; that is, at a fixed support. A possible misinterpretation of reactions is suggested by Fig. 3.11-3d. If solid elements have midedge nodes, uniformly distributed load on a face of the FE model is associated with nodal forces of differing directions. Thus tensile force at a corner does not necessarily imply that the distributed surface load is tensile at the corner (see also the discussion associated with Fig. 10.8-2).

In linear problems, loads maintain their original orientations in space, regardless of the magnitudes of computed displacements and rotations. Loads that maintain their orientation with respect to the structure as it deforms are called *follower forces*. An example is pressure applied to a membrane, such as a balloon. Hydrostatic pressure always acts normal to the membrane. A nonlinear analysis is required if the deformation is appreciable or if the membrane is initially flat and has practically no bending stiffness.

In describing temperatures for a thermal-stress analysis, one must know whether the software uses nodal temperatures or element temperatures. The distinction becomes important if there is a step change of temperature across an interelement boundary, as might occur in the simulation of a shrink fit. Temperatures in adjacent elements that are interpolated from temperatures at shared nodes do not describe a step change.

10.7 CONNECTIONS IN STRUCTURES

Little is said about connections in most courses and books about stress analysis, yet connections are often the weakest parts of a structure, and their elastic or inelastic behavior can significantly influence behavior in other parts of the structure. A connection may involve complicated geometry, misalignment, different materials, prestress, making or breaking of contacts, friction and slippage, plastic action, and damage to the material from bending, welding, and punching holes. These complexities are usually ignored or greatly simplified unless the connection itself is the object of study. Simplification is typically intended to approximate the effect of the connection on the rest of the structure, and may involve merely representing a connector by a standard element of reduced elastic modulus.

A connection is usually stiffest when loaded in the direction of the static load it is designed to carry. Dynamic displacements may load connections in their more flexible directions. If little is known about these lesser stiffnesses, so that they are carelessly modeled, dynamic behavior of the structure may not be well modeled [10.6].

References devoted to connections include books such as [10.8,10.9] and papers devoted to their numerical analysis such as [10.10–10.12]. In what follows we consider a few simple topics related to connections.

Mismatches. With rare exceptions, a connection between a plane FE model and an axisymmetric FE model is physically meaningless, even if software accepts such a user-defined connection without complaint. Such a connection is depicted in Fig. 10.7-1a, where the plane mesh may be intended to represent a cooling fin on a tube. As shown in cross section, the axisymmetric mesh appears two-dimensional, but its elements are rings, and what appear to be nodal points are nodal circles. If an input data flag has called for axisymmetric analysis, the intended plane mesh will be treated as axisymmetric by the software. To avoid an axis mismatch in axisymmetric analysis, one must know which coordinate direction is understood by the software to be the axial direction.

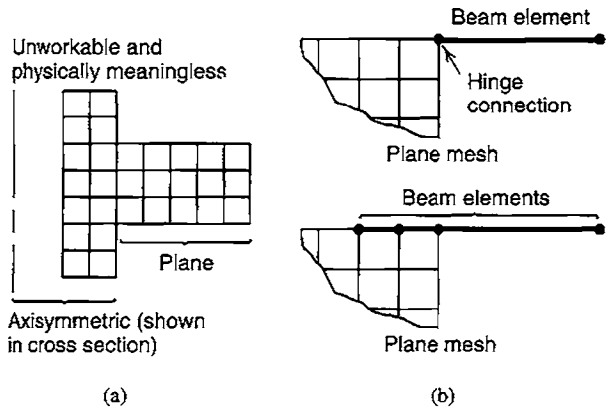

Figure 10.7-1. (a) Plane and axisymmetric FE models *cannot* be connected. (b) A hinge mechanism (upper sketch) is avoided by extending the beam into the plane mesh (lower sketch).

Response of an axisymmetric geometry to nonaxisymmetric loading can be analyzed by a superposition method that uses Fourier series components of the loading. By extending this procedure, the plane-to-solid connection depicted in Fig. 10.7-1a can be accommodated, but the method is not simple and is not part of standard FE software.

If elements with rotational d.o.f. are connected to elements without them, the connecting node acts as a hinge, which may not be what is intended. A case in point is depicted in Fig. 10.7-1b. The hinge connection can be avoided either by extending the beam into the plane mesh as shown, or by imposing a constraint relation among d.o.f., as discussed in Section 8.5. Stresses will not be realistic in the immediate neighborhood of such connections. The same devices can be applied to axisymmetric problems. Thus in Fig. 10.7-1b the beam element becomes the cross section of an annular plate, and the plane mesh becomes the cross section of an axisymmetric solid like that in Fig 10.7-1a.

Bolted Pipe Joint. A bolted joint in a pipe, Fig. 10.7-2, is axisymmetric in geometry except for the bolts. As an approximation, one can "smear" bolts around the bolt circle. The trick is to replace the bolts by an axisymmetric solid of radius r_b and length L that has the same stiffness in the axial direction as bolts it replaces but *zero* stiffness in the circumferential direction (because bolts have no circumferential continuity). Consider axial load on the pipe. Let there be n bolts around the bolt circle, each of elastic modulus E_b. Net axial stiffness from all bolts together is $k_b = A_b E_b/L$, where $A_b = n(\pi d^2/4)$. The replacement solid has axial stiffness $k_s = A_s E_s/L$. The condition $k_b = k_s$ yields $A_s E_s = n(\pi d^2/4)E_b$. The replacement solid is connected only to nodes on flange surfaces; that is, to nodal circles AA and BB in Fig. 10.7-2c. The replacement solid can be a single element; indeed, input data could describe it as a two-node bar element between nodes A and B. This device does not violate the rule that bodies with and without axial symmetry cannot be connected because we are only using the data and input description of a nonaxisymmetric element to obtain the required axisymmetric element.

Axial stress in a bolt is computed by multiplying its computed axial strain by its actual elastic modulus, E_b. To account for bending of bolts due, for example, to axial load on the pipe, one might similarly smear the flexural stiffness of individual bolts, include flexural stiffness in the replacement solid, and recover flexural stresses from computed displacements and cross-sectional properties of an individual bolt.

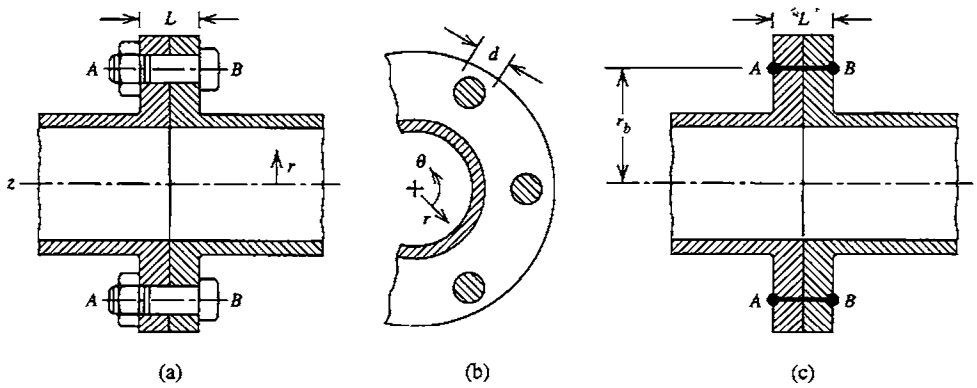

Figure 10.7-2. (a) Bolted pipe connection, side view. (b) Axial view. (c) As an approximation, axisymmetric connector AB replaces the bolts.

Prestress. Prestress produced by a known amount of interference can be simulated by temperature change. As a simple example, imagine that a circular ring is to be shrink-fitted onto a bar of circular cross section. Initially, when bar and ring are unconnected and at the same temperature, the inside diameter of the ring is a small but known amount less than the diameter of the bar. Physically, the shrink-fit can be accomplished by heating the ring, slipping it onto the bar, and allowing it to cool. For analysis, bar and ring comprise one axisymmetric model, initially stress-free and at uniform temperature. Then the ring portion alone is cooled an amount that would produce the required diameter difference if the ring were not attached to the bar and thus were free to contract. Note that modeling the bar and ring as a single axisymmetric solid prohibits axial slip between them.

Simulating a prescribed amount of prestress force in an elastic structure by means of temperature change ΔT is not as easily accomplished. In Fig. 10.7-2, let P be a known prestress force required from all bolts combined, so that P/n is the required prestress force in a single bolt. We seek the temperature drop ΔT in the bolts that produces the required force. When ΔT is applied, bolts and flange must contract the same amount. That is, with contraction taken as positive, and A_b the sum of bolt cross-sectional areas,

$$\alpha L\,\Delta T - \frac{PL}{A_b E_b} = \frac{PL}{A_f E_f} \tag{10.7-1}$$

where $A_f E_f / L$ is the stiffness of both flanges together as seen by the bolts. To calculate this stiffness, one can remove the bolts, apply an axisymmetric clamping force F across both flanges, and compute δ_{AB}, which is the resulting relative displacement between flange faces. Then

$$\delta_{AB} = \frac{FL}{A_f E_f} \qquad \text{from which} \qquad \frac{A_f E_f}{L} = \frac{F}{\delta_{AB}} \tag{10.7-2}$$

Now that $A_f E_f / L$ is known, Eq. 10.7-1 yields the required ΔT. Calculation details appear in [10.13].

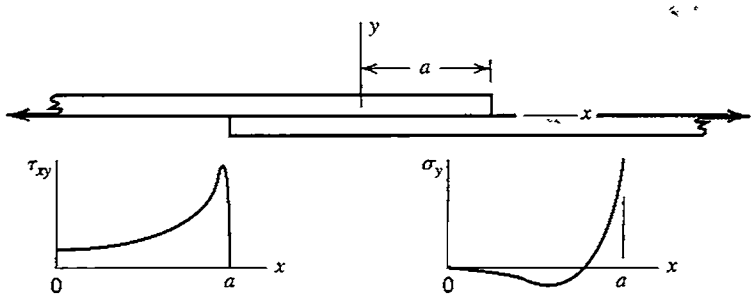

Figure 10.7-3. Lap joint loaded in tension. Plots are qualitative representations of shear stress and normal stress in the right half of the glue layer.

Because pipe flanges are more massive than the connecting bolts, elastic stiffness in the connection is due mostly to the flanges. If there is a gasket between flanges, bolt tension tends to "roll" the flanges relative to each other, bending the bolts, and perhaps resulting in partial loss of contact with the gasket during prestressing, with further loss when internal pressure is applied. A load-dependent contact area renders the problem nonlinear [10.9,10.14]. If flanges are connected without a gasket, even large bolt tensions would not produce joint stiffness as large as would be provided by continuous material, owing to the near impossibility of achieving a perfect fit and preventing any slip.

Glued Lap Joint. A glued lap joint is shown in Fig. 10.7-3. Very simplified analysis, as performed in a first course in stress analysis, makes the assumption that shear stress in the glue layer is uniform. The actual distribution is much different, as shown [10.8]. Note in particular the large "peel stress" σ_y at ends of the glue layer, which may initiate a crack that then propagates toward the center of the joint. As compared with other kinds of joints, glued joints benefit from comparative simplicity of geometry, if not simplicity of behavior.

Misalignment. Oversimplification of a connection can exclude joint loadings that increase stresses in the connection and in the members connected. Thus, in Fig. 10.7-4, the "poor model" arbitrarily superposes connections that are actually only adjacent, and does not capture bending moments that actually arise.

Release. A *release* is the disconnection of element d.o.f. that would ordinarily be shared at a node where elements meet. As an example, imagine that in Fig. 10.7-4b the structural

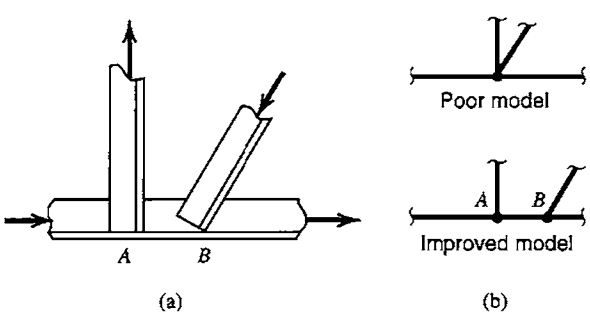

Figure 10.7-4. (a) Portion of a plane frame built of angle sections. Members are not concurrent at a single point. (b) Possible 2D models of the joint.

members are represented by beam elements, but we wish to make the connection at node A a hinge connection. Therefore, we wish to say that at A the connected elements have the same translational d.o.f. but independent rotational d.o.f. This can be accomplished by condensing the affected rotational d.o.f. in element matrices before assembly (Section 6.7). Condensed rows and columns of element matrices are replaced by zeros so that no unwanted stiffness coefficients are carried into the structure stiffness matrix. However, when n members meet at a hinge, rotational d.o.f. must be condensed in only $n - 1$ members, lest rotational d.o.f. of the structure node be completely unattached, which would make the structure stiffness matrix singular [2.21,10.15].

10.8 BOUNDARY CONDITIONS

Boundary conditions, also called support conditions in structural mechanics, are often misrepresented in the mathematical model or misstated as input data to FE software. Care is needed because changes in support conditions that appear minor can have a major effect on computed results. For example, if deflections are small and the beams in Figs. 10.8-1a and 10.8-1b are not too short, computed results differ only in that local stresses associated with supports appear at different locations on end cross sections. But supports in Fig. 10.8-1c prevent elongation along the bottom of the beam, thereby applying horizontal forces that affect response throughout the beam. If the FE model consists of standard two-node beam elements along the horizontal centerline, physical behavior in Fig. 10.8-1c can be approximated by use of rigid links that extend from each support up to beam nodes on the centerline (Section 8.5).

Boundary conditions are not often obvious in a real-world problem. To see that even a simple problem presents many choices and uncertainties, consider stress analysis of a tabletop under uniform downward load. Let the tabletop be a flat rectangular plate supported by prismatic vertical legs at four corners. If the top is analyzed alone, simple supports at corners make the model too flexible, while fixity at corners makes it too stiff. If legs are included in the model, legs may be fixed at the floor, pinned, or free to slide. Connections between legs and the tabletop may be loose. A leg may be too short, or the floor uneven.

If the physical problem does not present a clear choice of appropriate boundary conditions, it may be possible to bound the correct result by two analyses. For example, imagine that rotations at ends of a uniformly loaded and simply supported beam are elastically restrained to an uncertain degree. Two analyses, one with simple supports and another with fixed supports, will respectively overestimate and underestimate the magnitude of the actual bending moment at midspan. Similarly, if there is sliding with an uncertain amount of friction, an analysis with no sliding and another with free sliding may bound the correct result. In some problems, of course, relaxation of fixity or friction may make the model unstable.

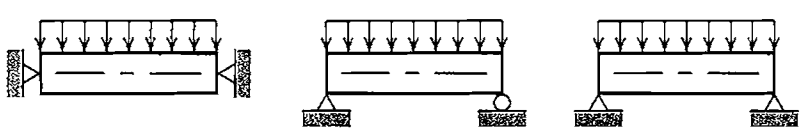

(a) (b) (c)

Figure 10.8-1. (a,b) Possible models of a beam with simple supports. (c) A beam with hinge supports.

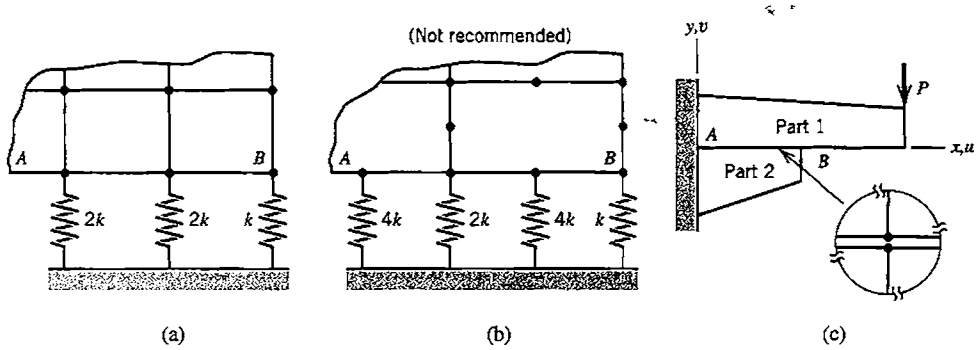

Figure 10.8-2. (a,b) Spring supports intended to simulate a uniform elastic foundation. (c) Two plane regions with sliding contact along *AB*. Inset shows typical adjacent nodes in FE models of parts 1 and 2.

Some support conditions are dictated by FE technology rather than by physical considerations. A restraint, such as prescription of zero displacement or rotation, should appear *at* a node rather than between nodes. (Otherwise, one must invoke constraint conditions that relate d.o.f. at adjacent nodes on the boundary of the FE model.) Also, global d.o.f. not active in the FE model must be suppressed, whether or not they are on the boundary. Thus for a plane structure modeled in the *xy* plane, d.o.f. w, θ_x, and θ_y must be set to zero to prevent singularity of the structure stiffness matrix. Software may do so automatically when instructed that the problem is planar, but the software user should verify (not assume) that this is so. Some details of the matter are discussed in Sections 2.6 and 2.7. Restraint of d.o.f. in directions other than the *xy* directions can be addressed by transformation operations, and by use of rigid links (Figs. 8.4-1 and 8.5-4).

It is risky to simulate a uniform elastic foundation by means of discrete springs (Fig. 10.8-2a,b). Nodal forces consistent with uniform pressure should result when edge *AB* is translated vertically downward. For this to happen, stiffnesses of uniformly spaced discrete springs in a plane model must have the relative magnitudes shown. If instead the model were three-dimensional, with element faces parallel to the foundation having midside nodes as well as corner nodes, the required spring stiffnesses are counterintuitive. That is, as suggested by Fig. 3.11-3d, each spring located at an element corner node must have negative stiffness! It is conceivable that an FE model will display negative diagonal coefficients in [**K**]. Clearly, there is ample opportunity for confusion and mistakes in this kind of foundation model. It is safer to use a consistent formulation, such as described by Eq. 8.8-2. If software supplies the consistent formulation only in association with beam or plate elements, it may be acceptable to add beam or plate elements to the plane or solid model, using very small moduli for the added elements (but proper moduli for the foundation they bring with them).

In Fig. 10.8-2c, it may not be obvious that a gap opens along *AB* when load *P* is applied. A pilot study that allows sliding contact all along *AB* can settle the matter. A sliding contact between FE meshes of parts 1 and 2 requires that adjacent nodes on either side of *AB* have the same vertical displacement but unrestrained horizontal displacement. Constraints of this kind are discussed in Section 8.5. For the geometry and loading shown, computed results will show tensile σ_y along *AB*, thus indicating that contact appears only at *B*. Another option is to impose sliding contact only at *B* but connect other adjacent nodes on either side of *AB* by very soft linear springs. Computation will show tensile forces in these springs, thus indicating that a gap opens. If the springs are sufficiently soft, their effect on stresses in parts 1 and 2 will be negligible.

Numerical error may be provoked by adding a very stiff spring, either within the FE model or as part of a boundary condition treatment. The matter is discussed in Section 9.2. In particular, see Fig. 9.2-3c,d, where a stiff spring is added to simulate an inclined roller support. The stiff spring could also be used as part of an ad hoc procedure for imposing a prescribed nonzero displacement. For example, imagine that instead of the roller support shown in Fig. 9.2-3b, prescribed displacement D'_A in the x' direction is to be imposed. In Fig. 9.2-3c,d, a force kD'_A can be applied parallel to the spring of large stiffness k. The stiffness seen by this force is k plus a small contribution from the comparatively flimsy structure. Computed displacement in the x' direction will be only slightly less than D'_A. Dangers of this procedure are the same as described in Section 9.2.

Input data as understood by the software can easily be checked. Graphical preprocessors can depict boundary conditions at each node, using symbols that show the direction of restraint and its type (displacement or rotation). These displays should be carefully checked for physical reasonableness and for data input blunders.

10.9 REPETITIVE SYMMETRY

Repetitive symmetry exists when a number of identical regions are connected together in identical fashion so as to form a pattern that repeats several times. Boundary conditions and applied loads must also be identical on each region so as to display a repetitive pattern. When repeating regions fit together around a complete circle, repetitive symmetry is also called cyclic symmetry, sectorial symmetry, or rotational periodicity. As an example, a centrifugal pump impeller displays cyclic symmetry. The existence of repetitive or cyclic symmetry permits response of the entire assembly to be obtained from analysis of a single repeating region [10.16]. (Reduction in problem size is also made possible by reflective and skew symmetry, which are discussed in Section 2.11.)

An example of cyclic symmetry appears in Fig. 10.9-1a. A complete solution can be obtained by analysis of one repeating portion, such as that in Fig. 10.9-1b (alternative

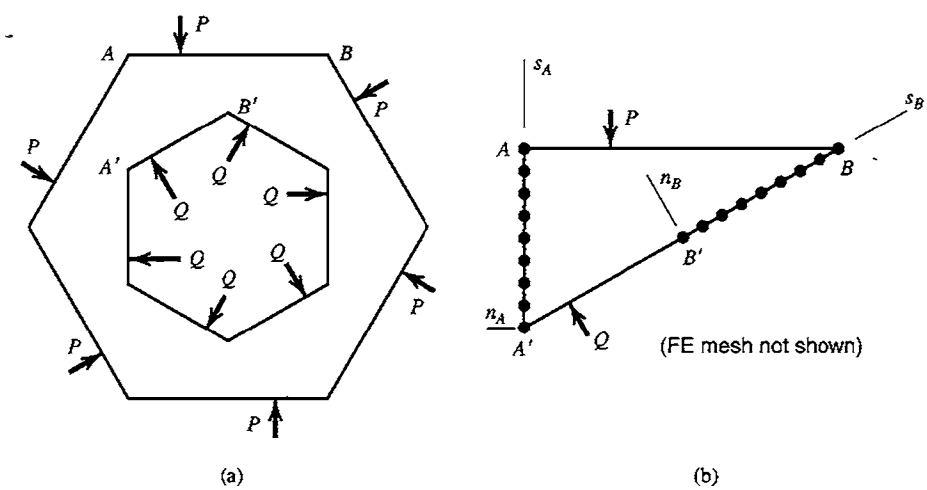

Figure 10.9-1. (a) A plane structure that exhibits cyclic symmetry. Loads are P and Q. Supports, not shown, exert no force. (b) Typical repeating portion. Mesh, not shown, has "attachment" nodes shown on AA' and BB'.

choices of the portion to be analyzed are possible). Although only one such portion is needed for analysis, it is convenient to refer to "attachment" d.o.f. along AA' and BB'. Nodes on these lines of attachment d.o.f. must correspond exactly—in number, placement, type, and orientation—because d.o.f. along AA' and BB' must be constrained to have identical displacements. Thus, in their respective ns coordinate systems, $n_A s_A$ and $n_B s_B$, nodes A and B have the same n component of displacement and the same s component of displacement, and similarly for every other homologous pair of nodes. Similar remarks apply to more general cases of cyclic symmetry, where in general nodes associated with attachment d.o.f. constitute homologous pairs on congruent curved surfaces.

To formulate the problem, we consider one repeating portion, such as that in Fig. 10.9-1b, which we now elect to call a *substructure*. Let $[\mathbf{K}]\{\mathbf{D}\} = \{\mathbf{R}\}$ represent the FE model of one substructure, where $\{\mathbf{D}\}$ includes all d.o.f. of the substructure. In partitioned form, equations $[\mathbf{K}]\{\mathbf{D}\} = \{\mathbf{R}\}$ are

$$\begin{bmatrix} \mathbf{K}_{II} & \mathbf{K}_{IA} & \mathbf{K}_{IB} \\ \mathbf{K}_{IA}^T & \mathbf{K}_{AA} & \mathbf{K}_{AB} \\ \mathbf{K}_{IB}^T & \mathbf{K}_{AB}^T & \mathbf{K}_{BB} \end{bmatrix} \begin{Bmatrix} \mathbf{D}_I \\ \mathbf{D}_A \\ \mathbf{D}_B \end{Bmatrix} = \begin{Bmatrix} \mathbf{R}_I \\ \mathbf{R}_A \\ \mathbf{0} \end{Bmatrix} + \begin{Bmatrix} \mathbf{0} \\ \mathbf{F}_A \\ \mathbf{F}_B \end{Bmatrix} \tag{10.9-1}$$

where $\{\mathbf{D}_A\}$ and $\{\mathbf{D}_B\}$ contain d.o.f. on interface boundaries AA' and BB', respectively, and $\{\mathbf{D}_I\}$ contains all remaining d.o.f. of the substructure. Interface loads $\{\mathbf{F}_A\}$ and $\{\mathbf{F}_B\}$ result from elastic deformations and are applied by neighboring substructures. Loads $\{\mathbf{R}_I\}$ and $\{\mathbf{R}_A\}$ are imposed loads, caused perhaps by rotation or externally applied forces, or by uneven (but cyclically symmetric) heating. Loads $\{\mathbf{R}_B\}$ are absent because imposed loads must appear on only one interface. If mistakenly placed on both, the substructure receives twice the load intended. For the particular example shown in Fig. 10.9-1, forces P and Q appear in $\{\mathbf{R}_I\}$, and loads $\{\mathbf{R}_A\}$ are zero. Because all repeating substructures are identical,

$$\{\mathbf{D}_B\} = \{\mathbf{D}_A\} \quad \text{and} \quad \{\mathbf{F}_B\} = -\{\mathbf{F}_A\} \tag{10.9-2}$$

in which it is assumed that d.o.f. and loads along AA' and BB' are expressed in their respective coordinate systems rather than in a global coordinate system. Using transformation formulations explained in Chapter 8, we write

$$\begin{Bmatrix} \mathbf{D}_I \\ \mathbf{D}_A \\ \mathbf{D}_B \end{Bmatrix} = [\mathbf{T}] \begin{Bmatrix} \mathbf{D}_I \\ \mathbf{D}_A \end{Bmatrix} \qquad \text{in which} \qquad [\mathbf{T}] = \begin{bmatrix} \mathbf{I} & \mathbf{0} \\ \mathbf{0} & \mathbf{I} \\ \mathbf{0} & \mathbf{I} \end{bmatrix} \tag{10.9-3}$$

where each $[\mathbf{I}]$ is a unit matrix and each $[\mathbf{0}]$ is a block of zeros. The operations $[\mathbf{T}]^T[\mathbf{K}][\mathbf{T}]$ and $[\mathbf{T}]^T\{\mathbf{R}\}$, applied to $[\mathbf{K}]$ and $\{\mathbf{R}\}$ of Eq. 10.9-1, yield

$$\begin{bmatrix} \mathbf{K}_{II} & \mathbf{K}_{IA} + \mathbf{K}_{IB} \\ \mathbf{K}_{IA}^T + \mathbf{K}_{IB}^T & \mathbf{K}_{AA} + \mathbf{K}_{AB} + \mathbf{K}_{AB}^T + \mathbf{K}_{BB} \end{bmatrix} \begin{Bmatrix} \mathbf{D}_I \\ \mathbf{D}_A \end{Bmatrix} = \begin{Bmatrix} \mathbf{R}_I \\ \mathbf{R}_A \end{Bmatrix} \tag{10.9-4}$$

in which $\{\mathbf{F}_A\}$ and $\{\mathbf{F}_B\}$ do not appear because of Eq. 10.9-2. Solution for nodal d.o.f. and stresses now proceeds in the usual way.

Equation 10.9-4 can be produced automatically by the assembly process, thus avoiding the transformation of Eq. 10.9-3. The trick is to assign the same node number to each pair of homologous nodes along AA' and BB'; for example, nodes A and B would both be given the number (say) 125. Thus, additions seen in Eq. 10.9-4 are produced automatically when elements of the substructure are assembled. One must of course use actual nodal coordinates in the formulation of element matrices.

10.10 STRESS CONCENTRATIONS. SUBMODELS

Stress Concentrations. A common source of structural failure is a stress raiser, in the form of a hole, fillet, groove, crack, or other geometric irregularity, singly or in combination. FEA is not well-suited to economical modeling of these small details unless special elements are used. If each stress raiser is surrounded by a profusion of small elements, meshing becomes tedious and computational demands become large. An attractive alternative is to use a tabulated stress concentration factor (SCF), simply by applying a tabulated SCF to the stress field in an FE model that does not include the stress raiser. Thus in Fig. 10.3-4a we might determine the bending moment M at the corner, look up the SCF for the known fillet radius, and multiply the nominal flexural stress Mc/I by the SCF. Or, in the neighborhood of an isolated circular hole in plane stress conditions, if in-plane principal stresses σ_1 and σ_2 exist when the hole is not present, tabulated SCF data show that maximum and minimum stresses tangent to the edge of the hole are $3\sigma_1 - \sigma_2$ and $3\sigma_2 - \sigma_1$.

If the needed SCF is not available, the following alternative can sometimes be used as an economical alternative to highly refined meshing [10.17]. The geometric discontinuity is modeled by a coarse "local" mesh and peak stress is computed. To compensate for mesh coarseness, the peak stress must be multiplied by a scale factor SF. To determine SF, we use the same local mesh to solve a problem for which results are known. SF is computed as the ratio of exact peak stress to computed peak stress in the secondary problem. Success of the method relies on the availability of a secondary case that is "close" to the primary case and the ability of the analyst to recognize it.

As an example, consider stress at point E in Fig. 10.10-1a. The mesh of four-node plane elements is very coarse. For this mesh and the load P used, the stress of largest magnitude at E is -221 (the units do not matter here). The same local mesh is embedded in a tensile strip, Fig. 10.10-1b, as a suitable secondary case for which the SCF is known. For the load applied, the secondary case provides a peak stress of 130 at E by applying the known SCF to the nominal stress $\sigma_{\text{nom}} = P/A_{\text{net}}$, while according to FEA the peak stress at E is 92.8. Hence the scale factor is SF $= 130/92.8 = 1.40$. The final estimate of stress at E in Fig. 10.10-1a is therefore $-221(1.40) = -310$. To obtain the final estimate of -310 *without* use of SF, the 2 by 2 mesh in Fig. 10.10-1a must be replaced by an 8 by 8 mesh. A peak stress of -337 at E in Fig. 10.10-1a is provided by a highly refined mesh.

Submodels. When geometry, material properties, loads, or boundary conditions are such that a tabulated SCF cannot be applied, or when results in addition to peak stress are required, more elements and/or improved elements must be used. However, it is not necessary to revise and reanalyze the entire FE model. Refinement can be strictly local. This procedure is called *submodeling* or a *global-local* approach. Submodeling has features in common with sub*structuring* (Section 10.11). Here we describe the traditional procedure of submodeling, and note its shortcomings.

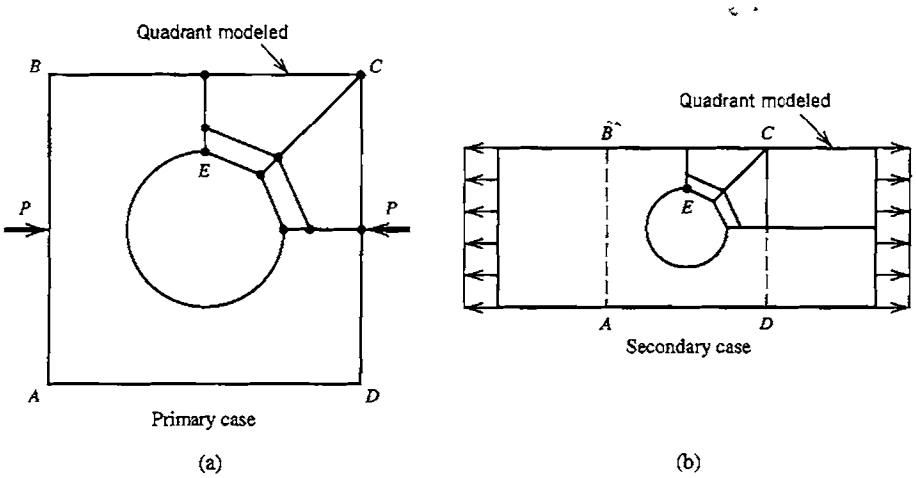

Figure 10.10-1. (a) A plane square region with a central hole, loaded by pinching forces *P*. (b) "Secondary" case having locally similar geometry, for which results are known.

As an example, consider a plate with a hole, Fig. 10.10-2a. Only a portion of the entire FE mesh is shown in Fig. 10.10-2a. We assume that this mesh is too coarse to provide accurate stresses on the boundary of the hole, but fine enough to provide reasonably accurate stresses *near* the hole. A possible submodel is shown in Fig. 10.10-2b. A submodel is subjected to prescribed *displacements* at all nodes along its "cut boundary," which in the present example is comprised of lines *BC* and *DA* and arc *CD*. Displacements to be imposed on the submodel are obtained from the coarse mesh. For submodel nodes on the cut boundary that do not exist in the coarse mesh, displacements must be obtained by interpolation from coarse-mesh nodal d.o.f. The submodel can be refined repeatedly without ever changing the coarse-mesh model.

Commercial software usually includes a procedure for obtaining d.o.f. on the cut boundary of the submodel from d.o.f. of the coarse-mesh model. Obtaining these d.o.f. by an algorithmic procedure seems preferable to the time-consuming alternative of devising a transitional mesh

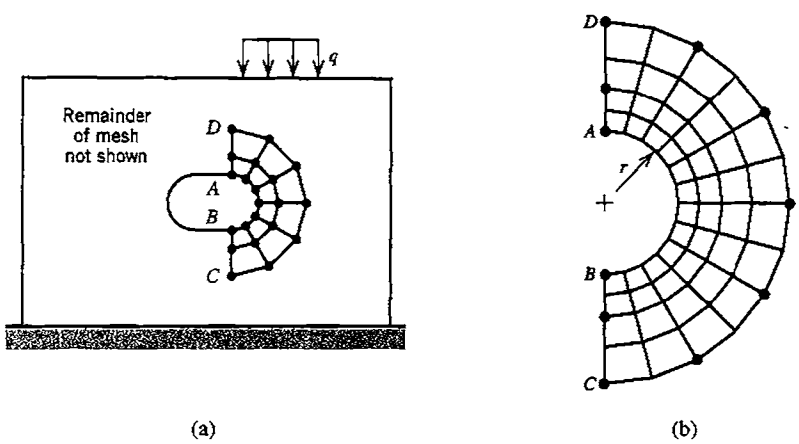

Figure 10.10-2. (a) Plate with a hole, showing a portion of a coarse-mesh plane FE discretization. (b) A submodel. Dots show nodes on the cut boundary that also appear in the coarse mesh.

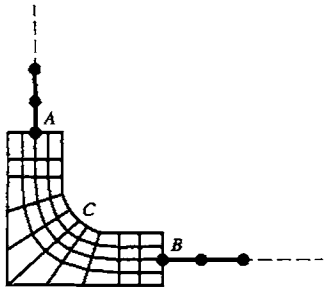

Figure 10.10-3. A submodel for the corner connection in Fig. 10.3-4a, using plane elements and beam elements.

to couple a submodel to a coarse mesh. Various algorithms for joining independent or dissimilar meshes have been proposed, including some that do not require any coincident nodes on a cut boundary, or even a good geometric match along it. References include [10.18–10.22].

Submodeling can be applied to the plane intersection shown in Fig. 10.3-4, in the manner shown by Fig. 10.10-3. Plane elements and beam elements must be connected at points A and B. This connection can be accomplished by imposing constraints (Section 8.5) or by extending the beam into the mesh (Fig. 10.7-1b). Special transition elements for this purpose have also been devised [10.23].

In the foregoing discussion of traditional submodeling we have assumed that regardless of improvement provided by the submodel, the coarse-mesh model is unaffected; thus it always provides the same d.o.f. to the cut boundary of the submodel. For this assumption to be reasonable, the coarse mesh must not be *too* coarse, and the cut boundary must be far enough from the local disturbance that is to be more carefully modeled. In Fig. 10.10-2, "far enough" means that d.o.f. along the cut boundary would be almost the same if they were computed using a mesh refinement of the entire plate. As a partial check, stresses along the cut boundary can be computed in both the coarse mesh and in the submodel; if these stresses are much the same, we have some indication that the cut boundary placement is acceptable. Even when carefully done, submodeling may underestimate peak stresses because the coarse-mesh model is likely to err by being too stiff, which means that the d.o.f. imposed on the submodel will be underestimated.

10.11 SUBSTRUCTURES

Over time, and as procedures for coupling different meshes together have become more capable [10.18–10.22], the distinction between submodels and substructures has become less precise. For the following discussion we will say that submodeling is a method of substituting an improved mesh into an existing FE structure when and where needed, while substructuring is division of the original structure into components, planned at the outset and usually adopted as a way to manage a large FE analysis project or as a way to fit the analysis into limited computer resources. With traditional submodeling, as described in Section 10.10, submodel behavior does not influence the coarse-mesh model. With substructuring, separate substructures interact. A time-independent analysis using substructures proceeds as follows [10.24].

1. Divide the FE model into two or more parts (substructures). The division should be made where parts have few interconnections. Thus, as we will see, reduced substructure matrices will not be large. For example, in Fig. 10.11-1a, division is made along the shaded lines rather than along the fuselage or lengthwise along wings.

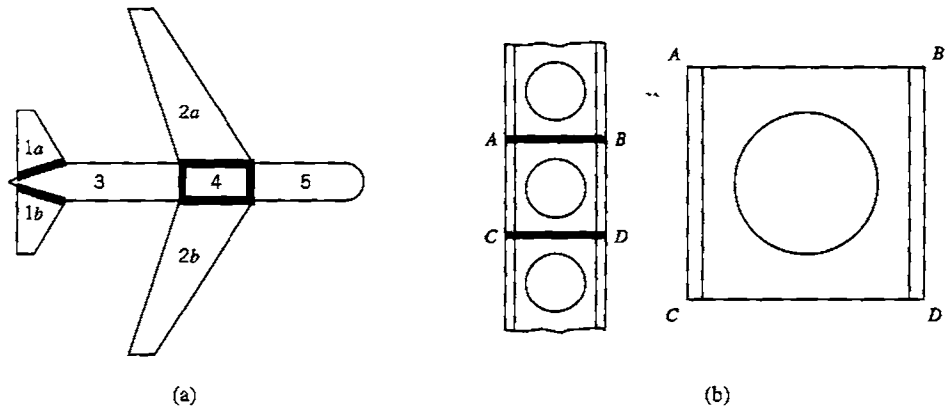

Figure 10.11-1. (a) Possible substructures 1a, 1b, ..., 5 of a hypothetical aircraft. (b) Castellated beam, with typical repeating substructure *ABCD*. Elements in substructures are not shown.

2. For each substructure, create an FE model and generate its global equations $[\mathbf{K}_s]\{\mathbf{D}_s\} = \{\mathbf{R}_s\}$. Begin to solve each such set of equations, say by Gauss elimination, until only "attachment" d.o.f. $\{\mathbf{D}_a\}$ of interconnection nodes remain. $\{\mathbf{D}_a\}$ is a small subset of $\{\mathbf{D}_s\}$. We symbolize the reduced equation set for a single substructure by $[\mathbf{K}_a]\{\mathbf{D}_a\} = \{\mathbf{R}_a\}$.
3. Assemble the reduced equation sets of all substructures to obtain global equations $[\mathbf{K}_A]\{\mathbf{D}_A\} = \{\mathbf{R}_A\}$, where $\{\mathbf{D}_A\}$ contains all attachment d.o.f. $\{\mathbf{D}_a\}$ of all substructures. (This equation set would also be produced by including all d.o.f. of the assembled structure in global equations $[\mathbf{K}]\{\mathbf{D}\} = \{\mathbf{R}\}$, then applying elimination until only attachment d.o.f. $\{\mathbf{D}_A\}$ remain.)
4. Solve equations $[\mathbf{K}_A]\{\mathbf{D}_A\} = \{\mathbf{R}_A\}$ for $\{\mathbf{D}_A\}$. Thus attachment d.o.f. $\{\mathbf{D}_a\}$ are known for each substructure. Return to substructure equations $[\mathbf{K}_s]\{\mathbf{D}_s\} = \{\mathbf{R}_s\}$ created and partially solved in step 2: now solve for the remaining d.o.f. in $\{\mathbf{D}_s\}$ by back substitution. Finally, postprocess to obtain gradients (such as stresses) in elements.

The process just described is that of static condensation prior to assembly, which is discussed in Section 6.7. Thus a substructure is regarded as a single element that happens to have a great many internal d.o.f. The name "superelement" is sometimes used to describe a substructure. Additional terminology may refer to attachment d.o.f. as "masters" and internal d.o.f. as "slaves."

The foregoing description implies that in order for substructures to attach to one another, attachment d.o.f. on mating boundaries of adjacent substructures must match in number, location, type, and orientation. With more recently developed methods, substructures (or entire structures whose connection had not been anticipated) can be connected when neither node patterns nor element types match along interfaces [10.18–10.22]. Thus substructuring can be used as an alternative to submodeling, most conveniently if the region to be refined is planned in advance.

There is particular advantage to substructuring if the FE model contains many repetitions of the same geometry (Fig. 10.11-1b). Then the same reduced substructure stiffness matrix $[\mathbf{K}_a]$ applies to every substructure. Repeated assembly of the same $[\mathbf{K}_a]$ array, with appropriate global node numbers, provides stiffness matrix $[\mathbf{K}_A]$ of the assembled substructures.

In time-independent analysis, substructuring introduces no additional approximation into the FE model. In dynamic analysis, the procedure analogous to substructuring is called *component mode synthesis,* which *does* introduce additional approximation. Again in time-independent analysis, if the advantage of repeating substructures cannot be exploited, substructuring does not reduce the computational effort of a *single analysis* of the complete structure. Indeed, substructuring requires somewhat *more* effort because of the additional bookkeeping involved. In practice it is unlikely that a single analysis will suffice, as almost certainly there will be errors to correct and changes to be made. Advantages of substructuring for large problems include the following.

If attachment d.o.f. $\{\mathbf{D}_A\}$ are not much affected by design changes, analysis and design of individual substructures can proceed independently, with only occasional assembly of substructures to update $\{\mathbf{D}_A\}$. Different design groups, indeed different subcontractors, can be assigned to different substructures. By not having to bring the entire assembled structure into calculations, each group can more quickly and easily correct errors, refine the substructure discretization as necessary, explore "what if" questions, and revise the substructure design.

Nonlinearity requires an iterative solution, which can be very expensive if the entire structure is used in calculations. If nonlinearity is confined to a single substructure, with the remainder of the structure reduced to attached substructures, the number of calculations per iterative cycle is greatly reduced.

Substructuring provides a systematic and orderly way of managing the analysis and design of a large structure. A large number of computer files is generated, especially if substructures are themselves substructured. Software must be coded in a way that helps the user with bookkeeping and data management chores. Even so the user is advised to plan carefully and keep records.

10.12 PLANNING AN ANALYSIS

In order to plan an FE analysis, the analyst must have a good grasp of the physical problem, understand the behavior and limitations of elements, and be aware of options and limitations presented by the software. Otherwise the problem may not be well defined, the FE model may not capture its important features, loading and support conditions may be inappropriate, and too much faith may be placed in computed results. A preprocessor may generate a mesh that represents geometry but is inappropriate to analysis requirements, and a postprocessor can present an attractive display that hides a need for mesh revision. Many users overestimate their FEA skills, underestimate the care required, and produce FE analyses so flawed that a competent analysis based on tools such as statics and elementary mechanics of materials would be more reliable.

An analyst competent in the problem area should plan the work, whose purpose may range from evaluation of a trial design to analysis of why an existing design has failed. In any case the analyst is likely to have some knowledge of the purpose of analysis, what information is sought, and what accuracy is required. This knowledge influences the number and type of assumptions and simplifications incorporated in mathematical models and in FE models. It is better to start with such considerations and a plan, which will almost certainly be revised as more is learned, than to start without a clear direction. Planning an FE project involves the following considerations.

Understanding the Problem. The broad goal of any analysis is to obtain adequate answers at reasonable cost in time and effort. In early steps the analyst surveys what is known and what is desired, considers simplifying assumptions, makes sketches, and gathers information. Users comfortable with computers but new to FEA may proceed too quickly, seeking answers to poorly defined questions. "Instant gratification" results are probably wrong. The process of preparing for FEA may sound tedious, but is likely to save more time than it takes, especially if the problem is complicated—and it probably *is* complicated if FEA is to be undertaken.

Questions about physical behavior include the following. Is time-independent analysis appropriate? Does the problem involve vibration or shock loading? If time-dependent, can damping be ignored? If not, how should it be represented? Are coupled fields involved, as when displacements of an immersed structure interact with fluid motion? If material properties are temperature-dependent or anisotropic, is material data available? Are there nonlinearities, due to material behavior, gaps that may open or close, or displacements large enough to alter the way loads are applied or transmitted? Answers to these questions decide the general nature of the analysis project.

In devising a mathematical model, one attempts to predict physical behavior. Response to the loads applied may be three-dimensional or perhaps essentially planar, and if planar, may be classified as plane stress or plane strain. An axisymmetric vessel may be considered thin-walled or thick-walled. These distinctions are important because they influence the mathematical theory adopted as descriptive of anticipated physical behavior, and hence the kinds of elements chosen to implement the theory: plane elements cannot represent three-dimensional behavior; thin shell elements cannot represent thickness-direction stress.

More detailed questions also influence the nature of the mathematical model and its discretization. Do load cases involve concentrated or distributed loads, or body forces from self-weight or spinning about an axis? Are loads fixed in direction or do their directions change as load increases? Can symmetry be exploited? Are there elastic supports or connections of uncertain stiffness? Are there cutouts that act as stress raisers, perhaps on a scale below mesh size? How reliable is data about geometry, loads, boundary conditions, and material properties?

Preliminary Analysis. Prior to performing FEA, some of the computed results should be anticipated qualitatively or quantitatively but preferably both. A preliminary analysis may be based on elementary theory, formulas from handbooks, analytical work, or experimental evidence. In almost all situations there is some way to obtain approximate answers to be compared with FEA results subsequently obtained. Even a crude preliminary analysis should be adequate to detect a computed displacement in the wrong direction, a strange pattern in a computed stress or temperature field, or a computed result in error by orders of magnitude. Often, strange FEA output results from a blunder in data input rather than from a serious misunderstanding.

There is a natural tendency to defend results that require considerable effort to obtain, as is the case for FEA results. For this reason, we recommend that approximate results, produced with comparatively little effort, be obtained *before* undertaking FEA. In addition to their use in checking FEA results, preliminary solutions provide insight that improves the FE model and sharpens analytical skills.

Start with Simple FE Models and Improve Them. An adequate FE model is likely to develop from a sequence of models, each of which contains improvements suggested by results provided by previous models, until the last one includes enough detail and contains suitable elements in a suitable mesh. The term "sequence of models" may suggest a great deal of effort. However, the sequence may not be long and some models may differ little from one another. The sequential approach builds confidence in the final result. It also takes less time overall than an attempt to construct a very detailed model at the outset, only to discover that it is inadequate or inappropriate because of behavior that was not foreseen. As FE software becomes more widely available, pre- and post-processors improve, and computing costs decline, there is a tendency to use more and more elements in FE models. This is unwise if done as a substitute for understanding.

Any set of rules for FE modeling is likely to have exceptions. This said, the following rules are often helpful. Include all of the structure in the FE model; do not omit part of it on the assumption that it is lightly stressed or does not influence the remainder of the structure. Use a finer mesh to obtain stresses (or mode shapes of vibration) than to obtain displacements (or natural frequencies of vibration). Use a finer mesh for thermal stress analysis than for temperature analysis of the same object. If the problem involves nonlinearity or anisotropy, analyze a linear or isotropic version of the problem first. If there are dynamic effects, do a static analysis first, using loads that approximate the major dynamic loads. Linear and static analyses are easier to perform and interpret, and may disclose flaws in the FE model that also affect nonlinear and dynamic analyses. A linear analysis may also disclose that local buckling is possible, or that stresses are so large that plastic action will develop. At present, software will not automatically decide that a buckling or elastic-plastic analysis is needed and then proceed to do it. Instead the analyst must make the decision and activate the type of analysis required.

The foregoing suggestions lead naturally to a sequence of FE models and analyses. Small detail such as fillets and oil holes have very little influence on overall behavior and can sometimes be taken into account by stress concentration factors rather than by refined FEA. Detail is likely to be added to subsequent models, as the mesh is refined or otherwise revised in regions of interest and in regions that influence overall behavior. Sometimes it is possible to begin the sequence with a "stick model," which is a model built of a few bar or beam elements. We do not suggest that the initial model be crude, only that it be comparatively simple. Some models in the sequence, probably the later models, may be produced by adaptive meshing, as described in Section 9.11. The analyst should not trust that adaptive meshing will always work properly. It cannot converge toward correct results for the problem intended if, due to user mistakes, it operates on a model that represents a different problem. It cannot convert a stick model to a plane model or a plane model to a solid model, or resurrect geometric detail initially discarded. Enough elements must be used to adequately model geometry. If shapes are complicated, this consideration may favor use of many elements with few nodes each rather than higher-order elements. The simpler elements may also provide better accuracy per unit of computational expense. It may happen that adequate geometric representation produces a very large number of d.o.f., especially if the model is a 3D solid. Where possible, 3D solid models (if needed) should be the final models in a sequence because they are the most tedious to prepare and the most demanding of computer resources.

Check the Model and the Results. Defects of modeling that prevent execution are often identified by error messages from the software. Defects that produce unreliable results usually must be detected by the analyst. Computed results must be carefully examined. These important matters are discussed in Sections 10.13 to 10.15.

Numerical Experiments in Design. In improving a design, one may want to learn how a quantity of interest is affected by changes in certain design variables. For example, we might have the goal of reducing a high stress or a high temperature, and have reason to believe that the goal can be accomplished by changes in a certain thickness, a certain material property, and a certain hole radius. Analyses using different numerical values of the design variables can be undertaken after the FE model is deemed acceptable (provided that changes in design variables are not so great that the model is no longer appropriate). By doing analyses in which each design variable is altered, we hope to learn the sensitivity of the quantity of interest to changes in each design variable, and to changes made in combination, so as to select the most favorable values. Procedures for planning these numerical experiments and interpreting results are part of the study called *design of experiments,* which for many years has been applied to physical experiments in an effort to obtain as much information as possible from a small number of tests. Many books are available; also see [10.25] for an introduction. See also Section 10.16, which summarizes automation of the design process.

10.13 COMMON MISTAKES

In this section we cite common errors in FE modeling and blunders in data preparation. Section 10.14 surveys more systematic searches for errors. Corrections for the errors are either obvious or are discussed elsewhere.

Broadly speaking, mistakes in modeling result from insufficient familiarity: with the physical problem, with element behavior, with analysis limitations, and with software. Failure to correct mistakes results from the same causes, from disregard of warning messages produced by software, and from insufficient discipline to check computed results.

An element matrix $[\mathbf{k}]$ is null if a common multiplier such as element thickness is zero. If unspecified, element thickness may default to unity, depending on the software. As element stiffness matrices are generated, division by zero will occur if Poisson's ratio is 0.5 in a plane strain, axisymmetric, or 3D solid problem. A global matrix $[\mathbf{K}]$ that is singular or nearly so may be caused by any of the following items, many of which can result from blunders in data input.

- Material properties such as elastic moduli are zero in all elements that share a node.
- One or more structure nodes are not connected to any element.
- One or more parts of a structure are not connected to the remainder.
- Boundary conditions are unspecified or are insufficient.
- A spurious mode (mechanism) is possible because of inadequate connections (as in the hinge connection of Fig. 10.7-1b).
- Too many releases are prescribed at a joint.
- There are large stiffness differences, as described in Section 9.2.

- Part of the structure has buckled. (This is possible if "stress stiffening" is included and negative stiffening has reduced a net stiffness coefficient to zero or less.)
- In nonlinear analysis, supports or connections have reached zero stiffness, so that part or all of the structure is inadequately supported.

Some instances of these blunders are as follows. Independently meshed parts of a structure may have coincident nodes, but software may not have been instructed that coincident nodes are to be considered identical. Instead these nodes are left unconnected. With 3D models, it is easy to forget that six rigid-body motions are possible, and thus forget to provide adequate support conditions. If a structural member that acts as a bar is modeled by several bar elements end to end (which is quite probably pointless), elements are connected with translational d.o.f. only. Like a chain, the bar assembly is then a mechanism many times over.

If software reports that [**K**] is singular but the cause is not apparent, it may help to analyze the model for its lowest vibration modes (perhaps as many as six modes for a 3D problem). Vibration analysis does not require that [**K**] be nonsingular. Any mode that has zero frequency is made possible by restraints that are inadequate for static analysis. An animated plot of such a mode may quickly suggest what additional restraint is required.

A singular [**K**] usually triggers a warning message and halts execution. If execution stops, or continues but produces bizarre results, it is clear that something is wrong and that a search for the cause is needed. The situation is more dangerous if there are errors that lead to results that appear reasonable upon casual inspection but in fact are seriously flawed. Errors in this category include the following.

- Elements are of the wrong type; for example, shell elements used where 3D solid elements are required.
- The mesh is too coarse, or element capability is too limited.
- Boundary conditions are wrong in location, type, or direction. (Supports can be too many as well as too few. They may impose complete fixity rather than a hinge, or may overconstrain rather than merely impose symmetry).
- Loads are wrong in location, type, direction, or magnitude. If symmetry is exploited, load in a plane of symmetry may not have been divided by 2, or stiffness of a beam that straddles a plane of symmetry may not have been divided by 2.
- Decimal points may be misplaced or units may be mixed. It is easy to supply a data item with the wrong power of 10. Angular velocity might be supplied as radians per second rather than revolutions per second (or vice versa), or feet may not have been converted to inches.
- An element may have been defined twice. Duplication may be overlooked because it is not seen on a display of the mesh. The result is a "stiff spot" in the FE model.
- Element connections may be poor (Fig. 10.3-3) or physically meaningless (Fig. 10.7-1a).
- Data provided for an axisymmetric analysis uses z as the axis of revolution, while software uses the y axis.

It is important to keep records of the status and progress of a project. Files should be identified with the name of the project, date created, date modified, nature of modification, the name of the analyst, and the name and version of software used. Records should be kept of information sources, assumptions made, pilot studies conducted, load cases treated, and checks performed. Small but important items that are easily forgotten should

be recorded. Records become important if work must be resumed after interruption or must be reviewed by someone else or some time after completion. Without records there is confusion. Where did data used to prepare the model come from? Did I remember to make changes X, Y, and Z or not? Which data files correspond to which model? Does the title line of the analysis refer to the current model or to a previous model?

10.14 CHECKING THE MODEL

A model should be checked prior to computation, both to make success more likely and to avoid making the task more distasteful by postponing it. Some checking can be done as the model is being prepared, using graphical features of preprocessors. It is easier to locate and correct mistakes as soon as they appear than to do so later. Mistakes can be made anywhere, even with simple data. Undetected mistakes can prevent execution, or lead to bizarre results, or lead to results that are plausible but wrong.

Checking Done by the Analyst. A mesh can be generated automatically, based on input data that describes the type of element to be used, the region to be meshed, and the mesh density required in selected parts of the region. The plotted mesh should be examined, to see if it "looks right"; that is, to see if the overall geometry is correct, if mesh densities seem appropriate, and if element shapes are not greatly distorted. Overly distorted elements are likely to be flagged by the software, but software examines separate details, while the analyst can survey the whole. The domain can be remeshed if necessary, or its unsatisfactory details corrected. If fine detail such as certain node locations are important, a numerical list of data should be examined as well as the graphical display. A numerical list *must* be examined to check material properties and cross-sectional properties of beams.

Graphical display can provide more than a plot of structure geometry with a mesh drawn on it. An exploded view, or a "shrink plot" in which individual elements are reduced in size about 20% (Fig. 10.14-1b), shows immediately if an element is missing. Mesh checking becomes more difficult for 3D models, but additional graphical devices can help, by including views of sections through the FE model, views from various directions, perspective, and enlargement of a chosen portion. Selective scaling is possible, so that only the smaller dimension of a slender model may be enlarged. Support conditions are usually identified by special symbols that indicate direction and type (displacement or rotation) at each support. Loads can be displayed in similar fashion. The boundary of a plane model can be plotted. If part of it looks like a crack in the model, then some nodes are adjacent or coincident but unconnected, perhaps intentionally but perhaps not. For easy identification, it may be possible to assign different colors to regions of different modulus, or to independently generated meshes that are connected in some way to form an assembly.

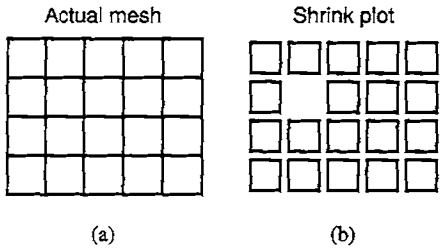

Figure 10.14-1. A shrink plot shows that an element has not been defined.

Checking Done by the Software. Commercial software does some checking automatically. In particular, element geometry is compared with internally stored numerical limits that define acceptability. Excessive distortions of the types shown in Fig. 10.3-1 are flagged, typically with each element graded "pass," "pass with warning," or "fail." Anything but "pass" produces a warning message or an error message; "fail" may also prevent execution. Numerical limits are somewhat arbitrary. What is unacceptable in one situation may be acceptable in another. Nevertheless all warning and error messages should be taken seriously, and changes made as required. Conditions that software may check include the following.

- A node is not connected to any element.
- Nodes are close or even coincident but unconnected. This circumstance does not necessarily indicate an error. The check may be most useful for a large 3D model. Some preprocessors can automatically connect nodes discovered to be close together.
- Elements share a node but do not use the same set of d.o.f. at that node.
- Corner and side nodes are connected; that is, there is a "bad connection" as in Fig. 10.3-3.
- Element shapes depart too greatly from the ideal, as in Fig. 10.3-1. Additional tests of element geometry, some using Jacobians of isoparametric elements, have been proposed [6.21,10.26–10.28]. See also Section 6.11.
- No loads have been supplied, or no boundary conditions, or no material properties.
- Prior to execution, software may be able to estimate the execution time and the amount of storage that will be required.

Automatic checking cannot disclose whether the problem intended has actually been defined, whether material property data is correct and units are consistent, whether loads and supports are properly located, and so on. The analyst must be vigilant.

Some additional tests of element geometry can be noted. A method of element stress smoothing provides a graphical display that shows the effects of shape distortion (Section 9.9, [9.17]). A similar test that compares element gradients with those obtained by patch recovery (Section 9.9) has been proposed [10.29]. This test requires that element stresses or other gradient information be computed, and therefore is not an a priori test. However, it can warn of excessive shape distortion based on actual performance, while a priori tests coded in a preprocessor offer only prediction based on element shape.

Software usually includes a *restart* capability, so that execution can be halted at various stages, then resumed. Execution might be halted by the software where an error is detected. The analyst might halt execution to investigate a warning message that has appeared, to examine intermediate results of an iterative solution, or to back up files. If an unanticipated load case must be investigated later, backup files may save time because most of the total computational effort precedes the processing of a load vector.

10.15 CRITIQUE OF COMPUTED RESULTS

Engineering errors can be expensive or even disastrous, so a solution should be checked in as many ways as reasonably possible. A single solution should not be trusted. As a first step in checking the results of FEA, we ask if they "look strange." For example, we ask if displacements are in unexpected places, unexpected directions, or are amazingly small or large; if support reactions have unexpected directions; if a stress disturbance appears in an unexpected

place; if heat seems to be flowing from cold to hot; and so on. Preanalysis planning should have provided at least qualitative expectations for checks such as these. If nothing is obviously wrong, we proceed to more detailed and quantitative checks, some of which are suggested in what follows. If trouble is suspected, we must seek its source, which is typically in the FE solution, but might also be in preliminary analysis or in physical understanding of the problem. In any case the trouble must be identified and corrected, and work repeated (see Fig. 1.5-3). When the current analysis is considered satisfactory, one must decide if further analysis is required, and if so, how it should be influenced by the current analysis.

In comparing FE results with results obtained otherwise—from approximate solution, handbook formulas, alternative software, existing similar structures, or experiment—one must be sure that the physical situation that produces the various results is substantially the same. Between FE and experimental analysis, for example, it is not uncommon to discover differences in loading, boundary conditions, and even structure geometry, especially if analysts and experimentalists do not communicate well.

In structural mechanics, displacements should be examined first, scaled up in plots so as to be easily visible, and preferably animated so the structure appears to oscillate between its deformed and undeformed configurations. (Typically, software plots only straight lines between nodes, so curved shapes assumed by beam elements are not shown.) One should see that displacements agree with intended boundary conditions; for example, that displacements are tangent to a roller support, or are zero at a fixed boundary. A gap should not "overclose"; adjacent parts cannot interpenetrate. One can also plot contours of selected displacements or rotations.

In plotting deformations produced by temperature, software may assume that the undeformed configuration exists at zero temperature. The analyst probably considers that the undeformed configuration exists at the prescribed reference temperature, which need not be zero. This impediment, if encountered, can be avoided by choosing zero as the reference temperature.

Software may automatically compute the sum of support reactions along each coordinate axis, and the net moment of reactions about each coordinate axis. If support forces and moments are found not to balance the intended load, it is more likely that load was incorrectly applied than that reactions have been incorrectly computed. Note that each reaction in the sum must be referred to the same coordinate system, and that constraint relations (if used) may introduce fictitious forces.

Recall that a linear solution is based on equilibrium equations written with respect to the initial *undeformed* geometry. In Fig. 10.15-1b, a physically possible rotation of the block requires tension in the spring. Standard linear analysis provides *compressive* force $F = Ph/b$ in the spring, regardless of the final configuration. For small rotation, $F = Ph/b$ is a satisfactory solution. Then the configuration in Fig. 10.15-1b may be misleading if it is the result of exaggerating actual displacements so as to make them visible when plotted. If displacements are *actually* this large, a nonlinear analysis is required.

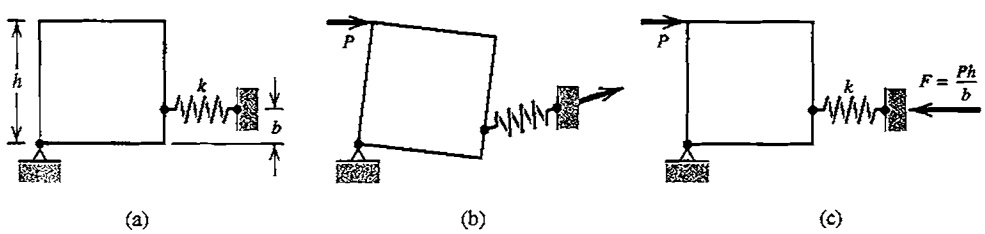

Figure 10.15-1. (a) Block supported by a hinge and a soft spring. (b) Possible displaced geometry produced by load P. (c) Reaction F computed by linear analysis.

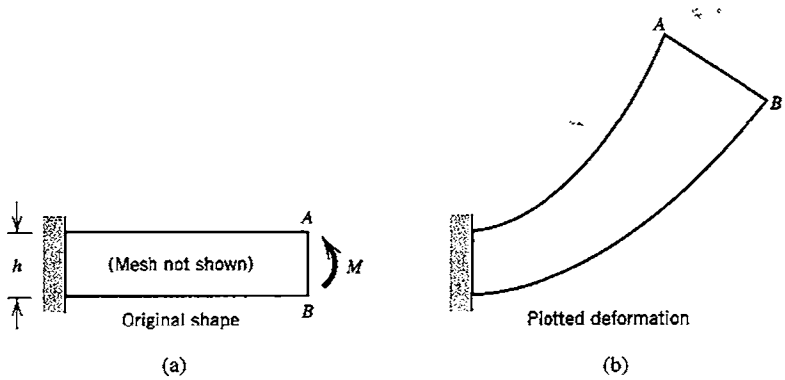

Figure 10.15-2. (a) Cantilever beam, loaded by tip moment. (b) Deformation from linear analysis, greatly exaggerated, as may be plotted by FE software.

Figure 10.15-2b shows a similar plot that may mislead. A small-deflection solution, which may be quite acceptable, has been scaled up a great amount. As plotted, it appears that the beam has gotten longer and that depth h has increased toward the right end. Closer inspection reveals that points A and B maintain their vertical separation and that the horizontal span of the beam centerline has not changed. The analyst must recognize that Fig. 10.15-2b does not represent a large-deflection solution, which can be obtained only by nonlinear analysis, in which equations to be solved must be based on the deformed configuration. A nonlinear solution iteratively constructs both the deformed configuration and matrix equations that describe it.

In conventional software, stresses are computed from displacement gradients, which means they are typically less accurate than computed displacements (see, however, the discussion in Section 9.9). In any case stresses should not be trusted if displacements are suspect. In vibration analysis, mode shapes should not be trusted if vibration frequencies are suspect. In heat conduction analysis, flux should not be trusted if temperatures are suspect.

Before examining stresses or other gradients, the analyst must understand how they are presented by the software. Are they referred to global or local axes? If local, how are these axes oriented? Are stress resultants (such as bending moments) presented? If so, they must not be mistaken for stresses. Are stresses averaged at nodes? This is incorrect if coordinate systems do not match or if there are discontinuities of element thickness or material properties (Fig. 3.12-2). In beam, plate, and shell elements, stresses may be available at upper, middle, and lower element surfaces. In these elements, what surface is the upper surface as understood by the software? A given surface of a plate of shell structure may contain both "upper" and "lower" element surfaces, with obvious opportunity for confusion about stresses on structure surfaces (see Section 15.1).

Remarks about calculation and interpretation of stresses (or other gradients) appear in Sections 1.5, 3.12, 6.10, and 9.9. These remarks are not repeated here, except for the recommendation that *un*averaged rather than averaged contours or bands be examined. Note also that if the model contains a plane of symmetry (of the FE mesh as well as loads, boundary conditions, and material properties), then contours will be continuous across that plane even if the mesh is far too coarse. A stress contour, which is the locus of points that have the same magnitude of a stress, contains no information about stress direction. Directional information is contained in *stress trajectories* (lines tangent to a principal stress direction), which may be plotted as arrows, with the length of each arrow proportional to the magnitude of principal stress at the tail of the arrow. In heat

conduction, analogous arrows represent heat flux. Stresses and other gradients can be viewed on user-defined cross sections of 3D solid models. Software may be able to report that a user-defined allowable stress has been exceeded, by how much and at what location. More specialized software can report on whether the model and computed results satisfy code requirements of a particular industry.

Some characteristics of an accurate stress field are as follows. At a boundary loaded only by normal pressure p, one of the principal stresses should be negative p (or zero for the common case of a load-free boundary). Principal stress trajectories should be normal or tangent to such boundaries. In an axially symmetric problem, radial and circumferential stresses should be equal on the axis of revolution. None of these conditions is likely to be met perfectly. The amount of imperfection is an indication of the amount of discretization error in the FE model.

Checking results in the manner described is likely to be most useful for the earliest models in a sequence, when blunders are most likely and the appropriateness of some assumptions may still be in question. Checking also provides insight as to how the model can be improved. Interelement discontinuity of gradient contours is one guide. The *closeness* of contours is another. Refinement is often advisable when an element spans several contours. Possibly the scope of analysis will have to be revised. This may happen if initial assumptions such as no buckling, no gap closure, or no plastic action are inconsistent with computed magnitudes of displacements and stresses.

10.16 DESIGN OPTIMIZATION

An optimal design might be defined as a design in which weight or cost is minimized. Other definitions of optimality are possible. To achieve an optimal design, design variables such as dimensions of its parts can be varied, with the constraint that allowable displacements and/or allowable stresses cannot be exceeded. An optimum is achieved by analyzing a trial design, making helpful changes, reanalyzing, and repeating the cycle until convergence. This iterative process can be automated, and provision for it appears in some software.

Stated in more detail, the goal of design optimization is to minimize an *objective function* by selecting appropriate values of the design variables. The objective function may be weight, a certain frequency, or any other quantity that can be calculated by the software. To minimize cost, the designer must be able to provide a formula for it in terms of the design variables. If desired, a quantity can be maximized; in that case we minimize its negative. Design variables may include cross-sectional areas, thicknesses of plates, and radii of major cut-outs. The number of design variables should number less than roughly 15 in order to reduce computer cost and to avoid converging to a local minimum rather than a global minimum. Hence, for example, a thickness is likely to be represented by a single design variable rather than by several parameters that would permit a continuous variation of thickness. The minimum sought is the minimum permitted by changes in the design variables adopted. The objective function is usually subject to constraints, such as limits on displacement or stress at several locations, and limits on design variables (such as a minimum allowable thickness). Many optimization algorithms have been devised, about which the interested reader will find many books and papers.

Related to optimal design is *fully stressed design,* defined as a design in which each member reaches its allowable stress under at least one of the applied load conditions. A fully stressed design is not necessarily a least weight design; indeed, no objective function is invoked. However, a fully stressed design can be calculated more quickly than an optimal design, and is a good starting configuration for optimization. Procedures of fully stressed design are iterative, and can be automated.

10.17 SOFTWARE

Several commercial software packages provide power, versatility, and conveniences for preparation of input and examination of output. A choice among them should be made with care. It takes time to learn to use a large software package with competence and facility, and having made the investment of time and money there is reluctance to change unless the software is found to have unacceptable shortcomings. Here we do not attempt to identify and compare popular programs, whose capabilities continually change [2.20,10.30]. Instead we offer some remarks that seem to have durability.

Development and Documentation. Programs are written (for different reasons) by researchers, students, and software vendors. Programs are not written by the typical analyst. The cost of programming includes planning, coding, testing, and documentation. Including time spent on all these tasks, a study showed that the average programmer produces only 200 lines of code per month [10.31]. In another study involving several programmers, the ratio of best to worst in coding speed was 25 to 1, and there was no correlation between productivity and experience [10.32]. Such anecdotes discourage an in-house programming project.

A large commercial analysis package may contain well over 150,000 lines of code and may represent an investment of tens of millions of dollars for development, maintenance, and support. New analysis packages appear infrequently. Not only are costs high, but engineering software has few buyers in comparison with software for other purposes. A vendor must work for years to penetrate a market in which users remain loyal to software they already know. Resistance to change may be justified. If there is little assurance that the vendor will remain in business and provide maintenance and support for several years, the cost of acquiring new software and learning to use it properly may not be warranted.

The language of most FE software has been Fortran. Not only has a large investment already been made in Fortran coding, but it remains powerful and portable, and it continues to evolve [10.33].

Documentation is usually provided both on paper and interactively via pull-down menus. It may be written by development staff familiar with the coding, but it is needed by less knowledgeable users, who are often confused and raise questions not anticipated by those who write the documentation. The writing of documentation may be regarded as an unpleasant labor, and perhaps postponed until software testing is well underway or even completed. It is preferable to regard the combination of documentation and software as the system to be tested [10.34]. The process of deciding which software system to buy should include study of the documentation.

Software Selection. In choosing a software vendor, a company may compile a list of candidates from advertisements in monthly magazines of engineering societies and by talking with associates at other companies. The list is shortened by discarding products that do not meet specific needs. Software that remains on the list is tested to see if it meets promotional claims and if it can solve the company's everyday problems. Compatibility with CAD systems currently in use may be important. The first package tested may stand out: if it is complicated, others may seem insufficiently comprehensive; if it is comparatively easy to use, others may seem too difficult.

Major vendors notify users when errors are detected in their software, and continue to correct, update, and extend the software. User support is provided, so that when users get into trouble, perhaps by exercising elements, options, and procedures in combinations not anticipated by developers, the telephone is answered. Major vendors also send periodic newsletters, provide training courses, and organize user conferences. Advice on software selection is plentiful; references include [2.20,10.34–10.37]. Reference 10.37 also contains extensive discussion of modeling, pre- and post-processing, and integration with CAD.

10.18 CONCLUDING REMARKS

Even now, many years after FEA began to be used in industry, its most common use may be to certify a design already completed or to study a design that has failed [10.25,10.38]. This is due at least in part to the time required for an FE analysis project. Users say it takes too long to prepare input data, even with automatic meshers. In one study, the time required for an FEA project averaged 15 man-days, with a median of 5 man-days, so that FEA may retard projects rather than accelerate them, and may not be used in early phases of design, where its capabilities might be most helpful. Despite increasing use of FEA, the rate of prototype failures seems unaffected [10.38].

Software that is easier to use and employs adaptive meshing may result in more productive use of FEA. More capable software may also make it easier for less capable users to obtain results, whether or not the modeling describes the intended problem and of course whether or not the intended problem addresses questions that should have been posed. The software provider is not responsible for decisions prompted by its use, even if the software contains serious errors. Engineers and analysts establish the mathematical model, choose software and solution methods, check results and interpret them, and the engineer of record assumes liability for all of the work [10.39]. It remains necessary to be vigilant and objective, despite the versatility of FEA and the effort expended in obtaining results. Again we recommend that the analyst understand the physical problem, plan ahead, check carefully, revise as needed, and understand how finite elements behave.

ANALYTICAL PROBLEMS

10.9-1 The three-node truss shown carries radial loads P. All of its bars are identical and each has axial stiffness $k = AE/L$. Use cyclic symmetry methods to determine the radial displacement at a typical node. Check results by use of elementary methods. *Suggestion:* Write a stiffness matrix that operates on radial displacements at (say) nodes 1 and 2, then enforce their equality.

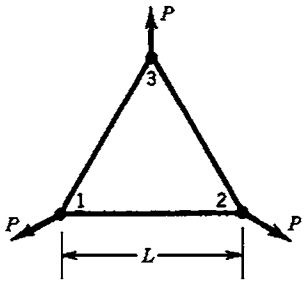

Problem 10.9-1

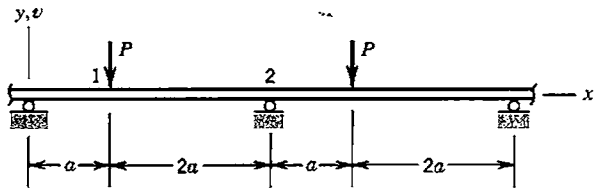

Problem 10.9-2

10.9-2 A long, uniform beam is supported and loaded in a repetitive pattern, as shown. Use cyclic symmetry methods to determine lateral displacement v_1 and in-plane rotations θ_1 and θ_2 at nodes 1 and 2 in terms of P, a, E, and I. Check results by use of elementary methods. *Suggestion:* Write a structure stiffness matrix that operates on nodal d.o.f. in a typical span between supports, then enforce equality of rotations at ends of the span.

COMPUTATIONAL PROBLEMS

C10.1 Apply uniform pressure to one face of a rectangular 20-node brick. Support the opposite face by discrete springs at nodes, in the manner depicted by Fig. 10.8-2, so as to mimic uniform foundation pressure (see also Fig. 3.11-3d). Is uniform stress computed in the element? Investigate what happens if (a) the element is made vastly stiffer than the foundation, and (b) the foundation is made vastly stiffer than the element. Explain the results obtained.

C10.2 For each of the two plane structures shown, determine the principal stress of largest magnitude by using a coarse mesh and the method suggested in connection with Fig. 10.10-1. Choose dimensions that approximately preserve the proportions shown. Then refine the mesh as needed to assess the adequacy of the result.

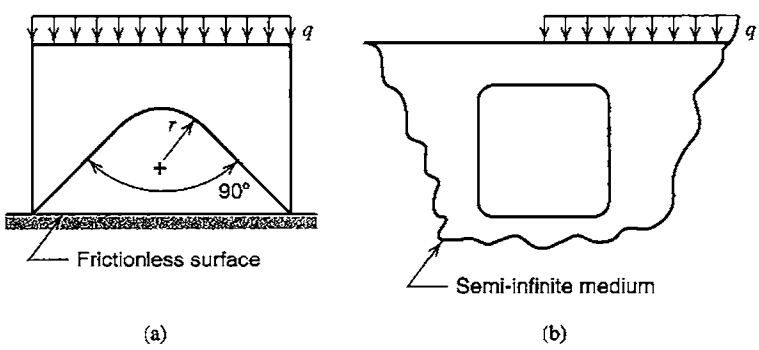

Problem C10.2

CHAPTER 11

FINITE ELEMENTS IN STRUCTURAL DYNAMICS AND VIBRATIONS

Formulation and solution of time-dependent structural problems are discussed in a finite element context. Alternatives for representation of mass and damping are described. Problems of structural dynamics are categorized, practical solution methods are considered, and suggestions for modeling are presented.

11.1 INTRODUCTION

Structural response is time-dependent if loading is time-dependent. However, if loading is cyclic and of frequency less than roughly one-quarter the structure's lowest natural frequency of vibration, dynamic response is scarcely larger than static response (only 7% larger for a single-d.o.f. spring-mass system). Then the problem can probably be classified as quasistatic and analyzed by methods discussed in preceding chapters. If loading is of higher frequency or is applied suddenly, dynamic analysis is required. Dynamic analysis uses the same stiffness matrix as static analysis, but also requires mass and damping matrices. For a given magnitude of loading, dynamic response may be greater or less than static response. It will be much greater if loading is cyclic with frequency close to a natural frequency of the structure. Some questions often posed in dynamic analysis are as follows.

- What are the natural frequencies of vibration and their mode shapes? Frequencies and mode shapes must be known in order to use some methods of dynamic response analysis. In applications, one may seek a design whose natural frequencies are well-separated from frequencies of applied loading. To calculate frequencies and modes we solve an *eigenvalue problem,* which is an algebraic form that also appears in buckling analysis. A short discussion of the vibration eigenvalue problem appears in the present chapter. A more general discussion of eigenvalue problems appears in Appendix C.
- What is the response to harmonic loading? Harmonic loading varies with time as a sine or cosine function, and may be applied by rotating machinery attached to the structure. In harmonic analysis, transient response to the initiation of loading is ignored. Instead we seek the steady-state response (here "steady-state" means response that repeats in equal time intervals). Calculation methods for harmonic response use vibration frequencies and modes.
- What is the time-varying response to loading that is not periodic or is suddenly applied? Here we seek the transient response, which we call the *response history* (known also by the curious name "time history"). Solution requires that differential equations of motion be integrated in time. If loading excites only a few of the lowest frequencies and response must be calculated over a time span equal to several multiples of the longest period of vibration, as is the case for earthquake loading, either the

mode superposition method or an implicit method of direct integration may be appropriate. If loading excites many frequencies and response must be calculated for no more than a few multiples of the longest period, as is the case for impact loading, explicit direct integration may be appropriate.

- What is the *maximum* response to loading that is not periodic or is suddenly applied? The question is answered by *response spectrum analysis*. It makes use of vibration frequencies and modes of the structure, and the response history of a single-d.o.f. spring mass system subject to the given time-varying pattern of loading. The method is approximate but can serve as an economical substitute for calculating the response history of a multiple-d.o.f. structure.

Answers to the foregoing questions require that the loading be known as a function of time. When loading is random, additional analysis tools are needed, which are beyond the scope of this book.

Structural dynamics has an extensive literature, and many textbooks such as [11.1–11.3]. Calculation methods are largely independent of FEA because these methods presume the availability of stiffness, mass, and damping matrices but do not demand that they arise from FE discretization. Indeed, many methods still in use were developed before the advent of FEA, when finite difference discretization was the numerical method of choice. Today, analysis methods are tailored to fit FE models. In addition to methods for calculation of frequencies and response history, methods that reduce the number of d.o.f. needed in these calculations have also been devised, in order to lessen computational requirements. Analysis tools discussed in the present chapter are common in FE software.

11.2 DYNAMIC EQUATIONS. MASS AND DAMPING MATRICES

Single-d.o.f. System. Each system shown in Fig. 11.2-1 has a single mass m, a single linear spring of stiffness k, and a single viscous damper. The viscous damper, shown by the conventional dashpot symbol, provides a resisting force proportional to rate of deformation. Motion is described by the single d.o.f. $u = u(t)$ and is governed by Newton's second law, $f = ma$ for one-dimensional motion. In conventional notation, velocity is $\dot{u} = du/dt$ and acceleration is $a = \ddot{u} = d^2u/dt^2$. Thus, in Fig. 11.2-1a,

$$f = ma \qquad \text{becomes} \qquad r - ku - c\dot{u} = m\ddot{u} \qquad \text{or} \qquad m\ddot{u} + c\dot{u} + ku = r \tag{11.2-1}$$

where $r = r(t)$ is an externally applied load that varies with time in a known fashion. Dynamic load r may also be known as a *forcing function, excitation,* or *external load.* Force ku of the spring may be called an *internal force.*

In Fig. 11.2-1b, force r is removed, and what was a fixed support in Fig. 11.2-1a is now given a prescribed motion $u_g = u_g(t)$. Displacement of mass m is u relative to the support but is $s = u + u_g$ relative to a fixed reference frame. Elastic and damping forces depend on relative motion, while inertia force depends on absolute acceleration $a = d^2s/dt^2$. Therefore $f = ma$ yields

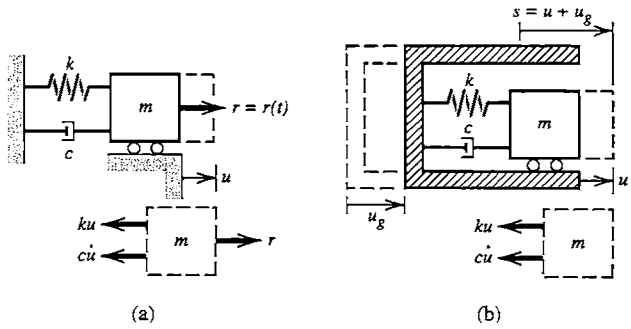

Figure 11.2-1. Single-d.o.f. systems, with displaced configurations shown by dashed lines. (a) Loading by time-varying force r. (b) Loading provided by support excitation.

$$-ku - c\dot{u} = m(\ddot{u} + \ddot{u}_g) \qquad \text{or} \qquad m\ddot{u} + c\dot{u} + ku = -m\ddot{u}_g \tag{11.2-2}$$

which is the same as Eq. 11.2-1 if $r = -m\ddot{u}_g$. Equation 11.2-2 is convenient when $\ddot{u}_g = \ddot{u}_g(t)$ is the known acceleration of an earthquake and displacement u is measured relative to the shaking earth.

General. The governing equation for structural dynamics, derived below, provides general expressions for structural mass and damping. Computationally effective formulations for mass and damping are examined in more detail in Sections 11.3 and 11.5.

We choose to derive the equation of motion by requiring that work done by externally applied loads be equal to the sum of work absorbed by inertial, dissipative, and internal forces for any virtual displacement (that is, for any imagined small motion that satisfies compatibility and essential boundary conditions). For a single element of volume V and surface area S, this work balance becomes

$$\begin{aligned} &\int \{\delta\mathbf{u}\}^T\{\mathbf{F}\}\, dV + \int \{\delta\mathbf{u}\}^T\{\mathbf{\Phi}\}\, dS + \sum_{i=1}^{n} \{\delta\mathbf{u}\}_i^T\{\mathbf{p}\}_i \\ &= \int \Big(\{\delta\mathbf{u}\}^T \rho\{\ddot{\mathbf{u}}\} + \{\delta\mathbf{u}\}^T c\{\dot{\mathbf{u}}\} + \{\delta\boldsymbol{\varepsilon}\}^T\{\boldsymbol{\sigma}\} \Big)\, dV \end{aligned} \tag{11.2-3}$$

where $\{\mathbf{F}\}$ and $\{\mathbf{\Phi}\}$ represent prescribed body forces and surface tractions, $\{\mathbf{p}\}_i$ and $\{\delta\mathbf{u}\}_i$ represent prescribed concentrated loads and their corresponding virtual displacements at a total of n points, ρ represents mass density, and c is a damping parameter analogous to viscosity. Also, $\{\delta\mathbf{u}\}$ and $\{\delta\boldsymbol{\varepsilon}\}$ represent virtual displacements and their corresponding strains, as explained in Section 3.3. In customary notation, FE discretization provides

$$\{\mathbf{u}\} = [\mathbf{N}]\{\mathbf{d}\} \qquad \{\dot{\mathbf{u}}\} = [\mathbf{N}]\{\dot{\mathbf{d}}\} \qquad \{\ddot{\mathbf{u}}\} = [\mathbf{N}]\{\ddot{\mathbf{d}}\} \qquad \{\boldsymbol{\varepsilon}\} = [\mathbf{B}]\{\mathbf{d}\} \tag{11.2-4}$$

Shape functions $[\mathbf{N}]$ are functions of space while nodal d.o.f. $\{\mathbf{d}\}$ are functions of time. Thus Eqs. 11.2-4 represent a local separation of variables. Combination of Eqs. 11.2-3 and 11.2-4 yields

$$\{\delta\mathbf{d}\}^T\left[\int \rho[\mathbf{N}]^T[\mathbf{N}]\,dV\,\{\ddot{\mathbf{d}}\} + \int c[\mathbf{N}]^T[\mathbf{N}]\,dV\,\{\dot{\mathbf{d}}\}\right.$$
$$\left. + \int [\mathbf{B}]^T\{\boldsymbol{\sigma}\}\,dV - \int [\mathbf{N}]^T\{\mathbf{F}\}\,dV - \int [\mathbf{N}]^T\{\boldsymbol{\Phi}\}\,dS - \sum_{i=1}^{n}\{\mathbf{p}\}_i\right] = 0 \tag{11.2-5}$$

in which it is assumed that concentrated loads $\{\mathbf{p}\}_i$ are located at nodes. The first two integrals in Eq. 11.2-5 are identified as "consistent" element mass and damping matrices:

$$[\mathbf{m}] = \int \rho[\mathbf{N}]^T[\mathbf{N}]\,dV \qquad [\mathbf{c}] = \int c[\mathbf{N}]^T[\mathbf{N}]\,dV \tag{11.2-6}$$

The word "consistent" emphasizes that these forms follow directly from FE discretization, and use the same shape functions as the element stiffness matrix. We define the element internal force vector $\{\mathbf{r}^{\text{int}}\}$ as forces—and also moments, if the element has rotational d.o.f.—applied to the element by nodes to resist stresses within the element.

$$\{\mathbf{r}^{\text{int}}\} = \int [\mathbf{B}]^T\{\boldsymbol{\sigma}\}\,dV \tag{11.2-7}$$

which is the negative of a term in Eq. 3.3-8. Similar notation is used to identify forces (and perhaps also moments) applied to nodes as a result of externally-applied loads on the element.

$$\{\mathbf{r}^{\text{ext}}\} = \int [\mathbf{N}]^T\{\mathbf{F}\}\,dV + \int [\mathbf{N}]^T\{\boldsymbol{\Phi}\}\,dS + \sum_{i=1}^{n}\{\mathbf{p}\}_i \tag{11.2-8}$$

The bracketed expression in Eq. 11.2-5 must vanish if the equation is to be true for arbitrary $\{\delta\mathbf{d}\}$. Thus, in the notation of Eqs. 11.2-6 to 11.2-8, Eq. 11.2-5 yields

$$[\mathbf{m}]\{\ddot{\mathbf{d}}\} + [\mathbf{c}]\{\dot{\mathbf{d}}\} + \{\mathbf{r}^{\text{int}}\} = \{\mathbf{r}^{\text{ext}}\} \tag{11.2-9}$$

Equations 11.2-7 and 11.2-9 are valid for both linear and nonlinear material properties. If the material is linearly elastic, then loads associated with element stresses are $\{\mathbf{r}^{\text{int}}\} = [\mathbf{k}]\{\mathbf{d}\}$, where $[\mathbf{k}]$ is the conventional element stiffness matrix, and Eq. 11.2-9 becomes

$$[\mathbf{m}]\{\ddot{\mathbf{d}}\} + [\mathbf{c}]\{\dot{\mathbf{d}}\} + [\mathbf{k}]\{\mathbf{d}\} = \{\mathbf{r}^{\text{ext}}\} \tag{11.2-10}$$

If $[\mathbf{m}]\{\ddot{\mathbf{d}}\}$ is isolated on one side of the equation, Eqs. 11.2-9 and 11.2-10 can be regarded as multidimensional forms of Newton's second law, $\mathbf{F} = m\mathbf{a}$. Global forms of Eqs. 11.2-9 and 11.2-10, for a multi-element structure, are respectively

$$[\mathbf{M}]\{\ddot{\mathbf{D}}\} + [\mathbf{C}]\{\dot{\mathbf{D}}\} + \{\mathbf{R}^{\text{int}}\} = \{\mathbf{R}^{\text{ext}}\} \tag{11.2-11}$$

$$[\mathbf{M}]\{\ddot{\mathbf{D}}\} + [\mathbf{C}]\{\dot{\mathbf{D}}\} + [\mathbf{K}]\{\mathbf{D}\} = \{\mathbf{R}^{\text{ext}}\} \tag{11.2-12}$$

Both of these equations state that external loads are resisted, or dynamically equilibrated, by a combination of inertia forces, damping forces, and internal stresses. The first form, Eq. 11.2-11, is convenient for nonlinear material properties, but can be used whenever it seems appropriate to compute internal forces by assembling element stress contributions rather than by using a global stiffness matrix.

Remarks. Equations 11.2-11 and 11.2-12 are each a system of coupled, second-order ordinary differential equations in time. Each constitutes a *semidiscretization:* nodal d.o.f. $\{\mathbf{D}\}$ are discrete functions of space but continuous functions of time. In a solution by direct integration, the equations are also discretized in time.

Consistent mass and damping matrices, Eqs. 11.2-6, are both symmetric, full, and positive definite. Nonconsistent forms are also used; they are described subsequently. Global matrices $[\mathbf{M}]$ and $[\mathbf{C}]$ have the same sparse topology as $[\mathbf{K}]$. They can be constructed by conceptual expansion of element matrices $[\mathbf{m}]$ and $[\mathbf{c}]$ to "structure size" and summation of overlapping terms, in the same way that $[\mathbf{K}]$ is constructed from element $[\mathbf{k}]$ matrices, as explained in Section 2.5.

Although structural damping is not viscous, it is usually small enough that a viscous representation is acceptable, and specific forms of $[\mathbf{c}]$ are chosen mainly for computational convenience (Section 11.5).

11.3 MASS MATRICES: CONSISTENT, DIAGONAL, AND OTHER

A mass matrix is a discrete representation of a continuous mass distribution. The consistent discrete representation is defined by Eq. 11.2-6. Simpler and historically earlier is the ad hoc "lumped" mass matrix obtained by placing particle masses at nodes. A lumped mass matrix is diagonal; a consistent mass matrix is not. The two representations have different merits, so that a particular analysis procedure may be best served by one or the other, or a combination of the two. An obvious advantage of lumping is computational; less storage space and processing time are required.

Particle Mass Lumping. Consider a uniform two-node bar element having length L, cross-sectional area A, and mass density ρ. Total element mass is therefore $m = \rho AL$. Particle lumping places a particle of mass $m/2$ at each node. As shown in Fig. 11.3-1a, this lumping implies a discontinuous displacement field in which the two halves of the element translate separately. Thus for an element of mass m the lumped element mass matrix, and inertia forces associated with nodal accelerations $\ddot{v}_1$ and $\ddot{v}_2$, are

$$[\mathbf{m}] = \frac{m}{2}\begin{bmatrix} 1 & 0 \\ 0 & 1 \end{bmatrix} \qquad \text{so that} \qquad [\mathbf{m}]\begin{Bmatrix} \ddot{v}_1 \\ \ddot{v}_2 \end{Bmatrix} = \begin{Bmatrix} F_1 \\ F_2 \end{Bmatrix} \tag{11.3-1}$$

Inertia forces are equilibrated by nodal forces F_1 and F_2 shown in Fig. 11.3-1a. The form of $[\mathbf{m}]$ in Eq. 11.3-1 prevails whether displacement is axial or lateral. If the two-node bar element is allowed to move in 3D space, its (diagonal) lumped mass matrix and nodal displacement vector are

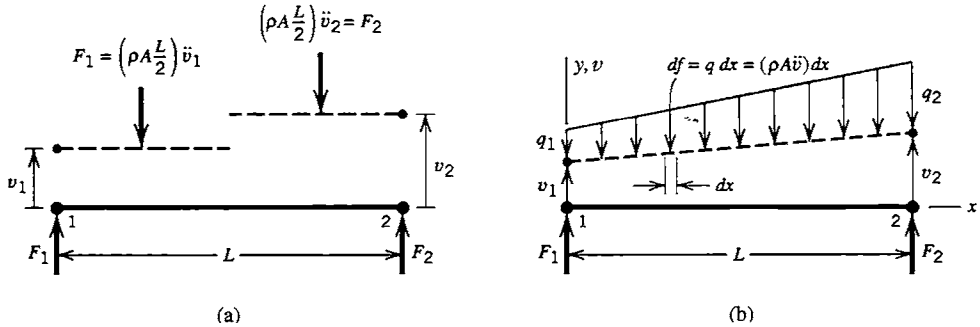

Figure 11.3-1. Lateral displacements of a two-node bar element are shown by dashed lines. (a) Implied by ad hoc lumping. F_1 and F_2 are inertia forces. (b) Linear displacement field provides the consistent [**m**] of a bar element.

$$[\mathbf{m}] = \frac{m}{2}\lceil 1 \quad 1 \quad 1 \quad 1 \quad 1 \quad 1 \rfloor \qquad \{\mathbf{d}\} = \lfloor u_1 \quad v_1 \quad w_1 \quad u_2 \quad v_2 \quad w_2 \rfloor^T \tag{11.3-2}$$

Thus for translational acceleration a in any coordinate direction, the total inertia force associated with the element is ma.

For an arbitrarily shaped three-node triangular element of area A and uniform thickness t, particle lumping places particles of mass $\rho At/3$ at each vertex. An eight-node rectangular hexahedron of volume V would have particles of mass $\rho V/8$ at each node.

Rotational d.o.f., in elements that have them, are not supplied with rotational inertia by the mere presence of mass particles. Rotational inertia must be added separately. Consider, for example, y-direction lateral displacement of a uniform two-node beam element, Fig. 2.3-1. Nodal d.o.f. are $\{\mathbf{d}\} = \lfloor v_1 \quad \theta_{z1} \quad v_2 \quad \theta_{z2} \rfloor^T$. With α a number to be selected, lumped mass matrices for an element of total mass m are

Beam without rotary inertia: Beam with rotary inertia:

$$[\mathbf{m}] = m\lceil 1/2 \quad 0 \quad 1/2 \quad 0 \rfloor \qquad [\mathbf{m}] = m\lceil 1/2 \quad \alpha L^2 \quad 1/2 \quad \alpha L^2 \rfloor \tag{11.3-3}$$

An ad hoc way to prescribe α is to imagine that a uniform slender bar of length $L/2$ and mass $m/2$ is attached to each node and rotates with it. The associated mass moment of inertia is $I = (m/2)(L/2)^2/3$, for which $\alpha = 1/24$.

Consistent Mass Matrix. Displacement of the two-node bar element in Fig. 11.3-1b is linear in the axial coordinate. If y-direction lateral displacement v is the only displacement, for a uniform element of total mass $m = \rho AL$, from Eq. 11.2-6,

$$\text{Bar:} \quad [\mathbf{N}] = \begin{bmatrix} \frac{L-x}{L} & \frac{x}{L} \end{bmatrix} \qquad [\mathbf{m}] = \int_0^L [\mathbf{N}]^T[\mathbf{N}]\rho A\,dx = \frac{m}{6}\begin{bmatrix} 2 & 1 \\ 1 & 2 \end{bmatrix} \tag{11.3-4}$$

which operates on the nodal acceleration vector $\{\ddot{\mathbf{d}}\} = \lfloor \ddot{v}_1 \quad \ddot{v}_2 \rfloor^T$.

For a uniform two-node beam element with d.o.f. $\{\mathbf{d}\} = \lfloor v_1 \quad \theta_{z1} \quad v_2 \quad \theta_{z2} \rfloor^T$, Fig. 2.3-1, shape functions are stated in Fig. 2.3-1 and in Fig. 3.2-4, and the consistent mass matrix is

$$\text{Beam:} \quad [\mathbf{m}] = \int_0^L [\mathbf{N}]^T[\mathbf{N}]\rho A\, dx = \frac{m}{420}\begin{bmatrix} 156 & 22L & 54 & -13L \\ 22L & 4L^2 & 13L & -3L^2 \\ 54 & 13L & 156 & -22L \\ -13L & -3L^2 & -22L & 4L^2 \end{bmatrix} \tag{11.3-5}$$

where $m = \rho AL$ is the total element mass. If the beam element stiffness matrix accounts for transverse shear deformation, as in Eq. 2.3-6, it is implied that shape functions differ from those used to obtain Eq. 11.3-5. Consequently additional terms appear in the mass matrix, expressions for which may be found in [11.4,11.5].

As final examples, consider an arbitrarily shaped three-node triangle and a four-node rectangle, namely element CST (Sections 3.4 and 7.1, Eq. 7.3-7) and element Q4 (Section 3.6). For motion in a single coordinate direction, with m the total mass of each element, consistent mass matrices for elements of uniform density and thickness are

$$\text{CST:} \quad [\mathbf{m}] = \frac{m}{12}\begin{bmatrix} 2 & 1 & 1 \\ 1 & 2 & 1 \\ 1 & 1 & 2 \end{bmatrix} \qquad \text{Q4:} \quad [\mathbf{m}] = \frac{m}{36}\begin{bmatrix} 4 & 2 & 1 & 2 \\ 2 & 4 & 2 & 1 \\ 1 & 2 & 4 & 2 \\ 2 & 1 & 2 & 4 \end{bmatrix} \tag{11.3-6}$$

If motion is allowed in all three coordinate directions, mass matrices are enlarged, with repetition of terms already present, in the same way that $[\mathbf{m}]$ of Eq. 11.3-1 is enlarged to become $[\mathbf{m}]$ of Eq. 11.3-2.

Combination Matrices. For a given number of elements in the FE model, computed vibration frequencies are often found to be more accurate if lumped and consistent mass matrices are combined. Taking the bar element as an example, with a number β in the range $0 \le \beta \le 1$, we obtain from Eqs. 11.3-1 and 11.3-4

$$(1-\beta)*\text{lumped} + \beta*\text{consistent:} \qquad \text{Average, } \beta = 0.5:$$

$$[\mathbf{m}] = \frac{m}{6}\begin{bmatrix} 3-\beta & \beta \\ \beta & 3-\beta \end{bmatrix} \qquad [\mathbf{m}] = \frac{m}{12}\begin{bmatrix} 5 & 1 \\ 1 & 5 \end{bmatrix} \tag{11.3-7}$$

A combination $[\mathbf{m}]$ for a beam element can be similarly constructed from Eqs. 11.3-3 and 11.3-5. Various combinations for various element types have been explored [11.6,11.7]. Selected results, in the form of computed vibration frequencies, appear in Table 11.3-1. For these bar and beam examples—but not in all problems—natural frequencies are underestimated by a particle-lumped $[\mathbf{m}]$ and overestimated by a consistent $[\mathbf{m}]$, by nearly equal amounts for the bar, but not so for the beam. Respectively, the bar and beam structures have 8 and 10 d.o.f., so modes 8 and 10 are the highest modes these models can provide. With particle masses, the beam has only four active d.o.f. with mass, so modes higher than four have infinite frequency. Note that the number of modes with adequate accuracy is roughly half the number of active d.o.f., at least in these examples.

TABLE 11.3-1. PERCENTAGE ERRORS OF COMPUTED NATURAL FREQUENCIES, USING DIFFERENT MASS MATRICES [11.7]. FOR BEAM ELEMENTS WITH PARTICLE-MASS LUMPING, $\alpha = 0$ IN EQ. 11.3-3. STRUCTURES ARE UNIFORM AND MODELED BY ELEMENTS OF EQUAL LENGTH.

Mode	Type of mass matrix used		
number	Particle-mass lumps (%)	Average [**m**] (%)	Consistent [**m**] (%)
	Axial vibration of an eight-element bar, one end fixed, the other free		
1	−0.16	0.00	+0.16
2	−1.44	−0.03	+1.45
3	−3.97	−0.20	+4.05
4	−7.69	−0.79	+7.92
8	−32.42	−17.43	+15.94
	Flexural vibration of a five-element cantilever beam		
1	−1.80	−0.91	0.00
2	−5.90	−3.07	+0.05
3	−9.31	−5.03	+0.36
4	−13.62	−7.69	+1.17
10	Unavailable	+91.77	+67.83

With h a measure of element length, it has been found that lumped and consistent mass formulations for the bar element each provide natural frequency errors of order h^2 (in opposite directions) and that the average formulation provides error of order h^4 [2.13]. Thus the convergence rate with mesh refinement is much faster when the average formulation is used. A similar improvement is possible with the beam element [2.13].

HRZ Lumping. The name "HRZ" identifies the authors of the procedure [11.8]. It is an ad hoc method but appears to be quite successful. The essential idea is to compute only diagonal terms of the consistent element mass matrix, then scale them so as to preserve the total element mass. The result is a diagonal mass matrix. Recognizing that there may be both translational and rotational d.o.f., which may describe motion in one, two, or three coordinate directions, the following steps might be followed for an element of total mass m.

1. Compute only diagonal coefficients m_{ii} of the consistent element mass matrix.
2. For each coordinate direction in which motion is described by the element d.o.f.:
   a. Determine a number s by adding the m_{ii} associated with translational d.o.f. (but not rotational d.o.f.).
   b. Multiply *all* coefficients m_{ii} associated with this direction by the ratio m/s.

Applying this procedure to [**m**] of the bar element, Eq. 11.3-4, we obtain [**m**] of Eq. 11.3-1. From [**m**] of the beam element, Eq. 11.3-5, we obtain the HRZ lumping

$$[\mathbf{m}] = m\lceil 1/2 \quad L^2/78 \quad 1/2 \quad L^2/78 \rfloor \tag{11.3-8}$$

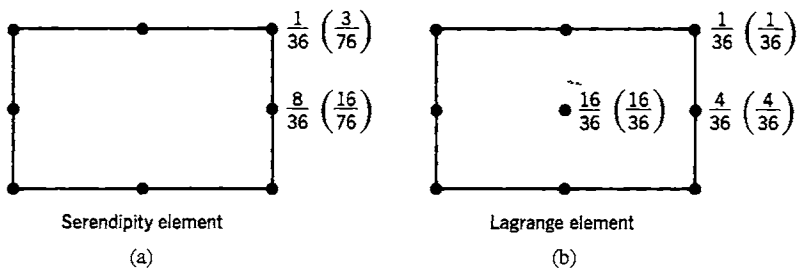

Figure 11.3-2. Rectangular plane elements, showing the fraction of total element mass associated with diagonal terms m_{ii} in HRZ lumping. First number: based on 2 by 2 Gauss quadrature. Second number (in parentheses): based on 3 by 3 Gauss quadrature.

Examples of HRZ lumping for plane elements having no rotational d.o.f. appear in Fig. 11.3-2.

Computed vibration frequencies of a plate appear in Table 11.3-2 [11.8]. Elements have eight nodes each, and each node has one lateral translational d.o.f. and two rotational d.o.f. The ad hoc lumping used consists of equal mass particles at each element node. Half the plate was modeled, using a 4 by 2 mesh of square elements. In the "modes" column, l_w and n_w are the number of half-waves in each direction over the entire plate.

Optimal Lumping. Mass lumping can be regarded as the result of using an appropriate quadrature rule to evaluate $\int \rho\, [\mathbf{N}]^T [\mathbf{N}]\, dV$. If integration points coincide with nodes of an element having translational d.o.f. only, then no off-diagonal terms are generated, so the resulting mass matrix is diagonal. If rotational d.o.f. are also present, blocks of terms appear along the diagonal. In what follows we consider elements having translational d.o.f. only.

TABLE 11.3-2. PERCENTAGE ERRORS OF COMPUTED NATURAL FREQUENCIES FOR LATERAL VIBRATION OF A SIMPLY SUPPORTED THICK SQUARE PLATE, USING DIFFERENT MASS MATRICES [11.8]. REDUCED INTEGRATION WAS USED TO OBTAIN ELEMENT STIFFNESS MATRICES.

Mode		Type of mass matrix used		
l_w	n_w	Ad hoc lumping (%)	HRZ lumping (%)	Consistent [**m**] (%)
1	1	+0.32	+0.32	−0.11
2	1	−0.45	+0.45	−0.40
2	2	−4.12	−2.75	−0.35
3	1	−5.75	+0.05	+5.18
3	2	−10.15	−2.96	+4.68
3	3	−19.42	−5.18	+13.78
4	2	+31.70	+1.53	+16.88

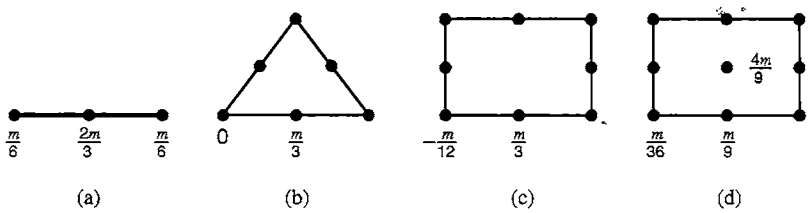

Figure 11.3-3. Optimal mass lumping for a uniform bar element, a triangular element, and two rectangular elements [11.11]. The total element mass of each element is m. Plane elements have uniform density and thickness.

Let p be the degree of the highest-order complete polynomial contained in $[\mathbf{N}]$ and m_d the highest-order derivative in the strain energy expression ($m_d = 1$ for elasticity, $m_d = 2$ for bending). It has been shown that a quadrature rule with degree of precision at least $2(p - m_d)$ will provide comparable accuracy and no loss in convergence rate relative to use of the consistent mass matrix [11.9,11.10]. A diagonal mass matrix integrated in this way is said to be *optimally lumped.*

As an example of optimal lumping, consider the three-node bar element shown in Fig. 6.1-1, for which $p = 2$ and $m_d = 1$. Let the element be uniform and have uniformly spaced nodes. The minimum order of integration for optimal lumping is $n = 2(2 - 1) = 2$. Simpson's integration rule is appropriate, as it has cubic precision, which is more than is required, and it has sampling points coincident with element nodes. In numerical integration, shape function products N_iN_j are zero when $i \neq j$; that is, when i and j designate different nodes. Therefore, the mass matrix is diagonal, and an element of total mass m has diagonal entries $m/6$ for end nodes and $2m/3$ for the center node (Fig. 11.3-3a).

Nodes of Lagrangian elements coincide with sampling points of the Lobatto quadrature rule [2.13]. Results for the plane quadratic Lagrange element are shown in Fig. 11.3-3d. Additional results appear in [11.11]. In higher-order Lagrange elements, nodal masses are positive but nodes must be at special positions in the element. For other element types, optimal lumping may produce zero or negative nodal masses. Sometimes HRZ and optimal lumpings are the same; this is the case for the quadratic Lagrange element, as seen in Figs. 11.3-2b and 11.3-3d. For higher-order elements, HRZ and optimal lumpings differ, but such elements are rarely used in structural dynamics. For all elements in Fig. 11.3-3, the fractional mass allocation is the same as the fractional load allocation for uniformly distributed axial load or uniform surface pressure (Fig. 3.11-3).

Remarks. With any mass matrix, the product $[\mathbf{m}]\{\ddot{\mathbf{d}}\}$ must provide the correct total force on an element according to Newton's second law $\mathbf{F} = m\mathbf{a}$ when $\{\ddot{\mathbf{d}}\}$ represents a rigid-body translational acceleration. This is the only motion experienced by an element if the mesh has been indefinitely refined.

A consistent mass matrix is positive definite. A lumped mass matrix is positive semidefinite or indefinite if zero or negative masses, respectively, appear on its diagonal. Zeros on the diagonal may or may not make analysis awkward, depending on the algorithm, and negative masses usually require special solution algorithms.

If the FE mesh correctly represents the structure volume and geometry, elements are compatible and their stiffnesses not softened by low-order integration rules, and mass matrices are consistent, then computed natural frequencies are upper bounds to exact frequencies

of the mathematical model. If any of these restrictions is violated, a bound cannot be guaranteed [5.1]. Thus in Table 11.3-2, where stiffness matrices are evaluated using reduced integration, we see that not even the consistent mass matrix always produces an upper bound.

With consistent mass matrices, the order of error of natural frequencies is $O(h^{2(p+1-m)})$ where, as in Section 9.6, h is a linear measure of element size, p is the degree of the highest-order complete polynomial in the approximating displacement field, and $2m$ is the highest-order displacement derivative in the governing differential equation [2.13]. For a two-node bar element, $p + 1 - m = 1 + 1 - 1 = 1$; for a standard cubic beam element, $p + 1 - m = 3 + 1 - 2 = 2$. Thus with consistent $[\mathbf{m}]$ and a mesh that is not too coarse, doubling the number of elements by uniform mesh refinement reduces frequency errors by factors of 4 for bars and 16 for beams.

Elements integrated by one-point quadrature require stabilization, as summarized in Section 6.8. An assembly of such elements may contain nonphysical modes of lower frequency than the realistic modes, depending on how stabilization is accomplished and what mass matrix is used. This defect can produce misleading results in vibration analysis and in response history analysis. One way to address the problem is to devise a mass matrix such that no kinetic energy is associated with nonphysical modes, so that nonphysical modes are shifted to the high end of the natural frequency spectrum [11.12].

Neither the lumped nor the consistent formulation is best for all problems. Consistent mass matrices are more accurate for flexural problems, such as beams and plates, and can bound frequencies from above, as previously noted. Lumped mass matrices usually, but not always, underestimate natural frequencies. In wave propagation problems, lumped masses provide greater accuracy because of fewer spurious oscillations. Lumped mass matrices are simpler to form and require less storage space. Some algorithms become prohibitively expensive unless $[\mathbf{M}]$ is lumped, while others accommodate a consistent $[\mathbf{M}]$ with very little added expense. The need for economy is much greater in response history analysis than in vibration analysis.

Throughout this section we have considered only the mass of elements themselves. Commonly there is also nonstructural mass that may exceed the structural mass. Nonstructural mass may be present in the form of attached machinery, snow, and so on. An attached machine might be modeled as a rigid mass or even a mass particle, while snow constitutes a distributed mass. A surrounding fluid such as water contributes added mass as described in Section 12.8, and also contributes to damping.

11.4 NATURAL FREQUENCIES AND MODES

We first review vibration of a simple spring-mass system, with and without damping. Next, undamped vibration of multiple-d.o.f. FE structures is discussed. Damping is considered further in Section 11.5, and is included in modal methods for analysis of response history and harmonic response, which are discussed in Sections 11.7 and 11.10.

Single-d.o.f. Free Vibration. "Free" vibration means that load r in Fig. 11.2-1 is zero. If there is no damping, motion is described by $u = \bar{u} \sin \omega t$, where $\bar{u}$ is the amplitude of vibration and ω is its *circular frequency* (radians per second). The *cyclic frequency* is $f = \omega/2\pi$ (Hertz; cycles per second) and the *period* is $T = 1/f$ (seconds). Substitution of $c = 0$, $r = 0$, and $u = \bar{u} \sin \omega t$ into Eq. 11.2-1 yields

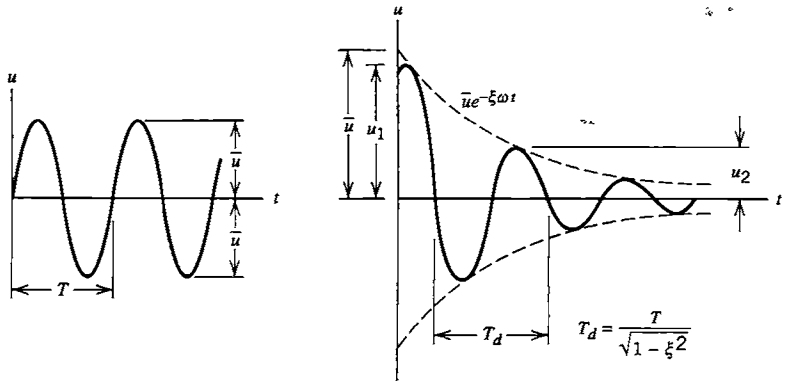

Figure 11.4-1. (a) Undamped free vibration. (b) Damped free vibration, with $c < c_c$.

$$k\bar{u}\ \sin \omega t - m\bar{u}\,\omega^2 \sin \omega t = 0 \qquad \text{from which} \qquad \omega = \sqrt{k/m} \tag{11.4-1}$$

In general, natural frequencies are independent of amplitude if conditions remain linearly elastic, gaps do not open or close, and amplitudes are small in comparison with structural dimensions so that geometric nonlinearity does not appear.

If damping is present ($c \neq 0$ in Eq. 11.2-1), basic vibration theory shows that there is a "critical" value $c_c = 2m\sqrt{k/m}$. If $c > c_c$, motion decays without oscillation; if $c < c_c$, the motion is oscillatory, and decays with time as shown in Fig. 11.4-1b. For $c < c_c$, the damped vibration frequency ω_d is less than the natural frequency $\omega = \sqrt{k/m}$; specifically

$$\omega_d = \omega\sqrt{1-\xi^2} \qquad \text{where} \qquad \xi = \frac{c}{c_c} \qquad \text{and} \qquad c_c = 2m\sqrt{k/m} = 2m\omega \tag{11.4-2}$$

where ξ, the fraction of critical damping, is called the *damping ratio.* Structural damping is usually small – typically $\xi < 0.15$ – so that $\omega_d \approx \omega$. For small damping, the ratio of any two consecutive displacement peaks, u_2/u_1 in Fig. 11.4-1b, is related to ξ by the equation $\delta = \ln(u_2/u_1) \approx -2\pi\xi$, where δ is called the *logarithmic decrement.* Thus the amplitude of motion is reduced by about half in one cycle of damped free vibration if $\xi = 0.10$, and reduced about 10% per cycle if $\xi = 0.02$. Damping is considered in more detail in Section 11.5.

For subsequent use (Section 11.7), we divide Eq. 11.2-1 by mass m and make use of Eqs. 11.4-2. Thus

$$\ddot{u} + \frac{c}{m}\dot{u} + \frac{k}{m}u = \frac{r}{m} \qquad \text{becomes} \qquad \ddot{u} + 2\xi\omega\dot{u} + \omega^2 u = \frac{r}{m} \tag{11.4-3}$$

Undamped Multiple-d.o.f. Free Vibration. We ask for natural frequencies of vibration and their associated modes, without regard to which of them may be important in application or how motion is initiated. Without damping, all d.o.f. move in phase with one another and at the same frequency ω. Vibratory motion consists of nodal amplitudes $\{\bar{\mathbf{D}}\}$ that vary sinusoidally with time relative to static equilibrium displacements $\{\mathbf{D}_{st}\}$ produced by time-independent loads. If these loads are zero, then $\{\mathbf{D}_{st}\} = \{\mathbf{0}\}$ and $\{\bar{\mathbf{D}}\}$ rep-

resents excursions from the unstressed configuration. Otherwise vibration produces displacements and stresses that are superposed on displacements and stresses associated with static load. Natural frequencies in a linear problem are independent of $\{\mathbf{D}_{st}\}$. However, nonstructural mass that may be associated with static loads must be represented in $[\mathbf{M}]$. Nodal displacements and accelerations associated with vibration are

$$\{\mathbf{D}\} = \{\bar{\mathbf{D}}\} \sin \omega t \qquad \{\ddot{\mathbf{D}}\} = -\omega^2 \{\bar{\mathbf{D}}\} \sin \omega t \tag{11.4-4}$$

With damping matrix $[\mathbf{C}]$ omitted, Eqs. 11.2-12 and 11.4-4 yield the eigenproblem

$$\text{Undamped free vibration:} \quad \Big([\mathbf{K}] - \omega^2 [\mathbf{M}] \Big) \{\bar{\mathbf{D}}\} = \{\mathbf{0}\} \tag{11.4-5}$$

where ω^2 is an eigenvalue, and ω is a natural frequency. Matrix $[\mathbf{K}] - \omega^2[\mathbf{M}]$ is called a *dynamic stiffness matrix.* A physical interpretation of vibration comes from writing Eq. 11.4-5 in the form $[\mathbf{K}]\{\bar{\mathbf{D}}\} = \omega^2[\mathbf{M}]\{\bar{\mathbf{D}}\}$. It says that a vibration mode is a configuration in which elastic resistances are in balance with inertia loads.

Let $\{\bar{\mathbf{D}}\}$ contain only d.o.f. that may assume nonzero values after all rigid-body modes and mechanisms (if any) are suppressed. Thus $[\mathbf{K}]$ is positive definite. If element mass matrices are consistent, or lumped with strictly positive diagonal coefficients, $[\mathbf{M}]$ is also positive definite. Then the number of nonzero ω_i is equal to the number of d.o.f. in $\{\bar{\mathbf{D}}\}$. Occasionally two or more ω_i are numerically equal. Then their associated vibration modes $\{\bar{\mathbf{D}}\}_i$ are not unique, but mutually orthogonal modes for the repeated ω_i can be established [2.14]. A partly or completely unconstrained structure, or a structure that contains a mechanism, has a positive semidefinite $[\mathbf{K}]$ and a zero eigenvalue associated with each possible rigid-body motion or mechanism. The associated mode shape describes the rigid-body motion or the mechanism motion. If $[\mathbf{M}]$ is lumped with some zero diagonal coefficients, an infinite eigenvalue is associated with each zero M_{ii}. Degrees of freedom associated with zero M_{ii} can be removed by static condensation before extracting eigenvalues, without affecting the remaining eigenvalues and mode shapes.

Eigenproblems and solution methods are surveyed in Appendix C. The following examples illustrate calculation of natural frequencies and modes in structural mechanics (acoustic modes are discussed in Section 12.7). The eigenvalue extraction method used in these examples is suitable only for hand calculation with very few d.o.f.

Example 1. A uniform slender cantilever beam is modeled by a single element (Fig. 11.4-2). Only flexural motion in the plane of the figure is considered. Degrees of freedom at node 1 are suppressed; only d.o.f. at node 2 are active. We elect to use the consistent mass matrix, Eq. 11.3-5. The element stiffness matrix is given by Eq. 2.3-5 (and by Eq. 3.3-14). Thus we obtain

$$\left(\frac{EI}{L^3} \begin{bmatrix} 12 & -6L \\ -6L & 4L^2 \end{bmatrix} - \omega^2 \frac{m}{420} \begin{bmatrix} 156 & -22L \\ -22L & 4L^2 \end{bmatrix} \right) \begin{Bmatrix} \bar{v}_2 \\ \bar{\theta}_{z2} \end{Bmatrix} = \begin{Bmatrix} 0 \\ 0 \end{Bmatrix} \tag{11.4-6}$$

where m is the total element mass. If there is to be a solution other than $\bar{v}_2 = \bar{\theta}_{z2} = 0$, the determinant of the complete matrix that multiplies these d.o.f. must vanish; that is

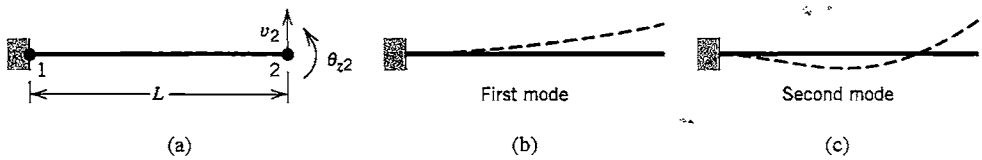

Figure 11.4-2. (a) One-element model of a cantilever beam. (b,c) Shapes of the two modes of lowest frequency.

$$\begin{vmatrix} 12-156a & -6L+22La \\ -6L+22La & 4L^2-4L^2a \end{vmatrix} = 0 \qquad \text{where} \qquad a = \frac{\omega^2 mL^3}{420EI} \tag{11.4-7}$$

Solving for a and then evaluating the latter equation for ω^2, we obtain the frequencies of modes 1 and 2 in the mathematical model.

$$\omega_1 = 3.533\left(\frac{EI}{mL^3}\right)^{1/2} \qquad \omega_2 = 34.81\left(\frac{EI}{mL^3}\right)^{1/2} \tag{11.4-8}$$

Theory of vibration for continuous systems shows that the exact multipliers of $(EI/mL^3)^{1/2}$ are 3.516 for mode 1 and 22.03 for mode 2. As expected, the approximate ω_1 is more accurate than the approximate ω_2, and use of the consistent mass matrix has produced upper bounds.

To obtain the eigenvector corresponding to a frequency ω_i by hand calculation, we first substitute ω_i into Eq. 11.4-6. Because ω_i makes the determinant of the coefficient matrix zero, one row is a constant times the other and a unique solution for $\lfloor \bar{v}_2 \;\; \bar{\theta}_{z2} \rfloor^T$ is not possible. A simple tactic is to substitute unity for one of the two d.o.f. (If applied to an arbitrary multiple-d.o.f. system, it is possible that the d.o.f. set to unity is actually zero. Then a solution will not be obtained, and another d.o.f. must be set to unity.) In the present example, for the first mode $\omega = \omega_1$ and we may set $\bar{v}_2 = 1$. Thus we obtain

$$\left(\frac{EI}{L^3}\begin{bmatrix} 12 & -6L \\ -6L & 4L^2 \end{bmatrix} - \frac{EI}{33.65L^3}\begin{bmatrix} 156 & -22L \\ -22L & 4L^2 \end{bmatrix}\right)\begin{Bmatrix} 1 \\ \bar{\theta}_{z2} \end{Bmatrix} = \begin{Bmatrix} 0 \\ 0 \end{Bmatrix}, \qquad \begin{Bmatrix} \bar{v}_1 \\ \bar{\theta}_{z2} \end{Bmatrix} = \begin{Bmatrix} 1 \\ 1.38/L \end{Bmatrix} \tag{11.4-9}$$

Similar calculation for the second mode yields $\bar{v}_2 = 1$, $\bar{\theta}_{z2} = 7.62/L$. Note that if $\{\bar{\mathbf{D}}\}_i$ is an eigenvector, so is $c\{\bar{\mathbf{D}}\}_i$, where c is a positive or negative constant. Hence any $\{\bar{\mathbf{D}}\}_i$ can be normalized (scaled), perhaps to satisfy Eq. C.3-13 of Appendix C. Mode shapes are shown by dashed lines in Fig. 11.4-2. These lines show only one extreme position; the other is obtained by reversing the algebraic signs of all d.o.f. Software graphics may be able to display only straight lines between nodes, and so may plot a straight line for both modes.

If particle masses are used, mass $m/2$ is associated with d.o.f. $\bar{v}_2$ only, so $[\mathbf{m}] = \lceil m/2 \;\; 0 \rfloor$. With this modification, $\omega_2 = \infty$, the second of Eqs. 11.4-6 yields $\bar{\theta}_{z2} = 3\bar{v}_2/2L$, and the first equation yields $\omega_1 = 2.45\sqrt{EI/mL^3}$. HRZ lumping, Eq. 11.3-8, fares even worse for ω_1 in this example, giving $\omega_1 = 2.38\sqrt{EI/mL^3}$ and $\omega_2 = 18.2\sqrt{EI/mL^3}$.

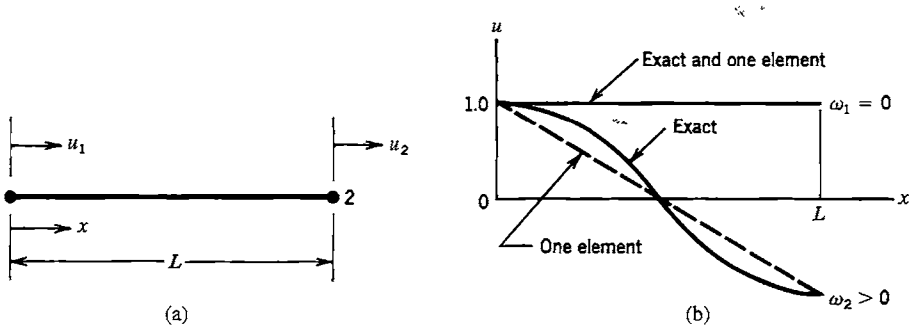

Figure 11.4-3. (a) Unsupported two-d.o.f. uniform bar. (b) Modes for $\omega_1 = 0$ (rigid-body translation) and $\omega_2 > 0$ (axial straining mode).

Example 2. Consider axial vibration of the unsupported one-element bar of mass m shown in Fig. 11.4-3. We elect to use the consistent mass matrix, Eq. 11.3-4. The eigenvalue problem, and the statement that the determinant of the expression in parentheses must vanish, are

$$\left(\frac{AE}{L}\begin{bmatrix} 1 & -1 \\ -1 & 1 \end{bmatrix} - \omega^2 \frac{m}{6}\begin{bmatrix} 2 & 1 \\ 1 & 2 \end{bmatrix}\right)\begin{Bmatrix} \bar{u}_1 \\ \bar{u}_2 \end{Bmatrix} = \begin{Bmatrix} 0 \\ 0 \end{Bmatrix} \qquad \text{and} \qquad \omega^2\left(m\omega^2 - 12AE/L\right) = 0 \tag{11.4-10}$$

Two eigenvalues and two eigenvectors can be computed by the same methods used in Example 1. Thus

First mode: Second mode:

$$\omega_1 = 0, \quad \begin{Bmatrix} \bar{u}_1 \\ \bar{u}_2 \end{Bmatrix} = \begin{Bmatrix} 1 \\ 1 \end{Bmatrix} \qquad \omega_2 = 3.464\sqrt{AE/mL}, \quad \begin{Bmatrix} \bar{u}_1 \\ \bar{u}_2 \end{Bmatrix} = \begin{Bmatrix} 1 \\ -1 \end{Bmatrix} \tag{11.4-11}$$

The first mode is rigid-body translation and is computed exactly. The exact frequency of the second mode is $\omega_2 = \pi\sqrt{AE/mL}$. If instead we use lumped masses, [**m**] in Eq. 11.4-10 becomes the diagonal mass matrix $m\lceil 1/2 \quad 1/2 \rfloor$, and we obtain $\omega_1 = 0$ and $\omega_2 = 2\sqrt{AE/mL}$. Frequency ω_2 is not an upper bound.

Rayleigh Quotient. Let Eq. 11.4-5 be premultiplied by $\{\bar{\mathbf{D}}\}^T$. Thus for any mode i

$$\{\bar{\mathbf{D}}\}_i^T[\mathbf{K}]\{\bar{\mathbf{D}}\}_i = \omega_i^2\{\bar{\mathbf{D}}\}_i^T[\mathbf{M}]\{\bar{\mathbf{D}}\}_i \tag{11.4-12}$$

This equation can be regarded as stating that, in any mode i, twice the maximum strain energy (when displacement is greatest and velocity is zero) equals twice the maximum kinetic energy (when velocity is greatest and displacement is zero). Solution of Eq. 11.4-12 for ω_i^2 yields

$$\text{Rayleigh quotient:} \qquad \omega_i^2 = \frac{\{\bar{\mathbf{D}}\}_i^T[\mathbf{K}]\{\bar{\mathbf{D}}\}_i}{\{\bar{\mathbf{D}}\}_i^T[\mathbf{M}]\{\bar{\mathbf{D}}\}_i} \tag{11.4-13}$$

It can be shown [2.14] that when an approximation for $\{\bar{\mathbf{D}}\}_i$ is used, the maximum and minimum ω_i values provided by the Rayleigh quotient are respectively less than the exact maximum ω of the mathematical model and greater than its exact minimum ω. Also, if $\{\bar{\mathbf{D}}\}_i$ approximates an exact eigenvector with first-order error, the Rayleigh quotient provides an ω_i that has only second-order error. Finally, the Rayleigh quotient is stationary (typically a relative maximum or minimum) when $\{\bar{\mathbf{D}}\}_i$ varies in the neighborhood of an exact eigenvector [5.1].

Remarks. Eigenvectors that correspond to different frequencies are orthogonal with respect to both stiffness and mass matrices; that is

$$\{\bar{\mathbf{D}}\}_i^T[\mathbf{K}]\{\bar{\mathbf{D}}\}_j = 0 \quad \text{and} \quad \{\bar{\mathbf{D}}\}_i^T[\mathbf{M}]\{\bar{\mathbf{D}}\}_j = 0 \quad \text{for} \quad i \neq j \tag{11.4-14}$$

The argument that provides this result appears in Appendix C. It requires that $\omega_i \neq \omega_j$. A 3D case for which $\omega_i = \omega_j$ in different modes $(i \neq j)$ is provided by a straight cantilever beam of circular cross section that lies along the x axis. Lateral vibration can take place in the xy plane or in the xz plane. A mode shape in one plane is repeated in the other, with the same frequency, but the modes are different because they appear in different planes, and eigenvectors that satisfy Eqs. 11.4-14 can be written.

In static analysis, one way to exploit symmetry is to analyze half the structure. However, mirror symmetry of structure and supports does not imply that all vibration modes are symmetric about the symmetry plane. By imposing mirror symmetry we exclude all antisymmetric modes. For this reason symmetry conditions should be used sparingly or not at all in vibration problems.

Spinning structures require special care. Tensile stress produced by rotation produces "stress stiffening" and raises natural frequencies. The effect is taken into account by a matrix that augments the conventional stiffness matrix (see Chapter 18). In some situations a "spin softening" acts to *reduce* natural frequencies (Section 18.6). Sometimes Coriolis forces are present. They multiply velocities and produce a skew-symmetric gyroscopic matrix $(G_{ij} = -G_{ji})$ that transfers energy from one mode to another. References include [11.13–11.19].

11.5 DAMPING

Damping dissipates energy, causing the amplitude of free vibration to decay with time, and limiting the amplitude of vibration produced by a loading whose frequency coincides with a natural frequency. Damping can be inherent or deliberately added, perhaps to limit peak response. Damping that influences structural dynamics can be categorized as follows.

- Viscous damping exerts force proportional to velocity, as exhibited by the term $c\dot{u}$ in Eq. 11.2-1. A formulation for this kind of damping was developed by Rayleigh [11.20]. Energy dissipated per cycle is proportional to frequency and to the square of amplitude. Viscous damping is supplied by surrounding gas or liquid or by viscous dampers added to the structure.
- Hysteresis damping, or solid damping, is inherent in the material and may result from plastic action on a very small scale, with nominal stresses in the elastic range. Energy dissipated per cycle is independent of frequency.

- Coulomb damping resembles hysteresis damping but is associated with dry friction, such as slippage in joints.
- Radiation damping refers to energy loss to a practically unbounded medium, such as soil that supports a structure [8.18]. Note that a surrounding medium also contributes mass. (Some analysis options for infinite media are noted in Section 8.8, and Section 12.7 discusses radiation damping in acoustics.)

Further discussion of structural damping appears in references such as [2.21,11.1–11.3, 11.21,11.22]. With direct time integration methods of response analysis there is also the possibility of *algorithmic damping* or *numerical dissipation,* which is artificial damping introduced by the solution algorithm (Section 11.13).

Of the foregoing kinds of physical damping, only viscous damping is easy to represent in dynamic equations. Fortunately, damping in structural problems is usually small enough that, regardless of its actual source, its effect on structural response is modeled well enough by regarding it as viscous. "Small enough" usually means that damping forces $[\mathbf{C}]\{\dot{\mathbf{D}}\}$ are less than roughly 10% of the other forces in Eq. 11.2-11 or 11.2-12. Such is the case for the majority of structures loaded in the elastic range.

Two devices commonly used to represent viscous damping are called *proportional damping* and *modal damping*. Either is a computationally convenient choice, unless damping characteristics are different in different parts of the structure [11.1,11.3].

Proportional Damping. This device, also known as *Rayleigh damping,* defines the global damping matrix $[\mathbf{C}]$ as a linear combination of the global mass and stiffness matrices.

$$[\mathbf{C}] = \alpha[\mathbf{M}] + \beta[\mathbf{K}] \tag{11.5-1}$$

This equation makes damping frequency-dependent, as shown in Fig. 11.5-1. For a single-d.o.f. system, Eq. 11.4-3, proportional damping becomes $c = \alpha m + \beta k$, which yields the fraction of critical damping.

$$\frac{1}{m}(\alpha m + \beta k) = 2\xi\omega \qquad \text{hence} \qquad \xi = \frac{1}{2}\left(\frac{\alpha}{\omega} + \beta\omega\right) \tag{11.5-2}$$

By selecting a design spectrum, identified as the frequency range of interest in Fig. 11.5-1, and choosing values of the desired ξ at points 1 and 2, we obtain from Eq. 11.5-2

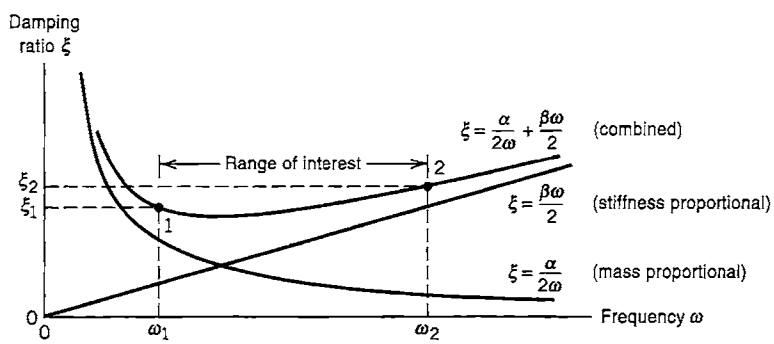

Figure 11.5-1. Fraction of critical damping for the proportional-damping scheme.

$$\begin{aligned} \alpha &= 2\omega_1\omega_2(\xi_1\omega_2 - \xi_2\omega_1)/(\omega_2^2 - \omega_1^2) \\ \beta &= 2(\xi_2\omega_2 - \xi_1\omega_1)/(\omega_2^2 - \omega_1^2) \end{aligned} \tag{11.5-3}$$

An important property of proportional damping is that vibration modes are then orthogonal with respect to [**C**] (this kind of orthogonality is described in Appendix C). Therefore the set of coupled equations, Eq. 11.2-12, can be transformed to a set of uncoupled equations, as described in Section 11.7.

The α[**M**] contribution damps lowest modes most heavily, while the β[**K**] contribution damps highest modes most heavily. Proportional damping can be imagined as immersion of the structure in a nonphysical fluid whose viscosity becomes infinite for rigid-body motion of the structure ($\omega = 0$). For higher-frequency modes, viscosity acts to damp relative motion of d.o.f., with increasing effect as ω increases. Therefore the β[**K**] term may be used to damp nonphysical high-frequency vibrations (noise) from response simulations. Noise may also be reduced by modal damping and by algorithmic damping (Section 11.13).

Modal Damping. When dynamic equations are decoupled by the modal method, an equation having the second form in Eq. 11.4-3 appears for each individual natural frequency of the structure. Each frequency may be assigned its own value of damping ratio ξ. See Section 11.7 for details.

11.6 REDUCTION OF THE NUMBER OF D.O.F.

General Summary. Analyses in dynamics often require repeated operations, each involving the computational effort of a single static solution for a single load vector. To reduce the amount of computation, it is sometimes helpful to reduce the size of matrices being manipulated. Reduction is accomplished by using a smaller set of d.o.f. to represent the full set of d.o.f. in the FE model. The two sets of d.o.f. are related by a transformation whose form depends on how the reduced set is constructed. D.o.f. in the reduced set need not be nodal d.o.f. of the FE model. They may be generalized d.o.f., like those used in the classical Rayleigh-Ritz method. Ideally, reduction is accomplished economically, without requiring decisions of the FE user, with little sacrifice in accuracy, and in a form that is easily implemented in subsequent dynamic analysis [11.23,11.24].

Various kinds of reduction can be identified. Each can be regarded as either a way of imposing an elastic constraint or as a way of providing a "reduced basis." A *basis* is a set of linearly independent vectors that can be combined in various proportions to represent or approximate other vectors. In the context of structural vibration, "other vectors" implies the complete set of eigenvectors of the FE model. A basis is called "reduced" if it includes fewer vectors than the complete set.

Reduction can be accomplished by methods that range from intuitive to semi-rigorous. In Guyan reduction, discussed below, mass associated with some d.o.f. is ignored, and these d.o.f. are constrained to displace as dictated by elastic properties and displacements of other d.o.f. called "masters." The reduced problem contains only master d.o.f., and its vibration modes constitute a reduced basis. In solving the eigenproblem (Appendix C), the set of trial vectors used in the Lanczos and subspace iteration methods can be regarded as

a reduced basis for the entire set of eigenvectors. In the modal method of response history analysis (Section 11.7), one uses several of the lowest modes rather than the entire set. Component mode synthesis (Section 11.9) forms a reduced basis by assembling selected information from component substructures.

It is not easy to say how many d.o.f. must appear in the reduced set. Similar concerns arise in modal analysis; see Section 11.7. There should be enough d.o.f. to represent the lowest vibration modes, as they are almost certain to be important. Few d.o.f. may be needed if the loading is simple in its spatial distribution, has only low-frequency content, and only displacement response is needed. If loading has complicated spatial distribution, or is suddenly applied, more d.o.f. are needed. More d.o.f. are needed to calculate velocity response, and yet more for acceleration response. In addition to the danger that the reduced set may have too few d.o.f., it is possible that the reduced set may not be able to represent a mode in the range of interest, while adequately representing modes of both lower and higher frequencies [11.21].

Why create an FE model having a great many d.o.f., then do additional work to obtain a reduced-basis model from it? A coarse-mesh FE model may not have sufficient detail in its stiffness and mass representations. Stress calculation often requires greater detail than dynamic analysis. A detailed FE model may already be available from previous analyses for static stresses.

Guyan Reduction. In this method, d.o.f. of the FE model are designated as either *slaves* or *masters*. Slave d.o.f. are required to move as dictated by the motion of masters and the content of [**K**], with inertia ignored, as is the case in static (or quasistatic) analysis. Only masters appear in the reduced equation set, whose order is equal to the number of masters.

To describe the method, we begin with the equation of undamped free vibration, Eq. 11.4-5, partitioned according to master d.o.f. $\{\bar{\mathbf{D}}_m\}$ and slave d.o.f. $\{\bar{\mathbf{D}}_s\}$.

$$\left(\begin{bmatrix} \mathbf{K}_{mm} & \mathbf{K}_{ms} \\ \mathbf{K}_{ms}^T & \mathbf{K}_{ss} \end{bmatrix} - \omega^2 \begin{bmatrix} \mathbf{M}_{mm} & \mathbf{M}_{ms} \\ \mathbf{M}_{ms}^T & \mathbf{M}_{ss} \end{bmatrix}\right) \begin{Bmatrix} \bar{\mathbf{D}}_m \\ \bar{\mathbf{D}}_s \end{Bmatrix} = \begin{Bmatrix} \mathbf{0} \\ \mathbf{0} \end{Bmatrix} \tag{11.6-1}$$

We might solve the lower partition for $\{\bar{\mathbf{D}}_s\}$ and substitute into the upper partition, thus obtaining a smaller system that has only $\{\bar{\mathbf{D}}_m\}$ as d.o.f., but matrices of such a reduced system would be frequency-dependent. To obtain a frequency-independent transformation, Guyan [11.25] and Irons [11.26] suggested that the relation between slaves and masters be dictated *entirely by stiffness coefficients*. Accordingly, we ignore all mass coefficients in the lower partition of Eq. 11.6-1 and obtain from it

$$\{\mathbf{D}_s\} = -[\mathbf{K}_{ss}]^{-1}[\mathbf{K}_{ms}]^T\{\mathbf{D}_m\} \tag{11.6-2}$$

Overbars have been omitted in Eq. 11.6-2 because the master-slave transformation can be applied generally; its use is not restricted to eigenvalue problems. The entire set of d.o.f. is expressed in terms of masters by the equation

$$\{\mathbf{D}\} = \begin{Bmatrix} \mathbf{D}_m \\ \mathbf{D}_s \end{Bmatrix} = [\mathbf{T}]\{\mathbf{D}_m\} \qquad \text{where} \qquad [\mathbf{T}] = \begin{bmatrix} \mathbf{I} \\ -\mathbf{K}_{ss}^{-1}\mathbf{K}_{ms}^T \end{bmatrix} \tag{11.6-3}$$

where $\lceil \mathbf{I} \rfloor$ is a (diagonal) unit matrix. Physically, the jth column of $[\mathbf{T}]$ represents the static displacement of the structure when the jth master has unit displacement and all other masters have zero displacement. This displacement state is sometimes called a *constraint mode.*

Substitution of Eq. 11.6-3 into Eq. 11.4-5, followed by premultiplication by $[\mathbf{T}]^T$, yields the reduced eigenproblem.

$$\Big([\mathbf{K}_r] - \omega^2[\mathbf{M}_r]\Big)\{\bar{\mathbf{D}}_m\} = \{\mathbf{0}\} \qquad \text{where} \qquad \begin{aligned} [\mathbf{K}_r] &= [\mathbf{T}]^T[\mathbf{K}][\mathbf{T}] \\ [\mathbf{M}_r] &= [\mathbf{T}]^T[\mathbf{M}][\mathbf{T}] \end{aligned} \tag{11.6-4}$$

Similar transformation of the basic equation of structural dynamics, Eq. 11.2-12, yields

$$[\mathbf{M}_r]\{\ddot{\mathbf{D}}_m\} + [\mathbf{C}_r]\{\dot{\mathbf{D}}_m\} + [\mathbf{K}_r]\{\mathbf{D}_m\} = \{\mathbf{R}_r^{\text{ext}}\} \qquad \text{where} \qquad \begin{aligned} [\mathbf{C}_r] &= [\mathbf{T}]^T[\mathbf{C}][\mathbf{T}] \\ \{\mathbf{R}_r^{\text{ext}}\} &= [\mathbf{T}]^T\{\mathbf{R}^{\text{ext}}\} \end{aligned} \tag{11.6-5}$$

Equations 11.6-4 and 11.6-5 show that reduced mass and damping matrices are full, even if the original $[\mathbf{C}]$ and $[\mathbf{M}]$ matrices are sparse or diagonal. Therefore slaves must appreciably outnumber masters if Guyan reduction is to decrease overall cost rather than increase it. Also, because slave d.o.f. are not credited with mass, Guyan reduction produces a $[\mathbf{K}_r]$ identical to that produced by static condensation, Section 6.7. This observation may suggest an alternative to Guyan reduction: choose master d.o.f., lump masses at only these d.o.f., and reduce $[\mathbf{K}]$ by static condensation. However, this alternative is often less accurate, and requires expertise of the analyst.

If slave d.o.f. are to be recovered after solving for masters, one may use Eq. 11.6-2. For better accuracy in eigenvalue problems, one can recover slave d.o.f. of the ith mode from the lower partition of Eq. 11.6-1 with all mass coefficients retained [11.27]. Thus

$$\{\bar{\mathbf{D}}_s\}_i = -\Big[\mathbf{K}_{ss} - \omega_i^2\mathbf{M}_{ss}\Big]^{-1}\Big[\mathbf{K}_{ms}^T - \omega_i^2\mathbf{M}_{ms}^T\Big]\{\bar{\mathbf{D}}_m\}_i \tag{11.6-6}$$

The example application in Fig. 11.6-1 shows that considerable reduction of order is possible. Reduction raises frequencies of the lowest modes because of displacement constraints imposed on the full system. Usually no more than the lower half of frequencies available from the reduced system have adequate accuracy. Accuracy can be estimated by reanalysis using more masters, or perhaps fewer.

Choice of Masters. In practice, the number of masters used in Guyan reduction may range from about one-tenth to one-half the total number of d.o.f. Some guidelines for choice of masters are:

- A master should have large mass, large deflection in modes of interest, or both. Large deflection implies a large mass-to-stiffness ratio. Accordingly masters are usually d.o.f. normal to the surface of a plate or a shell rather than tangent to it, and rotational d.o.f. are usually not masters.

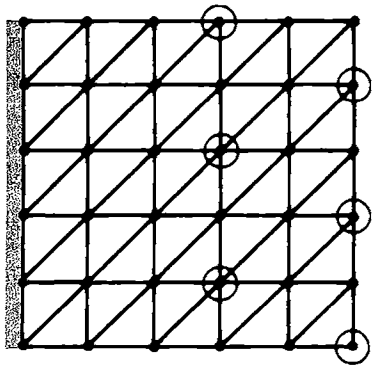

Full system, 90 d.o.f. (one displacement and two rotations at each node)	$\omega_1 = 3.469$ $\omega_2 = 8.535$ $\omega_3 = 21.450$ $\omega_4 = 27.059$
Reduced system, 6 master d.o.f. (lateral displacements at nodes circled)	$\omega_1 = 3.473$ $\omega_2 = 8.604$ $\omega_3 = 22.690$ $\omega_4 = 29.490$

Figure 11.6-1. The first four vibration frequencies of a thin, square, cantilever plate of side length a and thickness t [11.28]. The number reported is the multiplier of $\sqrt{D/\rho t a^4}$.

- Masters should not be clustered in a portion of the structure. With clustering, some modes may be poorly represented and others not represented at all.
- D.o.f. at which time-varying forces or displacements are to be prescribed should be retained as masters.

It is possible to automate the choice of masters, as described in what follows. If some choices made by software seem inappropriate or inadequate, the analyst may override or supplement them, based on good judgment and familiarity with the problem at hand.

Automatic selection of masters is based on heuristic argument. If d.o.f. with large mass-to-stiffness ratio should be masters, then d.o.f. with small mass-to-stiffness ratio should be slaves. An algorithm can scan diagonal entries in [**K**] and [**M**], searching for the d.o.f. i that has the smallest ratio M_{ii}/K_{ii}. This d.o.f. is removed by condensation, yielding reduced matrices [$\mathbf{K}_r$] and [$\mathbf{M}_r$] one order smaller than [**K**] and [**M**]. The reduced matrices are now scanned for d.o.f. with the smallest M_{rii}/K_{rii}, and the reduction process repeated, again reducing matrix order by one.. The process continues until a user-prescribed number of d.o.f. remain; these are the master d.o.f. Alternatively, if frequency content alone governs the number of masters needed, the process can be stopped when the next d.o.f. to be eliminated has a mass-to-stiffness ratio m/k such that $\sqrt{m/k}$ represents a frequency about three times the largest frequency considered important. Symbolically, the foregoing one-at-a-time reduction amounts to repeated application of the transformation in Eq. 11.6-4, although this is not a computationally efficient way to organize the manipulations. Discussion and numerical examples appear in [11.29–11.31].

Example. A one-element uniform beam is shown in Fig. 11.6-2. Nodal amplitudes of vibration are $\bar{v}_1$ and $\bar{\theta}_{z2}$. Using the conventional beam element stiffness matrix and consistent mass matrix, we obtain the eigenproblem

$$\left(\frac{EI}{L^3}\begin{bmatrix} 12 & 6L \\ 6L & 4L^2 \end{bmatrix} - \omega^2 \frac{m}{420}\begin{bmatrix} 156 & -13L \\ -13L & 4L^2 \end{bmatrix}\right)\begin{Bmatrix} \bar{v}_1 \\ \bar{\theta}_{x2} \end{Bmatrix} = \begin{Bmatrix} 0 \\ 0 \end{Bmatrix} \tag{11.6-7}$$

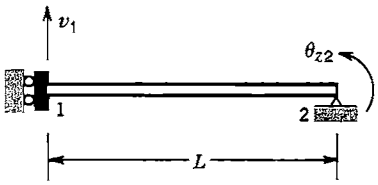

Figure 11.6-2. A uniform beam. The left end is allowed to displace but not to rotate. The right end is simply supported.

where m is the total mass of the element. For the first mode, exact results provided by beam theory, and approximate results provided by Eq. 11.6-7, are

$$\begin{array}{ll} \text{Exact, by beam theory:} & \text{Approximate, by FEA:} \\ \omega_1^2 = 6.0881EI/mL^3 & \omega_1^2 = 6.1362EI/mL^3 \\ \bar{v}_1 = 1, \quad \bar{\theta}_{z2} = -1.5708/L & \bar{v}_1 = 1, \quad \bar{\theta}_{z2} = -1.5704/L \end{array} \tag{11.6-8}$$

For Guyan reduction, we elect $\bar{v}_1$ as master and $\bar{\theta}_{z2}$ as slave, in accord with the guidelines. Using Eqs. 11.6-3 and 11.6-4, with $K_{ss} = 4EI/L$ and $K_{ms} = 6EI/L^2$, we obtain

$$[\mathbf{T}] = \begin{bmatrix} 1 \\ -3/2L \end{bmatrix} \quad \text{and} \quad \left(\frac{3EI}{L^3} - \omega_1^2 \frac{204m}{420}\right)\bar{v}_1 = 0 \tag{11.6-9}$$

from which the fundamental frequency is $\omega_1^2 = 6.1765EI/mL^3$. As expected, this result is higher than the approximate frequency in Eq. 11.6-8. With $\bar{v}_1$ set to unity, recovery of $\bar{\theta}_{z2}$ from Eqs. 11.6-2 and 11.6-6 respectively yields the mode shapes

$$\bar{v}_1 = 1, \; \bar{\theta}_{z2} = -1.5000/L \quad \text{and} \quad \bar{v}_1 = 1, \; \bar{\theta}_{z2} = -1.5709/L \tag{11.6-10}$$

A more accurate frequency than the approximate value in Eq. 11.6-8 can be obtained by substituting $\{\bar{\mathbf{D}}\} = \lfloor 1 \quad -1.5709/L \rfloor^T$ into the Rayleigh quotient, Eq. 11.4-13, with $[\mathbf{K}]$ and $[\mathbf{M}]$ taken from Eq. 11.6-7. The result is $\omega_1^2 = 6.1362EI/mL^3$, as is also obtained from Eq. 11.6-7 without reduction. Note that the Rayleigh quotient would provide no improvement if we were to use the first of Eqs. 11.6-10, so that $\{\bar{\mathbf{D}}\} = \lfloor 1 \quad -1.5000/L \rfloor^T$.

For this problem, we can obtain a fundamental frequency based on a particle-lumped $[\mathbf{m}]$ without formal use of FEA. We place a particle mass $m_1 = m/2$ at node 1. The lateral stiffness coefficient associated with node 1 is obtained by applying a lateral force F_1 at node 1, using beam theory to obtain the resulting lateral displacement $v_1 = F_1L^3/3EI$, from which the lateral stiffness coefficient at node 1 is $K_1 = F_1/v_1 = 3EI/L^3$. Hence the lumped-mass fundamental frequency is $\omega_1^2 = K_1/m_1 = 6EI/mL^3$. Note that this result is not an upper bound.

11.7 RESPONSE HISTORY: MODAL METHODS

Response History. The question posed is this: given a loading of known distribution in space and known variation with time, what is the resulting motion? That is, what are the accelerations, velocities, and displacements of d.o.f. as functions of time? Modal methods, and related Ritz vector methods, answer the question by using an alternative (and reduced)

set of d.o.f., solving for these d.o.f. as functions of time, then transforming back to the original physical d.o.f. Direct integration methods answer the question by retaining the original d.o.f. and integrating the equations of motion using time increments Δt. In practice, methods may be combined, as by using a direct method to integrate the reduced equation set of a modal method. Discussion of methods for calculating response history begins in this section and continues in Sections 11.8 and 11.11 to 11.14.

Modal Equations. Let each eigenvector $\{\bar{\mathbf{D}}\}_i$ of Eq. 11.4-5 be normalized with respect to the mass matrix; that is, scaled so that the denominator of the Rayleigh quotient, Eq. 11.4-13, is unity. Thus

$$\text{if} \quad \{\bar{\mathbf{D}}\}_i^T [\mathbf{M}]\{\bar{\mathbf{D}}\}_i = 1 \quad \text{then} \quad \{\bar{\mathbf{D}}\}_i^T [\mathbf{K}]\{\bar{\mathbf{D}}\}_i = \omega_i^2 \tag{11.7-1}$$

We define a *modal matrix* $[\mathbf{\Phi}]$ whose columns are the eigenvectors, normalized with respect to the mass matrix, and a diagonal *spectral matrix* $\lceil \boldsymbol{\omega}^2 \rfloor$ whose entries are the squared natural frequencies of vibration.

$$[\mathbf{\Phi}] = [\bar{\mathbf{D}}_1 \quad \bar{\mathbf{D}}_2 \quad \cdots \quad \bar{\mathbf{D}}_n] \qquad \lceil \boldsymbol{\omega}^2 \rfloor = \lceil \omega_1^2 \quad \omega_2^2 \qquad \omega_n^2 \rfloor \tag{11.7-2}$$

where n is the total number of d.o.f. not suppressed by boundary conditions or constraints. In Section C.3 of Appendix C it is shown that $\{\bar{\mathbf{D}}\}_i^T [\mathbf{M}]\{\bar{\mathbf{D}}\}_j = 0$ and $\{\bar{\mathbf{D}}\}_i^T [\mathbf{K}]\{\bar{\mathbf{D}}\}_j = 0$ when $i \neq j$; that is when $\{\bar{\mathbf{D}}\}_i$ and $\{\bar{\mathbf{D}}\}_j$ are eigenvectors of different modes. Therefore, from Eqs. 11.7-1 and 11.7-2,

$$[\mathbf{\Phi}]^T[\mathbf{M}][\mathbf{\Phi}] = \lceil \mathbf{I} \rfloor \qquad \text{and} \qquad [\mathbf{\Phi}]^T[\mathbf{K}][\mathbf{\Phi}] = \lceil \boldsymbol{\omega}^2 \rfloor \tag{11.7-3}$$

where $\lceil \mathbf{I} \rfloor$ is a unit matrix. An arbitrary displacement vector $\{\mathbf{D}\}$ can be expressed as a linear combination of the eigenvectors; that is, as $\{\mathbf{D}\} = \{\bar{\mathbf{D}}\}_1 Z_1 + \{\bar{\mathbf{D}}\}_2 Z_2 + \cdots + \{\bar{\mathbf{D}}\}_n Z_n$. Thus

$$\{\mathbf{D}\} = [\mathbf{\Phi}]\{\mathbf{Z}\} \qquad \{\dot{\mathbf{D}}\} = [\mathbf{\Phi}]\{\dot{\mathbf{Z}}\} \qquad \{\ddot{\mathbf{D}}\} = [\mathbf{\Phi}]\{\ddot{\mathbf{Z}}\} \tag{11.7-4}$$

The Z_i are generalized d.o.f., often called *modal coordinates* or *modal displacements*. They define the fraction of each eigenvector that contributes to $\{\mathbf{D}\}$. We propose to calculate the Z_i as functions of time, then use Eqs. 11.7-4 to obtain $\{\mathbf{D}\}$ as a function of time. Because of the modal combination expressed by Eqs. 11.7-4, the modal method is often called *mode superposition.*

For the time being we retain all n d.o.f. in the equations. By substituting Eqs. 11.7-4 into Eqs. 11.2-12, premultiplying by $[\mathbf{\Phi}]^T$, and taking note of Eqs. 11.7-3, we obtain

$$\{\ddot{\mathbf{Z}}\} + [\mathbf{C}_\Phi]\{\dot{\mathbf{Z}}\} + \lceil \boldsymbol{\omega}^2 \rfloor\{\mathbf{Z}\} = \{\mathbf{R}_\Phi\} \qquad \text{where} \qquad \{\mathbf{R}_\Phi\} = [\mathbf{\Phi}]^T\{\mathbf{R}^{\text{ext}}\} \tag{11.7-5}$$

If the proportional damping of Eq. 11.5-1 is used, $[\mathbf{C}_\Phi]$ is the *diagonal* matrix $[\mathbf{C}_\Phi] = \alpha\lceil \mathbf{I} \rfloor + \beta\lceil \boldsymbol{\omega}^2 \rfloor$. More often, the modal method uses *modal* damping, which is another representation of viscous damping that has as much (or as little) physical justification as proportional damping. To obtain modal damping we arbitrarily define $[\mathbf{C}_\Phi]$ in Eq. 11.7-5 as a diagonal matrix whose ith diagonal coefficient is $2\xi_i\omega_i$, where ξ_i is the damping ratio

for mode i prescribed by the analyst. Thus it becomes possible to use an appropriate or experimentally-determined ξ_i for each mode, or to selectively damp higher modes.

Because the damping matrix and $\lceil \boldsymbol{\omega}^2 \rfloor$ are both diagonal, Eqs. 11.7-5 are *uncoupled.* With modal damping, the generic equation for any mode i is

$$\ddot{Z}_i + 2\xi_i\omega_i\dot{Z}_i + \omega_i^2 Z_i = P_i \qquad \text{where} \qquad P_i = \{\boldsymbol{\Phi}\}_i^T\{\mathbf{R}^{\text{ext}}\} \tag{11.7-6}$$

Here $\{\boldsymbol{\Phi}\}_i$ is the ith column of $[\boldsymbol{\Phi}]$. Thus $\{\boldsymbol{\Phi}\}_i$ is the ith eigenvector $\{\bar{\mathbf{D}}\}_i$, scaled so that the first of Eqs. 11.7-1 is satisfied. Modal load P_i is therefore a known function of time. Equation 11.7-6 has the same form as Eq. 11.4-3, which is derived for a single-d.o.f. system. For each i, Eq. 11.7-6 must be integrated in time. Exact integration is possible for some kinds of loading [11.1–11.3]. For general loading, direct integration as described in Section 11.13 can be used. Initial conditions are needed to begin integration. They are obtained by inverting Eqs. 11.7-4. If the first of Eqs. 11.7-3 is postmultiplied by $[\boldsymbol{\Phi}]^{-1}$, we see that $[\boldsymbol{\Phi}]^{-1} = [\boldsymbol{\Phi}]^T[\mathbf{M}]$. Therefore

$$\{\mathbf{Z}\} = [\boldsymbol{\Phi}]^T[\mathbf{M}]\{\mathbf{D}\} \qquad \{\dot{\mathbf{Z}}\} = [\boldsymbol{\Phi}]^T[\mathbf{M}]\{\dot{\mathbf{D}}\} \tag{11.7-7}$$

from which $\{\mathbf{Z}\}$ and $\{\dot{\mathbf{Z}}\}$ at time $t = 0$ can be determined from known values of $\{\mathbf{D}\}$ and $\{\dot{\mathbf{D}}\}$ at time $t = 0$.

If the structure is partly or completely unconstrained, up to the first six columns of modal matrix $[\boldsymbol{\Phi}]$ are rigid-body modes, which activate no elastic forces in the physical structure. If these modes have no damping, which is the usual case, Eq. 11.7-6 becomes simply $\ddot{Z}_i = P_i$ for rigid-body motion. If desired, this contribution to total response can be evaluated separately from the deformation response [11.1].

Reduction of Order. With all n modes retained, Eqs. 11.7-6 are a mathematically exact representation of Eqs. 11.2-12. Only the form has been changed. The benefit of modal analysis is that, for many practical problems, *only the lowest portion of the eigenspectrum need be retained.* Thus in place of Eqs. 11.7-4 we write

$$\{\mathbf{D}\} \approx \sum_{i=1}^{m} \{\boldsymbol{\Phi}\}_i Z_i \qquad \text{where } \{\mathbf{D}\} \text{ and } \{\boldsymbol{\Phi}\}_i \text{ are } n\times 1 \text{ and typically } m << n \tag{11.7-8}$$

In effect, $[\boldsymbol{\Phi}]$ is used as an n by m matrix rather than as an n by n matrix, so that its first few columns constitute a reduced basis. In many problems $m << n$ provides the required accuracy. For a structure loaded by earthquake, m may be less than 20 while n exceeds 1000. Thus the eigensolver need extract only a few frequencies and modes from Eq. 11.4-5, and Eqs. 11.7-6 are few in number. Calculation of $\{\mathbf{D}\}$ from computed Z_i according to Eq. 11.7-8 may then be called *expansion.*

A measure of the error involved in modal analysis with $m < n$ can be obtained from Eq. 11.2-12 [2.14]:

$$e(t) = \frac{\left\|\{\mathbf{R}^{\text{ext}}\} - [\mathbf{M}]\{\ddot{\mathbf{D}}\} - [\mathbf{C}]\{\dot{\mathbf{D}}\} - [\mathbf{K}]\{\mathbf{D}\}\right\|}{\left\|\{\mathbf{R}^{\text{ext}}\}\right\|} \tag{11.7-9}$$

where $\{\mathbf{D}\}$ and its time derivatives are obtained from Eq. 11.7-8, and $||\cdot||$ denotes any vector norm. The numerator is a measure of the difference between actual load and load generated by a truncated mode set. It is assumed that $\{\mathbf{R}^{\text{ext}}\} \neq \{\mathbf{0}\}$ at the instant $e(t)$ is computed. At other times, the numerator should approach zero. For the entire duration of the analysis, $e(t)$ should be small (less than 1%, as a conjecture).

The reduced mode set must include all lower modes, without omission, up to a mode with a chosen frequency. But what frequency? Perhaps double the highest important frequency contained in the loading. But this answer is simplistic, because the number of modes required depends not only on the frequency content of the loading, but also on its spatial complexity, whether results in addition to displacements are required, and with what accuracy. Modes retained must have frequencies that span the temporal variation of loading. Mode shapes of free vibration are unrelated to the complexity of loading, so enough modes must be retained to approximate displacements associated with the spatial variation of loading and such displacement derivatives as may be needed to obtain stresses. (Obviously the FE mesh must be fine enough to provide these modes and their frequencies to a good approximation.) Therefore, more modes are needed as the loading becomes more abrupt in time, more irregular in space, when bending moments and transverse shears must be calculated, and when velocities and accelerations must be computed using Eqs. 11.7-4. Further discussion appears in Section 11.16. References include [2.14,2.21,10.6,11.3,11.21].

Static Correction. With a truncated mode set, $\{\mathbf{R}_\Phi\}$ in Eq. 11.7-5 is an approximate load vector, associated with lower modes, and producing a response representable by these modes. At any instant of time, the exact load vector minus the approximate load vector is a difference vector that contains load patterns having a more complicated spatial distribution than can be represented by modes retained. If modes retained span an adequate frequency range, the difference vector would produce little velocity or acceleration if even more modes were retained. Accordingly, response to the difference vector can be calculated by static analysis, and added as a correction to dynamic response calculated by the foregoing modal method. By including the correction, the spatial distribution of load is given better representation, and accuracy is increased for a given number of modes. Or, equivalent accuracy is obtained using fewer modes.

The correction can be accomplished by any of several methods. One group of methods is called *mode acceleration methods* [11.1,11.3,11.32–11.34]. This name distinguishes them from the foregoing modal method, which may be called the *mode displacement method.* The essential idea is to transform only the acceleration and velocity terms in Eq. 11.2-12 by modal transformation, leaving a contribution to $\{\mathbf{D}\}$ to be computed as $[\mathbf{K}]^{-1}\{\mathbf{R}^{\text{ext}}\}$.

Results comparable or even identical to those provided by the mode acceleration method can be obtained by *static correction.* The method is useful in treating a loading whose spatial complexity would require many modes but whose temporal complexity can be represented by a smaller number of modes [11.3]. The method appears in more than one form [2.14,11.3,11.33–11.35]. For a simple form, consider the load term in Eq. 11.7-5, with all modes retained, and make use of the first of Eqs. 11.7-3. Thus

$$\{\mathbf{R}_\Phi\} = [\Phi]^T\{\mathbf{R}^{\text{ext}}\} = [\Phi]^T[\mathbf{M}][\Phi]\{\mathbf{R}_\Phi\} \qquad \text{hence} \qquad \{\mathbf{R}^{\text{ext}}\} = [\mathbf{M}][\Phi]\{\mathbf{R}_\Phi\} \tag{11.7-10}$$

If the truncated mode set is used, the latter equation is the approximate load vector $\{\mathbf{R}^{\text{ext}}\}_{\text{approx}}$ represented by modes retained. The static correction $\{\Delta\mathbf{D}\}$, to be added to the $\{\mathbf{D}\}$ calculated by mode superposition, is

$$[\mathbf{K}]\{\Delta\mathbf{D}\} = \{\mathbf{R}^{\text{ext}}\} - \{\mathbf{R}^{\text{ext}}\}_{\text{approx}} \quad \text{where} \quad \underset{n\times 1}{\{\mathbf{R}^{\text{ext}}\}_{\text{approx}}} = \underset{n\times n}{[\mathbf{M}]}\,\underset{n\times m}{[\mathbf{\Phi}]}\,\underset{m\times n}{[\mathbf{\Phi}]^T}\underset{n\times 1}{\{\mathbf{R}^{\text{ext}}\}} \tag{11.7-11}$$

The structure must be supported so that $[\mathbf{K}]$ in Eq. 11.7-11 is nonsingular. Matrix $[\mathbf{K}]$ need be reduced for equation-solving only once, although $\{\Delta\mathbf{D}\}$ must be computed at each instant of time for which the correction is desired. If $\{\mathbf{R}^{\text{ext}}\}$ represents a loading of fixed spatial distribution whose intensity changes with time, $\{\Delta\mathbf{D}\}$ need only be scaled from one time instant to another.

Nonlinear Problems. Material nonlinearity makes $[\mathbf{K}]$ (and possibly $[\mathbf{C}]$) time-dependent. Modal analysis according to Eqs. 11.7-1 to 11.7-8 becomes inapplicable because natural frequencies and modes cease to be independent of time and because the principle of superposition ceases to be valid. However, nonlinearity can be accommodated by taking nonlinear terms to the right hand side and incorporating them with load vector $\{\mathbf{R}^{\text{ext}}\}$. At each time step, Eqs. 11.7-4 must be applied (because physical d.o.f. are needed to update the nonlinear terms) and modal loads $\{\mathbf{R}_\Phi\}$ must be recalculated. Thus the process may resemble repeated coordinate transformation more than conventional mode superposition. This method may be appropriate when nonlinearities are neither severe nor widespread. Otherwise a direct integration method may be more appropriate. References include [11.36–11.38].

11.8 RESPONSE HISTORY: RITZ VECTORS

The modal method described in Section 11.7 has disadvantages. It incurs the computational expense of solving an eigenproblem. Eigenvectors are unrelated to the spatial distribution of applied loading, so it is hard to foresee how many of them will be needed. An eigenvector whose frequency is contained in the loading will not contribute to response if it is orthogonal to the loading.

Rather than using eigenvectors as the basis for reduction, one can use Ritz vectors constructed from the loading. Static correction, a beneficial addition to the modal method, is automatically included in Ritz vectors. The Ritz vector method is in a sense opposite to the modal method: the modal method spans the frequency content of loading but approximates its spatial distribution, while the Ritz vector method spans the spatial distribution of loading but approximates its frequency content [11.34]. In one study, Ritz vectors were generated in one-tenth the time needed to determine eigenvectors, and the overall Ritz vector method required one-third the time of modal analysis [11.39]. However, natural frequencies and modes will probably be computed anyway, to better understand structure behavior, and for use in harmonic response and response spectra analyses.

In what follows we summarize Ritz vectors in their original form [11.40]. Improvements, such as predetermining how many are needed and error analysis, are left to references [11.3,11.24,11.40,11.41].

Generation of Ritz Vectors. Consider a time-dependent external loading that can be represented as

$$\{\mathbf{R}^{\text{ext}}\} = s\{\mathbf{S}\} \tag{11.8-1}$$

where $\{\mathbf{S}\}$ describes the spatial distribution of $\{\mathbf{R}^{\text{ext}}\}$ and $s = s(t)$ is a scalar function of time that describes its amplitude. Let structural response to the loading be described by

$$\{\mathbf{D}\} = [\mathbf{W}]\{\mathbf{a}\} \qquad \{\dot{\mathbf{D}}\} = [\mathbf{W}]\{\dot{\mathbf{a}}\} \qquad \{\ddot{\mathbf{D}}\} = [\mathbf{W}]\{\ddot{\mathbf{a}}\} \tag{11.8-2}$$

where $[\mathbf{W}]$ is a matrix whose columns are Ritz vectors and $\{\mathbf{a}\}$ is a vector of generalized d.o.f. whose individual terms a_i are amplitudes of the corresponding Ritz vector. Like the truncated mode set in Eq. 11.7-8, $[\mathbf{W}]$ constitutes a reduced basis. The size of $[\mathbf{W}]$ is n by m, where n is the order of the full system and m is the number of Ritz vectors, where $m << n$ in practice.

A more complicated external loading might have to be represented by superposing two or more loads of the type $s\{\mathbf{S}\}$. For linear conditions, structural response to each such load component can be superposed with response to another component. If l components are required to represent the loading, Eq. 11.8-1 and the first of Eqs. 11.8-2 are replaced by

$$\{\mathbf{R}^{\text{ext}}\} = \sum_{j=1}^{l} s_j\{\mathbf{S}\}_j \quad \text{and} \quad \{\mathbf{D}\} = \sum_{j=1}^{l} \{\mathbf{D}\}_j = \sum_{j=1}^{l} [\mathbf{W}]_j\{\mathbf{a}\}_j \tag{11.8-3}$$

Usually l is small; indeed $l = 1$ is often used for earthquake loading. In what follows we omit subscript j, with the understanding that $\{\mathbf{S}\}$ may represent any $\{\mathbf{S}\}_j$.

With $[\mathbf{K}]$ the n by n global stiffness matrix, we apply $\{\mathbf{S}\}$ as a static load and solve for the resulting displacement vector $\{\mathbf{w}^*\}_1$. When normalized with respect to the mass matrix, $\{\mathbf{w}^*\}_1$ becomes the first Ritz vector $\{\mathbf{w}\}_1$, which is entered as the first column of $[\mathbf{W}]$. Thus

$$[\mathbf{K}]\{\mathbf{w}^*\}_1 = \{\mathbf{S}\} \qquad b^2 = \{\mathbf{w}^*\}_1^T[\mathbf{M}]\{\mathbf{w}^*\}_1 \qquad \{\mathbf{w}\}_1 = \frac{1}{b}\{\mathbf{w}^*\}_1 \tag{11.8-4}$$

With ω an arbitrary vibration frequency, $\omega^2[\mathbf{M}]\{\mathbf{w}\}_1$ represents a vector of inertia-force loads not taken into account by Eq. 11.8-4. These loads can be regarded as an error vector, and applied as a static load in order to generate the next Ritz vector, $\{\mathbf{w}\}_2$. In similar fashion $\omega^2[\mathbf{M}]\{\mathbf{w}\}_2$ can be regarded as an error vector and used to generate $\{\mathbf{w}\}_3$, and so on. By this process all Ritz vectors generated have a form excited by the particular loading applied [11.40]. To generate Ritz vectors after the first, the following calculations are performed. For $i = 2, 3, \ldots, m$,

$$[\mathbf{K}]\{\mathbf{w}^*\}_i = [\mathbf{M}]\{\mathbf{w}\}_{i-1} \qquad \text{solve for } \{\mathbf{w}^*\}_i \tag{11.8-5a}$$

$$\{\mathbf{w}^{**}\}_i = \{\mathbf{w}^*\}_i - \sum_{k=1}^{i-1} c_k\{\mathbf{w}\}_k \qquad \text{where} \qquad c_k = \{\mathbf{w}\}_k^T[\mathbf{M}]\{\mathbf{w}^*\}_i \tag{11.8-5b}$$

$$\{\mathbf{w}\}_i = \frac{1}{b}\{\mathbf{w}^{**}\}_i \qquad \text{where} \qquad b^2 = \{\mathbf{w}^{**}\}_i^T[\mathbf{M}]\{\mathbf{w}^{**}\}_i \tag{11.8-5c}$$

In Eq. 11.8-5a, note that [**K**] need be reduced for equation-solving only once, but it must be nonsingular, so the structure cannot have rigid-body modes or mechanisms. Equation 11.8-5b makes each Ritz vector orthogonal to those preceding. Explanation of this orthogonalization and remarks on possible shortcomings appear in [11.3,11.41].

Substitution of Eqs. 11.8-1 and 11.8-2 into Eq. 11.2-12, followed by premultiplication by $[\mathbf{W}]^T$, yields the reduced system

$$\{\ddot{\mathbf{a}}\} + [\mathbf{C}_a]\{\dot{\mathbf{a}}\} + [\mathbf{K}_a]\{\mathbf{a}\} = s[\mathbf{W}]^T\{\mathbf{S}\} \qquad \text{where} \qquad \begin{aligned}[\mathbf{C}_a] &= [\mathbf{W}]^T[\mathbf{C}][\mathbf{W}] \\ [\mathbf{K}_a] &= [\mathbf{W}]^T[\mathbf{K}][\mathbf{W}]\end{aligned} \tag{11.8-6}$$

in which the coefficient of $\{\ddot{\mathbf{a}}\}$ is an implied unit matrix because Ritz vectors have been made mass-matrix orthogonal. Matrices $[\mathbf{C}_a]$ and $[\mathbf{K}_a]$ are full and of order m, but m is small, so dynamic response analysis by direct integration may be economical. Alternatively, and perhaps preferably, eigenvectors of the reduced system can be extracted, and modal analysis applied to the reduced system. Eigenvectors of the original system are approximately [**W**] times eigenvectors of the reduced system.

If loading $\{\mathbf{S}\}$ is zero, as for a structure that moves freely after initial velocities $\{\dot{\mathbf{D}}\}_0$ are prescribed, Eqs. 11.8-4 fail to provide $\{\mathbf{w}\}_1$. In this case one might simply set $\{\mathbf{w}^*\}_1$ equal to $\{\dot{\mathbf{D}}\}_0$, then go to Eqs. 11.8-5.

11.9 COMPONENT MODE SYNTHESIS (CMS)

Alternative names for component mode synthesis (CMS) are *modal synthesis, substructure synthesis,* and *dynamic substructuring.* The method is analogous to static substructuring, Section 10.11, but dynamic substructuring does not preserve the full information content of the complete system. As in static analysis, motivations for use of CMS in dynamics are partly economic and partly managerial. Reduction of order may be necessary for economical computation. Substructuring becomes all the more attractive when a structural form is repeated several times. It is convenient for different design groups or organizations to work on different substructures. Redesign of one substructure does not affect component modes of others. After assembly of components, the reduced system can be used for the usual purposes of structural dynamics: calculating frequencies and modes of the complete structure, response history analysis, and so on.

Many variants of CMS are available; [2.20,11.1,11.21,11.42–11.46] are a few of the many references. Here we summarize only the Craig-Bampton method, which is the method most widely used [11.1]. Terminology is as follows.

Attachment d.o.f. are d.o.f. at nodes on lines or surfaces where substructures are connected together. *Component modes* are vibration modes of individual substructures with their attachment d.o.f. fixed. *Constraint modes* are static displacement patterns of individual substructures produced by applying a unit displacement to each attachment d.o.f. in turn while all other attachment d.o.f. are kept fixed. (Any additional d.o.f. subjected to concentrated external loading should be treated like attachment d.o.f. in these calculations.)

In brief, CMS represents the many d.o.f. of a substructure by a much smaller number of constraint modes and component modes. The process of reducing substructure matrices can be regarded as a Ritz vector transformation, similar to that of Eqs. 11.8-6. The complete structure, in reduced form, is "synthesized" by assembling substructures along shared attachment nodes, in the same way that individual finite elements are assembled by connecting them at shared nodes. D.o.f. of the synthesized structure are its attachment d.o.f. and the component modes of substructures, which play the role of internal nodeless d.o.f. The method somewhat resembles Guyan reduction, Section 11.6, but with component modes as additional generalized d.o.f. Guyan reduction as described in Section 11.6 would be inappropriate because master d.o.f. would appear along lines or surfaces of attachment d.o.f., which would cluster them unfavorably. As in static substructuring, division into substructures for CMS should be made along shorter structural dimensions, so as to reduce the number of attachment d.o.f. (Fig. 10.11-1a). *Unlike* static analysis, internal d.o.f. cannot be statically condensed, as described in Section 6.7, because their motion is determined by inertia forces as well as by elastic forces.

To obtain natural frequencies of the complete structure, we solve an eigenvalue problem of the form

$$\left([\mathbf{K}]_{\mathrm{CMS}} - \omega_i^2\,[\mathbf{M}]_{\mathrm{CMS}}\right)\{\bar{\mathbf{z}}\}_i = \{\mathbf{0}\} \tag{11.9-1}$$

where i is the mode number, square matrices are stiffness and mass matrices of the synthesized structure, and $\{\bar{\mathbf{z}}\}$ is a vector of amplitudes of component modes and attachment d.o.f. We desire that the order of $\{\bar{\mathbf{z}}\}$ be much less than the number of d.o.f. in the original structure. Because constraints are imposed to obtain Eq. 11.9-1, it yields eigenvalues higher than corresponding eigenvalues of the original FE structure, for which all d.o.f. are retained. Conceivably, all Ritz vectors used in obtaining the matrices of Eq. 11.9-1 are orthogonal to an eigenvector of the actual structure, in which case that mode will not be represented by Eq. 11.9-1. The possibility that an important lower mode will be missed becomes more remote as the number of component modes retained in analysis increases.

Formulation. Component modes of a typical substructure j are obtained by fixing all substructure attachment d.o.f. and solving the usual undamped vibration problem

$$\left([\mathbf{K}_{nn}]_j - \omega_l^2\,[\mathbf{M}_{nn}]_j\right)\{\bar{\mathbf{D}}_l\}_j = \{\mathbf{0}\} \qquad [\mathbf{\Phi}]_j = [\bar{\mathbf{D}}_1 \;\; \bar{\mathbf{D}}_2 \;\; \cdots \;\; \bar{\mathbf{D}}_k]_j \tag{11.9-2}$$

where subscript n is used to indicate those substructure d.o.f. that are not attachment d.o.f. Subscript l identifies a component (substructure) mode and k is the number of modes retained in modal matrix $[\mathbf{\Phi}]_j$. The number of modes retained is at the discretion of the analyst, but is typically much less than the number of d.o.f. in the substructure. With n non-attachment d.o.f., $[\mathbf{\Phi}]_j$ is an n by k array.

Constraint modes of substructure j are obtained by static analysis, using the stiffness matrix of the substructure with attachment d.o.f. included. Subscript a identifies attachment d.o.f., and subscript n identifies all other substructure d.o.f., which are regarded as internal d.o.f.

$$\left[\begin{array}{c|c} \mathbf{K}_{nn} & \mathbf{K}_{na} \\ \hline \mathbf{K}_{na}^T & \mathbf{K}_{aa} \end{array}\right]_j \left[\begin{array}{c} \mathbf{\Psi} \\ \hline \mathbf{I} \end{array}\right]_j = \left[\begin{array}{c} \mathbf{0} \\ \hline \mathbf{R} \end{array}\right]_j \tag{11.9-3}$$

Here $\lceil \mathbf{I} \rfloor$ is a unit matrix, of size a by a if the substructure has a attachment d.o.f. Matrix $\lceil \mathbf{I} \rfloor$ describes unit displacement of each attachment d.o.f. in turn while others are held fixed. For a unit displacement of the mth attachment d.o.f., column m of $[\mathbf{\Psi}]$ is the resulting vector of internal d.o.f., and column m of $[\mathbf{R}]$ is the resulting vector of reactions at attachment d.o.f. The upper partition of Eq. 11.9-3 yields

$$[\mathbf{\Psi}]_j = -[\mathbf{K}_{nn}]_j^{-1}\,[\mathbf{K}_{na}]_j \tag{11.9-4}$$

The transformation between original d.o.f. $\{\mathbf{D}\}_j$ of substructure j and substitute d.o.f. used for synthesis is

$$\{\mathbf{D}\}_j = \begin{Bmatrix} \mathbf{D}_n \\ \mathbf{D}_a \end{Bmatrix}_j = [\mathbf{W}]_j \begin{Bmatrix} \mathbf{a} \\ \mathbf{D}_a \end{Bmatrix}_j \qquad \text{where} \qquad [\mathbf{W}]_j = \begin{bmatrix} \mathbf{\Phi} & \mathbf{\Psi} \\ \mathbf{0} & \mathbf{I} \end{bmatrix}_j \tag{11.9-5}$$

where $\{\mathbf{a}\}_j$ is a vector of modal coordinates analogous to $\{\mathbf{Z}\}$ of Eq. 11.7-4, $\{\mathbf{D}_n\}$ contains substructure d.o.f. other than attachment d.o.f., and $\{\mathbf{D}_a\}$ contains attachment d.o.f. Equation 11.9-5 resembles Eq. 11.6-3 of Guyan reduction, but with internal vibration modes added. The number of modes retained is at the discretion of the analyst. For the jth substructure, reduced stiffness and mass matrices are $[\mathbf{W}]_j^T\,[\mathbf{K}][\mathbf{W}]_j$ and $[\mathbf{W}]_j^T\,[\mathbf{M}][\mathbf{W}]_j$, which operate on modal amplitudes $\{\mathbf{a}\}_j$ and attachment d.o.f. $\{\mathbf{D}_a\}_j$. Assembly of reduced matrices yields Eq. 11.9-1. The process is illustrated by the following numerical example.

With lowest modes included in $[\mathbf{\Phi}]$, CMS is effective at representing lower modes of the assembled structure. Success in representing higher modes near a chosen ω_i can be enhanced by including an adjustment analogous to that of Eq. 11.6-6 [11.46].

Example. Consider axial vibration of the nonuniform bar shown in Fig. 11.9-1. Stiffness and lumped mass matrices of the entire structure are

$$[\mathbf{K}] = \frac{AE}{L}\begin{bmatrix} 1 & -1 & 0 & 0 & 0 \\ -1 & 2 & -1 & 0 & 0 \\ 0 & -1 & 3 & -2 & 0 \\ 0 & 0 & -2 & 4 & -2 \\ 0 & 0 & 0 & -2 & 4 \end{bmatrix} \qquad [\mathbf{M}] = \frac{\rho AL}{2}\begin{bmatrix} 1 & 0 & 0 & 0 & 0 \\ 0 & 2 & 0 & 0 & 0 \\ 0 & 0 & 3 & 0 & 0 \\ 0 & 0 & 0 & 4 & 0 \\ 0 & 0 & 0 & 0 & 4 \end{bmatrix} \tag{11.9-6}$$

Two substructures are selected. The first consists of elements 1 and 2; the second of elements 3, 4, and 5. Node 3 provides the only attachment d.o.f. With node 3 fixed, matrices for substructure 1 are

$$[\mathbf{K}_{nn}]_1 = \frac{AE}{L}\begin{bmatrix} 1 & -1 \\ -1 & 2 \end{bmatrix} \qquad [\mathbf{M}_{nn}]_1 = \frac{\rho AL}{2}\begin{bmatrix} 1 & 0 \\ 0 & 2 \end{bmatrix} \tag{11.9-7}$$

With node 3 and the right end fixed, matrices for substructure 2 are

$$[\mathbf{K}_{nn}]_2 = \frac{AE}{L}\begin{bmatrix} 4 & -2 \\ -2 & 4 \end{bmatrix} \qquad [\mathbf{M}_{nn}]_2 = \frac{\rho AL}{2}\begin{bmatrix} 4 & 0 \\ 0 & 4 \end{bmatrix} \tag{11.9-8}$$

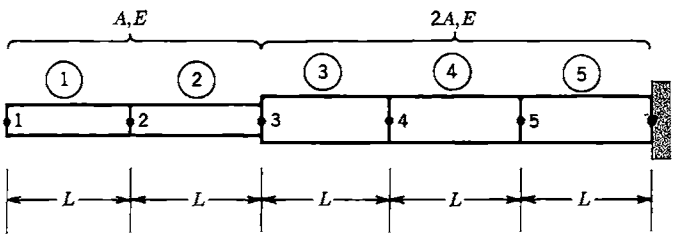

Figure 11.9-1. Bar of stepped cross section, modeled by five elements, each uniform and of length L.

For simplicity in what follows, we assume that $AE/L = 1$ and $\rho AL/2 = 1$. For substructure 1, the eigenproblem of Eq. 11.9-2 is solved with the matrices of Eqs. 11.9-7. The result is

$$\omega_1^2 = 0.293 \qquad \omega_2^2 = 1.707 \qquad \{\bar{\mathbf{D}}_1\}_1 = \begin{Bmatrix} 1 \\ \sqrt{2}/2 \end{Bmatrix} \qquad \{\bar{\mathbf{D}}_2\}_1 = \begin{Bmatrix} 1 \\ -\sqrt{2}/2 \end{Bmatrix} \tag{11.9-9}$$

where eigenvectors are normalized so that the first coefficient has unit amplitude. Similar solution, now for substructure 2 and with the matrices of Eqs. 11.9-8, yields

$$\omega_1^2 = 0.500 \qquad \omega_2^2 = 1.500 \qquad \{\bar{\mathbf{D}}_1\}_2 = \begin{Bmatrix} 1 \\ 1 \end{Bmatrix} \qquad \{\bar{\mathbf{D}}_2\}_2 = \begin{Bmatrix} 1 \\ -1 \end{Bmatrix} \tag{11.9-10}$$

Next, we write the first substructure stiffness matrix, partitioned as in Eq. 11.9-3, and use Eq. 11.9-4 to obtain Eq. 11.9-5. Labels u_1, u_2, and u_3 are appended merely to indicate the d.o.f. involved. We elect to retain only the first component mode.

$$\begin{bmatrix} 1 & -1 & 0 \\ -1 & 2 & -1 \\ 0 & -1 & 1 \end{bmatrix} \begin{matrix} u_1 \\ u_2 \\ u_3 \end{matrix} \qquad [\mathbf{\Psi}]_1 = -\begin{bmatrix} 1 & -1 \\ -1 & 2 \end{bmatrix}^{-1} \begin{Bmatrix} 0 \\ -1 \end{Bmatrix} = \begin{Bmatrix} 1 \\ 1 \end{Bmatrix} \qquad [\mathbf{W}]_1 = \begin{bmatrix} 1 & 1 \\ \sqrt{2}/2 & 1 \\ 0 & 1 \end{bmatrix} \tag{11.9-11}$$

The first substructure has no fixed boundary. Therefore $[\mathbf{\Psi}]_1$, which appears in the second column of $[\mathbf{W}]_1$, represents rigid-body translation.

The second substructure is treated similarly. Attachment d.o.f. u_3 now precedes internal d.o.f. u_4 and u_5, so to construct $[\mathbf{W}]_2$ the submatrices in $[\mathbf{W}]_j$ of Eq. 11.9-5 are rearranged by interchanging the two rows and the two columns. Again we elect to retain only the first component mode.

$$\begin{bmatrix} 2 & -2 & 0 \\ -2 & 4 & -2 \\ 0 & -2 & 4 \end{bmatrix} \begin{matrix} u_3 \\ u_4 \\ u_5 \end{matrix} \qquad [\mathbf{\Psi}]_2 = -\begin{bmatrix} 4 & -2 \\ -2 & 4 \end{bmatrix}^{-1} \begin{Bmatrix} -2 \\ 0 \end{Bmatrix} = \begin{Bmatrix} 2/3 \\ 1/3 \end{Bmatrix}$$

$$[\mathbf{W}]_2 = \begin{bmatrix} 1 & 0 \\ 2/3 & 1 \\ 1/3 & 1 \end{bmatrix} \tag{11.9-12}$$

With no node fixed, reduced stiffness and mass matrices of substructure 1 are respectively

$$
\begin{aligned}
[\mathbf{W}]_1^T \begin{bmatrix} 1 & -1 & 0 \\ -1 & 2 & -1 \\ 0 & -1 & 1 \end{bmatrix} [\mathbf{W}]_1 &= \begin{bmatrix} 0.5858 & 0 \\ 0 & 0 \end{bmatrix} \\
[\mathbf{W}]_1^T \begin{bmatrix} 1 & 0 & 0 \\ 0 & 2 & 0 \\ 0 & 0 & 1 \end{bmatrix} [\mathbf{W}]_1 &= \begin{bmatrix} 2.000 & 2.414 \\ 2.414 & 4.000 \end{bmatrix}
\end{aligned}
\tag{11.9-13}
$$

With only the rightmost node fixed, reduced stiffness and mass matrices of substructure 2 are respectively

$$
[\mathbf{W}]_2^T \begin{bmatrix} 2 & -2 & 0 \\ -2 & 4 & -2 \\ 0 & -2 & 4 \end{bmatrix} [\mathbf{W}]_2 = \begin{bmatrix} 2/3 & 0 \\ 0 & 4 \end{bmatrix}, \quad [\mathbf{W}]_2^T \begin{bmatrix} 2 & 0 & 0 \\ 0 & 4 & 0 \\ 0 & 0 & 4 \end{bmatrix} [\mathbf{W}]_2 = \begin{bmatrix} 4.222 & 4.000 \\ 4.000 & 8.000 \end{bmatrix}
\tag{11.9-14}
$$

Node 3 is shared by the two substructures, whose matrices are assembled by overlapping them at the common d.o.f. u_3. Vibration of the synthesized structure, Eq. 11.9-1, is described by the following equation, in which the first matrix is diagonal because there is only one attachment d.o.f. in this example.

$$
\left(\begin{bmatrix} 0.5858 & 0 & 0 \\ 0 & 0.6667 & 0 \\ 0 & 0 & 4.000 \end{bmatrix} - \omega_i^2 \begin{bmatrix} 2.000 & 2.414 & 0 \\ 2.414 & 8.222 & 4.000 \\ 0 & 4.000 & 8.000 \end{bmatrix} \right) \begin{Bmatrix} a_1 \\ u_3 \\ a_2 \end{Bmatrix}_i = \begin{Bmatrix} 0 \\ 0 \\ 0 \end{Bmatrix}
\tag{11.9-15}
$$

Results obtained are shown in Table 11.9-1. As expected, the reduced model yields higher frequencies than the original model.

If we were to retain both component modes of both substructures, the transformation matrices would become, instead of Eqs. 11.9-11 and 11.9-12,

TABLE 11.9-1. NATURAL FREQUENCIES OF THE STRUCTURE IN FIG. 11.9-1, FOR THE ORIGINAL STRUCTURE AND AS COMPUTED BY COMPONENT MODE SYNTHESIS.

Procedure	ω_1	ω_2	ω_3
Original structure (five d.o.f.)	0.2651	0.6156	1.000
CMS (2 component modes; three d.o.f.)	0.2653	0.6161	1.051
CMS (4 component modes; five d.o.f.)	0.2651	0.6156	1.000

$$[\mathbf{W}]_1 = \begin{bmatrix} 1 & 1 & 1 \\ \sqrt{2}/2 & -\sqrt{2}/2 & 1 \\ 0 & 0 & 1 \end{bmatrix} \qquad [\mathbf{W}]_2 = \begin{bmatrix} 1 & 0 & 0 \\ 2/3 & 1 & 1 \\ 1/3 & 1 & -1 \end{bmatrix} \tag{11.9-16}$$

Of course, there is no practical reason for retaining all modes, because the "reduced" problem is then the same size as the original, but it is reassuring that in this case CMS incurs no loss of accuracy (Table 11.9-1).

11.10 HARMONIC RESPONSE

Harmonic response analysis seeks the amplitude of response to a load of known amplitude that varies sinusoidally with time at known frequency. Alternative names include *frequency response analysis* and *forced vibration,* with the understanding that the forcing function varies harmonically. Harmonic loading may be applied to a structure by attached machinery that runs at constant speed. Harmonic response refers to vibration that continues at constant amplitude and at the frequency of the forcing function after initial transients have disappeared because of damping (Fig. 11.10-1). In what follows we outline the modal method of harmonic response analysis. Results obtained from an application appear in Section 11.17.

To begin, consider the single-d.o.f. system of Fig. 11.2-1a, with loading $r = F_0 \sin \Omega t$, where force F_0 and frequency Ω are both constant. As shown in basic vibration theory [11.1–11.3], the harmonic response is

$$\bar{u} = \frac{1}{\left[\left(1-\beta^2\right)^2 + (2\xi\beta)^2\right]^{1/2}}\left(\frac{F_0}{k}\right) \qquad \text{where} \qquad \alpha = \arctan\frac{2\xi\beta}{1-\beta^2}$$

$$u = \bar{u}\sin(\Omega t - \alpha) \qquad \beta = \Omega/\omega \qquad \omega = \sqrt{k/m} \tag{11.10-1}$$

and ξ is the damping ratio (Eq. 11.4-2). Harmonic response amplitude $\bar{u}$ is proportional to static displacement F_0/k, modified by a *dynamic magnification factor* that depends on β and ξ. Plots of amplitude $\bar{u}$ versus β for several values of ξ appear in Fig. 11.10-2. Response u lags forcing function r by phase angle α. Static displacement F_0/k is most greatly amplified when $\Omega \approx \omega$. The Ω for which amplification is greatest is called the *resonant frequency* [11.3]. We see that large amplitudes are possible when $\xi < 0.1$, as is the case in most structures. At a resonant frequency, damping is all that prevents vibration

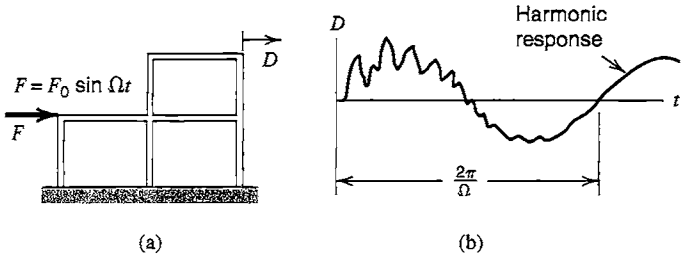

Figure 11.10-1. (a) A building frame, harmonically loaded. (b) Possible response of a particular d.o.f., showing decay of the transient component.

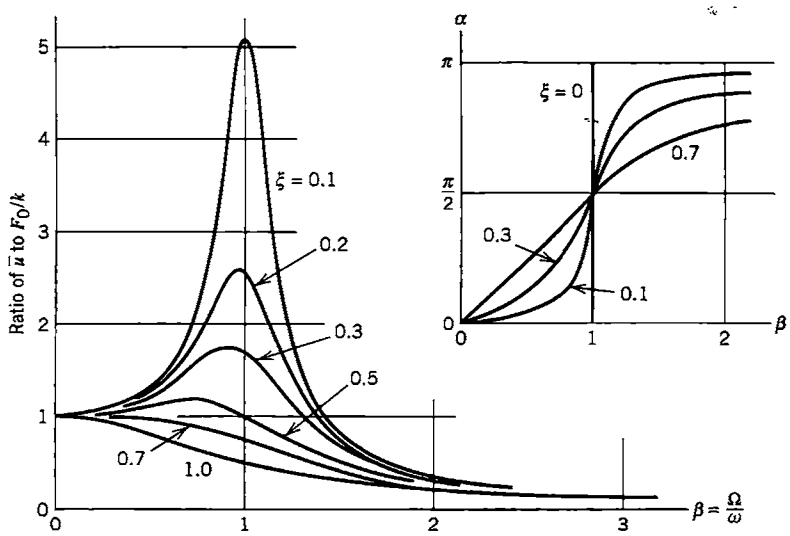

Figure 11.10-2. Ratio of dynamic displacement amplitude $\bar{u}$ to static displacement F_0/k, and phase angle α, for the single-d.o.f. system of Fig. 11.2-1a with $r = F_0 \sin \Omega t$.

amplitude from growing without limit, although at large amplitudes response may be limited by nonlinearities that develop. On the other hand, $\bar{u} < F_0/k$ when $\beta^2 > 2$, regardless of ξ. When β is large, the load changes direction so rapidly that the mass can scarcely respond.

A multiple-d.o.f. structure behaves qualitatively in the manner just described. The forced vibration amplitude of any d.o.f. selected can be plotted versus frequency Ω of the forcing function. The structure has as many natural frequencies as there are unrestrained d.o.f., so a plot analogous to Fig. 11.10-2 displays many peak amplitudes rather than only one. Peak amplitudes tend to decrease as Ω increases. Each peak receives greatest contribution from the structure mode whose frequency is closest to Ω. Contributions of other modes are much smaller but not necessarily negligible. This circumstance is conveniently accommodated by modal analysis, as follows.

Modal Analysis. As in any modal analysis, the first step is to obtain the lower frequencies and modes of the structure by solving an undamped eigenproblem. In the uncoupled modal equations, Eqs. 11.7-6, all terms in $\{\mathbf{R}^{\text{ext}}\}$ are in the form of a magnitude times $\sin \Omega t$. The solution of a generic modal equation has, of course, the same form as Eq. 11.10-1:

$$\bar{Z}_i = \frac{1}{\left[\left(1-\beta_i^2\right)^2 + (2\xi_i\beta_i)^2\right]^{1/2}}\left(\frac{\bar{P}_i}{\omega_i^2}\right) \quad \text{where} \quad \alpha = \arctan\frac{2\xi_i\beta_i}{1-\beta_i^2} \qquad (11.10\text{-}2)$$

$$Z_i = \bar{Z}_i \sin(\Omega t - \alpha_i) \qquad \beta_i = \Omega/\omega_i$$

where $\bar{P}_i$ is the amplitude of the sinusoidally varying modal load, obtained from the second of Eqs. 11.7-6. Equations 11.7-4 then provide physical displacements $\{\mathbf{D}\}$ from modal displacements Z_i. Phase angles α_i differ from one mode to another, so the Ω that

provides a peak amplitude is not known *a priori*. To find it, software may try several Ω's on either side of a natural frequency ω_i of the structure. In constructing a plot of response versus Ω (such as Fig. 11.17-3b), for each Ω the harmonic response is calculated using all structural modes up to and including at least one mode whose frequency exceeds Ω.

It is possible for loading to be periodic but not sinusoidal. Such a loading can be expressed as a sum of its Fourier series components, the foregoing analysis applied to each component, and results combined (Section 11.15).

11.11 RESPONSE HISTORY: DIRECT INTEGRATION METHODS

Direct integration refers to calculation of response history using step-by-step integration in time, without first changing the form of dynamic equations, as is necessary in modal methods. Response is evaluated at instants separated by time increments Δt, so we compute structure displacements at times Δt, $2\,\Delta t$, $3\,\Delta t$, ..., $n\,\Delta t$, and so on. At the nth time step, the equation of motion, Eq. 11.2-11 or Eq. 11.2-12, is

$$\begin{aligned} &[\mathbf{M}]\{\ddot{\mathbf{D}}\}_n + [\mathbf{C}]\{\dot{\mathbf{D}}\}_n + \{\mathbf{R}^{\text{int}}\}_n = \{\mathbf{R}^{\text{ext}}\}_n \\ \text{or}\quad &[\mathbf{M}]\{\ddot{\mathbf{D}}\}_n + [\mathbf{C}]\{\dot{\mathbf{D}}\}_n + [\mathbf{K}]\{\mathbf{D}\}_n = \{\mathbf{R}^{\text{ext}}\}_n \end{aligned} \tag{11.11-1}$$

The first form is better suited to a nonlinear problem in which $[\mathbf{K}]$ may change from one time step to the next.

Discretization in time is accomplished by using finite difference approximations of time derivatives. Many ways of doing so have been proposed. In this section we introduce the subject in a qualitative way. Details of some commonly used methods are discussed in the following three sections. In this discussion we assume that $[\mathbf{M}]$ is positive definite, but that (unless otherwise stated) $[\mathbf{K}]$ need only be positive semidefinite. Thus the structure is allowed to have rigid-body motion as part of its response. Similarly, a mechanism can be present, provided that it is not without mass. However, if there is a mechanism associated with an element instability, it may produce such large nonphysical displacements that results are unsatisfactory.

Methods of direct integration calculate conditions at time step $n + 1$ from the equation of motion, a difference expression, and known conditions at one or more preceding time steps. Algorithms can be classified as *explicit* or *implicit*. An *explicit* algorithm uses a difference expression of the general form

$$\{\mathbf{D}\}_{n+1} = f(\{\mathbf{D}\}_n, \{\dot{\mathbf{D}}\}_n, \{\ddot{\mathbf{D}}\}_n, \{\mathbf{D}\}_{n-1}, \ldots) \tag{11.11-2}$$

which contains only historical information on its right-hand side. The difference expression is combined with the equation of motion, Eq, 11.11-1, at time step n. An *implicit* algorithm uses a difference expression of the general form

$$\{\mathbf{D}\}_{n+1} = f(\{\dot{\mathbf{D}}\}_{n+1}, \{\ddot{\mathbf{D}}\}_{n+1}, \{\mathbf{D}\}_n, \{\dot{\mathbf{D}}\}_n, \{\ddot{\mathbf{D}}\}_n, \ldots) \tag{11.11-3}$$

which is combined with the equation of motion at time step $n + 1$.

Methods that originate with Eq. 11.11-2 or 11.11-3 are called *single-step* if the right-hand side contains information dating back to time step n, or *two-step* if the information dates back to time step $n-1$, and so on. We will discuss the *central difference method,* a two-step explicit method, and Newmark's method, a single-step implicit method.

In practical application, important differences between explicit and implicit methods are related to stability and economy. Explicit methods are conditionally stable, which means there is a "critical" time step Δt_{cr} that must not be exceeded if the numerical process is not to "blow up" by becoming unstable. Because Δt_{cr} is quite small, a great many time steps are needed, but each is executed quickly. Commonly used implicit methods are *unconditionally stable,* which means that calculations remain stable regardless of how large Δt becomes (although accuracy will suffer). In explicit methods, the coefficient matrix of $\{\mathbf{D}\}_{n+1}$ can be made diagonal, so that $\{\mathbf{D}\}_{n+1}$ is cheaply calculated in each time step. In implicit methods, the coefficient matrix of $\{\mathbf{D}\}_{n+1}$ cannot be made diagonal, so that cost per time step is greater, increasingly so as the FE mesh increases in dimensionality. As examples, using nonlinear test problems, the number of multiplications required per time step has been counted as an approximate indicator of computational effort [11.47,11.48]. The ratio of number of multiplications required, implicit/explicit per time step, was about 1.8 for the computationally one-dimensional problem of an axisymmetric shell, from 15 to 150 for two-dimensional problems, and 4000 for a three-dimensional problem. The ratio increases with dimensionality because matrices used in the implicit method become less narrowly banded. Another consequence of the difference in matrix topology is that an implicit method requires much more computer storage space than an explicit method.

Thus in direct integration we must choose between an explicit method, with low cost per time step but many steps required, and an implicit method, with higher cost per time step but fewer steps required. To make an appropriate choice we categorize a problem as of the *wave propagation* type or of the *structural dynamics* (or *inertial*) type.

A wave propagation problem is created by blast or impact loading, as in vehicle crashworthiness analysis. High-frequency modes must be represented in analysis. The number of significant modes may be large; perhaps two-thirds the number of d.o.f., or more if we wish to calculate accelerations as functions of time [2.14]. Response analysis usually need span only a small time interval.

A structural dynamics problem is created by loads that vary more slowly, such as loads created by an earthquake. Response is dominated by the lower modes; modes higher than the tenth may be insignificant in some applications, regardless of the number of d.o.f. in the structure. Response analysis may have to span several periods of the lowest frequency. If the rise time and duration of the load exceeds a few multiples of the time required for a sound wave to travel through the structure, the problem is probably of the structural dynamics type [11.48].

The following characteristics of methods may help in making an appropriate choice.

- The modal method, Section 11.7, is suited to structural dynamics problems. A major expense of the method is in solving the eigenproblem, so efficiency is greatest when very few modes are needed. If the loading versus time relation can be idealized as a series of straight segments, integration of modal equations in time can be done analytically and exactly. Cost per time step becomes low. An additional loading function can be analyzed cheaply because the eigenproblem need be solved only once, regardless of the number of loadings. It is relatively awkward to accommodate nonlinearity in the modal method.

- Implicit direct integration is suited to structural dynamics problems. It competes with the modal method, and may be cheaper where many modes would be needed in the modal method and when the analysis need not span as great a time. Cost per time step is substantial in 2D and 3D problems, but, in contrast with explicit direct integration, the size of Δt is limited by considerations of accuracy rather than numerical stability. As compared with the modal method, implicit direct integration has the advantage that vibration frequencies and modes need not be computed; however, they are often computed anyway for other reasons. An additional loading function constitutes a new problem, without a cost-saving carryover from the preceding problem other than reuse of the previously computed $[\mathbf{K}^{\text{eff}}]$ in its forward-reduced form for equation-solving. Nonlinearity can be accommodated without great trouble.
- Explicit direct integration is best suited to wave propagation problems. Computer storage requirements are low. Cost per time step is small, but so is the critical time step, so the method is not well suited to structural dynamics problems. As is the case with implicit direct integration, frequencies and modes need not be computed, and an additional loading function constitutes a new problem. Nonlinearity can be accommodated with relative ease.

11.12 EXPLICIT DIRECT INTEGRATION

In this section we consider two forms of the central difference method, discuss selection of an appropriate time step, and present computational examples.

Classical Central Differences. With Δt the time step, velocity and acceleration at time step n are approximated by the conventional central difference equations

$$\{\dot{\mathbf{D}}\}_n = \frac{1}{2\,\Delta t}\Big(\{\mathbf{D}\}_{n+1} - \{\mathbf{D}\}_{n-1}\Big) \quad \text{or} \quad \{\mathbf{D}\}_{n+1} = \{\mathbf{D}\}_{n-1} + 2\,\Delta t\{\dot{\mathbf{D}}\}_n \tag{11.12-1a}$$

$$\{\ddot{\mathbf{D}}\}_n = \frac{1}{\Delta t^2}\Big(\{\mathbf{D}\}_{n+1} - 2\{\mathbf{D}\}_n + \{\mathbf{D}\}_{n-1}\Big) \tag{11.12-1b}$$

(Acceleration can be related to velocities as shown by Eqs. 11.12-4.) Equations 11.12-1 can be obtained from Taylor series expansions of $\{\mathbf{D}\}_{n+1}$ and $\{\mathbf{D}\}_{n-1}$ about time $n\,\Delta t$:

$$\{\mathbf{D}\}_{n+1} = \{\mathbf{D}\}_n + \Delta t\{\dot{\mathbf{D}}\}_n + \frac{\Delta t^2}{2}\{\ddot{\mathbf{D}}\}_n + \frac{\Delta t^3}{6}\{\dddot{\mathbf{D}}\}_n + \cdots \tag{11.12-2a}$$

$$\{\mathbf{D}\}_{n-1} = \{\mathbf{D}\}_n - \Delta t\{\dot{\mathbf{D}}\}_n + \frac{\Delta t^2}{2}\{\ddot{\mathbf{D}}\}_n - \frac{\Delta t^3}{6}\{\dddot{\mathbf{D}}\}_n + \cdots \tag{11.12-2b}$$

Subtracting the latter equation from the former yields Eq. 11.12-1a, while adding the two equations yields Eq. 11.12-1b. In both cases, terms that contain Δt to powers higher than second are discarded. The primary error term is therefore proportional to Δt^2. This suggests that $\{\mathbf{D}\}$ has second-order accuracy, so halving the time step should approximately quarter the error. Realistically, adequate accuracy in all but the inconsequential highest modes is likely to be provided by the small Δt needed for computational stability.

Substitution of Eqs. 11.12-1 into the first of Eqs. 11.11-1 provides

$$\left[\frac{1}{\Delta t^2}\mathbf{M}+\frac{1}{2\,\Delta t}\mathbf{C}\right]\{\mathbf{D}\}_{n+1} = \{\mathbf{R}^{\text{ext}}\}_n - \{\mathbf{R}^{\text{int}}\}_n + \frac{2}{\Delta t^2}[\mathbf{M}]\{\mathbf{D}\}_n - \left[\frac{1}{\Delta t^2}\mathbf{M}-\frac{1}{2\,\Delta t}\mathbf{C}\right]\{\mathbf{D}\}_{n-1} \tag{11.12-3}$$

where, if linear conditions prevail, $\{\mathbf{R}^{\text{int}}\}_n = [\mathbf{K}]\{\mathbf{D}\}_n$.

Half-Step Central Differences. In place of Eqs. 11.12-1, we write [11.48,11.49]

$$\{\dot{\mathbf{D}}\}_{n-1/2} = \frac{1}{\Delta t}\Big(\{\mathbf{D}\}_n - \{\mathbf{D}\}_{n-1}\Big) \quad \text{and} \quad \{\dot{\mathbf{D}}\}_{n+1/2} = \frac{1}{\Delta t}\Big(\{\mathbf{D}\}_{n+1} - \{\mathbf{D}\}_n\Big) \tag{11.12-4a}$$

$$\{\ddot{\mathbf{D}}\}_n = \frac{1}{\Delta t}\Big(\{\dot{\mathbf{D}}\}_{n+1/2} - \{\dot{\mathbf{D}}\}_{n-1/2}\Big) = \frac{1}{\Delta t^2}\Big(\{\mathbf{D}\}_{n+1} - 2\{\mathbf{D}\}_n + \{\mathbf{D}\}_{n-1}\Big) \tag{11.12-4b}$$

Also, we rewrite the equation of motion, Eq. 11.11-1, with velocity lagging by half a time step. Thus for the half-step method we use the equations

$$\{\mathbf{D}\}_{n+1} = \{\mathbf{D}\}_n + \Delta t\{\dot{\mathbf{D}}\}_{n+1/2} \tag{11.12-5a}$$

$$\{\dot{\mathbf{D}}\}_{n+1/2} = \{\dot{\mathbf{D}}\}_{n-1/2} + \Delta t\{\ddot{\mathbf{D}}\}_n \tag{11.12-5b}$$

$$[\mathbf{M}]\{\ddot{\mathbf{D}}\}_n + [\mathbf{C}]\{\dot{\mathbf{D}}\}_{n-1/2} + \{\mathbf{R}^{\text{int}}\}_n = \{\mathbf{R}^{\text{ext}}\}_n \tag{11.12-5c}$$

Equations 11.12-5a and 11.12-5b are like Eqs. 11.12-2, but with half-step velocities. Combination of Eqs. 11.12-5 provides

$$\frac{1}{\Delta t^2}[\mathbf{M}]\{\mathbf{D}\}_{n+1} = \{\mathbf{R}^{\text{ext}}\}_n - \{\mathbf{R}^{\text{int}}\}_n + \frac{1}{\Delta t^2}[\mathbf{M}]\Big(\{\mathbf{D}\}_n + \Delta t\{\dot{\mathbf{D}}\}_{n-1/2}\Big) - [\mathbf{C}]\{\dot{\mathbf{D}}\}_{n-1/2} \tag{11.12-6}$$

For an alternative derivation of Eq. 11.12-6, let damping terms in Eq. 11.12-3 be gathered together and approximated, as follows.

$$\frac{1}{2\,\Delta t}[\mathbf{C}]\Big(\{\mathbf{D}\}_{n-1} - \{\mathbf{D}\}_{n+1}\Big) \approx \frac{1}{\Delta t}[\mathbf{C}]\Big(\{\mathbf{D}\}_{n-1} - \{\mathbf{D}\}_n\Big) \tag{11.12-7}$$

With this substitution, Eq. 11.12-3 provides the following equation. It agrees with Eq. 11.12-6, but is in a different form (write Eq. 11.12-5a one time step earlier, and substitute the half-step quantity into Eq. 11.12-6).

$$\frac{1}{\Delta t^2}[\mathbf{M}]\{\mathbf{D}\}_{n+1} = \{\mathbf{R}^{\text{ext}}\}_n - \{\mathbf{R}^{\text{int}}\}_n + \left[\frac{2}{\Delta t^2}\mathbf{M}-\frac{1}{\Delta t}\mathbf{C}\right]\{\mathbf{D}\}_n - \left[\frac{1}{\Delta t^2}\mathbf{M}-\frac{1}{\Delta t}\mathbf{C}\right]\{\mathbf{D}\}_{n-1} \tag{11.12-8}$$

In contrast to Eq. 11.12-3, Eqs. 11.12-6 and 11.12-8 can only be guaranteed to have first-order accuracy because of the lagging viscous forces. For practical structures that have light damping and require a very small time step, classical and half-step central difference methods have almost the same accuracy.

Remarks.

1. If [**M**] is diagonal in Eq. 11.12-6 or Eq. 11.12-8, as from lumped masses, each time step is executed very quickly because the solution of simultaneous equations is not required. The same is true of Eq. 11.12-3 if [**C**] is either zero or diagonal. However, we see from Eq. 11.5-1 that diagonal [**C**] corresponds to mass-proportional damping α[**M**] with diagonal [**M**], which damps lower modes most heavily. If damping is included, it is likely that stiffness-proportional damping β[**K**] is also desired in order to damp high-frequency numerical noise, but then Eq. 11.12-3 requires the solution of simultaneous equations, which greatly increases cost per time step. Therefore, for general use, Eq. 11.12-6 or Eq. 11.12-8 is the preferred form of the central difference method.
2. Equation 11.12-3 is *conditionally stable;* that is, calculations "blow up" unless

$$\Delta t \le \frac{2}{\omega_{\max}} = \Delta t_{cr} \quad \text{or, since} \quad \omega = 2\pi f = \frac{2\pi}{T}, \quad \text{then} \quad \Delta t \le \frac{T_{\min}}{\pi} \tag{11.12-9}$$

where frequency $\omega_{\max}$ and its period $T_{\min}$ correspond to the highest natural frequency of $([\mathbf{K}] - \omega^2[\mathbf{M}])\{\mathbf{D}\} = \{\mathbf{0}\}$. The critical time step for Eq. 11.12-3, $\Delta t_{\text{cr}} = 2/\omega_{\max}$, is independent of damping. Instability caused by too large a time step is recognized by an unbounded solution that may grow by orders of magnitude per time step, is obviously wrong (although instability in a nonlinear problem may be as obvious), and causes the computer program to stop due to overflow.

The case $\Delta t = 2/\omega_{\max}$ might be called "limiting stability." At $\Delta t = 2/\omega_{\max}$ the solution may diverge in certain cases, but only in arithmetic fashion. If $\Delta t > 2/\omega_{\max}$ divergence is exponential. Further discussion of this matter appears in Section 11.14.

The critical Δt for Eqs. 11.2-6 and 11.12-8 depends on damping ratio ξ. With i the mode number and ξ_i the damping ratio in that mode, numerical stability requires [11.48]

$$\Delta t \le \min\left[\frac{2}{\omega_i}\left(\sqrt{1-\xi_i^2} - \xi_i\right)\right] \qquad \text{but usually} \qquad \Delta t \le \frac{2}{\omega_{\max}}\left(\sqrt{1-\xi^2} - \xi\right) \tag{11.12-10}$$

where, in the latter equation, ξ is the damping ratio in the $\omega_{\max}$ mode. The latter equation usually prevails because ξ is likely to be small for all modes, so that $\omega_{\max}$ and its ξ dominate. When damping is not zero, Eq. 11.12-10 is more restrictive than Eq. 11.12-9.

3. For a small FE model, [**K**] of the entire structure can be formed and stored in fast computer memory, and internal forces at any time step n obtained by the multiplication

$\{\mathbf{R}^{\text{int}}\}_n = [\mathbf{K}]\{\mathbf{D}\}_n$. An attractive alternative, especially for a nonlinear problem, is to generate $\{\mathbf{R}^{\text{int}}\}_n$ in element-by-element fashion, by summing element contributions:

$$\{\mathbf{R}^{\text{int}}\}_n = \sum_{i=1}^{N_{\text{els}}} \left(\{\mathbf{r}^{\text{int}}\}_n\right)_i \qquad \text{where} \qquad \{\mathbf{r}^{\text{int}}\}_n = \int [\mathbf{B}]^T \{\boldsymbol{\sigma}\}_n \, dV \tag{11.12-11}$$

For rate-independent plasticity, element stresses $\{\boldsymbol{\sigma}\}$ are not linearly related to element strains but can be calculated using element displacements contained in $\{\mathbf{D}\}_n$. Similar remarks can be made for stiffness-proportional damping, if present. Because element $[\mathbf{k}]$ and $[\mathbf{c}]$ matrices need be neither formed nor stored, explicit methods can treat even large three-dimensional FE models with comparatively modest computer storage requirements.

Evaluation of the integral in Eq. 11.12-11 requires the same order of quadrature as the element stiffness matrix. Calculation of $\{\mathbf{R}^{\text{int}}\}$ is a large portion of the per-time-step cost of explicit integration, so one seeks to minimize the number of quadrature points per element. For example, use of one point rather than four, if possible, quarters the cost. Use of one-point quadrature demands attention to stress fields related to element instabilities; see the summary in Section 6.8 and papers, many by Belytschko, cited in Chapters 6, 15, and 16.

4. With $n = 0$, $\{\mathbf{D}\}_1$ appears on the left-hand side of Eq. 11.12-6, and to compute it, $\{\dot{\mathbf{D}}\}_{-1/2}$ is needed on the right-hand side. A backward difference approximation yields

$$\{\ddot{\mathbf{D}}\}_0 = \frac{1}{\Delta t/2}\left(\{\dot{\mathbf{D}}\}_0 - \{\dot{\mathbf{D}}\}_{-1/2}\right) \quad \text{hence} \quad \{\dot{\mathbf{D}}\}_{-1/2} = \{\dot{\mathbf{D}}\}_0 - \frac{\Delta t}{2}\{\ddot{\mathbf{D}}\}_0 \tag{11.12-12}$$

where $\{\ddot{\mathbf{D}}\}_0$ is obtained by evaluating Eq. 11.11-1 at $n = 0$, which provides

$$\{\ddot{\mathbf{D}}\}_0 = [\mathbf{M}]^{-1}\left(\{\mathbf{R}^{\text{ext}}\}_0 - [\mathbf{K}]\{\mathbf{D}\}_0 - [\mathbf{C}]\{\dot{\mathbf{D}}\}_0\right) \tag{11.12-13}$$

Thus $\{\dot{\mathbf{D}}\}_{-1/2}$ can be determined from known initial values of $\{\mathbf{R}^{\text{ext}}\}$, $\{\mathbf{D}\}$, and $\{\dot{\mathbf{D}}\}$.

To use Eq. 11.12-8 as an alternative form of Eq. 11.12-6, or to use Eq. 11.12-3, $\{\mathbf{D}\}_{-1}$ is needed on the right hand side to start the procedure. It is obtained from Eq. 11.12-2b, with powers of Δt higher than second omitted.

$$\{\mathbf{D}\}_{-1} = \{\mathbf{D}\}_0 - \Delta t\{\dot{\mathbf{D}}\}_0 + \frac{\Delta t^2}{2}\{\ddot{\mathbf{D}}\}_0 \tag{11.12-14}$$

where $\{\ddot{\mathbf{D}}\}_0$ comes from Eq. 11.12-13.

5. Conceivably, one may know conditions at present and require conditions in the past. The central difference method can be run in reverse, using a negative time step. Stability criteria then apply to the *magnitude* of Δt.

Stability: Estimation of Δt_{cr}. If Δt is too large, explicit integration fails; if Δt is unnecessarily small, calculations are too expensive. Therefore it is necessary to determine $\omega_{\max}$, or

accurately bound it, for use in Eq. 11.12-9 or Eq. 11.12-10. An analyst may wish to avoid calculating the exact ω_{max}, because [**K**] must be assembled and an eigenvalue problem solved.

One way to bound ω_{max} of the FE mesh is to note that it must be less than the largest ω_{max} of any unassembled and unsupported element of the mesh [11.48,11.50]. The latter frequency can sometimes be obtained by hand calculation. Consider the unsupported two-node bar element of Fig. 11.4-3a. With lumped masses, the highest frequency is calculated in Example 2 of Section 11.4 to be

$$\omega_{max} = 2\sqrt{\frac{AE}{mL}} \quad \text{but} \quad m = \rho AL \quad \text{so} \quad \omega_{max} = \frac{2}{L}\sqrt{\frac{E}{\rho}} = \frac{2c}{L} \tag{11.12-15}$$

where $c = \sqrt{E/\rho}$ is the speed of sound in the material. With this estimate, the critical time step $2/\omega_{max}$ for an undamped material is

$$\Delta t_{cr} \leq \frac{L}{c} \tag{11.12-16}$$

which is called the *CFL condition* after Courant, Friedrichs, and Lewy [11.51,11.52]. The physical interpretation is that Δt must be small enough that information does not propagate more than the distance between adjacent nodes during a single time step. Unfortunately, this estimate is not conservative for all clement types, and it is inconvenient to calculate L for all adjacent pairs of nodes [11.50]. Also, if elements have rotational d.o.f., Δt_{cr} may be governed by flexural modes, whose natural frequencies do not depend on nodal separation alone [2.14]. Formulas adapted to particular elements are available; see [11.53] and references it cites. If there is plastic action, ω_{max} is unchanged in elements that remain elastic, and not increased in elements that yield, so the global estimate of ω_{max} need not be revised if there is yielding.

Use of the highest element frequency to approximate ω_{max} suggests an important observation. Example 2 of Section 11.4 shows that changing from lumped masses to the consistent mass formulation raises the highest natural frequency of the unsupported bar element by a factor of 1.732 and consequently decreases Δt_{cr} by a factor of 0.577, according to the element-frequency estimate of ω_{max}. Thus, as compared with the consistent mass formulation, lumped masses not only reduce the cost per time step, they also increase the allowable time step. In Section 11.14 we argue that lumped masses are also likely to provide better accuracy.

An alternative estimate of ω_{max} is provided by the *Gerschgorin bound* [11.52], which may be stated in the following form for a lumped (diagonal) mass matrix.

$$\omega_{max}^2 \leq \max_i \left(\frac{1}{M_{ii}} \sum_{j=1}^{n} |K_{ij}| \right) \qquad \text{where} \qquad i = 1, 2, \ldots, n \tag{11.12-17}$$

where n is the matrix order; that is, the number of d.o.f. Thus for each row we add magnitudes of stiffness coefficients, divide by the corresponding lumped mass, and identify the largest such result as an upper bound of the correct ω_{max}.

A convenient measure of the time step actually used is the *Courant number*, defined as

$$C_n = \frac{\Delta t_{\text{actual}}}{\Delta t_{\text{cr}}} \tag{11.12-18}$$

where Δt_{cr} is the maximum time step consistent with numerical stability. Use of a smaller Δt may actually *decrease* accuracy [2.13,2.14].

Higher-order elements have higher frequencies than lower-order elements and tend to produce noise when stress waves move across an FE mesh. For these reasons, it may be best to avoid higher-order elements when using explicit integration. Similarly, one should avoid penalty constraints, and very small lumped masses, either of which make $\omega_{\max}$ very large. Note that a single small element (with its large stiffness) or a single small mass may seriously reduce Δt_{cr} for the entire FE mesh, even if the physical significance of a small element or a small mass may be negligible.

Example: Wave Propagation. Consider a uniform steel bar, without damping and initially at rest, loaded by a suddenly applied axial tip force (Fig. 11.12-1). The FE model consists of 40 two-node bar elements of equal length, so that each uniform-strain element has length $L = L_T/40 = 0.50$ in. Using the algorithm of Eq. 11.12-6 with a lumped mass matrix, we will calculate axial stress versus time at $x = 9.75$ in, which is the middle of the twentieth element (nodes and elements are numbered left to right). Conditions are assumed to be linearly elastic.

In this example, $\{\mathbf{R}^{\text{int}}\}$ is assembled as follows. Let u denote axial displacement and subscripts indicate node and element numbers. Axial force F_i in the ith element, positive in tension, is computed for all elements. $\{\mathbf{R}^{\text{int}}\}$ receives a contribution from only the first element at node 1, but from two elements at internal nodes. Thus

$$F_i = A\sigma_i = AE\frac{u_{i+1} - u_i}{L} \qquad R_1^{\text{int}} = -F_1 \quad R_i^{\text{int}} = F_{i-1} - F_i \quad \text{for} \quad i = 2, 3, \ldots, 20 \tag{11.12-19}$$

The highest element frequency is given by Eq. 11.12-15 as

$$(\omega_{\max})_e = \frac{2}{0.50}\sqrt{\frac{E}{\rho}} = \frac{2}{0.50}\sqrt{\frac{30(10^6)}{7.4(10^{-4})}} = 8.0539(10^5) \text{ rad/s} \tag{11.12-20}$$

The same value is obtained from Eq. 11.12-17 (however, it is rare that element and Gerschgorin bounds are identical). This value is very close to the computed maximum frequency of the FE model, which is $\omega_{\max} = 8.0523(10^5)$ rad/s. Using this $\omega_{\max}$ in Eq. 11.12-10 with $\xi = 0$, we obtain $\Delta t = 2/8.0523(10^5) = 2.484(10^{-6})$ s as the critical

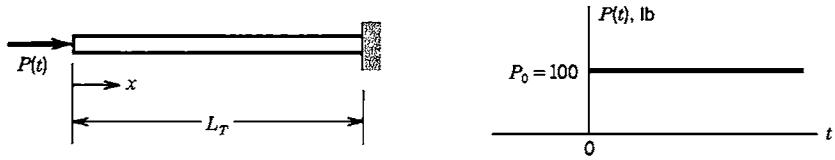

Figure 11.12-1. One-dimensional uniform bar with instantaneous axial tip loading. $A = 1.0$ in^2, $E = 30(10^6)$ psi, $\rho = 7.4(10^{-4})$ lb-s^2/in^4, $L_T = 20$ in. Load $P_0 = 100$ lb is applied at $t = 0$.

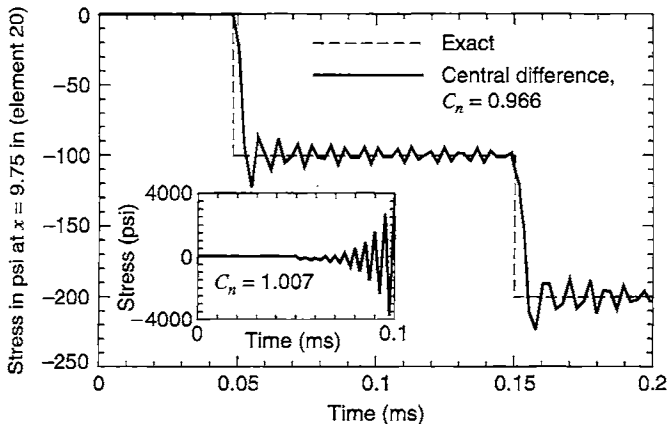

Figure 11.12-2. Axial stress versus time for a 40-element model of the bar in Fig. 11.12-1. Central difference solution with $\Delta t = 2.400(10^{-6})$ s ($C_n = 0.966$). Inset shows instability that results from too large a Δt ($\Delta t = 2.500(10^{-6})$ s, for which $C_n = 1.007$).

time step. Calculations are begun from at-rest initial conditions. Equation 11.12-6 is used, with $\{\dot{\mathbf{D}}\}_{-1/2}$ obtained from Eq. 11.12-12.

Results computed using $\Delta t = 2.400(10^{-6})$ s, for which $C_n = 0.966$, are shown in Fig. 11.12-2. The analysis duration of 83 time steps allows a stress wave to travel the length of the bar and back again. Stress at $x = 9.75$ in. is zero until the time required for a stress wave to travel from the left end to this location (0.048 milliseconds). The change in mean stress from −100 psi to −200 psi at 0.15 ms is due to wave reflection from the fixed end. The inset in Fig. 11.12-2 shows that a Δt only slightly greater than the stability limit produces a solution that soon increases wildly with each time step until the computer terminates execution due to overflow.

Figure 11.12-3a shows the result of using a Δt barely under the stability limit. Numerical noise is scarcely noticeable. Comparison with Fig. 11.12-2 shows that accuracy is *reduced* by using a smaller Δt (with an implicit method, accuracy increases as Δt is reduced). Figure 11.12-3b shows that large oscillations appear if Eq. 11.12-12 is ignored, which results in taking $\{\dot{\mathbf{D}}\}_{-1/2}$ as zero. Figure 11.12-4 shows what happens if the tip load

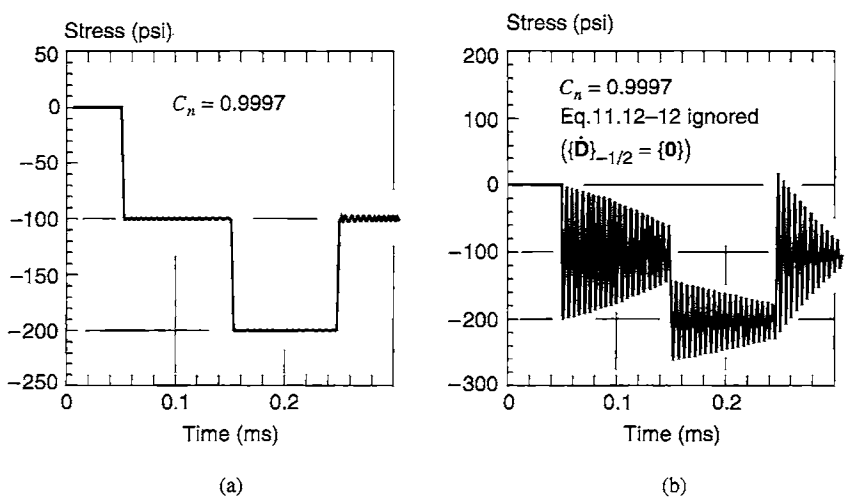

Figure 11.12-3. Central difference solutions for axial stress versus time for a 40-element model of the bar in Fig. 11.12-1. $\Delta t = 2.483(10^{-6})$ s ($C_n = 0.9997$), proper and improper initial conditions.

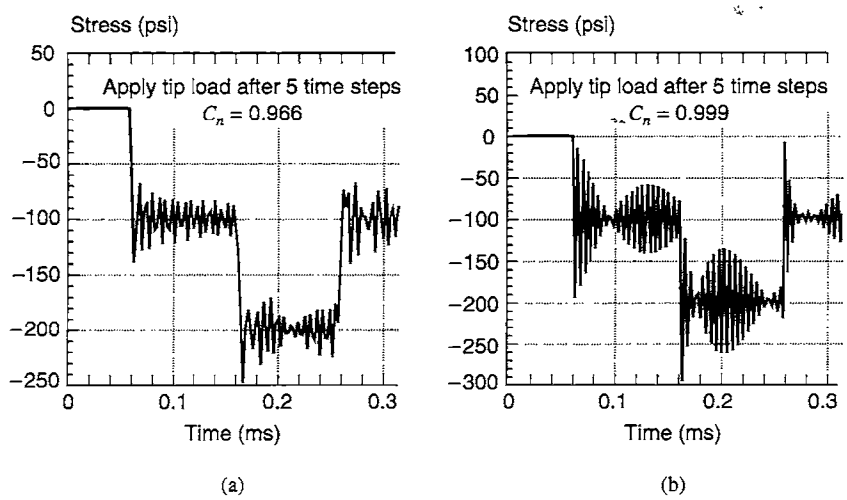

Figure 11.12-4. Central difference solutions for axial stress versus time for a 40-element model of the bar in Fig. 11.12-1. Zero initial velocity; load applied after starting.

is applied after five time steps rather than initially. Thus $\{\dot{\mathbf{D}}\}_{-1/2}$ is taken as zero. From collected results such as those in Figs. 11.12-3 and 11.12-4, we conclude that values of C_n in the range 0.95 to 0.98 may be best for general use.

Concluding Remarks. When an explicit method is used to solve a *single* ordinary differential equation, accuracy depends strongly on the time step. For a *system* of FE equations, perhaps any number greater than 20, it is typically observed that a Δt only slightly less than Δt_{cr} provides excellent accuracy. The reason is that the stability criterion is based on the *highest*-frequency, or *smallest-timescale* phenomenon that the FE mesh can represent, and the mesh contains a broad frequency spectrum. Motions associated with the smallest timescale are not accurately resolved, as evidenced by oscillations in Figs. 11.12-2 to 11.12-4. Fortunately, these oscillations contribute little to structural response, which is usually dominated by lower-frequency, longer-timescale phenomena that *are* accurately resolved. In other words, *we do not require that the highest-frequency phenomena be accurately resolved; all we ask is that they be stably integrated.* Thus a Δt adequate for stability is likely to guarantee accuracy. Even so, the maximum allowable Δt is so small that a great many time steps may be needed to span the required duration of an analysis.

11.13 IMPLICIT DIRECT INTEGRATION

Some implicit methods are conditionally stable, but those in common use are *unconditionally stable:* even very large values of Δt do not make calculations blow up (but may destroy accuracy). Conditionally stable implicit methods are rarely used in practice because of the severe constraint placed on Δt and the substantial cost per time step of an implicit method in 2D and 3D problems.

In what follows we emphasize the Newmark family of methods. It includes the constant- or average-acceleration method, which is unconditionally stable in linear problems and is

probably the most widely used implicit method. Numerical results produced by this method appear in Section 11.18.

Some Single-d.o.f. Formulas. Let τ be a value of time t within a typical time step Δt, so that $0 \le \tau \le \Delta t$ and $\Delta t = t_{n+1} - t_n$. Also let $u = u(t)$ be a dependent variable such as axial displacement of a bar. Let us assume that acceleration is constant over a time step, and equal to the average of final and initial values. Thus

$$\ddot{u}(\tau) = \frac{1}{2}(\ddot{u}_{n+1} + \ddot{u}_n) \tag{11.13-1a}$$

Integration and the initial condition $\dot{u}(\tau) = \dot{u}_n$ at $\tau = 0$ yield

$$\dot{u}(\tau) = \dot{u}_n + \frac{\tau}{2}(\ddot{u}_{n+1} + \ddot{u}_n) \tag{11.13-1b}$$

Integration and the initial condition $u(\tau) = u_n$ at $\tau = 0$ yield

$$u(\tau) = u_n + \tau\dot{u}_n + \frac{\tau^2}{4}(\ddot{u}_{n+1} + \ddot{u}_n) \tag{11.13-1c}$$

Alternatively, we might assume that acceleration is linear over a time step. Then Eqs. 11.13-1 are replaced by

$$\ddot{u}(\tau) = \ddot{u}_n + \frac{\tau}{\Delta t}(\ddot{u}_{n+1} - \ddot{u}_n) \tag{11.13-2a}$$

$$\dot{u}(\tau) = \dot{u}_n + \tau\ddot{u}_n + \frac{\tau^2}{2\,\Delta t}(\ddot{u}_{n+1} - \ddot{u}_n) \tag{11.13-2b}$$

$$u(\tau) = u_n + \tau\dot{u}_n + \frac{\tau^2}{2}\ddot{u}_n + \frac{\tau^3}{6\,\Delta t}(\ddot{u}_{n+1} - \ddot{u}_n) \tag{11.13-2c}$$

If the foregoing equations for velocity and displacement are evaluated at time step $n + 1$, where $\tau = \Delta t$, we obtain the following results.

Average Acceleration (Eqs. 11.13-1):

$$\dot{u}_{n+1} = \dot{u}_n + \frac{1}{2}\Delta t(\ddot{u}_{n+1} + \ddot{u}_n)$$

$$u_{n+1} = u_n + \Delta t\,\dot{u}_n + \frac{1}{4}\Delta t^2(\ddot{u}_{n+1} + \ddot{u}_n)$$

Linear Acceleration (Eqs. 11.13-2):

$$\dot{u}_{n+1} = \dot{u}_n + \frac{1}{2}\Delta t(\ddot{u}_{n+1} + \ddot{u}_n)$$

$$u_{n+1} = u_n + \Delta t\,\dot{u}_n + \Delta t^2\left(\frac{1}{6}\ddot{u}_{n+1} + \frac{1}{3}\ddot{u}_n\right)$$

These difference equations are implicit because calculation of u_{n+1} and $\dot{u}_{n+1}$ requires knowledge of $\ddot{u}_{n+1}$. That is, u_{n+1} and $\dot{u}_{n+1}$ depend on more than only historical information. By combining equations for the average acceleration algorithm so as to eliminate second-derivative terms, we obtain $u_{n+1} = u_n + \frac{1}{2}\Delta t(\dot{u}_{n+1} + \dot{u}_n)$, in which the latter set of

terms represents a trapezoidal area in a plot of $\dot{u}$ versus t. For this reason the average acceleration method is often called the *trapezoidal rule.*

Generalization. The foregoing relations can be regarded as special cases of the Newmark method [11.54], which contains numerical factors γ and β that control characteristics of the algorithm such as accuracy, numerical stability, and the amount of algorithmic damping. With $\{\mathbf{D}\}$ the vector of d.o.f., Newmark relations are

$$\{\dot{\mathbf{D}}\}_{n+1} = \{\dot{\mathbf{D}}\}_n + \Delta t\left[\gamma\{\ddot{\mathbf{D}}\}_{n+1} + (1-\gamma)\{\ddot{\mathbf{D}}\}_n\right] \tag{11.13-3a}$$

$$\{\mathbf{D}\}_{n+1} = \{\mathbf{D}\}_n + \Delta t\{\dot{\mathbf{D}}\}_n + \frac{1}{2}\Delta t^2\left[2\beta\{\ddot{\mathbf{D}}\}_{n+1} + (1-2\beta)\{\ddot{\mathbf{D}}\}_n\right] \tag{11.13-3b}$$

Respectively, the average acceleration and linear acceleration methods are given by $\gamma = \frac{1}{2}, \beta = \frac{1}{4}$ and by $\gamma = \frac{1}{2}, \beta = \frac{1}{6}$. By solving Eq. 11.13-3b for $\{\ddot{\mathbf{D}}\}_{n+1}$, then substituting this expression into Eq. 11.13-3a, we obtain

$$\{\ddot{\mathbf{D}}\}_{n+1} = \frac{1}{\beta\Delta t^2}\left(\{\mathbf{D}\}_{n+1} - \{\mathbf{D}\}_n - \Delta t\{\dot{\mathbf{D}}\}_n\right) - \left(\frac{1}{2\beta} - 1\right)\{\ddot{\mathbf{D}}\}_n \tag{11.13-4a}$$

$$\{\dot{\mathbf{D}}\}_{n+1} = \frac{\gamma}{\beta\Delta t}\left(\{\mathbf{D}\}_{n+1} - \{\mathbf{D}\}_n\right) - \left(\frac{\gamma}{\beta} - 1\right)\{\dot{\mathbf{D}}\}_n - \Delta t\left(\frac{\gamma}{2\beta} - 1\right)\{\ddot{\mathbf{D}}\}_n \tag{11.13-4b}$$

These equations are substituted into the equation of motion, Eq. 11.2-12, written at time step $n + 1$, and then solved for $\{\mathbf{D}\}_{n+1}$. The result is

$$[\mathbf{K}^{\text{eff}}]\{\mathbf{D}\}_{n+1} = \{\mathbf{R}^{\text{ext}}\}_{n+1} + [\mathbf{M}]\left\{\frac{1}{\beta\Delta t^2}\{\mathbf{D}\}_n + \frac{1}{\beta\Delta t}\{\dot{\mathbf{D}}\}_n + \left(\frac{1}{2\beta} - 1\right)\{\ddot{\mathbf{D}}\}_n\right\}$$

$$+ [\mathbf{C}]\left\{\frac{\gamma}{\beta\Delta t}\{\mathbf{D}\}_n + \left(\frac{\gamma}{\beta} - 1\right)\{\dot{\mathbf{D}}\}_n + \Delta t\left(\frac{\gamma}{2\beta} - 1\right)\{\ddot{\mathbf{D}}\}_n\right\} \tag{11.13-5a}$$

where

$$[\mathbf{K}^{\text{eff}}] = \frac{1}{\beta\Delta t^2}[\mathbf{M}] + \frac{\gamma}{\beta\Delta t}[\mathbf{C}] + [\mathbf{K}] \tag{11.13-5b}$$

Note that $[\mathbf{K}^{\text{eff}}]$ cannot be a diagonal matrix, because it contains $[\mathbf{K}]$. Therefore a diagonal mass matrix provides little computational economy. Indeed, as argued in Section 11.14, an implicit method is usually more accurate when $[\mathbf{M}]$ is the consistent mass matrix. If $[\mathbf{M}]$ is positive definite, then $[\mathbf{K}^{\text{eff}}]$ is nonsingular even if the structure is unsupported or contains a mechanism.

If there are no nonlinearities and time step Δt is not changed during an analysis, $[\mathbf{K}^{\text{eff}}]$ can be evaluated and factored for equation-solving at the outset, and thereafter need not be updated or re-factored. To begin calculation we require $\{\ddot{\mathbf{D}}\}_0$, which can be obtained from Eq. 11.12-13. Equation 11.13-5a is then solved for $\{\mathbf{D}\}_1$ as if solving a set of static equations with known load vector and stiffness matrix, and Eqs. 11.13-4 used to obtain $\{\ddot{\mathbf{D}}\}_1$ and $\{\dot{\mathbf{D}}\}_1$. In the next step Eq. 11.13-5a is solved for $\{\mathbf{D}\}_2$, and so on.

The α *method* proposed by Hilber, Hughes, and Taylor [2.13,11.55] can be regarded as a generalization of Newmark methods. It is based on the Newmark difference relations, Eqs. 11.13-3, and the modified equation of motion

$$[\mathbf{M}]\{\ddot{\mathbf{D}}\}_{n+1} + (1+\alpha)[\mathbf{C}]\{\dot{\mathbf{D}}\}_{n+1} - \alpha[\mathbf{C}]\{\dot{\mathbf{D}}\}_n + (1+\alpha)[\mathbf{K}]\{\mathbf{D}\}_{n+1} - \alpha[\mathbf{K}]\{\mathbf{D}\}_n = \{\mathbf{R}_\alpha^{\text{ext}}\} \tag{11.13-6}$$

where $\{\mathbf{R}_\alpha^{\text{ext}}\}$ is $\{\mathbf{R}^{\text{ext}}\}$ evaluated at time $(1+\alpha)t_{n+1} - \alpha t_n = t_{n+1} + \alpha\,\Delta t$. If loads vary linearly over a time step, this is the same as $\{\mathbf{R}_\alpha^{\text{ext}}\} = (1+\alpha)\{\mathbf{R}^{\text{ext}}\}_{n+1} - \alpha\{\mathbf{R}^{\text{ext}}\}_n$. If $\alpha = 0$, Eq. 11.13-6 reduces to the equation used in Newmark methods. Algorithmic damping is introduced by using $\alpha < 0$. Algorithmic damping can be introduced in Newmark methods, but only first-order accuracy can be guaranteed. That is, the order of error in computed displacements may decline from $O(\Delta t^2)$ to $O(\Delta t)$. The α method allows algorithmic damping while retaining second-order accuracy.

Rather than calculating total displacements, as in Eqs. 11.13-5, implicit integration formulas can be restated so as to calculate displacement increments [2.14,11.3]. Incremental forms are effective for nonlinear problems, where $[\mathbf{K}^{\text{eff}}]$ changes from one time step to the next (Section 17.7).

Accuracy, Stability, Damping. To obtain starting conditions for direct integration we must solve Eq. 11.12-13 for $\{\ddot{\mathbf{D}}\}_0$. This calculation requires that $[\mathbf{M}]$ be assembled and reduced for equation-solving. With an implicit method the calculation is not trivial, because the $[\mathbf{M}]$ used is usually not diagonal. It is tempting to skip these calculations and set $\{\ddot{\mathbf{D}}\}_0 = \{\mathbf{0}\}$. Unfortunately, doing so may reduce accuracy from second-order to first-order [11.56]. In a two-d.o.f. example in which Δt is 10 times the smaller period of vibration [2.14], setting initial accelerations to zero leads to computed displacements that are scarcely more than half the values computed when the correct initial accelerations are used.

It can be shown [2.13,11.57] that Newmark methods have *unconditional stability* when

$$2\beta \geq \gamma \geq \frac{1}{2} \tag{11.13-7}$$

and *conditional stability* when

$$\gamma \geq \frac{1}{2} \qquad \beta < \frac{1}{2}\gamma \qquad \Delta t \leq \frac{\Omega_{\text{crit}}}{\omega_{\max}} = \frac{\Omega_{\text{crit}} T_{\min}}{2\pi} \tag{11.13-8}$$

where $\omega_{\max}$ and $T_{\min}$ have the same meanings as in Eq. 11.12-9, and Ω_{crit} is defined as

$$\Omega_{\text{crit}} = \frac{\xi\left(\gamma - \frac{1}{2}\right) + \sqrt{\gamma/2 - \beta + \xi^2\left(\gamma - \frac{1}{2}\right)^2}}{\gamma/2 - \beta} \tag{11.13-9}$$

in which ξ is the damping ratio (Eq. 11.4-2). We see that damping has no effect on stability when $\gamma = \frac{1}{2}$, and that when $\gamma > \frac{1}{2}$ the allowable time step is increased by damping. (In

contrast, damping *decreases* the allowable Δt of an *explicit* method such as Eqs. 11.12-6 or Eq. 11.12-8.) In Eq. 11.13-9, small damping has small effect, so when damping is uncertain, a conservative Ω_{crit} is obtained by using $\xi = 0$, for which $\Omega_{\text{crit}} = (\gamma/2 - \beta)^{-1/2}$.

Some results of stability and accuracy analysis appear in Table 11.13-1. When $\xi > 0$ accuracy is likely to decline, at most from $O(\Delta t^2)$ to $O(\Delta t)$, or from $O(\Delta t^4)$ to $O(\Delta t^2)$ in the case of the Fox-Goodwin version. Stability is discussed further in Section 11.14.

To damp high-frequency modes, which may be of little interest or constitute only undesirable nonphysical oscillations associated with discretization, it is natural to consider the arbitrary addition of viscous damping, by increasing ξ. Hughes [2.13] shows that using this strategy with the average-acceleration method may damp mainly the *middle* modes, leaving the highest and lowest almost unaffected. It is better to use algorithmic damping.

When $\gamma > \frac{1}{2}$, Newmark methods display algorithmic damping, at the cost of reducing guaranteed accuracy from second-order to first-order. To obtain the highest possible high-frequency dissipation, while retaining unconditional stability, the following choice of β is appropriate [2.13].

$$\text{for} \qquad \gamma \geq \frac{1}{2} \qquad \text{use} \qquad \beta = \frac{1}{4}\left(\gamma + \frac{1}{2}\right)^2 \tag{11.13-10}$$

In the α method of Eq. 11.13-6, to introduce algorithmic damping and retain unconditional stability, $-\frac{1}{3} \leq \alpha \leq 0$ is recommended, with γ and β chosen as indicated in Table 11.13-1. Although both the Newmark method and the α method can effectively damp higher modes, the α method introduces less damping in lower modes, thus tending to preserve their accuracy (Fig. 11.13-1).

Operator Splitting. It may happen that mass and stiffness characteristics are quite different in different parts of a mathematical model. This may happen in a fluid-structure interaction problem, where response may be regarded as wave propagation in the fluid and vibration in the structure [2.14]. Also, nonlinearity such as gap closure may be confined to a part of the structure, which suggests use of an explicit method for that part alone and an

TABLE 11.13-1. STABILITY AND ACCURACY OF SELECTED IMPLICIT DIRECT INTEGRATION METHODS.

Version [or references]	γ	β	Stability condition	Error in $\{\mathbf{D}\}$ for $\xi = 0$
		Newmark Methods		
Average acceleration	$\frac{1}{2}$	$\frac{1}{4}$	Unconditional	$O(\Delta t^2)$
Linear acceleration	$\frac{1}{2}$	$\frac{1}{6}$	$\Omega_{\text{crit}} = 3.464$ if $\xi = 0$	$O(\Delta t^2)$
Fox-Goodwin	$\frac{1}{2}$	$\frac{1}{12}$	$\Omega_{\text{crit}} = 2.449$ if $\xi = 0$	$O(\Delta t^4)$
Algorithmically damped	$\geq \frac{1}{2}$	$\geq \frac{1}{4}(\gamma + \frac{1}{2})^2$	Unconditional	$O(\Delta t)$
		Hilber-Hughes-Taylor (α-method), $-\frac{1}{3} \leq \alpha \leq 0$		
[2.13,11.55]	$\frac{1}{2}(1 - 2\alpha)$	$\frac{1}{4}(1 - \alpha)^2$	Unconditional	$O(\Delta t^2)$

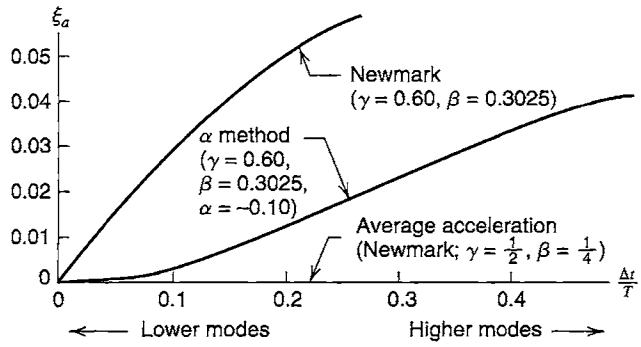

Figure 11.13-1. Algorithmic damping ratios ξ_a provided by implicit integration methods, where T is the period of the mode for which ξ_a is depicted [11.57].

implicit method elsewhere. Use of a mixture of explicit and implicit temporal integration methods in a single problem, so as to make best use of the characteristics of each, is known as *operator splitting* or *mixed time integration.* References include [2.13,2.14,11.48,11.57–11.61].

11.14 DIRECT INTEGRATION: STABILITY AND ACCURACY ANALYSIS

To examine stability, it is sufficient to let $\{\mathbf{R}^{\text{ext}}\} = \{\mathbf{0}\}$ in the equation of motion, for the reason that if an algorithm is stable for $\{\mathbf{R}^{\text{ext}}\} = \{\mathbf{0}\}$, it is also stable when $\{\mathbf{R}^{\text{ext}}\}$ is nonzero but bounded. Broadly speaking, stability can be analyzed by two methods. One is *spectral* or *Fourier* stability analysis, which examines the equation of motion of a single d.o.f. The justification is that a single equation is representative of a typical modal equation, and modal decomposition of a multiple-d.o.f. structure represents the structure exactly if all modes are retained. The second method is *energy* stability analysis, which examines equations of the original system and establishes conditions under which a norm of the solution is bounded as time increases. Spectral stability usually provides more insight and sometimes more precise results, while energy stability can be applied to more complicated problems. References include [2.13,11.57,11.59,11.61,11.62].

In what follows we consider the (explicit) central difference method and the (implicit) average acceleration method, both without damping.

Central Difference Method: Spectral Stability. Let us apply the central difference method to undamped motion of a single d.o.f. With zero external load, we obtain from the generic modal equation (Eq. 11.7-6), with subscript i omitted for simplicity,

$$\ddot{Z} + \omega^2 Z = 0 \tag{11.14-1}$$

This equation describes oscillatory motion (Eq. 11.14-14b). A central difference approximation is obtained by substituting Eq. 11.12-1b into Eq. 11.14-1 written at time step n. Thus

$$Z_{n+1} + (\omega^2 \Delta t^2 - 2)Z_n + Z_{n-1} = 0 \tag{11.14-2}$$

We seek a solution of the form $Z = \lambda^n$. Thus $Z_{n+1} = \lambda^{n+1}$ and $Z_{n-1} = \lambda^{n-1}$. Making these substitutions and dividing by λ^{n-1}, we obtain

$$\lambda^2 + (\omega^2 \Delta t^2 - 2)\lambda + 1 = 0 \tag{11.14-3}$$

which is called the *characteristic equation*. Solving this quadratic equation for its roots λ_1 and λ_2, we obtain

$$\lambda_{1,2} = \frac{1}{2}\left(2 - \omega^2 \Delta t^2 \pm \omega \, \Delta t \sqrt{\omega^2 \Delta t^2 - 4}\right) \tag{11.14-4}$$

Roots may be real or complex. For the time being, we assume that roots are distinct, $\lambda_1 \neq \lambda_2$. Then the solution of Eq. 11.4-2 is

$$Z_n = C_1 \lambda_1^n + C_2 \lambda_2^n \qquad \text{when} \qquad \lambda_1 \neq \lambda_2 \tag{11.14-5}$$

If $|\lambda_1| \leq 1$ and $|\lambda_2| \leq 1$, then Z_n decays or remains steady with time, providing stable computation. But if $|\lambda_1| > 1$ or if $|\lambda_2| > 1$, then Z_n becomes unbounded; this is instability. To investigate these possibilities we note that roots of the quadratic equation $a\lambda^2 + b\lambda + c = 0$ satisfy the relation $\lambda_1 \lambda_2 = c/a$, where $c/a = 1$ for Eq. 11.14-3. If the radicand in Eq. 11.14-4 is positive, then both λ_1 and λ_2 are real, and, with our assumption that λ_1 and λ_2 are distinct, $\lambda_1 \lambda_2 = 1$ indicates that one root is greater than unity while the other is less. Thus instability results. But if the radicand in Eq. 11.14-4 is negative, then λ_1 and λ_2 are complex conjugates, each of unit modulus (that is, each of unit magnitude) by virtue of $\lambda_1 \lambda_2 = 1$. Thus stable computation always results if the radicand in Eq. 11.14-4 is negative. Hence

$$\omega^2 \Delta t^2 - 4 < 0 \qquad \text{yields} \qquad \Delta t < \frac{2}{\omega} \tag{11.14-6}$$

Next consider the case of repeated roots. If the radicand in Eq. 11.14-4 is zero, then $\omega \, \Delta t = 2$, $\lambda_1 = \lambda_2 = -1$, and the solution of Eq. 11.4-2 is [11.63]

$$Z_n = C_1 \lambda_1^n + n \, \Delta t \, C_2 \lambda_1^n \qquad \text{when} \qquad \lambda_1 = \lambda_2 \tag{11.14-7}$$

Because n appears linearly in the second term of this equation, Z_n diverges in arithmetic fashion.

Recall that Eq. 11.14-1 is but one of many uncoupled modal equations that represent the complete structure. Our intent is to use direct integration to solve a system of *coupled* equations that represents the complete structure. The allowable Δt is governed by the modal equation that is most restrictive. Therefore, we must consider all natural frequencies of the numerical model and use the largest in Eq. 11.14-6. Thus we obtain the stability condition

$$\Delta t < \frac{2}{\omega_{\max}} \tag{11.14-8}$$

Equation 11.14-8 is usually stated in the literature as $\Delta t \leq 2/\omega_{\max}$. This equation ignores the possibility of arithmetic divergence due to repeated roots, Eq. 11.14-7. In practice this

situation is not likely to be encountered, especially when $\omega_{\max}$ is bounded from above by an approximation such as the Gerschgorin bound, Eq. 11.12-17.

Average Acceleration: Spectral Stability. We begin by writing the undamped, single-d.o.f. equation of motion, Eq. 11.14-1, at time steps n, $n + 1$, and $n + 2$, and adding the three equations that result. Thus

$$\ddot{Z}_{n+2} + 2\ddot{Z}_{n+1} + \ddot{Z}_n + \omega^2(Z_{n+2} + 2Z_{n+1} + Z_n) = 0 \tag{11.14-9}$$

The average acceleration method is given by $\gamma = 1/2$ and $\beta = 1/4$ in Eqs. 11.13-3. For the present argument we replace $\{\mathbf{D}\}$ by the single dependent variable Z. Thus Eq. 11.13-3b expresses Z_{n+1}. We also express Z_{n+2} by advancing the time step, then write $Z_{n+2} - Z_{n+1}$. The result contains $\dot{Z}_{n+1} - \dot{Z}_n$, which, from Eq. 11.13-3a, is $\Delta t\,(\ddot{Z}_{n+1} + \ddot{Z}_n)/2$. Thus Eqs. 11.13-3 yield

$$Z_{n+2} - 2Z_{n+1} + Z_n = \frac{\Delta t^2}{4}\left(\ddot{Z}_{n+2} + 2\ddot{Z}_{n+1} + \ddot{Z}_n\right) \tag{11.14-10}$$

Use of Eq. 11.14-9 to eliminate acceleration terms in Eq. 11.14-10 yields

$$(1 + h)Z_{n+2} + (2h - 2)Z_{n+1} + (1 + h)Z_n = 0 \qquad \text{where} \qquad h = \frac{\omega^2 \Delta t^2}{4} \tag{11.14-11}$$

We seek a solution of the form $Z = \lambda^n$. Thus $Z_{n+2} = \lambda^{n+2}$ and $Z_{n+1} = \lambda^{n+1}$. Making these substitutions and dividing by λ^n, we obtain

$$(1 + h)\lambda^2 + (2h - 2)\lambda + (1 + h) = 0 \tag{11.14-12}$$

Solving this quadratic equation for its roots λ_1 and λ_2, we obtain

$$\lambda_{1,2} = \frac{1 - h \pm 2\sqrt{-h}}{1 + h} \qquad \text{where} \qquad h = \frac{\omega^2 \Delta t^2}{4} \tag{11.14-13}$$

The equation for Z_n is Eq. 11.14-5. Applying the argument that follows Eq. 11.14-5, we obtain $\lambda_1\lambda_2 = 1$ for the average acceleration method. In addition, the radicand of Eq. 11.14-13 is always negative. Therefore λ_1 and λ_2 are complex conjugates, hence distinct, and each of unit modulus. Thus $|\lambda_1| = |\lambda_2| = 1$ regardless of the value of h, and Z_n does not grow as n increases. Accordingly, computation is stable regardless of the value of h (and hence of Δt). The same is true when damping is included, although we have not proved it here.

Amplitude and Period Errors. An approximate solution obtained by direct integration may display amplitude error and/or period error, as illustrated in Fig. 11.14-1. Amplitude error can be either amplitude increase, which is the same as instability, or amplitude decay, which is called algorithmic damping. Period error can consist of either period elongation or period contraction.

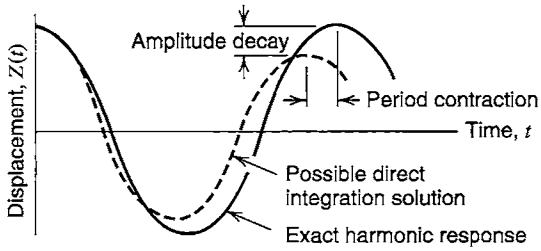

Figure 11.14-1. Possible amplitude and period errors in direct integration.

To investigate these errors, in both central difference and average acceleration methods, we again consider the undamped equation of motion of a single d.o.f., Eq. 11.14-1. The solution is harmonic, and can be written either in polar form or in trigonometric form:

$$Z^{\text{exact}} = \tilde{C}_1 e^{i\omega t} + \tilde{C}_2 e^{-i\omega t} \qquad \text{where} \qquad i = \sqrt{-1} \tag{11.14-14a}$$

$$Z^{\text{exact}} = \tilde{C}_1(\cos\omega t + i\sin\omega t) + \tilde{C}_2(\cos\omega t - i\sin\omega t) \tag{11.14-14b}$$

in which $\tilde{C}_1$ and $\tilde{C}_2$ are determined by initial conditions. For $\omega\,\Delta t < 2$, Eq. 11.14-4 of the central difference method can be written as

$$\lambda_{1,2} = x \pm iy \qquad \text{where} \qquad \begin{aligned} x &= \frac{1}{2}\left(2 - \omega^2\Delta t^2\right) \\ y &= \frac{1}{2}\omega\,\Delta t\sqrt{4 - \omega^2\Delta t^2} \end{aligned} \tag{11.14-15}$$

By proper choice of real constants a and b, we can write λ_1 and λ_2 as

$$\lambda_1 = e^{(a+ib)\,\Delta t} = e^{a\,\Delta t}e^{ib\,\Delta t} = e^{a\,\Delta t}(\cos b\Delta t + i\sin b\Delta t) \tag{11.14-16a}$$

$$\lambda_2 = e^{(a-ib)\,\Delta t} = e^{a\,\Delta t}e^{-ib\,\Delta t} = e^{a\,\Delta t}(\cos b\Delta t - i\sin b\Delta t) \tag{11.14-16b}$$

Hence Eq. 11.14-5 becomes

$$Z_n = C_1 e^{an\,\Delta t}(\cos bn\Delta t + i\sin bn\Delta t) + C_2 e^{an\,\Delta t}(\cos bn\Delta t - i\sin bn\Delta t) \tag{11.14-17}$$

With $n\,\Delta t = t$ in Eq. 11.14-17, comparison of Eqs. 11.14-14b and 11.14-17 shows that amplitude error will result unless $a = 0$ and period error will result unless $b = \omega$. Period error is addressed first.

Period Error. We define period error P as

$$P = \frac{P_{\text{approx}}}{P_{\text{exact}}} = \frac{2\pi/b}{2\pi/\omega} = \frac{\omega}{b} \qquad \text{where} \qquad \begin{aligned} &P > 1 \text{ period elongation} \\ &P = 1 \text{ no period error} \\ &P < 1 \text{ period contraction} \end{aligned} \tag{11.14-18}$$

From Eqs. 11.14-15, 11.14-16, and 11.14-17, with $n = 1$,

$$\tan b\Delta t = \frac{\sin b\,\Delta t}{\cos b\,\Delta t} = \frac{y}{x} \qquad \text{hence} \quad b = \frac{1}{\Delta t}\arctan\frac{\omega\Delta t\sqrt{4-\omega^2\Delta t^2}}{2-\omega^2\Delta t^2} \tag{11.14-19}$$

$$P = \frac{\omega}{b} = \omega\,\Delta t\left[\arctan\frac{\omega\,\Delta t\sqrt{4-\omega^2\Delta t^2}}{2-\omega^2\Delta t^2}\right]^{-1} \tag{11.14-20}$$

in which the angle obtained from the arctangent function is required to be positive. Equation 11.14-20 represents period contraction; it is plotted in Fig. 11.14-2.

For the average acceleration method, derivation of period errors is the same except that x and y in Eq. 11.14-15 must be redefined to agree with Eq. 11.14-13. Specifically, we now have

$$x = \frac{1-h}{1+h} \qquad y = \frac{2\sqrt{h}}{1+h} \qquad \tan b\Delta t = \frac{2\sqrt{h}}{1-h} \qquad P = \omega\Delta t\left[\arctan\frac{4\omega\,\Delta t}{4-\omega^2\Delta t^2}\right]^{-1} \tag{11.14-21}$$

in which the angle obtained from the arctangent function is required to be positive. Equation 11.14-21 represents period elongation; it is plotted in Fig. 11.14-2.

We emphasize that Fig. 11.14-2 pertains to the mode whose frequency is ω. A multiple-d.o.f. structure has many modes. For numerical analysis one should select a Δt such that $\omega\,\Delta t$ is small for all modes of practical interest.

Figure 11.14-2 provides guidance as to the choice of mass matrix in direct integration. Use of a lumped mass matrix often underestimates natural frequencies, which means that a lumped mass matrix often elongates periods. This discretization error partially compensates for the algorithmic error of period contraction in the central difference method. With

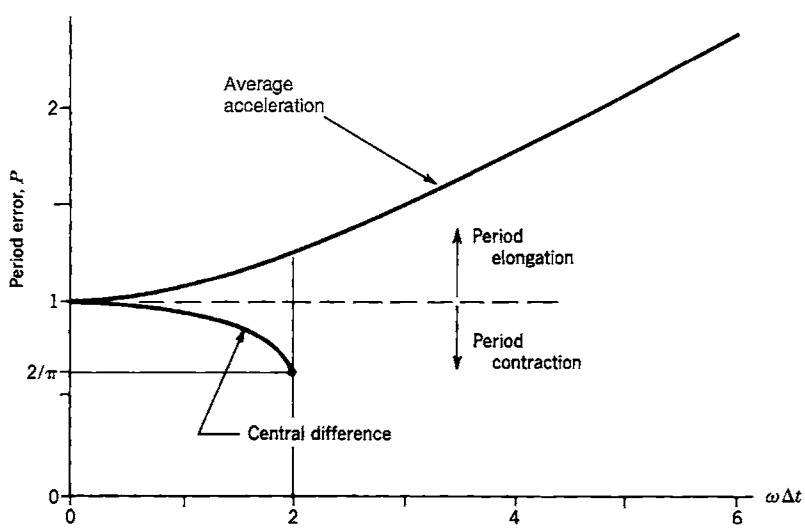

Figure 11.14-2. Period errors of central difference and average-acceleration methods.

the average acceleration method, the situation is reversed: consistent mass matrices overestimate frequencies and thus contract periods, which partially compensates for the algorithmic error of period elongation in the average acceleration method. Respectively, these observations are true of explicit methods and implicit methods in general. It is fortunate that these choices of mass matrix, lumped for explicit and consistent for implicit, are not only beneficial to accuracy but are also beneficial to computational economy (or, in implicit methods, not very detrimental). *Poor choices* would be consistent [**M**] with explicit methods and lumped [**M**] with implicit methods.

Amplitude Error. The central difference and average acceleration methods are both free of amplitude error, as may be seen by review of arguments pertaining to stability. For both methods, Z_n is given by Eq. 11.14-5. As argued following Eqs. 11.14-5 and 11.14-13, λ_1 and λ_2 are complex conjugates of unit modulus. Therefore Eq. 11.14-5 shows that Z_n neither grows nor decays as n increases.

To show in another way that the central difference method has no amplitude error, consider the sum $\lambda_1 + \lambda_2$, which may be written in two ways, first using Eq. 11.14-4, then using Eq. 11.14-16 with the polar forms of $e^{ib\,\Delta t}$ and $e^{-ib\,\Delta t}$. Thus

$$2 - \omega^2 \Delta t^2 = 2e^{a\,\Delta t} \cos b\,\Delta t \tag{11.14-22}$$

Substituting for $b\,\Delta t$ from Eq. 11.14-19 provides an equation for $a\,\Delta t$ that reduces to $a\,\Delta t = 0$ for all values of $\omega\,\Delta t$ (with $\omega\,\Delta t < 2$ for stability). For the average acceleration method, we use an equation analogous to Eq. 11.14-22, obtained by combining Eqs. 11.14-13 and 11.14-16, then substitute for $b\,\Delta t$ from Eq. 11.14-21, and after manipulation similarly conclude that $a\,\Delta t = 0$ for all values of $\omega\,\Delta t$. Completion of these arguments is left as an exercise.

Saying that the central difference method has no amplitude error does not mean that computed amplitudes will be exact. We argue as follows. When λ_1 and λ_2 are appreciably different, C_1 and C_2 in Eq. 11.14-17 are approximately the same as $\tilde{C}_1$ and $\tilde{C}_2$ in Eq. 11.14-14b. But when Δt is very close to the stability limit, λ_1 and λ_2 are almost equal, and the two parenthetic expressions in Eq. 11.14-17 are almost equal. In this situation, C_1 and C_2 may differ greatly from $\tilde{C}_1$ and $\tilde{C}_2$. What is meant by the statement that the central difference method has no amplitude error is that the envelope of the numerical solution does not grow or decay.

11.15 ANALYSIS BY RESPONSE SPECTRA

Imagine that a trial design is to be analyzed for its response to an anticipated dynamic loading of known form (other than harmonic loading, for which harmonic response analysis is appropriate). Then analysis may seek the *maximum* displacement, stress, or acceleration at one or more locations in a structure, regardless of when the maximum appears during the response history. A possible method is to use the modal method or direct integration to calculate the entire response history, then discard all results except the single maximum value. Maxima can be calculated more directly by using *response spectra,* especially if they are already available, as is the case for "standard" earthquake excitation. If response analysis must be preceded by calculation of response spectra, it is not clear that overall effort and computational expense will be less than that of modal analysis or direct integration.

In brief, response spectra are used to calculate the maximum response of each structural mode to a given excitation, then modal maxima are combined in such a way as to estimate the maximum response of the structure itself. In the following summary, conditions are presumed to be linearly elastic. Textbook references include [†1.2,11.3,11.64–11.66]. Widely used FE software supports use of response spectra in calculations.

Response Spectra. A *response spectrum* is a plot, for a prescribed dynamic loading and *for a single-d.o.f. system,* of the maximum magnitude of response versus either the natural frequency of the system or its period. "Response" may be any calculated quantity. Typically, displacement and acceleration are plotted. If the dynamic loading is a single impulse load, a response spectrum may be called a "shock response spectrum" or simply a "shock spectrum."

Consider a single-d.o.f. system, Fig. 11.15-1a, and its equation of motion (Eq. 11.2-1 or Eq. 11.4-3) Assume that response spectra for displacement are required. The natural frequency of the system is $\omega = \sqrt{k/m}$. A value of ω is selected, and the displacement response history produced by the known forcing function $r = r(t)$ is calculated by any appropriate method (perhaps by direct integration). Results are scanned for the maximum magnitude of displacement, at whatever time it appears. Thus we obtain a single point in the plot of $u^{\max}$ versus ω. Another value of ω is selected and calculations repeated to obtain a second point. The second point represents a $u^{\max}$ that probably appears at a different time than the first. Times at which maxima appear play no role in the construction of response spectra (but may be tabulated separately). After calculating a great many points we connect the points to obtain one response spectrum, such as one of the $u^{\max}$ versus ω curves shown in Fig. 11.15-1. The entire process can be repeated with a different value of damping ratio ξ to obtain the curve that represents another response spectrum. The ordinate may be stated not as $u^{\max}$ but as an amplification factor, $S = S(\omega)$, which is the ratio of $u^{\max} = u^{\max}(\omega)$ to the static displacement $u_{st} = r^{\max}/k$, where $r^{\max}$ is the maximum magnitude of $r = r(t)$. Thus, S is independent of the magnitude of forcing function r; only its variation with time is of importance.

Note that the abscissa for plotted spectra is not time, but either *frequency* or *period.* Recall that ω is the natural frequency of the single-d.o.f. system and has nothing to do with frequencies that may be present in the forcing function. Figure 11.10-2 shows response spectra for sinusoidal loading. A harmonic response plot, such as the example in Fig. 11.17-3b, is not a response spectrum. It depicts displacement of a particular d.o.f. in a multiple-d.o.f. system

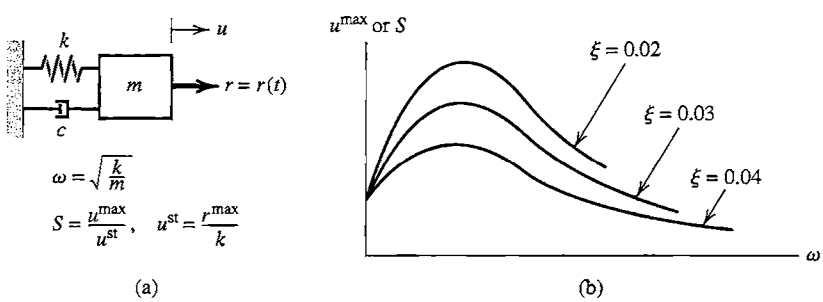

Figure 11.15-1. (a) Single-d.o.f. system with forcing function $r = r(t)$. (b) Hypothetical displacement response spectra for a known (but here unspecified) forcing function.

rather than displacement of a single-d.o.f. system, and the abscissa is frequency of an applied sinusoidal load rather than a frequency of the system.

For earthquake excitation, ground acceleration $\ddot{u}_g$ is known from recorded seismic data. Therefore forcing function $-m\ddot{u}_g$ in Eq. 11.2-2 is known, and a response spectrum for this forcing function and a prescribed damping ratio ξ can be constructed. Different earthquakes yield different spectra, but when plotted on the same axes there is a similarity among them. A "standard" spectrum can be obtained from the spectra of several earthquakes, perhaps by drawing a smooth bounding line or by a statistical smoothing process. The exercise can be repeated for other values of ξ. The resulting spectra can be used for design of any structure subjected to the same earthquake loading. Clearly, despite having a single-d.o.f. system, construction of response spectra requires considerable computation. For each ξ, hundreds of single-d.o.f. equations must be integrated (each based on a different ω), with hundreds of time steps per equation if direct integration is used. However, once calculated, spectra for a given forcing function need never be recalculated, and may be applied to any linear multiple-d.o.f. structure excited by the same forcing function, regardless of the structure's form or how many d.o.f. it has.

As a simple single-d.o.f. application, imagine a water tank atop a prismatic pipe. What, approximately, is the maximum flexural stress in the pipe due to an earthquake whose response spectrum is known? Let us idealize the structure as a particle mass m at the end of a massless cantilever beam of length L. The natural frequency is $\omega = \sqrt{k/m} = \sqrt{3EI/mL^3}$. A response spectrum provides $u^{\max}$ for this ω, where $u^{\max}$ represents lateral tip displacement relative to the ground in this case. The static lateral tip load that would produce $u^{\max}$ is $P = 3EIu^{\max}/L^3$; bending moment at the base is $M = PL$; flexural stress is Mc/I. An increase in pipe diameter may increase or decrease flexural stress, depending on the shape of the spectrum.

Modal Combination Rules. Response spectra derived for a single-d.o.f. system can be applied to a multiple-d.o.f. structure loaded by the same excitation under the assumption that *each individual mode of the structure responds like the single-d.o.f. system.* We also assume that individual nodal loads in $\{\mathbf{R}^{\text{ext}}\}$ all vary with time in the same way, so that $r = r(t)$ can represent these loads. For any mode of frequency ω_i and damping ratio ξ_i, a response spectrum provides displacement amplification factor S_i. From Eq. 11.4-3 the maximum magnitude of displacement is

$$u_i^{\max} = S_i u_i^{\text{st}} = S_i \frac{r_i^{\max}}{k} = S_i \frac{r_i^{\max}/m}{k/m} = S_i \frac{r_i^{\max}/m}{\omega_i^2} \tag{11.15-1}$$

For a multiple-d.o.f. structure we use modal quantities rather than physical quantities. So, in similar fashion to Eq. 11.15-1, we apply S_i to Eq. 11.7-6. With $P_i^{\max}$ the maximum magnitude of modal load, we obtain the modal maximum

$$Z_i^{\max} = S_i Z_i^{\text{st}} = S_i \frac{P_i^{\max}}{\omega_i^2} \tag{11.15-2}$$

With $\lfloor \Phi \rfloor_j$ the jth row of the mass-normalized modal matrix, Eq. 11.7-4 yields

$$D_j = \lfloor \Phi \rfloor_j \{Z\} \quad \text{or} \quad D_j = \sum_i \Delta_{ji} \quad \text{where} \quad \Delta_{ji} = \Phi_{ji} Z_i \tag{11.15-3}$$

in which Z_i and consequently Δ_{ji} are functions of time. Now consider the Δ_{ji} at a particular time, specifically when $Z_i^{\max}$ appears. The associated Δ_{ji}, denoted by an overbar, is

$$\bar{\Delta}_{ji} = \Phi_{ji} Z_i^{\max} \tag{11.15-4}$$

For example, $\bar{\Delta}_{32}$ is the value of d.o.f. D_3 produced by $Z_2^{\max}$ of the second mode. Because Φ_{ji} may be positive or negative, so may $\bar{\Delta}_{32}$. To obtain an estimate of the largest magnitude of D_3 at *any* instant of time, the contributions of all $\bar{\Delta}_{3i}$ must be included. We cannot simply add them, as may be suggested by Eq. 11.15-3, because for different modes i the $\bar{\Delta}_{3i}$ values associated with the various $Z_i^{\max}$ values in general appear at different times. However, by doing so we obtain an upper bound on the maximum magnitude of displacement d.o.f.

$$\text{Upper bound:} \quad D_j^{\max} = \sum_i |\bar{\Delta}_{ji}| \qquad \text{In general:} \quad D_j^{\max} \le \sum_i |\bar{\Delta}_{ji}| \tag{11.15-5}$$

There is no mathematically rigorous method for combining modal maxima to produce the physical maximum. If frequencies of contributing modes are well-separated, good results are often obtained by using the square root of the sum of the squares (SRSS):

$$\text{SRSS method:} \quad D_j^{\max} = \sqrt{\sum_i (\bar{\Delta}_{ji})^2} \tag{11.15-6}$$

The NRL-Sum method [11.67] uses the mode of largest magnitude, which we call $|\bar{\Delta}_{jm}|$, and applies SRSS to all other modes:

$$\text{NRL-Sum method:} \quad D_j^{\max} = |\bar{\Delta}_{jm}| + \sqrt{\sum_{i \ne m} \left(\bar{\Delta}_{ji}\right)^2} \tag{11.15-7}$$

Additional combination methods are discussed in other references.

Chopra [11.3] warns against a pitfall in calculating a quantity that depends on relative nodal displacements, such as curvature in a beam element, from which flexural stress is calculated. The correct way is to combine modal contributions to the same response quantity, in this case to curvature, and calculate its maximum. It would be incorrect to calculate curvature from separate maxima of the d.o.f. that contribute to curvature.

The foregoing discussion tacitly assumes that the forcing function has a single spatial component. That is, it might be the north-south component of earthquake motion. East-west and vertical components, and even rotational components, may also be present. Discussion of such complications appears in [11.65].

Some calculation details appear in the latter part of Section 11.18.

11.16 REMARKS. MODELING CONSIDERATIONS

Dynamic analysis is more complicated than static analysis. Loadings have the additional dimension of time, goals of analysis may be more varied, and there are more computational

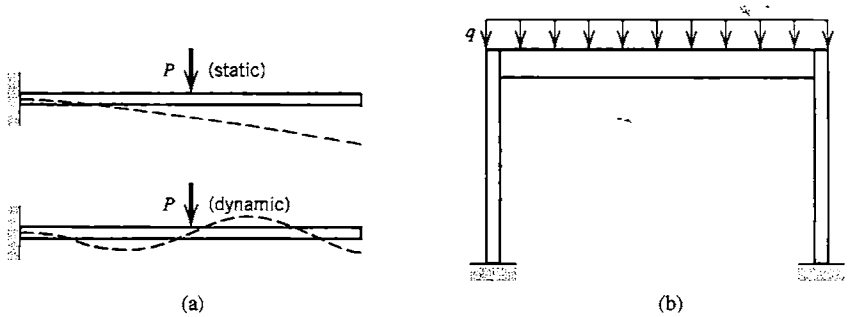

Figure 11.16-1. (a) Cantilever beams under static and dynamic loads. (b) Portal frame under static load q.

procedures that may lead to each goal. Dynamic analysis is more expensive than static analysis, both in demands on the analyst's time and demands on computer resources. It is more difficult to anticipate structural response, so it is more difficult to do preliminary analysis, plan the numerical work, and judge the quality of computed results.

Nevertheless, general advice like that given in Chapter 10 is appropriate. Understand the physical problem, structural dynamics concepts, and analysis procedures. Study software documentation and heed warning messages produced by software. Start simply, with pilot studies and coarse-mesh models. Expect to revise and improve models. Critically examine computed results. Keep records of data sources, assumptions made, pilot studies conducted, load cases considered, and methods used. The reader may wish to review Chapter 10 for additional advice that may be applied to dynamics as well as to statics.

Static and dynamic loads may create quite different responses in a given structure. In Fig. 11.16-1a, the right-hand part of the beam contributes nothing to static response due to load P. *Dynamically,* the right-hand part contributes substantially. For a given magnitude of P, dynamic stresses may substantially exceed their static counterparts, and their spatial distribution will probably not be obvious. In Fig. 11.16-1b, dynamic analysis is influenced by the frame's stiffness, which is less in horizontal directions than the vertical direction, and is reduced by connections to an extent that special connection modeling may be used [11.68]. Static analysis may emphasize stresses produced by vertical loading, but earthquake excitation is more likely to produce horizontal loading. Similarly, a structure may have flat panels that act as membranes to carry static load, but vibrate laterally with bending deformation under dynamic loading.

If dynamic analysis must be undertaken, several preliminary questions must be answered [2.21]. What is the goal of analysis? How much accuracy is required? What simplifications are possible? Is damping important? If so, how should it be represented? Are there material or geometric nonlinearities? What frequencies are implicitly contained in the loads, and what frequencies are important in the structure? What computational procedures are appropriate, and are they available in the software to be used? What output is appropriate? How will the large volume of output be sorted, stored, displayed, and checked?

Subsections that follow remark on practical aspects of matters discussed previously and add modeling suggestions.

Mass Representation. The mass matrix of a finite element can be written in various ways, such as particle-lumped (diagonal), diagonalized by algorithm, or consistent (full). Which way is best? Some considerations that influence the choice are as follows.

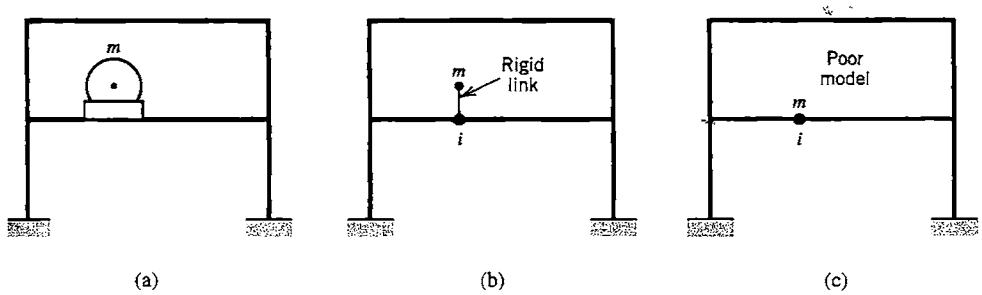

Figure 11.16-2. (a) Stiff machine of mass m attached to a building frame. (b) Acceptable model. (c) Poor model.

If element deformation fields are interelement-compatible, stiffness matrices are not softened by low-order quadrature rules, and mass matrices are consistent, then the FE model will provide natural frequencies of vibration that are upper bounds on the exact frequencies of the mathematical model. Particle-lumped mass matrices often (but not always) produce natural frequencies that are *lower* than exact. A solution algorithm that demands nonzero diagonal entries in [**M**] will fail if [**M**] is particle-lumped and there are rotational d.o.f., unless rotary inertia is arbitrarily assigned to rotational d.o.f. Usually the value assigned need not be accurate, because rotary inertia has little influence on the important lower modes of the FE model. However, for direct integration by a conditionally stable method, rotary inertia should not be so small as to make the allowable time step less than that dictated by the particle masses. With explicit direct integration, a lumped [**M**] is preferred for accuracy and is needed for economy. With implicit direct integration, a consistent [**M**] is preferred for accuracy and is only slightly detrimental to economy.

The frame in Fig. 11.16-2 supports a heavy machine of mass m, which is a "nonstructural" mass because it is considered practically rigid in comparison with the frame. It is acceptable to model the machine as a particle mass attached to the frame by a rigid link. To avoid the artificial introduction of a high-frequency mode, the link should be rigid, not merely of large stiffness (Sections 8.5 and 9.2). Motion of m is governed by both translational and rotational d.o.f. at node i, so off-diagonal terms appear in [**M**]. An ad hoc diagonalization scheme should not result in simply placing m at node i, as in Fig. 11.16-2c, as then realistic interaction between rotational and translational d.o.f. at node i would be lost. More generally, but for the same reason, a multi-point constraint that rigidly couples d.o.f. with mass should retain d.o.f. at the mass center of the rigid assembly as master d.o.f. [11.21].

Vibration Calculations. The eigenvalue problem, Eq. 11.4-5, can be solved by various algorithms (Appendix C). They differ in applicability and efficiency according to matrix sparsity, matrix topology, the number of frequencies to be calculated, and other factors. Software typically offers a choice of algorithms. Usually only the several lowest frequencies are calculated, perhaps the lowest 10% or so, as no more are needed for many analyses.

If a structure is not fully supported or has mechanisms, [**K**] will be singular, and each possible rigid-body mode or mechanism mode will display zero frequency. This circumstance may indicate modeling error. When [**K**] is intentionally singular, the user may have to invoke an "eigenvalue shift" to enable computation. If singularities have been avoided by introduction of a low-stiffness stabilization device, the important lower eigenspectrum will be cluttered with nonphysical low-frequency modes. At the other extreme, if [**M**] is

singular because it is diagonal and has some zero coefficients M_{ii}, an infinite frequency is implied by each such occurrence, and the eigensolver may balk.

Different modes may have the same frequency. The common example is a 3D cantilever beam of circular cross section, where each mode in one transverse plane has a mode of the same shape and frequency in the perpendicular transverse plane. This simple problem can be used as a test case to see if the eigensolver can detect repeated frequencies and can separate the associated modes. A Sturm sequence check (Appendix C) can discover if the eigensolver has missed any natural frequencies. If so, the solution can be repeated, this time with a greater number of frequencies requested. The missed frequencies may now appear [11.21].

Preliminary Frequency Estimates. As part of preliminary analysis that precedes FEA, it is sometimes possible to approximate the fundamental frequency using simple calculation, by reducing the system to an equivalent mass m supported by an equivalent spring of stiffness k. Both k and m may be approximate. Example applications of this method appear at the end of Section 11.6 and in Section 11.17. The Rayleigh quotient, Eq. 11.4-13, can also be used with an assumed mode shape.

If an equivalent stiffness k cannot be easily obtained by hand calculation, it can be obtained from the FE model itself, by applying a static load P. Load P must be located and directed so as to produce a deflected shape that resembles the anticipated mode shape. If Δ is the computed static displacement of P, the desired stiffness is $k = P/\Delta$. Software can compute total structure mass and the mass center location.

The Rayleigh quotient (Eq. 11.4-13) can sometimes be used to rank the frequencies of possible modes. The magnitude of $\{\bar{\mathbf{D}}\}_i$ does not matter, so it is convenient to imagine that each mode has the same maximum displacement. Thus, if we compare modes 1 and 2 in Fig. 11.16-3, we see that curvatures are greater for mode 2, which indicates that mode 2 produces the greater numerator in a Rayleigh quotient. Also, mode 2 has a point of zero displacement that mode 1 does not, which produces a smaller denominator. Thus we conclude that $\omega_1 < \omega_2$. Similar comparisons that involve mode 3 can be made [11.7].

Stress concentrations are local effects that have little influence on overall displacement modes. Accordingly, in view of the Rayleigh quotient, they have little influence on vibration frequencies, and, depending on analysis goals, might be modeled crudely, at least in initial analyses.

Response History: Modal Analysis. The greatest computational expense is likely to be solving the eigenproblem for the necessary mode and frequency information. This information may be available from a previous phase of the investigation. Uncoupled modal equations are cheaply integrated. By adjustment of modal damping ratios, algorithmic damping can be supplied to higher modes without affecting lower modes. The modal method is especially attractive if the effects of several different time-dependent loadings

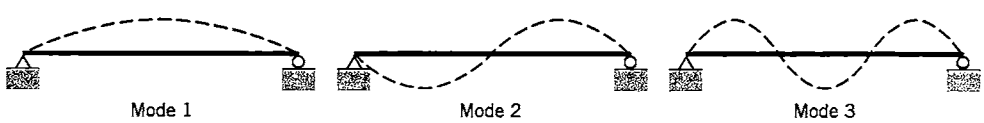

Figure 11.16-3. The first three vibration modes of a simply supported beam. Displacements are exaggerated.

are to be studied, because the same modes and frequencies are used for each. In contrast, direct integration requires complete re-solution for each different loading.

The modal method is best suited to structural dynamics problems, such as associated with earthquake loading, where only the lowest several modes are needed to calculate response. Modal analysis is not suited to wave propagation problems, such as associated with blast or impact loading, because the large number of modes needed would make the method uneconomical.

How many modes are needed? No easy answer is available. Some considerations that influence the decision appear in Section 11.7. Considering only the frequency content of the applied loading, some suggestions are as follows [2.14,2.21,10.6,11.3,11.21]. Let Ω_u be the circular frequency of the highest significant component in the loading, as determined from a Fourier series representation of the loading. The response spectrum appropriate to the quantity of interest, be it displacement, velocity, or acceleration, may be useful in identifying Ω_u. As shown by a single-d.o.f. system under sinusoidal loading, structural modes of frequency higher than about $4\Omega_u$ respond to load in almost static fashion, while modes of frequency less than $4\Omega_u$ respond dynamically. A "cutoff" frequency Ω_{co} identifies the highest modal frequency that need be used in most analyses, where $\Omega_{co} = 1.5\Omega_u$ (at least) or $\Omega_{co} = 4\Omega_u$ (at most). The larger values of Ω_{co} are used if velocities or accelerations must be computed in addition to displacements.

The highest frequency the FE mesh must be able to represent may also be taken as Ω_{co}. However, if the *spatial* distribution of the load is complicated, or if stresses as well as displacements must be computed, a finer mesh may be needed in order to allow a more complicated deformation state, and enough modes must be retained to represent that state. Obviously an ultra-coarse mesh will not suffice if the load distribution is complicated, even if the load varies with time in simple sinusoidal fashion, nor will very few modes unless static correction is applied.

Response History: Direct Integration. With a direct method, there is no need to calculate modes and frequencies (although they may be calculated anyway for other reasons). If there are several different time-dependent loadings, a separate direct integration solution must be undertaken for each.

Again, direct integration may be *explicit* or *implicit*. Differences between the two methods, and problems for which each is best suited, are summarized in Section 11.11. Explicit methods are conditionally stable. Implicit methods used in practice are unconditionally stable.

The time step Δt used in a conditionally stable method is limited by a stability criterion. The largest stable Δt provides adequate temporal discretization; indeed, in the central difference method (CDM), use of a smaller Δt may *decrease* accuracy rather than increase it [2.14]. If $[\mathbf{M}]$ is diagonal, the CDM (Eq. 11.12-6 or Eq. 11.12-8) requires very little computer storage and very little computation per time step, especially if $[\mathbf{C}]$ is also diagonal. However the allowable Δt is so small that most practical application of CDM is to short-time-scale phenomena such as blast and impact problems. Such problems often involve nonlinearity, which is accommodated with greater ease and efficiency by CDM than by an implicit method, because there is no need to repeatedly form and factor a changing stiffness matrix, and stiffness-related terms can instead be taken into account by summing element contributions that are based on historical information.

With CDM, a uniform mesh allows waves to propagate uniformly in all directions. Abrupt element size changes create numerical noise and artificial wave reflections [11.69].

Low-order elements are better than higher-order elements at modeling a shock wavefront. A lumped [**M**] creates fewer spurious oscillations than a consistent [**M**] and also allows a larger Δt. The trick of using a very stiff element as a support (Section 9.2) has the effect of raising $\omega_{\max}$, thus decreasing the allowable Δt, and should therefore be avoided. Reduction (Sections 11.6 and 11.8) should also be avoided because it discards higher-frequency information that is needed for a wave-propagation problem.

With an unconditionally stable implicit method (USIM), Δt is limited only by considerations of accuracy. USIM may be competitive with the modal method, but less so when more than one time-dependent load must be investigated. Cost per time step in USIM is high because the coefficient matrix ([$\mathbf{K}^{\text{eff}}$] of Eq. 11.13-5) is not diagonal, and in a nonlinear problem changes from one time step to the next, thus requiring repeated factorization. A consistent [**M**] is helpful to accuracy and only slightly detrimental to economy. With USIM one uses the largest Δt consistent with the accuracy required. From 10 to 30 time steps per period of cut-off frequency Ω_{co} have been suggested, where Ω_{co} is defined in foregoing remarks about modal analysis. Thus one would use Δt in the range $2\pi/30\ \Omega_{co} < \Delta t < 2\pi/10\ \Omega_{co}$. As a partial check for accuracy, analysis can be repeated with a smaller time step. If computed results are much the same, the original time step was probably small enough.

Symmetry. In static analysis, symmetry of geometry, material properties, boundary conditions, and loads makes it possible to analyze part of a structure as representative of the whole. Symmetry can also be exploited in vibration analysis, but it is easy to overlook modes. For example, let the left half of a simply supported beam be modeled. If the right end of this model is simply supported, only antisymmetric modes of the original beam are represented. To capture symmetric modes, the left-half model must be analyzed again, this time with its right end allowed to displace laterally but not allowed to rotate. A shell of revolution might be modeled as axisymmetric in static analysis, but most of its vibration modes will display waves around the circumference. It is recommended that symmetry conditions not be used in vibration problems or other dynamic analysis.

Stress Calculation. If provided with an approximate mode shape, the Rayleigh quotient, Eq. 11.4-13, produces a frequency that has less error than the mode shape. Because stresses are calculated from the mode shape, we conclude that accurate stresses require a finer mesh than accurate frequencies. A computed vibration mode defines relative amplitudes of d.o.f. it contains, but does not state actual displacement magnitudes. Unless the mode is scaled to agree with the actual displacement amplitude, magnitudes of stresses computed from the mode are not physically meaningful.

Stresses can be computed from nodal d.o.f., just as in static analysis. For beam elements, accuracy can be improved by superposing stresses that result from loading the element by inertia load associated with its motion. The procedure is described for static load in connection with Figs. 2.9-1 and 2.9-2.

Checking for Errors. Errors and blunders of static analysis, and more, are possible with dynamic analysis. As in static analysis one can check that nodes are suitably placed, that supports are of the proper type and properly located, and so on. Data blunders are more likely in dynamic analysis because more data is needed. Mass must be specified, in units consistent with other data, and ρ may mean mass density or weight density, depending on the software. Damping ratios must be provided, as fractions or percentages as software

requires. Computed ω's must not be interpreted as circular frequency if they are presented as cyclic frequency.

An FE model should first be analyzed statically, using a load that seems likely to produce an approximation of the lowest vibration mode. Static analysis is comparatively easy and cheap, and may disclose modeling errors that affect dynamic response as well. One can direct software to compute total structure mass and the mass center location. Results should have reasonable agreement with expectations. Vibration frequencies and modes can also be computed even if the analysis contemplated does not require them, as a further check and to gain insight needed to make decisions demanded by harmonic response, response history, and response spectrum analyses. Zero frequencies indicate a lack of support (which may be intentional) or the presence of a mechanism. Absurdly high or low frequencies suggest an error in data. Modes should be plotted, animated, and viewed from different directions if the model is not planar. Are the modes compatible with intended support conditions, and are they physically reasonable?

In dynamics, it may be difficult for even an experienced analyst to predict the nature of response. Modeling may therefore be difficult, and it may even be hard to foresee what sort of response should be investigated. Thus it is recommended that an unfamiliar analysis project begin with pilot studies. One may also make use of a restart option in software. For example, results of dynamic response analysis can be examined after a short time and computation resumed only if it seems to be working properly.

Comparison with Experiment. Experimentalists and analysts must work together to ensure that both groups address the same problem. They must agree on geometry, elastic properties, damping, structural mass, nonstructural mass (magnitude, location, and method of attachment), supports (hinged, elastic, or other, and location), excitation (type, magnitude, location, and direction), response to be investigated (type, location, and direction), and perhaps other considerations [11.21]. The structure is no doubt more complicated than its FE model, so the model may not represent some vibration modes of the structure. Nodes of the FE model should appear at locations where measurements are to be taken from the structure. Perhaps the FE model is linear but the structure is not. To find out, the structure could be subjected to two or more levels of excitation at a given frequency, and results plotted to see if response is directly proportional to excitation level.

Miscellaneous. A dynamic load may move over a structure rather than acting at a fixed location on it. For example, if a heavy vehicle moves along a beam, it loads the beam in a way that depends on vehicle speed, mass, suspension stiffness and damping, and the shape of the path followed (that is, on the deflection of the beam). A rolling tire is loaded by localized pressure that moves around the circumference relative to the tire. References for such problems include [11.70–11.74].

To avoid complete re-solution of a revised model, or as part of a design process to achieve desired dynamic behavior, it is helpful to predict rates of change of eigenvalues and eigenvectors with respect to changes in system parameters. This study is known as sensitivity analysis. Somewhat related is the improvement of an FE model, based on test data, so that FEA predictions agree better with observed behavior. This study is known by several names, perhaps primarily as system identification, but also as structural identification, model updating, parameter updating, parameter estimation, and the inverse problem of dynamics. A few references, of a great many available, are [11.75–11.79].

For some static problems, such as uniform beams under concentrated loads, FEA can solve the mathematical model exactly. Such is not the case in dynamics because elements based on polynomial fields cannot represent a mode shape exactly (the lateral displacement mode of a vibrating beam is sinusoidal, not cubic as in the standard beam element). Thus there is discretization error in stiffness representation. Mass representation also has discretization error. Lumped masses, which often produce frequencies that are too low, tend to compensate for the overstiffness inherent in compatible displacement-based elements. If, for a given FE mesh, the eigenproblem is solved twice, using a lumped [**M**] and then a consistent [**M**], good agreement of the two eigensolutions suggests that there is little discretization error. Mesh discretization error has not been so well-studied in dynamics as in statics. References include [11.80–11.83].

Estimates of error associated with the time step used in implicit direct integration are available, and can be used to automatically adjust the time step as solution proceeds [11.83–11.85].

Cautionary Remarks. Remarks in [11.86] about numerical modeling of impact phenomena can also be applied, with little modification, to FEA in general. The paper advises thorough understanding of the physics of the problem, of dynamics, and of numerical modeling. Otherwise the numerical problem may differ considerably from the physical problem. "In no way can today's computer programs for wave propagation and impact be treated as 'black boxes.' A minimum of 6 months to 2 years of experience is needed to be able to use such programs successfully. There is no shortcut, no royal road, to this process." The reference also warns against using a mesh more suited to computational convenience than to the physics of the problem, and ascribing a physical cause to numerical artifacts or instabilities that are not recognized as such.

11.17 AN APPLICATION: VIBRATION AND HARMONIC RESPONSE

The structure we consider is the right-angle frame *ABC* shown in Fig. 11.17-1a. The frame is uniform, pinned at *A*, and roller-supported at *C*. It is modeled by 50 beam elements, each of length 1.0 m. Selected nodes of the discretization (not shown in Fig. 11.17-1) are numbered. Displacements are confined to the plane of the paper. The simplicity of the structure allows us to emphasize dynamics rather than geometric modeling and to display results easily. We will calculate natural frequencies of vibration, then harmonic response with $\xi = 0.02$ as the damping ratio for all modes. Lumped masses with rotary inertia are generated by the software used, but its documentation offers no details about the formulation.

Preliminary Analysis. The fundamental vibration frequency is easy to estimate by reducing the problem to a single d.o.f., then calculating $\omega_1 \approx \sqrt{k/m}$. Let us assume that the fundamental vibration mode resembles static deformation that results from applying horizontal load F at C (Fig. 11.17-1). Static deflection u_C can be obtained using either simple energy methods or beam theory, and is

$$u_C = \frac{15Fa^3}{EI} \qquad \text{hence} \qquad k = \frac{F}{u_C} = \frac{EI}{15a^3} = 111{,}100 \text{ N/m} \tag{11.17-1}$$

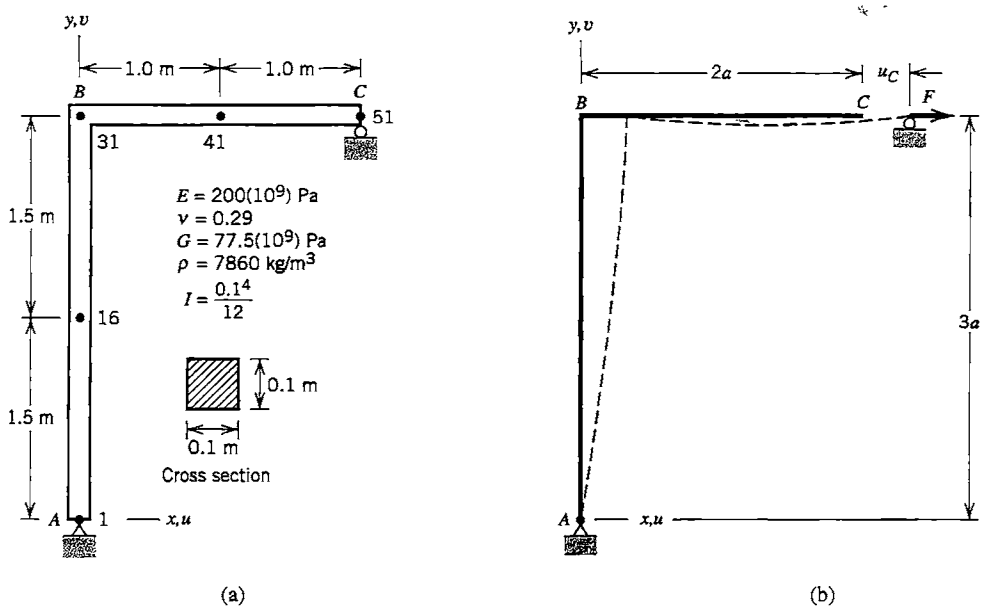

Figure 11.17-1. (a) Plane frame structure and its properties. Numbers 1, 16, 31, 41, and 51 are node numbers used in the FE model. (b) Static loading used in preliminary analysis. Here $a = 1.0$ m.

All the mass of BC has horizontal displacement u_C, but only some of the mass of AB. An accurate evaluation based on deflected shape can be made but it is not worth the trouble. We will arbitrarily assume that *half* the mass of AB has horizontal displacement u_C. Thus, multiplying mass density by volume, we obtain $7860(2.0 + 1.5)(0.1)(0.1) = 275$ kg as the effective mass m. Hence

$$\omega_1 \approx \sqrt{k/m} = 20.1/\text{s} \qquad \text{and} \qquad f_1 = \omega_1/2\pi \approx 3.20 \text{ Hz} \tag{11.17-2}$$

Frequencies and shapes of higher modes become increasingly difficult to estimate. As for harmonic response, we expect a peak response when the forcing function has frequency almost equal to a natural frequency.

Critique of Vibration Results. The first five frequencies and modes computed by FEA are shown in Fig. 11.17-2. There is excellent agreement between f_1 as computed by FEA and the preliminary estimate (Eq. 11.17-2). Displacement amplitudes, having been exaggerated for plotting, have no significance. Recalling the argument associated with Fig. 11.16-3, we see

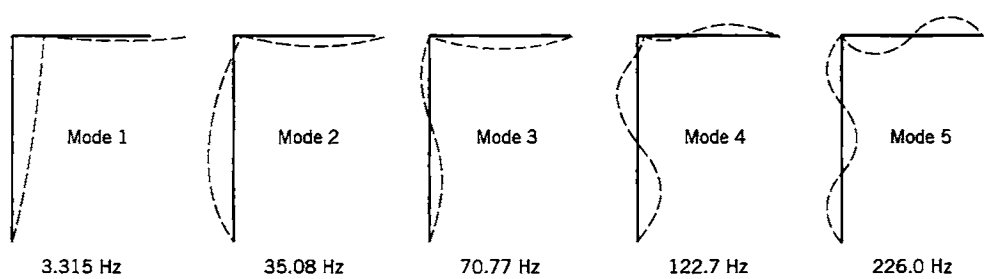

Figure 11.17-2. Computed mode shapes and cyclic frequencies $f = \omega/2\pi$.

TABLE 11.17-1. VIBRATION OF THE FRAME IN FIG. 11.17-1: SELECTED TERMS OF THE MASS-NORMALIZED EIGENVECTOR $\{\bar{\mathbf{D}}\}_i$ (THAT IS, NODAL AMPLITUDES IN MODE i, WITH EQ. 11.7-1 SATISFIED) FOR SELECTED NODES, EACH MULTIPLIED BY 1000.

d.o.f.	Node	Mode 1	Mode 2	Mode 3	Mode 4	Mode 5
$\bar{u}$	16	38.6	−81.5	23.8	−27.7	62.7
$\bar{\theta}_z$	41	1.0	7.0	−19.4	52.6	248.9
$\bar{u}$	51	62.3	33.1	−3.4	21.6	9.2

that modes shown in Fig. 11.17-2 imply an ordering of frequencies that agrees with values computed. Each wave of these modes is spanned by several elements, so the FE mesh appears adequate for these modes, and seems likely to be adequate up to at least mode 25, for which each complete sine wave of displacement would be spanned by four elements. Additional computed frequencies in hertz (Hz) are $f_6 = 269.4$, $f_7 = 396.6$, $f_8 = 420.8$, $f_9 = 552.3$, and $f_{10} = 649.6$. The FE model has a total of 150 frequencies. Amplitudes of selected d.o.f. in the first five modes, [M]-normalized according to Eq. 11.7-1, appear in Table 11.17-1. Algebraic signs in this table agree with what is shown in Fig. 11.17-2.

Harmonic Response Analysis. Let force $F = 3000 \sin \Omega t$, in units of newtons, act in the horizontal direction at node 51. Harmonic response is to be computed for each of several load frequencies Ω. The damping ratio is $\xi = 0.02$ for all modes. Figure 11.17-3a shows the forced vibration mode for $\Omega = 122$ Hz, which is not quite equal to the natural frequency of mode 4. By solving Eq. 11.10-2 for each of several values of Ω and converting from modal amplitude to physical amplitude, a plot that shows physical amplitude versus Ω can be constructed for any chosen d.o.f. Figure 11.17-3b shows such a plot for the amplitude of horizontal motion at node 16, over an arbitrarily chosen range of Ω. As expected, peaks are observed near $\Omega = \omega_3$ and near $\Omega = \omega_4$. Only five modes were used in the modal analysis, so results for $\Omega > \omega_4$ are questionable. However, reanalysis with only four modes produced almost identical results in the range plotted.

Using modal data from Table 11.17-1, peak amplitudes in Fig. 11.17-3b can be checked. Consider the contribution of mode 4 to the peak near 122.7 Hz. The only nonzero entry in the load amplitude vector $\{\mathbf{R}^{\text{ext}}\}$ is 3000 N rightward at node 51. Therefore, from Table 11.17-1 and Eq. 11.7-6, the amplitude of modal load in mode 4 is $\bar{P}_4 = 0.0216(3000) = 64.8$. With $\omega_4 = 2\pi(122.7) = 770.9$/s, $\xi_4 = 0.02$, and $\beta_4 = 1.0$, Eq. 11.10-2 yields

$$\bar{Z}_4 = \frac{\bar{P}_4/\omega_4^2}{2\xi_4} = \frac{64.8/770.9^2}{2(0.02)} = 0.00273 \tag{11.17-3}$$

Finally, to calculate the horizontal amplitude at node 16 due to mode 4, we read the top line of Table 11.17-1, and obtain $0.0277\bar{Z}_4 = 75.5(10^{-6})$ m. This value agrees fairly well with the peak value in Fig. 11.17-3b, which suggests that other modes contribute little to this peak. *Static* deflection due to the 3000-N load would be over 300 times

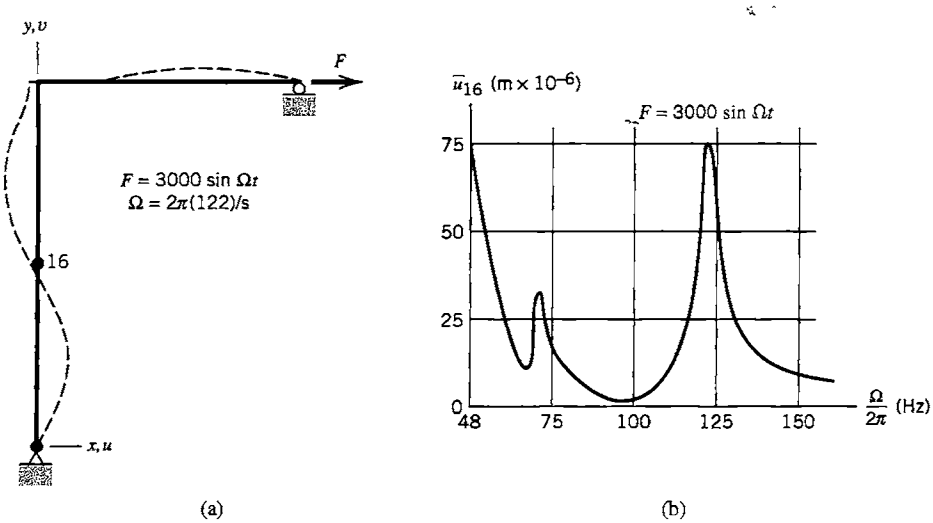

Figure 11.17-3. Harmonic response. (a) Vibration shape for forcing function frequency $f = 122$ Hz. (b) Amplitude of horizontal displacement at node 16 versus frequency Ω of the forcing function in an arbitrarily selected range of Ω.

greater. However, the amplitude of horizontal reaction at node 1 was found to be about 4800 N when $\Omega = \omega_4$; that is, about 1.6 times the amplitude of the forcing function.

Note: Data in this section and the next come from three different computer programs because none of the programs available at the time provided all results desired. All three provided modes and frequencies, but they did not quite agree. For this reason there are slight inconsistencies in numerical results reported.

11.18 AN APPLICATION: RESPONSE HISTORY

In this section, we consider impulse loading of the frame whose data appears in Fig. 11.17-1. As shown in Fig. 11.18-1, a horizontal force of 100,000 N is applied at node 51 for 0.01 seconds. The structure is initially undeformed and at rest. We will consider the response history of displacement and velocity, using both the modal method and direct integration by the average-acceleration (implicit) method. Because the load is suddenly applied it is a shock

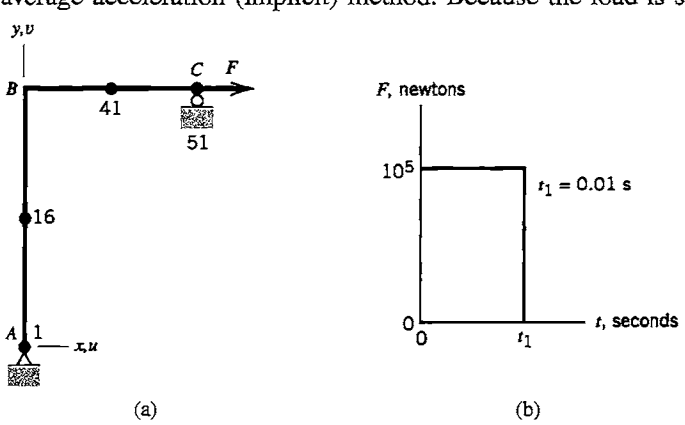

Figure 11.18-1. (a) Frame loaded at point C by horizontal force F. (b) Prescribed variation of force F with time.

loading, *for which the modal method is not well suited.* We use it anyway to show how it fares when applied to such a problem. The purpose of these analyses is more to illustrate the behavior of methods than to solve the problem.

Preliminary Analysis. We continue the analysis begun with Eq. 11.17-1, and now estimate the maximum horizontal acceleration, velocity, and displacement of node 51. Over the 0.01-second time span of loading, displacements are as yet so small that elastic forces have almost no influence on the horizontal acceleration of portion *BC*. Accordingly we use simple equations of particle dynamics. Newton's second law $\mathbf{F} = m\mathbf{a}$ provides acceleration at time $t = 0$ as

$$\ddot{u}_{51} = F/m \approx 100{,}000/275 = 364 \text{ m/s}^2 \tag{11.18-1}$$

Impulse Ft_1 is equal to the change of linear momentum, which we take to be $m\dot{u}_{51}$. Hence at $t = t_1$

$$\dot{u}_{51} = Ft_1/m \approx 100{,}000(0.01)/275 = 3.64 \text{ m/s} \tag{11.18-2}$$

To estimate maximum displacement, we equate maximum kinetic and maximum strain energies in mode 1, whose approximate stiffness k is available from Eq. 11.17-1. Thus

$$\frac{1}{2}m\dot{u}_{51}^2 = \frac{1}{2}ku_{51}^2 \qquad \text{hence} \quad u_{51} = \left[\frac{m\dot{u}_{51}^2}{k}\right]^{1/2} \approx \left[\frac{275(3.64)^2}{111{,}100}\right]^{1/2} = 0.181 \text{ m} \tag{11.18-3}$$

Finite Element Analysis. The FE discretization is the same as used in Section 11.17. For modal analysis, we use frequencies and modes computed in Section 11.17, and damping ratio $\xi = 0.02$. To investigate the effects of retaining different numbers of modes in the analysis, response history is computed several times by the modal method, each time adding another mode to the modal matrix, up to a total of 15 modes retained. The frequency of mode 15 is $f_{15} = 1268$ Hz. In each analysis the time step used for direct integration of Eq. 11.7-6 is $\Delta t = 0.0001$ s, which is about 7.9 time steps per period of mode 15.

The same problem is also solved by direct integration, using Eqs. 11.13-5 with $\gamma = 0.50$ and $\beta = 0.25$. The form of damping used in modal analysis, $\xi = 0.02$ for each mode, is not available in direct integration. If Eqs. 11.5-3 are used, with $\xi_1 = \xi_2 = 0.02$ and ω_1 and ω_2 the frequencies of modes 1 and 15, the α and β obtained provide a minimum ξ of 0.002 at $\omega = 407$/s ($f = 64.8$ Hz) from Eq. 11.5-2. We elect to omit damping. Its effects may be negligible over the short time span to which we will apply direct integration. Results produced using different time steps will be shown; the shortest time step used is $\Delta t = 20(10^{-6})$ s.

Would explicit direct integration be faster? To answer, we must estimate Δt_{cr} for explicit integration. Consider a typical element of the frame. The element bound for axial deformation, Eq. 11.12-15, gives $\omega = 2c/L = 0.10(10^6)$/s. But flexure yields a higher frequency. Vibration analysis of a single beam element with shear deformation neglected and both ends simply supported, for the higher of its two modes, yields the maximum frequency $\omega = 0.73(10^6)$/s, for which Eq. 11.12-9 yields $\Delta t_{cr} = 2/\omega_{max} = 2.7(10^{-6})$ s as the largest time step allowed in the central difference method. If $\Delta t = 20(10^{-6})$ s is the

smallest time step actually desired, and the cost-per-time-step ratio noted in Section 11.11 for a one-dimensional problem is accepted, the implicit method is faster (not accounting for the one-time cost of factoring [**K**] in the implicit method). The implicit method would be uneconomical if the problem were two- or three-dimensional.

Critique of Results. Computed maxima of horizontal acceleration, velocity, and displacement at node 51, from modal analysis with 15 modes retained, are respectively 173 m/s^2, 4.27 m/s, and 0.181 m. The agreement of velocity and displacement with Eqs. 11.8-2 and 11.8-3 is good to excellent. The agreement of acceleration with Eq. 11.18-1 is poor, and reflects the inappropriateness of modal analysis for shock loading.

We arbitrarily decide to present computed results for displacement, velocity, and acceleration of the rotational d.o.f. at node 41. Figure 11.18-2a, with only two modes retained in modal analysis, shows that the higher mode decays more quickly. This is reasonable in view of the discussion that follows Eq. 11.4-2, according to which damping $\xi = 0.02$ reduces amplitude about 10% per cycle. Mode 2 executes more cycles than mode 1 in a given time, so it decays sooner.

The initial portion of Fig. 11.18-2a is shown in Fig. 11.18-2b, but with 15 modes used. The contribution of modes higher than second is evident, but it appears that most of the *maximum* displacement is represented by the first two modes. Similar results computed by direct integration appear as Figs. 11.18-2c and 11.18-2d. The latter results suggest that yet more modes would be advisable in modal analysis, and that damping may have a noticeable effect, even in the small time span displayed.

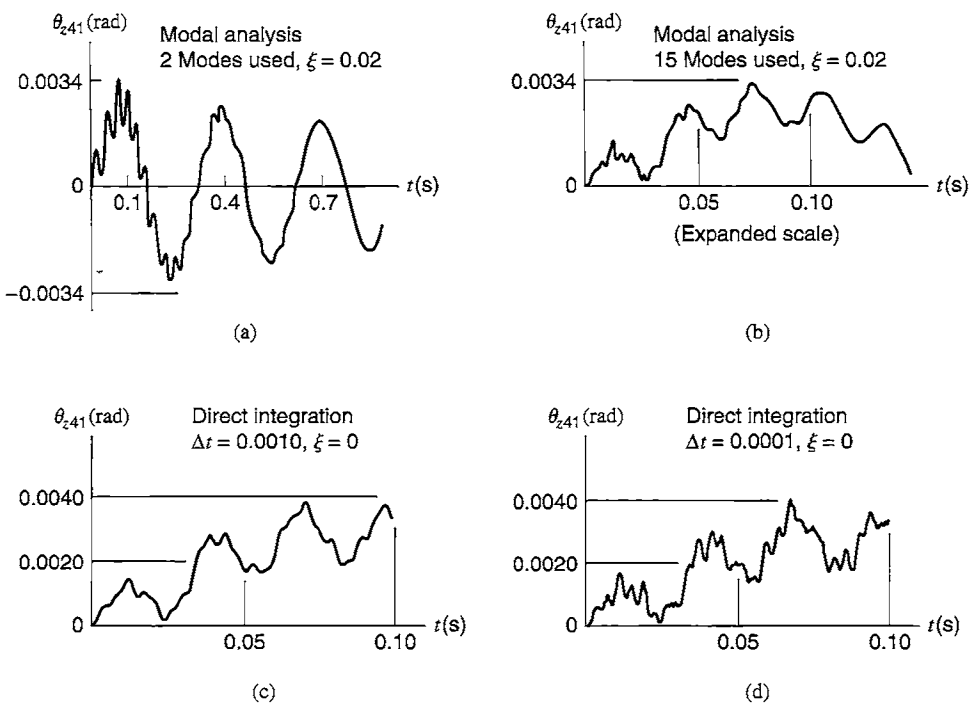

Figure 11.18-2. Rotation θ_z (radians) at node 41 versus time t (seconds) for the loading of Fig. 11.18-1b. (a,b) Computed by modal analysis. (c,d) Computed by direct integration, average acceleration method.

TABLE 11.18-1. ROTATION θ_z AT NODE 41 IN FIG. 11.18-1: MAXIMUM MAGNITUDES OF θ_{z41} (RADIANS) AND ITS TIME DERIVATIVES $d\theta_{z41}/dt$ AND $d^2\theta_{z41}/dt^2$, IN TIME RANGES INDICATED, COMPUTED BY MODAL ANALYSIS AND BY IMPLICIT DIRECT INTEGRATION.

		Modal analysis		Average acceleration method		
Quantity	Range of t	2 modes	15 modes	$\Delta t = 10^{-3}$ s	$\Delta t = 10^{-4}$ s	$\Delta t = 2(10^{-5})$ s
θ_{z41}	0 to 0.10 s	0.00337	0.00347	0.00386	0.00413	0.00410
$\dot{\theta}_{z41}$	0 to 0.02 s	0.15	0.60	0.24	0.84	1.44
$\ddot{\theta}_{z41}$	0 to 0.02 s	40	1524	171	3402	21,790

Similar plots, now for rotational velocity at node 41, appear in Fig. 11.18-3. Clearly, two modes are utterly inadequate for computation of $\dot{\theta}_{z41}$. Indeed, direct integration results show that 15 modes are also inadequate, and suggest that a yet smaller time step should be used for direct integration analysis. Results for acceleration $\ddot{\theta}_{z41}$, not shown graphically, display even greater disparities, as shown by data in Table 11.18-1. Again the conclusion is that *modal analysis is not suited to shock loading* and that smaller time steps are needed in direct integration, at least if velocities and accelerations are to be calculated.

Response Spectrum Analysis. If we require only the maximum magnitude of response, without regard to when it appears, we can obtain estimates by response spectrum analysis (Section 11.15). Such calculations are supported by FE software, but for illustration we will do them by hand. The preliminary modal analysis has been done; results appear in Table 11.17-1. This information is applied to rotation θ_z at node 41 as follows.

For the rectangular pulse load in Fig. 11.18-1b, amplification factor S_i of Eq. 11.15-2 is given by an analytical formula [11.2,11.3,11.66]:

$$S_i = 2\sin\pi t_1 f_i \quad \text{for} \quad t_1 f_i < 0.5 \qquad S_i = 2 \quad \text{for} \quad t_1 f_i > 0.5 \tag{11.18-4}$$

Thus for frequencies f_i reported in Fig. 11.17-2,

$$S_1 = 2\sin\pi(0.01)(3.315) = 0.208 \qquad S_2 = 2\sin\pi(0.01)(35.08) = 1.784 \tag{11.18-5}$$

and $S_3 = S_4 = \cdots = 2.000$. Using Eq. 11.7-6 and data in Table 11.17-1, we obtain modal loads

$$\begin{aligned} P_1 &= \{\Phi\}_1^T\{\mathbf{R}^{\text{ext}}\} = 0.0623(100{,}000) = 6230, \\ P_2 &= \{\Phi\}_2^T\{\mathbf{R}^{\text{ext}}\} = 0.0331(100{,}000) = 3310, \end{aligned} \tag{11.18-6}$$

and so on. Modal maxima, from Eq. 11.15-2, are

$$Z_1^{\max} = 0.208\frac{6230}{(2\pi\, 3.315)^2} = 2.99, \qquad Z_2^{\max} = 1.784\frac{3310}{(2\pi\, 35.08)^2} = 0.122, \tag{11.18-7}$$

and so on. To apply these results to θ_z at node 41, we use the middle line in Table 11.17-1 and Eq. 11.15-4. Let $(\bar{\Delta}_{41})_i$ represent rotation at node 41 due to $Z_1^{\max}$. Thus

$$(\bar{\Delta}_{41})_1 = 0.0010(2.99) = 299(10^{-5}), \qquad (\bar{\Delta}_{41})_2 = 0.0070(0.122) = 85(10^{-5}), \quad (11.18\text{-}8)$$

and so on (magnitudes of $\bar{\Delta}_{41}$ for modes 3 through 15, all multiplied by 10^{-5}, are 7, 38, 22, 22, 0, 3, 0, 3, 4, 1, 1, 0, and 1). Finally we combine modes according the procedures of Eqs. 11.15-5 to 11.15-7. Thus, estimates of the maximum magnitude of rotation θ_z at node 41 are, using the first 5 modes and then the first 15 modes,

$$\begin{array}{llll} \text{Upper bound:} & \theta_{z41}^{\max} = 0.00451 \text{ (5 modes)}, & \theta_{z41}^{\max} = 0.00486 \text{ (15 modes)} & \\ \text{SRSS:} & \theta_{z41}^{\max} = 0.00314 \text{ (5 modes)}, & \theta_{z41}^{\max} = 0.00315 \text{ (15 modes)} & (11.18\text{-}9) \\ \text{NRL:} & \theta_{z41}^{\max} = 0.00395 \text{ (5 modes)}, & \theta_{z41}^{\max} = 0.00398 \text{ (15 modes)} & \end{array}$$

Note that modal amplitudes of θ_{z41} in Table 11.17-1 increase strongly with ω, while modal amplitudes of u do not. This suggests that results for displacements will be better-behaved than results for rotations.

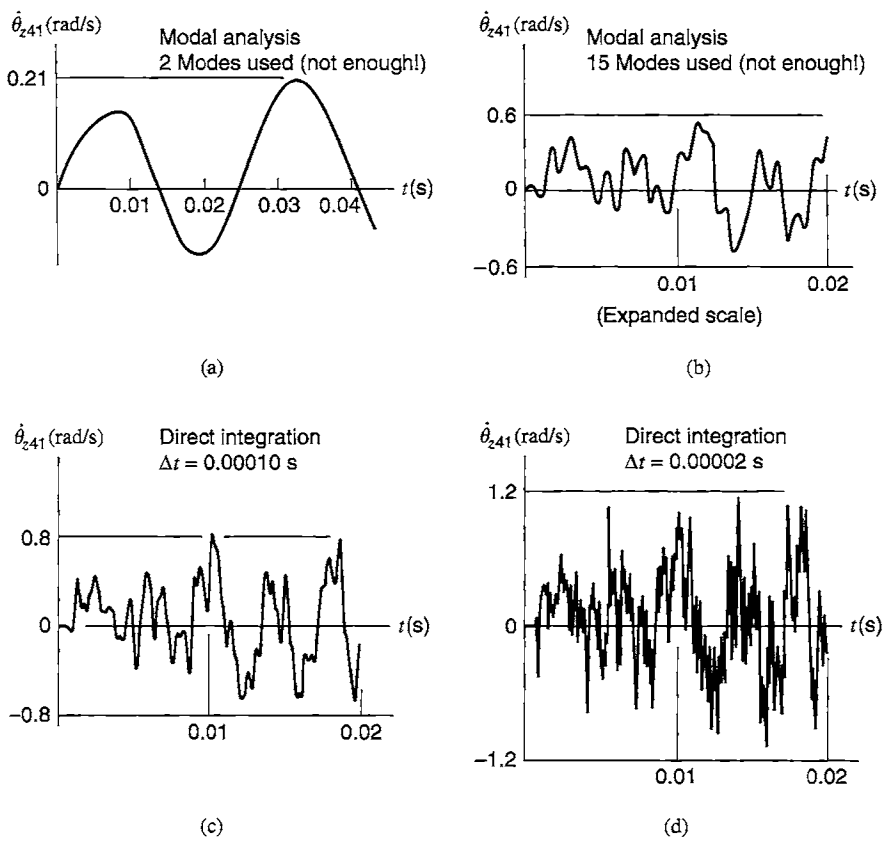

Figure 11.18-3. Angular velocity $\dot{\theta}_z$ (rad/s) at node 41 versus time t (s) for the loading of Fig. 11.18-1b. (a,b) Computed by modal analysis. (c,d) Computed by direct integration, average acceleration method.

ANALYTICAL PROBLEMS

11.2-1 A differential element having mass dm and velocity v has kinetic energy $v^2 dm/2$. Show that the kinetic energy of a finite element is therefore $\{\dot{\mathbf{d}}\}^T [\mathbf{m}] \{\dot{\mathbf{d}}\}/2$, where $[\mathbf{m}]$ is the consistent element mass matrix and $\{\mathbf{d}\}$ is the vector of element nodal d.o.f.

11.2-2 Show that with nodal accelerations $\{\ddot{\mathbf{d}}\}$, element nodal inertial loads $[\mathbf{m}]\{\ddot{\mathbf{d}}\}$ are the same as body force loads given by Eq. 3.3-8 (and by Eq. 4.8-15b).

11.3-1 (a) Is it possible to have a negative diagonal coefficient in a consistent mass matrix? Explain.
(b) Imagine that a uniform straight beam vibrates in such a way that inflection points of the vibration mode coincide with nodes of the FE mesh. What ω is obtained by using the second $[\mathbf{m}]$ in Eq. 11.3-3 with $\alpha = 1/24$? The exact result is $\omega = \pi^2\sqrt{EI/mL^3}$, where L and m are respectively the distance and mass between nodes.

11.3-2 Consider the kinetic energies of two-node elements in the following three rigid-body plane motions: lateral translation, rotation about the mass center, and rotation about the left end. Do the following mass matrices provide the correct kinetic energies or not?
(a) Bar element, lumped mass matrix (Eq. 11.3-1).
(b) Bar element, consistent mass matrix (Eq. 11.3-4).
(c) Beam element, consistent mass matrix (Eq. 11.3-5).

11.3-3 Cross-sectional area of the bar shown varies linearly from A_0 at the left end to γA_0 at the right end, where γ is a constant. Determine the consistent mass matrix that operates on axial d.o.f. u_1 and u_2.

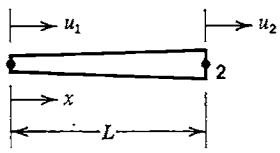

Problem 11.3-3

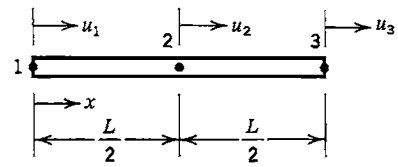

Problem 11.3-4

11.3-4 For the uniform quadratic-displacement bar shown, derive the consistent mass matrix that operates on axial d.o.f. u_1, u_2, and u_3.

11.3-5 Let a uniform beam element rotate about its mass center. What are the percentage errors in kinetic energy associated with HRZ lumping (Eq. 11.3-8) and with particle-mass lumping ($\alpha = 0$ in Eq. 11.3-3)?

11.3-6 Determine α in Eq. 11.3-3 such that a uniform beam element has the correct kinetic energy of rotation about its mass center. Then consider use of the resulting $\lceil \mathbf{m} \rfloor$ to model a simply supported beam by one element and determine its natural frequencies of vibration. What conclusion can be drawn from this example?

11.3-7 (a) By derivation, verify the CST mass matrix stated in Eq. 11.3-6. The element has uniform density and thickness.
(b) Expand this mass matrix to obtain a form applicable to motion in the xy plane, with nodal d.o.f. in the order $\{\mathbf{d}\} = \lfloor u_1 \; v_1 \; u_2 \; v_2 \; u_3 \; v_3 \rfloor^T$.

11.3-8 The four-node parallelogram element shown has uniform density and thickness. Shape functions are given by Eqs. 6.2-3. By integration, determine the consistent mass matrix.

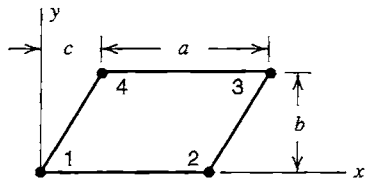

Problem 11.3-8

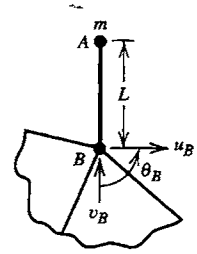

Problem 11.3-9

11.3-9 Rigid and massless link AB in the sketch connects a particle mass m at A to node B. In terms of d.o.f. shown at node B, what is the 3 by 3 mass matrix associated with m? *Suggestion:* Recall Section 8.3. Physically and qualitatively, what sort of error would be associated with a diagonalized form of this matrix?

11.3-10 Verify the nodal masses shown in parentheses in (a) Fig. 11.3-2a, and (b) Fig. 11.3-2b.

11.3-11 For a uniform beam element having the usual d.o.f. $\{\mathbf{d}\} = \lfloor\, v_1 \;\; \theta_{z1} \;\; v_2 \;\; \theta_{z2} \,\rfloor^T$ in two dimensions, consider the following lateral displacement function, in which $\xi = x/L$.

$$v = \left\lfloor \left(1-\xi\right) \quad \left(\xi-\xi^2\right)L/2 \quad \xi \quad \left(-\xi+\xi^2\right)L/2 \right\rfloor \{\mathbf{d}\}$$

(a) Show that v is linear in x if $\theta_{z1} = \theta_{z2}$. Also show that this field yields the correct forms for lateral displacement v and curvature $v_{,xx}$ when nodal d.o.f. are consistent with pure bending.
(b) Use this function and Eq. 11.2-6 to evaluate the mass matrix.
(c) Hence, obtain a diagonal mass matrix by the HRZ procedure.

11.4-1 Imagine that a redesign produces small changes in [**M**] and [**K**]. Hence, the natural frequency ω_i of each mode is slightly changed, by an amount $\Delta\lambda_i$, where $\lambda_i = \omega_i^2$. Using the Rayleigh quotient and neglecting terms of higher order, derive an expression for $\Delta\lambda_i$ in terms of λ_i, $\{\bar{\mathbf{D}}\}_i$, [**M**], [Δ**K**], and [Δ**M**].

11.4-2 (a) Let the following matrices be applicable to a certain problem of axial vibration with two d.o.f.:

$$[\mathbf{K}] = \begin{bmatrix} 2 & -2 \\ -2 & 5 \end{bmatrix} \qquad [\mathbf{M}] = \begin{bmatrix} 1 & 0 \\ 0 & 1 \end{bmatrix}$$

Exact eigenvalues and eigenvectors are $\lambda_1 = 1$ and $\{\bar{\mathbf{D}}\}_1 = \lfloor\, 2 \;\; 1 \,\rfloor^T$ for mode 1 and $\lambda_2 = 6$ and $\{\bar{\mathbf{D}}\}_2 = \lfloor\, 1 \;\; -2 \,\rfloor^T$ for mode 2. Consider the approximate eigenvectors $\lfloor\, 1.7 \;\; 1.0 \,\rfloor^T$ and $\lfloor\, 1.2 \;\; -2.0 \,\rfloor^T$, and show that the Rayleigh quotient provides good estimates of λ_1 and λ_2 (in Eq. 11.4-13, $\lambda_i = \omega_i^2$).
(b) In Example 1 of Section 11.4, estimate the fundamental frequency by using the Rayleigh quotient and a reasonable guess for the vibration mode.

11.4-3 Consider axial vibration of a uniform bar of length L and mass $m = \rho AL$, free at one end and fixed at the other. Using two-node elements, model the bar first by one element, then by two elements of equal length $L/2$. For each mesh, calculate the lowest natural frequency using the following mass matrix formulations. (The exact result is $\omega_1 = (\pi/2)\sqrt{AE/mL}$.)
(a) The consistent [**m**], Eq. 11.3-4.
(b) The lumped [**m**], Eq. 11.3-1.
(c) The average [**m**], Eq. 11.3-7.
(d) For what value of β in Eq. 11.3-7 does a one-element model produce the exact ω_1?

11.4-4 In Problem 11.4-3, consider the convergence rates of ω_1 as the mesh is refined. Do they agree with rates predicted in the discussion that follows Eq. 11.3-7?

11.4-5 The stiffness, consistent mass, and HRZ-lumped mass matrices for the three-node bar element shown in Problem 11.3-4 are respectively

$$\frac{AE}{3L}\begin{bmatrix} 7 & -8 & 1 \\ -8 & 16 & -8 \\ 1 & -8 & 7 \end{bmatrix} \qquad \frac{m}{30}\begin{bmatrix} 4 & 2 & -1 \\ 2 & 16 & 2 \\ -1 & 2 & 4 \end{bmatrix} \qquad \frac{m}{6}\begin{bmatrix} 1 & 0 & 0 \\ 0 & 4 & 0 \\ 0 & 0 & 1 \end{bmatrix}$$

where m is the total element mass. Exact natural frequencies of axial vibration of an unsupported uniform bar of length L are $\omega_1 = 0$, $\omega_2 = \pi\sqrt{AE/mL}$, and $\omega_3 = 2\omega_2$.
(a) Determine the mode shapes and percentage errors of calculated frequencies provided by the consistent mass matrix.
(b) Repeat part (a) using the HRZ-lumped mass matrix.

11.4-6 Fix the left end of the three-node bar element treated in Problem 11.4-5. Determine the two natural frequencies of axial vibration and their mode shapes.
(a) Use the consistent mass matrix.
(b) Use the HRZ-lumped mass matrix.
(c) Use ad hoc lumping: place a particle of mass $m/3$ at each of the three nodes.
(d) For each of parts (a), (b), and (c), estimate the lowest frequency by means of the Rayleigh quotient and the assumed displacement mode $u_1 = 0$, $u_2 = 1$, $u_3 = 2$.

11.4-7 Model a simply supported uniform beam of length $2L$ by a single element. Calculate natural frequencies of vibration, where possible, by using the mass matrices cited. The element [**k**] is given by Eq. 2.3-5 (and by Eq. 3.3-14). The exact fundamental frequency for a beam of length $2L$ is $\omega_1 = (\pi/2L)^2\sqrt{EI/\rho A}$.
(a) The consistent [**m**], Eq. 11.3-5.
(b) The lumped [**m**] of Eq. 11.3-3 with $\alpha = 0$.
(c) The lumped [**m**] of Eq. 11.3-3 with $\alpha = 1/24$.
(d) The HRZ-lumped [**m**] of Eq. 11.3-8.
(e) The [**m**] calculated in Problem 11.3-11(b).

11.4-8 Model a uniform cantilever beam of mass m and length L by a single element. Repeat parts (c) and (e) of Problem 11.4-7. The exact fundamental frequency is $\omega_1 = 3.516\sqrt{EI/mL^3}$.

11.4-9 An argument given in Section C.3 of Appendix C shows that different modes are mass-matrix orthogonal, but the argument presumes that different modes have different frequencies. Consider a one-element model of a cantilever beam of circular cross section, and two modes that have the same frequency and are identical in shape but appear in different planes. Demonstrate that the two modes are mass-matrix orthogonal.

11.4-10 Consider axial vibration of a uniform bar of mass m, fixed at one end and free at the other. The squared fundamental frequency is $\omega_1^2 = cAE/mL$, where $c = \pi^2/4$ for the exact result. For meshes $N = 1$ and $N = 2$ respectively, calculated values of c in Problem 11.4-3 (using consistent, lumped, and average mass matrices) are (a) 3.000 and 2.597, (b) 2.000 and 2.343, and (c) 2.400 and 2.463. Use Eq. 9.7-1 to extrapolate to $N = \infty$ for each of the three sequences of two values.

11.5-1 (a) Determine proportional damping parameters α and β for $\xi = 0.03$ at 5 Hz and $\xi = 0.20$ at 15 Hz.
(b) For these values of α and β, sketch a graph like Fig. 11.5-1. Comment on the combined ξ at frequencies less than 5 Hz and greater than 15 Hz. Is caution indicated?

11.6-1 (a) Show that Eq. 11.6-4 yields $[\mathbf{K}_r] = [\mathbf{K}_{mm}] - [\mathbf{K}_{ms}][\mathbf{K}_{ss}]^{-1}[\mathbf{K}_{ms}]^T$. Where has this relation been seen before?
(b) Derive a similar expression for $[\mathbf{M}_r]$ in Eq. 11.6-4.

11.6-2 If $\omega^2[\mathbf{M}]\{\bar{\mathbf{D}}\}$ in Eq. 11.4-5 is regarded as a vector of inertia loads $\{\mathbf{R}\}$, and $[\mathbf{K}]$ is inverted to provide the flexibility matrix $[\mathbf{F}]$, we obtain $[\mathbf{F}]\{\mathbf{R}\} = \{\bar{\mathbf{D}}\}$.
(a) Partition this equation into m master and s slave d.o.f., as in Eq. 11.6-1, and let $\{\mathbf{R}_s\} = \{\mathbf{0}\}$. Then derive the transformation

$$\begin{Bmatrix} \bar{\mathbf{D}}_m \\ \bar{\mathbf{D}}_s \end{Bmatrix} = [\mathbf{T}]\{\bar{\mathbf{D}}_m\} \qquad \text{where} \qquad [\mathbf{T}] = \begin{bmatrix} \mathbf{I} \\ \mathbf{F}_{ms}^T\mathbf{F}_{mm}^{-1} \end{bmatrix}$$

(b) Show that this transformation is mathematically the same as that of Eq. 11.6-3.
(c) How can $[\mathbf{F}_{mm}]$ be computed from $[\mathbf{K}]$, and what is its physical meaning?
(d) Why is the transformation of part (a) likely to be more computationally efficient than the form used in Eq. 11.6-3?

11.6-3 Consider the two-d.o.f. unsupported bar of Fig. 11.4-3. What is the reduced stiffness matrix that results from taking u_2 as the slave d.o.f.? Is this result reasonable?

11.6-4 (a) In the example problem associated with Fig. 11.6-2, the choice is $\bar{v}_1$ as master and $\bar{\theta}_{z2}$ as slave. Is this choice consistent with the rule that masters have larger mass-to-stiffness ratio?
(b) Make the other choice, $\bar{\theta}_{z2}$ as master and $\bar{v}_1$ as slave, and compute the frequency and mode shape (analogous to Eqs. 11.6-9 and 11.6-10).
(c) Seek to improve the estimate of ω_1 by using the mode shape from part (b) in the Rayleigh quotient, with $[\mathbf{K}]$ and $[\mathbf{M}]$ taken from Eq. 11.6-7. Try Eq. 11.6-3 and then Eq. 11.6-6 for recovery of slave d.o.f.

11.6-5 Only axial motion is permitted in the system shown. Let $k = 1$ and $m = 2$. Determine the fundamental vibration frequency ω_1 of the given system. Then calculate ω_1 after condensing the system to a single d.o.f. Calculate the fundamental mode,

using first Eq. 11.6-3 and then Eq. 11.6-6 to recover slave d.o.f. Finally use these modes in the Rayleigh quotient to see if either produces an improved value of ω_1.

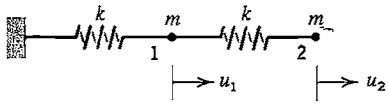

Problem 11.6-5

11.7-1 In terms of matrix products, determine the expression for damping matrix [**C**] in Eq. 11.2-12 that is implied by Eq. 11.7-6. (The resulting [**C**] is full, and depends on [$\mathbf{\Phi}$] and a diagonal matrix containing terms $2\xi_i\omega_i$.)

11.7-2 Consider the 2 by 2 stiffness and lumped mass matrices given in Problem 11.4-2a. Derive the system of two uncoupled differential equations for a modal analysis.

11.7-3 The sketch shows three equal particle masses connected by three springs, each of stiffness k. Only axial motion is permitted. Vibration modes, scaled so that the largest d.o.f. of each is unity, are $\{\bar{\mathbf{D}}\}_1 = \lfloor 1.000 \;\; 0.802 \;\; 0.445 \rfloor^T$, $\{\bar{\mathbf{D}}\}_2 = \lfloor -0.802 \;\; 0.445 \;\; 1.000 \rfloor^T$, and $\{\bar{\mathbf{D}}\}_3 = \lfloor -0.445 \;\; 1.000 \;\; -0.802 \rfloor^T$.
(a) Sketch these modes, and show by multiplication that they are mass-matrix orthogonal. Are they also stiffness matrix orthogonal?
(b) Let the two modes $\{\bar{\mathbf{D}}\}_1$ and $\{\bar{\mathbf{D}}\}_2$ be used to form modal matrix [$\mathbf{\Phi}$]. Also let $m = 1$ for each particle mass. What must be Z_2 if $Z_1 = 1$ and the physical displacement of node 1 is zero? Sketch the displaced shape of the structure thus obtained.
(c) For comparison, use u_1 and u_2 as masters in Guyan reduction (Section 11.6). For $u_1 = 0$ and $u_2 = 1$, sketch the displaced shape of the structure predicted by the reduced system.

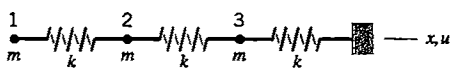

Problem 11.7-3

11.7-4 (a) In the sketch for Problem 11.6-5, let $k = m = 1$. Let the system be set in axial motion with initial conditions $u_1 = u_2 = \dot{u}_1 = 0$, $\dot{u}_2 = 1$. Calculate u_1 and u_2 at times $t = 1, 2, 3, 4$, and 5 by the modal method. Include both modes of the physical system in [$\mathbf{\Phi}$]. Note that the modal equations can be integrated exactly.
(b) Use results of part (a) to show that the numerator of the error expression, Eq. 11.7-9, is zero.
(c) Imagine now that only the lowest mode is retained, so that [$\mathbf{\Phi}$] becomes a column vector. Estimate the largest percentage errors in u_1 and u_2.

11.7-5 Again consider the two-spring, two-mass system treated in Problem 11.7-4. Let the system be undeformed and at rest at time $t = 0$. Steady axial force $F_2 = 1$ is applied to node 2 at $t = 0$. Use the modal method to calculate $u_1 = u_1(t)$ and $u_2 = u_2(t)$ at times $t = 2, 4, 6, 8$, and 10.
(a) Retain only the lowest mode in the transformation.
(b) Obtain similar results from the second mode, and add them to the results of part (a) to obtain the exact result. (Partial answer: $u_2 = 1.483$ at $t = 2$.)
(c) Evaluate the error estimate, Eq. 11.7-9, for part (a). What conclusion is indicated? What is $e(t)$ if both modes are used?

(d) Adjust results obtained in part (a) by applying the static correction, Eq. 11.7-11. What $e(t)$ is obtained if the static correction is included?

11.8-1 In the sketch for problem 11.6-5, let $k = m = 1$. Consider the application of Ritz vector analysis to this system, as follows.
(a) Externally-applied loads are zero, so arbitrarily assign $\{\mathbf{w}^*\}_1 = \lfloor 1 \;\; 0 \rfloor^T$. Hence, establish the 2 by 2 array $[\mathbf{W}]$ of Ritz vectors and the transformed system of Eq. 11.8-6.
(b) Repeat part (a), now using $\{\mathbf{w}^*\}_1 = \lfloor 0 \;\; 1 \rfloor^T$.
(c) If we arbitrarily assume that $\{\mathbf{w}^*\}_1 = \lfloor 1 \;\; 2 \rfloor^T$ and use no additional vectors, what is the resulting form of Eq. 11.8-6? What fundamental frequency does this equation yield? What other name identifies this method of calculation?

11.9-1 Consider axial vibration of the system of springs and masses shown, with $k = 1$ and $m = 1$. Natural frequencies are $\omega_1 = 0.9246$, $\omega_2 = 1.574$, and $\omega_3 = 2.381$. Create two substructures, one consisting of springs to the left of node 2, the other of springs to the right of node 2. Show that, in this case, component mode synthesis yields exact frequencies.

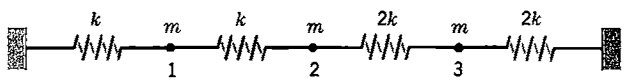

Problem 11.9-1

11.10-1 A single-d.o.f. spring-mass system without damping has natural frequency $\omega = \sqrt{k/m}$. It is excited by a force $P_0 \sin \Omega t$, where P_0 is a constant. For what range of the frequency ratio Ω/ω is the amplitude of motion more than 10% greater than the static displacement?

11.12-1 Forward and backward Euler direct integration methods are defined by

$$\text{Forward: } \{\mathbf{D}\}_{n+1} = \{\mathbf{D}\}_n + \Delta t \{\dot{\mathbf{D}}\}_n$$

$$\text{Backward: } \{\mathbf{D}\}_{n+1} = \{\mathbf{D}\}_n + \Delta t \{\dot{\mathbf{D}}\}_{n+1}$$

Determine the order of accuracy of these methods by using Taylor series expansion.

11.12-2 Show that Eq. 11.12-6 reduces to Eq. 11.12-3 if damping is zero.

11.12-3 Consider a single uniform two-node bar element with lumped masses and one end fixed. For this model, do the Gerschgorin bound, Eq. 11.12-17, and the element bound, Eq. 11.12-15, show good agreement with the exact frequency?

11.12-4 (a) Consider axial vibration of a uniform unsupported bar modeled by two-node elements of equal length. The maximum frequency of the entire model agrees with the maximum frequency of a single unconstrained element. Why?
(b) In the numerical example of Section 11.12, the element bound agrees almost exactly with the maximum mesh frequency. Should agreement be expected to improve or decline as the number of elements in the FE model is increased? Why?

11.12-5 A particle of unit mass is supported by a spring of unit stiffness, so $\omega = 1$. There is no damping or external load. At time $t = 0$, the particle has zero displacement, zero acceleration, but unit velocity. Use the central difference method, Eq. 11.12-3, to calculate displacement versus time over five time steps. Use (a) $\Delta t = 1$, (b) $\Delta t = \sqrt{2}$, (c) $\Delta t = 2$, and (d) $\Delta t = 3$.

11.12-6 A particle of unit mass is supported by a spring of unit stiffness, so $\omega = 1$. There is no damping. At time $t = 0$, when the particle has zero displacement and zero velocity, a unit force is applied and maintained. Use the central difference method, Eq. 11.12-3, to calculate displacement versus time over successive time steps as follows.

(a) Use $\Delta t = 0.5$ and go to $t = 7.0$.
(b) Use $\Delta t = 1.0$ and go to $t = 7.0$.
(c) Use $\Delta t = 2.0$ and go to $t = 10.0$.
(d) Use $\Delta t = 3.0$ and go to $t = 15.0$.
(e) Obtain the exact solution and compare the results of part (a) with it.

11.12-7 In the half-step central difference algorithm with proportional damping, viscous forces can be approximated as $\alpha[\mathbf{M}]\{\dot{\mathbf{D}}\}_n + \beta[\mathbf{K}]\{\dot{\mathbf{D}}\}_{n-1/2}$. For the mass-proportional portion, use Eq. 11.12-1a to approximate $\{\dot{\mathbf{D}}\}_n$. The stiffness-proportional portion can be obtained by summation of element contributions $\beta\int[\mathbf{B}]^T\{\dot{\boldsymbol{\sigma}}\}_{n-1/2}\,dV$ (verify that this is so). Thus obtain a revised form of Eq. 11.12-6.

11.13-1 Derive the equation $\dot{u}_{n+1} = \dot{u}_n + \frac{1}{2}\Delta t(\ddot{u}_{n+1} + \ddot{u}_n)$ by use of Taylor series, and show that $\dot{u}_{n-1}$ is approximated with error of $O(\Delta t^2)$. *Suggestion:* Write Taylor series for $\dot{u}_{n+1}$ about time $n\,\Delta t$, and for $\dot{u}_n$ about time $(n+1)\,\Delta t$, and combine results to obtain the desired relation plus higher-order terms.

11.13-2 Repeat Problem 11.12-5, but use the average acceleration method with four time steps, of magnitude (a) $\Delta t = 2.0$, and (b) $\Delta t = 1.0$.

11.14-1 Consider a single-d.o.f. equation of motion with damping but without inertia: $2\xi\omega\dot{Z} + \omega^2 Z = 0$. Investigate the stability criterion, if this equation is integrated by
(a) The central difference method, Eq. 11.12-1a.
(b) The average acceleration method. *Suggestion:* Write the equation of motion at time step n and at time step $n+1$, add the results, and use the equation $Z_{n+1} = Z_n + \frac{1}{2}\Delta t(\dot{Z}_{n+1} + \dot{Z}_n)$ to eliminate velocities.
(c) The forward Euler method, $Z_{n+1} = Z_n + \Delta t\,\dot{Z}_n$.
(d) The backward Euler method, $Z_{n+1} = Z_n + \Delta t\,\dot{Z}_{n+1}$.

11.14-2 Consider the central difference solutions obtained in Problem 11.12-5, parts (a), (b), and (c). What is the period error in each? Check that these values agree with Eq. 11.14-20.

11.14-3 Consider the average-acceleration solutions obtained in Problem 11.13-2, parts (a) and (b). Approximating as necessary, determine the period and period error of each. Check that these values agree with Eq. 11.14-21.

11.14-4 (a) For $\omega\,\Delta t = 0, 1, \sqrt{2}$, and 2, numerically evaluate Eq. 11.14-20 to obtain period errors of the central difference method.
(b) For $\omega\,\Delta t = 0, 1, 2$, and 4, numerically evaluate Eq. 11.14-21 to obtain period errors of the average acceleration method.

11.14-5 Derive equations requested in parts (a) and (b), and show that they reduce to forms that yield $a\,\Delta t = 0$ for all values of $\omega\,\Delta t$.
(a) The equation for the central difference method that results from using Eq. 11.14-22 in the manner described following that equation.
(b) The similar equation for the average acceleration method.

11.14-6 Consider Problem 11.12-5 again, in which the central difference method (Eq. 11.12-3) is applied to a spring-mass system for which $k = m = \omega = 1$. Now use $\Delta t = \sqrt{3.96}$, and start the algorithm using $u_0 = 0$ and $u_{-1} = -1$. Follow the motion for at least 30 time steps, and observe that the computed amplitude displays "beating" but no net growth.

11.17-1 Determine the contribution of mode 3 in Fig. 11.17-2 to the first peak in Fig. 11.17-3b. Use the method described in connection with Eq. 11.17-3.

COMPUTATIONAL PROBLEMS

Where dimensions, loads, or material properties are not assigned, choose values that seem reasonable or convenient. When additional assumptions are required, clearly state what they are. When mesh refinement is used, estimate the maximum percentage error of results provided by the finest FE mesh. Apply the analysis methodology suggested in Section 1.5.

C11.1 Let displacements of the structure shown be confined to the plane of the figure. The structure may be regarded as a truss (bar elements and pinned member connections) or a frame (beam elements and rigid member connections). For simplicity, assume that member cross sections are square, each h units on a side. One might, for example, use steel as the material, with $H = L = 6.0$ m and $h = 50$ mm. Using a single element to represent each of the ten members, investigate natural frequencies and modes under the following conditions.

(a) Truss model, consistent element mass matrices.
(b) Truss model, particle-lumped element mass matrices.
(c) Frame model, consistent element mass matrices.
(d) Frame model, particle-lumped element mass matrices.

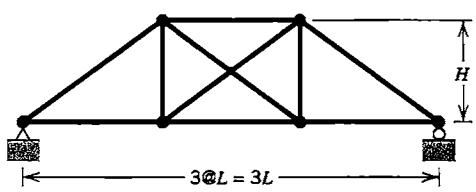

Problem C11.1

C11.2 (a) Repeat Problem C11.1, but remove the left support.
(b) Repeat Problem C11.1, this time using two or more elements of equal length to model each of the ten structural members.

C11.3 The sketch shows a building frame of n stories, each h units high. Investigate natural frequencies and modes.

C11.4 The structure shown consists of six identical slender bars of uniform circular cross section. The six bars are welded together with equal angles between them to form a plane structure with the weld at mass center C. Investigate the first eight nonzero natural frequencies and their modes. Confine displacements to the plane of the paper, and consider that center C is (a) unsupported, and (b) allowed to translate but not rotate.

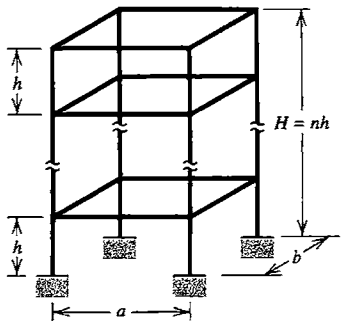

Problem C11.3

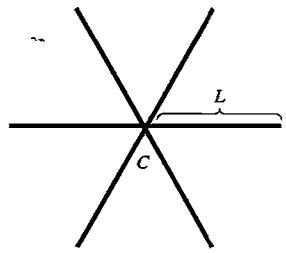

Problem C11.4

C11.5 (a) Repeat Problem C11.4 with three-dimensional motion allowed.
(b) Repeat Problem C11.4 with one of the bars doubled in mass.

C11.6 Repeat Problem C11.4, but with different support conditions: now provide simple support at the outer end of each bar and let center C be unsupported. Let displacements be (a) confined to the plane of the paper, and (b) allowed in any direction.

C11.7 By prescribing dimensions, design the steel tuning fork shown so that the sound heard has frequency 440 Hz.

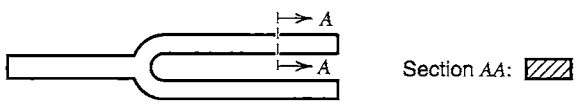

Problem C11.7

C11.8 Investigate natural frequencies and modes of a flat square panel of uniform-thickness material in the xy plane, with displacements confined to the xy plane. As boundary conditions, let edges be (a) all free, (b) all free but one, and (c) opposite edges free, the other two fixed.

C11.9 Investigate natural frequencies and modes of lateral vibration of flat plates. For comparison with computed results, analytically-determined results are available for many cases of rectangular and circular plates [11.66].

C11.10 Investigate the fundamental frequency and vibration mode of a plate on an elastic foundation (Section 15.6).
(a) Ignore the mass of the foundation.
(b) Include the mass of the foundation. Assume, for example, that it is an elastic layer between the plate and a parallel rigid plane. Approximate as seems appropriate.

C11.11 Look at sketches in other chapters, especially Chapter 16 (Shells). Many problems used as examples or test cases under static load may also be examined dynamically, for modes and frequencies, or response to time-varying loads. Great variety is possible in temporal variation and spatial distribution of forcing functions that may be chosen.

C11.12 Reduction can be applied to most dynamic problems. One might examine the change in results as progressively fewer modes or Ritz vectors are used, or as the

number of master d.o.f. in Guyan reduction is decreased. Also, a poor set of master d.o.f. might be deliberately chosen, and results compared with results produced by a good set and by the full system.

C11.13 The structure shown consists of equal-length lightweight beams *AE*, *BE*, *CE*, and *DE* that support heavy particles of slightly differing mass at *A*, *B*, *C*, and *D*. At *E*, the four beams are welded together and to a vertical beam *EF* that is fixed at *F*. Investigate the response history after an initial velocity is imparted to the particle at *A*. Let this velocity be in (a) the *y* direction, and (b) the *z* direction.

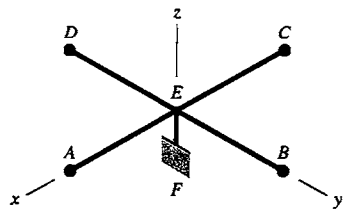

Problem C11.13

C11.14 Repeat the example problem of Section 11.12 (Fig. 11.12-1). Try using elements of unequal lengths (perhaps long in one half and short in the other), or consistent mass matrices, or substantially reducing the time step in a central difference solution. Try similar experiments with an implicit direct solution. Investigate the number of modes needed for accurate solution by the modal method.

C11.15 Apply response spectrum analysis to a problem for which response history has been computed. See if the maximum response is predicted with good accuracy.

CHAPTER 12

HEAT TRANSFER AND SELECTED FLUID PROBLEMS

Most of this chapter deals with the calculation of temperature distribution and heat flow in a solid body. Attention is given to both steady-state and transient conditions, and to nonlinearity associated with radiation boundary conditions. Other applications based on the same form of differential equation are noted. Acoustic modes in cavities, fluid-structure interaction, and plane incompressible irrotational flow are discussed.

12.1 HEAT TRANSFER: INTRODUCTION

Overview. In general, heat transfer analysis treats solids, liquids, and gases. Applications include heat exchangers, engines, electronic components, and chemical processes. When stress analysis is the goal, heat transfer calculations are applied to solids in order to determine a temperature field, so that associated thermal stresses may be determined. In FEA it is convenient, and usually possible, to use a single FE mesh for both temperature calculation and stress analysis by instructing software to transfer computed nodal temperatures to subsequent stress analysis. This two-step procedure is suited to the common case when coupling is sequential; that is, when temperature influences stress but stress has practically no influence on temperature.

Heat flows within a solid body by conduction. Heat is transferred to or from a solid body by convection of adjacent fluid and by radiation (Fig. 12.1-1). Also, heat may be generated internally, from such causes as resistance to electric current, absorption of microwave radiation, and radioactive decay. In a mathematical model of heat transfer, heat flow across a boundary and internal heat generation are respectively analogous to the stress analysis loads of surface traction and body force.

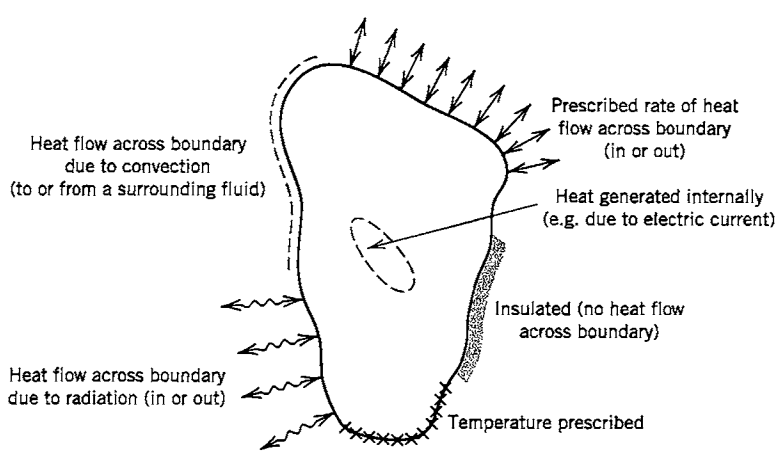

Figure 12.1-1. An arbitrary solid, showing various thermal loads and boundary conditions.

Conductivity and other thermal properties may be functions of temperature, just as elastic moduli may be temperature-dependent. Temperature-dependence does not make a stress analysis problem nonlinear, but *does* make a heat conduction problem nonlinear. A heat conduction problem is *certain* to be nonlinear if there is a radiation boundary condition because the associated heat flux depends on the difference of fourth powers of absolute temperature rather than on simple temperature differences. (Radiation is discussed in Section 12.3.)

The thermal problem we consider is that of determining the temperature field in a solid when physical properties are known and boundary conditions are prescribed. The temperature field may be steady-state or it may be transient, in which case we must determine the field as a function of time. In FEA, prominent matrices are a conductivity matrix [**K**], which is analogous to a stiffness matrix, and a heat capacity matrix [**C**], which is analogous to a mass matrix. Primary unknowns are nodal temperatures. Heat flux, if desired, is obtained from temperature gradients.

Nomenclature and Units. Quantities frequently used in subsequent discussion of heat transfer are as follows. In the SI system the unit of heat is the same as the unit of energy, namely the joule; 1 J = 1 N • m. The unit of power is the watt; 1 W = 1 J/s = 1 N • m/s. Temperature units are kelvins; degrees Celsius may be used instead unless radiation is involved (°C = K − 273).

c = specific heat (J/kg • K)

f = heat flux (W/m^2)

h = convective heat transfer coefficient (W/m^2 • K)

k = thermal conductivity (W/m • K)

Q = rate of internal heat generation per unit volume (W/m^3)

T = temperature (K; optionally °C if radiation is not involved)

T_{fl} = temperature of adjacent fluid outside the boundary layer (K)

$\dot{T}$ = $\partial T/\partial t$ (K/s)

t = time (s)

ρ = mass density (kg/m^3)

σ = Stefan-Boltzman constant (σ = 5.670 (10^{-8}) W/m^2 • K^4)

In the foregoing units, actual fluids and solids have numerical values in the approximate ranges $10^2 < c < 10^4$, $5 < h < 10^5$, and $0.01 < k < 300$ [12.1]. Large values of h are associated with boiling or condensation.

Flux across a boundary S due to convection is given by the following equation, which is called Newton's law of cooling:

$$f = h(T_{\text{fl}} - T_S) \tag{12.1-1}$$

where flux f is normal to the boundary and regarded as positive inward. Temperature in the fluid varies from T_{fl} to the surface temperature T_S through the thickness of a boundary layer adjacent to the solid. Typically h is determined by experiment, as its calculation presents a complicated problem of fluid mechanics, involving surface geometry and roughness, and the velocity, viscosity, density, and specific heat of the fluid, some of which may be temperature-dependent [12.2]. Tabulated data may state only a typical range of values for selected conditions.

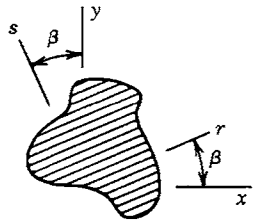

Figure 12.1-2. A layered material with principal directions r and s.

Governing Equations. Heat conduction analysis is based on the Fourier equation $f_s = -k\,(\partial T/\partial s)$, which states that heat flux in a direction s is proportional to temperature gradient, and flows in the opposite direction. In what follows we expand upon this relation, first for the two-dimensional case.

Consider a thermally orthotropic material, Fig. 12.1-2. Heat fluxes are

$$\begin{aligned} f_r &= -k_r T_{,r} \\ f_s &= -k_s T_{,s} \end{aligned} \quad \text{or} \quad \begin{Bmatrix} f_r \\ f_s \end{Bmatrix} = -\begin{bmatrix} k_r & 0 \\ 0 & k_s \end{bmatrix} \begin{Bmatrix} T_{,r} \\ T_{,s} \end{Bmatrix} \tag{12.1-2}$$

where k_r and k_s are thermal conductivities in principal material directions r and s. Temperature gradients $T_{,x}$ and $T_{,y}$ in x and y directions are related to temperature gradients $T_{,r}$ and $T_{,s}$ by chain rule differentiation:

$$\begin{Bmatrix} T_{,r} \\ T_{,s} \end{Bmatrix} = [\Lambda] \begin{Bmatrix} T_{,x} \\ T_{,y} \end{Bmatrix} \quad \text{where} \quad [\Lambda] = \begin{bmatrix} x_{,r} & y_{,r} \\ x_{,s} & y_{,s} \end{bmatrix} = \begin{bmatrix} \cos\beta & \sin\beta \\ -\sin\beta & \cos\beta \end{bmatrix} \tag{12.1-3}$$

Heat flux is a vector quantity and transforms in the same way as displacement; that is, $\lfloor f_x \;\; f_y \rfloor^T = [\Lambda]^T \lfloor f_r \;\; f_s \rfloor^T$. Combining this result with Eqs. 12.1-2 and 12.1-3, we obtain

$$\begin{Bmatrix} f_x \\ f_y \end{Bmatrix} = -[\kappa] \begin{Bmatrix} T_{,x} \\ T_{,y} \end{Bmatrix} \quad \text{where} \quad [\kappa] = \begin{bmatrix} k_x & k_{xy} \\ k_{xy} & k_y \end{bmatrix} = [\Lambda]^T \begin{bmatrix} k_r & 0 \\ 0 & k_s \end{bmatrix} [\Lambda] \tag{12.1-4}$$

Because temperature is a scalar quantity, not a vector, it requires no coordinate transformation.

For a body of unit thickness, the rate of heat generation in a differential element $dx\,dy$ is $Q\,dx\,dy$. Heat flux across sides of a differential element in the xy plane is shown in Fig. 12.1-3. For the time being we assume that lateral surfaces of the body (parallel to the xy plane) are insulated. Then the net rate of heat flow into a differential element of unit thickness is

$$Q\,dx\,dy - (f_{x,x}\,dx)\,dy - (f_{y,y}\,dy)\,dx \quad \text{or} \quad (Q - f_{x,x} - f_{y,y})\,dx\,dy \tag{12.1-5}$$

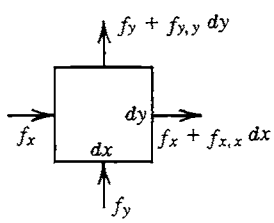

Figure 12.1-3. Heat flux through sides of a plane differential element.

Inward heat flow produces an increase of stored energy, specifically $c\rho\, dx\, dy\, \dot{T}$. Hence

$$Q - f_{x,x} - f_{y,y} = c\rho\dot{T} \tag{12.1-6}$$

Combination of Eqs. 12.1-4 and 12.1-6 provides, for a body of unit thickness,

$$\frac{\partial}{\partial x}(k_x T_{,x} + k_{xy} T_{,y}) + \frac{\partial}{\partial y}(k_{xy} T_{,x} + k_y T_{,y}) + Q - c\rho\dot{T} = 0 \tag{12.1-7}$$

If the medium is isotropic and homogeneous, then $k_{xy} = 0$ and $k_x = k_y = k$, and Eq. 12.1-7 reduces to

$$k(T_{,xx} + T_{,yy}) + Q - c\rho\dot{T} = 0 \tag{12.1-8}$$

If in addition $Q = 0$ and steady-state conditions prevail ($\dot{T} = 0$), we obtain Laplace's equation, $T_{,xx} + T_{,yy} = 0$.

Now let the thickness of the body be τ, where τ may be a function of x and y but is much smaller than dimensions in the xy plane. Also let lateral surfaces be uninsulated, with convection heat transfer to or from a surrounding fluid. Heat flux into the body across each uninsulated lateral surface is then $h(T_{\text{fl}} - T)$. If convection appears on *both* lateral surfaces, with h and T_{fl} the same on both, and T has negligible thickness-direction variation, then Eq. 12.1-7 is replaced by

$$\frac{\partial}{\partial x}(k_x \tau T_{,x} + k_{xy} \tau T_{,y}) + \frac{\partial}{\partial y}(k_{xy} \tau T_{,x} + k_y \tau T_{,y}) + \tau Q + 2h(T_{\text{fl}} - T) - c\rho\tau\dot{T} = 0 \tag{12.1-9}$$

This equation can be used to analyze a cooling fin, including one that is tapered. A similar equation, applicable to one-dimensional heat flow in a bar whose cross-sectional area A and perimeter p may vary with axial coordinate x, is

$$\frac{d}{dx}(AkT_{,x}) + AQ + hp(T_{\text{fl}} - T) - Ac\rho\dot{T} = 0 \tag{12.1-10}$$

This equation can be obtained by applying the same arguments as used to obtain Eq. 12.1-9, and can be used to analyze a "pin fin."

On boundary S of a plane region, Fig. 12.1-4, heat flux is related to temperature gradient as follows. If the body is thermally isotropic, flux in direction ν is $f_\nu = -kT_{,\nu}$. According to the chain rule,

$$T_{,\nu} = T_{,x} x_{,\nu} + T_{,y} y_{,\nu} \quad \text{or} \quad T_{,\nu} = T_{,x} l + T_{,y} m \tag{12.1-11}$$

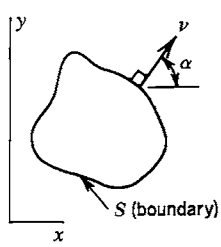

Figure 12.1-4. Plane region with outward normal direction ν on its boundary S.

where l and m are direction cosines of ν. Let f_B be boundary flux, positive when directed into the body, so that $f_B = -f_\nu$. Then for isotropic and orthotropic materials respectively, flux normal to boundary S is

$$\text{Isotropic:} \quad f_B = k(T_{,x}l + T_{,y}m) \tag{12.1-12a}$$

$$\text{Orthotropic:} \quad f_B = (k_x T_{,x} + k_{xy} T_{,y})l + (k_{xy} T_{,x} + k_y T_{,y})m \tag{12.1-13a}$$

The latter equation is obtained from Eq. 12.1-4 and the equation $f_B = -\lfloor l \;\; m \rfloor \lfloor f_x \;\; f_y \rfloor^T$. Flux f_B may be prescribed or may be associated with convection or radiation. Boundary temperature may also be prescribed, but not on the same portion of a boundary where f_B is prescribed.

In the foregoing formulation, boundary S is the edge of a plane region in a 2D problem and the ends of a bar in a 1D problem. More generally, convection is of much greater importance on *lateral* surfaces than on edges and ends. Surface S becomes an important convection surface for plates, shells, and solids.

Solid Bodies. Equations for solids are obtained by direct extension of the foregoing arguments. We choose to write equations in matrix format, using the following notation.

$$\{\partial\} = \begin{Bmatrix} \partial/\partial x \\ \partial/\partial y \\ \partial/\partial z \end{Bmatrix} \qquad \{\mathbf{T}_\partial\} = \begin{Bmatrix} T_{,x} \\ T_{,y} \\ T_{,z} \end{Bmatrix} \qquad \{\boldsymbol{\mu}\} = \begin{Bmatrix} l \\ m \\ n \end{Bmatrix} \tag{12.1-14}$$

where l, m, and n are direction cosines of a normal to the boundary. Also let $[\boldsymbol{\kappa}]$ be a 3 by 3 conductivity matrix. If the material is isotropic, then $[\boldsymbol{\kappa}] = k\lceil \mathbf{I} \rfloor$, where $\lceil \mathbf{I} \rfloor$ is a 3 by 3 unit matrix. If the material is orthotropic and has principal directions r, s, and t, then $[\boldsymbol{\kappa}] = [\boldsymbol{\Lambda}]^T \lceil k_r \;\; k_s \;\; k_t \rfloor [\boldsymbol{\Lambda}]$, where $[\boldsymbol{\Lambda}]$ is the transformation matrix stated in Eq. 8.1-1. Thus, for a solid body in rectangular Cartesian coordinates,

$$\text{Governing equation:} \quad \{\partial\}^T([\boldsymbol{\kappa}]\{\mathbf{T}_\partial\}) + Q - c\rho\dot{T} = 0 \tag{12.1-15a}$$

$$\text{Boundary condition:} \quad f_B = \{\boldsymbol{\mu}\}^T[\boldsymbol{\kappa}]\{\mathbf{T}_\partial\} \tag{12.1-15b}$$

in which, for example, $f_B = h(T_{\text{fl}} - T)$ for a convection condition with temperature T on boundary S. Equations 12.1-14 are analogous to Eqs. 12.1-7 and 12.1-12, and yield these equations if derivatives with respect to z are zero.

For a solid of revolution we adopt cylindrical coordinates. Equations 12.1-14 remain applicable if we use in place of Eqs. 12.1-13 the definitions

$$\{\partial\} = \begin{Bmatrix} (1/r) + \partial/\partial r \\ (1/r)\partial/\partial\theta \\ \partial/\partial z \end{Bmatrix} \qquad \{\mathbf{T}_\partial\} = \begin{Bmatrix} T_{,r} \\ T_{,\theta}/r \\ T_{,z} \end{Bmatrix} \qquad \{\boldsymbol{\mu}\} = \begin{Bmatrix} l \\ 0 \\ n \end{Bmatrix} \tag{12.1-16}$$

where r replaces x and z is the axis of revolution. If conditions are axisymmetric, derivatives with respect to θ vanish and the problem is mathematically two-dimensional, with

coordinates r and z playing the same role as coordinates x and y in a plane problem. If θ is a principal material direction, a temperature field that lacks axial symmetry can be analyzed by Fourier series, as explained for stress analysis in Sections 14.4 and 14.5. Thus the temperature field is expressed as $T = \sum \bar{T}_n \cos n\theta$. Here n is the harmonic number and temperature field $\bar{T}_n$ is a function of n, r, and z but is independent of θ. Solutions for $n = 0$, $n = 1$, $n = 2$, and so on are obtained separately and superposed to produce the final result.

12.2 FINITE ELEMENT FORMULATION

Applicable FE formulations have been seen in previous chapters. In Section 4.8, an FE formulation is obtained from a functional, for a plane isotropic body without convection boundary conditions. In Section 5.5, an FE formulation for the plane quasiharmonic problem (which includes the plane heat conduction problem) is obtained by the Galerkin method. In what follows we elect to use the more compact statements provided by a functional and the notation used in Eqs. 12.1-14. The functional is

$$\Pi = \int \left(\frac{1}{2} \{\mathbf{T}_\partial\}^T [\boldsymbol{\kappa}] \{\mathbf{T}_\partial\} - QT + c\rho T\dot{T} \right) dV - \int \left(f_B T + hT_{\mathrm{fl}} T - \frac{1}{2} hT^2 \right) dS \quad (12.2\text{-}1)$$

where, in the latter integral, T is evaluated on boundary S. Procedures discussed in Section 4.7 show that when T is subject to variation, $\delta\Pi = 0$ provides Eqs. 12.1-14. For FE formulation we use shape function interpolation to express T in an element in terms of element nodal temperatures $\{\mathbf{T}_e\}$. Thus

$$T = \lfloor \mathbf{N} \rfloor \{\mathbf{T}_e\} \quad \text{and} \quad \{\mathbf{T}_\partial\} = [\mathbf{B}]\{\mathbf{T}_e\} \quad \text{where} \quad [\mathbf{B}] = \{\partial\} \lfloor \mathbf{N} \rfloor \quad (12.2\text{-}2)$$

where $\{\partial\}$ is given by Eq. 12.1-3 in Cartesian coordinates, but differs from Eq. 12.1-5 in cylindrical coordinates, being $\{\partial\} = \lfloor \partial/\partial r \quad (1/r)\partial/\partial\theta \quad \partial/\partial z \rfloor^T$ in Eq. 12.2-2. Since $T = T^T$, $T^2 = T^T T$, and $\dot{T} = \lfloor \mathbf{N} \rfloor \{\dot{\mathbf{T}}_e\}$, Eq. 12.2-1 becomes, for one element,

$$\Pi_e = \frac{1}{2} \{\mathbf{T}_e\}^T \Big([\mathbf{k}] + [\mathbf{h}] \Big) \{\mathbf{T}_e\} + \{\mathbf{T}_e\}^T \Big([\mathbf{c}]\{\dot{\mathbf{T}}_e\} - \{\mathbf{r}_B\} - \{\mathbf{r}_h\} - \{\mathbf{r}_Q\} \Big) \quad (12.2\text{-}3)$$

where element matrices are

$$\begin{aligned}
[\mathbf{k}] &= \int_V [\mathbf{B}]^T [\boldsymbol{\kappa}] [\mathbf{B}]\, dV & \{\mathbf{r}_B\} &= \int_S \lfloor \mathbf{N} \rfloor^T f_B\, dS \\
[\mathbf{h}] &= \int_S \lfloor \mathbf{N} \rfloor^T \lfloor \mathbf{N} \rfloor h\, dS & \{\mathbf{r}_h\} &= \int_S \lfloor \mathbf{N} \rfloor^T h T_{\mathrm{fl}}\, dS \qquad (12.2\text{-}4) \\
[\mathbf{c}] &= \int_V \lfloor \mathbf{N} \rfloor^T \lfloor \mathbf{N} \rfloor c\rho\, dV & \{\mathbf{r}_Q\} &= \int_V \lfloor \mathbf{N} \rfloor^T Q\, dV
\end{aligned}$$

Here V is the element volume, and S is the area of the element surface if it forms part of the boundary of the body. Surface integrals are zero for interior elements. Addition of element

contributions Π_e provides Π of the assembled structure. Assembly implies the usual expansion of element arrays to "structure size," so that the array of global temperatures $\{\mathbf{T}\}$ replaces element arrays $\{\mathbf{T}_e\}$. Equations that make Π stationary are $\{\partial\Pi/\partial\mathbf{T}\} = \{\mathbf{0}\}$. Thus we obtain the following FE equation, in which assembled arrays are denoted by upper case letters.

$$[\mathbf{C}]\{\dot{\mathbf{T}}\} + [\mathbf{K}_T]\{\mathbf{T}\} = \{\mathbf{R}_T\} \qquad \text{where} \qquad \begin{aligned} [\mathbf{K}_T] &= [\mathbf{K}] + [\mathbf{H}] \\ \{\mathbf{R}_T\} &= \{\mathbf{R}_B\} + \{\mathbf{R}_h\} + \{\mathbf{R}_Q\} \end{aligned} \tag{12.2-5}$$

In a plane problem with convection heat transfer across a lateral surface, additional terms appear, as described in connection with Eq. 12.1-9. For convection heat transfer across a single lateral surface parallel to the xy plane, we define the element arrays

$$[\mathbf{h}_{\mathrm{ls}}] = \iint \lfloor \mathbf{N} \rfloor^T \lfloor \mathbf{N} \rfloor \, h \, dx \, dy \qquad \{\mathbf{r}_{\mathrm{ls}}\} = \iint \lfloor \mathbf{N} \rfloor^T h T_{\mathrm{fl}} \, dx \, dy \tag{12.2-6}$$

Upon assembly of elements, global arrays $[\mathbf{H}_{\mathrm{ls}}]\{\mathbf{T}\}$ and $\{\mathbf{R}_{\mathrm{ls}}\}$ are added to the left- and right-hand sides, respectively, of Eq. 12.2-5.

Remarks. We assign the following names to matrices and vectors defined by Eqs. 12.2-4, and note their analogues in matrices used in structural mechanics.

Matrix	Descriptive name	Structural analogue
$[\mathbf{k}]$	Conductivity matrix	Conventional stiffness matrix
$[\mathbf{h}]$	Boundary convection matrix	Elastic foundation stiffness matrix
$[\mathbf{c}]$	Specific heat (or capacity) matrix	Mass matrix
$\{\mathbf{r}_B\}$	Heat flux vector	Nodal loads due to surface traction
$\{\mathbf{r}_h\}$	Boundary convection vector	(no direct analogue)
$\{\mathbf{r}_Q\}$	Heat generation vector	Nodal loads due to body force

Note, however, that $[\mathbf{c}]$ multiplies *first* time derivatives of temperature while $[\mathbf{m}]$ in structural dynamics multiplies *second* time derivatives of displacement. Like a mass matrix, $[\mathbf{c}]$ is a full matrix if generated according to Eq. 12.2-4, but $[\mathbf{c}]$ can also be generated as a diagonal or "lumped" matrix, or diagonalized from its consistent form, as described for mass matrices in Section 11.3. The crudest diagonalization, for an element of volume V and n nodes, is to define diagonal terms as $c_{ii} = c\rho V/n$. Similarly, $[\mathbf{h}]$ may be diagonalized. A diagonal $[\mathbf{h}]$ is analogous to the elastic foundation stiffness matrix that arises from discrete springs at nodes rather than a continuous elastic support. One may regard $[\mathbf{h}]$ as associated with a zero-thickness "surface element" that is attached to a conventional element when needed, and whose function is only to supply terms associated with $[\mathbf{h}]$.

Arrays $[\mathbf{h}]$, $\{\mathbf{r}_B\}$, and $\{\mathbf{r}_h\}$ are null unless the element has an edge or face on boundary S and that portion of S is associated with either convection or prescribed flux f_B (or with radiation, as noted in Section 12.3). A portion of S where $\{\mathbf{r}_B\}$ or $\{\mathbf{r}_h\}$ is applied cannot also have a prescribed temperature. In other words, at a given node one can prescribe flux or temperature but not both, just as in structural mechanics one may prescribe displacement or load on a single d.o.f. but not both.

A prescribed nodal temperature can be treated like a prescribed nodal displacement d.o.f. in structural mechanics. Applicable treatments include manipulating the form of the coefficient matrix, as described in Section 2.7, and the penalty method, as described in Section 13.3. The thermal equivalent of the penalty-method treatment applied in Fig. 9.2-3d is to add a large conductivity K_D to the appropriate diagonal coefficient in [**K**] and augment the corresponding coefficient in the thermal load vector by $K_D\bar{T}$, where $\bar{T}$ is the desired nodal temperature. With one d.o.f. per node, large off-diagonal coefficients are not added to [**K**] and it does not become ill-conditioned. However, the treatment greatly increases the largest eigenvalue of [**K**] and may therefore require a very small time step if explicit direct integration is used to analyze thermal transients [12.3].

Example: Plane Element. Consider the isoparametric element depicted in Fig. 12.2-1. The element temperature field is $T = \lfloor \mathbf{N} \rfloor \{\mathbf{T}_e\} = N_1T_1 + N_2T_2 + N_3T_3 + N_4T_4$, where shape functions N_i are stated in Eq. 6.2-3. Temperature gradients are

$$\{\mathbf{T}_\partial\} = \begin{Bmatrix} T_{,x} \\ T_{,y} \end{Bmatrix} = [\mathbf{J}]^{-1}\begin{Bmatrix} T_{,\xi} \\ T_{,\eta} \end{Bmatrix} = \underbrace{[\mathbf{J}]^{-1}\begin{bmatrix} N_{1,\xi} & N_{2,\xi} & N_{3,\xi} & N_{4,\xi} \\ N_{1,\eta} & N_{2,\eta} & N_{3,\eta} & N_{4,\eta} \end{bmatrix}}_{[\mathbf{B}]}\begin{Bmatrix} T_1 \\ T_2 \\ T_3 \\ T_4 \end{Bmatrix} \tag{12.2-7}$$

where Jacobian matrix [**J**] is stated in Eq. 6.2-6. The conductivity matrix [**k**] for an element of thickness τ becomes

$$[\mathbf{k}] = \int_{-1}^{1}\int_{-1}^{1} [\mathbf{B}]^T[\boldsymbol{\kappa}][\mathbf{B}]\tau J \, d\xi \, d\eta \tag{12.2-8}$$

in which τ may be a function of ξ and η, and J is the determinant of [**J**].

Element boundary convection matrix [**h**] receives a contribution only from element side 3-4. Along side 3-4, $N_1 = N_2 = 0$, $N_3 = (1 + \xi)/2$, $N_4 = (1 - \xi)/2$, and $J = L_{34}/2$. Therefore, if τ and h are independent of ξ along side 3-4,

$$[\mathbf{h}] = \int_{-1}^{1} \lfloor \mathbf{N} \rfloor^T \lfloor \mathbf{N} \rfloor h\tau J \, d\xi = \frac{h\tau L_{34}}{6}\begin{bmatrix} 0 & 0 & 0 & 0 \\ 0 & 0 & 0 & 0 \\ 0 & 0 & 2 & 1 \\ 0 & 0 & 1 & 2 \end{bmatrix} \tag{12.2-9}$$

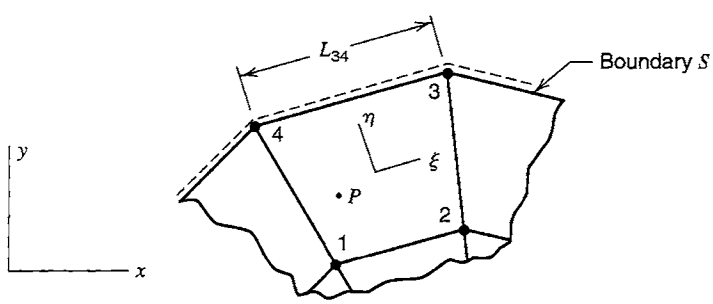

Figure 12.2-1. Bilinear isoparametric element adjacent to boundary S of a plane structure, where convection heat transfer occurs.

A lumped (diagonal) form of [**h**] is [**h**] $= (h\tau L_{34}/2)\lceil 0\ 0\ 1\ 1 \rfloor$. Boundary convection vector $\{\mathbf{r}_h\}$ is obtained in a fashion similar to [**h**] of Eq. 12.2-9:

$$\{\mathbf{r}_h\} = \int_{-1}^{1} \lfloor \mathbf{N} \rfloor^T h T_{fl} \tau J \, d\xi = T_{fl} \frac{h\tau L_{34}}{2} \begin{Bmatrix} 0 \\ 0 \\ 1 \\ 1 \end{Bmatrix} \tag{12.2-10}$$

Because nonzero terms in [**h**] and $\{\mathbf{r}_h\}$ are associated with surface nodes only, terms that contribute to [**H**] and $\{\mathbf{R}_h\}$ might be supplied by a surface element rather than by a surface of a 2D or 3D element. In Fig. 12.2-1, the appropriate surface element is a two-node element that connects nodes 3 and 4.

If heat input Q_P (units: W) is prescribed at an arbitrary point P in the element, we obtain the resulting heat generation vector $\{\mathbf{r}_Q\}$ from Eq. 12.2-4 by saying that $Q = 0$ except at point P. With $\lfloor \mathbf{N}_P \rfloor$ the value of $\lfloor \mathbf{N} \rfloor$ at point P,

$$\{\mathbf{r}_Q\} = \int \lfloor \mathbf{N} \rfloor^T Q \, dV = \lfloor \mathbf{N}_P \rfloor^T \int Q \, dV = \lfloor \mathbf{N}_P \rfloor^T Q_P \tag{12.2-11}$$

12.3 RADIATION. NONLINEAR HEAT TRANSFER PROBLEMS

Radiation. To introduce the subject of radiation, consider two parallel planes, both of infinite extent so that edge effects are not involved. Let each plane have uniform temperature, T_1 for plane 1 and T_2 for plane 2. Imagine that the planes are ideal blackbodies, so that each is a perfect absorber and a perfect radiator. Thus the plane of temperature T_1 absorbs heat flux σT_2^4 and radiates heat flux σT_1^4, where σ is the Stefan-Boltzmann constant and temperatures are measured on an absolute scale [12.1,12.4]. Net heat fluxes received by the surfaces of absolute temperatures T_1 and T_2 are respectively

$$f_1 = \sigma\left(T_2^4 - T_1^4\right) \quad \text{and} \quad f_2 = \sigma\left(T_1^4 - T_2^4\right) \tag{12.3-1}$$

If radiating and absorbing surfaces are not blackbodies, they are characterized by emissivities ε_1 and ε_2. Emissivity is defined as the ratio of actual emissive power to that of a blackbody of the same temperature. Thus $0 < \varepsilon < 1$. The value of ε depends on surface roughness, degree of oxidation (if metal), temperature, wavelength of emitted energy, and may vary with the direction of radiation relative to the surface normal. As examples, $\varepsilon \approx 0.05$ for aluminum foil, and $\varepsilon \approx 0.95$ for paper at room temperature [12.4]. Absorptivity α of a surface describes the fraction of radiant energy absorbed. It is defined similarly to emissivity and depends on the same factors. Sometimes heat transfer calculations can be simplified by assuming that $\varepsilon = \alpha$. For infinite parallel planes 1 and 2, it can be shown that f_1 of Eq. 12.3-1 is replaced by [12.1,12.4]

$$f_1 = \frac{\sigma}{(1/\varepsilon_1) + (1/\varepsilon_2) - 1}\left(T_2^4 - T_1^4\right) \tag{12.3-2}$$

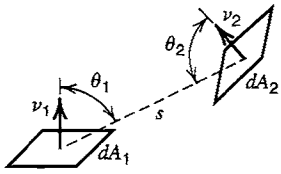

$$dF_{1-2} = \frac{\cos\theta_1 \cos\theta_2}{\pi s^2}\, dA_2$$

$$dF_{2-1} = \frac{\cos\theta_1 \cos\theta_2}{\pi s^2}\, dA_1$$

$$dF_{1-2}\, dA_1 = dF_{2-1} dA_2$$

Figure 12.3-1. View factor: differential relations, with s the center-to-center distance.

which reduces to Eq. 12.3-1 if $\varepsilon_1 = \varepsilon_2 = 1$. The next complication is that practical surfaces may not be parallel, are often not flat, and are certainly not infinite. These geometric complications are accounted for by a view factor F (also called a shape, angle, configuration, or interception factor). The view factor is a purely geometrical quantity that is unity for infinite parallel planes but zero for two surfaces that cannot "see" one another, as for coplanar areas and for areas hidden from one another by an intervening surface. Consider two differential areas dA_1 and dA_2 separated by distance s and having normal directions ν_1 and ν_2 (Fig. 12.3-1). Incremental view factor dF_{1-2} is the fraction of flux that leaves dA_1 and is intercepted by dA_2. In heat transfer calculation, large surfaces can be subdivided, and view factors can be considered constant over two finite subareas A_1 and A_2 if their separation is sufficiently great. In FEA, each element surface may be regarded as a subarea, and view factors may be calculated for each pair of subareas that exchange radiation with one another.

Let us symbolize the heat flux received by a surface of area A_1 and temperature T_1 as

$$f_1 = \psi\sigma\left(T_2^4 - T_1^4\right) \tag{12.3-3}$$

where ψ incorporates the view factor and emissivities appropriate to the surfaces in question. This equation can be written as many times as there are surfaces that exchange radiant energy with A_1. If A_1 is not large, f_1 can be regarded as constant over A_1. By factoring $T_2^4 - T_1^4$ in Eq. 12.3-3, we can write

$$f_1 = h_{\text{rad}}(T_2 - T_1) \qquad \text{where} \qquad h_{\text{rad}} = \psi\sigma\left(T_2^2 + T_1^2\right)(T_2 + T_1) \tag{12.3-4}$$

Comparing this equation with the convection equation, Eq. 12.1-1, we see that the flux expressions have the same form. Therefore FEA can account for radiation if matrices having the same form as convection matrices $[\mathbf{h}]$ and $\{\mathbf{r}_h\}$ in Eqs. 12.2-6 are added to the formulation, but with h replaced by h_{rad}. Note that h_{rad} is *temperature-dependent;* so much so that the heat transfer problem becomes highly nonlinear.

The foregoing is a brief summary of a large subject area. We have tacitly assumed that the medium between radiating surfaces is "nonparticipating;" that is, it does not radiate, absorb, or reflect. Such is the case for air, but certainly not for flames, and not for air contaminated with certain gases (H_2O, CO_2, and SO_2, for example).

Solution of Nonlinear Problems. If there are appreciable temperature differences within a body, thermal conductivity may have to be regarded as a function of T. Convection heat transfer coefficient h may also be temperature-dependent. For these reasons the problem may become nonlinear. The problem is *certain* to be nonlinear if radiation is involved, whether or not material properties are temperature-dependent. For nonlinear but steady-state conditions, Eq. 12.2-5 can be symbolized as

$$[\mathbf{K}_T]\{\mathbf{T}\} = \{\mathbf{R}_T\} \qquad \text{where} \qquad [\mathbf{K}_T] = [\mathbf{K}_T(T)] \qquad \text{and} \qquad \{\mathbf{R}_T\} = \{\mathbf{R}_T(T)\} \tag{12.3-5}$$

To solve for $\{\mathbf{T}\}$, methods described in Section 17.2 can be applied. The simplest of these is direct substitution, in which the starting $[\mathbf{K}_T]$ and $\{\mathbf{R}_T\}$ are generated based on an initial estimate of $\{\mathbf{T}\}$, a new $\{\mathbf{T}\}$ is computed from Eq. 12.3-5, then $[\mathbf{K}_T]$ and $\{\mathbf{R}_T\}$ are revised using Eq. 12.3-4, and so on. Thus we generate the sequence of solutions

$$\{\mathbf{T}_1\} = [\mathbf{K}_T(T_0)]^{-1}\{\mathbf{R}_T(T_0)\}, \quad \{\mathbf{T}_2\} = [\mathbf{K}_T(T_1)]^{-1}\{\mathbf{R}_T(T_1)\}, \quad \text{and so on} \tag{12.3-6}$$

A similar alternative is the initial stiffness method, which modifies Eq. 12.3-5 by splitting $[\mathbf{K}_T]$ into linear and nonlinear parts so that all nonlinear terms may be taken to the right-hand side. Strong linearity provided by radiation may require underrelaxation to prevent divergence (see Eq. 17.2-8, with $\mu = 0.5$, perhaps). To check for convergence one may examine temperatures, heat fluxes, or both. One might say that convergence is achieved when, at every node, the change in temperature from one iteration to the next is less than an assigned number such as one degree. Or, if testing flux, one might compare the out-of-balance flux with the total flux (see Eq. 17.2-10 and regard $\{\mathbf{R}\}$ as flux). Further discussion of time-independent nonlinear thermal problems appears in [12.5].

12.4 TRANSIENT THERMAL ANALYSIS

The problem to be solved is that of Eq. 12.2-5, here repeated:

$$[\mathbf{C}]\{\dot{\mathbf{T}}\} + [\mathbf{K}_T]\{\mathbf{T}\} = \{\mathbf{R}_T\} \tag{12.4-1}$$

where $\{\mathbf{R}_T\}$ is an array of thermal loads that may be time-dependent. If radiation is present or material properties are temperature-dependent, then $[\mathbf{C}]$ and $[\mathbf{K}_T]$ are also time-dependent, and the problem is nonlinear. In this section, unless stated otherwise, we presume that $[\mathbf{C}]$ and $[\mathbf{K}_T]$ are not time-dependent.

A time-varying solution may be obtained by the modal method or by direct time integration. The choice is guided by the same considerations that apply in structural mechanics. If the problem is linear and if the solution is dominated by lower eigenmodes and is required over an appreciable time span, the modal method is favored. If the problem is nonlinear or sharp transients must be represented in the solution, direct integration is favored. The following methods and equations will be recognized as similar to those described in Chapter 11.

Modal Method. The procedure is similar to that described in Section 11.7. It is outlined as follows. We first solve the eigenproblem

$$\Big([\mathbf{K}_T] - \lambda[\mathbf{C}]\Big)\{\bar{\mathbf{T}}\} = \{\mathbf{0}\} \tag{12.4-2}$$

Each eigenvector $\{\bar{\mathbf{T}}\}_i$ is normalized with respect to $[\mathbf{C}]$; in other words, it is scaled so that $\{\bar{\mathbf{T}}\}_i^T[\mathbf{C}]\{\bar{\mathbf{T}}\}_i = 1$. Let $[\boldsymbol{\phi}]$ be the modal matrix; that is, $[\boldsymbol{\phi}]$ is a square matrix whose ith column is the scaled eigenvector $\{\bar{\mathbf{T}}\}_i$. Then

$$[\boldsymbol{\phi}]^T[\mathbf{C}][\boldsymbol{\phi}] = \lceil \mathbf{I} \rfloor \quad \text{and} \quad [\boldsymbol{\phi}]^T[\mathbf{K}_T][\boldsymbol{\phi}] = \lceil \boldsymbol{\lambda} \rfloor \tag{12.4-3}$$

where $\lceil \mathbf{I} \rfloor$ is a unit matrix and $\lceil \boldsymbol{\lambda} \rfloor$ is the (diagonal) spectral matrix $\lceil \boldsymbol{\lambda} \rfloor \doteq \lceil \lambda_1 \ \lambda_2 \ \cdots \ \lambda_n \rfloor$. Nodal temperatures $\{\mathbf{T}\}$ are related to generalized temperatures $\{\mathbf{Z}\}$ by

$$\{\mathbf{T}\} = [\boldsymbol{\phi}]\{\mathbf{Z}\} \tag{12.4-4}$$

where the Z_i in $\{\mathbf{Z}\}$ state the fraction of each normalized eigenvector that contributes to $\{\mathbf{T}\}$. We substitute Eq. 12.4-4 into Eq. 12.4-1, premultiply by $[\boldsymbol{\phi}]^T$, and take note of Eqs. 12.4-3. Thus for an n by n system we obtain n uncoupled equations, each having the form

$$\dot{Z}_i + \lambda_i Z_i = p_i \qquad \text{where} \qquad p_i = \{\boldsymbol{\phi}\}_i^T \{\mathbf{R}_T\} \tag{12.4-5}$$

Here $\{\boldsymbol{\phi}\}_i$ is the ith column of $[\boldsymbol{\phi}]$, and i runs from 1 to m, where m is typically much less than the total number of d.o.f., so that only the first few columns of $[\boldsymbol{\phi}]$ are used in practical computation. After Eq. 12.4-5 is integrated with respect to time for each i used, $\{\mathbf{Z}\} = \{\mathbf{Z}(t)\}$ is known, and Eq. 12.4-4 yields $\{\mathbf{T}\} = \{\mathbf{T}(t)\}$.

Reduced-basis methods such as described for structural problems in Section 11.6 can also be applied to thermal problems [12.6].

Direct Integration. Consider two temperature states, separated by time Δt and denoted as $\{\mathbf{T}\}_n$ and $\{\mathbf{T}\}_{n+1}$. Temporal integration can be accomplished using the equation

$$\{\mathbf{T}\}_{n+1} = \{\mathbf{T}\}_n + \Delta t\left\{(1-\beta)\dot{\mathbf{T}}_n + \beta\dot{\mathbf{T}}_{n+1}\right\} \tag{12.4-6}$$

Like Newmark's method for the equations of structural dynamics, Eq. 12.4-6 contains a factor β that the analyst may choose. If the choice is $\beta = 0.5$, Eq. 12.4-6 is called the trapezoidal rule. We write Eq. 12.4-1 at time step n and again at time step $n + 1$, then multiply the first equation by $1 - \beta$ and the second by β. Thus

$$\begin{aligned} (1-\beta)\Big([\mathbf{C}]\{\dot{\mathbf{T}}\}_n + [\mathbf{K}_T]\{\mathbf{T}\}_n\Big) &= (1-\beta)\{\mathbf{R}_T\}_n \\ \beta\Big([\mathbf{C}]\{\dot{\mathbf{T}}\}_{n+1} + [\mathbf{K}_T]\{\mathbf{T}\}_{n+1}\Big) &= \beta\{\mathbf{R}_T\}_{n+1} \end{aligned} \tag{12.4-7}$$

If $[\mathbf{K}_T]$ and $[\mathbf{C}]$ do not change with time, we can add these two equations, then use Eq. 12.4-6 to eliminate time derivatives of temperature. The result is

$$\left(\frac{1}{\Delta t}[\mathbf{C}] + \beta[\mathbf{K}_T]\right)\{\mathbf{T}\}_{n+1} = \left(\frac{1}{\Delta t}[\mathbf{C}] - (1-\beta)[\mathbf{K}_T]\right)\{\mathbf{T}\}_n + (1-\beta)\{\mathbf{R}_T\}_n + \beta\{\mathbf{R}_T\}_{n+1} \tag{12.4-8}$$

Starting with a known $\{\mathbf{T}\}_0$ at $t = 0$, Eq. 12.4-8 provides $\{\mathbf{T}\}_1$ at $t = \Delta t$, then $\{\mathbf{T}\}_2$ at $t = 2\,\Delta t$, and so on. If Δt is not changed, the matrix that multiplies $\{\mathbf{T}\}_{n+1}$ need be generated and processed for equation-solving only once; the equation set is then repeatedly solved for a sequence of right-hand sides.

If $\beta < 0.5$ the algorithm is conditionally stable. The maximum time step for which it is numerically stable is [12.7]

$$\Delta t_{\text{cr}} = \frac{2}{(1-2\beta)\lambda_{\max}} \tag{12.4-9}$$

where λ_{max} is the largest eigenvalue of Eq. 12.4-2. If $\beta \geq 0.5$ the algorithm is unconditionally stable in linear problems; that is, numerical stability (but not accuracy!) is guaranteed as Δt becomes indefinitely large. Names associated with various values of β are

$\beta = 0$	Forward difference or Euler	(conditionally stable)
$\beta = \frac{1}{2}$	Crank-Nicolson or trapezoidal rule	(unconditionally stable)
$\beta = \frac{2}{3}$	Galerkin	(unconditionally stable)
$\beta = 1$	Backward difference	(unconditionally stable)

If $\beta = 0$ and $[\mathbf{C}]$ is diagonal, computational effort per time step is small, but so is Δt_{cr}. Among unconditionally stable methods, the Crank-Nicolson method is widely used. It is also second-order accurate. For $\beta \neq \frac{1}{2}$, only first-order accuracy can be guaranteed. Unconditional stability in a *nonlinear* problem requires $\beta = 1$ in Eq. 12.4-8 [12.7].

An incremental algorithm suitable for nonlinear thermal problems can be obtained in the same way as Eq. 17.7-5, which pertains to structural mechanics. We assume that $[\mathbf{C}]$ is constant but that $[\mathbf{K}_T]$ may be a function of temperature. At time step n, rather than $[\mathbf{K}_T]_n\{\mathbf{T}\}_n$, we introduce flux $\{\mathbf{f}\}$ within elements, and T and h on element boundaries, and write

$$\left\{\mathbf{R}_T^{\text{int}}\right\}_n = \sum\left\{-\int [\mathbf{B}]^T\{\mathbf{f}\}_n\, dV + \int \lfloor \mathbf{N} \rfloor^T T_n h_n\, dS\right\} \tag{12.4-10}$$

which sums element contributions and is appropriate when $[\boldsymbol{\kappa}]$ and h may be temperature-dependent. At time step $n + 1$, Eq. 12.4-1 becomes

$$[\mathbf{C}]\{\dot{\mathbf{T}}\}_{n+1} + \left\{\mathbf{R}_T^{\text{int}}\right\}_{n+1} = \{\mathbf{R}_T\}_{n+1} \tag{12.4-11}$$

With $\{\Delta\mathbf{T}\} = \{\mathbf{T}\}_{n+1} - \{\mathbf{T}\}_n$, we define

$$\left\{\mathbf{R}_T^{\text{int}}\right\}_{n+1} = \left\{\mathbf{R}_T^{\text{int}}\right\}_n + [\mathbf{K}_T]_n\{\Delta\mathbf{T}\} \qquad \text{and} \qquad \{\dot{\mathbf{T}}\}_{n+1} + \{\dot{\mathbf{T}}\}_n = \frac{2}{\Delta t}\{\Delta\mathbf{T}\} \tag{12.4-12}$$

Combination of Eqs. 12.4-11 and 12.4-12 yields

$$\left(\frac{2}{\Delta t}[\mathbf{C}] + [\mathbf{K}_T]_n\right)\{\Delta\mathbf{T}\} = \{\mathbf{R}_T\}_{n+1} - \left\{\mathbf{R}_T^{\text{int}}\right\}_n + [\mathbf{C}]\{\dot{\mathbf{T}}\}_n \tag{12.4-13}$$

which agrees with Eq. 17.7-5 if $[\mathbf{M}] = [\mathbf{0}]$, $\gamma = 1/2$, and $\beta = 1/4$. Strong nonlinearity may require iteration with a time step, as described in the latter portion of Section 17.7.

Finally, again for linear problems, we note that the Crank-Nicolson method displays annoying oscillations in response to suddenly imposed temperature changes. An improved algorithm is based on combining Eq. 12.4-6 with the equation [12.8]

$$[\mathbf{C}]\{\dot{\mathbf{T}}\}_{n+1} + [\mathbf{K}_T]\{(1+\alpha)\mathbf{T}_{n+1} - \alpha\mathbf{T}_n\} = (1+\alpha)\{\mathbf{R}_T\}_{n+1} - \alpha\{\mathbf{R}_T\}_n \tag{12.4-14}$$

The scheme is a form of the α method developed for structural dynamics, Eq. 11.13-6. Second-order accuracy is achieved if $\alpha + \beta = \frac{1}{2}$. Unconditional stability requires $\alpha \geq -\frac{1}{2}$ and $\beta \geq \frac{1}{2}$. The values $\alpha = -0.25$ and $\beta = 0.75$ are suggested [12.8].

12.5 MODELING CONSIDERATIONS. REMARKS

Element types, sizes, and shapes for a thermal FE model may be dictated less by thermal considerations than by subsequent stress analysis that is to be based on the same mesh and its associated nodal temperatures. Mesh requirements of stress analysis are usually more severe. A coarse mesh may adequately represent a temperature field having small gradients, yet associated thermal stresses may be large and display large gradients, especially near stress raisers such as holes and grooves, so that stress analysis typically requires a finer mesh. Accordingly, if thermal analysis and stress analysis are to use the same mesh, one should avoid three-node triangles and elements markedly elongated in a direction of little temperature change. The thermal mesh should be planned based on anticipated stresses.

A temperature field that is linear in rectangular Cartesian coordinates produces deformation but no stress in an unrestrained body that is isotropic or rectilinearly orthotropic. Thus a flat plate may become visibly curved when heated, yet be free of stress if temperature varies linearly from one lateral surface to the other. Temperature that varies linearly in the radial direction of cylindrical coordinates *does* produce stress. In a pipe of typical proportions, with fluids of different temperature inside and outside, temperature and stress have approximately linear variation through the wall thickness.

As with any FE analysis, computed results may be misleading if details are not treated with care. Dimensions, constants, and thermal loads must be stated in a consistent system of units. Orthotropic material properties must be assigned to correct directions of the model, using local axes if principal material axes do not coincide with global coordinate axes. Some loads or boundary conditions on bodies of revolution must be input for the entire circumference or on a per-radian basis, according to conventions of the software used. Absolute temperatures are needed if there is radiation heat transfer. Software may allow the user to state temperatures on a nonabsolute scale provided an "offset" temperature is also supplied so that temperature conversion can be accomplished internally by adding the offset to temperatures stated. Computed fluxes may be reported in a local coordinate system for some elements. Surface flux may be defined as positive inward or positive outward, depending on the software convention.

With all d.o.f. retained, a conductivity matrix [**K**] is singular. The analogous condition in structural mechanics is a stiffness matrix [**K**] that is singular because no d.o.f. have been prescribed as boundary conditions (that is, there are no supports). The necessary "support conditions" in thermal analysis can come from one or more prescribed nodal temperatures, from convection or radiation boundary conditions, or from some combination of these. In transient

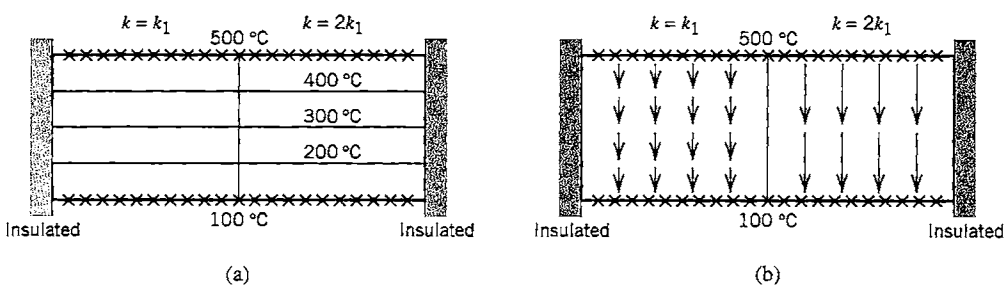

Figure 12.5-1. (a) Temperature contours and (b) heat flux in a two-dimensional bimaterial block with two isothermal boundaries and two insulated boundaries. Each material is isotropic.

thermal analysis a singular matrix $[\mathbf{K}_T]$ is acceptable, but *all* nodal temperatures must be prescribed as initial conditions. Typically, these temperatures are not all zero (in contrast to structural dynamics, where initial displacements and velocities are often all zero).

Only half (or less) of the structure need be modeled if there is symmetry of geometry, material properties, boundary conditions, and thermal loads with respect to one (or more) planes. Heat does not flow across a plane of symmetry, so nodes in a plane of symmetry become nodes on an insulated boundary of the portion of the structure that is modeled.

Boundary conditions are temperature-dependent if there is radiation or if convective heat transfer coefficients are temperature-dependent. Hence, in a transient problem, boundary conditions may be both temperature- and time-dependent. Sometimes boundary conditions are unclear [12.9]. Consider, for example, a rectangular plate, with two opposite edges at 0 °C and the other two opposite edges at 500 °C. Edges of different temperature meet at a corner. Should corner temperatures be left unassigned, or assigned as 0 °C, 250 °C, 500 °C, or something else? This problem is ill-posed and probably results from over-idealization of the physical situation. A similar uncertainty arises if temperature is prescribed along one edge and flux along an adjacent edge. At the node where two edges meet, which condition should be imposed? At a single node one can prescribe temperature or flux but not both.

As with structural FEA, a critique of computed results should begin by comparing computed results with a *previously obtained* approximation. Computed temperatures and fluxes at boundaries should be checked to verify that there are no disagreements with boundary conditions intended. Temperature contours (isotherms) should be parallel to a boundary of constant temperature, and normal to an insulated surface. Heat flux f can be plotted as a vector field, with each arrow pointing in the direction of local flux and having length proportional to the magnitude of flux. Computed flux should be parallel to insulated boundaries. These remarks are illustrated by Fig. 12.5-1. (Note that although the horizontal centerline is a line of geometric symmetry, the thermal problem is not symmetric with respect to this line because prescribed temperatures on horizontal boundaries are unequal.) Significant disagreement between results obtained and results expected suggests an error in understanding or an error in modeling. Stress analysis by FE and thermal analysis by FE are sufficiently similar that most remarks in Chapter 10 remain applicable in the present context. As with any problem area, thermal FEA is not likely to be successful if performed by someone unfamiliar with thermal analysis.

Temperature computed by thermal FEA is interelement-continuous, but flux may not be (unless spatial derivatives of temperature are included as nodal d.o.f.). In this way temperature is analogous to displacement and flux is analogous to stress, and concepts in Chapter 9 regarding discretization error in stress analysis can be applied to thermal analysis. Accordingly, flux contours should be plotted element-by-element, that is, *without nodal averaging*. Significant interelement discontinuities warn of a need for mesh refinement. The difference between the element-by-element flux field and the flux field produced by a smoothing scheme can be regarded as an error measure and used to drive adaptive meshing, in the manner described in Section 9.11. Each element should span roughly the same number of flux contours.

Note that a temperature field defined by nodal temperatures cannot display a step change across an interelement boundary with nodes shared by elements on either side of the boundary. Stress analysis that simulates a shrink fit by a prescribed temperature change must either use element temperatures or use separate nodes on a boundary between temperature zones.

Related Problems. Several physical phenomena are described by the same form of differential equation that describes conduction heat transfer. For simplicity of explanation, we specialize conditions to time-independence, isotropic material, and constant material properties. Let the dependent variable be $\phi = \phi(x,y,z)$. Consider the governing differential equation

$$k\nabla^2\phi + Q = 0 \tag{12.5-1}$$

which is the same as Eq. 12.1-8 for two dimensions, $\phi = T$, and $\dot{T} = 0$. Some additional phenomena described by Eq. 12.5-1 are as follows.

Groundwater flow (ϕ = hydraulic head)
Pressurized membrane (ϕ = lateral deflection)
Elastic torsion (ϕ = warping function or Prandtl stress function)
Electrostatics (ϕ = scalar potential)
Magnetostatics (ϕ = vector potential)
Potential flow (ϕ = velocity potential or stream function)

For the first three phenomena cited, k represents hydrodynamic conductivity, surface tension, and unity (for the warping function); Q is zero for simple ground water flow, represents lateral pressure on a membrane, and is zero for the torsional warping function. In electrostatics, scalar potential ϕ represents voltage, Q represents charge density, and k represents the dielectric property of the medium. In magnetostatics, ϕ represents magnetic vector potential, Q represents current density, and k represents the medium's response to a magnetic field.

With appropriate definition of quantities involved, a problem described by Eq. 12.5-1 can be addressed by software intended for thermal analysis. Obviously, great care must be exercised, as there may be subtle but important differences in how the equations are used in different disciplines. Software documentation is not likely to provide much guidance.

12.6 AN APPLICATION

Sections of a pipe are connected by a flanged joint (Fig. 12.6-1). Each flange has been slipped onto its section of pipe and attached to it by two circumferential welds. Bolts draw the flanges together and compress a gasket between them. Fluid in the pipe has temperature 0 °C. Vapor that condenses on the outside of the pipe has temperature 100 °C. Convection

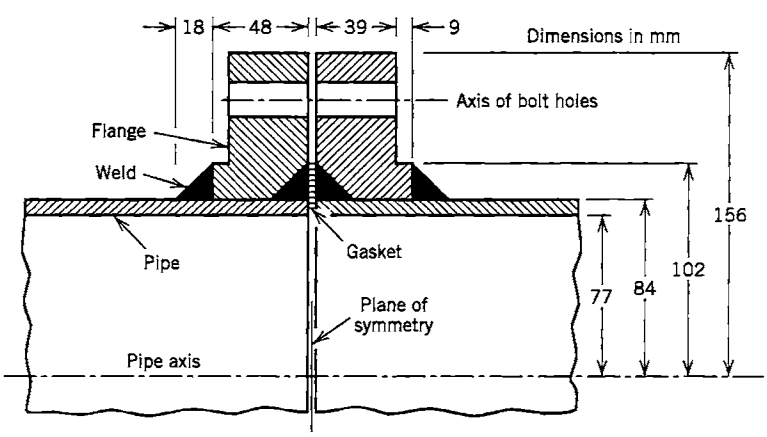

Figure 12.6-1. A flanged joint in a pipe, shown in cross section. Flanges are welded to the pipe. Welds are shown black in the figure.

heat transfer coefficients h are 5000 W/m^2 • °C inside the pipe and 20,000 W/m^2 • °C outside. Radiation heat transfer is neglected. Material of the pipe and flange has thermal conductivity k = 20 W/m • °C. Axisymmetric conditions are assumed to prevail. The steady-state temperature field distribution is required, for use in subsequent stress analysis.

Preliminary Analysis. We anticipate computed results as follows. Surfaces must be warmer than 0 °C inside and cooler than 100 °C outside. In Fig. 12.6-2, locations where these limits would be most closely approached should be near B and near D respectively. Heat flux should be largest where the pipe wall is thin, near HA in Fig. 12.6-2. The upper limit of flux through the pipe wall is easy to approximate by regarding the wall as plane and using the Fourier equation $f_r = -k(\partial T/\partial r)$ in radial direction r with the limiting surface temperatures:

$$f_{r\,\text{lim}} = -k\frac{\Delta T}{\Delta r} = -20\frac{100-0}{0.084-0.077} = -286{,}000\,\text{W/m}^2 \tag{12.6-1}$$

where the negative sign indicates that heat flows inward. In the flange the temperature gradient should be smaller, and temperature should increase with increasing radial and axial distance from B. Therefore flux should be directed mainly inward but should also have a component directed toward BC.

On the cylindrical surface between welds, IJ in Fig. 12.6-2a, pipe and flange touch only at isolated points, if at all, so heat conduction across this surface is very low as compared with conduction in continuous metal. We will assume that no heat is transferred across IJ, and will therefore model IJ as an insulator. This is a pessimistic assumption for subsequent stress analysis because it increases nearby temperature gradients, and large temperature gradients are often associated with large stresses.

Finite Element Analysis. The FE model is a solid of revolution, shown in cross section in Fig. 12.6-2b. The mesh shown was generated automatically by the software, based on data that locate the lettered boundary lines and state the desired element size near lettered points. Element sizes are made smaller where larger temperature gradients are expected. The mesh shown is rather coarse, especially if it is also to be used for subsequent stress analysis, as we shall discover. Elements are either six-node triangles or eight-node quadrilaterals. Each

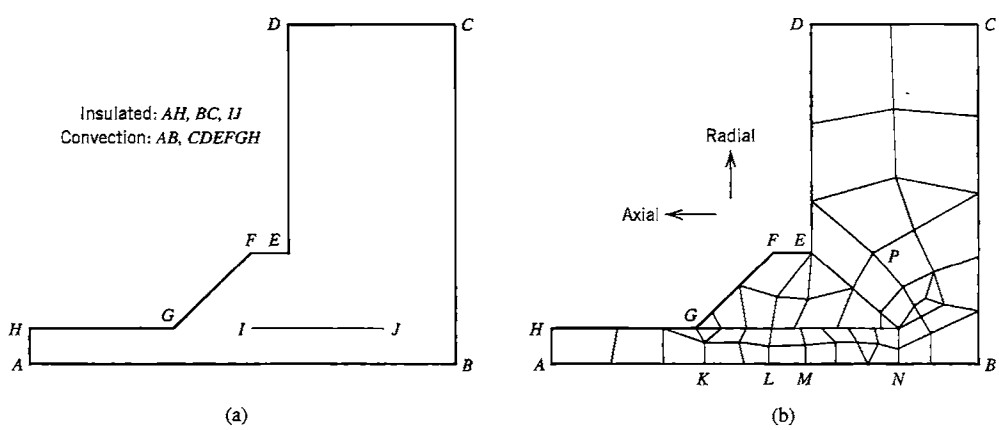

Figure 12.6-2. (a) Identification of conditions on surfaces in the left half of the structure. IJ is the unwelded pipe-flange interface. (b) FE mesh.

element is a solid of revolution rather than a plane figure (see Chapter 14 for details). The apparent discontinuity along *IJ* is intentional; sets of nodes on either side of *IJ* are left unconnected to model an interface that transfers no heat. For simplicity, bolts and bolt holes are replaced by continuous material. Temperature gradients are expected to be low at bolt locations. Fluid in the gap between adjacent flanges is also ignored because convection there is expected to be very low. Thus *BC* is regarded as a symmetry plane of the structure, across which no heat flows. Temperature is not prescribed at any node. Convection boundary conditions are prescribed along *AB* (inside) and along *CDEFGH* (outside).

Critique of Results. Computed temperature contours are shown in Fig. 12.6-3. Although six- and eight-node elements incorporate quadratic temperature fields, the software used plots temperature contours as straight line segnents. The lowest temperature is 3.59 °C along the right half of inside boundary *AB*. The highest temperature is 99.99 °C along the outer surface *CDEFG*. Temperature contours are interelement-continuous except along *IJ*, where the material is discontinuous. In the left portion of the model, temperature contours are parallel to the pipe axis, which suggests that if boundary *AH* were moved closer to *G*, computed temperatures would change very little. All these results agree with expectations. However, there are abrupt changes in contour directions near *I* and *J*, and contours are not quite normal to symmetry plane *BC*, so reanalysis with a finer mesh is indicated.

A vector plot of computed flux appears in Fig. 12.6-4a. Flux arrows are perpendicular to temperature contours because the material is isotropic. Arrows point in the direction of heat flow and arrow lengths are proportional to flux magnitude. Each arrow emanates from the center of an element. In the outer portion of the flange, flux is so small that arrows appear as dots. Computed radial flux near *AH* is 170,000 W/m^2, which, as expected, is less than the limiting magnitude of 286,000 W/m^2 (Eq. 12.6-1). Flux directions agree with expectations. Flux contours near *I*, Fig. 12.6-4b, show strong interelement discontinuities, again suggesting a need for mesh refinement, at least locally (some of the plotted contours coincide with interelement boundaries). Similar discontinuity appears near *J* and to a lesser extent near *G*. A relative error calculation, described in Section 9.10, provides $\eta = 0.03$ when it is based on all elements of the mesh. This value is a global error measure and does not indicate the accuracy of local results.

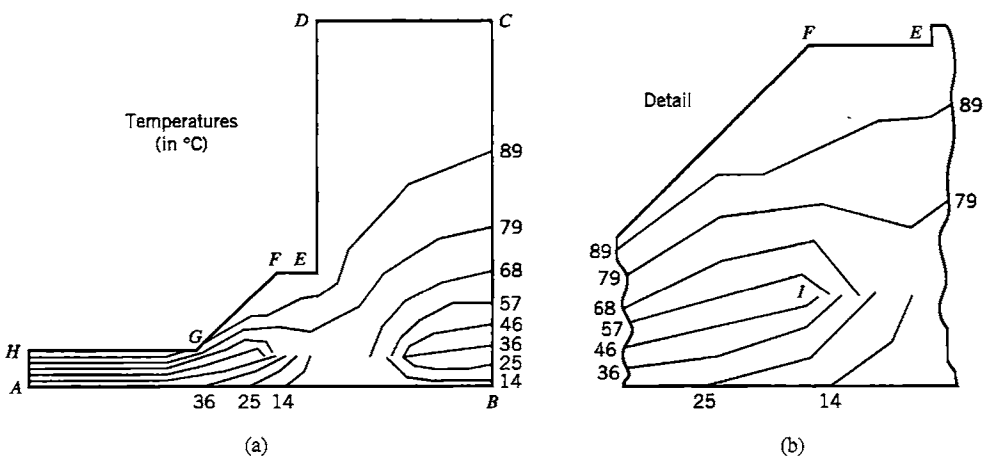

Figure 12.6-3. Computed temperature contours. (a) Contours in the entire FE model. (b) Detail of contours near point *I*.

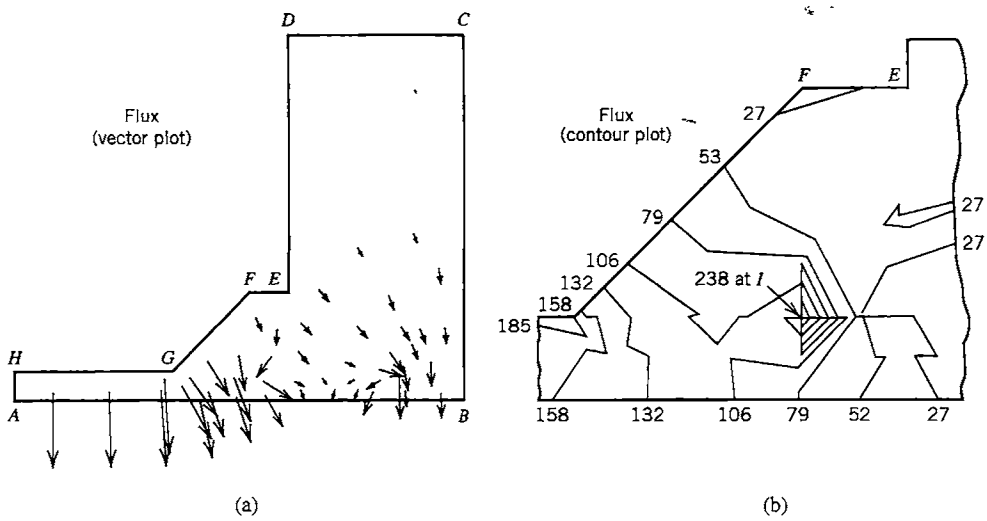

Figure 12.6-4. (a) Vector plot of the computed flux field. (b) Detail of computed flux contours near point I. Flux units are thousands of watts per square meter (10^3 W/m^2).

In summary, thermal results appear adequate except that refinement is needed near G, I, and J. Precisely *at* these locations there can never be enough refinement because flux is theoretically infinite at a sharp reentrant corner. We will ignore these shortcomings and proceed, in order to show how the same mesh behaves when used for stress analysis.

Subsequent Stress Analysis. We now use computed temperatures to calculate thermal stresses, assuming (incorrectly, as we will see) that the FE mesh of Fig. 12.6-2b is adequate for stress analysis. Load from bolt tensions could also be applied, as described in Section 10.7, but we will not do so here. There are two significant concerns about boundary conditions. First, should nodes along IJ be allowed to move independently? If opposite sides of the interface tend to separate, the answer is yes, but if sides tend to overlap, nodes along IJ should be allowed relative axial motion but not relative radial motion. Second, should all nodes along BC be fixed against axial motion? Allowing movement gives no credit to resistance provided by the gasket and bolts, while full fixity gives too much credit. We elect to calculate stresses twice, first allowing axial motion along BC and second preventing it. Thus, were it not for discretization error, we would expect to bracket the correct results. Material data is taken as $E = 200$ GPa, $\nu = 0.3$, and $\alpha = 12(10^{-6})/°\text{C}$.

Before performing FEA we make the following predictions, which apply to both sets of boundary conditions. The cooler inside surface should contract relative to the warmer surrounding material, pulling material toward the inside and opening a gap along IJ. As seen in Fig. 12.6-3a, material between IJ and inner surface AB has relatively massive surroundings, which implies that its contraction is considerably restrained, both radially and axially. Material *fully* restrained, uniaxially stressed, and cooled 100 °C relative to its supports would have the tensile stress $\sigma = \alpha E \Delta T = 12(10^{-6}) \times 200(10^9) \times 100 = 240$ MPa. We expect that material between IJ and the inside surface may display stresses that approach this value. Similarly, temperatures at A and H are about 30 °C and 90 °C respectively, that is, each is 30 °C different from the average temperature of 60 °C at the pipe midsurface. Therefore we expect circumferential and axial stresses to be about $\sigma = \alpha E \Delta T = 12(10^{-6}) \times 200(10^9) \times 30 = 72$ MPa, tensile inside and compressive outside.

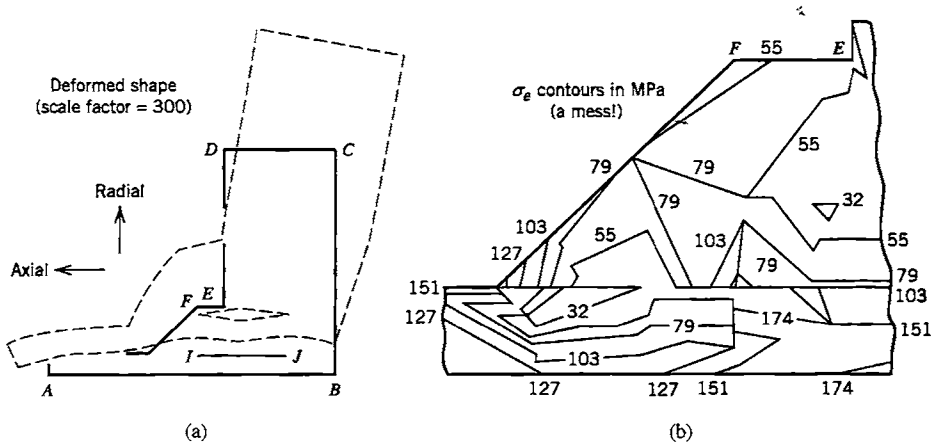

Figure 12.6-5. (a) Displaced shape with axial displacement prevented only at point B. The magnification factor is 300. (b) Detail of computed contours of von Mises stress σ_e near point I. (The mesh is *much* too coarse.)

In the first analysis, axial motion is prevented only at B, in order to suppress rigid-body axial translation. Computed deformation, exaggerated for plotting, is shown dashed in Fig. 12.6-5a, superposed on the undeformed geometry. The software used assumes that the undeformed shape prevails at the reference temperature, which has been chosen as 0 °C in this application. Point C is found to move less than 0.1 mm to the right, which is probably not enough to meet its neighboring point on the other flange and create a gap-closure problem. In the first analysis (and in the second, in which axial motion is prevented all along BC), a gap opens along IJ, as expected, which confirms the assumption made in thermal analysis that there is no conduction across IJ. The left portion of the deformed FE model, near AH, is not parallel to the pipe axis, which indicates that this portion is too short for accurate stress analysis. Circumferential and axial stresses at A and H are found to be approximately ±72 MPa, as predicted. Other computed stresses appear in Table 12.6-1, and again have approximately the values predicted. Unfortunately, stress contours have gross interelement discontinuities (Fig. 12.6-5b). Similar results (not plotted) are produced by the second analysis, in which there is axial fixity of all nodes along BC. In each analysis, the computed stress field has a relative energy error of $\eta = 0.28$, far larger than the $\eta = 0.03$ obtained in thermal analysis. Clearly, considerable mesh refinement is needed. Generalizing, we conclude that a mesh adequate for thermal analysis may be quite inadequate for stress analysis.

TABLE 12.6-1. MAXIMUM AND MINIMUM STRESSES (IN MPa) FOR DIFFERENT CASES OF AXIAL RESTRAINT ALONG BC. STRESSES ARE σ_r (RADIAL), σ_θ (CIRCUMFERENTIAL), σ_z (AXIAL), AND σ_e (VON MISES). LOCATIONS ARE IDENTIFIED BY LETTER IN FIG. 12.6-2. STRESSES COME FROM A COARSE MESH (FIG. 12.6-2B).

	Only node B axially restrained				All nodes on BC axially restrained			
	σ_r	σ_θ	σ_z	σ_e	σ_r	σ_θ	σ_z	σ_e
Maximum stress	113	216	244	222	105	229	257	242
Location of max.	*I,J*	*L-N*	*I,J*	*J*	*I,J*	*M-B*	*I,J,K*	*G,J*
Minimum stress	−68	−142	−199	8	−107	−225	−279	18
Location of min.	*G*	*G*	*G*	*P*	*G*	*G*	*G*	*C*

12.7 ACOUSTIC FREQUENCIES AND MODES

We consider a compressible fluid having no viscosity and no net flow, and whose density is uniform except for the small changes associated with sound waves. This idealization is satisfactory for calculation of acoustic vibrations in cavities. Areas of application include architectural enclosures and vehicle passenger compartments.

Wave Equation. Small motions of the fluid are associated with small pressure variations p relative to hydrostatic pressure. Pressure gradients in coordinate directions x, y, and z are related to accelerations $\ddot{u}$, $\ddot{v}$, and $\ddot{w}$ in these directions, as shown for the x direction in Fig. 12.7-1. Collected results for all three coordinate directions are

$$p_{,x} = -\rho\ddot{u} \qquad p_{,y} = -\rho\ddot{v} \qquad p_{,z} = -\rho\ddot{w} \tag{12.7-1}$$

where ρ is the fluid mass density. We differentiate each of Eqs. 12.7-1 with respect to its own spatial coordinate, and add results. Thus

$$p_{,xx} + p_{,yy} + p_{,zz} = -\rho(\ddot{u}_{,x} + \ddot{v}_{,y} + \ddot{w}_{,z}) \quad \text{or} \quad \nabla^2 p = -\rho\frac{d^2}{dt^2}(\varepsilon_x + \varepsilon_y + \varepsilon_z) \tag{12.7-2}$$

where $\varepsilon_x = u_{,x}$, and so on. Bulk modulus B is defined as the ratio of pressure to the fractional volume change it produces:

$$B = -\frac{p}{dV/V} = -\frac{p}{\varepsilon_x + \varepsilon_y + \varepsilon_z} \tag{12.7-3}$$

The negative sign appears because positive pressure is associated with a decrease in volume. Equations 12.7-2 and 12.7-3 yield the nondissipative wave equation

$$\nabla^2 p = \frac{\rho}{B}\ddot{p} \qquad \text{or} \qquad \nabla^2 p = \frac{1}{c^2}\ddot{p} \tag{12.7-4}$$

where c is the speed of sound in the medium, $c = \sqrt{B/\rho}$.

Equation 12.7-4 is to be solved in a volume V, subject to boundary conditions on its surface S. The essential boundary condition is $p = 0$, which prevails on the free surface of a liquid surface with negligible surface waves. The nonessential boundary condition, which prevails on the solid boundary of a cavity, is

$$\frac{\partial p}{\partial n} = -\rho\ddot{u}_n \tag{12.7-5}$$

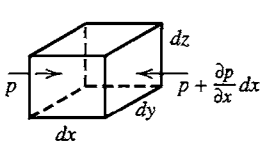

$$F_x = ma_x$$
$$p\,dy\,dz - \left(p + \frac{\partial p}{\partial x}dx\right)dy\,dz = (\rho\,dx\,dy\,dz)\ddot{u}$$
$$\frac{\partial p}{\partial x} = -\rho\ddot{u}$$

Figure 12.7-1. The x component of acceleration of a differential element of mass density ρ.

where n is the outward normal direction and $\ddot{u}_n$ is the acceleration of the boundary in direction n. For a rigid boundary, $\ddot{u}_n = 0$, so $\partial p/\partial n = 0$. Both of these boundary conditions, $p = 0$ and $\partial p/\partial n = 0$, reflect waves without absorbing energy.

A functional for a problem having uniform mass density is

$$\Pi = \int\left(\frac{p_{,x}^2 + p_{,y}^2 + p_{,z}^2}{2} + \frac{1}{c^2}p\ddot{p}\right) dV + \rho\int \ddot{u}_n p \, dS \tag{12.7-6}$$

As in Eq. 12.7-4, $1/c^2$ may be replaced by ρ/B. The stationary condition $\delta\Pi = 0$ yields the governing differential equation and natural boundary condition, Eqs. 12.7-4 and 12.7-5 (see Section 4.7).

An FE formulation follows the familiar pattern. Pressure p within an element is interpolated from the vector of element d.o.f., $\{\mathbf{P}_e\}$, which contains nodal pressures, and optionally spatial derivatives of nodal pressures as well. Thus

$$p = \lfloor \mathbf{N}_F \rfloor \{\mathbf{P}_e\} \quad \text{and} \quad \ddot{p} = \lfloor \mathbf{N}_F \rfloor \{\ddot{\mathbf{P}}_e\} \tag{12.7-7}$$

We define the following global matrices, where summation signs indicate assembly of element matrices.

$$\begin{aligned} [\mathbf{K}_F] &= \sum\int\left(\lfloor \mathbf{N}_{F,x}\rfloor^T\lfloor \mathbf{N}_{F,x}\rfloor + \lfloor \mathbf{N}_{F,y}\rfloor^T\lfloor \mathbf{N}_{F,y}\rfloor + \lfloor \mathbf{N}_{F,z}\rfloor^T\lfloor \mathbf{N}_{F,z}\rfloor\right) dV \\ [\mathbf{M}_F] &= \frac{1}{c^2}\sum\int\lfloor \mathbf{N}_F\rfloor^T\lfloor \mathbf{N}_F\rfloor \, dV \qquad \{\mathbf{R}_F\} = \rho\sum\int\lfloor \mathbf{N}_F\rfloor^T\ddot{u}_n \, dS \end{aligned} \tag{12.7-8}$$

In the latter integral, $\lfloor \mathbf{N} \rfloor$ is evaluated on the surface that experiences acceleration. After FE discretization, Eq. 12.7-6 is

$$\Pi = \{\mathbf{P}\}^T[\mathbf{M}_F]\{\ddot{\mathbf{P}}\} + \frac{1}{2}\{\mathbf{P}\}^T[\mathbf{K}_F]\{\mathbf{P}\} + \{\mathbf{P}\}^T\{\mathbf{R}_F\} \tag{12.7-9}$$

where $\{\mathbf{P}\}$ is the global array of nodal pressure d.o.f. The stationary condition $\{\partial\Pi/\partial\mathbf{P}\} = \{\mathbf{0}\}$ yields the finite element formulation

$$[\mathbf{M}_F]\{\ddot{\mathbf{P}}\} + [\mathbf{K}_F]\{\mathbf{P}\} = -\{\mathbf{R}_F\} \tag{12.7-10}$$

Acoustic Modes. Let walls of a cavity be rigid and stationary, so that $\ddot{u}_n = 0$. Thus the forcing function becomes zero, and the medium vibrates in one of its natural modes. Pressure becomes $p = \bar{p}\sin\omega t$, where ω is the circular frequency of a mode and its amplitude $\bar{p}$ is a function of spatial coordinates but is independent of time. Equation 12.7-4 becomes

$$\nabla^2\bar{p} + \omega^2\frac{\rho}{B}\bar{p} = 0 \qquad \text{or} \qquad \nabla^2\bar{p} + \omega^2\frac{1}{c^2}\bar{p} = 0 \tag{12.7-11}$$

Equation 12.7-11 is known as the *Helmholtz equation*. To obtain the corresponding FE formulation we substitute $\{\mathbf{R}_F\} = \{\mathbf{0}\}$ and $\{\mathbf{P}\} = \{\bar{\mathbf{P}}\}\sin\omega t$ in Eq. 12.7-10, and obtain

$$\left([\mathbf{K}_F] - \omega^2[\mathbf{M}_F]\right)\{\bar{\mathbf{P}}\} = \{\mathbf{0}\} \tag{12.7-12}$$

Solution of this eigenvalue problem yields natural frequencies ω_i and corresponding pressure modes $\{\bar{\mathbf{P}}\}_i$. If the cavity has no openings, the boundary condition $p = 0$ is not imposed at any node, so $[\mathbf{K}_F]$ is singular because all d.o.f. in $\{\bar{\mathbf{P}}\}$ are retained. Then the lowest mode produced by Eq. 12.7-12 is the trivial solution $\omega = 0$, for which all nodal pressures are equal. In subsequent modes, which are physically meaningful, nodal pressures represent departures from a mean pressure.

One-Dimensional Case. A piping system may have curves and branches. The foregoing formulation can be applied with one-dimensional elements if transverse dimensions of the pipe are small in comparison with the wavelength [12.10]. Let x be the lengthwise coordinate and A the cross-sectional area, where $A = A(x)$. If derivatives with respect to y and z are discarded from Eqs. 12.7-8 we obtain, for a single element,

$$[\mathbf{k}_F] = \int \lfloor \mathbf{N}_{F,x} \rfloor^T \lfloor \mathbf{N}_{F,x} \rfloor A\, dx \qquad [\mathbf{m}_F] = \frac{1}{c^2} \int \lfloor \mathbf{N}_F \rfloor^T \lfloor \mathbf{N}_F \rfloor A\, dx \tag{12.7-13}$$

Possible elements include two-node and three-node elements (Fig. 12.7-2a,b), whose shape functions appear in Eqs. 3.3-9 and 6.1-4, respectively. Element matrices for the case $A = A(x)$ appear in [12.10]. For a three-node element of constant cross-sectional area, with the internal node a distance $L/2$ from either end,

$$[\mathbf{k}_F] = \frac{A}{3L} \begin{bmatrix} 7 & -8 & 1 \\ -8 & 16 & -8 \\ 1 & -8 & 7 \end{bmatrix} \qquad [\mathbf{m}_F] = \frac{AL}{30c^2} \begin{bmatrix} 4 & 2 & -1 \\ 2 & 16 & 2 \\ -1 & 2 & 4 \end{bmatrix} \tag{12.7-14}$$

Figure 12.7-2c shows a two-element model of a pipe of uniform cross section. At a closed end, pressure amplitude is unknown. If both ends are closed in Fig. 12.7-2c the FE model corresponding to Eq. 12.7-12 has five d.o.f. and five eigenvalues, including the trivial solution $\omega = 0$, which corresponds to the same pressure amplitude at all nodes. At an open end, $p = 0$. If both ends are open in Fig. 12.7-2c, the FE model has three d.o.f., and the lowest mode (for which $p_2 = p_4$) is $\omega_1 = 1.5767c/L$. The mathematically exact result is $\omega_1 = 1.5708c/L$. Results from this FE model are upper bounds because elements are compatible and the consistent form of matrix $[\mathbf{m}_F]$ is used.

Boundary Absorption. In applications, walls of a cavity may be lined with sound-absorbing material that reduces the sound level produced by forced vibration. In an *unbounded* medium, waves generated by a vibrating structure radiate outward and do not return. A practical FE model of an unbounded medium must have an absorbing boundary at finite distance from the disturbance. A simple way of modeling an absorbing boundary is as follows.

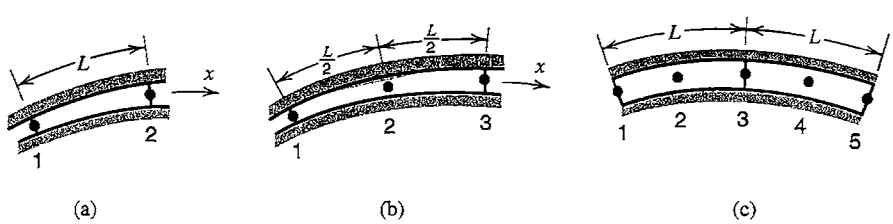

Figure 12.7-2. One-dimensional acoustic elements. (a) Two nodes. (b) Three nodes. (c) Two three-node elements.

The one-dimensional form of Eq. 12.7-4 is

$$\frac{\partial^2 p}{\partial n^2} = \frac{1}{c^2}\frac{\partial^2 p}{\partial t^2} \tag{12.7-15}$$

where n is the direction of propagation, which in the present discussion is normal to the boundary. The solution of this wave equation is

$$p = f_o(n - ct) + f_r(n + ct) \tag{12.7-16}$$

where functions f_o and f_r represent arbitrary disturbances, respectively traveling outward from and returning toward the source of disturbance. To eliminate the returning wave we set $f_r = 0$. Thus $p = f_o(\psi)$, where $\psi = n - ct$, so

$$\frac{\partial p}{\partial n} = \frac{\partial f_o}{\partial \psi} \quad \text{and} \quad \frac{\partial p}{\partial t} = -c\frac{\partial f_o}{\partial \psi} \quad \text{hence} \quad \frac{\partial p}{\partial n} = -\frac{1}{c}\frac{\partial p}{\partial t} \tag{12.7-17}$$

The latter equation is sometimes called the *Sommerfeld radiation condition*. Invoked as a boundary condition, it absorbs outgoing waves with no reflection. To incorporate the condition in FE formulation, in a way that permits a variable amount of absorption of waves normal to a boundary, we augment Π of Eq. 12.7-6 by a dissipation term. A numerical factor β that can be determined by experiment is arbitrarily included, such that $\beta = 0$ indicates no absorption. Thus Eq. 12.7-6 becomes

$$\Pi = \int\left(\frac{p_{,x}^2 + p_{,y}^2 + p_{,z}^2}{2} + \frac{1}{c^2}p\ddot{p}\right)dV + \rho\int \ddot{u}_n p\, dS + \frac{\beta}{c}\int p\dot{p}\, dS \tag{12.7-18}$$

The stationary condition $\delta\Pi = 0$ yields Eqs. 12.7-4, 12.7-5, and $\partial p/\partial n = -(\beta/c)\dot{p}$ on a dissipating surface S. To represent Eq. 12.7-18, Eq. 12.7-9 is augmented by the term $\{\mathbf{P}\}^T[\mathbf{C}_F]\{\dot{\mathbf{P}}\}$, where

$$[\mathbf{C}_F] = \frac{\beta}{c}\sum\int \lfloor \mathbf{N}_F \rfloor^T \lfloor \mathbf{N}_F \rfloor\, dS \tag{12.7-19}$$

in which the summation sign indicates assembly of elements and $\lfloor \mathbf{N}_F \rfloor$ is evaluated on the surface in question. Equation 12.7-10 becomes

$$[\mathbf{M}_F]\{\ddot{\mathbf{P}}\} + [\mathbf{C}_F]\{\dot{\mathbf{P}}\} + [\mathbf{K}_F]\{\mathbf{P}\} = -\{\mathbf{R}_F\} \tag{12.7-20}$$

The damping matrix can also be implemented by infinite elements (Section 8.8). Discussion and formulations of damping at a boundary appear in [12.11–12.15].

12.8 FLUID-STRUCTURE INTERACTION

In this section we formulate equations applicable to such problems as vibration of a floating structure and earthquake loading of a totally or partially immersed structure. In contrast to the sequential coupling found in thermal stress analysis, where (typically) temperature

influences stress but not vice versa, motions of structure and fluid are directly coupled and must be considered simultaneously. A byproduct of the following formulation is an expression for the added "hydrodynamic" mass that is in effect attached to the structure because the structure drags fluid with it as it moves. Equations developed in Section 12.7 are used; therefore the following development incorporates the assumptions and restrictions of Section 12.7.

Time-varying nodal loads on the fluid, $\{\mathbf{R}_F\}$ in Eq. 12.7-20, are regarded as produced by motion of the structure, which is in contact with some surfaces of the acoustic FE mesh, and imparts displacement u_n and acceleration $\ddot{u}_n$ to these surfaces. Let an element of the structure have nodal d.o.f. $\{\mathbf{d}\}$, and the usual displacement components u, v, and w in coordinate directions. Also let $\lfloor l \;\; m \;\; n \rfloor$ be the array of direction cosines of the normal to the element surface (in this array only, n does not indicate the outward normal to an acoustic surface). Hence

$$u_n = \lfloor l \;\; m \;\; n \rfloor \begin{Bmatrix} u \\ v \\ w \end{Bmatrix} = \underbrace{\lfloor l \;\; m \;\; n \rfloor [\mathbf{N}]}_{\lfloor \bar{\mathbf{N}} \rfloor} \{\mathbf{d}\} \tag{12.8-1}$$

where shape function matrix $[\mathbf{N}]$ is evaluated on the structure surface in contact with the fluid. Then, from Eqs. 12.7-8 and 12.8-1,

$$\{\mathbf{R}_F\} = \rho \sum \left\{ \underbrace{\int \lfloor \mathbf{N}_F \rfloor^T \lfloor \bar{\mathbf{N}} \rfloor \, dS}_{[\mathbf{s}]} \{\ddot{\mathbf{d}}\} \right\} = \rho \sum \Big([\mathbf{s}] \{\ddot{\mathbf{d}}\} \Big) = \rho [\mathbf{S}] \{\ddot{\mathbf{D}}\} \tag{12.8-2}$$

where the summation sign indicates assembly of elements. Equation 12.7-20 becomes

$$[\mathbf{M}_F]\{\ddot{\mathbf{P}}\} + [\mathbf{C}_F]\{\dot{\mathbf{P}}\} + [\mathbf{K}_F]\{\mathbf{P}\} = -\rho [\mathbf{S}] \{\ddot{\mathbf{D}}\} \tag{12.8-3}$$

Loads applied to the structure surface by fluid pressure p of Eq. 12.7-7 are

$$\{\mathbf{R}\} = \sum \int \lfloor \bar{\mathbf{N}} \rfloor^T p \, dS = \sum \underbrace{\int \lfloor \bar{\mathbf{N}} \rfloor^T \lfloor \mathbf{N}_F \rfloor \, dS}_{[\mathbf{s}]^T} \{\mathbf{P}_e\} = [\mathbf{S}]^T \{\mathbf{P}\} \tag{12.8-4}$$

The dynamic equation of the structure, Eq. 11.2-12, becomes

$$[\mathbf{M}]\{\ddot{\mathbf{D}}\} + [\mathbf{C}]\{\dot{\mathbf{D}}\} + [\mathbf{K}]\{\mathbf{D}\} = \{\mathbf{R}^{\text{ext}}\} + [\mathbf{S}]^T \{\mathbf{P}\} \tag{12.8-5}$$

The coupled problem, from Eqs. 12.8-3 and 12.8-5, is

$$\begin{bmatrix} \mathbf{M} & \mathbf{0} \\ \rho \mathbf{S} & \mathbf{M}_F \end{bmatrix} \begin{Bmatrix} \ddot{\mathbf{D}} \\ \ddot{\mathbf{P}} \end{Bmatrix} + \begin{bmatrix} \mathbf{C} & \mathbf{0} \\ \mathbf{0} & \mathbf{C}_F \end{bmatrix} \begin{Bmatrix} \dot{\mathbf{D}} \\ \dot{\mathbf{P}} \end{Bmatrix} + \begin{bmatrix} \mathbf{K} & -\mathbf{S}^T \\ \mathbf{0} & \mathbf{K}_F \end{bmatrix} \begin{Bmatrix} \mathbf{D} \\ \mathbf{P} \end{Bmatrix} = \begin{Bmatrix} \mathbf{R}^{\text{ext}} \\ \mathbf{0} \end{Bmatrix} \tag{12.8-6}$$

Surface Waves. Let there be small-amplitude waves, with elevation w_s relative to the mean surface level. Small waves are associated with pressure $p = \rho g w_s$, where g is the acceleration of gravity. Combining this pressure with $p_{,z} = -\rho \ddot{w}_s$ from Eq. 12.7-5, where z is the vertical coordinate, we obtain $p_{,z} = -\ddot{p}/g$ as the surface boundary condition when there are small-amplitude waves. To account for this term, the surface integral $\int (p\ddot{p}/g)\, dS$ is added to Π of Eq. 12.7-18. The result of this addition is that the matrix that multiplies $\{\ddot{\mathbf{P}}\}$ in Eq. 12.7-20 contains another contribution; it becomes

$$[\mathbf{M}_F + \mathbf{W}_F] \qquad \text{where} \qquad [\mathbf{W}_F] = \frac{1}{g}\sum \int \lfloor \mathbf{N}_F \rfloor^T \lfloor \mathbf{N}_F \rfloor \, dS \tag{12.8-7}$$

Only element surfaces that coincide with the fluid surface make a contribution to $[\mathbf{W}_F]$.

Added Mass. A simple but approximate expression for the fluid mass that the structure mobilizes as it moves can be obtained by saying that the fluid is incompressible, has neither surface waves nor boundary damping, and does not separate from the structure (cavitate). Thus $[\mathbf{M}_F] = [\mathbf{W}_F] = [\mathbf{C}_F] = [\mathbf{0}]$. The lower partition of Eq. 12.8-6 becomes

$$\rho[\mathbf{S}]\{\ddot{\mathbf{D}}\} + [\mathbf{K}_F]\{\mathbf{P}\} = \{\mathbf{0}\} \qquad \text{hence} \qquad \{\mathbf{P}\} = -\rho[\mathbf{K}_F]^{-1}[\mathbf{S}]\{\ddot{\mathbf{D}}\} \tag{12.8-8}$$

Substitution of this $\{\mathbf{P}\}$ into the upper partition of Eq. 12.8-6 yields, if $[\mathbf{C}] = [\mathbf{0}]$,

$$\left([\mathbf{M}] + \underbrace{\rho[\mathbf{S}]^T[\mathbf{K}_F]^{-1}[\mathbf{S}]}_{\text{added mass}} \right)\{\ddot{\mathbf{D}}\} + [\mathbf{K}]\{\mathbf{D}\} = \{\mathbf{R}^{\text{ext}}\} \tag{12.8-9}$$

The entire coefficient matrix that multiplies $\{\ddot{\mathbf{D}}\}$ is sometimes called the "virtual mass." If there is simple harmonic motion, so that $\{\mathbf{D}\} = \{\bar{\mathbf{D}}\} \sin \omega t$, Eq. 12.8-9 yields an eigenvalue problem analogous to Eq. 12.7-12.

The condition $p = 0$ is imposed on a fluid surface without waves. Thus matrix $[\mathbf{K}_F]$ is rendered nonsingular and the inverse of $[\mathbf{K}_F]$ exists. Matrix $[\mathbf{S}]$ is sparse, so implementation will probably exploit sparse matrix techniques and an equation-solving strategy rather than the formal inversion and subsequent triple product computation indicated in Eq. 12.8-9. If physical behavior depends more on properties of the structure than of the fluid, a relatively coarse mesh may be adopted for the fluid, so that a single fluid element may contact two or more structure elements [12.16].

Equation 12.8-9 may be used to analyze the vibration of a ship hull. However, it is known that surface effects make the added mass frequency-dependent, especially for motions whose frequency is close to the dominant frequency of surface waves, so that low-frequency vibration has a much larger added mass than higher frequencies [12.17]. Indeed if surface-wave matrix $[\mathbf{W}_F]$ of Eq. 12.8-7 is retained and both $\{\mathbf{D}\}$ and $\{\mathbf{P}\}$ are assumed to vary with time as $\sin \omega t$, the manipulations of Eqs. 12.8-8 and 12.8-9 produce an added mass expression that depends on ω. Frequency dependence is observed to decrease with increasing frequency, so Eq. 12.8-9 may be acceptable for analysis of hull vibration produced by a mechanical excitation, whose frequency is much higher than wave frequencies. As structural frequency increases, the amount of fluid set in motion decreases, until only a boundary layer adjacent to the structure is involved.

The assumption of incompressibility, used in obtaining Eq. 12.8-9, is not always acceptable. Analyses of dam-reservoir systems show that compressibility may greatly increase the fundamental vibration period when the fundamental frequency of water in the reservoir is less than the fundamental frequency of the dam with reservoir empty [12.18]. Also, pressure load on the dam displays a large increase when the period of dam vibration is comparable to the time taken by sound in the fluid to travel twice the height of the dam [12.19].

Nevertheless there are many applications where surface waves are unimportant and for which Eq. 12.8-9 may be satisfactory.

An Alternative Formulation. An obvious disadvantage of Eq. 12.8-6 is that matrices are not symmetric. Symmetric matrices are produced by a formulation that uses displacement d.o.f. rather than pressure d.o.f. for the fluid. It is summarized as follows.

A fluid element can be formulated using the same nodal d.o.f. and shape functions as are used for a structural element. A fluid element and its structural counterpart have the same mass matrix. In formulating the fluid element stiffness matrix, material property matrix [**E**] is replaced by bulk modulus B, so that fluid elements resist volume change but not shearing deformation. A mesh of these fluid elements may have several zero-frequency "circulation modes," especially if elements are underintegrated. To suppress them a penalty matrix can be added to each element matrix. Structure matrices that describe a coupled fluid-structure problem are symmetric, but for a given number of nodes are larger in size than matrices in Eq. 12.8-6; each fluid node has three d.o.f. in a 3D problem. References include [12.20–12.22].

The displacement-based fluid model has worked well for hydrostatics, for acoustic modes in rigid cavities, and for dynamics of a fluid in a flexible container. Unfortunately, it has not worked well at predicting vibration frequencies of an eleastic structure surrounded by fluid [12.22].

12.9 PLANE INCOMPRESSIBLE IRROTATIONAL FLOW

We briefly describe formulations for steady, irrotational flow of an incompressible fluid. Let u and v represent flow velocities in x and y directions, respectively. The conditions of irrotationality and continuity are stated by the equations

$$\text{Irrotationality:} \quad u_{,y} - v_{,x} = 0 \qquad \text{Continuity:} \quad u_{,x} + v_{,y} = 0 \tag{12.9-1}$$

If u and v were displacement components rather than flow velocities, rotation would be defined as $\omega = (v_{,x} - u_{,y})/2$ in the theory of elasticity. Thus the irrotationality condition would be stated as $d\omega/dt = 0$. The continuity condition is conceptually the same as the equation of heat flux, Eq. 12.1-6, with Q and $\dot{T}$ both zero.

For analysis, we can use either a potential function $\phi = \phi(x,y)$ or a stream function $\psi = \psi(x,y)$. Flow velocities are given by derivatives, as follows.

$$\text{Potential function:} \quad u = \phi_{,x} \quad \text{and} \quad v = \phi_{,y} \tag{12.9-2a}$$

$$\text{Stream function:} \quad u = \psi_{,y} \quad \text{and} \quad v = -\psi_{,x} \tag{12.9-2b}$$

(Some authors prefer to write $u = -\psi_{,y}$ and $v = \psi_{,x}$.) If orthogonal coordinates ns were to replace coordinates xy in Eqs. 12.9-2, $\phi_{,n}$ would represent flow velocity in the n direction and $\psi_{,n}$ would represent flow velocity in the negative s direction. Substitution of either Eq. 12.9-2a or 12.9-2b into Eq. 12.9-1 yields $0 \equiv 0$ for one equation and Laplace's equation for the other, so the problem is described by

$$\nabla^2\phi = 0 \quad \text{or by} \quad \nabla^2\psi = 0 \quad \text{where} \quad \nabla^2 = \frac{\partial^2}{\partial x^2} + \frac{\partial^2}{\partial y^2} \tag{12.9-3}$$

Thus the governing equation for incompressible irrotational flow has the same form as the thermal equation $\nabla^2 T = 0$, which describes steady-state heat flow in an isotropic medium without internal heat generation. A finite element occupies a fixed region of space through which fluid flows and uses nodal values of ϕ or ψ as d.o.f. Global equations of an FE formulation are

$$\left(\sum [\mathbf{k}]\right)\{\boldsymbol{\phi}\} = \sum \{\mathbf{r}\} \qquad \text{or} \qquad \left(\sum [\mathbf{k}]\right)\{\boldsymbol{\psi}\} = \sum \{\mathbf{r}\} \tag{12.9-4}$$

where summation signs indicate assembly of elements. The element characteristic matrix $[\mathbf{k}]$ given by the first of Eqs. 12.2-4, with $[\boldsymbol{\kappa}]$ a unit matrix. Load terms $\{\mathbf{r}\}$ come from $\{\mathbf{r}_B\}$ in Eq. 12.2-4, with f_B now representing inward flow rate normal to a boundary.

An example application is depicted in Fig. 12.9-1. Uniform x-direction flow at velocity u_0 enters at the left. Flow velocities in the neighborhood of the cylindrical obstacle are desired. Because of symmetry about horizontal and vertical centerlines, only one quadrant need be modeled. A coarse mesh of quadrilateral elements is shown. Known symmetries of the flow, when associated with Eqs. 12.9-2, dictate the boundary conditions shown. For

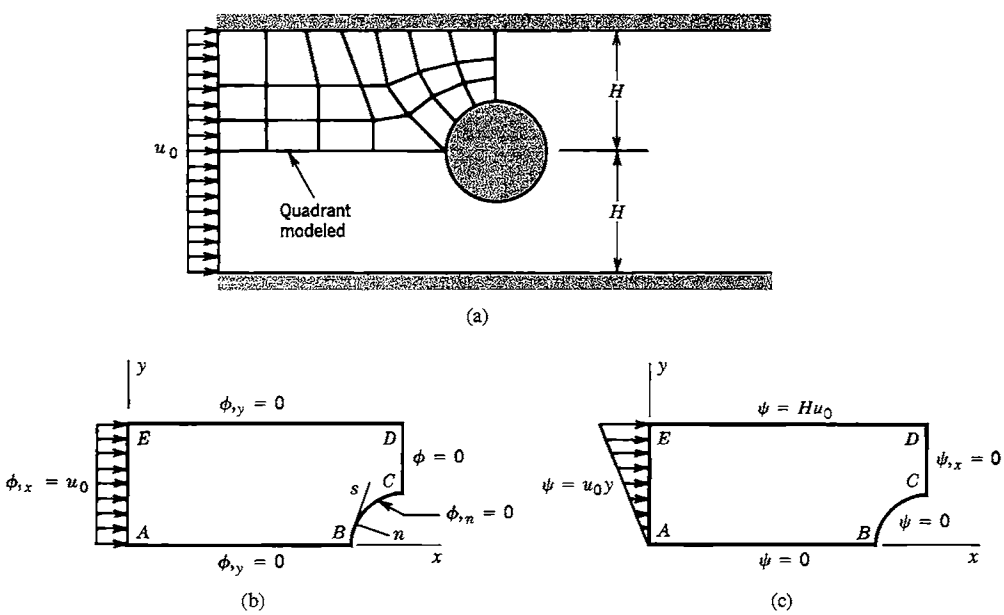

Figure 12.9-1. (a) Flow around a cylindrical obstacle. (b,c) Boundary conditions associated with use of ϕ and ψ in the quadrant modeled.

example, $v = 0$ along AB, CD, and DE; therefore $\phi_{,y} = 0$ along these boundaries. Velocity normal to the cylinder is zero; therefore $\phi_{,n} = 0$ along BC. To make the coefficient matrix nonsingular, ϕ must be prescribed at some node. The numerical value assigned is added to all other d.o.f. in the solution vector $\{\boldsymbol{\phi}\}$, but the numerical value is arbitrary because only derivatives of ϕ are of interest. If $\phi = 0$ is prescribed at C, the value $\phi = 0$ is dictated at all nodes along CD because of the condition $\phi_{,y} = 0$ along CD. These are the only d.o.f. prescribed. Loads $\{\mathbf{r}\}$ are prescribed along AE. Analogous remarks apply to use of ψ rather than ϕ. Then ψ is prescribed at all boundary nodes but those along CD, and $\{\mathbf{r}\} = \{\mathbf{0}\}$.

When all d.o.f. are known, gradients are calculated (see Eq. 12.2-2, with nodal temperatures replaced by nodal values of ϕ or ψ), and flow velocities are then known according to Eqs. 12.9-2.

ANALYTICAL PROBLEMS

12.1-1 Derive Eq. 12.1-10, using the kind of argument that produces Eq. 12.1-6.

12.1-2 Show that the plane flux transformation is as stated in the sentence that follows Eq. 12.1-3.

12.1-3 Devise an example that shows why θ must be a principal material direction if temperature T in a solid of revolution is to be symmetric with respect to the $\theta = 0$ plane.

12.1-4 Using conventional scalar notation (such as that in Eq. 12.1-9), write Eqs. 12.1-14 for the following special cases.
(a) Solid of revolution with axisymmetric temperature T and isotropic material.
(b) Plane problem in polar coordinates. Do not assume that the material is isotropic.

12.1-5 Derive the governing equation of Problem 12.1-4(b) from first principles; that is, by using the kind of argument that provides Eq. 12.1-7.

12.2-1 Use Eq. 4.7-6 to show that the volume integral in Eq. 12.2-1 provides Eq. 12.1-14(a) for a plane problem.

12.2-2 For a plane problem in xy coordinates, show that Eq. 12.2-1 yields the correct governing equation and natural boundary conditions from the variational statement $\delta\Pi = 0$.

12.2-3 For the one-dimensional problem of Eq. 12.1-10, use the Galerkin method to obtain formulas for FE matrices. Results should agree with Eqs. 12.2-4, specialized to the bar problem.

12.2-4 Assume that the three-node plane element shown is homogeneous, isotropic, and of unit thickness.
(a) Evaluate $[\mathbf{k}]$ in terms of conductivity k and nodal coordinates.
(b) Evaluate $[\mathbf{h}]$ in terms of heat transfer coefficient h and nodal coordinates, if only side 1-3 transfers heat by convection.
(c) Write the "lumped" forms of $[\mathbf{c}]$ and $[\mathbf{h}]$.
(d) Write an expression for $\{\mathbf{r}_Q\}$ if Q is constant over the element.

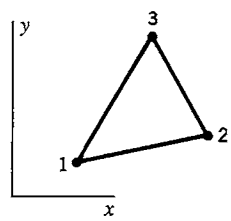

Problem 12.2-4

12.2-5 Repeat Problem 12.2-4, but regard the element as a solid of revolution, so that r replaces x and axis of revolution z replaces y.

12.2-6 The element shown in cross section is axisymmetric, homogeneous, isotropic, and of unit thickness in the z direction. Assume that lateral surfaces z = constant are insulated, that temperature in the element is a linear function of r, and that Q is uniform throughout the element. Evaluate matrices of Eqs. 12.2-4 in terms of element dimensions and physical constants.

12.2-7 Lateral surfaces of the uniform bar shown are insulated. The bar is modeled by two elements, each of cross-sectional area A and length L. Node 3 is maintained at temperature T_3. Constant heat flow $q_1 = Af_1$ is imposed at node 1. In terms of q_1, dimensions, and constants, what are T_1 and T_2 relative to T_3? Do these nodal temperatures provide the expected value of q at node 3? Make use of the conductivity matrix in the solution.

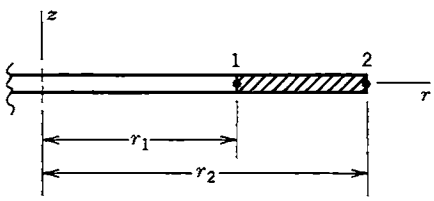

Problem 12.2-6

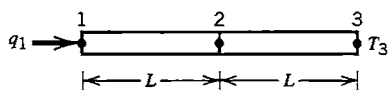

Problem 12.2-7

12.2-8 Repeat Problem 12.2-7, but use a stepped bar rather than a uniform bar. Let elements 1-2 and 2-3 have the respective cross-sectional areas A_o and $2A_o$.

12.2-9 Lateral surfaces of the uniform bar shown are insulated. The bar is modeled by three identical elements. Nodes 1 and 4 are maintained at the respective temperatures 0 °C and 300 °C. What are the temperatures at nodes 2 and 3? Make use of the conductivity matrix in the solution.

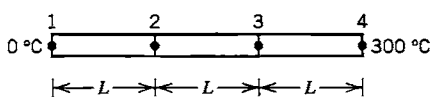

Problem 12.2-9

12.2-10 Repeat Problem 12.2-9, but use a stepped bar rather than a uniform bar. Let elements 1-2, 2-3, and 3-4 have the respective cross-sectional areas A_o, $2A_o$, and $3A_o$.

12.2-11 A uniform bar is modeled by two identical two-node elements, as shown. Node 1 is maintained at temperature T_1 = 0 °C. The bar is surrounded by fluid of temperature T_{fl} = 200 °C, which transfers heat across its cylindrical surface of area S. In units listed in Section 12.1, data are: $A = 300(10^{-6})$, $h = 600$, $k = 200$, and the surface area of the entire bar is $S = 0.020$.

(a) Formulate element matrices.

(b) Assemble element matrices, impose T_1 = 0 °C, and solve for T_2 and T_3.

(c) Repeat part (b), but alter the FE model so that the left element is half as long as the right element. The overall length remains 0.300 m.

(d) What conclusion might be drawn by comparing the results of parts (b) and (c)?

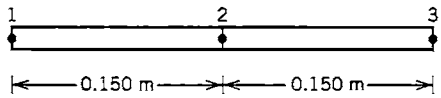

Problem 12.2-11

12.2-12 Imagine that nodal d.o.f. include first derivatives of temperature T as well as T itself, so that nodal d.o.f. in a plane problem are T, $T_{,x}$, and $T_{,y}$. Let the material be isotropic. For a straight boundary of the structure oriented normal to the x axis, state which of the three nodal d.o.f. are known (with the assistance of Eq. 12.1-4 if necessary), and which are unknown if the boundary is (a) insulated, (b) has prescribed temperature, (c) has prescribed normal heat flux, and (d) has convection heat transfer.

12.3-1 Over the temperature range 0 °C < T < 500 °C, the thermal conductivity of a certain metal in W/m • °C may be taken as $k = 73 - 0.06T$. Assume that lateral surfaces of the uniform bar shown are insulated and that ends are maintained at the respective temperatures 0 °C and 500 °C. Calculate nodal temperatures T_2 and T_3 and axial heat flux f. In calculation, let k be constant throughout an element and be determined based on the average of the element's two nodal temperatures. Carry out three iterations: assume that $T = T_0 = 0$ °C throughout to start, and use Eq. 12.3-6 to solve successively for nodal temperature vectors $\{\mathbf{T}_1\}$, $\{\mathbf{T}_2\}$, and $\{\mathbf{T}_3\}$.

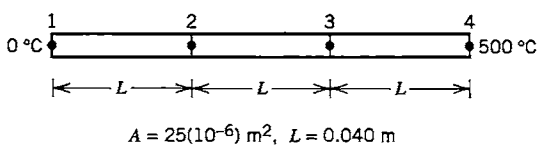

Problem 12.3-1

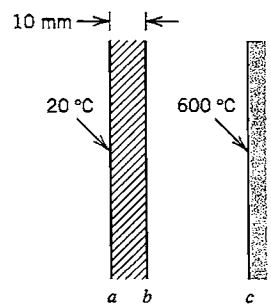

Problem 12.3-2

12.3-2 A flat plate ab of 10 mm thickness is shown in cross section. The plate is parallel to a flat wall c that radiates. Assume that k of the plate is 0.70 W/m • °C and that $\varepsilon_b = \varepsilon_c = 0.6$, all independent of temperature. If surfaces a and c are maintained at 20 °C and 600 °C respectively, what is the temperature of surface b? Solve iteratively by using Eq. 12.3-6 and h_{rad} of Eq. 12.3-4. Assume $T_b = 100$ °C to start the process.

12.4-1 Prove Eqs. 12.4-3.

12.4-2 Assume that the sketch shows the actual variation of temperature T with time at a certain node. Imagine that we start at point A and use Eq. 12.4-6 to predict T at time t_{n+1}. Consider $\beta = 0$, $\beta = 0.5$, and $\beta = 1.0$. Show on the sketch how the predicted temperature compares with T_B.

12.4-3 Let temperature T at a certain point be governed by the equation $2\dot{T} + 6T = 3$. Initially, $T = 0$. Compute T as a function of time according to the following instructions.
(a) To what temperature should $T(t)$ converge as t becomes large?
(b) What is the exact solution for $T = T(t)$?
(c) What is Δt_{cr} for Euler's method?

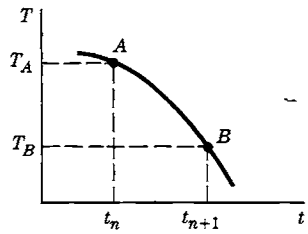

Problem 12.4-2

In what follows, use Eq. 12.4-8 with the values of β and Δt given. Take five time steps in each case. Compare computed temperatures with exact values.
(d–g) With $\Delta t = 0.1$, take β as (d) 0, (e) 1/2, (f) 2/3, and (g) 1.0.
(h–k) With $\Delta t = 1.0$, take β as (h) 0, (i) 1/2, (j) 2/3, and (k) 1.0.

12.4-4 Let temperature T at a certain point be governed by the equation $6\dot{T} + 2T = 8$. Initially, $T = 0$. Compute T as a function of time according to the following instructions.
(a) What is the exact solution for $T = T(t)$?
(b) Use Eq. 12.4-8 with $\beta = 0.5$. Take eight steps with $\Delta t = 1.0$.
(c) Use Eq. 12.4-8 with $\beta = 0.5$. Take eight steps with $\Delta t = 10.0$.

12.7-1 (a) Show that $dV/V = \varepsilon_x + \varepsilon_y + \varepsilon_z$, as claimed in Eq. 12.7-3.
(b) Show that with Π defined by Eq. 12.7-6, $\delta\Pi = 0$ yields Eqs. 12.7-4 and 12.7-5.
(c) Show that the functional $\Pi = \int [\bar{p}_{,x}^2 + \bar{p}_{,y}^2 + \bar{p}_{,z}^2 - (\omega\bar{p}/c)^2]\, dV$ yields Eq. 12.7-11 from the stationary condition $\delta\Pi = 0$.

12.7-2 Let a uniform pipe of length L have closed ends. Model the pipe by a single element. Determine the lowest nonzero acoustic frequency by the following FE formulations. The mathematically exact result is $\omega = \pi c/L$.
(a) Use the linear element of Fig. 12.7-2a.
(b) Use a four-d.o.f. element whose d.o.f. at each end are p and $p_{,x}$. See Eq. 18.2-6 for a matrix similar to the required $[\mathbf{k}_F]$.

12.7-3 Verify the result $\omega_1 = 1.5767c/L$ quoted following Eq. 12.7-14.

12.7-4 The sketch represents a three-node FE model of air in a uniform pipe. The left end is open. Determine the acoustic mode of lowest frequency by the following FE formulations. The mathematically exact result is $\omega = \pi c/2L$.
(a) Use two linear elements (Fig. 12.7-2a).
(b) Use a single quadratic element (Fig. 12.7-2b).

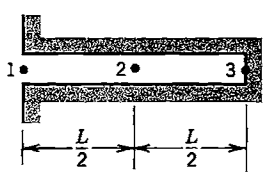

Problem 12.7-4

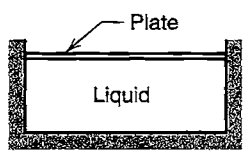

Problem 12.8-1

12.8-1 The sketch represents the cross section of a rigid rectangular tank of liquid. The liquid surface is in contact with a thin elastic plate whose four edges are attached to walls of the tank. Without calculation, sketch the two plate vibration modes of lowest frequency, assuming that all motion is parallel to the plane of the figure. Redo the sketches for the case when fluid is absent.

12.8-2 Retain the matrix $[\mathbf{W}_F]$ that accounts for surface waves. Then assume that $\{\mathbf{P}\} = \{\bar{\mathbf{P}}\}\sin \omega t$ and $\{\mathbf{D}\} = \{\bar{\mathbf{D}}\}\sin \omega t$ and derive the expression for added mass that results (see Eq. 12.8-9).

COMPUTATIONAL PROBLEMS

In thermal problems that follow, compute temperature and heat flux (acoustic and interaction problems carry their own instructions). Exploit symmetry where possible. Examine temperature contours, flux contours (unaveraged!), and vector plots of the flux field. When mesh refinement is used, estimate the maximum percentage error of results provided by the finest FE mesh. Apply the analysis methodology suggested in Section 1.5.

Unless otherwise stated, assume that plane models are homogeneous, isotropic, have unit thickness, and that steady-state conditions prevail. As an option, transient problems can be created by assuming that temperature is initially uniform and changes with time toward a steady-state condition. Each thermal analysis can be followed by stress analysis if so desired.

Where dimensions or loads are not assigned, choose values that seem reasonable or convenient. Handbooks provide data on material properties and their temperature-dependence.

C12.1 Let the plane annular sector shown be homogeneous ($k_1 = k_2$). Thus, in this problem, k_2, ϕ, β, c, and d have no meaning.
(a) Let boundaries AB and CD be insulated. Impose temperatures T_1 along AD and T_2 along BC.
(b) Let boundaries AD and AB be insulated. Impose heat flux f along BC and temperature T_1 along CD except at corner C.

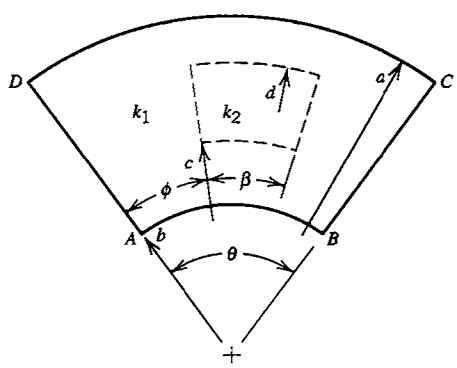

Problems C12.1 and C12.2

C12.2 Repeat Problem C12.1, but let the sector be inhomogeneous ($k_1 \neq k_2$).

C12.3 The plane annular sector shown is orthotropic. Principal material axes ns have constant orientation ϕ with respect to global Cartesian coordinates xy. Principal conductvities are k_n and $k_s = ck_n$, where c is a number greater than zero. Follow the instructions of parts (a) and (b) of Problem C12.1.

C12.4 The plane annular sector shown has prescribed temperature T_1 along BC, CD, and DA, and prescribed temperature T_2 along AB. (These conditions present the "undefined corner" difficulty noted in Section 12.5). Evaluate the temperature field and, in particular, the temperature at point E, whose radial coordinate is $(2b + a)/3$. Use coarse and fine meshes. At corners A and B, prescribe T_A and T_B as follows. (a) $T_A = T_B = T_1$. (b) $T_A = T_B = T_2$. (c) $T_A = T_B = (T_1 + T_2)/2$. (d) Let T_A and T_B be undefined (what then are their calculated values?).

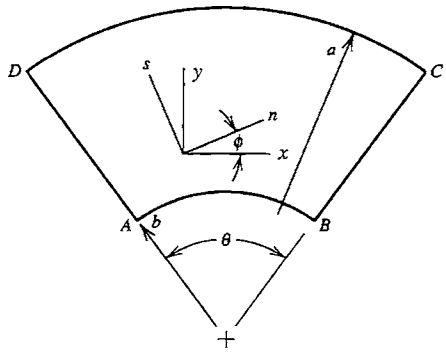

Problem C12.3

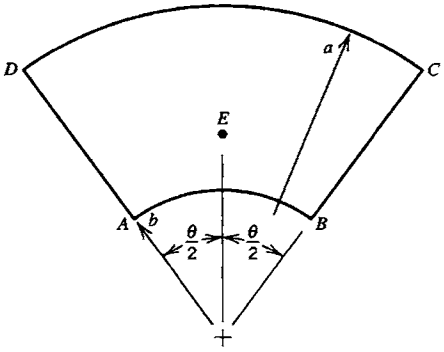

Problem C12.4

C12.5 Repeat Problem C12.4, but prescribe T_1 along AB, BC, and CD, and T_2 along DA. Parts (a) through (d) of the problem now refer to corners A and D.

C12.6 A long pipe, shown in cross section, has inner and outer radii a and b. Fluid of temperature T_i flows in the pipe. A covering of insulation has outer radius c and is surrounded by fluid of temperature T_o. Ignore radiation. Investigate how heat flux across the pipe wall is related to c/a and c/b.

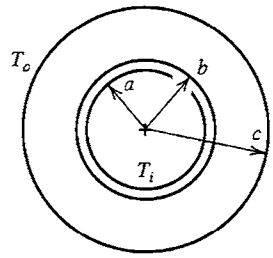

Problem C12.6

C12.7 In Problem C12.6, imagine that the outer pipe surface has emissivity 0.1 and the outer insulation surface has emissivity 0.9. Assume that $T_i = 100$ °C and $T_o = 0$ °C, and that outer surroundings do not reflect radiation. Heat is transferred by both convection and radiation. Investigate whether adding a thin layer of insulation reduces heat loss from the pipe. By numerical experiment, seek the insulation thickness c/b such that radiation and convection contribute equally to the heat loss.

C12.8 A spherical vessel has a cylindrical outlet (see the sketch for Problem C14.5). Water at temperature T_1 fills the vessel and its outlet. The vessel is surrounded by air at temperature T_2. Investigate the temperature field in the vessel.

C12.9 The sketch represents the cross section of a pipe. Initially the pipe and fluid flowing through it are at temperature T_1. At time $t = 0$ a closely spaced cylindrical surface

spanning angle ϕ assumes and then maintains temperature T_2, exchanging radiation with the outer surface of the pipe. Assume that conditions do not vary axially along the pipe. Compute (a) the transient solution, and (b) the steady-state solution.

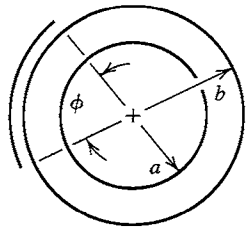

Problem C12.9

C12.10 Use the analogy between conduction heat transfer and torsion to investigate the torsional stiffness and shear stress in prismatic shafts of noncircular cross section.

C12.11 For acoustic analysis assume that the Y-shaped region shown has unit thickness perpendicular to the plane of the figure and that the three arms are slender enough that one-dimensional finite elements can be used. Ends are shown closed but one or more may be opened if desired. Investigate acoustic frequencies and modes.

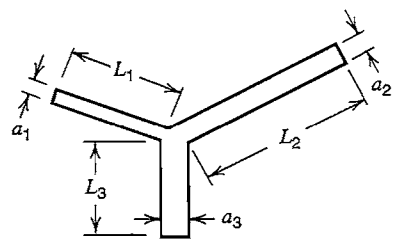

Problem C12.11

C12.12 Repeat Problem C12.11 using two-dimensional acoustic elements. Thus non-slender arms may be used, or the error associated with use of one-dimensional elements may be studied.

C12.13 The sketch represents water of depth H in a rectangular tank of span L. Two beams are shown, one horizontal and floating, the other vertical and cantilevered from the bottom. Vibration frequencies of the coupled fluid-structure problem are to be investigated. Assume that the problem may be regarded as two-dimensional.
(a) Omit the floating beam. (b) Omit the cantilevered beam. (c) Omit neither beam.

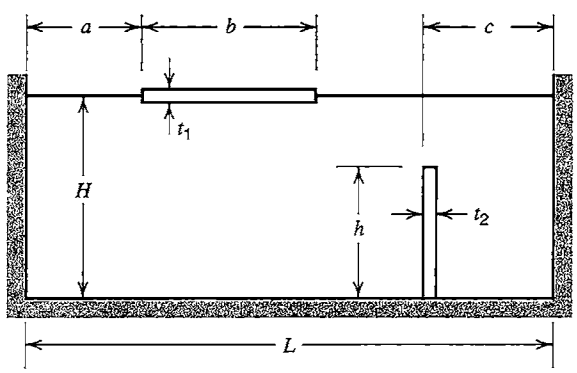

Problem C12.13

CHAPTER 13

CONSTRAINTS: PENALTY FORMS, LOCKING, AND CONSTRAINT COUNTING

Constraint conditions dictate values of d.o.f. or impose relationships among d.o.f. Explicit constraints can be imposed by transformation equations, Lagrange multipliers, or penalty functions. Implicit constraints, constraint counting, and treatment of nearly incompressible materials are also discussed.

13.1 EXPLICIT CONSTRAINTS. TRANSFORMATION EQUATIONS

Explicit constraints serve to dictate values of d.o.f., to impose an additional relationship among d.o.f. already related by global equations $[\mathbf{K}]\{\mathbf{D}\} = \{\mathbf{R}\}$, or to couple separate elements or separate substructures together. (Subsequently, in Section 13.4, we encounter *implicit* constraints, which we define as constraints contained in the existing global equations.) A *single-point constraint* sets a single d.o.f. to a known value (often zero), while a *multipoint constraint* imposes a relationship among two or more d.o.f. For the three-bar truss depicted in Fig. 2.5-2, setting $u_2 = v_2 = u_3 = 0$ as support conditions constitutes three single-point constraints. In Fig. 9.2-2a, d.o.f. u_B and u_C are already related by structural equations $[\mathbf{K}]\{\mathbf{D}\} = \{\mathbf{R}\}$, but to avoid possible numerical error we impose the *supplementary* relation $u_B = u_C$ as a multipoint constraint. In submodeling and substructuring, multipoint constraints are used to couple d.o.f. along shared boundaries.

Some problems of constraint can be formulated directly as a coordinate transformation, as in Section 8.5. Then, for each equation of explicit constraint, one d.o.f. can be eliminated from the vector of unknowns, but doing so may require considerable bookkeeping in software and rearrangement of coefficients, especially for multipoint constraints. In the present section, constraints are formulated in a more general way, which also leads to transformation operations. Alternative constraint procedures—Lagrange multipliers and the penalty method—are described in subsequent sections. The Lagrange multiplier method *adds* to the number of equations but requires less manipulation. The penalty method leaves the number of unknowns unchanged but may produce an ill-conditioned set of equations.

Transformation Equations to Enforce Constraints. Constraint equations that relate d.o.f. in $\{\mathbf{D}\}$ can be written in the form

$$[\mathbf{C}]\{\mathbf{D}\} - \{\mathbf{Q}\} = \{\mathbf{0}\} \tag{13.1-1}$$

where $[\mathbf{C}]$ and $\{\mathbf{Q}\}$ contain constants. There are more d.o.f. in $\{\mathbf{D}\}$ than constraint equations, so $[\mathbf{C}]$ has more columns than rows. For discussion, we imagine that $\{\mathbf{D}\}$ is partitioned, so that Eq. 13.1-1 becomes

$$[\mathbf{C}_r \quad \mathbf{C}_c]\{\mathbf{D}\} - \{\mathbf{Q}\} = \{\mathbf{0}\} \qquad \text{where} \qquad \{\mathbf{D}\} = \begin{Bmatrix} \mathbf{D}_r \\ \mathbf{D}_c \end{Bmatrix} \tag{13.1-2}$$

in which $\{\mathbf{D}_r\}$ and $\{\mathbf{D}_c\}$ are, respectively, d.o.f. to be retained and d.o.f. to be eliminated or "condensed out."

Because there are as many d.o.f. $\{\mathbf{D}_c\}$ as there are independent equations of constraint, matrix $[\mathbf{C}_c]$ is square and nonsingular. After solving Eq. 13.1-2 for $\{\mathbf{D}_c\}$, the complete array of d.o.f. can be written in the form

$$\begin{Bmatrix} \mathbf{D}_r \\ \mathbf{D}_c \end{Bmatrix} = \begin{bmatrix} \mathbf{I} \\ -\mathbf{C}_c^{-1}\mathbf{C}_r \end{bmatrix}\{\mathbf{D}_r\} + \begin{Bmatrix} \mathbf{0} \\ \mathbf{C}_c^{-1}\mathbf{Q} \end{Bmatrix} \quad \text{or} \quad \{\mathbf{D}\} = [\mathbf{T}]\{\mathbf{D}_r\} + \{\mathbf{Q}_0\} \tag{13.1-3}$$

where $[\mathbf{I}]$ is a unit matrix. For a specific example of Eq. 13.1-3, see Eq. 8.5-6, in which $[\mathbf{T}]$ is obtained by direct geometric argument.

The original global equations are $[\mathbf{K}]\{\mathbf{D}\} = \{\mathbf{R}\}$. Let $\{\mathbf{D}\}$ be partitioned as in Eq. 13.1-2. Premultiplying the global equations by $[\mathbf{T}]^T$ and substituting for $\{\mathbf{D}\}$ from Eq. 13.1-3, we obtain the reduced equation set

$$[\mathbf{K}_r]\{\mathbf{D}_r\} = \{\mathbf{R}_r\} \qquad \text{where} \qquad \begin{aligned} [\mathbf{K}_r] &= [\mathbf{T}]^T[\mathbf{K}][\mathbf{T}] \\ \{\mathbf{R}_r\} &= [\mathbf{T}]^T\Big(\{\mathbf{R}\} - [\mathbf{K}]\{\mathbf{Q}_0\}\Big) \end{aligned} \tag{13.1-4}$$

After $\{\mathbf{D}_r\}$ is calculated from the first of Eqs. 13.1-4, Eq. 13.1-3 yields $\{\mathbf{D}_c\}$.

Although $\{\mathbf{D}_c\}$ are termed "d.o.f. to be condensed," Eq. 13.1-4 differs from static condensation, Section 6.7. Equation 13.1-4 imposes additional relations among d.o.f., while static condensation uses only relations already contained in global equations $[\mathbf{K}]\{\mathbf{D}\} = \{\mathbf{R}\}$.

For single-point constraints, $[\mathbf{C}_r]$ is null and $[\mathbf{C}_c]$ is a unit matrix, so d.o.f. $\{\mathbf{D}_c\}$ have the prescribed value $\{\mathbf{Q}\}$. Thus, in effect, the reduced equation set of Eq. 13.1-4 is the result of taking known constants associated with $\{\mathbf{D}_c\}$ to the right-hand side, then discarding rows and columns of $[\mathbf{K}]$ associated with d.o.f. $\{\mathbf{D}_c\}$, as described in Eqs. 2.7-1 to 2.7-3. For multipoint constraints, the choice of which d.o.f. to place in $\{\mathbf{D}_c\}$ is not unique, but different choices should lead to the same final results.

Equation 13.1-4 requires partitioning of matrices and reordering of coefficients. In software these operations can be avoided by suitable coding [13.1], or by applying constraints at the element level before assembly of global equations, when matrices are smaller and more manageable [13.2].

Example. Consider the three-element structure of Fig. 13.1-1. With only axial deformation allowed, and after the boundary condition $u = 0$ at $x = 0$ is imposed, structural equations $[\mathbf{K}]\{\mathbf{D}\} = \{\mathbf{R}\}$ are

$$\begin{bmatrix} 2k & -k & 0 \\ -k & 2k & -k \\ 0 & -k & k \end{bmatrix}\begin{Bmatrix} u_1 \\ u_2 \\ u_3 \end{Bmatrix} = \begin{Bmatrix} P \\ P \\ P \end{Bmatrix} \tag{13.1-5}$$

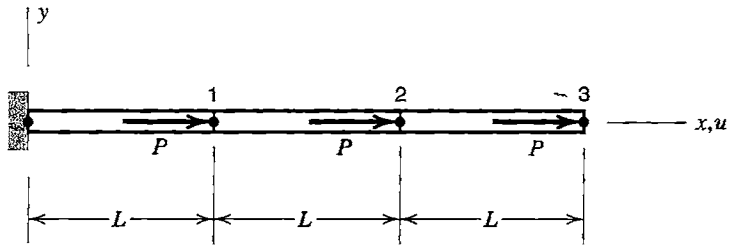

Figure 13.1-1. Three identical bar elements, each of axial stiffness $k = AE/L$.

Imagine that the multipoint constraint $u_2 = u_3$ is to be imposed. With the choice $D_c = u_3$, Eqs. 13.1-1 and 13.1-2 become

$$[0 \;\; 1 \,\vdots\, -1]\begin{Bmatrix} u_1 \\ u_2 \\ \hdashline u_3 \end{Bmatrix} = 0 \quad \text{in which} \quad [\mathbf{C}_r] = [0 \;\; 1],\ [\mathbf{C}_c] = -1, \text{ and } \{\mathbf{Q}\} = 0 \tag{13.1-6}$$

The transformation matrix and the reduced equation system of Eqs. 13.1-3 and 13.1-4 are

$$[\mathbf{T}] = \begin{bmatrix} 1 & 0 \\ 0 & 1 \\ 0 & 1 \end{bmatrix} \quad \text{and} \quad \begin{bmatrix} 2k & -k \\ -k & k \end{bmatrix}\begin{Bmatrix} u_1 \\ u_2 \end{Bmatrix} = \begin{Bmatrix} P \\ 2P \end{Bmatrix} \tag{13.1-7}$$

Solving Eq. 13.1-7 for u_1 and u_2 and then Eq. 13.1-6 for u_3, we obtain

$$\lfloor u_1 \;\; u_2 \;\; u_3 \rfloor = \left\lfloor \frac{3P}{k} \;\; \frac{5P}{k} \;\; \frac{5P}{k} \right\rfloor \tag{13.1-8}$$

Remark. When equilibrium equations $[\mathbf{K}]\{\mathbf{D}\} = \{\mathbf{R}\}$ are modified by application of multipoint constraints, the resulting solution may appear to violate equilibrium conditions. The problem depicted in Fig. 13.1-2 is a case in point. With only y-direction displacements allowed, the original equation system, and the equation that results from application of the constraint $u_1 = u_2$, are

$$\text{Original:} \quad \begin{bmatrix} k & 0 \\ 0 & k \end{bmatrix}\begin{Bmatrix} v_1 \\ v_2 \end{Bmatrix} = \begin{Bmatrix} P \\ 0 \end{Bmatrix} \qquad \text{Constrained:} \quad (2k)v_1 = P \tag{13.1-9}$$

Hence $v_1 = v_2 = P/2k$, and forces carried by the springs are $kv_1 = kv_2 = P/2$. Net forces applied to the rigid bar, Fig. 13.1-2b, satisfy equilibrium of y-direction forces but not equilibrium of moments. Of course, the condensed structure is not the original structure of Fig. 13.1-2a; it is a single spring of stiffness $2k$, loaded by force P.

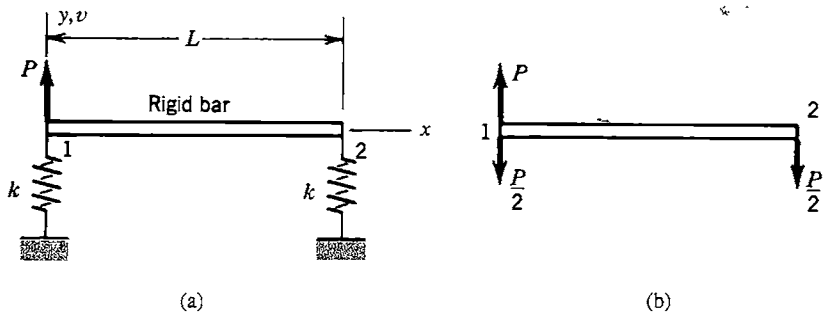

Figure 13.1-2. (a) Rigid bar supported by two springs. (b) External and elastic forces applied after the constraint $v_1 = v_2$ is imposed. Forces of constraint are not shown.

13.2 LAGRANGE MULTIPLIERS TO ENFORCE CONSTRAINTS

Lagrange's method of undetermined multipliers can be used to determine the maximum or minimum of a function of two or more variables that are not independent but must satisfy prescribed relations. In structural mechanics the function is potential energy Π_p, the variables are d.o.f. in $\{\mathbf{D}\}$, and the prescribed relations are multipoint constraints. System unknowns become $\{\mathbf{D}\}$ *and* the Lagrange multipliers.

To impose constraints by Lagrange multipliers, we premultiply the left-hand side of the constraint equations, Eq. 13.1-1, by a row vector $\{\boldsymbol{\lambda}\}^T$ that contains as many Lagrange multipliers λ_i as there are constraint equations, and add this expression to the potential energy expression, Eq. 4.8-20. Thus

$$\Pi_p = \frac{1}{2}\{\mathbf{D}\}^T[\mathbf{K}]\{\mathbf{D}\} - \{\mathbf{D}\}^T\{\mathbf{R}\} + \{\boldsymbol{\lambda}\}^T\Big([\mathbf{C}]\{\mathbf{D}\} - \{\mathbf{Q}\}\Big) \tag{13.2-1}$$

The expression in parentheses is zero, so we have "added nothing" to Π_p. Next, Π_p is made stationary by writing the equations $\{\partial\Pi_p/\partial\mathbf{D}\} = \{\mathbf{0}\}$ and $\{\partial\Pi_p/\partial\boldsymbol{\lambda}\} = \{\mathbf{0}\}$. Using differentiation rules stated in Appendix A, we obtain the set of algebraic equations

$$\begin{bmatrix} \mathbf{K} & \mathbf{C}^T \\ \mathbf{C} & \mathbf{0} \end{bmatrix} \begin{Bmatrix} \mathbf{D} \\ \boldsymbol{\lambda} \end{Bmatrix} = \begin{Bmatrix} \mathbf{R} \\ \mathbf{Q} \end{Bmatrix} \tag{13.2-2}$$

The lower partition of Eq. 13.2-2 is Eq. 13.1-1, the equations of constraint. Equations 13.2-2 are solved for $\{\mathbf{D}\}$ and $\{\boldsymbol{\lambda}\}$. The λ_i may be interpreted as forces of constraint (see the following example).

The null submatrix in Eq. 13.2-2 becomes nonzero in the course of a Gauss elimination solution for unknowns, and the solution process proceeds normally if $[\mathbf{K}]$ is by itself positive definite. In contrast to the method of constraint equations, the number of unknowns is increased by the method of Lagrange multipliers, which suggests that the method is better-suited to problems in which there are few multipoint constraints. An advantage of Eq. 13.2-2 is that the original $[\mathbf{K}]$ is not altered when constraints are applied. Therefore constraints can be changed without having to refactor $[\mathbf{K}]$. This property can be helpful in problems where different load cases involve different constraints, or in a contact problem where constraints increase in number as the load level increases [10.6].

Example. Again we impose the multipoint constraint $u_2 = u_3$ on the structure of Fig. 13.1-1. The constraint equation is the first of Eqs. 13.1-6. A single Lagrange multiplier is needed. Equation 13.2-2 becomes

$$\begin{bmatrix} 2k & -k & 0 & 0 \\ -k & 2k & -k & 1 \\ 0 & -k & k & -1 \\ 0 & 1 & -1 & 0 \end{bmatrix} \begin{Bmatrix} u_1 \\ u_2 \\ u_3 \\ \lambda \end{Bmatrix} = \begin{Bmatrix} P \\ P \\ P \\ 0 \end{Bmatrix} \tag{13.2-3}$$

which has the solution

$$\lfloor u_1 \;\; u_2 \;\; u_3 \;\; \lambda \rfloor = \left\lfloor \frac{3P}{k} \;\; \frac{5P}{k} \;\; \frac{5P}{k} \;\; -P \right\rfloor \tag{13.2-4}$$

The result $\lambda = -P$ can be interpreted as the force of constraint applied through element 2-3, which now acts as a rigid link. The algebraic sign of λ is not significant: had we used $[\mathbf{C}] = [0 \;\; -1 \;\; 1]$ in Eq. 13.1-6, we would have obtained $\lambda = +P$ but the same values of u_1, u_2, and u_3.

13.3 PENALTY FUNCTIONS TO ENFORCE CONSTRAINTS

From the constraint relation, Eq. 13.1-1, we define

$$\{\mathbf{t}\} = [\mathbf{C}]\{\mathbf{D}\} - \{\mathbf{Q}\} \tag{13.3-1}$$

so that $\{\mathbf{t}\} = \{\mathbf{0}\}$ defines satisfaction of the constraints. The usual potential energy function Π_p can be augmented by a *penalty function* $\{\mathbf{t}\}^T \lceil \boldsymbol{\alpha} \rfloor \{\mathbf{t}\}/2$, where $\lceil \boldsymbol{\alpha} \rfloor$ is a diagonal matrix of "penalty numbers" α_i. Thus

$$\Pi_p = \frac{1}{2}\{\mathbf{D}\}^T[\mathbf{K}]\{\mathbf{D}\} - \{\mathbf{D}\}^T\{\mathbf{R}\} + \frac{1}{2}\{\mathbf{t}\}^T \lceil \boldsymbol{\alpha} \rfloor \{\mathbf{t}\} \tag{13.3-2}$$

The penalty of constraint violation becomes greater as $\lceil \boldsymbol{\alpha} \rfloor$ increases. From Eqs. 13.3-1 and 13.3-2 and the minimum condition $\{\partial \Pi_p / \partial \mathbf{D}\} = \{\mathbf{0}\}$, we obtain

$$\Big([\mathbf{K}] + [\mathbf{C}]^T \lceil \boldsymbol{\alpha} \rfloor [\mathbf{C}]\Big)\{\mathbf{D}\} = \{\mathbf{R}\} + [\mathbf{C}]^T \lceil \boldsymbol{\alpha} \rfloor \{\mathbf{Q}\} \tag{13.3-3}$$

in which $[\mathbf{C}]^T \lceil \boldsymbol{\alpha} \rfloor [\mathbf{C}]$ can be called a *penalty matrix.* If $\lceil \boldsymbol{\alpha} \rfloor$ is null, constraints are ignored. As $\lceil \boldsymbol{\alpha} \rfloor$ grows, $\{\mathbf{D}\}$changes in such a way that constraints are more nearly satisfied. The analyst is responsible for selecting appropriate values of the α_i. For a positive definite $[\mathbf{K}]$, positive penalty numbers are used. If all penalty numbers are the same, then $\lceil \boldsymbol{\alpha} \rfloor = \alpha \lceil \mathbf{I} \rfloor$, where $\lceil \mathbf{I} \rfloor$ is a unit matrix, and Eq. 13.3-3 simplifies slightly.

The penalty method does not increase the number of unknowns. However, it may alter the topology of the coefficient matrix and thus affect bookkeeping procedures in software. It also may cause error due to ill-conditioning, as discussed in remarks that follow.

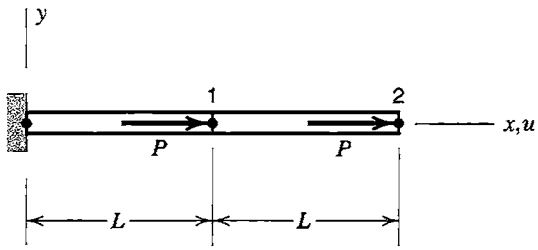

Figure 13.3-1. A two-element structure. Each bar has axial stiffness $k = AE/L$.

Example. Use the penalty method to apply the multipoint constraint $u_1 = u_2$ to the two-bar structure depicted in Fig. 13.3-1.

There is no unique way to write the constraint relation. We will write $[\mathbf{C}]$ in such a way that penalty numbers are dimensionless. Thus

$$[\mathbf{C}] = \lfloor \sqrt{k} \quad -\sqrt{k} \rfloor \qquad \{\mathbf{D}\} = \begin{Bmatrix} u_1 \\ u_2 \end{Bmatrix} \qquad \{\mathbf{Q}\} = \begin{Bmatrix} 0 \\ 0 \end{Bmatrix} \tag{13.3-4}$$

where $k = AE/L$. There is only one constraint equation, so $\lceil \boldsymbol{\alpha} \rfloor = \alpha$, a scalar. Equation 13.3-3 becomes

$$\left(\begin{bmatrix} 2k & -k \\ -k & k \end{bmatrix} + \alpha \begin{bmatrix} k & -k \\ -k & k \end{bmatrix} \right) \begin{Bmatrix} u_1 \\ u_2 \end{Bmatrix} = \begin{Bmatrix} P \\ P \end{Bmatrix} \tag{13.3-5}$$

which has the solution

$$u_1 = \frac{2P}{k} \quad \text{and} \quad u_2 = \frac{3 + 2\alpha}{1 + \alpha} \left(\frac{P}{k} \right) \tag{13.3-6}$$

If $\alpha = 0$, then $u_2 = 3P/k$, as expected in the absence of constraint. As α becomes large, u_2 approaches the value $2P/k$, which is correct for the constrained system. Vector $\{\mathbf{t}\}$ is $\{\mathbf{t}\} = t = \sqrt{k}(u_1 - u_2)$, and Eqs 13.3-6 yield $u_1 - u_2 = -(P/k)/(1 + \alpha)$. Thus we see that the coefficient of α in the penalty function, namely $t^2/2 = k(u_1 - u_2)^2/2$ in the present example, approaches zero as α approaches infinity.

Remarks. Equations 13.3-6 are obtained by symbolic manipulations and are exact. If calculations are done numerically, there may be substantial error due to ill-conditioning. The second square matrix in Eq. 13.3-5 is recognized as the stiffness matrix of a bar element connected to nodes 1 and 2. That is, the penalty method has in effect added a bar of axial stiffness αk to the structure. As α grows, the augmented structure becomes the error-prone case of a stiff region supported by a flexible region. The perils of this circumstance are discussed in Section 9.2. Indeed, we now recognize the boundary condition treatment depicted in Fig. 9.2-3c as a single-point penalty constraint. The penalty method of imposing constraints requires penalty numbers α_i that are large enough to be effective but not so large as to provoke numerical error. If numerical difficulties arise, iteration can improve accuracy [13.3].

If multipoint constraints do not couple all d.o.f. in $\{\mathbf{D}\}$, then $[\mathbf{C}]$ has more columns than rows, and $[\mathbf{C}]^T\lceil\boldsymbol{\alpha}\rfloor[\mathbf{C}]$ is certain to be a singular matrix. We *want* this matrix to be singular, as the following argument illustrates. For simplicity, let all α_i in $\lceil\boldsymbol{\alpha}\rfloor$ have the value α. Also let $\{\mathbf{Q}\} = \{\mathbf{0}\}$. Then, as α becomes large, Eq. 13.3-3 becomes

$$\left([\mathbf{C}]^T[\mathbf{C}]\right)\{\mathbf{D}\} \approx \frac{1}{\alpha}\{\mathbf{R}\} \tag{13.3-7}$$

Equation 13.3-7 shows that if $[\mathbf{C}]^T[\mathbf{C}]$ is nonsingular, then as α grows, the solution vector $\{\mathbf{D}\}$ approaches zero. In other words, the mesh *locks.* When $[\mathbf{C}]^T[\mathbf{C}]$ is *singular,* $\{\mathbf{D}\}$ can be nonzero, and the number of independent $\{\mathbf{D}\}$'s that satisfy Eq. 13.3-7 is equal to the order of $[\mathbf{C}]^T[\mathbf{C}]$ minus its rank. The significance of this conclusion is particularly important when dealing with implicit penalty constraints, discussed in sections that follow.

13.4 IMPLICIT PENALTY CONSTRAINTS AND LOCKING

In Section 13.3, multipoint constraints are imposed by explicit addition of a penalty matrix to an existing coefficient matrix $[\mathbf{K}]$. It is possible that $[\mathbf{K}]$ already contains a contribution that can be identified as a penalty matrix. An *implicit* constraint is inherent in the formulation, either because of characteristics of the numerical model or the nature of the physical problem. In this section we discuss two such formulations: transverse shear in beams (and, by extension, also in plates and shells), and incompressible media. Both can produce locking of the mesh for some choices of element type and integration rule. Physical interpretation of penalty constraints leads to understanding of reasons for locking and to ways of avoiding it. In the present section we describe the constraints, and in the following section we describe how to count them.

Mindlin Beam Element. A Mindlin beam element uses independent interpolation fields for lateral deflection and rotation of a cross section, and therefore takes transverse shear deformation into account. The element is a special case of similar formulations of plate and shell elements, and is not intended as a substitute for the beam element of Eq. 2.3-6. In formulating a Mindlin beam element it is assumed that plane cross sections initially normal to the beam axis remain plane but not necessarily normal to the deformed axis. Anticipating application to plates, we call the lateral deflection w rather than v. Figure 13.4-1b shows that axial displacement u and axial strain ε_x depend only on rotation ψ of cross sections, while transverse shear strain γ_{zx} depends on both ψ and w. Specifically

$$\varepsilon_x = u_{,x} = -z\psi_{,x} \quad \text{and} \quad \gamma_{zx} = w_{,x} - \psi \tag{13.4-1}$$

Thus, axial strain and the associated bending moment are coupled to lateral deflection only by transverse shear strain. For the two-node element shown in Fig. 13.4-1a, $w = w(x)$ is linearly interpolated between w_1 and w_2, and $\psi = \psi(x)$ is linearly interpolated between ψ_1 and ψ_2. Element strain energies U_b in bending and U_s in transverse shear, and associated contributions to the element stiffness matrix $[\mathbf{k}] = [\mathbf{k}_b] + [\mathbf{k}_s]$, are

$$U_b = \iint_0^L \frac{1}{2}E\varepsilon_x^2\,dx\,dA = \int_0^L \frac{1}{2}EI\psi_{,x}^2\,dx = \frac{1}{2}\{\mathbf{d}\}^T[\mathbf{k}_b]\{\mathbf{d}\} \tag{13.4-2a}$$

$$U_s = \iint_0^L \frac{1}{2}G\gamma_{zx}^2\,dx\,dA = \int_0^L \frac{1}{2}GA_s(w_{,x} - \psi)^2\,dx = \frac{1}{2}\{\mathbf{d}\}^T[\mathbf{k}_s]\{\mathbf{d}\} \tag{13.4-2b}$$

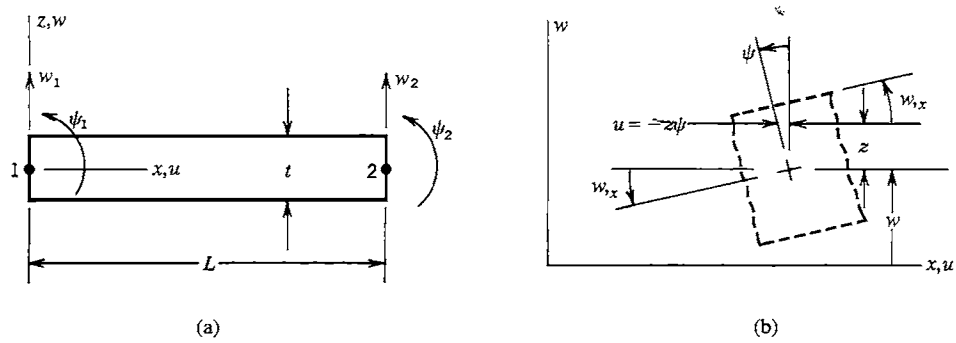

Figure 13.4-1. (a) Mindlin beam element. (b) Displacements and rotations.

where A is the cross-sectional area and A_s is the "effective" cross-sectional area of the beam in resisting transverse shear deformation. For a rectangular cross section, γ_{zx} varies parabolically over dimension t in Fig. 13.4-1, and $A_s = 5A/6$. If the distinction between $[\mathbf{k}_b]$ and $[\mathbf{k}_s]$ is maintained during assembly of elements, structural equations have the form

$$\Big([\mathbf{K}_b] + [\mathbf{K}_s]\Big)\{\mathbf{D}\} = \{\mathbf{R}\} \tag{13.4-3}$$

Details of the formulation are discussed in Section 15.4, in connection with elements for plate bending. There it is found that, in a one-element Mindlin cantilever beam, the contribution of bending to total deflection is reduced by the factor $(t/L)^2$. Thus, as elements become more and more slender, $[\mathbf{K}_s]$ acts as a penalty matrix that forces Eq. 13.4-3 to yield $\{\mathbf{D}\} \approx \{\mathbf{0}\}$—*unless* $[\mathbf{K}_s]$ *is singular,* a condition achievable by use of selective or reduced integration. For a two-node Mindlin beam element this means integrating $[\mathbf{k}_s]$ by using a single Gauss point rather than two (for further details, see Sections 13.5 and 15.4).

The foregoing development explains shear locking as an instance of penalty constraint. An alternative explanation, in terms of "parasitic shear," appears in Section 3.6. Inclusion of transverse shear deformation does not automatically make a beam element susceptible to shear locking; it depends upon the formulation. The beam element of Eq. 2.3-6 has neither tendency to lock nor ill-conditioning of $[\mathbf{k}]$ as a beam becomes indefinitely slender.

Incompressible Materials. In terms of E and ν, shear modulus G and bulk modulus B are

$$G = \frac{E}{2(1+\nu)} \qquad B = \frac{E}{3(1-2\nu)} \tag{13.4-4}$$

Modulus B expresses the ratio of hydrostatic pressure to the fractional volume change $\Delta V/V$ it produces, where $\Delta V/V = \varepsilon_x + \varepsilon_y + \varepsilon_z$ if strains are small. That is, $B = -p/(\Delta V/V)$, where $\Delta V < 0$ for positive pressure p. For an incompressible material, $\Delta V = 0$ and $B = \infty$. Thus an incompressible isotropic material is characterized by $\nu = 0.50$. Although no real material is completely incompressible, B in a rubberlike material is so much larger than G that the assumption of incompressibility is appropriate for most practical problems.

In terms of G and B, material property matrix $[\mathbf{E}]$ can be written in the form

$$[\mathbf{E}] = G\begin{bmatrix} \frac{4}{3} & -\frac{2}{3} & -\frac{2}{3} & 0 & 0 & 0 \\ -\frac{2}{3} & \frac{4}{3} & -\frac{2}{3} & 0 & 0 & 0 \\ -\frac{2}{3} & -\frac{2}{3} & \frac{4}{3} & 0 & 0 & 0 \\ 0 & 0 & 0 & 1 & 0 & 0 \\ 0 & 0 & 0 & 0 & 1 & 0 \\ 0 & 0 & 0 & 0 & 0 & 1 \end{bmatrix} + B\begin{bmatrix} 1 & 1 & 1 & 0 & 0 & 0 \\ 1 & 1 & 1 & 0 & 0 & 0 \\ 1 & 1 & 1 & 0 & 0 & 0 \\ 0 & 0 & 0 & 0 & 0 & 0 \\ 0 & 0 & 0 & 0 & 0 & 0 \\ 0 & 0 & 0 & 0 & 0 & 0 \end{bmatrix} \tag{13.4-5}$$

Terms of $[\mathbf{E}]$ in conventional format are stated in Eq. 3.1-5. In more compact notation, we write Eq. 13.4-5 as $[\mathbf{E}] = G[\mathbf{E}_G] + B[\mathbf{E}_B]$. Thus the element stiffness matrix, Eq. 3.3-7 or 4.8-15a, becomes

$$[\mathbf{k}] = G\int [\mathbf{B}]^T[\mathbf{E}_G][\mathbf{B}]\, dV + B\int [\mathbf{B}]^T[\mathbf{E}_B]\,[\mathbf{B}]\, dV$$

$$\text{or} \qquad [\mathbf{k}] = G[\mathbf{k}_G] + B[\mathbf{k}_B] \tag{13.4-6}$$

and structural equations have the form

$$\Big(G[\mathbf{K}_G] + B[\mathbf{K}_B]\Big)\{\mathbf{D}\} = \{\mathbf{R}\} \tag{13.4-7}$$

As ν approaches 0.50, matrix $B[\mathbf{K}_B]$ dominates the equation, thus acting as a penalty constraint and, unless $[\mathbf{K}_B]$ is singular, locking the mesh. This behavior is called "volumetric" or "dilatational" locking, and is explained by physical argument in connection with Fig. 3.4-3. It is tempting to model a rubberlike material by arbitrarily choosing a value of ν slightly less than 0.50, and not worrying about whether $[\mathbf{K}_B]$ is singular, but stresses are sensitive to small changes in ν when ν is close to 0.50.

Remarks. Equations 13.4-3 and 13.4-7 correspond to homogeneous constraints; that is, to $\{\mathbf{Q}\} = \{\mathbf{0}\}$ in Eq. 13.1-1. These constraints arise naturally from minimization of potential energy Π_p that can be stated in the form

$$\Pi_p = \beta\int (F + \alpha H)\, dV + P \tag{13.4-8}$$

Here F and H are proportional to strain energy densities, H is associated with implicit constraint, β is a common factor of F and H, α is a mesh-independent penalty number, and P represents work done by loads of all types. A typical problem presents no unique way to write Eq. 13.4-8, but if possible, β should be defined in a way that makes α dimensionless. A dimensionless α makes it easier to prescribe a suitable numerical value for it (see guidelines at the end of the present section). If the correct Π_p is to be closely approximated, a large α must be associated with a near-zero value of H.

For a Mindlin beam, the correspondence between Eqs. 13.4-2 and 13.4-8 can be written as follows. Let the cross section be rectangular, of width b and depth t. Replace dV by dx in Eq. 13.4-8, and let

$$F = \frac{E}{2}\psi_{,x}^2 \qquad H = \frac{E}{2L_T^2}(w_{,x} - \psi)^2$$
$$\beta = \frac{bt^3}{12} \qquad \alpha = \frac{10GL_T^2}{Et^2} = \frac{5}{1+\nu}\left(\frac{L_T}{t}\right)^2 \tag{13.4-9}$$

We use L_T rather than element length L because no discretization has yet been made. We see that α is proportional to $(L_T/t)^2$. The penalty constraint enforced is $w_{,x} = \psi$, for which $H = 0$.

The incompressible case, Eq. 13.4-7, is obtained from Eq. 13.4-8 if

$$F = \frac{E}{4(1+\nu)}\{\boldsymbol{\varepsilon}\}^T[\mathbf{E}_G]\{\boldsymbol{\varepsilon}\} \qquad H = \frac{E}{2}\{\boldsymbol{\varepsilon}\}^T[\mathbf{E}_B]\{\boldsymbol{\varepsilon}\}$$
$$\beta = 1 \qquad \alpha = \frac{1}{3(1-2\nu)} \tag{13.4-10}$$

Penalty number α becomes large as ν approaches the incompressibility value $\nu = 0.50$. Volumetric strain ε_V is $\varepsilon_V = \Delta V/V = \varepsilon_x + \varepsilon_y + \varepsilon_z$, hence $H = E\varepsilon_V^2/2$. Therefore, enforcing the constraint of incompressibility makes $H = 0$.

Locking. Locking occurs when, due to such particulars as displacement interpolation used and quadrature rule chosen, a physically realistic displacement mode tends to be "locked out" of element response because the mode activates extraneous strains that require much greater energy input than do strains of the realistic mode. The Mindlin beam element develops large shear stress when bent. So does the plane Q4 element of Fig. 3.6-2b. Thus shear locking appears in these elements. If used to analyze a rubberlike material in a state of plane strain ($\varepsilon_z = 0$), bending of the Q4 element also produces volumetric strain $\Delta V/V = \varepsilon_x + \varepsilon_y$, which is strongly resisted as ν approaches 0.50. Thus dilatational locking appears. However, in all these examples there are locations in elements where the unwanted strains are zero: at the midpoint of the Mindlin beam element and at the center of the Q4 element in Fig. 3.6-2b. Thus, locking might be avoided by reduced or selective integration, as described in the next section.

In common parlance, "locking" does not necessarily mean complete rigidity. The term can refer to unwanted high-stiffness behavior that influences the solution but does not overwhelm it, so that convergence with mesh refinement is slowed but not prevented. Thus, a slender beam modeled by Mindlin elements can provide accurate results if enough elements are used, even when $[\mathbf{k}_s]$ is fully integrated. In other words, a large value of α in Eqs. 13.4-9 does not preclude convergence. However, to obtain satisfactory results with a fully integrated $[\mathbf{k}_s]$, the L/t ratio of individual beam elements may have to be less than unity. When a single Gauss point is used to integrate $[\mathbf{k}_s]$, a large α enforces the condition $w_{,x} - \psi \approx 0$, as is appropriate for a beam for which L_T/t is large, but without producing a tendency to lock the mesh.

Locking behavior may be associated with ill-conditioning of the global equations. In computer solutions, trouble due to ill-conditioning is associated with loss of information required for a unique solution, as essential information in stiffness coefficients is lost when large penalty numbers are added to these coefficients. Although this description may well apply to various implicit penalty constraints, in general, locking and ill-conditioning are *not* the same. A mesh may lock even if its global equations are well-conditioned. On the other hand, when a penalty matrix is made singular in order to avoid locking while yet enforcing the penalty constraint, ill-conditioning is likely.

Guideline for Choice of α. If the penalty matrix is singular and computer words represent approximately d decimal digits, experience has shown that α should not exceed $10^{d/2}$ if numerical trouble associated with ill-conditioning is to be avoided. If this guideline is followed, coefficients of $[\mathbf{K}]$ in Eq. 13.3-3 influence the latter $d/2$ digits in computer words used to store the complete matrix $[\mathbf{K} + \mathbf{C}^T\boldsymbol{\alpha}\mathbf{C}]$. Typically $10^{d/2}$ is 10^3 or 10^4 in single precision and 10^6 or 10^7 in double precision. If numerical data provides a larger value of α, it is appropriate to arbitrarily reduce it. In preceding examples, this amounts to arbitrary reduction of L_T/t in Eq. 13.4-9 or of ν in Eq. 13.4-10.

13.5 CONSTRAINT COUNTING

We seek criteria for choosing a suitable numerical integration formula in a problem where penalty constraints are inherent in the formulation. Specifically, if the number of constraints is proportional to the number of sampling points used to integrate the penalty matrix, how many points per element should be used?

In what follows we assume that all weight factors in quadrature rules are positive. Otherwise, it is possible that terms in a summation would cancel one another. This would confuse the counting rule.

Constraints and Quadrature Points. Numerical integration of matrices in Eqs. 13.4-2 and 13.4-6 corresponds to evaluation of energy Π_p by numerical integration. Accordingly Eq. 13.4-8 can be written as

$$\Pi_p \approx \beta \sum_{I=1}^{N_{\text{els}}} \left[\sum_{i=1}^{n} (F_I J_I)_i W_i + \alpha \sum_{j=1}^{m} (H_I J_I)_j T_j \right] + P \tag{13.5-1}$$

where $(F_I J_I)_i$ and $(H_I J_I)_j$ are values of functions F and H times Jacobian J, each evaluated at the ith or jth sampling point, and W_i and T_j are positive weights (or weight products) appropriate to the integration rule. If $n = m$ and sampling points i and j are the same, the integration scheme is *uniform;* otherwise it is *selective.* If the number of sampling points is adequate to provide exact integration of all stiffness coefficients when the element shape happens to be undistorted—such as rectangular with straight sides and midside nodes—the integration scheme is called *full* (even when the actual element shape is distorted). If fewer sampling points are used—that is, if n or m is reduced—the integration scheme is called *reduced* and Π_p is said to be *underintegrated.* There is no need to discuss use of *more* sampling points than required for full integration, which would only provide

redundant constraint relations. In what follows we assume that spurious modes (mechanisms) are either impossible or are suppressed by boundary conditions. (Discussion of reduced integration and spurious modes appears in Section 6.8).

Consider the effect of letting α become large in Eq. 13.4-8. In order for the term αH to yield a finite result, such as a finite limit of dilatational strain energy in a nearly incompressible medium, a large value of α must be associated with a near-zero value of the second summation in Eq. 13.5-1. Because $(J_I)_j$ and T_j are both positive, the implied condition is that $(H_I)_j = 0$. Equations 13.4-9 and 13.4-10 show that $H = 0$ implies satisfaction of the constraint.

For the problems described by Eqs. 13.4-9 and 13.4-10, *each sampling point used to integrate the penalty matrix imposes a constraint at that point.* Therefore, the total number of constraints in the structure equals the number of elements times the number of penalty integration points per element. The number of "free" d.o.f. available to model structure behavior equals the total number of d.o.f. minus the number of d.o.f. imposed to satisfy boundary conditions and minus the number of penalty constraints. In choosing a selective integration rule, we seek to use a sufficient number of points for integration of the penalty matrix to adequately enforce constraints, but not so many as to either lock the mesh or leave so few free d.o.f. that structure behavior is poorly represented.

In other problems, each sampling point may impose more than one penalty constraint. For example, in a Mindlin plate element (Chapter 15), the matrix analogous to $[\mathbf{k}_s]$ in Eq. 13.4-2b is associated with *two* transverse shear strains, and each sampling point imposes penalty constraints on both of them. In the remainder of the present chapter, unless stated otherwise, we assume that each sampling point imposes a single penalty constraint.

Constraint Counting and Constraint Ratios. Let the cantilever beam in Fig. 13.5-1a be built of the Mindlin elements described in Section 13.4. Boundary conditions suppress w and ψ at the leftmost node, leaving $2N_{\text{els}}$ active d.o.f. in $\{\mathbf{D}\}$. If $[\mathbf{K}_s]$ of Eq. 13.4-3 is exactly integrated, by use of two sampling points per element, there are $2N_{\text{els}}$ penalty constraints in the structure. Thus, if L_T/t is large, all d.o.f. are occupied in satisfying the constraint $w_{,x} - \psi = 0$ and the computed deflection of load P is nearly zero (unless an extremely large number of elements is used).

A similar situation prevails if the beam is built of a single layer of four-node plane Q4 elements, as in Fig. 3.6-3, and elements are fully integrated by using a 2 by 2 Gauss rule. There are $4N_{\text{els}}$ active d.o.f. but also $4N_{\text{els}}$ "parasitic shear" constraints that lock the mesh when elements have large aspect ratio.

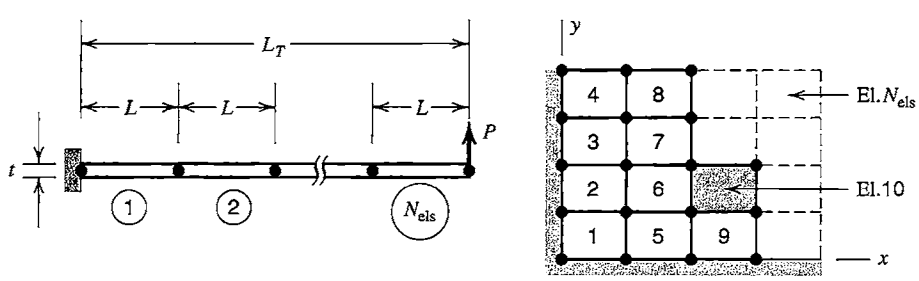

(a) (b)

Figure 13.5-1. Meshes that contain N_{els} elements. (a) Cantilever beam. (b) Mesh of four-node plane elements. A typical element (element 10; shaded) is being added to elements 1 through 9 already in place.

Let plane strain conditions prevail in Fig. 13.5-1b, so that $\varepsilon_z = 0$. Then the volumetric strain is $\Delta V/V = u_{,x} + v_{,y}$. Structural equations are Eqs. 13.4-7. With bilinear elements, no rotational d.o.f. at nodes, and full integration, there are $4N_{\text{els}}$ penalty constraints as ν approaches 0.50, and only $2N_{\text{els}}$ active d.o.f., so the mesh is locked. In similar fashion, constraint counting shows that, for plane strain conditions, the mesh of three-node triangles in Fig. 3.4-3 is locked.

Locking can be avoided in the foregoing examples by use of selective integration, so that the penalty matrix is underintegrated. Thus to establish $[\mathbf{K}_s]$ of Eq. 13.4-3 for Mindlin beam elements, and to establish $[\mathbf{K}_B]$ of Eq. 13.4-7 for bilinear elements, a single integration point is used. For the Mindlin beam of Fig. 13.5-1a, there are now $2N_{\text{els}}$ active d.o.f. and N_{els} penalty constraints. Here the *constraint ratio,* which is the number of active d.o.f. divided by the number of penalty constraints, is $r = 2/1$. For the plane strain example of Fig. 13.5-1b, the same numbers apply: $2N_{\text{els}}$ active d.o.f. and N_{els} penalty constraints, so again $r = 2/1$. With *full* integration the respective constraint ratios would be $1/1$ and $1/2$.

The same numbers can be obtained more easily by considering the numbers of d.o.f. and penalty constraints brought to the mesh when a single element is added. In Fig. 13.5-1b for example, when element 10 is added with elements 1 to 9 already in place, the added element brings with it two active d.o.f. and either one or four penalty constraints, depending on whether the integration rule for the penalty matrix is reduced or full. Thus we obtain $r = 2/1$ or $r = 1/2$, as before. These numbers remain approximately correct if boundary conditions are changed, provided that N_{els} is large. Henceforth we will assume that this is so, and do constraint counting by examining the number of *additional* d.o.f. and penalty constraints brought to a mesh by a single element, or perhaps by a single "superelement" built of two or more subelements.

Desirable Constraint Ratios. Examples. If constraint ratio r exceeds unity only slightly, the mesh is nearly locked. If r is much larger than unity, constraints are not sufficiently enforced. For incompressible media, Hughes [2.13] conjectures that the best value of r equals n_{de}, the number of differential equations of equilibrium, divided by the number of constraints to be applied to these equations. For 2D and 3D solids respectively, $n_{\text{de}} = 2$ and $n_{\text{de}} = 3$, and in each case there is one constraint ($\Delta V = 0$). Thus the proposed optimal r for near-incompressibility equals the spatial dimension of the problem.

Some examples pertinent to nearly incompressible media are as follows. Let n_{dof} and n_{pc} refer to the number of d.o.f. and the number of penalty constraints brought to the mesh by a single element. Thus $r = n_{\text{dof}}/n_{\text{pc}}$. Let us consider 2D and 3D elements that have no rotational d.o.f. For bilinear elements, Fig. 13.5-1b, $n_{\text{dof}} = 2$ and $n_{\text{pc}} = 1$ if one-point integration is used to evaluate $[\mathbf{K}_B]$, so the constraint ratio is $r = 2/1$, which is the conjectured optimal value. With 2 by 2 integration, the QM6 element described in Section 6.6 also works well [13.4]: the counts are $n_{\text{dof}} = 6$ and $n_{\text{pc}} = 4$. For the trilinear solid element without internal d.o.f., Fig. 13.5-2a, one-point integration of $[\mathbf{K}_B]$ provides $r = 3/1$, the conjectured optimal value. Four-point integration of $[\mathbf{K}_B]$ in Fig. 13.5-2b yields $n_{\text{pc}} = 4$. For eight- and nine-node versions of the element respectively, $n_{\text{dof}} = 6$ and $n_{\text{dof}} = 8$, for which the respective constraint ratios are $r = 3/2$ and $r = 2/1$. With one-point integration of $[\mathbf{K}_B]$ in each subtriangle of the two-triangle superelement in Fig. 13.5-2c, $n_{\text{pc}} = 2$. Depending on whether the internal node is omitted or included, $r = 1/1$ (so that the mesh is locked) or $r = 2/1$. With three-point integration of $[\mathbf{K}_B]$ in each subtriangle of the superelement in Fig. 13.5-2d, $n_{\text{pc}} = 6$. Because $n_{\text{dof}} = 12$ for the superelement, $r = 2$.

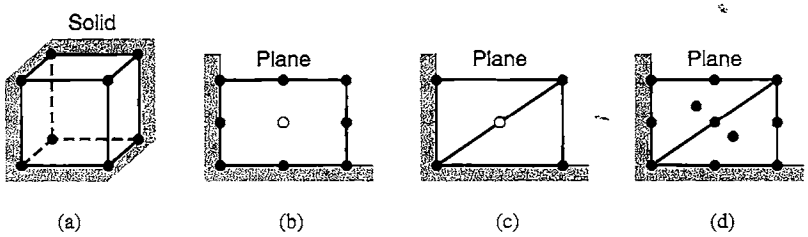

Figure 13.5-2. Solid element, and plane elements in plane strain conditions. For the purpose of constraint counting, elements shown are regarded as being added to a mesh. Nodes associated with open circles are optional.

Recall that the foregoing 2D examples are for plane *strain* conditions. For plane *stress* conditions, there is no locking or ill-conditioning even when $\nu = 0.50$.

If the conjecture regarding the optimal value of r is extended to the Mindlin beam, we count two differential equations of equilibrium (one for bending, one for transverse shear) and one constraint condition (that $w_{,x} - \psi = 0$ when the beam is slender). Thus $r = 2$ may be the optimal value, and this value is achieved in Fig. 13.5-1a by use of a single sampling point per element to evaluate $[\mathbf{K}_s]$ of Eq. 13.4-3. In the analogous Mindlin *plate* element, there are three equilibrium equations, two for moment and one for transverse shear. There are two constraints per sampling point used to evaluate $[\mathbf{K}_s]$, because two transverse shear strains, γ_{zx} and γ_{yz}, are both forced toward zero as elements become thin. We conjecture that $r = 3/2$ is optimal for a Mindlin plate [2.13].

If elements in a mesh have distorted shapes, a reduced integration rule may not be able to represent element volume exactly. This defect tends to disappear with mesh refinement by subdivision of elements because elements tend to become parallelograms (2D) or parallelepipeds (3D), as shown by Fig. 6.13-1b. Reduced integration may have to be accompanied by an element stabilization device in order to avoid spurious modes.

13.6 REMARKS ABOUT TECHNIQUES FOR INCOMPRESSIBLE MEDIA

In notation introduced following Eq. 13.4-5, a state of stress $\{\boldsymbol{\sigma}\}$ can be written as

$$\{\boldsymbol{\sigma}\} = \{\boldsymbol{\sigma}_D\} + \{\boldsymbol{\sigma}_V\} \quad \text{where} \quad \{\boldsymbol{\sigma}_D\} = G[\mathbf{E}_G]\{\boldsymbol{\varepsilon}\} \quad \text{and} \quad \{\boldsymbol{\sigma}_V\} = B[\mathbf{E}_B]\{\boldsymbol{\varepsilon}\} \tag{13.6-1}$$

where $\{\boldsymbol{\sigma}_D\}$ is a *deviatoric state* (which produces no change of volume) and $\{\boldsymbol{\sigma}_V\}$ is a *dilatational state* (which produces no change of shape). Equations 13.4-5 and 13.6-1 show that, regardless of the state of strain, $\{\boldsymbol{\sigma}_V\}$ contains three equal normal stresses and no shear stresses. The first of Eqs. 13.6-1 becomes

$$\{\boldsymbol{\sigma}\} = \{\boldsymbol{\sigma}_D\} + \lambda\lfloor 1 \;\; 1 \;\; 1 \;\; 0 \;\; 0 \;\; 0 \rfloor^T \tag{13.6-2}$$

where λ is a hydrostatic stress (the same in all directions) that prevents volumetric strain when B approaches infinity. From Eqs. 13.4-5, 13.4-10, and 13.6-2 we obtain $H = \frac{1}{2}\lambda\varepsilon_V$. Because λ and ε_V have the same sign, H is positive whether the hydrostatic state is tensile or compressive.

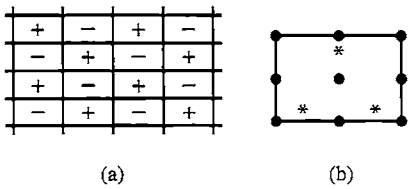

Figure 13.6-1. (a) "Checkerboard" pressure oscillations in a plane mesh. (b) Plane element with nine nodes and three pressure points, used in a consistent penalty method.

One may argue that the incompressible pressure field is, at each material point, the limit of the slightly compressible pressure λ computed from Eq. 13.6-2. The penalty method provides a way to slightly "perturb" the exactly incompressible solution and thus obtain a good approximation of it.

Pressure Calculation in the Penalty Method. One can calculate pressure λ by evaluating ε_V from the displacement field and then using Eq. 13.6-1. The error in λ associated with use of a penalty constraint rather than an exact constraint is of order $10^{-d/2}$ if α is chosen as $10^{d/2}$, as suggested at the end of Section 13.4 [13.5]. However, this error estimate is valid only when λ is calculated at locations where the constraint is enforced, namely at sampling points used to integrate element matrices $[\mathbf{k}_B]$. Thus, in the penalty method, the (reduced) volumetric integration points in Eq. 13.5-1 play more than one role: they are integration points, constraint points, and "pressure points."

Many element types may allow pressure oscillations in the mesh. For example, with one-point integration for $[\mathbf{k}_B]$, the bilinear elements of Fig. 13.5-1b may display "checkerboarding," which is a pattern of spurious pressures superposed on the desired pressures (Fig. 13.6-1a). This disorder is analogous to the "hourglassing" that can appear in conventional stress analysis under some conditions (Fig. 6.8-2). Pressure oscillations can be smoothed using techniques like those described for stress fields in Section 9.9 [2.13,13.6,13.7].

Consistent Penalty Method. In this method, selective integration is not required. Hydrostatic pressure is not derived from the displacement field. Instead it becomes an additional variable that functions as a Lagrange multiplier on the incompressibility constraint. The method may also be called a "mixed penalty method," and regarded as a special case of the "B-bar method" [13.8,13.9]. Displacement and pressure are independently interpolated; displacements in the usual way from nodal d.o.f., and pressure from "pressure points" that may reside entirely within an element. Because pressure is not differentiated in the functional used for the method, pressure need not be continuous between elements; it can be a C^{-1} field [13.10].

Like the method associated with Eqs. 13.4-10, the consistent penalty method can, depending on the penalty parameter and interpolations chosen, display locking, ill-conditioning of equations, and spurious pressure modes [2.20]. System equations that result resemble Eq. 13.2-2, except that $\{\mathbf{Q}\} = \{\mathbf{0}\}$ and the $[\mathbf{0}]$ submatrix is replaced by a nonsingular square matrix that represents slight compressibility. However, an important advantage of the method is that element pressure points are not shared by adjacent elements, even if they appear on element boundaries, so pressure d.o.f. can be condensed before assembly of elements and recovered after global equations are solved, as described in Section 6.7. The result is a set of equations like Eq. 13.4-7.

Perhaps the best plane pressure-point element is that depicted in Fig. 13.6-1b [2.13,2.20]. Displacements are interpolated from u and v at the nine nodes shown by dots and pressures are interpolated from the three internal pressure points. The constraint count, which now indicates the ratio of active displacement d.o.f. to pressure d.o.f., is 8/3 rather than the conjectured optimal value of 2/1. Nevertheless, the element behaves well, does not display spurious pressure modes, and passes the patch test [13.11]. There are rigorous error bounds for the element, which show that pressure is as accurate as strains in compressible elasticity [13.12]. Unfortunately, an element of comparable quality for 3D problems does not seem to be available.

ANALYTICAL PROBLEMS

13.1-1 Let a plane eight-node element have straight sides and midside nodes (Fig. 6.4-1a). Consider the constraint that displacement components u and v of each midside node are to be the average of u and v at the two adjacent corner nodes. Write the appropriate form of [**T**] in Eq. 13.1-3. For simplicity, consider displacement u only. Then, with $\lfloor \mathbf{N} \rfloor$ the list of shape functions of the eight-node element, write $\lfloor \mathbf{N} \rfloor [\mathbf{T}]$ to obtain the new set of shape functions. What element is produced?

13.1-2 In the plane frame shown, let all three members be identical. Assume that fixity at the base and the conditions $v_A = v_B = 0$ have already been imposed, so that [**K**] operates on d.o.f. u_A, θ_A, u_B, and θ_B. Write [**K**] in terms of A, E, I, and L. Then transform [**K**] by imposing the constraint $u_A = u_B$, so that the new d.o.f. are u_A, θ_A, and θ_B.

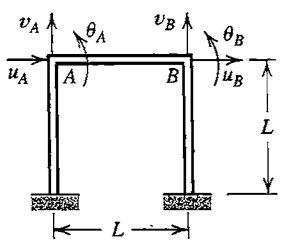

Problem 13.1-2

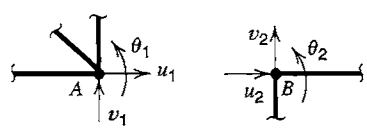

Problem 13.1-3

13.1-3 The sketch shows small portions of two separate plane frames. The frames are to be connected by superposing nodes A and B in such a way that a hinge connection results. For simplicity consider only the d.o.f. shown, and write an appropriate form of Eq. 13.1-2. Identify matrices $[\mathbf{C}_r]$ and $[\mathbf{C}_c]$ in this result.

13.1-4 Write Eq. 8.5-6 in the form of Eq. 13.1-2. How many equations of constraint are there?

13.1-5 The two-node bar shown has axial stiffness AE/L and is initially unsupported. Write the 2 by 2 [**k**], then obtain the form of Eq. 13.1-4 and solve for u_1 if the constraint imposed is (a) $u_2 = 0$, and (b) $u_2 = \bar{u}$, a constant.

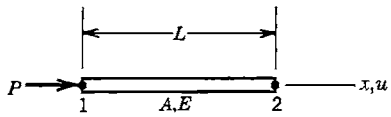

Problem 13.1-5

13.1-6 Two rigid links AB and BC are connected by a hinge at B and are supported by identical springs at A, B, and C, as shown. Write structural equations that use vertical displacements at A, B, and C as d.o.f. Then impose the constraint that the hinge is locked and so allows no relative rotation between the rigid links. Finally, solve for the three d.o.f. v_A, v_B, and v_C.

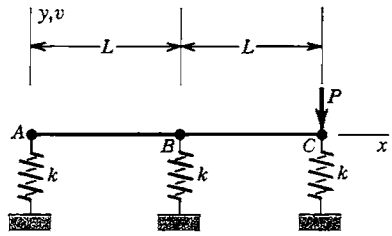

Problem 13.1-6

13.1-7 Imagine that three nodes lie on an x axis at coordinates x_1, x_2, and x_3. Write a relation in the form of Eq. 13.1-1 that constrains their x-direction displacements to be directly proportional to x.

13.1-8 Write the 4 by 4 [**K**] for bending of the two-element uniform cantilever beam shown. Use conventional beam elements and ignore transverse shear deformation. Then impose the constraint that element 2-3 is to be made rigid. Thus eliminate d.o.f. at node 3. Solve for d.o.f. at node 2. Compare results with results obtained from elementary beam theory.

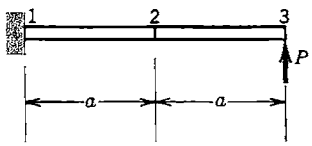

Problem 13.1-8

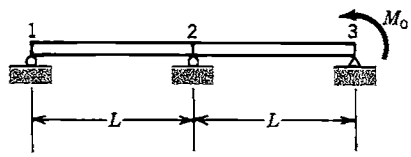

Problem 13.1-9

13.1-9 The uniform beam shown is modeled by two conventional beam elements and is simply supported at nodes 1, 2, and 3. Ignore transverse shear deformation. Write the 3 by 3 [**K**] that operates on nodal rotations.
(a) Impose the constraint that nodal rotations at nodes 2 and 3 are equal. Then solve for all three nodal rotations in terms of M_0, E, I, and L.
(b) Draw a free-body diagram, showing all externally applied forces and moments on the beam.

13.2-1 The following question is strictly mathematical, and serves as a review of the Lagrange multiplier method. In terms of a and b, what is the area of the largest rectangle that can be inscribed in the ellipse $(x/a)^2 + (y/b)^2 - 1 = 0$?

13.2-2 Solve the problem of Fig. 13.1-2. That is, impose the constraint $v_1 = v_2$ by means of a Lagrange multiplier λ, and solve for v_1, v_2, and λ.

13.2-3 A two-node bar has axial stiffness $k = AE/L$ and axial nodal d.o.f. u_1 and u_2 at left and right ends respectively. Rightward force $P = 3$ is applied to node 2. Use the Lagrange multiplier method to impose displacement $u_1 = 2$. Solve for u_2.

13.2-4 Model a uniform cantilever beam by a single conventional beam element, fixed at its left end. Neglect transverse shear deformation. For the following constraint

conditions, use the Lagrange multiplier method to determine the deflection of a transverse load P applied at the right end.
(a) The right end is to remain tangent to a straight line between the two ends. (The line rotates as the beam deforms.)
(b) The right end is to rotate half as much as the midpoint of the beam, but in the opposite direction.

13.2-5 Consider the equations $8u_1 - 4u_2 = -20$, $-4u_1 + 8u_2 = 4$.
(a) To what simple arrangement of identical springs does this equation correspond?
(b) Impose the constraint $u_1 = 0$ by the Lagrange multiplier method. Solve for u_2 and λ and interpret the meaning of λ.
(c) Impose the constraint $u_1 = -1$ by the Lagrange multiplier method. Solve for u_2 and λ, and interpret the meaning of λ.

13.3-1 (a) Verify that Eq. 13.3-3 follows from Eqs. 13.3-1 and 13.3-2.
(b) Revise the argument associated with Eq. 13.3-7: do not assume that all penalty numbers are equal or that $\{\mathbf{Q}\} = \{\mathbf{0}\}$. Is the same conclusion about locking obtained?

13.3-2 Solve the problem of Fig. 13.1-2. That is, impose the constraint $v_1 = v_2$ by means of a penalty number, and solve for v_1 and v_2. Check the limiting cases $\alpha = 0$ and $\alpha = \infty$.

13.3-3 Solve Problem 13.2-3, but use a penalty number rather than a Lagrange multiplier. For $k = 1$, tabulate computed values of u_1 and u_2 for the multiplier values $\alpha = 1$, 4, 10, and 100.

13.3-4 Use the penalty method to solve (a) Problem 13.2-4(a), and (b) Problem 13.2-4(b).

13.4-1 (a) Let a single Mindlin beam element be simply supported at nodes 1 and 2 and loaded in pure bending. Use Eqs. 13.4-2 to show that exact integration gives an element strain energy U consistent with an effective moment of inertia $I_e = I(1 + GL^2/1.2Et^2)$, where $I = bt^3/12$ for a rectangular cross section.
(b) What is the effective moment of inertia if U_s is integrated by one-point quadrature?

13.4-2 Use one Mindlin beam element to model a cantilever loaded by tip moment (see Fig. 15.4-1b; replace P by M_2). The stiffness matrix appears in Eq. 15.4-5, in which $l = L/3$ for exact integration and $A_s = 5bt/6$ for a rectangular cross section. If $\nu = 0$, for what value of L/t does the exactly integrated element provide a lateral deflection at node 2 that is 90% of the correct value?

13.4-3 The constraint of no net volume change in a plane element under plane strain conditions is $\iint (\varepsilon_x + \varepsilon_y)\, dx\, dy = 0$. For a rectangular bilinear element (Section 3.6), show that the same result is produced by setting $\varepsilon_x + \varepsilon_y = 0$ in a one-point quadrature rule.

13.5-1 Plane triangles (a) and (b) shown have homogeneous material, uniform thickness, straight sides, and uniformly spaced side nodes. Their stiffness matrices can be exactly integrated, by a six-point rule for triangle (a) and by a ten-point rule for triangle (b). In a refined mesh, for an incompressible material, what constraint ratios do the respective elements provide?

13.5-2 (a) Show that λ of Eq. 13.6-2 is $\lambda = (\sigma_x + \sigma_y + \sigma_z)/3$.
(b) Show that $\beta\alpha H$ in Eq. 13.4-8 can be expressed as $B\varepsilon_V^2/2$.

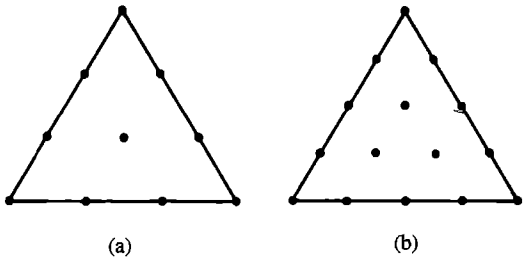

Problem 13.5-1

CHAPTER 14

SOLIDS OF REVOLUTION

Methods for analysis of axisymmetric solids are described in this chapter. The formulation for axisymmetric loading is described first, then the formulation for loads without axial symmetry. Stress analysis is emphasized; see Chapter 12 for other axisymmetric field problems.

14.1 INTRODUCTION. ELASTICITY RELATIONS FOR AXIAL SYMMETRY

A solid of revolution is generated by revolving a planar area about an axis in the same plane. Everyday examples include a hose nozzle and a light bulb, although the light bulb has a thin wall and would be classified as a *shell* of revolution for analysis purposes. Convenient coordinates for axisymmetric geometry are r (radial), θ (circumferential), and z (axial). When geometry, elastic properties, loads, and boundary conditions are all axisymmetric, nothing varies in the θ direction and material points have only the displacement components u and w, in radial and axial directions respectively. Thus the problem is *mathematically* two-dimensional. Indeed, an FE mesh for an axisymmetric problem resembles a plane mesh, and minor changes in software allow subroutines originally intended for plane problems to apply also to axisymmetric problems. Due to the close relation between plane and axisymmetric FE analyses, software may require an axisymmetric mesh to be constructed using axis labels x and y rather than axis labels r and z, which are favored in classical theory and are used in the present chapter.

Figure 14.1-1 depicts a single axisymmetric element of rectangular cross section. Element geometry is toroidal, with nodal circles rather than nodal points. The cross section

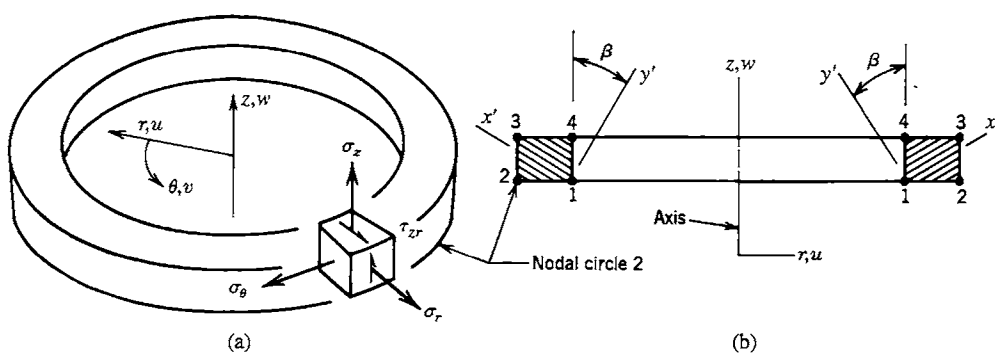

Figure 14.1-1. (a) An axisymmetric finite element, showing stresses associated with axisymmetric loading. (b) Hatching in the element cross section suggests an orthotropic material whose principal axes are x', y', and θ.

of an axisymmetric solid meshed by elements of triangular cross section is depicted in Fig. 1.4-1. By avoiding division into elements in the circumferential direction—that is, by not using a 3D mesh—computational demands are greatly reduced.

If the problem involves vibration or buckling, both symmetric and *un*symmetric displacement modes are possible, even if geometry, elastic properties, and boundary conditions are all axisymmetric. Unsymmetric modes are often the most important, and would be excluded by axisymmetric analysis.

Elasticity Relations. As usual, constitutive relations of a linearly elastic material can be written in the forms

$$\{\boldsymbol{\sigma}\} = [\mathbf{E}]\{\boldsymbol{\varepsilon}\} + \{\boldsymbol{\sigma}_0\} \text{ or } \{\boldsymbol{\sigma}\} = [\mathbf{E}](\{\boldsymbol{\varepsilon}\} - \{\boldsymbol{\varepsilon}_0\}) \text{ where } \{\boldsymbol{\sigma}_0\} = -[\mathbf{E}]\{\boldsymbol{\varepsilon}_0\} \quad (14.1\text{-}1)$$

If the trivial relations $\tau_{r\theta} = 0$ and $\tau_{\theta z} = 0$ are omitted, the most general axisymmetric form of Eq. 14.1-1 is

$$\begin{Bmatrix} \sigma_r \\ \sigma_\theta \\ \sigma_z \\ \tau_{zr} \end{Bmatrix} = \begin{bmatrix} E_{11} & E_{12} & E_{13} & E_{14} \\ & E_{22} & E_{23} & E_{24} \\ & & E_{33} & E_{34} \\ \text{symm.} & & & E_{44} \end{bmatrix} \left(\begin{Bmatrix} \varepsilon_r \\ \varepsilon_\theta \\ \varepsilon_z \\ \gamma_{zr} \end{Bmatrix} - \{\boldsymbol{\varepsilon}_0\} \right) \quad (14.1\text{-}2)$$

If the material is orthotropic, Fig. 14.1-1b, principal material axes x' and y' must not change direction with θ, and the third principal material axis must not form a helix about the axis of revolution. If $\beta = 0$ in Fig. 14.1-1b, then $E_{14} = E_{24} = E_{34} = 0$. Finally, for the case of isotropy and thermal loading, Eq. 14.1-2 becomes

$$\begin{Bmatrix} \sigma_r \\ \sigma_\theta \\ \sigma_z \\ \tau_{zr} \end{Bmatrix} = \frac{(1-\nu)E}{(1+\nu)(1-2\nu)} \begin{bmatrix} 1 & f & f & 0 \\ & 1 & f & 0 \\ & & 1 & 0 \\ \text{symm.} & & & g \end{bmatrix} \left(\begin{Bmatrix} \varepsilon_r \\ \varepsilon_\theta \\ \varepsilon_z \\ \gamma_{zr} \end{Bmatrix} - \begin{Bmatrix} \alpha T \\ \alpha T \\ \alpha T \\ 0 \end{Bmatrix} \right) \quad (14.1\text{-}3a)$$

in which

$$f = \frac{\nu}{1-\nu} \quad \text{and} \quad g = \frac{1-2\nu}{2(1-\nu)} \quad (14.1\text{-}3b)$$

Here T is temperature change, usually relative to a reference temperature at which the body is considered free of stress, and α is a temperature-independent coefficient of thermal expansion. Remarks on a temperature-dependent α appear in Section 3.1. For isotropy, E_{44} in Eq. 14.1-2 becomes G, the shear modulus.

At arbitrary radius r, circumferential strain is change in circumference divided by original circumference:

$$\varepsilon_\theta = \frac{2\pi(r+u) - 2\pi r}{2\pi r} = \frac{u}{r} \quad (14.1\text{-}4)$$

The complete strain-displacement relations for axisymmetric conditions are

$$\begin{Bmatrix} \varepsilon_r \\ \varepsilon_\theta \\ \varepsilon_z \\ \gamma_{zr} \end{Bmatrix} = [\partial]\begin{Bmatrix} u \\ w \end{Bmatrix} \qquad \text{where} \qquad [\partial] = \begin{bmatrix} \partial/\partial r & 0 \\ 1/r & 0 \\ 0 & \partial/\partial z \\ \partial/\partial z & \partial/\partial r \end{bmatrix} \tag{14.1-5}$$

Except for the change in axis labels and the addition of circumferential strain ε_θ, these relations are the same as the first of Eqs. 3.1-9.

14.2 AXISYMMETRIC SOLID ELEMENTS

In the formulation of element matrices, axisymmetric elements and plane elements differ only in details. The displacement field of a four-node, eight-d.o.f. bilinear element is

$$\begin{Bmatrix} u \\ w \end{Bmatrix} = \underbrace{\begin{bmatrix} N_1 & 0 & N_2 & 0 & N_3 & 0 & N_4 & 0 \\ 0 & N_1 & 0 & N_2 & 0 & N_3 & 0 & N_4 \end{bmatrix}}_{[\mathbf{N}]} \begin{Bmatrix} u_1 \\ w_1 \\ u_2 \\ \vdots \\ w_4 \end{Bmatrix} \tag{14.2-1}$$

For a rectangular cross section, Fig. 14.2-1, individual shape functions N_i are as stated in Eqs. 3.6-4. The strain-displacement matrix is $[\mathbf{B}] = [\partial][\mathbf{N}]$. Operator matrix $[\partial]$ is given by Eq. 14.1-5, in which, for local axis labels x and y adopted in Fig. 14.2-1, $r = r_m + x$, $\partial/\partial x$ replaces $\partial/\partial r$, and $\partial/\partial y$ replaces $\partial/\partial z$. Thus, using Eq. 3.3-7, the element stiffness matrix is

$$\underset{8\times 8}{[\mathbf{k}]} = \int_{-b}^{b}\int_{-a}^{a}\int_{-\pi}^{\pi} \underset{8\times 4}{[\mathbf{B}]^T}\underset{4\times 4}{[\mathbf{E}]}\underset{4\times 8}{[\mathbf{B}]}\, r\, d\theta\, dx\, dy \qquad \text{where} \qquad r = r_m + x \tag{14.2-2}$$

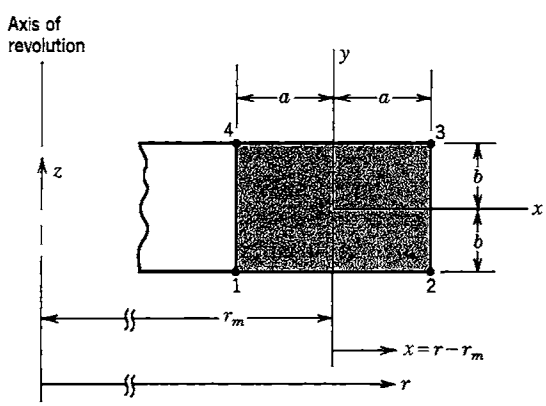

Figure 14.2-1. Geometry of an element of rectangular cross section.

This formula is much the same as the [**k**] formula for a plane element, Eq. 3.6-7. For axial symmetry the integrand is independent of θ, so the limits of circumferential integration in Eq. 14.2-2 can be changed from $-\pi,\pi$ to 0,1 if desired, provided that load terms are also formulated for a one-radian segment. If the axisymmetric element is isoparametric, its equation for [**k**] resembles Eq. 6.2-12 in the same way that Eq. 14.2-2 resembles Eq. 3.6-7. Thus, in changing from plane geometry to axisymmetric geometry, arrays in the integrand are expanded, circumferential integration is added, and $r\,d\theta$ appears instead of thickness t, but the number of d.o.f. per element is not changed. Broadly speaking, *any* axisymmetric element differs from its plane relative by accounting for circumferential strain ε_θ, which in terms of element shape functions N_i and radial displacements u_i in an element having n nodes is

$$\varepsilon_\theta = \frac{1}{r}(N_1u_1 + N_2u_2 + \cdots + N_nu_n) \tag{14.2-3}$$

Remarks. If the four-node element in Fig. 14.2-2a were *plane* rather than axisymmetric, it would have a rigid-body mode and could not support moment load M. For an axisymmetric element, M is a "ring rolling" moment, or moment per unit of circumferential length, whose dimensions are force • length/length or simply force. Ring rolling is resisted by circumferential strains, which for the direction of M shown are compressive around the upper portion, tensile around the lower portion, and vary linearly in the z direction [1.16,2.6].

If $r_m >> 2a$ in Fig. 14.2-2a, element circumferential stiffness becomes much less than the stiffness with which the element resists deformation of its cross section in an rz plane. That is, we encounter the case of a large stiffness supported by a small stiffness, which tends to make equations ill-conditioned, as described in Section 9.2. Thus, mesh refinement that makes elements extremely slender may decrease accuracy rather than increase it [14.1].

Some displacement-based elements contain incompatible modes. Let the QM6 element described in Section 6.6 be formulated as axisymmetric. When loaded radially as shown in Fig. 14.2-2b, internal d.o.f. are activated, creating the spurious bulge shown [14.2]. The bulge is associated with spurious shear strain γ_{zr} at all points in the element but its horizontal centerline, which suggests that during postprocessing γ_{zr} should be evaluated only at the center of a QM6 element. The bulge approaches zero for $r_m >> 2a$.

Some terms in the stiffness matrix integrand contain radius r in the denominator. With Gauss quadrature these terms do not become infinite because there are no Gauss points at $r = 0$. However, for elements close to the z axis, accuracy may be improved by use of more Gauss points in the radial direction than would be used for analogous plane elements. If [**k**] is to be integrated explicitly and the element has nodes on the z axis, one can formulate special "core" elements by using a displacement field in which $u = 0$ at $r = 0$ and using L'Hôpital's rule to evaluate indeterminate forms 0/0.

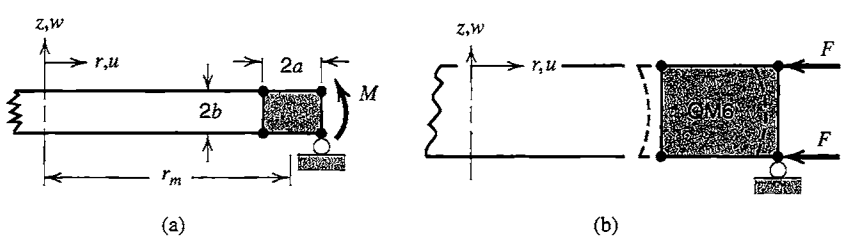

Figure 14.2-2. (a) A single axisymmetric element loaded by moment M.
(b) Radial loads F on an axisymmetric element having incompatible modes. Dashed lines show the displaced shape.

A uniform line load of intensity q around a circle of radius r is described as a force of magnitude $2\pi rq$, even if the load is radially directed so that its resultant is statically equivalent to zero. If integration spans one radian rather than the entire circle, the force is described as rq rather than $2\pi rq$. For spinning at angular velocity ω about the z axis, element nodal loads are, from Eq. 3.3-8,

$$\{\mathbf{r}_e\} = \iint_{-\pi}^{\pi} [\mathbf{N}]^T \begin{Bmatrix} \rho r \omega^2 \\ 0 \end{Bmatrix} r \, d\theta \, dA \tag{14.2-4}$$

where ρ is the mass density and A is the element cross-sectional area. For dynamic analysis, an element mass matrix is needed. From Eq. 11.2-6,

$$[\mathbf{m}] = \iint_{-\pi}^{\pi} [\mathbf{N}]^T [\mathbf{N}] \rho r \, d\theta \, dA \tag{14.2-5}$$

Note, however, that problems of vibration and dynamics are almost certain to require that nonaxisymmetric modes be taken into account.

As for boundary conditions, restraint of axial displacement w on a single nodal circle is sufficient to prevent rigid-body motion, as suggested for single elements in Fig. 14.2-2. Radial displacement u should be suppressed at all nodes that lie on the axis of revolution. Otherwise, $u \neq 0$ at these nodes implies existence of a pinhole, which doubles the circumferential stress at $r = 0$. General-purpose software may be coded so that the condition $u = 0$ is automatically assigned to nodes for which $r = 0$.

In calculation of strain and stress in elements that touch the axis of revolution, if strains are calculated at $r = 0$ rather than being extrapolated to $r = 0$ from Gauss point stresses, we encounter the calculation $\varepsilon_\theta = 0/0$. The situation can be avoided by instead calculating $\varepsilon_r = \partial u/\partial r$ at $r = 0$, then equating ε_θ to ε_r. This trick exploits the theoretical requirement that $\varepsilon_\theta = \varepsilon_r$ for points on $r = 0$. In software these considerations are hidden from the user, and it may be of interest to run a simple test case with isotropic material to discover if indeed $\sigma_r = \sigma_\theta$ is computed at $r = 0$.

In a curved beam or pipe loaded by pure moment (Figs. 6.15-1 and 10.2-2), structure geometry is axisymmetric but the analysis problem is not because displacements have circumferential components as well as radial and axial components. An FE analysis that requires no discretization in the circumferential direction is available [14.3,14.4], but it requires that the usual array of nodal d.o.f. be augmented by a single "global" d.o.f. that is associated with all elements, so the method is not contained in standard software, and a 3D analysis like that described in Section 6.15 may be required.

14.3 AN APPLICATION

Figure 14.3-1 depicts the cross section of an axisymmetric structure, already meshed with eight-node quadrilateral elements. The structure consists of an outer disk *BEFC* of uniform thickness, attached to a tapered inner disk *DABE* of the same material by means of a shrink fit. Physically, the shrink fit is accomplished by heating the outer disk, slipping it over the inner disk, then allowing the entire structure to return to the uniform initial temperature. Dimensions

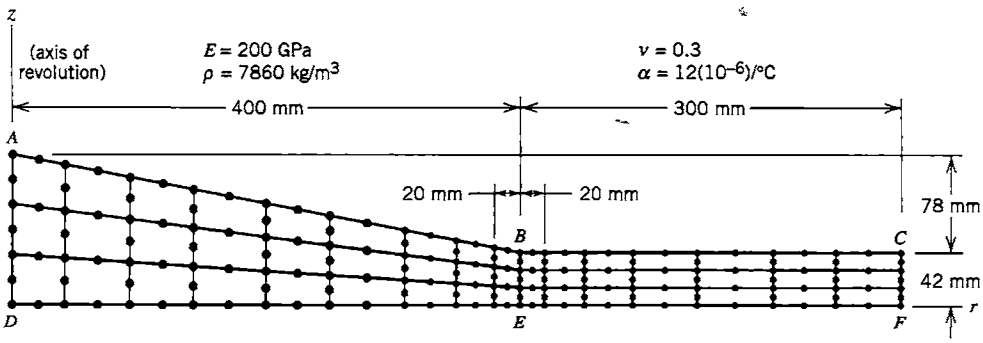

Figure 14.3-1. Mesh of eight-node elements on the cross section of a solid of revolution.

are such that when the outer disk is 100 °C hotter than the inner disk, the inner radius of the outer disk and the outer radius of the inner disk are both precisely 400 mm. We ask

1. What contact stresses along BE are produced by the shrink fit?
2. If the assemblage is set spinning about the z axis, at what angular velocity will the shrink fit loosen?

In seeking answers we will discover that question 1 has aspects not likely to be anticipated without careful thought, and that question 2 is not well posed and requires some analytical thinking.

Preliminary Analysis. Consider first the contact pressure p produced by the shrink fit. For a simple approximation we choose a mathematical model in which inner and outer disks have the same uniform thickness (Fig. 14.3-2). For analysis we assume that dimension h is small enough that the outer disk can be treated by simple formulas applicable to a thin ring. Thus, with R the mean radius of the outer disk, $\sigma_\theta = pR/h$, $\sigma_r = 0$, $\varepsilon_\theta = (\sigma_\theta - \nu\sigma_r)/E = pR/Eh$, and $u_i = r_i\varepsilon_\theta = pRr_i/Eh$ is the approximate radial displacement at the inner edge of the outer disk due to p. In addition, temperature change produces radial displacement $u_i = \alpha r_i T$ at the same location, where the temperature change is $T = -100$ °C in our case. In the inner disk, $\sigma_\theta = \sigma_r = -p$, and radial displacement at $r = r_i$ is $u_i = r_i\varepsilon_\theta = r_i(\sigma_\theta - \nu\sigma_r)/E = -pr_i(1 - \nu)/E$. Equating the u_i expressions, we obtain

$$\frac{pRr_i}{Eh} + \alpha r_i T = -\frac{pr_i}{E}(1 - \nu) \qquad \text{hence} \qquad p = -\frac{E\alpha T}{(1 - \nu) + \dfrac{R}{h}} \tag{14.3-1}$$

from which $p = 95$ MPa for the data of Figs. 14.3-1 and 14.3-2. Hence, in the outer disk, $\sigma_\theta \approx pR/h = 174$ MPa.

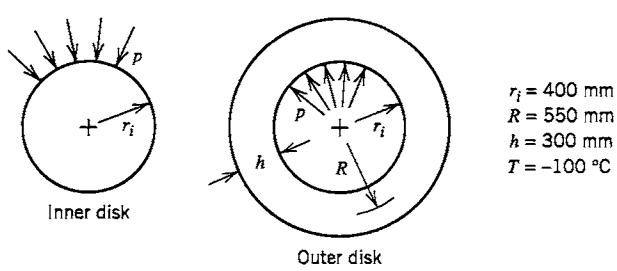

Figure 14.3-2. Model for approximate analysis of shrink fit pressure p.

For approximate analysis of stresses due to spinning, we use the same mathematical model and a handbook formula for radial stress in a thin flat disk with no central hole, of outer radius a, mass density ρ, spinning at angular velocity ω [1.16,2.6]:

$$\sigma_r = \frac{3+\nu}{8}\rho\omega^2(a^2 - r^2) \tag{14.3-2}$$

Using $a = 0.700$ m and setting $\sigma_r = 95$ MPa at $r = 0.400$ m, we obtain $\omega = 298$ rad/s as the approximate angular velocity at which the shrink fit should loosen.

Of course the inner disk is thicker and therefore stiffer than assumed in the foregoing approximation, which means that the actual shrink fit p is expected to be larger than 95 MPa. Also, the structure is not symmetric about a z = constant plane. The shape in Fig. 14.3-1 leads us to expect that the outer part will bend *downward* due to the shrink fit and *upward* due to spinning. Near point E, radial flexural stress will increase the magnitude of (compressive) shrink fit contact stress and increase the magnitude of (tensile) radial stress due to spinning.

Finite Element Analysis. The FE mesh in Fig. 14.3-1 is perhaps overly refined for an initial model, but is easy to generate. Each node has two d.o.f., namely radial and axial displacements. Both are set to zero at node D. At other nodes along AD, only radial displacement is set to zero. All nodes not on the z axis are unrestrained. Shrink fit loading is produced by stating that portion $BEFC$ is uniformly decreased in temperature by 100 °C. Implicit in this procedure is the assumption that there is no slipping in the axial direction on the surface of contact. Spinning is treated as a separate load case. Spinning creates inertia (body force) loading, for which appropriate radial forces on individual nodes are computed automatically by the software. Details of the analysis for spinning are discussed in what follows.

Critique of Results. By inspection, deflected shapes (not shown) are found to agree with expectations. More specifically, animation of deflections shows that nodes along AD move only axially, as intended. The cross section shown in Fig. 14.3-1 deflects like a beam cantilevered from AD, downward for the shrink fit and upward due to spinning. In addition, tip CF moves radially a small amount, inward for the shrink fit and outward due to spinning.

Contours of radial stress σ_r produced by the shrink fit are shown in Fig. 14.3-3a. Along BE the average magnitude of σ_r is in rough agreement with the predicted value of –95 MPa, but contours show severe interelement discontinuities. Is something wrong? Our FE model implies that a bond is created as soon as inner and outer disks make contact, and that the bond is thereafter unbroken. Therefore, the disks apply both r-direction *and* z-direction forces to one another across interface BE. In simplifying the problem to obtain Eq. 14.3-1 we have ignored the z-direction forces. They arise because temperature decrease in the outer disk causes it to contract axially as well as radially. Additionally, circumferential stresses in inner and outer disks are, respectively, compressive and tensile. The associated Poisson-effect axial strains are, respectively, tensile and compressive, and therefore add to axial thermal strains. To maintain identical z-direction lengths along BE, as the foregoing FE model demands, inner and outer disks must apply z-direction forces to one another along BE. These forces perturb the stress field locally. Mesh refinement is needed in this region to provide more detail. Computed results for a bimetal problem, Fig. 3.15-3b, lead us to suspect that stress singularities exist at B and E.

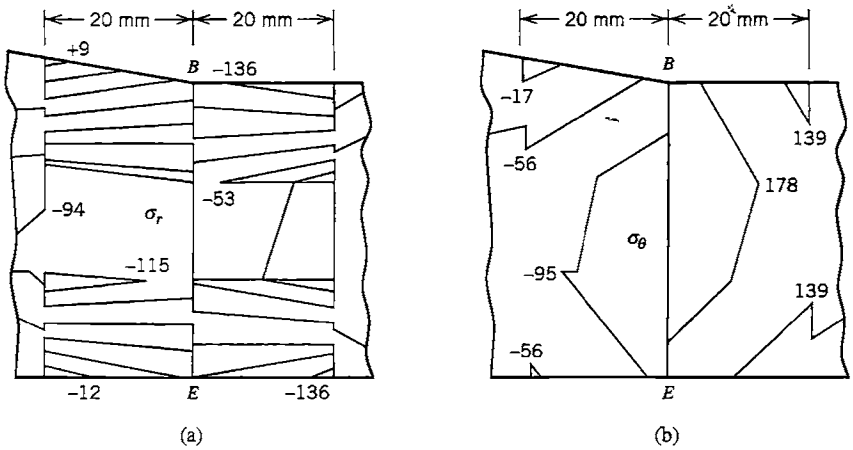

Figure 14.3-3. Stresses due to shrink fit: unaveraged stress contours from FEA in MPa. (a) Radial stress σ_r. (b) Circumferential stress σ_θ.

Circumferential stresses σ_θ produced by the shrink fit appear to be reliable (Fig. 14.3-3b). Viewing inner and outer disks separately, we see that interelement continuity of σ_θ stress contours is fair to good near *BE*. Continuity of σ_θ across *BE* is neither seen nor expected. The relative error defined in Eq. 9.10-7 is $\eta = 0.28$, which is quite high—but this is for the *entire* FE model, which represents a misapplication of the error estimate, which should not include discontinuities such as the known discontinuity of σ_θ across *BE*. The error estimate can legitimately be applied to the meshes of inner and outer disks separately, for which the respective values are $\eta = 0.17$ and $\eta = 0.09$. If we exclude from each mesh the three elements nearest *BE* (six elements altogether), we obtain the respective values $\eta = 0.04$ and $\eta = 0.02$. Clearly, mesh refinement is needed near *BE*. For the case of spinning, discussed in what follows, no discontinuity of stress appears across *BE*, and $\eta = 0.004$ for the entire mesh.

Next consider spinning at $\omega = 298$ rad/s, which is the approximate loosening speed calculated after Eq. 14.3-2. Stress contours due to this loading alone are shown in Fig. 14.3-4. Interelement continuity is good, and these plots give no reason to doubt the results. Radial

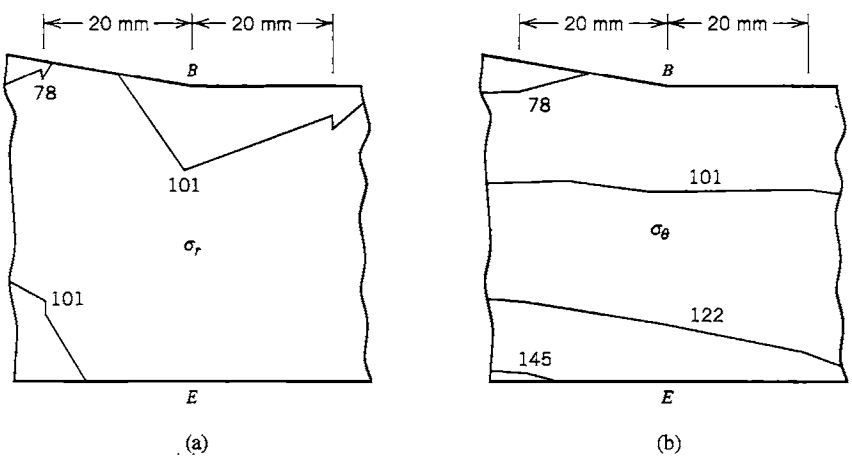

Figure 14.3-4. Stresses due to spinning about the z axis at $\omega = 298$ rad/s: unaveraged stress contours from FEA in MPa. (a) Radial stress σ_r. (b) Circumferential stress σ_θ.

stress near BE is approximately 100 MPa, about what is needed to cancel the compressive radial stress due to the shrink fit. Does this mean that $\omega = 298$ rad/s is indeed the ω at which the shrink fit will loosen? Because σ_r is not uniform along BE, we now realize that we have been unclear about what is meant by "loosen." Is it when contact along BE is completely broken, or is it when the superposed results of shrink fit and spinning give zero σ_r at some point along BE? The speed for complete separation along BE can be obtained by writing an equation analogous to Eq. 14.3-1 and solving for ω.

$$\omega^2\delta_1 = \omega^2\delta_2 + \alpha r_i T \tag{14.3-3}$$

where δ_1 is the largest radial deflection in the inner disk along BE, computed by FEA applied to the inner disk *alone* spinning at $\omega = 1$ rad/s, and δ_2 is the radial deflection along BE in the outer disk *alone* spinning at $\omega = 1$ rad/s, calculated by an available formula for spinning of a thin flat disk with a central hole [1.16]. In Eq. 14.3-3 we use ω^2, not ω, because stresses and displacements are proportional to the square of angular velocity. As in Eq. 14.3-1, $T = -100$ °C.

The other question, about the lowest speed for which the net σ_r falls to zero at some point along BE, requires accurate values of σ_r along BE due to shrink fit loading. At a node j along BE, let us symbolize shrink fit radial stress values by $[(\sigma_r)_T]_j$. Let $[(\sigma_r)_\omega]_j$ represent radial stress at node j due to spinning (of the *entire* disk) at angular velocity $\omega = 1$ rad/s. The latter stress is easily determined by dividing a nodal σ_r previously obtained by the ω^2 used to compute it. The ω for which loosening would appear at node j is obtained by solving for ω in the equation

$$\omega^2\left[(\sigma_r)_\omega\right]_j + \left[(\sigma_r)_T\right]_j = 0 \tag{14.3-4}$$

The calculation must be done for all nodes j along BE. The smallest of the several calculated values of ω is chosen as the desired result. Note that Eq. 14.3-4 is not applicable after the onset of loosening, as the continuity presumed by the FE model is then lost.

14.4 LOADS WITHOUT AXIAL SYMMETRY: INTRODUCTION

If geometry and material properties are axisymmetric but loads and/or boundary conditions are not, the problem is three-dimensional in the sense that every field quantity is a function of all three coordinates. Thus displacement components u (radial), v (circumferential), and w (axial) are each functions of r, θ, and z. Similarly, all six possible stress components (Fig. 14.4-1) are in general nonzero and are functions of r, θ, and z.

In what follows we consider how a load can be represented by components in the form of trigonometric series, an analysis made for each component separately, and results combined to produce the solution for the original loading. Commercial software provides for this kind of analysis. Its advantage is that no division into elements in the θ direction is required, so that instead of solving one large 3D problem, we instead solve a few 2D problems and combine results. Thus, data preparation is simplified and the analysis is much less demanding of computer resources.

In the present section we discuss basic relations of the analysis method. Specifics pertinent to FEA appear in Section 14.5.

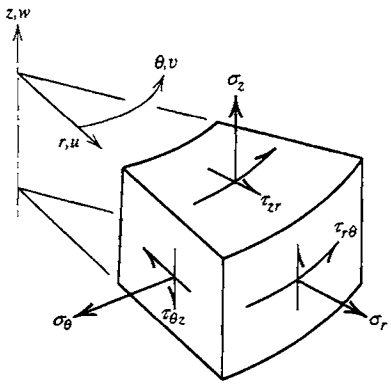

Figure 14.4-1. Stresses and displacements in an axisymmetric body with nonaxisymmetric loads.

Loads. Loading applied to a solid or shell of revolution can be described as the sum of its series components. Let q represent load in general, such as normal pressure, line load, or temperature in thermal stress analysis. A Fourier series representation of q is

$$q = \sum_{n=0}^{\infty} q_n^c \cos n\theta + \sum_{n=0}^{\infty} q_n^s \sin n\theta \tag{14.4-1}$$

where q_n^c and q_n^s are load amplitudes that depend on n (but not on θ). Here n is an integer that represents the harmonic number. Loads described by q can be radial, axial, or circumferential. A load state symmetric with respect to the $\theta = 0$ plane is described by the cosine series for radial and axial loads and by the sine series for circumferential loads. By locating the $\theta = 0$ plane appropriately, it often happens that only one of the two series is needed. Typical problems are solved accurately enough by using only the first few terms of the load series.

An example of a load series appears in Fig. 14.4-2a, where a radial load q, partly outward and partly inward but otherwise uniform, is represented by the sine series. Cosine terms of Eq. 14.4-1 are not needed (although the loading could be described by cosine terms alone if the $\theta = 0$ plane were placed 90° to the position shown). Load components associated with the first two nonzero terms of the sine series are shown in Fig. 14.4-2b,c. The initial term, Fig. 14.4-2b, might be used alone as a simple approximation of wind loading on (say) a power plant cooling tower.

Additional examples appear in Fig. 14.4-3. The radial load of Fig. 14.4-3a is described by the initial term ($n = 0$) of the cosine series. Here the load is axisymmetric and so is the structure's response to it. The load of Fig. 14.4-3b is also described by the initial term of the cosine series, but because the load is torsional, the structure's response is not symmetric with respect to the $\theta = 0$ plane or any other radial plane. In Fig. 14.4-3c, concentrated loads P at $\theta = \pm\pi/2$, both radially outward, are represented by the series

$$q = \frac{2P}{\pi a t}\left(\frac{1}{2} + \sum_{n=2,4,6,\ldots}^{\infty} \cos\frac{n\pi}{2}\cos n\theta\right) \tag{14.4-2}$$

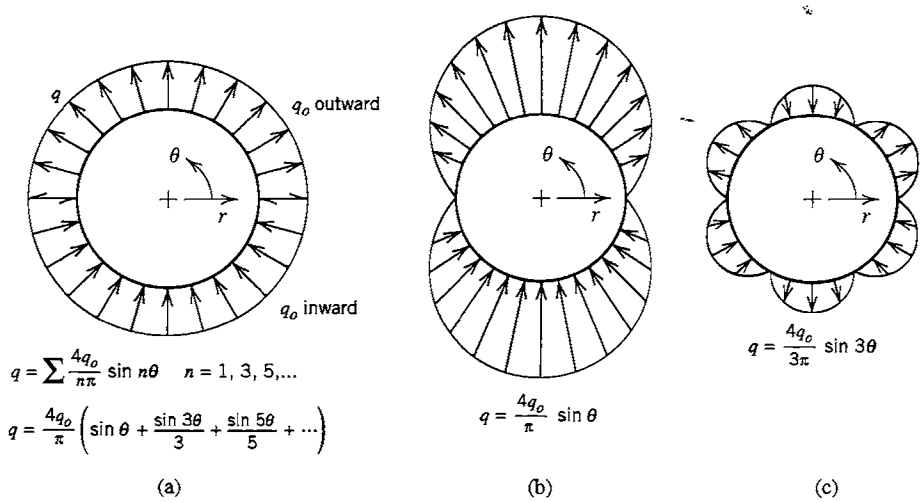

Figure 14.4-2. (a) A uniformly distributed load, alternately inward and outward, and its representation by a Fourier series. (b,c) Loads associated with the first two nonzero series terms.

In deriving this formula we imagine that a radial stress σ acts on an area that spans t units axially and $2a\theta_0$ units circumferentially at each load location, then let $2\sigma a\theta_0 t$ approach P as θ_0 approaches zero. The load becomes concentrated, rather than distributed along a strip of length t in an rz plane, as t approaches zero. The series of Eq. 14.4-2 does not converge, but it leads to convergent displacements and stresses in FEA. When loads are concentrated, many series terms may be needed for adequate accuracy. Loads that vary more gradually in the θ direction require fewer series terms.

A load described by Eq. 14.4-1 may vary with r or z, or may be applied to a single nodal circle, in which case it represents a circumferential line load or perhaps one or more concentrated loads (as in Eq. 14.4-2). Prescribed nonzero displacements in the coordinate directions can be described by similar series. The series representation of a prescribed load or displacement function can be calculated by standard methods of Fourier series analysis. Results applicable to some common loadings may be found in standard mathematical tables. Typically, the software user can either calculate series terms and provide them as input data, or ask the software to calculate them from a description of the loading.

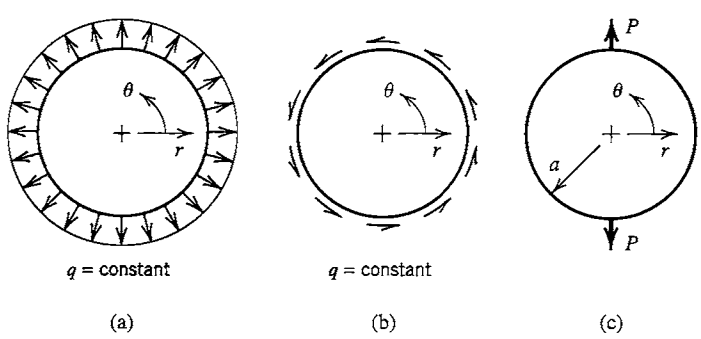

Figure 14.4-3. Further examples of loads. The second is a torsional load.

Stresses, Strains, and Displacements. With θ a principal material direction, the most general stress-strain relation $\{\boldsymbol{\sigma}\} = [\mathbf{E}]\{\boldsymbol{\varepsilon}\}$ is

$$\begin{Bmatrix} \sigma_r \\ \sigma_\theta \\ \sigma_z \\ \tau_{zr} \\ \tau_{r\theta} \\ \tau_{\theta z} \end{Bmatrix} = \begin{bmatrix} E_{11} & E_{12} & E_{13} & E_{14} & 0 & 0 \\ & E_{22} & E_{23} & E_{24} & 0 & 0 \\ & & E_{33} & E_{34} & 0 & 0 \\ & & & E_{44} & 0 & 0 \\ & \text{symmetric} & & & E_{55} & E_{56} \\ & & & & & E_{66} \end{bmatrix} \begin{Bmatrix} \varepsilon_r \\ \varepsilon_\theta \\ \varepsilon_z \\ \gamma_{zr} \\ \gamma_{r\theta} \\ \gamma_{\theta z} \end{Bmatrix} \tag{14.4-3}$$

If r and z are also principal material directions, or if the material is isotropic, then $E_{14} = E_{24} = E_{34} = E_{56} = 0$. If the material is isotropic, then $E_{55} = E_{66} = G$, where G is the shear modulus.

Strain-displacement relations in cylindrical coordinates are [3.1]

$$\begin{Bmatrix} \varepsilon_r \\ \varepsilon_\theta \\ \varepsilon_z \\ \gamma_{zr} \\ \gamma_{r\theta} \\ \gamma_{\theta z} \end{Bmatrix} = [\partial]\begin{Bmatrix} u \\ v \\ w \end{Bmatrix} \quad \text{where} \quad [\partial] = \begin{bmatrix} \partial/\partial r & 0 & 0 \\ 1/r & (\partial/\partial\theta)/r & 0 \\ 0 & 0 & \partial/\partial z \\ \partial/\partial z & 0 & \partial/\partial r \\ (\partial/\partial\theta)/r & (\partial/\partial r - 1/r) & 0 \\ 0 & \partial/\partial z & (\partial/\partial\theta)/r \end{bmatrix} \tag{14.4-4}$$

These relations are independent of material properties. Displacements u, v, and w may or may not be described by series.

Let displacement components be described by sine and cosine series:

Radial displacement: $$u = \sum_{n=0}^{\infty} \bar{u}_n \cos n\theta + \sum_{n=0}^{\infty} \bar{\bar{u}}_n \sin n\theta \tag{14.4-5a}$$

Circumferential displacement: $$v = \sum_{n=0}^{\infty} \bar{v}_n \sin n\theta - \sum_{n=0}^{\infty} \bar{\bar{v}}_n \cos n\theta \tag{14.4-5b}$$

Axial displacement: $$w = \sum_{n=0}^{\infty} \bar{w}_n \cos n\theta + \sum_{n=0}^{\infty} \bar{\bar{w}}_n \sin n\theta \tag{14.4-5c}$$

where $\bar{u}_n$, $\bar{\bar{u}}_n$, ..., $\bar{\bar{w}}_n$ are amplitudes of displacement that in general depend on r, z, and n but are independent of θ. Single-barred series describe displacement states that are symmetric with respect to $\theta = 0$; double-barred series describe displacement states that are antisymmetric with respect to $\theta = 0$. The motivation for the arbitrarily chosen negative sign in Eq. 14.4-5b is explained in remarks that follow Eq. 14.5-9.

Consider a typical harmonic of displacement, say the nth. If we substitute Eqs. 14.4-5 into Eqs. 14.4-4 and the resulting strains into Eq. 14.4-3, we find that stresses of the nth harmonic of the single-barred series have the form

$$\lfloor \sigma_{rn} \ \sigma_{\theta n} \ \sigma_{zn} \ \tau_{zrn} \rfloor = \lfloor \bar{\sigma}_{rn} \ \bar{\sigma}_{\theta n} \ \bar{\sigma}_{zn} \ \bar{\tau}_{zrn} \rfloor \cos n\theta \tag{14.4-6a}$$

$$\lfloor \tau_{r\theta n} \ \tau_{\theta zn} \rfloor = \lfloor \bar{\tau}_{r\theta n} \ \bar{\tau}_{\theta zn} \rfloor \sin n\theta \tag{14.4-6b}$$

where the barred terms are functions of r, z, and n but not θ. Analogous expressions are obtained from the double-barred series. When Eqs. 14.4-6 are substituted into the three differential equations of equilibrium expressed in cylindrical coordinates [3.1], we obtain expressions having the forms

$$\bar{Q}_1 \cos n\theta = 0 \qquad \bar{Q}_2 \cos n\theta = 0 \qquad \bar{Q}_3 \sin n\theta = 0 \tag{14.4-7}$$

where the $\bar{Q}_i$ are functions of r, z, and n but not θ. Equations 14.4-7 must prevail for all θ; hence $\bar{Q}_1 = \bar{Q}_2 = \bar{Q}_3 = 0$. In the FE context, equations analogous to the equations $\bar{Q}_1 = \bar{Q}_2 = \bar{Q}_3 = 0$ are

$$[\mathbf{K}_n]\{\bar{\mathbf{D}}_n\} - \{\bar{\mathbf{R}}_n\} = \{\mathbf{0}\} \tag{14.4-8}$$

in which $[\mathbf{K}_n]$ is independent of θ, and $\{\bar{\mathbf{D}}_n\}$ and $\{\bar{\mathbf{R}}_n\}$ respectively contain amplitudes of nodal d.o.f. and nodal load in the nth harmonic. The size of $[\mathbf{K}_n]$ is $3N$ by $3N$ for an FE model having N nodes and translational d.o.f. only. The same is true if double-barred series were used instead. If both series are used simultaneously, the size of $[\mathbf{K}_n]$ is doubled. But in all these cases, Eq. 14.4-8 pertains to a single harmonic. Harmonic n of load produces only harmonic n of displacement; that is, *the different Fourier harmonics are not coupled.* A single FE mesh is used for analysis of each harmonic. Equation 14.4-8 is generated and solved for $n = 1$, then for $n = 2$, and so on. The number of harmonics needed depends on the accuracy required and the nature of the loading. Nodal amplitudes provided by the separate analyses must be superposed according to Eqs. 14.4-5, but no division into elements in the circumferential direction is required.

Related Problems. The Fourier series treatment has been used in classical plate theory for well over 100 years. When applied to plates in an FE context, the Fourier series method is known as the *finite strip method* [14.5]. For a brief explanation, consider finite strip analysis of a rectangular plate in the xy plane with its two x-parallel edges simply supported. By making cuts parallel to the y axis, the plate is sliced into narrow strips. In the y direction, a sine series for lateral deflection satisfies simply supported boundary conditions. The pattern of loading in the y direction can also be expressed by a sine series. In the x direction, FE shape functions are used, so that each strip element has four d.o.f. A typical problem is solved by superposing solutions for a few of the lowest harmonics of load. In its more general form, the finite strip method does not require that opposite edges of a plate be simply supported. The method is also well suited to folded plates and to box beams, either straight or curved.

Prismatic solids can be analyzed by Fourier series, in which case the method may be called a "finite prism method" [14.5,14.6]. Conceptually, a prismatic geometry can be

obtained by straightening an axially symmetric solid. This viewpoint suggests that a prismatic solid might be idealized as axisymmetric if it is described as a toroidal ring of very large radius. However, equations of the resulting FE structure may be ill-conditioned, as suggested in remarks that follow Eq. 14.2-3.

14.5 LOADS WITHOUT AXIAL SYMMETRY: SOME DETAILS OF FEA

In the following discussion we give greatest attention to the single-barred displacement series of Eqs. 14.4-5. Within an element, one can interpolate Fourier amplitudes $\bar{u}_n$, $\bar{v}_n$, and $\bar{w}_n$ from *nodal* Fourier amplitudes $\bar{u}_{in}$, $\bar{v}_{in}$, and $\bar{w}_{in}$, where n is the harmonic number and i is the element node number. We symbolize this relation as $\{\bar{\mathbf{u}}_n\} = [\bar{\mathbf{N}}]\{\bar{\mathbf{d}}_n\}$, where $[\bar{\mathbf{N}}]$ contains the same shape functions as would be used in a plane problem. For example, for harmonic n and the four-node element of Fig. 14.2-1, the relation resembles Eq. 14.2-1:

$$\begin{Bmatrix} \bar{u}_n \\ \bar{v}_n \\ \bar{w}_n \end{Bmatrix} = \left[\begin{array}{ccc|ccc|c|c} N_1 & 0 & 0 & N_2 & 0 & 0 & \cdots & \cdots \\ 0 & N_1 & 0 & 0 & N_2 & 0 & \cdots & \cdots \\ 0 & 0 & N_1 & 0 & 0 & N_2 & \cdots & \cdots \end{array}\right] \{\bar{\mathbf{d}}_n\} \tag{14.5-1a}$$

$$\underbrace{\qquad\qquad}_{1} \quad \underbrace{\qquad\qquad}_{2} \quad \underbrace{\quad}_{3} \quad \underbrace{\quad}_{4}$$

where $$\{\bar{\mathbf{d}}_n\} = \begin{bmatrix} \bar{u}_{1n} & \bar{v}_{1n} & \bar{w}_{1n} & \bar{u}_{2n} & \bar{v}_{2n} & \bar{w}_{2n} & \cdots & \bar{w}_{4n} \end{bmatrix}^T \tag{14.5-1b}$$

An element having more than four nodes has more partitions in Eq. 14.5-1a and more d.o.f. in $\{\bar{\mathbf{d}}_n\}$ and of course uses different shape functions. For a given element, regardless of the number of nodes it contains, different displacement components and different harmonics can all use the same shape functions N_i.

Summation of the various Fourier harmonics provides displacements as stated by Eqs. 14.4-5. These displacements can be stated in matrix format by attaching $\cos n\theta$ to rows 1 and 3 in Eq. 14.5-1a and $\sin n\theta$ to row 2, then summing the harmonics. Thus, for a typical element,

$$\begin{Bmatrix} u \\ v \\ w \end{Bmatrix} = \sum_{n=0}^{\infty} \begin{Bmatrix} \bar{u}_n \cos n\theta \\ \bar{v}_n \sin n\theta \\ \bar{w}_n \cos n\theta \end{Bmatrix} = \sum_{n=0}^{\infty} \underbrace{\begin{bmatrix} N_1 \cos n\theta & 0 & 0 & N_2 \cos n\theta & \cdots \\ 0 & N_1 \sin n\theta & 0 & 0 & \cdots \\ 0 & 0 & N_1 \cos n\theta & 0 & \cdots \end{bmatrix}}_{[\mathbf{N}_n]} \{\bar{\mathbf{d}}_n\} \tag{14.5-2}$$

in which n is the harmonic number and numerical subscripts on italic N's indicate element node numbers. With the summation written out, Eq. 14.5-2 is

$$\begin{Bmatrix} u \\ v \\ w \end{Bmatrix} = \begin{bmatrix} \mathbf{N}_0 & \mathbf{N}_1 & \mathbf{N}_2 & \cdots \end{bmatrix} \begin{Bmatrix} \bar{\mathbf{d}}_0 \\ \bar{\mathbf{d}}_1 \\ \bar{\mathbf{d}}_2 \\ \vdots \end{Bmatrix} \quad \text{or} \quad \begin{Bmatrix} u \\ v \\ w \end{Bmatrix} = [\mathbf{N}]\{\bar{\mathbf{d}}\} = \sum_n [\mathbf{N}_n]\{\bar{\mathbf{d}}_n\} \tag{14.5-3}$$

in which subscripts on bold **N**'s and $\bar{\mathbf{d}}$'s represent harmonic numbers. Column vector $\{\bar{\mathbf{d}}\}$ lists nodal Fourier amplitudes from all element nodes and all harmonics. The first harmonic, $n = 0$, represents the axisymmetric case. From Eqs. 14.4-4 and 14.5-3,

$$\{\boldsymbol{\varepsilon}\} = [\partial]\begin{Bmatrix} u \\ v \\ w \end{Bmatrix} = \underbrace{[\partial][\mathbf{N}_0 \quad \mathbf{N}_1 \quad \mathbf{N}_2 \quad \cdots]}_{[\mathbf{B}]=[\mathbf{B}_0 \ \mathbf{B}_1 \ \mathbf{B}_2 \ \cdots]} \{\bar{\mathbf{d}}\} = \sum_n [\mathbf{B}_n]\{\bar{\mathbf{d}}_n\} \tag{14.5-4}$$

where $[\mathbf{B}]$ is the strain-displacement matrix, with submatrix $[\mathbf{B}_n]$ for harmonic n. With partitioning according to element nodes, element strains in the nth harmonic are, from Eqs. 14.4-4 and 14.5-4,

$$\begin{Bmatrix} \varepsilon_{rn} \\ \varepsilon_{\theta n} \\ \varepsilon_{zn} \\ \gamma_{zrn} \\ \gamma_{r\theta n} \\ \gamma_{\theta zn} \end{Bmatrix} = \left[\begin{array}{ccc|c} N_{1,r}\cos n\theta & 0 & 0 & \cdots \\ \dfrac{N_1}{r}\cos n\theta & \dfrac{nN_1}{r}\cos n\theta & 0 & \cdots \\ 0 & 0 & N_{1,z}\cos n\theta & \cdots \\ N_{1,z}\cos n\theta & 0 & N_{1,r}\cos n\theta & \cdots \\ -\dfrac{nN_1}{r}\sin n\theta & \left(N_{1,r}-\dfrac{N_1}{r}\right)\sin n\theta & 0 & \cdots \\ 0 & N_{1,z}\sin n\theta & -\dfrac{nN_1}{r}\sin n\theta & \cdots \end{array}\right] \begin{Bmatrix} \bar{u}_{1n} \\ \bar{v}_{1n} \\ \bar{w}_{1n} \\ \hline \bar{u}_{2n} \\ \bar{v}_{2n} \\ \vdots \end{Bmatrix} \tag{14.5-5}$$

$$\underbrace{\qquad\qquad\qquad\qquad}_{1} \quad \underbrace{\quad}_{2,3,4\ldots}$$

where numerical subscripts indicate the node number and a comma indicates differentiation with respect to the following literal subscript. Element shape functions N_i depend on r and z. Therefore $[\mathbf{B}]$ is a function of r, z, n, and θ.

The element stiffness matrix is given by Eq. 14.2-2, but with arrays of larger size. Let there be J nodes per element and M harmonics included. Then the integrand matrix $[\mathbf{B}]^T[\mathbf{E}][\mathbf{B}]$ is full and of size $3JM$ by $3JM$. It is composed of an M by M array of $3J$ by $3J$ submatrices. Off-diagonal submatrices contain $\sin m\theta \sin n\theta$ or $\cos m\theta \cos n\theta$ in every term, where m and n are *different* integers that represent different harmonics. With limits $-\pi$ to π, integrals of these terms are zero. We are left with only M submatrices on the diagonal, which means that different Fourier harmonics are uncoupled. Each on-diagonal submatrix is $3J$ by $3J$ and contains $\sin^2 n\theta$ or $\cos^2 n\theta$ in every term. With limits $-\pi$ to π, $\sin^2 n\theta$ and $\cos^2 n\theta$ each integrate to π (or to 2π for $\cos^2 n\theta$ when $n = 0$). Integration with respect to r and z is done in the same way as for an axisymmetric problem. In similar fashion, the element mass matrix for harmonic n is, from Eqs. 14.2-5 and 14.5-2,

$$[\mathbf{m}] = \iint_{-\pi}^{\pi} \underbrace{\begin{bmatrix} N_1^2\cos^2 n\theta & 0 & 0 & N_1N_2\cos^2 n\theta & \cdots \\ 0 & N_1^2\sin^2 n\theta & 0 & 0 & \cdots \\ 0 & 0 & N_1^2\cos^2 n\theta & 0 & \cdots \\ \vdots & \vdots & \vdots & \vdots & \end{bmatrix}}_{3J\times 3J} \rho r\, d\theta\, dA \tag{14.5-6}$$

After assembly of elements in the usual way, structural equations for a time-independent problem have the form

$$\begin{bmatrix} \mathbf{K}_0 & & & \\ & \mathbf{K}_1 & & \\ & & \mathbf{K}_2 & \\ & & & \ddots \end{bmatrix} \begin{Bmatrix} \bar{\mathbf{D}}_0 \\ \bar{\mathbf{D}}_1 \\ \bar{\mathbf{D}}_2 \\ \vdots \end{Bmatrix} = \begin{Bmatrix} \bar{\mathbf{R}}_0 \\ \bar{\mathbf{R}}_1 \\ \bar{\mathbf{R}}_2 \\ \vdots \end{Bmatrix} \quad \text{or} \quad [\mathbf{K}]\{\mathbf{D}\} = \{\mathbf{R}\} \tag{14.5-7}$$

where subscripts indicate the harmonic number, and barred quantities are Fourier amplitudes. The several terms in a stiffness submatrix $[\mathbf{K}_n]$ are either independent of n or contain n or n^2 as a multiplier. Accordingly, some stiffness coefficients increase as n increases. It is for this reason that a nonconvergent series for load such as that of Eq. 14.4-2, which provides nodal loads that merely alternate in sign from one harmonic to the next, can produce convergent results for displacement and stress. In practice we do not construct a stiffness matrix that contains all harmonics, as in Eq. 14.5-7; instead the separate subproblems $[\mathbf{K}_n]\{\bar{\mathbf{D}}_n\} = \{\bar{\mathbf{R}}_n\}$ are constructed and solved serially. Final displacements are given by Eq. 14.5-3, final strains by Eq. 14.5-4, and final stresses by Eq. 14.4-3.

For M harmonics, element nodal loads, Eq. 3.3-8, include contributions such as

$$\iint_{-\pi}^{\pi} \underset{3JM\times 3}{[\mathbf{N}]^T} \underset{3\times 1}{\{\mathbf{F}\}} r \, d\theta \, dA \qquad \text{and} \qquad \iint_{-\pi}^{\pi} \underset{3JM\times 6}{[\mathbf{B}]^T} \underset{6\times 1}{\{\boldsymbol{\sigma}_0\}} r \, d\theta \, dA \tag{14.5-8}$$

where $[\mathbf{N}]$ and $[\mathbf{B}]$ are given by Eqs. 14.5-3 and 14.5-4. For example, body forces associated with symmetric deformation have the form

$$\{\mathbf{F}\} = \begin{Bmatrix} \bar{F}_{r0} + \bar{F}_{r1}\cos\theta + \bar{F}_{r2}\cos 2\theta + \cdots \\ 0 + \bar{F}_{\theta 1}\sin\theta + \bar{F}_{\theta 2}\sin 2\theta + \cdots \\ \bar{F}_{z0} + \bar{F}_{z1}\cos\theta + \bar{F}_{z2}\cos 2\theta + \cdots \end{Bmatrix} \tag{14.5-9}$$

Integration of Eq. 14.5-8 is accomplished in the manner described above Eq. 14.5-6. Thus we obtain $\{\mathbf{R}\}$ of Eq. 14.5-7, in which $\{\bar{\mathbf{R}}_0\}$ contains only the zero-harmonic (axisymmetric) load terms, $\{\bar{\mathbf{R}}_1\}$ contains only the first-harmonic load terms, and so on.

Remarks. If the double-barred series is used rather than the single-barred series, one finds that $\sin n\theta$ and $\cos n\theta$ are interchanged in Eqs. 14.5-2, 14.5-5, 14.5-6, and 14.5-9. Also, algebraic signs are reversed in the last two rows of the rectangular matrix of Eq. 14.5-5. However, for $n > 0$, submatrices $[\mathbf{K}_n]$ in Eq. 14.5-7 turn out to be the same as those produced by the single-barred series. This convenience is the motivation for the arbitrarily chosen negative sign in Eq. 14.4-5b. If the sign were taken as positive, submatrices would differ between single- and double-barred series.

For $n = 0$, d.o.f. $\bar{v}_{ni}$, $\bar{\bar{u}}_{ni}$, and $\bar{\bar{w}}_{ni}$ have no stiffness associated with them. These d.o.f. must be suppressed at every node i to avoid a singular stiffness matrix. Also, for $n = 0$, axial translation must be suppressed on at least one nodal circle in order to prevent axial translation. For $n = 1$, rigid-body translations parallel to the $r\theta$ plane are possible, and also rigid-body rotations about axes in this plane. As an example, small rotation ϕ about the axis

$\theta = \pi/2$ produces displacement components $u = \phi z \cos\theta$, $v = -\phi z \sin\theta$, and $w = -\phi r \cos\theta$. To prevent singularity of $[\mathbf{K}_1]$ these motions must be suppressed. For bodies with nodes on the z axis, additional conditions on Fourier displacement amplitudes can be deduced from the requirement that strains remain finite at $r = 0$ [14.7]. If these conditions are ignored, some stiffness coefficients may be far larger than others. In dynamic analysis by explicit integration, this circumstance may dictate that a very small time step be used.

If θ is not a principal material direction, $[\mathbf{E}]$ in Eq. 14.4-3 becomes a full matrix. Barred and double-barred terms of Eqs. 14.4-5 become coupled in each harmonic, but different harmonics remain uncoupled [14.8]. If elastic moduli vary circumferentially, as for example when moduli are temperature-dependent and temperature varies with θ, Fourier series can again be used, but all harmonics are coupled [14.9,14.10].

ANALYTICAL PROBLEMS

14.1-1 If analysis of a solid of revolution is to be mathematically two-dimensional, circumferential displacement v must be zero. Devise an example in which $v \neq 0$ when θ is not a principal material direction, despite axisymmetric loading.

14.2-1 In Fig. 6.8-1, dashed lines represent displaced positions of a four-node bilinear element. If the element is axisymmetric rather than plane, x represents the radial direction and y is parallel to the axis of revolution (not shown). Which of the eight displacement modes are associated with zero strain energy in the element and which are not? Answer for each of the following situations.
(a) The element is plane and $[\mathbf{k}]$ is integrated by one Gauss point.
(b) The element is plane and $[\mathbf{k}]$ is integrated by four Gauss points.
(c) The element is axisymmetric and $[\mathbf{k}]$ is integrated by one Gauss point.
(d) The element is axisymmetric and $[\mathbf{k}]$ is integrated by four Gauss points.

14.2-2 The sketch represents three nodes on a z = constant face of an axisymmetric quadratic element. Nodes shown are uniformly spaced. Determine the consistent nodal load vector if z-direction traction Φ_z is applied to this face as follows.
(a) Φ_z has the constant value p over the face.
(b) $\Phi_z = \frac{1}{2}(\xi^2 - \xi)p_4 + (1 - \xi^2)p_7 + \frac{1}{2}(\xi^2 + \xi)p_3$, which is a parabolic variation based on nodal values p_4, p_7, and p_3.

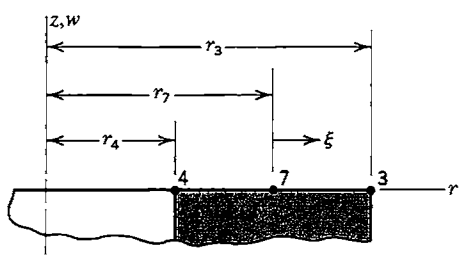

Problem 14.2-2

14.2-3 In the sketch for Problem 14.2-2, let $r_4 = 0$, and imagine that $w_4 > 0$ and $w_7 = w_3 = 0$. Is such a deformation mode reasonable? Consider shear strain γ_{zr} at $r = 0$.

14.2-4 Devise an argument that demonstrates the relation $\varepsilon_r = \varepsilon_\theta$ at $r = 0$ in an axisymmetric problem. *Suggestion:* Consider the radial displacement series $u = c_1 r + c_2 z + c_3 r^2 + c_4 rz + \cdots$.

14.2-5 Devise an argument or an example that confirms the existence of a large stiffness difference in the case of a very slender element, as noted following Eq. 14.2-3.

14.2-6 The sketch shows the cross section of an element of uniform thickness t, shaped like a metal washer. D.o.f. are radial displacements u_1 and u_2 at nodal circles 1 and 2. The material is isotropic and only in-plane strains ε_r and ε_θ need be considered.
(a) Formulate matrices [**N**] and [**B**].
(b) Let $\nu = 0$, and generate [**k**] by explicit integration over a one-radian segment.
(c) Let $L = r_2 - r_1$ and $r_m = (r_1 + r_2)/2$. Simplify integration by assuming that $r = r_m$. Hence, determine [**k**] for a nonzero Poisson's ratio. For what geometry is this [**k**] a good approximation?
(d) Show that the [**k**]'s of parts (b) and (c) agree when $\nu = 0$ and $r_m >> L$.
(e) From part (b), obtain [**k**] for the special case $\nu = r_1 = u_1 = 0$.
(f) From part (c), obtain [**k**] for the special case $\nu = r_1 = u_1 = 0$.

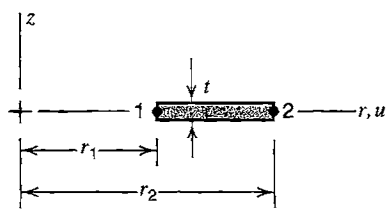

Problem 14.2-6

14.2-7 For the four-node, eight-d.o.f. axisymmetric element shown in Fig. 14.2-1, evaluate nodal loads $\{\mathbf{r}_e\}$ produced by spinning at angular velocity ω about the z axis. Include detail, but stop after setting up a triple integral over $d\theta\, dx\, dy$.

14.4-1 (a) In Fig. 14.4-2a, rotate the r axis 90° counterclockwise, so that the $\theta = 0$ plane is vertical in the figure. Do not reposition the load. Write the Fourier series for load that applies to this arrangement.
(b) Hence write a load series that applies to the following radial load: $q = q_o$ outward over $0 < \theta < \pi/2$, $q = q_o$ inward over $\pi < \theta < 3\pi/2$, and $q = 0$ over the remaining two quadrants, where q_o is a constant.
(c) For the loading described in part (b), how might the $\theta = 0$ plane be positioned so that only the cosine series is needed?

14.4-2 A flat plate contains a circular hole of radius R and is loaded by axial force P and in-plane bending moment M, as shown. The region enclosed by the dashed line of radius c is to be isolated and analyzed as a solid of revolution. If t = plate thickness and $c >> R$, what load terms from Eq. 14.4-1 should be used in analysis? Express answers in terms of P, M, h, t, r, n, and θ.
(a) Consider P only (let $M = 0$).
(b) Consider M only (let $P = 0$).

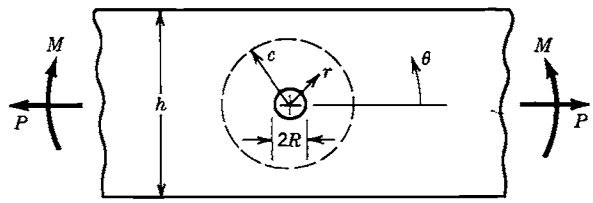

Problem 14.4-2

14.4-3 Write special forms of Eqs. 14.4-5 so as to describe each of the following rigid-body motions.
(a) Translation in the z direction.
(b) Translation in a radial direction and parallel to the plane $\theta = 0$.
(c) Translation in a radial direction and parallel to the plane $\theta = \pi/2$.
(d) Small rotation about the r axis located at $\theta = 0$.

14.4-4 If $\{\boldsymbol{\varepsilon}\} = \{\mathbf{0}\}$, Eqs. 14.4-4 have the solution

$$\begin{Bmatrix} u \\ v \\ w \end{Bmatrix} = \begin{bmatrix} 0 & \cos\theta & z\cos\theta & 0 & \sin\theta & z\sin\theta \\ 0 & -\sin\theta & -z\sin\theta & r & \cos\theta & z\cos\theta \\ 1 & 0 & -r\cos\theta & 0 & 0 & -r\sin\theta \end{bmatrix} \begin{Bmatrix} a_1 \\ a_2 \\ \vdots \\ a_6 \end{Bmatrix}$$

where the a_i are constants. A displacement field that contains all these terms can represent all possible rigid-body motions.
(a) Show that this field does indeed yield $\{\boldsymbol{\varepsilon}\} = \{\mathbf{0}\}$.
(b) Compare this field with Eqs. 14.4-5: identify columns of the rectangular matrix as to the value of n and as belonging to the single-barred series or to the double-barred series.
(c) Describe the physical meaning of the displacement mode associated with each of the a_i.

14.4-5 It can be shown that the sinusoidal loading $q_n = q_n^s \sin(n\pi x/L)$ on the uniform simply supported beam shown produces lateral deflection v that is also sinusoidal and is given by

$$v_n = \frac{q_n^s L^4}{EIn^4\pi^4}\sin\frac{n\pi x}{L}$$

A Fourier series for load is $q = \sum q_n^s$ and the associated lateral deflection is $v = \sum v_n$. At midspan, for each of the following loadings, evaluate the lateral deflection and bending moment and their percentage errors. Use one, then two, then three series terms.
(a) Uniformly distributed load q_o, for which $q_n^s = 4q_o/n\pi$ and $n = 1,3,5,\ldots$.
(b) Concentrated force P at midspan, for which $q_n^s = (2P/L)\sin(n\pi/2)$ and $n = 1,2,3,\ldots$.

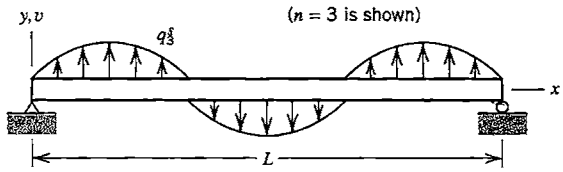

Problem 14.4-5

14.5-1 Repeat Problem 14.2-5, but now consider nonaxisymmetric deformation. More specifically, consider radial pressure $q = q_2^c \cos 2\theta$ and the associated radial displacement $u = \bar{u}_2 \cos 2\theta$. *Suggestion:* Equate strain energy in bending to work done by the load, thus obtain $\bar{u}_2$, define a flexural stiffness using $\bar{u}_2$, and compare it with circumferential stiffness. Assume that curvature is d^2u/ds^2, where $s = r\theta$.

14.5-2 (a) Write the form of the rectangular matrix in Eq. 14.5-5 appropriate to antisymmetric displacements (the double-barred series in Eqs. 14.4-5).
(b) Show that, for $n > 0$, submatrices $[\mathbf{K}_n]$ in Eq. 14.5-7 are identical to those obtained when using the single-barred series. (Note that it is not necessary to write terms extraneous to the question posed.)
(c) Show that the conclusion reached in part (b) would not be true if the negative sign in Eq. 14.4-5b were changed to positive.

14.5-3 Assume that a certain axisymmetric pressure vessel can be adequately modeled by four-node elements having translational d.o.f. only (as in Fig. 14.2-1b). Let the mesh be 20 by 1, with one element spanning the wall thickness and 20 elements spanning the axial dimension. Assume that loading is adequately described by harmonics 1 through 6 of the sine series in Eq. 14.4-1. Alternatively, one might contemplate a fully 3D analysis with a 20 by 1 by m mesh of eight-node solid elements, where m is the number of elements around the circumference.
(a) Estimate m so that the 3D model and the series solution have comparable accuracy. Assume that three elements per half-wave of displacement are acceptable.
(b) Estimate the cost ratio of the 3D solution to the series solution. Determine cost by estimating the number of multiplications needed to generate stiffness matrices by use of an order 2 Gauss rule.
(c) Repeat part (b), but now determine cost by estimating the number of multiplications needed to solve equations by Gauss elimination with a banded solver.

14.5-4 Consider the flat element of Problem 14.2-6. However, now allow circumferential displacement as well as radial displacement, so that nonaxisymmetric loads can be treated. Element nodal d.o.f. become u_1, v_1, u_2, and v_2. Let $\theta = 0$ be a plane of symmetry for displacements. Formulate the strain-displacement matrix of this element (for harmonic n, as in the rectangular matrix of Eq. 14.5-5, but including partitions for both nodes).

COMPUTATIONAL PROBLEMS

In the following problems, compute peak values of displacement and stress. Exploit symmetry where possible. When mesh refinement is used, estimate the maximum percentage error of results provided by the finest FE mesh. Where dimensions or loads are not assigned, choose values that seem reasonable or convenient. Where material properties are needed but not stated, use properties of steel (and aluminum if necessary). Apply the analysis methodology suggested in Section 1.5.

C14.1 (a) The sketch shows, in cross section, an axisymmetric FE model of an isotropic circular disk. The outer edge is prevented from rotating in the rz plane and is loaded by total axial force $2P$, uniformly distributed around the circumference. Compare computed results with theory [1.16,2.6] and with results proved by an improved mesh having the same number of elements (see Fig. 10.3-2). Are σ_r and σ_θ equal at $r = 0$, as expected?
(b) Many other loadings on circular plates are possible, both symmetric and unsymmetric, for which solutions are provided by handbook formulas [1.16]. (Solid of revolution elements can be used, but axisymmetric plate elements are more appropriate for thin plates.)

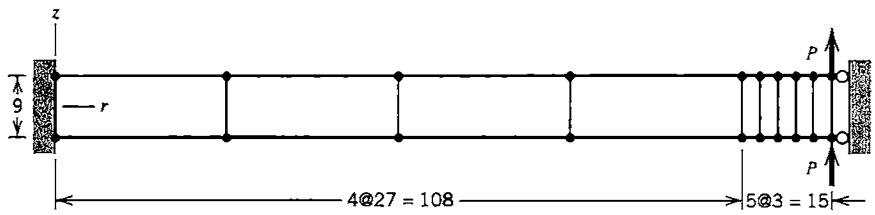

Problem C14.1

C14.2 Consider a long, thick-walled cylindrical pressure vessel. Let one end be fixed, the other unsupported. Analyze for the following loadings. (a) Internal pressure. (b) Spinning about the axis at constant speed (in this case let both ends be unsupported). (c) Pure torque about the axis. (d) Force at the unsupported end directed normal to the axis.

C14.3 Analyze a thick-walled spherical pressure vessel loaded by (a) internal pressure, and (b) spinning about the axis at constant speed.

C14.4 The sketch shows the cross section of a truncated cone built of two different materials. The cone becomes a cylinder if $R_1 = R_2$ and a disk if $R_1 - R_2 = L_1 + L_2$. Loading is by temperature change T and/or by uniform circumferential line loads F_1 and F_2.
(a) Let T be uniform and $F_1 = F_2 = 0$.
(b) Let T vary linearly with s and $F_1 = F_2 = 0$.
(c) Let T vary linearly in the direction of thickness t and $F_1 = F_2 = 0$.
(d) Let both materials be the same, $T = 0$, $F_1 = 0$, and F_2 directed radially.
(e) Let $T = 0$ and let loads F_1 and F_2 be directed axially with $F_1R_1 = F_2R_2$.

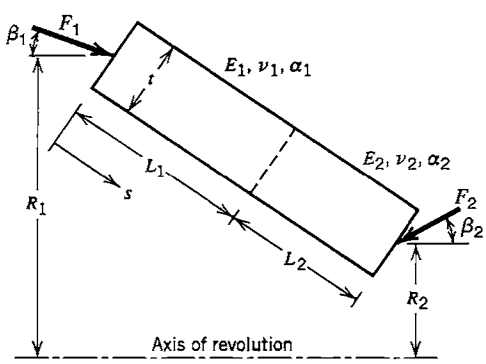

Problem C14.4

C14.5 A spherical vessel has a radially directed cylindrical outlet, as shown in cross section. The inside and/or outside may be reinforced by the axisymmetric enlargements shown: on the inside by AB perpendicular to the axis of the cylindrical part; on the outside by CD tangent to the outer surface of the spherical part. Let $t_c = 2t_s r_c / r_s$. Consider the following loadings.

(a) Internal pressure.

(b) Fluid temperatures T_i inside and T_o outside (see Chapter 12 for temperature field analysis).

(c) Torque applied to the nozzle (twisting about the z axis).

(d) Bending moment applied to the nozzle.

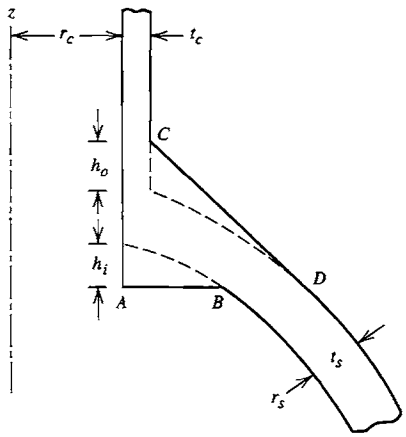

Problem C14.5

C14.6 (a,b) Solve Problem 14.4-2, parts (a) and (b). Apply the theory described in Sections 14.4 and 14.5.

C14.7 (a) A slender plane ring is pinched along a diameter by forces P (reverse the directions of forces shown in Fig. 14.4-3c). Apply the theory described in Sections 14.4 and 14.5.

(b) Similarly, a hollow sphere is pinched by diametral forces P.

(c) A pipe rests lengthwise on a horizontal surface, loaded by its own weight.

(d) A hollow sphere rests on a horizontal surface, loaded by its own weight.

CHAPTER 15

PLATE BENDING

Elementary plate bending theory is reviewed in this chapter. Concepts used in formulating a variety of plate elements are presented. Defects of selected formulations are considered, as well as some methods of overcoming the defects. Boundary conditions and test cases for plates are discussed, and an example application is presented.

15.1 INTRODUCTION. PLATE BEHAVIOR

By *plate* we mean a flat body whose thickness is much smaller than its other dimensions. Because of this geometry, 3D finite elements are not used for analysis of plate bending. If 3D elements were made thin in only the thickness direction there would be problems of shear locking and ill-conditioning, but if these problems were avoided by using a great many compact 3D elements, an FE structure would have far too many d.o.f. The problem of too many d.o.f. is avoided by basing elements on plate theory. Depending on the type of plate theory adopted, special formulation devices may be needed to avoid shear locking.

A flat plate, like a straight beam, carries lateral load by bending. In general, a plate develops bending moments in two directions and also a twisting moment. Because it is easy to formulate a satisfactory beam element, it might be supposed that the same is true of a plate element. Such is not the case. Early plate elements were plagued by troubles such as locking, a need for higher-order d.o.f. or many side nodes, differing d.o.f. arrangements at different nodes of a single element, patch test failure, instability due to spurious modes, shape restrictions, or simply poor performance.

In this chapter we discuss two plate theories. The first prohibits transverse shear deformation; the second accounts for it. In both, normal stress in the thickness direction is taken as zero. The first is called *thin-plate theory* or *Kirchhoff theory,* in recognition of Kirchhoff's research on plate theory in 1850. The second dates from about 1950 and is usually known as *Mindlin theory,* although the names Mindlin-Reissner and Reissner-Mindlin are also used [15.1,15.2]. Either of the two theories provides a mathematical model that can be solved by FEA, using appropriately formulated plate elements. Each theory has been used to develop a great many finite elements. Formulation procedures include displacement-based models, hybrid and mixed models, devices introduced to avoid difficulties, and more devices introduced to overcome new troubles associated with the previous devices. A 1984 survey paper cites some 150 FE formulations for plates [15.3]. Since then, the pace of development seems to have increased. A comprehensive survey is not undertaken in this chapter. Instead, we consider the more fundamental concepts and methods that have been widely used in FE plate theory, and cite useful references for further details, extensions, and improvements. The reference list is not intended to imply priority of discovery.

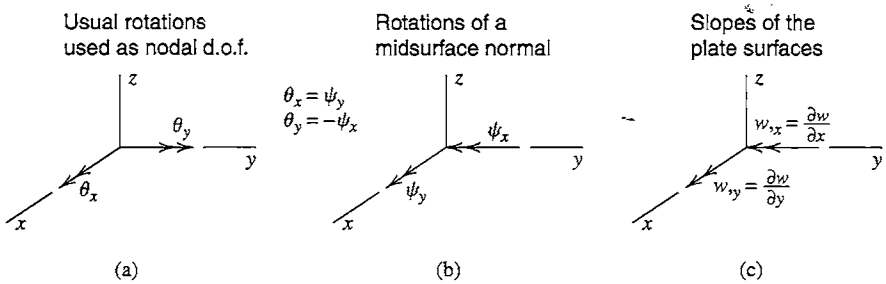

Figure 15.1-1. Notation for rotation components of a midsurface-normal and slopes of a plate surface.

Most FE users who wish to improve the accuracy and reliability of computed results will profit more from careful use of available formulations and software than from a search for the optimal element.

Notation. We place plates in the xy plane. In preceding chapters, arrows that represent rotations θ_x and θ_y according to the right-hand rule are considered positive when they point in positive x and y directions respectively (Fig. 15.1-1). Representation of plate surface slopes $w_{,x}$ and $w_{,y}$ by the right-hand rule produces arrows that point in the negative y and positive x directions respectively. We need both rotations and surface slopes to discuss plate elements. To reduce confusion, in the present chapter we reconcile signs and subscripts of rotations and slopes by replacing θ_x by ψ_y and θ_y by negative ψ_x, as shown in Fig. 15.1-1b.

Plate Theory. A brief summary of plate theory and plate behavior is as follows [3.2,10.2]. A plate of thickness t has a *midsurface* at distance $t/2$ from each lateral surface. For analysis, we locate the xy plane in the plate midsurface (Fig. 15.1-2a), so that $z = 0$ identifies the midsurface. In elementary plate bending theory it is assumed that bending of a homogeneous plate makes the midsurface a *neutral* surface; that is, $\varepsilon_x = \varepsilon_y = \gamma_{xy} = 0$ at $z = 0$. If in-plane loading is present, perhaps associated with large lateral deflection, midsurface strains are not zero.

Behavior is idealized by saying that a line that is straight and normal to the midsurface before load is applied remains straight but not necessarily normal to the deformed midsurface. Rotation of this straight line has components ψ_x and ψ_y. Thus a point not on the midsurface has the x-direction displacement u shown in Fig. 15.1-2b. A similar cross section,

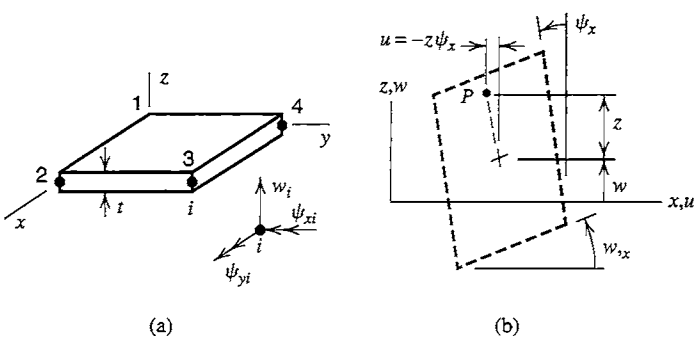

Figure 15.1-2. (a) A plate element with corner nodes, showing typical nodal d.o.f. (b) A deformed plate cross section, viewed in the $+y$ direction. Thickness-direction lines are assumed to remain straight.

viewed in the negative x direction, provides y-direction displacement v. Hence, for *small* displacements and rotations, strains are obtained from Eqs. 3.1-9:

$$\begin{aligned} u &= -z\psi_x & \varepsilon_x &= -z\psi_{x,x} & \gamma_{xy} &= -z(\psi_{x,y} + \psi_{y,x}) \\ v &= -z\psi_y & \varepsilon_y &= -z\psi_{y,y} & \gamma_{yz} &= w_{,y} - \psi_y \\ & & & & \gamma_{zx} &= w_{,x} - \psi_x \end{aligned} \tag{15.1-1}$$

where a comma denotes differentiation with respect to the following subscript and w is the lateral (z-direction) deflection of the midsurface. An expression for thickness-direction strain ε_z is not needed. Equations 15.1-1 are the basis of Mindlin plate theory, which allows transverse shear deformation; that is, strains γ_{yz} and γ_{zx} need not be zero. In Kirchhoff plate theory, a straight line normal to the undeformed midsurface is assumed to remain straight *and normal* to the deformed midsurface. Thus $w_{,y} = \psi_y$ and $w_{,x} = \psi_x$, and transverse shear deformation is zero throughout a Kirchhoff plate (although transverse shear *forces* remain present). Many practical plates can be regarded as Kirchhoff plates because they are thin enough for transverse shear deformation to be negligible.

Stresses on cross sections are depicted in Fig. 15.1-3a. It is customary to associate these stresses with moments and forces *per unit of length* in the xy plane. For example, an increment of M_x is $dM_x = z(\sigma_x\, dA)$, where $dA = (1)dz$ is an increment of cross-sectional area a distance z from the deformed midsurface. Thus

$$M_x = \int_{-t/2}^{t/2} \sigma_x z\, dz \qquad M_y = \int_{-t/2}^{t/2} \sigma_y z\, dz \qquad M_{xy} = \int_{-t/2}^{t/2} \tau_{xy} z\, dz \tag{15.1-2a}$$

$$Q_x = \int_{-t/2}^{t/2} \tau_{zx}\, dz \qquad Q_y = \int_{-t/2}^{t/2} \tau_{yz}\, dz \tag{15.1-2b}$$

These quantities are depicted in Fig. 15.1-3b, in directions consistent with stress directions in Fig. 15.1-3a. Moments M_x and M_y are bending moments, while M_{xy} is a twisting moment. Like stresses in Fig. 3.1-2a, quantities in Fig. 15.1-3b have rates of change with respect to the coordinates, although for simplicity they are not shown here. Deformation

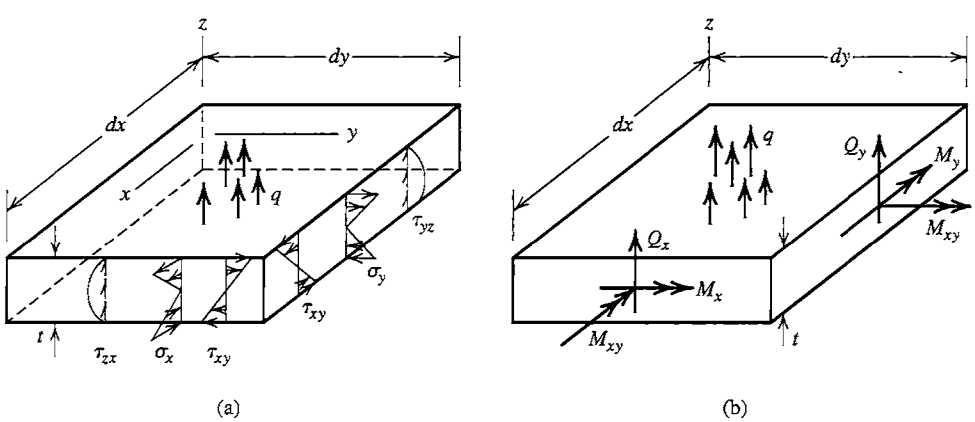

Figure 15.1-3. (a) Stresses and distributed lateral force q on a differential element of a plate. (b) Moments and transverse shear forces associated with stresses in part (a).

such as that depicted in Fig. 15.1-2b, in which lines originally normal to the midsurface are assumed to remain straight, produces stresses σ_x, σ_y, and τ_{xy} that vary linearly with z, as shown in Fig. 15.1-3a. Thus, for homogeneous material, Eqs. 15.1-2a yield stresses $\pm 6M_x/t^2$, $\pm 6M_y/t^2$, and $\pm 6M_{xy}/t^2$ at plate surfaces $z = \pm t/2$, as if the flexure formula $\sigma = Mc/I$ had been applied to a rectangular cross section of depth t and unit width. Transverse shear stresses τ_{yz} and τ_{zx} are usually small in comparison with σ_x, σ_y, and τ_{xy}. For homogeneous material they vary parabolically through the thickness and have greatest magnitude at $z = 0$, where $\tau_{yz} = 1.5Q_y/t$ and $\tau_{zx} = 1.5Q_x/t$.

Customarily, normal stress σ_z is considered negligible in comparison with σ_x, σ_y, and τ_{xy}. Then, for a linearly elastic and isotropic material, the stress-strain relation in each z-parallel layer of the plate is the familiar plane-stress expression

$$\begin{Bmatrix} \sigma_x \\ \sigma_y \\ \tau_{xy} \end{Bmatrix} = \frac{E}{1-\nu^2}\begin{bmatrix} 1 & \nu & 0 \\ \nu & 1 & 0 \\ 0 & 0 & \dfrac{1-\nu}{2} \end{bmatrix}\left(\begin{Bmatrix} \varepsilon_x \\ \varepsilon_x \\ \gamma_{xy} \end{Bmatrix} - \begin{Bmatrix} \varepsilon_{x0} \\ \varepsilon_{y0} \\ 0 \end{Bmatrix}\right) \tag{15.1-3}$$

where ε_{x0} and ε_{y0} are initial strains. If material properties are not isotropic, the square matrix in Eq. 15.1-3 is in general a full matrix. Transformation of material properties, if required, can be accomplished as described in Section 8.2.

Kirchhoff Plate Theory. Transverse shear deformation is prohibited, so $w_{,x} = \psi_x$ and $w_{,y} = \psi_y$ in Eqs. 15.1-1; hence $\varepsilon_x = -zw_{,xx}$, $\varepsilon_y = -zw_{,yy}$, and $\gamma_{xy} = -2zw_{,xy}$. These strain-curvature relations may be substituted into Eq. 15.1-3 and the resulting expressions for stress into Eqs. 15.1-2. Thus the moment-curvature relations for a homogeneous and isotropic Kirchhoff plate are

$$\{\mathbf{M}\} = -[\mathbf{D}]\Big(\{\boldsymbol{\kappa}\} - \{\boldsymbol{\kappa}_0\}\Big) \qquad \text{or, written out,} \tag{15.1-4a}$$

$$\begin{Bmatrix} M_x \\ M_y \\ M_{xy} \end{Bmatrix} = -\begin{bmatrix} D & \nu D & 0 \\ \nu D & D & 0 \\ 0 & 0 & \dfrac{(1-\nu)D}{2} \end{bmatrix}\left(\begin{Bmatrix} w_{,xx} \\ w_{,yy} \\ 2w_{,xy} \end{Bmatrix} - \{\boldsymbol{\kappa}_0\}\right) \tag{15.1-4b}$$

where $$D = \frac{Et^3}{12(1-\nu^2)} \qquad (D \text{ is called } \textit{flexural rigidity}) \tag{15.1-4c}$$

D is analogous to flexural stiffness EI of a beam. Indeed, for a unit width and $\nu = 0$, $D = EI = Et^3/12$. As an example of initial curvatures $\{\boldsymbol{\kappa}_0\}$, let temperature vary linearly with z from T_o at $z = -t/2$ to $-T_o$ at $z = t/2$. Then, with α the coefficient of thermal expansion, $\{\boldsymbol{\kappa}_0\} = \lfloor 2\alpha T_o/t \quad 2\alpha T_o/t \quad 0 \rfloor^T$. The state of deformation and stress throughout a Kirchhoff plate are completely described by a single field, namely lateral deflection $w = w(x,y)$ of the midsurface.

Let a plate be bent to a cylindrical surface by moment M_y, as shown in Fig. 15.1-4a. Here $w_{,yy}$ is constant and $w_{,xx} = w_{,xy} = 0$. Equation 15.1-4b shows that M_x appears as

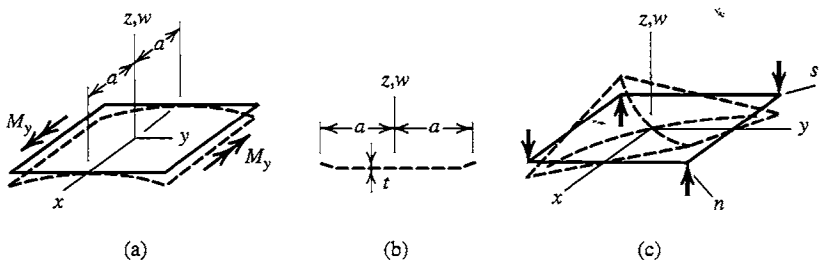

Figure 15.1-4. (a) Bending to the cylindrical surface $w \propto y^2$. (b) Cross section exposed by the xz plane, showing deformation if $M_x = 0$ on edges $x = \pm a$. (c) A state of pure twist, $w \propto xy$.

well as M_y, with $M_x = \nu M_y$. The associated flexural stresses are $\sigma_x = \nu\sigma_y$. If dimension a were comparable to thickness t the structure would behave as a beam lying along the y axis, so that $\sigma_x \approx 0$ and z-parallel sides of the beam would rotate with respect to one another. Similarly, if edges $x = \pm a$ of the plate are free, so that σ_x and M_x are both zero on edges $x = \pm a$, these edges curl slightly as shown in Fig. 15.1-4b, so that the displaced shape is not cylindrical near edges $x = \pm a$. Throughout most of the plate, the induced stress $\sigma_x = \nu\sigma_y$ constrains the plate from displaying the curvature $w_{,xx}$ that a beam would have, thereby stiffening the plate in comparison with a beam. In Eqs. 15.1-4, this stiffening effect appears as the divisor $1 - \nu^2$.

In Fig. 15.1-4c, lateral forces are applied to corners in alternating directions, so that the plate assumes a state of pure twist, namely $w \propto xy$, so that $w_{,xy} > 0$ with $w_{,xx} = w_{,yy} = 0$. Within the twisted plate, from Eq. 15.1-4b, M_{xy} is a negative constant while M_x and M_y are both zero. In coordinates ns oriented at 45 degrees to coordinates xy in Fig. 15.1-4c, the twisted plate appears saddle-shaped, with equal and opposite curvatures $w_{,nn}$ and $w_{,ss}$ but no twist $w_{,ns}$ and with moments $M_n = -M_s$ and $M_{ns} = 0$.

Mindlin Plate Theory. *Three* fields—w, ψ_x, and ψ_y—must each be expressed in terms of x and y in order to describe the state of deformation and stress throughout a Mindlin plate. With w, ψ_x, and ψ_y retained as independent quantities in Eqs. 15.1-1, the process that yields Eq. 15.1-4 can be repeated. Thus, for homogeneous, isotropic, and linearly elastic material, relations analogous to Eqs. 15.1-4 but for a Mindlin plate are

$$\begin{Bmatrix} M_x \\ M_y \\ M_{xy} \\ Q_x \\ Q_y \end{Bmatrix} = -\underbrace{\begin{bmatrix} & & & 0 & 0 \\ & \underset{3\times 3}{[\mathbf{D}]} & & 0 & 0 \\ & & & 0 & 0 \\ 0 & 0 & 0 & kGt & 0 \\ 0 & 0 & 0 & 0 & kGt \end{bmatrix}}_{[\mathbf{D}_M]} \left(\underbrace{\begin{Bmatrix} \psi_{x,x} \\ \psi_{y,y} \\ \psi_{x,y} + \psi_{y,x} \\ \psi_x - w_{,x} \\ \psi_y - w_{,y} \end{Bmatrix}}_{\{\boldsymbol{\kappa}_M\}} - \{\boldsymbol{\kappa}_0\} \right) \tag{15.1-5}$$

in which $[\mathbf{D}]$ is the same square matrix seen in Eq. 15.1-4. Factor k accounts for the parabolic z-direction variation of transverse shear stress, and kt can be regarded as the effective thickness for transverse shear deformation. The accepted value of k for a homogeneous

plate is $k = 5/6$. In Mindlin theory, not only are three fields involved, but the lateral deflection field is coupled to the rotation fields only by transverse shear deformation. Such a theory might seem more complicated than Kirchhoff theory but in fact makes it easier to obtain a variety of workable finite elements, although there are difficulties such as shear locking that must be overcome.

Remarks. As usual, material properties need not be isotropic. If principal directions of the material are other than x and y, a transformed $[\mathbf{D}]$ can be obtained in the same way that a transformed $[\mathbf{E}]$ is obtained (Section 8.2). A transformed lower-right 2 by 2 submatrix in Eq. 15.1-5 can be established as follows. Imagine that an orthotropic material has principal directions n and s in the xy plane, so that a matrix $[\mathbf{G}']$ relates Q_n and Q_s to $w_{,n} - \psi_n$ and $w_{,s} - \psi_s$. Equilibrium of z-direction forces relates $\{\mathbf{Q}'\} = \lfloor Q_n \; Q_s \rfloor^T$ to $\{\mathbf{Q}\} = \lfloor Q_x \; Q_y \rfloor^T$ of Fig. 15.1-3b, so the relation $\{\mathbf{Q}\} = [\mathbf{T}]^T\{\mathbf{Q}'\}$ can be written in terms of direction cosines between axes. If the required 2 by 2 submatrix in xy coordinates is called $[\mathbf{G}]$, it has the form $[\mathbf{G}] = [\mathbf{T}]^T[\mathbf{G}'][\mathbf{T}]$.

Because the material need not be homogeneous or isotropic, sandwich plates and other layered or fiber-reinforced construction can be accommodated. If material properties are symmetric with respect to the midsurface, the midsurface remains a neutral surface when the plate is bent. But in general, different layers may have different properties and may be anisotropic, so that locations where strains are zero depend on the loading applied. That is, bending and membrane states are coupled. Then in-plane displacements u and v must be added to the list of dependent variables. The coupling effect is pronounced in two-layer laminated plates [15.4]. Special elements for layered plates appear in commercial software. Such elements may use one node or several nodes on a thickness-direction line, depending on the theory used in element formulation. Computational models for sandwich and layered plates are surveyed in [15.5]. For such plates, transverse shear deformation is often important.

Cylinders and cones are singly-curved surfaces and are *developable,* meaning that they can be unrolled to become flat. A doubly-curved surface such as a sphere is not developable. Stated in reverse, a flat sheet of paper is easily rolled into a cylinder or a cone, but cannot be wrapped around a sphere (without wrinkling the paper). In terms of lateral deflection of an initially flat plate, a cylindrical or conical shape may have negligible membrane stress, but a spherical shape *must* develop membrane stress, perhaps enough for the plate to wrinkle (buckle). In most situations, the deflected plate midsurface is not developable, so that even if lateral deflection is small, membrane stresses arise, even when supports allow in-plane displacement. Membrane stresses support part of the lateral load, making lateral deflection smaller than it would be if load were supported by only by bending moments and transverse shear forces. If membrane stresses have appreciable effect, the situation is called a "large deflection" plate problem and is nonlinear because the intensity and distribution of membrane stresses are not known at the outset. In unfavorable circumstances, lateral deflection may be "large" if it is as little as half the plate thickness, the exact amount being dependent on the particulars of loading, support, and solution accuracy required. Similar remarks apply to a plate that is not initially flat: depending on the initial curvature and the nature of applied load, membrane stresses may be tensile or compressive, and buckling may be a concern. In summary, an analyst must be aware that linear plate analysis allows little departure from flatness, either before or after load is applied.

Transverse shear deformation becomes negligible in a plate whose span is much greater than its thickness. Plate elements should reflect this behavior, and not fail if the FE plate model is made extremely thin. However, failure by shear locking, in which computed deflections approach zero as thickness approaches zero, must be overcome in Mindlin plate elements. Failure may seem academic if it happens only when thickness is (say) a millionth of the element span, as no practical plate is this thin. Nevertheless such elements obviously are not foolproof, and software developers avoid them.

In the element library of FE software, one may find that plate elements are not identified as such, because shell elements serve as plate elements. A shell element is capable of modeling membrane action and bending action, either separately or in combination. A shell element functions as a plate-bending element if it is flat and if d.o.f. that model in-plane deformation of the midsurface are set to zero. These d.o.f. are nodal displacements u and v and drilling d.o.f. θ_z (if present).

When applying loads and examining computed results, analysts must understand the software's definition of "upper surface" and its sign conventions for nodal rotations and bending moments. Shell elements in an FE model may have various orientations in global coordinates, and stresses tangent to element surfaces are desired, so an "upper surface" is defined using local information for each element. Software may define the upper surface of an element by applying the right-hand rule when element node numbers are taken in numerical order. Thus the (local) $+z$ surface in Fig. 15.1-2a would be called the upper surface. A graphic display option may show the local $+z$ direction of each element by an arrow. One desires that arrows of contiguous elements all point in the same direction if the model is a plate, or all point outward (or perhaps all inward) if the model is a shell. An automatic mesh generator may produce a mesh for a plate or shell such that element upper surfaces (however defined) are not all on the same side of the plate or shell. Thus, on a surface of a plate or shell, a contour plot constructed from upper-surface element stresses would display extreme interelement discontinuities. Software may provide a way to alter definitions after mesh generation, so that upper surfaces of all elements appear on the same side of the plate or shell. Reversal of upper and lower surface definitions also reverses the direction of distributed load, which, for a shell, may change the loading from internal pressure to external pressure. In any case, analysts must be particularly cautious with FE models of plates and shells until they are familiar with software behavior.

15.2 C^1 (KIRCHHOFF) PLATE ELEMENTS

Transverse shear deformation is prohibited by Kirchhoff plate theory. Therefore, a plate problem is solved when lateral deflection $w = w(x,y)$ of the midsurface has been determined. Strain energy U in the plate due to nodal displacements can be expressed in terms of curvatures $\{\boldsymbol{\kappa}\} = \lfloor w_{,xx} \;\; w_{,yy} \;\; 2w_{,xy} \rfloor^T$ by setting $\gamma_{yz} = \gamma_{zx} = 0$ in Eqs. 15.1-1, substituting strains into the general expression for U (Eq. 4.4-5), and integrating through the plate thickness. Thus, with initial curvature terms omitted,

$$U = \int \frac{1}{2} \{\boldsymbol{\varepsilon}\}^T [\mathbf{E}] \{\boldsymbol{\varepsilon}\} \, dV \qquad \text{becomes} \qquad U = \int \frac{1}{2} \{\boldsymbol{\kappa}\}^T [\mathbf{D}] \{\boldsymbol{\kappa}\} \, dA \tag{15.2-1}$$

where A is the midsurface area and $[\mathbf{D}]$ is given by Eqs. 15.1-4 for a homogeneous and isotropic plate. Following the usual procedure for formulation of a displacement-based

element, we define displacement over an element by shape-function interpolation from nodal d.o.f. $\{\mathbf{d}\}$.

$$w = \lfloor \mathbf{N} \rfloor \{\mathbf{d}\} \quad \text{hence} \quad \{\boldsymbol{\kappa}\} = [\mathbf{B}]\{\mathbf{d}\} \quad \text{where} \quad [\mathbf{B}] = \begin{Bmatrix} -\partial^2/\partial x^2 \\ \partial^2/\partial y^2 \\ 2\partial^2/\partial x\,\partial y \end{Bmatrix} \lfloor \mathbf{N} \rfloor \tag{15.2-2}$$

Hence, with integration confined to a single element, Eq. 15.2-1 provides the element strain energy and element stiffness matrix $[\mathbf{k}]$.

$$U = \frac{1}{2}\{\mathbf{d}\}^T[\mathbf{k}]\{\mathbf{d}\} \qquad \text{where} \qquad [\mathbf{k}] = \int [\mathbf{B}]^T[\mathbf{D}][\mathbf{B}]\,dA \tag{15.2-3}$$

Typically, but not necessarily, $\{\mathbf{d}\}$ contains three d.o.f. per node, as shown in Fig. 15.1-2a, with $\psi_{xi} = w_{,xi}$ and $\psi_{yi} = w_{,yi}$ for a Kirchhoff element. A displacement field expressed in terms of generalized d.o.f. a_i can be expressed in terms of d.o.f. $\{\mathbf{d}\}$ by applying procedures described in Section 3.2. Because U involves second derivatives of w, continuity requires that first derivatives of w be interelement-continuous, at least in the limit of mesh refinement. Thus a Kirchhoff element is a C^1 element.

If a Kirchhoff element uses only the three d.o.f. per node shown in Fig. 15.1-2a, it has been shown that an element can either achieve interelement continuity of slopes $w_{,x}$ and $w_{,y}$ or a unique definition of twist $w_{,xy}$ at corners, but not both at once, regardless of element shape [15.6]. The difficulty can be overcome by adding $w_{,xy}$ to the list of nodal d.o.f. This option has not been widely used because boundary conditions become awkward and excessive interelement continuity may be enforced, as described in Section 8.6.

Development of Kirchhoff Elements. Early plate elements were 12-d.o.f. rectangles, with a node at each corner and three d.o.f. per node. One proposal for $w = w(x,y)$ was the "crossed beam" function, which extends to two dimensions the cubic shape functions $N_i(x)$ used for a beam along the x axis. Interelement compatibility of displacement and slope is obtained. However, inspection of the shape functions shows that the $w = xy$ term is missing, so that a state of constant twist is not possible [2.2]. Thus the element fails a patch test and is unacceptable.

Another early proposal for a 12-d.o.f. rectangular element was the following 12-term polynomial, which is an incomplete quartic.

$$w = \lfloor 1 \quad x \quad y \quad x^2 \quad xy \quad y^2 \quad x^3 \quad x^2y \quad xy^2 \quad y^3 \quad x^3y \quad xy^3 \rfloor \{\mathbf{a}\} \tag{15.2-4}$$

where the twelve a_i in $\{\mathbf{a}\}$ are generalized d.o.f.. This element is incompatible in normal slope; for example, along a shared side x = constant, adjacent elements generally display different values of $w_{,x}$. Incompatibilities approach zero with mesh refinement and the element performs satisfactorily, but the element cannot be generalized to nonrectangular shapes [3.3,15.7].

Triangular elements present different difficulties [3.3,15.7,15.8]. With three d.o.f. per node and vertex nodes only, nine d.o.f. are required. A complete cubic polynomial has 10 terms, including the cubic terms x^3, x^2y, xy^2, and y^3. If any one of them is omitted, the polynomial is unbalanced: the lateral displacement polynomial along an element side depends on the orientation of the side in xy coordinates, and the resulting element lacks geometric isotropy. If the middle two cubic terms are combined to form the term $x^2y + xy^2$, the transformation $\{\mathbf{d}\} = [\mathbf{A}]\{\mathbf{a}\}$, described in Section 3.2, produces a singular matrix $[\mathbf{A}]$ for some element

shapes. If the nine vertex d.o.f. are supplemented by lateral displacement at the centroid, so as to use all 10 terms, the element fails to converge. The aforementioned troubles can be avoided by representing $w = w(x,y)$ as a complete quartic (15 terms), but now an unfavorable arrangement of nodal d.o.f. is required, such as supplementing the usual nine d.o.f. by vertex d.o.f. $w_{,xy}$ and normal rotations at midsides. If midside d.o.f. are acceptable, a simple option is a six-d.o.f. constant-curvature element, based on a complete quadratic polynomial, but having an awkward arrangement of d.o.f.: lateral displacement at vertex nodes and normal rotations at midsides [15.9]. This element has a "mixed" form, also with six d.o.f., in which moment d.o.f. appear in place of rotational d.o.f., but this arrangement is even more awkward [15.10]. Remedies for some of these troubles include using area coordinates (Section 7.3) to assure geometric isotropy (Section 3.9), augmenting area-coordinate cubic terms by complicated quartic terms, and dividing the triangle into 10-d.o.f. subtriangles while enforcing continuity relations between subtriangles.

Efforts such as these have produced many elements that pass patch tests and converge properly with mesh refinement. They are all "strict" Kirchhoff elements, in which transverse shear strain is zero throughout the element. In practice, such elements seem to have been supplanted by "discrete" Kirchhoff elements, in which the constraint of zero transverse shear strain is enforced only at selected locations.

Discrete Kirchhoff (DK) Elements. Names often applied to these elements are DKT for a triangle and DKQ for a quadrilateral. Formulation begins with *independent* fields for lateral displacement and for rotation of a midsurface-normal line. In this respect, DK elements resemble Mindlin elements. However, in Mindlin elements the fields are implicitly coupled by transverse shear stiffness of the material, while in DK elements the fields are explicitly coupled by enforcing zero transverse shear strain at selected locations. Formulation of a DKT element is summarized as follows [15.11].

The starting point is a straight-sided triangle having vertex and midside nodes (Fig. 15.2-1a). Rotation components of a thickness-direction line are interpolated from nodal rotations ψ_{xi} and ψ_{yi}, and are given by complete quadratic polynomials.

$$\psi_x = \sum_{i=1}^{6} N_i \psi_{xi} \quad \text{and} \quad \psi_y = \sum_{i=1}^{6} N_i \psi_{yi} \tag{15.2-5}$$

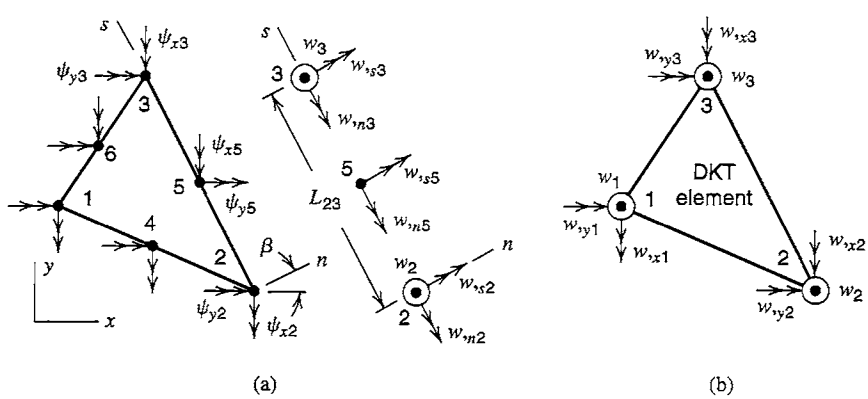

Figure 15.2-1. (a) D.o.f. used in the formulation of a DKT element. (b) The final DKT element, which has the nine d.o.f. shown.

Shape functions N_i are given by Eqs. 7.1-2 or 7.3-4. Lateral deflection w is defined only on element sides, using d.o.f. of vertex nodes. On each side w is a cubic in the side-tangent coordinate s. Slope $w_{,s}$ at midside can be obtained from beam shape functions, Fig. 2.3-1 (or Fig. 3.2-4), by differentiating once and evaluating at midspan. Thus, at the middle of side 2-3 for example,

$$w_{,s5} = \frac{3}{2L_{23}}(w_3 - w_2) - \frac{1}{4}(w_{,s2} + w_{,s3}) \tag{15.2-6}$$

Similar expressions are written for each of the two remaining sides. Slope $w_{,s}$ is related to slopes $w_{,x}$ and $w_{,y}$ by the relation $w_{,s} = -w_{,x}\sin\beta + w_{,y}\cos\beta$. Thus Eq. 15.2-6 relates $w_{,s5}$ to values of w, $w_{,x}$ and $w_{,y}$ at nodes 2 and 3. Slopes $w_{,s}$ at midsides are not introduced as additional d.o.f. but are needed in step 2 below.

At this point we have introduced 21 d.o.f.: ψ_{xi} and ψ_{yi} at each of six nodes, and w_i, $w_{,xi}$ and $w_{,yi}$ at each of the three vertex nodes. To obtain a nine-d.o.f. element, whose d.o.f. are w_i, $w_{,xi}$ and $w_{,yi}$ at each of the three vertex nodes, 12 constraints must be imposed. They are as follows.

1. Transverse shear strains γ_{zx} and γ_{yz} vanish at the vertex nodes. Thus, from Eqs. 15.1-1, we obtain the six constraints

$$\psi_{xi} = w_{,xi} \quad \text{and} \quad \psi_{yi} = w_{,yi} \quad \text{for} \quad i = 1,2,3 \tag{15.2-7}$$

2. Transverse shear strain γ_{sz} vanishes at midsides. Thus we obtain the three constraints

$$\psi_{si} = w_{,si} \quad \text{for} \quad i = 4,5,6 \quad \text{where} \quad \psi_s = -\psi_x \sin\beta + \psi_y \cos\beta \tag{15.2-8}$$

3. Normal slopes vary linearly along each side. Therefore

$$\psi_{n4} = \frac{1}{2}(w_{,n1} + w_{,n2}) \quad \psi_{n5} = \frac{1}{2}(w_{,n2} + w_{,n3}) \quad \psi_{n6} = \frac{1}{2}(w_{,n3} + w_{,n1}) \tag{15.2-9}$$

$$\text{where} \quad \psi_n = \psi_x \cos\beta + \psi_y \sin\beta \quad \text{and} \quad w_{,n} = w_{,x}\cos\beta + w_{,y}\sin\beta$$

After the foregoing 12 constraints have been applied, the 12 nodal rotations, ψ_{xi} and ψ_{yi} for $i = 1,2,\ldots,6$, are expressed in terms of the nine w_i, $w_{,xi}$, and $w_{,yi}$ at vertex nodes. Symbolically, using a transformation matrix as in Chapter 8, this relation is

$$\lfloor \psi_{x1} \;\; \psi_{y1} \;\; \psi_{x2} \;\; \cdots \;\; \psi_{y6} \rfloor^T = \underset{12\times 9}{[\mathbf{T}]} \lfloor w_1 \;\; w_{,x1} \;\; w_{,y1} \;\; w_2 \;\; \cdots \;\; w_{,y3} \rfloor^T \tag{15.2-10}$$

Element strains, from Eqs. 15.1-1, are

$$\begin{Bmatrix} \varepsilon_x \\ \varepsilon_y \\ \gamma_{xy} \end{Bmatrix} = -z[\partial]\begin{Bmatrix} \psi_x \\ \psi_y \end{Bmatrix} \quad \text{where} \quad [\partial] = \begin{bmatrix} \partial/\partial x & 0 \\ 0 & \partial/\partial y \\ \partial/\partial y & \partial/\partial x \end{bmatrix} \tag{15.2-11}$$

Equations 15.2-5, 15.2-10, and 15.2-11 yield strains $\{\boldsymbol{\varepsilon}\} = \lfloor \varepsilon_x \;\; \varepsilon_y \;\; \gamma_{xy} \rfloor^T$.

$$\{\boldsymbol{\varepsilon}\} = \underbrace{-z[\partial]\begin{bmatrix} N_1 & 0 & N_2 & 0 & \cdots & N_6 & 0 \\ 0 & N_1 & 0 & N_2 & \cdots & 0 & N_6 \end{bmatrix}[\mathbf{T}]}_{[\mathbf{B}]} \underbrace{\lfloor w_1 \;\; w_{,x1} \;\; w_{,y1} \;\; w_2 \;\; \cdots \;\; w_{,y3} \rfloor^T}_{\{\mathbf{d}\}} \tag{15.2-12}$$

Expressions such as Eq. 7.2-9 are used in forming derivatives of the N_i. Strain energy in the element is given by the first of Eqs. 15.2-1. After integration through the thickness, the 9 by 9 element stiffness matrix [**k**] is given by Eq. 15.2-3, in which, for an isotropic material, [**D**] is given by Eq. 15.1-4. Degrees of freedom {**d**} of Eq. 15.2-12 are shown in Fig. 15.2-1b. Degrees of freedom used in software may be θ_{xi} in place of $w_{,yi}$ and $-\theta_{yi}$ in place of $w_{,xi}$. After nodal d.o.f. {**d**} have been computed by solving the FE model, Eq. 15.2-12 yields strains, Eq. 15.1-3 yields stresses, and Eq. 15.1-2 yields bending moments.

For an element of uniform thickness, [**k**] is exactly integrated by a three-point quadrature rule. An explicit formulation is available [15.12], and Fortran coding for [**k**] appears in [15.13]. The original DKT formulation [15.14] was found to remain one of the best three-node plate elements over 10 years after its introduction [15.11]. By extending the foregoing formulation procedure to four sides, a quadrilateral element DKQ is produced [2.17]. Modifications of DKT and DKQ elements are reported in [2.17,15.15–15.17], with Fortran coding in [15.15].

Because w is defined only along element sides, consistent formulations for an element load vector and an elastic foundation stiffness matrix are not available. Serviceable forms can be obtained by defining $w = w(x,y)$ in an ad hoc manner. Also, there is an alternative formulation of the DKT element that defines w within the element [2.17].

Numerical results produced by the DKT element, extracted from [15.14,15.17], are shown in Table 15.2-1. Meshes are uniform and use N_{es} elements per side of a plate quadrant, Fig. 15.2-2a. In each test case all four edges of the complete plate have the same boundary conditions, either clamped or simply supported (soft form; see Section 15.5). Distributed loads are lumped by assigning one-third the total force on an element to each of its vertex nodes. Results in Table 15.2-1 are for $\nu = 0.3$ and are reported as the ratio of computed deflection to the exact deflection as stated in [10.2]. Additional results, reported in [15.11,15.12], show that the DKT element performs well at large aspect ratios and satisfactorily solves the "twisted strip" test case.

In software, an element that purports to be a quadrilateral may actually be composed of two or four triangles. With two triangles, Fig. 15.2-2a, division is made along the shorter diagonal if the quadrilateral is not rectangular. With four triangles, Fig.15.2-2b, both diagonals are used, producing two sets of triangles that overlap. Overlapping represents the quadrilateral twice, so the resulting stiffness matrix must be divided by two. Alternatively, four

TABLE 15.2-1. CENTER DEFLECTION w_c AND CENTER BENDING MOMENT M_c IN A SQUARE PLATE, CALCULATED BY DKT ELEMENTS [15.14,15.17]. EXACT VALUE = 1.000. SEE TEXT FOR DESCRIPTION.

Mesh	Uniformly loaded				Concentrated center load	
Fig. 15.2-2a	Simply supported		Clamped		Simply supported	Clamped
	w_c	M_c	w_c	M_c	w_c	w_c
$N_{es} = 1$	1.025	1.355	1.500	2.258	1.076	1.012
$N_{es} = 2$	0.999	1.078	1.228	1.330	1.008	1.046
$N_{es} = 4$	1.001	1.017	1.069	1.089	1.003	1.019
$N_{es} = 8$	1.001	——	1.021	——	1.001	1.007

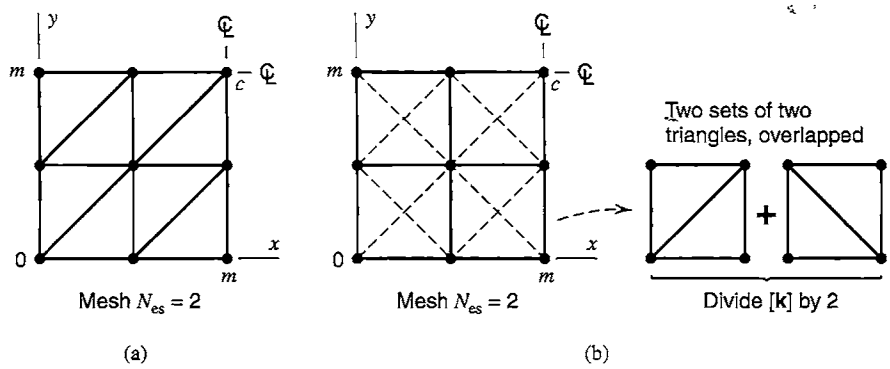

Figure 15.2-2. Mesh in one quadrant of a square plate. Sides $x = 0$ and $y = 0$ are supported and there is symmetry about both centerlines. (a) Triangles or two-triangle quadrilaterals. (b) Quadrilaterals, each built of four overlapping triangles.

nonoverlapping triangles might share an internal node, whose d.o.f. are condensed prior to assembling the quadrilateral into the FE structure. Four-triangle arrangements avoid some of the directional bias that can appear with two-triangle arrangements. Table 15.2-2 lists results provided by uniform meshes of quadrilaterals built of four overlapping DKT triangles, as shown in Fig. 15.2-2b. We see that this arrangement is not as flexible as that of Fig. 15.2-2a. This behavior is at least partly explained by noting that the triangle whose 90° angle is at $x = y = 0$ is more completely constrained by supports than are other triangles in the quadrilateral element; indeed for the clamped-edge case this triangle has no deformation at all. Also, the central plate node receives less load in Fig. 15.2-2b for the following reason. Let uniformly distributed load produce a force F on each triangle in Fig. 15.2-2a, so that force $F/3$ is applied to each triangle vertex. Consider the upper-right node in Fig. 15.2-2. It receives force $2(F/3)$ in Fig. 15.2-2a, and force $3(F/3)/2 = 1.5(F/3)$ in Fig. 15.2-2b.

TABLE 15.2-2. UNIFORMLY LOADED SQUARE PLATES. ELEMENTS ARE FOUR-TRIANGLE QUADRILATERALS (FIG. 15.2-2b). w_c = CENTER DEFLECTION, M_c = CENTER BENDING MOMENT, M_{xy0} = TWISTING MOMENT AT $x = y = 0$, M_m = BENDING MOMENT AT MIDEDGE. EXACT VALUE = 1.000.

Mesh	Simply supported edges			Clamped edges		
Fig. 15.2-2b	w_c	M_c	M_{xy0}	w_c	M_c	M_m
$N_{es} = 1$	0.803	1.367	0.488	1.177	1.878	0.689
$N_{es} = 2$	0.945	1.095	0.849	1.084	1.277	0.935
$N_{es} = 4$	0.986	1.024	0.955	1.025	1.064	0.942
$N_{es} = 8$	0.997	1.006	0.987	1.010	1.010	0.961
$N_{es} = 16$	1.000	1.001	0.996	1.006	0.996	0.979

15.3 C^0 (MINDLIN) PLATE ELEMENTS

Early plate elements were Kirchhoff elements because of the influence of classical plate theory. Mindlin elements appeared later, as special forms of isoparametric elements for 3D solids. The 3D "parent" element of the plate element shown in Fig. 15.1-2a is an eight-node solid element having $8 \times 3 = 24$ d.o.f. The lateral displacement and rotation fields of a Mindlin plate element having n nodes can be stated as

$$\begin{Bmatrix} w \\ \psi_x \\ \psi_y \end{Bmatrix} = \sum_{i=1}^{n} \begin{bmatrix} N_i & 0 & 0 \\ 0 & N_i & 0 \\ 0 & 0 & N_i \end{bmatrix} \begin{Bmatrix} w_i \\ \psi_{xi} \\ \psi_{yi} \end{Bmatrix} \quad \text{or} \quad \{\mathbf{u}\} = [\mathbf{N}]\{\mathbf{d}\} \tag{15.3-1}$$

Here the same shape functions are used for each displacement component. This is the simplest and most obvious arrangement, but not the only arrangement possible and not necessarily the best. Strain ε_z is present in the parent 3D element, but Eqs. 15.1-1 and 15.3-1 leave strain ε_z undefined in the plate element, which avoids ill-conditioning due to small thickness. A plate element based on Eq. 15.3-1 is formulated in much the same way as a 2D isoparametric element.

A Mindlin plate element and its 3D parent element are subject to the same disorders, such as shear locking when the element is thin and spurious modes when elements are underintegrated. Thus, despite conceptual simplicity, it is not easy to produce a Mindlin element robust enough for inclusion in user-oriented software. In the present section we describe element formulation, and some disorders discovered and remedies proposed soon after Mindlin elements were introduced. Additional remedies are summarized in Section 15.4.

Formulation. Terms for both curvature and transverse shear strain appear in array $\{\boldsymbol{\kappa}_M\}$ of Eq. 15.1-5. With $\{\mathbf{u}\} = \lfloor w \;\; \psi_x \;\; \psi_y \rfloor^T$, we obtain from Eqs. 15.1-1 and 15.1-5

$$\{\boldsymbol{\kappa}_M\} = \begin{Bmatrix} \psi_{x,x} \\ \psi_{y,y} \\ \psi_{x,y} + \psi_{y,x} \\ \psi_x - w_{,x} \\ \psi_y - w_{,y} \end{Bmatrix} = [\boldsymbol{\partial}]\{\mathbf{u}\} \quad \text{where} \quad [\boldsymbol{\partial}] = \begin{bmatrix} 0 & \partial/\partial x & 0 \\ 0 & 0 & \partial/\partial y \\ 0 & \partial/\partial y & \partial/\partial x \\ -\partial/\partial x & 1 & 0 \\ -\partial/\partial y & 0 & 1 \end{bmatrix} \tag{15.3-2}$$

From Eqs. 15.3-1 and 15.3-2, for an element having n nodes,

$$\{\boldsymbol{\kappa}_M\} = \underset{5\times 3n}{[\mathbf{B}_M]}\{\mathbf{d}\} \quad \text{where} \quad [\mathbf{B}_M] = [\boldsymbol{\partial}][\mathbf{N}] = \begin{bmatrix} 0 & N_{1,x} & 0 & 0 \\ 0 & 0 & N_{1,y} & N_{n,y} \\ 0 & N_{1,y} & N_{1,x} & N_{n,x} \\ -N_{1,x} & N_1 & 0 & 0 \\ -N_{1,y} & 0 & N_1 & N_n \end{bmatrix} \tag{15.3-3}$$

Strain energy U in the element due to nodal displacements, and the element stiffness matrix, are

$$U = \frac{1}{2}\{\mathbf{d}\}^T[\mathbf{k}]\{\mathbf{d}\} \quad \text{and} \quad [\mathbf{k}] = \int [\mathbf{B}_M]^T[\mathbf{D}_M][\mathbf{B}_M]\,dA \tag{15.3-4}$$

where $[\mathbf{D}_M]$ is stated in Eq. 15.1-5. In general, isoparametric coordinates ξ and η are used in the midsurface, so $dA = J\,d\xi\,d\eta$, where J is the Jacobian determinant. For four- and eight-node plate elements respectively, shape functions $N_i = N_i(\xi,\eta)$ are given by Eqs. 6.2-3 and 6.4-1. Shape function derivatives, needed in Eq. 15.3-3, are given by the usual transformation (Eq. 6.2-7):

$$N_{i,x} = \Gamma_{11}N_{i,\xi} + \Gamma_{12}N_{i,\eta} \qquad N_{i,y} = \Gamma_{21}N_{i,\xi} + \Gamma_{22}N_{i,\eta} \tag{15.3-5}$$

The element stiffness matrix can be represented as the sum of a bending stiffness $[\mathbf{k}_b]$ and a transverse shear stiffness $[\mathbf{k}_s]$. To represent $[\mathbf{B}_M]$ as the sum of bending terms and transverse shear terms, we define $[\mathbf{B}_b]$ as $[\mathbf{B}_M]$ but with the last two rows null, and define $[\mathbf{B}_s]$ as $[\mathbf{B}_M]$ but with the first three rows null, so that $[\mathbf{B}_M] = [\mathbf{B}_b] + [\mathbf{B}_s]$. Then from Eq. 15.3-4,

$$[\mathbf{k}] = \underbrace{\int [\mathbf{B}_b]^T[\mathbf{D}_M][\mathbf{B}_b]\,dA}_{[\mathbf{k}_b]} + \underbrace{\int [\mathbf{B}_s]^T[\mathbf{D}_M][\mathbf{B}_s]\,dA}_{[\mathbf{k}_s]} \tag{15.3-6}$$

Coupling terms $[\mathbf{B}_b]^T[\mathbf{D}_M][\mathbf{B}_s]$ and $[\mathbf{B}_s]^T[\mathbf{D}_M][\mathbf{B}_b]$ vanish because of the distribution of zeros in $[\mathbf{D}_M]$. The following discussion describes how separate consideration of $[\mathbf{k}_b]$ and $[\mathbf{k}_s]$ permits some (but not all) element defects to be overcome. Some details related to Eq. 15.3-6 appear in Section 15.4.

Element Behavior. Elements depicted in the first column of Fig. 15.3-1 are viewed edgewise, parallel to their midsurfaces, and are either bilinear (4 nodes) or quadratic (8 or 9 nodes). They are loaded by prescribed rotations on opposite sides, so that displacements do not vary with y. A bilinear element and three quadratic elements are shown in plan view in Table 15.3-1, along with terminology for quadrature. For states of pure bending and pure twist, the contribution of $[\mathbf{k}_b]$ is correctly evaluated by all quadrature rules. Trouble arises from $[\mathbf{k}_s]$ of Eq. 15.3-6. Figure 15.3-1 suggests the order of Gauss quadrature needed to avoid shear locking. In the first example, pure bending of a bilinear element, transverse shear strain γ_{zx} is correct only at $x = L/2$. This observation suggests that $[\mathbf{k}_s]$ should be integrated using a single Gauss point at the element center. If instead $[\mathbf{k}_s]$ were integrated using 2 by 2 Gauss quadrature, the element would display shear locking due to the element's need to display transverse shear in order to represent bending. This behavior is exactly as described for a plane element in Section 3.6. Thus Eq. 3.6-11 shows that as a bilinear plate element becomes thin, 2 by 2 Gauss quadrature overestimates its bending stiffness by a factor of about $(L/t)^2$. If the bilinear element is asked to display linearly varying moment—the second example in Fig. 15.3-1—there is *no* integration rule that avoids the element's overestimate of γ_{zx}.

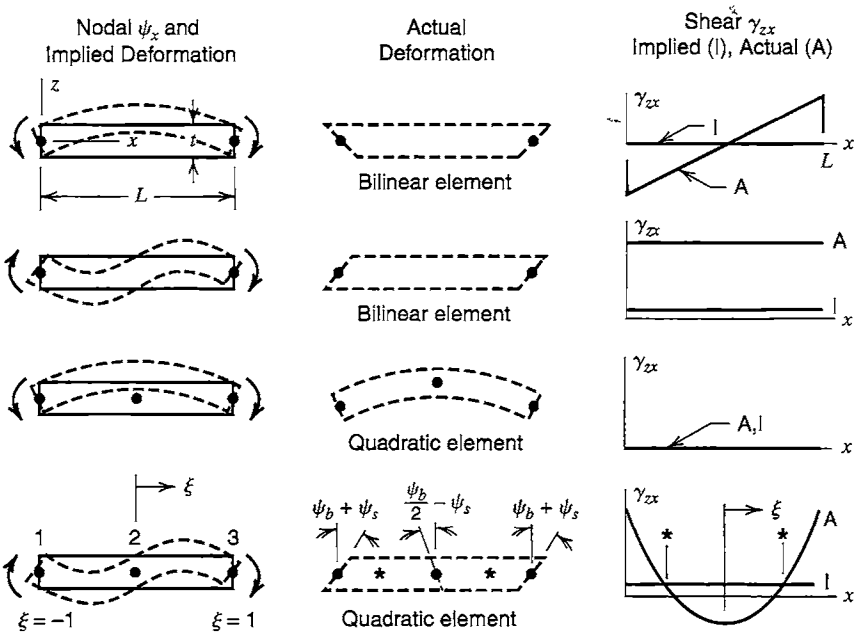

Figure 15.3-1. Edge views of Mindlin plate elements whose y-parallel sides are caused to rotate as shown. Elements are viewed parallel to the y axis.

Each Gauss point used in formulation of a Mindlin plate element introduces *shear constraints,* which force transverse shear strains γ_{yz} and γ_{zx} at the Gauss point to approach zero as the span-to-thickness ratio becomes large. In other words $[\mathbf{k}_s]$ functions as a penalty matrix, as described in Chapter 13.

The latter two examples in Fig. 15.3-1 illustrate uniform bending and linearly varying bending of a quadratic element. We see that uniform bending can be correctly represented regardless of the quadrature rule. In the quadratic element, linearly varying bending is correctly represented only by an order 2 Gauss rule. To see that this is so, note that linearly-varying bending is accompanied by constant transverse shear force, which is associated with constant transverse shear rotation ψ_s as shown in the last row of Fig. 15.3-1. A beam behaves in the same way, and elementary beam theory shows that if rotation due to bending is ψ_b at ends, it is $-\psi_b/2$ at midspan. Thus, using shape functions from Eq. 6.1-4, rotation ψ as a function of dimensionless coordinate ξ is

$$\psi = \frac{1}{2}(-\xi + \xi^2)(\psi_b + \psi_s) + (1 - \xi^2)\left(-\frac{1}{2}\psi_b + \psi_s\right) + \frac{1}{2}(\xi + \xi^2)(\psi_b + \psi_s) \qquad (15.3\text{-}7)$$

where $\xi = \pm 1$ at beam ends and ψ is taken as positive clockwise in this exercise. Curvature $\psi_{,x} = (2/L)\psi_{,\xi}$ and bending moment M vanish at midspan, as beam theory requires. But $w = 0$ throughout the element because $w = 0$ at all nodes, so transverse shear strain γ_{zx} is due entirely to ψ. We set $\psi = \psi_s$ to determine values of ξ where γ_{zx} is correctly represented, and from Eq. 15.3-7 obtain $\xi = \pm 1/\sqrt{3}$, which are Gauss point locations of an order 2 rule.

The foregoing discussion suggests that reduced integration should be used to generate stiffness matrices of Mindlin plate elements. Reduced integration of *both* $[\mathbf{k}_b]$ and $[\mathbf{k}_s]$ causes rank deficiency of $[\mathbf{k}]$ due to spurious modes (mechanisms). One-point integration of the four-node bilinear element introduces only two shear constraints, one each on γ_{yz}

TABLE 15.3-1. DATA FOR SELECTED MINDLIN PLATE ELEMENTS. INTEGRATION: R = REDUCED, S = SELECTIVE, F = FULL; n_{sc} = NUMBER OF SHEAR CONSTRAINTS PER ELEMENT; n_{dof} = NUMBER OF D.O.F. ADDED TO A LARGE MESH BY ONE ELEMENT; n_{mech} = NUMBER OF MECHANISMS PER *UNSUPPORTED* ELEMENT.

Element type		Integration rule Type	$[\mathbf{k}_b]$	$[\mathbf{k}_s]$	n_{sc}	n_{dof}	n_{mech}
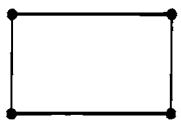	Bilinear:	R	1×1	1×1	2	3	4
	4 nodes	S	2×2	1×1	2	3	2
	12 d.o.f.	F	2×2	2×2	8	3	0
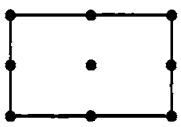	Lagrange:	R	2×2	2×2	8	12	4
	9 nodes	S	3×3	2×2	8	12	1
	27 d.o.f.	F	3×3	3×3	18	12	0
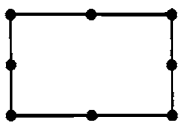	Serendipity:	R	2×2	2×2	8	9	1
	8 nodes	S	3×3	2×2	8	9	0
	24 d.o.f.	F	3×3	3×3	18	9	0
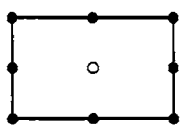	Heterosis:	S	3×3	2×2	8	11	0
	9 nodes	(Ref. [2.13]. D.o.f. w at the center node is					
	26 d.o.f.	omitted; d.o.f. there are ψ_x and ψ_y only.)					

and γ_{zx}, and allows four mechanisms to remain. For an element in which $x = y = 0$ at the center and with constants c_i, these mechanisms are: (1) $w = \psi_y = 0$, $\psi_x = c_1 xy$, which resembles the first example in Fig. 15.3-1 but with y variation; (2) the similar mode $w = \psi_x = 0$, $\psi_y = c_2 xy$; (3) $w = 0$, $\psi_x = -c_3 y$, $\psi_y = c_3 x$, in which upper and lower element surfaces rotate in opposite directions about the z axis; and (4) the w-hourglass mode $w = c_4 xy$, $\psi_x = \psi_y = 0$, which resembles the pure twist mode of Fig. 15.1-4c except that midsurface-normal lines do not rotate. The economy of one-point integration can be important in dynamic and nonlinear applications, with spurious modes suppressed by "stabilization" matrices, as described for plates in [15.18,15.19] and for other problems in [3.3,6.13–6.15].

Reduced (2 by 2) integration of quadratic plate elements does not suppress mechanisms that also appear in plane elements (for plate elements, substitute $u = -z\psi_x$ and $v = -z\psi_y$ in Fig. 6.8-3). These modes comprise the single mechanism possible in a serendipity element and three mechanisms possible in a Lagrange element. The fourth mechanism possible

in a Lagrange plate element, most simply stated for a square element two units on a side in which $x = y = 0$ at the center, is $\psi_x = \psi_y = 0$, $w = c(3x^2y^2 - x^2 - y^2)$, where c is a constant. This mechanism can cause displacement oscillations in comparatively thick Lagrange elements [2.13], but is not possible in the "heterosis" element of Table 15.3-1 because the term x^2y^2 is not present in its w field.

Some troublesome mechanisms can be avoided by the device of *selective* integration, in which $[\mathbf{k}_s]$ is integrated by a rule of lower order than the rule used for $[\mathbf{k}_b]$. The effect of using selective integration is seen in Table 15.3-1. The two mechanisms that remain in the bilinear element are those identified as (3) and (4) in the second preceding paragraph. Mechanism (3) is not communicable between elements, and so causes no trouble in a mesh of more than one element. Mechanism (4) *is* communicable. The remaining mechanism of the Lagrange element is the aforementioned mechanism $\psi_x = \psi_y = 0$, $w = c(3x^2y^2 - x^2 - y^2)$, which also is communicable. Communicable mechanisms can be troublesome, as when a load pattern excites the mechanism in elements distant from restraint that may be provided by supports.

The behavior of elements cited in Table 15.3-1 is shown in Fig. 15.3-2, which uses an 8 by 8 mesh on a clamped square plate. Shear locking is in evidence. As a plate becomes thin, bilinear elements with full integration, and serendipity elements with any integration rule, all fail by grossly underestimating the center deflection. An explanation can be extracted from Table 15.3-1, using the same "constraint-counting" argument that is applied to Fig. 13.5-1b. Consider the addition of a single element to a large mesh, in the manner of adding element 10 in Fig. 13.5-1b. Each added plate element brings n_{dof} d.o.f. and n_{sc} shear constraints to the mesh. If $n_{\text{dof}} - n_{\text{sc}}$ is zero or negative, all added d.o.f. are occupied in satisfying shear constraints, with none left over to model structural response. However, some elements fail in Fig. 15.3-2, even though the "element count" is $n_{\text{dof}} - n_{\text{sc}} = +1$. This happens because boundary conditions impose enough additional constraints to make the corresponding

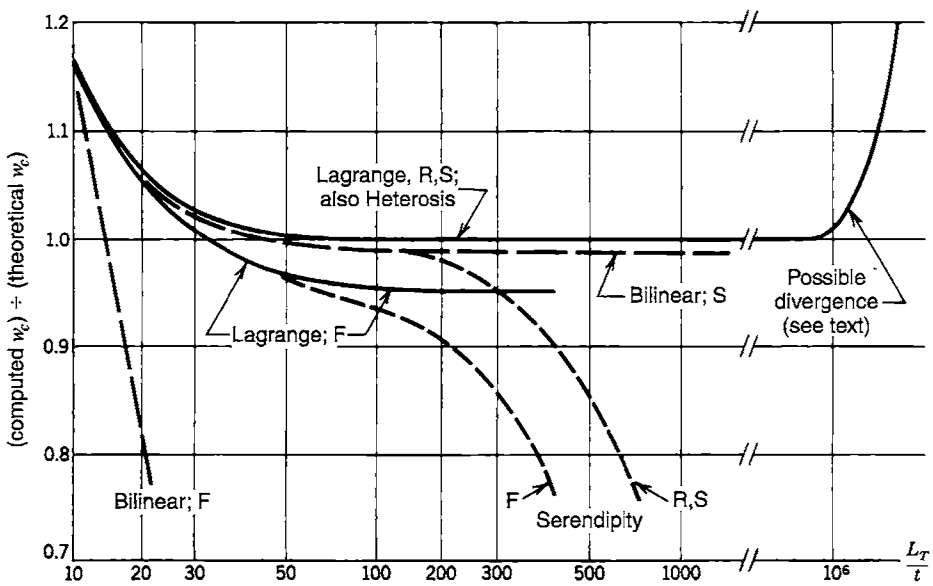

Figure 15.3-2. Center deflection of a uniformly loaded square plate of side length L_T with all edges clamped, modeled by an 8 by 8 mesh [15.20,15.21]. Notation for integration rules appears in Table 15.3-1.

"structure count" zero or negative, thus locking the mesh. For the serendipity element with selective integration, an N by N mesh on the entire plate, and clamped edges, the structure count is negative unless N is 12 or more [15.22]. Only the heterosis element is free of troublesome mechanisms and is satisfactory in Fig. 15.3-2. But the heterosis element fails patch tests for elements shapes that are not rectangles or parallelograms [2.17,3.3]. Also, Lagrange and heterosis elements have side nodes and require more computation to formulate than a bilinear element. The expense may be detrimental in dynamic and nonlinear applications.

The indefinitely rising curve in the right hand part of Fig. 15.3-2 suggests divergence to numerical ill-conditioning in a mesh that does not suffer from shear locking. As penalty matrix $[\mathbf{k}_s]$ becomes numerically large, it may overwhelm the useful information in $[\mathbf{k}_b]$. This kind of potential difficulty is also seen in the example problem of Section 13.3. Although associated with matrix $[\mathbf{k}_s]$, this behavior is not locking because it is not caused by locking out a desired deformation mode.

We conclude that despite selective integration, *none* of the C^0 elements discussed in this section is entirely adequate. More devices used in the search for good C^0 plate elements are summarized in the next section.

15.4 MINDLIN BEAM. MORE DEVICES FOR C^0 PLATE ELEMENTS

For all the troubles of Mindlin plate elements, developers have preferred them to Kirchhoff elements because they provide more options for possible improvement and because they are more readily extended to become shell elements. The goal is an element free of shear locking and spurious modes, which passes patch tests, is accurate without great mesh refinement, and loses little accuracy when element shapes are distorted. As might be expected, many devices have been explored, singly and in combination. In what follows we note some of them. Papers cited list many more references. A survey is included in [15.23].

We begin with analysis of a homogeneous and isotropic Mindlin beam element. The beam illustrates, in a simple way, some details of formulation and some devices for improvement that are also used in Mindlin plate elements.

Mindlin Beam. For the two-node plane Mindlin beam element in Fig. 15.4-1, lateral displacement and rotation fields are

$$\begin{aligned} w &= \lfloor N_1 \;\; 0 \;\; N_2 \;\; 0 \rfloor \{\mathbf{d}\} \\ \psi &= \lfloor 0 \;\; N_1 \;\; 0 \;\; N_2 \rfloor \{\mathbf{d}\} \end{aligned} \qquad \text{where} \qquad \begin{aligned} N_1 &= \frac{L-x}{L} \qquad N_2 = \frac{x}{L} \\ \{\mathbf{d}\} &= \lfloor w_1 \;\; \psi_1 \;\; w_2 \;\; \psi_2 \rfloor^T \end{aligned} \tag{15.4-1}$$

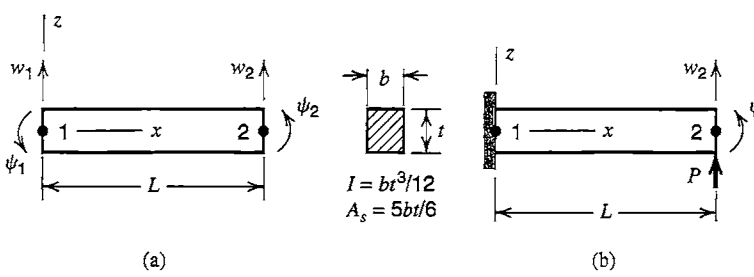

Figure 15.4-1. (a) Mindlin beam element of rectangular cross section. (b) Tip-loaded cantilever beam.

Strains are $\varepsilon_x = -z\psi_{,x}$ and $\gamma_{zx} = w_{,x} - \psi$. Element strain energies U_b in bending and U_s in transverse shear are

$$U_b = \iint_0^L \frac{1}{2}E\varepsilon_x^2\,dx\,dA = \int_0^L \frac{1}{2}EI\psi_{,x}^2\,dx = \frac{1}{2}\{\mathbf{d}\}^T[\mathbf{k}_b]\{\mathbf{d}\} \tag{15.4-2a}$$

$$U_s = \iint_0^L \frac{1}{2}G\gamma_{zx}^2\,dx\,dA = \int_0^L \frac{1}{2}GA_s(w_{,x} - \psi)^2\,dx = \frac{1}{2}\{\mathbf{d}\}^T[\mathbf{k}_s]\{\mathbf{d}\} \tag{15.4-2b}$$

where A is the cross-sectional area and A_s is the "effective" cross-sectional area of the beam in resisting transverse shear deformation. For a rectangular cross section, γ_{zx} varies parabolically over dimension t in Fig. 15.4-1, and $A_s = 5A/6$. With a uniform beam and exact integration, Eqs. 15.4-1 and 15.4-2 yield

$$[\mathbf{k}_b] = EI\begin{bmatrix} 0 & 0 & 0 & 0 \\ 0 & 1/L & 0 & -1/L \\ 0 & 0 & 0 & 0 \\ 0 & -1/L & 0 & 1/L \end{bmatrix}, \quad [\mathbf{k}_s] = GA_s\begin{bmatrix} 1/L & 1/2 & -1/L & 1/2 \\ 1/2 & L/3 & -1/2 & L/6 \\ -1/L & -1/2 & 1/L & -1/2 \\ 1/2 & L/6 & -1/2 & L/3 \end{bmatrix} \tag{15.4-3}$$

The same result is given by two-point Gauss quadrature. With one-point Gauss quadrature, Eqs. 15.4-1 and 15.4-2 yield

$$[\mathbf{k}_b] = EI\begin{bmatrix} 0 & 0 & 0 & 0 \\ 0 & 1/L & 0 & -1/L \\ 0 & 0 & 0 & 0 \\ 0 & -1/L & 0 & 1/L \end{bmatrix}, \quad [\mathbf{k}_s] = GA_s\begin{bmatrix} 1/L & 1/2 & -1/L & 1/2 \\ 1/2 & L/4 & -1/2 & L/4 \\ -1/L & -1/2 & 1/L & -1/2 \\ 1/2 & L/4 & -1/2 & L/4 \end{bmatrix} \tag{15.4-4}$$

One-point quadrature provides the exact $[\mathbf{k}_b]$ of a beam element but not of a plate element because a plate is two-dimensional.

Locking. Consider the one-element cantilever beam problem of Fig. 15.4-1b, for which

$$\left(EI\begin{bmatrix} 0 & 0 \\ 0 & 1/L \end{bmatrix} + GA_s\begin{bmatrix} 1/L & -1/2 \\ -1/2 & l \end{bmatrix}\right)\begin{Bmatrix} w_2 \\ \psi_2 \end{Bmatrix} = \begin{Bmatrix} P \\ 0 \end{Bmatrix} \tag{15.4-5}$$

where $l = L/3$ for exact integration and $l = L/4$ for one-point integration. With exact integration, $l = L/3$, Eq. 15.4-5 yields

$$w_2 = \frac{12EI + 4GA_sL^2}{12EI + GA_sL^2}\left(\frac{PL}{GA_s}\right) \qquad \psi_2 = \frac{6PL^2}{12EI + GA_sL^2} \tag{15.4-6}$$

The significance of Eq. 15.4-6 is easier to see if we set $\nu = 0$, so that $E = 2G$, and consider a rectanglar cross section, for which we substitute $I = bt^3/12$ and $A_s = 5bt/6$ in the large fraction terms. Thus

$$w_2 = \frac{12(t/L)^2 + 20}{12(t/L)^2 + 5}\left(\frac{PL}{GA_s}\right) \qquad \psi_2 = \frac{30}{12(t/L)^2 + 5}\left(\frac{P}{GA_s}\right) \tag{15.4-7}$$

For a very deep beam the t/L terms dominate, and w_2 approaches the correct transverse shear deformation, PL/GA_s. But for a slender beam t/L is small, and w_2 then approaches $4PL/GA_s$, with no contribution from bending. This result is a clear indication of shear locking. In contrast, with reduced integration, for which $l = L/4$ in Eq. 15.4-5, we obtain

$$w_2 = \left(1 + \frac{4EI}{GA_s L^2}\right)\frac{PL^3}{4EI} \qquad \psi_2 = \frac{PL^2}{2EI} \tag{15.4-8}$$

Here ψ_2 is correct and is independent of A_s. As the beam becomes slender, I approaches zero faster than A_s, and while the limiting deflection $PL^3/4EI$ is incorrect (it should be $PL^3/3EI$) there is no locking behavior. This is the motivation for use of reduced integration to calculate $[\mathbf{k}_s]$ of Mindlin elements for beams and plates. As argued following Eq. 13.4-3, $[\mathbf{k}_s]$ is a penalty matrix, which we wish to make singular, a goal achieved by one-point quadrature.

Modified Properties. It happens that Eqs. 15.4-8 produce correct results for both deep beams and slender beams if a modified shear stiffness GA^* is used in place of GA_s. We can obtain an expression for GA^* by requiring that Eq. 15.4-8 produce the exact deflection when GA_s is replaced by GA^*. Thus

$$w_2 = \left(1 + \frac{3EI}{GA_s L^2}\right)\frac{PL^3}{3EI} = \left(1 + \frac{4EI}{GA^* L^2}\right)\frac{PL^3}{4EI} \quad \text{hence}$$

$$GA^* = \left(\frac{L^2}{12EI} + \frac{1}{GA_s}\right)^{-1} \tag{15.4-9}$$

MacNeal [3.3] calls this correction "residual bending flexibility" and dates the idea to no later than 1953. Thus modified, the Mindlin beam with one-point integration for $[\mathbf{k}_s]$ behaves like the Timoshenko beam described by Eq. 2.3-6, not only for the tip-loaded cantilever, but for arbitrary supports and loads at ends of a two-node element. This kind of correction plays a role in several plate elements, including those of [15.24–15.28]. Use of GA^* also prevents terms in $[\mathbf{k}_s]$ from becoming far larger than terms in $[\mathbf{k}_b]$ as the beam becomes very slender.

The use of such adjustment factors is somewhat distasteful, and appropriate choices may be unclear if the material is inhomogeneous, anisotropic, or nonlinear.

Substitute Displacement Fields. In a Mindlin beam, transverse shear deformation is $\gamma_{zx} = w_{,x} - \psi$. In Eq. 15.4-1, w and ψ are defined by linear shape functions, so that $w_{,x}$ is constant and ψ is linear in x. One can say that shear locking results from this mismatch. By adopting the same quadratic used in Eq. 3.10-1 we can write lateral deflection as a quadratic, while retaining the linear expression for ψ. Thus

$$w = \frac{L-x}{L}w_1 + \frac{x}{L}w_2 + \frac{x(L-x)}{2L}(\psi_1 - \psi_2) \qquad \psi = \frac{L-x}{L}\psi_1 + \frac{x}{L}\psi_2 \tag{15.4-10}$$

Hence

$$\gamma_{zx} = w_{,x} - \psi = \frac{w_2 - w_1}{L} - \frac{\psi_1 + \psi_2}{2} \tag{15.4-11}$$

The same result is obtained by using linear interpolation for both w and ψ and evaluating the average γ_{zx}, namely $1/L$ times the integral of $w_{,x} - \psi$ over length L. The γ_{zx} at midspan provided by Eqs. 15.4-1, and by use of a single Gauss point for integration, is provided throughout the Mindlin beam by Eq. 15.4-11. Now selective integration is of no benefit; one may proceed in more straightforward fashion by using full integration for both $[\mathbf{k}_b]$ and $[\mathbf{k}_s]$. More elaborate substitute fields have been suggested for plates; references include [15.27,15.29,15.30]. Quadrilateral plate elements may use substitute fields that depend on transverse shear strains at midside locations or at interior points on the ξ and η axes of isoparametric coordinates [2.13,2.14,3.3,15.29,15.31]. The addition of nonconforming displacement modes has also been explored [15.32].

'Discrete Shear' Elements. Instead of enforcing *zero* transverse shear deformation at selected points, as in discrete Kirchhoff elements, the *correct* shear deformation can be enforced at these points. An example of this approach is the "discrete shear triangle," or DST plate element [15.33]. To explain the idea in terms of a beam we must imagine that the beam element of Fig. 15.4-1a has a node at midspan where rotation ψ_m is defined, so that rotation ψ is a quadratic function of x, expressed in terms of nodal d.o.f. ψ_1, ψ_m, and ψ_2. Lateral deflection is initially taken as cubic in x, expressed in terms of w and $w_{,x}$ at end nodes 1 and 2. Let signs of bending moment M and transverse shear force Q have positive senses shown in Fig. 15.1-3. The equilibrium equation of transverse force and the moment-curvature relation are

$$\left.\begin{aligned} Q &= \frac{dM}{dx} \\ M &= -EI\frac{d\psi}{dx} \end{aligned}\right\} \quad \text{hence} \quad Q = -EI\,\frac{d^2\psi}{dx^2} \quad \text{and} \quad \gamma_{zx} = \frac{Q}{GA_s} = -\frac{EI}{GA_s}\frac{d^2\psi}{dx^2} \qquad (15.4\text{-}12)$$

But also, as in Eq. 15.4-2b, $\gamma_{zx} = w_{,x} - \psi$. By equating the two expressions for γ_{zx} at each of the three beam nodes, we can eliminate $w_{,x1}$, $w_{,x2}$, and midpoint rotation ψ_m, so that element d.o.f. remaining are w_1, ψ_1, w_2, and ψ_2. As the beam becomes indefinitely slender, the Kirchhoff constraint $w_{,x} = \psi$ is enforced at both ends and at the center, without the appearance of large penalty constraint coefficients analogous to matrix $[\mathbf{k}_s]$ of Eq. 15.4-4. For a triangular plate element [15.33], as thickness becomes small the formulation provides a nine d.o.f. element that reduces to the DKT element described in Section 15.2.

Other Variational Principles. Elements having displacement d.o.f. need not be based on the principle of stationary potential energy. Good plate elements have arisen from mixed and hybrid principles in their various forms, which allow independent assumptions of internal stresses, or strains, or displacements, or combinations of them; which permit equilibrium equations within an element to be satisfied explicitly by the forms used or implicitly by Lagrange multipliers; and which allow freedom in the forms of boundary fields assumed. Devices summarized earlier in this section can be used with mixed and hybrid elements as well as with displacement-based elements. A shear-flexible beam element is formulated by a hybrid principle in the latter part of Section 4.10. From that development we see an advantage easily provided by the hybrid approach: as a beam becomes slender, or a plate becomes thin, there is no shear locking and no large penalty terms appear in the stiffness matrix. Papers that discuss mixed and hybrid plate elements include [15.23,15.27,15.29,15.30,15.34].

15.5 BOUNDARY CONDITIONS. TEST PROBLEMS

Boundary Conditions. The support condition at an edge of a plate may be free, clamped, or simply supported. A single support condition need not prevail along the entire plate boundary. If a plate contains a line of symmetry or antisymmetry, that line may become an edge of the FE model, with appropriate boundary conditions imposed. In the notation of Fig. 15.5-1, plate boundary conditions are as follows.

Free:	$M_n = 0$	$M_{ns} = 0$	$Q_n = 0$	(15.5-1a)
Clamped:	$w = 0$	$\psi_s = 0$	$\psi_n = 0$	(15.5-1b)
Simply Supported:	$w = 0$	$M_{ns} = 0$	$M_n = 0$	(15.5-1c)
Symmetric about s axis:	$\psi_n = 0$	$M_{ns} = 0$	$Q_n = 0$	(15.5-1d)
Antisymmetric about s axis:	$w = 0$	$\psi_s = 0$	$M_n = 0$	(15.5-1e)

In typical FE formulations, only displacement d.o.f. appear in $\{\mathbf{D}\}$, so that the M's and Q's constitute load terms.

A practical interpretation of the foregoing conditions might allow some nonzero values. For example, along a plate edge, prescribed displacement can make $w \neq 0$ but leave $M_{ns} = M_n = 0$, or the edge might carry externally-applied moment M_n while w remains zero there because the edge is supported. Physically, such an edge might be regarded as simply supported because the support applies no moment. Similarly, a line load Q might be applied along a free edge of a plate, just as a transverse force might be applied to the unrestrained end of a cantilever beam.

Simply supported conditions listed in Eq. 15.5-1c are called "soft" simple supports. Classical thin-plate theory uses $\psi_s = 0$ in place of $M_{ns} = 0$, producing the "hard" simply supported conditions $w = \psi_s = 0$. Unless simply supported edges are straight and intersect one another at right angles, hard simple supports overconstrain an FE model, so that a parallelogram-shaped plate behaves as if corners were clamped, and the piecewise-linear model of a continuously curved edge behaves as if the entire edge were clamped [2.13]. Although "hard" and "soft" simple supports provide comparable results for rectangular plates, in general it is recommended that simple supports be modeled as "soft," so that $w = 0$ is the only boundary d.o.f. prescribed.

There is another reason to use soft rather than hard conditions to describe a simply supported edge. In Mindlin theory there is a "boundary layer," extending into the plate a distance

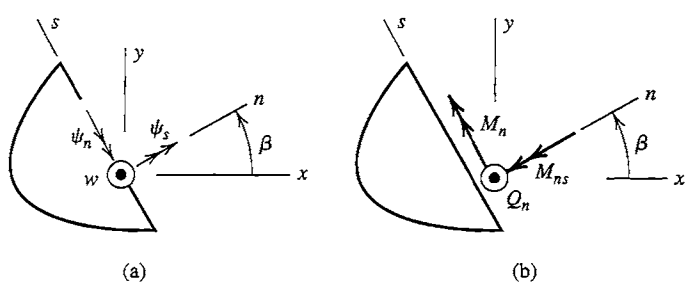

Figure 15.5-1. An arbitrarily oriented edge of a plate, with edge-tangent coordinate s. Displacement d.o.f and associated force and moments are shown.

roughly equal to thickness t, in which Q_n and M_{ns} have large gradients. The gradients are captured by soft supports but not by hard supports [15.35–15.37]. Kirchhoff plate theory excludes the boundary layer by its restrictive assumption of zero transverse shear deformation. Instead, edges of Kirchhoff plates carry the net shear force $V_n = Q_n + \partial M_{ns}/\partial s$, which leads to concentrated corner reactions, of magnitude twice the value of M_{ns} at corners [10.2]. In FEA of a Mindlin plate with soft simple supports there is a pronounced increase of Q_n near corners, which is more realistic than concentrated corner reactions. The pronounced increase does not appear in FEA with hard simple supports [15.35,15.36].

Patch Tests. Stress Calculation. A patch of Kirchhoff elements must be able to display constant states of M_x, M_y, and M_{xy}. A patch of Mindlin elements must be able to display constant states of M_x, M_y, M_{xy}, Q_x, and Q_y. In testing for (say) the curvature state $w_{,xx}$ = constant (or $\psi_{x,x}$ = constant in a Mindlin plate), which should provide constant M_x and $M_y = \nu M_x$, it will be necessary to set $\psi_y = 0$ at nodes on x-parallel boundaries of the patch. In testing for constant states of Q_x and Q_y, rotations at all nodes must be suppressed in order to prevent bending moments from developing.

In plates, "stress calculation" implies calculation of M_x, M_y, M_{xy} and possibly Q_x and Q_y as well. Equations 15.1-4 or 15.1-5 may be used, or an alternative method such as that described in the latter portion of Section 6.10. When using Mindlin elements and Eqs. 15.1-5, we are likely to find that moments are most accurately calculated at Gauss points used in integration of $[\mathbf{k}_b]$. Similarly, as suggested by Fig. 15.3-1, we are likely to find that transverse shear forces are most accurately calculated at Gauss points used in reduced or selective integration of $[\mathbf{k}_s]$. Jirousek notes that Eq. 15.1-5 may provide inaccurate values of shear forces Q, especially when plate thickness t is small, and suggests that more accurate values can be obtained from deflections of a stiff elastic edge support that provides $w \approx 0$ on a supported edge [15.35,15.38]. Of course, values of Q are often not of interest.

One expects that elements in commercial software have been patch-tested by developers and found satisfactory. A user may wish to do patch tests anyway to provide confidence in the software. Patch tests, like test cases described below, may also be helpful in learning to use unfamiliar software.

Test Cases. Rectangular and circular plates, Fig. 15.5-2a and 15.5-2b, are commonly used test cases for plate elements. For comparison with computed results, analytically determined formulas for lateral deflection and bending moments are readily available, for various loadings and boundary conditions [1.16,10.2].

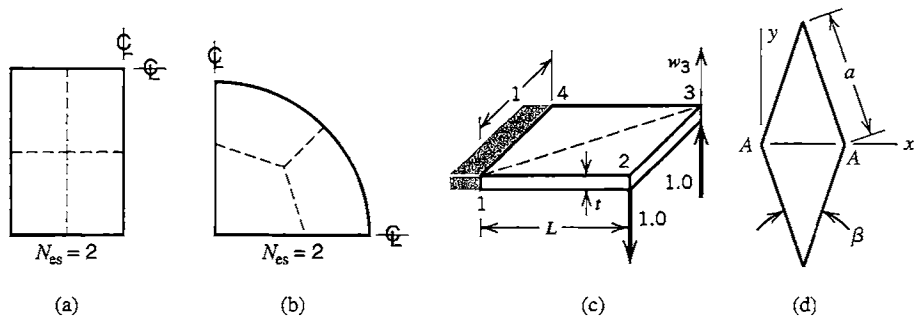

Figure 15.5-2. Test cases for plate elements. Coarse meshes are suggested by dashed lines. (a,b) Quadrants of rectangular and circular plates. N_{es} = number of elements per side. (c) Twisted strip. (d) Simply supported rhombic plate.

The twisted strip test case, Fig. 15.5-2c, is often modeled by one rectangular element or two triangular elements, to test the effect of element aspect ratio as length L increases. There is a statically equivalent loading in which each unit force is replaced by a half-unit couple whose vector is directed parallel to dimension L. For either loading, with $E = 10^7$, $\nu = 0.25$, and $t = 0.05$, the correct corner deflection w_3 is very nearly $w_3 = (3.0L - 0.6)10^{-3}$ [15.12]. The deflection is not simply $w_3 = 3.0L(10^{-3})$ because nodal rotation is suppressed at the fixed support, but this restraint is felt only very close to the support. Some proposed elements have done badly in this test case, displaying a w_3 that is almost independent of L.

The simply supported rhombic plate, Fig. 15.5-2d, is sometimes used as a test for skew element geometry. Under uniform load, with $\beta = 30°$ and $\nu = 0.3$, analytically-determined results at the center of the plate are: $w = 4.08(10^{-4})qa^4/D$, $M_x = 0.0191qa^2$, and $M_y = 0.0108qa^2$ [15.39]. At obtuse corners A, M_x is negative infinity and M_y is positive infinity. If "hard" simple supports are used for this test case, results may be poor, even for a fine mesh. This problem is not a good test case for skewness because the singularities at corners A strongly influence the solution. Finite elements without built-in singularities are not very accurate near a singularity, where gradients change rapidly.

15.6 AN APPLICATION

A flat plate of large span and uniform thickness is loaded by a lateral force, applied at a point well away from plate edges. The only support is an elastic layer that exerts lateral pressure k_0 MPa on the plate for each millimeter of lateral deflection (Fig. 15.6-1a). Data is as follows:

$$E = 200\text{ GPa} \qquad L = 1650\text{ mm} \qquad k_0 = 0.20\text{ MPa/mm}$$

$$\nu = 0.3 \qquad t = 30\text{ mm} \qquad P = 1.0\text{ N}$$

The states of deformation and stress in the plate are to be examined. A unit load P is convenient in computation because a different load is accommodated by multiplying computed results by that load. The choice $L = 1650$ mm is somewhat arbitrary and is explained in what follows.

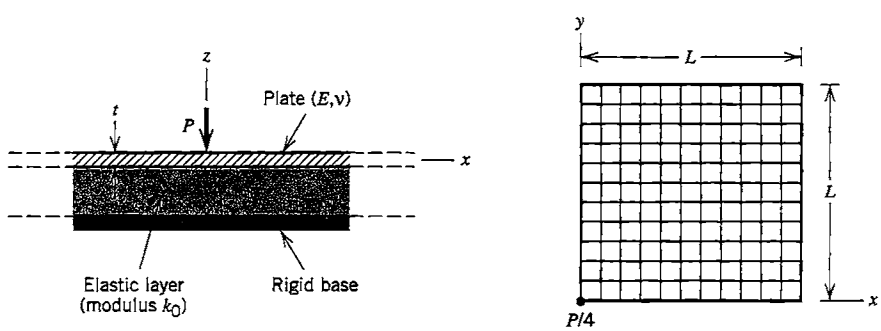

(a) (b)

Figure 15.6-1. (a) Cross section of a plate on an elastic foundation. (b) FE mesh on a quadrant, with z-direction force $P/4$ at $x = y = 0$.

Preliminary Analysis. We know that the plate has a large span, which implies that its outer portion, far from the load, is essentially undeflected and unstressed. How great a span should be modeled for FEA? Textbooks and handbooks provide formulas for elastically supported beams, but not for elastically supported plates. To plan the initial FE model, we make the bold assumption that a cross section containing load P has the same extent of downward deflection as an infinitely long *beam,* elastically supported and loaded by concentrated lateral force. A beam whose cross section has width b and depth 30 mm has moment of inertia $I = 2250b$ mm^4 and elastic foundation modulus $k = bk_0$. Pursuing the beam analysis in its usual terminology [1.16,2.6], we obtain $\beta = 0.00325$/mm and $x = 3\pi/4\beta = 726$ mm as the distance from the load at which deflection changes from downward to upward. For an initial FE model we guess that the mesh need span no more than about twice this distance.

To obtain an estimate of maximum deflection, for comparison with subsequent FE results, we will approximate the deflected shape of the plate, then write an equation stating that load P is equal to the force provided by foundation pressure on the plate. A simple assumption for deflected shape, in terms of radial distance r from load P, appears in Fig. 15.6-2a. We also assume that $|w|$ is negligible for $r > R$. The foundation pressure is $p = -k_0 w$. The minus sign is needed so that negative (downward) w will produce positive (upward) pressure on the plate. For equilibrium of vertical forces,

$$\int_0^{2\pi}\int_0^R pr\,dr\,d\theta - P = 0 \qquad \text{hence} \qquad w_0 = \frac{2\pi P}{(\pi^2-4)k_0R^2} \tag{15.6-1}$$

With $R = 726$ mm, as calculated above, we obtain $w_0 = 10.2(10^{-6})$ mm as the estimated deflection of load P. It seems pointless to also estimate bending moments using the cosine shape because d^2w/dr^2 is needed. In Fig.15.6-2a, d^2w/dr^2 has the same magnitude at $r = R$ as at $r = 0$, and clearly the actual d^2w/dr^2 will have much larger magnitude at $r = 0$.

Finite Element Analysis. The problem has symmetry about the z axis, so the model could be a single row of elements in the shape of a narrow wedge, with rotations about radial lines restrained at all nodes. For illustrative purposes, we choose instead to use Cartesian coordinates and rectangular elements. Figure 15.6-1b shows a quadrant of the plate, modeled by an 11 by 11 mesh of four-node plate elements, each a 150 mm square, built of four overlapping DKT elements, as shown in Fig. 15.2-2b. Thus $L = 1650$ mm in Fig. 16.6-1b. The software used allows an elastic foundation to be included with element formulation. We adopt a uniform mesh because it is very easy to prepare and at this stage we are unsure about details of

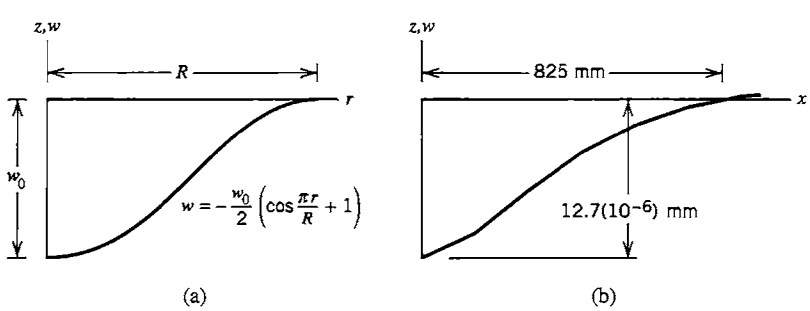

Figure 15.6-2. (a) Deflected shape assumed in preliminary analysis.
(b) Deflected shape along $y = 0$, from FEA with the mesh of Fig. 15.6-lb.

an improved mesh. Load $P/4$ is applied at $x = y = 0$ on the quadrant modeled. Symmetry is imposed by preventing rotation about the x axis for nodes on the x axis and rotation about the y axis for nodes on the y axis. Deflection w is unrestrained at all nodes.

Critique of Results. Software plots the deflected shape shown in Fig. 15.6-2b, with straight lines rather than curves between nodes. The computed deflection at $x = y = 0$ is $12.7(10^{-6})$ mm downward, in good agreement with the estimate $w_0 = 10.2(10^{-6})$ mm from preliminary analysis. The computed deflection curve crosses the x axis at $x = 825$ mm, also in good agreement with the preliminary guess of 726 mm. The largest upward deflection is $0.2(10^{-6})$ mm and appears far from $x = y = 0$, but within the quadrant modeled rather than at its boundaries.

Computed stress contours are shown in Fig. 15.6-3. As should be expected, contours of von Mises stress σ_e are symmetric about the line $x = y$, which implies only that we have not blundered in imposing loads and boundary conditions. Contours of σ_e should be concentric circles. Interelement continuity of the contours is fair. Were we to model the entire plate with a mesh symmetric with respect to both x and y axes, we would see perfect continuity of contours across x and y axes, but this continuity would have nothing to do with whether results are accurate or not. Similar remarks might be made regarding σ_x contours, Fig. 15.6-3b, although these contours are not expected to be concentric circles. If we had exploited symmetry using a single wedge-shaped row of elements, contour discontinuties of the kind shown in Fig. 15.6-3 would not be available.

We conclude that results are reasonable for an initial coarse-mesh analysis. Error measure η, Eq. 9.10-7, is 0.20 for the entire mesh, which is too large for comfort. However, plate theory says that bending moments and stresses are infinite at a concentrated load. Elements nearest the load contribute most to η. Standard plate elements will not represent the singularity, regardless of mesh refinement, so it would be better to omit these elements from the calculation of η. But a truly concentrated load does not exist in reality. It is possible that applying the load as a distribution over a small area would be more realistic. An improved analysis would certainly use a finer mesh near $x = y = 0$, and would probably not suffer if a coarser mesh were used at more distant locations.

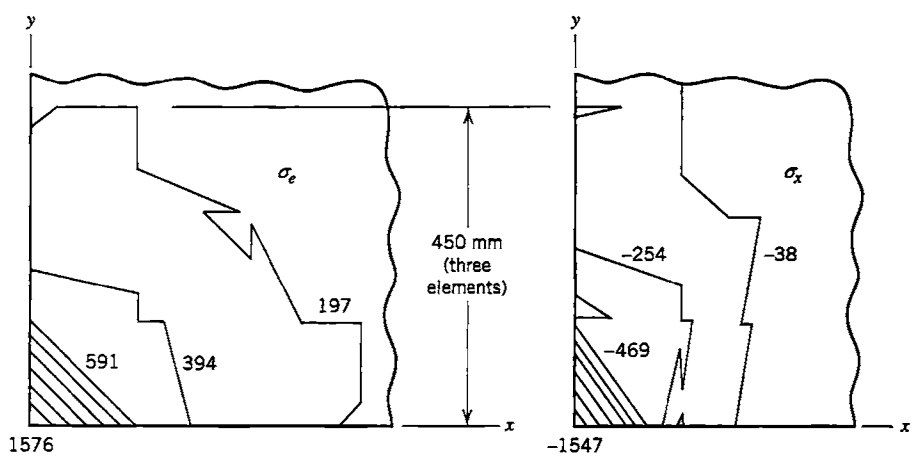

Figure 15.6-3. Contours of stresses σ_e and σ_x on the upper surface of the plate near $x = y = 0$ in Fig. 15.6-lb. Stress units are Pa.

Note that the foundation is assumed to remain in contact with the plate, and to pull down wherever the plate deflects upward. If only upward foundation pressure is possible because the plate can lift off its foundation, an iterative (nonlinear) analysis is required because in effect we do not know where to place the foundation until a cycle of calculation has told us (approximately) where w is upward and where it is downward. In the present problem, lift-off may make little difference in results, judging by the relatively small magnitude of upward deflection.

ANALYTICAL PROBLEMS

15.1-1 (a) Use Eq. 15.1-2 to show that, if σ_x is linear in z, then σ_x has magnitude $6M_x/t^2$ at plate surfaces.
(b) Use Eq. 15.1-2 to show that, if τ_{yz} is parabolic in z, then τ_{yz} has magnitude $1.5Q_y/t$ at the plate midsurface.

15.1-2 In a plane problem, an equation used for stress transformation between xy axes and an axis n in the xy plane is $\sigma_n = \frac{1}{2}(\sigma_x + \sigma_y) + \frac{1}{2}(\sigma_x - \sigma_y)\cos 2\theta + \tau_{xy}\sin 2\theta$. What analogous expression relates bending moment M_n to bending and twisting moments M_x, M_y, and M_{xy}?

15.1-3 (a) In Fig. 15.1-3b, presume that the M's and Q's are functions of x and y, so that $M_x\,dy$ acts along edge $x = 0$ and $(M_x + M_{x,x}\,dx)\,dy$ acts along the parallel edge, and so on. Show that the equilibrium equations are $Q_{x,x} + Q_{y,y} = -q$, $M_{x,x} + M_{xy,y} = Q_x$, and $M_{xy,x} + M_{y,y} = Q_y$.
(b) Hence, show that $M_{x,xx} + 2M_{xy,xy} + M_{y,yy} + q = 0$.
(c) Use the result of part (b) and Eq. 15.1-4b to show that $\nabla^4 w = q/D$, where ∇^4 is the biharmonic operator.

15.1-4 An isotropic thin rectangular plate has dimension a parallel to the x axis and dimension b parallel to the y axis. The x-parallel edges are simply supported; the y-parallel edges are free. Uniform downward pressure p is applied to the upper surface. What are the principal stresses at the middle of the lower surface? What is the lateral deflection at the center of the plate?

15.1-5 An expression for $\{\kappa_0\}$ in terms of T_o is stated following Eqs. 15.1-4. Verify the correctness of this expression.

15.1-6 Consider an isotropic thin square plate, with edges parallel to x and y axes, loaded only along its edges. Describe loads applied to the edges if the lateral deflection is (a) $w = c_1(x^2 + y^2)$, and (b) $w = c_2(y^2 - x^2)$, where c_1 and c_2 are constants.

15.1-7 One sometimes wonders how wide a beam can be before it should be regarded as a plate. How would you decide? Or what would you do if unable to decide?

15.1-8 Establish coordinates ns, rotated by angle β with respect to xy coordinates (as in Fig. 15.5-1, for example). Let n and s be principal axes of an orthotropic material. Express transverse shear coefficients in Eq. 15.1-5 in terms of β and principal shear moduli G_n and G_s. A procedure is suggested in the text.

15.1-9 Let a slender beam of length L and rectangular cross section (width b and depth t) carry uniformly distributed lateral load q. Supports at either end allow rotation but prevent beam ends from moving laterally or axially.
(a) Assume that lateral deflection w has the parabolic distribution $w = 4w_c x(L - x)/L^2$, where w_c is the midspan deflection. Show that the fraction of q

supported by axial (membrane) stress is $q_m = (64/3)(Ebt^4/L^4)(w_c/t)^3$. *Suggestions:* Assume that tensile force is independent of x, and recall that for $w_c << L$ the change in centerline length is the integral of $0.5(dw/dx)^2dx$ over length L.
(b) Approximate net load q as $q = q_m + q_b$, where q_b is supported by bending as in a simply supported beam. Show that when $w_c/t = 0.5$, membrane and bending actions each support roughly half the load.

15.2-1 (a) Let the element in Fig. 15.1-2a be a rectangular Kirchhoff element with the lateral displacement field of Eq. 15.2-4. Without expressing w in terms of nodal d.o.f., devise an argument to show that interelement compatibility of normal slopes is lacking. For example, show that $w_{,y}$ along side 3-4 does not depend only on $w_{,y}$ at nodes 3 and 4.
(b) What can be said about interelement continuity of w and $w_{,x}$ along side 3-4?
(c) In Eq. 15.2-4, terms $a_{11}x^3y$ and $a_{12}xy^3$ might be replaced by $a_{11}x^4$ and $a_{12}y^4$, but it is not wise to do so. Why?

15.2-2 Imagine that lateral deflection w of a triangular Kirchhoff element is taken as a complete quintic in x and y (21 terms). For each of the two elements shown, and without calculation, allocate d.o.f. to nodes in a way that seems acceptable. Use higher-order d.o.f. as needed. Is interelement compatibility achieved?—without expressing w in terms of nodal d.o.f., answer by considering compatibility conditions on edge $x = 0$.

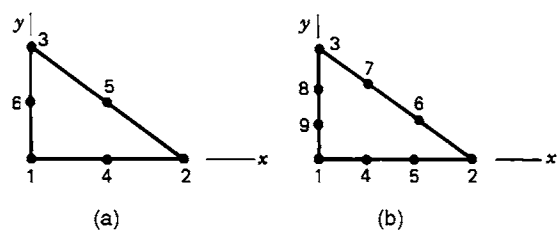

Problem 15.2-2

15.2-3 In Fig. 15.2-1, let side 2-3 of the element be parallel to the y axis. By eliminating $w_{,y}$ at midside, express a quadratic variation of ψ_y along this side in terms of L_{23}, w_2, $w_{,y2}$, w_3, $w_{,y3}$, and ξ, where ξ is a dimensionless coordinate such that $\xi = -1$ at node 2 and $\xi = +1$ at node 3.

15.2-4 Imagine that, for the DKT element, a plausible if inexact formula has been devised for assigning nodal loads (a formula analogous to Eq. 3.3-8 or Eq. 4.8-15b). The imagined formula can provide nodal moments as well as nodal forces when distributed lateral load is applied.
(a) Which results in Table 15.2-1 would certainly *not* be changed by application of this formula?
(b) Which results would perhaps not be changed, or changed very little?
(c) Which results would probably be noticeably changed, and how?

15.2-5 Assume that the formula referred to in Problem 15.2-4 is based on interpolation of lateral displacement w over the triangle from the three d.o.f. at each vertex node. Begin construction of this displacement field by using a quadratic w function along an edge of length L (see Eq. 15.4-10, for example). Hence, express the w field in

terms of nodal values of w, $w_{,x}$, and $w_{,y}$, nodal x and y coordinates, and area coordinates of the triangle (see Eqs. 7.3-1).

15.2-6 In constructing $[\mathbf{k}]$ of the DKT element, why is numerical integration with three sampling points adequate to provide exact results?

15.2-7 (a) In Table 15.2-1, convergence is not monotonic for all deflections and moments listed. What might explain this behavior?
(b) Where a steady rate of monotonic convergence seems indicated in Table 15.2-1, what is the apparent order of error? That is, what is m in $O(h^m)$, where h is the length of an element side?
(c) Repeat part (b) for the "simply supported edges" results in Table 15.2-2.

15.3-1 Imagine that the four-node plate element of Fig. 15.1-2a is to be obtained by specialization of the eight-node solid element of Fig. 6.5-1a and Eq. 6.5-4. Describe the substitutions required. For simplicity, consider only terms corresponding to $i = 1$ in Eq. 15.3-1.

15.3-2 Show that Eq. 15.3-6 follows from Eq. 15.3-4 when $[\mathbf{B}_b]$ and $[\mathbf{B}_s]$ are defined as stated in the text.

15.3-3 A uniformly distributed lateral load q acts upward on a rectangular C^0 plate element of side lengths $2a$ and $2b$. In the vector of consistent nodal loads, do nodal moments appear? Why? For each of the four elements listed in Table 15.3-1, what are the consistent loads at nodes?

15.3-4 A rectangular plate with all edges clamped is to be analyzed. (All d.o.f. are suppressed at a clamped boundary.) The loading is symmetric about both centerlines of the plate, so only one quadrant is modeled for FEA. Consider use of each element type depicted in Table 15.3-1, with selective integration, to model the quadrant. After displacement boundary conditions are imposed, how many unknown d.o.f. appear in $\{\mathbf{D}\}$? And how many remain after subtracting the number of d.o.f. occupied in satisfying transverse shear constraints? Model the quadrant by (a) one element, (b) a 2 by 2 mesh, and (c) a 4 by 4 mesh.

15.3-5 Consider the latter three elements in Table 15.3-1. For what states of displacement or deformation will γ_{zx} and γ_{yz} be correctly evaluated at all points in the element?

15.3-6 (a) Let a rectangular Lagrange element have side lengths $2a$ and $2b$. Sketch the element in its deformed state if displacements are described by $\psi_x = \psi_y = 0$, $w = c(3\xi^2\eta^2 - \xi^2 - \eta^2)$, where c is a constant, and $\xi = x/a$ and $\eta = y/b$, with $\xi = \eta = 0$ at the element center.
(b) Show that this deformation mode yields zero strains at Gauss points of a 2 by 2 integration rule.

15.3-7 Sketch an unsupported 2 by 3 mesh of rectangular bilinear elements, viewed in the same perspective as the element in Fig. 15.1-2a. Superposed on this sketch, show the mesh with elements deformed into the w-hourglass mode.

15.3-8 Use Eq. 15.3-2 to evaluate $\{\boldsymbol{\kappa}_M\}$ for each of the four spurious modes possible in the bilinear element with reduced (one-point) integration of all terms. Hence, explain why two of these modes cease to be mechanisms when selective integration is used.

15.3-9 Imagine that the serendipity element of Table 15.3-1 is to be given a "discrete Kirchhoff" treatment by explicitly enforcing zero transverse shear strain at Gauss points of

a 2 by 2 rule, and eliminating some nodal d.o.f. as a result. How many d.o.f. can be eliminated? Which d.o.f. do you think it appropriate to retain in $\{\mathbf{d}\}$, and why?

15.4-1 Verify that one-point quadrature produces Eqs. 15.4-4 from Eqs. 15.4-1 and 15.4-2.

15.4-2 Use a single uniform two-node Mindlin beam element to solve for nodal displacement or rotation in each of the two beam problems shown. Use one-point integration and the modified shear properties GA^* defined by Eq. 15.4-9. Where possible, compare the solution with results provided by elementary beam theory.

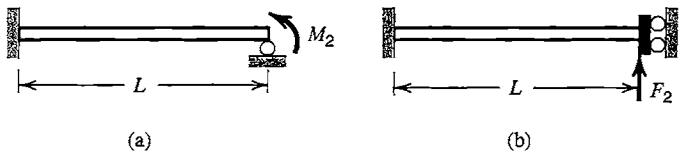

Problem 15.4-2

15.4-3 A single quadratic (three-node) Mindlin beam element is used to model a uniform and uniformly loaded beam fixed at each end, as shown. What GA^* value, analogous to that in Eq. 15.4-9, is required if the exact midspan deflection is to be obtained as the beam becomes more and more slender? Use two-point Gauss quadrature to evaluate the stiffness coefficient (there is only one nonzero d.o.f.).

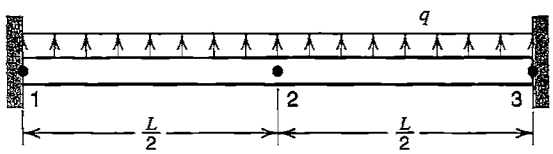

Problem 15.4-3

15.6-1 Assume that a plate is not bonded to an elastic foundation that supports it, so that portions of the plate may lift off when load is applied. Describe a simple algorithm that may converge to the correct solution.

COMPUTATIONAL PROBLEMS

In the following problems compute significant values of displacement, moment, or stress, as appropriate. Exploit symmetry where possible. When mesh refinement is used, estimate the maximum percentage error of results provided by the finest FE mesh. Where dimensions or loads are not assigned, choose values that seem reasonable or convenient. Where material properties are needed but not stated, use properties of steel. Apply the analysis methodology suggested in Section 1.5.

C15.1 Patch-test the plate elements provided in software you use. Does it appear that transverse shear deformation is taken into account by any of these elements?

C15.2 (a-b) Solve problems depicted as test cases in parts (a) and (b) of Fig. 15.5-2. Use uniform meshes $N_{es} = 1$, $N_{es} = 2$, and $N_{es} = 4$, and determine, if possible, the convergence rate of computed deflection and bending moment versus N_{es}.
(c) Where loading is by concentrated force at the plate center, try using a refined mesh near the load point. Does it appear that displacements and/or bending moments converge with mesh refinement?
(d) In Fig. 15.5-2d, try using both "soft" and "hard" simple supports. Also, with mesh refinement, do bending moments at corners A seem to diverge in the manner expected?

C15.3 If C^0 elements are available, solve the problem of a uniformly loaded rectangular plate with clamped edges, using (say) a 6 by 6 mesh over the entire plate. If the software allows choice in integration rules, try using different numbers of Gauss points. What is the effect of changing the plate thickness, from perhaps one-eighth the length of the shorter side to very small? Is there evidence of locking?

C15.4 The plate shown has two supported edges, which are clamped and include angle 2ϕ, and two free edges. A uniformly distributed line load in the z direction is applied along span $2c$ of the longer free edge.

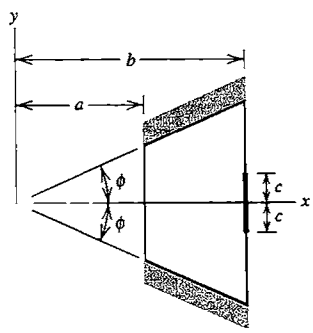

Problem C15.4

C15.5 Solve the problem of an elastically-supported plate, either finite, semi-infinite, or infinite, under loadings such as:
(a) Uniform pressure over a circle of radius R.
(b) Uniformly distributed line load around a circle of radius R.
(c) Uniformly distributed line load along part of the edge of a finite or semi-infinite plate.

C15.6 The foregoing problems admit many modifications, such as:
(a) Add reinforcing beams to one side of the plate, along one or more edges or in other locations.
(b) Use orthotropic material properties.
(c) Load the plate by a temperature field of the form $T = zf$, where f is either a constant or a function of x and/or y.

CHAPTER 16

SHELLS

Shell behavior is summarized in this chapter. FE formulations for arches are discussed first, as an introduction to similar difficulties and techniques of shell elements. We consider elements for shells of revolution, then both flat and curved elements for shells of general shape. Test cases for FE formulations and an axisymmetric application are presented.

16.1 INTRODUCTION

Familiar examples of shells are an eggshell and a water tank. A shell has curved inner and outer surfaces separated by a thickness t that is small in comparison with overall dimensions of the shell. The *midsurface* is a distance $t/2$ from both inner and outer surfaces. Thickness t may be constant or may vary either gradually or abruptly.

Stresses in a shell generate membrane forces N, which are forces per unit of length measured tangent to the shell surface:

$$N_x = \int_{-t/2}^{t/2} \sigma_x \, dz \qquad N_y = \int_{-t/2}^{t/2} \sigma_y \, dz \qquad N_{xy} = \int_{-t/2}^{t/2} \tau_{xy} \, dz \tag{16.1-1}$$

where z is a direction normal to the midsurface and x and y are axes tangent to the midsurface. Bending and twisting moments, described for a plate by Eqs. 15.1-2a, are also present in a shell. The state of stress in x and y directions can be represented as the superposition of *membrane* stresses and *flexural* or *bending* stresses. If the shell is thin-walled and its material is linearly elastic and homogeneous, then (for practical purposes) membrane stresses are independent of z and flexural stresses vary linearly with z. Thus, the net surface-tangent stresses at arbitrary z are

$$\sigma_x = \frac{N_x}{t} + \frac{M_x z}{t^3/12} \qquad \sigma_y = \frac{N_y}{t} + \frac{M_y z}{t^3/12} \qquad \tau_{xy} = \frac{N_{xy}}{t} + \frac{M_{xy} z}{t^3/12} \tag{16.1-2}$$

Flexural stresses at shell surfaces are $\sigma_x = \pm 6M_x/t^2$, and so on. Flexural stresses are often large, and may be quite localized near loads or disturbances that cause them. Consider, for example, axisymmetric loads at the end of a cylindrical shell, Fig. 16.1-1a. Dimensions of these loads are force/length for V_0 and force • length/length for M_0. The theory of cylindrical shells [1.16,2.6,10.2] shows that expressions for x-direction flexural stresses at inner and outer surfaces contain the terms $e^{-\lambda x} \sin \lambda x$ and $e^{-\lambda x} \cos \lambda x$, where $\lambda = [3(1-\nu^2)/R^2t^2]^{1/4}$. When $R/t = 250$, for example, the exponential term $e^{-\lambda x}$ at $x = 0.15R$ is only about 5% of its value at $x = 0$, which means that large flexural stresses are confined to a very small

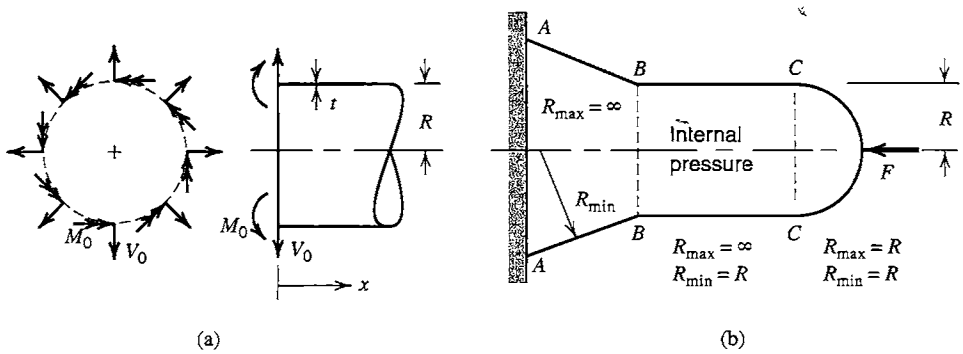

Figure 16.1-1. (a) Axisymmetric end loads on a cylindrical shell. (b) A shell of revolution having conical, cylindrical, and spherical parts.

length of the shell. An unwary FE user may not use a fine enough mesh in the neighborhood of such disturbances to model them properly.

Loads *without* axial symmetry create disturbances that propagate far along a thin cylindrical shell. This behavior does not contradict Saint-Venant's principle, which is applicable to relatively compact 2D and 3D isotropic bodies but not to general loading of thin-walled or highly anisotropic bodies.

A shell has two principal radii of curvature at every point. Each is measured normal to the shell, and each is the radius of a small arc drawn in the shell midsurface. The small arcs intersect at right angles. One radius is the largest, the other the smallest, of the radii of all possible arcs in the midsurface where the arcs intersect. In a conical shell, one principal radius of curvature is infinite and the other increases with distance from the apex of the cone (Fig. 16.1-1b). In a cylindrical shell, one radius is infinite and the other is constant. In a spherical shell, the two principal radii are equal and constant. When only one principal radius is finite, the shell is called *singly curved;* when both are finite the shell is called *doubly curved.* A shell is usually regarded as thin if the magnitude of R_{min}/t is greater than about 20. For an eggshell, R_{min}/t is roughly 50. For constructed shells, R_{min}/t may approach 1000.

A shell can carry a large load if membrane stresses dominate, just as a thin wire can sustain a large axial load but only a small load in bending. Thus, a shell is much stronger than a flat plate made of the same volume of the same material. Like a thin wire, a shell is susceptible to buckling if membrane stresses are compressive in all or part of the shell: *Unlike* a wire or a cable, whose curved shape must change when the pattern of lateral loading changes, a doubly curved shell of a given shape can carry a distributed lateral load of almost any pattern while displaying very little bending except near supports.

An abrupt change in radius of curvature creates local bending stresses, as would an abrupt change in thickness. Thus, in Fig. 16.1-1b we expect to find bending stresses close to circumferential lines *BB* and *CC*. Load *F* will produce bending, as will support conditions at circumferential line *AA*, where loads applied to the shell by the support include a distributed axial load as well as the distributed shear and moment loads shown in Fig. 16.1-1a. These remarks apply to shells in general, not only to shells of revolution. In the argument that follows Eq.16.1-2, a half-wave of $\sin\lambda x$ or $\cos\lambda x$ is provided by $\lambda x = \pi$, for which $x \approx 2.4\sqrt{Rt}$. This result suggests a rough guideline for FE modeling of any shell: even an initial coarse-mesh model should use *at least* two elements within a distance of $\sqrt{Rt}$ from a

concentrated load, a line load, or a geometric discontinuity, where R is the smaller principal radius of curvature.

The preceding discussion uses axisymmetric shells as simple examples, but the goal of shell analysis, especially by FEA, is to analyze a shell of arbitrary shape. In a general shell, membrane and bending actions are both present, so a successful shell element must surmount possible shortcomings of plane elements (Chapters 3 and 6) and of plate elements (Chapter 15), *and* new diffculties that may arise because curved shell geometry causes membrane and bending actions to interact. Also, the membrane stiffness of a thin shell is much greater than its bending stiffness, which means that FE equations may be ill-conditioned, as described in Section 9.2.

Three approaches to finite elements for shells have been pursued:

1. Flat elements, formed by combining a plane membrane element with a plate bending element.
2. "Degenerated" solid elements, formed from 3D elements by specialization. The procedure is analogous to that used for Mindlin plate elements, Section 15.3.
3. Curved elements based on classical shell theory.

Merits of the first approach include simplicity, acceptable performance, and easy accommodation of standard beam elements as ribs and edge stiffeners. The second approach offers a better fit of curved shell geometry and can perform acceptably despite many possible element disorders, especially locking. The third approach has been much less productive than the first two and will not be discussed here.

A very large body of literature is devoted to shell analysis, both by classical methods and by FEA. Surveys include [16.1–16.6]; [16.2] is a quite readable account of element development. As with plate elements in Chapter 15, we make no attempt to be comprehensive. Instead we consider some concepts and methods that have been useful in formulating shell elements. References are cited for further details, extensions, and improvements. The reference list is not intended to represent priority of discovery.

16.2 CIRCULAR ARCHES AND ARCH ELEMENTS

We discuss arches prior to shells because arches display many of the difficulties encountered in analysis of shells, but in a simpler context. Devices used to improve arch elements have also been used to improve shell elements. In this section we assume that arch radius R is constant and that loads and deformations are confined to the plane of the arch. Initially we assume that the arch is slender enough that transverse shear deformation can be ignored.

Arch Theory. A point on the arch midline has s-direction (tangential) displacement u- and z-direction (radial) displacement w (Fig. 16.2-1). Let ε_s represent tangential strain at an arbitrary point, a distance z from the midline. With the aid of Fig. 16.2-2, we write

$$\varepsilon_s = \frac{d}{ds}(\delta_a + \delta_c) + \frac{w}{R} \qquad \text{hence} \qquad \varepsilon_s = u_{,s} + \frac{w}{R} + z\left(\frac{u_{,s}}{R} - w_{,ss}\right) \tag{16.2-1}$$

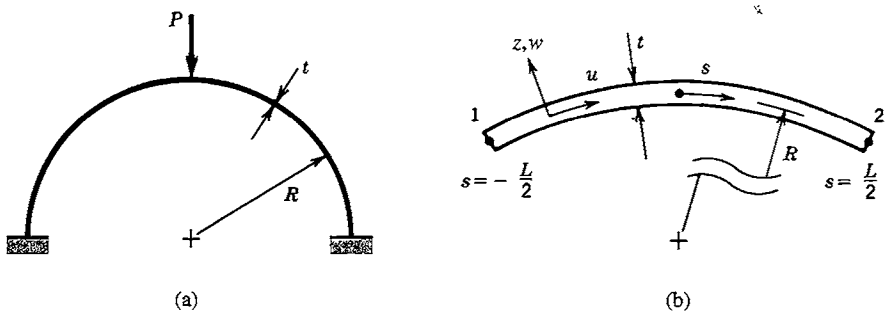

Figure 16.2-1. (a) Semicircular arch with clamped ends and concentrated center load. (b) Arch element of arc length L.

where s is the tangential coordinate. Not all authors agree on the form of these equations; some may simply write $\delta_a = u$ in Fig. 16.2-2a or may not make the approximation shown in Fig. 16.2-2b [16.7]. In alternative notation, Eq. 16.2-1 is

$$\varepsilon_s = \varepsilon_m + z\kappa \qquad \text{where} \qquad \varepsilon_m = u_{,s} + \frac{w}{R} \tag{16.2-2a}$$

$$\kappa = \frac{u_{,s}}{R} - w_{,ss} \tag{16.2-2b}$$

Membrane strain ε_m appears along the arch midline and is associated with membrane force, which acts in the s direction. Curvature change κ is associated with bending moment and is here considered positive when the radius of curvature decreases.

Strain energy U receives contributions from ε_m and from κ. For a linearly elastic and homogeneous element of arc length L,

$$U = U_m + U_b = \int_{-L/2}^{L/2} \frac{1}{2} EA\varepsilon_m^2 ds + \int_{-L/2}^{L/2} \frac{1}{2} EI\kappa^2 ds \tag{16.2-3}$$

where E = elastic modulus, A = cross-sectional area, and I = moment of inertia of A about the neutral axis of bending. The expression for U can be derived by integration of

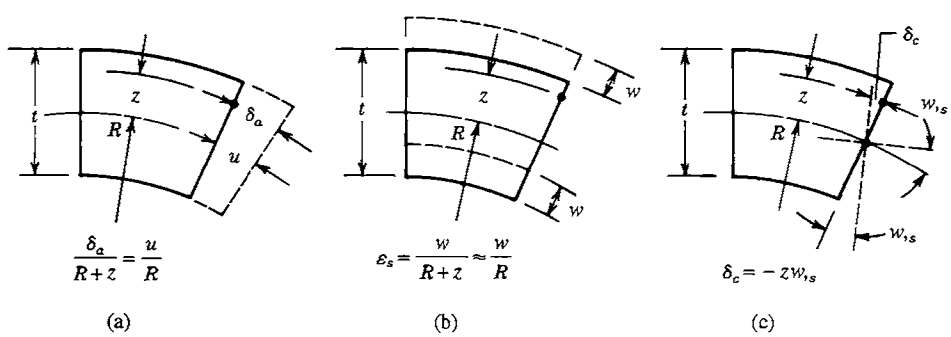

Figure 16.2-2. Axial, radial, and rotational deformations of a thin arch ($R >> t$). Rotation $w_{,s}$ is presumed small and transverse shear deformation is neglected.

strain energy density $E\varepsilon_s^2/2$ through the arch thickness t. A term linear in z disappears, and terms shown in Eq. 16.2-3 remain. A stiffness matrix is obtained from U in the usual way (as in Section 4.8, for example).

For rigid-body motion, $\varepsilon_m = 0$ and $\kappa = 0$. By combining Eqs. 16.2-2 and integrating, we obtain the displacement field for rigid-body motion of a circular segment:

$$u = b_1 \cos\phi + b_2 \sin\phi + b_3 \tag{16.2-4a}$$

$$w = b_1 \sin\phi - b_2 \cos\phi \tag{16.2-4b}$$

where $\phi = s/R$. The b_i are constants; b_1 and b_2 represent translations normal and tangent to the radial line $\phi = 0$ and b_3 represents rotation about the center of curvature.

Under most loadings, a slender arch bends but has very little membrane strain. In the limit of slenderness, from Eq. 16.2-2a,

$$\varepsilon_m = 0 \qquad \text{implies} \qquad u_{,s} + \frac{w}{R} = 0 \tag{16.2-5}$$

which is known as the *inextensibility condition.*

Straight Elements. A straight arch element is identical to a beam element that includes axial stiffness. One combines stiffness matrices of straight bar and straight beam elements, as in Eq. 2.3-6. In the notation of Fig. 16.2-3a, this result is the six-d.o.f. element

$$[\mathbf{k}]\{\mathbf{d}\} = \left[\begin{array}{c|c} \mathbf{k}_m & \mathbf{0} \\ \hline \mathbf{0} & \mathbf{k}_b \end{array}\right] \left\{\begin{array}{c} \mathbf{d}_m \\ \hline \mathbf{d}_b \end{array}\right\} \quad \text{where} \quad \{\mathbf{d}_m\} = \begin{Bmatrix} u_1 \\ u_2 \end{Bmatrix} \quad \text{and} \quad \{\mathbf{d}_b\} = \begin{Bmatrix} w_1 \\ \psi_1 \\ w_2 \\ \psi_2 \end{Bmatrix} \tag{16.2-6}$$

where subscripts m and b refer to membrane (bar) and bending (beam) contributions, respectively. Rotational d.o.f. are called ψ in anticipation of treating rotational d.o.f. in shells in the same way as they are treated in plates (see Fig. 15.1-1).

To assemble straight elements of different orientation, a common set of d.o.f. is needed at each node, as in Fig. 16.2-3b. The choice of directions for translational d.o.f. D is not

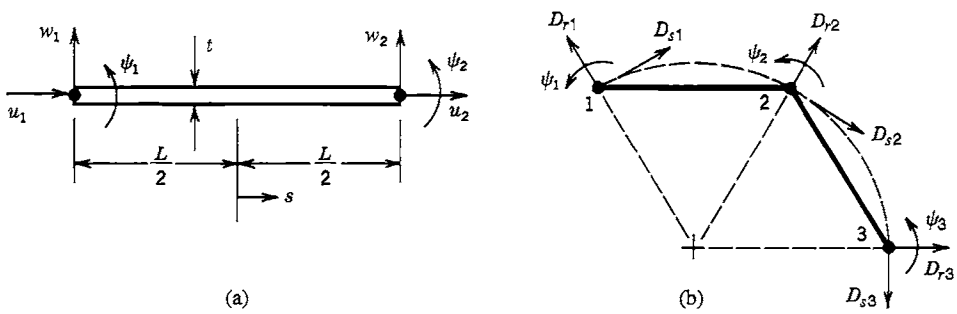

Figure 16.2-3. (a) Straight element, showing d.o.f. in the local coordinate system. (b) A possible choice of directions for global d.o.f. D.

unique. Whatever the choice, procedures described in Section 8.3 serve to replace u and w d.o.f. by D_s and D_r d.o.f. Because the problem is planar, d.o.f. ψ are not transformed.

It can be rigorously shown that a straight-element model of a curved arch converges to exact results. Indeed, for a given number of elements, the straight-element model is more accurate than the model provided by many formulations for curved elements [16.7–16.9]. The absence of membrane-bending coupling within a straight element, evidenced by the null off-diagonal submatrices in Eq. 16.2-6, does not prevent the element from working properly. Coupling between membrane and bending actions occurs in the assembled structure because adjacent elements are not collinear. For example, axial force in element 2-3 of Fig. 16.2-3b applies force to node 2 that element 1-2 sees as having a lateral component, which bends element 1-2.

In Fig. 16.2-3b, nodes lie on the circular arc of the actual arch, which implies an FE model in which element lengths are chords of the arc. This error of geometry makes the model somewhat stiff. In formulating $[\mathbf{k}]$, it is better to take element length as the actual arc length. For example, let $R/t = 40$ for the arch of Fig. 16.2-1a, and let the entire arch be modeled by four straight elements, each of chord length $L = 2R \sin 22.5°$. The computed displacement of load P is about 10% low. If instead the arc length $L = \pi R/4$ is used, the error is only about 2%.

A way to introduce membrane-bending coupling into a straight element is suggested by a membrane strain equation used for shallow shells. Consider the shallow parabolic arch shown in Fig. 16.2-4a. Membrane strain ε_m according to Marguerre shallow shell theory [16.10], and its average value over length L, are

$$\varepsilon_m = \frac{du}{dx} + \frac{dz}{dx}\frac{dw}{dx} \qquad \varepsilon_{m(\text{ave})} = \frac{1}{L}\int_0^L \varepsilon_m \, dx \tag{16.2-7}$$

An expression for arch elevation z is given in Fig. 16.2-4. Let axial displacement be interpolated in the usual linear fashion, $u = (1 - x/L)u_1 + (x/L)u_2$, and lateral displacement w by the usual cubic (Fig. 2.3-1 or Fig. 3.2-4). Thus we obtain the axial strain expression

$$\varepsilon_{m(\text{ave})} = \frac{1}{L}(u_2 - u_1) + \frac{2h}{3L}(\psi_1 - \psi_2) \tag{16.2-8}$$

The latter term in Eq. 16.2-8 can also be obtained by loading the arch in pure bending by nodal moments M, calculating the resulting x-direction separation of nodes by integration

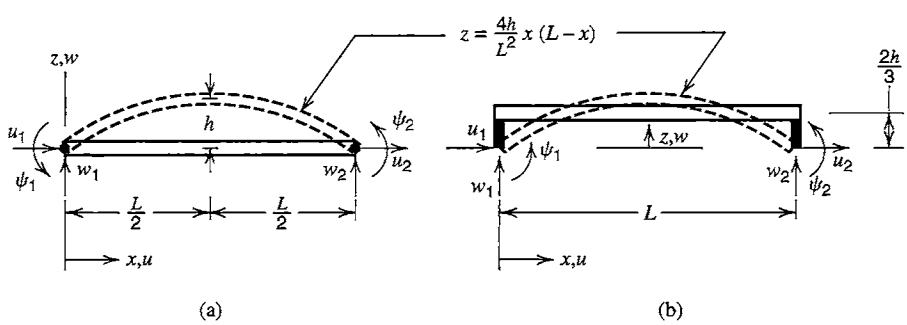

Figure 16.2-4. (a) Straight element used to model arch segment shown by dashed lines. (b) Element geometry implied by use of Eq. 16.2-8.

of $z(M\,dx/EI)$ over length L, dividing the result by L, and replacing M by its equivalent in terms of relative nodal rotation $\psi_2 - \psi_1$. A physical interpretation of Eq. 16.2-8 is that the element remains straight, but that its nodes are offset from the element axis by rigid offsets of length $2h/3$ (Fig. 16.2-4b). Equation 16.2-8 is used for ε_m in the first integral of Eq. 16.2-3 and the usual cubic for κ is used in the second integral. In contrast to many curved elements that use Eqs. 16.2-2 in their formulation, the element of Eq. 16.2-8 does not display the membrane locking described below.

With differing details in implementation, the shallow-shell concept has also been used to "add curvature" to conical axisymmetric shell elements [16.11] and to flat general shell elements [16.12–16.15]. In [16.12], z is taken as cubic in x and defined by slopes dz/dx at either end. The price paid for adding curvature is having to provide extra input data that defines $z = z(x)$, for all arch elements or for all edges of shell elements.

Membrane Locking. The term "membrane locking" refers to excessive stiffness in bending. Not all curved elements suffer from this disorder. In those that do, strain fields in the element interact unfavorably, so that nodal displacements that should be resisted only by bending are resisted by membrane deformation as well. Because membrane stiffness is far greater than bending stiffness in a slender arch (and in a thin shell), the desired bending mode tends to be excluded from element response to load. Straight arch elements do not suffer from membrane locking. Neither does the element of Eq. 16.2-8: when $\psi_1 \neq \psi_2$, the two terms on the right-hand side can have equal magnitude but opposite sign, so that $\varepsilon_{m(\text{ave})} = 0$.

The two-node element of Fig. 16.2-1b provides an example of membrane locking that may arise in a curved element based on low-order displacement fields. By analogy with displacement fields used for a straight beam, one might employ the radial and axial displacement fields

$$u = a_1 + a_2 s \tag{16.2-9a}$$

$$w = a_3 + a_4 s + a_5 s^2 + a_6 s^3 \tag{16.2-9b}$$

where the a_i are generalized d.o.f. From Eqs. 16.2-2 and 16.2-9, membrane strain ε_m and curvature change κ are

$$\varepsilon_m = \left(a_2 + \frac{a_3}{R}\right) + \frac{a_4}{R}s + \frac{a_5}{R}s^2 + \frac{a_6}{R}s^3 \qquad \kappa = \frac{a_2}{R} - 2a_5 - 6a_6 s \tag{16.2-10}$$

Inextensibility (Eq. 16.2-5) is enforced as an arch becomes indefinitely slender. The condition $\varepsilon_m = 0$ for all s requires that

$$\left(a_2 + \frac{a_3}{R}\right) = 0 \qquad a_4 = 0 \qquad a_5 = 0 \qquad a_6 = 0 \tag{16.2-11}$$

If the conditions $a_2 + a_3/R = a_5 = a_6 = 0$ are enforced, then the only contribution to κ comes from the membrane term a_2. Stated another way, if the element is forced to bend, then nonzero values of the a_i in Eq.16.2-11 produce nonzero ε_m, whose associated strain energy and stiffness are very large for a slender element. Thus, when bending load is applied, bending deformation tends to be "locked out"of element response. With a straight element, $R = \infty$ and locking does not occur.

Membrane locking is also indicated by constraint counting (Section 13.5). When a curved arch element of the type associated with Eqs. 16.2-9 is added to the structure, it brings three d.o.f. with it. But Eqs. 16.2-11 comprise four constraints. All d.o.f. are occupied in satisfying constraints, so none are left to model structure behavior. With $R/t = 40$ and four fully integrated two-node curved elements used to model the arch of Fig. 16.2-1a, the computed displacement of load P is less than 5% of its correct value [16.16].

Equations 16.2-10 suggest the device of selective integration. If the U_m term in Eq. 16.2-3 is integrated by one quadrature point (at the center, $s = 0$), then a_4, a_5, and a_6 do not appear in ε_m, and inextensibility enforces only the first of Eqs. 16.2-11, thus making curved elements behave more like straight elements. Now constraint counting shows that two d.o.f. per additional element are available to model structure behavior. This curved element does not suffer from membrane locking, and has about the same accuracy as a straight element [16.16].

Other Curved Elements. Exactly integrated curved elements can behave well if element fields are properly designed. For example, consider axial and radial displacement fields of the form [16.17]

$$u = a_1 + a_2\phi + a_3\phi^2 + a_4\phi^3 + a_5\phi^4 + a_6\phi^5 \tag{16.2-12a}$$

$$w = -a_2 - 2a_3\phi - 3a_4\phi^2 - 4a_5\phi^3 - 5a_6\phi^4 \tag{16.2-12b}$$

where $\phi = s/R$. These equations satisfy the inextensibility condition $\varepsilon_m = 0$ for all s. Because $\varepsilon_m = 0$, the element stiffness matrix comes entirely from bending stiffness. Equations 16.2-12 indicate that if displacement fields are to have enough d.o.f. for a six-d.o.f. curved arch element and are also to display $\varepsilon_m = 0$ for all ϕ, the axial field must be at least quintic and the radial displacement field one degree lower. By adding an internal d.o.f. a_7 to Eq. 16.2-12b the element can display nonzero ε_m. Either way, computed results for the displacement of load P in Fig. 16.2-1a are less than 1% in error for a two-element solution in which each element spans a 90° arc [16.17]. However, it appears that such a high-order polynomial may cause difficulty in nonlinear analysis [16.13].

Neither the curved element of Eqs. 16.2-9 nor the curved element of Eqs. 16.2-12 explicitly includes the capability for rigid-body motion with strain. In series expansions of sine and cosine terms in the rigid-body motion equations, Eqs. 16.2-4, one sees terms that also appear in Eqs. 16.2-9 and 16.2-12. Thus one can argue that Eqs. 16.2-9 and 16.2-12 include the initial series terms required, and indeed rigid-body motion capability is recovered with mesh refinement. Early in the development of curved elements for arches and shells, it was assumed that poor performance was due to inability of elements to model rigid-body motion with little or no strain. But the good performance of elements based on Eqs. 16.2-12, as well as other studies [16.16,16.18,16.19], show that membrane locking is far more detrimental.

Mindlin Arch Elements. Displacements used in formulating a Mindlin arch element are tangential and radial displacements u and w of the arch midline and rotation ψ of a cross section that was radial before deformation. Strain energy is $U = U_m + U_b + U_s$, in which the respective contributions to U are due to membrane strain ε_m, curvature change κ, and transverse shear strain γ_{zs}. For an arch of midline length L, constant radius R, and cross-section rotations ψ directed as shown in Fig. 16.2-3 [16.20],

$$U_m = \int_{-L/2}^{L/2} \frac{1}{2} EA\varepsilon_m^2 \, ds \qquad \text{where} \qquad \varepsilon_m = u_{,s} + \frac{w}{R} \tag{16.2-13a}$$

$$U_b = \int_{-L/2}^{L/2} \frac{1}{2} EI\kappa^2 \, ds \qquad \text{where} \qquad \kappa = \frac{u_{,s}}{R} - \psi_{,s} \tag{16.2-13b}$$

$$U_s = \int_{-L/2}^{L/2} \frac{1}{2} GA_s \gamma_{zs}^2 \, ds \qquad \text{where} \qquad \gamma_{zs} = w_{,s} - \psi \tag{16.2-13c}$$

where A_s is the "effective" cross-sectional area that resists transverse shear deformation ($A_s = 5A/6$ for homogeneous material and a rectangular cross section).

A linear element, whether curved (Fig. 16.2-1b) or straight (Fig. 16.2-3a), can be based on the linear shape functions $N_1 = 0.5 - s/L$ and $N_2 = 0.5 + s/L$. Thus, with generalized d.o.f. a_i, linear interpolations are

$$u = a_1 + a_2 s \quad \text{or} \quad u = N_1 u_1 + N_2 u_2 \tag{16.2-14a}$$

$$w = a_3 + a_4 s \quad \text{or} \quad w = N_1 w_1 + N_2 w_2 \tag{16.2-14b}$$

$$\psi = a_5 + a_6 s \quad \text{or} \quad \psi = N_1 \psi_1 + N_2 \psi_2 \tag{16.2-14c}$$

Arguments related to locking of this element are very similar to arguments made in connection with Eqs. 16.2-9 to 16.2-11 and are summarized as follows. As arch thickness t approaches zero, all strain energy should be contained in bending, so that ε_m and γ_{zs} should vanish for all s, which implies, for a curved element,

$$a_2 + \frac{a_3}{R} = 0 \qquad a_4 = 0 \qquad a_5 = 0 \qquad a_6 = 0 \tag{16.2-15}$$

or for a straight element ($R = \infty$),

$$a_2 = 0 \qquad a_4 - a_5 = 0 \qquad a_6 = 0 \tag{16.2-16}$$

In both cases, an element added to a thin arch brings three d.o.f. with it, but all are occupied in satisfying constraints, and the mesh is locked. However, if U_m and U_s are integrated with a single sampling point at $s = 0$, only two constraints are imposed per element, one each on ε_m and γ_{zs}, and locking is avoided. Details of the two-node arch element are very similar to those of the Mindlin beam element discussed in Section 15.4, and formulation options discussed there can also be applied to arch elements.

A quadratic Mindlin arch element has three nodes, one at either end ($s = \pm L/2$) and one at the middle ($s = 0$). It is based on the displacement fields

$$\begin{Bmatrix} u \\ w \\ \psi \end{Bmatrix} = \begin{Bmatrix} a_1 \\ a_4 \\ a_7 \end{Bmatrix} + \begin{Bmatrix} a_2 \\ a_5 \\ a_8 \end{Bmatrix} \xi + \begin{Bmatrix} a_3 \\ a_6 \\ a_9 \end{Bmatrix} \xi^2 \qquad \text{where} \qquad \xi = \frac{s}{L/2} \tag{16.2-17}$$

Equations 16.2-13a and 16.2-17 yield the membrane strain

$$\varepsilon_m = \left(\frac{2a_2}{L} + \frac{a_4}{R} \right) + \left(\frac{4a_3}{L} + \frac{a_5}{R} \right) \xi + \frac{a_6}{R} \xi^2 \tag{16.2-18}$$

To satisfy the inextensibility condition for all ξ, the two parenthetic expressions must vanish, as must a_6. The constraint $a_6 = 0$ implies membrane locking, as it implies that $w_{,ss}$ is zero (note that $w_{,ss} \approx \psi_{,s}$ when the arch is slender). Reduced integration offers a remedy [16.20,16.21]. Equation 16.2-18 can be rewritten in the form

$$\varepsilon_m = \left(\frac{2a_2}{L} + \frac{a_4}{R} + \frac{a_6}{3R}\right) + \left(\frac{4a_3}{L} + \frac{a_5}{R}\right)\xi + \frac{a_6}{R}\left[\xi^2 - \frac{1}{3}\right] \tag{16.2-19}$$

If integration of membrane energy U_m is performed by two-point Gauss quadrature, for which sampling points are at $\xi = \pm 1/\sqrt{3}$, the bracketed expression vanishes. Thus the constraint $a_6 = 0$ is not enforced.

A similar argument can be applied to transverse shear strain. The condition $\gamma_{zs} = 0$ implies that $\psi_{,ss} = 0$ in the quadratic element. This is not a locking condition, but it degrades element performance. Again the remedy is reduced integration; a two-point Gauss rule is recommended for the stiffness contribution of γ_{zs}.

The quadratic element does not explicitly contain the rigid-body motion capability described by Eqs. 16.2-4. However, these equations pertain to a *circular* geometry, and the shape of a three-node arch element is parabolic. The equations are approximately satisfied by an element that is not sharply curved. The capability for rigid-body motion without strain is not provided by all numerical integration procedures; see below Eq. 16.5-15.

Remarks. When reduced integration is used to evaluate strains in the process of generating [**k**], the same sampling points should be used to evaluate these strains when computing stresses in the postprocessing phase. Large spurious strains may appear at other locations, as in the examples of Figs. 6.8-2, 6.10-1, and 15.3-1.

Again we note that *straight* elements include rigid-body motion capability and are free of membrane locking. So are arch elements associated with Eq. 16.2-8 and initially flat shell elements that receive analogous modification. In a nonlinear problem where large displacements are possible, an initially straight element may *become* curved and thus have a tendency to lock if the element is of a type for which locking is possible.

Even when locking is avoided, a slender arch (or a thin shell) has a high ratio of membrane stiffness to bending stiffness. Thus the structure stiffness equations tend to be ill-conditioned, as discussed in Section 9.2.

Despite the large number of curved arch and beam elements available, new curved elements are continually developed, many based on hybrid and mixed variational principles. More recent contributions include [16.22–16.24]. Anti-locking devices cited in Section 15.4 can be applied to arch elements, and of course to shell elements as well.

16.3 SHELLS OF REVOLUTION

The midsurface of a shell of revolution is generated by revolving a planar line about an axis in the same plane. If the line is straight, the shell is conical or cylindrical. A *meridian* is the intersection of the midsurface with a plane containing the axis. A *parallel* or *parallel circle* is the intersection of the midsurface with a plane normal to the axis. If geometry, loads, supports, and material properties are axisymmetric, so is response, and the problem

is mathematically two-dimensional. Loads without axial symmetry can be treated by expressing the load in terms of its Fourier series components, analyzing for response due to each load component, and superposing results, as discussed for solids of revolution in Sections 14.4 and 14.5.

Formulation options for axisymmetric shell elements are similar to options for arch elements, discussed in Section 16.2. Details of implementation resemble details used for solids of revolution, discussed in Section 14.2. Accordingly we will be brief, and consider only the axisymmetric case, and only elements having a straight meridian. Thus each element is a conical frustum, which has been shown to work well for a continuously curved shell, just as straight beam elements have been shown to work well for an arch. Further details and references for curved shell-of-revolution elements appear in [15.7].

Numerical analysis of shells of revolution need not be done by FEA. A versatile computer program based on the finite difference method [16.25] has capability for stress, vibration, buckling, nonaxisymmetric response, creep, plastic action, and large deflection.

Thin-Shell Formulation. Equations 16.1-1 and 16.1-2 describe stresses in a shell of revolution, Fig. 16.3-1, if we replace x by s and y by θ, where s and θ designate meridional and circumferential directions. Shear force $N_{s\theta}$ and twisting moment $M_{s\theta}$ are zero for axisymmetric conditions. Forces and moments per unit length are related to membrane strains ε_m and curvature changes κ, in s and θ directions, by the relations

$$\begin{Bmatrix} N_s \\ N_\theta \end{Bmatrix} = [\mathbf{E}_m]\begin{Bmatrix} \varepsilon_{ms} \\ \varepsilon_{m\theta} \end{Bmatrix} \quad \text{and} \quad \begin{Bmatrix} M_s \\ M_\theta \end{Bmatrix} = -[\mathbf{D}_b]\begin{Bmatrix} \kappa_s \\ \kappa_\theta \end{Bmatrix} \tag{16.3-1}$$

in which, for an isotropic material of elastic modulus E and Poisson's ratio ν,

$$[\mathbf{E}_m] = \frac{Et}{(1-\nu^2)}\begin{bmatrix} 1 & \nu \\ \nu & 1 \end{bmatrix} \qquad [\mathbf{D}_b] = \frac{Et^3}{12(1-\nu^2)}\begin{bmatrix} 1 & \nu \\ \nu & 1 \end{bmatrix} \tag{16.3-2}$$

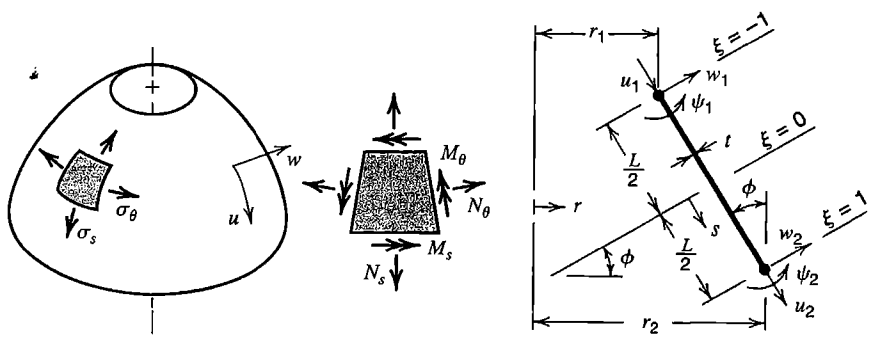

(a)

Figure 16.3-1. (a) Shell of revolution, showing normal stresses and associated membrane forces and moments when loading is axisymmetric. (b) Meridian of a conical frustum element. $\xi = 2s/L$.

Let u and w be displacements, respectively tangent and normal to the meridian, Fig. 16.3-1a. For axisymmetric conditions and a conical element such as that in Fig. 16.3-1b, the strain-displacement relation is [10.2]

$$\begin{Bmatrix} \boldsymbol{\varepsilon} \\ \boldsymbol{\kappa} \end{Bmatrix} = [\partial]\{\mathbf{u}\} \qquad \text{or} \qquad \begin{Bmatrix} \varepsilon_{ms} \\ \varepsilon_{m\theta} \\ \kappa_s \\ \kappa_\theta \end{Bmatrix} = \begin{bmatrix} \dfrac{d}{ds} & 0 \\ \dfrac{\sin\phi}{r} & \dfrac{\cos\phi}{r} \\ 0 & \dfrac{d^2}{ds^2} \\ 0 & \dfrac{\sin\phi}{r}\dfrac{d}{ds} \end{bmatrix} \begin{Bmatrix} u \\ w \end{Bmatrix} \tag{16.3-3}$$

For the two-node conical element in Fig.16.3-1b, a suitable displacement field is, with $\xi = 2s/L$,

$$u = \frac{1}{2}(1-\xi)u_1 + \frac{1}{2}(1+\xi)u_2 + \left(1-\xi^2\right)a_1 \tag{16.3-4a}$$

$$w = \frac{1}{4}\left[\left(2-3\xi+\xi^3\right)w_1 + \left(2+3\xi-\xi^3\right)w_2\right] + \frac{L}{8}\left[\left(1-\xi-\xi^2+\xi^3\right)\psi_1 - \left(1+\xi-\xi^2-\xi^3\right)\psi_2\right] \tag{16.3-4b}$$

where a_1 is an optional nodeless d.o.f., whose associated mode serves to improve element performance when $\phi \neq 0$ and $u_1 \neq u_2$, and which is to be condensed before assembly of elements [16.19]. (For application to nonaxisymmetric cases, with added modes in u and also in circumferential displacement v, see [16.26].) Cubic polynomials in Eq. 16.3-4b are the standard cubic expressions, Fig. 2.3-1 or Fig. 3.2-4, here written with the substitution $x = (1+\xi)L/2$. Strain energy in the element is

$$U = \frac{1}{2}\int_{-1}^{1} \begin{Bmatrix} \boldsymbol{\varepsilon} \\ \boldsymbol{\kappa} \end{Bmatrix}^T \begin{bmatrix} \mathbf{E}_m & \mathbf{0} \\ \mathbf{0} & \mathbf{D}_b \end{bmatrix} \begin{Bmatrix} \boldsymbol{\varepsilon} \\ \boldsymbol{\kappa} \end{Bmatrix} 2\pi r \frac{L}{2}\, d\xi \tag{16.3-5}$$

where $r = \frac{1}{2}(1-\xi)r_1 + \frac{1}{2}(1+\xi)r_2$. The relation $\{\boldsymbol{\varepsilon}\} = [\mathbf{B}]\{\mathbf{d}\}$, where $\{\mathbf{d}\}$contains element d.o.f., can be constructed from Eqs. 16.3-3 and 16.3-4. All ingredients are now at hand to produce element stiffness matrix $[\mathbf{k}]$, as described in Section 3.3 and in Section 4.8. Radius r appears in denominators of strain expressions, Eqs. 16.3-3, so a conical element with one end much closer to the axis of revolution than the other may benefit from more integration points than would be used if the element were cylindrical. Otherwise, two-point Gauss quadrature is effective. With optional internal d.o.f. a_1 included, $[\mathbf{k}]$ is a 7 by 7 matrix, to be condensed to a 6 by 6 matrix that operates on the nodal d.o.f. shown in Fig. 16.3-1b. If the factor 2π is omitted, $[\mathbf{k}]$ applies to a one-radian segment. For assembly with other elements, a common set of translational d.o.f. is required—typically radial and axial—which requires a transformation of the form $[\mathbf{T}]^T[\mathbf{k}][\mathbf{T}]$, as described in Section 8.3. For final stress calculation

in directions tangent to the midsurface, element d.o.f. in the local element coordinate system are obtained by coordinate transformation of the appropriate global d.o.f.

As special cases, the foregoing formulation applies to thin cylindrical shells if $\phi = 0$ for all elements, and to thin circular plates if $\phi = \pi/2$ for all elements. If transverse shear deformation must be taken into account, one may do so in the context of the foregoing development [16.27]. Or, one may use a Mindlin-type formulation, much as that described for beams in Section 15.4 and for arches in Section 16.2.

Mindlin-Shell Formulation. The following formulation takes transverse shear deformation into account. For a two-node conical shell element, Fig. 16.3-1b may again be used. Now shell-normal displacement w is interpolated independently of cross-sectional rotation ψ. Consequently, curvature changes κ_s and κ_θ now depend on ψ and its first derivative rather than on the first and second derivatives of w, and transverse shear strain is $\gamma = (dw/ds) - \psi$. The strain-displacement matrix of Eq. 16.3-3 becomes

$$\begin{Bmatrix} \varepsilon_{ms} \\ \varepsilon_{m\theta} \\ \kappa_s \\ \kappa_\theta \\ \gamma \end{Bmatrix} = \begin{bmatrix} \dfrac{d}{ds} & 0 & 0 \\ \dfrac{\sin\phi}{r} & \dfrac{\cos\phi}{r} & 0 \\ 0 & 0 & \dfrac{d}{ds} \\ 0 & 0 & \dfrac{\sin\phi}{r} \\ 0 & \dfrac{d}{ds} & -1 \end{bmatrix} \begin{Bmatrix} u \\ w \\ \psi \end{Bmatrix} \tag{16.3-6}$$

The element displacement field can be taken as

$$\begin{aligned} u &= N_1 u_1 + N_2 u_2 \\ w &= N_1 w_1 + N_2 w_2 + \frac{L}{8}\left(1 - \xi^2\right)(\psi_1 - \psi_2) \\ \psi &= N_1 \psi_1 + N_2 \psi_2 \end{aligned} \qquad \begin{aligned} N_1 &= \tfrac{1}{2}(1 - \xi) \\ N_2 &= \tfrac{1}{2}(1 + \xi) \end{aligned} \tag{16.3-7}$$

where $\xi = 2s/L$. The expression for w comes from Eq. 15.4-10 (with coordinate x instead of ξ), where it is presented as an option for formulation of a Mindlin beam element. The linear w of Eq. 16.2-14b could be used instead, but would require selective integration to avoid shear locking. Symbolically, Eq. 16.3-5 still applies, but the square matrix now becomes the 5 by 5 matrix

$$\begin{bmatrix} \mathbf{E}_m & \mathbf{0} & 0 \\ \mathbf{0} & \mathbf{D}_b & 0 \\ 0 & 0 & 5Gt/6 \end{bmatrix} \tag{16.3-8}$$

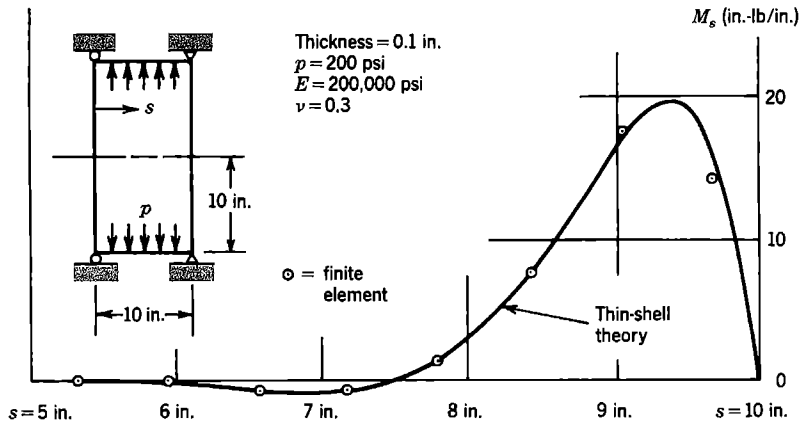

Figure 16.3-2. (a) Meridional bending moment M_s at element centers in a cylindrical shell with simply supported ends under uniform internal pressure [16.28]. Each element spans 0.625 in. axially.

where G is the shear modulus and $5t/6$ is the effective thickness in accounting for transverse shear deformation in homogeneous material. Again all ingredients are now at hand to produce a 6 by 6 element stiffness matrix [**k**] that operates on the six nodal d.o.f. shown in Fig. 16.3-1b. Tests of the element [16.28] show good accuracy (for example, Fig. 16.3-2). For the shell in Fig. 16.3-2, $\sqrt{Rt}$ = 1.0 in., and because less than two elements span this distance, the mesh near the end would be considered very coarse.

16.4 GENERAL SHELLS: THREE- AND FOUR-NODE ELEMENTS

In this section we consider three-node triangles and four-node quadrilaterals, whose membrane and bending stiffnesses come from the corresponding plane and plate bending elements. These elements are formulated as flat, although an optional adjustment like that of Eq. 16.2-8 can couple membrane and bending stiffnesses within an element. A more necessary adjustment is invoked when nodes of a quadrilateral element are not coplanar. A nominally flat element is formulated in a local coordinate system, then transformed for assembly of elements based on d.o.f. in a global system. Shell elements formulated as "degraded" isoparametric solids, which are often curved elements having eight or nine nodes, are discussed in Section 16.5.

Triangular Elements. Physically, modeling a shell by triangles connected at their vertices converts a doubly curved shell into a surface of triangular facets. With three translational and three rotational d.o.f. per node and vertex nodes only, each element has 18 d.o.f. Element matrices are most conveniently generated by placing the element in a local coordinate system such as shown in Fig. 16.4-1, for which the element stiffness matrix can be written as

$$[\mathbf{k}]\{\mathbf{d}\} = \left[\begin{array}{c|c} \underset{9\times 9}{[\mathbf{k}_m]} & \underset{9\times 9}{[\mathbf{0}]} \\ \hline \underset{9\times 9}{[\mathbf{0}]} & \underset{9\times 9}{[\mathbf{k}_b]} \end{array}\right] \left\{\begin{array}{c} \mathbf{d}_m \\ \hline \mathbf{d}_b \end{array}\right\} \quad \text{where} \quad \{\mathbf{d}_m\} = \begin{Bmatrix} \mathbf{u}_i \\ \mathbf{v}_i \\ \boldsymbol{\theta}_{zi} \end{Bmatrix} \quad \text{and} \quad \{\mathbf{d}_b\} = \begin{Bmatrix} \mathbf{w}_i \\ \boldsymbol{\Psi}_{xi} \\ \boldsymbol{\Psi}_{yi} \end{Bmatrix} \tag{16.4-1}$$

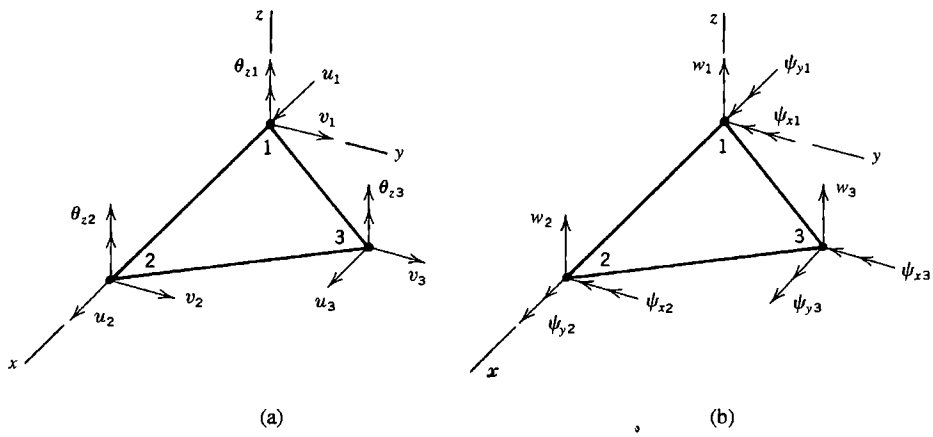

Figure 16.4-1. Flat triangular element in a local xy plane. (a) Degrees of freedom associated with membrane deformation. (b) Degrees of freedom associated with bending deformation.

in which, for convenience of notation only, d.o.f. have been grouped as shown; $\{\mathbf{u}_i\} = \lfloor u_1 \;\; u_2 \;\; u_3 \rfloor^T$, and so on. Degrees of freedom $\{\mathbf{d}_m\}$ and $\{\mathbf{d}_b\}$ are respectively the nodal d.o.f. associated with membrane and bending deformations. Use of ψ for nodal rotation corresponds to the nodal rotation used for plates in Fig. 15.2-1a. Matrix $[\mathbf{k}_b]$ represents any good plate-bending element, such as element DKT described in Section 15.2, or the shear-flexible DST element noted in Section 15.4. Matrix $[\mathbf{k}_m]$ represents a plane element, most simply the CST (constant-strain triangle) described in Section 3.4, although a better choice is a good element that has "drilling" d.o.f.; see Section 3.10 and [16.29,16.30]. If $[\mathbf{k}_m]$ represents the CST, element drilling d.o.f. $\{\boldsymbol{\theta}_{zi}\}$ have no stiffness associated with them, and $[\mathbf{k}_m]$ contains a 3 by 3 null submatrix. Thus, if any structure node happens to be surrounded by coplanar elements, the structure stiffness matrix is singular because rotation about the shell normal at that node is not resisted. When elements are *not* coplanar, resistance exists because normal rotation at a node in one element has a component that is resisted by bending stiffness in an adjacent element.

Shell elements that lack resistance to drilling d.o.f. have been troublesome. One remedy is to supply the required resistance in ad hoc fashion. Zienkiewicz suggested the relation [15.7]

$$\begin{Bmatrix} M_{z1} \\ M_{z2} \\ M_{z3} \end{Bmatrix} = \alpha EAt \begin{bmatrix} 1.0 & -0.5 & -0.5 \\ -0.5 & 1.0 & -0.5 \\ -0.5 & -0.5 & 1.0 \end{bmatrix} \begin{Bmatrix} \theta_{z1} \\ \theta_{z2} \\ \theta_{z3} \end{Bmatrix} \tag{16.4-2}$$

where E = elastic modulus, A = element area, t = element thickness, and α is an arbitrarily chosen number, perhaps 0.3 or less. The matrix of Eq.16.4-2 with its multiplier αEAt replaces what would otherwise be a null submatrix in $[\mathbf{k}_m]$. The ad hoc stiffness offers no resistance to the mode $\theta_{z1} = \theta_{z2} = \theta_{z3}$ or to any other rigid-body motion. Hence an element with drilling d.o.f. must not allow $\theta_{z1} = \theta_{z2} = \theta_{z3}$ to be a spurious mode in $[\mathbf{k}_m]$.

Another option, when shell elements have no resistance of their own to drilling d.o.f., is to omit rotation about the shell normal from the list of structure d.o.f. However, if elements (either flat or curved) do not have a common tangent plane at a node they share, the global shell-normal rotation d.o.f. has stiffness even without ad hoc additions to elements such as those in Eq. 16.42. Then suppression of the shell-normal rotation constitutes constraint, and constraint implies a stiffening of the structure. Where plates meet at a sharp angle, as along a ridge line in a folded plate, any amount of such a constraint is overconstraint [16.31]. Indeed, along such a ridge line, or at a node where elements do not share a common tangent plane, how is the shell-normal direction to be defined? One option is to define the shell-normal direction as an average of element normals at the shared node. The shell-normal rotation at that node can be restrained when elements are "almost" coplanar according to some definition [3.3,16.31]. Here "restrain" can mean insertion of an arbitrary small stiffness, or setting the d.o.f. to zero, which may be acceptable because fixity of a d.o.f. that has almost no stiffness associated with it has little effect on the structure.

Membrane-bending coupling can be added to a triangular element. The modification resembles that used for a straight arch element in Eqs. 16.2-7 and 16.2-8 [16.12,16.14]. Results of several test cases show that original and modified triangular elements have comparable accuracy in most cases [16.14]. An exception is the test case shown in Fig. 16.4-2, where the original formulation does not do well [16.12]. However, the poor result in Fig. 16.4-2a is explained by noting that in this example all nodes are placed on the surface of the actual shell, so that each four-element patch of straight-sided elements forms a shallow surface in the shape of a pyramid, which is much stiffer than desired. The modified formulation, Fig. 16.4-2b, handles this node placement without difficulty. If center nodes in Fig. 16.4-2a are moved inward so that all triangles of a four-element patch are coplanar, the original formulation behaves well. In practical application, the modified formulation reduces chances for error, as it is common practice to locate all nodes on the midsurface of the actual shell.

Transformation of [**k**] from the local coordinates of Fig. 16.4-1 to global coordinates is as described in Section 8.3, and as applied to a beam element in Section 2.4. Rows of matrix [Λ], seen in Eqs. 2.4-9 and 8.1-1, can be regarded as direction cosines between local-direction vectors $\mathbf{V}_x$, $\mathbf{V}_y$, and $\mathbf{V}_z$ and global axes. These vectors are easily established. Using global coordinates of nodes 1, 2, and 3 in Fig. 16.4-1, we use vector cross products to determine

$$\mathbf{V}_x = \mathbf{V}_{1-2} \qquad \mathbf{V}_z = \mathbf{V}_x \times \mathbf{V}_{1-3} \qquad \mathbf{V}_y = \mathbf{V}_z \times \mathbf{V}_x \tag{16.4-3}$$

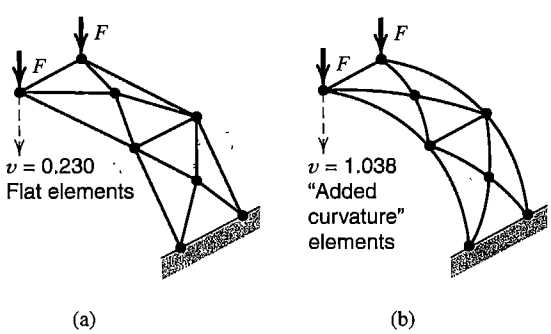

Figure 16.4-2. Quarter-circle segment of a cylindrical shell, modeled by triangular elements. Exact deflection is $v = 1.000$. All nodes are located on the cylindrical surface.

where, for example, $\mathbf{V}_{1-2} = (x_2 - x_1)\mathbf{i} + (y_2 - y_1)\mathbf{j} + (z_2 - z_1)\mathbf{k}$ in *global* coordinates, where **i**, **j**, and **k** are unit vectors in the global x, y, and z directions. Division of each vector **V** by its magnitude provides the required direction cosines. For final stress calculation in directions tangent to the midsurface, element d.o.f. in the local element coordinate system are recovered by coordinate transformation of the appropriate global d.o.f.

Quadrilateral Elements. As with triangular elements, a flat quadrilateral shell element is a combination of membrane and bending stiffnesses. Usually it is not so simple as would be suggested by changing labels "9 × 9" in Eq. 16.4-1 to "12 × 12," because many ad hoc adjustments are apt to be required in order to achieve good performance. Among four-node elements that appear to work well are those of [15.29,15.34,16.32]. Various formulations use assumed displacement fields, assumed strain fields, and mixed and hybrid variational principles. There are also elements that use one-point quadrature, intended primarily for use in dynamic and nonlinear applications where economy of element formulation is important [16.33,16.34].

In general the four nodes of a quadrilateral shell element do not lie in the same plane; that is, the element is warped (Fig. 16.4-3a). When the element stiffness matrix is formulated as if the element were flat and in a reference plane, shown shaded in Fig. 16.4-3a, additional adjustment is needed. Without it, computed results may be orders of magnitude in error. What is needed is a transformation that changes stiffness properties from lettered nodes to numbered nodes in Fig. 16.4-3. The matter is not as simple as connecting each lettered node to its adjacent numbered node by a rigid link, as was done for a beam element in Section 8.5. Doing so for a warped quadrilateral would create physically inappropriate bending moments. Instead, z-direction forces are introduced to resist couples created by membrane forces. For example, on edge AB in Fig. 16.4-3c, edge-parallel forces f_{12} and f_{21} are each the sum of components of x-parallel and y-parallel nodal forces. Couples associated with these forces and couples associated with the z-direction forces must be equal, that is

$$f_{zA} = f_{zB} = \frac{H}{L_{AB}}(f_{12} + f_{21}) \tag{16.4-4}$$

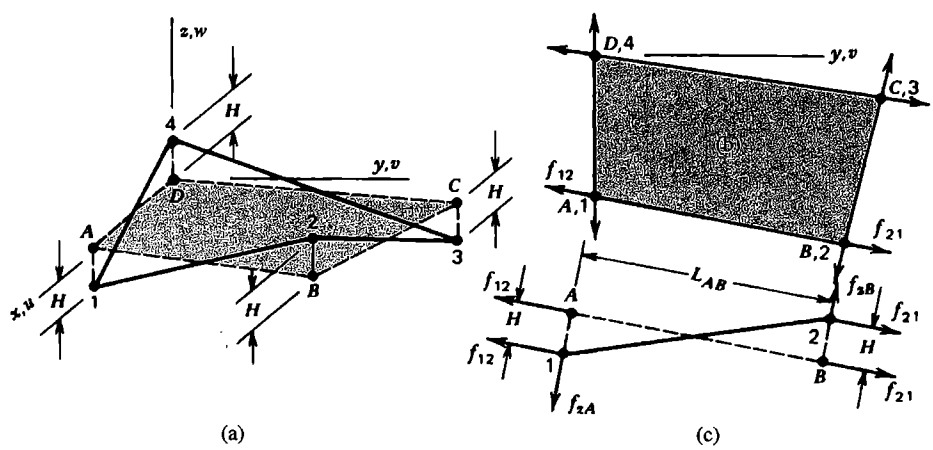

Figure 16.4-3. (a) A warped quadrilateral 1234 in local coordinates xyz. (b) Projection of the element onto the xy plane yields flat element $ABCD$. (c) A view parallel to the xy plane and normal to edge AB.

Also, it is possible that adjacent warped elements may display different bending moments along their shared edge, which would create physically unrealistic couples normal to element reference planes. The remedy, applied to each element edge, is to balance couples by added couple-forces parallel to the element reference plane. Details of procedures appear in [3.3,16.35]. The various corrections can be incorporated in one or more transformation matrices, which are applied to individual elements prior to assembly.

16.5 GENERAL SHELLS: CURVED ISOPARAMETRIC ELEMENTS

Summary. It is possible to model a shell of general shape by three-dimensional solid elements that (typically) have a thickness dimension considerably smaller than their other dimensions, as shown in Fig. 16.5-1a. However, unless the shell is so thick that it should be regarded as a solid rather than a shell, three thickness-direction nodes at each corner supply more d.o.f. than needed. Elimination of midsurface nodes yields the element of Fig. 16.5-1b. Here thickness-direction lines remain straight but can rotate with respect to the shell midsurface, which is the behavior postulated in generating Mindlin elements for beams, arches, plates, and shells. In Figs. 16.5-1a and 16.5-1b, as an element becomes thinner, thickness-direction stiffness coefficients become much larger than other coefficients of the stiffness matrix, which produces ill-conditioning (Section 9.2). If in Fig. 16.5-1b we constrain each pair of nodes on a thickness-direction line to have the same thickness-direction displacement, we are left with five translational d.o.f. per pair of nodes. Finally, we halve the number of nodes by replacing surface nodes by midsurface nodes, Fig. 16.5-1c, where each midsurface node has three translational d.o.f. and two rotational d.o.f.

In the following development, we begin with the type of element shown in Fig. 16.5-1c. We make no restriction as to the number of nodes per element, although eight- or nine-node elements are often used. As with other Mindlin-type elements, troubles with spurious modes and locking may be provoked (or avoided) by interrelated actions of element geometry, number of nodes, formulation procedure, and numerical integration scheme.

Element Geometry. At a typical node i, Fig. 16.5-2a, a thickness-direction vector $\mathbf{V}_{3i}$ is

$$\mathbf{V}_{3i} = t_i \begin{Bmatrix} l_{3i} \\ m_{3i} \\ n_{3i} \end{Bmatrix} \quad \text{where} \quad \begin{Bmatrix} l_{3i} \\ m_{3i} \\ n_{3i} \end{Bmatrix} = \frac{1}{t_i} \begin{Bmatrix} x_j - x_k \\ y_j - y_k \\ z_j - z_k \end{Bmatrix} \tag{16.5-1}$$

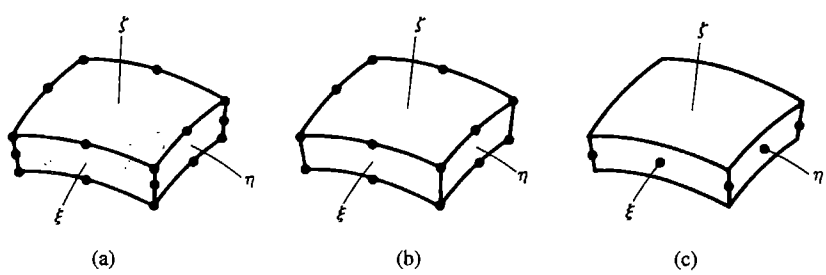

Figure 16.5-1. (a) A 20-node solid element. (b) Elimination of four midedge nodes yields a 16-node element. (c) Further constraint yields an eight-node element.

in which l_{3i}, m_{3i}, and n_{3i} are direction cosines of the midsurface-normal line kij and xyz is a global coordinate system. Global coordinates of an arbitrary point in the element are

$$\begin{Bmatrix} x \\ y \\ z \end{Bmatrix} = \sum N_i \begin{Bmatrix} x_i \\ y_i \\ z_i \end{Bmatrix} + \sum N_i \zeta \frac{t_i}{2} \begin{Bmatrix} l_{3i} \\ m_{3i} \\ n_{3i} \end{Bmatrix} \tag{16.5-2}$$

where summation spans all element nodes and $\xi\eta\zeta$ is the usual coordinate system used for isoparametric elements (Chapter 6). Midsurface coordinates are $x_i = (x_j + x_k)/2$, and so on. Shape functions N_i depend on ξ and η but are independent of ζ. For example, the N_i of Eqs. 6.4-1 are appropriate for the eight-node element of Fig. 16.5-1c. To define element geometry, one can either provide the global coordinates of all nodes j and k, or supply x_i, y_i, z_i, t_i, and the direction cosines of $\mathbf{V}_{3i}$ for all nodes i.

Vectors $\mathbf{V}_{1i}$ and $\mathbf{V}_{2i}$ in Fig. 16.5-2 are perpendicular to each other and to $\mathbf{V}_{3i}$. Thus $\mathbf{V}_{1i}$ and $\mathbf{V}_{2i}$ are tangent to the element midsurface at node i, but they are not required to have any particular orientation with respect to global coordinate directions. $\mathbf{V}_{1i}$ and $\mathbf{V}_{2i}$ are used to define directions of nodal rotation d.o.f. α_i and β_i. Directions of α_i and β_i may differ from node to node in a single element, and may differ between elements at a node the elements share. Before elements are assembled, each element $[\mathbf{k}]$ must be transformed to suit a global set of d.o.f. at structure nodes.

One way to define $\mathbf{V}_{1i}$ and $\mathbf{V}_{2i}$ is to establish $\mathbf{V}_{1i}$ normal to both $\mathbf{V}_{3i}$ and the global y direction by writing the cross product $\mathbf{V}_{1i} = \mathbf{j} \times \mathbf{V}_{3i}$, where $\mathbf{j}$ is a unit vector in the y direction. Then $\mathbf{V}_{2i} = \mathbf{V}_{3i} \times \mathbf{V}_{1i}$. (The calculation $\mathbf{V}_{1i} = \mathbf{j} \times \mathbf{V}_{3i}$ fails if $\mathbf{j}$ and $\mathbf{V}_{3i}$ are parallel. In programming, one can test for this condition, and if it is encountered substitute the calculations $\mathbf{V}_{2i} = \mathbf{V}_{3i} \times \mathbf{i}$ and $\mathbf{V}_{1i} = \mathbf{V}_{2i} \times \mathbf{V}_{3i}$.) For subsequent use, we define the following matrix of direction cosines.

$$\left[\boldsymbol{\mu}_i\right] = \begin{bmatrix} -\dfrac{\mathbf{V}_{2i}}{V_{2i}} & \dfrac{\mathbf{V}_{1i}}{V_{1i}} \end{bmatrix} = \begin{bmatrix} -l_{2i} & l_{1i} \\ -m_{2i} & m_{1i} \\ -n_{2i} & n_{1i} \end{bmatrix} \tag{16.5-3}$$

where V_{1i} and V_{2i} are the magnitudes of $\mathbf{V}_{1i}$ and $\mathbf{V}_{2i}$.

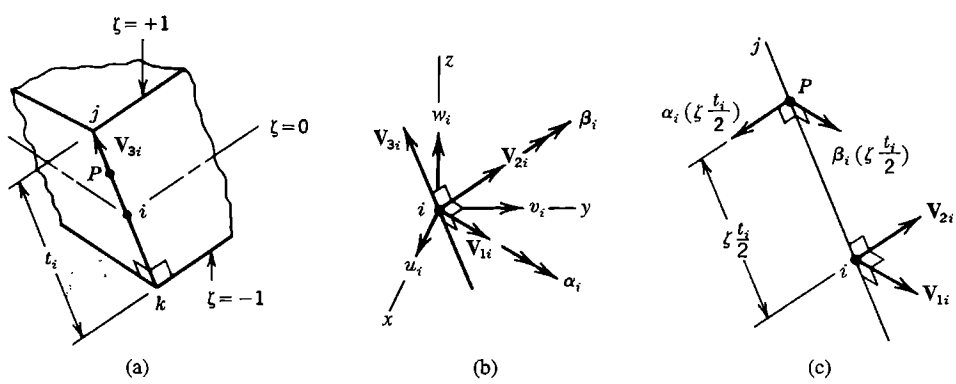

Figure 16.5-2. (a) Typical node i, and thickness-direction vector $\mathbf{V}_{3i}$ (b) Orthogonal vectors at node i, and nodal d.o.f. (c) Displacements at an arbitrary point P on $\mathbf{V}_{3i}$ due to small nodal rotations α_i and β_i.

From Eq. 16.5-2, the first column of Jacobian matrix [**J**], Eq. 6.5-2, contains

$$
\begin{aligned}
x_{,\xi} &= \sum N_{i,\xi}(x_i + \zeta\, t_i l_{3i}/2) \\
x_{,\eta} &= \sum N_{i,\eta}(x_i + \zeta\, t_i l_{3i}/2) \\
x_{,\zeta} &= \sum N_i(t_i l_{3i}/2)
\end{aligned}
\tag{16.5-4}
$$

Expressions for the second and third columns of [**J**] are similar.

Strain-Displacement Relation. The displacement of a point P on vector $\mathbf{V}_{3i}$, Fig. 16.5-2c, consists of the displacement of node i plus the displacement of P relative to i created by rotation of $\mathbf{V}_{3i}$ through small angles α_i and β_i. The relative displacement must be resolved into x, y, and z components before being added to displacement components of node i. For example, point P has the x-direction displacement

$$
u_P = u_i - \alpha_i\left(\zeta\frac{t_i}{2}\right)l_{2i} + \beta_i\left(\zeta\frac{t_i}{2}\right)l_{1i} \tag{16.5-5}
$$

Hence, by shape function interpolation, displacements of an arbitrary point in the element are

$$
\begin{Bmatrix} u \\ v \\ w \end{Bmatrix} = \sum N_i\left(\begin{Bmatrix} u_i \\ v_i \\ w_i \end{Bmatrix} + \zeta\frac{t_i}{2}[\boldsymbol{\mu}_i]\begin{Bmatrix} \alpha_i \\ \beta_i \end{Bmatrix}\right) \tag{16.5-6}
$$

Following standard procedures explained in Chapter 6, we express strains in terms of displacement derivatives:

$$
\lfloor \varepsilon_x \;\; \varepsilon_y \;\; \varepsilon_z \;\; \gamma_{xy} \;\; \gamma_{yz} \;\; \gamma_{zx} \rfloor^T = [\mathbf{H}]\lfloor u_{,x} \;\; u_{,y} \;\; u_{,z} \;\; v_{,x} \;\; \cdots \;\; w_{,z} \rfloor^T \tag{16.5-7}
$$

$$
\begin{Bmatrix} u_{,x} \\ u_{,y} \\ u_{,z} \\ v_{,x} \\ \vdots \\ w_{,z} \end{Bmatrix} = \begin{bmatrix} \mathbf{J}^{-1} & \mathbf{0} & \mathbf{0} \\ \mathbf{0} & \mathbf{J}^{-1} & \mathbf{0} \\ \mathbf{0} & \mathbf{0} & \mathbf{J}^{-1} \end{bmatrix} \begin{Bmatrix} u_{,\xi} \\ u_{,\eta} \\ u_{,\zeta} \\ v_{,\xi} \\ \vdots \\ w_{,\zeta} \end{Bmatrix} \tag{16.5-8}
$$

where [**H**] is the rectangular matrix in Eq. 6.5-3 and $[\mathbf{J}]^{-1}$ is the inverse of the 3 by 3 Jacobian matrix [**J**]. Strains in Eq. 16.5-7 are with reference to global coordinate directions xyz.

All six strains are included because the shell midsurface may have any orientation with respect to global directions. The condition that plane stress conditions prevail in midsurface-parallel layers will be introduced subsequently, via the stress-strain relation. From Eq. 16.5-6 we obtain

$$\begin{Bmatrix} u_{,\xi} \\ u_{,\eta} \\ u_{,\zeta} \\ v_{,\xi} \\ \vdots \\ w_{,\zeta} \end{Bmatrix} = \sum \begin{bmatrix} N_{i,\xi} & 0 & 0 & -\zeta t_i N_{i,\xi} l_{2i}/2 & \zeta t_i N_{i,\xi} l_{1i}/2 \\ N_{i,\eta} & 0 & 0 & -\zeta t_i N_{i,\eta} l_{2i}/2 & \zeta t_i N_{i,\eta} l_{1i}/2 \\ 0 & 0 & 0 & -t_i N_i l_{2i}/2 & t_i N_i l_{1i}/2 \\ 0 & N_{i,\xi} & 0 & -\zeta t_i N_{i,\xi} m_{2i}/2 & \zeta t_i N_{i,\xi} m_{1i}/2 \\ \vdots & \vdots & \vdots & \vdots & \vdots \\ 0 & 0 & 0 & -t_i N_i n_{2i}/2 & t_i N_i n_{1i}/2 \end{bmatrix} \begin{Bmatrix} u_i \\ v_i \\ w_i \\ \alpha_i \\ \beta_i \end{Bmatrix} \tag{16.5-9}$$

Combination of Eqs. 16.5-7, 16.5-8, and 16.5-9 yields

$$\lfloor \varepsilon_x \;\; \varepsilon_y \;\; \varepsilon_z \;\; \gamma_{xy} \;\; \gamma_{yz} \;\; \gamma_{zx} \rfloor^T = \sum [\mathbf{B}_i] \lfloor u_i \;\; v_i \;\; w_i \;\; \alpha_i \;\; \beta_i \rfloor^T \tag{16.5-10}$$

The complete strain-displacement matrix $[\mathbf{B}]$ is built of as many 6 by 5 blocks $[\mathbf{B}_i]$ as there are nodes in the element.

Stress-Strain Relation. The stress-strain relation can be stated as

$$\{\boldsymbol{\sigma}\} = [\mathbf{E}]\{\boldsymbol{\varepsilon}\} \qquad \text{or as} \qquad \{\boldsymbol{\sigma}'\} = [\mathbf{E}']\{\boldsymbol{\varepsilon}'\} \tag{16.5-11}$$

where $\{\boldsymbol{\sigma}\}$contains stresses in the global coordinate system xyz and $\{\boldsymbol{\sigma}'\}$ contains stresses in a local coordinate system we shall call 123, where directions 1 and 2 are tangent to the midsurface and direction 3 is normal to it. For an isotropic material, the relation $\{\boldsymbol{\sigma}'\} = [\mathbf{E}']\{\boldsymbol{\varepsilon}'\}$ is

$$\begin{Bmatrix} \sigma_1 \\ \sigma_2 \\ \sigma_3 \\ \tau_{12} \\ \tau_{23} \\ \tau_{31} \end{Bmatrix} = \begin{bmatrix} E' & \nu E' & 0 & 0 & 0 & 0 \\ \nu E' & E' & 0 & 0 & 0 & 0 \\ 0 & 0 & 0 & 0 & 0 & 0 \\ 0 & 0 & 0 & G & 0 & 0 \\ 0 & 0 & 0 & 0 & G^* & 0 \\ 0 & 0 & 0 & 0 & 0 & G^* \end{bmatrix} \begin{Bmatrix} \varepsilon_1 \\ \varepsilon_2 \\ \varepsilon_3 \\ \gamma_{12} \\ \gamma_{23} \\ \gamma_{31} \end{Bmatrix} \tag{16.5-12}$$

where $E' = E/(1 - \nu^2)$, $G = 0.5E/(1 + \nu)$, and $G^* = 5G/6$ in homogeneous material, where the factor of $5/6$ accounts for the thickness-direction variation of transverse shear strain, which is more nearly parabolic than the constant value associated with Mindlin theory. Note that Eq. 16.5-12 is contrived to make $\sigma_3 = 0$ and provide plane stress conditions in each thickness-direction layer. Matrix $[\mathbf{E}]$ is obtained from $[\mathbf{E}']$ by the coordinate transformation $[\mathbf{E}] = [\mathbf{T}_\varepsilon]^T[\mathbf{E}'][\mathbf{T}_\varepsilon]$ (see Eq. 8.2-10). In numerical integration, this transformation must be carried out at each sampling point for which ξ and η differ (multiple

sampling points on the same thickness-direction line have the same [**E**] if the material is homogeneous). Direction cosines needed in $[\mathbf{T}_\varepsilon]$ are direction cosines of vectors $\mathbf{V}_1$, $\mathbf{V}_2$, and $\mathbf{V}_3$ at the sampling point. In turn, these vectors can be established by shape function interpolation from nodal values:

$$\mathbf{V}_1 = \sum N_i \mathbf{V}_{1i} \quad \mathbf{V}_2 = \sum N_i \mathbf{V}_{2i} \quad \mathbf{V}_3 = \sum N_i \mathbf{V}_{3i} \tag{16.5-13}$$

in which the N_i are evaluated at the sampling point in question.

Stiffness Matrix [k]. The element stiffness matrix is, with N the number of nodes per element,

$$\underset{5N\times 5N}{[\mathbf{k}]} = \int_{-1}^{1}\int_{-1}^{1}\int_{-1}^{1} \underset{5N\times 6}{[\mathbf{B}]^T} \underset{6\times 6}{[\mathbf{E}]} \underset{6\times 5N}{[\mathbf{B}]} \det[\mathbf{J}]\, d\xi\, d\eta\, d\zeta \tag{16.5-14}$$

An alternative form for the product $[\mathbf{B}]^T[\mathbf{E}][\mathbf{B}]$ is $[\mathbf{B}']^T[\mathbf{E}'][\mathbf{B}']$, where $[\mathbf{B}'] = [\mathbf{T}_\varepsilon][\mathbf{B}]$. In this form one can omit null terms associated with midsurface-normal strain ε_3 and write $[\mathbf{E}']$ as a 5 by 5 matrix and $[\mathbf{B}']$ as a 5 by $5N$ matrix, thus making computations more efficient.

Equation 16.5-14 is most economically integrated by assuming that the ratio of element thickness to element span is sufficiently small that the dependence of [**J**] on ζ can be ignored. Thus [**J**] is evaluated on the midsurface and [**B**] can be written as $[\mathbf{B}] = [\mathbf{B}_0] + \zeta[\mathbf{B}_1]$, where $[\mathbf{B}_0]$ and $[\mathbf{B}_1]$ are independent of ζ. Also let [**E**] be constant. Then, after explicit integration in the thickness direction, Eq. 16.5-14 becomes

$$[\mathbf{k}] = \int_{-1}^{1}\int_{-1}^{1}\left(2[\mathbf{B}_0]^T[\mathbf{E}][\mathbf{B}_0] + \frac{2}{3}[\mathbf{B}_1]^T[\mathbf{E}][\mathbf{B}_1]\right)\det[\mathbf{J}]\, d\xi\, d\eta \tag{16.5-15}$$

However, even if thin, elements do not display rigid-body motion without strain unless their curvature is zero or thickness-direction integration is exact. And, of course, Eq. 16.5-15 includes the assumption that [**E**] is independent of ζ, so that material inhomogeneity or layered construction is not taken into account. Details of thickness-direction integration are addressed in [3.3,16.36–16.39].

Element nodal loads come from the usual sources. Those associated with initial strains are, because $\{\boldsymbol{\varepsilon}_0'\} = [\mathbf{T}_\varepsilon]\{\boldsymbol{\varepsilon}_0\}$ and $[\mathbf{E}] = [\mathbf{T}_\varepsilon]^T[\mathbf{E}'][\mathbf{T}_\varepsilon]$,

$$\int [\mathbf{B}]^T[\mathbf{E}]\{\boldsymbol{\varepsilon}_0\}\, dV = \int_{-1}^{1}\int_{-1}^{1}\int_{-1}^{1} [\mathbf{B}]^T[\mathbf{T}_\varepsilon]^T[\mathbf{E}']\{\boldsymbol{\varepsilon}_0'\} \det[\mathbf{J}]\, d\xi\, d\eta\, d\zeta \tag{16.5-16}$$

Computed stresses referred to local directions 123 are

$$\{\boldsymbol{\sigma}'\} = [\mathbf{E}']\Big([\mathbf{T}_\varepsilon][\mathbf{B}]\{\mathbf{d}\} - \{\boldsymbol{\varepsilon}_0'\}\Big) \tag{16.5-17}$$

Remarks. Membrane and bending actions are coupled in the foregoing shell element when it is curved. Accordingly, one may encounter membrane locking, as described in Section 16.2, as well as shear locking, as described for plane elements in Section 3.6 and for plate elements in Section 15.3. Remedies for locking include devices used for plane

and plate elements, such as reduced integration, which may introduce spurious modes, and reduced integration with a device for stabilization [16.39,16.40]. Reduced integration reduces membrane-flexural coupling, thus making curved elements behave more like straight elements [16.41].

In the formulation described by the preceding equations, elements have five d.o.f. per node. If drilling d.o.f. (nodal rotations about the midsurface normal) are introduced as global d.o.f., a zero stiffness arises at a node if surrounding elements happen to be coplanar, unless drilling d.o.f. are included in the basic element formulation or a stabilization matrix is added. A related difficulty is that of deciding what d.o.f. are appropriate if elements meet at an angle, as in a folded plate (see the discussion that follows Eq. 16.4-2). In this context we note that elements intended to model a cylindrical or spherical surface actually do not share a common tangent across an interelement boundary because three-node element edges are parabolic rather than circular. For the same reason, a computed vector $\mathbf{V}_3$ at an arbitrary location in an element may not be precisely normal to the actual midsurface intended. The geometric discrepancies disappear as arcs subtended by elements approach zero.

A nine-node curved shell element based on assumed strains (rather than assumed displacements) has been devised [16.42]. It performs well, but does not pass patch tests for constant curvature [3.3]. The formulation of Eqs. 16.5-1 to 16.5-17 accommodates any number of nodes. The question of whether nine nodes are better than eight has not been settled [3.3,16.43].

16.6 TEST CASES. REMARKS

Test Cases. Elements for shells of general shape are among the most difficult elements to formulate. In practical applications, shell behavior is often difficult to anticipate, and various element types found in FE software may behave rather differently. Therefore, one may wish to test elements in software to be sure of their validity, sensitivity to shape distortion, and behavior in problems for which correct results are already known. If geometry is flat, a shell element should be able to solve either plane stress or plate bending problems, and should pass patch tests for both. Arch problems, such as those in Figs. 16.2-1a and 16.4-2 and others tabulated [1.16], can be solved by shell elements of cylindrical shape.

Some other test cases for general shell elements are shown in Fig. 16.6-1 [16.14,16.39]. The shell roof is loaded by its own weight of $q = 90$ per unit area (we present data in consistent but unspecified units). Straight edges are free and curved edges have "diaphragm" support, which means that translational d.o.f. in the plane of the curve are prohibited but translational d.o.f. normal to this plane and all rotational d.o.f. are unrestrained. Loads on the pinched cylinder are $F = 1.0$, and circular ends have diaphragm support. A pinched cylinder with free ends is sometimes used, but it is not a challenging test case. The hemisphere has a free edge, is restrained only against rigid-body motion, and has radial loads $F = 2.0$ at the equator. The twisted strip is cantilevered and there are two load cases, $F_1 = 10^{-6}$ and $F_2 = 10^{-6}$. Commonly used numerical data, and accepted displacements Δ_A of point A in the direction of the load, are as follows:

Problem	R or b	L	t	E	ν	Δ_A
Shell roof	25	50	0.25	$432(10^6)$	0.00	0.3024
Pinched cylinder	300	600	3.00	$3(10^6)$	0.30	$0.1825(10^{-4})$
Hemisphere	10	—	0.04	$68.25(10^6)$	0.30	0.0924
Twisted strip (F_1)	1.1	12	0.0032	$29(10^6)$	0.22	$5256(10^{-6})$
Twisted strip (F_2)	1.1	12	0.0032	$29(10^6)$	0.22	$1294(10^{-6})$

Symmetry can be exploited: one need model only one quadrant of the roof and one octant of the pinched cylinder. Exploiting both symmetry and antisymmetry, one might analyze an octant of the hemisphere, but a quadrant may be an easier choice. A similar test case cuts an 18° cap off the top of the hemisphere, so that the shell extends from the equator to latitude 72°; for this problem, $\Delta_A = 0.094$ [16.12]. A twisted strip with thickness $t = 0.32$ is sometimes used, but this test case is less demanding than the case $t = 0.0032$.

The foregoing cases test different aspects of element behavior. Membrane action dominates in the shell roof, bending dominates in the hemisphere, and both actions are present in the pinched cylinder. Sensitivity to warping is tested if quadrilateral elements are used to model the twisted strip. Experience shows that a particular element may do very well in two or three of these test cases but quite poorly in one or two others.

The test case depicted in Fig. 16.6-2 is a curved strip of material, fixed at one end, and loaded at the other end by a force parallel to the longer dimension of the cross section. It has been called the "Raasch challenge problem" after I. Raasch, who experimented with various formulations of flat shell elements, both with and without the capability for transverse shear deformation in the plate-bending portion of the stiffness matrix. He found that answers became *worse* with mesh refinement unless transverse shear deformation capability was omitted from the element formulation [16.44]. Tip deflection computed from a 20 by 136 by 2 mesh of eight-node hybrid solid elements is 4.9366 when t-direction thickness changes are unrestrained at the fixed end, while 20 by 136 by 1 meshes of shear-flexible shell elements predict two to five times this value, depending on the type of element used [16.44]. MacNeal's analysis of the trouble [16.31] concludes that the manner of transfer of twisting moment from element to element produces spurious transverse shear deformation whose strain energy is proportional to $(1 + t^2/w^2)$. Thus, decreasing t improves accuracy,

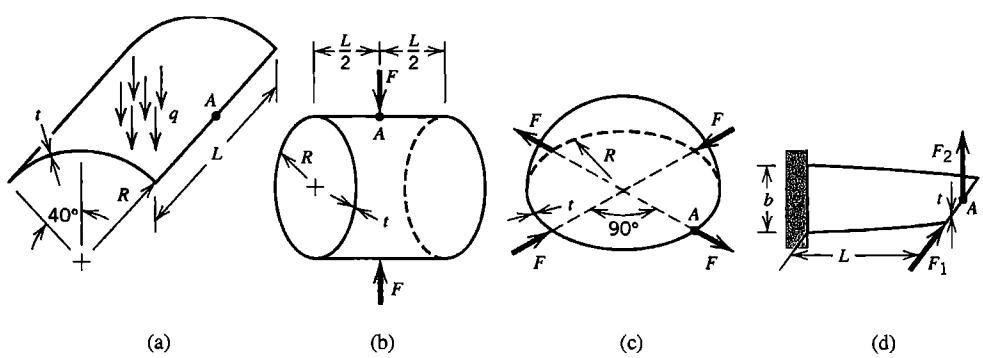

Figure 16.6-1. (a) Cylindrical shell roof loaded by its own weight. (b) Pinched cylinder. (c) Hemisphere loaded by four uniformly spaced radial forces in the equatorial plane. (d) Strip with a 90° twist over length L.

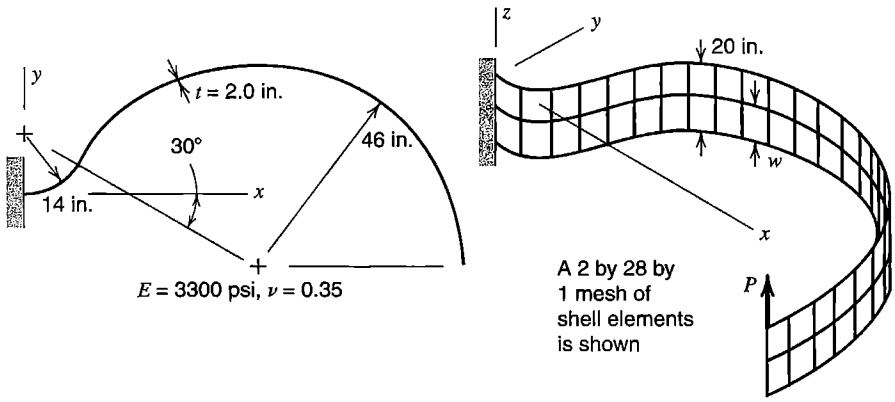

Figure 16.6-2. A strip of material bent into a hook shape, seen in edge view and in isometric view.

as is shown by numerical experiment, and reducing w (as by refining the mesh) reduces accuracy. The remedy proposed involves examining the relation between element normals at each shared node, then ensuring that the moment about the defined shell normal is zero before restraining the corresponding rotational d.o.f. The Raasch test case reminds us to be wary: some elements that failed the test had been in service for years and were thought to be working properly.

Remarks. When loads are distributed, as from applied pressure, the nodal load vector should not contain moment terms, for reasons discussed in the latter part of Section 2.9. For proper application of pressure loads, and for proper interpretation of computed stresses, one must pay attention to the "upper surface" problem discussed at the end of Section 15.1.

For acceptable accuracy, a shell element should not subtend a large angle. The allowable angle depends on the element type, the problem at hand, and the accuracy required. As rough guidelines, triangular and quadrilateral elements might subtend no more than 15°, and conical elements no more than 12°, or perhaps 5° if near the axis of revolution.

Near shell intersections, such as a T intersection of pipes or a pressure vessel outlet, behavior may be sufficiently complicated that 3D solid elements should be used rather than shell elements, especially if the shell is rather thick. Shell elements may yet be appropriate farther from the intersection, with the shell-to-solid transition modeled in a fashion similar to the beam-to-plane transition depicted in Fig. 10.10-3. Special-purpose elements for shell intersections are available [16.45]. Similarly, there are special pipe elbow elements, that account for such effects as ovalization of the cross section due to applied bending moment and the stiffening effect of internal pressure [16.46]. Elbow elements appear in software capable of piping system analysis.

Materials need not be homogeneous, isotropic, or linearly elastic. Then thickness-direction integration requires more sampling points or other special attention [16.38]. Elements that account for thickness-direction variation of material properties may or may not use several nodes through the thickness, depending on the theory adopted [15.5].

A shell so thin that its bending stiffness is negligible may be analyzed as a membrane by including only midsurface displacements and nodal translations as d.o.f. Thus, for example, we discard κ and $[\mathbf{k}_b]$ in Section 16.2, $[\mathbf{D}_b]$ in Section 16.3, $[\mathbf{k}_b]$ in Section 16.4, and $[\mathbf{B}_1]$ in Section 16.5. Stress stiffening, discussed in Chapter 18, is commonly included. Without it, a flat membrane would have no resistance to lateral load. Possible wrinkling of

a membrane can be accommodated, most simply (and perhaps crudely) by using a material property matrix [E] that provides no stiffness in the direction of a compressive principal stress. Of course, one must first detect the onset of compressive stress and establish its direction; accordingly the solution must be obtained by iterative cycles of analysis and revision of material properties. Iteration is also needed to define stress stiffening, as it depends on membrane stresses that are not usually known in advance. References include [15.5,16.47–16.50].

16.7 AN AXISYMMETRIC SHELL APPLICATION

The structure we consider is a segment of a thin spherical shell, Fig. 16.7-1a. It is fixed to a rigid support at the equator and is loaded by a uniformly distributed downward force around the 30° parallel, which is unrestrained. The state of stress is to be investigated.

Preliminary Analysis. Axial symmetry prevails. Compressive membrane force in the meridional direction is expected throughout. Meridional bending moment is also expected, near the 30° parallel because load q has a component normal to the shell, and near the equator because the fixed support suppresses any tendency to displace or rotate. Meridional membrane force at the equator is easy to calculate by statics. Equilibrium of vertical forces requires

$$2\pi R N_B = 2\pi(R\cos 30°)q \qquad \text{hence} \qquad N_B = 0.866q = 4.33\ \text{N/mm} \tag{16.7-1}$$

Meridional membrane stress $N_B/t = 4.33$ MPa (compressive) is present on the shell midsurface at B. If radial displacement were unrestrained at B, a circumferential tensile stress of equal magnitude would appear in order to provide equilibrium of forces normal to the shell [2.6]. Thus the shell wants to expand around the equator, but is restrained by the support, which applies inward radial line load V_B around the equator. Load V_B tries to rotate the shell inward; the support prevents rotation by applying meridional moment M_B distributed around the equator. Around the top of the shell, there is no support to oppose the shell-normal component of load q.

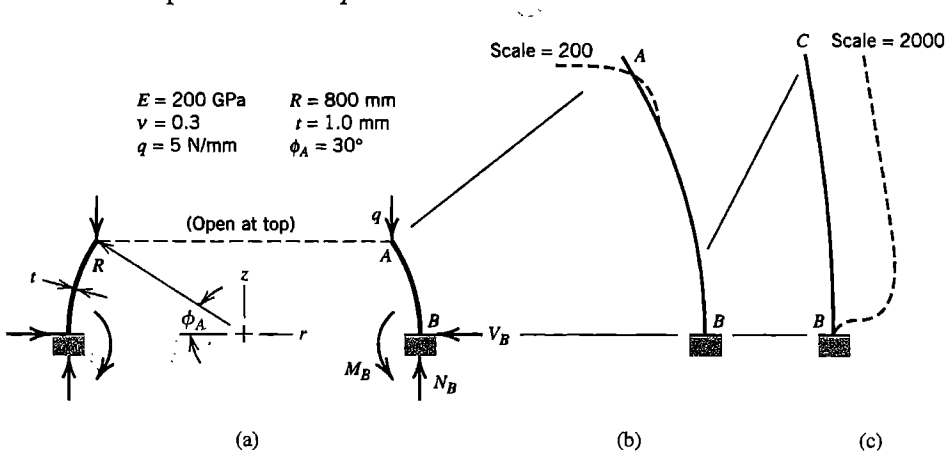

Figure 16.7-1. (a) Geometry, loading, and properties of a shell of revolution. (b) Computed displacements along AB, multiplied by 200. (c) Computed displacements along lower quarter of AB, multiplied by 2000.

Summing up, we expect computed results to display large inward deflection near A, where no support opposes the inward component of applied load. We expect no meridional bending moment at A because this edge is free. Slightly downward from A, because of inward bending, meridional bending stress should be tensile on the outside surface. At the equator, meridional membrane stress should be the predicted value, 4.33 MPa compressive. We expect N_B, V_B, and M_B to be in the directions shown, and meridional bending stress at B to be tensile on the inside surface.

Finite Element Analysis. The appropriate shell elements are axisymmetric. We elect to use two-node conical elements, described by Fig. 16.3-1b and Eqs. 16.3-3 and 16.3-4. Within a meridional distance of $\sqrt{Rt} = \sqrt{800 \cdot 1} = 28$ mm from A and B, the mesh should include at least two elements even in a coarse mesh. For the present analysis, the software is instructed to mesh the arc from A to B automatically, using element lengths of 4 mm at A and B and 20 mm at the middle of the arc. The result is 65 nodes and 64 elements with graduated element lengths along the arc. All three d.o.f. at B are set to zero; all other d.o.f. of the mesh are unrestrained.

Critique of Results. Computed displacements are found to have the qualitative behavior expected (Fig. 16.7-1b,c), and reactions N_B, V_B, and M_B are found to have the directions expected. Computed meridional membrane stress at B is -4.33 MPa, exactly as predicted. Meridional bending moment M near the top and bottom is shown in Fig. 16.7-2. The sign convention is that of the software used, namely that M is positive when it creates tensile flexural stress on the inside of the shell (opposite to the direction of M_s shown in Fig. 16.3-1a). As expected, $M = 0$ at A. The largest meridional flexural stress is $\pm 6M/t^2 = \pm 6(17.7)/1^2 = \pm 106$ MPa, about 17 mm from the top. At this location, the meridional membrane stress is only about -6 MPa and the net meridional stress is about -112 MPa, on the inside of the shell. Net meridional stresses at the equator are comparatively small, being about 6 MPa on the inside and -15 MPa on the outside. The largest magnitude of stress is found at the top, where the large inward displacement creates a circumferential membrane stress of -175 MPa. So large a compressive stress in a thin shell suggests that buckling is possible, for which a separate analysis would be required.

For this type of element, the software used does not provide a relative energy error based on interelement stress discontinuities. Even if the estimate were available, it might not alert

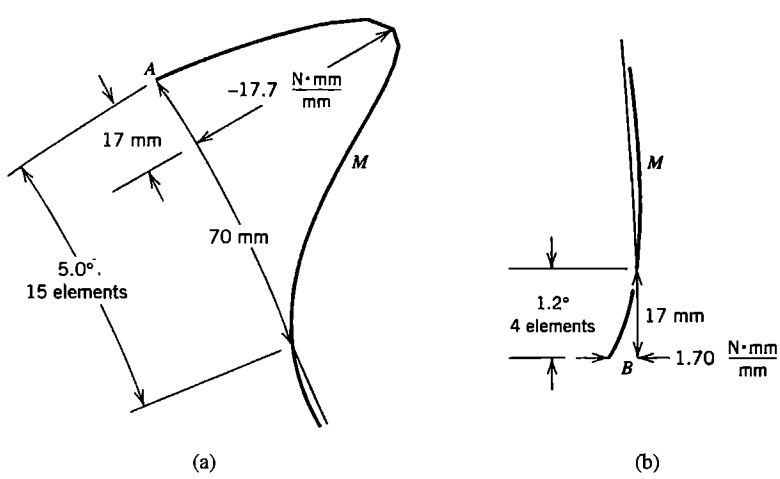

Figure 16.7-2. Meridional bending moments in the shell of Fig. 16.7-1, computed by FEA. (a) Near the top. (b) Near the bottom.

us to trouble if we were to use elements spanning arcs so large that local behavior near shell edges A and B could not be captured.

It is known that edge effects in axisymmetric shell problems are represented by damped sine and cosine functions, in the manner described for a cylindrical shell following Eq. 16.1-2. This is indeed the behavior seen in Figs. 16.7-1 and 16.7-2. The smoothness of the plotted curve in Fig. 16.7-2 suggests that mesh refinement would change results very little.

It happens that there are tabulated formulas applicable to this problem, although they are tedious to apply in hand calculation [1.16, 2.6]. These formulas give values of V_B, M_B, and largest meridional bending moment less than 1% different from those computed by FEA.

ANALYTICAL PROBLEMS

16.1-1 (a) Let x and y be meridional and circumferential directions in a cylindrical shell of revolution with hemispherical end caps. Internal pressure is applied. According to Eqs. 16.1-1 and elementary pressure vessel formulas, what are N_x, N_y, and N_{xy} in the cylinder and in its end caps?
(b) Imagine that a garden hose has an elliptical cross section. Why does increasing pressure make the cross section almost circular? Around the external circumference, sketch the approximate variation of circumferential flexural stress due to internal pressure.

16.1-2 The cylindrical tank shown contains a step change in thickness and is capped by a hemispherical shell. Loads consist of axial force Q and internal pressure.
(a) Explain why load Q cannot be supported by membrane action alone.
(b) Remove fixity at CC and divide the vessel into three parts by making circumferential cuts around parallels AA and BB. Then sketch the deformation each part would have if it sustained only the membrane stresses caused by pressure p.
(c) Show by sketches the loads (applied by one part to another) needed to restore continuity of displacements and rotations.

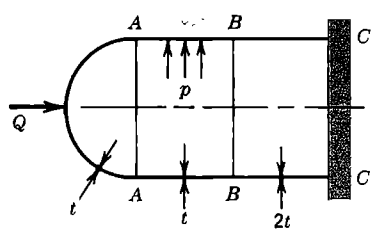

Problem 16.1-2

16.2-1 Write an expression for strain ε_s, analogous to Eqs. 16.2-2, if arch radius R is a function of s.

16.2-2 (a) Derive Eqs. 16.2-4.
(b) Consider a quarter-circle arch that occupies the first quadrant of rectangular coordinates. By three separate sketches, show displacement fields associated with b_1, b_2, and b_3 in Eqs. 16.2-4.

16.2-3 For element 1-2 in Fig. 16.2-3b, write the coordinate transformation of nodal d.o.f. from part (a) to part (b). That is, define all necessary coefficients in terms of L and R. Assume that local d.o.f. are ordered as shown in Eq. 16.2-6, and that global d.o.f. in Fig. 16.2-3b have the order $\lfloor D_{s1} \;\; D_{r1} \;\; \psi_1 \;\; D_{s2} \;\; D_{r2} \;\; \psi_2 \rfloor^T$.

16.2-4 Model a complete circular ring by four straight elements of equal length. The FE model is therefore a square, as shown. Calculate the relative separation of loads P, accounting for deformation due to bending only. Take the element length as (a) chord length $L = \sqrt{2}R$, and (b) arc length $L = \pi R/2$. The exact result is $0.1488PR^3/EI$. *Suggestion:* Apply elementary beam theory.

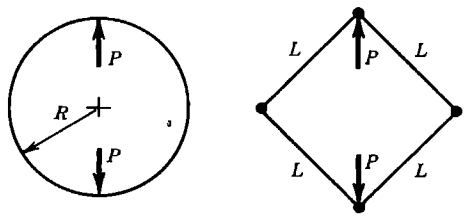

Problem 16.2-4

16.2-5 For an arch of constant radius, integrate U_m of Eq. 16.2-3 using the displacement field of Eq. 16.2-9. Hence, show that the condition $U_m = 0$ implies Eqs. 16.2-11.

16.2-6 Using displacement fields cited in (a) and (b) below for an arch of constant radius, establish the relation between nodal d.o.f. and generalized d.o.f. a_i. That is, determine [**A**] in the relation

$$\lfloor u_1 \;\; w_1 \;\; \psi_1 \;\; u_2 \;\; w_2 \;\; \psi_2 \rfloor^T = [\mathbf{A}] \lfloor a_1 \;\; a_2 \;\; a_3 \;\; a_4 \;\; a_5 \;\; a_6 \rfloor^T$$

where $\psi = dw/ds$ for a thin arch. (a) Use Eqs. 16.2-9. (b) Use Eqs. 16.2-12.

16.2-7 In [**k**] of the element associated with Eqs. 16.2-12, the diagonal and off-diagonal coefficients associated with radial deflections at nodes are

$$k_{22} = k_{55} = \frac{24}{\beta^3} - \frac{192}{35\beta} + \frac{16\beta}{35} \quad \text{and} \quad k_{25} = k_{52} = \frac{21}{\beta^3} - \frac{108}{35\beta} - \frac{\beta}{35}$$

where $\beta = L/2R$ for an element of arc length L [16.17]. Use this information to analyze the ring of Problem 16.2-4, again using a single element per quadrant.

16.2-8 In formulating an element stiffness matrix [**k**] from Eqs. 16.2-12, strain energy U_m makes no contribution to [**k**]. Why cannot U_m simply be discarded in the formulation of other arch elements, such as the one associated with Eq. 16.2-9?

16.2-9 (a) Verify the correctness of Eqs. 16.2-15 and 16.2-16.
(b) Determine the analogous equations of constraint associated with use of a single sampling point to numerically integrate U_m and U_s.

16.2-10 Investigate the $\gamma_{zs} = 0$ condition and the effect of reduced integration on a three-node Mindlin arch element (obtain equations analogous to Eqs. 16.2-17 and 16.2-18).

16.3-1 Consider a thin cylindrical shell of radius R whose midsurface meridional strain ε_{ms} is unrestrained. By considering the energy associated with membrane strains

ε_{ms} and $\varepsilon_{m\theta}$ show that radial displacement w is in effect resisted by an elastic foundation of modulus Et/R^2 (as well as being resisted by bending stiffness).

16.3-2 Consider a cylindrical shell, thin-walled and symmetrically loaded, but without axial loads. Thus $N_s = 0$, membrane strains have the relation $\varepsilon_{ms} = -\nu\varepsilon_{m\theta}$, and meridional displacement u need not be considered. Use a cubic w field, and determine the 4 by 4 element stiffness matrix that operates on nodal d.o.f. w_i and ψ_i.

16.3-3 Let uniform pressure p be applied to the inner surface of the element described by Eqs. 16.3-7. Evaluate the consistent element nodal load vector.

16.3-4 A cylindrical pipe terminates in a heavy flange. The pipe is modeled by shell of revolution elements, the flange by four-node solid of revolution elements. At the juncture shown in cross section, nodes A and B are on the flange and node C is on the pipe. What transformation matrix [**T**] should be written so that d.o.f. of node C can be replaced by d.o.f. of nodes A and B?
(a) Let the problem be axisymmetric.
(b) Let the problem be without axial symmetry.
(c) Repeat part (b), but state the relation by writing a constraint matrix [**C**] instead of transformation matrix [**T**] (see Section 13.1).

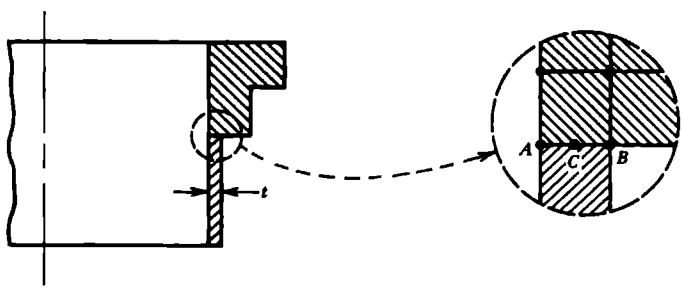

Problem 16.3-4

16.4-1 Let a doubly curved shell be modeled by flat triangular elements, each with vertex nodes but without drilling d.o.f. In what way are interelement displacements incompatible? Give a plausible argument to the effect that mesh refinement nevertheless provides convergence to correct results.

16.4-2 Imagine that each side of a rectangular box is modeled by a mesh of flat shell elements. Internal pressure is applied. Along edges where sides intersect, what d.o.f. can probably be set to zero, and why?

16.5-1 Write an equation analogous to Eq. 16.5-2 but applicable to the element of Fig. 16.5-1b. (Each shape function should depend on ξ and η and should be multiplied by a linear function of ζ.)

16.5-2 (a) Define terms in Jacobian matrix [**J**] in terms of ζ, N_i, $N_{i,\xi}$, $N_{i,\eta}$, nodal coordinates, and components of $\mathbf{V}_{3i}$.
(b) Specialize the results of part (a) for an element that is flat, of uniform thickness, and whose midsurface coincides with the xy plane.

16.5-3 (a) Imagine that instead of rotational d.o.f. α_i and β_i about local directions (Fig. 16.5-2), we choose to use rotational d.o.f. β_{xi}, β_{yi}, and β_{zi}, which are small rotations about global axes x, y, and z. Write the appropriate form of Eq. 16.5-6 and define terms in the direction cosine matrix suited to this representation.
(b) Check that the result of part (a) agrees with Eq. 16.5-6 for three special cases: all vectors $\mathbf{V}_{3i}$ parallel to the x axis, then all parallel to the y axis, and finally all parallel to the z axis.

16.5-4 Let a typical $[\mathbf{B}_i]$ in Eq. 16.5-10 have the form $[\mathbf{B}_i] = [\mathbf{H}][\bar{\mathbf{B}}_i]$, where $[\mathbf{H}]$ is the 6 by 9 matrix defined by Eq. 6.5-3 and $[\bar{\mathbf{B}}_i]$ is a 9 by 5 matrix. Express $[\bar{\mathbf{B}}_i]$ as a function of ζ, t_i, N_i, $N_{i,\xi}$, $N_{i,\eta}$, direction cosines, and the Γ_{ij} in $[\mathbf{\Gamma}] = [\mathbf{J}]^{-1}$.

16.5-5 The sketch represents an end of an isoparametric *beam* element, whose geometry is defined by the position of nodes along its centerline and vectors $\mathbf{V}_{2i}$ and $\mathbf{V}_{3i}$ that span its rectangular cross section.
(a) Write an equation of geometry analogous to Eq. 16.5-2.
(b) Write an equation of displacement analogous to Eq. 16.5-6.

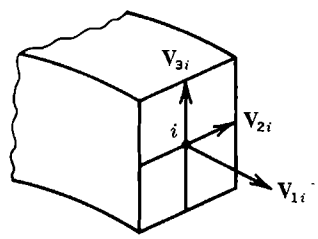

Problem 16.5-5

COMPUTATIONAL PROBLEMS

In the following problems, compute significant values of displacement, moment, or stress, as appropriate. Exploit symmetry where possible. When mesh refinement is used, estimate the maximum percentage error of results provided by the finest FE mesh. Where dimensions or loads are not assigned, choose values that seem reasonable or convenient. Where material properties are needed but not stated, use properties of steel. Apply the analysis methodology suggested in Section 1.5.

C16.1 A thin shell of revolution in the shape of a truncated cone is simply supported around its base, as shown. A uniformly distributed line load q is applied around the top parallel. (If the cone is rather flat, it is also known as a "Belleville spring" and has a nonlinear load versus deflection response.)

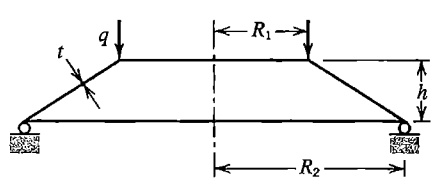

Problem C16.1

C16.2 Possible modifications of Problem C16.1 include the following:
(a) Add a reinforcing ring (such as the flange in Problem 16.3-4) to the top and/or bottom.
(b) Uniformly heat the upper half or the lower half.
(c) Apply load q around only half of the top parallel.
(d) Reorient load q so that it is directed circumferentially and acts to twist the shell.
(e) Uniformly heat only half the circumference.

C16.3 (a) The sketch shows an end closure on a cylindrical pressure vessel of radius R_c. The closure consists of a toroidal "knuckle" of radius R_t and a spherical cap of radius R_s. Investigate stresses that result from internal pressure or from temperature that varies linearly through the wall thickness.
(b) Rather than using a toroidal knuckle of constant radius R_t, the cylinder and its spherical-segment cap can be connected by a transition shell of varying radius. Seek the shape of a transition shell that is "best" in some sense. (References on pressure vessel design may be useful.)

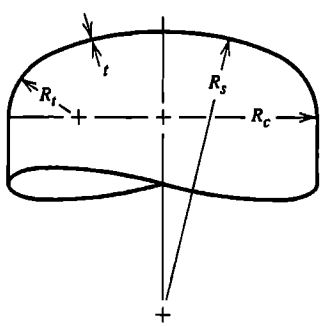

Problem C16.3

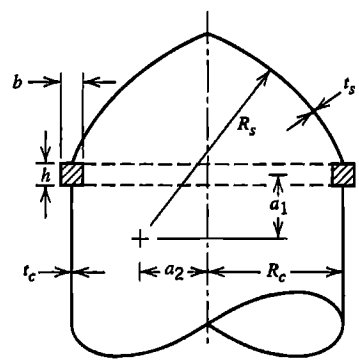

Problem C16.4

C16.4 Let a thin-walled shell of revolution consist of a cylindrical portion of radius R_c capped by a closure whose meridian is a circular arc of radius R_s, as shown. As an option, the juncture may be reinforced by a ring of rectangular cross section, as shown. Let cylinder and cap intersect the ring (if present) at midwidth, a distance $b/2$ from each side. The base of the cylindrical shell (not shown) may be considered fixed. Loads may be (1) internal pressure, (2) self-weight, with axis vertical as shown, (3) self-weight with axis horizontal. Some geometries of possible interest are
(a) $a_1 = a_2 = 0, R_s = R_c$ (hemispherical end cap).
(b) $a_1 = \sqrt{3}R_c, a_2 = 0, R_s = 2R_c$ (shallow end cap subtends a 60° angle).
(c) $a_1 = -\sqrt{3}R_c, a_2 = 0, R_s = 2R_c$ (like part (b), but with cap "dished in").

C16.5 Solve the circular ring problem of Fig. 2.13-2 by means of a single shell of revolution element, using Fourier series to represent the loads.

C16.6 Consider cantilever beams that are slender and thin-walled. Some possible cross sections are shown as (a), (b), and (c) of the sketch. Loading shown is by transverse tip force F. As options, F might be applied at other cross sections along length L, or at other locations on a cross section.

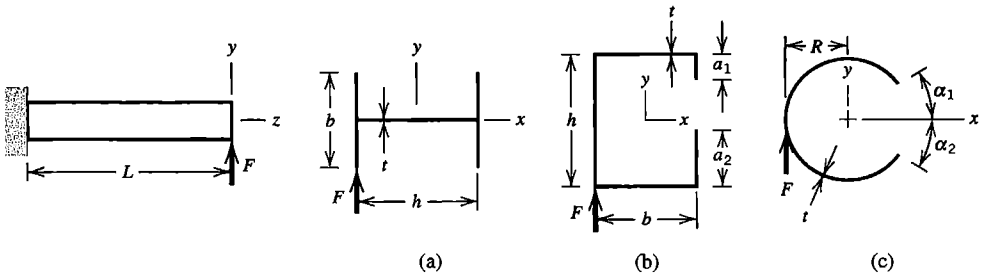

Problem C16.6

C16.7 In Problem C16.6, determine the x coordinate of the y-parallel force F such that the beam will bend without twisting (that is, determine the x coordinate of the shear center).

C16.8 In Problem C16.6, cross sections (b) and (c), replace transverse force F by self-equilibrating axial forces. For example, on cross section (a), apply z-direction forces $+P$ to lower left and upper right flange tips, and z-direction forces $-P$ to upper left and lower right flange tips. An alternative support condition is one that prevents rigid-body motion but does not restrain deformation.

C16.9 In Problem C16.6, let beam axis z be curved rather than straight. Cross sections may be oriented as shown or rotated 90 degrees. Possible loadings include transverse tip force, acting either in the plane of curvature or normal to it.

C16.10 Thin-walled pipes of circular cross section intersect at a right angle, as shown. As an option, the ellipse formed by the intersection may be reinforced by a stiffening member on the outside of the shell. Stresses at and near the intersection are of interest. Obtain a separate solution for each of the six loadings shown. For convenience, a force or moment load may be applied to the center of a circular disk on the end of the structure.

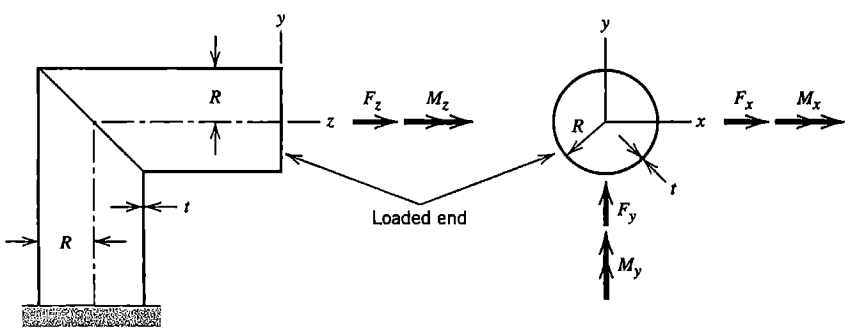

Problem C16.10

C16.11 Test cases shown in Fig. 16.6-1 may be analyzed to determine rate of convergence with mesh refinement (as well as the ability of the software to produce correct results). Thus one might use 1, 4, 16, etc. quadrilaterals per quadrant (or per octant) of the structure. For the pinched cylinder and hemisphere test cases, one might also solve using axisymmetic elements and Fourier series representation of loads, and assess convergence rate with number of harmonics used.

C16.12 Attach a reinforcing beam to each straight edge of the shell roof in Fig. 16.6-1a. As another option, cantilever the roof from one end, leaving the other end free.

C16.13 A segment of a circular cylindrical shell is fixed on two straight edges, as shown. Uniform line load q acts on one of the curved edges and is radially directed.

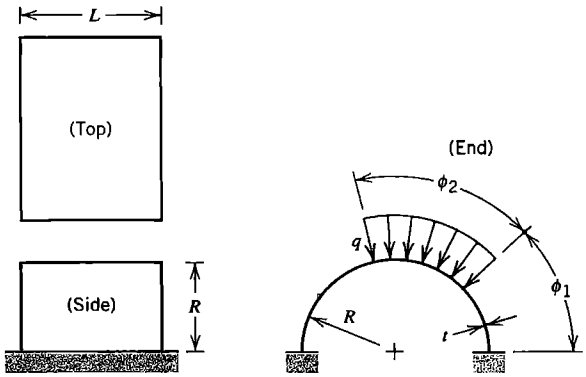

Problem C16.13

C16.14 A square tube and a circular tube are connected by a conical transition section, as shown. Possible loads include internal pressure p, temperature gradient, bending, axial force, and torque about the longitudinal axis.

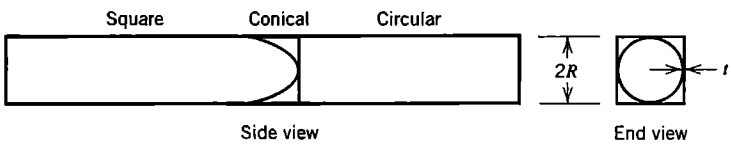

Problem C16.14

CHAPTER 17

NONLINEARITY: AN INTRODUCTION

Selected nonlinear problems are described and given a finite element formulation. Solution procedures for nonlinear equations are discussed. In discussions of material and geometric nonlinearity, emphasis is given to elastic-plastic problems and to large-deflection elastic problems. Modeling suggestions for nonlinear analysis are included.

17.1 NONLINEAR PROBLEMS

To identify behavior as nonlinear is only to say what the behavior is not. Nonlinear behavior admits a wide variety of phenomena, possibly interacting with one another, and each perhaps difficult to formulate. It is fortunate that linear models provide satisfactory approximations for many problems of practical interest. However, substantial departure from linearity is common. In heat transfer analysis, material properties are often temperature-dependent; phase change absorbs or liberates heat and changes properties; radiation makes analysis highly nonlinear because it depends on the fourth power of absolute temperature. In structural mechanics, material may yield or creep; local buckling may arise; gaps may open or close. Nonlinear problems pose the difficulty of describing phenomena by realistic mathematical and numerical models and the difficulty of solving nonlinear equations that result. Effort required of the analyst increases substantially when a problem becomes nonlinear. Computational cost may also be a concern, despite the growing capability of computers. Nevertheless, nonlinear analyses are undertaken more and more often because software has become more capable and more widely available, computational costs have declined, more demands are placed upon structures, and more understanding of manufacturing processes is required.

In structural mechanics, types of nonlinearity include the following:

- *Material nonlinearity,* in which material properties are functions of the state of stress or strain. Examples include nonlinear elasticity, plasticity, and creep.
- *Contact nonlinearity,* in which a gap between adjacent parts may open or close, the contact area between parts changes as the contact force changes, or there is sliding contact with frictional forces.
- *Geometric nonlinearity,* in which deformation is large enough that equilibrium equations must be written with respect to the deformed structural geometry. Also, loads may change direction as they increase, as when pressure inflates a membrane.

Problems in these categories are nonlinear because stiffness, and perhaps loads as well, become functions of displacement or deformation. Thus, in structural equations $[\mathbf{K}]\{\mathbf{D}\} = \{\mathbf{R}\}$, coefficient matrix $[\mathbf{K}]$ and perhaps load vector $\{\mathbf{R}\}$ become functions of $\{\mathbf{D}\}$. We cannot immediately solve for $\{\mathbf{D}\}$ because information needed to construct $[\mathbf{K}]$ and

$\{\mathbf{R}\}$ is not known in advance. An iterative process is required to obtain $\{\mathbf{D}\}$ and its associated $[\mathbf{K}]$ and $\{\mathbf{R}\}$ such that the product $[\mathbf{K}]\{\mathbf{D}\}$ is in equilibrium with $\{\mathbf{R}\}$.

When equations $[\mathbf{K}]\{\mathbf{D}\} = \{\mathbf{R}\}$ are nonlinear the principle of superposition *does not apply.* That is, we cannot scale results in proportion to load or superpose results of different load cases. Each different load case requires a separate analysis. Also, for a given set of loads there may be more than one solution $\{\mathbf{D}\}$. If a load case consists of (say) two portions that are sequentially applied, reversing the sequence of application may produce different results.

A substantial literature is devoted to FEA in nonlinear problems. In structural mechanics, currently available books have some 670 pages [11.49], 370 pages [17.1], 340 pages [17.2], and 490 pages [17.3]. The present chapter is of course more limited. The following section describes some equation-solving techniques applicable to time-independent nonlinear equations. Subsequent sections contain introductory discussions of plasticity, contact problems, and geometric nonlinearity. Successful nonlinear FEA requires—as usual—a grasp of the physical problem, but also more understanding of equation-solving procedures than is required for linear analysis, because a single strategy may not work for all problems. Satisfactory results may appear only after several attempts and a change of strategy.

17.2 SOME SOLUTION METHODS

In this section we summarize commonly-used methods of solving time-independent equations $[\mathbf{K}]\{\mathbf{D}\} = \{\mathbf{R}\}$ for d.o.f. $\{\mathbf{D}\}$ when $[\mathbf{K}]$ is a function of $\{\mathbf{D}\}$. The source of nonlinearity is not important in the present discussion. In order to depict procedures as two-dimensional plots of load versus response, we apply solution methods to a special case, namely the single nonlinear equation $f(u,x) = 0$ for $u = u(x)$, where u is the only dependent variable. A physical problem that leads to this equation is that of a single force applied to a nonlinear spring, Fig. 17.2-1a. The relation between load P and displacement u is

$$ku = P \quad \text{or} \quad (k_0 + k_N)\,u = P \quad \text{where} \quad k_N = k_N(u) \tag{17.2-1}$$

In order that this single-d.o.f. problem correspond to a realistic multiple-d.o.f. problem $[\mathbf{K}]\{\mathbf{D}\} = \{\mathbf{R}\}$, we imagine that k, and hence spring force ku, can be calculated for any given value of u, but that it is not possible to explicitly solve for u when P is prescribed. Instead u is obtained by taking a series of linear steps, each of which corresponds to a change in load. Calculation procedures may use the *tangent stiffness,* which is defined as $k_t = dP/du$ and represents the slope of the P versus u plot.

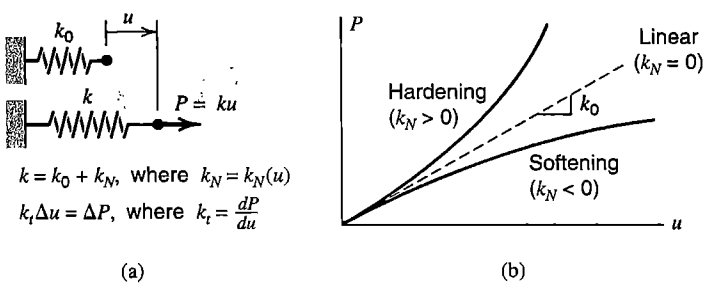

Figure 17.2-1. (a) Single-d.o.f problem of a nonlinear spring. (b) Hardening and softening behavior.

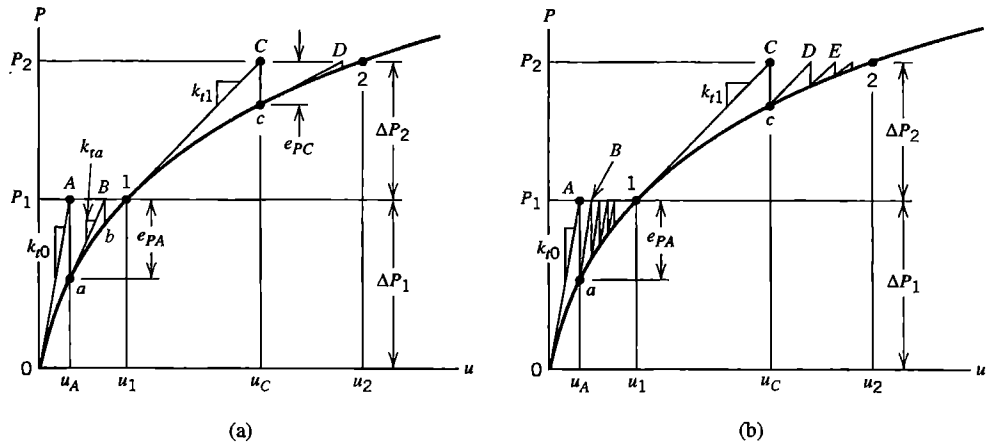

Figure 17.2-2. Iterations to convergence at each of load levels P_1 and P_2. (a) Newton-Raphson iterations. (b) Modified Newton-Raphson iterations.

In the one-dimensional nonlinear spring analogy, stiffness is a function of u, but a prescribed load is simply a value of P, independent of u. In a multidimensional problem, both $[\mathbf{K}]$ *and* $\{\mathbf{R}\}$ may be functions of $\{\mathbf{D}\}$. Examples include a geometrically nonlinear problem in which a prescribed pressure creates nodal loads that change direction as the structure deforms, and a heat transfer problem in which radiation from a source having prescribed temperature creates nodal flux loads that depend on nodal temperatures.

Some of the many solution methods are as follows. It is often effective to use the methods in combination, although some combinations may be detrimental rather than helpful.

Newton-Raphson (N-R). In calculus texts, this method may be known as Newton's method, and may be explained as a way of extracting a root of a polynomial. Here we describe it as a way of generating the P versus u curve, whose shape is not known at the outset.

In Eq. 17.2-1, imagine that initially $u = 0$. Then a load P_1 is applied and we seek the corresponding displacement u_1. The initial tangent stiffness is called k_{t0} in Fig. 17.2-2a, and the initial load increment is the load itself; $\Delta P_1 = P_1$ because we have chosen to start from zero load. We calculate the current displacement increment and update the solution:

$$k_{t0}\,\Delta u = \Delta P_1 \qquad \Delta u = k_{t0}^{-1}\Delta P_1 \qquad u_A = 0 + \Delta u \tag{17.2-2}$$

Here u_A is the current estimate of the desired result u_1. This estimate is not exact because the deformed spring does not yet exert a force that equilibrates load P_1. The current force error (or load imbalance) e_{PA} is

$$e_{PA} = P_1 - ku_A \qquad \text{where } k = k(u) \text{ is evaluated using displacement } u_A \tag{17.2-3}$$

Here ku_A is the resisting force provided by the structure in its current deformation state. (In specific applications, such as plastic analysis, resisting forces may be calculated directly from element stresses, without generating a stiffness matrix in the process.)

We now commence "equilibrium iterations" intended to eventually reduce the imbalance to zero. While keeping P_1 constant we take another step, starting at point a in

Fig. 17.2-2a and moving along a tangent to the curve at point a. Thus we obtain a more accurate displacement u_B.

$$k_{ta}\,\Delta u = e_{PA} \qquad \Delta u = k_{ta}^{-1} e_{PA} \qquad u_B = u_A + \Delta u \tag{17.2-4}$$

The spring force still does not equilibrate applied load P_1. The current force error is

$$e_{PB} = P_1 - ku_B \qquad \text{where } k = k(u) \text{ is evaluated using displacement } u_B \tag{17.2-5}$$

The next step moves along a tangent to the curve at point b and provides another displacement increment Δu and the updated displacement $u_B + \Delta u$. Although this method is not guaranteed to converge for all nonlinear problems, continued iteration typically causes force errors to decrease, successive displacement increments Δu to approach zero, and the updated solution to approach the correct value u_1.

Another load increment ΔP_2 can now be added, and iteration begun again to seek displacement u_2, which corresponds to the total applied load P_2. Equations corresponding to Eqs. 17.2-2 and 17.2-3 are

$$k_{t1}\,\Delta u = \Delta P_2 \qquad \Delta u = k_{t1}^{-1}\Delta P_2 \qquad u_C = u_1 + \Delta u \tag{17.2-6}$$

$$e_{PC} = P_2 - ku_C \qquad \text{where } k = k(u) \text{ is evaluated using displacement } u_C \tag{17.2-7}$$

Clearly, by applying a sequence of increasing load levels, and iterating to convergence for each, we can locate as many points 1, 2, 3, ... as are needed to construct an adequate representation of the P versus u curve. The likelihood of convergence to a correct solution at each load level is enhanced by taking small load steps.

Modified Newton-Raphson. Rather than updating tangent stiffness k_t prior to each calculation of a displacement increment Δu, the same tangent stiffness can be used in many iterative cycles. The procedure is depicted in Fig. 17.2-2b, where initial tangent stiffness k_{t0} is used until convergence at load level P_1, then updated to k_{t1} and maintained at k_{t1} until convergence at load level P_2. This alternative choice of tangent stiffness is the only alteration needed in Eqs. 17.2-2 to 17.2-7.

Cost reduction is the motivation for adopting the modified N-R method. In a multidimensional problem, the original N-R method requires that a new tangent stiffness matrix $[\mathbf{K}_t]$ be generated prior to each calculation of d.o.f. increments $\{\Delta\mathbf{D}\}$, and the actual calculation of $\{\Delta\mathbf{D}\}$ requires factorization of $[\mathbf{K}_t]$ in order to solve the simultaneous algebraic equations. Modified N-R avoids repeated generation of $[\mathbf{K}_t]$, and each calculation of $\{\Delta\mathbf{D}\}$ after the first requires only the processing of a new right-hand side. Thus, although the modified N-R method requires more iterations than the original N-R method, each iteration is accomplished more quickly, and the cost savings can be appreciable. Overall computational cost is usually lowest when $[\mathbf{K}_t]$ is updated occasionally, typically when a load increment is added, as shown in Fig. 17.2-2b.

Other Methods. The most elementary solution method may be *direct substitution.* This method does not use a tangent stiffness matrix. Instead the coefficient matrix is repeatedly updated and the entire solution repeated. Thus, for the case in which $\{\mathbf{R}\}$ is constant, we begin with an initial assumption $\{\mathbf{D}\}_0$ for the d.o.f. (perhaps with all D_i equal to zero),

establish the corresponding $[\mathbf{K}]_0$, and solve equations $[\mathbf{K}]_0\{\mathbf{D}\}_1 = \{\mathbf{R}\}$ for $\{\mathbf{D}\}_1$, which is presumably a more accurate solution than $\{\mathbf{D}\}_0$. Then we establish $[\mathbf{K}]_1$ based on $\{\mathbf{D}\}_1$ and solve for $\{\mathbf{D}\}_2$, and so on. The method is often inefficient, and is more likely to encounter convergence difficulties than tangent stiffness methods.

The *initial stiffness* method uses stiffness matrix $[\mathbf{K}_0]$ throughout, regardless of the load level. Nonlinearities are taken to the right-hand side and repeatedly updated until convergence. In notation analogous to that of Eq. 17.2-1, the method is $[\mathbf{K}_0]\{\mathbf{D}\}_i = \{\mathbf{R}\} - [\mathbf{K}_N]\{\mathbf{D}\}_{i-1}$, where $[\mathbf{K}] = [\mathbf{K}_0 + \mathbf{K}_N]$, and $[\mathbf{K}_0]$ and $[\mathbf{K}_N]$ are respectively constant and displacement-dependent matrices. Because $[\mathbf{K}_0]$ is the same as $[\mathbf{K}_t]$ when displacements are zero, the initial stiffness matrix is a modified N-R method in which the tangent stiffness is never updated. Like the direct substitution method, the initial stiffness method may converge slowly or not at all, depending on details of the problem at hand.

Load versus deflection relations depicted in Fig. 17.2-3a are troublesome for one or both N-R solution methods. Each curve displays a "limit point," labeled L in Fig. 17.2-3a, which is a relative maximum on the load versus displacement plot, where the tangent stiffness is zero. Physically, for the nonlinear spring problem, each curve could be generated by displacement control, gradually increasing u and applying whatever P is needed. (Computationally, the method would not be as simple for a multiple-d.o.f. nonlinear problem because the relationship among d.o.f. in $\{\mathbf{D}\}$ for a given load vector is not known in advance.) Both curves in Fig. 17.2-3a are characteristic of snap-through buckling: when a limit point is reached under gradually increasing load and displacement is not controlled, displacement suddenly jumps to a much larger value on the rising part of the curve. Curve OB also characterizes some fracture problems. In computation, if load P_c slightly greater than the limit point load of curve OA is applied, N-R iterations give very large increments Δu as point L is approached, and negative increments Δu as soon as point L is passed. The process may fail to converge to point c. Modified N-R iterations succeed, but slowly. Portions L-1 and L-2 of the curves cannot be calculated by either of the N-R methods depicted in Fig. 17.2-2. (Indeed, static analysis ignores the dynamic reality of snap-through, which may be of importance in the actual structure.) A method that usually succeeds for both curves is known as the *arc-length method* [15.7,17.1–17.6]. As depicted for a one-dimensional problem in Fig. 17.2-3b, the arc-length method is a form of N-R iteration in which, within each new level of external load, iterative increments of load and displacement are adjusted in such a way that iterative steps 1A, aB, bC, and so on cause points A, B, C, and so on in Fig. 17.2-3b to lie on a curve of radius Δl centered at initial point 1. The method incorporates a way to keep the process from doubling back on itself when the curve acquires a negative slope. Because of adjustments inherent in the method, computed displacements correspond to a load level that is adjusted by computation and is slightly less than the load level used to start the process.

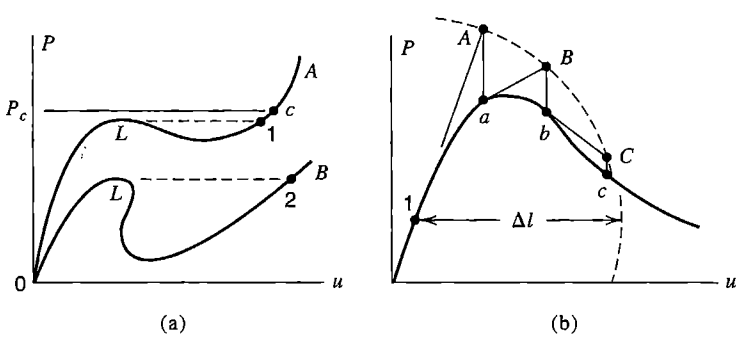

Figure 17.2-3. (a) More complicated load-displacement curves. Both are physically possible. Each peak L is a limit point. (b) Successive iterations in the arc-length method.

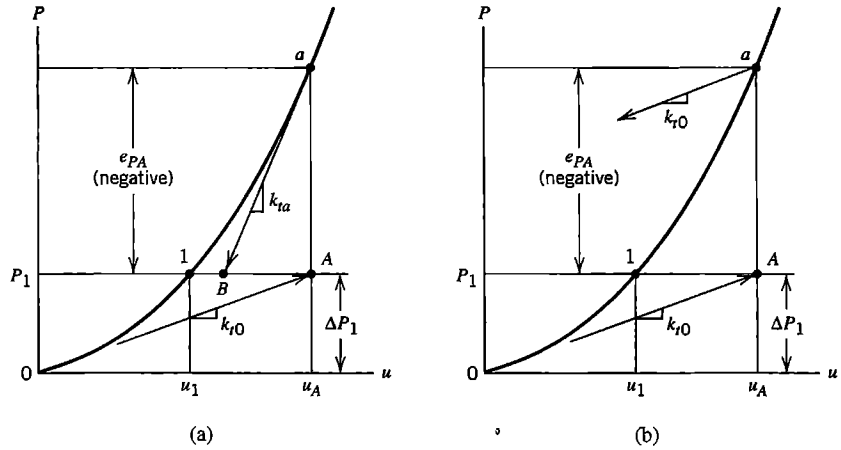

Figure 17.2-4. A hardening curve, showing the first two calculation steps, starting from zero load. (a) N-R method. (b) Modified N-R method.

In preceding descriptions we have emphasized softening curves. Figure 17.2-4 depicts the application of N-R and modified N-R iterations to a hardening curve. We see that, for the particular curve depicted, the N-R method at first overestimates displacement but converges in subsequent iterations. The second iteration of the *modified* N-R method uses such an erroneous tangent stiffness that subsequent iterations may diverge or become stuck in an endless loop. The modified N-R method is more likely to fail with hardening behavior than with softening behavior, especially if load steps are large. Sometimes computational stability can be restored by *underrelaxation*. Thus, rather than updating the previous solution by the entire current increment Δu, we update by a fraction of it:

$$u_{\text{new}} = u_{\text{old}} + \mu\,\Delta u \quad \text{or} \quad \{\mathbf{D}\}_{\text{new}} = \{\mathbf{D}\}_{\text{old}} + \mu\{\Delta\mathbf{D}\} \quad \text{where} \quad 0 < \mu < 1 \qquad (17.2\text{-}8)$$

Procedures for determining a good choice of μ are known as *line search algorithms* [17.1–17.3].

Increasingly, methods known by the names *quasi-Newton* and *secant stiffness* are being used. Consider Fig. 17.2-5a, and imagine that two cycles of modified N-R iteration have

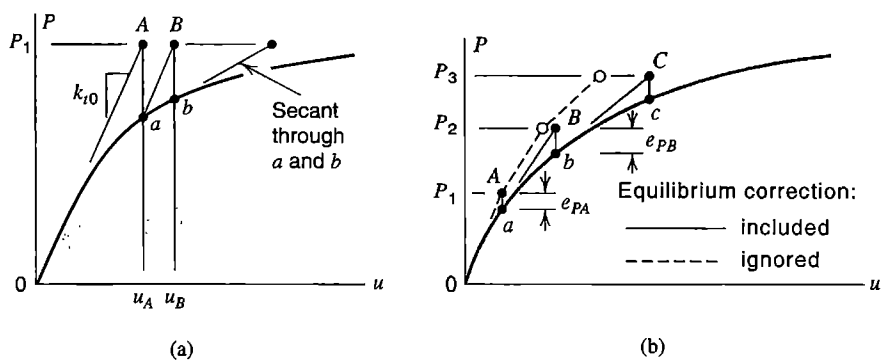

Figure 17.2-5. (a) Secant step following two modified N-R iterations. (b) Incremental solution, with and without equilibrium corrections.

produced displacements u_A and u_B. A much-improved solution is obtained by taking the next step along a secant through points a and b. The method is robust, and an important consideration for multiple-d.o.f. problems is that the inverse of the secant stiffness matrix can be obtained by updating the preceding tangent-stiffness inverse $[\mathbf{K}_t]^{-1}$ (which in Fig. 17.2-5a corresponds to $1/k_t$ at zero load). Thus the equation-solving cost of the secant step is greatly reduced, which more than pays for the cost of generating the secant-stiffness inverse matrix. References include [2.14,17.2,17.7,17.8].

Open circles in Fig. 17.2-5b depict results of purely incremental steps, with an increase in external load at each step and without equilibrium iterations at each load level. The initial step takes us to point A, where the force imbalance is e_{PA}. If we include such imbalances in succeeding steps, we obtain the sequence of displacements

$$\begin{aligned} u_A &= k_{t0}\,\Delta P && \text{where} \quad \Delta P = P_1 \\ u_B &= u_A + k_{ta}^{-1}[\Delta P + e_{PA}] && \text{where} \quad \Delta P = P_2 - P_1 \\ u_C &= u_B + k_{ta}^{-1}[\Delta P + e_{PB}] && \text{where} \quad \Delta P = P_3 - P_2 \end{aligned} \tag{17.2-9}$$

and so on. Thus we obtain points A, B, C, and so on, which serve as points through which an approximation of the correct curve can be constructed. If load imbalance terms e_{PA} and e_{PB} are omitted from the equations, displacement errors accumulate, providing the inferior approximation indicated by the dashed line and open circles in Fig. 17.2-5b. The dashed line is recognized as an instance of Euler's method of numerically solving a first-order differential equation.

As a solution approaches a limit point (Fig. 17.2-3a) under gradually increasing load, the physical structure often approaches collapse. The determinant of $[\mathbf{K}_t]$ approaches zero and displacement increments become very large. Just past a limit point, $[\mathbf{K}_t]$ has a negative determinant, which may cause failure of the equation solver (depending on the algorithm used). Reaching a limit point can also be signaled by a near-zero value of the *current stiffness parameter,* which is a scalar stiffness measure constructed from previously computed force and displacement increments [17.1].

It is possible to solve a time-independent problem by using methods intended for structural dynamics. A fictitious damping matrix is assigned to the structure, and displacements are computed as a function of time. When the structure stops moving, the time-independent solution has been obtained. Physically, one can imagine that this method amounts to immersing the structure in a viscous fluid, which damps strong geometric nonlinearities such as the sudden jump of snap-through buckling. The method is known as *dynamic relaxation* or as *viscous relaxation,* depending on whether or not a mass matrix is included in the numerical model. References include [17.3,17.9-17.12].

Convergence Criteria. Equilibrium iterations at a given load level can cease when the result is "close enough" according to one or more criteria that can be applied automatically by software. Two plausible criteria are that the current force imbalance be a small fraction of the total applied force in the current load level and that the current displacement increment be a small fraction of the initial displacement increment. Thus, for a multiple-d.o.f. structure having displacement vector $\{\mathbf{D}\}$, applied loads $\{\mathbf{R}\}$, and displacement-dependent stiffness $[\mathbf{K}]$, the force imbalance is $\{\mathbf{e}_R\} = \{\mathbf{R}\} - [\mathbf{K}]\{\mathbf{D}\}$, and two convergence criteria are

$$\begin{aligned} &\text{Force convergence:} && \|\mathbf{e}_R\| < \varepsilon_R \|\mathbf{R}\| \\ &\text{Displacement convergence:} && \|\Delta\mathbf{D}\| < \varepsilon_D \|\Delta\mathbf{D}_0\| \end{aligned} \tag{17.2-10}$$

where, in the preceding one-dimensional description of the N-R method, $\{\mathbf{e}_R\}$ and $\{\Delta\mathbf{D}\}$ correspond to the most recently determined values of e_P and Δu. Tolerances ε_R and ε_D might be in the range 0.001 to 0.01, but actual values adopted may be quite different, depending on the nature of the problem, the accuracy required, and the expense of continued iteration. If the norm adopted is the Euclidean norm, then $\|\mathbf{R}\| = \sqrt{\{\mathbf{R}\}^T\{\mathbf{R}\}}$ and so on. In the displacement criterion, $\|\Delta\mathbf{D}_0\|$ indicates the initial displacement increment of the current load step. If accumulated displacements $\{\mathbf{D}\}$ were used instead, the convergence test would become less and less demanding as displacements accumulate.

In general, $\{\mathbf{R}\}$ contains both forces and moments. As written, Eq. 17.2-10 ignores the mismatch in dimension of the R_i. Moment terms may dominate $\|\mathbf{e}_R\|$ and $\|\mathbf{R}\|$ if length units are millimeters but not if length units are meters. This difficulty can be avoided by including only forces in the first of Eqs. 17.2-10, or can be reduced by dividing each term in $\{\mathbf{e}_R\}$ and $\{\mathbf{R}\}$ by the square root of the corresponding diagonal term in the original global stiffness matrix [17.1]. In commonplace systems of units, rotation terms are not likely to become large enough to dominate $\|\Delta\mathbf{D}\|$ and $\|\mathbf{D}\|$.

Occasionally, it is difficult to satisfy the force convergence criterion because of localized force imbalances that have little effect on overall structural behavior [17.1]. However, experience has shown that the displacement criterion is usually not a satisfactory substitute. The displacement criterion may terminate iterations merely because convergence is slow, or may indicate convergence when substantial force imbalance remains. For example, if in Fig. 17.2-4a the curve is almost vertical at point a, distance AB may be small in comparison with displacement u_A although point B is associated with large force imbalance. Usually, if the displacement convergence criterion is used, it should be supplemented by the force convergence criterion [17.2]. If underrelaxation (Eq. 17.2-8) has been used, $\|\Delta\mathbf{D}_0\|$ in Eqs. 17.2-10 should be multiplied by μ so that convergence will not be indicated merely because a small increment $\mu\{\Delta\mathbf{D}\}$ has been used [17.1].

Usually a limit is placed on the number of iterations or on the computational time. Reaching one of these limits before convergence may indicate that not enough iteration or enough time was allowed, that the convergence tolerance is too tight, or that the solution algorithm has run into trouble. One might then restart the process from the previous load level but with a smaller load increment. Otherwise the analyst must decide how to proceed. Options include changing the iteration limit, changing convergence tolerances, and selecting a different solution algorithm. Software may have the capability to automatically alter the solution algorithm, restart from a lower load, and alter the step size [17.13,17.14].

17.3 PLASTICITY: INTRODUCTION

Plasticity refers to deformation that is not recovered if loads are removed. Conventionally, and in this book, plasticity is regarded as time-independent. Thus, creep is excluded, and strain *rate* plays no role in plasticity calculations. (Nevertheless, some authors prefer to state plasticity equations in terms of strain rates. Thus, fictitious time increments are used

merely as a way of counting successive increments of load, stress, and strain.) As might be expected, there are several mathematical alternatives for describing physical behavior, and there are many calculation methods and variants of methods. In the present section we consider one-dimensional elastic-plastic relations. Multidimensional relations are presented in Section 17.4 and specialized in Section 17.5 to a form appropriate for initially isotropic metals such as steel and aluminum. In Section 17.6 an incremental method of calculation that uses a tangent stiffness matrix is presented. Many references are available, including [17.1–17.3,17.8,17.15–17.19].

Uniaxial Stress. Let σ be a uniaxial stress, such as the axial stress in a tensile test specimen, and ε the corresponding axial strain. For simplicity of explanation we temporarily idealize the stress-strain relation as bilinear (Fig. 17.3-1). As σ increases from zero, yielding begins at stress σ_Y and the corresponding strain ε_Y. In general formulations, yielding is defined by $F = 0$, where F is called a "yield function." For uniaxial stress σ, $F = |\sigma| - \sigma_Y$, where σ_Y is always taken as positive.

For strains larger than ε_Y, a strain increment $d\varepsilon$ can be regarded as composed of an elastic contribution $d\varepsilon^e$ and a plastic contribution $d\varepsilon^p$ (here we exclude thermal strain and creep strain). When $\varepsilon > \varepsilon_Y$, increment $d\varepsilon^e$ exists only when $E_t \neq 0$, and is associated with an increment of stress $d\sigma$, which can be written in various ways. For strain in the plastic range, with $d\varepsilon = d\varepsilon^e + d\varepsilon^p$,

$$d\sigma = E\,d\varepsilon^e \qquad d\sigma = E(d\varepsilon - d\varepsilon^p) \qquad d\sigma = E_t\,d\varepsilon \qquad d\sigma = H_p\,d\varepsilon^p \tag{17.3-1}$$

where H_p may be called the *strain-hardening parameter* or the *plastic modulus*. Substitution of the second and fourth of Eqs. 17.3-1 into the third yields

$$H_p = \frac{E_t}{1-(E_t/E)} \qquad \text{or} \qquad E_t = E\left(1-\frac{E}{E+H_p}\right) \tag{17.3-2}$$

When the expression for tangent modulus E_t is written in this form, it is similar to a more general form used for multiaxial states of stress. If $H_p = 0$, for which $E_t = 0$, the material

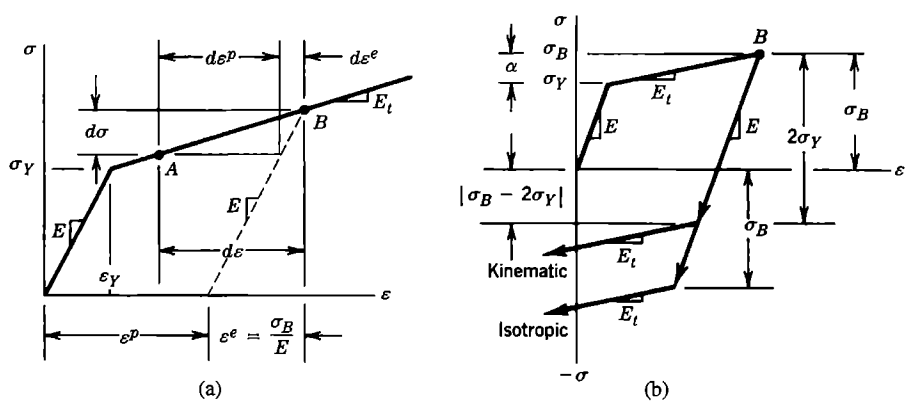

Figure 17.3-1. (a) Stress-strain relation for uniaxial stress, idealized as bilinear (two straight lines), where σ_Y is the stress at first onset of yielding. (b) Isotropic and kinematic hardening rules.

is called "elastic–perfectly plastic." If the material has not yet yielded or is unloading, then $E_t = E$ and H_p is not used in the calculation. As illustrated in Fig. 17.3-1b, unloading from a plastic stress σ_B takes place elastically. Conditions remain elastic until either stress σ_B is exceeded for reloading in the same direction or a stress of magnitude σ_B (at most) is reached in reversed loading. The span of this elastic range is defined by the hardening rule.

Two common rules for hardening are *isotropic hardening* and *kinematic hardening*. Upon reaching uniaxial stress σ_B in the plastic range, Fig. 17.3-1b, according to the isotropic hardening rule the elastic range has expanded from the initial value $2\sigma_Y$ to the value $2\sigma_B$. Thus the experimentally observed Bauschinger effect is ignored. The kinematic hardening rule accounts for the Bauschinger effect by preserving an elastic range of $2\sigma_Y$, but ignores the possibility that the elastic range might increase. In practice the two rules may be used in combination. Uniaxial yield criteria, as modified by application of hardening rules, can be stated in the forms

$$\text{Isotropic:} \quad F = |\sigma| - \sigma_0 \qquad\qquad \text{Kinematic:} \quad F = |\sigma - \alpha| - \sigma_Y \tag{17.3-3}$$

where $\sigma_0 = \sigma_Y + \alpha$ is the largest magnitude of uniaxial stress reached in previous plastic straining, and α, called the "kinematic shift" when used in the kinematic hardening rule, is shown in Fig. 17.3-1b. Prior to initial yielding, $\alpha = 0$ and $\sigma_0 = \sigma_Y$. Elastic conditions are predicted when σ and α are such that $F < 0$, and yielding when $F = 0$. The case $F > 0$ is not physically possible. Continued or renewed plastic action with strain hardening alters α and therefore modifies the yield criterion. In multiaxial states of stress, isotropic hardening preserves initial isotropy, while kinematic hardening leads to a different anisotropic material after each increment of plastic strain. Here anisotropy pertains to yield behavior, not to elastic moduli.

Different forms of yield criterion, flow rule, and hardening rule are used for different materials. Thus rules that work well for copper do not work well for concrete. The observed behavior of commonly used metals is predicted fairly well by the von Mises yield criterion and its associated flow rule (Section 17.5).

Calculations in Uniaxial Stress. Consider the uniaxial stress-strain relation shown in Fig. 17.3-2, and let it pertain to axial stress in a bar element in a structure under load. Assume that, as the result of a load increment applied to the structure, strain increment $\Delta\varepsilon = \varepsilon_B - \varepsilon_A$ has taken place. Stress σ_A is known and σ_B must be calculated. So that this calculation will resemble what must be done in a multiaxial state of stress, here we imagine that we cannot simply "read the curve" to obtain σ_B when ε_B is known. Instead, we

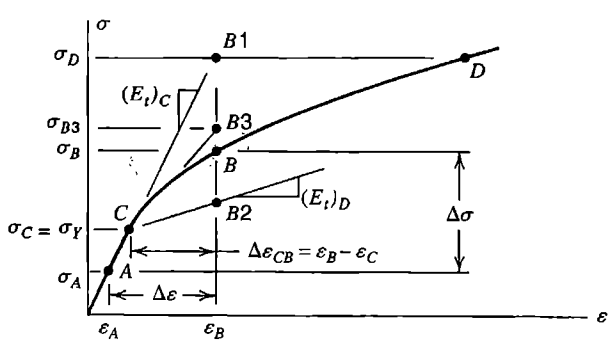

Figure 17.3-2. A stress-strain relation for uniaxial stress. Stress at A is known; stress σ_B corresponding to ε_B is desired.

proceed as follows, calculating first the portion of stress increment $\Delta\sigma$ associated with elastic strains, then the portion associated with post-yield strains.

Point A happens to lie in the linearly elastic range, so that $(E_t)_C = E$. Therefore strain increment $\Delta\varepsilon = \varepsilon_B - \varepsilon_A$ gives a trial stress increment $\Delta\sigma_{\text{trial}} = \sigma_D - \sigma_A = E\Delta\varepsilon$. A fractional step, $\beta\,\Delta\sigma_{\text{trial}}$, where $0 < \beta < 1$, lies in the elastic range and places the material on the verge of yield, at point C. To determine β we use $\sigma_0 = \sigma_Y$ in Eq. 17.3-3.

$$F_C = |\sigma_A + \beta\,\Delta\sigma_{\text{trial}}| - \sigma_Y = 0 \qquad \text{hence} \qquad \beta = \frac{\sigma_Y - \sigma_A}{\sigma_D - \sigma_A} = \frac{F_A}{F_A - F_D} \tag{17.3-4}$$

$$\text{where} \qquad \Delta\sigma_{\text{trial}} = \sigma_D - \sigma_A$$

In uniaxial stress, these calculations are a roundabout way of stating what may be obvious. In multiaxial stress states, analogous calculations provide results that are not obvious.

Starting from point C in Fig. 17.3-2, the post-yield stress increment from C to B can be estimated by two-step Euler integration, as follows. At point C in this particular example, the slope of the curve is the elastic modulus E, and the strain increment from C to B is $\Delta\varepsilon_{CB} = \varepsilon_B - \varepsilon_C = \varepsilon_B - (\sigma_C/E)$. Therefore, with $(E_t)_C = E$, first estimates of the stress increment from C to B and the stress at B are

$$(\Delta\sigma)_1 = (E_t)_C\,(\varepsilon_B - \varepsilon_C) = \sigma_D - \sigma_C \quad \text{and} \quad \sigma_{B1} \approx \sigma_C + (\Delta\sigma)_1 = \sigma_D \tag{17.3-5}$$

Next, the calculation is repeated, now using the tangent modulus that corresponds to the estimate σ_{B1}, namely E_t at point D in the present example [17.17]. Thus second estimates of the stress increment from C to B and the stress at B are

$$(\Delta\sigma)_2 = (E_t)_D\,(\varepsilon_B - \varepsilon_C) \quad \text{and} \quad \sigma_{B2} \approx \sigma_C + (\Delta\sigma)_2 \tag{17.3-6}$$

Averaging the two estimates, we obtain $\sigma_B \approx \sigma_{B3}$, where

$$\sigma_{B3} = \sigma_C + \frac{1}{2}\Big[(\Delta\sigma)_1 + (\Delta\sigma)_2\Big] \quad \text{or} \quad \sigma_{B3} = \sigma_C + \frac{1}{2}\Big[(E_t)_C + (E_t)_D\Big]\,\Delta\varepsilon_{CB} \tag{17.3-7}$$

Inexactness in Eq. 17.3-7 can be reduced by reducing the size of the load step and by dividing the calculation of $\Delta\sigma$ into subincrements. The multiaxial form of Eqs. 17.3-5 to 17.3-7 appears in Section 17.6.

Readers familiar with numerical methods will recognize Eq. 17.3-7 as the result of numerical integration by the trapezoidal rule. As written for integration of the equation $y = f(x)$, the *generalized* trapezoidal rule is

$$y_{n+1} = y_n + \Big[(1-\gamma)(dy/dx)_n + \gamma(dy/dx)_{n+1}\Big]\,\Delta x \tag{17.3-8}$$

where $0 \le \gamma \le 1$. Starting from the known (or approximated) value y_n, we seek the value y_{n+1} that results from taking a step Δx. The cases $\gamma = 0$ and $\gamma = 1$ are respectively called forward and backward Euler integration. The case $\gamma = 0.5$ is the conventional trapezoidal rule, and is sometimes also identified as a form of second-order Runge-Kutta method [17.20]. Use of $\gamma = 0.5$ provides second-order accuracy; that is, the error in $\Delta y = y_{n+1} - y_n$ is proportional to $(\Delta x)^2$ [2.14,5.1].

17.4 PLASTICITY: GENERAL FORMULATION FOR SMALL STRAINS

Prior to any yielding, many materials display almost linear and elastic response, so that stresses can be calculated by knowing elastic constants and strains. When there is yielding, not only are load, deformation, and stress nonlinearly related, they are also history-dependent. That is, changing the load history en route to a particular final load state is likely to change final results. For an arbitrary load history, the final state of stress and deformation can be determined only by accounting for the history of stress and strain. In calculation, history is taken into account by formulations that relate increments of stress to increments of strain. In this section we summarize such a formulation, in sufficiently general terms that it can be applied to various materials. More specialized forms, appropriate for commonly used metals, appear in Section 17.5. Details and theoretical background may be found in references such as [17.1–17.3,17.15,17.16].

Incremental theory is not the only valid theory for all plasticity problems. Stresses can also be determined from *total* strains if loading is proportional; that is, if loading increases all components of the state of stress by the same factor. Thus, under increasing load, a problem is solved as if material properties were elastic but nonlinear. In applications where an unloading phase occurs, it must be separated from the loading phase. The assumption that loading is proportional may be adequate for many engineering problems that involve plastic action [17.15].

In this and subsequent sections we continue to use the engineering definition of shear strain; $\gamma_{xy} = u_{,y} + v_{,x}$ and so on. In textbooks devoted to plasticity, the tensor definition $\varepsilon_{xy} = \gamma_{xy}/2$ is usually adopted.

Incremental Plasticity Relations. As in Section 17.3, strain increments are regarded as composed of recoverable (elastic) and nonrecoverable (plastic) components,

$$\{d\boldsymbol{\varepsilon}\} = \{d\boldsymbol{\varepsilon}^e\} + \{d\boldsymbol{\varepsilon}^p\} \tag{17.4-1}$$

where superscripts e and p denote *elastic* and *plastic,* respectively. Stress increments are associated with only the elastic component.

$$\{d\boldsymbol{\sigma}\} = [\mathbf{E}]\{d\boldsymbol{\varepsilon}^e\} \quad \text{or} \quad \{d\boldsymbol{\sigma}\} = [\mathbf{E}]\Big(\{d\boldsymbol{\varepsilon}\} - \{d\boldsymbol{\varepsilon}^p\}\Big) \tag{17.4-2}$$

where $[\mathbf{E}]$ is the elastic material property matrix. In general, $\{d\boldsymbol{\sigma}\}$ contains increments of all six components of stress, $\{d\boldsymbol{\sigma}\} = \lfloor d\sigma_x \;\; d\sigma_y \;\; d\sigma_z \;\; d\tau_{xy} \;\; d\tau_{yz} \;\; d\tau_{zx} \rfloor^T$.

The three essential ingredients of elastic-plastic analysis are a *yield criterion,* a *flow rule,* and a *hardening rule.* The yield criterion relates the state of stress to the onset of yielding. The flow rule relates the state of stress $\{\boldsymbol{\sigma}\}$ to the corresponding six increments of plastic strain $\{d\boldsymbol{\varepsilon}^p\}$ when an increment of plastic flow occurs. The hardening rule describes how the yield criterion is modified by straining beyond initial yield.

Let the yield function be written as

$$F = F\Big(\{\boldsymbol{\sigma}\},\{\boldsymbol{\alpha}\},W_p\Big) \tag{17.4-3}$$

where $\{\boldsymbol{\alpha}\}$ and W_p account for hardening by describing how a "yield surface" in multidimensional stress space is altered, by changes in location or size, in response to plastic

strains (Eqs. 17.4-5 and 17.4-6). Examples of F for a uniaxial state of stress appear in Eq. 17.3-3. Elastic conditions prevail when $F < 0$. When stresses are such that $F = 0$, yielding impends or is in progress. The case $F > 0$ is not physically possible. Starting from the state $F = 0$, plastic flow is associated with changes in $\{\boldsymbol{\sigma}\}$ and changes in $\{\boldsymbol{\alpha}\}$ and/or W_p. During plastic flow, stresses remain on the yield surface (which may be changing in shape and/or location as required by the hardening rule); hence $dF = 0$. When there is unloading, $dF < 0$, which signals a return to elastic behavior.

The flow rule is stated in terms of a function Q, which has units of stress and is called a "plastic potential." With $d\lambda$ a scalar that may be called a "plastic multiplier," plastic strain increments are given by

$$\{d\boldsymbol{\varepsilon}^p\} = \left\{\frac{\partial Q}{\partial \boldsymbol{\sigma}}\right\} d\lambda \tag{17.4-4}$$

Thus $d\varepsilon_x^p = (\partial Q/\partial \sigma_x)\, d\lambda$, and so on. The flow rule is called "associated" if $Q = F$ and "nonassociated" otherwise. Associated flow rules are commonly used for ductile metals. Nonassociated rules are better suited to soil and granular materials.

Hardening can be modeled as isotropic or as kinematic, either separately or in combination. Isotropic hardening can be represented by plastic work per unit volume W_p, which describes growth of the yield surface. Kinematic hardening can be represented by a vector $\{\boldsymbol{\alpha}\}$, which accounts for translation of the yield surface in stress space. Symbolically,

Isotropic hardening: Kinematic hardening:

$$W_p = \int \{\boldsymbol{\sigma}\}^T \{d\boldsymbol{\varepsilon}^p\} \qquad \{\boldsymbol{\alpha}\} = \int \lceil \mathbf{C} \rfloor \{d\boldsymbol{\varepsilon}^p\} \tag{17.4-5}$$

where the latter expression follows from integration of

$$\{d\boldsymbol{\alpha}\} = \lceil \mathbf{C} \rfloor \{d\boldsymbol{\varepsilon}^p\} \quad \text{in which} \quad \lceil \mathbf{C} \rfloor = \frac{2}{3} H_p \begin{bmatrix} 1 & 1 & 1 & \frac{1}{2} & \frac{1}{2} & \frac{1}{2} \end{bmatrix} \tag{17.4-6}$$

and H_p is the plastic modulus H_p, first seen in Eq. 17.3-1. The reason for the factor of 2/3 cannot be explained briefly. In general, H_p is not constant. It can be related to stress or strain by experiment. The diagonal matrix $\lceil \mathbf{C} \rfloor$ is not a unit matrix because we write $\{d\boldsymbol{\varepsilon}\}$ using the engineering definition of shear strain rather than the tensor definition. Plastic flow takes place at constant volume, $d\varepsilon_x^p + d\varepsilon_y^p + d\varepsilon_z^p = 0$; hence $\lfloor 1 \;\; 1 \;\; 1 \;\; 0 \;\; 0 \;\; 0 \rfloor \{\boldsymbol{\alpha}\} = \alpha_x + \alpha_y + \alpha_z = 0$.

Incremental Stress-Strain Relations. During an increment of plastic straining, $dF = 0$, so we obtain from Eq. 17.4-3

$$\left\{\frac{\partial F}{\partial \boldsymbol{\sigma}}\right\}^T \{d\boldsymbol{\sigma}\} + \left\{\frac{\partial F}{\partial \boldsymbol{\alpha}}\right\}^T \{d\boldsymbol{\alpha}\} + \frac{\partial F}{\partial W_p} dW_p = 0 \tag{17.4-7}$$

Substitution of Eq. 17.4-4 into Eqs. 17.4-2, 17.4-5, and 17.4-6 provides

$$\{d\boldsymbol{\sigma}\} = [\mathbf{E}]\left(\{d\boldsymbol{\varepsilon}\} - \left\{\frac{\partial Q}{\partial \boldsymbol{\sigma}}\right\} d\lambda\right), \quad dW_p = \{\boldsymbol{\sigma}\}^T \left\{\frac{\partial Q}{\partial \boldsymbol{\sigma}}\right\} d\lambda, \quad \{d\boldsymbol{\alpha}\} = \lceil \mathbf{C} \rfloor \left\{\frac{\partial Q}{\partial \boldsymbol{\alpha}}\right\} d\lambda \tag{17.4-8}$$

These expressions are substituted into Eq. 17.4-7 and the resulting equation solved for the plastic multiplier $d\lambda$. Thus we obtain

$$d\lambda = \lfloor \mathbf{P}_\lambda \rfloor \{d\boldsymbol{\varepsilon}\} \tag{17.4-9}$$

where $\lfloor \mathbf{P}_\lambda \rfloor$ is the row matrix

$$\lfloor \mathbf{P}_\lambda \rfloor = \frac{\left\{\dfrac{\partial F}{\partial \boldsymbol{\sigma}}\right\}^T [\mathbf{E}]}{\left\{\dfrac{\partial F}{\partial \boldsymbol{\sigma}}\right\}^T [\mathbf{E}] \left\{\dfrac{\partial Q}{\partial \boldsymbol{\sigma}}\right\} - \left\{\dfrac{\partial F}{\partial \boldsymbol{\alpha}}\right\}^T \lceil \mathbf{C} \rfloor \left\{\dfrac{\partial Q}{\partial \boldsymbol{\alpha}}\right\} - \dfrac{\partial F}{\partial W_p} \{\boldsymbol{\sigma}\}^T \left\{\dfrac{\partial Q}{\partial \boldsymbol{\sigma}}\right\}} \tag{17.4-10}$$

Although both work hardening and strain hardening are included in this equation, practical applications will probably use one or the other, or perhaps a fraction of each (Eq. 17.5-6). Finally, from Eqs. 17.4-8 and 17.4-9 we obtain

$$\{d\boldsymbol{\sigma}\} = [\mathbf{E}_{ep}]\{d\boldsymbol{\varepsilon}\} \quad \text{where} \quad [\mathbf{E}_{ep}] = [\mathbf{E}]\left(\lceil \mathbf{I} \rfloor - \left\{\frac{\partial Q}{\partial \boldsymbol{\sigma}}\right\} \lfloor \mathbf{P}_\lambda \rfloor\right) \tag{17.4-11}$$

where $\lceil \mathbf{I} \rfloor$ is a unit matrix. The elastic-plastic matrix $[\mathbf{E}_{ep}]$ can be regarded as a generalized form of tangent modulus E_t. It is a symmetric matrix for an associated flow rule ($Q = F$). For unloading from a plastic state ($F = 0$ and $dF < 0$) or when yielding has yet to appear ($F < 0$), the latter term in Eq. 17.4-11 is set to zero so that $[\mathbf{E}_{ep}] = [\mathbf{E}]$.

Use of $[\mathbf{E}_{ep}]$ rather than $[\mathbf{E}]$ in element formulation provides the tangent stiffness matrix

$$[\mathbf{k}_t] = \int [\mathbf{B}]^T [\mathbf{E}_{ep}][\mathbf{B}]\, dV \tag{17.4-12}$$

One may use simple elements, with $[\mathbf{E}_{ep}]$ assumed constant over the element. Otherwise $[\mathbf{E}_{ep}]$ varies from one sampling point to another. Assembled equations for an FE structure are $[\mathbf{K}_t]\{d\mathbf{D}\} = \{d\mathbf{R}\}$. They provide displacement increments $\{d\mathbf{D}\}$ produced by a load increment $\{d\mathbf{R}\}$ when there is plastic straining.

Uniaxial Stress. For uniaxial stress σ, associative plasticity, and kinematic hardening, we write

$$F = Q = \left[(\sigma - \alpha)^2\right]^{1/2} - \sigma_Y \qquad W_P = 0 \tag{17.4-13}$$

where σ_Y is the initial yield stress, always taken as positive. Hence

$$\frac{\partial F}{\partial \sigma} = \frac{\partial Q}{\partial \sigma} = -\frac{\partial F}{\partial \alpha} = \frac{1}{2}\frac{2(\sigma - \alpha)}{\left[(\sigma - \alpha)^2\right]^{1/2}} = \frac{\sigma - \alpha}{\sigma_Y} \tag{17.4-14}$$

in which σ_Y can be introduced in the denominator because $F = 0$ during yielding. In one-dimensional form, $\lfloor \mathbf{P}_\lambda \rfloor$ in Eq. 17.4-10 becomes the scalar P_λ, $[\mathbf{E}]$ becomes E, and $\lceil \mathbf{C} \rfloor$ is replaced by H_p. Thus, letting r represent $(\sigma - \alpha)/\sigma_Y$, Eqs. 17.4-10 and 17.4-11 provide

$$P_\lambda = \frac{rE}{r^2E + r^2H_p} = \frac{E}{r(E+H_p)} \qquad \text{and} \qquad E_t = E\left(1 - \frac{E}{E+H_p}\right) \tag{17.4-15}$$

where E_t is the one-dimensional form of $[\mathbf{E}_{ep}]$. The latter result agrees with Eq. 17.3-2.

17.5 PLASTICITY: FORMULATION FOR VON MISES THEORY

By "von Mises theory" we mean associative plasticity ($F = Q$) in which yielding is postulated to take place when the von Mises or "effective" stress σ_e reaches a limiting value, where

$$\sigma_e = \frac{1}{\sqrt{2}}\left[(\sigma_x - \sigma_y)^2 + (\sigma_y - \sigma_z)^2 + (\sigma_z - \sigma_x)^2 + 6\left(\tau_{xy}^2 + \tau_{yz}^2 + \tau_{xy}^2\right)\right]^{1/2} \tag{17.5-1}$$

The positive root is intended. Von Mises theory works well in describing the plastic behavior of common metals. Note that if the state of stress is uniaxial, then σ_e reduces to the magnitude of the uniaxial stress.

Deviatoric stresses play a prominent role in von Mises theory. Any stress state can be represented as the sum of a hydrostatic state and a deviatoric state. A hydrostatic state produces no change of shape. A deviatoric state produces no change of volume. Deviatoric shear stresses are the same as actual shear stresses. Deviatoric normal stresses are actual normal stresses minus the mean normal stress σ_m, where $\sigma_m = (\sigma_x + \sigma_y + \sigma_z)/3$. Adopting the symbol s for deviatoric stresses, we have

$$\{\mathbf{s}_\sigma\} = \begin{Bmatrix} s_x \\ s_y \\ s_z \end{Bmatrix} = \begin{Bmatrix} \sigma_x - \sigma_m \\ \sigma_y - \sigma_m \\ \sigma_z - \sigma_m \end{Bmatrix} = \frac{1}{3}\begin{Bmatrix} 2\sigma_x - \sigma_y - \sigma_z \\ 2\sigma_y - \sigma_z - \sigma_x \\ 2\sigma_z - \sigma_x - \sigma_y \end{Bmatrix} \qquad \{\mathbf{s}_\tau\} = \begin{Bmatrix} s_{xy} \\ s_{yz} \\ s_{zx} \end{Bmatrix} = \begin{Bmatrix} \tau_{xy} \\ \tau_{yz} \\ \tau_{zx} \end{Bmatrix} \tag{17.5-2}$$

Thus $s_x + s_y + s_z = 0$. In terms of deviatoric stresses, stress σ_e of Eq. 17.5-1 has the form

$$\sigma_e = \sqrt{\frac{3}{2}}\left[s_x^2 + s_y^2 + s_z^2 + 2\left(s_{xy}^2 + s_{yz}^2 + s_{zx}^2\right)\right]^{1/2} \tag{17.5-3}$$

Formulation. What follows is a specialization of the plasticity theory summarized in Section 17.4. As before, we present a summary and leave details and theoretical background to references such as [17.3,17.15,17.16].

For von Mises theory, plastic multiplier $d\lambda$ is the same as the increment of effective plastic strain that corresponds to σ_e. Thus

$$d\lambda = d\varepsilon_e^p = \sqrt{\frac{2}{3}}\left[\left(d\varepsilon_x^p\right)^2 + \left(d\varepsilon_y^p\right)^2 + \left(d\varepsilon_z^p\right)^2 + \frac{1}{2}\left\langle\left(d\gamma_{xy}^p\right)^2 + \left(d\gamma_{yz}^p\right)^2 + \left(d\gamma_{zx}^p\right)^2\right\rangle\right]^{1/2} \quad (17.5\text{-}4)$$

Because Poisson's ratio is 0.5 in plastic flow, $d\varepsilon_x^p + d\varepsilon_y^p + d\varepsilon_z^p = 0$. For uniaxial stress σ_x, $d\varepsilon_y^p = d\varepsilon_z^p = -0.5d\varepsilon_x^p$, and we obtain $d\varepsilon_e^p = d\varepsilon_x^p$. Therefore a plot of σ_e versus ε_e^p is the same as a uniaxial stress-strain plot.

For von Mises theory, it can be shown that isotropic hardening can be described by either a strain hardening expression or a work hardening expression. The resulting expression for the yield function for isotropic hardening is

$$F = \sigma_e - \sigma_0 \quad , \quad (17.5\text{-}5)$$

where σ_0 is the largest value of σ_e reached in previous plastic straining. The case $F < 0$ describes elastic conditions. The case $F = 0$ defines yielding. The case $F > 0$ is not physically possible.

We choose to write a "mixed" hardening rule, including both isotropic and kinematic hardening, by introducing a number η, where $0 \le \eta \le 1$. Thus

$$F = \left[\frac{3}{2}\left\langle(s_x - \eta\alpha_x)^2 + (s_y - \eta\alpha_y)^2 + (s_z - \eta\alpha_z)^2\right\rangle + 3\left\langle(s_{xy} - \eta\alpha_{xy})^2 + (s_{yz} - \eta\alpha_{yz})^2 + (s_{zx} - \eta\alpha_{zx})^2\right\rangle\right]^{1/2} - \eta\sigma_Y - (1-\eta)\sigma_0 \quad (17.5\text{-}6)$$

where σ_Y is the von Mises stress σ_e, or the magnitude of uniaxial stress, at initial yield. Translation of the yield surface is controlled by $\{\boldsymbol{\alpha}\}$, where $\{\boldsymbol{\alpha}\} = \lfloor\alpha_x \;\; \alpha_y \;\; \alpha_z \;\; \alpha_{xy} \;\; \alpha_{yz} \;\; \alpha_{zx}\rfloor^T$. Hardening is purely isotropic if $\eta = 0$ and purely kinematic if $\eta = 1$ (Fig. 17.5-1).

The last term in Eq. 17.4-7, $\{\partial F/\partial W_p\}dW_p$, is replaced by

$$\frac{\partial F}{\partial \sigma_0}d\sigma_0 \quad \text{where} \quad \frac{\partial F}{\partial \sigma_0} = -(1-\eta) \quad \text{and} \quad d\sigma_0 = H_p\,d\lambda \quad (17.5\text{-}7)$$

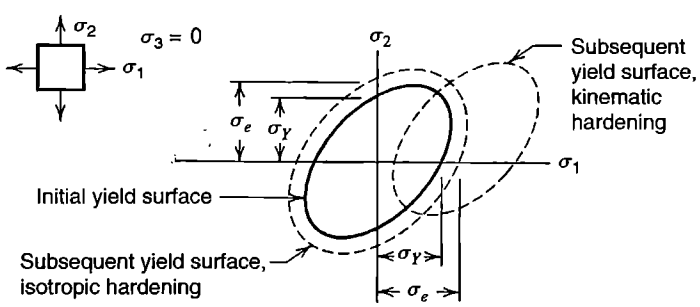

Figure 17.5-1. Hardening rules, illustrated for the case of plane stress with nonzero principal stresses σ_1 and σ_2. Stresses within the ellipse are elastic.

We see that $\{\partial F/\partial \boldsymbol{\alpha}\} = -\eta\,\{\partial F/\partial \boldsymbol{\sigma}\}$. Therefore the same manipulations that produced Eq. 17.4-10 now provide, with $F = Q$,

$$\lfloor \mathbf{P}_\lambda \rfloor = \frac{\left\{\dfrac{\partial F}{\partial \boldsymbol{\sigma}}\right\}^T [\mathbf{E}]}{\left\{\dfrac{\partial F}{\partial \boldsymbol{\sigma}}\right\}^T \Big([\mathbf{E}] + \eta\lceil \mathbf{C} \rfloor\Big)\left\{\dfrac{\partial F}{\partial \boldsymbol{\sigma}}\right\} + (1-\eta)H_p} \tag{17.5-8}$$

Differentiation of F with respect to $\{\boldsymbol{\sigma}\}$ is accomplished as follows.

$$\left\{\frac{\partial F}{\partial \boldsymbol{\sigma}}\right\} = \frac{1}{2[\cdots]^{1/2}}\left\{\frac{\partial}{\partial \boldsymbol{\sigma}}[\cdots]\right\} = \frac{1}{2\left[\eta\sigma_Y + (1-\eta)\sigma_0\right]}\left\{\frac{\partial}{\partial \boldsymbol{\sigma}}[\cdots]\right\} \tag{17.5-9}$$

where $[\cdots]$ represents the expression within brackets in Eq. 17.5-6. The substitute denominator in the latter form of Eq. 17.5-9 is allowed because $F = 0$ during yielding. The first term in $\{\partial[\cdots]/\partial\sigma\}$ is evaluated as follows, with the aid of Eqs. 17.5-2.

$$\frac{\partial}{\partial \sigma_x}[\cdots] = 3\left[(s_x - \eta\alpha_x)\frac{\partial s_x}{\partial \sigma_x} + (s_y - \eta\alpha_y)\frac{\partial s_y}{\partial \sigma_x} + (s_z - \eta\alpha_z)\frac{\partial s_z}{\partial \sigma_x}\right] \tag{17.5-10a}$$

$$\frac{\partial}{\partial \sigma_x}[\cdots] = 3\left[(s_x - \eta\alpha_x)\frac{2}{3} - (s_y - \eta\alpha_y)\frac{1}{3} - (s_z - \eta\alpha_z)\frac{1}{3}\right] \tag{17.5-10b}$$

Differentiation with respect to σ_y and σ_z is accomplished similarly, and differentiation with respect to shear stresses is simple. From Eqs. 17.5-2, $2s_x - s_y - s_z = 3s_x$ and similarly for other deviatoric normal stresses and the corresponding α terms. Thus we obtain the 6 by 1 vector needed in Eq. 17.5-8.

$$\left\{\frac{\partial F}{\partial \boldsymbol{\sigma}}\right\} = \frac{3}{\eta\sigma_Y + (1-\eta)\sigma_0}\left(\frac{1}{2}\begin{Bmatrix}\mathbf{s}_\sigma - \eta\boldsymbol{\alpha}_\sigma \\ \mathbf{0}\end{Bmatrix} + \begin{Bmatrix}\mathbf{0} \\ \mathbf{s}_\tau - \eta\boldsymbol{\alpha}_\tau\end{Bmatrix}\right)$$

$$\text{where} \qquad \{\boldsymbol{\alpha}\} = \begin{Bmatrix}\boldsymbol{\alpha}_\sigma \\ \boldsymbol{\alpha}_\tau\end{Bmatrix} \tag{17.5-11}$$

Finally, $[\mathbf{E}_{ep}]$ and $[\mathbf{k}_t]$ can be obtained from Eqs. 17.4-11 and 17.4-12.

With $Q = F$ and isotropic hardening ($\eta = 0$), Eqs. 17.4-4 and 17.5-11 state that $d\varepsilon_x^p = (3s_x/2\sigma_0)\,d\lambda, \ldots, d\gamma_{zx}^p = (3s_{zx}/\sigma_0)\,d\lambda$. If we temporarily adopt tensor notation for shear strains ($\varepsilon_{xy} = \gamma_{xy}/2$, and so on), these relations have the form

$$\frac{d\varepsilon_x^p}{s_x} = \frac{d\varepsilon_y^p}{s_y} = \frac{d\varepsilon_z^p}{s_z} = \frac{d\varepsilon_{xy}^p}{s_{xy}} = \frac{d\varepsilon_{yz}^p}{s_{yz}} = \frac{d\varepsilon_{zx}^p}{s_{zx}} = \frac{3}{2\sigma_0}\,d\lambda \tag{17.5-12}$$

Equations 17.5-12 are known as the Prandtl-Reuss relations. They state that during plastic flow, each plastic strain increment is proportional to its corresponding deviatoric stress.

Thus, principal axes of strain increments coincide with principal stress directions. For uniaxial stress σ_x we have $s_x = 2\sigma_x/3$ and $\sigma_x = \sigma_0$, so Eq. 17.4-12 yields $d\varepsilon_x^p = d\lambda$.

17.6 PLASTICITY: SOME COMPUTATIONAL PROCEDURES

In this section we discuss some calculation procedures for time-independent plastic analysis based on equations of Sections 17.4 and 17.5. We assume that the goal of analysis is to determine nodal displacements $\{\mathbf{D}\}$ and stresses $\{\boldsymbol{\sigma}\}$ during the course of a loading program described by a known external load vector $\{\mathbf{R}\}$, which changes with time in quasistatic fashion. Practical software may add procedures or bypass procedures discussed in favor of others. We do not attempt to describe or even mention all methods, variants, and combinations that have been advocated.

Except for solving for global displacement increments (Eq. 17.6-1) and selecting the next load increment to be applied, calculations described in this section are performed at each sampling point. These points are likely to be the same as Gauss points used to formulate element matrices. To reduce computational expense, analysts may prefer elements that require only one Gauss point per element. Most such elements must be stabilized to suppress spurious modes. Elements must not be susceptible to dilatational locking when material becomes incompressible, as it does during plastic flow.

We presume that a laboratory test of the material's uniaxial stress-strain relation has been made and is stored in numerical form. Thus, for a von Mises material the stored data provides H_p for a given value of σ_e. Elastic modulus E and initial yield stress σ_Y are also stored. To follow changing displacements the current $\{\mathbf{D}\}$ must be stored, and updated as the solution progresses. In the following calculation steps, quantities that must be available at each sampling point, and updated as the solution progresses, are stresses $\{\boldsymbol{\sigma}\}$ and, depending on the hardening rule used, $\{\boldsymbol{\alpha}\}$ and/or W_p (or σ_0 for a von Mises material).

If starting from zero load, the initial load step should place the structure on the verge of yield. This is easily accomplished: apply an arbitrary magnitude of load, use linear analysis to determine σ_e at the most highly stressed point, then scale the load and all computed results by the ratio σ_Y/σ_e. In subsequent load increments, an individual sampling point may remain elastic, remain plastic, or make the elastic-plastic transition.

In what follows we assume that preceding calculations have produced a state of deformation and stress that does not violate equilibrium conditions, compatibility conditions, or the yield criterion, at least to an acceptable approximation. We will call this condition *state A*. We now apply the following steps to determine conditions in *state B*, which is produced by adding an increment $\{\Delta\mathbf{R}\}_{AB}$ of external load.

Increment of Displacement and Strain. Generate the global tangent stiffness matrix, $[\mathbf{K}_t] = \sum[\mathbf{k}_t]$. See Eq. 17.4-12 for $[\mathbf{k}_t]$. To correct for possible equilibrium errors that may remain in state A, augment load increment $\{\Delta\mathbf{R}\}_{AB}$ by the imbalance between applied loads and loads applied to nodes by existing stresses (see the one-dimensional example of Eq. 17.2-3; also Eq. 3.3-8 or Eq. 4.8-15b and Eq. 11.2-7). Thus

$$[\mathbf{K}_t]_A\{\Delta\mathbf{D}\}_{AB} = \{\Delta\mathbf{R}\} \qquad \text{where} \qquad \{\Delta\mathbf{R}\} = \{\Delta\mathbf{R}\}_{AB} + \left(\{\mathbf{R}\}_A - \sum\int[\mathbf{B}]^T\{\boldsymbol{\sigma}\}_A\,dV\right) \tag{17.6-1}$$

where dV is an increment of element volume and summation spans all elements, with the usual expansion of element arrays to "structure size." Solve for $\{\Delta\mathbf{D}\}_{AB}$. Update displacements and obtain strain increments at a sampling point in an element.

$$\{\mathbf{D}\}_B = \{\mathbf{D}\}_A + \{\Delta\mathbf{D}\}_{AB} \qquad \{\Delta\boldsymbol{\varepsilon}\}_{AB} = [\mathbf{B}]\{\Delta\mathbf{d}\}_{AB} \tag{17.6-2}$$

where element d.o.f. $\{\Delta\mathbf{d}\}_{AB}$ are extracted from global d.o.f. $\{\Delta\mathbf{D}\}_{AB}$. Next comes the major task of updating the state of stress at each sampling point.

Partly Plastic Increment. If the sampling point was elastic in state A, determine if it remains elastic. Therefore compute

$$\text{Trial elastic update:} \qquad \{\boldsymbol{\sigma}\}_{\text{trial}} = \{\boldsymbol{\sigma}\}_A + [\mathbf{E}]\{\Delta\boldsymbol{\varepsilon}\}_{AB} \tag{17.6-3}$$

Check the yield criterion: if $F = F_{\text{trial}} < 0$ for stresses $\{\boldsymbol{\sigma}\}_{\text{trial}}$, then conditions remain elastic, so accept these stresses as correct; that is, $\{\boldsymbol{\sigma}\}_B = \{\boldsymbol{\sigma}\}_{\text{trial}}$ (Fig. 17.6-1a). If $F_{\text{trial}} > 0$, determine the fraction β of the step that is elastic. The one-dimensional form of this problem is linear and is easily solved (Eq. 17.3-4), but here we must solve for β in the nonlinear problem

$$F_C = F(\{\boldsymbol{\sigma}\}_C) = 0 \qquad \text{where} \qquad \{\boldsymbol{\sigma}\}_C = \{\boldsymbol{\sigma}\}_A + \beta\,[\mathbf{E}]\{\Delta\boldsymbol{\varepsilon}\}_{AB} \tag{17.6-4}$$

where stresses $\{\boldsymbol{\sigma}\}_C$ are on the "yield surface" (Fig. 17.6-1b). The same argument as used in Eq. 17.3-4 yields a first approximation for β.

$$\beta \approx \frac{F_A}{F_A - F_{\text{trial}}} = \beta_1 \qquad \text{hence} \qquad \{\boldsymbol{\sigma}\}_{C1} \approx \{\boldsymbol{\sigma}\}_A + \beta_1[\mathbf{E}]\{\Delta\boldsymbol{\varepsilon}\}_{AB} \tag{17.6-5}$$

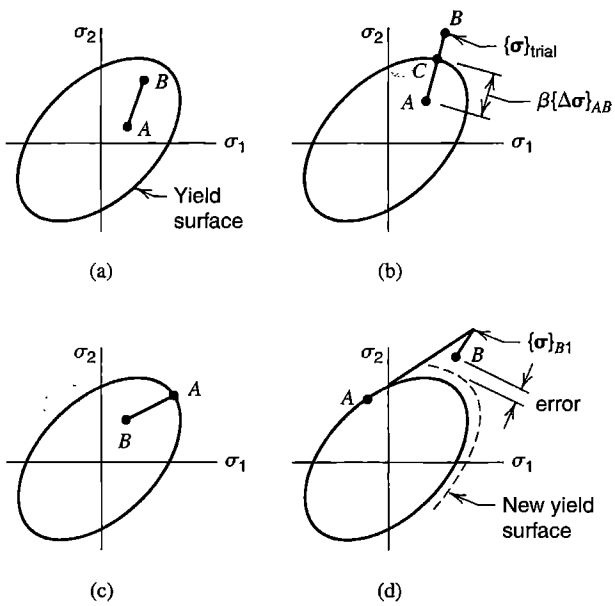

Figure 17.6-1. Possible stress changes from state A to state B, illustrated for the case of plane stress with nonzero principal stresses σ_1 and σ_2. (a) Entirely elastic. (b) Partially elastic. (c) Elastic unloading. (d) Entirely plastic.

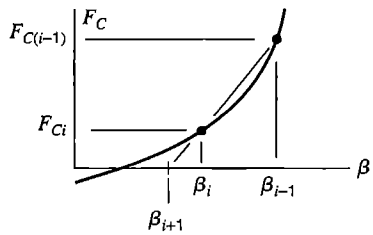

Figure 17.6-2. Secant iteration to determine β for which $F_C = 0$.

where stresses $\{\boldsymbol{\sigma}\}_{C1}$ are estimated stresses that result from the entirely elastic portion of the increment. More accurate results are provided by secant iteration [17.17], which resembles a classical Newton-Raphson solution. Thus with i the iteration number, we write (see Fig. 17.6-2)

$$\{\boldsymbol{\sigma}\}_{Ci} = \{\boldsymbol{\sigma}\}_A + \beta_i[\mathbf{E}]\{\Delta\boldsymbol{\varepsilon}\}_{AB} \tag{17.6-6a}$$

$$\beta_{i+1} = \beta_i - \frac{F_{Ci}}{\Delta F_C/\Delta\beta} \qquad \text{where} \qquad \frac{\Delta F_C}{\Delta\beta} = \frac{F_{C(i-1)} - F_{Ci}}{\beta_{i-1} - \beta_i} \tag{17.6-6b}$$

Starting values are $i = 1$, $\beta_0 = 0$, $\{\boldsymbol{\sigma}\}_{C0} = \{\boldsymbol{\sigma}\}_A$, and β_1 and $\{\boldsymbol{\sigma}\}_{C1}$ from Eq. 17.6-5. Only four or five iterations are needed, even with a strict convergence tolerance [17.17]. The final yield-condition state of stress is $\{\boldsymbol{\sigma}\}_{C(i+1)}$. From this state, the remainder of the strain increment is $(1-\beta)\{\Delta\boldsymbol{\varepsilon}\}_{AB}$, which is a plastic increment that is treated as described next for an entirely plastic strain increment that is called $\{\Delta\boldsymbol{\varepsilon}\}_{AB}$.

Plastic Increment. Consider a sampling point for which stresses $\{\boldsymbol{\sigma}\}_A$ satisfy the yield criterion $F_A = 0$. Stresses $\{\boldsymbol{\sigma}\}_B$ at the end of the current increment are desired. Plastic multiplier $\Delta\lambda$ is needed. From Eqs. 17.4-4 and 17.4-9,

$$\{\Delta\boldsymbol{\varepsilon}^p\}_{AB} = \left\{\frac{\partial Q}{\partial\boldsymbol{\sigma}}\right\}\Delta\lambda \qquad \Delta\lambda = \lfloor\mathbf{P}_\lambda\rfloor\{\Delta\boldsymbol{\varepsilon}\}_{AB} \tag{17.6-7}$$

in which, as an initial guess, $\lfloor\mathbf{P}_\lambda\rfloor$ is evaluated at state A. Then, if $\Delta\lambda \le 0$, unloading has taken place, and stresses at the end of the step are obtained from Eq. 17.6-3, with $\{\boldsymbol{\sigma}\}_{\text{trial}} = \{\boldsymbol{\sigma}\}_B$ in this case (Fig. 17.6-1c). But if $\Delta\lambda \ge 0$, the step is plastic, and in Eqs. 17.6-7 we have the question of where to evaluate $\{\partial Q/\partial\boldsymbol{\sigma}\}$ and $\lfloor\mathbf{P}_\lambda\rfloor$, which vary along the path from A to B. We may write the following expression, which is a multidimensional form of Eq. 17.3-8.

$$\{\Delta\boldsymbol{\varepsilon}^p\}_{AB} = \left[(1-\gamma)\left\{\frac{\partial Q}{\partial\boldsymbol{\sigma}}\right\}_A\lfloor\mathbf{P}_\lambda\rfloor_A + \gamma\left\{\frac{\partial Q}{\partial\boldsymbol{\sigma}}\right\}_B\lfloor\mathbf{P}_\lambda\rfloor_B\right]\{\Delta\boldsymbol{\varepsilon}\}_{AB} \tag{17.6-8}$$

Forward Euler integration is given by $\gamma = 0$ and is called *explicit* because it uses only information at the start of the increment. Backward Euler integration is given by $\gamma = 1$ and is called *implicit* because it uses information at the end of the increment. End-point information is not known in advance, so the equation is implemented in predictor-corrector form. The predictor uses start-point information to obtain first estimates of the plastic strain increment and end-point stresses. From Eqs. 17.4-2, 17.4-4, and 17.4-9,

$$\{\Delta\boldsymbol{\varepsilon}^p\}_{AB1} = \left\{\frac{\partial Q}{\partial \boldsymbol{\sigma}}\right\}_A \lfloor \mathbf{P}_\lambda \rfloor_A \{\Delta\boldsymbol{\varepsilon}\}_{AB} \qquad \{\Delta\boldsymbol{\sigma}\}_{AB1} = [\mathbf{E}]\Big(\{\Delta\boldsymbol{\varepsilon}\}_{AB} - \{\Delta\boldsymbol{\varepsilon}^p\}_{AB1}\Big) \tag{17.6-9}$$

Estimated end-point stresses are currently $\{\boldsymbol{\sigma}\}_{B1} \approx \{\boldsymbol{\sigma}\}_A + \{\Delta\boldsymbol{\sigma}\}_{AB1}$ (Fig. 17.6-1d). Using these stresses and $\{\Delta\boldsymbol{\varepsilon}^p\}_{AB1}$ we can update the several quantities in Eq. 17.4-10 to obtain the estimated end-point array $\lfloor \mathbf{P}_\lambda \rfloor_{B1}$. Second estimates of the plastic strain increment and end-point stresses are

$$\{\Delta\boldsymbol{\varepsilon}^p\}_{AB2} = \left\{\frac{\partial Q}{\partial \boldsymbol{\sigma}}\right\}_{B1} \lfloor \mathbf{P}_\lambda \rfloor_{B1} \{\Delta\boldsymbol{\varepsilon}\}_{AB}, \quad \{\Delta\boldsymbol{\sigma}\}_{AB2} = [\mathbf{E}]\Big(\{\Delta\boldsymbol{\varepsilon}\}_{AB} - \{\Delta\boldsymbol{\varepsilon}^p\}_{AB2}\Big) \tag{17.6-10}$$

By using $\gamma = 1/2$ in Eq. 17.6-8 we average the two estimates. Thus we obtain

$$\{\Delta\boldsymbol{\varepsilon}^p\}_{AB} \approx \frac{1}{2}\Big(\{\Delta\boldsymbol{\varepsilon}^p\}_{AB1} + \{\Delta\boldsymbol{\varepsilon}^p\}_{AB2}\Big) \tag{17.6-11}$$

$$\{\boldsymbol{\sigma}\}_B \approx \{\boldsymbol{\sigma}\}_A + \frac{1}{2}\Big(\{\Delta\boldsymbol{\sigma}\}_{AB1} + \{\Delta\boldsymbol{\sigma}\}_{AB2}\Big) \tag{17.6-12}$$

Error can be reduced by reducing the size of the load increment.

Return to Yield Surface. Stresses $\{\boldsymbol{\sigma}\}_B$ provided by Eq. 17.6-12 usually do not satisfy the yield condition $F_B = 0$, although error may be much smaller than suggested by an exaggerated sketch (Fig. 17.6-1d). Several methods of returning stresses to the yield surface have been suggested. A widely used method is to keep total strains constant while allowing small plastic strain increments to take place [17.2]. Thus, using the symbol δ to indicate the return adjustment, we set $\{\delta\boldsymbol{\varepsilon}\} = \{\mathbf{0}\}$ and seek plastic strain increments $\{\delta\boldsymbol{\varepsilon}^p\}$ such that $F_B + \delta F = 0$. A first-order Taylor series expression for $F_B + \delta F$ yields, with $F_B + \delta F = 0$,

$$0 = F_B + \left\{\frac{\partial F}{\partial \boldsymbol{\sigma}}\right\}^T \{\delta\boldsymbol{\sigma}\} + \left\{\frac{\partial F}{\partial \boldsymbol{\alpha}}\right\}^T \{\delta\boldsymbol{\alpha}\} + \frac{\partial F}{\partial W_p}\,\delta W_p \tag{17.6-13}$$

Using Eqs. 17.4-2, 17.4-4, 17.4-6, and 17.4-8 with $\{d\boldsymbol{\varepsilon}\} = \{\mathbf{0}\}$, we obtain

$$\delta\lambda = \frac{F_B}{[\text{denom}]_B} \tag{17.6-14}$$

where $[\text{denom}]_B$ is the denominator of Eq. 17.4-10, evaluated at state B. Updated stresses can be obtained from Eq. 17.4-8 with $\{d\boldsymbol{\varepsilon}\} = \{\mathbf{0}\}$. Thus

$$\{\boldsymbol{\sigma}\}_{B(\text{new})} = \{\boldsymbol{\sigma}\}_B - [\mathbf{E}]\left\{\frac{\partial Q}{\partial \boldsymbol{\sigma}}\right\}_B \delta\lambda \tag{17.6-15}$$

For improved accuracy, Eqs. 17.6-14 and 17.6-15 can be applied iteratively, with updates of [denom] prior to each additional iteration, until (for a von Mises material) $F_{B(\text{new})}/\sigma_0$ is

in the range 0.01 to 0.001 [17.21]. However, some investigators consider a single adjustment adequate or omit the adjustment altogether, preferring to subdivide incremental steps as needed to satisfy an error criterion [17.17].

Size of Load Increment. The size of a load increment can be adjusted to meet an error criterion. One suggestion is that the current load step be subdivided if the first-estimate stress increment $\{\Delta\boldsymbol{\sigma}\}_{AB1}$ of Eq. 17.6-9 causes yield function F to change by more than about 10% [17.21]. Another suggestion [17.22] is that the number of substeps NS be related to the error of initial-estimate stresses $\{\boldsymbol{\sigma}\}_{B1}$. Estimated stress errors in $\{\boldsymbol{\sigma}\}_{B1}$ are

$$\{\Delta\boldsymbol{\sigma}^{\text{err}}\} = \{\boldsymbol{\sigma}\}_{B1} - \{\boldsymbol{\sigma}\}_B \approx \frac{1}{2}\Big(\{\Delta\boldsymbol{\sigma}\}_{AB1} - \{\Delta\boldsymbol{\sigma}\}_{AB2}\Big) \tag{17.6-16}$$

This error vector is then represented by a scalar e, which is used to estimate an appropriate number of substeps, NS:

$$e = 2\frac{\Delta\sigma_e^{\text{err}}}{\sigma_e} \quad \text{and} \quad NS = 20e \tag{17.6-17}$$

Here $\Delta\sigma_e^{\text{err}}$ is calculated from Eq. 17.5-1, but with stresses replaced by stress changes $\{\Delta\boldsymbol{\sigma}^{\text{err}}\}$ of Eq. 17.6-16. Additional substepping schemes with error control are suggested in [17.17]. Discretization error and automatic mesh refinement have also been studied in the context of elastic-plastic analysis [17.18,17.19].

Finally, having updated $\{\boldsymbol{\sigma}\}$, $\{\boldsymbol{\alpha}\}$, and W_p (or σ_0 for a von Mises material), we obtain new element tangent stiffness matrices using Eq. 17.4-12, assemble a new structure matrix $[\mathbf{K}_t]$, and return to Eq. 17.6-1 with another load increment $\{\Delta\mathbf{R}\}$.

17.7 NONLINEAR DYNAMIC PROBLEMS

If the frequency of excitation exceeds roughly one-quarter the structure's lowest natural frequency of vibration, inertia becomes important and the problem must be analyzed as dynamic rather than quasistatic. Explicit and implicit integration methods discussed in Chapter 11 remain applicable when nonlinearity is present. Explicit methods accommodate nonlinearity more easily than implicit methods. Explicit methods require little computation per time step but demand a small time step because they are conditionally stable, and so are best suited to short-duration loads such as impact. Implicit methods require considerable computation per time step but allow a much larger time step, and so are best suited to long-duration loads such as provided by an earthquake. Methods that are unconditionally stable when applied to a linear problem are not necessarily so when applied to a nonlinear problem.

In what follows we presume familiarity with Sections 11.11 to 11.13. Also, we presume that nonlinearity affects the stiffness matrix but leaves mass and damping matrices unchanged.

Explicit Methods. Consider the central difference method, (Eq. 11.12-3, 11.12-6, or 11.12-8). In a linearly elastic problem, the term $\{\mathbf{R}^{\text{int}}\}_n$ represents forces needed to equil-

ibrate elastic stresses within the structure. To accommodate material nonlinearity, this term can be computed as

$$\{\mathbf{R}^{\text{int}}\}_n = \sum \{\mathbf{r}^{\text{int}}\}_n \quad \text{where} \quad \{\mathbf{r}^{\text{int}}\}_n = \int [\mathbf{B}]^T \{\boldsymbol{\sigma}\}_n \, dV \tag{17.7-1}$$

Here $\{\boldsymbol{\sigma}\}_n$ represents elastic and/or plastic stresses in an element at the end of step n and summation spans all elements of the structure, with the usual expansion of the element arrays to "structure size." Procedures for updating $\{\boldsymbol{\sigma}\}_n$ are explained in Section 17.6, where the respective states A and B correspond to states $n-1$ and n in the present discussion.

For nonlinear problems as well as linear problems, when time step Δt is small enough to ensure computational stability of an explicit method, adequate accuracy is usually assured. Computational experience suggests that the stability criteria of Eqs. 11.12-9 and 11.12-10 also apply to nonlinear problems provided that one uses the instantaneous value of $\omega_{\max}$, which for material nonlinearity is a function of changing material properties. In softening materials, whose tangent modulus E_t decreases with increasing stress or strain, the instantaneous value of $\omega_{\max}$ usually does not exceed the $\omega_{\max}$ of linearly elastic response [17.23]. Thus a Δt that provides stability for elastic response will also provide stability for elastic-plastic response. Although it is possible that the allowable Δt may increase, the amount of increase is usually small, as $\omega_{\max}$ is often governed by elements of the mesh that experience little or no plastic deformation. With a stiffening material, it is usually necessary to monitor $\omega_{\max}$ as the solution progresses, perhaps using Eq. 11.12-15, and reduce Δt as necessary.

Numerical instability is usually easy to detect in a linear problem because the solution grows without limit (Fig. 11.12-2). With elastic-plastic or other energy-dissipating nonlinear material behavior, energy that is artificially introduced by numerical instability may be dissipated by the material to such an extent that the instability is arrested [11.48]. An "arrested instability" is often difficult to detect because the solution may appear to be reasonable despite being in error by 10% to 100% or even more.

When an explicit method is used for nonlinear dynamics, it is usually prudent to perform an energy balance check to warn of possible numerical instability. A formula based on strain energy, kinetic energy, and the work of external forces has been proposed [2.20,11.48].

Example: Dynamic Plasticity, Explicit Algorithm. We reconsider the example presented in Section 11.12, but now use the elastic-plastic hardening model depicted in Fig. 17.3-1b, with $E = 30(10^6)$ psi, $E_t = E/4$, and $\sigma_Y = 40(10^3)$ psi. The 20-in. bar, shown in Fig. 11.12-1, is initially at rest and is modeled by 40 equal-length two-node elements, so $L = L_T/40 = 0.5$ in. Axial tip loading is as shown in Fig. 11.12-1, except that its magnitude is now taken as $P_0 = 2A\sigma_Y = 80(10^3)$ lbs. Because $E_t < E$, a time step stable for elastic analysis remains stable when yielding appears. Hence we assume that the critical time step is $\Delta t = 2.484(10^{-6})$ s, as calculated following Eq. 11.12-20. In calculation we elect to use $\Delta t = 2.400(10^{-6})$ s (for which the Courant number is $C_n = 0.966$), and take 83 time steps. In summary, calculations are the same as in Section 11.12 except that $\{\mathbf{R}^{\text{int}}\}$ is computed from stresses in elastic-plastic elements rather than from the elastic conditions stated in Eq. 11.12-19.

Figure 17.7-1 shows the resulting history of stress at $x = 9.75$ in., which is the midpoint of element 20. Two separate stress waves arrive at different times. They are an elastic wave

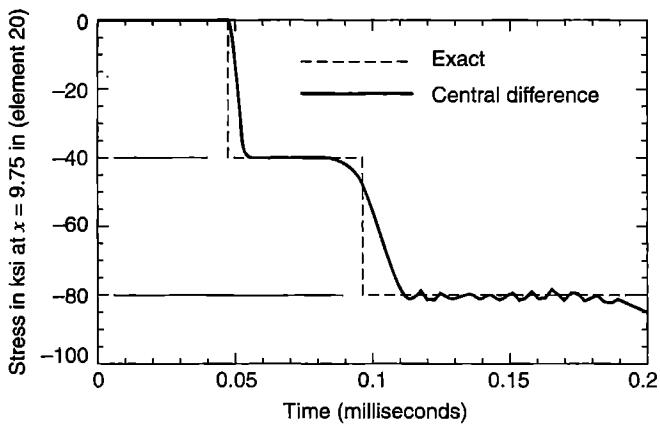

Figure 17.7-1. Stress versus time at $x = 9.75$ in. for a 40-element model of a 20 in. bar of elastic-plastic material, with $\Delta t = 2.400(10^{-6})$ s, for which $C_n = 0.966$. Figure 11.12-1 applies, except that $P_0 = 80{,}000$ lb.

traveling at speed $c_e = \sqrt{E/\rho}$, which arrives first, followed by a plastic wave traveling at speed $c_p = \sqrt{E_t/\rho} = c_e/2$. Thus, at $x = 9.75$ in., an elastic wave arrives at $t = 0.0484$ ms and a plastic wave arrives at $t = 0.0968$ ms.

The solution at $x = 9.75$ in. is smooth until the plastic wave passes, then it displays oscillations. The reason is that as the elastic wave travels along the bar, numerical noise creates stress excursions beyond the initial yield stress. These excursions are transmitted at plastic wave speed and hence do not arrive at $x = 9.75$ in. until approximately 0.11 ms have elapsed.

Computer time needed for practical vehicle crash analysis can be large. Reference [15.7] cites an analysis that used 14,805 shell elements with $\Delta t = 8(10^{-9})$ s, and required 17 hours on a Cray supercomputer.

Tangent-Stiffness (Implicit) Method. The advantage of an implicit method over an explicit method is the large time step permitted by commonly used implicit methods. Note, however, that unconditional stability in a linear problem does not guarantee unconditional stability in a nonlinear problem. Nonlinearity presents the same difficulty to both static and implicit dynamic solution algorithms: stiffness is a function of displacements, which are not known in advance. Methods for addressing this difficulty in dynamics are analogous to similar methods in statics (Section 17.6).

A first-order approximation that uses the tangent stiffness matrix is [11.47]

$$\{\mathbf{R}^{\text{int}}\}_{n+1} = \{\mathbf{R}^{\text{int}}\}_n + [\mathbf{K}_t]_n\{\Delta\mathbf{D}\} \qquad \text{where} \qquad \{\Delta\mathbf{D}\} = \{\mathbf{D}\}_{n+1} - \{\mathbf{D}\}_n \tag{17.7-2}$$

Thus, at time $(n + 1)\,\Delta t$ the equation of motion, Eq. 11.2-11, becomes

$$[\mathbf{M}]\{\ddot{\mathbf{D}}\}_{n+1} + [\mathbf{C}]\{\dot{\mathbf{D}}\}_{n+1} + \{\mathbf{R}^{\text{int}}\}_n + [\mathbf{K}_t]_n\{\Delta\mathbf{D}\} = \{\mathbf{R}^{\text{ext}}\}_{n+1} \tag{17.7-3}$$

Acceleration and velocity at time $(n + 1)\,\Delta t$, from Eqs. 11.13-4, are now substituted into Eq. 17.7-3, with $\{\mathbf{D}\}_{n+1} - \{\mathbf{D}\}_n = \{\Delta\mathbf{D}\}$. Thus

$$\left(\frac{1}{\beta\,\Delta t^2}[\mathbf{M}] + \frac{\gamma}{\beta\,\Delta t}[\mathbf{C}] + [\mathbf{K}_t]_n\right)\{\Delta\mathbf{D}\} = \{\mathbf{R}^{\text{ext}}\}_{n+1} - \{\mathbf{R}^{\text{int}}\}_n \tag{17.7-4}$$

$$+ [\mathbf{M}]\left\{\frac{1}{\beta\Delta t}\{\dot{\mathbf{D}}\}_n + \left(\frac{1}{2\beta} - 1\right)\{\ddot{\mathbf{D}}\}_n\right\} + [\mathbf{C}]\left\{\left(\frac{\gamma}{\beta} - 1\right)\{\dot{\mathbf{D}}\}_n + \Delta t\left(\frac{\gamma}{2\beta} - 1\right)\{\ddot{\mathbf{D}}\}_n\right\}$$

Because $[\mathbf{K}_t]$ changes, each new calculation of $\{\Delta\mathbf{D}\}$ according to Eq. 17.7-4 requires factorization of the coefficient matrix. An alternative form of the right-hand side is used in [11.3].

Next we *provisionally* update nodal d.o.f., to $\{\mathbf{D}\}_{n+1} = \{\mathbf{D}\}_n + \{\Delta\mathbf{D}\}$, obtain $\{\dot{\mathbf{D}}\}_{n+1}$ and $\{\ddot{\mathbf{D}}\}_{n+1}$ from Eqs. 11.13-4, and use an error measure such as described below before accepting the updated d.o.f. as correct. Using the provisional d.o.f., stresses can be updated, and used to compute $\{\mathbf{R}^{\text{int}}\}_{n+1}$ (Eq. 17.7-1 with subscripts $n + 1$). Hence from Eq. 11.2-11 at time $(n + 1)\,\Delta t$,

$$\{\mathbf{R}^{\text{err}}\}_{n+1} = \{\mathbf{R}^{\text{ext}}\}_{n+1} - [\mathbf{M}]\{\ddot{\mathbf{D}}\}_{n+1} - [\mathbf{C}]\{\dot{\mathbf{D}}\}_{n+1} - \{\mathbf{R}^{\text{int}}\}_{n+1} \tag{17.7-5}$$

An energy error can be defined as

$$W^{\text{err}} = \frac{1}{2}\{\Delta\mathbf{D}\}^T\Big(\{\mathbf{R}^{\text{err}}\}_n + \{\mathbf{R}^{\text{err}}\}_{n+1}\Big) \approx \Delta t\{\dot{\mathbf{D}}\}_{n+1}^T\{\mathbf{R}^{\text{err}}\}_{n+1} \tag{17.7-6}$$

to be applied for $n > 1$. In numerical examples [17.24], W^{err} is not allowed to exceed $10^{-6}\,W$, where W is the sum of current kinetic energy and the accumulated work done by external forces up to the current time. If the error tolerance is exceeded, $\{\mathbf{R}^{\text{err}}\}$ is added to $\{\mathbf{R}^{\text{ext}}\}_{n+1}$ in Eq. 17.7-4 and the calculation of $\{\Delta\mathbf{D}\}$ repeated, and repeated again if necessary to meet the error tolerance. Thus, within a time step we pursue "equilibrium iterations," as described in connection with Eqs. 17.2-4 and 17.2-5.

If error control is not used, $\{\mathbf{R}^{\text{err}}\}$ may become unbounded, and the solution will then diverge in a manner similar to divergence of the central-difference method with a time step larger than the critical value. If W^{err} is bounded throughout the analysis the trapezoidal rule algorithm ($\gamma = 1/2$, $\beta = 1/4$) is unconditionally stable [17.24], but it is not necessarily accurate if W^{err} is too large. Confidence in computed results is increased if substantially the same results are obtained when a smaller time step is used. Further discussion of energy-conserving algorithms appears in [17.25].

17.8 PROBLEMS OF GAPS AND CONTACT

The *contact problem* is a kind of geometrically nonlinear problem that arises when different structures, or different surfaces of a single structure, either come into contact or separate or slide on one another with friction. Contact forces, either gained or lost, must be determined in order to calculate structural behavior. The location and extent of contact may not be known in advance, and must also be determined. Usually, friction between contacting surfaces must be taken into account, and a representation other than the familiar Coulomb rule may be appropriate. Sometimes a flow of heat or electric current takes place at a contact, and may itself be the subject of analysis, or may have to be represented because it influences structural behavior. Problems may be quasi-static or time-dependent. In this section we merely introduce the subject area, which is extensive [17.3,17.26–17.29].

One type of contact problem is the shrink fit application discussed in Section 14.3, where nodes of mating FE structures line up and surfaces that come into contact can be

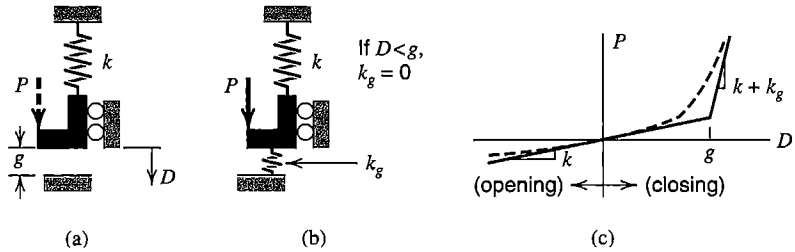

Figure 17.8-1. (a) Mathematical model: a rigid L-shaped block makes contact with a rigid horizontal surface when $D = g$. (b) Computational model: a stiff nonlinear spring is installed. (c) Load versus displacement behaviors of computational models.

identified in advance (however, in Section 14.3 it is merely *assumed* that there is no relative axial motion between mating parts). In Section 14.3 both contacting surfaces are regarded as deformable, as would also be appropriate in rolling contact of machine parts and threaded connections. In a metal forming process one surface might be regarded as rigid. Considerable detail may be needed in a contact zone if conditions in that zone are of concern. Much less local detail is needed if one needs only to discover the effect of a contact on the remainder of the structure. A formulation for contact problems that involve friction results in equations similar to plasticity equations in Section 17.4. Contact problems are nonlinear, often highly so because of large and sudden stiffness changes when contact is made.

The computational difficulty posed by a contact problem is suggested by the very simple problem shown in Fig. 17.8-1a. In the mathematical model, when $D = g$ and $P = kg$, a rigid block makes contact with a rigid horizontal surface. Further increases in P produce no further deflection. A computational model, Fig. 17.8-1b, has an added spring of stiffness k_g. This is a "mathematical spring" that need have no physical size. The spring is nonlinear because it has zero stiffness for $D < g$ but very large stiffness for $D > g$. The resulting load versus deflection behavior is shown by solid lines in Fig. 17.8-1c, and in equation form is

$$kD = P \qquad \text{for} \qquad P < kg \tag{17.8-1a}$$

$$(k + k_g)D = P \qquad \text{for} \qquad P > kg \tag{17.8-1b}$$

Thus the constraint $D \le g$ is approximately enforced in penalty fashion (Section 13.3). If k_g is too small, the gap "overcloses." On the other hand, too large a k_g may produce convergence difficulties or even "bouncing" convergence failure as the numerical solution alternates between $D < g$ and a contact condition in successive iterations.

As an alternative, the constraint can be enforced exactly by the method of Lagrange multipliers (Section 13.2). Thus $P = kD$ for $P < kg$, then

$$\begin{bmatrix} k & 1 \\ 1 & 0 \end{bmatrix} \begin{Bmatrix} D \\ \lambda \end{Bmatrix} = \begin{Bmatrix} P \\ g \end{Bmatrix} \qquad \text{for } P > kg \qquad \text{hence} \qquad \begin{aligned} D &= g \\ \lambda &= P - kg \end{aligned} \tag{17.8-2}$$

where $\lambda = P - kg$ is the force of constraint. Among computational options, an "augmented Lagrange method" is currently favored, in which penalty terms are added to the Lagrange method.

The dashed line in Fig. 17.8-1c results when the spring of stiffness k_g is always active and is defined as having an ad hoc nonlinear stiffness. This representation is intended to reduce abrupt stiffness changes associated with Eqs. 17.8-1 and 17.8-2. The dashed line may be realistic for joints in rock, where crushable material may exist between adjacent solid rock surfaces.

In general, surface nodes of one FE discretization do not become coincident with surface nodes of a second when contact is made. Consequently, if it happens that uniform contact pressure is physically realistic, the FE model may not provide it.

Contact algorithms in FE analysis may allow "contact elements" to be attached to the surface of one of two FE discretizations that are expected to come in contact. A contact element is not a conventional finite element. Its function is to sense contact and then supply a penalty stiffness or activate some other scheme for preventing or limiting interpenetration. Also, a gap algorithm can be applied "in reverse" to resist the further opening of a gap rather than its closing. Thus one can model the effect of a cable, which has very low stiffness when slack and much greater stiffness when taut.

17.9 GEOMETRIC NONLINEARITY

Geometric nonlinearity arises when deformations are large enough to alter the distribution or orientation of applied loads, or the orientation of internal resisting forces and moments. Relevant examples include elastic contact in a roller bearing, where contact pressure is spread over an increasing area as load increases, and a vaulter's pole, which resists load mainly with P/A stress or mainly with My/I stress directed tangent to the pole, depending on whether it is almost straight or is severely bent. Note that geometric nonlinearity may not involve large displacement. In the elastic contact problem, displacements are small, and in so-called "large displacement" plate analysis, lateral deflection may be less than the plate thickness. The essential difficulty of geometrically nonlinear analysis is that equilibrium equations must be written with respect to the *deformed* geometry—which is not known in advance.

Problems that display geometric nonlinearity may simultaneously display contact nonlinearity and plasticity, as for example in vehicle crash analysis. A discussion of geometric nonlinearity leads naturally to problems of instability and buckling, but we defer this discussion to Chapter 18. The present section is limited to simple concepts and procedures that may be applied to problems of geometric nonlinearity.

Green Strain. Of many strain measures used in large-deformation analysis, we introduce only one. (For each geometrically nonlinear strain measure there is a conjugate stress measure, such that stress times strain always provides the same strain energy.) Green strain has the following definition. Consider line segment AB in Fig. 17.9-1a, which moves from position AB to position $A'B'$ as a result of deformation. Its axial strain can be defined as

$$\varepsilon_G = \frac{1}{2}\left(\frac{ds^2 - ds_o^2}{ds_o^2}\right) \tag{17.9-1}$$

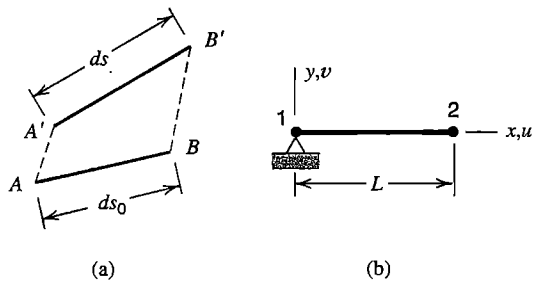

Figure 17.9-1. (a) Displacement and distortion of a line segment. (b) A bar hinged at node 1 and initially horizontal.

This expression leads to the following expressions for strain components in terms of the usual displacement components u, v, and w in coordinate directions x, y, and z [2.14, 3.2,4.3,17.2].

$$\varepsilon_x = u_{,x} + \frac{1}{2}\left(u_{,x}^2 + v_{,x}^2 + w_{,x}^2\right) \tag{17.9-2a}$$

$$\varepsilon_y = v_{,y} + \frac{1}{2}\left(u_{,y}^2 + v_{,y}^2 + w_{,y}^2\right) \tag{17.9-2b}$$

$$\varepsilon_z = w_{,z} + \frac{1}{2}\left(u_{,z}^2 + v_{,z}^2 + w_{,z}^2\right) \tag{17.9-2c}$$

$$\gamma_{xy} = u_{,y} + v_{,x} + (u_{,x}\,u_{,y} + v_{,x}\,v_{,y} + w_{,x}\,w_{,y}) \tag{17.9-2d}$$

$$\gamma_{yz} = v_{,z} + w_{,y} + (u_{,y}\,u_{,z} + v_{,y}\,v_{,z} + w_{,y}\,w_{,z}) \tag{17.9-2e}$$

$$\gamma_{zx} = w_{,x} + u_{,z} + (u_{,z}\,u_{,x} + v_{,z}\,v_{,x} + w_{,z}\,w_{,x}) \tag{17.9-2f}$$

in which the parenthetic expressions augment conventional linear expressions.

Let Eq. 17.9-2a be applied to plane motion of the bar in Fig. 17.9-1b, with $u_1 = v_1 = 0$ at node 1, displacements u_2 and v_2 of node 2, and linear interpolation of displacements along the bar. Thus

$$\begin{aligned} u &= (x/L)u_2 \\ v &= (x/L)v_2 \end{aligned} \qquad \text{yields} \qquad \varepsilon_x = \frac{u_2}{L} + \frac{1}{2}\left(\frac{u_2^2}{L^2} + \frac{v_2^2}{L^2}\right) \tag{17.9-3}$$

If $u_2 << L$ and $v_2 << L$ we obtain the conventional engineering definition, $\varepsilon_x = u_2/L$. For rigid-body rotation about node 1, no matter how large, $\varepsilon_x = 0$. As examples, consider a 90° rotation ($u_2 = -L$ and $v_2 = L$) or a 180° rotation ($u_2 = -2L$ and $v_2 = 0$).

The expression for ε_x in Eq. 17.9-3 corresponds to a "Lagrangian" description, in which displacements are referred to the *original* coordinate system. Thus in Fig. 17.9-1b, regardless of how much the bar may have rotated, node 2 of the bar is located by coordinates $x = L$ and $y = 0$, and horizontal coordinate x is used in displacement fields $u = (x/L)u_2$ and $v = (x/L)v_2$. Although the bar may have rotated a large amount, its axial strain is called ε_x and is defined by Eq. 17.9-3. In summary, in a Lagrangian formulation a structure is not described in terms of where it *is*, but in terms of where it originally *was*.

Corotational Formulation. Corotational coordinates may also be called "convected coordinates." A local coordinate system is attached to each element, and translates and rotates with the element as deformation proceeds. The global coordinate system remains fixed. Element deformation is decomposed into a rigid-body component, which is identical

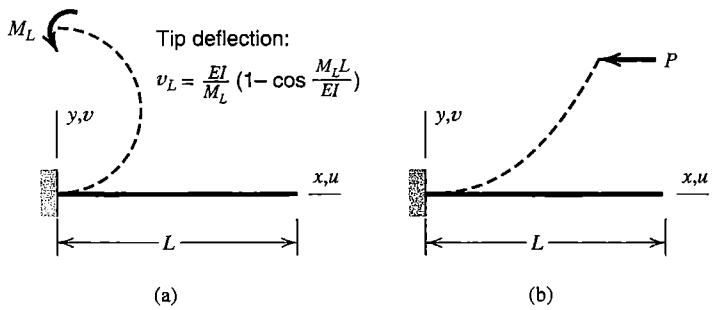

Figure 17.9-2. Large deformation in the xy plane of a cantilever beam under (a) tip moment, and (b) tip force P in the negative x direction.

to rigid-body motion of the local system, and a straining component that can be described by d.o.f. measured in the local system. Having separated the components, they can be addressed independently.

If elements are sufficiently small relative to the complexity of the deformation field, and do not change much in size and shape as deformation accumulates, then element matrices can be formulated *in the local system* using conventional theory for small strains and small rotations. Therefore, Green strain is not needed. After formulation, element matrices are coordinate-transformed so that they operate on global d.o.f., and assembled into the global stiffness matrix. Thus the global stiffness matrix, and global equilibrium equations, pertain to the deformed structural geometry. As this geometry is not known in advance, iterative solution is required. References include [17.2,17.3,17.30–17.32].

In this section we limit explanation of the method to time-independent plane problems of frames modeled by beam elements that resist stretching and bending. The material is assumed to remain linearly elastic. As simple applications, large-deflection behaviors of beams shown in Fig. 17.9-2 might be calculated. The restriction to plane motion makes it easy to establish a local coordinate system for each element and follow its motion. The analogous three-dimensional case is not nearly as simple, because large rotations do not combine in vectorial fashion [17.32]. This is easily shown by rotating a book through 90° angles about axes x, y, and z in that order, then rotating a second book through 90° angles about the axes in reverse order. Final orientations of the books differ.

Before describing a computational algorithm we explain the establishment of a local coordinate system, determination of forces applied to nodes by the deformed element, and transformation of these loads and the element stiffness matrix to global coordinates. In Fig. 17.9-3a, element 1-2 is shown in its original configuration, before any deformation of

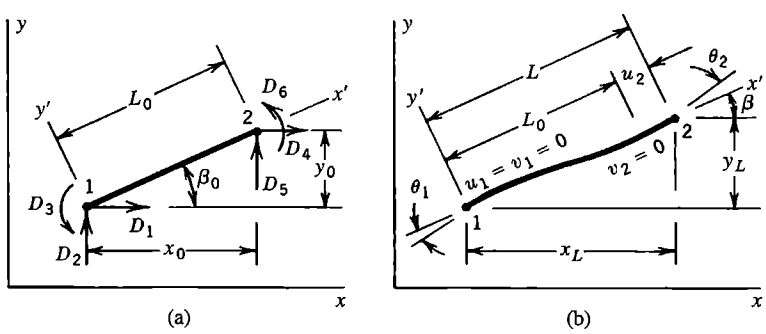

Figure 17.9-3. (a) Plane beam element before deformation, identifying subsequent nonzero global d.o.f. D_1 to D_6. (b) The same element after deformation. Nonzero local d.o.f. are θ_1, u_2, and θ_2.

the structure has taken place (thus for all elements that would be used to model the beams in Fig. 17.9-2, $\beta_0 = 0$). The same element, after deformation defined by global d.o.f. D_1 to D_6, is shown in Fig. 17.9-3b. Local system $x'y'$ moves with the element, with origin at node 1, and node 2 on the x' axis. Thus d.o.f. u_1, v_1, and v_2 are always zero in the local system. From original nodal locations and global d.o.f. D_1 to D_6 we must determine nonzero local d.o.f. θ_1, θ_2, u_2 and angle β of the x' axis. We presume that elements are small enough that $|\theta_1| << 1$ and $|\theta_2| << 1$.

After deformation, element length projections on global xy axes and orientation β of local axis x' are

$$x_L = x_0 + D_{41} \qquad y_L = y_0 + D_{52} \qquad \beta = \arctan(y_L/x_L) \tag{17.9-4a}$$

where

$$D_{41} = D_4 - D_1 \quad \text{and} \quad D_{52} = D_5 - D_2 \tag{17.9-4b}$$

Element d.o.f. in local system $x'y'$ are $\{\mathbf{d}'\} = \lfloor 0 \;\; 0 \;\; \theta_1 \;\; u_2 \;\; 0 \;\; \theta_2 \rfloor^T$, in which

$$\theta_1 = D_3 - (\beta - \beta_0) \qquad \theta_2 = D_6 - (\beta - \beta_0) \qquad u_2 = L - L_0 \tag{17.9-5a}$$

where $L^2 = x_L^2 + y_L^2$ and $L_0^2 = x_0^2 + y_0^2$. However, u_2 may have considerable cancellation error if computed as $u_2 = L - L_0$. An improved expression for numerical calculation is obtained by substituting from Eq. 17.9-4a in the L^2 expression, forming $L^2 - L_0^2$, and writing $L^2 - L_0^2 = (L - L_0)(L + L_0) = u_2(L + L_0)$. Thus [17.31]

$$u_2 = \frac{1}{L + L_0}\left[(2x_0 + D_{41})D_{41} + (2y_0 + D_{52})D_{52}\right] \tag{17.9-5b}$$

Because $u_2 << L$, the denominator could as well be written as $2L_0$.

In local system $x'y'$, nodal loads $\{\mathbf{r}'\}$ needed to equilibrate element deformations can be computed either from the local element stiffness matrix or from element stresses. In general,

$$\{\mathbf{r}'\} = [\mathbf{k}']\{\mathbf{d}'\} \quad \text{or} \quad \{\mathbf{r}'\} = \int \lfloor \mathbf{B} \rfloor^T \{\boldsymbol{\sigma}\}\, dV \tag{17.9-6}$$

In the present application $[\mathbf{k}']$ can be taken from Eq. 2.3-6, reduced to a 3 by 3 matrix if desired because u_1, v_1, and v_2 are always zero in Fig. 17.9-3b. Transformation through angle β to global coordinates is

$$[\mathbf{k}] = [\mathbf{T}]^T[\mathbf{k}'][\mathbf{T}] \quad \text{and} \quad \{\mathbf{r}\} = [\mathbf{T}]^T\{\mathbf{r}'\} \tag{17.9-7}$$

where $[\mathbf{T}]$ is as described in Section 8.3. Next the tangent-stiffness matrix and the array of internal nodal forces of the structure in its current configuration are obtained by the usual assembly process, with element arrays expanded to "structure size."

$$[\mathbf{K}_t] = \sum [\mathbf{k}] \quad \text{and} \quad \{\mathbf{R}^{\text{int}}\} = \sum \{\mathbf{r}\} \tag{17.9-8}$$

A summary of a computational algorithm is as follows. We assume that an external load has been applied, and a converged solution for that load has been obtained. Another increment of external load is now added, thus changing the net external load to $\{\mathbf{R}^{\text{ext}}\}$. The new configuration is to be determined by iterative calculation. Let i denote the iteration number. Tangent stiffness $[\mathbf{K}_t]_1$, global d.o.f. $\{\mathbf{D}\}_1$, and internal loads $\{\mathbf{R}^{\text{int}}\}_1$ are known from the existing converged solution. We solve for the displacement increment produced by the new increment of external load and update the solution, starting with $i = 1$.

$$\{\Delta\mathbf{D}\}_{i+1} = [\mathbf{K}_t]_i^{-1}\Big(\{\mathbf{R}^{\text{ext}}\} - \{\mathbf{R}^{\text{int}}\}_i\Big) \qquad \{\mathbf{D}\}_{i+1} = \{\mathbf{D}\}_i + \{\Delta\mathbf{D}\}_{i+1} \tag{17.9-9}$$

Using $\{\mathbf{D}\}_{i+1}$, updated arrays $[\mathbf{K}_t]_{i+1}$ and $\{\mathbf{R}^{\text{int}}\}_{i+1}$ can be established. We return to Eq. 17.9-9, now with $i = 2$. Iteration continues until convergence, when $\{\Delta\mathbf{D}\}_{i+1} \approx \{\mathbf{0}\}$ and $\{\mathbf{D}\}_{i+1}$ is such that the *deformed* structure has a configuration that can support loads $\{\mathbf{R}^{\text{ext}}\}$. The solution process is Newton-Raphson iteration that drives the load imbalance in Eq. 17.9-9 toward zero. One might choose to update $[\mathbf{K}_t]$ only when a new load increment is added, thus using the modified N-R method during iterations at a given load level.

Remarks. Other Problems. When stresses are such as to place the structure near a buckling condition, "stress stiffening" should be included. A simple example of stress stiffening is as follows (a more complete discussion appears in Chapter 18). In Fig. 17.9-4a, a spring-supported rigid bar carries axial load P. Lateral displacement due to added lateral force F is shown in Fig. 17.9-4b. By taking moments about node 1, with $v_2 << L$, we obtain

$$(k + k_\sigma)v_2 = F \qquad \text{where} \qquad k_\sigma = \frac{P}{L} \tag{17.9-10}$$

where k_σ is the "stress stiffness." The effect of a *compressive* force P is to decrease the net stiffness $k + k_\sigma$. Indeed $k + k_\sigma = 0$ when $P = -kL$, which defines a buckling condition. Despite the name "stress stiffening," the effect is of more concern when it reduces stiffness. In multiple-d.o.f. problems the analogue of k_σ is an element matrix $[\mathbf{k}_\sigma]$ that augments the conventional stiffness matrix $[\mathbf{k}]$. The effect of stress stiffening is automatically included in a formulation based on the complete Green strain expressions, but must be added to a corotational formulation by including $[\mathbf{k}_\sigma]$ matrices. In Fig. 17.9-2b, stress stiffening is an important part of the numerical model if load P is roughly equal to the column buckling load P_{cr}, but is much less important for yet larger values of P.

If the strains of Eqs. 17.9-2 are incorporated in stiffness matrix formulation, results can be written in the form $[\mathbf{k}] = [\mathbf{k}_0] + [\mathbf{k}_1] + [\mathbf{k}_2]$, where subscripts indicate the order of displacements contained. Thus $[\mathbf{k}_0]$ is the conventional small-displacement stiffness matrix,

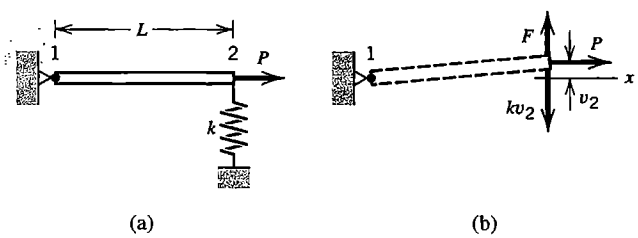

Figure 17.9-4. (a) Rigid bar supported by a linear spring at one end and carrying axial force P. (b) The rigid bar displaced by lateral force F.

independent of displacements. Matrix $[\mathbf{k}_1]$ contains displacements to the first power. If displacements in $[\mathbf{k}_1]$ are replaced by their associated stresses within the element, $[\mathbf{k}_1]$ can be identified as a stress stiffness matrix $[\mathbf{k}_\sigma]$. Matrix $[\mathbf{k}_2]$ contains displacements to the second power and is sometimes called an "initial-displacement stiffness matrix."

A geometrically nonlinear structure may have more than one equilibrium configuration. In Fig. 17.9-2b, for example, for $P > P_{cr}$ the structure is in equilibrium when bent up, bent down, or straight. The straight configuration is unstable equilibrium, but a numerical solution may converge to it. Especially near a buckling condition, small load increments may be appropriate, and small auxiliary lateral loads may be temporarily applied to start the structure moving in the desired direction. The column problem with $P > P_{cr}$ is a classic problem called the *elastica*. It provides a convenient test case. The problem was solved analytically by Euler in 1744. Theory and numerical results appear in [17.33,17.34].

An initially flat and unstressed membrane has no stiffness with which to resist lateral load. To avoid singularity in the first cycle of a tangent-stiffness analysis under lateral loading, one might temporarily impose a fictitious membrane stress so that a nonsingular stress stiffness matrix $[\mathbf{K}_\sigma]$ is present at the outset. The *actual* $[\mathbf{K}_\sigma]$, based on computed stresses, can be used in subsequent iterative cycles.

If deflections are quite large, as in inflating a balloon, there are several sources of nonlinearity. The material has a nonlinear stress-strain relation. Deflections are large and elements grow substantially in size; consequently external force on each element grows because the element grows, and the force changes in direction as the element rotates [17.35]. Because of element growth and distortion, Green strain may be needed and a corotational formulation may not be appropriate. References include [16.47–16.50].

Cable problems are roughly similar to membrane problems, because of the near-absence of flexural stiffness, the need to account for stress stiffening, and the possibility of large deflections. One might model a cable by many standard two-node elements, but such a model may have convergence difficulties because displacements may be on the order of the structure dimensions, and may be computationally expensive when it does succeed. Formulations based on exact catenary equations effectively represent an entire cable between support points as a single element, and seem more appropriate [17.36–17.38]. Extensions to dynamics are available [17.39]. By adding some flexural stiffness, a "long flexible beam element" is produced [17.40].

17.10 MODELING CONSIDERATIONS. REMARKS

As compared with linear analysis, nonlinear analysis is likely to be much more demanding of computer resources and the analyst's time and expertise. Goals of analysis may be more varied and there are more computational paths from which to choose. It is harder to foresee structural response. A good understanding of the response and how to compute it may develop only after performing trial analyses. Modeling advice of Section 1.5 and Chapter 10 remains applicable: try to understand the physical problem and concepts that underlie analysis procedures; study software documentation; expect to use a sequence of models; critically examine computed results; keep records of what is done in each analysis and what is learned from it; and so on. Before undertaking a nonlinear analysis one should be satisfied that it is really necessary.

Recall that the principle of superposition is not applicable to nonlinear problems. Double the load produces more, or less, than double the response. Results of different load cases cannot be algebraically or vectorially added. If different loads are applied sequentially, the final state of stress and deformation may depend on the order in which loads are applied.

Strategy. Much more than in linear analysis, the nature of a nonlinear problem may become clear only after trying to solve it. At the outset, the types and extent of nonlinearities may not be apparent, and even if they are, the appropriate elements, mesh layout, solution algorithm, and load steps may not be. An attempt to solve a nonlinear problem in "one go" is likely to fail, producing confusion and frustration. As always, it is desirable to anticipate FE results by doing a simplified preliminary analysis. Nonlinear analysis should make liberal use of test cases and pilot studies. Linear analysis should precede nonlinear analysis. Linear analysis can detect modeling blunders that would also afflict nonlinear analysis and can test the adequacy of the initial discretization. It may also suggest the location and extent of yielding, or what gaps are likely to open or close, or the approximate load and deformation state of actual collapse. If nonlinearity is produced by different sources, it may be possible to add them one at a time, so as to better understand their effects and how to treat them [2.14]. Initial models in a sequence may use a relatively coarse mesh, large load steps, and a liberal convergence tolerance. Subsequently all of these can be refined. Usually a final load must be approached in several steps. Too large a load step can slow convergence or produce an abrupt change in a load versus displacement plot that can be mistaken for actual physical behavior. Convergence failure may be due to a numerical difficulty, perhaps provoked by too large a load step, or it may correctly indicate that a collapse state has been reached.

Once past early trials, the remainder of the analysis should be planned, as to what is to be done in each stage and why. Each load step can produce as much output as a complete linear analysis, so it pays to anticipate what output to request and how it will be examined. Output should be examined in at least a cursory way after each load step. Status reports and warnings produced by the software should be taken seriously and understood. One may wish to go on to the next load level only if the analysis seems to be behaving satisfactorily. Accordingly, sufficient data should be stored to allow restart from the current load level. At restart the analyst may call for changes in load increment, convergence tolerance, or other aspects of the solution algorithm.

Modeling. Modeling suggestions noted in Chapters 1, 10, and 11 might be reviewed, as they contain suggestions applicable to nonlinear analysis. Miscellaneous suggestions are as follows. A follower load, which maintains the same orientation with respect to a deforming surface, must be identified as such so that it will not be treated as the more common case of a load whose orientation is fixed in space. Software may automatically treat fluid pressure as a follower load, but the analyst must verify, not assume, that this is so. Residual or initial stresses may be present before external load is applied. Residual stresses are appreciable in standard rolled steel beams and have the effect of reducing the external load at which yielding begins. Initial stresses may also arise because of assembly procedures, and, like stresses accumulated during deformation, may make a structure either stiffer or more flexible via the stress stiffening effect.

If a structure can be divided into linear and nonlinear parts, the linear parts can be represented by one or more substructures. Matrices that represent linear parts need not

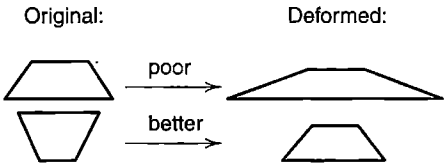

Figure 17.10-1. Possible distortion of element shape produced by large deformation.

change from one iteration to the next. As compared with a full model, fewer d.o.f. are needed because linear substructures can be represented by their attachment d.o.f. Most d.o.f. retained in the assembly can be in the nonlinear part, whose matrices *must* change from one iteration to the next.

Symmetry and antisymmetry conditions must be used with caution or avoided altogether. In a *linear* problem (other than buckling or vibration) symmetry of geometry, supports, elastic properties, and loads allows a portion of the structure to be modeled with symmetry conditions imposed. In a *non*linear problem, such symmetries may disappear as load increases, depending on details of the model and its subsequent loading.

Large strains may deform a mesh so greatly that well-shaped elements become poorly shaped. A revised initial mesh allows element shapes to remain acceptable despite large deformation (Fig. 17.10-1). It is also appropriate to refine the mesh as deformation accumulates. With large deformations and rotations, stresses and strains may have to be defined differently from what one is accustomed to in linear analysis. Computed stresses and strains may be reported with reference to global directions or rotated element directions. Software documentation must be studied to discover what output is presented and what it means.

With large displacements, the orientation of a spring or a bar that links nodes is controlled by positions of nodes to which it is connected. Thus, in Fig. 17.10-2 if it is intended that the link exert only forces normal to adjacent surfaces, such may not be the case after deformation. If the problem is one of contact, a better representation is provided by a frictionless contact element that resists interpenetration of adjacent surfaces. Note that *linear* analysis of the model in Fig. 17.10-2 is based on the original vertical orientation of the link, regardless of the magnitude of displacements computed.

In elastic-plastic analysis, the initial load step can be large if it takes the structure to the initiation of yield but not beyond. Detecting the onset of yield and tracking its spread demands an adequately refined mesh and adequate distribution of sampling points in

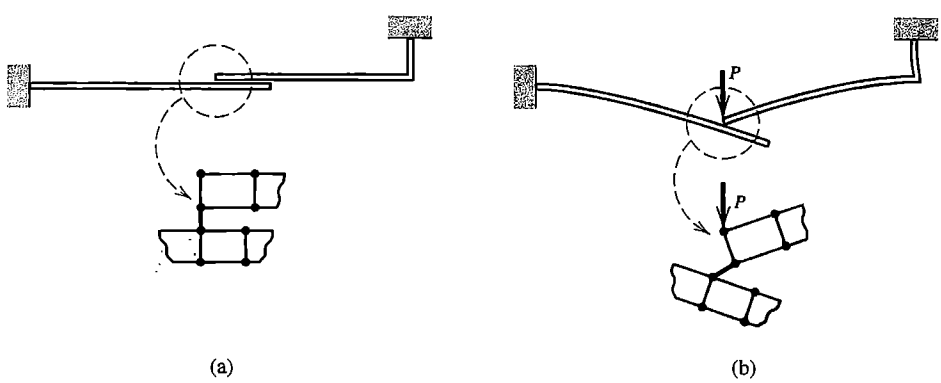

Figure 17.10-2. A spring or link connects nodes across a gap. (a) Before loading: link normal to adjacent surfaces. (b) After large deformation: link no longer normal to surfaces.

affected elements, with perhaps more than the usual number of points if elements become severely distorted. A part that bends requires sampling points on its surface, where yielding begins, and enough thickness-direction sampling points to permit a satisfactory calcuation of bending moment. The plastic strain increment $\Delta\lambda$ should not exceed about 5% in any load increment [8.7]. In examining results it is usually helpful to plot the deformed structure and also plot the extent of plastic action as load increases.

Elements can be activated or deactivated (called element "birth" and "death" in [8.7]). An element can be deactivated by setting its stiffness to nearly zero, as might be appropriate if calculation shows too large a stress in a material that crumbles. Mass remains unless it is also set to zero, as might be done for material that melts and flows away. Conversely, elements initially inactive might be activated when a structure grows, due to causes such as solidification, spray deposition, or filament winding.

Nonlinear dynamic analysis is usually performed by direct integration, as most software lacks devices needed to enable a modal method to deal with nonlinearity. In dynamic analysis of a contact problem by the central difference method, the allowable time step is substantially reduced if large stiffnesses are introduced, because they produce high natural frequencies. Regardless of the method of direct integration, perhaps 30 time steps per period of the highest frequency may be needed to prevent the algorithm from dissipating energy in a collision [8.7].

Convergence. Equilibrium conditions become satisfied only at convergence. Slow convergence, or failure to converge, may have various causes. In an elastic-plastic problem, concentrated loads and point supports are associated with high local stresses. In trying to resolve conditions at these locations, the algorithm may use many iterations, which are wasted if the region of interest lies elsewhere. The difficulty can be avoided by assigning a very high yield stress to elements adjacent to concentrated loads and point supports. Or, convergence failure may indicate that the structure has reached its load-carrying capacity, perhaps due to buckling, the exhaustion of strain-hardening capacity in plasticity, or a gap that opens permanently so that part of the structure "floats away." When approaching a collapse condition or a limit point (Fig. 17.2-3a), displacement increments become large. At a collapse condition or a limit point, and for some distance beyond it, tangent stiffness matrix $[\mathbf{K}_t]$ is not positive definite, usually provoking software to halt execution and issue an error message.

Various tactics are possible when convergence fails. The number of iterations usually allowed per load step may be roughly 20, or perhaps over 80 for a problem of gaps and contact. These limits can be increased. The size of load increments can be reduced. One can search for badly shaped elements, adopt a continuously curved stress-strain relation to replace a bilinear relation, or relax the convergence tolerance [10.37]. Alternative algorithms and combinations of computational paths that the software may provide can be explored. If convergence is eventually obtained, computed results must be carefully examined to see if the given problem has been altered by the computational tactics. If difficulties remain, expert advice can be sought.

A converged solution may not be a physically realistic solution. For a given load there may be more than one equilibrium configuration, and a numerical solution may converge to any one of them, even if the configuration is physically unstable.

Buckling. Buckling may be defined as a condition in which the stability of equilibrium is lost. The simplest elastic cases are those of initially straight columns under axial load

and initially flat plates under in-plane load, for which there is no lateral deflection until the solution "bifurcates" at the critical load. An actual structure is more likely to display lateral deflection from the outset of loading, perhaps nonlinearly related to load. Buckling may be by bifurcation or it may be associated with a limit point (Fig. 17.2-3a). There may or may not be postbuckling strength. Clearly, nonlinear analysis plays a role in buckling investigations. These matters are discussed in Chapter 18.

ANALYTICAL PROBLEMS

17.2-1 (a) In Fig. 17.2-1a, let $k = 0.2 - u$ and $P = 0.006$. Starting with $u = 0$, apply three cycles of the direct substitution algorithm.
(b) In the manner of Fig. 17.2-2, qualitatively sketch the progress of the algorithm on a plot of P versus u.
(c) What is the expression for tangent stiffness k_t in terms of u?

17.2-2 The sketch shows a nonlinear relation $P = P(D)$. In the following parts of this problem we pretend that P and dP/dD can be determined when D is known, but that an explicit expression for D in terms of P is not available. In each part, numerically solve for D by the method indicated, using data provided. Sketch the progress of each solution on a plot of P versus D.
(a) Let $P = 8$. What D is predicted by five cycles of N-R iteration, starting from $D = 0$?
(b) Let $P = 8$. What D is predicted by five cycles of modified N-R iteration, starting from $D = 3$?
(c) Repeat part (b) but use three cycles and update the tangent stiffness after the first cycle only.
(d) What D is predicted by four purely incremental steps (Euler's method) of $\Delta P = 2$, starting from $P = 1$ (where $D = 0.1111$) and going to $P = 9$?
(e) Repeat part (d) but include the force imbalance correction at every step.
(f) Let $P = 8$. What D is predicted by five cycles of the direct substitution algorithm, starting from $D = 0$?

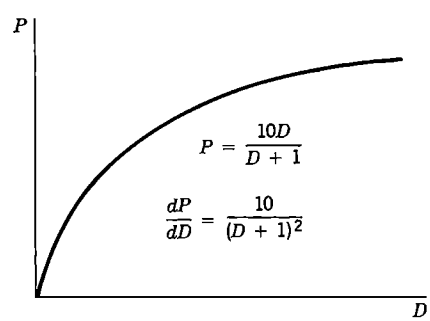

Problem 17.2-2

17.2-3 Apply the introductory remarks of Problem 17.2-2, now with reference to the hardening curve shown.
(a) Let $P = 0.8$. What D is predicted by five cycles of N-R iteration, starting from $D = 0$?
(b) Let $P = 3$. What D is predicted by five cycles of modified N-R iteration, starting from $D = 6$?
(c) Repeat part (b), but now update displacements according to Eq. 17.2-8, with $\mu = 0.6$.
(d) Repeat part (b) but use four cycles and update the tangent stiffness after the first cycle only.
(e) What D is predicted by three purely incremental steps (Euler's method) of $\Delta P = 1$, starting from $P = 1.5$ (where $D = 6$) and going to $P = 4.5$?
(f) Repeat part (e) but include the force imbalance correction at every step.
(g) Let $P = 4$. What D is predicted by four cycles of the direct substitution algorithm, starting from $D = 0$?

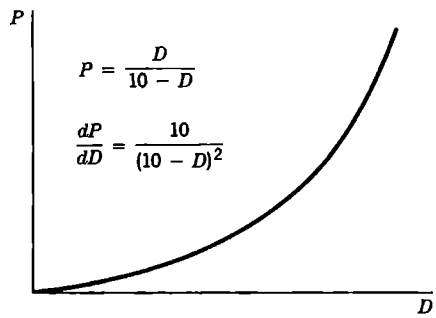

Problem 17.2-3

17.2-4 The bar shown is of length L when unstressed, where $L^2 = a^2 + c^2$. Let $a >> c$. When load P is zero, so is displacement D. The bar has axial stiffness AE/L, rolls without friction at B, and does not buckle as a column. Assume that the roller is constrained to remain in contact with the wall and in the plane of the figure.
(a) For $a >> c$, show that potential energy $\Pi_p = U - PD$ is

$$\Pi_p = (AE/8a^3)(D^2 - 2cD)^2 - PD.$$

(b) Show that equilibrium values of D are given by roots of the equation

$$P = (AE/2a^3)(2cD - D^2)(c - D).$$

(c) Determine expressions for the secant stiffness $k_{sec} = P/D$ and the tangent stiffness.
(d) Show that limit points are at $D = c(1 \pm 1/\sqrt{3})$.
(e) Let constants of the system be such that points A and F on the P versus D curve shown are at $P_A = 241$, $D_A = 0.211$, $P_F = 250$, and $D_F = 1.080$. After convergence at $P = 200$, P is increased to 250, and the following sequence of displacements D is generated by the N-R algorithm: 0.173, 0.219, 0.071, 0.143, 0.190, 0.249, 0.199, 0.294, 0.235, 0.175, 0.222, 0.108, 0.166, 0.210, 1.178, 1.096, 1.080, 1.080. Explain this path to convergence by sketching it on the P versus D plot.

(f) Sketch the path that would be taken by the *modified* N-R algorithm for P = 250, starting from D = 0.

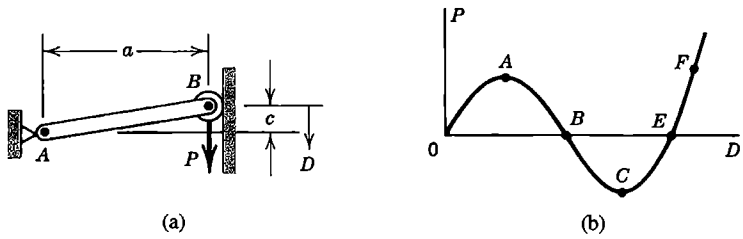

Problem 17.2-4

17.2-5 Let loads P_1 and P_2 be functions of displacements D_1 and D_2; that is, $P_1 = f_1(D_1,D_2)$ and $P_2 = f_2(D_1,D_2)$. Let D_A and D_B be exact values of D_1 and D_2 produced by loads P_A and P_B. Let D_A^* and D_B^* be approximations of D_A and D_B. Assume that $D_A = D_A^* + \Delta D_A$ and $D_B = D_B^* + \Delta D_B$. Derive the following equations of the N-R method:

$$\begin{bmatrix} \partial P_1/\partial D_1 & \partial P_1/\partial D_2 \\ \partial P_2/\partial D_1 & \partial P_2/\partial D_2 \end{bmatrix}_{D_A^*,D_B^*} \begin{Bmatrix} \Delta D_A \\ \Delta D_B \end{Bmatrix} = \begin{Bmatrix} P_A - f_1(D_A^*, D_B^*) \\ P_B - f_2(D_A^*, D_B^*) \end{Bmatrix}$$

17.2-6 Consider a function $g(x) = x - [f(x)/f'(x)]$, where a prime indicates differentiation with respect to x. To solve the equation $f(x) = 0$ by the N-R method, we seek a solution x^* that satisfies $x^* = g(x^*)$ by starting with a given x_0 and iterating; that is, $x_{i+1} = g(x_i)$. A second-order Taylor series for $g(x)$ is

$$g(x) = g(x^*) + g'(x^*)(x - x^*) + \frac{1}{2} g''(\bar{x})(x - x^*)^2$$

where $\bar{x}$ lies between x and x^*. Hence, show that the N-R method terminates quadratically.

17.3-1 The two bars shown are fixed to rigid walls at their outer ends and are welded together where load P is applied. Material behavior is shown in the second part of the sketch. Use a tangent-stiffness method. Starting from zero load, apply successive load increments $\Delta P = 20$, $\Delta P = 10$, and $\Delta P = -30$. Determine the corresponding values of displacement D. Show results on a plot of P versus D.

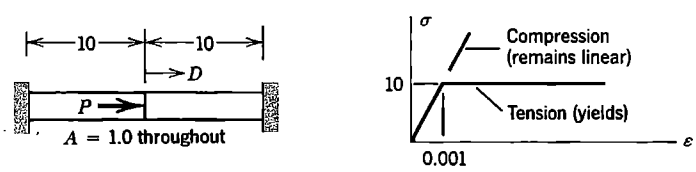

Problem 17.3-1

17.3-2 For the bar of Problem 17.3-1, apply the single load increment $\Delta P = 10$ after the yield-point value of load P is reached. Determine the value of displacement D predicted by five cycles of the initial-stiffness method.

17.3-3 Imagine that the horizontal bar in the sketch is rigid and is constrained to remain horizontal as load P and displacement v increase. The three vertical bars are elastic–perfectly plastic, with $A = 1$, $E = 1$, and $L = 2$. Bars have the respective yield-point loads $F_1 = 2$, $F_2 = 4$, and $F_3 = 6$. Use three steps of a tangent stiffness method to generate the P versus v relation. Scale the result of each step so that one bar begins to yield at the beginning of the next step.

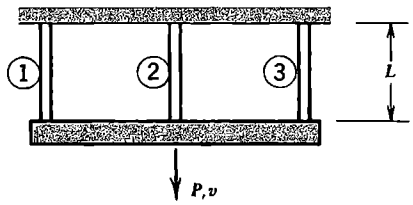

Problem 17.3-3

17.3-4 The weightless, rigid block B shown is pushed down in a frictionless guide by force P. The force versus deflection plot for each of the two supporting bars is given in the sketch. Solve for displacement D of block B due to a force $P = 24$ N, as follows.

(a) Determine the exact solution.

(b) Use a tangent-stiffness method. Let $\Delta P = 19$ N be the initial load increment, and $\Delta P = 5$ N be the second and final load increment.

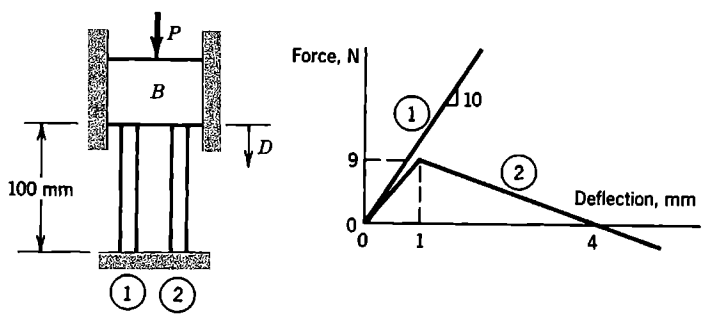

Problem 17.3-4

17.3-5 Assume that members of a truss carry only uniaxial stress, and that members in compression will buckle elastically at their critical loads without ever yielding. Assume that members in tension have elastic–perfectly plastic behavior. Outline a tangent-stiffness algorithm for computation of displacements produced by monotonically increasing loads.

17.3-6 Let a uniaxial stress-strain relation have the equation $\sigma^2 = 10^6\varepsilon$. Starting on the curve at $\sigma = 1000$, use the procedure of Eqs. 17.3-5 to 17.3-7 to determine the stress predicted by strain increment $\Delta\varepsilon = 3$. What is the percentage error of the result?

17.5-1 Assume that plastic action in bending is to be modeled and that several sampling points are used in the thickness direction (dimension d in the sketch).

(a) Why might a trapezoidal rule or a Simpson quadrature rule be preferable to a Gauss rule?

(b) Imagine that the stress distribution shown prevails across depth d of a beam of rectangular cross section. What is the percentage error of the computed bending moment M_c, if M_c is integrated from the stress distribution using a two-point Gauss rule? And what error for a three-point Gauss rule?
(c) Similarly, determine percentage errors associated with trapezoidal rules that use 3, 5, 7, and 9 sampling points.

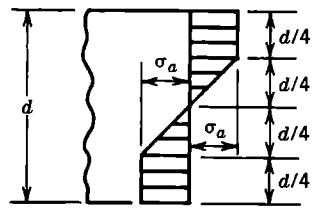

Problem 17.5-1

17.5-2 Imagine that a state of uniaxial stress produces a plastic strain increment $d\varepsilon^p$ in the direction of the stress. Show that Eq. 17.5-4 yields $d\varepsilon_e^p = d\varepsilon^p$ if the stress acts at 45° to x and y axes.

17.5-3 Describe steps of a tangent-stiffness solution algorithm in which each load increment causes a single additional sampling point to be brought to the initiation of yielding. Assume that load increases monotonically and that the material is elastic–perfectly plastic.

17.5-4 Consider an FE model of a plane structure. The material is isotropic, linearly elastic, and brittle: it cracks when tensile stress in any direction exceeds the value σ_t. Outline a plausible tangent-stiffness algorithm for predicting deformations caused by monotonically increasing load. How will a collapse condition be detected by this algorithm?

17.9-1 Consider axial strain of the bar in Fig. 17.9-1b. For what value of u_2/L does the engineering definition $\varepsilon_x = u_2/L$ differ by more than 5% from the ε_x definition of Green strain, Eq. 17.9-3? Consider (a) $v_2 = 0$, (b) $v_2 = u_2$, and (c) $v_2 = 100u_2$.

17.9-2 In Eqs. 17.9-2, let $w = 0$ to obtain expressions for Green strain in the xy plane. Show that these strains are zero for general rigid-body plane motion, Eq. 4.9-1 and Fig. 4.9-1.

17.9-3 Frame ABC is loaded by moment M_B at B, as shown. Assume that there is no yielding. For the following situations, sketch deflected shapes with sufficient care that they look different (if indeed they *are* different).

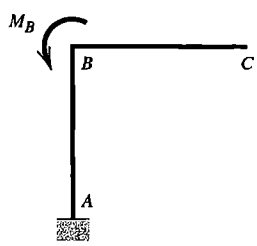

Problem 17.9-3

(a) The software is directed to scale up a linear (small deflection) solution by a large amount, so that corner B appears to rotate about 60°.
(b) M_B is large enough to produce an *actual* rotation of about 60° at corner B.
(c) Repeat parts (a) and (b), now assuming that a frictionless vertical wall prevents horizontal motion at B.

17.9-4 When load P is zero, displacement D shown in the sketch is zero and the springs are collinear and unstressed. Spring stiffness k_0 is constant.
(a) Determine the secant stiffness $k_{sec} = P/D$, in terms of k, L, and D.
(b) What is k_{sec} for small values of D ($D << L$)?
(c) What is the tangent stiffness for small values of D?
(d) Let $P = 1$ N, $L = 10$ mm, and $k_0 = 800$ N/mm. Then $D = 0.5$ mm. Now increase P by $\Delta P = 7$ N, and apply three cycles of N-R iteration to approximate the resulting D.

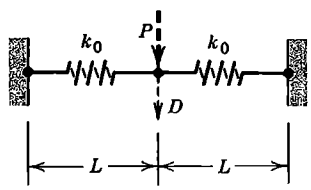

Problem 17.9-4

17.9-5 In Eq. 17.9-5b, show that $u_2 = 0$ for large rigid-body rotation of the element about node 1, starting from $\beta_0 = 0$ in Fig. 17.9-3.

17.9-6 In Fig. 17.9-2a, let the beam be uniform and linearly elastic. Derive the expression for y-direction tip displacement v_L as a function of M, L, E, and I, valid for any value of M. Show that this expression reduces to the standard linear relation when M is small.

17.9-7 When not loaded, the uniform slender beam shown has constant radius of curvature R, where $R >> a$. Its left end is tangent to the rigid horizontal surface. Vertical force F is then applied to the right end. If the beam remains linearly elastic, what value of F reduces curvature at the left to zero? For larger F, at what distance x does the beam depart from the horizontal surface? Use mechanics of materials methods.

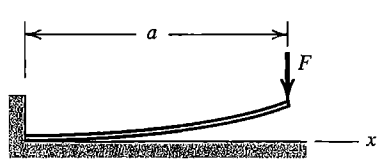

Problem 17.9-7

17.9-8 The angle frame shown has uniform flexural stiffness EI and may be regarded as weightless. At C, a small frictionless roller contacts a rigid vertical surface.

Determine the vertical deflection at C due to force F, using mechanics of materials methods. Assume that this deflection is small.

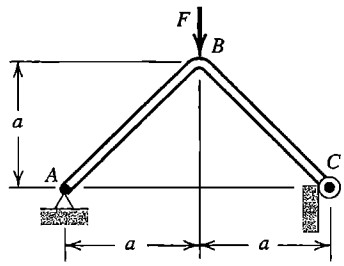

Problem 17.9-8

COMPUTATIONAL PROBLEMS

In the following problems compute significant values of displacement, moment or stress, as appropriate. Exploit symmetry where possible. When mesh refinement is used, estimate the maximum percentage error of results provided by the finest FE mesh. Where dimensions, loads, or material properties are not assigned, choose values that seem reasonable or convenient. When additional assumptions are required, clearly state what they are. Apply the analysis methodology suggested in Section 1.5.

C17.1 Numerically solve the analytical problems of (a) Problem 17.9-3, (b) Problem 17.9-7, and (c) Problem 17.9-8.

C17.2 Plane rectangular strips are loaded in tension. Apply uniform far-field stress σ as shown. Identify zones that become plastic as load increases [15.7].

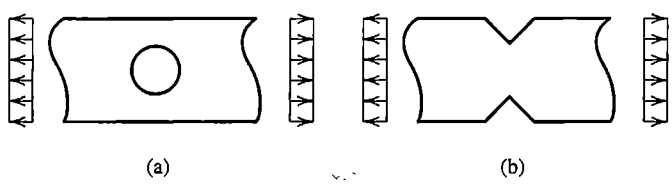

Problem C17.2

C17.3 Each of the plane bodies shown may be loaded by force F and/or moment M. Apply load sufficient to produce yielding. Investigate the extent of yielding and residual stresses upon unloading.

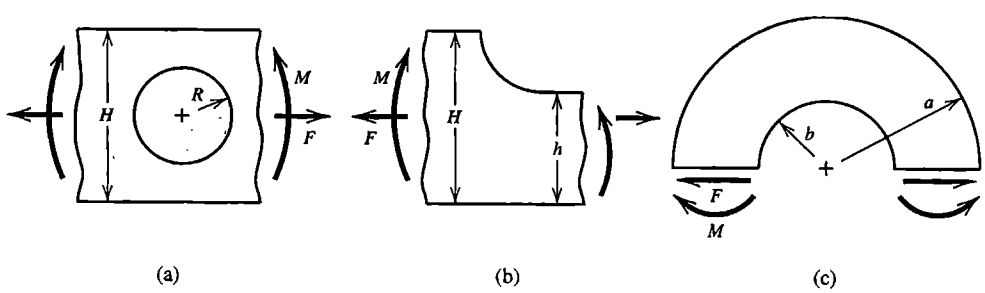

Problem C17.3

C17.4 (a) An elastic beam is loaded by lateral force P, as shown. The beam rests on an elastic foundation that can push against the beam but cannot pull on it. Investigate the extent and intensity of the contact pressure between beam and foundation.
(b) As in part (a), but now consider a rectangular plate that rests on an elastic foundation.

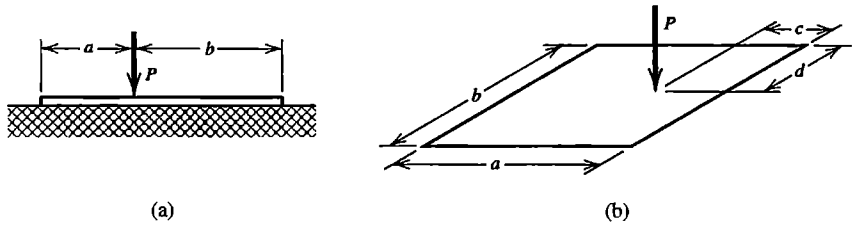

Problem C17.4

C17.5 Two plane elastic blocks are pressed together, as shown. Assume that friction between blocks is zero, and investigate the extent and intensity of contact pressure between blocks.

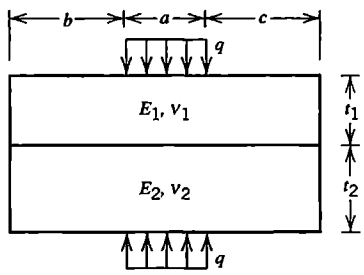

Problem C17.5

C17.6 The sketch represents an idealized drum brake problem. Curved elastic bar AB is hinged at A and is pressed against a rigid circular brake drum by force F. The drum rotates with angular velocity Ω. Investigate how torque required to rotate the drum varies with angle α, the coefficient of friction, and dimension h. Analyses may be repeated with the direction of rotation reversed.

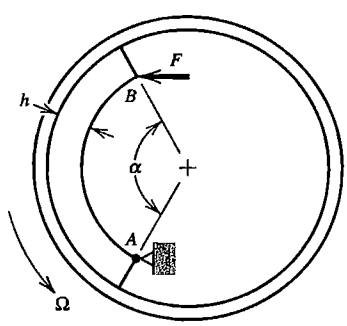

Problem C17.6

C17.7 A slender, elastic, circular ring is to be pulled through a smaller opening, as shown. The coefficient of friction between ring and opening is μ. Investigate the relation between force P and its displacement. Analysis may be repeated with P applied at A rather than at B.

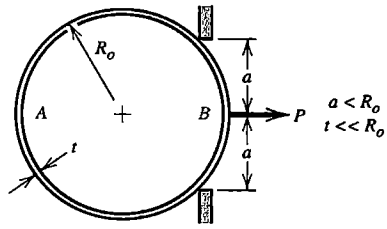

Problem C17.7

C17.8 (a) In Fig. 17.9-2a, investigate the relation between load M_L and displacement components of the beam tip.
(b) In Fig. 17.9-2b, investigate the relation between an x-parallel tip load P and displacement components of the beam tip when P exceeds the column buckling load. Add a very small lateral force to get lateral deflection started.
(c) Investigate deflections of an initially unstressed elastic membrane loaded by uniform lateral pressure p. (For a square membrane of side length L, thickness t, Poisson's ratio 0.3, and slopes everywhere much less than unity, [17.41] reports lateral center deflection $w_c = 0.2866t[(p/E)(L/t)^4]^{1/3}$)

C17.9 Investigate the force versus deflection relation of an archery bow.

C17.10 The sketch shows a thin, flat piece of metal fixed to a rigid support at $x = 0$. Initially, the structure midsurface and force P lie in the xy plane. Investigate large deflection elastic behavior that involves displacement components normal to the xy plane. Add a very small force normal to the xy plane to get lateral deflection started.

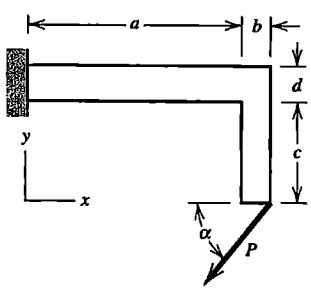

Problem C17.10

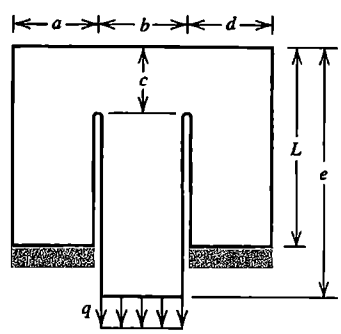

Problem C17.11

C17.11 The sketch shows a thin, flat piece of metal in a vertical plane. The vertical slots are very narrow. Lower ends of the outer legs are fixed and a vertical distributed load q is applied to the bottom of the center leg. Investigate large-deflection elastic behavior that involves displacement components normal to the plane of the paper. Load q may act either downward, as shown, or upward. Add a very small lateral force to get lateral deflection started.

CHAPTER 18

STRESS STIFFNESS AND BUCKLING

Matrices that account for the effect of membrane forces on bending stiffness are formulated. Applications include buckling problems. Various types of buckling problems are reviewed. Risks of oversimplifying the computational problem are noted.

18.1 INTRODUCTION. ENERGY CONSIDERATIONS

The term *stress stiffening* refers to the influence of membrane forces on lateral deflection, especially the lateral deflection associated with bending of beams, plates, and shells. Membrane forces, and associated membrane stresses, act along the axis of a bar or a beam and tangent to the midsurface of a plate or a shell. Despite the name "stress stiffening," resistance to bending deformation is *reduced* when membrane forces are compressive rather than tensile, as when a column carries compressive axial load.

Buckling means loss of the stability of an equilibrium configuration, without fracture or separation of the material or at least prior to it. *Bifurcation buckling* is the kind of buckling familiar from elementary column theory in which, for an axial compressive load of magnitude P_{cr}, called the *critical load,* the straight pre-buckling configuration ceases to be a stable state of equilibrium and an alternative buckled configuration is also possible at load P_{cr}. Buckling may also appear without bifurcation, as at a limit point, where there is no alternative and infinitesimally close equilibrium configuration (Fig. 17.2-3a).

Bifurcation buckling occurs when a member or structure converts membrane strain energy into bending strain energy with no change in externally applied load. In slender columns and thin plates or shells, membrane stiffness is much greater than bending stiffness, and large membrane strain energy can be stored with small deformations. When buckling occurs, comparatively large bending deformations are needed to absorb membrane strain energy released.

In FEA, the effects of membrane stresses on lateral deflection are accounted for by a matrix $[\mathbf{k}_\sigma]$, which augments the conventional stiffness matrix $[\mathbf{k}]$. Matrix $[\mathbf{k}_\sigma]$ is a function of an element's geometry, displacement field, and state of membrane stress. We call $[\mathbf{k}_\sigma]$ the *stress stiffness matrix.* Other names include "initial stress stiffness matrix" (although membrane stresses may change as deformation accumulates) and "geometric stiffness matrix" (although the conventional stiffness matrix also depends on geometry).

Matrix $[\mathbf{k}_\sigma]$ is independent of material properties and is therefore applicable despite possible anisotropy and yielding. Element $[\mathbf{k}_\sigma]$ matrices are assembled to provide structural matrix $[\mathbf{K}_\sigma]$, in the same way that conventional element stiffness matrices $[\mathbf{k}]$ are assembled to provide $[\mathbf{K}]$. Bifurcation buckling is an eigenvalue problem, having the same form as a vibrations problem, but with mass matrix $[\mathbf{M}]$ replaced by $[\mathbf{K}_\sigma]$.

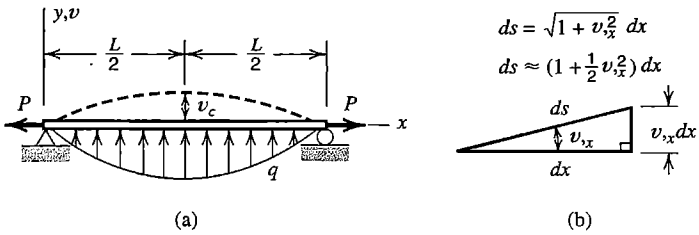

Figure 18.1-1.
(a) A uniform beam on simple supports.
(b) Geometric relations for a differential element of original length dx.

Analysis of a Beam-Column. To illustrate concepts of stress stiffness and bifurcation buckling calculation, we consider a simply supported beam (Fig. 18.1-1a). Axial force P, positive in tension in this example, is regarded as imposed at the outset, perhaps by a change in temperature while ends of the bar are not allowed to move axially. An analysis based on energy concepts is as follows.

For small lateral displacement $v = v(x)$, strain energy in bending is given by the standard expression in terms of curvature $v_{,xx}$.

$$U_b = \frac{1}{2}\int_0^L EI_z v_{,xx}^2\, dx \tag{18.1-1}$$

Imagine that $v = v(x)$ takes place without any axial displacement u. Each differential length dx becomes a new differential length ds, where $ds > dx$. The expression for ds, and an approximation based on the first two terms of a binomial expansion and valid for $|v_{,x}| << 1$, are shown in Fig. 18.1-1b. Axial membrane strain in the bar is therefore

$$\varepsilon_m = \frac{ds - dx}{dx} = \frac{ds}{dx} - 1 \qquad \text{hence} \qquad \varepsilon_m \approx \left(1 + \frac{1}{2}v_{,x}^2\right) - 1 = \frac{1}{2}v_{,x}^2 \tag{18.1-2}$$

Equation 17.9-2a, for ε_x based on Green strain, also gives $v_{,x}^2/2$ when v is the only displacement.

During small lateral displacement, axial force P remains essentially constant. As each elemental length dx lengthens an amount $\varepsilon_m\, dx$, tensile force P it carries does work, and stores strain energy, in the amount $P\varepsilon_m\, dx$. Thus the change in membrane energy is

$$U_m = \int_0^L P\varepsilon_m\, dx \quad \text{or} \quad U_m = \frac{1}{2}\int_0^L P v_{,x}^2\, dx \tag{18.1-3}$$

Let us assume that v varies as a half sine wave, $v = v_c \sin(\pi x/L)$, where v_c is the center deflection. Thus

$$U_b = \frac{\pi^4 EI_z}{4L^3} v_c^2 \qquad U_m = \frac{\pi^2 P}{4L} v_c^2 \tag{18.1-4}$$

If lateral load is also a half sine wave, $q = q_c \sin(\pi x/L)$, total potential is

$$\Pi_p = U_b + U_m + \Omega \qquad \text{where} \qquad \Omega = -\int_0^L vq\, dx = -\frac{q_c L}{2} v_c \tag{18.1-5}$$

The equilibrium state is given by $d\Pi_p/dv = 0$, from which

$$v_c = \frac{q_c L}{2(k + k_\sigma)} \qquad \text{where} \qquad k = \frac{\pi^4 EI_z}{2L^3} \quad \text{and} \quad k_\sigma = \frac{\pi^2 P}{2L} \tag{18.1-6}$$

Lateral deflection may be either decreased or increased by axial load P, depending on whether P is tensile or compressive.

Buckling occurs when P is such that v_c can be nonzero while $q_c = 0$. In other words, the effective flexural stiffness is reduced to zero when $P = P_{cr}$. From the equation $k + k_\sigma = 0$ we obtain $P_{cr} = -\pi^2 EI_z/L^2$, which is the classical Euler buckling load. Mathematically, we have solved the single-d.o.f. eigenvalue problem $(k + k_\sigma)v_c = 0$.

The same critical load is given by the following energy argument. When the infinitesimal lateral displacement of the buckling mode occurs, membrane energy is exchanged for bending energy without any work being done by applied loads. Thus

$$U_m + U_b = 0 \qquad \text{yields} \qquad P_{cr} = -\frac{\pi^2 EI_z}{L^2} \tag{18.1-7}$$

Caution. Imagine now that axial force P is not known *a priori*. It could be obtained as $P = AE\varepsilon_m$, where axial membrane strain ε_m is calculated from axial d.o.f. While this procedure is not needed with the simple beam example of Fig. 18.1-1a, it can be applied to a more complicated problem where membrane stresses are not known *a priori*, such as an irregularly shaped flat plate loaded by an irregular distribution of in-plane forces. After membrane stresses have been calculated by plane stress analysis, $[\mathbf{k}_\sigma]$ matrices can be constructed and used for buckling analysis or for response to lateral load.

However, this two-stage procedure is appropriate only if there is little or no coupling between membrane deformation and bending deformation. Such is likely to be the case only for initially straight columns and initially flat plates. Consider Fig. 18.1-2, in which initial imperfection e designates slight initial curvature or slight eccentricity of the compressive load P. The computed buckling load $P_{cr} = \pi^2 EI/L^2$ is correct only if $e = 0$ in the physical problem. As e increases, membrane and bending deformations become increasingly coupled, the column displays large displacements rather than buckling, and P_{cr} becomes less useful as a predictor of behavior. For most practical problems in which

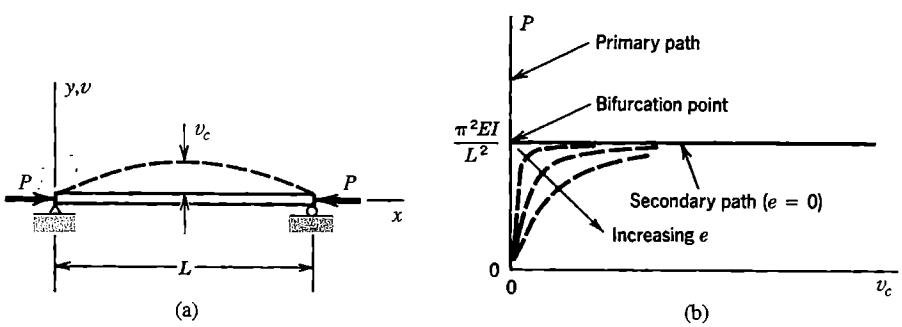

Figure 18.1-2. (a) Bar subjected to compressive axial load P. (b) The effect of an initial imperfection e.

buckling appears possible, membrane and bending actions are coupled, and linear bifurcation analysis may seriously overestimate the actual collapse load. Usually, nonlinear analysis is more appropriate, so that the coupling of membrane and bending actions is taken into account from the outset. Eventual collapse may be associated with bifurcation or with reaching a limit point, or collapse might be defined as excessive deflection.

These cautionary remarks do not obviate the usefulness of $[\mathbf{k}_\sigma]$ in analysis, whether $[\mathbf{k}_\sigma]$ acts to reduce bending stiffness (as in collapse analysis) or increase it (as in a spinning structure where there are tensile membrane stresses).

Additional Terminology. A *primary path* (Fig. 18.1-2b) is the original load-displacement line or curve and its extension. The *secondary path* is the alternative path that originates when the critical load is reached. The two paths intersect at the *bifurcation point.* Past the bifurcation point, the primary path is unstable: although it is possible mathematically, a real structure will follow the secondary path instead. If the secondary path rises, the structure has post-buckling strength. The secondary path shown in Fig. 18.1-2b is shown as a horizontal straight line because small-displacement assumptions are made in elementary column buckling analysis. Actually, the path is initially horizontal, then curves upward. A *limit point,* points L in Fig. 17.2-3a, is a maximum on a load-displacement curve. It is not a bifurcation point because there is no immediately adjacent equilibrium configuration. When a limit-point load is reached under increasing load, *snap-through buckling* occurs, as the structure assumes a new configuration by suddenly moving along path $L1$ or $L2$ in Fig. 17.2-3a. A *collapse load* is the maximum load a structure can sustain without gross deformation. It may be greater or less than a computed bifurcation buckling load. In common usage, *critical load* may refer to bifurcation load, limit-point load, or collapse load. Further remarks about these matters appear in Section 18.7.

18.2 BAR AND BEAM ELEMENTS

Let a straight bar or beam lie along the x axis, and let lateral displacement v and rotation $v_{,x}$ in the xy plane be determined by nodal d.o.f. $\{\mathbf{d}\}$. Thus

$$v = \lfloor \mathbf{N} \rfloor \{\mathbf{d}\} \quad \text{and} \quad v_{,x} = \lfloor \mathbf{G} \rfloor \{\mathbf{d}\} \qquad \text{where} \qquad \lfloor \mathbf{G} \rfloor = \frac{d}{dx} \lfloor \mathbf{N} \rfloor \tag{18.2-1}$$

Membrane strain energy U_m associated with lateral displacement v is given by Eq. 18.1-3. With axial force P considered positive in tension,

$$U_m = \frac{1}{2}\int_0^L P v_{,x}^2 \, dx = \frac{1}{2}\int_0^L v_{,x}^T P v_{,x} \, dx = \frac{1}{2}\{\mathbf{d}\}^T [\mathbf{k}_\sigma] \{\mathbf{d}\} \tag{18.2-2}$$

where stress stiffness matrix $[\mathbf{k}_\sigma]$ is given by

$$[\mathbf{k}_\sigma] = \int_0^L \lfloor \mathbf{G} \rfloor^T \lfloor \mathbf{G} \rfloor P \, dx \tag{18.2-3}$$

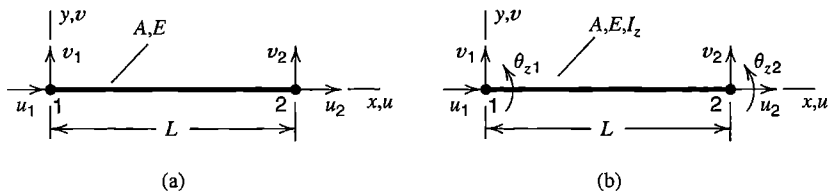

Figure 18.2-1. Plane bar and beam elements and their nodal d.o.f. A = cross-sectional area, E = elastic modulus, I_z = centroidal moment of inertia of A.

If lateral displacement is also allowed in the z direction, additional d.o.f. are needed in $\{\mathbf{d}\}$ and displacement w is included in calculations. The resulting $[\mathbf{k}_\sigma]$ matrices are very similar to those for plane deformation but contain more terms.

Bar Element. For plane motion of a bar, Fig. 18.2-1a,

$$v = \left\lfloor \frac{L-x}{L} \quad \frac{x}{L} \right\rfloor \begin{Bmatrix} v_1 \\ v_2 \end{Bmatrix} \qquad \text{hence} \qquad \begin{aligned} \lfloor \mathbf{G} \rfloor &= \frac{1}{L}\lfloor -1 \quad 1 \rfloor \\ [\mathbf{k}_\sigma] &= \frac{P}{L}\begin{bmatrix} 1 & -1 \\ -1 & 1 \end{bmatrix} \end{aligned} \tag{18.2-4}$$

in which axial force P is considered positive in tension. If z-direction motion is also allowed, additional P/L terms appear, associated with nodal d.o.f. w_1 and w_2. Or, if axial d.o.f. u_1 and u_2 are allowed with plane motion, zeros appear on the diagonal. Respectively, these results are

For $\{\mathbf{d}\} = \lfloor v_1 \; w_1 \; v_2 \; w_2 \rfloor^T$: For $\{\mathbf{d}\} = \lfloor u_1 \; v_1 \; u_2 \; v_2 \rfloor^T$:

$$[\mathbf{k}_\sigma] = \frac{P}{L}\begin{bmatrix} 1 & 0 & -1 & 0 \\ 0 & 1 & 0 & -1 \\ -1 & 0 & 1 & 0 \\ 0 & -1 & 0 & 1 \end{bmatrix} \qquad [\mathbf{k}_\sigma] = \frac{P}{L}\begin{bmatrix} 0 & 0 & 0 & 0 \\ 0 & 1 & 0 & -1 \\ 0 & 0 & 0 & 0 \\ 0 & -1 & 0 & 1 \end{bmatrix} \tag{18.2-5}$$

Beam Element. With deformation restricted to the xy plane, Fig. 18.2-1b, shape functions in $\lfloor \mathbf{N} \rfloor$ appear in Fig. 2.3-1 and in Fig. 3.2-4. Hence $\lfloor \mathbf{G} \rfloor$ is obtained from Eq. 18.2-1, and for P independent of x and positive in tension, Eq. 18.2-3 yields

$$[\mathbf{k}_\sigma] = \frac{P}{30L}\begin{bmatrix} 36 & 3L & -36 & 3L \\ 3L & 4L^2 & -3L & -L^2 \\ -36 & -3L & 36 & -3L \\ 3L & -L^2 & -3L & 4L^2 \end{bmatrix} \qquad \text{for} \qquad \{\mathbf{d}\} = \begin{Bmatrix} v_1 \\ \theta_{z1} \\ v_2 \\ \theta_{z2} \end{Bmatrix} \tag{18.2-6}$$

This result can be expanded in the same fashion as seen in Eqs. 18.2-5 if z-direction deformation or axial deformation is allowed.

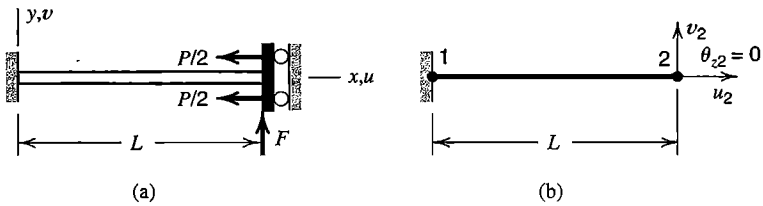

Figure 18.2-2. (a) Cantilever beam with zero rotation at the right end. (b) One-element FE model.

Force P might be regarded as a function of x for a column loaded by its own weight, but in practice it is more likely that axial force variation would be modeled by step changes in P from one element to the next.

In a beam of thin-walled open cross section, whether the beam is axially or laterally loaded, buckling usually occurs by a combination of twisting and bending. The stress stiffness matrix of Eq. 18.2-6 accounts only for flexural behavior of an initially straight prismatic beam. References for stress stiffening effects in beam elements with twisting and cross sectional warping include [15.8,18.1–18.4]. Rather than use special beam elements, a shell-element model like that in Fig. 10.2-1c might be used, although it has many more d.o.f.

Example. The following simple example illustrates use of $[\mathbf{k}_\sigma]$ in displacement calculation. Let a uniform beam be fixed at the left end and prevented from rotation at the right end, Fig. 18.2-2a. Displacements are confined to the xy plane. Axial compressive load P and lateral load F are applied. Deflection at the right end is to be calculated.

The net stiffness matrix is $[\mathbf{k}] + [\mathbf{k}_\sigma]$, where $[\mathbf{k}]$ for a plane beam without transverse shear deformation is stated in Eq. 2.3-5 and in Eq. 3.3-14. With d.o.f. u_2 and v_2 both retained, axial stiffness AE/L appears in $[\mathbf{k}]$. For $[\mathbf{k}_\sigma]$, we may use either the second of Eqs. 18.2-5 or Eq. 18.2-6, expanded to include axial d.o.f. The latter choice provides greater accuracy. For illustration we begin with the former. Thus, with P negative because it is compressive,

$$\left(\begin{bmatrix} AE/L & 0 \\ 0 & 12EI_z/L^3 \end{bmatrix} + \begin{bmatrix} 0 & 0 \\ 0 & -P/L \end{bmatrix}\right)\begin{Bmatrix} u_2 \\ v_2 \end{Bmatrix} = \begin{Bmatrix} -P \\ F \end{Bmatrix} \tag{18.2-7}$$

The equations for u_2 and v_2 are uncoupled. They yield

$$u_2 = -\frac{PL}{AE} \qquad v_2 = \frac{FL^3/12EI_z}{1 - PL^2/12EI_z} \tag{18.2-8}$$

If instead $[\mathbf{k}_\sigma]$ is taken from Eq. 18.2-6, we obtain $u_2 = -PL/AE$ and

$$\left(\frac{12EI_z}{L^3} - \frac{6P}{5L}\right)v_2 = F \qquad \text{from which} \qquad v_2 = \frac{FL^3/12EI_z}{1 - PL^2/10EI_z} \tag{18.2-9}$$

We see that v_2 is increased by compressive P, and according to Eq. 18.2-9 becomes infinite when $P = 10EI_z/L^2$, which is the predicted buckling load (the exact buckling load is $\pi^2 EI_z/L^2$).

18.3 PLATE ELEMENTS

For a flat plate, as for a straight bar or beam, an expression for $[\mathbf{k}_\sigma]$ can be obtained by examination of work done by constant membrane forces as they act through displacements associated with small lateral deflection. Membrane forces N_x, N_y, and N_{xy} are forces per unit length. They are shown in Fig. 18.3-1 and are stated in terms of membrane stresses σ_x, σ_y, and τ_{xy} by Eqs. 16.1-1. We presume that membrane forces are known, either *a priori* or from previous plane stress analysis.

Membrane strains associated with lateral deflection $w = w(x,y)$ of the plate are given by terms in Eqs. 17.9-2.

$$\varepsilon_x = \frac{1}{2}w_{,x}^2 \qquad \varepsilon_y = \frac{1}{2}w_{,y}^2 \qquad \gamma_{xy} = w_{,x}w_{,y} \tag{18.3-1}$$

The change in membrane strain energy associated with constant membrane forces and the strains of Eqs. 18.3-1 is written in a form analogous to Eq. 18.2-2 [17.33]:

$$U_m = \int\left(\frac{1}{2}N_x w_{,x}^2 + \frac{1}{2}N_y w_{,y}^2 + N_{xy}w_{,x}\,w_{,y}\right) dA \tag{18.3-2a}$$

or

$$U_m = \frac{1}{2}\iint \begin{Bmatrix} w_{,x} \\ w_{,y} \end{Bmatrix}^T \begin{bmatrix} N_x & N_{xy} \\ N_{xy} & N_y \end{bmatrix} \begin{Bmatrix} w_{,x} \\ w_{,y} \end{Bmatrix} dx\,dy = \frac{1}{2}\{\mathbf{d}\}^T[\mathbf{k}_\sigma]\{\mathbf{d}\} \tag{18.3-2b}$$

For an element that has n d.o.f.,

$$w = \underset{n\times 1}{\lfloor \mathbf{N} \rfloor\{\mathbf{d}\}} \qquad \text{yields} \qquad \begin{Bmatrix} w_{,x} \\ w_{,y} \end{Bmatrix} = \underset{2\times n}{[\mathbf{G}]}\,\{\mathbf{d}\} \tag{18.3-3}$$

Equations 18.3-2b and 18.3-3 yield

$$[\mathbf{k}_\sigma] = \iint [\mathbf{G}]^T \begin{bmatrix} N_x & N_{xy} \\ N_{xy} & N_y \end{bmatrix} [\mathbf{G}]\,dx\,dy \tag{18.3-4}$$

where integration spans the element area. If the element is of the isoparametric family, shape functions in $\lfloor \mathbf{N} \rfloor$ are expressed in terms of dimensionless coordinates ξ and η, and we must invoke Jacobian matrix $[\mathbf{J}]$ of Eq. 6.2-5. Thus

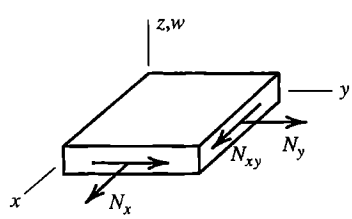

Figure 18.3-1. Differential element of a flat plate, showing membrane forces N_x, N_y, and N_{xy}.

$$\begin{Bmatrix} w_{,\xi} \\ w_{,\eta} \end{Bmatrix} = [\mathbf{G}_I]\{\mathbf{d}\} \quad \text{and} \quad \begin{Bmatrix} w_{,x} \\ w_{,y} \end{Bmatrix} = [\mathbf{J}]^{-1}\begin{Bmatrix} w_{,\xi} \\ w_{,\eta} \end{Bmatrix} \tag{18.3-5}$$

where $[\mathbf{G}_I]$ contains derivatives of the shape functions with respect to ξ and η. With $dx\,dy = J\,d\xi\,d\eta$, where J is the determinant of $[\mathbf{J}]$, Eqs. 18.3-2b and 18.3-5 yield

$$[\mathbf{k}_\sigma] = \int_{-1}^{1}\int_{-1}^{1} [\mathbf{G}_I]^T[\mathbf{J}]^{-T}\begin{bmatrix} N_x & N_{xy} \\ N_{xy} & N_y \end{bmatrix}[\mathbf{J}]^{-1}[\mathbf{G}_I]\,J\,d\xi\,d\eta \tag{18.3-6}$$

For triangular plate elements, a formulation for $[\mathbf{k}_\sigma]$ can be based on element boundary displacements alone [18.5]. It is slightly less accurate than a $[\mathbf{k}_\sigma]$ based on displacements within an element, but requires much less time to compute, which may be important in a nonlinear problem. A diagonal form of $[\mathbf{k}_\sigma]$ is also available [18.6].

18.4 A GENERAL FORMULATION

In Sections 18.2 and 18.3, each type of element is treated as a special case. It is desirable to also have a general formula for $[\mathbf{k}_\sigma]$, analogous to the formula for the conventional stiffness matrix (stated in Eqs. 3.3-7 and in Eq. 4.8-15a), that may be specialized to a particular geometry and displacement field. Such a formula is developed in the present section. As in preceding Sections 18.1 to 18.3, the resulting $[\mathbf{k}_\sigma]$ is limited to situations in which displacement gradients are much less than unity.

As an example problem in which such a formulation is useful, imagine that an I beam carries axial load and that its web and flanges are each modeled by flat shell elements. Let lateral deflection occur in a direction normal to the plane of the web. The $[\mathbf{k}_\sigma]$ developed in Section 18.3 would account for stress-stiffening effects on plate elements in the web, but not on plate elements in the flanges, which deform in their own planes. Additional stress stiffness terms are needed for these elements.

Imagine that a strain state $\{\boldsymbol{\varepsilon}_0\}$ and associated stresses $\{\boldsymbol{\sigma}_0\}$ prevail. Assume that $\{\boldsymbol{\sigma}_0\}$ remains constant as additional strains $\{\boldsymbol{\varepsilon}\}$ occur. Strains $\{\boldsymbol{\varepsilon}\}$ correspond to the second stage of the two-stage analysis summarized following Eq. 18.1-7. We assume that strains are small enough that the engineering definition of stress may still be used. Virtual work associated with the additional strains is

$$\int \{\boldsymbol{\varepsilon}\}^T\{\boldsymbol{\sigma}_0\}\,dV \qquad \text{where} \qquad \begin{aligned} \{\boldsymbol{\varepsilon}\}^T &= \begin{bmatrix} \varepsilon_x & \varepsilon_y & \cdots & \gamma_{zx} \end{bmatrix} \\ \{\boldsymbol{\sigma}_0\} &= \begin{bmatrix} \sigma_{x0} & \sigma_{y0} & \cdots & \tau_{zx0} \end{bmatrix}^T \end{aligned} \tag{18.4-1}$$

With $\{\boldsymbol{\varepsilon}\}$ the Green strains of Eqs. 17.9-2, the product $\{\boldsymbol{\varepsilon}\}^T\{\boldsymbol{\sigma}_0\}$ first displays the terms $u_{,x}\sigma_{x0} + v_{,y}\sigma_{y0} + \cdots$. These terms lead to nodal load terms associated with axial force in a column, or with membrane forces in a plate, and so on. Subsequent higher-order terms are associated with strain energy analogous to U_m in Eqs. 18.2-2 and 18.3-2. Here we call this energy U_σ, where

$$U_\sigma = \int \left[\frac{1}{2}(u_{,x}^2 + v_{,x}^2 + w_{,x}^2)\,\sigma_{x0} + \cdots + (u_{,z}u_{,x} + v_{,z}v_{,x} + w_{,z}w_{,x})\,\tau_{zx0} \right] dV \qquad (18.4\text{-}2)$$

If we define

$$\{\boldsymbol{\delta}\} = \lfloor\, u_{,x} \;\; u_{,y} \;\; u_{,z} \;\; v_{,x} \;\; v_{,y} \;\; v_{,z} \;\; w_{,x} \;\; w_{,y} \;\; w_{,z} \,\rfloor^T \qquad (18.4\text{-}3)$$

then Eq. 18.4-2 can be written in the form

$$U_\sigma = \frac{1}{2}\int \{\boldsymbol{\delta}\}^T \begin{bmatrix} \mathbf{s} & \mathbf{0} & \mathbf{0} \\ \mathbf{0} & \mathbf{s} & \mathbf{0} \\ \mathbf{0} & \mathbf{0} & \mathbf{s} \end{bmatrix} \{\boldsymbol{\delta}\}\, dV \quad , \quad \text{where} \quad [\mathbf{s}] = \begin{bmatrix} \sigma_{x0} & \tau_{xy0} & \tau_{zx0} \\ \tau_{xy0} & \sigma_{y0} & \tau_{yz0} \\ \tau_{zx0} & \tau_{yz0} & \sigma_{z0} \end{bmatrix} \qquad (18.4\text{-}4)$$

This expression is analogous to Eqs. 18.2-2 and 18.3-2b, and yields $[\mathbf{k}_\sigma]$ in an analogous way. Let the element displacement field be given by the usual expression $\{\mathbf{u}\} = [\mathbf{N}]\{\mathbf{d}\}$, where $\{\mathbf{u}\} = \lfloor u \;\; v \;\; w \rfloor^T$ and $\{\mathbf{d}\}$ contains element nodal d.o.f. Also let $\{\boldsymbol{\delta}\} = [\mathbf{G}]\{\mathbf{d}\}$, where terms in $[\mathbf{G}]$ are obtained from shape functions in $[\mathbf{N}]$ by appropriate differentiation and ordering of terms. Equation 18.4-4 becomes $U_\sigma = \{\mathbf{d}\}^T[\mathbf{k}_\sigma]\{\mathbf{d}\}/2$, where the element stress stiffness matrix is

$$[\mathbf{k}_\sigma] = \int [\mathbf{G}]^T \begin{bmatrix} \mathbf{s} & \mathbf{0} & \mathbf{0} \\ \mathbf{0} & \mathbf{s} & \mathbf{0} \\ \mathbf{0} & \mathbf{0} & \mathbf{s} \end{bmatrix} [\mathbf{G}]\, dV \qquad (18.4\text{-}5)$$

Example. Consider the bar of Fig. 18.2-1a, again with deformation restricted to the xy plane, so that $w = 0$. Initial stresses are zero except for axial stress σ_{x0}. We assume that u and v are linear in x. If Eq. 18.4-5 is written out in full, we find many zeros associated with nodal forces and displacements normal to the xy plane. With these terms discarded, and with shape functions $N_1 = (L - x)/L$ and $N_2 = x/L$, we obtain

$$\begin{aligned} u &= N_1 u_1 + N_2 u_2 \\ v &= N_1 v_1 + N_2 v_2 \end{aligned} \qquad \{\boldsymbol{\delta}\} = \begin{Bmatrix} u_{,x} \\ v_{,x} \end{Bmatrix} = \underbrace{\frac{1}{L}\begin{bmatrix} -1 & 0 & 1 & 0 \\ 0 & -1 & 0 & 1 \end{bmatrix}}_{[\mathbf{G}]} \begin{Bmatrix} u_1 \\ v_1 \\ u_2 \\ v_2 \end{Bmatrix} \qquad (18.4\text{-}6)$$

$$[\mathbf{k}_\sigma] = \int_0^L [\mathbf{G}]^T \begin{bmatrix} \sigma_{x0} & 0 \\ 0 & \sigma_{x0} \end{bmatrix} [\mathbf{G}]\, A\, dx = \frac{P}{L}\begin{bmatrix} 1 & 0 & -1 & 0 \\ 0 & 1 & 0 & -1 \\ -1 & 0 & 1 & 0 \\ 0 & -1 & 0 & 1 \end{bmatrix} \qquad (18.4\text{-}7)$$

where $P = \sigma_{x0}A$. This result is almost the same as the second of Eqs. 18.2-5, but contains four additional terms. The additional terms occupy the same positions as AE/L terms in

the conventional elastic stiffness matrix $[\mathbf{k}]$ of a bar element. Thus, in the net stiffness matrix $[\mathbf{k}] + [\mathbf{k}_\sigma]$, we see coefficients $\pm(AE + P)/L$ that multiply u_1 and u_2 and coefficients $\pm P/L$ that multiply v_1 and v_2. Because $AE \gg |P|$ in any practical elastic problem, the four "extra" P/L terms in Eq. 18.4-7 have negligible influence.

18.5 CALCULATION OF BUCKLING LOADS

We have defined buckling as a condition in which loads are large enough to destroy the stability of an equilibrium configuration. Buckling may occur by *bifurcation,* which means that a reference configuration of the structure and an infinitesimally close (buckled) configuration are both possible at the same load. Prior to bifurcation, the load versus deflection relation may or may not be linear. Buckling may also be associated with a *limit point* (points L in Fig. 17.2-3a), where stability is lost but there is no immediately adjacent equilibrium state. Limit-point buckling is inherently nonlinear.

Linear Bifurcation Buckling. In this subsection we discuss the kind of analysis that is commonly used for straight columns and flat plates. The first step is to load the structure by an arbitrary reference level of external load, $\{\mathbf{R}\}_{\text{ref}}$, and perform a standard linear analysis to determine element stresses such as membrane stresses in a plate. For stresses associated with load $\{\mathbf{R}\}_{\text{ref}}$, the stress stiffness matrix is $[\mathbf{K}_\sigma]_{\text{ref}}$. For some other load level, with λ a scalar multiplier,

$$[\mathbf{K}_\sigma] = \lambda[\mathbf{K}_\sigma]_{\text{ref}} \quad \text{when} \quad \{\mathbf{R}\} = \lambda\{\mathbf{R}\}_{\text{ref}} \tag{18.5-1}$$

Equations 18.5-1 imply that multiplication of all loads R_i in $\{\mathbf{R}\}$ by λ also multiplies the intensity of the stress field by λ but does not alter the distribution of stresses. Because the problem is presumed linear, the conventional stiffness matrix $[\mathbf{K}]$ is unchanged by loading. Let buckling displacements $\{\delta\mathbf{D}\}$ take place relative to displacements $\{\mathbf{D}\}_{\text{ref}}$ of the reference configuration. Because external loads do not change at a bifurcation point,

$$\begin{aligned} \Big([\mathbf{K}] + \lambda_{\text{cr}}[\mathbf{K}_\sigma]_{\text{ref}}\Big)\{\mathbf{D}\}_{\text{ref}} &= \lambda_{\text{cr}}\{\mathbf{R}\}_{\text{ref}} \\ \Big([\mathbf{K}] + \lambda_{\text{cr}}[\mathbf{K}_\sigma]_{\text{ref}}\Big)\{\mathbf{D}_{\text{ref}} + \delta\mathbf{D}\} &= \lambda_{\text{cr}}\{\mathbf{R}\}_{\text{ref}} \end{aligned} \tag{18.5-2}$$

Subtraction of the first equation from the second yields

$$\Big([\mathbf{K}] + \lambda_{\text{cr}}[\mathbf{K}_\sigma]_{\text{ref}}\Big)\{\delta\mathbf{D}\} = \{\mathbf{0}\} \tag{18.5-3}$$

Equation 18.5-3 is an eigenvalue problem whose smallest root λ_{cr} defines the smallest level of external load for which there is bifurcation, namely

$$\{\mathbf{R}\}_{\text{cr}} = \lambda_{\text{cr}}\{\mathbf{R}\}_{\text{ref}} \tag{18.5-4}$$

The eigenvector $\{\delta\mathbf{D}\}$ associated with λ_{cr} is the buckling mode. Because the magnitude of $\{\delta\mathbf{D}\}$ is indeterminate in a linear buckling problem, it defines shape but not amplitude.

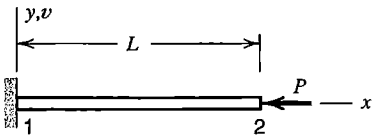

Figure 18.5-1. A uniform elastic column, fixed at $x = 0$ and free at $x = L$.

A physical interpretation of Eq. 18.5-3 is as follows. Terms in parentheses comprise a total or net stiffness $[\mathbf{K}_{\text{net}}]$. Because forces $[\mathbf{K}_{\text{net}}]\{\delta\mathbf{D}\}$ are zero, one can say that stresses of critical intensity reduce net stiffness to zero with respect to buckling mode $\{\delta\mathbf{D}\}$. Mathematically, $[\mathbf{K}_{\text{net}}]$ is singular and has a zero determinant.

Example: Linear Bifurcation. Consider the uniform column in Fig. 18.5-1. Let the FE model be a single beam element. We take $[\mathbf{k}]$ from Eq. 2.3-5 or Eq. 3.3-14 and $[\mathbf{k}_\sigma]$ from Eq. 18.2-6. We arbitrarily choose the reference load as $P_{\text{ref}} = -1.0$, where the negative sign indicates compression. From a similar example, Eq. 18.2-7, we realize that axial d.o.f. need not be included in the eigenvalue problem. At the right end of the column, nonzero d.o.f. associated with lateral displacement are v_2 and θ_{z2}. For buckling in the xy plane, Eq. 18.5-3 becomes

$$\left(\frac{EI_z}{L^3}\begin{bmatrix} 12 & -6L \\ -6L & 4L^2 \end{bmatrix} + \lambda_{\text{cr}}\frac{-1}{30L}\begin{bmatrix} 36 & -3L \\ -3L & 4L^2 \end{bmatrix}\right)\begin{Bmatrix} \delta v_2 \\ \delta\theta_{z2} \end{Bmatrix} = \begin{Bmatrix} 0 \\ 0 \end{Bmatrix} \tag{18.5-5}$$

A solution other than $\delta v_2 = 0$ and $\delta\theta_{z2} = 0$ requires that the expression in parentheses have a zero determinant. Therefore we may write the characteristic polynomial and extract its lowest root (this method is suitable for hand calculation with very few d.o.f.). The lowest root of Eq. 18.5-5 is

$$\lambda_{\text{cr}} = 2.4860EI_z/L^2 \qquad \text{hence} \qquad P_{\text{cr}} = \lambda_{\text{cr}}(-1.0) = -2.4860EI_z/L^2 \tag{18.5-6}$$

If instead $[\mathbf{k}_\sigma]$ were taken from Eq. 18.2-5, we would obtain $P_{\text{cr}} = -3EI_z/L^2$, which is less accurate than the result in Eq. 18.5-6. Both results are upper bounds to the correct result, $P_{\text{cr}} = -2.4674EI_z/L^2$ (remarks about bounds appear in Section 18.6).

The buckling mode that corresponds to λ_{cr} can be obtained from Eq. 18.5-6 by inserting $\lambda_{\text{cr}} = -2.4860EI_z/L^2$, choosing an arbitrary value for one of the d.o.f. (such as $\delta\theta_{z2} = 1.0$), and solving for the remaining d.o.f. Thus from Eq. 18.5-5 we obtain

$$\{\delta\mathbf{D}\} = \lfloor\, \delta v_2 \quad \delta\theta_{z2} \,\rfloor^T = \lfloor\, 0.6379L \quad 1 \,\rfloor^T \tag{18.5-7}$$

In general, $\{\delta\mathbf{D}\}$ represents displacements relative to displacements $\{\mathbf{D}\}_{\text{ref}}$ of the reference configuration that provides stresses used to construct $[\mathbf{K}_\sigma]$. In the present example, with d.o.f. u_2 omitted *a priori*, $\{\mathbf{D}\}_{\text{ref}} = \{\mathbf{0}\}$.

Example: Condensation of d.o.f. In structural dynamics, condensation can be used to reduce the size of an eigenvalue problem (Section 11.6). The same can be done in a buckling problem, with $[\mathbf{K}_\sigma]$ taking the place of mass matrix $[\mathbf{M}]$. In the preceding example, if

we choose to eliminate $\delta\theta_{z2}$ from Eq. 18.5-5, transformation matrix [**T**] is obtained by the calculations of Eq. 11.6-3:

$$\left[-\mathbf{K}_{ss}^{-1}\mathbf{K}_{ms}^{T}\right] = -\left(\frac{L}{4EI_z}\right)\left(-\frac{6EI_z}{L^2}\right) = \frac{3}{2L} \qquad \text{hence} \qquad [\mathbf{T}] = \begin{Bmatrix} 1 \\ 3/2L \end{Bmatrix} \tag{18.5-8}$$

The transformations of Eq. 11.6-4 convert Eq. 18.5-5 to

$$\left(\frac{3EI_z}{L^3} - \lambda_{\text{cr}}\frac{6}{5L}\right)\delta v_2 = 0 \qquad \text{hence} \qquad \lambda_{\text{cr}} = \frac{2.5EI_z}{L^2} \quad \text{and} \quad P_{\text{cr}} = -\frac{2.5EI_z}{L^2} \tag{18.5-9}$$

Condensation has slightly increased the magnitude of the computed buckling load.

Nonlinear Buckling. A buckling problem becomes nonlinear when there are significant prebuckling rotations. The problem can be addressed by methods described in Chapter 17. Thus we can form a tangent-stiffness matrix [$\mathbf{K}_t$], which includes the effect of changing geometry as well as the effect of stress stiffening. In calculation we might solve equations [$\mathbf{K}_t$]{$\Delta\mathbf{D}$} = {$\Delta\mathbf{R}$} by an incremental scheme using load increments {$\Delta\mathbf{R}$}, with load correction terms and updates of [$\mathbf{K}_t$] after each incremental step. As a limit point is approached, displacement increments {$\Delta\mathbf{D}$} become very large. At either a limit point or a bifurcation point, [$\mathbf{K}_t$] becomes singular. A way of solving a nonlinear buckling problem as a sequence of linearized trial solutions is described in [18.7].

In the foregoing discussion we have tacitly assumed that external loads {$\mathbf{R}$} are independent of deformation, thus providing the null right-hand side of Eq. 18.5-3. Such may not be the case, as when buckling occurs under hydrostatic pressure loading. Further remarks on nonlinearity in buckling appear in Sections 18.6 and 18.7.

18.6 REMARKS ON STRESS STIFFNESS AND ITS USES

Form of [$\mathbf{k}_\sigma$]. Bounds and Errors. A stress stiffness matrix can be termed "consistent" if it is based on the same shape functions as used to form the conventional stiffness matrix. Then, if elements are compatible and not softened by low-order integration rules, linear buckling analysis (Eq. 18.5-3) provides an upper bound on the linear bifurcation buckling load of the mathematical model. This behavior might be expected in view of the upper-bound nature of computed vibration frequencies (Section 11.3), which are obtained from a similar eigenproblem. Procedures for estimating the discretization error of buckling loads computed by FEA appear in [9.31,9.39].

An inconsistent [$\mathbf{k}_\sigma$] does not violate convergence requirements stated in Section 4.9, which apply to the conventional stiffness matrix [$\mathbf{k}$]. A one-element illustration of an inconsistent form appears in Eq. 18.2-7. If more elements were used in this problem, results would become quite accurate. Use of reduced integration in formulating [$\mathbf{k}_\sigma$] has the effect of basing it on a simplified displacement field. In the extreme of simplification,

a diagonal formulation for $[\mathbf{k}_\sigma]$ has been devised, which provides a lower bound on buckling loads in test cases [18.6]. The motivation for adopting a simplified form of $[\mathbf{k}_\sigma]$ is the possibility of a worthwhile cost saving in computation-intensive problems.

With the conventional stiffness matrix $[\mathbf{k}]$, the product $[\mathbf{k}]\{\mathbf{d}\}$ is null when nodal d.o.f. $\{\mathbf{d}\}$ represent rigid-body translation or (small) rigid-body rotation. With the stress stiffness matrix, the product $[\mathbf{k}_\sigma]\{\mathbf{d}\}$ provides nonzero nodal forces when $\{\mathbf{d}\}$ represents rigid-body rotation. This result is not incorrect. A simple example is that of Fig. 18.2-2 and Eq. 18.2-7, in which a bar element provides the stress stiffness term. Nodal displacement v_2 causes the bar element to rotate and consequently to apply y-direction force $(P/L)v_2$ at node 2. This force is resisted by the elastic force $(12EI_z/L^3)v_2$ due to bending. Hence this model provides $P_{cr} = 12EI_z/L^2$. More generally, one might interpret the buckling problem of Eq. 18.5-3 as requiring that pseudo-loads $\lambda_{cr}[\mathbf{K}_\sigma]_{ref}\{\delta\mathbf{D}\}$ be numerically equal to elastic resistances $[\mathbf{K}]\{\delta\mathbf{D}\}$.

The form of $[\mathbf{k}_\sigma]$ used in a bifurcation buckling analysis cannot be chosen independently of the application. In sandwich construction, where shear deformation of the core may be considerable, correct results require a match between fields on which $[\mathbf{k}]$ and $[\mathbf{k}_\sigma]$ are based [18.8]. A more important example is that of shells loaded by hydrostatic pressure: loaded surfaces rotate when a buckling mode appears, so the load changes direction (that is, hydrostatic pressure is a follower load). As a simple special case, consider a slender circular ring of radius R and uniform flexural stiffness EI. Let uniformly distributed line load q be applied to the circumference, acting inward. For the follower load of hydrostatic pressure, $q_{cr} = 3EI/R^3$. But if q has constant direction, $q_{cr} = 4EI/R^3$; and if q is always radially directed, $q_{cr} = 4.5EI/R^3$. If bifurcation buckling analysis is to provide correct buckling loads for hydrostatic loading, $[\mathbf{k}_\sigma]$ must be supplemented by a "pressure stiffness matrix." Moreover, the form of the pressure stiffness matrix must be related to the shell theory on which element stiffness matrices are based. In some situations the pressure stiffness matrix is unsymmetric, although there appears to be little error in many cases when the matrix is "symmetrized." References include [18.9–18.13].

Miscellaneous Applications. A shell of revolution usually has an asymmetric buckling mode even when geometry, supports, material properties and loading are all axisymmetric. The buckling mode will probably display many waves in each parallel circle. The problem can be addressed using a Fourier series method of the type described for solids of revolution in Sections 14.4 and 14.5 [18.14]. First the shell is discretized in the meridional direction, so that it is modeled by ring-shaped elements. Then one selects a specific number n of circumferential waves, and obtains the buckling load for that n. Analysis is repeated for $n + 1$ waves, for $n + 2$ waves, and so on. Provided that the initial n is sufficiently small, the lowest of the computed buckling loads can be identified as the desired result. It is not obvious which mode will govern, and several analyses may be needed: [18.15] cites a case in which buckling is associated with $n = 39$. If many waves also appear in the *meridional* direction, many ring-shaped elements are needed even if the shell has simple geometry.

An initially flat membrane has no initial resistance to lateral pressure unless stress stiffening is provided by initial stresses. A deflected membrane can resist pressure because of its shape, but stress stiffening effects remain important. Similar remarks apply to a cable network. A chainlike linkage of bars connected by frictionless hinges that hangs under its own weight would resist initial lateral load only because of stress stiffening, and lateral d.o.f. $\{\mathbf{D}\}$ would be obtained from the equations $[\mathbf{K}_\sigma]\{\mathbf{D}\} = \{\mathbf{R}\}$.

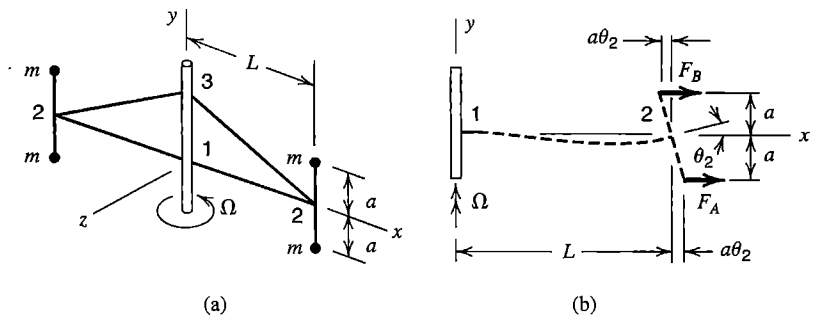

Figure 18.6-1. (a) Particles of mass m and weightless members attached to a shaft that rotates with angular velocity Ω. (b) Forces associated with rotation.

Linear dynamic analysis of an undamped structure with initial stresses is represented by the equations

$$\text{Dynamic response:} \quad [\mathbf{K} + \mathbf{K}_\sigma]\{\mathbf{D}\} + [\mathbf{M}]\{\ddot{\mathbf{D}}\} = \{\mathbf{R}^{\text{ext}}\} \tag{18.6-1}$$

$$\text{Natural frequencies:} \quad ([\mathbf{K} + \mathbf{K}_\sigma] - \omega^2[\mathbf{M}])\{\bar{\mathbf{D}}\} = \{\mathbf{0}\} \tag{18.6-2}$$

where $[\mathbf{M}]$ = mass matrix, $\{\ddot{\mathbf{D}}\}$ = accelerations of nodal d.o.f., ω = circular frequency, and $\{\bar{\mathbf{D}}\}$ = amplitudes of nodal d.o.f. Tensile membrane forces increase natural frequencies of vibration. Compressive membrane forces decrease them and produce a root $\omega = 0$ if buckling impends.

Spin Softening. Tensile stress induced by rotation has the effect of stiffening a member such as a fan blade. An opposing effect sometimes called "spin softening" or "centrifugal softening" may also arise. The effect is not related to matrix $[\mathbf{K}_\sigma]$. We explain the concept by using the simple example in Fig. 18.6-1. Four particle masses m are attached to rigid and massless y-parallel bars, which in turn are attached to massless x-parallel elastic beams 1-2. Massless rigid links 2-3 serve only to prevent axial (y-direction) motion of beam ends. The assembly rotates about the y axis with angular velocity Ω. If Ω is large enough, end 2 of a beam will rotate in a radial plane, just as a column will deflect laterally when axial compressive force reaches the buckling load. If rotation at node 2 is a small amount θ_2 in a radial plane, centrifugal forces on the particle masses become unequal, and thereby create a moment we shall call M_Ω.

$$\begin{aligned} F_A &= m(L + a\theta_2)\Omega^2 \\ F_B &= m(L - a\theta_2)\Omega^2 \end{aligned} \qquad M_\Omega = F_A a - F_B a = 2ma^2\Omega^2\theta_2 \tag{18.6-3}$$

Imagine now that member 1-2 is modeled by a single beam element, fixed at node 1 and simply supported at node 2 so that the only nonzero d.o.f. is θ_2. Stress stiffening is accounted for by the last term in Eq. 18.2-6, with axial force $P = 2mL\Omega^2$. Let external moment M_2 be applied at node 2. Thus

$$(k + k_\sigma)\theta_2 = M_2 + M_\Omega \qquad \text{where} \qquad k + k_\sigma = \frac{4EI_z}{L} + 2mL\Omega^2\frac{2L}{15} \tag{18.6-4}$$

From Eqs. 18.6-3 and 18.6-4,

$$\left[\frac{2EI_z}{L} + m\Omega^2\left(\frac{2L^2}{15} - a^2\right)\right]\theta_2 = \frac{M_2}{2} \tag{18.6-5}$$

We see that the effect of stress stiffening is reduced by spin softening. Indeed the bracketed expression may vanish for physically possible combinations of the quantities involved, so that the stability of equilibrium would be lost and θ_2 would be indeterminate. Rotation of node 2 about the x axis through a small angle θ_{x2} causes masses m to exert torque $2ma^2\Omega^2\theta_{x2}$ about the axis of member 1-2. Thus torsional stiffness of the x-parallel members is also effectively reduced by spin softening, but without a counteracting stress stiffening effect.

It is not hard to imagine that effects seen in this simple example may also appear in more realistic elastic structures. Usually stress stiffening has more influence on behavior than spin softening. Pertinent references for spinning structures include [11.13–11.19].

18.7 REMARKS AND EXAMPLES

The shallow plane truss in Fig. 18.7-1 illustrates possible types of secondary path [18.10]. Let displacements be confined to the plane of the figure. The problem is nonlinear; strongly so with extreme shallowness. The qualitative relation between load F and its displacement D can be understood without calculation. If the optional central spring is either absent or sufficiently soft, the primary path displays a limit point. But if beams that comprise the truss are slender, one or the other may buckle as a column before the limit point is reached. If the truss is sufficiently shallow and has no central spring, the column buckling load P_{cr} can be sustained with increasing D but decreasing F. Thus the secondary path descends, which is characteristic of a structure without post-buckling strength. In this case the bifurcation buckling load is a good indicator of maximum strength, although pre-buckling nonlinearity must be taken into account. By adding a central spring of suitable stiffness k the secondary path may be made to rise, Fig. 18.7-1b. Thus the structure has post-buckling strength. It does not collapse upon bifurcation, although the primary path ceases to be stable at point B.

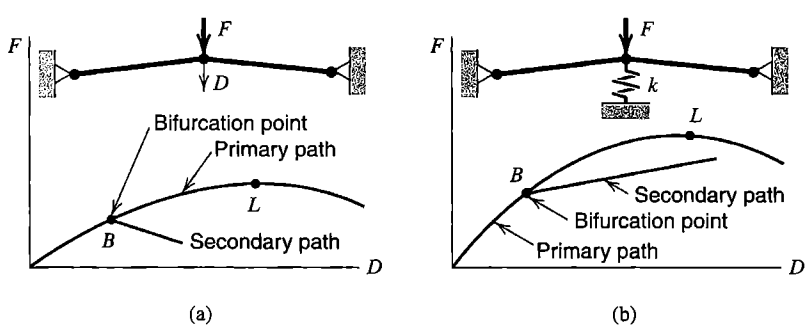

Figure 18.7-1. A shallow plane truss, with qualitative plots of load F versus its deflection D. (a) No supporting spring. (b) Supporting spring added.

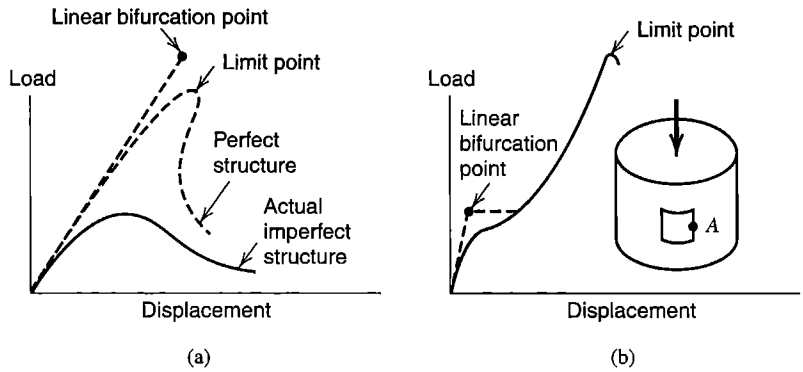

Figure 18.7-2. Qualitative load-deflection plots for thin shells. (a) Axial load and axial deflection in a cylindrical shell, or external pressure and radial deflection in a deep spherical cap. (b) Axial load and radial deflection at point A in a cylindrical shell with a cutout.

In the foregoing example, behavior can be strongly influenced by small changes in shallowness, column buckling strength, and stiffness of the central spring. The behavior of a thin shell is also sensitive to small changes. Figure 18.7-2a shows the qualitative behavior of axially compressed cylindrical shells and nonshallow spherical caps under external pressure. The buckling load predicted by linear bifurcation analysis overestimates the limit point load. Even the limit point load is a poor estimate of the actual collapse load if calculations are based on geometric perfection. A structure that displays the behavior shown is called *imperfection-sensitive,* which means that the collapse load is strongly affected by small changes in structure geometry, distribution or orientation of loads, or manner of support. The limit point load of the actual thin-walled shell, with its imperfections, may be only 10% of the buckling load computed by linear bifurcation analysis [18.16]. The percentage may rise to 50% in laboratory tests when heroic efforts are made to achieve perfection.

Small imperfections are easy to introduce into an FE model. They must be *deliberately* introduced; the small errors inherent in numerical calculation are not sufficient to direct computed behavior into an imperfect mode, or into an asymmetric mode when a symmetric mode is mathematically possible but actually unstable [18.11]. Geometric irregularities can be introduced directly. One of them might be the buckling mode predicted by linear bifurcation analysis. Or, it may be easier to apply small additional loads to create deformations similar to the initial geometric imperfections of interest.

A cutout may drastically alter the behavior of an axially compressed thin cylindrical shell (Fig. 18.7-2b). Here, linear bifurcation analysis seriously *under*estimates the actual limit load, where collapse occurs [18.16]. This example shows that bifurcation may be associated with a local buckling mode that has little influence on the mode that eventually produces collapse. For this structure, as with many practical structures, the actual geometry is imperfect and it may be unnecessary to add artificial imperfections.

Collapse analysis should be approached with the care and caution appropriate to any other nonlinear problem. Linear bifurcation analysis is comparatively easy, and may provide a useful first estimate, but it is rarely sufficient. It is easy to be misled, even in linear bifurcation analysis. For example, an axially compressed thin cylindrical shell modeled by triangular shell elements is an attractive test case for comparison with classical bifurcation

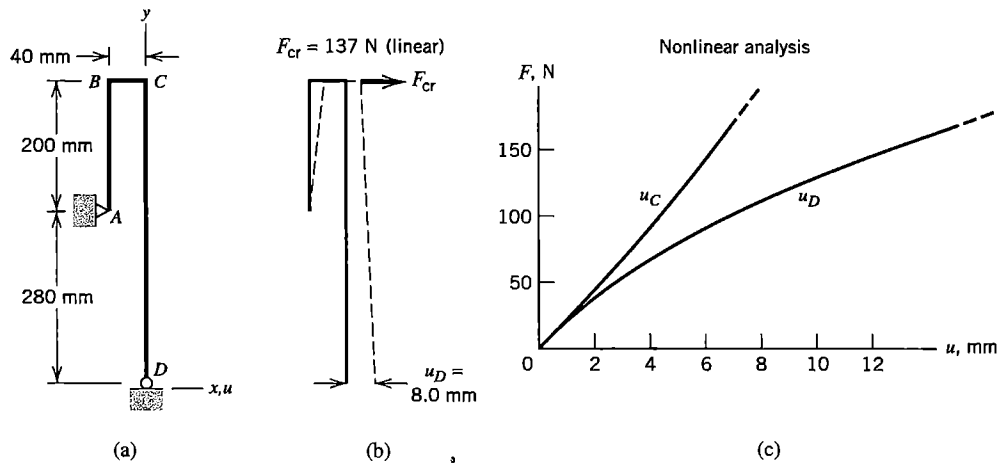

Figure 18.7-3. (a) Plane frame. (b) Displaced shape when $F = F_{cr}$ according to linear bifurcation analysis. (c) Load versus displacement relations computed by nonlinear analysis.

theory, but the problem is computationally difficult because several eigenvalues are clustered yet correspond to quite different eigenmodes. Even if software can negotiate the difficulties, computed results will be poor if, misled by the geometric simplicity of the structure, the analyst has employed so few d.o.f. that the many waves of the buckling mode cannot be properly modeled. Helpful observations appear in [18.17,18.18].

Numerical Example: Plane Frame. Bars of frame *ABCD* in Fig. 18.7-3a all have a square cross section 8 mm on a side. The material is assumed to remain linearly elastic at all times, with $E = 200$ GPa. Beam elements are used for the FE model: 5 along *AB*, 2 along *BC*, and 12 along *CD*. Node *A* is pinned, node *D* may displace horizontally without friction, and displacements are confined to the *xy* plane. Behavior produced by horizontal load *F* at node *C* is to be investigated.

Because members are slender, buckling appears possible. An approximate preliminary analysis might regard *CD* as a column of length 480 mm, fixed at *C* and free at *D*, so that the column buckling load is $P_{cr} = \pi^2 EI_z/4L^2$. In the original configuration, a vertical force $5F$ at node *D* is required for equilibrium. Hence, $5F = P_{cr}$ yields $F_{cr} = 146$ N. In FE computation, axial forces in members are determined by linear static analysis, and subsequent linear bifurcation buckling analysis using these forces provides $F_{cr} = 137$ N. Deformations that prevail when this F_{cr} is reached are shown in Fig. 18.7-3b. Results of *non*linear analysis, in which geometry is updated as load increases, are shown in Fig. 18.7-3c. Nonlinear analysis shows that the frame does not buckle at all. Instead, displacements continue to increase as load increases.

To illustrate the effect of a small geometric imperfection, the initial (unloaded) geometry is slightly altered by inclining the lowest element so that node *D* is 2 mm left of the centerline of member *CD*, as shown in Fig. 18.7-4a. In FE computation, linear static analysis followed by linear bifurcation buckling analysis now yields $F_{cr} = 114$ N and a configuration in which node *D* moves 2.6 mm leftward (Fig. 18.7-4b). Nonlinear analysis, Fig. 18.7-4c, shows that node *D* moves rightward at first, then reverses direction as load increases further. The frame collapses by snap-through buckling when $F = 86$ N. In this example, as is often the case, linear bifurcation analysis overestimates the collapse load.

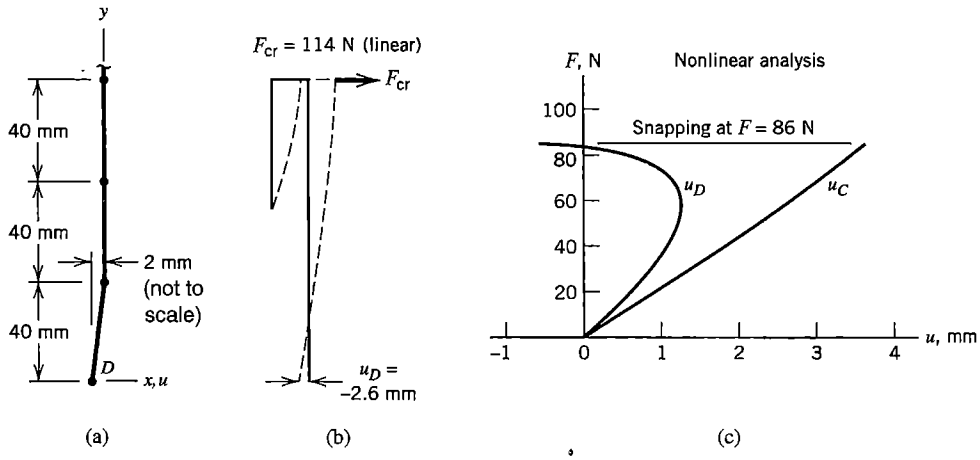

Figure 18.7-4. (a) Detail of altered initial geometry for the frame of Fig. 18.7-3a. (b) Displaced shape when $F = F_{cr}$ according to linear bifurcation analysis. (c) Load versus displacement relations computed by nonlinear analysis.

ANALYTICAL PROBLEMS

18.1-1 A straight wooden column has a central axial hole that fits closely but without friction around a threaded metal rod, as shown. Turning a nut at either end tensions the rod and compresses the column. Will the assembly buckle?

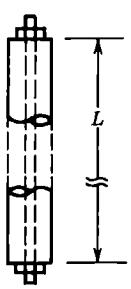

Problem 18.1-1

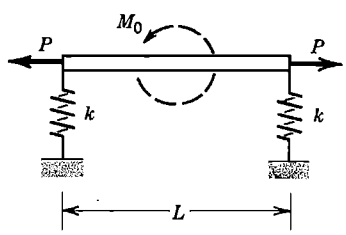

Problem 18.1-2

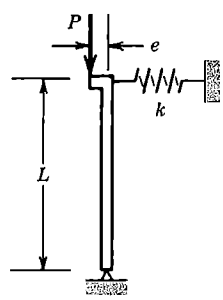

Problem 18.1-3

18.1-2 A rigid bar is supported by linear springs, as shown. Forces P are always horizontally directed. Moment load M_0 is applied. Displacements are confined to the plane of the figure. Consider work or energy associated with the forces, the moment, and the springs, and determine:
(a) the angle of rotation of the bar, in terms of M_0, P, k, and L.
(b) the (compressive) value of P for buckling (when $M_0 = 0$) in terms of k and L.

18.1-3 A rigid bar is pivoted at its lower end and attached to a linear spring at its upper end, as shown. Displacements are confined to the plane of the figure. Determine P_{cr} for central loading ($e = 0$). Then, for $e \neq 0$, use small-angle approximations to express lateral deflection Δ of the top in terms of P, e, k, and L. Plot Δ/L versus P/P_{cr} for $e/L = 0$, 0.01, and 0.02.

18.1-4 For the problem described by Fig. 18.1-1 and Eq. 18.1-6, let $P_{cr} = -\pi^2 EI_z/L^2$ and let v_{c0} represent the value of v_c produced by q alone (when $P = 0$). Plot v_c/v_{c0} versus P/P_{cr} as P goes from $P = P_{cr}$ (compressive) to $P = 5|P_{cr}|$ (tensile).

18.2-1 For a straight bar on the x axis that may stretch and bend in the xy plane, strain and strain energy for small displacements are given by

$$\varepsilon_x = u_{,x} + \frac{1}{2}v_x^2 - yv_{,xx} \qquad U = \int \frac{1}{2}E\varepsilon_x^2\, dV$$

Show how these expressions yield familiar conventional element stiffness matrices and a stress stiffness matrix.

18.2-2 Imagine that a bar element is tapered, so that its cross-sectional area is a continuous function of its axial coordinate. In which element matrices ($[\mathbf{k}]$ or $[\mathbf{k}_\sigma]$) does the effect of taper appear, and how is it taken into account?

18.2-3 Construct a 4 by 4 matrix $[\mathbf{k}_\sigma]$ for a uniform two-node beam element, analogous to Eq. 18.2-6, by using the quadratic lateral displacement field $v = (1 - \xi)v_1 + \xi v_2 + (1 - \xi)\xi L(\theta_{z1} - \theta_{z2})/2$, where $\xi = x/L$.

18.2-4 Obtain the P/L terms in the second $[\mathbf{k}_\sigma]$ matrix in Eq. 18.2-5 by appropriate specialization of $[\mathbf{k}_\sigma]$ in Eq. 18.2-6.

18.2-5 For the plane system shown, establish two matrix equations that could be used to determine lateral deflection and rotation at node 2 in terms of P, Q, E, I, L, and c. The connection at node 2 transmits no moment.

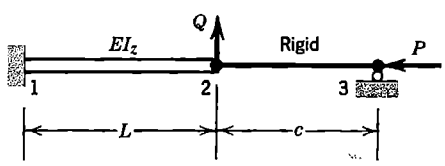

Problem 18.2-5

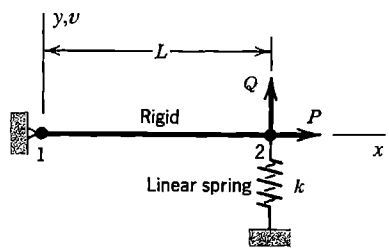

Problem 18.2-6

18.2-6 The bar shown is hinged at node 1 and may be considered rigid and weightless. Force P remains horizontal and motion is confined to the xy plane. In terms of P, Q, k, and L, what is deflection v_2 if P is (a) zero, (b) $0.96kL$ in tension, and (c) $0.96kL$ in compression?

18.2-7 Solve Problem 18.2-6(c), in which $P = -0.96kL$, by the following iterative method. For Q alone, $v_2 = Q/k$, and now a nonzero P will exert a moment about node 1. Another analysis, in which moments about node 1 are used, therefore yields a larger value of v_2. The process repeats.

18.2-8 The column shown is fixed at the left end. At the simply supported end, x-direction load P has offset e. Model the column by one element.
(a) Determine rotation θ_{z2} in terms of P, L, E, I, and e.
(b) If $e = 0$, what value of P makes θ_{z2} nonzero? What is the percentage error of this result?

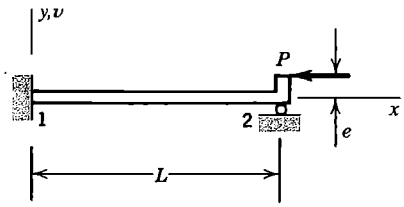

Problem 18.2-8

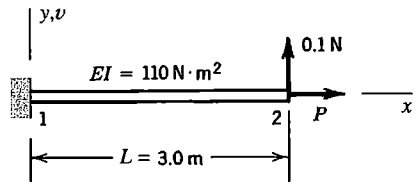

Problem 18.2-9

18.2-9 The x-direction force P on the cantilever beam shown may be either tensile or compressive. Model the beam by one element. Use v_2 and θ_{z2} as d.o.f. and take $[\mathbf{k}_\sigma]$ from Eq. 18.2-6. Determine v_2 if P is (a) zero, (b) 30 N in tension, and (c) 30 N in compression.

18.2-10 Repeat Problem 18.2-9, but use the $[\mathbf{k}_\sigma]$ developed in Problem 18.2-3.

18.2-11 In Problem 18.2-9(c), evaluate the bending moment at $x = 0$ by the calculation $M = EI[\mathbf{B}]\{\mathbf{d}\}$, where $[\mathbf{B}]$ is based on the usual cubic field and $\{\mathbf{d}\} = \lfloor 0 \quad 0 \quad v_2 \quad \theta_{z2} \rfloor^T$. Compare this M with that obtained by statics; that is, $M = 0.1L - Pv_2$, where $P = -30$ N in this case.

18.2-12 Diagonal mass matrices are discussed in Chapter 11. Why is an analogous diagonal stress stiffness matrix unacceptable if its nonzero terms operate on only translational d.o.f.?

18.4-1 For the eight-node trilinear solid isoparametric element, how many rows and columns are there in $[\mathbf{G}]$ of Eq. 18.4-5? Express the G_{ij} in terms of shape function derivatives and coefficients Γ_{ij} of the inverse Jacobian matrix. For convenience, let $\{\mathbf{d}\} = \lfloor u_1 \quad u_2 \quad \cdots \quad u_8 \quad v_1 \quad \cdots \quad w_8 \rfloor^T$.

18.4-2 (a) Consider a three-node triangular element that is constrained to move only in its plane. Write the formula for $[\mathbf{k}_\sigma]$ in terms of a 2 by 2 submatrix $[\mathbf{s}]$ and matrix $[\mathbf{B}]$ of Eq. 7.2-6. For convenience, order d.o.f. in $\{\mathbf{d}\}$ as $\lfloor u_1 \quad u_2 \quad u_3 \quad v_1 \quad v_2 \quad v_3 \rfloor^T$. (b) Now let the same element be allowed only small deflection $w = w(x,y)$ normal to its plane. What then is the formula for $[\mathbf{k}_\sigma]$? Let $\{\mathbf{d}\} = \lfloor w_1 \quad w_2 \quad w_3 \rfloor^T$.

18.5-1 Equation 18.5-5 has two roots, of which the lower root $\lambda = \lambda_{cr}$ is given by Eq. 18.5-6. What is the other root and the corresponding mode shape?

18.5-2 Using the $[\mathbf{k}_\sigma]$ derived in Problem 18.2-3, determine the critical load in Fig. 18.5-1. Use one element. The only d.o.f. needed are v_2 and θ_{z2}.

18.5-3 Assume that the two pin-connected bars shown are rigid and weightless. The linear springs each have stiffness k. Displacements are confined to the xy plane.

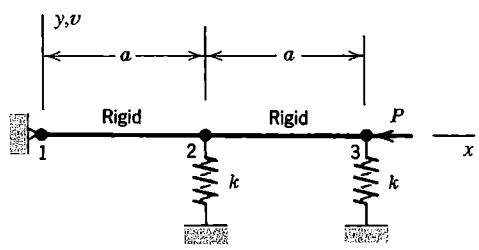

Problem 18.5-3

(a) Determine the buckling load P_{cr}.
(b) In the buckling mode, set $v_2 = 1$ and determine v_3. Sketch this mode, and show that laterally-directed forces $[\mathbf{K}_\sigma][v_2 \quad v_3]^T$ are equal in magnitude to forces in the deflected springs.

18.5-4 The uniform beam shown is fixed at its left end, simply supported at its right end, and divided into two identical beam elements, each of length a. Displacements are confined to the xy plane.
(a) Set up a three-equation system $[\mathbf{K} + \mathbf{K}_\sigma]\{\mathbf{D}\} = \{\mathbf{R}\}$, then eliminate d.o.f. θ_{z2} and θ_{z3} by condensation, leaving v_2 as the only d.o.f. retained.
(b) From this result, calculate P_{cr} (for the case $F = 0$) and its percentage error.
(c) For nonzero F, plot v_2/a versus P/P_{cr} if $F = 0.10EI/a^2$.

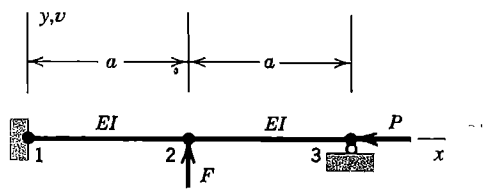

Problem 18.5-4

18.5-5 Assume that the uniform columns shown buckle in the plane of the figure. Express their buckling loads P_{cr} in terms of E, I, and L. Use the $[\mathbf{k}_\sigma]$ of Eq. 18.2-6.
(a) In Fig. (a), use θ_1 and θ_2 as d.o.f.
(b) In Fig. (b) there are two elements. Impose symmetry about node 2 (which is not a hinge), so that θ_1 and v_2 are the only d.o.f. needed.
(c) In Fig. (c), the lower end is fixed and the linear spring has stiffness $k = 2EI/L^3$.
(d) In Fig. (d), the lower end is fixed and the rotational spring has stiffness $k = EI/L$.
(e) Repeat part (c), letting $k \to \infty$ (top free to rotate but not translate).
(f) Repeat part (d), letting $k \to \infty$ (top free to translate but not rotate).

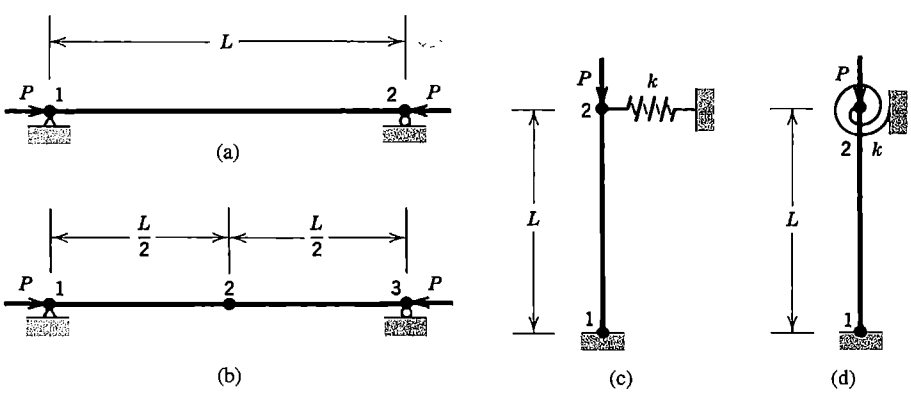

Problem 18.5-5

18.5-6 Repeat Problem 18.5-5, using the $[\mathbf{k}_\sigma]$ derived in Problem 18.2-3.

18.5-7 Repeat Problem 18.5-5, to the extent possible, using the $[\mathbf{k}_\sigma]$ for a bar element (Eq. 18.2-5).

18.5-8 (a) In using condensation for a buckling problem (as in Eqs. 18.5-8 and 18.5-9), how should one select the d.o.f. to be eliminated?
(b) Using condensation, solve Problem 18.2-9(b).
(c) Using condensation, solve Problem 18.2-9(c).
(d) Using condensation to eliminate θ_1, solve Problem 18.5-5(b).
(e) Using condensation to eliminate θ_1, solve Problem 18.5-6(b).

18.5-9 The two slender bars shown are of different lengths but otherwise identical. They are fixed at A and C and welded together at B, where they are simply supported and axial load P is applied. Investigate the possibility of buckling.

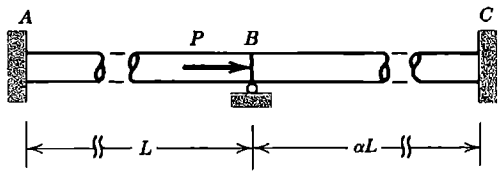

Problem 18.5-9

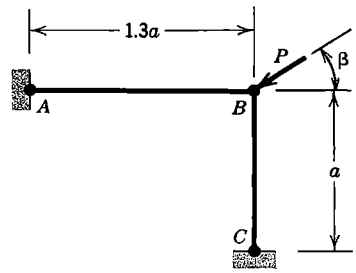

Problem 18.5-10

18.5-10 The two-element frame shown is fixed at A and C. Members are rigidly connected together at B and have the same EI throughout. For buckling in the plane of the figure, determine the angle β that minimizes the buckling load P_{cr}.

18.6-1 The massless string shown is horizontal and carries two particles, each of mass m. Assume that string tension T is not altered by small lateral deflection.
(a) Determine the static deflections of the particles caused by gravity.
(b) Determine the vibration frequencies and associated mode shapes.

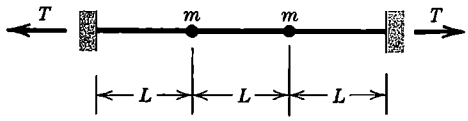

Problem 18.6-1

18.6-2 Repeat Problem 18.6-1, but increase the mass of the left-hand particle to $2m$.

18.6-3 The string shown has mass ρ per unit length. Assume that string tension T is not altered by small lateral deflection. Omit the conventional stiffness matrix $[\mathbf{K}]$ and use $[\mathbf{K}_\sigma]$ and $[\mathbf{M}]$ matrices associated with a cubic lateral displacement field. Determine the natural frequencies and associated mode shapes. (The exact fundamental frequency is $\omega_1^2 = \pi^2 T/4\rho a^2$.)
(a) Use one element. (Nonzero d.o.f. are then θ_1 and θ_2.)
(b) Use two elements and impose symmetry about the center. (What is a possible disadvantage of this procedure?)

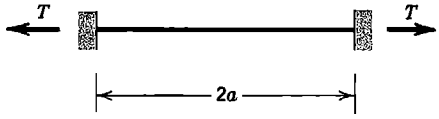

Problem 18.6-3

18.6-4 Repeat Problem 18.6-3, to the extent possible, using $[\mathbf{K}_\sigma]$ for a bar element (Eq. 18.2-5), and (a) $[\mathbf{M}]$ based on a cubic lateral displacement field, and (b) a lumped $[\mathbf{M}]$.

18.6-5 A massless flexible string of length $2L$ is attached to a ceiling. Two particles are attached to the string, each of mass m, one at the middle and one at the lower end.
(a) Determine the horizontal deflection at the lower end if a small horizontal force Q is applied there.
(b) Determine the natural frequencies and associated mode shapes.

18.6-6 Model a uniform simply supported beam by a single element. Let $L = 1.0$ m, $A = 0.0002$ m^2, $EI = 300.0$ N • m^2, and $\rho = 2100$ kg/m^3. Impose symmetry, thus reducing the problem to a single d.o.f., by setting $\theta_2 = -\theta_1$. Determine
(a) the fundamental vibration frequency if there is no axial force.
(b) the axial force that makes the vibration frequency 347 rad/s.
(c) the vibration frequency if compressive axial force 1200 N is imposed.

18.6-7 Let the members of length L in Fig. 18.6-1a have static torsional stiffness K. Ignore the possible effect of links 2-3. What rotational speed Ω effectively reduces torsional stiffness to zero? In other words, for what Ω are the members of length a no longer in a stable configuration when oriented parallel to the axis of spin?

COMPUTATIONAL PROBLEMS

In the following problems, compute the load associated with a bifurcation point and/or the load that actually causes collapse. Exploit symmetry where appropriate. When mesh refinement is used, estimate the maximum percentage error of results provided by the finest FE mesh. Where dimensions, loads, or material properties are not assigned, choose values that seem reasonable or convenient. Material nonlinearity may be considered. When additional assumptions are required, clearly state what they are. Apply the analysis methodology suggested in Section 1.5.

C18.1 Classical linear elastic bifurcation buckling loads are known for many problems, including straight columns, laterally loaded beams, and flat plates, with various load distributions and support conditions [1.16,17.33]. Such problems can be helpful in learning to use software and in showing the effects of mesh refinement.

C18.2 Reconsider the following problems, now with attention to the comparison between bifurcation load and collapse load. (a) Problem C17.10. (b) Problem C17.11.

C18.3 A thin, flat, circular plate rests on a soft elastic foundation. A central lateral force F pushes the plate against the foundation.

C18.4 A thin rectangular plate, initially flat, carries four lateral forces F, one at each corner. The forces act upward at two diagonally opposite corners and downward at the two remaining corners. Impose support conditions sufficient only to prevent rigid-body motion.

C18.5 Solve problem C16.1. Let height h be much less than radii R_1 and R_2, so that deformation is nonlinearly related to load q.

C18.6 A uniform bimetallic strip is manufactured with small initial curvature. Elastic properties of the two metals may differ, as may coefficients of thermal expansion α_1 and α_2. Ends of the strip are pinned to rigid walls, as shown. No force is exerted on the walls at initial temperature T_0. Loading is created by changing the temperature uniformly to a value T [18.19].

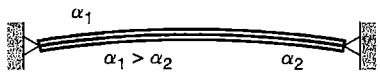

Problem C18.6

C18.7 Solve shell problems of the type discussed in connection with Fig. 18.7-2. For comparison with published results, consult references cited in this chapter.

C18.8 The cross section of a steel measuring tape forms a shallow arc of small thickness, so that a length of tape has the shape of a longitudinal strip cut from a thin cylindrical shell. Bend the strip by applying opposing moment loads at the curved ends. Moment vectors may be directed parallel to the chord of the cross-sectional arc or normal to it.

C18.9 A uniform cable hangs under its own weight. Investigate natural frequencies and modes of vibration.
(a) The cable hangs from one end; the other end is free.
(b) The cable is supported at both ends. The amount of sag and the elevation of one end with respect to the other may be chosen arbitrarily [18.20].

C18.10 A thin, flat, circular plate spins with angular velocity Ω about an axis normal to the disk and through its center. Investigate the effect of Ω on
(a) the frequencies of vibration.
(b) the temperature T_0 that causes buckling, where temperature T varies linearly with the radial coordinate, from zero at the center to T_0 at the rim.

C18.11 Idealize a fan blade as a thin flat rectangular plate, rigidly attached to a shaft at one end. Investigate the effect of rotational speed of the shaft on vibration frequencies of the plate. Investigate the effects of including (a) only stress stiffening, (b) only spin softening, and (c) both.

C18.12 Investigate buckling due to axial compression of an aluminum beer can, both with and without internal pressure.

APPENDIX A

MATRICES: SELECTED DEFINITIONS AND MANIPULATIONS

This appendix reviews matrix theory often used in FE theory. Symbols used are arbitrary and imply no particular physical meaning. Further explanation may be found in any of several references, including [9.8,17.20,A.1].

Definitions. A *matrix* is an array that contains numbers and/or symbols. Using symbols, we have for example

$$[\mathbf{A}] = \begin{bmatrix} A_{11} & A_{12} & \cdots & A_{1n} \\ A_{21} & A_{22} & \cdots & A_{2n} \\ \vdots & \vdots & & \vdots \\ A_{m1} & A_{m2} & \cdots & A_{mn} \end{bmatrix} \qquad \{\mathbf{b}\} = \begin{Bmatrix} b_1 \\ b_2 \\ \vdots \\ b_m \end{Bmatrix} \qquad \lfloor \mathbf{r} \rfloor = \lfloor r_1 \quad r_2 \qquad r_n \rfloor \tag{A.1}$$

Respectively, these matrices are called a *rectangular* matrix, a *column* matrix (or column vector), and a *row* matrix (or row vector). Conventionally, boldface type is used to denote a matrix. Brackets and braces are optional; we use them to indicate the type of matrix. If $m = n$, matrix [**A**] is *square,* and n is its *order.* Coefficients with like subscripts (A_{11}, A_{22}, and so on) are on the *principal diagonal* (also called simply the *diagonal*). A *unit* or *identity* matrix is a square matrix that has 1's on its diagonal and zeros elsewhere.

$$\lceil \mathbf{I} \rfloor = \begin{bmatrix} 1 & 0 & \cdots \\ 0 & 1 & \cdots \\ \vdots & \vdots & \end{bmatrix} \qquad \text{or} \qquad \lceil \mathbf{I} \rfloor = \lceil 1 \;\; 1 \cdots 1 \rfloor \tag{A.2}$$

A *null* matrix is filled entirely with zeros. The *trace* of a square matrix is the sum of its diagonal terms; for a matrix of order n, $\mathrm{tr}[\mathbf{A}] = A_{11} + A_{22} + \cdots + A_{nn}$.

The *transpose* of a matrix is produced by interchanging rows and columns. For matrices in Eq. A.1,

$$[\mathbf{A}]^T = \begin{bmatrix} A_{11} & A_{21} & \cdots \\ A_{12} & A_{22} & \cdots \\ \vdots & \vdots & \end{bmatrix} \qquad \{\mathbf{b}\}^T = \lfloor b_1 \, b_2 \cdots \rfloor \qquad \lfloor \mathbf{r} \rfloor^T = \begin{Bmatrix} r_1 \\ r_2 \\ \vdots \end{Bmatrix} \tag{A.3}$$

If $A_{12} = A_{21}, A_{13} = A_{31}$, and so on—that is, if $[\mathbf{A}]^T = [\mathbf{A}]$—then [**A**] is *symmetric.* A symmetric matrix must be square ($m = n$).

A matrix having all zeros above the diagonal is called *lower triangular;* a matrix having all zeros below the diagonal is called *upper triangular.* See, for example, [**L**] and [**U**] in Eq. A.7.

Addition and Multiplication. If matrices have the same m and the same n, they can be added or subtracted. The operation is performed term by term. Thus, $[\mathbf{C}] = [\mathbf{A}] + [\mathbf{B}]$ is computed as $C_{ij} = A_{ij} + B_{ij}$. Multiplication by a scalar β is also done term by term; thus $[\mathbf{D}] = \beta[\mathbf{C}]$ implies $D_{ij} = \beta C_{ij}$.

The product of two matrices is

$$\underset{l\times n}{[\mathbf{P}]} = \underset{l\times m}{[\mathbf{A}]}\,\underset{m\times n}{[\mathbf{B}]} \qquad \text{where} \qquad P_{ij} = \sum_{k=1}^{m} A_{ik}B_{kj} \tag{A.4}$$

For example, $P_{23} = A_{21}B_{13} + A_{22}B_{23} + A_{23}B_{33} + \cdots$. Matrices must be *conformable* for multiplication; that is, if $[\mathbf{A}]$ has m columns, then $[\mathbf{B}]$ must have m rows. Examples of matrix multiplication are

$$\lfloor 1 \quad 2 \rfloor \begin{Bmatrix} 3 \\ 4 \end{Bmatrix} = 11 \qquad \begin{Bmatrix} 1 \\ 2 \end{Bmatrix} \lfloor 3 \quad 4 \rfloor = \begin{bmatrix} 3 & 4 \\ 6 & 8 \end{bmatrix} \qquad \begin{bmatrix} 1 & 2 \\ 3 & 4 \end{bmatrix}\begin{bmatrix} 5 & 6 & 7 \\ 8 & 9 & 0 \end{bmatrix} = \begin{bmatrix} 21 & 24 & 7 \\ 47 & 54 & 21 \end{bmatrix} \tag{A.5}$$

In general, $[\mathbf{A}][\mathbf{B}] \neq [\mathbf{B}][\mathbf{A}]$; that is, except for some special forms, matrix multiplication is not commutative. The following properties may be stated (provided, of course, that matrices are conformable for the operation stated).

$$\begin{aligned} &[\mathbf{A}]\Big([\mathbf{B}] + [\mathbf{C}]\Big) = [\mathbf{A}][\mathbf{B}] + [\mathbf{A}][\mathbf{C}] && [\mathbf{A}]\Big([\mathbf{B}][\mathbf{C}]\Big) = \Big([\mathbf{A}][\mathbf{B}]\Big)[\mathbf{C}] \\ &\Big([\mathbf{A}] + [\mathbf{B}]\Big)[\mathbf{C}] = [\mathbf{A}][\mathbf{C}] + [\mathbf{B}][\mathbf{C}] && \Big([\mathbf{A}] + [\mathbf{B}]\Big)^T = [\mathbf{A}]^T + [\mathbf{B}]^T \\ &[\mathbf{A}]\lceil \mathbf{I} \rfloor = \lceil \mathbf{I} \rfloor[\mathbf{A}] = [\mathbf{A}] && \Big([\mathbf{A}][\mathbf{B}]\cdots[\mathbf{Z}]\Big)^T = [\mathbf{Z}]^T\cdots[\mathbf{B}]^T[\mathbf{A}]^T \end{aligned} \tag{A.6}$$

The last equation is often used in FEA: *the transpose of a product is the product of the transposes* <u>*in reverse order*</u>.

If $[\mathbf{B}]$ is square and symmetric, so is the product matrix $[\mathbf{P}] = [\mathbf{A}]^T[\mathbf{B}][\mathbf{A}]$. If $[\mathbf{A}]$ is a column vector, $[\mathbf{P}]$ is a scalar.

Sometimes it is convenient to *partition* a matrix into submatrices, as indicated in the following example.

$$[\mathbf{L}][\mathbf{U}] = \left[\begin{array}{c|cc} 1 & 0 & 0 \\ \hline a & 1 & 0 \\ b & c & 1 \end{array}\right]\left[\begin{array}{c|cc} d & e & f \\ \hline 0 & g & h \\ 0 & 0 & i \end{array}\right] = \left[\begin{array}{c} \mathbf{A} \\ \hline \mathbf{B} \end{array}\right]\left[\begin{array}{c|c} \mathbf{C} & \mathbf{D} \end{array}\right] = \begin{bmatrix} \mathbf{AC} & \mathbf{AD} \\ \mathbf{BC} & \mathbf{BD} \end{bmatrix} \tag{A.7}$$

As shown, submatrices can be multiplied as if they were matrices in their own right, provided that they are conformable.

Inverse. The inverse of a square matrix is another square matrix of the same order such that its product with the original matrix yields a unit matrix.

$$[\mathbf{A}][\mathbf{A}]^{-1} = [\mathbf{A}]^{-1}[\mathbf{A}] = \lceil \mathbf{I} \rfloor \tag{A.8}$$

The inverse of a 2 by 2 matrix is simple enough to be stated explicitly:

$$[\mathbf{A}] = \begin{bmatrix} a & b \\ c & d \end{bmatrix} \qquad [\mathbf{A}]^{-1} = \frac{1}{|\mathbf{A}|}\begin{bmatrix} d & -b \\ -c & a \end{bmatrix} \qquad \text{where} \qquad |\mathbf{A}| = ad - bc \tag{A.9}$$

in which $|\mathbf{A}|$ is the determinant of $[\mathbf{A}]$. (Numerical evaluation of $|\mathbf{A}|$ is discussed in Appendix B.) Properties of the inverse include

$$\Big([\mathbf{A}][\mathbf{B}]\Big)^{-1} = [\mathbf{B}]^{-1}[\mathbf{A}]^{-1} \quad \text{and} \quad \Big([\mathbf{A}]^{-1}\Big)^{T} = \Big([\mathbf{A}]^{T}\Big)^{-1} \tag{A.10}$$

Thus, the inverse of a product is the product of the inverses *in reverse order,* and the transpose of an inverse is the inverse of the transpose.

Symbolically, a set of algebraic equations and its solution for unknowns $\{\mathbf{x}\}$ is

$$[\mathbf{A}]\{\mathbf{x}\} = \{\mathbf{b}\} \qquad \{\mathbf{x}\} = [\mathbf{A}]^{-1}\{\mathbf{b}\} \tag{A.11}$$

In FEA, matrix $[\mathbf{A}]$ is typically large and sparse. It would be wasteful of storage and time to invert it. Thus, the statement $\{\mathbf{x}\} = [\mathbf{A}]^{-1}\{\mathbf{b}\}$ usually means only "solve for unknowns," typically by Gauss elimination or an iterative method (see Appendix B).

A matrix is called *orthogonal* if its inverse is equal to its transpose. For example,

$$[\mathbf{A}] = \begin{bmatrix} 0.8 & 0.6 \\ -0.6 & 0.8 \end{bmatrix} \qquad [\mathbf{A}]^{T} = \begin{bmatrix} 0.8 & -0.6 \\ 0.6 & 0.8 \end{bmatrix} \qquad [\mathbf{A}][\mathbf{A}]^{T} = \begin{bmatrix} 1 & 0 \\ 0 & 1 \end{bmatrix} \tag{A.12}$$

Orthogonal matrices appear in some coordinate transformation operations.

Rank and Singularity. The *rank* of a matrix is the order of the largest nonzero determinant that can be formed from the matrix. One or more rows and an equal number of columns may have to be deleted from a square matrix in order to obtain a nonzero determinant from rows and columns that remain. Thus, one finds that matrices in Eqs. A.12 have rank 2, and the following matrices have ranks 2, 1, 1, and 1, respectively.

$$\begin{bmatrix} 7 & -8 & 1 \\ -8 & 16 & -8 \\ 1 & -8 & 7 \end{bmatrix} \qquad \begin{bmatrix} 1 & -1 \\ -1 & 1 \end{bmatrix} \qquad \begin{bmatrix} 2 & 4 & -2 \\ 1 & 2 & -1 \\ 3 & 6 & -3 \end{bmatrix} \qquad \begin{Bmatrix} a \\ b \\ c \end{Bmatrix} \tag{A.13}$$

In the first matrix, any row (or column) can be formed as a linear combination of the other two rows (or columns). In the second matrix, one row or column is the negative of the other row or column. Two such linear dependencies appear in the third matrix. The rank of a square matrix can also be defined as the maximum number of linearly independent rows or columns. A matrix whose rank is less than its order is called *rank-deficient.* A rank-deficient matrix is *singular* and has a zero determinant. A singular matrix has no inverse, and Eqs. A.11 have no unique solution for $\{\mathbf{x}\}$. If two matrices have ranks r_1 and r_2, with $r_1 < r_2$, their product has rank r_1. Thus, a square matrix $[\mathbf{A}] = \{\mathbf{a}\}\lfloor\mathbf{b}\rfloor$ has rank 1 or is null, regardless of its order.

Quadratic Forms. Consider a real square matrix $[\mathbf{A}]$ and a real vector $\{\mathbf{x}\}$ of the same order. Scalar F is called a quadratic form, where

$$F = \{\mathbf{x}\}^{T}[\mathbf{A}]\{\mathbf{x}\} \tag{A.14}$$

Imagine that all possible values of F are calculated by letting terms x_i in $\{\mathbf{x}\}$ assume any and all real values except for all x_i simultaneously zero. Then $[\mathbf{A}]$ is called

positive definite	if $F > 0$ for all $\{\mathbf{x}\}$
positive semidefinite	if $F \geq 0$ for all $\{\mathbf{x}\}$
indefinite	if $F > 0$ and $F < 0$ are both possible
negative semidefinite	if $F \leq 0$ for all $\{\mathbf{x}\}$
negative definite	if $F < 0$ for all $\{\mathbf{x}\}$

As examples, matrix [**A**] in Eq. A.12 is positive definite, and the first matrix in Eq. A.13 is positive semidefinite. If a square matrix is positive definite or negative definite, it is also nonsingular.

Differentiation. Differentiation of a matrix is accomplished by differentiating each of its terms. For example, if $\lfloor \mathbf{a} \rfloor = \lfloor 1 \;\; x^2 \rfloor$, then $d\lfloor \mathbf{a} \rfloor / dx = \lfloor 0 \;\; 2x \rfloor$.

Let $\{\mathbf{x}\} = \lfloor x_1 \;\; x_2 \;\; \cdots \;\; x_n \rfloor^T$ and let [**A**] be an arbitrary n by n square matrix that does not depend on the x_i. Suppose it is required to differentiate the quadratic form

$$\phi = \frac{1}{2}\{\mathbf{x}\}^T[\mathbf{A}]\{\mathbf{x}\} \tag{A.15}$$

with respect to each of the x_i. The result is conveniently stated as a vector:

$$\left\{\frac{\partial \phi}{\partial \mathbf{x}}\right\} = \left\lfloor \frac{\partial \phi}{\partial x_1} \;\; \frac{\partial \phi}{\partial x_2} \;\; \cdots \;\; \frac{\partial \phi}{\partial x_n} \right\rfloor^T = \frac{1}{2}\left([\mathbf{A}] + [\mathbf{A}]^T\right)\{\mathbf{x}\} \tag{A.16}$$

as may be verified by writing ϕ in terms of the x_i and the A_{ij}, taking the derivatives, and gathering terms. If [**A**] is *symmetric,* then

$$\left\{\frac{\partial \phi}{\partial \mathbf{x}}\right\} = [\mathbf{A}]\{\mathbf{x}\} \qquad \text{and} \qquad \frac{\partial^2 \phi}{\partial x_i \partial x_j} = A_{ij} = A_{ji} \tag{A.17}$$

As a special case, if [**A**] is a unit matrix, then $\{\partial\phi/\partial\mathbf{x}\} = \{\mathbf{x}\}$.

Let $\{\mathbf{x}\} = \lfloor x_1 \, x_2 \cdots x_m \rfloor^T$, $\{\mathbf{y}\} = \lfloor y_1 \, y_2 \cdots y_n \rfloor^T$, and [**A**] be an arbitrary m by n matrix that does not depend on the x_i. Imagine that the scalar $\psi = \{\mathbf{x}\}^T[\mathbf{A}]\{\mathbf{y}\}$ is to be differentiated with respect to each of the x_i. The result is conveniently stated as a vector:

$$\left\{\frac{\partial \psi}{\partial \mathbf{x}}\right\} = \left\lfloor \frac{\partial \psi}{\partial x_1} \;\; \frac{\partial \psi}{\partial x_2} \;\; \cdots \;\; \frac{\partial \psi}{\partial x_m} \right\rfloor^T = [\mathbf{A}]\{\mathbf{y}\} \tag{A.18}$$

As for differentiation with respect to each of the y_i, we note that because ψ is a scalar,

$$\psi = \psi^T = \{\mathbf{y}\}^T[\mathbf{A}]^T\{\mathbf{x}\} \tag{A.19}$$

Therefore, if [**A**] does not depend on the y_i,

$$\left\{\frac{\partial \psi}{\partial \mathbf{y}}\right\} = \left\lfloor \frac{\partial \psi}{\partial y_1} \;\; \frac{\partial \psi}{\partial y_2} \;\; \cdots \;\; \frac{\partial \psi}{\partial y_n} \right\rfloor^T = [\mathbf{A}]^T\{\mathbf{x}\} \tag{A.20}$$

As a special case, if [**A**] is a unit matrix, then $m = n$, and

$$\psi = \{\mathbf{x}\}^T\{\mathbf{y}\} = \{\mathbf{y}\}^T\{\mathbf{x}\} \qquad \left\{\frac{\partial \psi}{\partial \mathbf{x}}\right\} = \{\mathbf{y}\} \qquad \left\{\frac{\partial \psi}{\partial \mathbf{y}}\right\} = \{\mathbf{x}\} \tag{A.21}$$

Norms. A *norm* is a measure of the size of a matrix or vector. Norms are useful in measuring the convergence of numerical processes. For a vector $\{\mathbf{x}\}$ of order n, various vector norms can be

defined. The 1-norm, 2-norm, ∞-norm, and p-norm are identified by double bars with the appropriate subscript. (Single bars indicate the magnitude of a scalar.)

$$\|\mathbf{x}\|_1 = |x_1| + |x_2| + \cdots + |x_n| \qquad \|\mathbf{x}\|_2 = \left(x_1^2 + x_2^2 + \cdots + x_n^2\right)^{1/2}$$
$$\|\mathbf{x}\|_\infty = \max_i |x_i| \qquad \|\mathbf{x}\|_p = \left(|x_1|^p + |x_2|^p + \cdots + |x_n|^p\right)^{1/p} \tag{A.22}$$

The 2-norm is also called the *Euclidean norm.* For $n = 2$ and $n = 3$ respectively, the 2-norm is the length of $\{\mathbf{x}\}$ in 2D and 3D space. When the x_i are functions of spatial coordinates, a measure called the L_2 norm is defined over a volume V as

$$\|\mathbf{x}\|_{L_2} = \left[\int \{\mathbf{x}\}^T\{\mathbf{x}\}\, dV\right]^{1/2}, \qquad \text{where} \qquad \{\mathbf{x}\}^T = \lfloor x_1\ x_2 \cdots x_n \rfloor \tag{A.23}$$

Matrix norms are defined in a manner analogous to Eqs. A.22. For a square matrix $[\mathbf{A}]$ of order n,

$$\|\mathbf{A}\|_1 = \max_j \left(\sum_{i=1}^{n} |A_{ij}|\right) \qquad \|\mathbf{A}\|_2 = \sqrt{\lambda_{\max}} \qquad \|\mathbf{A}\|_\infty = \max_i \left(\sum_{j=1}^{n} |A_{ij}|\right) \tag{A.24}$$

where $\lambda_{\max}$ is the maximum eigenvalue of $[\mathbf{A}]^T[\mathbf{A}]$. The 1-norm is the absolute maximum column sum; the ∞-norm is the absolute maximum row sum.

Another measure of the size of a square matrix is the *spectral radius* $\rho(\mathbf{A})$. If μ_i are the eigenvalues of $[\mathbf{A}]$, spectral radius is defined as

$$\rho(\mathbf{A}) = \max_i |\mu_i| \tag{A.25}$$

For any norm defined in Eqs. A.24, $\rho(\mathbf{A}) \le \|\mathbf{A}\|$.

Let $[\mathbf{A}]$ and $[\mathbf{B}]$ be square matrices and $\{\mathbf{x}\}$ and $\{\mathbf{y}\}$ be vectors, of conformable order for multiplication and addition where indicated, and let s be a scalar. The following relations hold for any norm defined in Eqs. A.22 and A.24.

$$\|\mathbf{x} + \mathbf{y}\| \le \|\mathbf{x}\| + \|\mathbf{y}\| \qquad \|s\mathbf{x}\| = |s|\,\|\mathbf{x}\| \qquad \|\mathbf{A}\mathbf{x}\| \le \|\mathbf{A}\|\,\|\mathbf{x}\|$$
$$\|\mathbf{A} + \mathbf{B}\| \le \|\mathbf{A}\| + \|\mathbf{B}\| \qquad \|s\mathbf{A}\| = |s|\,\|\mathbf{A}\| \qquad \|\mathbf{A}\mathbf{B}\| \le \|\mathbf{A}\|\,\|\mathbf{B}\| \tag{A.26}$$

The first relation in Eq. A.26 is known as the *triangle inequality.* Another relation is that $\|\mathbf{A}\| > 0$ unless $[\mathbf{A}]$ is null, in which case $\|\mathbf{A}\| = 0$. Similarly, $\|\mathbf{x}\| > 0$ unless $\{\mathbf{x}\}$ is null.

APPENDIX B

SIMULTANEOUS ALGEBRAIC EQUATIONS

B.1 OVERVIEW

Computational methods produce large systems of simultaneous algebraic equations. In this appendix we represent the equation system as $[\mathbf{A}]\{\mathbf{x}\} = \{\mathbf{b}\}$, which is to be solved for $\{\mathbf{x}\}$, the vector of unknowns. In FEA, coefficient matrix $[\mathbf{A}]$ is often a stiffness matrix. A large coefficient matrix is likely to be sparse, with perhaps less than one nonzero term for every 100 zeros. The number and location of nonzero terms in $[\mathbf{A}]$ is called the *matrix topology.* Because $[\mathbf{A}]^{-1}$ is full even when $[\mathbf{A}]$ is sparse, formal inversion to obtain $\{\mathbf{x}\} = [\mathbf{A}]^{-1}\{\mathbf{b}\}$ is not a practical solution method.

The equation system is *linear* if $[\mathbf{A}]$ and $\{\mathbf{b}\}$ contain known constants, and *nonlinear* if $[\mathbf{A}]$ and/or $\{\mathbf{b}\}$ is a function of $\{\mathbf{x}\}$. In FEA we always deal with a linear equation system $[\mathbf{A}]\{\mathbf{x}\} = \{\mathbf{b}\}$, and solve a nonlinear *problem* by repeatedly updating $[\mathbf{A}]$ and/or $\{\mathbf{b}\}$ based on the most recently computed $\{\mathbf{x}\}$. Equation solving may consume the bulk of total computation time in a nonlinear problem.

Equation solvers can be classed as *direct* or *iterative.* A direct solver obtains the solution in a definite number of steps. The number can be predicted when the topology of $[\mathbf{A}]$ is known. Direct solvers deal effectively with multiple right-hand sides (multiple load cases in FEA) because by far the greatest computational effort is expended in the reduction of $[\mathbf{A}]$; each $\{\mathbf{b}\}$ is then treated very quickly. Direct solvers have the disadvantage of creating many "fills" by converting many zero coefficients A_{ij} to nonzero values, which must subsequently be processed and for which storage space must be allocated. An iterative solver repeats calculations until a convergence test is satisfied. The number of iterations required cannot be predicted. Iterative solvers create few fills (or none, depending on the method), but do not readily deal with multiple right-hand sides, and may converge slowly in some cases. In a nonlinear problem, it may be possible to reduce the number of iterations at a given load by using an incompletely converged $\{\mathbf{x}\}$ to update the equation system, with convergence required only in the final stage.

In each category, direct and indirect, there are many choices of solvers available. Assuming that competing methods fit in available storage space and obtain $\{\mathbf{x}\}$ with adequate accuracy, one seeks the fastest method. Factors that influence speed include matrix size and topology, whether size requires that data must frequently be swapped to and from disk storage, how many vectors $\{\mathbf{b}\}$ must be processed, the condition number of $[\mathbf{A}]$, and how skillfully the algorithms are coded. The choice of equation solver is important for large problems and for problems that require repeated solutions, such as nonlinear problems.

In what follows we undertake a brief and selective discussion of these matters. The discussion is intended to supplement Section 2.8.

B.2 DIRECT SOLVERS

Gauss Elimination. The arrangement of Gauss elimination we describe requires that $[\mathbf{A}]$ be nonsingular. Also, each diagonal coefficient must be nonzero when it is used as a divisor in an elimination step. Typically, diagonal coefficients A_{ii} are initially nonzero. An A_{ii} that is initially zero may be

converted to nonzero by preceding eliminations (as, for example, when Lagrange multipliers are used to enforce constraints).

To illustrate the systematic manipulations of Gauss elimination, we consider a 3 by 3 system $[\mathbf{A}]\{\mathbf{x}\} = \{\mathbf{b}\}$. Let unknowns be eliminated in numerical order. Accordingly, we solve the first equation for x_1 and obtain

$$x_1 = \frac{1}{A_{11}}(b_1 - A_{12}x_2 - A_{13}x_3) \tag{B.2-1}$$

Substitution of this expression for x_1 into the second and third equations eliminates x_1 from these equations.

$$\begin{bmatrix} A_{11} & A_{12} & A_{13} \\ 0 & A_{22}-(A_{21}/A_{11})A_{12} & A_{23}-(A_{21}/A_{11})A_{13} \\ 0 & A_{32}-(A_{31}/A_{11})A_{12} & A_{33}-(A_{31}/A_{11})A_{13} \end{bmatrix} \begin{Bmatrix} x_1 \\ x_2 \\ x_3 \end{Bmatrix} = \begin{Bmatrix} b_1 \\ b_2-(A_{21}/A_{11})b_1 \\ b_3-(A_{31}/A_{11})b_1 \end{Bmatrix} \tag{B.2-2}$$

The next elimination treats the southeast 2 by 2 system of Eq. B.2-2 in similar fashion, by solving the middle equation for x_2 and substituting the resulting expression into the last equation. Thus $[\mathbf{A}]$ is triangularized, and unknowns $\{\mathbf{x}\}$ can be determined in the order x_3, x_2, x_1 by back substitution. A numerical example of Gauss elimination, using a 4 by 4 system, appears in Fig. 2.8-3.

If Gauss elimination is applied to a 2 by 2 matrix $[\mathbf{A}]$, we obtain

$$\text{Original } [\mathbf{A}]: \begin{bmatrix} a & b \\ c & d \end{bmatrix} \qquad \text{Reduced } [\mathbf{A}]: \begin{bmatrix} a & b \\ 0 & d-bc/a \end{bmatrix} \tag{B.2-3}$$

The latter form will be compared with related forms in what follows.

Symmetric [A]. Next we consider Gauss elimination applied to the common case of $[\mathbf{A}]$ symmetric. Thus, only the upper triangle of $[\mathbf{A}]$ needs to be stored and processed. A solution algorithm for a symmetric system of n equations appears in Table B.2-1. It differs from Eq. B.2-2 in that where a

TABLE B.2-1 GAUSS ELIMINATION SOLUTION OF $[\mathbf{A}]\{\mathbf{x}\} = \{\mathbf{b}\}$, WITH n BY n SYMMETRIC $[\mathbf{A}]$. INPUT MATRICES $[\mathbf{A}]$ AND $\{\mathbf{b}\}$ ARE OVERWRITTEN BY THE REDUCED $[\mathbf{A}]$ AND SOLUTION $\{\mathbf{x}\}$. REDUCTION OF $[\mathbf{A}]$ MUST PRECEDE REDUCTION OF $\{\mathbf{b}\}$. THE = SIGN MEANS "IS REPLACED BY," AS IN PROGRAMMING.

1. Reduction of symmetric $[\mathbf{A}]$	**2.** Forward reduction of $\{\mathbf{b}\}$	**3.** Back substitution, $\{\mathbf{b}\} \leftarrow \{\mathbf{x}\}$
For $k = 1,2,3,\ldots,n-1$ For $i = k+1, k+2,\ldots,n$ $r = A_{ki}/A_{kk}$ For $j = i, i+1,\ldots,n$ $A_{ij} = A_{ij} - rA_{kj}$ $A_{ki} = r$ [Ratios $r = A_{ki}/A_{kk}$ are now stored, as A_{ki}, and all diagonals A_{kk} but the last are unity (implicitly)]	For $k = 1,2,3,\ldots,n-1$ For $i = k+1, k+2,\ldots,n$ $b_i = b_i - A_{ki}b_k$	$b_n = b_n/A_{nn}$ For $k = n-1, n-2,\ldots,1$ For $i = k+1, k+2,\ldots,n$ $b_k = b_k - A_{ki}b_i$

lower-diagonal term such as A_{21} appears in Eq. B.2-2, the algorithm uses its equivalent upper-triangle term A_{12} instead (because the portion of [**A**] not yet triangularized remains symmetric). Also, only information in the upper triangle of [**A**] is processed. The last line of Step 1, $A_{ki} = r$, overwrites the original A_{ki} by the ratio A_{ki}/A_{kk} after the original A_{ki} is no longer needed. Thus, the A_{ki}/A_{kk} values to be used in reduction of {**b**} are preserved, and any number of different {**b**} vectors can be treated without having to process [**A**] again. Finally, in back substitution, the solution vector overwrites the original {**b**}. In Steps 1 and 3, note that after forward reduction each row of [**A**] but the last has been divided by its diagonal coefficient, but without bothering to either store or process numerical values of unity on the diagonal.

An operation count shows that if n is large, efficient reduction of a full but symmetric [**A**] requires about $n^3/6$ multiplications, while forward reduction and back substitution of {**b**} each require about $n^2/2$ multiplications. Thus the cost of treating each load vector is about $6/n$ times the cost of reducing [**A**].

Choleski Method. The Choleski method of solving [**A**]{**x**} = {**b**}, with [**A**] symmetric, calls for factoring [**A**] into the product $[\mathbf{U}]^T[\mathbf{U}]$, where [**U**] is upper triangular. For example, if [**A**] is 2 by 2, we obtain

$$[\mathbf{A}] = \begin{bmatrix} a & b \\ b & d \end{bmatrix} = [\mathbf{U}]^T[\mathbf{U}] = \begin{bmatrix} \sqrt{a} & 0 \\ b/\sqrt{a} & \sqrt{d-(b^2/a)} \end{bmatrix} \begin{bmatrix} \sqrt{a} & b/\sqrt{a} \\ 0 & \sqrt{d-(b^2/a)} \end{bmatrix} \tag{B.2-4}$$

which may be compared to Eq. B.2-3 with $c = b$. Solution of [**A**]{**x**} = {**b**} for {**x**} proceeds as follows.

$$[\mathbf{U}]^T[\mathbf{U}]\{\mathbf{x}\} = \{\mathbf{b}\} \qquad \text{Define } [\mathbf{U}]\{\mathbf{x}\} = \{\mathbf{y}\} \tag{B.2-5a}$$

$$\text{Solve } [\mathbf{U}]^T\{\mathbf{y}\} = \{\mathbf{b}\} \text{ for } \{\mathbf{y}\} \qquad \text{(forward substitution)} \tag{B.2-5b}$$

$$\text{Solve } [\mathbf{U}]\{\mathbf{x}\} = \{\mathbf{y}\} \text{ for } \{\mathbf{x}\} \qquad \text{(backward substitution)} \tag{B.2-5c}$$

The algorithm for obtaining [**U**] for a symmetric [**A**] of order n is as follows.

$$U_{11} = \sqrt{A_{11}} \qquad U_{1j} = A_{1j}/U_{11} \quad \text{for } j = 2,3,\ldots,n \tag{B.2-6a}$$

$$U_{ii} = \left(A_{ii} - \sum_{k=1}^{i-1} U_{ki}^2 \right)^{1/2} \qquad \text{for } i = 2,3,\ldots,n \tag{B.2-6b}$$

$$U_{ij} = \frac{1}{U_{ii}} \left(A_{ij} - \sum_{k=1}^{i-1} U_{ki}U_{kj} \right) \qquad \text{for } j = i+1,\ldots,n \tag{B.2-6c}$$

Equations B.2-6b and B.2-6c are used alternately: as soon as a U_{ii} is calculated, the U_{ij} for the same i are then calculated. Matrix [**A**] is overwritten by [**U**].

A variant of the Choleski factorization is $[\mathbf{A}] = [\mathbf{U}_1]^T\lceil\mathbf{D}\rfloor[\mathbf{U}_1]$, where $[\mathbf{U}_1]$ is upper triangular with 1's on its diagonal and $\lceil\mathbf{D}\rfloor$ is a diagonal matrix. The Choleski method and its variants provide

equation solvers of efficiency comparable to Gauss elimination, with differences related to the organization of computational loops and data storage [B.1]. Choleski decomposition, or a variant of it, is often used as a "preconditioner" in the conjugate gradient iterative solver.

Determinant. From Eqs. B.2-3 we see that det[**A**], the determinant of [**A**], is the product of diagonal terms in the reduced [**A**]. The same is true when [**A**] is of arbitrary order. In Choleski factorization, Eqs. B.2-5a, the determinant of [**A**] is the product of the squared U_{ii}, and in the factorization $[\mathbf{A}] = [\mathbf{U}_1]^T \lceil \mathbf{D} \rfloor [\mathbf{U}_1]$ it is the product of the D_{ii} in $\lceil \mathbf{D} \rfloor$. Because the magnitude of det[**A**] is usually very large, the product of diagonals is likely to overflow in numerical computation. It is better to calculate the logarithm of the determinant by adding logarithms of diagonal coefficients.

Sparsity. The foregoing algorithms are stated for a full matrix [**A**], ignoring the fact that [**A**] is usually sparse in FEA. Contents of the global matrix [**A**] before reduction are often less than 5% nonzero, and perhaps less than 1% nonzero if there are thousands of d.o.f. During reduction of [**A**], a direct solver changes most zeros between the skyline and the diagonal to nonzero, but leaves zeros above the skyline intact, so the matrix remains sparse. FE software exploits sparsity by using compact storage formats, so that zeros above the skyline are neither stored nor processed, and by renumbering nodes (for internal processing only) in such a way that the compact storage format is effectively used. Here we make no attempt to further explore this extensive subject area. A brief discussion appears in Section 2.8. References include [2.16,B.2–B.4].

Frontal Method. A direct solver such as Gauss elimination does not require that the global matrix [**A**] be assembled before starting to solve equations. Steps of assembly can alternate with steps of solution. When enough elements have been assembled to complete the initial portion of the global matrix, solution begins, then temporarily ceases when more of the matrix must be built by assembly. Phases of partial assembly and partial solution alternate until the entire system has been assembled and solved. Names associated with this way of arranging the calculations are *frontal method* or *wavefront method,* because d.o.f. currently active in assembly and solution can be visualized as a "wave" or "front" that passes over the structure as the assembly-solution alternation progresses. When "wavefront" is used to indicate size, it refers to the number of d.o.f. currently active. Efficiency increases as front size decreases. The order in which equations are processed depends on element numbering, not node numbering, so we seek an effective numbering sequence for elements [B.4].

Development of the wavefront method was prompted by the desire to solve sizeable problems on machines with limited high-speed storage space. As compared with a solver that requires assembly of the entire coefficient matrix before solution begins, a frontal solver requires more internal bookkeeping. The overall efficiency of either arrangement is considerably influenced by the time needed to transfer data in and out of high-speed storage. A frontal solver offers no speed advantage if high-speed storage can accommodate the entire coefficient matrix.

Remark. Every solution algorithm has many variants, such as how coefficients are stored and whether computer coding is row-oriented or column-oriented. Such details are of no concern to the typical user of FEA. Interested readers may consult published coding. Some of many references are [2.13,2.14,4.4,B.2,B.5–B.10].

B.3 ITERATIVE SOLVERS

Numerical analysis textbooks discuss classical iterative methods such as the Gauss-Seidel method and successive over-relaxation [17.20]. These methods are too slow to be useful in FEA. In what follows we summarize the conjugate gradient method, which is currently in favor, and the multigrid method.

Conjugate Gradient (CG) Method. The problem is to solve equations $[\mathbf{A}]\{\mathbf{x}\} = \{\mathbf{b}\}$ for unknowns $\{\mathbf{x}\}$. In the following summary we assume that $[\mathbf{A}]$ is symmetric. The problem of solving for $\{\mathbf{x}\}$ may be stated as a minimization problem:

$$\text{Minimize} \quad \{\mathbf{r}\} = \{\mathbf{b}\} - [\mathbf{A}]\{\mathbf{x}\} \quad \text{or} \quad \text{minimize} \quad \Pi = \frac{1}{2}\{\mathbf{x}\}^T[\mathbf{A}]\{\mathbf{x}\} - \{\mathbf{x}\}^T\{\mathbf{b}\} \tag{B.3-1}$$

where $\{\mathbf{r}\}$ is the residual and, in structural mechanics, Π is potential energy. The conjugate gradient method can be regarded as a minimum-seeking procedure, and as such is part of optimization theory [B.11]. The gradient of Π is $-\{\mathbf{r}\}$, so (positive) $\{\mathbf{r}\}$ is the direction of steepest descent from a given approximate $\{\mathbf{x}\}$. The CG method uses search directions $\{\mathbf{p}\}$ that are close to directions of steepest descent, subject to the constraint that vectors $\{\mathbf{p}\}$ are *conjugate;* that is, orthogonal to $[\mathbf{A}]$, which means that $\{\mathbf{p}\}_i^T[\mathbf{A}]\{\mathbf{p}\}_j = 0$ for $i \neq j$. The solution is a weighted sum of the $\{\mathbf{p}\}$ vectors.

$$\{\mathbf{x}\} = \alpha_1\{\mathbf{p}\}_1 + \alpha_2\{\mathbf{p}\}_2 + \cdots + \alpha_m\{\mathbf{p}\}_m \tag{B.3-2}$$

If calculations could be done in exact arithmetic, the exact $\{\mathbf{x}\}$ would appear when $m = n$, where m is the number of search directions (or the number of iterations) and n is the order of the system of equations to be solved. Computer numbers have only finite precision, so n steps do not produce exact results. Computation is stopped when results are "close enough" according to a convergence test. For the method to be practical, the convergence test must be satisfied when m is much less than n.

Even the basic CG algorithm, reported in 1952 [B.12], has several variants. One of them is stated in the left-hand column of Table B.3-1. Storage space must be allocated for the upper or lower triangle of the original symmetric $[\mathbf{A}]$, doubtless in some sparse-matrix format, and for five vectors, including $\{\mathbf{x}\}$. The disadvantage of this algorithm is that more and more iterations are required as the condition number of $[\mathbf{A}]$ increases. For practical use, *preconditioning* is required.

Preconditioned CG Method. A preconditioner is a supplementary matrix, called $[\mathbf{C}]$ in Table B.3-1, which is inserted into the CG algorithm. Its role is to provide an approximate inverse of $[\mathbf{A}]$. Of course, the inverse is not constructed; equation-solving operations are used instead, to provide $\{\mathbf{z}\} = [\mathbf{C}]^{-1}\{\mathbf{r}\}$ in the right-hand column of Table B.3-1. These operations increase the computational effort per iterative cycle but reduce the number of cycles required. We do not use $[\mathbf{C}] = [\mathbf{A}]$ because that implies a full-blown direct solution, making iteration unnecessary. The desired attributes of $[\mathbf{C}]^{-1}$ are conflicting: it should be easily constructed, contain few nonzero terms, and be a good approximation of $[\mathbf{A}]^{-1}$.

In practice the approximation may be crude. In the simplest approximation, called Jacobi preconditioning, $[\mathbf{C}]$ is a diagonal matrix whose entries are the diagonal coefficients of $[\mathbf{A}]$. Thus we obtain the JCG method. More widely used is incomplete Choleski preconditioning, which provides the ICCG method. The ICCG method uses Choleski factors (Eqs. B.2-6 or one of the closely related Choleski variants), with the important difference that *fill-in terms are ignored.* Thus, the incomplete Choleski factor $[\mathbf{U}]$ requires only as much storage space as the unfactored $[\mathbf{A}]$. In a variant of the factorization, a fill-in term is ignored if its magnitude falls below a prescribed threshold [B.13–B.15]. Discarding fill-in terms may cause a negative diagonal to appear during factorization. Negative diagonals can be avoided by multiplying original diagonal terms by a number slightly greater than unity, typically less than 1.05 but perhaps as great as 1.5 [B.1,B.14,B.15]. When using the ICCG algorithm in Table B.3-1, the Choleski-factored $[\mathbf{A}]$ is used as preconditioner matrix $[\mathbf{C}]$, where $[\mathbf{C}] = [\mathbf{U}]^T[\mathbf{U}]$. Operations in Table B.3-1 that use $[\mathbf{C}]^{-1}$ call for direct equation-solving procedures, not actual inversion. The ICCG algorithm is preferable to the JCG algorithm if the problem is not well-conditioned. ICCG requires about twice as much storage space as JCG, but still much less storage than required by a direct solver. References include [2.14,2.20,12.15,B.16].

TABLE B.3-1 CONJUGATE GRADIENT ALGORITHMS THAT SOLVE FOR $\{\mathbf{x}\}$ IN THE EQUATION SYSTEM $[\mathbf{A}]\{\mathbf{x}\} = \{\mathbf{b}\}$, WITH SYMMETRIC $[\mathbf{A}]$. PRECONDITIONING MATRIX $[\mathbf{C}]$ IS USED IN THE PRECONDITIONED CG ALGORITHM.

Conjugate gradient (CG) algorithm	Preconditioned CG algorithm
Initialize:	Initialize:
Choose $\{\mathbf{x}\}_1$	Choose $\{\mathbf{x}\}_1$
$\{\mathbf{p}\}_1 = \{\mathbf{r}\}_1 = \{\mathbf{b}\} - [\mathbf{A}]\{\mathbf{x}\}_1$	$\{\mathbf{r}\}_1 = \{\mathbf{b}\} - [\mathbf{A}]\{\mathbf{x}\}_1$
	$\{\mathbf{p}\}_1 = \{\mathbf{z}\}_1 = [\mathbf{C}]^{-1}\{\mathbf{x}\}_1$
For $i = 1, 2, \ldots$, until convergence:	For $i = 1, 2, \ldots$, until convergence:
$\{\mathbf{v}\}_i = [\mathbf{A}]\{\mathbf{p}\}_i$	$\{\mathbf{v}\}_i = [\mathbf{A}]\{\mathbf{p}\}_i$
$\alpha_i = \dfrac{\{\mathbf{r}\}_i^T\{\mathbf{r}\}_i}{\{\mathbf{p}\}_i^T\{\mathbf{v}\}_i}$	$\alpha_i = \dfrac{\{\mathbf{z}\}_i^T\{\mathbf{r}\}_i}{\{\mathbf{p}\}_i^T\{\mathbf{v}\}_i}$
$\{\mathbf{x}\}_{i+1} = \{\mathbf{x}\}_i + \alpha_i\{\mathbf{p}\}_i$	$\{\mathbf{x}\}_{i+1} = \{\mathbf{x}\}_i + \alpha_i\{\mathbf{p}\}_i$
$\{\mathbf{r}\}_{i+1} = \{\mathbf{r}\}_i - \alpha_i\{\mathbf{v}\}_i$	$\{\mathbf{r}\}_{i+1} = \{\mathbf{r}\}_i - \alpha_i\{\mathbf{v}\}_i$
Stop if converged	Stop if converged
	$\{\mathbf{z}\}_{i+1} = [\mathbf{C}]^{-1}\{\mathbf{r}\}_{i+1}$
$\beta_i = \dfrac{\{\mathbf{r}\}_{i+1}^T\{\mathbf{r}\}_{i+1}}{\{\mathbf{r}\}_i^T\{\mathbf{r}\}_i}$	$\beta_i = \dfrac{\{\mathbf{z}\}_{i+1}^T\{\mathbf{r}\}_{i+1}}{\{\mathbf{z}\}_i^T\{\mathbf{r}\}_i}$
$\{\mathbf{p}\}_{i+1} = \{\mathbf{r}\}_{i+1} + \beta_i\{\mathbf{p}\}_i$	$\{\mathbf{p}\}_{i+1} = \{\mathbf{z}\}_{i+1} + \beta_i\{\mathbf{p}\}_i$
$i \leftarrow i+1$	$i \leftarrow i+1$

The convergence test may take various forms. One possibility is to stop iterations when the Euclidean norm of the residual vector is less than 10^{-6} times the Euclidean norm of $\{\mathbf{b}\}$ [B.17]. Here we presume that $\{\mathbf{b}\}$ is not null; accordingly, loads and/or boundary condition treatments must make contributions to $\{\mathbf{b}\}$. Criteria based on energy or entirely on displacements have also been proposed. One may require that two different criteria both be satisfied (see Eqs. 17.2-10, for example). Discussion appears in [2.17,B.17,B.18].

Test problems show that, for some problems, a direct solver may be worse than an ICCG solver by a factor of six for time required and a factor of 15 for storage space required [B.19]. Comparisons also appear in [B.1] and various other papers. Comparisons inevitably depend on specifics of the algorithms, how skillfully they are coded, the particular problems used as test cases, and the type of computer used.

Multigrid Methods. In structural terms, iterative methods are found to provide fast reduction of residuals associated with the most complicated displacement modes a mesh can represent, but much slower convergence for long-wavelength modes that span many elements. This observation suggests the use of both fine and coarse meshes to solve a single problem. Iteration is applied to equations that represent both meshes. Errors associated with short wavelengths are quickly reduced using the fine mesh, then remaining residuals (associated with long wavelengths) are transferred to a coarse mesh, where they are perceived as associated with short wavelengths due to the coarseness of the

mesh, and quickly reduced. Alternatively, a direct solver may be applied to the coarse mesh. Alternation between meshes proceeds until convergence.

Multigrid efficiency is claimed to be greater than JCG efficiency. As with most other iterative methods, each new $\{\mathbf{b}\}$ vector constitutes a new problem, and convergence is slower when the problem is ill-conditioned. Coding for iteration must be supplemented by coding that transfers residuals from fine mesh to coarse and transfers the updated solution from coarse mesh to fine. Accordingly, a multigrid solver cannot be divorced from the mesh, in contrast to direct and CG solvers. References include [B.17,B.20,B.21].

Remarks. In comparison with direct methods, CG methods are better suited to larger problems, say 50,000 d.o.f. or more, for which the coefficient matrix is well-conditioned. A CG method may be slower than a direct method if the coefficient matrix is not well-conditioned (difficulty has been reported for some shell problems and when elements are considerably elongated). Similar remarks apply to the comparison between direct methods and multigrid methods. If available storage is not great enough to accommodate a direct solver, there is little choice but to use an iterative solver.

Again, iterative solvers have the drawback that each new vector $\{\mathbf{b}\}$ constitutes a new problem, so that the time required is directly proportional to the number of right-hand sides. Another type of iterative solver, based on a preconditioned Lanczos method, fares better with multiple right-hand sides, but is not as fast as ICCG for a single right-hand side [2.17]. Iterative methods may be particularly appropriate in nonlinear problems, where each advance of the solution (as by incrementing the load) may produce only small changes, so that the previous solution vector is an excellent starting vector for the next solution.

There are connections among iterative methods, and between iterative and direct methods [B.12]. The preconditioner of the ICCG method, being an approximate inverse of $[\mathbf{A}]$, is dominated by lower eigenvalues of $[\mathbf{A}]$ (see Eq. 9.3-5 or Eq. C.2-4). In other words, the preconditioner reduces long-wavelength errors in the ICCG method, just as the coarse mesh reduces them in a multigrid solution. One might also say that the coarse mesh of a multigrid solution acts as a preconditioner for the fine mesh. Convergence of a viscous relaxation solution can also be speeded by applying the preconditioner concept (see Section 17.2 and [17.10]).

APPENDIX C

EIGENVALUES AND EIGENVECTORS

C.1 OVERVIEW

Let [**A**] and [**B**] be n by n square matrices. The eigenproblem asks for values of a scalar λ such that the matrix equation

$$\Big([\mathbf{A}] - \lambda[\mathbf{B}]\Big)\{\mathbf{x}\} = \{\mathbf{0}\} \tag{C.1-1}$$

has solutions other than the trivial solution $\{\mathbf{x}\} = \{\mathbf{0}\}$. There are at most n nonzero roots λ_i, not necessarily all distinct. The λ_i are called *eigenvalues* (alternative names include *characteristic values, latent roots, proper values, and principal values*). Corresponding to each λ_i is an $\{\mathbf{x}\}_i$ called an *eigenvector* (alternative names include *characteristic vector, proper vector, principal vector, principal mode, normal mode,* and *natural mode*). Together, λ_i and its associated $\{\mathbf{x}\}_i$ are called an *eigenpair.* Equation C.1-1 is called a *generalized eigenproblem* or simply an *eigenproblem.* If [**B**] happens to be the unit matrix $\lceil\mathbf{I}\rfloor$, Eq. C.1-1 is called a *standard eigenproblem* and the associated λ_i are called eigenvalues of [**A**].

A common physical problem characterized by Eq. C.1-1 is that of undamped mechanical vibration, where [**A**] is a stiffness matrix, [**B**] is a mass matrix, $\sqrt{\lambda_i} = \omega_i$ is a vibration frequency, and $\{\mathbf{x}\}_i$ is the associated mode of vibration. Elementary aspects of the vibration eigenproblem are discussed in Section 11.4.

In what follows we state some properties of eigenproblems, usually without proof, then briefly summarize some solution techniques, without providing details. The computational scene is complicated by the practice of using supplementary techniques to improve basic algorithms and by the use of basic algorithms in combination. Considerations that influence the choice of algorithm include the order of matrices involved, their topology, and how many eigenvalues are required.

The literature of eigenproblems is quite large, both for theoretical aspects and for numerical algorithms, and we cite only a small fraction of it. Some FE books contain extensive discussions [2.13,2.14,2.20]. Other books and review papers include [11.24,C.1–C.7].

C.2 THE STANDARD EIGENPROBLEM

Consider first an eigenproblem of the form

$$\Big([\mathbf{A}^*] - \lambda\lceil\mathbf{B}^*\rfloor\Big)\{\mathbf{x}^*\} = \{\mathbf{0}\} \tag{C.2-1}$$

where $[\mathbf{A}^*]$ is an arbitrary square matrix of order n and $\lceil\mathbf{B}^*\rfloor$ is diagonal, of the same order, and nonsingular. Thus, all of the B^*_{ii} must be nonzero. We define a diagonal matrix $\lceil\mathbf{T}\rfloor$ and a transformation of $\{\mathbf{x}^*\}$ by

$$T_{ii} = \frac{1}{\sqrt{B_{ii}}} \qquad \text{and} \qquad \{\mathbf{x}^*\} = \lceil\mathbf{T}\rfloor\{\mathbf{x}\} \tag{C.2-2}$$

Premultiplication of Eq. C.2-1 by $\lceil \mathbf{T} \rfloor$ and substitution from Eq. C.2-2 yields the *standard eigenproblem.*

$$\Big([\mathbf{A}] - \lambda \lceil \mathbf{I} \rfloor\Big)\{\mathbf{x}\} = \{\mathbf{0}\} \tag{C.2-3}$$

where $[\mathbf{A}] = \lceil \mathbf{T} \rfloor [\mathbf{A}^*] \lceil \mathbf{T} \rfloor$. Equations C.2-1 and C.2-3 have the same eigenvalues, and eigenvectors related by Eq. C.2-2. Properties of Eq. C.2-3 that may be useful in engineering applications are as follows, most of which can be deduced from information in [A.1].

1. If $[\mathbf{A}]$ is real and symmetric, the λ_i are real.
2. If $[\mathbf{A}]$ is real, symmetric, and positive semidefinite, there are no negative λ_i. The number of nonzero λ_i equals the rank of $[\mathbf{A}]$.
3. If $[\mathbf{A}]$ is real, symmetric, and positive definite, the λ_i are all positive.
4. If $[\mathbf{A}]$ is real and positive definite but unsymmetric, the matrix $[\mathbf{A}] + [\mathbf{A}]^T$ has positive eigenvalues.
5. The sum of the λ_i equals the trace of $[\mathbf{A}]$, and the product of the λ_i equals the determinant of $[\mathbf{A}]$.
6. If $\{\mathbf{x}\}_i$ is an eigenvector, so is $c\{\mathbf{x}\}_i$, where c is an arbitrary nonzero scalar.
7. If all λ_i are distinct, all eigenvectors are distinct and linearly independent.
8. If a λ_i is repeated k times, the associated eigenvectors are not unique, but a set of k mutually orthogonal eigenvectors can be constructed [2.14].
9. Let $[\mathbf{G}]$ be a square matrix, nonsingular and the same order as $[\mathbf{A}]$ but otherwise arbitrary. A matrix $[\mathbf{C}]$ obtained by the *similarity transformation* $[\mathbf{C}] = [\mathbf{G}]^{-1}[\mathbf{A}][\mathbf{G}]$ has the same eigenvalues as $[\mathbf{A}]$. If $\{\mathbf{x}_c\}$ is an eigenvector of $[\mathbf{C}]$, the corresponding eigenvector of $[\mathbf{A}]$ is $[\mathbf{G}]\{\mathbf{x}_c\}$.
10. If $[\mathbf{A}]$ is real and symmetric, its eigenvectors are orthogonal; that is, $\{\mathbf{x}\}_i^T\{\mathbf{x}\}_j = 0$ for $i \neq j$.
11. If an eigenvector is scaled so that $\{\mathbf{x}\}_i^T\{\mathbf{x}\}_i = 1$, then $\{\mathbf{x}\}_i^T[\mathbf{A}]\{\mathbf{x}\}_i = \lambda_i$ (see the Rayleigh quotient for the real symmetric case, Eq. 11.4-13 or Eq. C.3-11).
12. If each eigenvector is scaled so that $\{\mathbf{x}\}_i^T\{\mathbf{x}\}_i = 1$ and $[\mathbf{A}]$ is symmetric, positive definite, and of order n, then

$$[\mathbf{A}] = \sum_{i=1}^{n} \lambda_i \{\mathbf{x}\}_i\{\mathbf{x}\}_i^T \quad \text{and} \quad [\mathbf{A}]^{-1} = \sum_{i=1}^{n} \frac{1}{\lambda_i} \{\mathbf{x}\}_i\{\mathbf{x}\}_i^T \tag{C.2-4}$$

C.3 THE GENERAL EIGENPROBLEM

The *general eigenproblem* has the form

$$\Big([\mathbf{A}] - \lambda[\mathbf{B}]\Big)\{\mathbf{x}\} = \{\mathbf{0}\} \tag{C.3-1}$$

where $[\mathbf{A}]$ and $[\mathbf{B}]$ are square matrices of order n. In what follows we assume that $[\mathbf{A}]$ *and* $[\mathbf{B}]$ *are symmetric and not indefinite*. Such is the case in the great majority of FE applications. In structural mechanics, $[\mathbf{A}]$ is a stiffness matrix that is positive semidefinite, and positive definite if rigid-body motion and mechanisms are suppressed; and $[\mathbf{B}]$ is a mass matrix that is positive semidefinite if some d.o.f. have no mass, and positive definite if all d.o.f. are associated with positive mass. (Some optimal lumping schemes can produce negative masses and an indefinite $[\mathbf{B}]$; see [11.11,C.8]).

If Eq. C.3-1 is to be satisfied for nonzero $\{\mathbf{x}\}$, the determinant of the coefficient matrix must vanish.

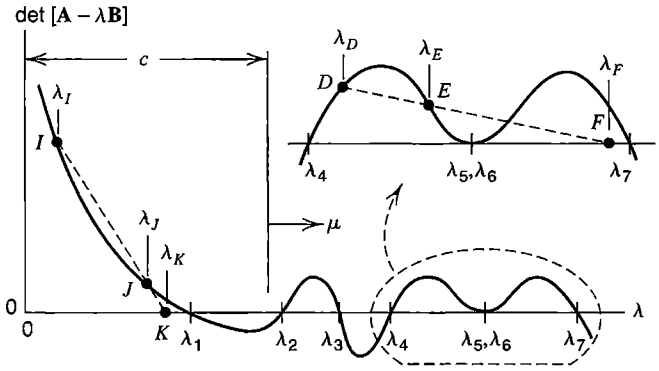

Figure C.3-1. The characteristic polynomial of Eq. C.3-2. Roots λ_i, for $i = 1,2,3,\ldots$ are eigenvalues. Distance c is an eigenvalue shift, Eq. C. 3-3.

$$\det[\mathbf{A} - \lambda\mathbf{B}] = 0 \tag{C.3-2}$$

Multiplied out, this determinant is a polynomial in λ of degree n, where n is the order of [**A**] and [**B**], and whose roots λ_i are the desired eigenvalues (Fig. C.3-1). Obtaining the λ_i by extracting polynomial roots is suitable for hand calculation if $n = 2$, but it is not a practical numerical method. Indeed for $n > 4$ no closed-form solution for polynomial roots exists. Accordingly, for $n > 4$, all eigenvalue extraction methods are iterative [2.14].

Shifting. If we substitute $\lambda = \mu + c$ into Eq. C.3-1, where c is a constant called the "eigenvalue shift," we obtain

$$\Big([\mathbf{A} - c\mathbf{B}] - \mu[\mathbf{B}]\Big)\{\mathbf{x}\} = \{\mathbf{0}\} \qquad \text{where} \qquad \mu = \lambda - c \tag{C.3-3}$$

Equation C.3-3 has the same eigenvectors as Eq. C.3-1, but eigenvalues are decreased by c (Fig. C.3-1). In structural mechanics, the physical interpretation of shifting is that a spring of stiffness $-cB_{ii}$ is added between each d.o.f. x_i and ground, thus preventing rigid-body motion. If [**A**] and [**B**] are positive semidefinite and c is a negative number, [**A** − c**B**] is almost always positive definite in practical problems. Therefore a possible application of shifting is to make it possible to use an eigensolver that cannot deal with a singular [**A**]. More often, a positive c is used, as in inverse iteration to obtain an eigenvalue λ other than the lowest eigenvalue. Although [**A** − c**B**] becomes ill-conditioned as c approaches an eigenvalue, the error created in $\{\mathbf{x}\}$ is proportional to $\{\mathbf{x}\}$, so no harm is done [11.21].

Reduction to Standard Form. If [**B**] in Eq. C.3-1 is positive definite, it may be factored according to Eqs. B.2-6. Let us do so, and also define a new vector $\{\mathbf{x}_U\}$. Thus,

$$[\mathbf{B}] = [\mathbf{U}]^T[\mathbf{U}] \qquad \text{and} \qquad \{\mathbf{x}_U\} = [\mathbf{U}]\{\mathbf{x}\} \qquad \text{so} \qquad \{\mathbf{x}\} = [\mathbf{U}]^{-1}\{\mathbf{x}_U\} \tag{C.3-4}$$

If Eq. C.3-1 is premultiplied by $[\mathbf{U}]^{-T}$ and Eqs. C.3-4 are substituted, we obtain

$$\Big([\mathbf{A}_U] - \lambda[\mathbf{I}]\Big)\{\mathbf{x}_U\} = \{\mathbf{0}\} \qquad \text{where} \qquad [\mathbf{A}_U] = [\mathbf{U}]^{-T}[\mathbf{A}][\mathbf{U}]^{-1} \tag{C.3-5}$$

This transformation, which is called a *congruence transformation,* alters eigenvectors but not eigenvalues. If [**B**] is diagonal, the transformation reduces to that of Eqs. C.2-2 and C.2-3. If [**B**] is singular but [**A**] is not, Eq. C.3-1 can be rewritten as

$$\left([\mathbf{B}] - \frac{1}{\lambda}[\mathbf{A}]\right)\{\mathbf{x}\} = \{\mathbf{0}\} \tag{C.3-6}$$

and the $[\mathbf{U}]^T[\mathbf{U}]$ factorization can be applied to $[\mathbf{A}]$. If a general eigenproblem can be converted to a standard eigenproblem, properties are those of the standard problem [2.14].

Eigenvector Orthogonality. Let Eq. C.3-1 be written for the ith eigenpair and again for the jth eigenpair.

$$\Big([\mathbf{A}] - \lambda_i[\mathbf{B}]\Big)\{\mathbf{x}\}_i = \{\mathbf{0}\} \qquad \Big([\mathbf{A}] - \lambda_j[\mathbf{B}]\Big)\{\mathbf{x}\}_j = \{\mathbf{0}\} \tag{C.3-7}$$

Next, premultiply the first equation by $\{\mathbf{x}\}_j^T$, the second by $\{\mathbf{x}\}_i^T$, and transpose the second equation, recalling that $[\mathbf{A}]$ and $[\mathbf{B}]$ are symmetric. Thus,

$$\{\mathbf{x}\}_j^T\Big([\mathbf{A}] - \lambda_i[\mathbf{B}]\Big)\{\mathbf{x}\}_i = 0 \qquad \{\mathbf{x}\}_j^T\Big([\mathbf{A}] - \lambda_j[\mathbf{B}]\Big)\{\mathbf{x}\}_i = 0 \tag{C.3-8}$$

Finally, subtract the first equation from the second, and assume for now that $\lambda_i - \lambda_j \neq 0$, as is usually the case. Thus,

$$(\lambda_i - \lambda_j)\{\mathbf{x}\}_j^T[\mathbf{B}]\{\mathbf{x}\}_i = 0 \qquad \text{therefore} \qquad \{\mathbf{x}\}_j^T[\mathbf{B}]\{\mathbf{x}\}_i = 0 \qquad \text{for } i \neq j \tag{C.3-9}$$

The latter equation states that eigenvectors are orthogonal with respect to matrix $[\mathbf{B}]$. In the event that $\lambda_i = \lambda_j$, the foregoing proof fails, but it is still possible to choose as many mutually orthogonal eigenvectors as there are multiplicities of an eigenvalue [2.14]. By repeating the argument, using Eq. C.3-6 instead of Eq. C.3-1, we show that eigenvectors are also orthogonal with respect to matrix $[\mathbf{A}]$.

$$\{\mathbf{x}\}_j^T[\mathbf{A}]\{\mathbf{x}\}_i = 0 \qquad \text{for} \quad i \neq j \tag{C.3-10}$$

Rayleigh Quotient. Let Eq. C.3-1 be written for the ith eigenpair. Then premultiply by $\{\mathbf{x}\}_i^T$ and solve for λ_i. The result is called the *Rayleigh quotient:*

$$\lambda_i = \frac{\{\mathbf{x}\}_i^T[\mathbf{A}]\{\mathbf{x}\}_i}{\{\mathbf{x}\}_i^T[\mathbf{B}]\{\mathbf{x}\}_i} \tag{C.3-11}$$

If $\{\mathbf{x}\}_i$ is an approximate eigenvector having first-order error, λ_i has second-order error. Thus, a casual approximation $\{\mathbf{x}\}_i$ may produce a λ_i of adequate accuracy. The Rayleigh quotient is, in fact, an extreme value when $\{\mathbf{x}\}_i$ varies in the neighborhood of its exact value. Therefore, extraction of an eigenvalue can be approached as a minimization problem. Maximum and minimum eigenvalues of Eq. C.3-1 bound the Rayleigh quotient; that is, for an *arbitrary* vector $\{\mathbf{v}\}$,

$$\lambda_{\min} \leq \frac{\{\mathbf{v}\}^T[\mathbf{A}]\{\mathbf{v}\}}{\{\mathbf{v}\}^T[\mathbf{B}]\{\mathbf{v}\}} \leq \lambda_{\max} \tag{C.3-12}$$

If $[\mathbf{B}]$ is indefinite or semidefinite, as may happen with optimal mass lumping or lumping with zero rotary inertia, the Rayleigh quotient may be positive or negative infinity for some choices of $\{\mathbf{v}\}$.

Normalized Eigenvectors. An eigenvector can be normalized with respect to [**B**] by scaling its terms by a constant a:

$$\text{Calculate:} \quad \{\mathbf{x}\}_i^T[\mathbf{B}]\{\mathbf{x}\}_i = a^2 \qquad \text{Normalized vector:} \quad \{\mathbf{x}_N\}_i = \frac{1}{a}\{\mathbf{x}\}_i \tag{C.3-13}$$

The normalized eigenvector reduces the Rayleigh quotient to $\lambda_i = \{\mathbf{x}_N\}_i^T[\mathbf{A}]\{\mathbf{x}_N\}_i$.

C.4 SOLUTION ALGORITHMS

Typically we seek only the lowermost eigenpairs of Eq. C.1-1. In structural dynamics, where [**A**] is a stiffness matrix and [**B**] is a mass matrix, the highest eigenpairs are not needed, and are not accurate anyway due to discretization error. Sometimes eigenpairs in a certain range of frequencies are desired. Extracting eigenpairs requires considerably more computation than solving equations. Many methods have been devised. Which algorithm is fastest depends on the size of arrays, their sparsity, how many eigenpairs are needed, computer architecture, and how skillfully algorithms are coded.

What follows is a brief survey of methods that have practical value. Details appear in references cited. Explanations pertain to Eq. C.3-1, but Eq. C.3-3 may be used instead, in which case *shifted* eigenvalues μ are computed.

Transformation Methods. Classical transformation methods apply to the standard eigenproblem, Eq. C.2-3. If [**B**] is diagonal, the standard form is readily obtained (Eqs. C.2-2), and the original topology of [**A**] is preserved. With a transformation method, one does not ask for the lowest several eigenvalues. *All* eigenvalues are extracted simultaneously. Therefore transformation methods are suited to comparatively small matrices.

The *Jacobi method* reduces [**A**] to a diagonal matrix whose terms are eigenvalues, and provides a supplementary matrix whose columns are eigenvectors. The method is simple and stable, and can deal with positive, negative, and zero eigenvalues. It is most efficient if [**A**] is narrowly banded. A modified form applies to the general eigenproblem, Eq. C.3-1 [2.14].

The *Householder-QR method* is more appropriate when [**A**] is more nearly a full matrix. The Householder transformation reduces [**A**] to a tridiagonal matrix, eigenvalues of which are extracted by the QR method [2.14]. The eigenvectors, if desired, can be obtained by another method such as inverse iteration, which converges rapidly because eigenvalues are already known.

Determinant Search. Determinant search is a "brute force" method best suited to extracting no more than a few eigenvalues of a narrowly banded matrix. The method exploits the property that the determinant of [$\mathbf{A} - \lambda\mathbf{B}$] is zero when λ is an eigenvalue. Starting with a trial value λ_I, the determinant is computed (a computational method is summarized in Section B.2). The determinant is then calculated using trial value λ_J. Thus we obtain points I and J in Fig. C.3-1. The secant, indicated by a dashed line, indicates trial value λ_K for the next determinant calculation, and so on until convergence at eigenvalue λ_1. Secant iteration can be accelerated [C.5]. For convergence of the process, one might require that $\Delta\lambda/\lambda$ be less than 10^{-5} or 10^{-6}, where $\Delta\lambda$ is the change between the current and previous estimates of λ, and λ is the current estimate. Eigenvectors, if desired, are obtained by another method such as inverse iteration, which converges rapidly because eigenvalues are already known. Determinant search may converge to a root other than the one desired, and secant iteration may skip over a root (see the inset in Fig. C.3-1).

Sturm Sequence. For a trial value of λ, let $[\mathbf{A} - \lambda\mathbf{B}]$ be converted to the upper triangular matrix $[\mathbf{U}_G]$ by Gauss elimination, or factored into the form $[\mathbf{U}_1]^T\lceil\mathbf{D}\rfloor[\mathbf{U}_1]$. (These operations would also be used if the determinant were to be evaluated.) The number of negative terms on the diagonal of $[\mathbf{U}_G]$, or in $\lceil\mathbf{D}\rfloor$, is equal to the number of eigenvalues smaller than the trial value of λ. This is the Sturm sequence property. It is useful in checking that an algorithm has not missed any roots. Thus, in the inset in Fig. C.3-1, we would be able to detect that there are two eigenvalues between trial values λ_E and λ_F.

Inverse Iteration. One starts with a trial vector and successively determines improved vectors. A computed vector is normalized after it is calculated. Then the eigenvalue is supplied by the Rayleigh quotient, whose denominator is unity because vectors are normalized. The kth iteration of the basic inverse-iteration algorithm is

$$\begin{aligned}
&\text{Determine } \{\mathbf{x}^k\}: && [\mathbf{A}]\{\mathbf{x}^k\} = [\mathbf{B}]\{\mathbf{x}_N^{k-1}\} \\
&\text{Normalize:} && \{\mathbf{x}_N^k\} = \frac{\{\mathbf{x}^k\}}{\left(\{\mathbf{x}^k\}^T[\mathbf{B}]\{\mathbf{x}^k\}\right)^{1/2}} \\
&\text{Obtain root:} && \lambda^k = \{\mathbf{x}_N^k\}^T[\mathbf{A}]\{\mathbf{x}_N^k\}
\end{aligned} \tag{C.4-1}$$

where, to begin, $k = 1$ and the initial trial vector might be arbitrarily taken as $\{\mathbf{x}_N^0\} = \lfloor 1\,0\,0 \ldots 0\rfloor^T$. Calculation of $\{\mathbf{x}^k\}$ involves equation-solving operations, not inversion of $[\mathbf{A}]$. The purpose of normalization is to prevent the eigenvector from shrinking or growing without limit, so any convenient normalization method will do. If the "normalize" method shown in Eqs. C.4-1 is substituted into the "obtain root" step, we see that λ^k is computed by the Rayleigh quotient, Eq. C.3-11.

Convergence of λ^k is to the smallest eigenvalue, or, if the shifted equation C.3-3 has been used, to the eigenvalue λ closest to shift point c. Convergence is speeded when c is close to the eigenvalue, which suggests that c be updated after a few iterations; however, the coefficient matrix must then be refactored for equation-solving. Details and computational improvements appear in [2.14]. Convergence may be assessed as described in connection with the determinant search method.

The method is called "inverse iteration" because there is a "forward iteration" method, in which $[\mathbf{A}]$ and $[\mathbf{B}]$ are interchanged in the first of Eqs. C.4-1. Forward iteration is very fast if $[\mathbf{B}]$ is diagonal, but the method converges to the *largest* eigenvalue of Eq. C.3-1.

Subspace Iteration. This method is widely used to obtain a prescribed number of the lowest eigenpairs. It is a generalization of inverse iteration, in which the single vector $\{\mathbf{x}\}$ is replaced by a matrix $[\mathbf{x}]$ whose columns function as Ritz vectors that span a subspace of the entire eigenproblem. If p accurate eigenpairs are desired, it is recommended that the number of columns in $[\mathbf{x}]$ be $2p$ or $p + 8$, whichever is smaller. A Sturm sequence check can detect whether the method has missed any eigenpairs. Details appear in [2.13,2.14,C.9].

Lanczos Method. Like subspace iteration, the Lanczos method is used to obtain a number of eigenpairs by using multiple vectors to span a subspace. The vectors are generated sequentially as iteration proceeds. The result is a tridiagonal matrix from which eigenvalues are extracted. The method requires comparative little storage and is claimed to be from two to ten times faster than subspace iteration [11.24]. The basic algorithm "can be easily misused and greatly improved" [C.10]. Indeed, its acceptance was preceded by years of tinkering and enhancements, and work continues. References include [2.13,2.14,11.24,C.3].

Other Methods. The conjugate gradient method, summarized in Section B.3 as an equation solver, can be used to minimize the residual vector $\{\mathbf{r}\}$ that remains when an approximate λ is used

in Eq. C.3-1 [11.24,C.11]. The QZ method is complicated, but can operate when [**A**] and/or [**B**] is indefinite. Methods are available for the damped eigenvalue problem [C.12,C.13]. New methods continue to be developed, each claiming a gain in efficiency [C.14,C.15]. Program listings, for older methods and for more recent methods, appear in several references, including [2.13,2.14,C.16–C.20].

REFERENCES

CHAPTER 1

1.1 E. L. Wilson, "Structural Analysis of Axisymmetric Solids," *AIAA Journal*, Vol. 3, No. 12, 1965, pp. 2269–2274.

1.2 F. Williamson, Jr., "A Historical Note on the Finite Element Method," *International Journal for Numerical Methods in Engineering*, Vol. 15, No. 6, 1980, pp. 930–934.

1.3 K. Wieghardt, "Über einen Grenzübergang der Elastizitätslehre und Seine Anwendung auf die Statik hochgradig statisch unbestimmter Fachwerke," *Verhandlungen des Vereins zur Beförderung des Gewehrbefliesses*, Vol. 85, 1906, pp. 139–176.

1.4 W. Riedel, "Beiträge zur Lösung des ebenen Problems eines elastischen Körpers mittels der Airyschen Spannungsfunktion," *Zeitschrift für angewandte Mathematik und Mechanik*, Vol. 7, No. 3, 1927, pp. 169–188 (discussion by C. Weber, Vol. 8, No. 2, 1928, pp. 159–160).

1.5 A. Hrennikoff, "Solution of Problems in Elasticity by the Framework Method," *ASME Journal of Applied Mechanics*, Vol. 8, No. 4, 1941, pp. A169–A175.

1.6 C. A. Felippa, "50 Year Classic Reprint: An Appreciation of R. Courant's 'Variational Methods for the Solution of Problems of Equilibrium and Vibrations,' 1943," *International Journal for Numerical Methods in Engineering*, Vol. 37, No. 13, 1994, pp. 2159–2187 [includes Courant's paper].

1.7 M. J. Turner, R. W. Clough, H. C. Martin, and L. J. Topp, "Stiffness and Deflection Analysis of Complex Structures," *Journal of the Aeronautical Sciences*, Vol. 23, No. 9, 1956, pp. 805–823.

1.8 J. Robinson, *Early FEM Pioneers*, Robinson and Associates, Dorset, UK, 1985.

1.9 J. H. Argyris and S. Kelsey, *Energy Theorems and Structural Analysis*, Butterworths, London, 1960 [collection of papers published in *Aircraft Engineering* in 1954 and 1955].

1.10 R. W. Clough, "The Finite Element Method after Twenty-Five Years: A Personal View," *Computers & Structures*, Vol. 12, No. 4, 1980, pp. 361–370.

1.11 R. W. Clough, "Original Formulation of the Finite Element Method," *Finite Elements in Analysis and Design*, Vol. 7, No. 2, 1990, pp. 89–101.

1.12 E. L. Wilson, "Automation of the Finite Element Method—A Personal Historical View," *Finite Elements in Analysis and Design*, Vol. 13, Nos. 2 & 3, 1993, pp. 91–104.

1.13 K. K. Gupta and J. L. Meek, "A Brief History of the Finite Element Method," *International Journal for Numerical Methods in Engineering*, Vol. 39, No. 22, 1996, pp. 3761–3774.

1.14 O. C. Zienkiewicz and Y. K. Cheung, *The Finite Element Method in Structural and Continuum Mechanics*, McGraw-Hill Publishing Co. Ltd., London, 1967.

1.15 J. Mackerle, "Some Remarks on Progress with Finite Elements," *Computers & Structures*, Vol. 55, No. 6, 1995, pp. 1101–1106.

1.16 W. C. Young, *Roark's Formulas for Stress and Strain*, 6th ed., McGraw-Hill, New York, 1989.

1.17 T. Sussman and K. J. Bathe, "Studies of Finite Element Procedures—Stress Band Plots and the Evaluation of Finite Element Meshes," *Engineering Computations*, Vol. 3, No. 3, 1986, pp. 178–191.

1.18 "Computer Misuse—Are We Dealing with a Time Bomb? Who Is to Blame and What Are We Doing about It? A Panel Discussion," in *Forensic Engineering*, Proceedings of the First Congress, K. L. Rens (ed.), American Society of Civil Engineers, Reston, VA, 1997, pp. 285–336.
1.19 P. S. Symonds and T. X. Yu, "Counterintuitive Behavior in a Problem of Elastic-Plastic Beam Dynamics," *ASME Journal of Applied Mechanics*, Vol. 52, No. 3, 1985, pp. 517–522.
1.20 G. E. Smith, "The Dangers of CAD," *Mechanical Engineering*, Vol. 108, No. 2, 1986, pp. 58–64.

CHAPTER 2

2.1 G. R. Cowper, "The Shear Coefficient in Timoshenko's Beam Theory," *ASME Journal of Applied Mechanics*, Vol. 33, No. 2, 1966, pp. 335–340.
2.2 J. S. Przemieneicki, *Theory of Matrix Structural Analysis*, McGraw-Hill, New York, 1968.
2.3 R. T. Severn, "Inclusion of Shear Deflection in the Stiffness Matrix for a Beam Element," *Journal of Strain Analysis*, Vol. 5, No. 4, 1970, pp. 239–241.
2.4 R. Narayanaswami and H. M. Adelman, "Inclusion of Transverse Shear Deformation in Finite Element Displacement Formulations," *AIAA Journal*, Vol. 12, No. 11, 1974, pp. 1613–1614 (discussion: Vol. 13, No. 9, 1975, pp. 1253–1254).
2.5 W. L. Cleghorn, B. Tabarrok, Y. Xiong, and T. W. Lee, "A Note on Some Exact Elements," *International Journal of Mechanical Engineering Education*, Vol. 19, No. 2, 1991, pp. 143–154.
2.6 R. D. Cook and W. C. Young, *Advanced Mechanics of Materials*, 2nd ed., Prentice Hall, Upper Saddle River, NJ, 1999.
2.7 J. W. Bull, ed., *Finite Element Applications to Thin-Walled Structures*, Elsevier Applied Science, London, 1990.
2.8 D. Krajcinovic, "A Consistent Discrete Elements Technique for Thinwalled Assemblages," *International Journal of Solids & Structures*, Vol. 5, No. 7, 1969, pp. 639–662.
2.9 P. W. Sharman, "Analysis of Structures with Thin-Walled Open Sections," *International Journal of Mechanical Sciences,* Vol. 27, No. 10, 1985, pp. 665–677.
2.10 H. Chen and G. E. Blandford, "A C^0 Finite Element Formulation for Thin-Walled Beams," *International Journal for Numerical Methods in Engineering*, Vol. 28, No. 10, 1989, pp. 2239–2255.
2.11 J. W. Wekezer, "Vibrational Analysis of Thin-Walled Bars with Open Cross Sections," *ASCE Journal of Structural Engineering*, Vol. 115, No. 12, 1989, pp. 2965–2978.
2.12 S. Y. Back and K. M. Will, "A Shear-Flexible Element with Warping for Thin-Walled Open Beams," *International Journal for Numerical Methods in Engineering*, Vol. 43, No. 7, 1998, pp. 1173–1191.
2.13 T. J. R. Hughes, *The Finite Element Method: Linear Static and Dynamic Finite Element Analysis*, Prentice Hall, Englewood Cliffs, NJ, 1987.
2.14 K. J. Bathe, *Finite Element Procedures*, Prentice Hall, Englewood Cliffs, NJ, 1996.
2.15 I. M. Smith and D. V. Griffiths, *Programming the Finite Element Method*, 3rd ed., John Wiley & Sons, Chichester, UK, 1998.
2.16 S. W. Sloan, "A Fortran Program for Profile and Wavefront Reduction," *International Journal for Numerical Methods in Engineering*, Vol. 28, No. 11, 1989, pp. 2651–2679 [includes program listing].
2.17 M. A. Crisfield, *Finite Elements and Solution Procedures for Structural Analysis*, Pineridge Press, Swansea, UK, 1986.
2.18 M. Papadrakakis and S. Smerou, "A New Implementation of the Lanczos Method in Linear Problems," *International Journal for Numerical Methods in Engineering*, Vol. 29, No. 1, 1990, pp. 141–159.

2.19 G. Prathap and B. P. Naganarayana, "Consistent Thermal Stress Evaluation in Finite Elements," *Computers & Structures*, Vol. 54, No. 3, 1995, pp. 415–426.
2.20 H. Kardestuncer, ed., *Finite Element Handbook*, McGraw-Hill, New York, 1987.
2.21 C. Meyer, ed., *Finite Element Idealization*, American Society of Civil Engineers, New York, 1987.
2.22 P. D. Mangalgiri, B. Dattaguru, and T. S. Ramamurthy, "Specification of Skew Conditions in Finite Element Formulation," *International Journal for Numerical Methods in Engineering*, Vol. 12, No. 6, 1978, pp. 1037–1041.
2.23 C. J. Burgoyne and R. Dilmaghanian, "Bicycle Wheel as Prestressed Structure," *ASCE Journal of Engineering Mechanics*, Vol. 119, No. 3, 1993, pp. 439–455.

CHAPTER 3

3.1 S. P. Timoshenko and J. N. Goodier, *Theory of Elasticity*, 3rd ed., McGraw-Hill, New York, 1970.
3.2 Y. C. Fung, *Foundations of Solid Mechanics*, Prentice Hall, Englewood Cliffs, NJ, 1965.
3.3 R. H. MacNeal, *Finite Elements: Their Design and Performance*, Marcel Dekker, New York, 1994.
3.4 C. A. Felippa, "Refined Finite Element Analysis of Linear and Nonlinear Two-Dimensional Structures," Ph.D. Dissertation, University of California, Berkeley, 1966 [also available as PB-178-418 and PB-178-419, N.T.I.S.; computer programs in the latter].
3.5 D. J. Allman, "A Compatible Triangular Element Including Vertex Rotations for Plane Elasticity Analysis," *Computers & Structures*, Vol. 19, No. 1–2, 1984, pp. 1–8.
3.6 K. Y. Sze and Y. S. Pan, "Hybrid Stress Tetrahedral Elements with Allman's Rotational D.O.F.," *International Journal for Numerical Methods in Engineering*, Vol. 48, No. 7, 2000, pp. 1055–1070.
3.7 K. Y. Sze, Chen Wanji, and Y. K. Cheung, "An Efficient Quadrilateral Plane Element with Drilling Degrees of Freedom Using Orthogonal Stress Modes," *Computers & Structures*, Vol. 42, No. 5, 1992, pp. 695–705.
3.8 M. Iura and S. N. Atluri, "Formulation of a Membrane Finite Element with Drilling Degrees of Freedom," *Computational Mechanics*, Vol. 9, No. 6, 1992, pp. 417–428.
3.9 Long Yuqiu and Xu Yin, "Generalized Conforming Triangular Membrane Element with Vertex Rigid Rotational Freedoms," *Finite Elements in Analysis and Design*, Vol. 17, No. 4, 1994, pp. 259–271.
3.10 T. J. R. Hughes, A. Masud, and I. Harari, "Numerical Assessment of Some Membrane Elements with Drilling Degrees of Freedom," *Computers & Structures*, Vol. 55, No. 2, 1995, pp. 297–314.
3.11 E. L. Wilson, R. L. Taylor, W. P. Doherty, and J. Ghaboussi, "Incompatible Displacement Models," in *Numerical and Computer Methods in Structural Mechanics*, S. J. Fenves et al., eds., Academic Press, New York, 1973, pp. 43–57.
3.12 I. U. Ojalvo, "Improved Thermal Stress Determination by Finite Element Methods," *AIAA Journal*, Vol. 12, No. 8, 1974, pp.1131-1132.
3.13 J. Pittr and H. Hartl, "Improved Stress Evaluation Under Thermal Load for Simple Elements," *International Journal for Numerical Methods in Engineering*, Vol. 15, No. 10, 1980, pp. 1507–1515.
3.14 D. Munz and Y. Y. Yang, "Stress Singularities at the Interface in Bonded Dissimilar Materials under Mechanical and Thermal Loading," *ASME Journal of Applied Mechanics*, Vol. 59, No. 4, 1992, pp. 857–861.
3.15 S. Ioka, S. Kubo, K. Ohji, and J. Kishimoto, "Thermal Residual Stresses in Bonded Dissimilar Materials and Their Singularities," *International Journal JSME, Series A: Mechanics and Materials Engineering*, Vol. 39, No. 2, 1996, pp. 197–203.

3.16 W. J. O'Donnell, "The Additional Deflection of a Cantilever Due to the Elasticity of the Support," *ASME Journal of Applied Mechanics*, Vol. 27, No. 3, 1960, pp. 461–464.

CHAPTER 4

4.1 H. L. Langhaar, *Energy Methods in Applied Mechanics*, John Wiley & Sons, New York, 1962.
4.2 K. Washizu, *Variational Methods in Elasticity and Plasticity*, 3rd ed., Pergamon Press, Oxford, UK, 1982.
4.3 J. N. Reddy, *Variational Methods in Applied Mechanics*, John Wiley & Sons, New York, 1984.
4.4 O. C. Zienkiewicz and R. L. Taylor, *The Finite Element Method*, 4th ed., Vol. 1, McGraw-Hill, London, 1989.
4.5 R. J. Melosh and D. W. Lobitz, "On a Numerical Sufficiency Test for Monotonic Convergence of Finite Element Models," *AIAA Journal*, Vol. 13, No. 5, 1975, pp. 675–678.
4.6 T. H. H. Pian, "Derivation of Element Stiffness Matrices by Assumed Stress Functions," *AIAA Journal*, Vol. 2, No. 7, 1964, pp. 1333–1336 (discussion: Vol. 3, No. 1, 1965, pp.186–187).
4.7 J. P. Wolf, "Alternate Hybrid Stress Finite Element Models," *International Journal for Numerical Methods in Engineering*, Vol. 9, No. 3, 1975, pp. 601–615.
4.8 T. H. H. Pian and C.-C. Wu, "A Rational Approach for Choosing Stress Terms for Hybrid Finite Element Formulations," *International Journal for Numerical Methods in Engineering*, Vol. 26, No. 10, 1988, pp. 2331–2343.
4.9 C. K. Lee and R. E. Hobbs, "Closed Form Stiffness Matrix Solutions for Some Commonly Used Hybrid Finite Elements," *Computers & Structures*, Vol. 67, No. 6, 1998, pp. 463–482.
4.10 K. Y. Sze, "On Immunizing Five-Beta Hybrid-Stress Models from 'Trapezoidal Locking' in Practical Analyses," *International Journal for Numerical Methods in Engineering*, Vol. 47, No. 4, 2000, pp. 907–920.
4.11 J. Jirousek and P. Teodorescu, "Large Finite Elements Method for the Solution of Problems in the Theory of Elasticity," *Computers & Structures*, Vol. 15, No. 5, 1982, pp. 575–587.
4.12 J. Jirousek and L. Guex, "The Hybrid-Trefftz Finite Element Model and Its Application to Plate Bending," *International Journal for Numerical Methods in Engineering*, Vol. 23, No. 4, 1986, pp. 651–693.
4.13 J. Jirousek and A. Wróblewski, "T-Elements: State of the Art and Future Trends," *Archives of Computational Methods in Engineering*, Vol. 3, No. 4, 1996, pp. 323–434.
4.14 J. Jirousek and A. P. Zielinski, "Survey of Trefftz-Type Element Formulations," *Computers & Structures*, Vol. 63, No. 2, 1997, pp. 225–242.
4.15 M. Fröier, L. Nilsson, and A. Samuelsson, "The Rectangular Plane Stress Element by Turner, Pian, and Wilson," *International Journal for Numerical Methods in Engineering*, Vol. 8, No. 2, 1974, pp. 433–437.

CHAPTER 5

5.1 S. H. Crandall, *Engineering Analysis*, McGraw-Hill, New York, 1956.
5.2 B. A. Finlayson and L. E. Scriven, "The Method of Weighted Residuals—A Review," *ASME Applied Mechanics Reviews*, Vol. 19, No. 9, 1966, pp. 735–748 [cites 187 refs.].
5.3 B. A. Finlayson, *The Method of Weighted Residuals and Variational Principles*, Academic Press, New York, 1972.
5.4 C. A. J. Fletcher, *Computational Galerkin Methods*, Springer-Verlag, Berlin, 1984.
5.5 E. D. Eason, "A Review of Least-Squares Methods for Solving Partial Differential Equations," *International Journal for Numerical Methods in Engineering*, Vol. 10, No. 5, 1976, pp. 1021–1046 [cites 241 refs.].

5.6 M. F. N. Mohsen, "Some Details of the Galerkin Finite Element Method," *Applied Mathematical Modelling*, Vol. 6, No. 3, 1982, pp. 165–170.
5.7 S. Kumaresan, S. Radhakrishnan, and N. Ganesan, "Mixed Models in Finite Element Analysis," *Computers & Structures*, Vol. 51, No. 1, 1994, pp. 117–123.
5.8 D. S. Malkus and T. J. R. Hughes, "Mixed Finite Element Methods—Reduced and Selective Integration Techniques: A Unification of Concepts," *Computer Methods in Applied Mechanics and Engineering*, Vol. 15, No. 1, 1978, pp. 63–81.
5.9 R. H. Gallagher, J. A. Liggett, and S. T. K. Chan, "Finite Element Shallow Lake Circulation Analysis," *ASCE Journal of the Hydraulics Division*, Vol. 99, No. HY7, 1973, pp. 1083–1096.

CHAPTER 6

6.1 B. M. Irons, "Engineering Applications of Numerical Integration in Stiffness Methods," *AIAA Journal*, Vol. 4, No. 11, 1966, pp. 2035–2037.
6.2 A. H. Stroud and D. Secrest, *Gaussian Quadrature Formulas*, Prentice Hall, Englewood Cliffs, NJ, 1966.
6.3 T. K. Hellen, "Effective Quadrature Rules for Quadratic Solid Isoparametric Elements," *International Journal for Numerical Methods in Engineering*, Vol. 4, No. 4, 1972, pp. 597–599.
6.4 G. Bedrosian, "Shape Functions and Integration Formulas for Three-Dimensional Finite Element Analysis," *International Journal for Numerical Methods in Engineering*, Vol. 35, No. 1, 1992, pp. 95–108.
6.5 J. Springer, "Shape-Derived Anisotropy Directions on Quadrangle and Brick Finite Elements," *Communications in Numerical Methods in Engineering,* Vol. 12, No. 6, 1996, pp. 351–357.
6.6 R. L. Taylor, J. C. Simo, O. C. Zienkiewicz, and A. C. H. Chan, "The Patch Test—A Condition for Assessing FEM Convergence," *International Journal for Numerical Methods in Engineering*, Vol. 22, No. 1, 1986, pp. 39–62.
6.7 R. L. Taylor, P. J. Beresford, and E. L. Wilson, "A Non-Conforming Element for Stress Analysis," *International Journal for Numerical Methods in Engineering,* Vol. 10, No. 6, 1976, pp. 1211–1219.
6.8 E. L. Wilson and A. Ibrahimbegovic, "Use of Incompatible Displacement Modes for the Calculation of Element Stiffnesses or Stresses," *Finite Elements in Analysis and Design*, Vol. 7, No. 3, 1990, pp. 229–241.
6.9 E. L. Wilson, "The Static Condensation Algorithm," *International Journal for Numerical Methods in Engineering,* Vol. 8, No. 1, 1974, pp. 198–203.
6.10 R. D. Cook and V. N. Shah, "A Cost Comparison of Two Static Condensation Algorithms," *International Journal for Numerical Methods in Engineering*, Vol. 12, No. 4, 1978, pp. 581–588.
6.11 N. Bicanic and E. Hinton, "Spurious Modes in Two-Dimensional Isoparametric Elements," *International Journal for Numerical Methods in Engineering*, Vol. 14, No. 10, 1979, pp. 1545–1557.
6.12 Y. H. Kim, R. F. Jones, and S. W. Lee, "Study of 20-Node Solid Element," *Communications in Applied Numerical Methods*, Vol. 6, No. 3, 1990, pp. 197–205.
6.13 W. K. Liu, Y. K. Hu, and T. Belytschko, "Multiple Quadrature Underintegrated Finite Elements," *International Journal for Numerical Methods in Engineering*, Vol. 37, No. 19, 1994, pp. 3263–3289.
6.14 K. Y. Sze, A. K. Soh, and Y. S. Sim, "Solid Elements with Rotational DOFs by Explicit Hybrid Stabilization," *International Journal for Numerical Methods in Engineering*, Vol. 39, No. 17, 1996, pp. 2987–3005.

6.15 M. A. Puso, "A Highly Efficient Enhanced Assumed Strain Physically Stabilized Hexahedral Element," *International Journal for Numerical Methods in Engineering*, Vol. 49, No. 8, 2000, pp. 1029–1064.
6.16 J. Barlow, "Optimal Stress Locations in Finite Element Models," *International Journal for Numerical Methods in Engineering*, Vol. 10, No. 2, 1976, pp. 243–251 (comment: Vol. 11, No. 3, 1977, p. 604).
6.17 J. Barlow, "More on Optimal Stress Points—Reduced Integration, Element Distortions and Error Estimation," *International Journal for Numerical Methods in Engineering*, Vol. 28, No. 7, 1989, pp. 1487–1504.
6.18 R. T. Tenchev, "Empirical Way to Improve Stress Accuracy at Stress Concentrations in Finite Element Analysis," *Communications in Numerical Methods in Engineering*, Vol. 10, No. 7, 1994, pp. 565–576.
6.19 I. Fried, "Accuracy of Complex Finite Elements," *AIAA Journal*, Vol. 10, No. 3, 1972, pp. 347–349.
6.20 N. S. Lee and K. J. Bathe, "Effects of Element Distortions on the Performance of Isoparametric Elements," *International Journal for Numerical Methods in Engineering*, Vol. 36, No. 20, 1993, pp. 3553–3576.
6.21 K. E. Barrett, "Jacobians for Isoparametric Elements," *Communications in Numerical Methods in Engineering*, Vol. 12, No. 11, 1996, pp. 755–766.
6.22 I. Ergatoudis, B. M. Irons, and O. C. Zienkiewicz, "Curved Isoparametric, 'Quadrilateral' Elements for Finite Element Analysis," *International Journal of Solids & Structures*, Vol. 4, No. 1, 1968, pp. 31–42.
6.23 T. Belytschko and D. Lasry, "A Fractal Patch Test," *International Journal for Numerical Methods in Engineering*, Vol. 26, No. 10, 1988, pp. 2199–2210.
6.24 W. D. Pilkey, *Peterson's Stress Concentration Factors*, 2nd ed., John Wiley & Sons, New York, 1997.
6.25 B. M. Irons, "Quadrature Rules for Brick Based Finite Elements," *International Journal for Numerical Methods in Engineering*, Vol. 3, No. 2, 1971, pp. 293–294.
6.26 R. H. MacNeal and R. L. Harder, "A Proposed Standard Set of Problems to Test Finite Element Accuracy," *Finite Elements in Analysis and Design*, Vol. 1, No. 1, 1985, pp. 3–20.

CHAPTER 7

7.1 R. E. Newton, "Degeneration of Brick-Type Isoparametric Elements," *International Journal for Numerical Methods in Engineering*, Vol. 7, No. 4, 1973, pp. 579–581.
7.2 B. M. Irons, "A Technique for Degenerating Brick-Type Isoparametric Elements Using Hierarchical Midside Nodes," *International Journal for Numerical Methods in Engineering*, Vol. 8, No. 1, 1974, pp. 203–209.
7.3 K. Moser and G. Swoboda, "Explicit Stiffness Matrix of the Linearly Varying Strain Triangular Element," *Computers & Structures*, Vol. 8, No. 2, 1978, pp. 311–314.
7.4 G. Subramanian and C. Jayachandra Bose, "Convenient Generation of Stiffness Matrices for the Family of Plane Triangular Elements," *Computers & Structures*, Vol. 15, No. 1, 1982, pp. 85–89.
7.5 P. S. Shiakolas, K. L. Lawrence, and R. V. Nambiar, "Closed-Form Expressions for the Linear and Quadratic Strain Tetrahedral Finite Elements," *Computers & Structures*, Vol. 50, No. 6, 1994, pp. 743–747.
7.6 N. M. Ferrers, *An Elementary Treatise on Trilinear Coordinates, the Method of Reciprocal Polars and the Theory of Projections*, Macmillan, London, 1861.
7.7 K. Bell, "A Refined Triangular Plate Bending Finite Element," *International Journal for Numerical Methods in Engineering*, Vol. 1, No. 1, 1969, pp. 101–122.

7.8 D. A. Dunavant, "High Degree Efficient Symmetrical Gaussian Quadrature Rules for the Triangle," *International Journal for Numerical Methods in Engineering*, Vol. 21, No. 6, 1985, pp. 1129–1148.
7.9 K. S. Sunder and R. A. Cookson, "Integration Points for Triangles and Tetrahedrons Obtained from the Gaussian Quadrature Points for a Line," *Computers & Structures*, Vol. 21, No. 5, 1985, pp. 881–885.
7.10 D. J. Naylor, "On Integration Formulas for Triangles," in *Numerical Methods in Geotechnical Engineering*, I. M. Smith, ed., A. A. Balkema, Rotterdam, 1994.
7.11 M. Gellert and R. Harbord, "Moderate Degree Cubature Formulas for 3-D Tetrahedral Finite Element Approximations," *Communications in Applied Numerical Methods*, Vol. 7, No. 6, 1991, pp. 487–495.
7.12 K. Y. Sze and D. Zhu, "On the Relative Merits of Three-Point Integration Rules for Six-Node Triangles," *Finite Elements in Analysis and Design*, Vol. 27, No. 4, 1997, pp. 335–343.
7.13 C. A. Felippa, "Programming the Isoparametric Six-Node Triangle," *Engineering Computations*, Vol. 7, No. 2, 1990, pp. 173–177.
7.14 P. Keast, "Moderate Degree Tetrahedral Quadrature Formulas," *Computer Methods in Applied Mechanics and Engineering*, Vol. 55, No. 3, 1986, pp. 339–348.

CHAPTER 8

8.1 A. Ranjbaran, "Mathematical Formulation of Embedded Reinforcements in 3D Brick Elements," *Communications in Numerical Methods in Engineering*, Vol. 12, No. 12, 1996, pp. 897–903.
8.2 R. D. Cook, "Beam Cantilevered from Elastic Support: Finite Element Modeling," *Communications in Applied Numerical Methods*, Vol. 7, No. 8, 1991, pp. 621–623.
8.3 A. K. Gupta and P. S. Ma, "Error in Eccentric Beam Formulation," *International Journal for Numerical Methods in Engineering*, Vol. 11, No. 9, 1977, pp. 1473–1477.
8.4 R. E. Miller, "Reduction of the Error in Eccentric Beam Modeling," *International Journal for Numerical Methods in Engineering*, Vol. 15, No. 4, 1980, pp. 575–582.
8.5 M. A. Crisfield, "The Eccentricity Issue in the Design of Plate and Shell Elements," *Communications in Applied Numerical Methods*, Vol. 7, No. 1, 1991, pp. 47–56.
8.6 M. F. Kanninen and C. H. Popelar, *Advanced Fracture Mechanics*, Oxford University Press, New York, 1985.
8.7 *ANSYS Structural Analysis Guide*, ANSYS, Inc., Canonsburg, PA, 1997.
8.8 L. Banks-Sills, "Application of the Finite Element Method to Linear Elastic Fracture Mechanics," *ASME Applied Mechanics Reviews*, Vol. 44, No. 10, 1991, pp. 447–461.
8.9 B. Y. Ting and E. F. Mockry, "Beam on Elastic Foundation Finite Element," *ASCE Journal of Structural Engineering*, Vol. 110, No. 10, 1984, pp. 2324–2339.
8.10 M. Eisenberger and D. Z. Yankelevsky, "Exact Stiffness Matrix for Beams on Elastic Foundation," *Computers & Structures*, Vol. 21, No. 6, 1985, pp. 1355–1359.
8.11 M. Eisenberger and J. Bielak, "Finite Beams on Infinite Two-Parameter Elastic Foundations," *Computers & Structures*, Vol. 42, No. 4, 1992, pp. 661–664.
8.12 M. S. Cheung, "A Simplified Finite Element Solution for the Plates on Elastic Foundation," *Computers & Structures*, Vol. 8, No. 1, 1978, pp. 139–145.
8.13 P. Bettess, *Infinite Elements*, Penshaw Press, Sunderland, UK, 1992.
8.14 J. M. C. Marques and D. R. J. Owen, "Infinite Elements in Quasi-Static Materially Nonlinear Problems," *Computers & Structures*, Vol. 18, No. 4, 1984, pp. 739–751.
8.15 S. Kay and P. Bettess, "Revised Mapping Functions for Three-Dimensional Serendipity Infinite Elements," *Communications in Numerical Methods in Engineering*, Vol. 12, No. 3, 1996, pp. 181–184.

8.16 W.-S. Park, C.-B. Yun, and C.-K. Pyun, "Infinite Elements for 3-Dimensional Wave-Structural Interaction Problems," *Engineering Structures*, Vol. 14, No. 5, 1992, pp. 335–346.
8.17 Y.-B. Yang, S.-R. Kuo, and H.-H. Hung, "Frequency-Independent Infinite Elements for Analysing Semi-Infinite Problems," *International Journal for Numerical Methods in Engineering*, Vol. 39, No. 20, 1996, pp. 3553–3596.
8.18 M. Cohen and P. C. Jennings, "Silent Boundary Methods for Transient Analysis," in *Computational Methods for Transient Analysis*, T. Belytschko and T. J. R. Hughes, eds., North-Holland, Amsterdam, 1983.
8.19 R. T. Fenner, "The Boundary Integral Equation (Boundary Element) Method in Engineering Stress Analysis," *Journal of Strain Analysis*, Vol. 18, No. 4, 1983, pp. 199–205.
8.20 D. E. Beskos, ed., *Boundary Element Methods in Mechanics*, North-Holland, Amsterdam, 1987.
8.21 J. Mackerle, "A Guide to the Literature on Finite and Boundary Element Techniques and Software," *Software for Engineering Workstations*, Vol. 4, No. 4, 1988, pp. 170–182.
8.22 G. Beer and J. O. Watson, *Introduction to Finite and Boundary Element Methods for Engineers*, John Wiley & Sons, Chichester, UK, 1992.
8.23 J. H. Kane, *Boundary Element Analysis in Engineering Continuum Mechanics*, Prentice Hall, Englewood Cliffs, NJ, 1994.
8.24 J. Ma and M. Le, "A New Method for Coupling of Boundary Element Method and Finite Element Method," *Applied Mathematical Modelling*, Vol. 16, No. 1, 1992, pp. 43–46.
8.25 C.-C. Lin, E. C. Lawton, J. A. Caliendo, and L. R. Anderson, "An Iterative Finite Element—Boundary Element Algorithm," *Computers & Structures*, Vol. 59, No. 5, 1996, pp. 899–909.
8.26 X. Li and Q. Du, " Recent Engineering Applications in China on Coupling Boundary Elements with Finite Elements," *ASME Applied Mechanics Reviews*, Vol. 50, No. 11, 1997, pp. 731–740.
8.27 S.-W. Wu, "Finite Elements with Nonreflecting Boundary Conditions Formulated by the Helmholtz Integral Equation," *ASME Journal of Vibration and Acoustics*, Vol. 121, No. 2, 1999, pp. 214–220.
8.28 C. Song and J. P. Wolf, "Consistent Infinitesimal Finite-Element Cell Method: Three-Dimensional Vector Wave Equation," *International Journal for Numerical Methods in Engineering*, Vol. 39, No. 13, 1996, pp. 2189–2208.
8.29 J. P. Wolf and C. Song, *Finite Element Modelling of Unbounded Media*, John Wiley & Sons, Chichester, UK, 1996.
8.30 C. Song and J. P. Wolf, "The Scaled Boundary Finite-Element Method—Alias Consistent Infinitesimal Finite-Element Cell Method—For Elastodynamics," *Computer Methods in Applied Mechanics and Engineering*, Vol. 147, No. 3–4, 1997, pp. 329–355.
8.31 C. Song and J. P. Wolf, "Consistent Infinitesimal Finite-Element Cell Method for Incompressible Unbounded Medium," *Communications in Numerical Methods in Engineering*, Vol. 13, No. 1, 1996, pp. 21–32.
8.32 J. S. Aurora, "Survey of Structural Reanalysis Techniques," *ASCE Journal of the Structural Division*, Vol. 102, No. ST4, 1976, pp. 783–802 [cites 89 refs.].
8.33 A. M. Abu Kassim and B. H. V. Topping, "Static Reanalysis: A Review," *ASCE Journal of Structural Engineering*, Vol. 113, No. 5, 1987, pp. 1029–1045 [cites 110 refs.].
8.34 E. Castillo, A. Cobo, A. Fernández-Canteli, F. Jubete, and E. Pruneda, "Updating Inverses in Matrix Analysis of Structures," *International Journal for Numerical Methods in Engineering*, Vol. 43, No. 8, 1998, pp. 1479–1504.
8.35 P. B. Nair, A. J. Keane, and R. S. Langley, "Improved First-Order Approximation of Eigenvalues and Eigenvectors," *AIAA Journal*, Vol. 36, No. 9, 1998, pp. 1721–1727.
8.36 U. Kirsch, "Efficient, Accurate Reanalysis for Structural Optimization," *AIAA Journal*, Vol. 37, No. 12, 1999, pp. 1663–1669.
8.37 W. M. Jenkins, "A Neural Network for Structural Re-Analysis," *Computers & Structures*, Vol. 72, No. 6, 1999, pp. 687–698.

8.38 G. L. Rigby and G. M. McNeice, "A Strain Energy Basis for Studies of Element Stiffness Matrices," *AIAA Journal*, Vol. 10, No. 11, 1972, pp. 1490–1493.
8.39 W. P. Doherty, E. L. Wilson, and R. L. Taylor, "Stress Analysis of Axisymmetric Solids Utilizing Higher-Order Quadrilateral Finite Elements," *Report UC-SESM-69-3*, Civil Engineering Dept., University of California, Berkeley, 1969 (PB-190-312, N.T.I.S.).
8.40 D. J. Kidger and I. M. Smith, "Eigenvalues of Element Stiffness Matrices. Part II: 3-D Solid Elements," *Engineering Computations*, Vol. 9, No. 3, 1992, pp. 317–328.
8.41 J. O. Dow, T. H. Ho, and H. D. Cabiness, "Generalized Finite Element Evaluation Procedure," *ASCE Journal of Structural Engineering*, Vol. 111, No. 6, 1985, pp. 435-452.
8.42 J. Robinson, "Element Shape Sensitivity Testing Using the CRE-Method and Without a FEM System," *Finite Elements in Analysis and Design*, Vol. 7, No. 1, 1990, pp. 73–84.

CHAPTER 9

9.1 R. A. Rosanoff, J. F. Gloudemann, and S. Levy, "Numerical Conditioning of Stiffness Matrix Formulations for Frame Structures," *Proceedings of the Second Conference on Matrix Methods in Structural Mechanics*, Wright-Patterson AFB, Ohio, 1968 (AFFDL-TR-68-150), pp. 1029–1060.
9.2 S. Utku and R. J. Melosh, "Estimating the Manipulation Errors in Finite Element Analysis, Part I," *Finite Elements in Analysis and Design*, Vol. 3, No. 4, 1987, pp. 285–295.
9.3 R. T. Haftka, "Stiffness-Matrix Condition Number and Shape Sensitivity Errors," *AIAA Journal*, Vol. 28, No. 7, 1990, pp. 1322–1324.
9.4 R. A. Rosanoff and T. A. Ginsburg, "Matrix Error Analysis for Engineers," *Proceedings of the Conference on Matrix Methods in Structural Mechanics*, Wright-Patterson AFB, Ohio, 1965 (AFFDL-TR-66-80), pp. 887–910.
9.5 I. Fried, "Condition of Finite Element Matrices generated from Nonuniform Meshes," *AIAA Journal*, Vol. 10, No. 2, 1972, pp. 219–221.
9.6 I. Fried, "Influence of Poisson's Ratio on the Condition of the Finite Element Stiffness Matrix," *International Journal of Solids & Structures*, Vol. 9, No. 3, 1973, pp. 323–329.
9.7 B. M. Irons, "Roundoff Criteria in Direct Stiffness Solutions," *AIAA Journal*, Vol. 6, No. 7, 1968, pp. 1308–1312.
9.8 B. Noble, *Applied Linear Algebra*, Prentice Hall, Englewood Cliffs, NJ, 1969.
9.9 G. Strang and G. J. Fix, *An Analysis of the Finite Element Method*, Prentice Hall, Englewood Cliffs, NJ, 1973.
9.10 C. Militello and C. A. Felippa, "*r*-Adaptive Methods Based on Element-Level Error Indicators for Parallel Analysis of Plates and Shells," *The 33rd AIAA/ASME/ASCE/AHS/ASC Structures, Structural Dynamics, and Materials Conference*, AIAA, Washington, DC, 1992, pp. 292–301a.
9.11 R. J. Melosh and P. V. Marcal, "Energy Basis for Mesh Refinement of Structural Continua," *International Journal for Numerical Methods in Engineering*, Vol. 11, No. 7, 1977, pp. 1083–1091.
9.12 D. J. Turke, "Characteristics of Piecewise Approximation in Numerical Analysis," in *Finite Element Grid Optimization*, M. S. Shephard and R. H. Gallagher, eds., ASME, New York, 1979, pp. 15–26.
9.13 J. Fish, "The *s*-Version of the Finite Element Method," *Computers & Structures*, Vol. 43, No. 3, 1992, pp. 539–547.
9.14 T. Belytschko, J. Fish, and A. Bayliss, "Spectral Overlay on Finite Elements for Problems with High Gradients," *Computer Methods in Applied Mechanics and Engineering*, Vol. 81, No. 1, 1990, pp. 71–89.

9.15 E. Rank and R. Krause, "A Multiscale Finite-Element Method," *Computers & Structures*, Vol. 64, Nos. 1–4, 1997, pp. 139–144.
9.16 E. Hinton and J. S. Campbell, "Local and Global Smoothing of Discontinuous Finite Element Functions Using a Least Squares Method," *International Journal for Numerical Methods in Engineering*, Vol. 8, No. 3, 1974, pp. 461–480.
9.17 M. Ulbin and T. K. Hellen, "Post-Processing Techniques for Assessing Element Distortion Errors," *Engineering Computations*, Vol. 6, No. 1, 1989, pp. 35–43.
9.18 J. Avrashi and R. D. Cook, "New Error Estimation for C^0 Eigenproblems in Finite Element Analysis," *Engineering Computations*, Vol. 10, No. 3, 1993, pp. 243–256.
9.19 J. Avrashi, "High Order Gradient Smoothing Towards Improved C^1 Eigenvalues," *Engineering Computations*, Vol. 12, No. 6, 1995, pp. 513–528.
9.20 G. Loubignac, G. Cantin, and G. Touzot, "Continuous Stress Fields in Finite Element Analysis," *AIAA Journal*, Vol. 15, No. 11, 1977, pp. 1645–1647.
9.21 O. C. Zienkiewicz and J. Z. Zhu, "The Superconvergent Patch Recovery and *A Posteriori* Error Estimates. Part 1: The Recovery Technique," *International Journal for Numerical Methods in Engineering*, Vol. 33, No. 7, 1992, pp. 1331–1364.
9.22 N. E. Wiberg, R. Bausys, and P. Hager, "Adaptive *h*-Version Eigenfrequency Analysis," *Computers & Structures*, Vol. 71, No. 5, 1999, pp. 565–584.
9.23 N. E. Wiberg and F. Abdulwahab, "Patch Recovery based on Superconvergent Derivatives and Equilibrium," *International Journal for Numerical Methods in Engineering*, Vol. 36, No. 16, 1993, pp. 2703–2724.
9.24 T. Blacker and T. Belytschko, "Superconvergent Patch Recovery with Equilibrium and Conjoint Interpolant Enhancements," *International Journal for Numerical Methods in Engineering*, Vol. 37, No. 3, 1994, pp. 517–536.
9.25 I. Babuška, T. Strouboulis, and C. S. Upadhyay, "A Model Study of the Quality of *A Posteriori* Error Estimators for Finite Element Solutions of Linear Elliptic Problems, with Particular Reference to the Behavior Near the Boundary," *International Journal for Numerical Methods in Engineering*, Vol. 40, No. 14, 1997, pp. 2521–2577.
9.26 N. E. Wiberg, F. Abdulwahab, and S. Ziukas, "Improved Element Stresses for Node and Element Patches Using Superconvergent Patch Recovery," *Communications in Numerical Methods in Engineering*, Vol. 11, No. 7, 1995, pp. 619–627.
9.27 H. C. Park, S.-H. Shin, and S. W. Lee, "A Superconvergent Stress Recovery Technique for Accurate Boundary Stress Extraction," *International Journal for Numerical Methods in Engineering*, Vol. 45, No. 9, 1999, pp. 1227–1242.
9.28 A. A. Yazdani, H. R. Riggs, and A. Tessler, "Stress Recovery and Error Estimation for Shell Structures," *International Journal for Numerical Methods in Engineering*, Vol. 47, No. 11, 2000, pp. 1825–1840.
9.29 A. Pica, R. D. Wood, A. O. Adekunle, and J. Bonet, "Smoothing Stress Resultants in Adaptive Finite Element Shell Analysis," *Computers & Structures*, Vol. 54, No. 5, 1995, pp. 835–849.
9.30 K. M. Okstad, T. Kvamsdal, and K. M. Mathisen, "Superconvergent Patch Recovery for Plate Problems Using Statically Admissible Stress Resultant Fields," *International Journal for Numerical Methods in Engineering*, Vol. 44, No. 5, 1999, pp. 697–727.
9.31 R. D. Cook, J. Avrashi, and C. H. Lin, "Buckling Analysis: Alternative Formulations, Error Estimation, and Adaptive Meshing," *Finite Elements in Analysis and Design*, Vol. 11, No. 1, 1992, pp. 55–65.
9.32 O. C. Zienkiewicz znd J. Z. Zhu, "A Simple Error Estimator and Adaptive Procedure for Practical Engineering Analysis," *International Journal for Numerical Methods in Engineering*, Vol. 24, No. 2, 1987, pp. 337–357.
9.33 O. C. Zienkiewicz and J. Z. Zhu, "The Superconvergent Patch Recovery and *A Posteriori* Error Estimates. Part 2: Error Estimates and Adaptivity," *International Journal for Numerical Methods in Engineering*, Vol. 33, No. 7, 1992, pp. 1365–1382.

9.34 M. K. Georges and M. S. Shephard, "Automated Adaptive Two-Dimensional System for the *hp*-Version of the Finite Element Method," *International Journal for Numerical Methods in Engineering,* Vol. 32, No. 4, 1991, pp. 867–893.
9.35 K. Jayaswal and I. R. Grosse, "Finite Element Error Estimation for Crack Tip Singular Elements," *Finite Elements in Analysis and Design*, Vol. 14, No. 1, 1993, pp. 17–35.
9.36 O. C. Zienkiewicz and J. Z. Zhu, "Error Estimates and Adaptive Refinement for Plate Bending Problems," *International Journal for Numerical Methods in Engineering*, Vol. 28, No. 12, 1989, pp. 2839–2853.
9.37 E. Hinton, M. Özakça, and N. V. R. Rao, "Adaptive Analysis of Thin Shells Using Facet Elements," *International Journal for Numerical Methods in Engineering*, Vol. 32, No. 6, 1991, pp. 1283–1301.
9.38 I. R. Grosse, P. Katragadda, and J. Bonoit, "An Adaptive Accuracy-Based *A Posteriori* Error Estimator," *Finite Elements in Analysis and Design*, Vol. 12, No. 1, 1992, pp. 75–90.
9.39 D. B. Stephen and G. P. Steven, "Error Estimation for Plate Buckling Elements," *Computers & Structures*, Vol. 61, No. 4, 1996, pp. 747–761.
9.40 A. Dutta, C. V. Ramakrishnan, and P. Mahajan, "Adaptive Finite Element Analysis of Structures Under Transient Dynamic Loading Using Modal Superposition," *Finite Elements in Analysis and Design*, Vol. 31, No. 4, 1999, pp. 255–272.
9.41 T. J. Baker, "Mesh Adaptation Strategies for Problems in Fluid Dynamics," *Finite Elements in Analysis and Design*, Vol. 25, Nos. 3–4, 1997, pp. 243–273.
9.42 E. Oñate and G. Bugeda, "A Study of Mesh Optimality Criteria in Adaptive Finite Element Analysis," *Engineering Computations*, Vol. 10, No. 4, 1993, pp. 307–321.
9.43 L. Y. Li, P. Bettess, J. W. Bull, and T. Bond, "Mesh Refinement Formulations in Adaptive Finite Element Methods," *Proceedings of the Institution of Mechanical Engineers*, Vol. 210, No. C4, 1996, pp. 353–361.
9.44 H. S. Oh and J. K. Lim, "Modified *h*-Method with Directional Error Estimate for Finite Element Stress Analysis," *Computers & Structures*, Vol. 65, No. 2, 1997, pp. 191–204.
9.45 *Computer Methods in Applied Mechanics and Engineering*, Vol. 33, Nos. 3–4, 1996 [special issue on *p*- and *hp*-methods].
9.46 *Finite Elements in Analysis and Design*, Vol. 25, Nos. 1–4, 1997 [special issue on adaptive meshing].
9.47 S. C. Cannan, S.-C. Lin, and A. V. Mobley, "Automatic 3D Surface Meshing to Address Today's Industrial Needs," *Finite Elements in Analysis and Design*, Vol. 25, Nos. 1–2, 1997, pp. 185–198.

CHAPTER 10

10.1 W. G. Dodge and S. E. Moore, "Stress Indices and Flexibility Factors for Moment Loadings on Elbows and Curved Pipes," *Welding Research Council Bulletin 179*, December 1972.
10.2 S. P. Timoshenko and S. Woinowsky-Krieger, *Theory of Plates and Shells*, 2nd ed., McGraw-Hill, New York, 1959.
10.3 R. D. Henshell, D. Walters, and G. B. Warburton, "A New Family of Curvilinear Plate Bending Elements for Vibration and Stability," *Journal of Sound and Vibration*, Vol. 20, No. 3, 1972, pp. 381–397 (discussion and authors' closure: Vol. 23, No. 4, 1972, pp. 507–513).
10.4 *The Standard NAFEMS Benchmarks* (Revision), National Agency for Finite Elements Methods and Standards, Glasgow, UK, 1989.
10.5 F. Osweiler, "Evolution and Synthesis of the Effective Elastic Constants Concept for the Design of Tubesheets," *ASME Journal of Pressure Vessel Technology*, Vol. 111, No. 3, 1989, pp. 209–217.

10.6 *A Finite Element Primer*, National Agency for Finite Elements Methods and Standards, Glasgow, UK, 1986.

10.7 D. P. Jones, J. L. Gordon, D. N. Hutula, J. E. Holliday, and W. D. Jandrasits, "Application of Equivalent Elastic Methods in Three-Dimensional Finite Element Analysis," *ASME Journal of Pressure Vessel Technology*, Vol. 121, No. 3, 1999, pp. 283–290.

10.8 R. D. Adams and W. C. Wake, *Structural Adhesive Joints in Engineering*, Elsevier Applied Science, London, 1984.

10.9 J. H. Bickford, *An Introduction to the Design and Behavior of Bolted Joints*, 3rd ed., Marcel Dekker, New York, 1995.

10.10 J. Bortman and B. A. Szabó, "Analysis of Fastened Structural Connections," *AIAA Journal*, Vol. 30, No. 11, 1992, pp. 2758–2764.

10.11 H. Chen and G. E. Blandford, "Finite-Element Model for Thin-Walled Space Frame Flexible Connection Behavior," *ASCE Journal of Structural Engineering*, Vol. 121, No. 10, 1995, pp. 1514–1521.

10.12 H. Shakourzadeh, Y. Q. Guo, and J. L. Batoz, "Modeling of Connections in the Analyses of Thin-Walled Space Frames," *Computers & Structures*, Vol. 71, No. 4, 1999, pp. 423–433.

10.13 J. M. Stallings and D. Y. Huang, "Modeling Pretensions in Bolted Connections," *Computers & Structures*, Vol. 45, No. 4, 1992, pp. 801–803.

10.14 E. Zhahavi, "A Finite Element Analysis of Flange Connections," *ASME Journal of Pressure Vessel Technology*, Vol. 115, No. 3, 1993, pp. 327–330.

10.15 J. M. Stallings, "Member End Releases in Framed Structures," *Computers & Structures*, Vol. 46, No. 3, 1993, pp. 443–449.

10.16 O. C. Zienkiewicz and F. C. Scott, "On the Principle of Repeatability and Its Application in Analysis of Turbine and Pump Impellers," *International Journal for Numerical Methods in Engineering*, Vol. 4, No. 3, 1972, pp. 445–448.

10.17 I. Taig, "Finite Element Analysis in Industry—Expertise or Efficiency?" in *Accuracy, Reliability, and Training in FEM Technology* (Proceedings of Fourth World Congress and Exhibition on Finite Element Methods), J. Robinson, ed., Robinson and Associates, Wimbourne, UK, 1984, pp. 56–70.

10.18 N. F. Knight, Jr., J. B. Ransom, O. H. Griffen, Jr., and D. M. Thompson, "Global/Local Methods Research Using a Common Structural Analysis Framework," *Finite Elements in Analysis and Design*, Vol. 9, No. 2, 1991, pp. 91–112.

10.19 J. B. Ransom, S. L. McCleary, and M. A. Aminpour, "A New Interface Element for Connecting Independently Modeled Substructures," *The 34th AIAA/ASME/ASCE/AHS/ASC Structures, Structural Dynamics, and Materials Conference*, AIAA, Washington, DC, 1993, pp. 1693–1703.

10.20 M. A. Aminpour, T. Krishnamurthy, and Y. Shin, "Coupling of Independently Modeled Three-Dimensional Finite Element Meshes with Non-Matching Arbitrary Shape Interface Boundaries," *AIAA/ASME/ASCE/AHS/ASC Structures, Structural Dynamics, and Materials Conference and Exhibit*, AIAA, Washington, DC, 1999, pp. 856–865.

10.21 C. Zhao, B. E. Hobbs, H. B. Mühlhaus, and A. Ord, "A Consistent Point-Searching Algorithm for Solution Interpolation in Unstructured Meshes Consisting of 4-Node Bilinear Quadrilateral Elements," *International Journal for Numerical Methods in Engineering*, Vol. 45, No. 10, 1999, pp. 1509–1526.

10.22 C. R. Dohrman, S. W. Key, and M. W. Heinstein, "A Method for Connecting Dissimilar Finite Element Meshes in Two Dimensions," *International Journal for Numerical Methods in Engineering*, Vol. 48, No. 5, 2000, pp. 655–678.

10.23 T. C. Gmür and R. H. Kauten, "Three-Dimensional Solid-to-Beam Transition Elements for Structural Dynamics Analysis," *International Journal for Numerical Methods in Engineering*, Vol. 36, No. 9, 1993, pp. 1429–1444.

10.24 J. S. Przemienicki, "Matrix Structural Analysis of Substructures," *AIAA Journal*, Vol. 1, No. 1, 1963, pp. 138–147.

10.25 A. J. Rizzo, "Quality Engineering with FEA and DOE," *Mechanical Engineering*, Vol. 116, No. 5, 1994, pp. 76–78.
10.26 J. Robinson, "Distortion Measures for Quadrilaterals with Curved Boundaries," *Finite Elements in Analysis and Design*, Vol. 4, No. 2, 1988, pp. 115–131.
10.27 D. A. Field, "Qualitative Measures for Initial Meshes," *International Journal for Numerical Methods in Engineering*, Vol. 47, No. 4, 2000, pp. 887–906.
10.28 A. El-Hamalawi, "A Simple and Effective Element Distortion Factor," *Computers & Structures*, Vol. 75, No. 5, 2000, pp. 507–513.
10.29 H. S. Oh and J. K. Lim, "A Simple Error Estimator for Size and Distortion of 2D Isoparametric Finite Elements," *Computers & Structures*, Vol. 59, No. 6, 1996, pp. 989–999.
10.30 G. Gendron, "A Review of Four PC Packages for FE Structural Analysis," *Finite Elements in Analysis and Design*, Vol. 28, No. 2, 1997, pp. 105–114.
10.31 J. R. Rice, *Numerical Methods, Software, and Analysis*, McGraw-Hill, New York, 1983.
10.32 P. Naur, B. Randell, and J. N. Buxton, *Software Engineering: Concepts and Techniques*, Petrocelli-Charter, New York, 1976.
10.33 K. Bell, "Some Thoughts on Design, Development and Maintenance of Engineering Software," *Advances in Engineering Software*, Vol. 8, No. 2, 1986, pp. 66–72.
10.34 J. T. Christian, "Verification and Documentation of Engineering Software," in *Reliability of Methods for Engineering Analysis*, K. J. Bathe and D. R. J. Owen, eds., Pineridge Press, Swansea, UK, 1986.
10.35 R. Evans, "Guidelines for the Selection of Analysis Software," *Mechanical Engineering*, Vol. 109, No. 3, 1987, pp. 42–43.
10.36 *Guide for Evaluating Engineering Software*, ASCE, New York, 1989.
10.37 V. Adams and A. Askenazi, *Building Better Products with Finite Element Analysis*, OnWord Press, Santa Fe, NM, 1999.
10.38 B. A. Szabó and R. L. Actis, "Finite Element Analysis in Professional Practice," *Computer Methods in Applied Mechanics and Engineering*, Vol. 133, Nos. 3–4, 1996, pp. 209–228.
10.39 L. Z. Emkin, "Computers in Structural Engineering Practice: The Issue of Quality," *Computers & Structures*, Vol. 30, No. 3, 1988, pp. 439–446.

CHAPTER 11

11.1 R. R. Craig Jr., *Structural Dynamics: An Introduction to Computer Methods*, John Wiley & Sons, New York, 1981.
11.2 R. W. Clough and J. Penzien, *Dynamics of Structures*, 2nd ed., McGraw-Hill, New York, 1993.
11.3 A. K. Chopra, *Dynamics of Structures: Theory and Applications to Earthquake Engineering*, Prentice Hall, Upper Saddle River, NJ, 1995.
11.4 J. S. Archer, "Consistent Matrix Formulations for Structural Analysis Using Finite Element Techniques," *AIAA Journal*, Vol. 3, No. 10, 1965, pp. 1910–1918.
11.5 T. Yokoyama, "Vibrations of a Hanging Timoshenko Beam Under Gravity," *Journal of Sound and Vibration*, Vol. 141, No. 2, 1990, pp. 245–258.
11.6 C. Stavrinidis, J. Clinckemaillie, and J. Dubois, "New Concepts for Finite-Element Mass Matrix Formulation," *AIAA Journal*, Vol. 27, No. 9, 1989, pp. 1249–1255.
11.7 K.-O. Kim, "A Review of Mass Matrices for Eigenproblems," *Computers & Structures*, Vol. 46, No. 6, 1993, pp. 1041–1048.
11.8 E. Hinton, T. Rock, and O. C. Zienkiewicz, "A Note on Mass Lumping and Related Processes in the Finite Element Method," *Earthquake Engineering and Structural Dynamics*, Vol. 4, No. 3, 1976, pp. 245–249.

11.9 G. J. Fix, "Effect of Quadrature Errors in Finite Element Approximation of Steady State Eigenvalue and Parabolic Problems," in *Mathematical Foundations of the Finite Element Method*, I. Babuška and A. K. Aziz, eds., Academic Press, New York, 1972, pp. 525–556.

11.10 I. Fried and D. S. Malkus, "Finite Element Mass Matrix Lumping by Numerical Integration With No Convergence Rate Loss," *International Journal of Solids & Structures*, Vol. 11, No. 4, 1975, pp. 461–466.

11.11 D. S. Malkus and M. E. Plesha, "Zero and Negative Masses in Finite Element Vibration and Transient Analysis," *Computer Methods in Applied Mechanics and Engineering*, Vol. 59, No. 3, 1986, pp. 281–306.

11.12 R. A. Brockman, "Dynamics of the Bilinear Mindlin Plate Element," *International Journal for Numerical Methods in Engineering*, Vol. 24, No. 12, 1987, pp. 2343–2356.

11.13 W. Carnegie, "Vibrations of Rotating Cantilever Blading: Theoretical Approaches to the Frequency Problem Based on Energy Methods," *Journal of Mechanical Engineering Science*, Vol. 1, No. 3, 1959, pp. 235–240.

11.14 R. M. Laurenson, "Modal Analysis of Rotating Flexible Structures," *AIAA Journal*, Vol. 14, No. 10, 1976, pp. 1444–1450.

11.15 W. H. Wittrick and F. W. Williams, "On the Free Vibration Analysis of Spinning Structures by Using Discrete or Distributed Mass Models," *Journal of Sound and Vibration*, Vol. 82, No. 1, 1982, pp. 1–15.

11.16 M. Geradin and N. Kill, "A New Approach to Finite Element Modelling of Flexible Rotors," *Engineering Computations*, Vol. 1, No. 1, 1984, pp. 52–64.

11.17 A. Y. T. Leung and T. C. Fung, "Spinning Finite Elements," *Journal of Sound and Vibration*, Vol. 125, No. 3, 1988, pp. 523–537 (discussion: Vol. 140, No. 2, 1990, pp. 341–347).

11.18 G. Sauer and M. Wolf, "Finite Element Analysis of Gyroscopic Effects," *Finite Elements in Analysis and Design*, Vol. 5, No. 2, 1989, pp. 131–140.

11.19 Q. H. Qin and C. X. Mao, "Coupled Torsional-Flexural Vibration of Shaft Systems in Mechanical Engineering—I. Finite Element Model," *Computers & Structures*, Vol. 58, No. 4, 1996, pp. 835–843.

11.20 J. W. S. Rayleigh, *The Theory of Sound*, 2nd ed., 1894 (reprinted by Dover Publications, New York, 1945), Vol. I, p. 102; Vol. II, p. 312.

11.21 D. Hitchings, ed., *A Finite Element Dynamics Primer*, NAFEMS, Glasgow, UK, 1992.

11.22 C. F. Beards, "Damping in Structural Joints," *Shock and Vibration Digest*, Vol. 24, No. 7, 1992, pp. 3–7.

11.23 A. K. Noor, "Recent Advances and Applications of Reduction Methods," *ASME Applied Mechanics Reviews*, Vol. 47, No. 5, 1994, pp. 125–146 [cites 235 refs.].

11.24 A. F. Bertolini, "Review of Eigensolution Procedures for Linear Dynamic Finite Element Analysis," *ASME Applied Mechanics Reviews*, Vol. 51, No. 2, 1998, pp. 155–172 [cites 320 refs.].

11.25 R. J. Guyan, "Reduction of Stiffness and Mass Matrices," *AIAA Journal*, Vol. 3, No. 2, 1965, p. 380.

11.26 B. Irons, "Structural Eigenvalue Problems: Elimination of Unwanted Variables," *AIAA Journal*, Vol. 3, No. 5, 1965, pp. 961–962.

11.27 R. L. Kidder, "Reduction of Structural Frequency Equations," *AIAA Journal*, Vol. 11, No. 6, 1973, p. 892 (discussion: Vol. 13, No. 5, 1975, pp. 701-703).

11.28 R. G. Anderson, B. M. Irons, and O. C. Zienkiewicz, "Vibration and Stability of Plates Using Finite Elements," *International Journal of Solids & Structures*, Vol. 4, No. 10, 1968, pp. 1031–1055.

11.29 V. N. Shah, and M. Raymund, "Analytical Selection of Masters for the Reduced Eigenvalue Problem," *International Journal for Numerical Methods in Engineering*, Vol. 18, No. 1, 1982, pp. 89–98.

11.30 J. H. Ong, "Improved Automatic Masters for Eigenvalue Economization," *Finite Elements in Analysis and Design*, Vol. 3, No. 2, 1987, pp. 149–160.

11.31 K.-O. Kim and M.-K. Kang, "Convergence Acceleration of Iterative Modal Reduction Methods," *AIAA Journal*, Vol. 39, No. 1, 2001, pp. 134–140.
11.32 R. E. Cornwell, R. R. Craig, Jr., and C. P. Johnson, "On the Application of the Mode-Acceleration Method to Structural Engineering Problems," *Earthquake Engineering and Structural Dynamics*, Vol. 11, No. 5, 1983, pp. 679–688.
11.33 H. L. Soriano and F. V. Filho, "On the Modal Acceleration Method in Structural Dynamics. Mode Truncation and Static Correction," *Computers & Structures*, Vol. 29, No. 5, 1988, pp. 777–782.
11.34 J. M. Dickens, J. M. Nakagawa, and M. J. Wittbrodt, "A Critique of Mode Acceleration and Modal Truncation Augmentation Methods for Modal Response Analysis," *Computers & Structures*, Vol. 62, No. 6, 1997, pp. 985–998.
11.35 O. E. Hansteen and K. Bell, "On the Accuracy of Mode Superposition Analysis in Structural Dynamics," *Earthquake Engineering and Structural Dynamics*, Vol. 7, No. 5, 1979, pp. 405–411.
11.36 V. N. Shah, G. J. Bohm, and A. N. Nahavandi, "Modal Superposition Method for Computationally Economical Nonlinear Structural Analysis," *ASME Journal of Pressure Vessel Technology*, Vol. 101, No. 2, 1979, pp. 134–141.
11.37 N. F. Knight Jr., "Nonlinear Structural Dynamic Analysis Using a Modified Modal Method," *AIAA Journal*, Vol. 23, No. 10, 1985, pp. 1594–1601.
11.38 R. Villaverde and M. M. Hanna, "Efficient Mode Superposition Algorithm for Seismic Analysis of Non-Linear Structures," *Earthquake Engineering and Structural Dynamics*, Vol. 21, No. 10, 1992, pp. 849–858.
11.39 R. R. Arnold, R. L. Citerly, M. Chargin, and D. Galant, "Application of Ritz Vectors for Dynamic Analysis of Large Structures," *Computers & Structures*, Vol. 21, No. 5, 1985, pp. 901–907.
11.40 E. L. Wilson, M.-W. Yuan, and J. M. Dickens, "Dynamic Analysis by Direct Superposition of Ritz Vectors," *Earthquake Engineering and Structural Dynamics*, Vol. 10, No. 6, 1982, pp. 813–821.
11.41 K.-J. Joo, E. L. Wilson, and P. Leger, "Ritz Vectors and Generation Criteria for Mode Superposition Analysis," *Earthquake Engineering and Structural Dynamics*, Vol. 18, No. 2, 1989, pp. 149–167.
11.42 R. R. Craig, Jr., "A Review of Time-Domain and Frequency-Domain Component-Mode Synthesis Methods," *International Journal of Analytical and Experimental Modal Analysis*, Vol. 2, No. 2, 1987, pp. 57–72.
11.43 A. Y. T. Leung, "A Simple Dynamic Substructure Method," *Earthquake Engineering and Structural Dynamics*, Vol. 16, No. 6, 1988, pp. 827–837.
11.44 L. Meirovitch and M. K. Kwak, "Rayleigh-Ritz Based Substructure Synthesis for Flexible Multibody Systems," *AIAA Journal*, Vol. 29, No. 10, 1991, pp.1709–1719.
11.45 L. E. Suarez and M. P. Singh, "Improved Fixed Interface Method for Modal Synthesis," *AIAA Journal*, Vol. 30, No. 12, 1992, pp. 2952–2958.
11.46 W.-H. Shyu, Z.-D. Ma, and G. M. Hulbert, "A New Component Mode Synthesis Method: Quasi-Static Mode Compensation," *Finite Elements in Analysis and Design*, Vol. 24, No. 4, 1997, pp. 271–281.
11.47 T. Belytschko, "A Survey of Numerical Methods and Computer Programs for Dynamic Structural Analysis," *Nuclear Engineering and Design*, Vol. 37, No. 1, 1976, pp. 23–34.
11.48 T. Belytschko, "An Overview of Semidiscretization and Time Integration Procedures," in *Computational Methods for Transient Analysis*, T. Belytschko and T. J. R. Hughes, eds., North-Holland, Amsterdam, 1983, pp. 1–65.
11.49 T. Belytschko, W. K. Liu, and B. Moran, *Nonlinear Finite Elements for Continua and Structures*, John Wiley & Sons, Chichester, UK, 2000.
11.50 D. P. Flanagan and T. Belytschko, "Eigenvalues and Stable Time Steps for the Uniform Strain Hexahedron and Quadrilateral," *ASME Journal of Applied Mechanics*, Vol. 51, No. 1, 1984, pp. 35–40.

11.51 R. Courant, K. O. Friedrichs, and H. Lewy, "Über die Partiellen Differenzengleichungen der Mathematischen Physik," *Mathematische Annalen*, Vol. 100, 1928, pp. 32–74.
11.52 E. Isaacson and H. B. Keller, *Analysis of Numerical Methods*, John Wiley & Sons, New York, 1966.
11.53 J. I. Lin, "Bounds on Eigenvalues of Finite Element Systems," *International Journal for Numerical Methods in Engineering*, Vol. 32, No. 5, 1991, pp. 957–967.
11.54 N. M. Newmark, "A Method of Computation for Structural Dynamics," *ASCE Journal of the Engineering Mechanics Division*, Vol. 5, No. EM3, 1959, pp. 67–94.
11.55 H. M. Hilber, T. J. R. Hughes, and R. L. Taylor, "Improved Numerical Dissipation for Time Integration Algorithms in Structural Dynamics," *Earthquake Engineering and Structural Dynamics*, Vol. 5, No. 3, 1977, pp. 283–292.
11.56 G. M. Hulbert and T. J. R. Hughes, "An Error Analysis of Truncated Starting Conditions in Step-by-Step Time Integration: Consequences for Structural Dynamics," *Earthquake Engineering and Structural Dynamics*, Vol. 15, No. 7, 1987, pp. 901–910.
11.57 T. J. R. Hughes, "Analysis of Transient Algorithms with Particular Reference to Stability Behavior," in *Computational Methods for Transient Analysis*, T. Belytschko and T. J. R. Hughes, eds., North-Holland, Amsterdam, 1983, pp. 67–155.
11.58 T. Belytschko and R. Mullen, "Stability of Explicit-Implicit Mesh Partitions in Time Integration," *International Journal for Numerical Methods in Engineering*, Vol. 12, No. 10, 1978, pp. 1575–1586.
11.59 T. J. R. Hughes and W.-K. Liu, "Implicit-Explicit Finite Elements in Transient Analysis: Stability Theory," *ASME Journal of Applied Mechanics*, Vol. 45, No. 2, 1978, pp. 371–374.
11.60 T. J. R. Hughes and W.-K. Liu, "Implicit-Explicit Finite Elements in Transient Analysis: Implementation and Numerical Examples," *ASME Journal of Applied Mechanics*, Vol. 45, No. 2, 1978, pp. 375–378.
11.61 T. J. R. Hughes, K. S. Pister, and R. L. Taylor, "Implicit-Explicit Finite Elements in Nonlinear Transient Analysis," *Computer Methods in Applied Mechanics and Engineering*, Vol. 17/18, Part I, 1979, pp. 159-182.
11.62 G. L. Goudreau and R. L. Taylor, "Evaluation of Numerical Integration Methods in Elastodynamics," *Computer Methods in Applied Mechanics and Engineering*, Vol. 2, No. 1, 1972, pp. 69–97.
11.63 S. D. Conte and C. de Boor, *Elementary Numerical Analysis*, McGraw-Hill, New York, 3rd ed., 1980.
11.64 M. L. James, G. M. Smith, J. C. Wolford, and P. W. Whaley, *Vibration of Mechanical and Structural Systems*, 2nd ed., Harper Collins, New York, 1994.
11.65 A. K. Gupta, *Response Spectrum Method*, Blackwell Scientific, Boston, MA, 1990.
11.66 C. M. Harris, ed., *Shock and Vibration Handbook*, McGraw-Hill, New York, 1996.
11.67 G. J. O'Hara and R. O. Belsheim, *Interim Design Values for Shock Design of Shipboard Equipment*, NRL Memorandum Report 1396, U.S. Naval Research Laboratory, Washington, DC, 1963.
11.68 S. Kawashima and T. Fujimoto, "Vibration Analysis of Frames with Semi-Rigid Connections," *Computers & Structures*, Vol. 19, Nos. 1–2, 1984, pp. 85–92.
11.69 Z. P. Bazant and Z. Celep, "Spurious Reflection of Elastic Waves in Nonuniform Meshes of Constant and Linear Strain Finite Elements," *Computers & Structures*, Vol. 15, No. 4, 1982, pp. 451–459.
11.70 A. O. Cifuentes, "Dynamic Response of a Beam Excited by a Moving Mass," *Finite Elements in Analysis and Design*, Vol. 5, No. 3, 1989, pp. 327–346.
11.71 M. R. Taheri, E. C. Ting, and A. R. Kukreti, "Vehicle-Guideway Interactions: A Literature Review," *Shock and Vibration Digest*, Vol. 22, No. 6, 1990, pp. 3–9 [cites 47 refs.].
11.72 J. R. Rieker, Y.-H. Lin, and M. W. Trethewey, "Discretization Considerations in Moving Load Finite Element Beam Models," *Finite Elements in Analysis and Design*, Vol. 21, No. 3, 1996, pp. 129–144.

11.73 Y.-B. Yang and J.-D. Yau, "Vehicle-Bridge Interaction Element for Dynamic Analysis," *ASCE Journal of Structural Engineering*, Vol. 123, No. 11, 1997, pp. 1512–1518.
11.74 J. Padovan and I. Zeid, "On the Development of Traveling Load Finite Elements," *Computers & Structures*, Vol. 12, No. 1, 1980, pp. 77–83.
11.75 T. R. Sutter, C. J. Camarda, J. L. Walsh, and H. M. Adelman, "Comparison of Several Methods for Calculating Vibration Mode Shape Derivatives," *AIAA Journal*, Vol. 26, No. 12, 1988, pp. 1506–1511.
11.76 B. P. Wang, "Improved Approximate Methods for Calculating Eigenvector Derivatives in Structural Dynamics," *AIAA Journal*, Vol. 29, No. 6, 1991, pp. 1018–1020.
11.77 J. E. Mottershead and M. I. Friswell, "Model Updating in Structural Dynamics: A Survey," *Journal of Sound and Vibration*, Vol. 167, No. 2, 1993, pp. 347–375 [cites 243 refs.].
11.78 M. I. Friswell and J. E. Mottershead, *Finite Element Model Updating in Structural Dynamics*, Kluwer Academic Publishers, Dordrecht, 1995.
11.79 S. H. Chen and X. W. Yang, "Extended Kirsch Combined Method for Eigenvalue Reanalysis," *AIAA Journal*, Vol. 38, No. 5, 2000, pp. 927–930.
11.80 R. D. Cook and J. Avrashi, "Error Estimation and Adaptive Meshing for Vibration Problems," *Computers & Structures*, Vol. 44, No. 3, 1992, pp. 619–626.
11.81 Y. M. Xie and G. P. Steven, "Explicit Formulas for Correcting Finite Element Predictions of Natural Frequencies," *Communications in Numerical Methods Engineering*, Vol. 9, No. 8, 1993, pp. 671–680.
11.82 D. B. Stephen and G. P. Steven, "Error Estimation for Natural Frequency Finite Element Analysis," *Finite Elements in Analysis and Design*, Vol. 26, No. 1, 1997, pp. 21–40.
11.83 X. D. Li, L. F. Zeng, and N.-E. Wiberg, "A Simple Local Error Estimator and an Adaptive Time-Stepping Procedure for Direct Integration Method in Dynamic Analysis," *Communications in Numerical Methods in Engineering*, Vol. 9, No. 4, 1993, pp. 273–292.
11.84 N.-E. Wiberg and X. D. Li, "A Post-Processing Technique and an *A Posteriori* Error Estimate for the Newmark Method in Dynamic Analysis," *Earthquake Engineering and Structural Dynamics*, Vol. 22, No. 6, 1993, pp. 465–489.
11.85 C.-K. Choi and H.-J. Chung, "Error Estimates and Adaptive Time Stepping for Various Direct Time Integration Methods," *Computers & Structures*, Vol. 60, No. 6, 1996, pp. 923–944.
11.86 J. A. Zukas, "Some Common Problems in the Numerical Modeling of Impact Phenomena," *Computing Systems in Engineering*, Vol. 4, No. 1, 1993, pp. 43–58.

CHAPTER 12

12.1 K. D. Hagen, *Heat Transfer with Applications*, Prentice Hall, Upper Saddle River, NJ, 1999.
12.2 H.-C. Huang and A. S. Usmani, *Finite Element Analysis for Heat Transfer*, Springer-Verlag, London, 1994.
12.3 E. L. Wilson, K. J. Bathe, and F. E. Peterson, "Finite Element Analysis of Linear and Nonlinear Heat Transfer," *Nuclear Engineering and Design*, Vol. 29, No. 1, 1974, pp. 110–124.
12.4 R. Siegel and J. R. Howell, *Thermal Radiation Heat Transfer*, 3rd ed., Hemisphere Publishing Corp., Washington, DC, 1992.
12.5 J. F. Stelzer and R. Welzel, "Experiences in Non-Linear Analysis of Temperature Fields with Finite Elements," *International Journal for Numerical Methods in Engineering*, Vol. 24, No. 1, 1987, pp. 59–73.
12.6 B. Nour-Omid, "Lanczos Method for Heat Conduction Analysis," *International Journal for Numerical Methods in Engineering*, Vol. 24, No. 1, 1987, pp. 251–262.
12.7 T. J. R. Hughes, "Unconditionally Stable Algorithms for Nonlinear Heat Conduction," *Computer Methods in Applied Mechanics and Engineering*, Vol. 10, No. 2, 1977, pp. 135–139.

12.8 R. E. Cornwell and D. S. Malkus, "Improved Numerical Dissipation for Time Integration Algorithms in Conduction Heat Transfer," *Computer Methods in Applied Mechanics and Engineering*, Vol. 97, No. 2, 1992, pp. 149–156.
12.9 K. E. Barrett, D. M. Butterfield, J. H. Tabor, and S. Ellis, "Quadratic Elements for Heat Transfer—A Cautionary Tale," *International Journal of Mechanical Engineering Education*, Vol. 18, No. 1, 1990, pp. 59–74.
12.10 A. Craggs, "A Note on the Theory and Application of a Simple Pipe Acoustic Element," *Journal of Sound and Vibration*, Vol. 85, No. 2, 1982, pp. 292–295.
12.11 O. C. Zienkiewicz and R. E. Newton, "Coupled Vibrations of a Structure Submerged in a Compressible Fluid," in *Proceedings of the Symposium on Finite Element Techniques*, M. Sörensen, ed., University of Stuttgart, Germany, 1969, pp. 359–379.
12.12 O. C. Zienkiewicz and P. Bettess, "Fluid-Structure Dynamic Interaction and Wave Forces. An Introduction to Numerical Treatment," *International Journal for Numerical Methods in Engineering*, Vol. 13, No. 1, 1978, pp. 1–16.
12.13 R. J. Astley and W. Eversman, "Finite Element Formulations for Acoustical Radiation," *Journal of Sound and Vibration*, Vol. 88, No. 1, 1983, pp. 47–64.
12.14 A. Craggs, "A Finite Element Model for Acoustically Lined Small Rooms," *Journal of Sound and Vibration*, Vol. 108, No. 2, 1986, pp. 327–337.
12.15 *ANSYS Theory Reference*, Release 5.4, ANSYS Inc. Canonsburg, PA, 1997.
12.16 O. C. Zienkiewicz, "Coupled Problems and their Numerical Solution," in *Numerical Methods in Coupled Systems*, R. W. Lewis, P. Bettess, and E. Hinton, eds., John Wiley & Sons, Chichester, UK, 1984, pp. 35–58.
12.17 R. E. D. Bishop and W. G. Price, *Hydroelasticity of Ships*, Cambridge University Press, Cambridge, UK, 1979.
12.18 A. K. Chopra and P. Chakrabarti, "Dynamics of Gravity Dams—Significance of Compressibility of Water and Three-Dimensional Effects," *Earthquake Engineering and Structural Dynamics*, Vol. 2, No. 1, 1973, pp. 103–104.
12.19 O. C. Zienkiewicz and P. Bettess, "Dynamic Fluid-Structure Interaction. Numerical Modelling of the Coupled Problem," in *Numerical Methods in Offshore Engineering*, O. C. Zienkiewicz, R. W. Lewis, and K. G. Stagg, eds., John Wiley & Sons, Chichester, UK, 1978, pp. 185–193.
12.20 L. Kiefling and G. C. Feng, "Fluid-Structure Finite Element Vibrational Analysis," *AIAA Journal*, Vol. 14, No. 2, 1976, pp. 199–203.
12.21 M. A. Hamdi, Y. Ousset, and G. Verchery, " A Displacement Method for the Analysis of Vibrations of Coupled Fluid-Structure Systems," *International Journal for Numerical Methods in Engineering*, Vol. 13, No. 1, 1978, pp. 130–150.
12.22 L. G. Olson and K.-J. Bathe, "A Study of Displacement-Based Fluid Finite Elements for Calculating Frequencies of Fluid and Fluid-Structure Systems," *Nuclear Engineering and Design*, Vol. 76, No. 2, 1983, pp. 137–151.

CHAPTER 13

13.1 J. F. Abel and M. S. Shephard, "An Algorithm for Multipoint Constraints in Finite Element Analysis," *International Journal for Numerical Methods in Engineering*, Vol. 14, No. 3, 1979, pp. 464–467.
13.2 S.-C. Chang and T.-W. Lin, "Constraint Relation Implementation for Finite Element Analysis from an Element Basis," *Advances in Engineering Software*, Vol. 10, No. 4, 1988, pp. 191–194.
13.3 C. A. Felippa, "Iterative Procedures for Improving Penalty Function Solutions of Algebraic Equations," *International Journal for Numerical Methods in Engineering*, Vol. 12, No. 5, 1978, pp. 821–836.

13.4 U. Hueck, H. L. Schreyer, and P. Wriggers, "On the Incompressible Constraint of the Four-Node Quadrilateral Element," *International Journal for Numerical Methods in Engineering*, Vol. 38, No. 17, 1995, pp. 3039–3053.
13.5 D. S. Malkus, *Finite element Analysis of Incompressible Solids*, Ph.D. Dissertation, Boston University, Boston, MA, 1976.
13.6 T. J. R. Hughes, W. K. Liu, and A. Brooks, "Finite Element Analysis of Incompressible Viscous Flows by the Penalty Function Formulation," *Journal of Computational Physics*, Vol. 30, No. 1, 1979, pp. 1–60.
13.7 C. Johnson and J. Pitikäranta, "Analysis of Some Mixed Finite Element Methods Related to Reduced Integration," *Mathematics of Computation*, Vol. 38, No. 158, 1982, pp. 375–400.
13.8 J. C. Simo, R. L. Taylor, and K. S. Pister, "Variational and Projection Methods for the Volume Constraint in Finite Deformation Plasticity," *Computer Methods in Applied Mechanics and Engineering*, Vol. 51, Nos. 1–3, 1985, pp. 177–208.
13.9 T. J. R. Hughes, "Generalization of Selective Integration Procedures to Anisotropic and Nonlinear Media," *International Journal for Numerical Methods in Engineering*, Vol. 15, No. 9, 1980, pp. 1413–1418.
13.10 J. Donea and T. Belytschko, "Advances in Computational Mechanics," *Nuclear Engineering and Design*, Vol. 134, No. 1, 1992, pp. 1–22.
13.11 O. C. Zienkiewicz and R. L. Taylor, "The Finite Element Patch Test Revisited: A Computer Test for Convergence, Validation and Error Estimates," *Computer Methods in Applied Mechanics and Engineering*, Vol. 149, Nos. 1–4, 1997, pp. 223–254.
13.12 M. Engelman, R. L. Sani, P. M. Gresho, and M. Bercovier, "Consistent vs. Reduced Integration Penalty Methods for Incompressible Media Using Several Old and New Elements," *International Journal for Numerical Methods in Fluids*, Vol. 2, No. 1, 1982, pp. 25–42.

CHAPTER 14

14.1 *ANSYS News*, Swanson Analysis Systems Inc., Houston, PA, Third Issue, 1989.
14.2 R. D. Cook, "A Note on Certain Incompatible Elements," *International Journal for Numerical Methods in Engineering,* Vol. 6, No. 1, 1973, pp. 146–147.
14.3 R. D. Cook, "Axisymmetric Finite Element Analysis for Pure Moment Loading of Curved Beams and Pipe Bends," *Computers & Structures*, Vol. 33, No. 2, 1989, pp. 483–487.
14.4 R. D. Cook, "Pure Bending of Curved Beams of Thin-Walled Rectangular Box Section," *ASME Journal of Applied Mechanics*, Vol. 58, No. 1, 1991, pp. 154–156.
14.5 Y. K. Cheung and L. G. Tham, *Finite Strip Method*, CRC Press, Boca Raton, Florida, 1998.
14.6 O. C. Zienkiewicz and J. M. Too, "The Finite Prism in Analysis of Thick Simply Supported Box Bridges," *Proceedings of the Institution of Civil Engineers*, Vol. 53, Part 2, 1972, pp. 147–172.
14.7 T. Belytschko, "Finite Elements for Axisymmetric Solids Under Arbitrary Loadings with Nodes on Origin," *AIAA Journal*, Vol. 10, No. 11, 1972, pp. 1532–1533 (discussion and closure: Vol. 11, No. 9, 1973, pp. 1357–1358).
14.8 J. Padovan, "Quasi-Analytical Finite Element Procedures for Axisymmetric Anisotropic Shells and Solids," *Computers & Structures*, Vol. 4, No. 3, 1974, pp. 467–483.
14.9 J. G. Crose, "Stress Analysis of Axisymmetric Solids with Asymmetric Properties," *AIAA Journal*, Vol. 10, No. 7, 1972, pp. 866–871.
14.10 M. Sedaghat and L. R. Herrmann, "A Nonlinear, Semi-Analytical Finite Element Analysis for Nearly Axisymmetric Solids," *Computers & Structures*, Vol. 17, No. 3, 1983, pp. 389–401.

CHAPTER 15

15.1 E. Reissner, "On Bending of Elastic Plates," *Quarterly of Applied Mathematics*, Vol. 5, No. 1, 1947, pp. 55–68.

15.2 R. D. Mindlin, "Influence of Rotary Inertia and Shear On Flexural Motions of Isotropic Elastic Plates," *ASME Journal of Applied Mechanics*, Vol. 18, No. 1, 1951, pp. 31–38.

15.3 M. M. Hrabok and T. M. Hrudey, "A Review and Catalog of Plate Bending Finite Elements," *Computers & Structures*, Vol. 19, No. 3, 1984, pp. 479–495.

15.4 J. M. Whitney and A. W. Leissa, "Analysis of Heterogeneous Anisotropic Plates," *ASME Journal of Applied Mechanics*, Vol. 36, No. 2, 1969, pp. 261–266.

15.5 A. K. Noor, W. S. Burton, and C. W. Bert, "Computational Models for Sandwich Panels and Shells," *ASME Applied Mechanics Reviews*, Vol. 49, No. 3, 1996, pp. 155–199 [cites 1376 refs.].

15.6 B. M. Irons and K. J. Draper, "Inadequacy of Nodal Connections in a Stiffness Solution for Plate Bending," *AIAA Journal*, Vol. 3, No. 5, 1965, p. 961.

15.7 O. C. Zienkiewicz and R. L. Taylor, *The Finite Element Method*, 4th ed., Vol. 2, McGraw-Hill, London, 1991.

15.8 R. H. Gallagher, *Finite Element Analysis: Fundamentals*, Prentice Hall, Englewood Cliffs, NJ, 1975.

15.9 L. S. D. Morley, "The Constant-Moment Plate-Bending Element," *Journal of Strain Analysis*, Vol. 6, No. 1, 1971, pp. 20–24.

15.10 L. R. Herrmann, "Finite-Element Bending Analysis for Plates," *ASCE Journal of the Engineering Mechanics Division*, Vol. 93, No. EM5, 1967, pp. 13–26.

15.11 J.-L. Batoz, K.-J. Bathe, and L. W. Ho, "A Study of Three-Node Triangular Plate Bending Elements," *International Journal for Numerical Methods in Engineering*, Vol. 15, No. 12, 1980, pp. 1771–1812.

15.12 J.-L. Batoz, "An Explicit Formulation for an Efficient Triangular Plate Bending Element," *International Journal for Numerical Methods in Engineering*, Vol. 18, No. 7, 1982, pp. 1077–1089.

15.13 C. Jayachandrabose, J. Kirkhope, and C. R. Babu, "An Alternative Formulation for the DKT Plate Bending Element," *International Journal for Numerical Methods in Engineering*, Vol. 21, No. 7, 1985, pp. 1289–1293.

15.14 J. A. Stricklin, W. E. Haisler, P. R. Tisdale, and R. Gunderson, "A Rapidly Converging Triangular Plate Element," *AIAA Journal*, Vol. 7, No. 1, 1969, pp. 180–181.

15.15 C. Jayachandrabose and J. Kirkhope, "Construction of New Efficient Three-Node Triangular Thin-Plate Bending Elements," *Computers & Structures*, Vol. 23, No. 5, 1986, pp. 587–603.

15.16 C. Wanji and Y. K. Cheung, "Refined Quadrilateral Discrete Kirchhoff Thin Plate Bending Element," *International Journal for Numerical Methods in Engineering*, Vol. 40, No. 21, 1997, pp. 3937–3953.

15.17 C. Wanji and Y. K. Cheung, "Refined Triangular Discrete Kirchhoff Plate Element for Thin Plate Bending, Vibration and Buckling Analysis," *International Journal for Numerical Methods in Engineering*, Vol. 41, No. 8, 1998, pp. 1507–1525.

15.18 T. Belytschko, C.-S. Tsay, and W. K. Liu, "A Stabilization Matrix for the Bilinear Mindlin Plate Element," *Computer Methods in Applied Mechanics and Engineering*, Vol. 29, No. 3, 1981, pp. 313–327.

15.19 T. Belytschko and C.-S. Tsay, "A Stabilization Procedure for the Quadrilateral Plate Element with One-Point Quadrature," *International Journal for Numerical Methods in Engineering*, Vol. 19, No. 3, 1983, pp. 405–419.

15.20 E. Hinton and H. C. Huang, "A Family of Quadrilateral Mindlin Plate Elements with Substitute Shear Strain Fields," *Computers & Structures*, Vol. 23, No. 3, 1986, pp. 409–431.

15.21 E. D. Pugh, E. R. Hinton, and O. C. Zienkiewicz, "A Study of Quadrilateral Plate Bending Elements with 'Reduced' Integration," *International Journal for Numerical Methods in Engineering,* Vol. 12, No. 7, 1978, pp. 1059–1079.

15.22 M. Dhainaut, " A Comparison Between Serendipity and Lagrange Plate Elements in the Finite Element Method," *Communications in Numerical Methods in Engineering,* Vol. 13, No. 5, 1997, pp. 343–353.

15.23 A. F. Saleeb and T. Y. Chang, "An Efficient Quadrilateral Element for Plate Bending Analysis," *International Journal for Numerical Methods in Engineering,* Vol. 24, No. 6, 1987, pp. 1123–1155.

15.24 H. Parisch, " A Critical Survey of the 9-Node Degenerated Shell Element with Special Emphasis on Thin Shell Application and Reduced Integration," *Computer Methods in Applied Mechanics and Engineering*, Vol. 20, No. 3, 1979, pp. 323–350.

15.25 A. Tessler and T. J. R. Hughes, "A Three-Node Mindlin Plate Element with Improved Transverse Shear," *Computer Methods in Applied Mechanics and Engineering*, Vol. 50, No. 1, 1985, pp. 71–101.

15.26 N. Carpenter, T. Belytschko, and H. Stolarski, "Locking and Shear Scaling Factors in C^0 Bending Elements," *Computers & Structures*, Vol. 22, No. 1, 1986, pp. 39–52.

15.27 G. Shi and P. Tong, "Assumed Stress C^0 Quadrilateral/Triangular Plate Elements by Interrelated Edge Displacements," *International Journal for Numerical Methods in Engineering,* Vol. 39, No. 6, 1996, pp. 1041–1051.

15.28 A. K. Soh, L. Zhifei, and C. Song, "A Mindlin Plate Triangular Element with Improved Interpolation Based on Timoshenko's Beam Theory," *Communications in Numerical Methods in Engineering,* Vol. 15, No. 7, 1999, pp. 527–532.

15.29 K. Y. Sze and C. L. Chow, "A Mixed Formulation of a Four-Node Mindlin Shell/Plate with Interpolated Covariant Transverse Shear Strains," *Computers & Structures*, Vol. 40, No. 3, 1991, pp. 775–784.

15.30 F. Auricchio and R. L. Taylor, "A Triangular Thick Plate Finite Element with an Exact Thin Limit," *Finite Elements in Analysis and Design*, Vol. 19, Nos. 1-2, 1995, pp. 57–68.

15.31 K.-J. Bathe and E. N. Dvorkin, "A Four-Node Plate Bending Element Based on Mindlin/ Reissner Plate Theory and a Mixed Interpolation," *International Journal for Numerical Methods in Engineering,* Vol. 21, No. 2, 1985, pp. 367–383.

15.32 C. K. Choi, S. H. Kim, Y. M. Park, and H. J. Chung, "The Best of the Enhanced Displacement Non-conforming Plate/shell Elements," *Archives of Computational Methods in Engineering*, Vol. 7, No. 1, 2000, pp. 3–18.

15.33 J. L. Batoz and P. Lardeur, "A Discrete Shear Triangular Nine D.O.F. Element for the Analysis of Thick to Very Thin Plates," *International Journal for Numerical Methods in Engineering,* Vol. 28, No. 3, 1989, pp. 533–560.

15.34 Y. K. Cheung and W. Chen, "Generalized Hybrid Degenerated Elements for Plates and Shells," *Computers & Structures*, Vol. 36, No. 2, 1990, pp. 279–290.

15.35 J. Jirousek, "Comment on Evaluation of Shear Forces and Reactions from Transverse Shear Deformations by using Isoparametric Quadratic Mindlin Plate Elements," *Computers & Structures*, Vol. 19, No. 5/6, 1984, pp. 899–903.

15.36 K.-J. Bathe, N.-S. Lee, and M. L. Bucalem, "On the Use of Hierarchical Models in Engineering Analysis," *Computer Methods in Applied Mechanics and Engineering*, Vol. 82, No. 1/3, 1990, pp. 5–26.

15.37 A. Selman, E. Hinton, and W. Atamaz-Sibai, "Edge Effects in Mindlin-Reissner Plates using Adaptive Mesh Refinement," *Engineering Computations*, Vol. 7, No. 3, 1990, pp. 217–226.

15.38 J. Jirousek and M. N'Diaye, "Accurate Evaluation of Support Reaction in Finite Element Plate-Bending Analysis," *Computers & Structures*, Vol. 38, No. 5/6, 1991, pp. 653–658.

15.39 L. S. D. Morley, *Skew Plates and Structures*, Macmillan, New York, 1963.

CHAPTER 16

16.1 G. Wempner, "Mechanics and Finite Elements of Shells," *ASME Applied Mechanics Reviews*, Vol. 42, No. 5, 1989, pp. 129–142 [cites 148 refs.].

16.2 R. H. MacNeal, "The Evolution of Lower Order Plate and Shell Elements in MSC/NASTRAN," *Finite Elements in Analysis and Design*, Vol. 5, No. 3, 1989, pp. 197–222.

16.3 A. K. Noor, "Bibliography of Monographs and Surveys on Shells," *ASME Applied Mechanics Reviews*, Vol. 43, No. 9, 1990, pp. 223–234 [cites 538 refs.].

16.4 W. Gilewski and M. Radwanska, "A Survey of Finite Element Models for the Analysis of Moderately Thick Shells," *Finite Elements in Analysis and Design*, Vol. 9, No. 1, 1991, pp.1–21 [cites 329 refs.].

16.5 M. L. Bucalem and K. J. Bathe, "Finite Element Analysis of Shell Structures," *Archives of Computational Methods in Engineering*, Vol. 4, No. 1, 1997, pp. 3–61.

16.6 H. T. Y. Yang, S. Saigal, A. Masud, and R. K. Kapania, "A Survey of Recent Shell Finite Elements," *International Journal for Numerical Methods in Engineering*, Vol. 47, Nos. 1–3, 2000, pp. 101–127 [cites 379 refs.].

16.7 T. Moan, "A Note on the Convergence of Finite Element Approximations for Problems Formulated in Curvilinear Coordinate Systems," *Computer Methods in Applied Mechanics and Engineering*, Vol. 3, No. 2, 1974, pp. 209–235.

16.8 F. Kikuchi, "On the Validity of the Finite Element Analysis of Circular Arches Represented by an Assemblage of Beam Elements," *Computer Methods in Applied Mechanics and Engineering*, Vol. 5, No. 3, 1975, pp. 253–276.

16.9 F. Kikuchi and K. Tanizawa, "Accuracy and Locking-Free Property of the Beam Element Approximation for Arch Problems," *Computers & Structures*, Vol. 19, Nos. 1–2, 1984, pp. 103–110.

16.10 K. Marguerre, " Zur Theorie der Gekrümmten Platte Grosser Formänderung," in *Proceedings of the 5th International Congress for Applied Mechanics*, J. P. Den Hartog and H. Peters, eds., John Wiley & Sons, New York, 1939, pp. 93–101.

16.11 R. D. Cook, "Simulating Curved Elements by Offsets: Rationale and Application to Shells of Revolution," *Engineering Computations*, Vol. 7, No. 1, 1990, pp. 79–80.

16.12 H. Stolarski, T. Belytschko, N. Carpenter, and J. M. Kennedy, "A Simple Triangular Curved Shell Element," *Engineering Computations*, Vol. 1, No. 3, 1984, pp. 210–218.

16.13 T. Belytschko, H. Stolarski, W. K. Liu, N. Carpenter, and S.-J. Ong, "Stress Projection for Membrane and Shear Locking in Shell Finite Elements," *Computer Methods in Applied Mechanics and Engineering*, Vol. 51, Nos. 1–3, 1985, pp. 221–258.

16.14 N. Carpenter, H. Stolarski, and T. Belytschko, "Improvements in Three-Node Triangular Shell Elements," *International Journal for Numerical Methods in Engineering*, Vol. 23, No. 9, 1986, pp. 1643–1667.

16.15 R. D. Cook, "Further Development of a Three-Node Triangular Shell Element," *International Journal for Numerical Methods in Engineering*, Vol. 36, No. 8, 1993, pp. 1413–1425.

16.16 G. Prathap, "The Curved Beam/Deep Arch/Finite Ring Element Revisited," *International Journal for Numerical Methods in Engineering*, Vol. 21, No. 3, 1985, pp. 389–407.

16.17 H. Meck, "An Accurate Polynomial Displacement Function for Finite Ring Elements," *Computers & Structures*, Vol. 11, No. 4, 1980, pp. 265–269.

16.18 W. E. Haisler and J. L. Stricklin, "Rigid-Body Displacements of Curved Elements in the Analysis of Shells by the Matrix-Displacement Method," *AIAA Journal*, Vol. 5, No. 8, 1967, pp. 1525–1527.

16.19 P. M. Mebane and J. L. Stricklin, "Implicit Rigid-Body Motion in Curved Finite Elements," *AIAA Journal*, Vol. 9, No. 2, 1971, pp. 344–345.

16.20 G. Prathap and C. R. Babu, "An Isoparametric Quadratic Thick Curved Beam Element," *International Journal for Numerical Methods in Engineering*, Vol. 23, No. 9, 1986, pp. 1583–1600.

16.21 S. F. Pawsey and R. W. Clough, "Improved Numerical Integration of Thick Shell Finite Elements," *International Journal for Numerical Methods in Engineering*, Vol. 3, No. 4, 1971, pp. 575–586.

16.22 P.-G. Lee and H.-C. Sin, "Locking-Free Curved Beam Element Based on Curvature," *International Journal for Numerical Methods in Engineering*, Vol. 37, No. 6, 1994, pp. 989–1007.

16.23 J. G. Kim and Y. Y. Kim, "A New Higher-Order Hybrid-Mixed Curved Beam Element," *International Journal for Numerical Methods in Engineering*, Vol. 43, No. 5, 1998, pp. 925–940.

16.24 P. Raveendranath, G. Singh, and B. Pradhan, "A Two-Noded Locking-Free Shear Flexible Curved Beam Element," *International Journal for Numerical Methods in Engineering*, Vol. 44, No. 2, 1999, pp. 265–280.

16.25 D. Bushnell, "Stress, Buckling and Vibration of Hybrid Bodies of Revolution," *Computers & Structures*, Vol. 7, No. 4, 1977, pp. 517–537.

16.26 J. A. Stricklin, W. E. Haisler, and W. A. Von Riesemann, "Large-Deflection Elastic-Plastic Dynamic Response of Stiffened Shells of Revolution," *ASME Journal of Pressure Vessel Technology*, Vol. 96, No. 2, 1974, pp. 87–95.

16.27 V. Paramasivam and D. Muthiah Raj, "Shear-Deformable Axisymmetric Conical Shell Element with 6-DOF and Convergence of $O(h^4)$," *Computer Methods in Applied Mechanics and Engineering*, Vol. 113, Nos. 1–2, 1994, pp. 47–54.

16.28 A. Tessler, "An Efficient, Conforming Axisymmetric Shell Element Including Transverse Shear and Rotary Inertia," *Computers & Structures*, Vol. 15, No. 5, 1982, pp. 567–574.

16.29 N. Carpenter, H. Stolarski, and T. Belytschko, "A Flat Triangular Shell Element with Improved Membrane Interpolation," *Communications in Applied Numerical Methods*, Vol. 1, No. 4, 1985, pp. 161–168.

16.30 E. Providas and M. A. Kattis, "An Assessment of Two Fundamental Flat Triangular Shell Elements with Drilling Rotations," *Computers & Structures*, Vol. 77, No. 2, 2000, pp. 129–139.

16.31 R. H. MacNeal, C. T. Wilson, R. H. Harder, and C. C. Hoff, "Treatment of Shell Normals in Finite Element Analysis," *Finite Elements in Analysis and Design*, Vol. 30, No. 3, 1998, pp. 235–242.

16.32 R. H. MacNeal, "Derivation of Element Stiffness Matrices by Assumed Strain Distributions," *Nuclear Engineering and Design*, Vol. 70, No. 1, 1982, pp. 3–12.

16.33 T. Belytschko, B. L. Wong, and H.-Y. Chiang, "Advances in One-Point Quadrature Shell Elements," *Computer Methods in Applied Mechanics and Engineering*, Vol. 96, No. 1, 1992, pp. 93–107.

16.34 Y. G. Zhu and T. Zacharia, "A New One-Point Quadrature, Quadrilateral Shell Element with Drilling Degrees of Freedom," *Computer Methods in Applied Mechanics and Engineering*, Vol. 136, Nos. 1–2, 1996, pp. 165–203.

16.35 B. P. Naganarayana and G. Prathap, "Force and Moment Corrections for the Warped Four-Node Quadrilateral Plane Shell Element," *Computers & Structures*, Vol. 33, No. 4, 1989 pp. 1107–1115.

16.36 R. V. Milford and W. C. Schnobrich, "Degenerated Isoparametric Finite Elements Using Explicit Integration," *International Journal for Numerical Methods in Engineering*, Vol. 23, No. 1, 1986, pp. 133–154.

16.37 M. A. Crisfield, "Explicit Integration and the Isoparametric Arch and Shell Elements," *Communications in Applied Numerical Methods*, Vol. 2, No. 2, 1986, pp. 181–187.

16.38 S. M. Yunus, P. Kohnke, and S. Saigal, "An Efficient Through-Thickness Integration Scheme in an Unlimited Layer Doubly Curved Isoparametric Composite Shell Element," *International Journal for Numerical Methods in Engineering*, Vol. 28, No. 12, 1989, pp. 2777–2793.

16.39 T. Belytschko and B. L. Wong, "Assumed Strain Stabilization Procedure for the 9-Node Lagrange Shell Element," *International Journal for Numerical Methods in Engineering*, Vol. 28, No. 2, 1989, pp. 385–414.
16.40 T. Belytschko, W. -K. Liu, J. S. –J. Ong, and D. Lam, "Implementation and Application of a 9-Node Lagrange Shell Element with Spurious Mode Control," *Computers & Structures*, Vol. 20, Nos. 1–3, 1985, pp. 121–128.
16.41 H. Stolarski and T. Belytschko, "Shear and Membrane Locking in Curved C^0 Elements," *Computer Methods in Applied Mechanics and Engineering*, Vol. 41, No. 3, 1983, pp. 279–296.
16.42 K. C. Park and G. M. Stanley, "A Curved C^0 Shell Element Based on Assumed Natural-Coordinate Strains," *ASME Journal of Applied Mechanics*, Vol. 53, No. 2, 1986, pp. 278–290.
16.43 R. H. MacNeal and R. L. Harder, "Eight Nodes or Nine?," *International Journal for Numerical Methods in Engineering*, Vol. 33, No. 5, 1992, pp. 1049–1058.
16.44 N. F. Knight, Jr., "Raasch Challenge for Shell Elements," *AIAA Journal*, Vol. 35, No. 2, 1997, pp. 375–381.
16.45 W. J. Koves and S. Nair, "A Finite Element for the Analysis of Shell Intersections," *ASME Journal of Pressure Vessel Technology*, Vol. 118, No. 4, 1996, pp. 399–406.
16.46 A. M. Yan, R. J. Jospin, and D. H. Nguyen, "An Enhanced Pipe Elbow Element—Application in Plastic Limit Analysis of Pipe Structures," *International Journal for Numerical Methods in Engineering*, Vol. 46, No. 3, 1999, pp. 409–431.
16.47 W. R. Spillers, M. Schlogel, and D. Pilla, "A Simple Membrane Finite Element," *Computers & Structures*, Vol. 45, No. 1, 1992, pp. 181–183.
16.48 F. Muttin, "A Finite Element for Wrinkled Curved Elastic Membranes, and Its Application to Sails," *Communications in Numerical Methods in Engineering*, Vol. 12, No. 11, 1996, pp. 775–785.
16.49 Y. F. Zhao, T. N. Wong, S. T. Tan, and W. J. Chen, "A Model for Simulating Flexible Surfaces of Cloth Objects," *Computers & Structures*, Vol. 63, No. 1, 1997, pp. 133–147.
16.50 S. Kang and S. Im, "Finite Element Analysis of Wrinkling Membranes," *ASME Journal of Applied Mechanics*, Vol. 64, No. 2, 1997, pp. 263–269.

CHAPTER 17

17.1 E. Hinton, ed., *NAFEMS Introduction to Nonlinear Analysis*, NAFEMS, Glasgow, UK, 1992.
17.2 M. A. Crisfield, *Non-linear Finite Element Analysis of Solids and Structures, Vol. 1: Essentials*, John Wiley & Sons, Chichester, UK, 1991.
17.3 M. A. Crisfield, *Non-linear Finite Element Analysis of Solids and Structures, Vol. 2: Advanced Topics*, John Wiley & Sons, Chichester, UK, 1997.
17.4 E. Riks, "Progress in Collapse Analyses," *ASME Journal of Pressure Vessel Technology*, Vol. 109, No. 1, 1987, pp. 33–41.
17.5 H.-B. Hellweg and M. A. Crisfield, "A New Arc-Length Method for Handling Sharp Snap-Backs," *Computers & Structures*, Vol. 66, No. 5, 1998, pp. 705–709.
17.6 P. X. Bellini and A. Chulya, "An Improved Automatic Incremental Algorithm for the Efficient Solution of Nonlinear Finite Element Equations," *Computers & Structures*, Vol. 26, Nos. 1/2, 1987, pp. 99–110.
17.7 C.-C. Chang, "Periodically Restarted Quasi-Newton Updates in Constant Arc-Length Method," *Computers & Structures*, Vol. 41, No. 5, 1991, pp. 963–972.
17.8 C.-C. Chang, "Consistent-Stiffness Iteration Method for Elastic-Plastic Analysis," *Computers & Structures*, Vol. 43, No. 2, 1992, pp. 255–263.
17.9 P. Underwood, "Dynamic Relaxation," in *Computational Methods for Transient Analysis*, T. Belytschko and T. J. R. Hughes, eds., North-Holland, Amsterdam, 1983, pp. 245–265.

17.10 O. C. Zienkiewicz and R. Löhner, "Accelerated 'Relaxation' or Direct Solution? Future Prospects for FEM," *International Journal for Numerical Methods in Engineering*, Vol. 21, No. 1, 1985, pp. 1–11.
17.11 L. C. Zhang, M. Kadkhodayan, and Y.-W. Mai, "Development of the maDR Method," *Computers & Structures*, Vol. 52, No. 1, 1994, pp. 1–8.
17.12 L. M. Kutt, A. B. Pifko, J. A. Nardiello, and J. M. Papazian, "Slow-Dynamic Finite Element Simulation of Manufacturing Processes," *Computers & Structures*, Vol. 66, No. 1, 1998, pp. 1–17.
17.13 M. M. Abdel-Gaffar, D. W. White, and W.-F. Chen, "An Error Estimate and Step Size Control Method for Nonlinear Solution Techniques," *Finite Elements in Analysis and Design*, Vol. 13, Nos. 2–3, 1993, pp. 137–148.
17.14 A. J. Abbo and S. W. Sloan, "An Automatic Load Stepping Algorithm with Error Control," *International Journal for Numerical Methods in Engineering*, Vol. 39, No. 10, 1996, pp. 1737–1759.
17.15 A. Mendelson, *Plasticity: Theory and Application*, Macmillan Co., New York, 1968.
17.16 W. F. Chen and D. J. Han, *Plasticity for Structural Engineers*, Springer-Verlag, New York, 1988.
17.17 S. W. Sloan, "Substepping Schemes for the Numerical Integration of Elastoplastic Stress-Strain Relations," *International Journal for Numerical Methods in Engineering*, Vol. 24, No. 5, 1987, pp. 893–911.
17.18 N.-S. Lee and K.-J. Bathe, "Error Indicators and Adaptive Remeshing in Large Deformation Finite Element Analysis," *Finite Elements in Analysis and Design*, Vol. 16, No. 2, 1994, pp. 99–139.
17.19 L.-Y. Li and P. Bettess, "Error Estimates and Adaptive Remeshing Techniques in Elasto-Plasticity," *Communications in Numerical Methods in Engineering*, Vol. 13, No. 4, 1997, pp. 285–299.
17.20 J. D. Hoffman, *Numerical Methods for Engineers and Scientists*, McGraw-Hill, New York, 1992.
17.21 J. M. C. Marques, "Stress Computation in Elastoplasticity," *Engineering Computations*, Vol. 1, No. 1, 1984, pp. 42–51.
17.22 C. Nyssen, "An Efficient and Accurate Iterative Method, Allowing Large Incremental Steps, to Solve Elasto-Plastic Problems," *Computers & Structures*, Vol. 13, Nos. 1–3, 1981, pp. 63–71.
17.23 M. E. Plesha, "Eigenvalue Estimation for Dynamic Contact Problems," *ASCE Journal of Engineering Mechanics*, Vol. 113, No. 3, 1987, pp. 457–462.
17.24 T. Belytschko and D. F. Schoeberle, "On the Unconditional Stability of an Implicit Algorithm for Nonlinear Structural Dynamics," *ASME Journal of Applied Mechanics*, Vol. 42, No. 4, 1975, pp. 865–869.
17.25 D. Kuhl and M. A. Crisfield, "Energy-Conserving and Decaying Algorithms in Non-Linear Structural Dynamics," *International Journal for Numerical Methods in Engineering*, Vol. 45, No. 5, 1999, pp. 569–599.
17.26 Z.-Z. Zhong and J. Mackerle, "Static Contact Problems—A Review," *Engineering Computations*, Vol. 9, No. 1, 1992, pp. 3–37 [cites 629 refs.].
17.27 D. Peric and D. R. J. Owen, "Computational Model for 3-D Contact Problems with Friction Based on the Penalty Method," *International Journal for Numerical Methods in Engineering*, Vol. 35, No. 6, 1992, pp. 1289–1309.
17.28 M. Oldenburg and L. Nilsson, "The Position Code Algorithm for Contact Searching," *International Journal for Numerical Methods in Engineering*, Vol. 37, No. 3, 1994, pp. 359–386.
17.29 V. Chawla and T. A. Laursen, "Energy Consistent Algorithms for Frictional Contact Problems," *International Journal for Numerical Methods in Engineering*, Vol. 42, No. 5, 1998, pp. 799–827.
17.30 D. W. Murray and E. L. Wilson, "Finite-Element Large Deflection Analysis of Plates," *ASCE Journal of the Engineering Mechanics Division*, Vol. 95, No. EM1, 1969, pp. 143–165.

17.31 T. Belytschko and B. J. Hsieh, "Non-Linear Transient Finite Element Analysis with Convected Coordinates," *International Journal for Numerical Methods in Engineering*, Vol. 7, No. 3, 1973, pp. 255–271.
17.32 K.-M. Hsiao, H.-J. Horng, and Y.-R. Chen, "A Corotational Procedure that Handles Large Rotations of Spatial Beam Structures," *Computers & Structures*, Vol. 27, No. 6, 1987, pp. 769–781.
17.33 S. P. Timoshenko and J. M. Gere, *Theory of Elastic Stability*, 2nd ed., McGraw-Hill, New York, 1961.
17.34 K. E. Bisshopp and D. C. Drucker, "Large Deflection of Cantilever Beam," *Quarterly of Applied Mathematics*, Vol. 3, No. 3, 1945, pp. 272–275.
17.35 K. Schweizerhof and E. Ramm, "Displacement Dependent Pressure Loads in Nonlinear Finite Element Analysis," *Computers & Structures*, Vol. 18, No. 6, 1984, pp. 1099–1114.
17.36 A. H. Peyrot and A. M. Goulois, "Analysis of Cable Structures," *Computers & Structures*, Vol. 10, No. 5, 1979, pp. 805–813.
17.37 H. B. Jayaraman and W. C. Knudson, "A Curved Element for the Analysis of Cable Structures," *Computers & Structures*, Vol. 14, Nos. 3–4, 1981, pp. 325–333.
17.38 B. M. McDonald and A. H. Peyrot, "Analysis of Cables Suspended in Sheaves," *ASCE Journal of Structural Engineering*, Vol. 114, No. 3, 1988, pp. 693–706.
17.39 U. Starossek, "Dynamic Stiffness Matrix of Sagging Cable," *ASCE Journal of Engineering Mechanics*, Vol. 117, No. 12, 1991, pp. 2815–2829.
17.40 A. H. Peyrot, "Large Deflection Analysis of Beams, Pipes, or Poles," *Engineering Structures*, Vol. 4, No. 1, 1982, pp. 11–16.
17.41 P. Seide, "Large Deflections of Rectangular Membranes under Uniform Pressure," *International Journal of Non-Linear Mechanics*, Vol. 12, No. 6, 1977, pp. 397–406.

CHAPTER 18

18.1 R. S. Barsoum and R. H. Gallagher, "Finite Element Analysis of Torsional and Torsional-Flexural Stability Problems," *International Journal for Numerical Methods in Engineering*, Vol. 2, No. 3, 1970, pp. 335–352.
18.2 M. M. Attard, "Lateral Buckling Analysis of Beams by the FEM," *Computers & Structures*, Vol. 23, No. 2, 1986, pp. 217–231.
18.3 F. Laudiero and D. Zaccaria, "Finite Element Analysis of Stability of Thin-Walled Beam of Open Section," *Computers & Structures*, Vol. 30, No. 8, 1988, pp. 543–557.
18.4 C. H. Yoo, Y. J. Kang, and J. S. Davidson, "Buckling Analysis of Curved Beams by Finite-Element Discretization," *ASCE Journal of Engineering Mechanics*, Vol. 122, No. 8, 1996, pp. 762–770.
18.5 H. K. Stolarski and N. J. Carpenter, "An Alternative Formulation of the Geometric Stiffness Matrix for Plate Elements," *Computers & Structures*, Vol. 24, No. 6, 1986, pp. 935–940.
18.6 S. J. Shah and W. D. Pilkey, "Lumped-Parameter Approach to Stability Analysis," *ASCE Journal of Engineering Mechanics*, Vol. 119, No. 10, 1993, pp. 2109–2129.
18.7 S.-C. Chang and J.-J. Chen, "Effectiveness of Linear Bifurcation Analysis for Predicting the Nonlinear Stability Limits of Structures," *International Journal for Numerical Methods in Engineering*, Vol. 23, No. 5, 1986, pp. 831–846.
18.8 R. D. Cook, "Finite Element Buckling Analysis of Homogeneous and Sandwich Plates," *International Journal for Numerical Methods in Engineering*, Vol. 9, No. 1, 1975, pp. 39–50.
18.9 S. R. Bodner, "On the Conservativeness of Various Distributed Force Systems," *Journal of the Aeronautical Sciences*, Vol. 25, No. 1, 1958, pp. 132–133.
18.10 D. O. Brush and B. O. Almroth, *Buckling of Bars, Plates, and Shells*, McGraw-Hill, New York, 1975.

18.11 R. F. Jones, Jr., M. G. Costello, and T. E. Reynolds, "Buckling of Pressure Loaded Rings and Shells by the Finite Element Method," *Computers & Structures*, Vol. 7, No. 2, 1977, pp. 267–274.
18.12 H. A. Mang, "Symmetricability of Pressure Stiffness Matrices for Shells with Loaded Free Edges," *International Journal for Numerical Methods in Engineering*, Vol. 15, No. 7, 1980, pp. 981–990.
18.13 T. Q. Ye and R. H. Gallagher, "Instability Analysis of Pressure-Loaded Thin Arches of Arbitrary Shape," *ASME Journal of Applied Mechanics*, Vol. 50, No. 2, 1983, pp. 315–320.
18.14 D. Bushnell, "Analysis of Ring-Stiffened Shells of Revolution under Combined Thermal and Mechanical Loadings," *AIAA Journal*, Vol. 9, No. 3, 1971, pp. 401–410.
18.15 D. R. Navaratna, T. H. H. Pian, and E. Witmer, "Analysis of Elastic Stability of Shells of Revolution by the Finite Element Method," *AIAA Journal*, Vol. 6, No. 2, 1968, pp. 355–361.
18.16 B. O. Almroth and F. A. Brogan, "Bifurcation Buckling as an Approximation of the Collapse Load for General Shells," *AIAA Journal*, Vol. 10, No. 4, 1972, pp. 463–467.
18.17 D. Bushnell, "Buckling of Shells—Pitfall for Designers," *AIAA Journal*, Vol. 19, No. 9, 1981, pp. 1183–1226.
18.18 D. Bushnell, *Computerized Buckling Analysis of Shells*, Marinus Nijhoff, Dordrecht, 1985.
18.19 W. C. Orthwein, "Thermal Buckling of a Bimetallic Strip," *ASME Journal of Vibrations, Acoustics, Stress, and Reliability in Design*, Vol. 106, No. 4, 1984, pp. 538–542.
18.20 J. G. Gale and C. E. Smith, "Vibrations of Suspended Cables," *ASME Journal of Applied Mechanics*, Vol. 50, No. 3, 1983, pp. 687–689.

APPENDIX A

A.1 G. Strang, *Linear Algebra and Its Applications*, 3rd ed., Harcourt-Brace-Jovanovich, San Diego, CA, 1988.

APPENDIX B

B.1 E. L. Poole, "Comparing Direct and Iterative Equation Solvers in a Large Structural Analysis Software System," *Computing Systems in Engineering*, Vol. 2, No. 4, 1991, pp. 397–408.
B.2 D. J. Rose, G. G. Whitten, A. H. Sherman, and R. E. Tarjan, "Algorithms and Software for In-Core Factorization of Sparse Symmetric Positive Definite Matrices," *Computers & Structures*, Vol. 11, No. 6, 1980, pp. 597–608.
B.3 J. K. Reid and J. A. Scott, "Ordering Symmetric Sparse Matrices for Small Profile and Wavefront," *International Journal for Numerical Methods in Engineering*, Vol. 45, No. 12, 1999, pp. 1737–1755.
B.4 J. A. Scott, "On Ordering Elements for a Frontal Solver," *Communications in Numerical Methods in Engineering*, Vol. 15, No. 5, 1999, pp. 309–323.
B.5 D. P. Mondkar and G. H. Powell, "Towards Optimal In-Core Equation Solving," *Computers & Structures*, Vol. 4, No. 3, 1974, pp. 531–548.
B.6 C. A. Felippa, "Solution of Linear Equations with Skyline-Stored Symmetric Matrix," *Computers & Structures*, Vol. 5, No. 1, 1975, pp. 13–29.
B.7 E. L. Wilson and H. H. Dovey, "Solution or Reduction of Equilibrium Equations for Large Complex Structural Systems," *Advances in Engineering Software*, Vol. 1, No. 1, 1978, pp. 19–25.
B.8 E. Mendelssohn and M. Baruch, "Solution of Linear Equations with a Skyline-Stored Nonsymmetric Matrix," *Computers & Structures*, Vol. 18, No. 2, 1984, pp. 215–246.

B.9 S. H. Lo, "On Bandsolver Using Skyline Storage," *Computers & Structures*, Vol. 44, No. 6, 1992, pp. 1187–1196.

B.10 M. Klisinski and K. Runesson, "Improved Symmetric and Non-Symmetric Solvers for FE Calculations," *Advances in Engineering Software*, Vol. 18, No. 1, 1993, pp. 41–51.

B.11 S. S. Rao, *Engineering Optimization: Theory and Practice*, 3rd ed., John Wiley & Sons, New York, 1996.

B.12 M. R. Hestenes and E. Stiefel, "Methods of Conjugate Gradients for Solving Linear Systems," *Journal of Research of the National Bureau of Standards*, Vol. 49, No. 6, 1952, pp. 409–436.

B.13 E. Graham and P. A. Forsyth, "Preconditioning Methods for Very Ill-Conditioned Three-Dimensional Linear Elasticity Problems," *International Journal for Numerical Methods in Engineering*, Vol. 44, No. 1, 1999, pp. 77–99.

B.14 P. Saint-George, G. Warzee, Y. Notay, and R. Beauwens, "Problem-Dependent Preconditioners for Iterative Solvers in FE Elastostatics," *Computers & Structures*, Vol. 73, Nos. 1–5, 1999, pp. 33–43.

B.15 J. K. Dickenson and P. A. Forsyth, "Preconditioned Conjugate Gradient Methods for Three-Dimensional Linear Elasticity," *International Journal for Numerical Methods in Engineering*, Vol. 37, No. 13, 1994, pp. 2211–2234.

B.16 G. H. Golub and C. F. Van Loan, *Matrix Computations*, 3rd ed., Johns Hopkins University Press, Baltimore, MD, 1996.

B.17 C. E. Jouglard and A. L. G. A. Coutinho, "A Comparison of Iterative Multi-Level Finite Element Solvers," *Computers & Structures*, Vol. 69, No. 5, 1998, pp. 655–670.

B.18 A. Jennings and G. M. Malik, "The Solution of Sparse Linear Equations by the Conjugate Gradient Method," *International Journal for Numerical Methods in Engineering*, Vol. 12, No. 1, 1978, pp. 141–158.

B.19 K. J. Bathe, J. Walczak, and H. Zhang, "Some Recent Advances for Practical Finite Element Analysis," *Computers & Structures*, Vol. 47, Nos. 4/5, 1993, pp. 511–521.

B.20 I. D. Parsons and J. F. Hall, "The Multigrid Method in Solid Mechanics: Part I—Algorithm Description and Behavior," *International Journal for Numerical Methods in Engineering*, Vol. 29, No. 4, 1990, pp. 719–737.

B.21 D. Braess, *Finite Elements: Theory, Fast Solvers, and Applications in Structural Mechanics*, Cambridge University Press, Cambridge, 1997.

APPENDIX C

C.1 J. H. Wilkinson, *The Algebraic Eigenvalue Problem*, Clarendon Press, Oxford, UK, 1965.

C.2 B. N. Parlett, *The Symmetric Eigenvalue Problem*, Prentice-Hall, Englewood Cliffs, NJ, 1980.

C.3 N. S. Sehmi, *Large Order Structural Eigenanalysis Techniques*, Ellis Horwood Ltd., Chichester, UK, 1989.

C.4 Y. K. Cheung and A. Y. T. Leung, *Finite Element Methods in Dynamics*, Kluwer Academic Publishers, Dordrecht, 1991.

C.5 K.-J. Bathe and E. L. Wilson, "Solution Methods for Eigenvalue Problems in Structural Mechanics," *International Journal for Numerical Methods in Engineering*, Vol. 6, No. 2, 1973, pp. 213–226.

C.6 A. Jennings, "Eigenvalue Methods for Vibration Analysis," *Shock and Vibration Digest*, Vol. 16, No. 1, 1984, pp. 25–33.

C.7 V. A. Tischler and V. B. Venkayya, "Evaluation of Eigenvalue Routines for Large Scale Applications," *Shock and Vibration*, Vol. 1, No. 3, 1994, pp. 201–216.

C.8 D. S. Malkus and X. Qui, "Divisor Structure of Finite Element Eigenproblems Arising from Zero and Negative Masses," *Computer Methods in Applied Mechanics and Engineering*, Vol. 66, No. 3, 1988, pp. 365–368.

C.9 X. Wang and J. Zhou, "An Accelerated Subspace Iteration Method for Generalized Eigenproblems," *Computers & Structures*, Vol. 71, No. 3, 1999, pp. 293–301.

C.10 I. U. Ojalvo, "Proper Use of Lanczos Vectors for Large Eigenvalue Problems," *Computers & Structures*, Vol. 20, Nos. 1–3, 1985, pp. 115–120.

C.11 D. T. Nguyen and J. S. Arora, "An Algorithm for Solution of Large Eigenvalue Problems," *Computers & Structures*, Vol. 24, No. 4, 1986, pp. 645–650.

C.12 I.-W. Lee, M.-C. Kim, and A. R. Robinson, "Efficient Solution Method of Eigenproblems for Damped Structural Systems Using Modified Newton-Raphson Technique," *ASCE Journal of Engineering Mechanics*, Vol. 124, No. 5, 1998, pp. 576–580.

C.13 M.-C. Kim and I.-W. Lee, "A Computationally Efficient Algorithm for the Solution of Eigenproblems for Large Structures with Non-Proportional Damping Using Lanczos Method," *Earthquake Engineering and Structural Dynamics*, Vol. 28, No. 2, 1999, pp. 157–172.

C.14 K. K. Gupta and C. L. Lawson, "Development and Application of a Progressive Simultaneous Iteration (PSI) Method for Vibration Analysis of Structures," *39th AIAA/ASME/ASCE/AHS/ASC Structures, Structural Dynamics and Materials Conference and Exhibit and AIAA/ASME/AHS Adaptive Structures Forum*, Long Beach, CA, 1998, pp. 2609–2613.

C.15 I.-W. Lee, H.-J. Jung, M.-C. Kim, and A. R. Robinson, "Eigensolution Method for Structures with Multiple or Close Eigenvalues," *ASCE Journal of Engineering Mechanics*, Vol. 125, No. 11, 1999, pp. 1286–1292.

C.16 W. Weaver, Jr. and D. M. Yoshida, "The Eigenvalue Problem for Banded Matrices," *Computers & Structures*, Vol. 1, No. 4, 1971, pp. 651–654.

C.17 K. K. Gupta, "Eigenproblem Solution by a Combined Sturm Sequence and Inverse Iteration Technique," *International Journal for Numerical Methods in Engineering*, Vol. 7, No. 1, 1973, pp. 17–42 (discussion: Vol. 11, No. 4, 1977, pp. 759–764).

C.18 K. K. Gupta, "Eigenproblem Solution of Damped Structural Systems," *International Journal for Numerical Methods in Engineering*, Vol. 8, No. 4, 1974, pp. 877–911.

C.19 P. C. Chowdhury, "The Truncated Lanczos Algorithm for Partial Solution of the Symmetric Eigenproblem," *Computers & Structures*, Vol. 6, No. 6, 1976, pp. 439–446.

C.20 R. B. Corr and A. Jennings, "A Simultaneous Iteration Algorithm for Symmetric Eigenvalue Problems," *International Journal for Numerical Methods in Engineering*, Vol. 10, No. 3, 1976, pp. 647–663.

INDEX

Accuracy, *see* Bounds; Convergence; Error
Acoustics, 474–477
Active column storage, 43
Adaptive meshing, 329–331
Added mass, 383, 431, 479
Admissible displacement or field, 88, 138
Analogies, problem areas, 469
Anisotropy of element behavior, 105
Arches, theory and elements, 563–570
Arc-length method, 599
Area coordinates, 264–265
Assembly of elements
  congruent transformation, 160–161
  direct stiffness method, 23, 32–36
  matching of d.o.f., 28
Attachment d.o.f. and modes, 359, 400
Average acceleration algorithm, 417–418, 420–426
Axial symmetry
  strain-displacement relations, 510, 512
  stress-strain relation, 509
  see also Shells; Solids of revolution

Bandwidth, of matrix, 44
Bar element
  heat conduction, 21–22
  mass matrices, 377–378
  stress stiffness matrix, 643
  three nodes, 203–205
  two nodes, 20–21, 29–31, 47–48, 89–90, 186–188
Basis, reduced, 390–391
Basis function, 84
Beam, curved, 244–247, 338–339, 341
Beam element
  beam-column, 640–641
  connection to solid, 279, 349
  Euler-Bernoulli beam, defined, 24
  limitations of, 28–29, 338
  mass matrices, 378–379
  Mindlin element, 495–496, 547–550
  standard element, 24–29, 32, 49–52, 90–91, 145, 170–171
  stress stiffness matrix, 643
  Timoshenko beam, defined, 24
Bilinear element, 96–100, 205–209
Bimoment, 29
Biquadratic element, 101–102, 213–215
Blast loading, 408
Body force, *see* Loads
Boundary conditions
  computational procedures, 40–42, 276–277, 305, 354
  essential (principal), 137, 151–152, 155
  in heat transfer, 457–463
  inadequate support, 38–39, 364, 523–524
  in modeling, 352–354
  nonessential (natural), 137, 151–152, 155
  for plate bending, 551–552
  for solids of revolution, 512, 523–524
  on stress, 82, 119
  for symmetry, various types, 54–57, 354–356
Boundary elements, 290–291
Bounds
  on bifurcation buckling load, 650
  Gerschgorin, 413
  with hybrid elements, 168
  with incompatible elements, 110, 221
  by modeling choices, 352, 436
  on Rayleigh quotient, 678
  on Rayleigh-Ritz solutions, 150–151
  with reduced integration, 223
  on vibration frequencies, 382–383
Box beams, 520
Brick element, 102–104, 217–219
Bubble function, 215
Buckling
  bifurcation, 641–642, 648, 653–655
  bounds, on bifurcation load, 650
  collapse, 627, 642, 654, 655
  imperfection sensitivity, 654
  limit point, 599, 642, 653–654
  nature of, 639, 642
  nonlinearities, 650, 653–656
  pressure load, 651
  snap-through, 599, 642, 655
  symmetry, use of, 57
  thin-walled structures, 651, 654
  see also Stress stiffening
Bulk modulus, 496

Cables and chains, 626, 651
Central difference methods, 409–416, 421–426
Centrifugal softening, 652–653
CFL condition, 413
Characteristic matrix, 19
Checkerboarding, 503
Checking for mistakes, 13–15, 236–237, 363–369
Choleski method, 670–671
Circulation modes, 480
C^m continuity, defined, 84
Collapse load, 642, 654
Collocation residual method, 183
Compatibility
  in elasticity, 81
  extent satisfied in FEA, 118–119
  interelement, 105
  see also Incompatible elements
Completeness
  convergence and, 149–150, 313
  of polynomial field, 105–106, 313
Component mode synthesis, 400–405
Condensation (reduction of order)
  in buckling problems, 649–650
  in dynamic problems, 390–394, 396, 399, 400–405
  in modal methods, 396
  by Ritz vectors, 399
  in static problems, 221–222, 352, 359, 490
Condition number, 44, 306–308
  see also Ill-conditioning
Conduction, *see* Heat conduction and transfer
Congruence transformation, 160–161, 677
Conjugate gradient solution, 672–674
Connections
  of dissimilar elements, 279–282, 349, 358
  interelement, 117–118, 342
  partial, at nodes, 39
  in structures, 348–352
Conservative system, defined, 137
Consistent penalty method, 503
Constant-strain triangle, 93–95, 102, 262–263
Constitutive matrix, *see* Stress-strain relations
Constraint modes, 400
Constraints
  consistent penalty method, 503
  counting of, 226, 500–502, 546–547, 568–569
  incompressibility, 94, 496–497, 502–504
  and Lagrange multipliers, 492–493, 620–621
  multipoint, 281, 489
  penalty, explicit, 493–495, 621
  penalty, implicit, 495–499
  and quadrature rule, 498–500
  ratios, 501–502
  shear, beams and plates, 495–496, 544–547
  single-point, 489
  transformation methods for, 276–282, 489–491
  see also Locking
Contact, sliding, 353
Contact problems, 340, 492, 595, 619–621
Continuity, degree of, 84
Convected coordinates, 622
Convergence
  equilibrium iterations for, 597–598
  extrapolation for, 315–318
  h-refinement, 318–320
  monotonic, 162–163, 315–316
  in nonlinear problems, 601–602, 626, 629
  p-refinement, 318–320
  rate of, dynamics, 388, 409, 411, 419–420
  rate of, statics, 164–165, 310–315, 325, 383
  of Rayleigh-Ritz method, 149–151
  requirements for, in FEA, 104, 161–163
  see also Bounds; Error
Coordinate transformation, *see* Transformation
Corotational formulation, 622–625
Coupled field problems
  defined, 3
  fluid-structure, 477–480
Courant number, 414
Cracks, fracture and, 283–286
Craig-Bampton method, 400–405
Critical load, defined, 639
CST element, 93–95, 102, 262–263
Curved beam, 244–247, 338–339, 341

D.o.f., *see* Degrees of freedom
Damping
  algorithmic, 389, 419–421, 423–426
  consistent matrix for, 376
  modal, 390, 395
  proportional, 389–390
  ratio, 384
  Rayleigh, 389–390
  types of, 388–389
Degenerate (degraded) elements, 264, 285, 563
Degrees of freedom
  defined, 8
  generalized, 7–8, 146, 157
  hierarchic, 305–306, 319
  higher derivatives as, 282–283
  nodeless, 109, 219
  relative, 109, 305–306, 319

Design of experiments, 363
Determinant, calculation of, 671
Developable surface, 535
Diagonal decay test, 308–309
Direct integration in dynamics
  accuracy of, 414–416, 419–420, 423–426, 434
  algorithmic damping and, 389, 419–421, 423–426
  average acceleration algorithm, 417–418, 420–426
  central difference methods, 409–416, 421–426
  cost of, relative, 408
  error, control of, 436, 619
  error, order of, 409, 411, 419–420
  explicit methods, 407–416, 616–618
  in heat transfer, 465–466
  implicit methods, 407–409, 416–421, 618–619
  initial conditions, 412, 415–416, 418, 419
  mass matrix for, 411, 413, 425–426, 434
  mixed time integration, 421
  Newmark methods, 416–421
  nonlinear problems, 616–619, 629
  operator splitting, 421
  overview, 407–409
  spurious modes and, 227, 383, 407, 412, 431
  stability of, 411, 419–420, 421–423, 466, 617
  trapezoidal rule, 418
Direct stiffness method, 23, 32–36, 161
Discrete Kirchhoff elements, 538–541
Discretization, 4
Distorted elements, 234–236, 238, 340–342, 366, 570, 577–578
Divergence theorem, 191–192
Drilling d.o.f., 106–108
Dynamic problems
  basic equations, 189, 374–376
  classified, 373–374, 455
  inverse problem (identification), 435
  see also Damping; Direct integration in dynamics; Eigenproblems; Harmonic response; Mass and mass matrices; Modal methods; Response history; Response spectra; Vibration
Dynamic relaxation, 601
Dynamic stiffness matrix, 385

Effective stress, 117, 232–233, 609
Eigenproblems
  buckling, 648–650
  hand calculation, 385–387
  orthogonality of modes, 395, 678
  Rayleigh quotient, 387–388, 432, 678–679
  theory and algorithms, 675–681
  vibration, 385
Eigenvalue test of elements, 293–294
Elastica, 626
Elastic support, 286–288, 353
Energy
  in buckling problems, 639–641
  complementary, 167
  conservation of, 139–140
  error measure, use in, 294, 326–328
  in nonlinear dynamics, 617, 619
  stationary principle, 137–140
  strain energy density, 142–143
  in terms of d.o.f., 160
  in vibration (Rayleigh quotient), 387
Equation solving, 42–46, 668–674
Equilibrium
  differential equations of, 81–82, 156
  extent satisfied in FEA, 88, 119, 194
  iteration to satisfy, 322, 597–598, 619, 625
  nodal, 33–34
  in patch stress recovery, 325
Error
  a posteriori error estimate, 326–328
  checking, in modeling, 363–364
  discretization, 4, 165–166, 301, 310–315
  extrapolation to reduce, 315–318
  indicator, eigenproblems, 328, 436, 650
  indicator, flux or stress, 14, 326, 328, 468
  indicator, modal methods, 396–397
  indicator, nonlinear dynamics, 619
  iterative reduction of, 310, 597–598, 619, 625
  modeling, 3–4, 300–301
  numerical, 4, 301–310
  order of, dynamics, 383, 388, 409, 411, 419–420
  order of, statics, 165–166, 310–315, 325
  of Rayleigh quotient, 388, 678
  singularities, 314–315
  sources, classified, 300–301
  tests for, 301–302, 306–310, 326–328, 436, 601–602, 619
  ZZ error estimate, 326–328
  see also Bounds; Convergence; Ill-conditioning; Locking
Euler equations, 152–153
Examples, application of FEA
  axisymmetric shell, 586–588

axisymmetric solid, 469–473, 512–516
beam element structure, 59–62
buckling, nonlinear, 655–656
elastic foundation, 553–556
harmonic response, 438–439
heat transfer, 469–472
plane, 119–124, 240–244
plate bending, 553–556
response history, 439–442
response spectra, 442–443
shrink fit, 512–516
solid, 3D, 244–247
spinning disk, 512–516
thermal stress, 121–124, 472–473
vibration, 436–438
wave propagation, 414–416, 617–618
Excitation, 374
Experiment
comparison with, 367, 435
numerical, 363
Extrapolation, multimesh, 315–318

Fills, in equation solving, 43, 44, 46, 671
Finite element method
advantages of, 1–2, 9–10
analysis procedure, 13, 15, 20
dangers of, 15–16, 331, 371, 436
defined, 5, 7
history of, 10–11
nature of, 5–8, 118–119, 150, 161
see also Modeling
Finite prism method, 521
Finite strip method, 520
Flexural rigidity, 533
Fluid flow, 480–482
Fluid-structure interaction, 477–480
Follower force, 348, 626, 651
Forced vibration, 373, 405–407, 438–439
Forcing function, 374
Foundation, elastic, 286–288, 353
Fourier series, 516–524
Fracture mechanics, 283–286
Frame invariance, 105, 227
Framework analogy, 10
Frequency response analysis, 405–407, 438–439
Frontal solution, 44, 671
Fully stressed design, 370
Functionals, various, 136, 143, 152–153, 197–198, 459

Galerkin method, 156, 179–197
Gaps and contact, 288, 340, 353, 595, 619–621
Gauss elimination, 45–46, 668–670
Gauss quadrature, 209–213
Generalized d.o.f., described, 7–8, 146
Geometric isotropy, 105, 227
Geometric nonlinearity, 340, 367–368, 535, 595, 621–626, 653–656
Geometry, element, 234–236, 238, 340–342, 366, 570, 577–578
Gerschgorin bound, 413
Global stiffness, defined, 22
Global-local model, 356–358
Green strain, 621–622
Guyan reduction, 390–394
Gyroscopic effects, 388

Harmonic function, 193
Harmonic response, 373, 405–407, 438–439
Heat conduction and transfer
bar element, 21–22, 190–191
boundary conditions, 457–463
error measure, 328
formulation, 153, 157–159, 456–462
modeling considerations, 467–468
nomenclature and units, 454–455
radiation, 462–463
transients, 464–466
Helmholtz equation, 475
Hilbert matrix, 302
Hinge, 39, 58, 279, 349, 351–352
History of FEA, 10–11
Hourglass mode, *see* Spurious modes
Hybrid formulation, 165–171, 233

Ill-conditioning
condition number, 306–308
in equation solving, 44–45, 302, 303, 672, 674
in least squares methods, 184
modeling situations, 281, 303–308, 494, 511
with slender ring elements, 511
Impact loading, 408
Imperfection sensitivity, 654
Incompatible elements, 7, 105, 109–111, 117–118, 219–221, 537
Incompressible materials, 94, 308, 496–497, 502–504
Inextensibility condition, 565
Infinite elements and media, 286–291
Initial stiffness method, 599
Initial stress and strain
bar elements, 52–54
calculation procedure, 52, 115
element load formula, 89

energy expression, 143
stress calculation, 53, 115
stress-strain relation, 78–79
Instability, *see* Buckling; Mechanisms; Spurious modes
Integration
analytical, triangles and tetrahedra, 264–266
by parts, 154, 156, 181, 191–192
see also Numerical integration
Interaction
fluid-structure, 477–480
in general, 3
Internal forces, 374, 412, 617
Interpolation
choice of functions, 104–106
defined, 83
Hermitian (C^1), 86–87
Lagrange's formula (C^0), 85–86
Intrinsic coordinates, 203, 205–206, 259, 264–265
Inverse iteration, 680
Isoparametric elements
bar example, 203–205
basics, plane, 205–209
basics, solid, 217–218
defined, 202
shells, 578–583
triangles and tetrahedra, 259–264
validity of, 237–240
see also Numerical integration
Iterative improvement, 310, 322, 329–331, 369–370, 597–598, 625

Jacobian, 204, 207, 218, 262, 582
Joints, *see* Connections

Kinematic mode, *see* Spurious modes
Kirchhoff plate elements, 536–541

Lagrange elements, 97, 101, 215, 219, 545–547, 583
Lagrange multipliers, 492–493
Lagrange's interpolation formula, 85–86
Lanczos method, 390, 674, 680
Lap joint, 351
Laplace's equation, 193
Large displacement and strain, 38, 57, 163–164, 535, 570, 621–623, 628
Least squares residual methods, 183
Least squares solution, 184, 185, 233, 324
Limit point, 599, 653–654
Loads
acceleration, 82
axisymmetric, 347, 512
body force, 81, 113–114
concentrated, 90, 112–114, 347
consistent, 47, 49, 51, 89, 111–115
in contact problems, 619–621
corrective (imbalance), 397–398, 597–601, 612, 615, 625
distributed, and pressure, 47–49, 344, 348, 626, 651
by element, to element, 21, 33
follower forces, 348, 626, 651
Fourier series for, 517–518
gravity, 46, 113–114
on incompatible elements, 111–112, 220, 221
inertia, 378
initial strain and stress, 52, 89, 145–146, 160
mesh layout, effect of, 344, 541
moment (couple), 114, 279, 347
moving, 435
multiple load cases, 45–46, 668, 674
on plates and shells, 536, 541
prestress, 350
reduced (lumped), 46, 49, 51–52
spinning, 512
symmetry and, 55–57, 355
thermal, 52–53, 79, 89–90, 145–146, 348
tractions (surface), 82, 112–114, 227–230
work-equivalent, 111–115
Locking
constraint counting and, 500–502, 546–547, 568–569
dilatational, 94, 497, 612
discussed, 93–95, 498–500
incompressibility and, 94, 497
membrane, 567–570, 582–583
penalty constraints, implicit, 495–500
quadrature rule and, 498–500
selective integration and, 227, 500–501, 543–549, 568–570
shear, 98, 99, 496, 543, 546, 548–549
volumetric, 94, 497, 612
LST element, 95–96, 102, 107, 263

Marguerre shell theory, 566
Mass and mass matrices
added mass, 287, 383, 431, 479
choice of, modeling, 382–383, 411, 413, 426, 430–431, 434, 436
condensation of, 390–394
consistent, 376, 378–379
HRZ lumping, 380–381
nonstructural, 287, 383, 431, 479

optimal lumping, 381–382
particle-lumped, 377–378
Master d.o.f., 359, 391
Material nonlinearity, *see* Plasticity
Material properties, *see* Stress-strain relations
Mathematical model, defined, 3
Matrices, definitions and manipulations, 663–667
Mechanisms, *see* Spurious modes
Membrane-bending coupling, 535, 563, 566–567
Membranes, 585–586, 651
Mesh generation and revision, 242, 318–320, 329–331, 341–342
Mindlin elements
arches, 568–570
beams, 495–496, 547–550
plates, 534–535, 542–550
shells, 573–574, 578–583
Mistakes, common, 363–365
Mixed formulation, 166, 195–197, 538
Modal methods
error correction for, 396–398
in harmonic response, 406–407
in heat transfer, 464–465
modal synthesis, 400–405
mode acceleration method, 397
in nonlinear problems, 398
number of modes needed, 397, 433, 442
orthogonality of modes, 388, 395, 678
problem type for, 408, 433
spurious modes and, 227, 412, 431
static correction, 397–398
theory of, 395–397
versus Ritz vectors, 398
Modeling
dynamic problems, 429–436
element selection, 337–339
error of, 3–4, 300–301
general procedure, 11–13, 336–337, 360–363
heat transfer, 467–468
mathematical model, 3
nonlinear problems, 596, 626–629, 651–654
see also specific problem areas
Modification, of structures, 292–293, 363
Multigrid methods, 320, 673–674

Natural coordinates, 203, 205–206, 259, 264–265
Natural frequencies, *see* Vibration
Newmark methods, 416–421, 425–426
Newton-Raphson methods, 597–598
Nodeless d.o.f., 109, 219
Nonconforming elements, *see* Incompatible elements
Nonlinearity
convergence, and criteria for, 601–602, 629
in dynamic problems, 398, 409, 412, 616–619, 629
gaps and contact, 288, 340, 353, 595, 619–621
geometric, 340, 367–368, 535, 595, 621–626, 653–656
material, 340, 595, 606, 627
modeling, 596, 626–629, 602
radiation heat transfer, 463–464
solution methods, general, 464, 596–602
sources of, 288, 340, 463, 535, 595
substructures, value of, 360
see also Buckling; Plasticity
Norms, matrix, 666–667
Numerical dissipation, *see* Damping, algorithmic
Numerical experiments, 363
Numerical integration
and accuracy, 213, 235–236
full, 223, 499
Gauss quadrature, 209–213
reduced and selective, 221, 223–227, 499–500, 543–547, 569–570
thickness direction, 213, 582, 585, 629
shell elements, 582
triangles and tetrahedra, 266–268
see also Locking; Spurious modes

Offsets, 280–281
Optimization, design, 369–370
Ovalization, 338–339, 585
Overlays, 320

Parasitic shear, 98–100, 227, 496
see also Locking
Patch recovery for gradients, 323–326
Patch test, 238–240, 552
Penalty function, 493
Perforated plate, 345–346
Petrov-Galerkin method, 182
Pilot studies, 344
Pipe bend, 338–339, 585

Plasticity
calculations, general, 612–616
flow rule, 606–608, 611
formulation, general, 606–609
hardening rule, 604, 606–607, 610

uniaxial, 603–605, 608–609
von Mises theory, 609–612
yield criterion, 604, 606–607, 609
Plate bending and plate elements
boundary conditions, 551–552
discrete shear elements, 550
FE surface definition, 368, 536
finite strip method, 520
folded plates, 520, 576, 583
Kirchhoff (C^1) elements, 536–541
layered, 535
limitations of, 530, 535
membrane-bending coupling, 535
Mindlin (C^0) elements, 542–550
stress calculation, 552
test cases, 552–553
theory of plates, 531–535
various formulations, 550
Poisson equation, 193
Postprocessing, 13, 365–369
Potential energy principle, 138–140
Potential function (fluids), 480
Prandtl-Reuss relations, 611
Preliminary analysis, 13, 337, 361
Preprocessing, 13
Pressure, *see* Loads
Pressure calculation, 503–504
Prestress, 350, 513–514
see also Initial stress and strain
Profile, of matrix, 43, 44
Programs and programming, 370–371

Q4 element, 96–100, 102, 168–170, 205–209
Q6 and QM6 elements, 109–111, 219–221
Q8 and Q9 elements, 100–102, 213–217
Quadrature, *see* Numerical integration
Quarter-point elements, 284–286
Quasiharmonic equation, 193–194
Quasi-Newton methods, 600–601

Raasch problem, 584–585
Radiation (acoustics), 476–477
Radiation, *see* Heat conduction and transfer
Rank deficiency, 213, 223, 226, 665
Rayleigh quotient, 387–388, 678–679
Rayleigh-Ritz method, 136, 146–150, 156–161
Reanalysis, after modifications, 292–293
Reciprocal theorem, 37, 344
Recordkeeping, 360, 364–365
Reduction of order, *see* Condensation
Refinement methods, mesh, 318–320, 329–331
Reflection, of waves, 287, 290, 476–477
Release of d.o.f., 351–352
Repetition of form, 354–356, 359
Residual bending flexibility, 549
Residuals
in dynamics, 396–398, 619
as error measure, 309–310
in nonlinear problems, 597–598, 601–602, 625
weighted residual methods, 155–156, 179–197
Resonant frequency, 405
Response history
choice of method, 373–374, 408–409, 432–434
defined, 373–374
response spectra, 426–429, 442–443
Ritz vectors for, 398–400
see also Direct integration; Modal methods
Response spectra, 426–429, 442–443
Restart capability, 366
Richardson extrapolation, 315–316
Rigid body motion, 38, 104, 163–164, 293, 364, 385, 396, 407, 523–524
Rigid links and elements, 278–282
Ritz vectors, 398–400
Rotational periodicity, 354–356

Sampling points, *see* Numerical Integration
Secant stiffness methods, 600–601
Serendipity elements, 100, 215, 219, 545–546, 583
Shape function, meaning of, 84
Shear center, 29, 338
Shear deformation, *see* Transverse shear deformation
Shear lag, 338
Shells
arches, as special case, 563–570
axisymmetric, 339, 561–562, 570–574
behavior of, 561–562
C^0 elements, 573–574, 578–583
C^1 elements, 571–573, 574–578
FE surface definition, 368, 536
isoparametric elements for, 578–583
layered, 585
Marguerre theory, 566
mechanisms in elements, 575–576
membrane locking, 567–570
membrane-bending coupling, 566–567, 576
modeling suggestions, 562–563, 576, 585–586
test cases, 583–585
warped quadrilateral elements, 577–578
Shock loading, 408

Shock spectrum, 427
Shrink fit, 350, 468, 513–514
Single element test, 294
Singularities
  and convergence, 314–315
  elements for, 284–286
  of field quantity, 124, 283–284, 290, 291, 329, 330, 341, 347
  stiffness matrix, causes of, 38–39, 108, 364, 523–524, 599, 651
Skyline, of matrix, 42–43
Slave d.o.f., 280, 359, 391
Software, remarks about, 370–371
Solids of revolution
  finite elements for, 510–512
  nonaxisymmetric conditions, 516–524
  strain-displacement relations, 510–512, 519
  stress-strain relation, 509, 519
Sparsity, matrix, 37, 42–44, 671
Spectral matrix, 395
Spectral stability, 421–423
Spin softening, 652–653
Spurious modes
  communicable, 224–227, 546
  definition and terminology, 39, 223
  drilling d.o.f. and, 108, 575, 583
  in dynamics, 227, 383, 407, 412, 431
  plates and shells, 544–546, 575–576, 583
  pressure (checkerboarding), 503
  stabilization of, 227, 383, 412, 431, 545, 575, 583
  tests for, 240, 293, 364
  see also Hinge
Stationary principles, *see* Variational methods
Stiff region, 281–282, 302–306, 494
Stiffener, eccentric, 280–281
Stiffness matrix
  assembly of, 23, 32–36, 51, 160–161
  formula for, derived, 88–89, 159–160, 194–195
  formula for, from eigensolution, 307, 676
  numerically integrated, 209–213
  physical meaning of, 21
  properties of, 36–39, 141–142
  see also Stress stiffening
Strain energy density, 142–143
Strain-displacement relations
  arches, 564
  Cartesian coordinates, 80
  large strains, 621–622
  plate bending, 532, 537, 542
  shell of revolution, 572, 573
  solid of revolution, 510, 512, 519
Stream function, 480
Stress and stress calculation
  accuracy of, 6, 115, 151, 314, 325
  averaging and smoothing, 114, 116, 320–326
  bars and beams, 47–54
  best locations for, 6, 225, 230–231, 266, 323
  concentrations, 119–121, 356–357
  contours, as error indicator, 14
  deviatoric, 502, 609
  discontinuous, 116–118
  effective stress, 117, 232–233, 609
  element geometry, effect of, 234–236, 238, 340–342, 366, 577–578
  extrapolation from Gauss points, 231–232
  with incompatible elements, 221
  intensity factor, 283–284, 286
  invariants of, 116–117
  iteration for improvement, 322
  from nodal displacements, 115
  from nodal forces, 233–234
  patch recovery, 323–326
  residual, 627
  singularities, 124, 283–286, 290, 329, 330, 341, 347
  superconvergence, 314, 325
  surface definition and, 368, 536
  thermal stress, 52–54, 115, 234, 467
  trajectories, 368
  von Mises stress, 117, 232–233, 609
Stress stiffening
  bar, beam, plate elements, 643, 645–646
  discussed, 625, 639
  forms of matrix, 650–651
  general formulation, 646–648
  spin softening, 652–653
Stress-strain relations
  anisotropic, 78, 344–345, 509, 519, 535
  isotropic, 79, 94, 509, 519
  plane strain, 94
  plane stress, 79, 533, 581
  plates and shells, 533–535, 571, 581
  substitute, 345–347, 549
  temperature-dependent, 79
Strong form, 136, 151–156
Structure, defined, 1
Sturm sequence, 680
Sub- and super-parametric elements, 202, 238
Subdomain residual method, 183
Submodels, 356–358
Subspace iteration, 390, 680
Substructures

discussed, 358–360
dynamic, 400–405
repeating, 355, 359–360
Superelement, 359
Supports, *see* Boundary conditions
Surface tractions, 82
Surface waves, 479
Symmetry conditions
antisymmetry, 55–57
buckling problems and, 57
cyclic, 354–356
heat transfer, 468
nonlinear problems and, 57, 628
reflective, 54–56
repetitive, 354–356
skew, 56–57
vibration problems and, 57, 434
System, defined, 137

Test cases, in general, 342–344
Thermal stress calculation, 52–54, 79, 115, 234, 467
Thermal transients, 464–466
Thin-walled construction, 337–339
see also Shells
Transformation
isoparametric, 204, 206–208, 218, 262
of material properties, 275
modeling applications, 276–282
of stiffness matrix, 29–32, 276
of stress and strain, 273–274
of support directions, 276–277
of vectors, 271–273
see also Constraints
Transition elements, 215–216, 358, 585
Transverse shear deformation
beams, 26–27, 170–171, 495–496, 549
plates, 533–535
Trapezoidal rule, 418, 605
Trefftz elements, 166
Trilinear solid element, 102–103

Underrelaxation, 600
Unsupported structure, 38, 364, 385, 396, 407

Variational methods, 136–171
Vibration
acoustical, 474–477
bars, 380, 387
beams and frames, 380, 385–386, 436–437
bound on frequencies, 382–383
computational considerations, 431–432
forced vibration, 405–407, 438–439
frequency estimates, 432, 437
harmonic response, 373, 405–407, 438–439
multiple d.o.f., 384–385
order of error, 383
plates, 381, 393
single d.o.f., 383–384
spurious modes and, 227, 383, 412, 431
symmetry, use of, 57, 434
see also Eigenproblems
Virtual work principle, 88, 156
Viscous relaxation, 601
Von Mises stress, 117, 232–233, 609

Warped elements, 341, 574, 577–578, 584
Wave equation, 474, 477
Wavefront solution method, 44, 671
Wave propagation, 408, 414–416, 433–434, 617–618
see also Response history
Waves, fluid surface, 479
Weak form, 136, 151–156
Weight, *see* Loads
Weighted residual methods, 179–198
Winkler foundation, 287–288, 353
Work, *see* Energy

Zero energy mode, *see* Spurious modes